13th International Conference on

Magnetically Levitated Systems and Linear Drives

Maglev '93

May 19 - 21, 1993

Argonne National Laboratory
9700 S. Cass Avenue
Argonne, Illinois 60439 USA

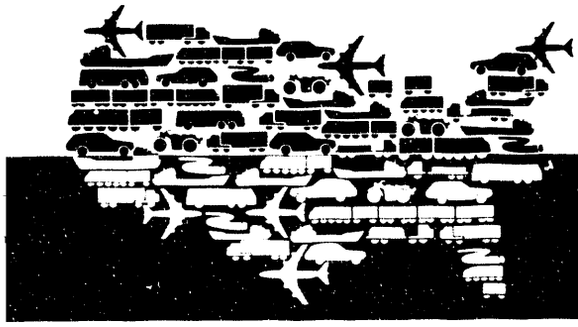

Center for Transportation Research

Energy Systems Division
ARGONNE NATIONAL LABORATORY

Sponsored by: **Argonne National Laboratory**
U.S. Department of Energy
Federal Railroad Administration
U.S. Army Corps of Engineers

CONFERENCE COMMITTEE

Co-Chairmen
Dr. Donald M. Rote, Dr. Howard T. Coffey

Argonne National Laboratory:

Dr. Larry Johnson	Dr. Jianliang He
Dr. John Hull	Dr. Thomas Mulcahy
Dr. Shoei-Sheng Chen	Mr. Lawrence Blow

United States Committee Members

Dr. John Harding	U.S. Federal Railroad Administration
Mr. Stu Kissinger	U.S. Army Corps of Engineers
Mr. Patrick Sutton	U.S. Department of Energy

Foreign Committee Members

Prof. Anthony R. Eastham	Queen's University, Ontario, Canada
Prof. Ji San Lian	Southwest Jiaotong University, People's Republic of China
Mr. Dieter Rogg	Dornier GmbH, Germany
Mr. K. Kurian John	Bharat Heavy Electricals Ltd., India
Prof. Augusto Morini	University of Padova, Italy
Prof. Eisuke Masada	University of Tokyo, Japan
Dr. Yong-Joo Kim	Korea Electrotechnology Research Institute
Prof. J.L. Mahtani	Coventry Polytechnic, The United Kingdom
Prof. Eugeny Yu Klimenkl	Kurchatov Institute of Atomic Energy, Russia

PREFACE

Traditionally the site of this conference has rotated from Asia to Europe to North America. In keeping with this tradition, this 13th Conference on Magnetically Levitated Systems and Linear Drives is being held at Argonne National Laboratory in the United States. The 11th and 12th Conferences, Maglev '89 and Maglev '92, were held in conjunction with the 5th and 6th World Conferences on Transportation Research in Yokohama, Japan and Lyon, France. Anticipating greater participation this year, Maglev '93 was organized as an independent conference. Indeed, for the first time in many years, U.S. investigators joined their Japanese and German colleagues in contributing the majority of the manuscripts received. In addition to these papers, we were gratified to receive contributions from China, Korea, Russia, Ukraine, Italy, Canada, and the United Kingdom. The many papers from countries around the world confirms the continued and renewed worldwide interest in this topic. It is as a result of your efforts that we have been able to assemble this program and organize this conference.

After a brief period in which the Japanese MLU-002 was rebuilt and changes were made to the Transrapid test track at Emsland, testing is resuming at both sites and this conference finds renewed activity and interest in maglev technologies. The substantial growth in U.S. participation is due to the R&D program supported by the National Maglev Initiative in 1991 and 1992, and the anticipation that a National Maglev Prototype Development Program will begin later this year.

We have been honored to serve this conference as co-chairmen and hope that you will find it to be intellectually stimulating and rewarding. At the conference dinner, and on the dinner cruise aboard the *Spirit of Chicago* on Lake Michigan, you will have an opportunity to become acquainted with your maglev colleagues from other countries. We look forward to visiting with our old maglev friends and colleagues and to meeting those of you whom we do not yet know.

Donald M. Rote

Howard T. Coffey

ACKNOWLEDGEMENTS

It is a pleasure to acknowledge the advice and cooperation of Dr. Larry Johnson and Dr. John Hull of Argonne National Laboratory who served with the co-chairmen as the Conference Organizing Committee. Ms. Laverne Franek served as Secretary of the Conference, and with the help of Ms. Christine McGhee and Ms. Carolyn Kowalski has patiently answered questions from participants, prepared the materials mailed to each of you, and assembled this volume of proceedings.

The conference program could not have been assembled without the help of the Conference Committeemen from around the world who successfully solicited manuscripts for this conference from their countrymen and encouraged them to be here today. After receipt, the manuscripts were forwarded to the Chairmen of the various sessions of the conference for review prior to publication in these proceedings. Our thanks are due to these Session Chairmen who conducted the business of the conference and deserve the credit for the quality of the sessions.

We are deeply grateful to Ms. Joan Brunsvold and Ms. Jackie Habenicht of Argonne's Conference Services Department for capably handling the logistics of the conference, including the booking of hotel rooms, arranging for buses, organizing the dinner and dinner cruise, for the coffee breaks, the poster boards, the audio-visual equipment and all the other minor details which together make a successful conference.

Finally, we wish to express our appreciation to the authors of the manuscripts contained in these proceedings. We are well aware of the difficulties that many of them encountered in complying with our space, time and format constraints.

The Co-Chairmen

TABLE OF CONTENTS

Development of Maglev Transportation in Japan : Present State and Future Prospects

Eisuke Masada
Department of Electrical Engineering, The University of Tokyo
Hongo, Tokyo 113, Japan

Abstract - The present state of developments is overviewed on the maglev transportation systems and the related technologies in Japan. Both EDS and EMS systems are at the final stage of development for practical applications. Their prospects are explained for future application fields in relation with their own features.

I. Introduction

The railway systems have been well developed in Japan as the mass transports for public. The urban networks withsubways and suburban systems have covered over many large cities. The Shinkansen system has extended with longer than 1,800km track connecting cities over our main land with highspeed as 270km/h. They have contributed to support socio-economical activities in Japan and assist industrial growth.

Our land is narrow and long extended over 2000km from north-east to south-west. The need for superspeed ground transportation system is considered as the growth of the demand of the Shinkansen system, especially for the connection between Tokyo and Osaka. However, the rail system has its own limit of operational velocity due to maintenance efforts to keep it with high reliability and environmental influences on the area along its track. The problem is more severe in the metropolitan area.

Therefore the developments of the maglev transports were considered and started in late 60's, in order to solve the limits of the wheel and rail system. Begining with the basic research on the new concepts and the realization of necessary components, the developments have taken more than 20 years and are at their final stage for the practical applications.

II. Short History of Developments

At early 70's, after basic researches in institutes and universities, the Ministry of Transport, Japan (MOT), the Japan Air Lines (JAL) and the Japanese National Railways (JR) were interested on the maglev system as transports in future in different application fields respectively, and started practical development for their own purposes. MOT wished to solve the problem of public acceptance for the construction of new urban transportation systems needed from the rapid increase of the population in large cities with the reduction of environmental infringement due to the operation of transportation systems based on the principle of contactless maglev system. JAL intended to introduce a new high speed transport mean to connect airports with city centers in short time, in order to keep up with expansion of the domestic air network. JR concentrated to develop the superconducting maglev system, which could operate at the velocity up to 500-600km/h and was applicable as the next generation inter-city system replacing the Shinkansen.

MOT constructed a 166m test track at Tsukimino near Tokyo. A test vehicle EML-50 of 1.8t with the electromagentic suspension system (EMS) was made and operated. It verified the technical feasibility of the maglev system, but the original concept was based on too heavy vehicle for the urban application. The council for the transportation technologies of MOT approved the necessity of the urban maglev transports and recommended their staged development in cooperation with HSST project.

In 1973 JAL completed a 1.3km test track in Higashiohgishima, Kawasaki and carried out operational experiments of the High Speed Surface Transport (HSST) system with test vehicles HSST-01 and 02. HSST is based on the concept of the combined lift and guide type of EMS system utilizing U-shaped magnets and U-shaped rail in their cross section. The technical feasibility of the system was established with operational tests at the velocity up to 308km/h. The vehicle can be lightweighted due to rather simple EMS structure and is considered to be applicable to urban transports practically.

MOT supported further development of HSST for the urban transport. Then HSST-03 was demonstrated on 400m track in Expo'85 in Tsukuba for public. It satisfied more than 600,000 passengers with its excellent riding comforts and very low operational audible noise. It impressed them as a promising future transport in urban area. Continuously demonstrations of HSST-03 in Expo'86 in Vancouver and HSST-04 in Saitama attracted interests of many peoples. In 1989 on the occasion of Yokohama fair, HSST-05 was licenced for revenue service by MOT on the basis of operational results before as a demonstration transport operable up to 60km/h. Practical development for the urban transport is taken over by the project in Nagoya based on its success in Yokohama.

After the basic research on the principle of the superconducting electrodynamic suspension system and the superconducting magnets in Railway Technology Research Institute, JR constructed a 7km long test track in 1977 in Hyuuga, Miyazaki. ML-500 vehicle recorded the highest velocity of 517km/h in 1979 and verified the technical feasibility of the system. The guideway was modified into U-shape in 1980 and the manned operation was carried out thereafter with MLU-001 vehicle successfully. Though its operational velocity was limited due to original dimension of the guideway, it attained at the speed of 401km/h. Improvement of superconducting magnets was done to increase their reliability and better their characteristics to realize applicable ones to practical system.

Though JR was separated and put into private managements in 1987, the development was continued and transfered to RTRI. The prototype vehicle MLU-002 with the half size of the practical model and equipped with bogietracks, was introduced. Operational characteristics of superconducting magnets agaist complicated dynamic motion of bogies coupled with car body were measured and evaluated for the design of the full-scale train. On the basis of the concept of this this system, JR Central Japan proposed the Linear Express Project in 1989, which would connect Tokyo with Osaka in about an hour as a future system to measure the growth of demand in the 21st century. It was approved as a candidate system for the Chuoh Shinkansen Project which reinforthes Tokaido Shinkansen as a trunk line for the Tokyo-Osaka corridor. To prove the technical readiness of the superconducting system for the project, a new large scale test track was decided to be constructed in the south east of Koufu, Yamanashi in 1990 by MOT.(1)

III. Superconducting Maglev System

In order to evaluate technical completion to be applied to a practical system with the operational speed up to 500km/h, and clarify the economical basis of the investment, the Yamanashi test track is under

construction. Technical studies are carried out continuously in the Miyazaki test track for the design of the facilities in Yamanashi and improvement of the system. The final decision for the practical application will be done until March 1998 with the results of construction and operational tests in the new test track.

A. Linear Express Project

The ridership of Tokaido Shinkansen has grown steadily and the number of passengers per day has attained up to 360,000. It is foreseen that its transportation capacity will not be able to cope with the demand in the 21st century. The second connection between Tokyo and Osaka passing over mountainous area straight has planned as the Chuoh Shinkansen from this reason.

JR Central Japan proposed to introduce the superconducting maglev system into this connection and named it "Linear Express". (2) It is considered to connect Tokyo, Nagoya and Osaka with the operational velocity of 500km/h. 10 trains with 12-16 cars will operate per hour at most. It will share the passengers in Tokaido corridor with Tokaido Shinkansen and carry more than 200,000 passengers per day. The profitability of Linear express is estimated good, if it operates alone.

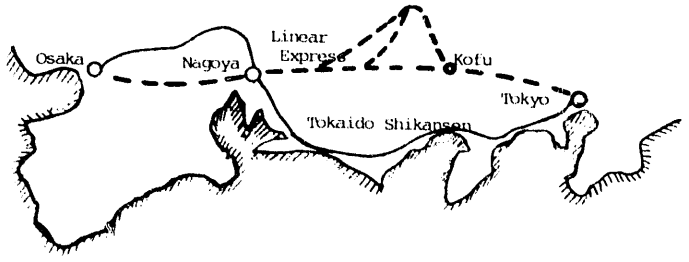

Fig.1 Linear Express Project

MOT instructed JR Central Japan and Railway Construction Corporation to investigate geographical and geological condition of the route for Chuoh Shinkansen on the basis of both conventional Shinkansen and linear express in 1990. The work will be completed in 1997. With the test results on the characteristics of the superconducting maglev system obtained at Yamanashi Test Track, the final decision for the realization of Linear Express project will be done in 1998.

B. Yamanashi Test Track

After ten years of basic develoments and operational tests in Miyazaki Test Track, MOT and JR groups decided to construct a full scale test track for the practical realization of the superconducting maglev system in 1989. The objectives of the project are:

- to complete the system technology necessary for practical application
- to evaluate economical feasibility of the system as a superspeed transportation system

To carry out enough operational tests to achieve these objectives, a new test track is needed, which has the length of about 40km, double tracks, tunnel and bridge, as well as steep gradient and curves. From three alternatives, Yamanashi Test Track located south east of Kofu was chosen. If the successful results will be got there and favorable decision will be given to the superconducting maglev system, the test track will be utilized as a part of the track of the linear express line.

The length of the test track is 42.8km, 35km of which is tunnel. Its central area of 24km is double track with a high speed switch. The highest gradient is 4%. The smallest radius of the curved track is 8,000m. The space between the center of double tracks is 5.8m. It has two substations, which feed variable frequency current to each train, and a depot for trains.

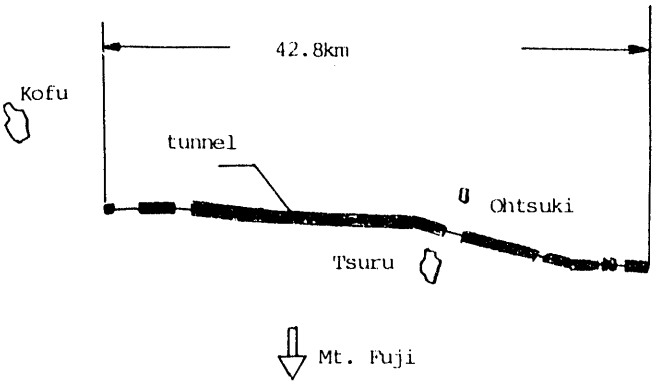

Fig.2 Yamanashi Test Track

The project was started in 1990. The construction began in 1991 and the operation will be carried out from 1995. The total amount of the project budget is 346 B¥. JR group shares main part of it. JR Central Japan invests 196 B¥. The government supports about 20% of it. 12% of it will be spent for the technical development program.

C. Definition of New System

On the definition of the system realized in Yamanashi the following improvements of the system characteristics are taken into account for practical application.

- reduction of energy consumption
- increase of system reliability

Then such modificatios are taken over the system used in Miyazaki test track before as:

- introduction of the sidewall levitation scheme
- two layer coil arrangement for the long stator of linear synchronous motor
- GTO inverter for the drive system
- coupled bogie structure for multi-section train

The basic design of Yamanashi Test Track was carried out on these concepts.

1) guideway: The long stator coils and levitation coils are installed on the side of the U-shaped guideway. In order to suppress disturbances in the magnetic field generated with the long stator and to increase operational reliability of superconducting magnets, the stator coils are equipped in two layers. The levitation coils are installed over them as shown in Fig. 3.

Three kinds of coil fixing structure and three types of beam structure of guideway will be tested in the new track for the study of economical construction of guideways. (6 combinations)

2) concept of train: Two train sets with 3 and 5 cars will be manufactured. The length and weight of the front car are 28m and 30t. Those of intermediate cars are 21.6m and 20t. The maximum operational velocity is supposed to be 550km/h. A superconducting magnet with 4 coils is installed in each side of a coupled bogie. Its magnetmotive force is 700kAT.

3) power supply station: Two power supply stations will be constructed, which can supply current independently for each train, as well as transfer powerfeed to a train between them. They have different capacity. The smaller one is equipped with a forced commutated converter to suppress disturbances to utility network. To supply variable frequency current to the long stator to accelerate or deaccelerate a train, the voltge source type, pulse-width modulated GTO inverter is utilized.

D. Technical Development Program

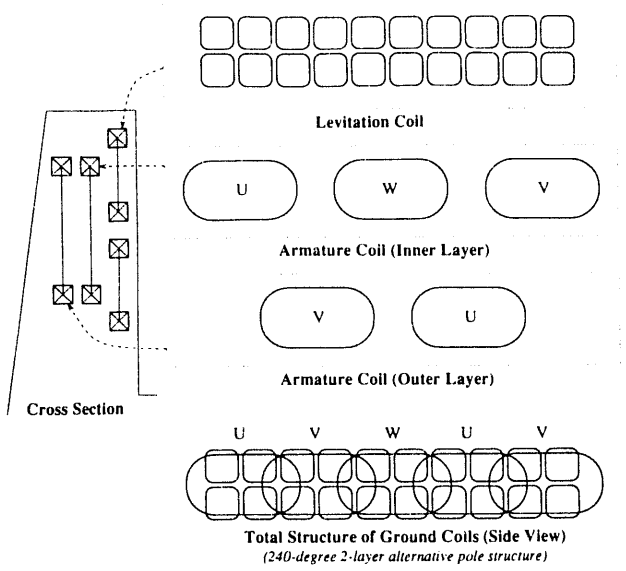

Fig. 3 Ground coil arrangement

Parallely with the construction of the new test track, RTRI has modified the facilities of Miyazaki Test Track and carried out operational tests to verify new concept and design.

1) improvement of superconducting magnets: In order to reduce the probability of quench of superconducting magnets, the mechanism of the generation of losses in them is analyzed in details. Both mechanical vibration tests and simulated vibration tests due to electromagnetic forces generated in the guideway were carried out at the bench test equipments with full size magnets in RTRI and manufacturers. Then it became clear that

- mechanical losses due to vibration in superconducting coils
- eddy current losses in the structure of the magnet caused by vibration

were influential to quench phenomena. New construction scheme is introduced to suppress these effects.

First bogie installed new designed magnets were equipped to MLU-002 and put into operation in June 1991. However, due to the interaction with the other old bogie, operational results of it were limited. The second new bogie was equipped in October 1991. Unfortunately on the first day of the operation of the new arrangement, the vehicle had a fire because of mechanical failure in a wheel and was completely distroyed.

2) sidewall levitation scheme: With EDS system, enough lift force cannot be obtained at low speed as less than 200km/h. The wheeled operation with rubber tires is required in this velocity range. If the levitation coils are installed on the surface of the base of the track, as in the original arrangement in Miyazaki, induction current flows in these coils even in wheeled operation and causes much energy losses due to low speed.

A new scheme to install these coils on the sidewall of the guideway is introduced to improve operational energy efficiency and named "sidewall levitation". If the superconducting magnet is positioned at the center of the 8-shaped levitation coil on the sidewall under wheeled operation, no induction current flows because of the null-flux principle. Then no losses are generated in them. Though the null-flux connection between coils on both sides of the guideway to provide lateral guidance force required wiring between each coil, the scheme is adopted for the practical system to reduce operational costs.

Several spans of guideways of Miyazaki have modified into this arrangement and operational tests showed successful results. Method of construction and practical installation of coils of this scheme were also studied with mock-up guideway models.

3) MLU-002N vehicle: Soon after the fire of MLU-002, MOT approved to restore it. A new vehicle MLU-002N was brought into Miyazaki at the end of December 1992 and has been operated from January 1993. Its basic configuration is the same as MLU-002, but countermeasures against fire are taken. Its features are as follows;

- aerodynamic brake is installed
- cabin material is Aluminium alloy
- without front windows
- no seats for passengers
- double frame, link coupled bogie
- 14-inch tire with the disk brake
- inframable hydraulic oil
- heat resistant piping
- sensor for inner pressure of tires
- guarding wheels

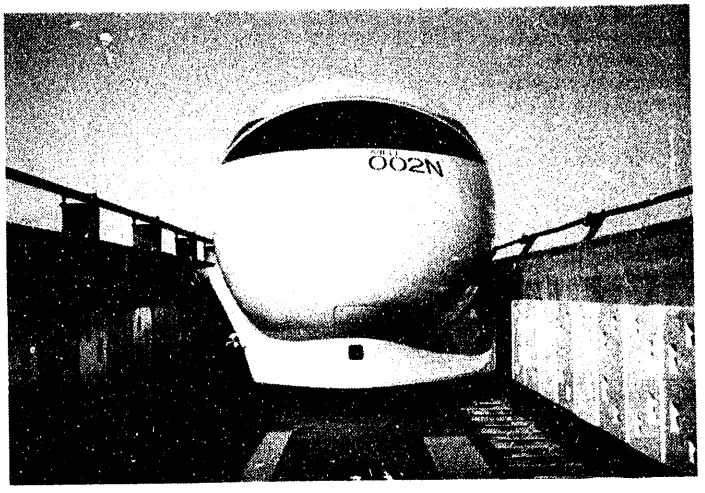

Photo 1 MLU-002N

E. Future Prospects

The future of the application of the superconducting maglev system depends strongly upon the results of construction and operational tests in Yamanashi Test Track for this several years. Though high speed rail developments are being carried out in Japan too and operation over 350km/h has been realized, their emission of audible noise to the environment is considered to be difficult to be solved for practical application. Also the problem related to the increase of air traffics over Japan should be taken into account. The superconducting maglev system has high potential as the future transportation system with larger capacity, better environmental influences and higher safety. The extension of Linear Express to further west to Fukuoka, the airport connection in Sapporo and others have been considered by local governments for possible application of the system.

IV. HSST Project

As the first stage of application of HSST, many local governments have been interested to use it for urban transports in city center. The maximum operational velocity less than 100km/h is considered to be enough, but negotiation with small radius curves and steep gradient track are required to be realizable. The con-

struction and operation costs should be evaluated in details. For its practical construction and operation, the official legislation and technical standardization should be established. The Nagoya project has been introduced for these aims.

A. Nagoya Project

For the evaluation of HSST system as an urban transport, HSST Co. (a subsidery of JAL), Nagoya Railways Co. and Aichi Prefecture formed a joint venture of Chubu HSST Development Co. (CHSST) in 1989. It constructed a new test track of 1.6km long in Nagoya, Aichi, utilizing an existing line of Nagoya Railways connecting Ohe with Nagoya Port in the south part of the city.

Various components needed for the realization of an urban transport with HSST have been installed and tested for two years.

1) guideway: The test track is constructed with a main single track and a short branch line connected with a bending switch. The main track has both elevated and grounded guideways. The latter part is used for the test section of various types of guideway construction and supporting rail fixings. Features of the main track are as follows:

- two gradient parts of 6% and 7%
- curving parts with radius of 100, 300, 1500m
- two elevated end stations
- a depot for the vehicle maintenance

The short branch line has a curve of very small radius of 25m, which should be negotiated with the operation of the vehicle in the case that the elevated guideway is constructed along the roads in urban area, using their right of way to make land acquisition for the track easy.

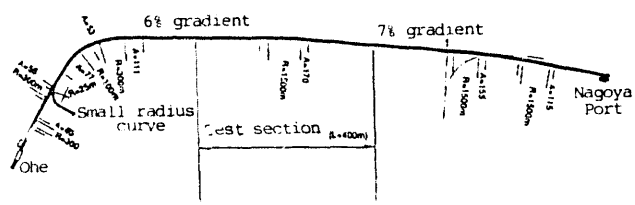

Fig. 4 CHSST Nagoya Test Track

2) vehicle: Assuming the application in the center of cities, a train unit with two cars (2-section vehicle) of rather small size has been tested. It is modeled as a half unit of the practical train unit, which consists of 4 cars and is applicable to the urban transport in a local city. The basic features of the train unit are:

- dimensions: 8.5m(L)x2.6m(W)x3.3m(H) per section
- weight of train: 18t(empty), 30t(max. allowable)
- no. of seats: 24 seats per section
- no. of passengers: 44 per section (normal)
  67 per section (max.)

HSST is based on the combined lift and guide EMS system and the short stator linear induction motor propulsion, which are integrated into a structure called "module". The basic features related to the module are:

- vertical gap length: 8mm
- 3 modules per side per section
- each module equipped with 4 magnets, a SLIM landing skids, hydraulic brakes and sensors
- modules in both sides of section are coupled each other through beams
- connected to the cabin with air springs
- max. lift force 5t

The propulsion of the vehicle is controlled with a GTO variable frequency variable voltage inverter, which regulates the stator current of 6 LIM's in each section. Both regenerative and reverse phase braking are applied directly to the vehicle by LIM's. The hydraulic brake is also operable as a back-up system and in very low velocity. The maximum acceleration and deceleration is 4.5km/h/s, but the latter can be increased up to 5.3km/h/s in emergency. The maximum operational velocity is 110km/h. The propulsion is automatically regulated based on the pre-programmed operation pattern. The protection of train operation is done with ATS and ATO.

3) Electrical system: The electrical power to the vehicle is supplied with 1500 v.d.c. from a substation at the end of the track. AL/SUS solid contact rails are equipped along a side of guideway beam. Through sliding collector the current is fed to the vehicle.

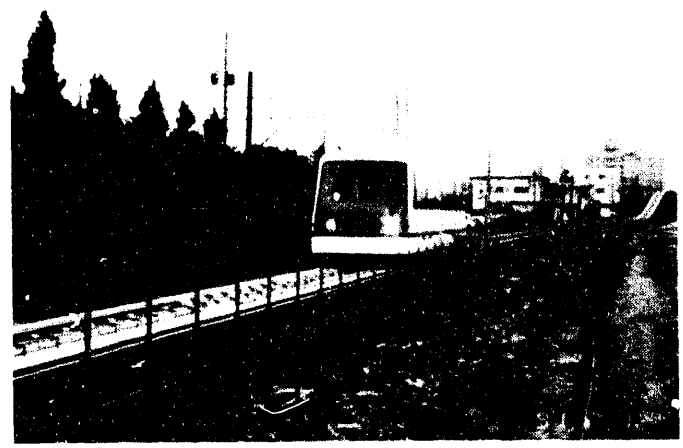

Photo 2. HSST Nagoya Test Track

It should be noted that the whole project is strongly intended to keep operational and technical compatibility with the conventional urban transportation system, as being understood from above explanation.

B. Operation and Tests in Nagoya Track

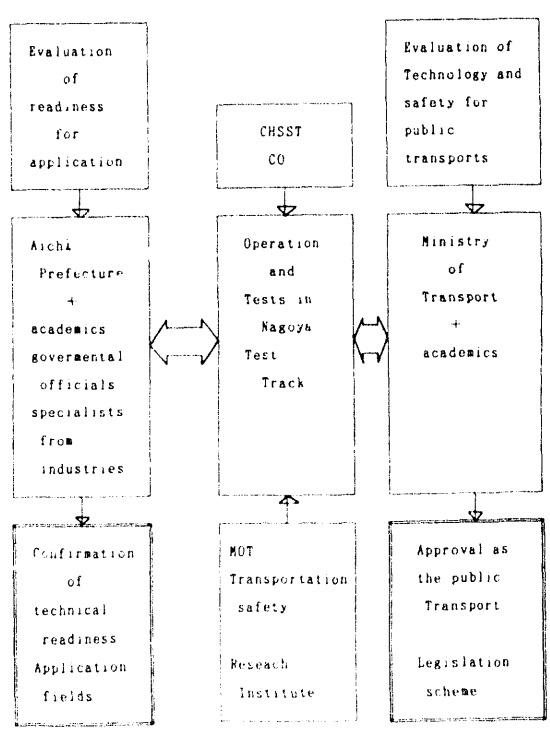

Fig. 5 Aims of Operation and Tests in Nagoya

The operation and tests in Nagoya have two objectives. Aichi prefecture has made a study on the technical evaluation of readiness as a practical system and the application field in it on the HSST, in cooperation with CHSST Co. MOT has carried out an investigation on the technology and safety of the EMS maglev system as the public transport. The program of tests was considered to satisfy both. The operation has been done by CHSST, as well as the main part of tests. The research institute on transportation safety of MOT has shared the tests related to the safety and influences on the environments.

The results of both studies are evaluated by the committee of academics and specialists respectively. The reports are completed at the end of March 1993.

C. Readiness for Application

The technology of HSST is decomposed into more than 140 items to evaluate its technical completion level and necessary investment costs to construct it as a practical system.

Since May 1991, the operational tests with HSST-100 were carried out to gather needed data for the evaluation stated above. After that the continuous operation test has been continued to attain the total length of more than 35,000km of operation. During the tests, some modifications are made both for the vehicle and guideways to improve the characteristics of the system and satisfy the requirements. The construction efforts on site and the maintenance experiences are analyzed in details to estimate expenses, too.

No important modification was needed in relation with the maglev system, other than the reinforcement of the fixing of the levitation rails.

The conclusion of the evaluation is as follows.
The only one item, the consumption of the skid for the emergency landing, is evaluated to be improved before the construction of the practical system. Other items are evaluated as technically enough completed.

On the basis of the results, the investment and operational costs of the system are calculated and compared with those of the monorail and the people mover, in relation with an assumed system of 10km long. The results show that the costs are less in the case of HSST than others, though the profits from revenue service will be obtained in longer time than the monorail due to the governmental supporting system in Japan.

Due to the higher velocity and the flexibility to negotiate smaller radius curves and higher gradients, the application fields of HSST-100 is considered to be mainly in the system, which has rather longer track as more than 10km and connects the city center to suburban residential area. Such characteristics of HSST are stressed as preferable urban transports compared with other alternative systems:

- smaller travelling time
- better riding comforts
- less audible noise to environments
- higher safety due to no-derailing structure
- robustness to weather conditions

It is also noted that the operation after the stacking of snow up to 4cm was also successfully experienced and proven to be satisfactory.

D. Evaluation as Public Transports

As a part of the technical investigation on the EMS maglev transport, MOT evaluates the technology and safety of HSST as a public transportation system. For this purpose, technical items, which are considered to be essential of the system, are listed up and related to necessary characteristics of the components, subsystem and system. These items are evaluated on the basis of test results, simulational studies, and theoretical studies. Mainly the matters on the safety and environment are studied in details.

The lateral guidance with magnets based on the combined lift and guide principle is a key item related to HSST, as an example. It is evaluated with the guidance characteristics in operation;

- performances at the irregular arrangement of rails
- operation over curved track with various velocity
- variation of gap length in normal operation

The experimental results and theoretical analysis of the motion of the module over small radius curves are examined. Then the item is decided acceptable as the public transport.

A few items related to the life of skid and brake materials are considered to be tested further before the practical application case, but the HSST is evaluated to be applicable as a public transportation system.

Even though HSST technology is considered to be applicable, it should also be based on the reasonable investment and operational costs. Then two practical cases of public transports are chosen and the costs related to HSST are calculated. The results show that HSST can also be constructed and oeprated in these cases with reasonable costs.

As a whole, MOT has concluded that HSST is applicable to practical transportation and is acceptable to be licenced as a public transport with operational velocity under 100km/h. In the case of the system with higher speed as 200km/h, further study as this project would be needed.

E. Prospects for Application in Future

Aichi prefecture studies eagerly to construct a HSST system in it on the basis of operational tests and results of the Nagoya project. As a possibility, a connection between a housing complex in the suburb and a metro station, or a transportation system from the city center to the planned expo site, both in Nagoya, is considered. HSST Co. studies also applications in urban area near Yokohama and an airport connection in Hiroshima. Hopefully one project might be realized before the turnover of the century.

V. Related Systems

The public interests on the new type of transportation system is much in Japan, but there exist some uncertain feeling on the technology. Then it is considered to be important to show publics its component technology practically and make them convince step by step. In this sense, as an intermediate stage to future transportation system, it is important to utilize its component technologies in conventional transportation system.

A. Linear Metro

The transportation authorities of metropolitan area both in Tokyo and Osaka have introduced the linear motor drive system in their subway systems. With the application of the short-stator, single-sided linear induction motor, though the basic configuration of the vehicle is basically same with the conventional inverter driven cars of the subway, the cross section of the tunnel is made small and the construction costs are reduced. The projects were also supported by MOT. Before practical utilization, similarly as the case of HSST, the operational tests of the system had been carried out with test track long time.

Though the influences of the normal forces cause by SLIM's on the wheels, the operational results in both systems have been satisfactory. Various types of the secondary of linear motors are also tested to evaluate their operational characteristics and costs. The successful operational experience of both systems have

given publics the applicability of linear drive system clearly.

B. Transportation Systems with Permanent Magnets

Other systems with magnets were demonstrated and under development too.

1) CTM: The continuous transportation system with magnets is the people mover, which is installed with permanent magnets on board and driven with moving ferro magnetic belts. The attractive force between magnets and the belt provides propulsive force to vehicle supported with rubber tires. Compared with people mover driven by the rope as the Otis system, it is considered to have more flexibility. A model system was tested in Yokohama. Another demonstration system was constructed and operated in the flower fair in Osaka in 1990.

2) ALPS: The rather shorter stator section version with electromagnets of EDS system had been also studied by RTRI.

Photo 3. Linear Metro in Osaka

The conceptional study of the suburban transportation system based on it was carried out as ALPS. The system utilizes rubber tires to lift and guide the vehicle. A new version with permanent magnets is also under study.

VI. Conclusion

The development of maglev transports are at their final stage for the practical application. The conclusion of the technical evaluation of systems based on the data obtained at test tracks are positive. The realization before the 21st century is expected hopefully in Japan. Some experiences obtained already with hybrid systems with conventional systems have given good results and proven as a good example.

Though the introduction and extension of high speed rail are also planned and developed, the maglev transport has high potential as the future system in the operational velocity, riding comforts and environmental influences, which are important features for the active society in the next century.

References

1. E. Masada et al.: "Technology of Maglev Transports" Ohm-sha (1992).

2. T. Doi et al: "Linear Express" Proc. Int. Conf. on Maglev Transports, Yokohama, (1989).

Status Quo of Development of Superconducting Maglev System in Japan

Shohiko Miyata
Maglev System Development Division, Railway Technical Research Institute, Shinjuku-ku, Tokyo, Japan

Kazuhisa Matsuda
Linear Express Research and Development Division, Central Japan Railway Company, Chuo-ku, Tokyo, Japan

Mamoru Minemoto
Japan Railway Construction Public Corporation, Minato-ku, Tokyo, Japan

Abstract - **Since 1970, Japanese National Railways have continued to promoted R&D of a superconducting maglev system. The epoch-making event for this system came in 1980 when it gained the status of a national-funded project in Japan. The government authorized a 42.8 km test line in Yamanashi Prefecture and R&D entered a new phase. The date for completion is set for the fiscal year of 1997. Our main objective is to upgrade the new test line's reliability and stability, and also to ensure commercial viability.**

This paper shows some background on R&D, the brief description of newly constructed test line and the future outlook of this system.

I. Introduction

The concept of a superconducting maglev system was advocated in the paper of ASME by Dr. Gorden Danby and Dr. James Powell of Brookhaven National Laboratory in 1966. We are most thankful for their pioneering work on this system.

Since 1970, Mr. Kyotani and his colleagues of Japanese National Railways have continued to promoted R & D of this system. He worked vigorously to establish the principle of maglev which means magnetic levitation system, by conducting many experiments from basic ones to more complex ones including the test of MLU001. His work confirmed the feasibility of this system.

The epoch-making event for maglev came in 1990 when it gained the status of a national-funded project in Japan. The Government authorized a 42.8 km test line in YAMANASHI prefecture. R & D entered a new phase. The project team consists of Railway Technical Research Institute, the Central Japan Railway Company and the Japan Railway Construction Public Corporation, was organized. The date for completion is set for the Fiscal year of 1997. Our main objective is to upgrade the new test line's reliability and stability, and also to ensure commercial viability.

Manuscript received March 15, 1993. The development of the superconducting maglev system has been financially supported by the Ministry of Transport of Japan.

II. Details of Development

In order to create a railway system which would far exceed the Shinkansen in speed, it was necessary to seek a new one. The maglev was born in the course of groping after the successor to the Shinkansen.

The following are the reasons why it has been examined.

(1) For the train to run at a high speed beyond 500 km/h, it is suspected that the conventional railway is limited by the adhesive force between rails and wheels.

(2) Adopting Linear Induction Motor (LIM) to be replaced later by Linear Synchronous Motor (LSM), will make it needless to mount a heavy motor on the vehicle.

(3) The height of levitation of about 100 mm ensures this system against earthquake.

(4) Because of non-contact, it is advantageous in maintenance.

(5) Noise and ground vibration caused by train are smaller and they are favorable for the preservation of environment.

Around 1967, the first experimental facilities that had a small

vehicle using permanent magnets and a short track with electromagnets were installed on the premises of the RTRI. It was the first step for the development. In 1972, marking the Railway Centennial in Japan, a vehicle of LIM system firstly succeeded in levitated running.

In order to prove the possibility of 500 km/h running, a test track with length of 7 km was constructed in MIYAZAKI prefecture, south-west of Japan, about 1,000 km away from TOKYO, in 1975.

In December 1979, an unmanned vehicle named ML-500 attained a maximum speed record of 517 km/h surpassing the target speed, which demonstrates the feasibility of high speed running. Subsequently, it was found that the straddled type vehicle had to be changed into more practical box type one to secure a room for the passengers, and the inverted-T shaped guideway was transformed into U shape. The manned vehicle named MLU001 after that transformation successfully attained a speed of 400.8 km/h in 1987.

The next vehicle MLU002 debuted in the same year, and the latest car MLU002N unveiled in January 1993. The tests of durability for YAMANASHI test line or practical use in future have been continued.

III. Comparison of Magnetically Levitated Vehicles

The magnetically levitated train system HSST of Japan and TRANSRAPID of Germany are levitated by attractive force using electromagnets, but the JR type maglev uses repulsive force using with superconducting magnets.

In MIYAZAKI test track, we have had the facing levitation method with the ground coils for levitation arranged on the slab of viaduct. But it was decided to change the levitation method from the facing to the side-wall type to reduce the magnetic resistance. In the side-wall levitation method, a ground coil for levitation ("8"-figured coil) formed by transposed connecting the small upper one with the lower one is set up on the side-wall of the guideway.

Though the magnetic resistance which influences electric consumption in running increases at low speed, the side-wall system, which is superior inefficiency of levitation force to the facing one, may reduce the electric drag.

Besides, there is merit that the high voltage at null-flux cables will be cut down by using the side-wall levitation coils for lateral guidance of the vehicle instead of as coils for propulsion.

The side-wall levitation method has already been set up on some sections in MIYAZAKI test track, and the data about the vehicle motion, riding comfort, etc. were collected.

This will be adopted in all sections of the newly constructed test line in YAMANASHI prefecture.

IV. Brief Description of New Test Line Construction

In order to put the vehicle to more practical use as means of railway, a new test line which has the sufficient facilities to promote the technological development related to the maglev will be needed in future. This is due to the facts that the MIYAZAKI test track is only 7 km in length with a single track and the structures consist of only viaducts and bridges, that it is impossible to carry out a running tests in tunnel sections.

Japan Ministry of Transport (MOT) made investigations and studies on the site suited for construction of a new test line and the step of pursuing the technological development for its realization.

Meanwhile, MOT set up an internal committee called "The Superconducting Magnetically Levitated Train Study Committee" (chairman: Prof. Dr. Eng. Yoshiji MATSUMOTO, Science University of TOKYO) in 1988.

The requirements for the new test line agreed upon by the Committee are as follows;

(1) There shall be a continuous straight section.

(2) There shall be a curve.

(3) There shall be a steep slope section.

(4) There shall be structures such as tunnels and viaducts.

(5) Besides fulfilling the above requirements, the test line shall have an overall length of some 40 km or so.

After the discussion being made concerning the test line construction site, the Committee selected YAMANASHI prefecture as the best one from the view point of feasibility of achieving the test objects, effective use in future and obtaining the cooperation of local authority concerned.

The plan for development of fundamental technology and the plan of YAMANASHI test line construction are approved by the Minister of Transport in June 1990, and these plans are being pursued.

The YAMANASHI test line has a length of 42.8 km including about 35 km length of tunnel sections, partially with double

tracks. And it has some sections with maximum gradient of 40 permillage (4 percent), and with minimum radius of curvature of 8,000 m. The distance between the centers of tracks is 5.8 m.

The following are main items to be tested;

(1) Stable run at 500 km/h with safety and comfort.

(2) Reliability and durability of vehicles including superconducting magnets and ground facilities.

(3) Structural standards specifying a minimum radius of curvature, the steepest gradient, etc.

(4) Distance between both guideways taking account of two trains passing each other.

(5) Vehicle performance related to tunnel cross section and to the pressure fluctuation in a tunnel.

(6) Turnout performance.

(7) Control system between substations.

(8) Multiple train operation control system.

(9) Safety operation system.

(10) Environmental preservation.

(11) Technical standards on maintenance.

(12) Investigation of cost performance, and grasp of construction and operation cost.

V. Condition of Proceeding

In September 1991, the ground-breaking ceremony was held for east-side section of KUKI Tunnel in Tsuru-City, which is to be about 1,670 m long, it was the first phase of the constructions. And now, the excavations in 9 tunnel sections are in process by the Japan Railway Construction Public Corporation and the Central Japan Railway Company. At open section, theworks for infrastructures such as bridge and viaduct will be started in already prepared section.

But progress in the works delayed about a year because of a difficulty in right-of-way purchase. Otherwise, with the improvements of specifications achieved such as boosting the blocking voltage in the ground coil for propulsion and enlarging the capacity of GTO inverter, a higher acceleration can be set in the run-curve.

In order to begin early the running test in some section where the construction was finished, it was concluded that "The Priority Section" which had a length of 18.4 km set up at midpoint including the main installations such as a substation, a test center and a car shed was constructed on priority basis. Although a test will remain for stability and durability over long period, prospects for the technology development have been confirmed by the running test in the priority section, with the stationary test and some simulations, will have to be planned with Fiscal Year 1997 target unchanged.

VI. Conclusion

We have been researching and developing a superconducting maglev system for 24 years. And we now are highly honored to be conducting a "national project" of this magnitude. But, several obstacles must be overcome before we have a commercially viable system. Two main ones are;

First, we have to ensure reliability and durability of the magnet system as well as the total system when it is running at super-high speeds for a long time. In order for us to do this plan to perform as many tests as possible at super-high speeds on the new YAMANASHI test line.

Second is the issue of cost. In order to reduce the running-cost we made a major improvement by shifting levitation ground coils from the floor of the U-shape track to side-wall, thus, reducing the running resistance. And we are also making an effort to reduce the construction costs of the total system.

The construction of the YAMANASHI test line is going on. Our anticipated success on this test line will be a major step towards building a "CENTRAL LINEAR EXPRESS" linking TOKYO and OSAKA. Because of this, the focus of much of our work is the national YAMANASHI test line project.

We are convinced that the superconducting maglev system will be an important transportation system in the next century. After all, it is an ideal system offering super-speed service, high energy efficiency and the least pollution of environment.

The Development of the Superconducting Maglev system

Kan-ichiro Kaminishi
Maglev System Development Division, Railway Technical Research Institute, Shinjuku-ku, Tokyo, Japan

Akio Seki
Linear Express Research and Development Division, Central Japan Railway Company, Chuo-ku, Tokyo, Japan

Hitoshi Tsuruga
Linear Express Research and Development Division, Central Japan Railway Company, Chuo-ku, Tokyo, Japan

Abstract - **Today, in Yamanashi Prefecture in Japan, we are constructing a 42.8km test line using a superconducting maglev system whose technology is based on the best results achieved by the efforts of the defunct Japanese National Railways (JNR) and Railway Technical Research Institute (RTRI). The new test line, having as many useful installations as possible to operate the revenue service, will be used for evaluating the practicability of a superconducting maglev system.**

This system features an electrodynamic levitation system (EDS) which enables a superhigh speed running without any special control device for levitating a coach as well as guiding one. Using this fundamental method, we developed and designed a new test line, which is mainly composed of vehicle, guideway, linear synchronous motor (LSM) and so on. To be a practical transport means in the 21st century for high speed operations, the maglev system requires high running stability and perfect safety, including the friendliness to the environment, even if it may involve all the possible risks which originate from outer disturbances or any other troubles. To fulfill these requirements, we conducted many laboratory works and full-scale running tests. Through these efforts, we have identified the problems, devised countermeasures to solve them, and developed subsystems. The design of the Yamanashi test line is based on these achievements so far gained. Today, the development is coming into a more practical phase of assessing the reliability, the durability, and the economic efficiency using a new long test line.

Manuscript received March 15, 1993. The development of the superconducting maglev system has been financially supported by the Ministry of Transport of Japan.

I. INTRODUCTION

Two years before Bullet Train of Tokaido Shinkansen came into being, JNR started basic research on super-high speed railway systems in 1962, which has led to the present superconducting maglev system composed of both LSM and EDS. During the past 30 years, the technology has made great advances; for example, superconductors, power electronics, engineering plastics, to name a few. This progress has made the manufacturing subsystems easier and more reliable. In the early stage, based on the experiments, we pursued feasibility studies vigorously. But, now, we are struggling with the problems concerning the manufacture, the maintenance and the environment.

In 1987, JNR was privatized and divided into seven Japan Railway companies (JRs) and so on. RTRI took over the work of R & D and also all the matters concerning the MAGLEV system from JNR. In 1990, the Government authorized constructing a 42.8km test line in Yamanashi Prefecture. To push ahead with this plan, a project team, which is composed of RTRI, Central Japan Railway Company (JRC) and Japan Railway Construction Public Corporation (JRCC) was organized. Now, this team is held responsible for the construction of the Yamanashi test line.

The facilities in the test line will be made using the best technology available and all the necessary equipment for the commercial maglev service will be furnished as far as possible. Using this test line, we shall evaluate the serviceability of this superconducting maglev system, that is, JR maglev system. As for the Miyazaki test track, full-scale test runs using it will

be kept up, and the results thereof will be reported to the committee of the Yamanashi project team.

II. JR Maglev's Feature And Principle

JR maglev system, using a superconducting magnet (SCM), features a super high speed running without any control process, which is achieved by the EDS. The utility of this system will be confirmed through the running tests on Yamanashi test line.

The principle of a superconducting maglev system is as follows:

An onboard SCM can be moved by a travelling magnetic field caused by the current of ground coils for propulsion. Thus a maglev train runs synchronized with the ground travelling magnetic field of a linear synchronous motor (LSM). A moving SCM produces an induced current in the ground coils for levitation, which generates a repulsive force between the ground coils and SCMs. This is an electrodynamic levitation system (EDS). As the train speeds up, the levitation force increases. But, at low speeds, the induced levitation force is not enough to lift a maglev train, which then needs rubber tires to support itself. A guidance force can be obtained by the current induced in the levitation ground coils, linking both side levitation coils by a null-flux cable. When a vehicle runs on the center of the guideway, no guidance current is induced. But, when it runs leaning to one side, a guidance current will be generated, which makes a guiding force. This is a null-flux guidance.

As for the braking, JR maglev normally uses a strong power-regenerative braking. However, against any trouble in the ground facilities or the vehicle, some safeguards will be available, such as a coil short-circuit braking, an aerodynamic braking and a wheel disc braking.

The running stability of SCM has been studied sufficiently. But, in the case of a quenching trouble with loss of the magnetomotive force of SCM, a null-flux guidance generates an unnecessary guidance force. To avoid this unnecessary force, both side pairing SCM will be discharged promptly. And besides, the onboard stopper wheel is provided to protect the side of the car body against abrasion. Even in this case, we can move the maglev train up to a safe place using other energized SCMs.

As a quenching trouble influences the system reliability, we performed stationary vibration tests using an electromagnetic field, in a simulation test. This equipment can generate an electromagnetic field which is equivalent to the actual electromagnetic field to which the running SCM is exposed on account of energized track coils. Through testing, we have acquired good prospects.

III. JR Maglev's Technical Difficulties

Aiming at the revenue service, we need to confirm the ability of the 14 subsystems, which are scheduled to be introduced in Yamanashi test line as many as possible (see Table 1). Table 1 reveals what is peculiar to JR maglev and what is different from the conventional iron-wheel system though it may look similar to the conventional system at a glance. Besides, the technology which is common to all systems is listed.

To commercialize JR maglev, not only the performance of each subsystem, but also its environmental compatibility, safety, reliability, durability and economic efficiency have to be well balanced and perfect. The Yamanashi project team is making efforts to put together all subsystems into an integrated well-balanced system, i.e., the best system.

Concerning the conventional rail-wheel system, we have sufficient know-how and standards. On the other hand, as for the superconducting maglev system, I regret to say, inexperienced matters remain. So, we are now making a review covering a wide area, such as all the design specifications, advance survey of the weak points in each part, the system safety in all the cases of failures which may occur. We have used some effective means of the failure mode and effect analysis (FMEA), the Fault Tree Analysis (FTA) and so on.

IV. Major Results To Be Utilized In Yamanashi Test Line

In the following, we present major results to be implemented in Yamanashi test line -the results derived from R & D up to now in vehicles, guideway, driving system and so on.

Progress is remarkable, especially in the stability and the efficiency of JR maglev system.

A. Development in the field of vehicles

TABLE 1
CONFIGURATION OF THE JR MAGLEV SYSTEM

Subsystem	Peculiar technology to JR maglev	Similar technology between new and conventional systems	Common technology between new and conventional systems
Running operation	Generating a running curve		Supervision of operation Management of diagram Control of route
Traffic control	Traffic control pursuing a train movement	Blocking control Train speed control with monitoring	
Telecommunications	Inductive wires for inductive radio transmission		Leakage coaxial cable Information system
Train position detector	Inductive wires for inductive radio transmission	Train position detector	
Power supply and driving	Driving control Propulsion coil Feeder section switch boundary section switch	Power converter Feeder	
Suspension and guidance	Coils for levitation and guidance Null flux cable		
Guideway	Running way Guiding way	Turnout	Tunnel Viaduct Bridge
Station	Platform		Information
Vehicle	SCM Magnetic shielding Auxilliary guiding wheel Auxilliary supporting wheel Onboard power supply	Track Onboard conrol unit Onboard braking equipment Coupling device	Car body
Cabin facilities		Ventilation facilities	Broadcasting Accommodation Onboard equipment
Car depot	Cooling system Exciter		
Distribution			Distributing Charger
Ground equipment			Protection for overrun Protective equipment Preventing disasters
Maintenance wagon		Inspection wagon Service wagon	

We have made some test vehicles which are listed in Table 2, in which we introduce the main results. Among the listed vehicles, the test vehicle coded ML-100 is one exclusively using the linear induction motor (LIM), having an onboard reaction plate and running on the active track. Other vehicles are driven by LSM. The car named ML-500R is the first one having an onboard refrigerator which re-liquefies the recovered evaporated helium gas. The truck of the car named ML-500 is applied to the car named ML-500R, whose car body has been made newly for the onboard refrigerator. As a more practical testing car with a box type cabin, we made a train set named MLU001 composed of three motor cars having 8 SCMs to one car. Running tests with a single car and with a train set have been carried out. Unfortunately, the car named MLU002 was

TABLE 2
THE TEST VEHICLES OF JR MAGLEV AND RESULTS

Year manufactured	Names of test vehicle	Typical results
1972	LSM200	Running by LSM
1972	ML-100	Verification of EDS
1975	ML-100A	Prototype of JR Maglev
1979	ML-500	Confirmation of high speed running at 500 km/h
1979	ML-500R	Onboard refrigerator
1986	MLU001	Running of train sets Testing of train motion
1987	MLU002	Concentrated arrangement of SCM on truck
1993	MLU002N	Elastic suspension of SCM

spoiled by a fire on last October 3rd in 1991. Using a new car named MLU002N which has two aerodynamic braking sets, test runs on Miyazaki test track have been resumed in Jan. '93.

Up to the present, we have developed a simpler I-type SCM; a lighter concentrated arrangement of SCM using a truck; a downsize onboard refrigerator to re-liquefy the evaporated helium gas; a track brake system with sliding frictional shoes for high speed running; an aerodynamic brake and so on.

Now, using MLU002N, we are completing with an elastic suspension truck system, a wheel disc braking which is available at a high speed of 500 km/h. These products are to be implemented in the new test cars for Yamanashi test line.

B. Development in the field of guideway

We began with a test using ML-500 on an inverted-T type guideway in Miyazaki test track in 1977. In 1980, the guideway was changed to a U-type and the testing car was changed to MLU001. Recently, we changed a normal flux levitation system to a null flux magnetic suspension system which reduces magnetic drag and increases levitation ability, which has been verified mainly by MLU002 since 1988. This change has borne fruits, which make it possible to simplify the maintenance work of guideway, that is, the re-alignment work is restricted to one face of the side-wall, having levitation coils and propulsion coils. Besides, the side-wall has become a "beam" fabricated to high precision as a precast concrete beam. Then manufacturing a side-wall beam has become much simpler, that is, we can manufacture side wall beams in a yard near the construction site. In the same yard, we can also set up all the ground coils. Therefore, with high accuracy and without laborious work, we can build a maintenance-free structure, that is, a side wall beam.

In the development of a turnout, we developed two different types, one of which is a traverse type for high speed running and the other is a side-wall concrete traversing one for a car depot.

C.Development in the field of propulsion system

The propulsion system is composed of a train position detector, an LSM propulsion control equipment, a power converter, a feeder, a feeder section switch, a propulsion coil and so on. The system configuration of a propulsion system is presented in Fig.1. When running on the guideway, a vehicle issues a signal. This makes it possible for us to know where the train is running using an inductive wire for inductive radio transmission. Using this position data, the LSM propulsion control equipment outputs which section must be energized and what power, that is, propulsion current must be supplied. A power is supplied to the appointed feeding section using a feeder section switch. This switch changes over as every train passes. As its frequency is very high being equal to the running frequency, we have developed a much more durable switching gear, for example, can be switched 300,000 times.

Even when a maglev train is crossing over the feeding section, to propel a train smoothly we have used a two-power converter system in Miyazaki test track. To improve the fault tolerability of the power supply system, we have decided to adopt a three-power converter system in Yamanashi test line. Using this system, we can drive a maglev train when one power converter fails. Besides, the total capacity of the power supply equipment will be reduced to three-fourths of a two-power

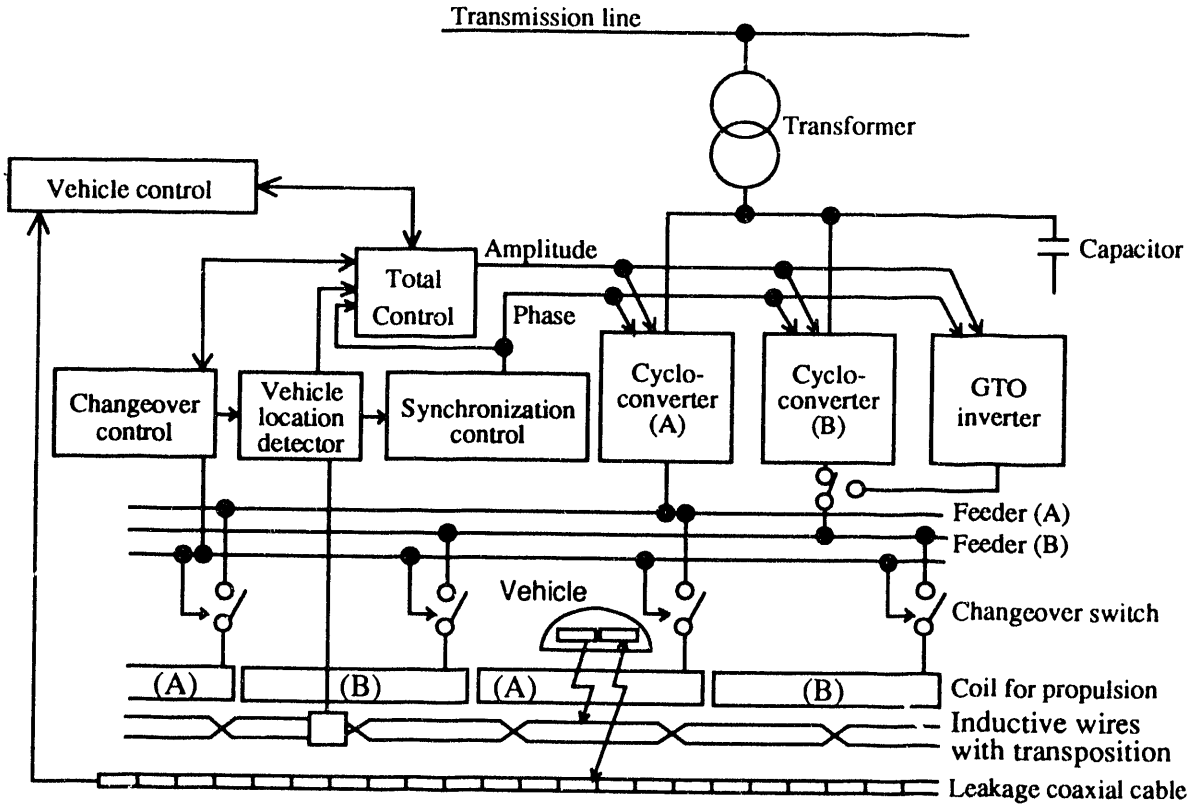

Fig. 1. Power supply system of Miyazaki test track

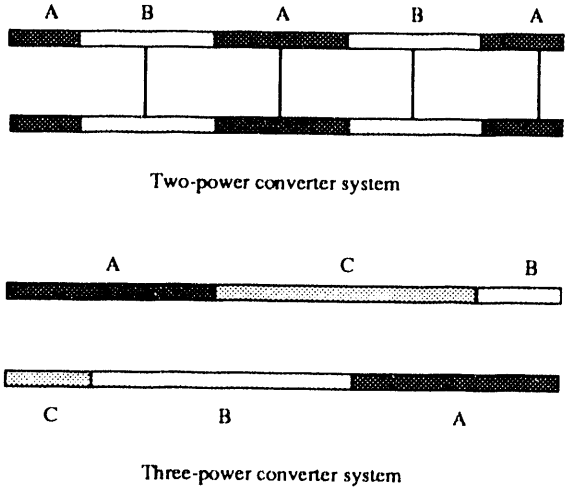

Fig. 2. Feeding Arrangement for propulsion coils

converter system.

The development of the power converter equipment is underway as follows:

At Miyazaki test facility, we have used a cycloconverter with a thyristor element. As this is a direct conversion type without intermediate direct current (DC) circuit, a characteristic of the load may influence the electric power system. Therefore, in the early stage, we have used a rotary type power converter with a motor-generator set as the first converter. The next converter is a circulating current type cycloconverter without a frequency converter as a motor-generator set, its capacity being 16 MVA. Even this type needs many capacitors to improve the power factor. And in an area with low power capacity, the cross influence between the load and the power system through the cycloconverter is undesirable.

Meanwhile, today, the technology of the large power gate turn-off thyristor (GTO thyristor) has progressed remarkably. So, we decided to develop a large power pulse width modulation (PWM) inverter as a power converter with DC circuit.

Using this type, unacceptable cross influence will not occur, being eliminated by intermediate DC circuit. After authorization of Yamanashi test line, we have installed a PWM inverter in Miyazaki test facility for testing, whose capacity is 10 MVA. The data derived from this inverter set are available for designing the new large inverter of Yamanashi test line, whose capacities are 20 MVA and 38 MVA.

V. Testing items in Yamanashi test line

As for the details of equipment installed in the new test line which are presented in the poster session, we have simplified the description. The technical assessment concerning the equipment is conducted in three steps as follows:

First, the basic running performance of each of two train sets is confirmed, such as the acceleration and the deceleration when running on a curve section, a gradient section, a tunnel section.

Second, considering the revenue service, the overall running performance is confirmed, such as passing each other test runs, substation cross-over test runs, simultaneous multiple trains operation tests, test runs with artificial failures.

Third, the continuous test run at high speeds is confirmed to assess the reliability and the durability of the total system.

In parallel with these tests, we conduct other tests concerning the passenger physiology, the influence on the environment, the economic efficiency, the maintenance specifications and so on.

ACKNOWLEDGMENT

We express our appreciation to all the people who have permitted us to participate in this '93 maglev conference and who have been in charge of business involved in our participation.

Outline of HSST-100 System and Test Line in Nagoya

Masaaki Fujino
Managing Director, Engineering
Chubu HSST Development Corporation (CHSST)

Abstract - **HSST–100 is an urban transit version of Maglev – HSST (High Speed Surface Transport) system, which has been tested for the sooner practical use by CHSST (Chubu HSST Development Corporation).**

This paper reports HSST–100 system and its test runs on the test line in Nagoya, Japan.

I. General and History of HSST

A. HSST Development before CHSST

HSST is nonwheeled maglev vehicle system which is supported and guided by attraction forces between electromagnets and iron rails, and propelled by LIM, Linear Induction Motor.

HSST development work was started by Japan Airlines in 1974, and has been succeeded by HSST Corporation since 1986.

Before CHSST establishment, five HSST vehicles from HSST-01 to HSST-05 were built, tested and operated.

Especially, HSST-05 was operated on the first maglev commercial line with Railroad license in Japan though it was a temporary operation at low speed in '89 Yokohama Expo site.

B. CHSST

HSST demonstrated its maglev operations at six expos (two International expos included), however, the operations were made at low speed due to limited track lengths available and the conditions were not enough for the complete system test.

To be certified as the public transit system, HSST has to demonstrate its system performance for safety, reliability, economy, etc through the repeated runs on the test line with sufficient length, necessary curves and slopes.

CHSST was founded in 1989 by Aichi Prefecture (a local government), Nagoya Railroad Company and HSST Corporation to conduct test runs of HSST-100 system.

Aichi Pref. conceives a plan to construct the 10km HSST commercial line in east of Nagoya City.

C. HSST development after CHSST

CHSST decided the specification of test line, then constructed it in Nagoya City. Two-year long HSST–100 test runs started in April 1991.

The special committee to evaluate HSST–100 System was organized by Aichi Pref. It consists of Chairman Prof. Masada and other professors, government specialists (Ministries of Transport and Construction, and Aichi Pref.) and engineers of manufacturing companies (vehicle, electric systems, signal systems etc) and construction companies. The committee also gives advices regarding test plans and test items.

Ministry of Transport (Japan) has formed another committee which discusses how to revise transportation regulations etc for the practical use of Maglev (normal conducting) systems.

II. Outline of HSST Test Line in Nagoya

A. General

Nagoya test line is 1530 m long single lane track including a track switch (turnout). Fig.1 shows a plan and profile of the test line that is capable to make all types of test runs for HSST–100 system and is equipped with steep slopes, small curves and a track switch. Maximum (design) speed is 110 kph for this line.

Table.1 shows major specifications of HSST–100 system and Nagoya test line.

B. Test Vehicle and Test Facilities

1) Vehicle: The test train consists of two HSST–100 cars which are called MC1 and MC2 respectively as shown in Fig.2, and the car bodies are made of aluminum alloy.

Modules are HSST's essential parts that are similar to the truck bogies of conventional train, and contain all of levitation magnets, LIMs, brake system etc. Each car has six modules which are connected to the car body with air springs and slide tables. Fig. 3 shows Modules.

LIM output (drive and brake forces) is controlled by VVVF Inverter (Variable Volt./ Variable Freq.) loaded

on MC2 car.

Normal brake system is LIM/Hydro-combined type with vehicle load compensation function, and it consists of LIM brake (Regenerative/Reverse phase) and Hydraulic (mechanical friction) brake which is applied in case of insufficient LIM brake.

2) Guideway and its structure: Test line has minimum curve of 100 m radius (8 degrees of cant angle or superelevation angle) on main line and 25 m radius on a branch line beyond a switch.

Main line has two steep slopes with 70/1000 and 60/1000 gradients respectively.

1000 m radius vertical curves are incorporated to smoothe the gradient change points.

Fig.4 shows a guideway structure for standard portion. Each rail has an inversed U-shape cross section and is covered with aluminum reaction plate on its upper surface. Rails are bolted onto PC girders with H-shaped steel cross arms in 1.20 m pitches.

Various combinations have been constructed to test the characteristics in the cost, maintenability, etc.

They are Rail installations onto :

- PC girder with Steel Cross arms (Basic)
- PC girder with PC Cross arms
- PC girder with Steel Bracket (not Cross arm)
- PC/Steel girder directly (without Cross arm/Bracket)

One track switch is installed on the test line, and it is 3-segmented level turn type. Major switch structure consists of one Main moving beam, two Dependent beams, Beam locking mechanisms and Transition rails.

Dependent beams are linked to the main beam in series, and all beams are driven electrical (AC) motor through link mechanism. Beam locking mechanism is to lock the moving rails in each switched position. Transition rails are provided to make rail cnnecting angles smoother. One switch operation from one position to another can be done within 15 seconds.

3) Electric power supply facility: A substation located along the test line supplies 1500 V DC to the trolley rails, and it is equipped with a power absorber unit which disposes energy regenerated by LIM brake.

Trolley rails are Aluminum-Stainless Steel combined rigid type with side contact surface, and two rails are installed on both sides of girder respectively.

4) Signal Facilities: Dual functions are provided for end station overrun protection. One is multi-step ATP (Automatic Train Protection) which activates an emergency brake in case of a train overrun condition detected, and the other is the normal automatic brake activation based on the normal operation pattern prior to an emergency brake.

Train detection is based on the continuous check-in/check-out method. Speed measurement is made through counting and processing pulses on the pattern belt (signal cable).

III. Test Runs

A. General of test runs

The purpose of the test runs is to collect the demonstration data which verify HSST-100 system is complete for the practical use. More than 100 items of test runs in various range have been conducted in these two years.

Major test items are:

a. Characteristics of Vehicle, Guideway, Electrical Power, Signal systems for levitation/guidance

b. Measurement to establish the design load conditions on guideway

c. Safety and Capability for operations in case of system failure, rescue of failed vehicle, etc.

d. Levitation characteristics and Ride quality to establish guideway precision tolerances (test for bad conditions)

e. Measurement of Ride quality, Noise, Vibration on ground, Mag field leakage, Electric field intensity

f. Measurement of Power consumption, Parts' wear, Maintenability, etc.

g. Endurance and Reliability of Vehicle system and Switch for long period/repeated operations

h. Operations in adverse weather conditions (wind, snowfall)

B. Schedule of Test Runs

Test runs began with preliminary test including unit car test and speed-up test, then the planned items were tested with both empty and fully loaded vehicles. Abnormal and bad conditions' tests and the long period run tests followed to check the system performance in safety, environmental aspect, reliability, maintenability, economy etc including emergency cases. Fig.5 shows the test run schedule.

Prior to vehicle test run, the function of power collector unit was tested at a speed over 100 kph with a rotating disc test machine.

In speed up test, speed was increased, step by step, up to 100 kph while confirming the safety and basic performance, and correcting discrepancy as necessary. After completion of speed up test in early October '91, to lessen yawing motions of vehicle, an oil damper was installed near the coupler portion between cars. Then, more than 100 items advised by the committee were started to test.

From March '92, tests of guideway, mainly for the on-ground (not elevated) experimental girders, including 100 m radius curve and a track switch, were conducted with both normal (levitated) and nonlevitated runs (sliding with skids).

Last test items with fully loaded train from August 1992 to September, were passing through the guideway in abnormal conditions such as displaced rail connection (with wide gaps in vertical/lateral) etc to obtain the data necessary to confirm the guideway precision tolerance (requirement).

The long period run tests through the days from morning to night for Endurance and Reliability, were started in October '92, and will be completed in June '93, targetting 20,000 km of train run distance (grand total 32,000 km).

The track switch was successfully completed 50,000 times' continuous operation tests, and the test is planned to last up to end of March '93 (estimated 80,000 times).

Ministry of Transport of Japan (MOT) has formed a special team to establish the standards for Maglev transit including HSST system, and Traffic Safety/Nuisanse Research Institute of MOT has conducted 7 times of evaluation test/measurements on HSST-100 since September '91.

IV. Results of Tests (part)

A. *Vehicle (Levitation/Guidance)*

5) Levitation gap and Guidance gap: At 100 kph run with full loaded weight, a levitation gap fluctuation was normally ±2 mm, and ±3 mm of peak values observed on passing through the rail connecting point with maximum tolerable rail displacement intentionally set. So they are well within ±6 mm of mechanical moving range and there is no possibility of contact with rails during runs.

Maximum lateral oscillation observed was 12 mm of a full amplitude (6 mm per side) and it is within lateral movable range (15 mm, contact with guidance skid).

6) Levitation characteristics for running speed: Fig.6 shows levitation gap fluctuations for various speeds (coast operation) with full loaded weight. RMS values (average of fluctuations at forward and aft of module) are proportional to square root of speed. At 100 kph, RMS of fluctuation is 0.8 mm, and a peak value is 3 mm or approximately 4 times of RMS.

Fig.7 shows magnet power consumption that is calculated from magnet resistance and measured magnet currents.

At 100 kph run, it is 0.88 kW/each tonne of train weight that is 1.3 times of power at zero speed.

B. *Signal (function and noise characteristics)*

Fig.8 shows the signal system of the test line. It consists of Normal Brake Pattern (similar to ATC indication) indicated to the train corresponding to the absolute train position, and Automatic Train Protection (ATP) system by equipment provided along the track.

Reliable and fail-safe speed detection for Overrun Protection is made by counting pulses on twisted loops of pattern belt (signal cable).

7) Normal Brake Pattern function test: It was verified that Brake Apply/Release actions were taken in 1.4" (design : 1.6") of response delays in both signal and actuation systems when the overspeed occurred.

8) ATP Emergency Brake function test: It was also verified to function in 1.3" (design : 1.6").

With both Normal and Emergency brake functions, Overrun Protection was verified as satisfactory.

9) Noise characteristics test: Pattern belt (signal cable on the girders) and antennas of signal system may inevitably pick up noises emitted by the potential onboard noise source equipment (levitation coil, LIM, power collector, electric cable, etc.), however, the measurement verified that the effects by equipment noises are within the acceptable range, for example, noise level in Train Detection system is below −60 dBv, or with 13 dB of reserved margin for the minimum required level.

C. *Infrastructure and Guideway*

Measurements were made mainly to establish the design load coditions and to check details of structure. Measured items were displacements, stresses (strains), acceleration, etc of rails and sturctures for both dynamic (vehicle test run) and static (temperature effect) conditions on nine (9) girders, four (4) piers and a track switch.

10) Temperature effect: Temperature of rail surface was highly corelated with the ambient temperature, as shown Fig.9 and below:

$$\text{RailTemp.}(^\circ\text{C}) = \text{AmbientTemp.}(^\circ\text{C}) \times 2.644 - 43.80$$

During daytime, the temperature on sunny side rail surface is hotter than on shaded side by 2 – 3 °C, and almost none of temperature difference at night.

Five (5) mm of the daily vertical displacement at mid point of 20 m span PC girder was observed (without train load, convex in daytime/36.3 °Cmax, and concave at night/25.1 °Cmin, due to difference of heat propagation for rail/PC girder).

11) Dynamic load test: As typical sample of tests to establish the load condition for structural design, Impact load factor is shown here.

In contrary to the wheeled systems, HSST is supported by levitation magnets with distributed load along almost full train length.

Train impact load (vertical) is defined as the product of Train load (max weight) and Impact load factor,i .

$$i = (d - s)/s$$

while,

d : stress or displacement by dynamic load

s : stress or displacement by static load

Fig.11 shows Impact load factor, i, calculated with the equation above and the measured stress and displacement of PC girder of test line, and also shows Impact load factors used for HSST test line design and for the design standard of other transit systems.

As shown, HSST's Impact load factors observed in test are much less than the standards of other transit systems.

V. Maturity of HSST-100

The evaluation committee has evaluated test results, item by item, and almost all items have been marked as "A" on A, B, C, D, E Scale. So far, none of serious technical problems have been left, and HSST-100 is evaluated to be acceptable for the practical use.

VI. Future Plan

The long period test run for endurance will be completed by the end of June 1993, and it is planned attain approximately 35,000 km of total run distance.

Further system improvement may be made according to experiences obtained during test runs, especially for better maintenability.

January 1993, HSST Development Corporation was founded by Japan Airlines, Nagoya Railroad, etc for the stronger formation to expedite the development for sooner practical use.

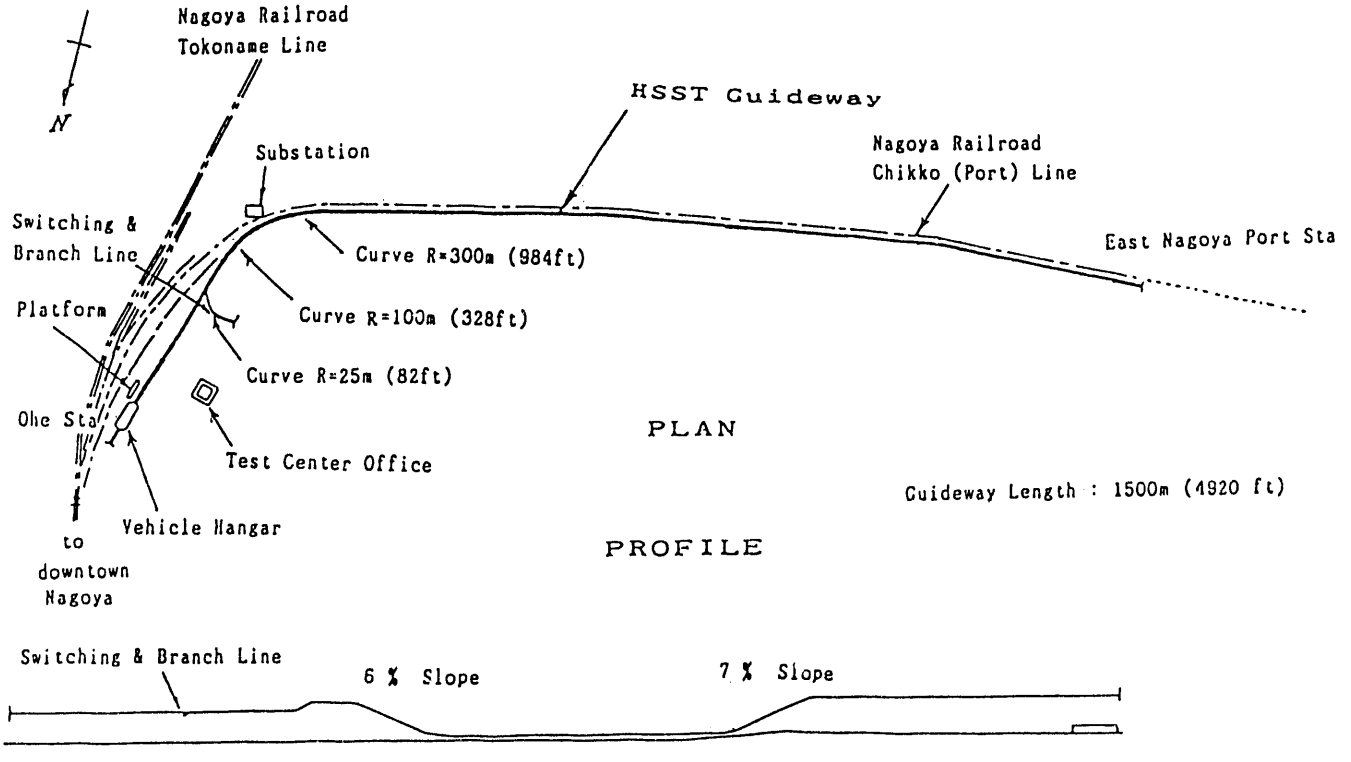

Fig.1 Plan and profile of test line

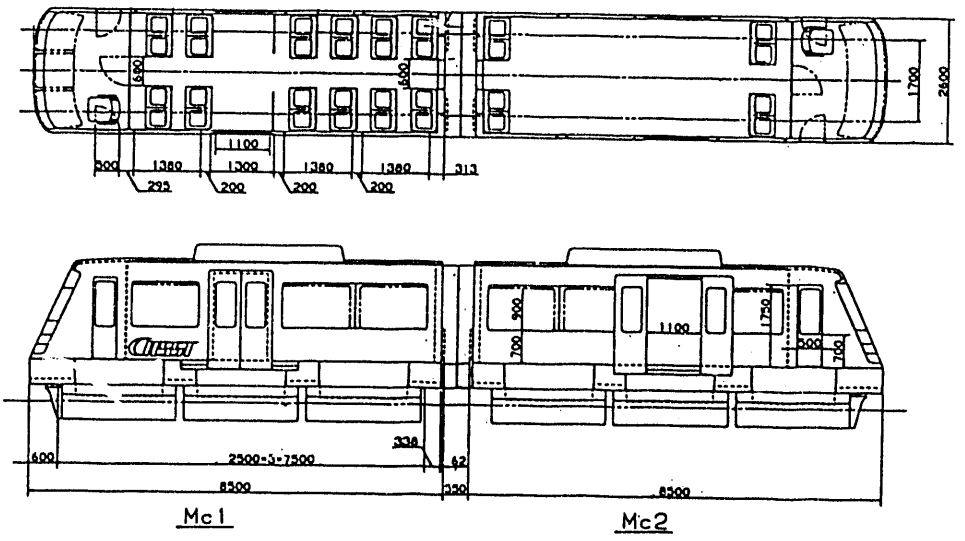

Fig.2 HSST-100 vehicle used for test

Tab.1 Specification of Test systems

items	specification
VEHICLE	
Formation	Two-car train (MC1+MC2)
Dimensions	8.5m(L)/car, 2.6m(W), 3.3m(H)
Train Weights (per two cars)	Empty 18,000 kg Maximum 30,000 kg
Capacity	44 (24 seats) per car (nominal) 67 (24 seats) " " (peak load)
Passenger Door	one bi-parting slide door per each side of car
Modules	six (or 3 pairs) per car in 2.5m pitch
Levitaion & Guidance	by attraction forces, of U-shaped elctromagnets
Levitat. Height	8mm (magnetic gap)
Power received	1500 V DC (by power collectors)
Propulsion	six Linear Induction Motors/car
" control	one VVVF inverter per train
Aux. power unit	one DC-DC Converter per train
Brake system	
Regular	LIM(Regenerative/Reverse phase) and Hydraulic brake (LIM-Hydro combined & Load compensated)
Emergency	Hydraulic brake
Air condition	Cooler/Heater
Couplers	Ends: none Between: Rod type coupler
Train control	ATP(Auto. Train Protection)
Train operation	Manual (with Auto. function)
TRAIN PERFORMANCE	
Maximum speed	110 kph
Acceleration	4.5 km/h/sec (maximum)
Deceleration	
Regular(max)	4.5 km/h/sec
Emergency	5.3 km/h/sec
GUIDEWAY	
Testline length	1530 m in total
Girder structur	Single Beam PC or Steel
Rail gauge	1.70 m (between rail centers)
Min curve radii	
(horizontal)	100 m (main line), 25 m (branch)
(vertical)	1000 m
Max Cant angle	8 degrees
Max Gradient	7 %
Switch	3-segment, horizontal turn type
SIGNAL SYSTEM	
Train control	ATP (Automatic Train Protection)
Switch control	Relay Interlocking
Train Overrun Protection	limited by phased speed ceiling
ELECTRIC POWER	
Trolley lines	AL/SUS Combined rigid rails (2)

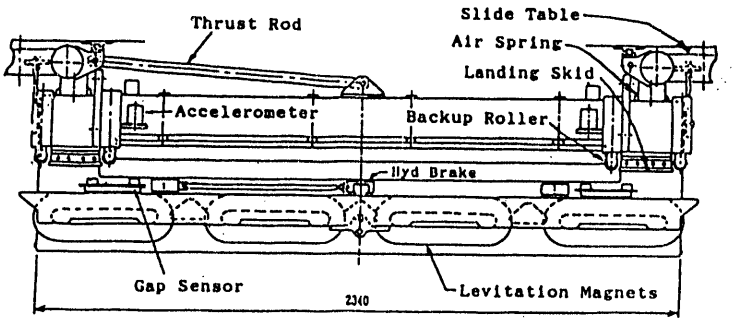

Fig.3 Module structure

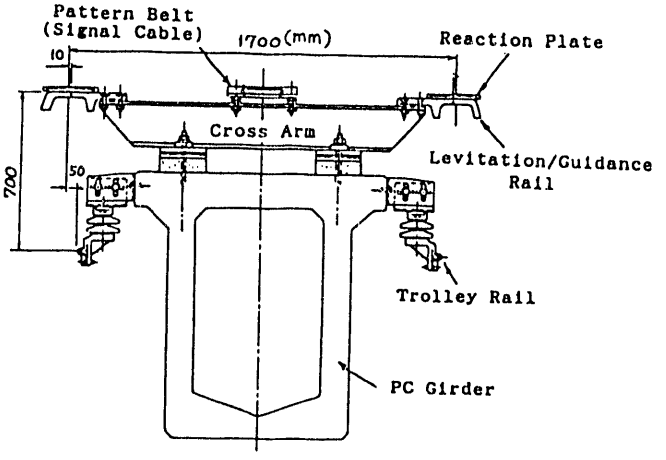

Fig.4 Cross section of guideway (standard)

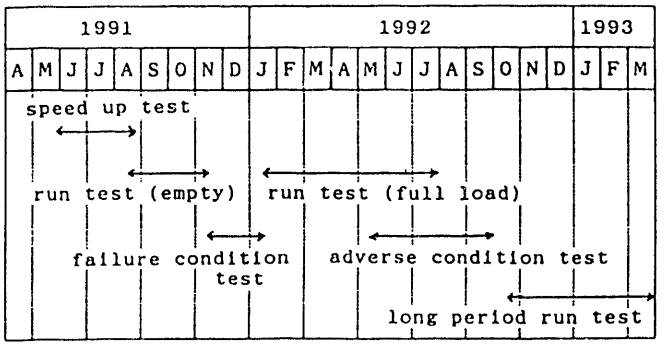

Fig.5 Test schedule

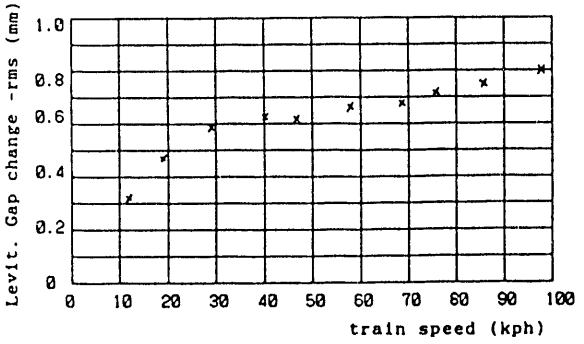

Fig.6 Levitation gap fluctuation vs. train speed

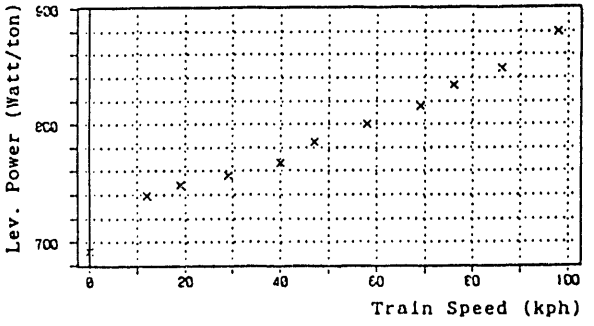

Fi.7 Levitation Power Consumption (per train weight)

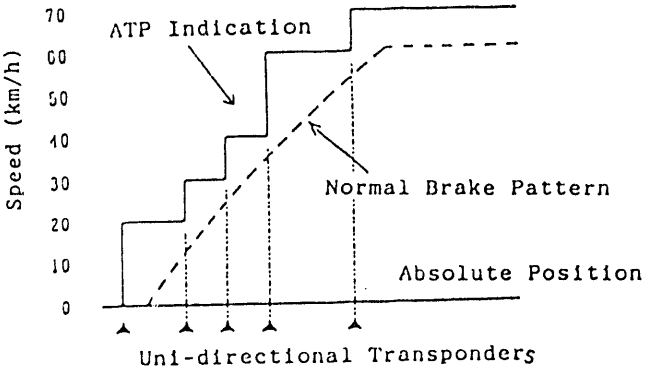

Fig.8 Overrun protection function

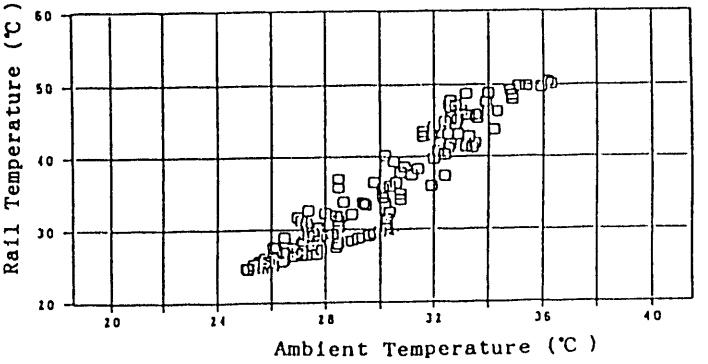

Fig.9 Rail Temperature vs Ambient Temperature

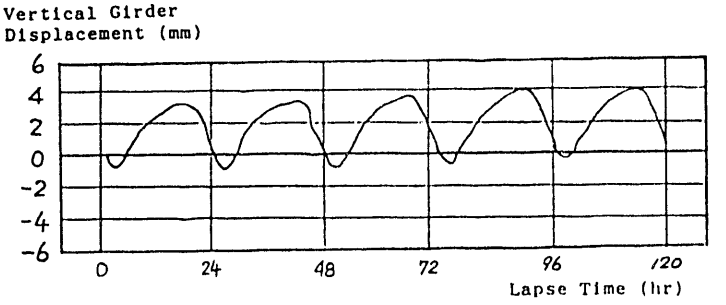

Fig.10 Daily change of Girder vertical displacement

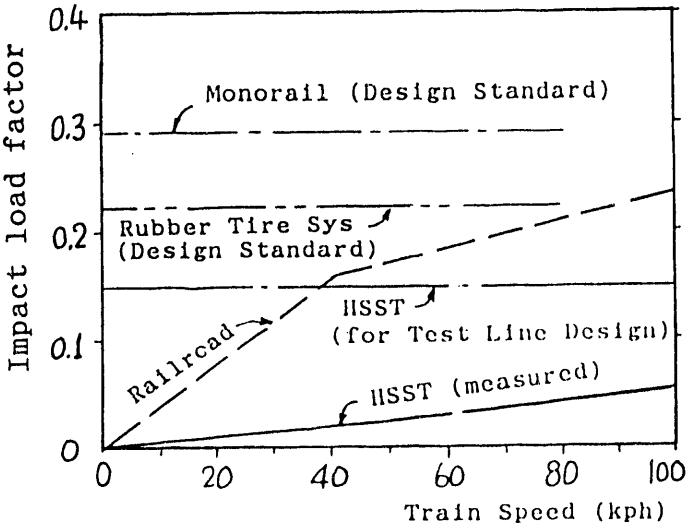

Fig.11 Impact load factor on PC girder

HIGH-SPEED MAGNETIC LEVITATION TRAIN TRANSRAPID, PLANNING OF THE DEVELOPMENT PROGRAM UNTIL 1995 AND PROSPECTS OF UTILIZATION IN THE FEDERAL REPUBLIC OF GERMANY

Ulrich WIESCHOLEK
Dipl.-Ing.
Fed. Ministry for Research and Technology, Ref. 514
D-5300 Bonn - GERMANY

Willi J. MAYER
Phys.-Ing.
Dornier GmbH, Dept. PBPE
D-7990 Friedrichshafen - GERMANY

Dieter ROGG
Dipl.-Ing
Dornier GmbH, Dept. PBPE
D-7990 Friedrichshafen - GERMANY

Abstract - The TRANSRAPID is a new high-speed transport system using levitation technology for speeds up to 500 km/h. It is supported and tracked by electromagnets. A synchronised linear motor provides the levitated propulsion.

In 1970, the development of a high speed magnetic train was begun in Germany. After more than 20 years of development, and after extensive investigations of the system, the TRANSRAPID was granted readiness for application by Deutsche Bundesbahn, at the end of 1991.

The first operational route in Germany was selected after an extensive selection process from five different routes in the new German states and three routes between Bonn and Berlin. The investigations showed the economically most promising results for the Berlin - Hamburg link which connects the two largest German cities, thereby permitting the close interconnection of these two industrial centers. It was therefore incorporated in the German transportation plan. An decision about the financing concept is expected in 1993. After completion of the planning phase, the construction of the operational route can begin in early 1996.

1. STATE OF DEVELOPMENT

1.1 Overview of the First Years of Development

The origins of electromagnetic levitation technology date back to the 1930's with Hermann Kemper, - a German inventor and engineer - who was already researching the possibilities of using electro-magnetic levitation technology for high-speed transport. The first form of electronic gap control to maintain electromagnets in a condition of levitation is accredited to him.

At the beginning of the 1970's, the German Ministry for Research and Technology launched an extensive development programme for tracked high-speed transport systems. The electromagnetic, electrodynamic and permanent-magnetic levitation methods as well as air-cushion technology were researched for their suitability in the use of high-speed trains. In 1977, after numerous investigations of the system and component testing, the electromagnetic levitation method using synchronised linear motors was selected as the definite development line. Two years later, the TRANSRAPID 5 - an experimental demonstration train in electromagnetic levitation technology - transported over 40,000 visitors at the International Transport Exhibition in Hamburg over a 1 km long stretch of track. Furthermore, the construction of the large scale TRANSRAPID test facility was started, in the same year, in the Emsland ((TVE).

1.2 Testing on the TRANSRAPID Test Facility in the Emsland (TVE)

This was the world's first MAGLEV test facility which enabled the full-scale testing of all principal components and of the complete system at high speeds and continuous operation. Main TVE components are the guideway, a high-speed straight section with guidewayloops on both ends, with an overall length of 31 km and with three switches; 2 vehicles, the TRANSRAPID 06 and 07, with a capacity of approximately 200 passengers each; the test center, power supply and the operations control system (fig. 1 and 2). The construction of the facility was begun in 1979 by an industrial consortium and started operations in 1984. One year later it was taken over by the Versuchs- und Planungsgesellschaft für Magnetbahnsysteme (MVP), a company founded by the Deutsche Bundesbahn, Lufthansa and IABG with the aim of testing the TRANSRAPID from an operator's point of view.

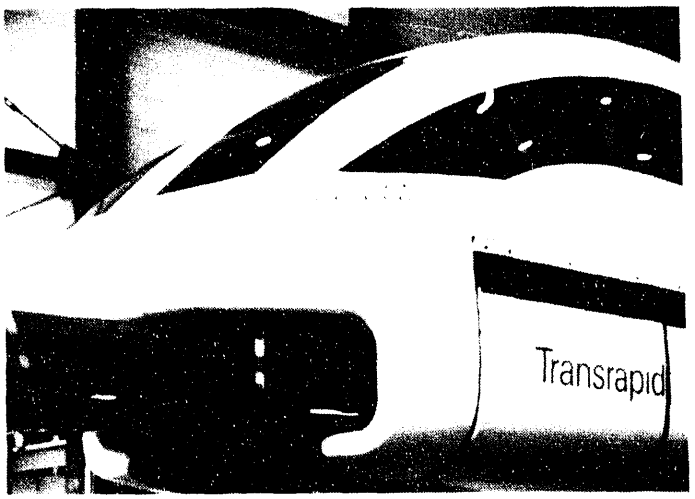

Fig. 1: Test vehicle TRANSRAPID 07

Testing was not without its technical setbacks, which, however, were almost never attributable to specific components of the magnetic levitation system. The objectives, however, were attained. Top speed could be increased from the design value of 400 km/h to 435 km/h. Extrapolations show that there are no limitations to this speed and that the system design is sufficient for operation at 500 km/h. In several endurance test campaigns, a total mileage of approximately 135,000 km was reached. The mileage record for a single day was about 2,500 km.

The tests included the qualification of the main hardware components of a complete new transport system in a prototype stage. The mechanical and electrical designs had to be scrutinized. But also software concepts and procedures which are necessary to operate a tracked high speed passenger transport system safely and economically have been included into the testing as far as possible. Special importance was attached to the gaining of data which are relevant for an operator of a revenue system, such as verification of safety, investment costs, maintenance, energy consumption, aerodynamic behavior, riding comfort and noise emission.

The overall results were as follows: The principle advantages of the TRANSRAPID could be confirmed to full extent. Fundamental redesigns have in no case been necessary. All problems arising during the test phase could be solved satisfactorily. A number of possibilities for further optimization could be brought to light. Continuation of the endurance testing is still necessary in order to complete and to corroborate the test results.

1.3 Qualification of Readiness for Application

This was initiated by the German Ministry for Research and Technology together with the Ministry of Transport and specifically designed to furnish proof of an adequate state of development. The Central Office of the Federal German Railway (BZA) was charged with testing and it presented at the end of 1991 the final report concluded as follows:

The criteria to be considered for technical readiness for application of the TRANSRAPID High Speed Maglev Train are satisfactorily fulfilled. That means, that

* the prerequisites for implementing the legal planning procedures are given;

* system risks and safety risks overall and in the subsystems are not present.

This also applies to technical solutions which have not yet been demonstrated for individual problems for which solution approaches exist and are being assessed.

Supplementary information and suggestions are given for the additional development work with regard to application.

Fig. 2: TRANSRAPID Test Facility Emsland (TVE), vehicle TRANSRAPID 07

2. DEVELOPMENT PROGRAM 1991 to 1995

The BZA expertise has provided an exactly defined development state so that development work which has still to be performed could be specified. In the negotiation of the coalition parties of the German Federal Parliament in January 1991, it was basically agreed to carry out the final development. As soon as these prerequisites had been settled, the final program was started. It will be executed in the 1991 to 1995 timeframe and consists of the main

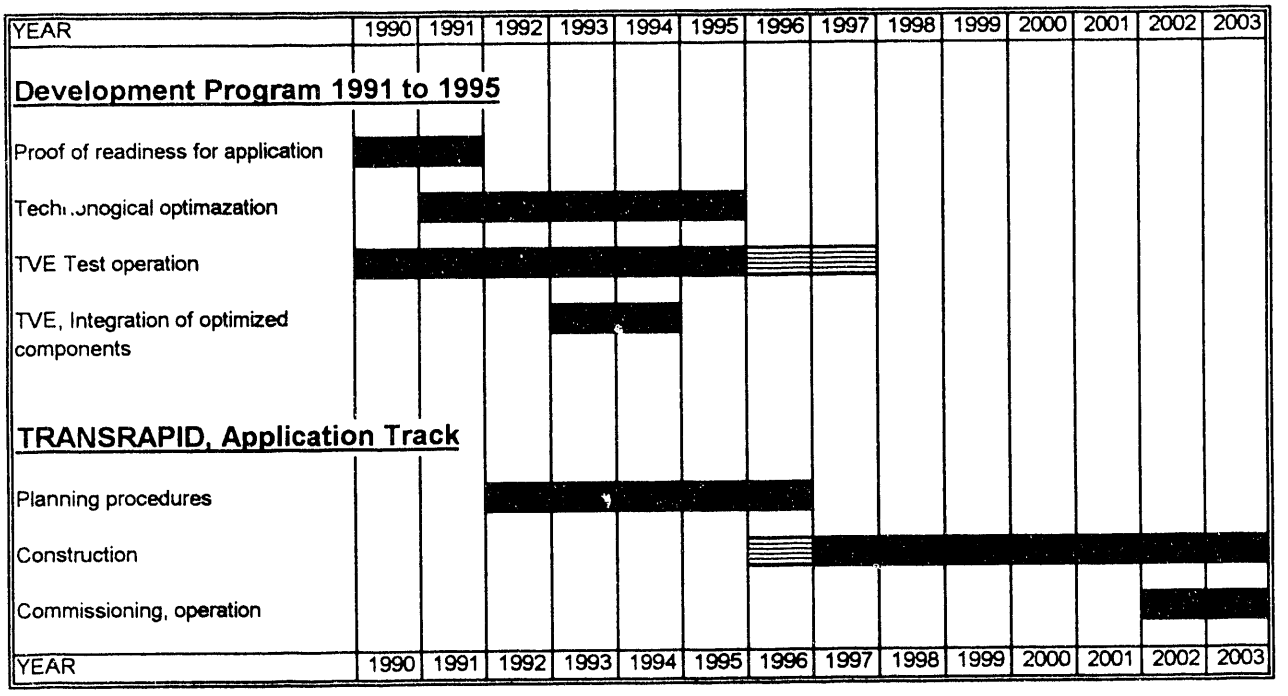

Fig. 3: TRANSRAPID, development program 1991 to 1995, planning and construction of a first application track in Germany

program parts (fig. 3):

* Final technological optimization with the keypoints high speed aerodynamics, utilization of the technological progress in electronics, further improvement of the availability and of the data which are relevant for environmental influences;

* Endurance testing on the TVE under all specified operating conditions, in order to gain more experience in operation and maintenance, with the aim to define and validate the regulations and operation instructions for revenue lines;

* Employment and testing of optimized components, especially for the vehicle, propulsion and signalling/control system and of auxiliary operation devices on the TVE;

* Basic research and companion studies and assessments.

3. TRANSRAPID - Characteristics and Application Fields

With electromagnetic levitation methods, the electromagnets act on both sides of the vehicle, from underneath on the magnetic armature rails on the track. The attracting forces lead to a stable levitation condition by means of an electronic gap control adjusted to the high acceleration and breaking ability.

The function of the linear motor corresponds to a conventional synchronous machine. For TRANSRAPID, the windings are accommodated on the track which, driven from a stationary substation with variable tension and frequency, generate travelling magnetic fields. The desired propulsion forces are generated through the interaction with the electromagnets on the vehicle.

On-board power is transmitted inductively to the vehicle via linear generator windings; the power is supplied and buffered in on-board batteries. The levitation, guidance, propulsion and brakes as well as the power transmission to the vehicle occur completely contact-free, i.e. without mechanical contact with the track. This provides some particularly good features compared to conventional rail systems. The resulting advantages of this design permit efficient and ecologically reasonable operation throughout the whole speed range:

* Low wear and maintenance cost

* Low guideway loads

* Comparatively low emission of noise and vibra-

tion, particularly in the speed range used for entering urban areas

* Comparatively low energy consumption because of low vehicle weight and complete aerodynamic fairing

* Flexible routing parameters

* Minimum interference with the landscape due to easy adaptation of the route to the topography

* Economical operation due to short vehicle travelling time per cycle

* High acceleration and deceleration by virtue of low vehicle mass and high propulsion power in those sections of the track where it is necessary. As a result, a high average speed can be achieved even when there are short distances between stops.

* High payload, nearly constant over the whole speed range

* Propulsion and braking systems are independent of wheather and friction

Short travelling times, high ride quality and high safety combined with competitive fares and an appealing image play a vital role in a passenger's choice of a transport system. As the TRANSRAPID fully meets all of these criteria, it can contribute to making public passenger transport systems more attractive.

4. Application of the TRANSRAPID System

4.1 German Transportation Plan

As a result of the German Federal cabinet's decision on 15th July 1992, a new Transportation Plan for both East and West Germany with a fixed programme up until 2010 has been submitted. This first Transportation Infrastructure Plan for the whole of Germany was consequential to the unification of the two parts of Germany and will improve the transport network in the direction East-West within the next twenty years.

The traffic forecasts carried out in the course of the Transportation Plan show a considerable increase in the traffic volume in the coming years.

The Federal Ministry of Transport calculated the following increases (reference year 1988):

* In total 80% more freight traffic and 30% more passenger traffic;

* Doubling of the transit freight traffic through Germany by 2010 and almost triple the amount of transit passenger traffic

* Within Germany, freight traffic between West and East will increase more than seven fold, passenger traffic almost eight fold

* The number of cars will increase to over 45 million -at the moment there are more than 36 million cars.

In order to cope with this traffic volume with regard for the economy and the environment, the extensive reshaping of public transport is a priority goal alongside the intended extension of the road network.

Therefore the 1992 Transportation Plan sets a new investment strategy to solve environmental and mobility problems by combining all the different transport means into one coordinated transport system.

In this plan, the TRANSRAPID has to play an important role. It should reduce, for economic and ecological reasons, undesirable short-range flights and long distance private vehicle traffic, as well as provide free capacities in the rail network for freight traffic.

To identify suitable lines for a first TRANSRAPID application the Federal Ministry of Research and Technology and the Federal Ministry of Transport started investigations in summer 1991.

4.2 Selection of Routes

In the selection process the following aspects had to be considered:

An established need for transport and a sufficient traffic volume; preferably no selection of routes that already yield high gains within the existing railroad network; preferably selection of routes with only a small effect or none at all on planned conventional rail links, prospects for subsequent extension, possibility of realising a TRANSRAPID track in successive construction phases; above all the TRANSRAPID should upgrade service in areas which so far have been underserviced.

With these criteria in mind the Federal Ministry of Transport proposed that the following links be analysed (fig.4):

T1:Hannover - Halle - Leipzig

T2:Hamburg - Berlin

T3:Hamburg - Parchim Airport - Berlin

T4:Berlin - Berlin Süd Airport - Dresden

T5:Stuttgart - Nürnberg - Dresden

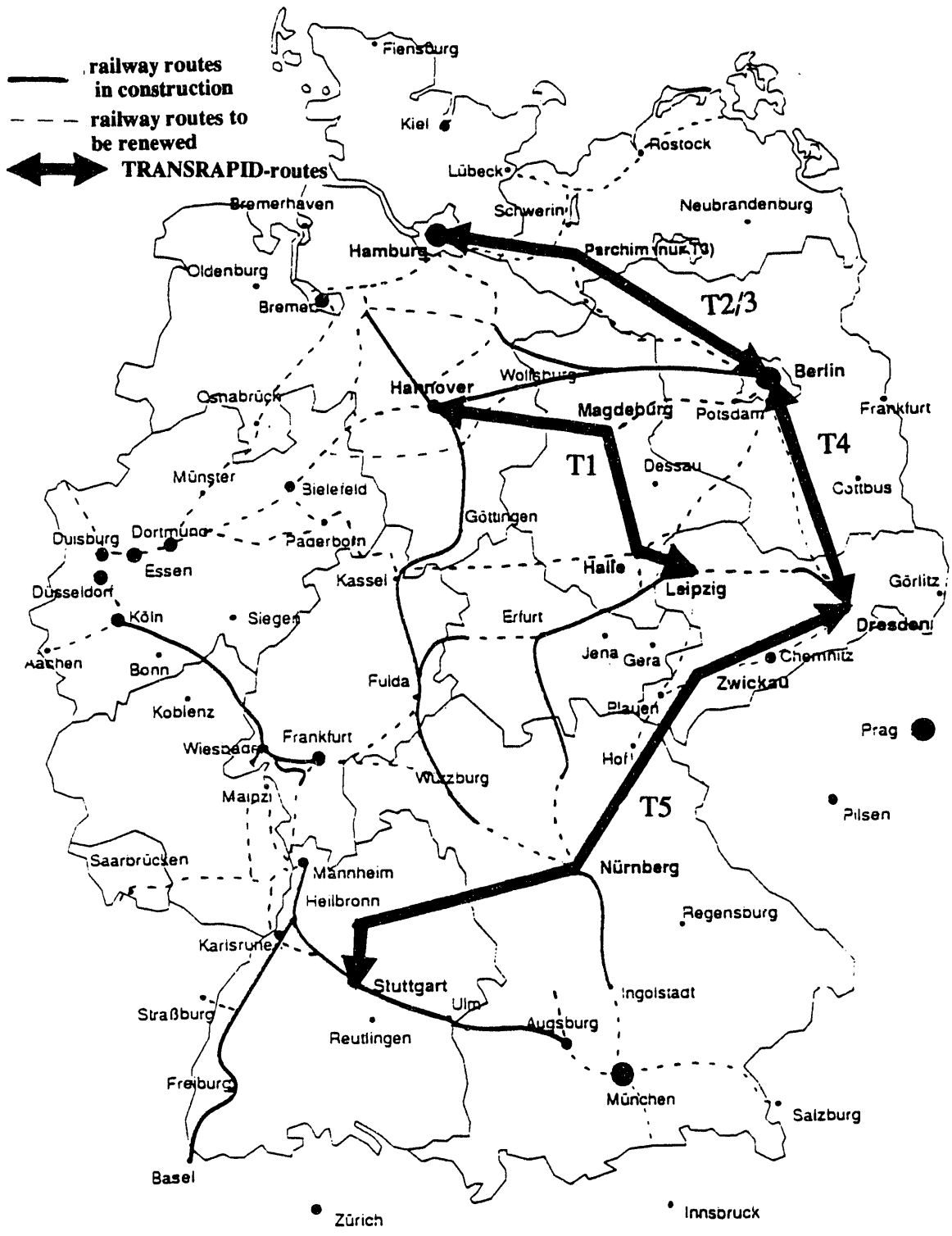

Fig.4: TRANSRAPID links in investigation with regard to the German traffic infrastructure planning

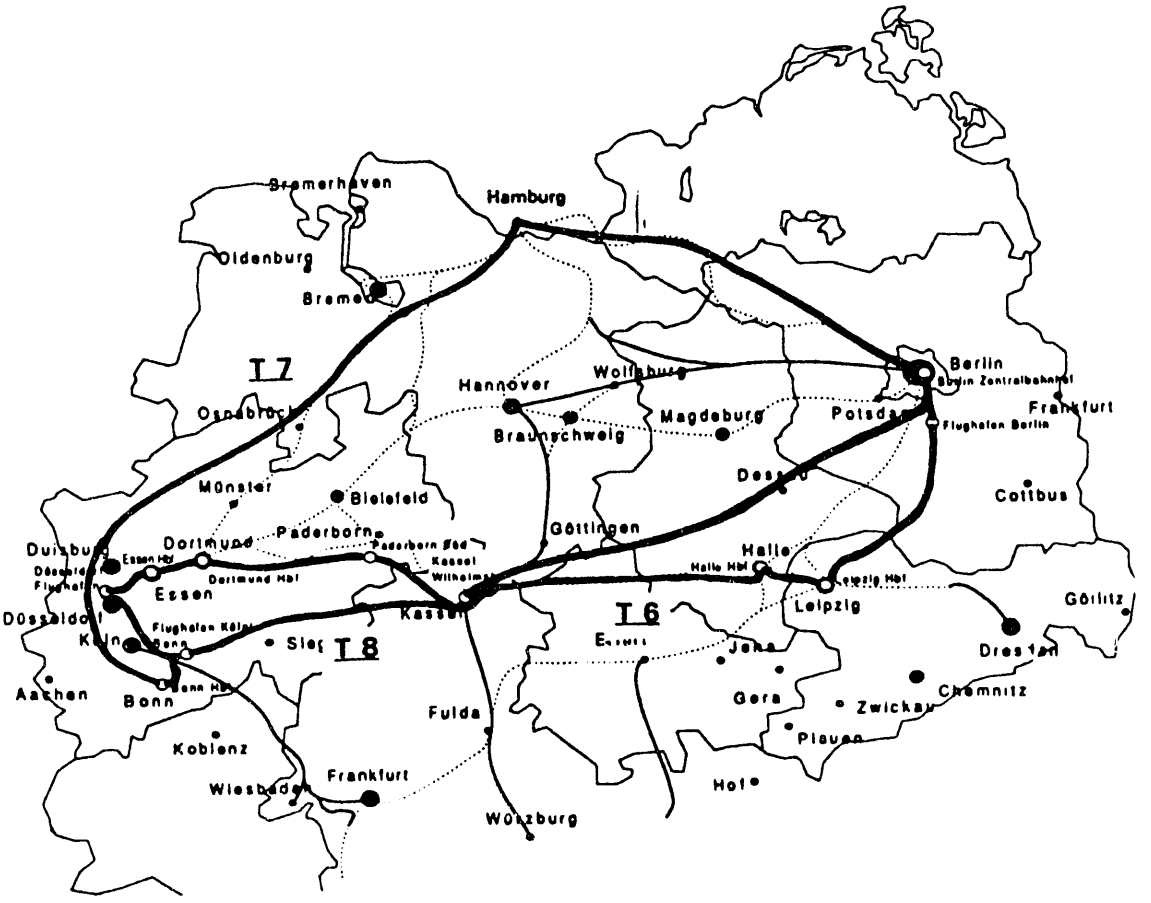

Fig.5: Alternative TRANSRAPID routes Bonn - Berlin.

In response to a recommendation by parliamentary working groups a link between Bonn and Berlin was also selected for detailed investigation (fig.5).

4.3 Procedure

The proposed routes were studied in a step by step analysis according to the general evaluation procedure which has to be performed before infrastructure projects can be included into the general traffic infrastructure planning:

* environmental impact assessment; such as use of land, segregation, noise emission

* alignment; with special regard for the environment as well as the topography and with the aim to attain a binding with existing infrastructure (rail and roads)

* forecast of passenger transport volume;

* service planning;

* dimensioning of the infrastructure;

* calculation of investment costs;

* calculation of operating costs;

* determination of effects on the existing passenger and freight transport network;

* evaluation of the effect on the whole national economy;

* evaluation of effects on the profitability of the German Rail.

The benefit/cost ratio resulting from these evaluations is decisive for the inclusion into the infrastructure planning.

4.4 Results of two selected Routes

4.4.1 Hamburg - Berlin

The Hamburg - Berlin route is of particular interest from the transport and economic point of view. First and foremost, this intercity line is to link the two biggest German cities as a kind of metroliner.

The length of the Hamburg - Berlin link is 287 km; travelling time is around 55 minutes. At a fixed cycle of one TRANSRAPID train every 10 minutes, the service would comprise 95 four-section trains with 332 seats each per day and direction.

The transport volume is estimated at about 15 million passengers and more than 4 billion passenger kilometres per year. The TRANSRAPID takes around half of these from air and road traffic, thus relieving the pressure on the environment. The increase in the capacity of freight trains on the existing railway lines was calculated to be some 430 million ton kilometres. The total investment costs for the infrastructure (guideway, energy supply, operation and maintenance facilities) amount to 6,700 million DM, the investment costs for the rolling stock to 600 million DM. The total yearly amount of the operating costs was estimated at 190 million DM. With a fare 30% higher than the Intercity Railway standard and 15% higher than the ICE-tariff the yearly revenues amount to approximately 800 million DM. The revenues can be further improved through optimization of the offer. The completed overall economic evaluation for the German Transportation Plan showed a benefit-cost ratio of 2.8. The favourable results led to this route being upheld in the Transportation Plan.

4.4.2 Bonn - Berlin

Three tracks for this link have been studied:

Bonn - Cologne/Bonn Airport - Düsseldorf Airport - Essen -Dortmund - Paderborn - Kassel - Leipzig - Berlin Airport -Berlin Central Station (710 km);

Bonn - western Ruhr area - Bremen - Hamburg - Berlin (750 km);

Bonn - Kassel - Berlin (direct route) (548 km)

Assuming a travelling time of 3 hours, a traffic volume of about 40 million passengers can be expected according to estimates with respect to the first version of the Bonn - Berlin link. Version 3 would offer the shortest travelling time of about 2 hours.

The Bonn - Hamburg - Berlin route can, with the transferral of the German parliament to Berlin, prove its worth.

4.5 Time Schedule for the Implementation of TRANSRAPID Application Tracks

The Hamburg - Berlin connection was incorporated in the German Transportation Plan as the first TRANSRAPID application track in Germany. New forms of operation are to be studied for the new transport system, the TRANSRAPID. The project should, as far as possible, be financed through private means. At present, under the incorporation of industry and banks, appropriate financial concepts are being developed. Following a decision on the financing and operator concept, which is still awaited in 1993, the legal planning procedures can be initiated. In this case the construction work may start in 1996. If all goes well, the TRANSRAPID can take up revenue service between Hamburg and Berlin around the year 2000.

A first step is hereby taken towards a promising new transport system which helps to avoid traffic congestion on the ground as well as in the air, and which causes less damage to the environment than other means of transport. In the future transport plan in Germany and Europe, the present demand forecasts and the comprehensive allocation of external costs of air and road traffic have to be taken into consideration. In particular, the political opening in eastern Europe and the expected long-term industrial development give the TRANSRAPID substantial opportunities, since large distance have to be covered and the infrastructure is still poorly developed.

Analysis of Prospective Transrapid Applications

Hans Georg Raschbichler
Luitpold Miller
Manfred Wackers
Thyssen Industrie AG Henschel, Anzinger Strasse 11, 8000 München 80, Federal Republic of Germany

Abstract – The high speed maglev system Transrapid will complement the existing transportation networks in a cost effective and environmentally acceptable way. According to expert opinion, the basic development is concluded and the readiness for application in revenue service of the Transrapid system is achieved. The paper describes the features of the Transrapid technology and its major advantages in future fields of application. The basic data have been verified by extensive testing of the TR07 vehicle in long term operation amounting to more than 130 000 km (80 000 miles) at speeds of up to 436 km/h (280 mph) at the Transrapid Test Facility in Emsland. A first analysis of the financial scheme of the most advanced German Transrapid project, the link between Berlin and Hamburg, shows the high efficiency and profitability of the Transrapid system.

I. Introduction

For more than 15 years, Thyssen Henschel has been involved in the development of magnetic levitation technology. Beginning with the first test vehicles for electromagnetic suspension (EMS), Thyssen has provided the leadership in consequently developing and optimizing this completely new transportation system.

In December 1991, a working group of experts from the Deutsche Bundesbahn (German Federal Railroad) in cooperation with renowned universities approved the technical readiness for application of the Transrapid.

That was one of the most important prerequisites for the German Federal Cabinet to include the magnetic levitation system in the new Federal Transportation Master Plan in 1992. The Cabinet also approved the route Berlin – Hamburg to be the first application of Transrapid in Germany, but with the condition of private or partially private financing. Three different financing models have been developed with the condition of relieving the public budget and presented to the Government.

The current project plan foresees the construction phase beginning in 1995/96.

II. System Description and Characteristics

The high speed transportation system Transrapid is a track–bound system, capable of revenue operation at speeds of 400 to 500 km/h (250 to 312 mph). The principle of attractive magnetic force is used for the suspension and guidance of the vehicle and a synchronous linear motor provides the propulsion and braking.

An overview of the system characteristics is shown in Table I.

TABLE I

Technical Data

Design Speed		500 km/h
Operating Speed		300 – 500 km/h
Passenger Vehicle		
Empty Weight		46,000 kg
Total Weight, allowed		55,000 kg
Cargo Vehicle		
Empty Weight		42,000 kg
Total Weight, allowed		58,500 kg
Acceleration		
0 – 100 km/h [1]	300 m	20 s
0 – 200 km/h [1]	2,000 m	60 s
0 – 300 km/h [2]	4,900 m	120 s
0 – 400 km/h [2]	9,300 m	165 s
Allowed Crosswind		
Standstill		60 m/s
200 km/h		40 m/s
400 km/h		30 m/s

[1] Commuter operation max. acceleration = 1.4 m/s²
[2] Long distance operation

A. Vehicle

Transrapid trainsets are composed of up to ten vehicle sections with each section having a length of 25.5 meters (84.2 feet). They are designed to transport passengers or superior express goods at speeds of up to 500 km/h (312 mph).

Flux–coupled electromagnets arranged in a redundant configuration and controlled in two degrees of freedom are used to levitate and guide the vehicle. A safe–life power supply for the vehicles is provided by linear generators independent of any external power supply. These generators convert part of the vehicles' kinetic energy into electrical energy. The safe–life behavior is achieved through sufficiently high redundancy. At low speeds (less than 80 km/h or 50 mph), the on–board power supply network is buffered by batteries.

Eddy–current brakes using modular design are provided to assure the safe–life braking function of the vehicle.

Skids are used to support the vehicle on the guideway at stand-

still and to stop the vehicle in the event the electromagnetic levitation system is deactivated.

The structure and design of the cabin correspond to the latest technological development and are comparable to modern railway coaches.

B. Propulsion System

The propulsion system is realized by a synchronous long stator linear motor. It consists of stator packs with a three–phase winding installed under the guideway (comparable to the stator of a rotating motor) and electromagnets mounted on the vehicle (corresponding to the rotor of a rotating motor).

C. Automatic Train Control

The communication and control system is fully automated. It maintains the trainset speed within the operating specifications (safe speed enforcement) and provides a safe and unobstructed travel path (route integrity). The system relies mainly on microprocessors which are designed and verified with fail–safe, fail–active, and fault–tolerant techniques.

D. Guideway

Various types of guideway structures are available for route planning with regard to cost efficiency and environmental concerns:

- Single or double track elevated guideways using steel or prestressed concrete beams mounted on 5 meter (16 feet) high piers (normal height)
- Single or double track at–grade guideways for tunnels, cuttings, bridges, and areas where this is required for better general acceptance

For guideway switching, bendable switches with maximum vehicle turnout speeds of 100 km/h (62 mph) and 200 km/h (125 mph) have been developed and tested.

Table II gives an overview of the guideway alignment data and parameters which are technically allowed. The land surface area reflects the foundations required for an elevated or at–grade guideway route. The land required (right of way) and the excavations are based on various representative reference alignments.

TABLE II

Track Alignment Data

Lateral Acceleration		$\leq$ 1.5 m/s^2
Vertical Acceleration	$\leq$ 0.6 m/s^2 (crest)	$\leq$ 1.2 m/s^2 (trough)
Omnidirectional Jerk		$\leq$ 1.0 m/s^3
Lateral Inclination		$\leq$ 16 °
Curvature Radii		
Minimum		350 m
200 km/h		705 m
300 km/h		1,590 m
400 km/h		2,825 m
Foundation Area (Double Track)		
Elevated Guideway		1.5 m^2/m
At–grade Guideway		11.8 m^2/m
Total Area (Double Track)		
Normal Case		12.0 m^2/m
Mountainous Region		22.8 m^2/m

E. Availability

High availability of all subsystems is essential to ensure that the Transrapid system maintains a high level of operating performance in revenue service.

This is achieved through:

- Error–tolerant behavior, i.e. mission accomplishment even in case of multiple component failures
- On–line diagnostics
- Automatic deactivation of components in case of failure and on–line self–diagnosis including reactivation routines
- Easy handling and maintainability
- Computer–aided equipment for preventive and corrective maintenance
- Insensitivity to environmental influences (outside temperature, winter conditions, lightning, crosswind, and earthquakes)

Development models of computer–aided equipment for preventive and corrective maintenance have been installed in the Transrapid Test Facility and undergo continuous testing in daily operation. The target data for reliability and availability have been verified during the long term operation at the test facility.

The summary of the operation performance at the test facility is given in Table III.

TABLE III

Operation Performance at the Transrapid Test Facility

Speed record	436	km/h
Total distance accumulated	over 130,000	km
Longest non–stop distance traveled	1,050	km
Maximum daily distance	2,500	km
Long term test		
Average daily distance	1,200	km
Portion of distance above 350 km/h	42	%

F. Safety

The Transrapid high speed transportation system has been subjected to a detailed and comprehensive safety analysis and evaluation. The methodology and procedures in the safety assessment relied on developed and verified techniques applied to analyze complex systems such as railways, air transportation networks, and chemical and power plants.

On the basis of quantitative criteria to decide acceptance or refusal of risk, safety measures have been defined and evaluated in a closed loop processing of risk assessment and evaluation. The end of the iterative process results in a final safety specification.

A comparison with other transportation systems demonstrates the high level of safety of the Transrapid. Using the number of fatalities per billion passenger–kilometers as a measure of safety, the Transrapid system is safer than air travel by a factor of 20, than conventional railroad by 250, and than road travel by 700.

The high level of safety in the Transrapid system can be explained as follows:

- As a new transportation system, the Transrapid profits from the experiences with existing systems, by avoiding from the outset known accident risks.
- The technique of magnetic levitation used in the Transrapid system does not introduce any new risks. It guarantees safe operation on the basis of the adopted technical and design measures.

Specific requirements for application in the U.S. were investigated through a U.S.–German cooperation, carried out by the Federal Railroad Administration and TÜV Rheinland. In this cooperation, project specific data and U.S. statistics were gathered and used as input for the safety analysis and evaluation, as well as for the definition of specific regulations for Transrapid applications in the U.S.

G. Environmental Compatibility and Performance Characteristics

Environmental acceptability has become more and more important for the implementation of transportation systems. Alignment parameters for the maglev train Transrapid are extremely favorable. Due to the vehicle's ability to climb steep gradients and travel tight curves, the guideway can be flexibly adapted to the landscape and co–located closely with existing roads and railroad tracks. Elevated or at–grade, the guideway requires less ground area than other transportation systems.

Transrapid is matchless in terms of quietness, especially within the range of those speeds utilized in densely populated areas or when approaching stations.

The high acceleration and deceleration ability permits the system:

- to serve as a commuter train in lightly populated areas
- to reduce cruising speed when passing noise sensitive areas or in tight curves without significant impact on overall travelling times

TABLE IV

Environmental Compatibility Data

Specific Secondary Energy Consumption	Constant Speed [watt hour per seat km]	Typical Trip [watt hour per seat km]
200 km/h	26	29
250 km/h	31	33
300 km/h	38	43
400 km/h	58	64

Noise Emission [1]	Distance 25 m	
200 km/h	79.0	dB (A)
250 km/h	82.5	dB (A)
300 km/h	86.5	dB (A)
400 km/h	93.5	dB (A)

Magnetic Field [2] Extreme Low Frequency (ELF) Fields [3]		
Passenger Compartment	10	μT
Near the Guideway	6.5 – 9.5	μT
Passenger Station	2	μT
Static Field [4]	0 – 33.5	μT

[1] Measured by TÜV Rheinland at elevated guideway. At–grade guideway reduces the level by 3–4 dB.
[2] Measured by Electric Research and Management,Inc.
In comparison to:
[3] Houshold appliances 1,000 μT (ELF)
[4] Earth's geomagnetic field 50 μT (static)

The environmental data and performance characteristics given in Table IV are derived from the evaluation of measurements of test rides at the Transrapid Test Facility in Emsland and from data provided by the Versuchs– und Planungsgesellschaft für Magnetbahnsysteme mbH (MVP).

The calculation of the vehicle specific data is based on a typical trainset configuration with eight vehicle sections and 702 seats. The secondary energy consumption refers to seat and kilometer when riding at constant speed and/or to a reference travel cycle, i.e. standstill – acceleration – constant speed – braking – standstill.

H. Economic Efficiency

The investment costs correspond to those required for a modern high speed train. The operating costs are significantly lower due to reduced expenditure for maintenance and repair.

The non–contact technical concept and aerodynamic optimization of the vehicles lead to lower drag coefficients which result for example in about 30 % lower energy consumption in comparison with modern railroads.

These characteristics enhance the opportunity for profitable operation at competitive ticket prices.

III. The German Transrapid Project between Berlin and Hamburg

As the world's first magnetic levitation train system, the Transrapid stands application–ready for use. The German government has recognized that the magnetic levitation train Transrapid, due to its innovative technology, can play an economically and environmentally sensible role in overcoming the continuously growing traffic volume in western Europe.

After the German reunification, the federal government investigated various magnetic levitation train routes in conjunction with the new federal states. The route Berlin – Hamburg showed itself to be particularly attractive. It was included in the federal cabinet's Federal Transportation Master Plan 1992 with the condition that private/partially private financing models be investigated for the financing of the route.

Since then, the corporations Thyssen Industrie AG, Siemens AG, and Daimler Benz AG/AEG AG in conjunction with the Deutsche Bank and the Kreditanstalt für Wiederaufbau (Credit Institute for Reconstruction), have developed three financing model alternatives for the government. Industry serves as the general contractor in all three models and is responsible for fulfilling the work to schedule and within budget while also guaranteeing the functionality of the system. This goes far beyond the historical role of industry in realising public railroad projects. The risks though, which result from public approval processes or acts of God, must be carried by the public authorities. This also goes for the political risks due to traffic politics, fares etc.

TABLE V

Operation and Base Data

Traffic Volume [1]	14.5	million passengers/year
Traffic Performance	4.1	billion passenger–km/year
Number of train trips per day and direction	96	
Trip frequency	10	minutes
Number of trainsets	19	
Number of vehicle sections per trainset	4	
Route length	283	km
Operational speed	400	km/h
Trip time	53	minutes
Operational performance	6.6	billion seat–km/year
Number of seats per trainset	332	
Average trainset utilization	63	%

[1] Basis: Gesellschaft für Transport –, Umwelt–, Kommunikationsanalyse mbH

A. Route Alignment and Operation Data

1) Route Alignment: The base case for the economic calculations is the planning case,

Berlin Westkreuz–Hamburg Hauptbahnhof (Main train station).

The suggested alignment route utilizes land areas in use in the existing traffic corridors. To avoid further cutting up of the landscape, the route will travel along the highway connecting the two cities, Berlin and Hamburg.

Ongoing deliberations point toward having central and peripheral stopping points in Berlin and in Hamburg. The establishment of an intermediate stop is also planned in one of the new federal states which are passed through by the route, such as near Schwerin, the state capital of Mecklenburg–Vorpommern.

2) Operation and Base Data: The significant results of the operational plans have been determined for the base case on the basis of the route specific traffic demand prognoses. These are shown in Table V.

B. Initial Data for the Profitability Calculation

The profitability calculation uses the following project data as a basis:

Route data:

Berlin Westkreuz – Hamburg Hauptbahnhof
283 km, 53 minutes trip time

Time period under review:

Approval process	1993 – 1995
Construction	1995 – 2002
Commissioning	2002
Operation	2002 – 2042

Investment cost (Basis 1989): 7.2 billion DM

Operation costs: 210 million DM p.a.

Ticket rates (basis 1992):	1st class	0,39 DM/km
	2nd class	0,26 DM/km

C. Financing Models

Three financing models have been developed:

1. Use reimbursement model
2. Capital market model
3. Structural reform model

Using different methods, these models achieve through the financing of the magnetic levitation train route Berlin – Hamburg

the following desired effects:

- an expeditious realization of the project
- a shifting of clearly defined risks onto the private economy
- an involvement of the public authorities in the risk while simultaneously relieving to a great extent the public budget

1) Use Reimbursement Model: In the use reimbursement model, the project will be realised through a private, non–profit project corporation. This corporation will receive the concession to build and operate the magnetic levitation train from the federal states involved, will apply in its own name for the required capital from the banks, and will contract an industry consortium as general contractor for the construction. Immediately after completion, the construction and the equipment will be transferred to the public sector. With the start of operation, or at the latest, with the start of the debt service, the complete project costs not related to the operation, will be amortized through over time distributed, use reimbursement payments. These use reimbursement payments will be paid for by the sale of travel tickets. These operation and traffic volume independent, use reimbursement payments will be insured through a utilization contract with the public authorities. Thus the credit risk for the capital market is given de facto to the public authorities. This type of government assurance is normal for privately–financed large projects that have public significance and is already in practice.

The project is divided into three phases:

- preparation phase
- planning and construction phase
- operation phase

After system acceptance, the operating corporation will begin operation and fare collection. If the operating and use reimbursement costs are not completely covered by the fares, then foreseen is that the federal government will guarantee the difference through a subsidy. The project corporation performs its debt service through the use reimbursement fees.

The profitability analysis yields: the magnetic levitation train connection Berlin – Hamburg is self supporting. The fares are sufficient during the entire life of the project to cover the operating costs and reimbursement fees. That means that demands on the public authorities and therefore a strain on the public budget would not occur. Moreover the tax receipts would constitute a considerable sum. The financal resources will be supplied entirely through bank credit.

2) Capital Market Model: As an alternative to the use reimbursement model, the capital market model differentiates itself mainly through the grounding of a stock corporation as project carrier which would be listed on the exchange. It will receive the grant from the federal states for the construction and operation concession. The shareholders of the corporation would be public stockholders, public authorities, states, etc. and interested industrial companies. The project stock corporation will finance the project through its own equity and outside capital. An industrial consortium would be contracted as general contractor. The project corporation would own the magnetic levitation train route and would carry the economic risk. An operator corporation, such as the Deutsche Bundesbahn (German Federal Railroad) or Lufthansa, would be trusted with operating the route. The operator will transfer the proceeds from operating the route, minus the costs, to the project corporation. After subtraction of all expenses, the remaining free cash flow is available for dividend distribution.

The following preconditions will be necessary in order to raise the owned equity on the capital market:

- a division of risk between industry and the public authorities
- a convincing concept for operating the route with the possibility of a route extension
- additional incentives for private and institutional investors

Such an additional incentive could be achieved through the earning of a stock connected, guaranteed minimum return in the form of a PUT option. This gives the stockholder the right between the start of operation and the distribution of the first dividend, within a specific time–limit, to offer the stock to the public authorities. The minimum return can be assessed as less than that of riskless investments (for ex. federal bonds of equal maturity).

The results of the profitability investigation based on the capital market model are: The funding necessary in the capital market model is less in comparison to the use reimbursement model, because of the availability to the project corporation of non–interest–bearing equity for the financing prior to the employment of outside capital. Dividend payments commence according to the plan in the third year of operation and result in comparatively good, rising returns over the time period considered. In addition to tax revenues which are larger than those foreseen in the use reimbursement model, the public authorities receive as stockholder, their portion of the dividends distributed.

The capital market model also offers the possibility, to distribute the budget load over a longer time period due to the individual participation of various corporate bodies (federal and state).

3) Structural Reform Model: This financing model corresponds to the future structure of the German railroad, which foresees a division between the railroad track (guideway) and the operation. The investments for the guideway fall in this case on the government. Thus the size of the investment costs differentiates this financing model from the others. The guideway will be created by an organized, legally private guideway corporation under direct and exclusive government participation. Through this is assured that the public legal approval process can be accomplished quickly. This corporation leases the guideway to a likewise organized, legally private operations corporation for a use–dependent reimbursement. This reimbursement, which will begin with the commissioning, will correspond to

the guideway depreciation rate. Interest expenses for the guideway corporation which could occur under certain circumstances, will not be calculated into the use–dependent reimbursements.

The profit–oriented operations corporation will aquire all of the magnetic levitation train economic goods, other than the guideway, required for operation and will operate the route in its own name and expense. It will carry the full economic operating risk. The operating costs and the funds to service its own equity and the outside capital will be acquired through the operation proceeds (ticket sales). The operations corporation will finance thereby its allocated investment volume with approximately 20 % owned equity and 80 % outside captial. Other than in the previous models, only the profitability of the operations corporation will be considered in the structural reform model. The operations corporation can support itself using the assumptions for the base case. In the case of a stock corporation and with the assumed development, the stock could be placed into the capital market. The operations corporation generates taxes for the public authorities at a level well above that for the use reimbursement model.

D. Opportunities and Risks

The operational revenues carry special significance in the profitability assessment for all of the models. They are influenced primarily by the traffic volume, the fare arrangement, and the potential for additional receipts.

The traffic volume prognoses used for the magnetic levitation train route Berlin – Hamburg are the same as those used in the 1992 Federal Transportation Master Plan. The traffic volume is assumed to remain constant after the prognosis limit for the year 2010. This assumption can be taken as conservative, since numerous indicators predict that the volume of track–bound traffic, particularly for the connections between the old and new federal states, will disproportionally increase mid and long term. Therefore it can be assumed that the traffic volume for a large portion of the time period considered, will lie well above the base values used in the profitability calculations.

In respect to the fare arrangement, the Deutsche Bundesbahn is working on a new fare system for passenger traffic, which specifically takes into account the individual competitive situation. After exhaustion of the speed potential, the Deutsche Bundesbahn will orient the train fares (1st class) using airfares as a guide. Higher revenues as compared to the planning case assumptions are also possible by optimizing the fare structure upon this new basis.

IV. Summary

The system characteristics and advantages of the magnetic levitation train Transrapid are well documented. With its readiness for application and the final development stage currently in progress, the time has come to integrate the system into the overall transportation network. As with the innovative technology used in the Transrapid, the financing required to achieve the success of the project will also break new ground for infrastructure projects.

The models presented here offer financing alternatives which relieve the public budget in different ways. They differentiate themselves fundamentally from the previous financing of public infrastructure projects. In all cases though, the public authorities must assume definite risks which can not be transferred to the private sector.

Intended is the stimulation of discussions between the private economic sector and the public authorities as to how the magnetic levitation train connection Berlin – Hamburg is to be financed.

V. References

[1] L. Miller and Dr. F. Loeser, "Safety Analysis of Transrapid System – Methodology and Results", 8th Int. Convention on High Speed Rail, Anaham, Calif., May 1991.

[2] H. G. Raschbichler and L. Miller, "Readiness for Application of the Transrapid Maglev System", RTR 33 (1991/1992). pp. 9–14.

[3] U.S. Department of Transportation, "Safety of High Speed Magnetic Levitation Transportation Systems: German High Speed Maglev Train Safety Requirements – Potential for Application in the United States", DOT/FRA/ORD–92/02, Interim Report, February 1992.

[4] U. Wiescholek, "High Speed Magnetic Levitation Train Transrapid – Planning of the final development program until 1995 and prospects of utilization in the FRG", 6th World Conference on Transport Research, Lyon, June 1992.

[5] Magnetschnellbahn Berlin–Hamburg GmbH (Thyssen Industrie AG, Siemens AG und Daimler–Benz AG/AEG AG unter Mitwirkung der Deutschen Bank AG und der Kreditanstalt für Wiederaufbau), "Finanzierungskonzepte – Magnetschnellbahn Berlin–Hamburg, Bericht an die Bundesministerien für Forschung und Technologie und Verkehr", München, März 1993.

RESULTS ON THE OPERATION OF THE TRANSRAPID TEST FACILITY IN EMSLAND, NORTH GERMANY

Fritz Polifka, Hans-Peter Friedrich
MVP Versuchs- und Planungsgesellschaft
für Magnetbahnsysteme mbH
Landsberger Straße 76
D-8000 München 2
Geramny

1. DESCRIPTION OF THE FACILITY

The decision to continue to investigate only the electromagnetic levitation system was linked to the decision for a large-scale test facility for the TRANSRAPID.

The task of this facility was initially the qualification of the magnetic levitation technology under realistic application conditions. The Emsland test facility thus created the possibility to travel at high speeds and to prove the running qualities uphill and in bends and the feasibility of switches. Adapted to the financial conditions and the factors pertaining to the site, the test facility was built as follows.

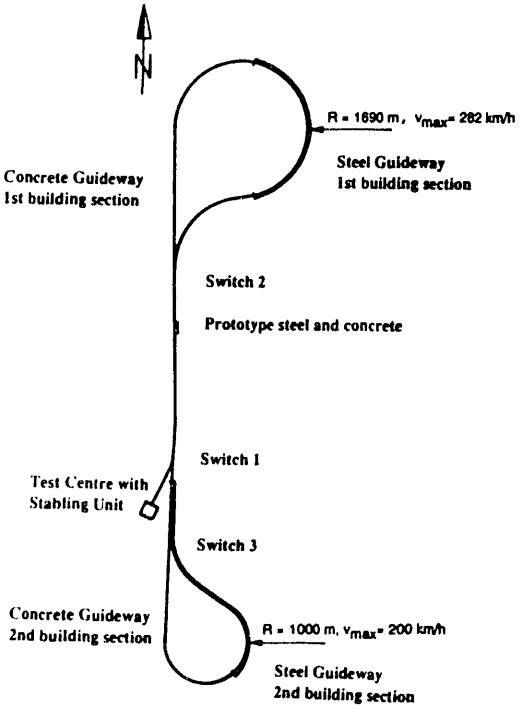

Fig. 1 Test Facility in Emsland

The test route consists of two loops, connected by a fairly straight stretch. The design speed on the straight is more than 400 km/h, for the two loops 280 and 200 km/h. The guideway is basically elevated, but there are sections with a height of 13 m and some ground level guideway. The longitudinal tilt is up to 3.5%, the maximum banking angle up to 12 degrees. There are three switches as part of the test facility with lengths between 67 and 150 meters. The test centre contains a traverser with stabling facility in addition to a hall for maintenance and repair.

The overall length of the guideway is 31.5 km; a complete circuit gives a distance of 38.7 km, whereby the straight between the two loops is covered twice. About 10 km of the route is steel guideway, 21.5 km concrete guideway. The vehicles available are the TRANSRAPID 06 (TR 06) and the TRANSRAPID 07 (TR 07). The basic test runs in recent years were undertaken with the TR 07, the newer vehicle. The TR 06 has been used for tests of individual components (e.g. tests on the runner surface). The propulsion is provided by a substation accommodated in the test facility. The control and safety of the test operation is undertaken from the control centre in the central test building.

2. QUALIFICATION OF THE TRANSRAPID SYSTEM

As has already been mentioned, the first important aim of the central test facility was the qualification of the magnetic levitation system. This was undertaken in the meantime in a convincing manner, even if

there were problems over a longer period of time with the availability of the guideway. These guideway problems are not Maglev-specific but concern the conventional part. They can be put down to the disregard of construction and engineering principles and will be corrected in accordance with the availability of funds by 1993.

The general qualification was the essential basis for the assessment of service readiness which the Bundesbahnzentralamt München (Federal Railway Central Office in Munich) confirmed as the independent assessor in 1991. 1.000 km per operating day were covered in an intensive operational phase for one month. The longest non-stop journey was 1.050 km. The longest journey in a day was 2.476 km. About 10% of the journeys were covered at top speeds over 400 km/h. In the course of this month, over 23.000 km were covered. In all the total distance covered with the magnetic levitation system amounts to 135.000 km. It should be noted that currently the aim is not to achieve as much distance as possible but lies in the achievement of selected test journeys for individual measurements.

The top speed achieved on the test route to date was 435 km/h.

About 25.000 visitors have travelled on Maglev as part of the qualification tests. It has to be stated here that, due to the priority accorded to tests, the runs with visitors have been handled very sparingly.

3. INDIVIDUAL COMPONENT FUNCTIONS

Besides the qualification of the general functionality of the magnetic levitation technology, the individual subsystems, vehicle, guideway, propulsion and operational control system were intensively tested at the test centre. The results from these detailed investigations have already led to optimisations of the components originally used at the centre. In 1989 the TR 07 was integrated into test centre operation as a further development of the TR 06 and a second generation of command and control technology is currently being integrated and tested. In the following is be given a brief overview of the tests to date back and their results.

Guideway

As has already been mentioned, differing guideway constructions have been compared at the test centre. This refers not only to the steel and concrete designs but also to the single span and two span girders. An important but also surprising result of the tests at the test facility in Emsland was the fact that the temperature differences between the upper and lower booms of the guideway girders were considerably higher than was specified in the generally applicable construction regulations (e.g. for road bridges). These temperature differences lead to guideway deformations, which have considerable effects on the follow-up behaviour on the support and guidance systems. As part of the service readiness assessment, in 1990 and 1991, both a steel and concrete two span girder were erected and tested positively at the test centre. In this case the girder deformations under temperature and load flows correspond to the specified loads. Actual the two span girder is envisaged for an application route.

The construction form of the single span girder, reveals unfavourable characteristics. Therefore in the last year started at the test facility a long term test with special absorption elements at a single span concrete girder. The previous results suggested an essential better behaviour.

A further result obtained from the test centre operations led in the new two span girder to a new fixture for the long stator on the guideway girder, which differs from the stator fixtures to date both in dimensions and by an additional redundant fixture. Already positive load qualifications have been carried out. Solely the question of resonances has to be considered in great detail in an optimisation

phase. Unfortunately, due to the given installation measures, it was not possible to incorporate this stator fixture in the other test centre girders.

Vehicle

As part of the vehicle tests to date, the speed range up to 435 km/h was tested. The magnetic support and guidance systems were tested positively concerning stability, sequential behaviour and failure tolerance in numerous test runs. Particular attention was paid to experimental function qualifications of the support and guidance systems at unusual guideway curvature points. Detailed investigations into the behaviour of various malfunctions were taken into consideration for the qualification of failure tolerance. These were in particular magnet failures and board network failures.

The faultless interaction with the other subsystems (propulsion, guideway and command and control) was proven in all essential points in comprehensive series of tests.

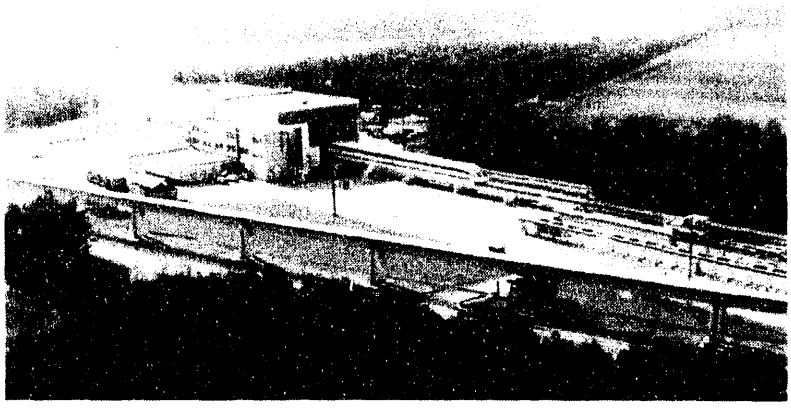

Fig. 2:
Test Center in the Emsland with the TR 07 in front of the hall

The interaction between contactless energy transmission and on board energy supply in the TR 07 could also be positively evaluated experimentally in comprehensive tests at the test centre.

Technical qualification of the braking concept, in particular with the eddy current brake system, which is applied as an emergency brake given a propulsion failure, were conducted as were design loads for support, guidance and propulsion forces.

In particular as part of the intensive long-term test operation, the optimisation potential of the support magnets was developed, which were implemented with the fitting of modified support magnets. The fitting of new magnets is planned to take place in Summer 1993.

Propulsion

The development of the propulsion has advanced since the initial introduction of the test facility in Emsland. The staggered arrangement of motor windings has been realised instead of the leapfrog method for the relaying of guideway sections and the digital propulsion control instead of the analog system on the test facility as on-going concepts.

All subsystems of the propulsion run satisfactorily over the whole speed range. The newly installed subsystems digital propulsion control and staggered arrangement of motor windings run without fault under operating conditions. In connection with the digital propulsion control, several vehicle position detection systems were tested. The investigations into the rotor

displacement angle start support and slip suspension detection could be concluded positively. Currently work is being carried out on an improvement in the braking precision. In the course of the investigations and development it has proved advantageous to set up simulation models for the propulsion system. For this purpose, experimental protective elements for the data to be collected in the simulation are implemented.

Operational Control System

An adaptation to the state-of-the-art has been undertaken in operations control. This new operational control system corresponds to electronic controlling unit technology for wheel-on-rail systems. The data transmission is undertaken with 40 GHz radio. As operations control has to accept the full safety responsibility for the test operations, not only the technical functions have to be proven in this instance but also the overall certification procedures for safety technology be completed. The technical functions have reached a satisfactory status after comprehensive tests. The certification process will take until the end of 1993.

Magnetic Field Strength

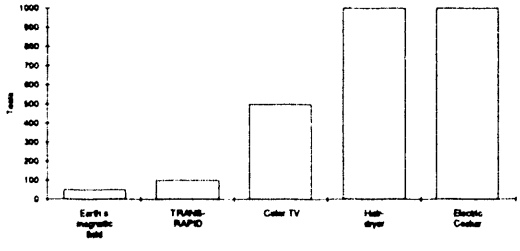

Fig. 3: Magnetic Field Strength

The results of the measurements of the magnetic field strength are shown in Fig. 3. The magnetic field of Transrapid lies near that of the natural earth magnetic field. So the influence is so slight that any negative effect even on passengers with heart pacemakers is completely ruled out.

Sound Measurements

The acceptance of modern highspeed trains is highly dependent on low noise emission. To achieve a quiet vehicle the knowledge of the dominant noise sources and their mechanism is necessary. Furthermore their position and strength have to be known to perform reliable calculations of the estimated noise immision for the area along a highspeed track.

In contrast to conventional rail/wheel systems there exists no primary knowledge of noise sources for the maglev train TRANSRAPID. Especially the strength of localized turbulence noise - and their position - with respect to the areal boundary layer noise is unknown. Therfore an experimental setup has been developed and installed at the TRANSRAPID test facility for the investigation of these questions.

On the basis of these measurements, the inclusion of the magnetically levitated system in Acoustics 03 - a public and legally recognised evaluation of acoustic radiation of rail systems - is still being worked on.

Fig. 4 shows a typical measurement of the noise source distribution for a velocity of 400 km/h in the frequency range 250-3150 Hz. Dominant noise emission occurs only at the lower part of the vehicle where the flaps are located which cover the propulsion and guiding magnets. They consist of segments with a basic length of 3 m which can move independently from each other to provide an optimum guide along the track. It is supposed that the edges of the flaps cause local aerodynamic turbulences leading to noise emission (a significant contribution of the propulsion system itself can be excluded for the high velocity range). The dominant peak occurs in the very front of the vehicle and is caused by a turbulence at the nose of the vehicle. The upper part of the vehicle (passenger cabin) which has a smooth surface without edges shows a much lower noise emission.

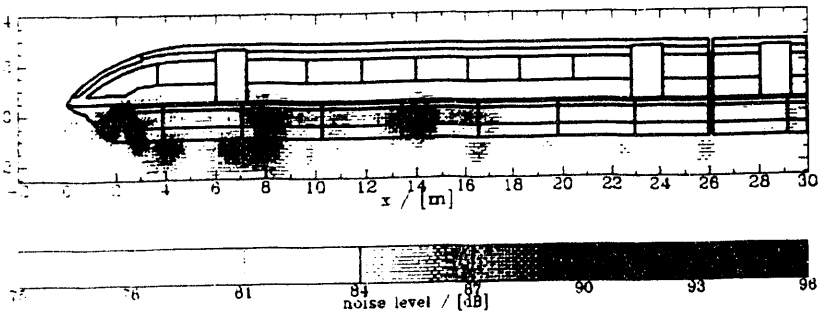

Fig. 4:

Noise emission of
the maglev train TRANSRAPID
during passby with 400 km/h.
(running direction right to left)

So one result of the noise measurement is that aerodynamic boundary layer noise is not the dominant noise source.

Aerodynamics

With the help of a measurement panel erected for this purpose parallel to the guideway on the test facility, the experimental pre-requisites for the assessment of two-way behaviour of two Maglev vehicles at high speed in accordance with recognised procedures.

The nose and tail of the TR 07 were investigated for this. As part of the aerodynamic measurements, the nose design of this vehicle was optimised. Experimentally secured statements for the pressure loads of the windows at high speeds also exist.

The most important topic for high speed vehicles of the positioning of inlet and outlet openings for the air conditioning system was similarly comprehensively investigated and corresponding modifications were undertaken.

Operational Observations

Parallel to the individual investigations and functional qualifications, the behaviour of the individual components is supervised and documented under operating conditions in order to be able to use the experience obtained on the test facility for the operation of a test route.

The aim of the observations on the test facility is to investigate procedures and actions for operations in terms of their rational sequence and handling. Included here are the maintenance of the system and the individual measures and the procedures concerned. There is considerable experience where this point is concerned. This has been implemented as realistic measures and procedures (e.g. maintenance vehicles for the guideway).

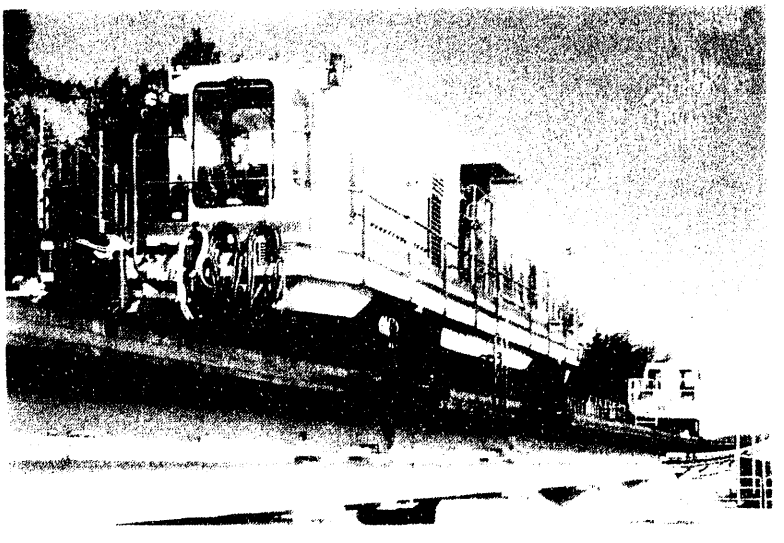

Fig. 5:
Maintenance vehicles
at the test facility

Intensive observations of the long-term behaviour and reliability of the individual components will only be possible when the test facility guideway is again fully available.

Overall it has to be stated that the experience and results of the test operation at the test centre have confirmed the course taken.

4. FUTURE PERSPECTIVE

The practicable applications and the tests conducted at the test centre in conjunction with the positive confirmation of service readiness show that all the basic factors for a decision for the use of the high-speed magnetic train in Germany have been created.

It is obvious that the Maglev developments will be carried on, in the course of which precise analyses of the transport market will be made, detailed operational concepts drawn up and optimisation of the system engineering will be undertaken.

Maglev Programs in Korea

In-Kun Kim
Mun-Whan Yoo
Korea Institute of Machinery and Metals
Daejon, Korea

Chanil Park
Hyun-Kap Chung
Korea Research Institute of Ships and Ocean Engineering
Daejon, Korea

Kook-Hun Kim
Korea Electrotechnology Research Institute
Changwon, Korea

Abstract - Korean Ministry of Science and Technology initiated a small R&D project in 1989 to assess the possibility of developing a magnetically levitated train system. This government project is closed to the end of its 1st phase in which the possibility was shown and a good progress was made toward the next phase. The project office is preparing for the 2nd phase which is more commercialization oriented.

The government project not only proved the possibility but also triggered the interest of Korean industry giants such as Hyundai and Daewoo, and they are now actively pursuing programs of their own. As a result, Hyundai is building a 40 person vehicle to exhibit during the Daejon Expo'93 and Daewoo is testing a similar size vehicle at the moment. The main focus of these programs is low to mid speed maglev technologies based on Electro-Magnetic Suspension (EMS) and Linear Induction Motor (LIM) drive. These maglev teams are in the process of forming a consortium to accelerate the delvelopment and commercialization efforts.

The Korean maglev program when successful will find its prime applications as urban guided transit. Korean government is conducting feasibility studies for a number of urban guided transit routes to alleviate traffic congestions in large cities. The prime candidate for the maglev application is connecting downtown Seoul and New International Airport under construction. The target date for the new airport transit operation is year 2001.

I. Introduction

Much of the previous interest in magnetically levitated train has centered on high speed systems but advantages of low friction and noise, and high reliablity showed promise for low speed applications such as urban transits also. The successful service of Birmingham People Mover (BPM) at Birmingham airport proved this possibility and recent development of HSST program to low speed applications provides a renewed hope for the future of the low speed maglev.

The government program started without clear target for application nor clear picture of system choice. During its 1st year (1989-1990), the program office compared various maglev systems and assessed them in terms of technical difficulties and available resources, and application. High Speed Systems of MLU (Japan) and TRANSRAPID (Germany), and mid to low speed systems of HSST, BPM and M-Bahn were looked into. From

application side, possibility of Seoul-Pusan Corridor (high speed) and urban transits for Seoul suburb (low speed) were assessed. It became immediately clear. The technology requirements for the high speed systems were to high and there were to many problems to slove for the time and resources available to this program. Furthermore, government (Ministry of Transportation) was pursuing construction of high speed train system (wheel-on-rail) with foreign technology and thus did not want any form of distraction. The only available choice for the government maglev team was low-to-mid speed system for urban transit application.

The large cities of Korea are experiencing aweful traffic and pollution problems due mainly to the rapid increase of automobiles during last decade and government is seriously considering various guided transit systems as a solution. This situation also played a role in the choice of system and application. Another factor contributed to this system choice. At the time of program formulation, Korean government was applying to hold an international exposition in 1993. A group of maglev people, which later formed the government maglev team, suggested maglev exhibition in the Exposition and this idea was adopted. Both Hyundai and Daewoo showed interest in the exhibition but the task was awarded to Hyundai while the government team was selected to supervise and coordinate the task in behalf of the Expo organizing committee. Daewoo continued their maglev program and developed a 40 person vehicle.

The program started with little maglev experience in the team. The team is composed of people from three government supported labs , Korea Inst. of Machinery and Metals(KIMM), Korea Electro-technology Research Inst.(KERI) and Korea Research Inst. of Ships and Ocean Engineering(KRISO) with the project office installed in KIMM. The project office took responsibility of the system engineering and integration, and vehicle dynamics. Levitation and propulsion tasks were given to KERI. Guide way designs and construction was assigned to KRISO which had years of experiences with large precision metal works.

II. System Choice

From the early stage of the project it was decided that Electromagnetic Suspension and LIM drive would be only possible choice of the system. Two test proven systems of HSST and BPM were used as models in the designs of levitation/propulsion modules.

During the 1st year, two small scale (~1/2 scale) modules were built, one after HSST and the other after BPM. The 1st one used staggered magnets with transverse magnetic flux paths and 2nd one used longitudinal flux paths.

Some of the important features of the modules are;

	1st	2nd
No. of Magnet	8	4
No. of LIM	2	1
Weight	1.0 ton	2 ton
Length	1.2 m	2.3 m
Gap	6 mm	8 mm
Guideway	15 m	15 m
Levitation Control	Analog	Analog
Power Collection	AC 220 V	DC 600 V

The modules executed the basic functions of levitation and propulsions successfully. The objective of these modules were to evaluate the design concepts and technical problems associated with them. These modules revealed many technical problems which we did not fully aware of. After the test of these modules, magnet arrangement with transverse flux paths is selected mainly from the guidance consideration.

Eventhough EMS/LIM drive was chosen early in the stage, we didn't have a good picture of full vehicle or components. Table 1 shows some of the ideas we had at the time of system choice. The arrow sign show the directions of progress.

Table 1 System Ideas

Levitaiton Control	: Analog→Digital
Propulsion Control	: Constant Slip→Speed pattern
Power Conversion	: Power TR→IGBT→GTO
Track	: Single Beam Steel → Concrete

III. Research and Development so far

The scale model tests provided some real insight into the maglev and the direction of future work. The tests with scale models couldn't provide much of the quantitative informations and problems associated with speed. The needs of full scale test was strongly raised.

The project office decided to construct full scale test bed. The full scale test bed was designed with the following concept.

1. Include as may test features as possible
2. Test track simulation to commercial one and room for extensions
3. Room for upgrade

The test bed includes :

1. 2 different size test modules
2. 100 m track with curved guideway
3. DC power supply facility

The two modules were orginally designed with the following specifications.

1st Module

Weight : 4 tons
Length : 3.7 m
Gap : 11 mm
Design Speed : 40 km/hr
Levitation Control : Analog
Inverter : Power TR (1 KHz)
Chopper : Power TR (2 KHz)
Power Cellection : DC 600V

2nd Module

Weight : 2.5 tons
Length : 2.5 m
Gap : 9 mm
Design Speed : 50 km/hr
Levitation Control : Digital
Inverter : speed pattern control IGBT (10 KHz)
Chopper : IGBT (10 KHz)
Power Collection : DC 600V

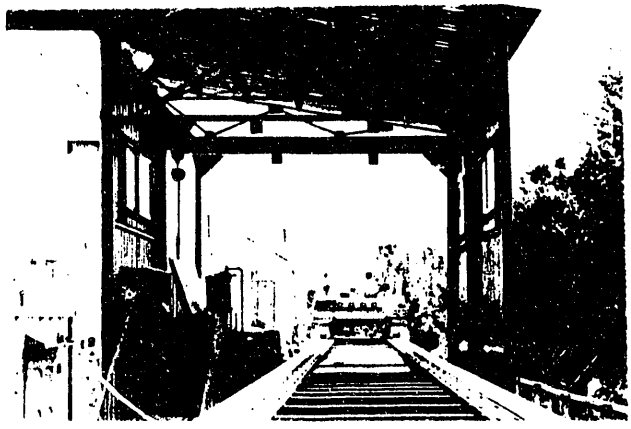

Fig. 1 Shows the Track and a Module

There was 9 months time separation between the two modules. Several changes were made in the 2nd module reflecting the progresses. Along with change of module length, new methods in levitation and propulsion controls were introduced and high frequency power conversion equipments were employed. Change of module length were made to investigate the curve negotiating characteristics of the modules. Digital levitation control made the management of control parameters during tests much easier. Various mode controls such as active guidance control, pitching control in addition to levitation were possible. High frequency power conversion equipments were introduced mainly to reduce the noise generated from to low frequency switching but new transistors allowed compact equipment design also.

Due to the length of the track, the maximum speed possible is only 10 km/hr, however, a smooth ride was noted for each of the modules. A 36

channel data acquisition system is being uesd to store all the test data. For the two-module tests, the 1st module will be upgrade with control and power equipments similar to those of the 2nd module.

Hyundai's Expo'93 Exhibition Program : Hyundai is the first to start maglev oriented research in Korea, 1985. This program was carried by small team of 3 -4 people until 1990. After small scale proof-of-principle test for levitation and LIM propulsion, they built 2 ton vehicle with 3 modules and demonstrated to public in January, 1991. This team was expanded to take up the development tasks of Expo maglev exhibition vehicle. This program is in its final stage with vehicle test coming up in April. Figure 2 shows the Expo track (520 m) with pyramid shaped Maglev pavillion behind and Table 1 shows specification of the vehicle. The exhibition will last 3 month (August 6 - November 10) and is expected to carry 1/4 million people.

Fig. 2 Hyundai's Expo Track

Table 2. Expo Vehicle Specification

Vehicle	L 17.6 m × W 3.0 m × H 3.8 m
Weight	28 tons
No. of Seats	40
Max. Speed	50 km/hr
Levitation	Attractive Magnets
Propulsion	Single-sided LIMs
Air Gap	12 mm
Track	520 m
Levitation Control	Analog

Daewoo's Maglev vehicle : Daewoo's maglev program is reported separately in this conference(PS 1~2). A short remark may be made here. Starting from scratch, Daewoo developed a full size vehicle in shortest time(~2 Year) and demonstrated successfully on 100m track. This vehicle is shown in Figure 3.

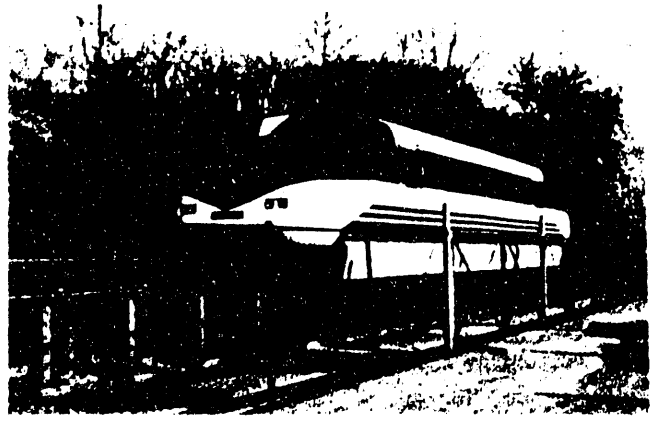

Fig. 3 Daewoo's Full size Vehicle

Ⅳ. Future Research and Development

Eventhough Korean maglev teams made remarkable progress in short time, major portion of the work remains for the future. The problem areas and future tasks are :

Power Conversion Equipments : The EMS/LIM driven maglev employs choppers and inverters to power magnets and LIM, respectively. Reliability of these equipments became major source of trouble during the tests. These equipments were not designed for vehicle mount and frequent failures of elements occured. These failures are caused due to the lack of protection circuits and exessive vibration during the tests. Our team of power electronics is working with selected equipment manufactures to improve the reliability.

Test Track : A vehicle can not be completed without proving its performance at the speed and track conditions similar to the commercial one. The test track we have is grossly inadequate for the kind of

tests required for the commercialization. The project office applied for the special funding for the construction of 1 km test track in 1992 and it was approved. The plan calls for completion of track in 3 years starting from 1993. Some of the important features of the track includes :

- Total length 1 km
- 400 m straight section
- Smallest radius of 60 m
- Two switchings
- Slopes between 3 % and 6 %
- Vertical curvatures of 1 km

This track, when completed will allow to test the vehicle up to a speed of 70 km/hr and various curve negotiating characteristic. The straight section of this track may be extented for higher speed later.

Test Vehicle : Two test vehicle are being designed and will be tested on the new test track from later part of 1995. These vehicles are going to be manufactured by Daewoo and Hyundai and tested as a train. These vehicles will reflect all the research and upgrade work done up to the end of 1994.

Non-Contacting speed detection : To operate maglev vehicle with given speed pattern, accurate speed detection through now-contacting method is required. Various tehnologies are under evaluation and a small scale test will be conducted later part of 1993.

V. Consortium

The remaining work for the Korean maglev teams to reach the commercialization level is too much for any one team to carry. It is thus a consortium is being formed to share the burden in a way the strength of each team can be best utilized. The basic research and, test and evaluation will be responsibility of the government team and vehicle design and manufacuring will be carried by the industrial teams. The first action of the consortium will be proposal writing to the government A proposal "Application of Magnetically Levitated Train for Seoul-New International Airport Transit" is being prepared by the consortium organizers.

VI. Conclusion

A development task of maglev scale can not be successful without clear picture of application and support from the user. Korean maglev program is not an exception. The users (government) want make sure the system is in applicable form before making any application decision but the system can not become fully applicable until the application picture is provide by the user. The future of Korean maglev program depends on how soon the government fully commits to the maglev application.

A General Survey of Chinese Maglev Train

J.S. Lian, J.W.Zhou, K.L. Zhang, and H. Jiang

Department of Electrical Engineering, Southwest Jiaotong University
Chengdu, Sichuan, China, 610031

Abstract - **China's present transportation status is briefly introduced in the paper first, which shows the heavy traffic in large cities and their suburbs and in some railway districts. Then, the necessity of developing a maglev train in China is proposed in detail. The scheme and status of research and development of the maglev system in China are described.**

I. INTRODUCTION

China's economy has developed rapidly with the reform and opening in the last ten years. The gross national product increased by 12% in 1992, and the per capita income increased by 10%. Prediction shows that the increase in 1993 will be even higher than that of 1992. But the communications and transportation have not caught up with the rapidly developing situations. Hence, the Chinese government gives the first priority to communication and transportation systems in its seven emphasized investment fields in 1993. It is well known that China's transportation system depends mainly on the railway which makes up about 60-70% of the total transport capacity and this situation can not be changed thoroughly within a relatively long period. Most of this 60-70% of the total freight volume is concentrated in the coastal area of east China, where heavy traffic results from the rapidly developing economy. Therefore, it is an important task to solve the problem of heavy cargo passenger traffic in this area.

Table 1 lists the railway districts that have a relatively higher density of passenger-cargo traffic on the basis of prediction for the year of 2000. The predicted carrying capacity required in these districts are shown in Table II. One can see from these Tables that the districts have a large and stable passenger flow. In order to meet the transport quotas in 2000, the carrying capacity must be enhanced. However, the conventional high-speed railway can not satisfy such a requirement because it occupies a lot of land which is not available in those areas.

The annual railway passenger traffic of China is about a billion person-trips at present. It is predicted that by the end of this century, the annual passenger traffic will reach 1.6 billion person-trip. In fact, passenger trains are often overloaded by 50-70% on the heavy trunk lines. One can hardly find a place to stand in the passenger train during the traditional Chinese Spring Festival

Metropolises all over the world are suffering from crowded traffic at present. There are 31 cities in China with a population of more than 1 million. The urban population increases very quickly along with the construction of satellite towns. Taking Beijing for example, the passenger traffic is now 6.86 times that of 1975. However, the number of vehicles is only 4.84 times that of 1975. The conventional city traffic causes environmental pollutions. For instance, in the city proper of Shanghai, the traffic noise accounts for 35% of the total environmental noise. In the busy section of Shanghai, the traffic noise level can reach 85 db.

The traffic character of large cities in China is the large number of bicycles. The number of bicycles in the whole country is nearly 400 millions and the number is increasing annually. Large numbers of bicycles result in a lot of problems. The ratio of the road area occupied by the bicycles to that occupied by the passenger bus is 12. The city roads are congested with bicycles which lead to traffic jams and increasing accidents. For example, the bus running speed in Chinese cities has dropped from 20 km/h in 1960's to 10 km/h at present. People take a long travel time to go to work and back home. This is not only waste of time, but also of vigor, and leads to low work efficiency. The large number of bicycles causes a marked increase of traffic accidents. Statistics show that the mortality rate is 4-6 people per thousand bicycles per year in Beijing, Shanghai, and Tianjing.

II NECESSITY OF DEVELOPING MAGLEV TRAIN IN CHINA.

The unreasonable structure of the transportation system in China is the main cause of crowded traffic and the difficulty to take trains or buses, whether looking at the traffic state in some railway district on the trunk lines or in the large cities. Passenger and freight transport should be separated, and special high-speed passenger transport railways should be constructed. The number of bicycle should be reduced in large cities. It is not realistic to drive a private car to go to work because of the large population. It is also difficult to increase the number of buses because the the roads have already been saturated with vehicles. There are subways, lignt-rail vehicles and maglev trains that can be chosen as solutions. The maglev train has some special advantages over other two means, such as large volume of traffic, reduced pollution, high speed, safety and comfort, beautification of cities, and relatively low costs. Subway, buses on surface, and elevated maglev railway together form a three-dimensional transport network which can relieve the traffic tension in large cities.

China is now a developing country, its economy and technology are still weak. However, the problem of communications and transportation is extremely serious. The Chinese government makes every effort to find a solution that tallies with the actual situation. From the longer viewpoint, it is rather favorable to consider the maglev train as a solution whether inside large cities or inter-cities. We chose the suburb of Beijing (Beijing-

Changping) to do the feasibility study in order to develop maglev train in China.

Beijing is the political, economic, cultural and transport center of China. It covers an area of 16800 square kilometers, in which the city proper covers 68 km^2. It has a population of more than ten million, about six million live in the city proper. The four center districts of the city have a population of 2.4 million, and the population density is nearly thirty thousand people per square kilometers. Beijing served as the capital of past successive dynasties in Chinese history, which left many historical sites and scenic views. Every year many domestic and foreign visitors come to the city. So the floating population is fairly considerable (about several hundred thousand each day), and in recent years, the satellite towns have flourished, all of which increase the load of transportation. Because of the shortage of land and other limited conditions in Beijing, the problem cannot be solved well if the traditional transport system is employed. But it is fairly suitable to adopt the maglev train.

According to the imagination of overall city plan, the total railway length of the Beijing-Changping district is about 40 km. There are many world famous scenes and four satellite towns along the railway line. These towns are the center of light and textile industry, the center of heavy industry, the center of higher education and research, and the center of tourism, respectively. Each town has about a half million people. On account of traffic, it is not convenient to travel from satellite towns to the city proper because the travel time is too long. Many people try very hard to move back to the city proper again although measures have been adopted to encourage people to live in the satellite town. Clearly, people would enjoy living in the satellite towns if the travel time could be controlled within a half-hour. Therefore, it is necessary to build a maglev railway to disperse the population in the city proper and promote prosperity in the satellite towns.

III. APPROACH TO BEIJING-CHANGPING MAGLEV RAILWAY

To plan a maglev railway with busy passenger traffic, the first thing to do is to analyze the passenger volume between the start and the end of the line. The next is to choose a suitable mathematic model to predict the traffic in future years. These are the primary conditions to decide the alignment of the line, station scale, number of cars in trains, operation management, and required numbers of facilities. These are also the important bases for the further appraisal of investment business income, business costs and the financial and economic analysis of the project.

There are highways and railways between Beijing and Changping. The transportation mainly relies on the highway which accounts for 95% of the total traffic. It takes about two hours to go from Beijing to Changping and vice versa. If the maglev train is adopted, the round-trip travel time will only be about a half-hour.

Table III shows the passenger traffic in Beijing-Changping district from 1978 to 1987. According to it the graph of passenger traffic on time sequence can be acquired, as shown in Fig. 1. Based on the preliminary regularity of Fig. 1, a quadratic polynomial model is adopted to do the prediction and analysis with the aid of a computer.

The prediction on the basis of the mathematical model shows that the passenger traffic will reach forty six million in Beijing-Changping district in the year 2000.

The passenger turnover volume is the product of passenger traffic and the average mileage of passengers completed in a certain time. It includes the factor of mileage and can reflect the passenger traffic well. It is one of the main quotas on the passenger transport operation, and also the main basis of calculating and analyzing the cost and income of passenger transport, and the labor productivity. Passenger's average mileage can be obtained from the ratio between the total turnover volume and the total passenger traffic of each year. In the Beijing-Changping district, the passenger's average mileage is 30 km.

To predict the turnover volume of the maglev train in the future, it is assumed that the absorb coefficient of the maglev train is 60%. Table IV shows the annual turnover volume of the district in the next ten years.

There are a number of maglev routes that can be chosen for the Beijing-Changping district. Two routes have been carefully compared. One is from Xizhimen to the north of Changping through the Summer Palace, having a total length of 42.1 km. The second is from Deshengmen to Changping, the total length being 38 km. Both routes can cooperate with the Beijing subway and other public traffic systems very well, making the traffic convenient for the residents, and ensuring enough passenger traffic. The railway is easy to built because of the smooth terrain along the railway line and a small amount of house movement. The first route begins at Xizhimen and goes through the city proper, but it is curvilineal and needs considerable investment. The second route begins at Deshengmen and goes a very short distance through the city proper. This line, being mostly straight, requires a smaller investment and should be adopted.

After the maglev route is determined, the organization of the train operation should be planned, the carrying capacity and other relative quotas should be checked or calculated in detail.

When planning the organization of the maglev train operation, the annual passenger traffic shown in Table IV should be considered first. The second to be considered is the unbalanced coefficient of the whole day passenger traffic to that of peak hours. According to the statistics of Beijing traffic, the peak hour accounts for 12% of the whole day passenger traffic in Beijing, i.e the unbalanced coefficient is 1.2. The operating hours of each day and the minimum interval time of trains should be decided on this basis. The organization of operating plan is as following:

- operating 18 hours everyday (5 am to 11 pm);
- Minimum interval time of trains: 3 minutes;
- Requirement of traffic:
  - single directional carrying capacity in year 2000: 27.5 million passengers
  - single directional carrying capacity per

day: 76.7 thousand passengers
- carrying capacity in each peak hour: 11.5 thousand passengers.

- Parameters of the maglev train:

• running speed (km/h)	200
• acceleration (m/s^2)	1
• acceleration in starting (m/s^2)	0.7
• deceleration in braking (m/s^2)	0.8
• starting time (s)	79.4
• distance of starting (m)	2205
• braking time (s)	69.5
• distance of braking (m)	1929

There will be two stations between Beijing and Changping: the Qinghe station and the Shahe station. The running time from the Deshengmen station to the Qinghe station is 4.48 minutes, and 5.1 minutes from Qinghe to Shahe or from Shahe to Changping. The detention time in each station is one minute. We have compared the single line with the double line. The results are listed in table V.

The construction of the Beijing-Changping maglev railway will remedy the crowded surface traffic greatly, decrease pollution, improve the environment, reduce traffic accidents, and more importantly save travel time. If the per capita income of Beijing residents is 1.2 yuan per person-hour, each person saves 1.5 hour travel time every day, and the daily average passenger traffic is 76.7 thousand passenger-time in 2000, then the value of the time saved is 50 million yuan/each year. On the contrary, if the same passenger traffic is completed by buses, and if it is assumed that the average running speed is 30 km/h, then 60 buses need to be added every day even if each bus can hold 150 persons. If we consider the cost of buying buses and auxiliary facilities, widening the roads and so on, the investment will not be less than that of the maglev railway. Therefore, from the point of social and economic benefits, it is favorable to build a maglev railway between Beijing and Changping. Of course, the economy and technology of China are still fairly weak, and the study of the maglev train is just in the beginning. It seems necessary to import the foreign investment and technology to build the maglev railway.

IV RESEARCH STATUS OF CHINESE MAGLEV TRAIN.

China began to study maglev trains in the early 1980's. Southwest Jiaotong University is a key comprehensive University which has a history of 97 years, and has brought up a large number of railway technical personnel. It began to study maglev trains in 1987, and has already successfully conducted experiments on maglev model. Then, in 1990 it began to develop a maglev train weighting one ton and holding 2-4 passengers on a 42 meter-long track. The assembly work is expected to be finished this year.

In 1991, the Chinese Science and Technology Committee made the maglev train a key item of China's 8th Five-Year Plan and appointed the Railway Ministry to organize and develop a maglev train weighting 14 ton, holding 46 passenger, with a 500-meter long track, and running at a speed of 50 km/h. The maglev vehicle will be tested in 1995 at the loop—track experiment base of Railway Science and Technology Institute (RSTI) in Beijing. The RSTI will be in charge of the project. Changchun Passenger Coaches Manufacture Plant will make the train. Southwest Jiaotong University is responsible for the basic research work.

V. CONCLUSION

As a result of the reform and opening, the Chinese economy has developed quickly in the last 14 years. The passenger and freight traffic have increased year by year. The intense state of communication and transportation is quite out standing. It needs to find a new transport means to relax the heavy traffic loads in large cities or between large cities and their satellite towns. It is an effective measure to adopt the overhead maglev train, which can satisfy the passenger traffic demands of China after 2000 year. According to the present economic and technological status of China, this paper presents the idea of giving first priority to developing the Beijing-Changping maglev railway.

REFERENCES

[1] H. Jiang and J. S. Lian, "The Development and Prospect of Maglev Train in the World", Journal of The China Railway Society, Vol. 13, No. 2, 1991.

[2] H. Jiang and J. S. Lian , "On the Control Principles for the Attraction Magnetic Suspension Vehicles", Journal of The China Railway Society. (Special Issue on Electrification and Automation of Railway Traction), 1991.

[3] B.V. Jayawant, Electromagnetic Levitation and Suspension Techniques," Edward Arnold Ltd, 1981.

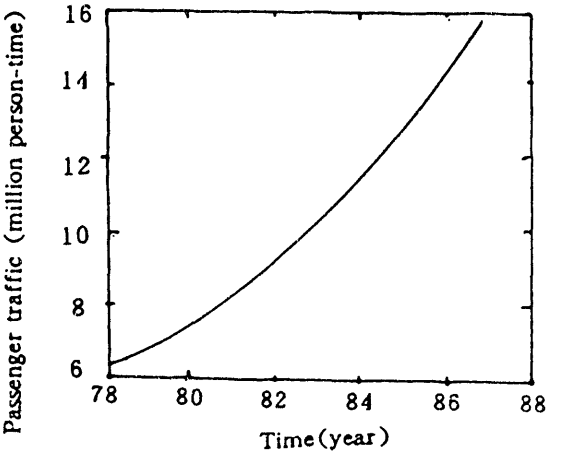

Fig. 1. Passenger traffic on time sequence

TABLE I

Higher density railway districts in China in 2000.

District	Mileage (km)	Passenger traffic density, up going (million person)/down going (million person)	Freight taffic density, up going (million ton)/down going (million ton)
Beijing-Tianjing	137	26.48/28.47	40.66/61.00
Nanjing-Changzhou	144	28.00/27.63	21.30/51.00
Chanzhou-Shanghai	167	29.42/29.26	21.10/47.00
Shanghai-Hangzhou	189	24.62/24.64	23.95/27.00

TABLE II

Required carrying capacity in some districts

District	Required number of pairs of trains		Required capacity in the simultaneous operation diagram			
	Passenger train[a]	Freight train[a]	Train succession (minute)	Passenger train	Freight train	Total capacity
Beijing-Tianjing	65	73	10	130	90	220
			8	163	95	258
Nanjing-Changzhou	64	61	10	128	75	203
			8	160	80	240
Changzhou-Shanghai	67	56	10	134	69	203
			8	168	74	242
Shanghai-Hangzhou	56	41	10	112	51	163
			8	140	54	194

a. The passenger train is calculated in 1200 person/each train.
The freight train is calculated in 5000 ton/each train.

TABLE III

The passenger traffic in Beijing-Changping district from 1978～1987

Year	Passenger traffic (thousand person-time)	Year	Passenge traffic (thousand person-time)
1978	6358.6	1983	10634.0
1979	7648.2	1984	12291.1
1980	7862.7	1985	13695.5
1981	8501.8	1986	13499.9
1982	9706.6	1987	16737.9

TABLE Ⅳ

Turnover volume in the future

Year	Total passenger traffic of single direction (thousand person-time)	Absorb coefficiant	Average mileage (km)	Bi-directional turnover volume (million person kilometer)
2000	46634.0	60%	30	1678.8240
2002	53045.7	60%	30	1909.6452
2004	59918.4	60%	30	2157.0624
2006	67234.6	60%	30	2420.4456
2008	75026.2	60%	30	2706.9432
2010	83278.6	60%	30	2998.0296

TABLE V

Comparison of single and double lines

Type / Year / Quota		Operating quotaes of single line.	Operating quotaes of double line
		In the year of 2000	
Whole day passenger traffic (thousand people)		76.7	76.7
Peak hour (morning or dusk)	Passenger traffic	11.5	11.5
	Overload rate	65%	65%
	Mashalling number and operating pairs of trains.	14 pairs, 10 cars in each train	58 pairs, 4 cars in each train
	Average interval	17 (minute)	4 (minute)
Normal hour	Operating pairs of trains of whole day	64	192
	Average interval of whole day	17 (minute)	7 (minute)
Necessary number of cars		40	30
Necessary number of staffs		200	330
Apprised investment (billion yuan)[a]		1.5	22
Recovery time of investment (years)		10	14

a. One yuan equals about 1/8 dollar

Present Status of Research for Maglev in Italy

G.Martinelli and A.Morini
Department of Electrical Engineering - University of Padova
Via Gradenigo 6/a - 35131 PADOVA (Italy)

Abstract - **In Italy the researches in the field of magnetic levitation transport systems are late as regards other industrialized countries: at present there is no MAGLEV practical realization. In the frame of the Progetto Finalizzato *Trasporti 2*, promoted by the National Research Council and at present operating, a research project has been financed to study MAGLEV systems driven by long-stator linear synchronous motors. The three-year research, begun in the second half of 1992, involves the Universities of Padova, Bologna, Palermo and the Polytechnic of Milan.**

I. Introduction

The Italian transportation system presents to-day heavy drawbacks, owing mainly to the following reasons:

- extreme concentration of goods traffic in the roads with consequent congestion of the main routes because of the low competitiveness of the rail transport and the increasing demand in transportation;
- deficiencies in the services of both the railroad and the harbors, due also to bureaucratic procedures not compatible with an operative management;
- high traffic congestion of the main airports, nearly saturated;
- high congestion of the great urban areas, because of the inadequate quality of the public utilities and of the absence of integration between individual and public transportations.

It is therefore plain that the social and economic growth of the country demands a more efficient transport system, both for passengers and goods, as well as a re-examination of the transport policy in order to find more satisfactory solutions.

The importance and urgency of the problem were acknowledged by the National Research Council (CNR), which promoted and financed the Progetto Finalizzato *Trasporti 2* (PFT2), following and completing the Progetto Finalizzato *Trasporti*. The main aim of the project is to seek for the most appropriate means of increasing the efficiency of the Italian transport system and of suitably responding to the rising demand in transportation. The attainment of such a target needs also the development of new technical solutions and from this point of view the chance of investigating the prospects of MAGLEV applications in Italy, as components of a balanced and integrated transport system, has been acknowledged. It follows that in the frame of the PFT2 a research on the high-speed MAGLEV systems driven by long-stator linear synchronous motors has been funded.

Manuscript received March 15, 1993. This work was supported by the Progetto Finalizzato CNR *Trasporti 2*.

II. Study of High-Speed Maglev Systems in the Frame of the Progetto Finalizzato Trasporti 2

The Progetto Finalizzato *Trasporti 2* is a five-year project: it began in the second half of 1992 and has been initially funded by the CNR with about 290 thousand million lire. The main targets of the Progetto are:

- to increase the efficiency of the transport system with regard to the technical and economic aspect, as well as to the fulfilment of the demand of transportation;
- to increase the harmonization between the territorial and transport policies in order to rationalize the movement of population;
- to protect the environment;
- to increase the safety and reliability and to reduce the vulnerability of the transport system;
- to improve the competitiveness of the transport industries;
- to contribute the creation of technical abilities in the field.

For the attainment of such purposes the strategy adopted by the PTF2 consists in the following points:

- development of system innovations;
- development of component innovations;
- transfer of advanced technologies to the field of transportation;
- incentive to the basic research and to the creation of specialized abilities;
- advice and support to the economic planning;
- methodological support to the planning, management and control of the transportation system.

Such strategy is followed by means of six sub-projects:

1. Management of mobility and Tools for planning
2. Vehicles
3. Support technological systems and Substructures
4. Urban transportation
5. Goods transportation
6. International programs

In the frame of the sub-project "Vehicles" the research topic "Guideway vehicles with non conventional sustentation and/or propulsion" is included; one of the research projects of this topic is entitled "Study of innovatory transportation systems with long-stator linear synchronous motors and magnetic levitation obtained by means of superconducting and/or conventional coils".

The aims of this three-year research project are:

- to study the high-speed MAGLEV systems with long-stator linear synchronous motors (LSM);
- to investigate on their possible applications in Italy;
- bearing in mind the results of the international researches on high-speed MAGLEV systems, to coagulate the Italian experiences and resources in the field in order to make actual proposals for such systems also in Italy.

The research is divided into the following points:

- technical and economic analysis of the MAGLEV systems, both electromagnetic (EMS-MAGLEV) and electrodynamic (EDS-MAGLEV);
- prospects of their application in Italy;
- design criteria of the levitation magnets as well as of the LSM windings, both in the case of superconducting field coils and in the case of conventional coils and iron core;
- design criteria of the supply and control system of the vehicle;
- preliminary design of a prototype and of the related supply and control systems;
- construction of a LSM model.

The final target is therefore the acquisition of specific abilities on the design criteria of high-speed MAGLEV systems and of their components (in particular the LSM) and the availability to transfer such criteria to national users for possible applications.

Four operating groups take part in the research program:

- Department of Electrical Engineering of the University of Padova;
- Institute of Electrotechnics of the University of Bologna;
- Department of Electrical Engineering of the University of Palermo;
- Department of Electrotechnics of the Polytechnic of Milan.

The activities of the research groups are closely connected and coordinated.

III. Present Status of the Research

The technical and economic analysis on the prospects of application of the high-speed MAGLEV systems in Italy is still under preparation. The first results seem to point out that such systems could be utilized for intercity travels, as an alternative to high-speed on-rail trains and to short-haul flights; they could also be utilized for shorter distances, to realize speedy connections between airports and downtown or between neighbouring towns.

In comparison with on-rail high-speed trains, MAGLEV systems offer the advantage of reduced travel time; such advantage is maintained in Italy also versus medium-haul aircraft flights (400÷800 km), bearing in mind the check-in and check-out operations, the airport congestions and the transferring times between airport and downtown.
Although detailed indications on the cost-competitivity of MAGLEV will be available only after the operation of the first commercial lines, nevertheless the preliminary analyses show that, in comparison with high-speed railways, MAGLEV systems should have lower operating costs and comparable capital costs [1,2].
In comparison with air transportation, the advantage of MAGLEV is given by lower specific energy consumptions and by the reduction in sky and airport congestion; due to the financing costs to construct a MAGLEV system, the cost comparison between MAGLEV and air flights must be done on the basis of the trip length and number of passengers/day.
For short distances, the advantage of MAGLEV versus motor cars is given by lower specific consumptions, by the reduction in road traffic (very congested in Italy) and by reduced travel times.

As regards a strictly technical point of view, the activities of the operating groups have been initially directed towards the comparative analysis of the functional and structural characteristics of the proposed high-speed MAGLEV systems (EMS and EDS systems) [3,4].
An integrated and coordinated set of calculation codes has also been defined and implemented; the codes are of different kind and characteristics (analytical and numerical methods, two- and three-dimensional methods, PC and workstation codes) and are to be utilized in the comparative analysis and calculation of the magnetic field and forces.
In particular, an analytical three-dimensional method has been proposed to calculate the magnetic field and the levitation, drag and propulsion forces acting in EDS-MAGLEV systems with superconducting coils for both levitation and LSM field; the method takes into account the most general coil arrangement [5,6].

At present the activity mainly concerns the definition of the design criteria and the optimization of the performance of the inverter-LSM drive, as well as the study of the dynamic stability of the system.

IV. Conclusions

For the time being there is no practical realization of MAGLEV systems in Italy.

A three-year research program on high-speed MAGLEV systems is under development, funded by the National Research Council in the frame of the Progetto Finalizzato *Trasporti 2*.

The scientific activity of the first months of the research mainly concerns the implementation of a set of calculation programs which will be utilized in the definition of the design criteria of the system and of its components.

The first results of the technical and economic analysis show that MAGLEV systems could be utilized in Italy for intercity travels, as an alternative to high-speed on-rail trains and to short-haul flights; they could also be utilized for shorter distances, to realize speedy connections between airports and downtown or between neighbouring towns.

A practical obstacle to the realization of intercity high-speed MAGLEV systems in Italy seems to be the difficult integration of such systems with the on-rail high-speed systems, particularly in view of a European railway network.

Moreover, the Italian political and industrial sensitiveness is probably not yet ready to deal with these new technologies. Nevertheless, the delayed starting of the reorganization of the Italian transport system as well as the development of MAGLEV researches in other industrialized countries may give the opportunity to partially correct the planning in the field of transportation: according to this, the possibility to realize, for some specific utilizations, innovative systems may be taken into account. In particular, the MAGLEV systems may be proposed as components of a balanced and integrated transport system, with the object of rationalizing the movement of population and increasing the high-technology know-how of the national transport industry.

References

[1] L.R.Johnson, D.M.Rote, J.R.Hull, H.T.Coffey, J.G.Daley and R.F.Giese, "MAGLEV Vehicles and Superconductor: Integration of High-Speed Ground Transportation into the Air Travel System", Argonne National Laboratory ANL/CNSV-67, April 1989.

[2] G.Martinelli and A.Morini, "Potential Markets and Economic Considerations for High-Speed MAGLEV Transportation", ETTIAS 1st School on European Training on *Technologies and Industrial Applications of Superconductivity*, World Scientific Publishing Co, Singapore 1992, pp. 489-503.

[3] G.Martinelli and A.Morini, "High Speed Transportation and Superconducting Technology", ETTIAS 1st School on European Training on *Technologies and Industrial Applications of Superconductivity*, World Scientific Publishing Co, Singapore 1992, pp. 463-488.

[4] A.Di Gerlando and M.Galasso, "Problematiche di alimentazione nei sistemi MAGLEV", National Workshop on *Electric Drives with Linear Motors*, Milan (Italy), April 13-14, 1992.

[5] M.Andriollo, G.Martinelli and A.Morini, "General expressions for forces acting in EDS-MAGLEV systems driven by linear synchronous motors", *Intern. Aegean Conf. on Electrical Machines and Power Electronics*, Kusadasi (Turkey), May 27-29, 1992.

[6] F.Albicini, M.Andriollo, G.Martinelli and A.Morini, "General expressions of propulsion force in EDS-MAGLEV systems with superconducting coils", *Applied Superconductivity Conference*, Chicago (USA), Aug. 23-28, 1992.

Status of Development and Future Prospects of DaeWoo Maglev System in Korea

In-Dae Chung
Rolling Stock R/D Center,
DaeWoo Heavy Industries LTD., Seoul, Korea

Prof. Dr. Dal-Ho Im
Hanyang University, Seoul, Korea

Chan-Il Park
Korea Institute of Machinery & Metals, Seoul, Korea

Abstract

This paper describes the development and technical details of DaeWoo Maglev System (DMV, DaeWoo Magnetically Levitated Vehicle). Some experimental results are also shown.

Introduction

DaeWoo Heavy Industries commenced a research and development program in 1989 with the objective of providing a new mass transportation system by means of magnetically levitated vehicles.

In October 1992 three full size maglev vehicles were successfully produced which passed all performance criteria measured on the test track in the DaeWoo plant.

Reliability trials are continuing to obtain life data and develop ride quality.

Initial trials were carried out on a one-third scale prototype model.

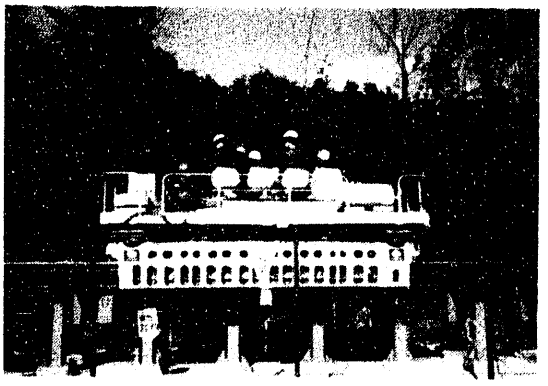

Fig. 1. First unit running test

History of research and development

Item		Period	Remarks
1) Design Team formation and data survey		Sept. 1989 to Sept. 1990	
2) Basic design with industry/university cooperation		Oct. 1990 to Nov. 1990	Han Yang Univ. (Prof. Dr. Dal-Ho Im)
3) Detail design		Dec. 1990 to May 1991	
4) Development of levitation controller with institutional partner		Apr. 1991 to July 1991	KIMM (General Manager, Chan-Il Park)
1st phase	5) Manufacture Prototype	July 1991 to Aug. 1991	13 seat capacity vehicle
	6) Prototype tests & trial running	Sept. 1991 to Nov. 1991	
2nd phase	7) Detail design	Dec. 1991 to Apr. 1992	40 seat capacity vehicle
	8) Manufacture full size vehicle	May 1992 to Sept. 1992	
	9) Tests & trial running	Oct. 1992	

Brief Specification of DaeWoo Maglev

Item		Specification
Typical Vehicle	Length x Width x Height	15m x 3m x 3m
	Weight (Gross)	18 ton
	Number of seats	40
Track	Length	100 m. straight-single mode
	Width	2.3 m
	Height	1.4 m
Speed	Designed max. speed	110 Km/h
	Operation speed on 100M test track	15 Km/h
Levitation	System	Electro-Magnetic Suspension
	Air gap	11 mm
	Power conversion method	Chopper & Controller
Propulsion	System	Single sided Linear Induction Motor
	Power conversion method	Variable Voltage Variable Frequency
Power Supply		DC 600 V

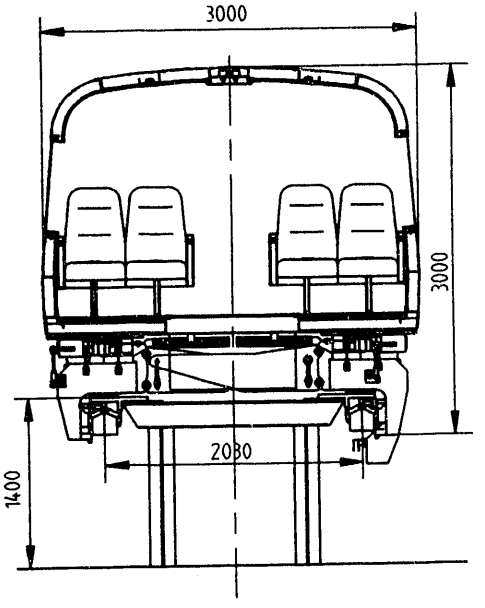

Fig. 3. Sectional View of the System

Guide Way

The height of the coulmn is 1.4m and the distance between columns is 1.2m. Two kinds of guide rail are used. one 4.8m long and the other 2.4m long. These are arranged in zig-zag formation.

The mass produced method would probably entail an extrusion. a welded structure was used for the development track.

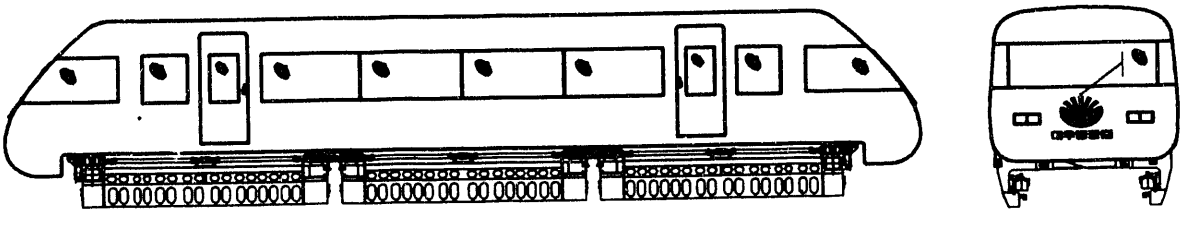

Fig. 2. DaeWoo Maglev vehicle

Fig. 4. Interior Design

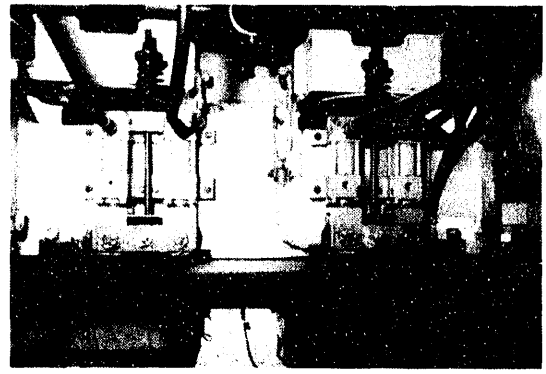

Fig. 6. Lifting Mechanism

Car body and Trim

The structure of the car body and end sections are mainly welded aluminium alloy covered with FRP.

Three large boxes under the cabin contain the electrical equipments (converter, inverters and choppers), hydraulic equipment and emergency back-up battery.

Interior trim is FRP-plated and there are two sliding doors on each side.

Maglev Module

Modules are aluminium alloy fabrications. The car body is supported by six modules each of which is equipped with four magnets, a linear induction motor, four hydraulic lifting mechanisms and emergency skids.

Anti-roll bars link pairs of modules to control ride quality

Secondary suspension is provided by four pneumatic dampers mounted on each module.

In emergency situations, rollers are hydraulically actuated to engage the rail and make the vehicle safe.

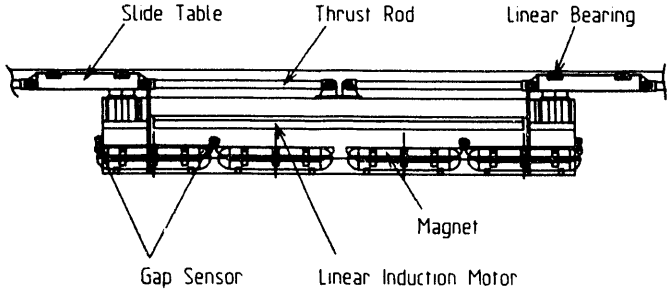

Fig. 5. Module Assembly

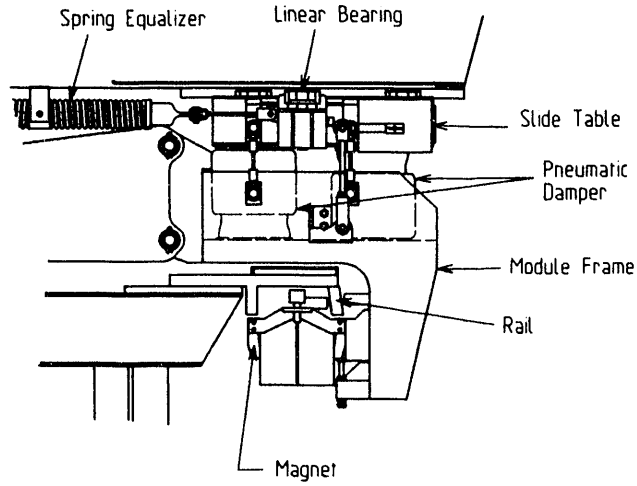

Fig. 7. Secondary Suspension

Secondary Suspension

Four pneumatic dampers per module provide support in the vertical direction.

Lateral movement of the car body is allowed for by the the slide table and linear bearing to which the dampers are connected.

Lateral movement of the module end of the damper is restricted by a spring equalizer.

The slide table is connected to the module frame by means of a thrust rod so enabling the transfer of the thrust force from the linear induction motor to the car body.

Levitation System

The levitation system comprises six modules. To control a module, four gap sensors, four accelerometers, two magnet drivers and two analog type levitation controllers are used.

A magnet driver controls two magnets each of which is laterally offset from the center line of the linear induction motor by 6 mm.

Each levitation controller unit uses four sensor signal inputs and provides two outputs.

Using four gap sensors per module, the vehicle can slide smoothly over the rail, even at the joint of two consecutive rails providing there is no difference in height.

A Programmable Logic Controller (PLC) actuates the levitation sequence in intervals of one second to reduce power consumption.

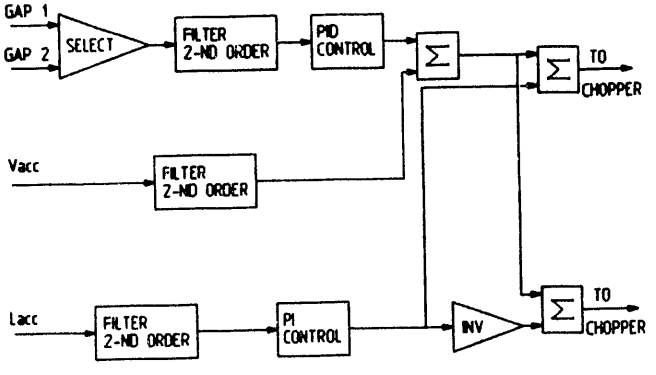

Fig. 8. Levitation Controller Block Diagram

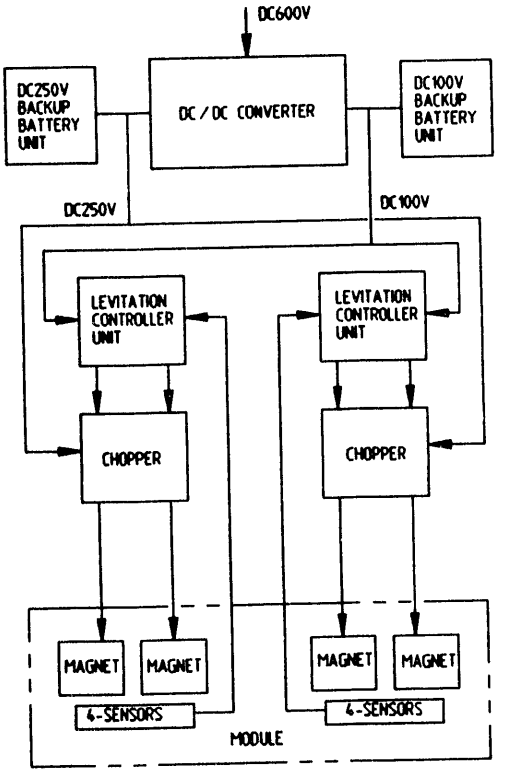

Fig. 9. Levitation System

Propulsion System

Two VVVF inverters using transistor modules as power switching devices are used to regulate six linear induction motors. Each inverter controls three linear induction motors which are connected in series.

The linear induction motor is designed for a maximum speed range of 110 Km/h. Due to the limit of track length the actual operating speed is 15 Km/h on the experimental track.

The propulsion power of the linear induction motor is 2KN/LIM. The nominal airgap between the primary and secondary side of the linear induction motor is 13 mm.

Driving sequence of DaeWoo Maglev System

The DMV can be driven in automatic or manual modes. Except for levitation and landing, which have to be operated manually, all other sequences are able to be carried out in eather mode.

Manual operation is as follows : On actuating the levitation switch, the P.L.C. sends "ready" signals to the choppers and receives "ready completion" in return ; if no response signal is received a warning signal is actuated. On receipt of the "ready completion" signals, triggering commands are passed to the levitation controller which allows the choppers to drive the levitation sequence.

On completion of levitation, the levitation controller signals the P.L.C. which starts the inverters. The driver can then move the vehicle by regulating the linear induction motors.

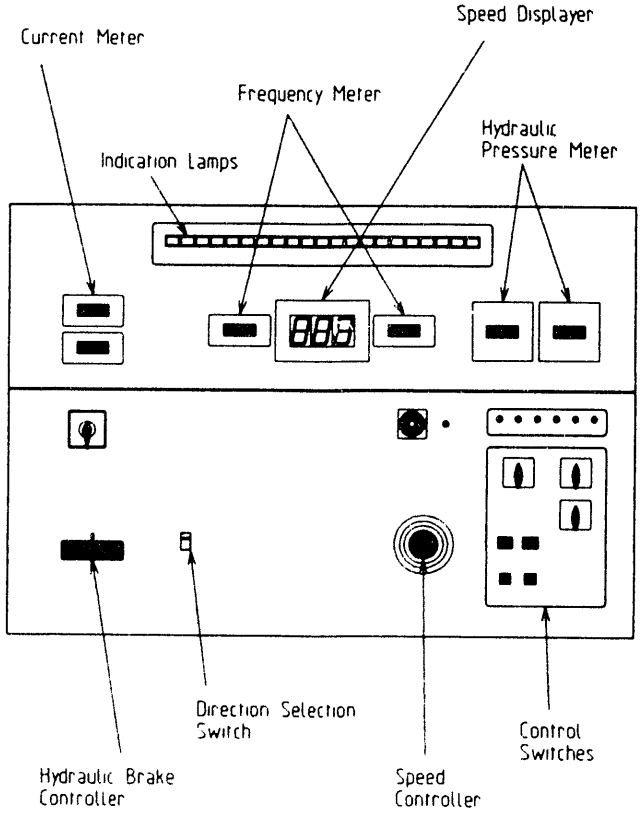

Fig. 10. The Arrangement of Dashboard

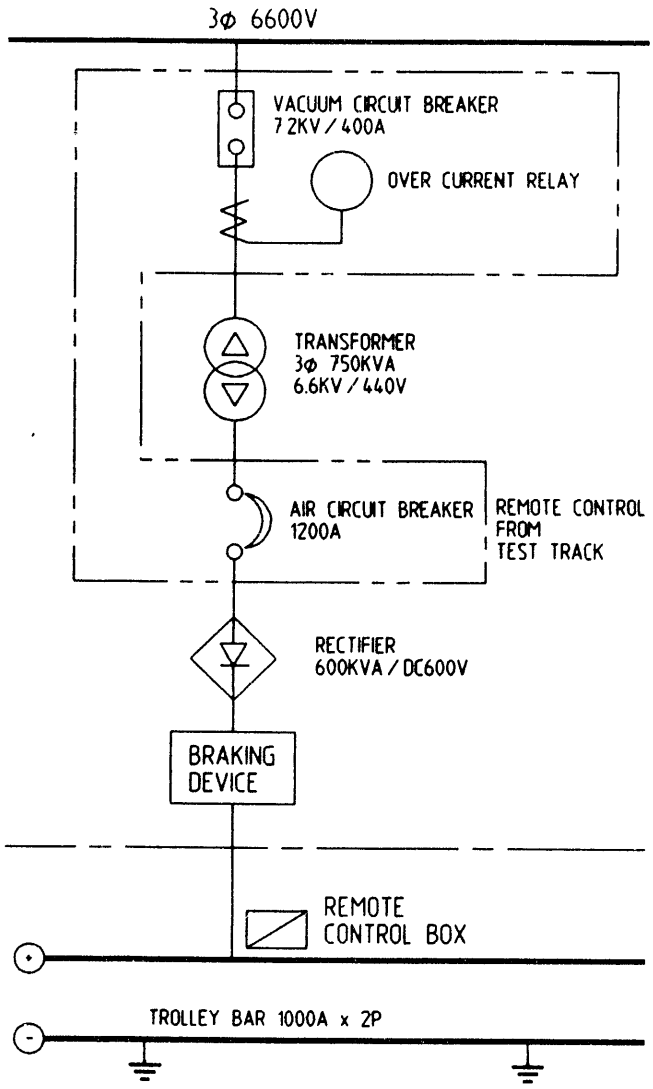

Fig. 11. Power System Schematic

Test results of magnet forces

The magnet of the DMV system has two windings which are connected in parallel. Serial connection was tried but parallel connection proved to provide better control.

The lifting and guiding forces of the magnet were simulated with a computer program, and after manufacturing a sample magnet, the forces were measured using a test bed.

Six load cells - four for lifting force, two for guiding force - were used to measure the forces of the magnet.

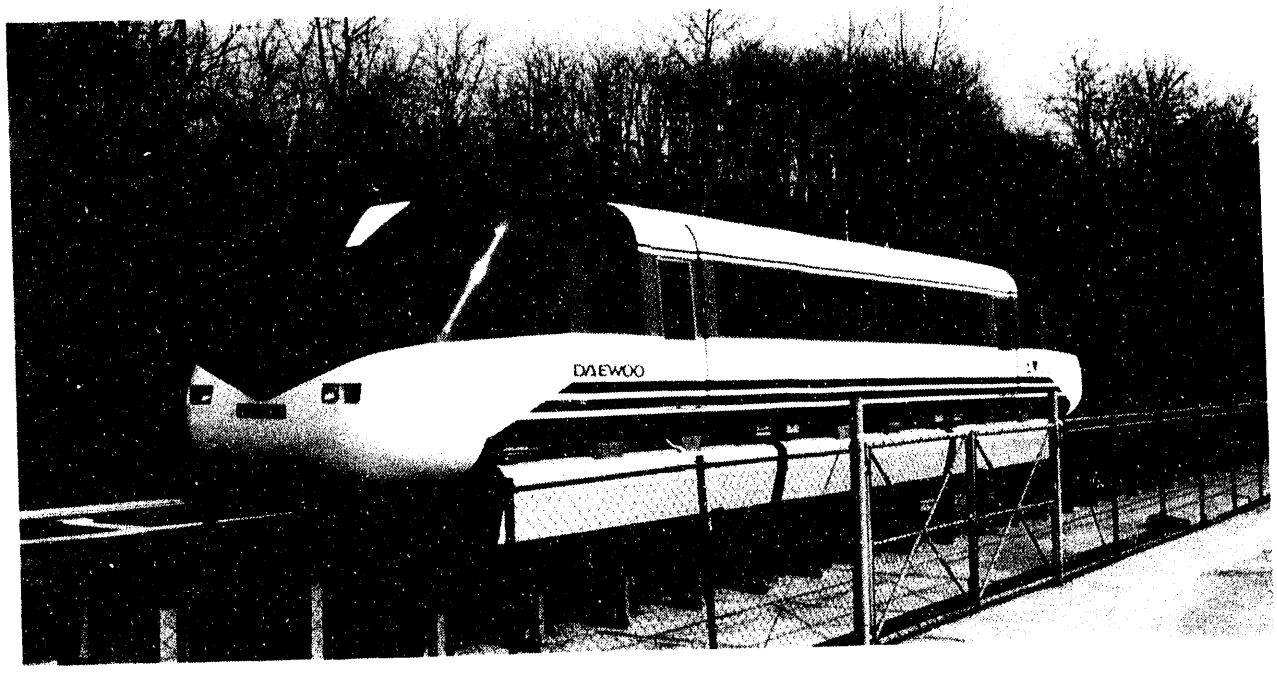

Fig. 12. Overview of the DaeWoo Maglev Vehicle

Fig. 13. denotes the simulated and the measured lifting forces of a magnet in several air gap conditions. The measured force of the magnet is about 80% of the simulated force.

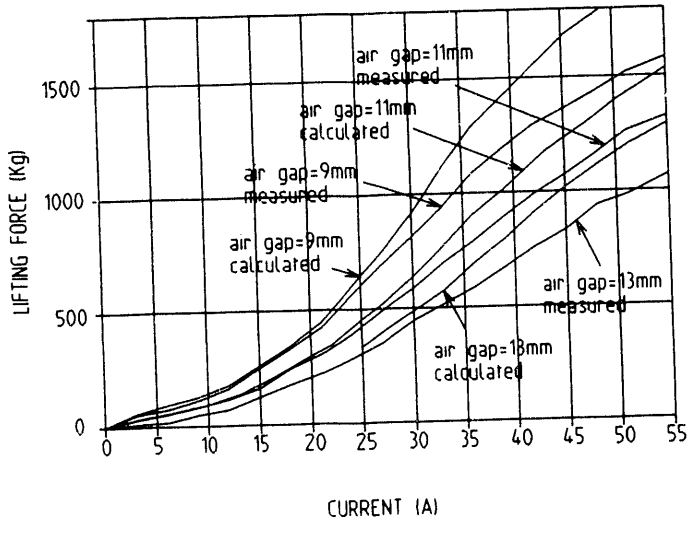

Fig. 13. Magnet Lifting Force

Future Plans

The DaeWoo Maglev system (DMV-'92) is designed for an intercity commuter service. such as between suburbs and city centers or between outlying airports and cities.

Reliability trials are under way and studies are being carried out on increased seat capacity to be provided by multi-units and/or lightweight vehicles.

Commencing in 1995 a 150 seat capacity vehicle will be manufactured as a two car system and this will be applied to a commercial operation.

New Structure Electro-magnetic Guideway for Maglev

Shunsuke Fujiwara, Kazuo Sawada
Railway Technical Research Institute

Hirotaka Natsuhara
Japan Railway Construction Public Corporation

Nobuhito Uchiyama
Central Japan Railway Company

Yukio Saitou
Hitachi Ltd.

Yoshitaka Kobayashi
Toshiba Corp.

Shigeya Oohama
Mitsubishi Electric Corp.

1. IN THE BEGINNING

Superconductive Maglev aims to be a super speed transportation system, that speed conventional rail system can never attain. One of the reason of superconductive Maglev's super speed ability is the large clearance between vehicle and the guideway, which is about 100 mm.

So, it is very important for superconductive Maglev to select the magnetic propulsion, levitation and guidance system.

In the process of superconductive Maglev development, We have changed the structure of guideway from inverted T type to U type. And in the U shaped guideway, we changed repulsive levitation to null-flux levitation. As for propulsion, we are now examining new structure. Recent tests in Miyazaki test track are directory related to the design of Yamanashi test line.

This paper describes the changes of electro-magnetic guideway in Miyazaki test track, the characteristics of the new structure which is now under examination and the prospect of the future including Yamanashi test line.

2. INVERTED T TYPE GUIDEWAY

Superconductive Maglev's test run started at 1977 on Miyazaki test track. At that time, guideway structure was inverted T type. Propulsion coils were installed on the both side walls of the center beam, and repulsive levitation coils were laid on track.

The peculiar point of this structure is the combined propulsion and guidance system which is attained by connecting the corresponding propulsion coils of both sides of center beam using "null flux cable." If vehicle shifts from the center line of the guideway, interlink fluxes of both side coils become different. So, currents are induced between the two coils, and which generates the guidance force.

To get a sufficient guidance force, the difference of interlink fluxes of both side coils must be enough large for the vehicle's displacement from the center of guideway. However in inverted T system, not only the distance between the coils of both sides but that between the superconducting magnets of both sides are also small. So inevitably the difference of interlink fluxes are few for certain displacement of the vehicle, if

the superconducting magnets of both sides are excited in the same polarity. Therefore both side magnets must be excited in opposite polarity. (Fig. 1)

As both side coils were fed from one feeder, and the corresponding SCM's polarities are opposite, two coils of both side must have opposite winding to generate the propulsion force of the same direction. That is "open" type and "cross" type.

3. U SHAPED GUIDEWAY

We adopted the inverted T type structure in order to minimize the air drag force, and to act the propulsion or guidance force near the center of gravity of the vehicle. This allowed high acceleration-deceleration or high speed run, so test vehicle recorded 517 km/h in spite of short test track length of 7 km. However, we had conceived that inverted T type to be inferior to U type for practical use. Because, the cross section area of commercial vehicle in inverted T type is larger than that in U type. As there will be many and long tunnel sections in Japanese revenue service line, it is very important for the cross section area of vehicle to be small to reduce the construction cost.

So we decided to change the guideway to U shape after completing the inverted T type examination. We used the existing propulsion and levitation coils again for U type guideway's ground coils to save the conversion cost.

In U type, the distance between coils of both side are large, so the polarity of SCM doesn't have large effect upon the guidance characteristics. But as the propulsion coils of both side walls were different i.e. "open type" and "cross type", SCMs of both side had to have opposite polarity. (Fig. 2)

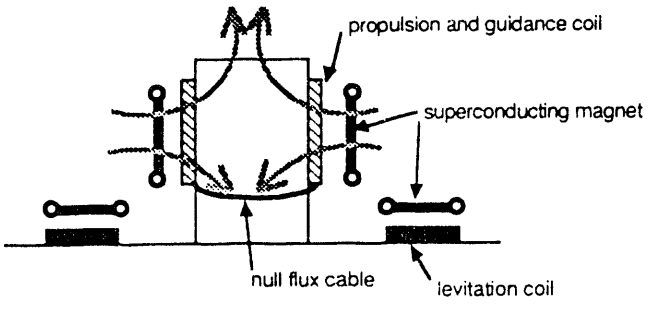

Fig. 1. Inverted T type guideway

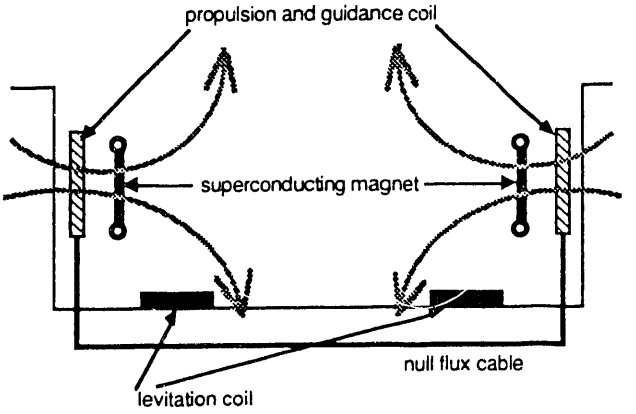

Fig. 2. U type guideway

With opposite polarity excitation, the magnetic flux is vertical on the center of floor, so the flux density of the cabin is rather large up to 200 gauss in Miyazaki test vehicle.

4. NULL FLUX LEVITATION SYSTEM

Null flux levitation and guidance system was invented by RTRI in 1988. In this system, "8" figured coils are installed on the side wall, and corresponding coils of both side walls are connected by null flux cable to generate a guidance force.

Compared with repulsive levitation, the characteristics are as follows,

1) Lower magnetic drag force: It is almost zero during the wheel running, on the contrary, there is a drag peak at low speed range in repulsive levitation system.

2) Larger levitation force.

3) Harder magnetic suspension: It means the vehicle is less sensitive to load weight, and means that more regularity of the guideway is required to gain the same ride quality.

4) Easier installation: All of the ground coils are installed on the side walls, so it is easier to get the guideway regularity than repulsive system.

5) Lower voltage guidance system: Levitation coil can function as guidance one. So the voltage of guidance

system is lower than that of combined propulsion and guidance system.

6) As for levitation coils and installation equipment, it is important to examine the strength, because the direction of the levitation force is different from the repulsive system, and the difference is estimated to be harder for them.

After comparing above-mentioned merits and demerits, we have decided to choose the null flux levitation system. We have appreciated especially the following two points, lower magnetic drag forces and larger levitation force.

Since 1989, we have remodeled Miyazaki test track into null-flux levitation successively. Recently, 1.5 km length track have completed and null-flux levitation section is now about 2.0 km.

So far there haven't been observed large difference between null-flux levitation and repulsive levitation as for ride quality. On the contrary, we can observe the clear difference of drag force between the two systems. (Fig. 3) We will check the drag force characteristics of null-flux levitation system at high speed range by new test vehicle MLU002N.

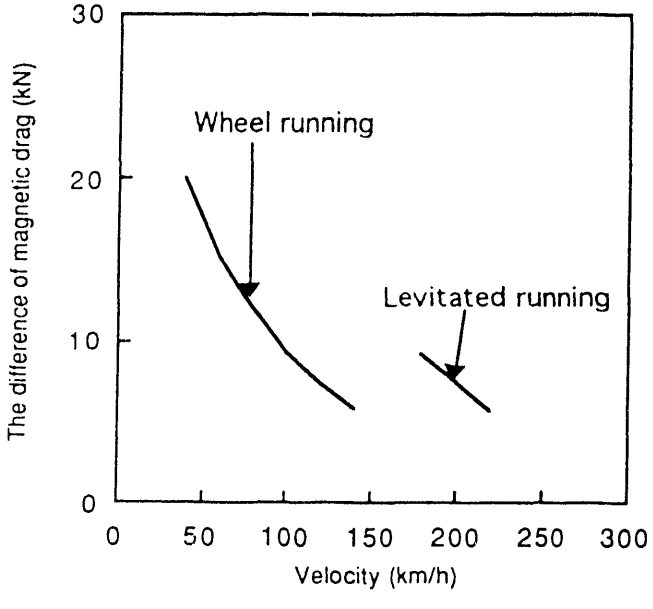

Fig. 3. The difference of magnetic drag

5. DOUBLE LAYERED PROPULSION COIL

At Miyazaki test track, propulsion coils are single layered and are installed every 120° electrical angle on the both side walls. This type is simple, but it became evident that the large harmonic magnetic field produced by single layered propulsion coils induces considerable temperature rise inside the superconducting magnets.

It is no matter for short run time operation like Miyazaki test vehicle, but as for long revenue service line, the operation will be difficult if the heat generated inside the superconducting magnet is larger than the capacity of on-board refrigerators.

So, we have tried to improve the magnetic fields produced by propulsion coils, by using bigger coils and double layered installation. One coil covers 180° electric angle, and coils are installed every 120° pitch along the side wall. The composite magnetic field produced by those double layered coils is as Fig. 4. The harmful change of magnetic field is reduced remarkably. As the distance from the superconducting magnet is different between the front propulsion coil and the back one, it is necessary to adjust the windings of coils between them.

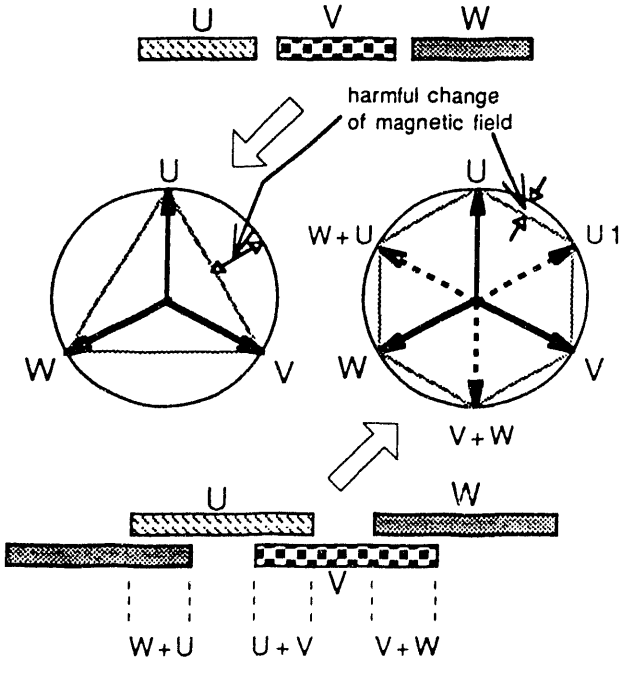

Fig.4 Double layered installation

So far propulsion coils at Miyazaki test track have been made of SMC molding, double layered propulsion coils are made of epoxy resin molding, which is applicable to future system's high voltage coils.

About 1 km section has been remodeled to double layered propulsion coils at Miyazaki test track, and we are now examining the characteristics of it using MLU002N.

6. Beam or panel system

In the new structure of guideway, triple layered coils are installed along the both side walls, that are null-flux levitation coil and double layered propulsion coils. It is fairly difficult to install the coils exactly in tunnel or on bridge. So we are examining another way, that is to make concrete beam or panel with high precision and install coils to them successively in a plant, then bring them to the point they should be installed. We have installed 6 beams and 2 panels on trial at Miyazaki test track, and had good result.

7. Electro-magnetic guideway of Yamanashi test line

The electro-magnetic guideway of Yamanashi test line is constructed based on the recent development in Miyazaki test track. That are double layered propulsion coils and null-flux combined levitation and guidance coil, and beam or panel system. But according to the recent advance on superconducting magnet, we will try the more simplified propulsion coil system partly.

Considering the magnetic field in the cabin, the polarity of superconducting magnet of both side is changed to same. Therefore propulsion coils of both side walls are also same.

As the pole pitch changes from Miyazaki system, basic dimension of coil changes correspondingly. According to the power up of LSM system, the voltage level of propulsion coil increases to 22 kV or 11 kV.

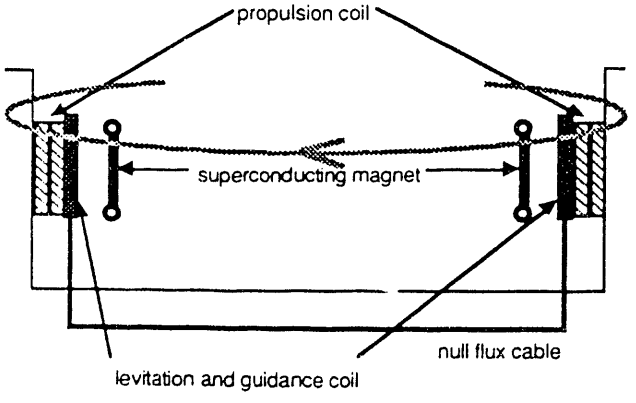

Fig. 5. Null-flux levitation + double layered propulsion system

8. Conclusions

We have showed the recent development of electromagnetic guideway in Miyazaki test track. These are all adopted in Yamanashi test line. This structure is considered to be suitable for rather large capacity LSM system, in which long trains will be operated frequently. Besides this, RTRI is developing various type electromagnetic guideways. As it is estimated that electromagnetic guideway cost will occupy the large proportion of Maglev system construction cost, to choose the most suitable guideway structure considering the characteristics of proper revenue service system is very important.

References

[1] J. R. Powell and G. R. Danby.: "Magnetically Suspended Trains: The applications of Superconductor to High Speed Transport." Cryogenics and Industrial Gases, 1669, p. 19

[2] S. Fujiwara.: "Characteristics of EDS Magnetic Levitation Having Ground Coils for Levitation Arranged on the Side Wall." Trans. IEEJ. Vol. 108-D, No. 5, May, 1988

[3] H. Weh.: "Supre-Acht-Differenzflussverfahren, eine neue Variante der elektrodynamischen Schwebetechnik" Deutche Patenttamt, 1974

[4] S. Fujiwara and T. Fujimoto.: "Characteristics of the Combined Levitation and Guidance System Using Ground Coils on the Side Wall of the Guideway." International Conference on Maglev '89, July 1989 Yokohama

Electrodynamic Forces of the Cross-Connected Figure-Eight Null-Flux Coil Suspension System

J.L. He, D.M. Rote, and H.T. Coffey

Center for Transportation Research
Energy Systems Division, Argonne National Laboratory
9700 S. Cass Ave., Argonne, IL 60439, U.S.A.

Abstract **- This paper analyzes the cross-connected figure-eight null-flux coil suspension system for maglev vehicles on the basis of dynamic circuit theory. The equivalent circuits and general magnetic force expressions for the system are developed. Simple analytical formulas for the magnetic force partitions on the basis of harmonic approximation are presented, and numerical results are also included.**

I. INTRODUCTION

The cross-connected null-flux coil suspension system has been under development in Japan for several years [1-3]. The system consists of two arrays of figure-eight-shaped null-flux coils mounted on the side walls of the guideway, each coil on the left side wall being cross-connected with another one on the right side wall to form a combined levitation and guidance system. Both the null-flux levitation and the null-flux guidance forces are generated from the interaction between two rows of superconducting coils, or superconducting magnets (SCMs), aboard the vehicle and two rows of null-flux coils on the guideway. The concept has become very popular in both Japan and the United States because of its several unique features, including high lift-to-drag and guidance-to-drag ratios, high suspension stiffness, and very low magnetic drag at low speed.

This paper discusses the electrodynamic performance of the cross-connected null-flux coil suspension system on the basis of the dynamic circuit model. The equivalent circuits of the system are presented, and the general expressions for the determination of magnetic forces acting on the SCMs and the current induced in the null-flux coils are derived. Closed-form formulas for the magnetic forces are derived using a harmonic approximation. These formulas are valuable for the design of maglev systems and for vehicle dynamic studies. The paper is organized into several sections: (1) introduction, (2) the equivalent circuit model, (3) harmonic circuit model, (4) numerical example and discussion, and (5) conclusion.

II. THE EQUIVALENT CIRCUIT MODEL

A. The Equivalent Circuit for a SCM Interacting with a Null-Flux Coil

The simplest model for a figure-eight null-flux coil interacting with a SCM can be described by an equivalent circuit containing one mesh with two branches, as shown in Fig. 1. Each branch having a resistance R and an inductance L represents a single loop of the null-flux coil. The coupling between the upper and lower loops is described by the mutual inductance M_{12}, and the couplings between the moving SCM and the upper and lower loops of the null-flux coil are modeled by two time- and space-dependent voltage sources e_1 and e_2, respectively. In Fig. 1, I_1 and I_2 stand for the currents flowing in the upper and lower loops, and i ($=I_1=-I_2$) is the current circulating in the null-flux coil.

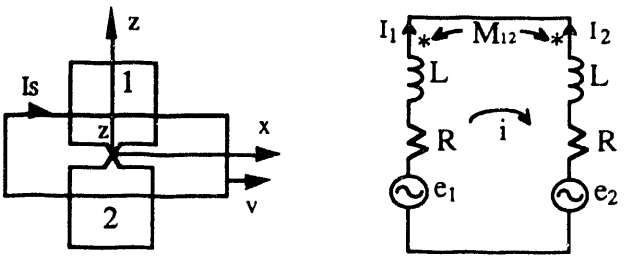

Fig. 1 Equivalent Circuit of a Single SCM Interacting with a Null-Flux Coil

Letting I_S and v be the current and speed of the SCM, and M_{s1} and M_{s2} be the mutual inductances between the SCM and the upper and lower loops of the null-flux coil, respectively, one can express e_1 and e_2 as:

$$e_1 = -I_s v \frac{\partial M_{s1}(x,y,z)}{\partial x} \tag{1}$$

$$e_2 = -I_s v \frac{\partial M_{s2}(x,y,z)}{\partial x} \tag{2}$$

The voltage equation for the system is:

$$2Ri + 2(L-M_{12})\frac{di}{dt} = e_1 - e_2 \tag{3}$$

The three components of time-dependent magnetic forces f_x, f_y, f_z existing between the moving SCM and the null-flux coil are

$$f_x = I_s I_1 \frac{\partial M_{s1}}{\partial x} + I_s I_2 \frac{\partial M_{s2}}{\partial x} = I_s i \left(\frac{\partial M_{s1}}{\partial x} - \frac{\partial M_{s2}}{\partial x} \right) \tag{4}$$

$$f_y = I_s I_1 \frac{\partial M_{s1}}{\partial y} + I_s I_2 \frac{\partial M_{s2}}{\partial y} = I_s i \left(\frac{\partial M_{s1}}{\partial y} - \frac{\partial M_{s2}}{\partial y} \right) \quad (5)$$

$$f_z = I_s I_1 \frac{\partial M_{s1}}{\partial z} + I_s I_2 \frac{\partial M_{s2}}{\partial z} = I_s i \left(\frac{\partial M_{s1}}{\partial z} - \frac{\partial M_{s2}}{\partial z} \right) \quad (6)$$

(1) to (6) can only be solved step by step numerically because M_{si} (i=1,2) is time- and space-dependent. The electrodynamic performance of the system is then predicted on the basis of the system solution. It is seen from (3) to (6) that the three components of magnetic force are proportional to the product of the circulating current i, SCM current I_S, and the difference of the mutual inductance derivatives between the SCM and upper and lower loops. Clearly, they vanish as the SCM moves to the equilibrium position (z=0).

B. The Equivalent Circuit Model for the Cross-Connected Null-Flux Coil Suspension

A pair of SCMs aboard the vehicle interacting with figure-eight null-flux coils that are cross-connected and mounted on the two sides of the guideway shown in Fig. 2 can be modeled by the equivalent circuit shown in Fig. 3. Similarly, each branch having a resistance R, an inductance L, and a voltage source e represents a single loop of the null-flux coil. The mutual inductance M_{12} between loops 1 and 2 equals the mutual inductance M_{34} between loops 3 and 4. I_i (i=1,4) and

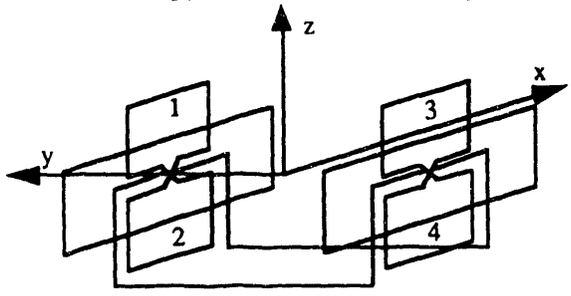

Fig. 2 Cross-Connected Figure-Eight Null-Flux Coils for Maglev Levitation and Guidance

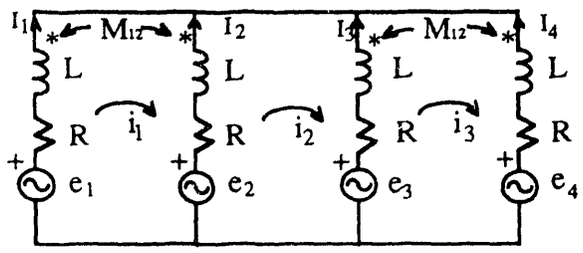

Fig. 3 Equivalent Circuit for the Cross-Connected Null-Flux Coil Suspension System

e_i (i=1,4) are the currents flowing in the loop, and the voltages induced in the loop, respectively. The mesh currents flowing in the circuit are i_1, i_2, and i_3. In particular, i_2 represents the current flowing in the cross-connecting cable across the guideway, and it contributes to the null-flux guidance. In Fig. 3, the resistance and inductance of the cross-connected cables are neglected. Similar to (1) and (2), the voltages induced in the loops 3 and 4 can be expressed in terms of the mutual inductances M_{s3} and M_{s4} between the SCM and loops 3 and 4, respectively:

$$e_3 = -I_s v \frac{\partial M_{s3}}{\partial x} \quad (7)$$

$$e_4 = -I_s v \frac{\partial M_{s4}}{\partial x} \quad (8)$$

Figure 3 can be simplified by eliminating the mutual inductances, M_{12}, between the upper and lower loops. Using Kirchhoff's voltage law, one can write voltage equations in terms of mesh currents for Fig. 3:

$$2Ri_1 + 2(L-M_{12})\frac{di_1}{dt} - Ri_2 - (L-M_{12})\frac{di_2}{dt} = e_1 - e_2 \quad (9)$$

$$-Ri_1 - (L-M_{12})\frac{di_1}{dt} + 2Ri_2 + 2L\frac{di_2}{dt} - Ri_3 - (L-M_{12})\frac{di_3}{dt} = e_2 - e_3 \quad (10)$$

$$-Ri_2 - (L-M_{12})\frac{di_2}{dt} + 2Ri_3 + 2(L-M_{12})\frac{di_3}{dt} = e_3 - e_4 \quad (11)$$

After solving mesh currents from (9) to (11), one can determine the three components of magnetic forces acting on the moving SCM:

$$f_x = \sum_{j=1}^{4} I_s I_j \frac{\partial M_{sj}}{\partial x} = I_s \left\{ i_1 \left(\frac{\partial M_{s1}}{\partial x} - \frac{\partial M_{s2}}{\partial x} \right) + i_2 \left(\frac{\partial M_{s2}}{\partial x} - \frac{\partial M_{s3}}{\partial x} \right) + i_3 \left(\frac{\partial M_{s3}}{\partial x} - \frac{\partial M_{s4}}{\partial x} \right) \right\} \quad (12)$$

$$f_y = \sum_{j=1}^{4} I_s I_j \frac{\partial M_{sj}}{\partial y} = I_s \left\{ i_1 \left(\frac{\partial M_{s1}}{\partial y_1} - \frac{\partial M_{s2}}{\partial y_1} \right) + i_2 \left(\frac{\partial M_{s2}}{\partial y_1} - \frac{\partial M_{s3}}{\partial y_2} \right) + i_3 \left(\frac{\partial M_{s3}}{\partial y_2} - \frac{\partial M_{s4}}{\partial y_2} \right) \right\} \quad (13)$$

$$f_z = \sum_{j=1}^{4} I_s I_j \frac{\partial M_{sj}}{\partial z} = I_s \left\{ i_1 \left(\frac{\partial M_{s1}}{\partial z} - \frac{\partial M_{s2}}{\partial z} \right) + i_2 \left(\frac{\partial M_{s2}}{\partial z} - \frac{\partial M_{s3}}{\partial z} \right) + i_3 \left(\frac{\partial M_{s3}}{\partial z} - \frac{\partial M_{s4}}{\partial z} \right) \right\} \quad (14)$$

where the relations between the mesh and branch currents, $I_1=i_1$, $I_2=i_3-i_1$, $I_3=i_3-i_2$, and $I_4=-i_3$, were used. Two different

lateral coordinates needed for the two lateral air gaps are specified by y_1 and y_2 in (13). Comparing (12) to (14) with (4) to (6), one notes that the three components of magnetic force in the cross-connected null-flux coil suspension system depend upon the current i_2 flowing between the two figure-eight null-flux coils. At the lateral equilibrium position, no current flows between the two figure-eight null-flux coils. In this case, the cross-connected null-flux coil suspension system becomes two independent conventional null-flux coil suspension systems. The guidance force of the cross-connected null-flux coil suspension system consists of two parts: one due to cross-connection, which follows the null-flux suspension principle, and the other due to the individual null-flux coils and the air gap difference. The latter can be determined from (4) to (6). To obtain the guidance force resulting from the cross-connection, one can first simplify Fig. 3 by eliminating the mutual inductances between the upper and lower loops, and then find a Thevenin equivalent circuit by eliminating meshes 1 and 3, as shown in Fig. 4.

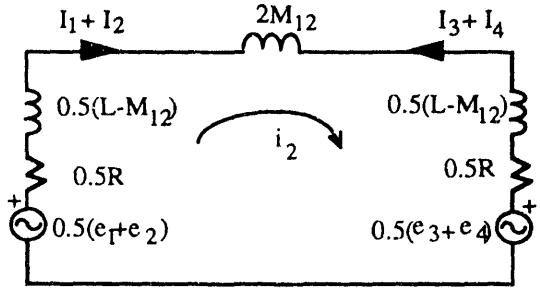

Fig. 4 Simplified Equivalent Circuit for Determining Null-Flux Guidance Force

Figure 4 shows that the voltage e_1 has the same polarity as e_2, and e_3 has the same polarity as e_4. The null-flux guidance force will be generated when the condition $e_1+e_2 \neq e_3+e_4$, or $I_1+I_2 \neq I_3+I_4$, is true. The current flowing in the cross-connecting cable between the two null-flux coils can be determined from Fig. 4 in terms of the voltage equation:

$$Ri_2 + (L-M)\frac{di_2}{dt} = \frac{1}{2}[(e_1 + e_2) - (e_3 + e_4)] \qquad (15)$$

The cross-connection part of the null-flux guidance force is:

$$f_y = \frac{1}{2} i_2 I_s\left[\left(\frac{\partial M_{s1}}{\partial y_1} + \frac{\partial M_{s2}}{\partial y_1}\right) - \left(\frac{\partial M_{s3}}{\partial y_2} + \frac{\partial M_{s4}}{\partial y_2}\right)\right] \qquad (16)$$

Because the null-flux suspension system usually operates near vertical equilibrium, it is a good approximation to assume that the derivatives of the mutual inductance M_{s1} with respect to y_1 is equal to that of M_{s2} with respect to y_1. Similarly, one may assume that the derivatives of mutual inductances M_{s3} and M_{s4} with respect to y_2 are also equal. Thus, (16) is simplified:

$$f_y = i_2 I_s\left[\frac{\partial M_{s1}}{\partial y_1} - \frac{\partial M_{s3}}{\partial y_2}\right] \qquad (17)$$

It should be noted that (16) and (17) represent only the guidance force resulting from the current flowing in the cross-connecting cable (i_2), while (13) gives a total guidance force.

Equations (9) to (15) can be numerically solved to obtain the transient currents induced in the null-flux coils and the time-dependent magnetic forces acting on the SCMs using an approach similar to that discussed previously [4-5].

III. HARMONIC APPROXIMATION

Exact solutions of (9) to (14) require a numerical approach because of the time- and space-dependence of the mutual inductances between the moving SCMs and the null-flux coils. It is difficult to gain physical insight and to conduct vehicle dynamic stability studies with numerical solutions. Thus, (9) to (14) are further developed on the basis of a harmonic approximation to obtain simplified analytical expressions that are very useful for preliminary system design. Because a maglev vehicle usually consists of several groups of SCMs, each of which has several SCMs arranged in one row with alternating polarities, the flux linkage through the null-flux coils varies its direction as the SCM row moves forward. It is a good approximation to express the mutual inductance between a group of SCMs and a null-flux coil by a harmonic function whose fundamental wave is:

$$M_{sj} = M_{pj}(y,z)\cos\frac{\pi}{\tau}x = M_{pj}(y,z)\cos\omega t \qquad j=1,4 \qquad (18)$$

where M_{pj} is the peak value of the mutual inductance between one SCM and the jth loop of the null-flux coil. It depends upon only displacements in the vertical (z-axis) and lateral (y-axis) directions. τ is the pole pitch of the SCMs, and $\omega=\pi v/\tau$ is the radian frequency. It should be noted that (18) is only an approximation, and high-order harmonics may be added to (18) for a higher accuracy.

Substituting (1), (2), (7), (8), and (18) into (9) to (11), one can solve for the sinusoidal current i_2 flowing in the cross-connecting cable:

$$i_2 = \frac{(E_1 + E_2) - (E_3 + E_4)}{2\sqrt{R^2 + \omega^2(L + M_{12})^2}}\sin(\omega t - \phi_2) \qquad (19)$$

where

$$\phi_2 = \tan^{-1}\frac{\omega t(L+M_{12})}{R} \qquad (20)$$

and

$$E_j = \omega I_s M_{pj} \qquad (21)$$

It is seen from (19) that i_2 depends only upon the lateral displacement. The current will flow through the cross-connecting cable as long as (E_1+E_2) is not equal to (E_3+E_4),

or there exists a lateral displacement. Mesh currents i_1 and i_2 are found to be

$$i_1 = \frac{E_1 - E_2}{2\sqrt{R^2 + \omega^2(L-M_{12})^2}} \sin(\omega t - \phi_1) + \frac{1}{2} i_2 \tag{22}$$

and

$$i_3 = \frac{E_3 - E_4}{2\sqrt{R^2 + \omega^2(L-M_{12})^2}} \sin(\omega t - \phi_1) + \frac{1}{2} i_2 \tag{23}$$

where

$$\phi_1 = \tan^{-1} \frac{\omega(L-M_{12})}{R} \tag{24}$$

Equations (22) and (23) show that the currents flowing through the figure-eight null-flux coil 1 and coil 2 consist of two parts: the first part resulting from the vertical displacement, and the second part due to the lateral displacement. At a vertical equilibrium position ($E_1=E_2$ and $E_3=E_4$), both i_1 and i_2 equal half of i_2. In this case, there still exists a null-flux guidance force as long as i_2 exists. This force does not exist in a conventional side wall null-flux suspension system, in which all magnetic forces vanish at vertical equilibrium even though there exists a lateral shift, while in a cross-connected null-flux coil system, magnetic forces disappear only at both lateral and vertical equilibrium positions.

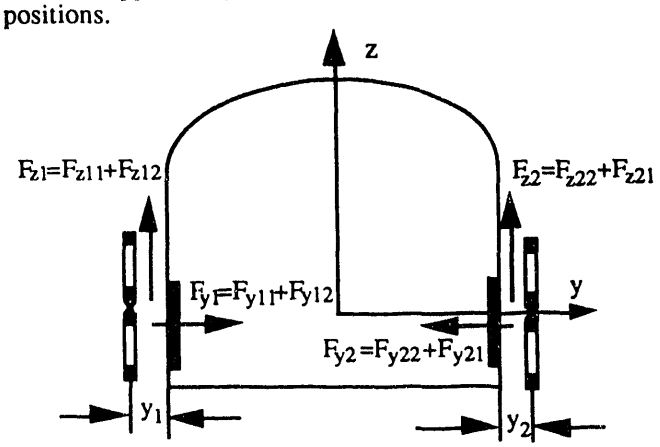

Fig 5 Cross-Sectional View of the Side-Wall Null-Flux Suspension System

Substituting (19), (22) and (23) into (12) to (14) and taking the integral with respect to time over a period, one can determine the time-average forces in terms of dynamic circuit parameters. Those forces can be grouped according to physical insight and the positions on which the forces act, as shown in Fig. 5. The time-average null-flux levitation force, F_z, between a pair of SCMs and a pair of cross-connected figure-eight null-flux coils is:

$$F_z = F_{z11} + F_{z12} + F_{z22} + F_{z21} \tag{25}$$

where F_{z11} and F_{z22} are the null-flux levitation forces from the interaction between the SCMs and the left- and right-hand side null-flux coils, respectively, when two coils are not cross-connected. They are given by:

$$F_{z11} = -\frac{I_s^2}{4} \frac{v^2}{v^2 + v_{c1}^2} \frac{M_{p1} - M_{p2}}{L-M_{12}} \left(\frac{\partial M_{p1}}{\partial z} - \frac{\partial M_{p2}}{\partial z} \right) \tag{26}$$

$$F_{z22} = -\frac{I_s^2}{4} \frac{v^2}{v^2 + v_{c1}^2} \frac{M_{p3} - M_{p4}}{L-M_{12}} \left(\frac{\partial M_{p3}}{\partial z} - \frac{\partial M_{p4}}{\partial z} \right) \tag{27}$$

and F_{z12} and F_{z21} are the additional levitation forces produced by the left- and right-hand side figure-eight null-flux coils resulting from the cross-connection:

$$F_{z12} = -\frac{I_s^2}{8} \frac{v^2}{v^2 + v_{c2}^2} \frac{(M_{p1} + M_{p2}) - (M_{p3} + M_{p4})}{L+M_{12}} \times \left(\frac{\partial M_{p1}}{\partial z} + \frac{\partial M_{p2}}{\partial z} \right) \tag{28}$$

$$F_{z21} = \frac{I_s^2}{8} \frac{v^2}{v^2 + v_{c2}^2} \frac{(M_{p1} + M_{p2}) - (M_{p3} + M_{p4})}{L+M_{12}} \times \left(\frac{\partial M_{p3}}{\partial z} + \frac{\partial M_{p4}}{\partial z} \right) \tag{29}$$

It should be noted that F_{z11} and F_{z22} are the dominant terms, and F_{z21} and F_{z12} are very small because the derivatives of the mutual inductances M_{s1} and M_{s2} with respect to vertical displacements have different signs, and so do those of M_{s3} and M_{s4}. The last terms of (28) and (29) are small. Similarly, one can group the magnetic drag:

$$F_x = F_{x11} + F_{x12} + F_{x22} + F_{x21} \tag{30}$$

where F_{x11} and F_{x22} are the magnetic drag produced by the left- and right-hand side figure-eight null-flux coils when they are not cross-connected:

$$F_{x11} = -\frac{I_s^2}{4} \frac{vv_{c1}}{v^2 + v_{c1}^2} \frac{\pi/\tau (M_{p1} - M_{p2})^2}{L-M_{12}} \tag{31}$$

$$F_{x22} = -\frac{I_s^2}{4} \frac{vv_{c1}}{v^2 + v_{c1}^2} \frac{\pi/\tau (M_{p3} - M_{p4})^2}{L-M_{12}} \tag{32}$$

and F_{x12} ($=F_{x21}$) is the additional drag resulting from the cross-connection:

$$F_{x12} = -\frac{I_s^2}{16}\frac{vv_{c2}}{v^2+v_{c2}^2}\frac{\pi/\tau\left[(M_{p1}+M_{p2})-(M_{p3}+M_{p4})\right]^2}{L+M_{12}} \quad (33)$$

Notice that since $F_{x12}=F_{x21}$, there is no torque in the yaw direction caused by this drag force component. The guidance force can also be grouped as:

$$F_y = F_{y11} + F_{y12} + F_{y22} + F_{y21} \quad (34)$$

where F_{y11} and F_{y22} are the guidance forces produced by the figure-eight null-flux coils on the left- and right-hand sides, respectively, when the two coils are not cross-connected:

$$F_{y11} = -\frac{I_s^2}{4}\frac{v^2}{v^2+v_{c1}^2}\frac{(M_{p1}-M_{p2})}{L-M_{12}}\left(\frac{\partial M_{p1}}{\partial y_1}-\frac{\partial M_{p2}}{\partial y_1}\right) \quad (35)$$

$$F_{y22} = -\frac{I_s^2}{4}\frac{v^2}{v^2+v_{c1}^2}\frac{(M_{p3}-M_{p4})}{L-M_{12}}\left(\frac{\partial M_{p3}}{\partial y_2}-\frac{\partial M_{p4}}{\partial y_2}\right) \quad (36)$$

F_{y12} and F_{y21} are the guidance forces resulting from the cross-connection; they are the major guidance forces, depending upon the lateral displacement and following the principle of null flux suspension. F_{y12} and F_{y21} are given by

$$F_{y12} = -\frac{I_s^2}{8}\frac{v^2}{v^2+v_{c2}^2}\frac{(M_{p1}+M_{p2}-M_{p3}-M_{p4})}{L+M_{12}} \times\left(\frac{\partial M_{p1}}{\partial y_1}+\frac{\partial M_{p2}}{\partial y_1}\right) \quad (37)$$

$$F_{y21} = \frac{I_s^2}{8}\frac{v^2}{v^2+v_{c2}^2}\frac{(M_{p1}+M_{p2}-M_{p3}-M_{p4})}{L+M_{12}} \times\left(\frac{\partial M_{p3}}{\partial y_1}+\frac{\partial M_{p4}}{\partial y_1}\right) \quad (38)$$

In (26) to (38), v_{c1} and v_{c2} are the characteristic speeds, which are defined as the speeds at which the magnetic drags F_{x11}, F_{x22}, and F_{x12}, F_{x21} approach their peaks, respectively. Due to cross-connection, there exist two major drag forces: one associated with the vertical displacement and characterized by v_{c1}, and another associated with lateral displacement and characterized by v_{c2}. They are

$$v_{c1} = \frac{\tau R}{\pi(L-M_{12})} \quad (39)$$

and

$$v_{c2} = \frac{\tau R}{\pi(L+M_{12})} \quad (40)$$

Up to now all magnetic forces for the cross-connected null-flux suspension system have been derived in terms of the dynamic circuit parameters on the basis of harmonic approximation. Clearly, these relations are straightforward and easy to use, because they are not a function of time. One needs only to determine the mutual inductances between one SCM and one loop of the null-flux coil at a fixed longitudinal coordinate, or at a plane transverse to the motion, and to determine the derivatives of the mutual inductance with respect to the lateral and vertical displacements.

IV. EXAMPLE AND DISCUSSION

To better understand the performance of the cross-connected figure-eight null-flux coil suspension system, it is necessary to consider a numerical example. Table 1 lists the dimensions and other parameters used for the example, which are similar to those used in paper [3].

Table 1 Data Used for the Example

Superconducting Magnet	
Length (m)	1.7
Height (m)	0.5
Current (kA)	700
Figure-Eight Null-Flux Coil	
Length (m)	0.55
Height/Loop (m)	0.31
Cross-Section/Conductor(cm^2)	1
Number of Turns	36
Vertical Space between the Two Loop Centers (m)	0.42
Conductivity of Al ($m^{-1}\Omega^{-1}$)	3×10^7
Resistance/Loop R (mΩ)	20.64
Inductance/Loop L (mH)	0.88
Mutual Inductance between Upper and Lower Loops (μH)	-65.8

Assuming a pole pitch of 2 m for the SCM and a vehicle speed of 138 m/s, one obtains v_{c1}=13.9 m/s and v_{c2}=16.1 m/s. The time constant of the coil is about 42.6 ms. Figure 6 shows the dependence of the null-flux lift force components on the vertical displacement with a lateral shift of -5 cm and an effective air gap of 20 cm. One can see that the lift forces F_{z11} and F_{z22} are dominant, and F_{z12} and F_{z21}, resulting from the cross-connection, are relatively small. It should be noted that F_{z11} is much larger than F_{z22} because the lateral shift makes the air gap on the left-hand side decrease to 15 cm, and that on the right-hand side increase to 25 cm. Clearly, such a large force difference between two null-flux coils could lead to a roll motion. The cross-connection between the two figure-eight coils may reduce such roll motion because F_{z12} is negative and F_{z21} is positive. The dimensions of the figure-eight null-flux coil and SCM may be designed to increase F_{z12} and F_{z21} and to improve vehicle stability. The lateral shift could be encountered while making a turn with the center of curvature to the right. The induced roll is in the correct direction for passenger comfort.

The guidance force as a function of vertical displacement at a lateral shift of -5 cm is illustrated in Fig. 7, where one can see that a guidance force of about 5 kN ($F_{y12}+F_{y21}$) resulting from the cross-connection is obtained at zero vertical offset. It should be noted that the main advantage of the cross-connected null-flux coil suspension system over a conventional null-flux suspension system is that it provides null-flux guidance for a large range of vertical displacement, including the vertical equilibrium position. The guidance forces, F_{y11} and F_{y22}, resulting from the difference of air gap without cross-connection depend upon the vertical displacement. They are relatively small at a small vertical displacement and increase rapidly at a large vertical displacement. Both guidance forces reach the same value at a vertical offset of about 5 cm. Because a maglev vehicle usually operates at a relatively small vertical offset, such as 2 to 4 cm, one can conclude that the guidance forces resulting from the cross-connection are dominant for normal maglev operations.

Total lift and guidance forces, lift-to-drag ratio, and guidance-to-drag ratio as a function of vertical displacement at a lateral shift of 5 cm are illustrated in Fig. 8, where it is interesting to note that the lift-to-drag ratio has a maximum value of 140 at about 2 cm, while the maximum value of the guidance-to-drag ratio appears at a zero vertical offset. Figure 9 shows the dependence of the lift-to-drag ratio on vertical displacement with lateral displacement as a parameter. It is seen from Figure 9 that the lift-to-drag ratio decreases monotonically as the lateral displacement increases, regardless of the vertical displacement. On the other hand, for a fixed value of lateral displacement the ratio goes through a maximum value as the vertical displacement increases. That is, at small vertical displacements, as the vertical displacement approaches zero the drag force increases in magnitude relative to the lift force. Only in the case where the lateral displacement is zero does the drag force decrease relative to the lift force as the vertical displacement approach zero. This is in contrast to the case where no cross-connection exists. In the later case the drag force diminishes in magnitude relative to the lift force as the vertical displacement approaches zero, regardless of the lateral displacement.

Guidance force as a function of lateral displacement with vertical offset as a parameter is shown in Fig. 10, where one can see that guidance force and lateral stiffness increase as the vertical offset increases. Maximum guidance forces are about 13 kN for a zero vertical offset and about 20 kN for a 3-cm vertical offset. Figure 11 shows the dependence of lift and guidance forces acting on each SCM on lateral displacement at a vertical offset of 3 cm, where a large change in lift can be observed as the maglev vehicle displaces laterally, while the guidance force changes are rather small. This implies that the lateral stiffnesses of the two forces are very different.

Assuming a coil pitch of 0.7 m for the figure-eight null-flux coil, one obtains a pitch ratio (SCM pitch over coil pitch) of 3. Thus, the total lift force from the interaction between a pair of SCMs and two rows of cross-connected figure-eight null-flux coils would be three times larger than that discussed above. Thus, according to Fig. 8, the lift force acting on a pair of SCMs at a vertical offset of 3 cm is about 51 kN. Twelve such SCMs can lift 31 metric tons at a vertical offset of 3 cm and 21.5 metric tons at a vertical offset of 2 cm. The guidance force associated with the twelve-SCM vehicle at a lateral shift of 5 cm is about 13 metric tons for a 3-cm vertical offset and 11 metric tons for a 2-cm vertical offset.

V. CONCLUSIONS

A simple dynamic circuit model for the cross-connected figure-eight null-flux coil suspension system has been developed. The model can be used for the determination of both transient and steady-state performance of the cross-connected null-flux coil levitation and guidance system. The closed-form expressions for the magnetic force components are obtained on the basis of a harmonic approximation. These simple relations are useful for vehicle dynamic stability studies. Numerical results show that a cross-connected null-flux suspension system has many advantages over the conventional null-flux coil levitation system. In particular, such a system can provide null-flux guidance at any vertical offset. On the other hand, in contrast to the non-cross-connected system, there is only one point where the drag force goes to zero; namely, when both the lateral and vertical displacements are zero.

ACKNOWLEDGMENT

This work was supported by the U.S. Army Corps of Engineers and the Federal Railroad Administration through interagency agreements E8691R001 and DTFR53-93-X-00047, respectively, with the U.S. Department of Energy.

REFERENCE

[1] S. Fujiwara and T. Fujimoto, "Characteristics of the Combined Levitation and Guidance System Using Ground Coils on the Side Wall of the Guideway," International Conference on Maglev '89, July 1989, pp 241-244.

[2] J. Fujie, "Current Status of Superconducting Maglev System," ISTEC Journal, Vol. 4, No. 4, 1991, pp 40-43.

[3] H. Tanaka, "Change in the Coil Distribution of Electrodynamic Suspension System," International Symposium on Magnetic Suspension Technology, NASA Langley Research Center, Hampton, Va., USA, Aug. 19-23, pp 813-825.

[4] J.L. He and D.M. Rote, "Computer Model Simulation of Null-Flux Magnetic Suspension and Guidance," the 6th World Conference on Transport Research, June 29 - July 3, 1992.

[5] J.L. He, D.M. Rote, and H.T. Coffey, "Computation of Magnetic Suspension of Maglev System Using Dynamic Circuit Theory," Proc. of International Symposium on Magnetic Suspension Technology, Hampton, Virginia, Aug. 1991, NASA Conference Publication 3152, pp 919-938.

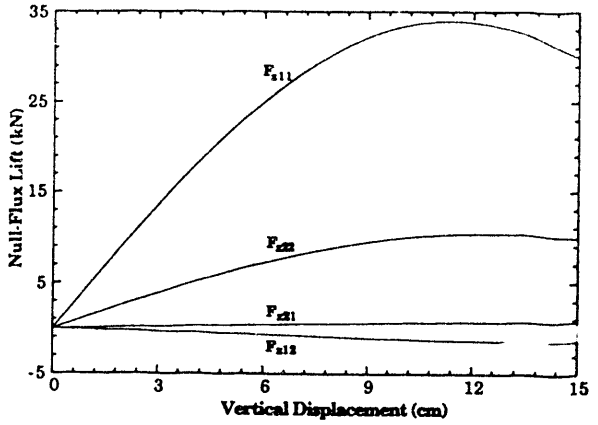

Fig. 6 Null-Flux Lift Force Components as a Function of Vertical Displacement. Speed: 138 m/s; Effective Gap: 20 cm; Lateral Shift: 5 cm. (See Table 1 for Other Parameters)

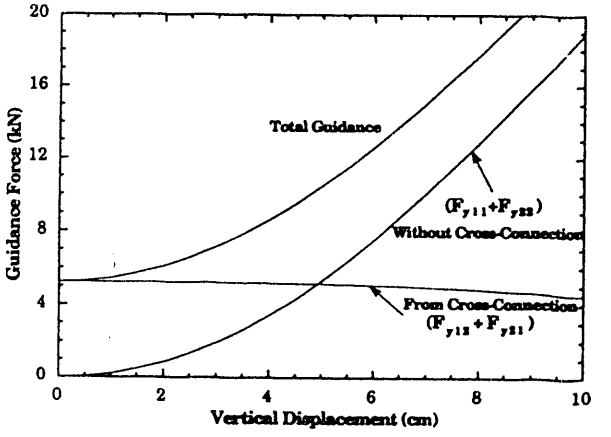

Fig. 7 Guidance Force Components vs Vertical Displacement. (See Table 1 and Fig. 6 for Other Parameters)

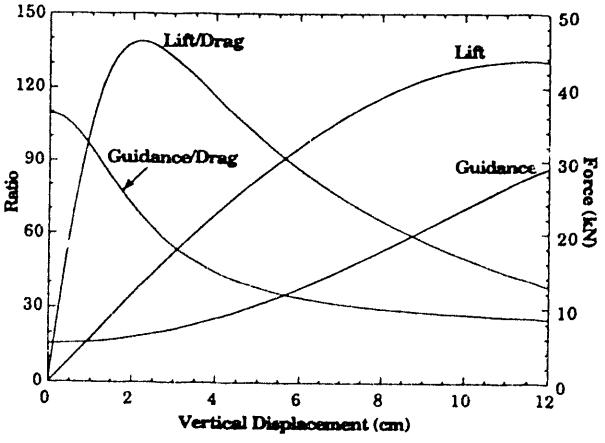

Fig. 8 Total Lift, Total Guidance, Lift/Drag, and Guidance/Drag as a Function of Vertical Displacement. (See Table 1 and Fig. 6 for Other Parameters)

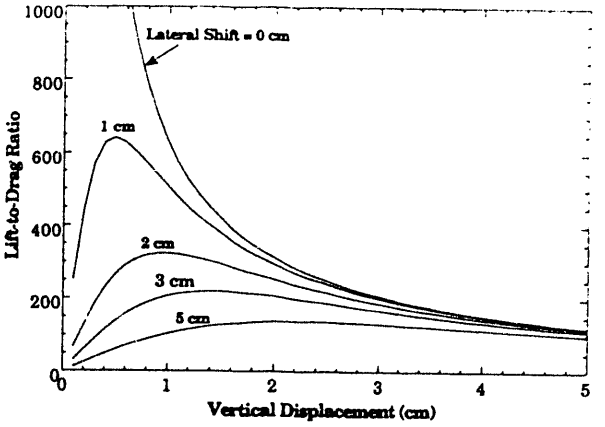

Fig. 9 Lift-to-Drag Ratio Profile as a Function of Vertical Displacement with Lateral Offset as a Parameter. Speed: 138 m/s; Effective Gap: 20 cm. (Ref. Table 1)

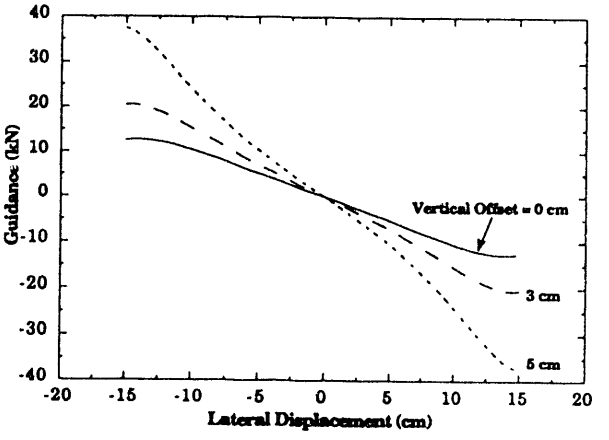

Fig. 10 Total Guidance Force vs Lateral Displacement with Vertical Offset as a Parameter. Speed: 138 m/s; Effective Gap: 20 cm; Vertical Offset: 3 cm. (Ref. Table 1)

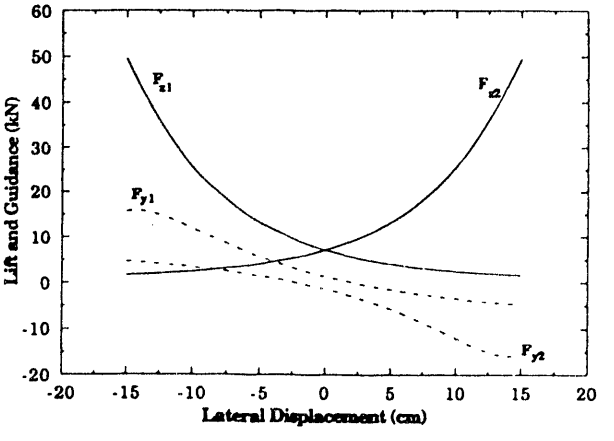

Fig. 11 Lift and Guidance Force Acting on Left- and Right-Hand Side SCMs as a Function of Lateral Displacement Speed: 138 m/s; Effective Gap: 20 cm; Vertical Offset: 3 cm (Also see Table 1 for Other Parameters)

Self Nulling Hybrid Maglev Suspension System

Richard Herbermann
Grumman Corp
Bethpage N.Y. 11714

*Abstract** - **This paper describes a system for using a superconducting coil on an iron core for the levitation of a Maglev vehicle using the electromagnetic or attractive suspension system (EMS). The control system outlined here overcomes the superconducting coil's inherent inability to tolerate rapid changes in current.**

I. INTRODUCTION

This design evolved from the need for a higher magnetomotive force (MMF) in an iron cored magnet than was possible with normal conducting coils. This requirement was generated by the desire to increase the air gap in an EMS Maglev system in order to reduce the tolerance requirements on the guideway. This concept was applied to the Grumman conceptual design in order to increase the air gap between the pole face and the iron rail from 1 to 4 cm [1]

The obvious solution to increasing the MMF driving the core was to use a superconducting coil. However, this was at conflict with the requirement for a 10 Hz bandwidth in order to control the gap width, of the inherently unstable EMS system, and give acceptable ride quality. Superconductors simply do not like high values of di/dt. This design concept allows the superconducting coil to supply most of the MMF and relegates the rapidly changing currents to normal copper coils. A technique was developed to allow the flux through the superconducting coil to change as the current in the normal coils is varied. In addition at a low bandwidth, which the superconductors can tolerate, the current in the superconductors is varied in such a manner as to drive the current in the normal coils to zero. This minimizes power dissipation in the normal coils while retaining the ability to rapidly vary the flux in the gap .

II. BACKGROUND

The EMS suspension system for a Maglev vehicle has been demonstrated by the German Transrapid system [2]. This approach has several advantages over the electrodynamic (EDS) or repulsive system. The vehicle is levitated at all speeds, the magnetic fields in the cabin and external to the vehicle are extremely low, owing to the fact that almost all of the flux is confined to the iron core and as a consequence of the flux confinement the mechanical force and flux density at the coil of the magnet are also very low. The latter fact makes these magnets extremely well suited for excitation by a superconducting coil. With the flux confined to the warm iron core all the lifting forces for the vehicle are reacted in the core which can be supported by heavy warm structure. With little or no force on the coil itself it can be supported by light cold structure thereby minimizing the heat leak from the cold coil to ambient. A second benefit of the low flux at the coil is a greater stability margin in the superconducting coil. Transrapid uses normal copper coils to create the MMF for their magnets. The problems of power consumption and coil heating force them to have a relatively small air gap between the core and the iron rail (≈ 1 cm). This in turn causes two other problems. First the guideway surface smoothness is driven by the small gap and second the small gap dictates an extremely stiff control system to prevent losing control authority. The latter condition mandates a secondary suspension system which is heavy and costly. Replacing the copper coils with superconducting coils permits a much higher MMF and consequently a much larger air gap (≈ 4 cm). This larger air gap reduces the requirements on guideway tolerances and allows an adaptive control system which gives an acceptable ride quality without the need for a secondary suspension system.

III. MAGNETIC CALCULATIONS

Let us assume that we have a normal copper coil magnet with the necessary lifting force to support our vehicle at an air gap of 1 cm. The lifting force as defined in (1) [3] is determined by B^2 assuming A and μ_0 remain constant

$$F = \frac{B^2 A}{2\mu_0} \qquad (1)$$

Where B is flux density, A is the total pole face area, μ_0 is the permeability of air and F is the force generated between the pole faces. Therefore in order to increase the gap and maintain the same lifting force all that is necessary is to keep the flux density in the gap constant. This can be accomplished by increasing the MMF supplied by the driving coil. A first order approximation indicates that all the MMF in a magnetic circuit with a large air gap is dropped across the gap. Assuming the reluctance of the gap is linear with distance (in fact as the distance gets large, leakage fluxes makes the reluctance go up even faster) then the MMF will go up directly as the ratio of the air gap increase. If we were to increase the Transrapid 1 cm air gap to the desired 4 cm air gap it would require 4 times the MMF presently used. This would greatly increase the weight and power consumption of the lifting magnets. A parametric study was made to evaluate the saving when using a superconducting coil. The weight summary for the two options is summarized in Table 1.

* Manuscript received March 15, 1993. This work was performed as part of the EMS Maglev System Concept Definition study supported by the U.S. Army Corps of Engineers under contract DTFR-92-C-000 04

TABLE 1
MAGNET PARAMETERS

PARAMETER	UNIT	AL	CU	SC
Lift per pole	Kg	1,470	1,470	1,470
SC coil weight	Kg			22
Cooling plant weight	Kg	N/A	N/A	20
Normal coil weight	Kg	87	190	
Power consumption per pole	kW	3.3	3	.35
Power cond. weight	Kg	66	60	10
Total weight	Kg	153	250	52

Both aluminum and copper conductors were considered for the normal coils. This study also included the weight of the cryogenic system and the weight of the power conditioning systems for both the normal and superconducting coils. The power conditioning was based on a weight of 20 Kg/kW. The superconducting coil option (on the basis of overall weight is a factor of 3 lighter than a aluminum coil and a factor of 5 lighter than a copper coil. In addition to the weight increase it would also be necessary to transfer additional power to the vehicle (264 kW for aluminum coils and 240 kW for copper coils). It is difficult to transfer this amount of power inductively at all speeds. The high power dissipation and confined locations of the normal coils would require them to be actively cooled. This cooling would require additional power consumption and add even more weight. It is estimated that in light of the cooling and power problems the normal coil option will look even less attractive.

However, stabilizing an inherently unstable attractive system requires that the current in the coil vary at rates of 10 or higher Hz. Rapid current changes at this rate causes heating in the superconductor which, at best, greatly increases the cooling requirements and which, at worst, quenches the magnet

IV. HYBRID MAGNET AND CONTROL SYSTEM

The hybrid magnet and control system shown in Fig. 1 allows the superconducting coil to supply most of the MMF necessary to levitate the vehicle while allowing the rapid flux variation necessary to stabilize the vehicle. The superconducting coil is mounted on the lower arm of the core and two normal copper coils are mounted on the legs. Two power supplies are provided. One is for the copper coils and the other is for the superconducting coil. The supply driving the superconducting coils is a constant current power supply. This type supply will automatically adjust it's output voltage to maintain load current constant in the face of large changes in load impedance. Looking at the supply from the load it looks like an infinite impedance. The copper coils are driven by a conventional regulated supply whose output current is set by a gap sensor which drives the gap to the desired spacing. There is a current sensor in the leads driving the copper coils and it's output is fed through a low pass filter to control the set point of the constant current power supply driving the superconducting coil.

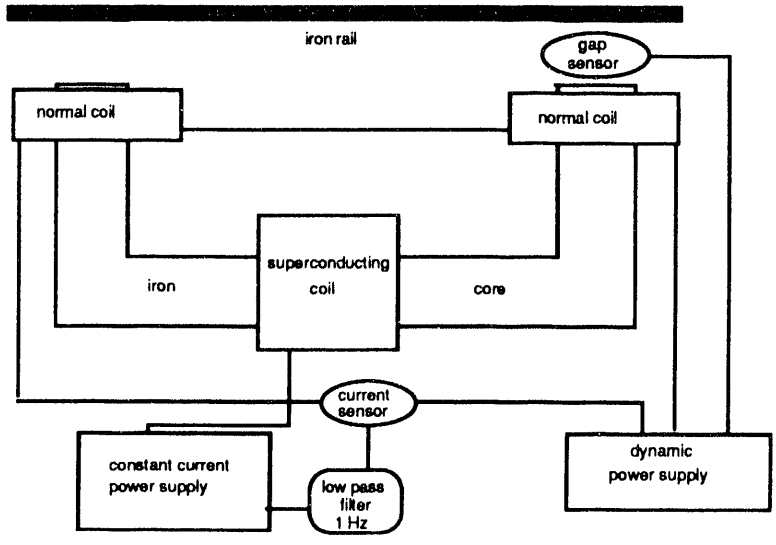

Fig 1

Hybrid magnet control system allows the superconducting coil to supply most of the MMF for lifting the vehicle while at the same time permitting the rapid flux changes required to stabilize the inherently unstable EMS system

The operation of the system is as follows. Upon energizing the system the current set points of both supplies is zero. The gap sensor detects a larger than desired gap and starts current flowing in the normal copper coils. At the same time the current sensor in the copper coil leads detects a current flow and commands current to flow in the superconducting coil. When sufficient MMF is generated by the copper and superconducting coils the vehicle will begin to levitate and the gap sensor will begin to indicate correct gap. This will cause the current in the copper coils to diminish to maintain the correct distance. At this point the entire MMF will be supplied by the superconducting coil and no current will flow in the copper coils. Should a disturbance such as an additional weight be placed on the vehicle the gap will begin to open and the sensor will detect the change. This will cause an immediate increase in the copper coil current maintaining the required lifting force. At the same time the current sensor will detect this current and begin to increase the current in the superconducting coil. The increased MMF will then begin to close the gap and the detector will start to lower the current in the copper coils until eventual equilibrium restored and no current is flowing in the copper coils and the current in the superconducting coils increased.

V. DYNAMIC ANALYSIS

The system was modeled using a single degree of freedom (DOF) analysis to estimate the effect of a 3 cm (1.2 in) gap step closure on the rail. This type of disturbance is represented by a ramp input to the servo since each magnet module (4 magnets) sees the step accruing consecutively over time intervals of 0.022 seconds for a vehicle traveling at 134 m/s (300 mph).

The results of this run are presented in Fig. 2 which demonstrates that for a ramp input disturbance of 3 cm (1.2 in) the gap error does not exceed 2.5 cm (1 inch). At the same time the control coil current does not exceed 15 kaT, well within it's allowable short time limit, and the superconducting coil current does not exceed 6 kaT, which is approximately 12% variation on the nominal 50 kaT. This is the result of the 1 Hz band pass filter. The reason that the currents in the normal control coil and the superconducting coil do not have to go higher is because, as the gap closes, the increase in attractive force approaches a constant value equivalent to the saturation level of the iron core. If this analysis were performed on a 5 DOF nonlinear simulation the results would be expected to be even less severe because each magnet module sees the disturbance in a consecutive manner

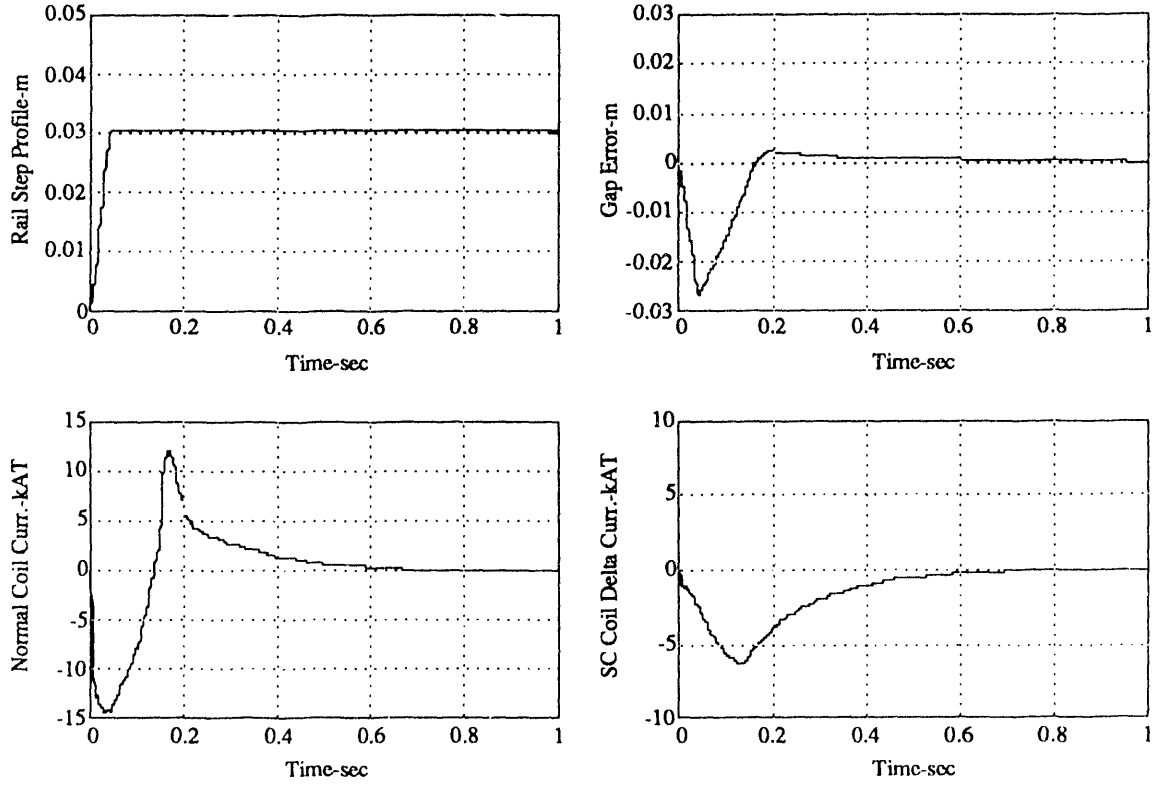

Fig. 2

Demonstration of effectiveness of control system in stabilizing vehicle in response to a step change in gap without requiring large rapid current changes in superconducting coil current

implying that by the time the last magnet has seen the disturbance the first one will already have recovered. From this analysis we can conclude that the system is very tolerant to extreme conditions like a 75% step closure in gap clearance.

References

[1] Michael Proise et al. System Concept Definition of the Grumman Superconducting Electromagnetic Suspension (EMS) Maglev Design, Unpublished, To be Presented at the Maglev 93 Conference, Argonne National Laboratory, May 19-21,1993 Paper OS4-4

[2] Dr.-Ing. Klaus Heinrich, Dipl.-Ing. Rolf Kretzschmar, Transrapid MagLev System, Hestra-Vverlag, Darmstadt

[3] William H. Timbe and Vannevar Bush, Principles of Electrical Engineering, Pg. 370, John Wiley & Sons, Inc. , New York Chapman & Hall, Limited, London 1951

Flux Canceling Maglev Suspension

Richard D. Thornton
Department of Electrical Engineering and Computer Science, MIT, Cambridge, Mass. 02139

Abstract - **This paper discusses the fundamental efficiency limits of EDS maglev and describes a new flux canceling system that achieves high efficiency for suspension and guidance in addition to rapid attenuation of field with distance and low ac losses in the superconductor. It has a drag peak that is relatively small and occurs at low enough speed that the vehicle can operate at speeds below 5 m/s.**

INTRODUCTION

This paper starts with a discussion of the theoretical issues that determine lift efficiency and a comparison of the efficiency of existing designs. The theory leads to a new *flux canceling* EDS system that requires a minimum volume of guideway conductors for a given efficiency. Guidance and propulsion are also discussed.

EDS DESIGN CONSIDERATIONS

Two dimensional field model

It is important to understand the fundamental limitations and tradeoffs that are inherent in Electro Dynamic Suspensions. There are several important limits, and they can be understood from analysis of relatively simple models.

Fig. 1 shows a two dimensional model which assumes all vehicle magnets are long and neglects any performance degradation from coil end turns. The vehicle magnet is represented as a pair of superconducting wires carrying current i_v and interacting with a corresponding pair of guideway conductors carrying current i_g. The vertical suspension force F_y is produced by the z-directed component of the magnetic field in the vicinity of the guideway conductors, B_g, interacting with the x directed component of the current in the guideway conductors, i_g. To maximize the field, the best we can do is space the vehicle conductors far enough apart so that the field in the guideway conductors is determined only by the nearest vehicle current element.

Considering only the field of the nearest vehicle wire, the z directed field B_g, the vertical force per unit length F_y, and the suspension power loss per unit length P_g are

$$B_z = \frac{\mu_0 i_v}{2\pi c}, \quad F_y = 2B_g i_g, \quad P_g = \frac{4\rho}{A} \tag{1}$$

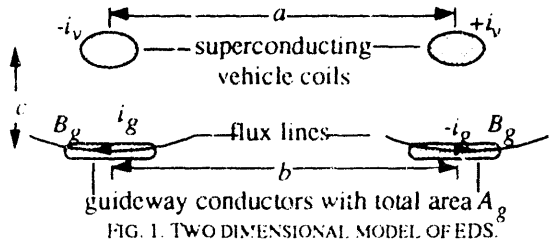

FIG. 1. TWO DIMENSIONAL MODEL OF EDS.

Manuscript received March 15, 1993. This work was supported by the MIT Department of Electrical Engineering and Computer Science, and by the U.S. Department of Transportation via a contract from Bechtel Corporation.

Eliminating B_g, the suspension loss per unit mass is

$$\frac{F_y}{P_g} = \frac{\mu_0}{4\pi\rho_g}\frac{A_g}{c}\frac{i_v}{i_g} \tag{2}$$

The design compromise is evident in (2). The first factor is a material property that offers very few options; copper has 60% of the resistivity of aluminum, but on a per unit cost basis it is more expensive, so most EDS designs use aluminum for the suspension components. The second factor shows the desirability of a large area of guideway conductor and close spacing between vehicle and guideway. The third factor shows the desirability of a high ratio of vehicle current to guideway current. Clearly, the desire for efficiency is in direct conflict with a desire for light vehicle magnets and low cost guideways with a wide gap suspension.

Inductance model

To complete the analysis we use the inductance model illustrated in Fig. 2 with the vehicle and guideway conductors modeled by closed loops carrying currents i_v and i_g, and with inductances used to model the magnetic energy storage. In Fig. 2 the coils are shown in a vertical plane with the vehicle assumed to be in motion in the x direction. The vehicle coil is assumed to be a port superconducting coil and the guideway coil is assumed to be mounted on the side of the supporting girder. The analysis can be extended to deal with more complex coils in any other plane,. but the chosen model is a good representation of our preferred design.

We want to determine the currents and forces when the vehicle is moving at a uniform velocity in the x direction,. The key problem is to determine y directed forces produced by induced currents in the guideway coil.

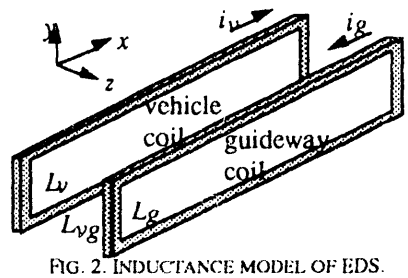

FIG. 2. INDUCTANCE MODEL OF EDS.

Later we will consider the effect of the resistivity ρ_g for the guideway coil, but for now assume the guideway conductor has no resistance. Then the model includes a vehicle coil self inductance L_v, a guideway coil self inductance L_g, a mutual inductance between them L_{vg}, the vehicle coil current i_v, and the guideway coil current i_g, and the flux linkages λ_v and λ_g. The directions of the currents were assigned such that in normal operation i_v and i_g have the same sign. Thus L_{vg} has a negative value and is assumed to be a function of y, the vertical displacement between the two coils. The important matrix relation is

$$\begin{bmatrix} L_v & L_{vg} \\ L_{vg} & L_g \end{bmatrix}\begin{bmatrix} i_v \\ i_g \end{bmatrix} = \begin{bmatrix} \lambda_v \\ \lambda_g \end{bmatrix} \tag{3}$$

If there is no resistance in either inductor, the flux linkages can not change from their initial value. The currents, however, will change and we can calculate them as functions of the flux linkages. Knowing the currents, we can calculate the total stored magnetic energy W, and from that compute the vertical suspension force F_y by computing the change in energy caused by a change in the vertical displacement.

$$\begin{bmatrix} i_v \\ i_g \end{bmatrix} = \frac{1}{L_v L_g - L_{vg}^2}\begin{bmatrix} L_g & -L_{vg} \\ -L_{vg} & L_v \end{bmatrix}\begin{bmatrix} \lambda_v \\ \lambda_g \end{bmatrix}$$
$$W = \frac{1}{2}\left(i_v\lambda_v + i_g\lambda_g\right),\ F_y = \left.\frac{\partial W}{\partial y}\right|_{\lambda_v,\lambda_g\ \text{const}} = i_v i_g \frac{\partial L_{vg}}{\partial y} \tag{4}$$

The vehicle flux linkage is set when the vehicle magnet is "fluxed" (this seems to be a more appropriate term than "charged"!) and if we assume the persistent current does not change, λ_v will never change. The guideway current is totally an induced current, so $\lambda_g = 0$, and we have the important result

$$\begin{bmatrix} i_v \\ i_g \end{bmatrix} = \frac{\lambda_v}{L_v L_g - L_{vg}^2}\begin{bmatrix} L_g \\ -L_{vg} \end{bmatrix},$$
$$\frac{i_g}{i_v} = -\frac{L_{vg}}{L_g},\ F_y = -L_g i_g^2 \frac{1}{L_{vg}}\frac{\partial L_{vg}}{\partial y}. \tag{5}$$

Three important facts are conveyed by (5).

- The ratio of guideway current to vehicle current is the ratio of the mutual inductance between vehicle and guideway coils to the self inductance of the guideway coil.
- The force is twice the product of the stored energy in the guideway inductance and the per unit dependence of mutual inductance on position. Storing more energy costs more, either in terms of using a larger and heavier guideway inductor or creating more loss in the *real* guideway coil which has finite resistance.
- Small L_{vg} is essential for low superconducting magnet power loss due to ac currents. For a given vertical oscillation, due for example to guideway bumps, the ac current induced in the vehicle magnet is proportional to this inductance and ac loss varies as the square of the induced ac current..

If we could construct a guideway with superconductors, then the forces could be computed exactly as described. With a superconducting guideway we would construct a maglev system comprising a configuration of coils on both sides of the vehicle and a guideway such that the vector sum of all forces produces stable equilibrium in the y and z directions and neutral equilibrium in the x direction. This is possible because the currents can change with relative position of the vehicle on the guideway, so Earnshaw's theorem is not applicable. This type of stable superconducting system has been given the name "Magnetic Potential Well" or MPW, but clearly any EDS system with stable suspension for moving vehicles becomes an MPW system if the guideway is constructed with superconductors. The principal virtue of the MPW idea is that it can help in the design and analysis of a practical system.

The effect of loss

We can compute lift efficiency by modeling guideway loss as a perturbation of the inductance model. If we define the guideway coil resistance as R_g then

$$P_g = i_g^2 R_g,\ \frac{F_y}{P_g} = -\frac{L_g}{R_g}\left(\frac{1}{L_{vg}}\frac{\partial L_{vg}}{\partial y}\right) \tag{6}$$

In (6) the negative sign indicates the force is in the direction of decreasing magnitude of L_{vg}., i.e. a repulsive force. The first factor on the right is the electrical time constant of the guideway coil when there is no vehicle present. The second factor is the per unit change in mutual inductance with changes is vertical position between vehicle and guideway. The only way to achieve high efficiency is to make one or both of these factors large.

Time constant of guideway coil

Consider first the problem of designing a guideway coil with a large electrical time constant. Assume that both coils in Fig. 2 are long in the x direction and neglect the effect of end turns and model the coils as transmission line as shown in Fig. 3 The inductance and resistance calculations are given by (7).

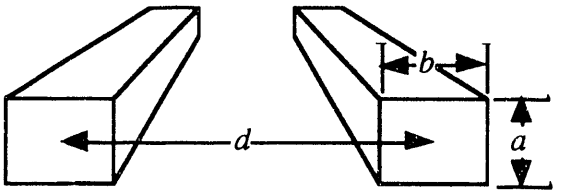

FIG. 3. TRANSMISSION LINE MODEL OF GUIDEWAY COILS.

$$L_g = \frac{\mu_0}{\pi}\left(\ln\frac{d}{a+b} + 1.5\right),\ R_g = \frac{2\rho_g}{ab} = \frac{4\rho_g}{A_g}$$
$$\tau_g = \frac{L_g}{R_g} = \frac{\mu_0 A_g}{4\pi\rho_g}\left(\ln\frac{d}{a+b} + 1.5\right) \tag{7}$$

To first order the inductance per unit length depends only on the perimeter of the wire and there is very little difference whether the cross section is round, square, or rectangular. In a practical design we would usually make the cross section rectangular with b somewhat greater than a in order to minimize the distance from the center of the guideway conductor to the center of the vehicle conductor. Since the dependence on d is only logarithmic, there is very little possibility to increase L. by increasing d. The only way to increase the time constant significantly is to reduce the resistance by using more conductor.

The conductors can be made with either aluminum or copper. These two materials cost about the same per unit mass and if the mass or cost is specified aluminum will produce a coil with a larger electrical time constant. For the suspension system the use of aluminum will normally lead to lower cost, but in cases where there is a limited space for the winding, such as in slots in an iron core machine, copper is better. Assuming aluminum conductors:

with $a = 0.02$ m, $b = 0.03$ m, $d = 0.35$ m:

$$\rho_g = 0.0282\ \mu\text{ohm-m},\ R_g = 47.0\ \mu\text{ohms/m}, \quad (8)$$

$$L_g = 1.378\ \mu\text{h/m},\ \tau_g = \frac{L_g}{R_g} = 29.3\ \text{msec.}$$

When end turns are considered, a practical guideway inductance time constant is in the range 15 to 30 msec.

The relation between efficiency and stiffness

We set an objective of realizing at least 1 Newton of lift for each watt of dissipation. This gives a lift power dissipation of 9.8 kW per tonne of vehicle mass and a lift to drag ratio of 135 for a vehicle velocity of 135 m/s. To achieve this lift efficiency, and assuming a guideway time constant of 25 ms, we need

$$\frac{F_y}{P_g} = -\frac{L_g}{R_g}\frac{1}{L_{vg}}\frac{\partial L_{vg}}{\partial y} = 1; \quad (9)$$

$$\text{if } \frac{L_g}{R_g} = 0.025\ \text{sec},\ \frac{1}{L_{vg}}\frac{\partial L_{vg}}{\partial y} = -40\ \text{m}^{-1}.$$

There are two generic types of EDS systems, ones that use a direct repulsion between opposing coils and ones that use the "shear" force between two sets of coils. that "slide" in parallel planes. This is shown by the two plots of Fig. 4.

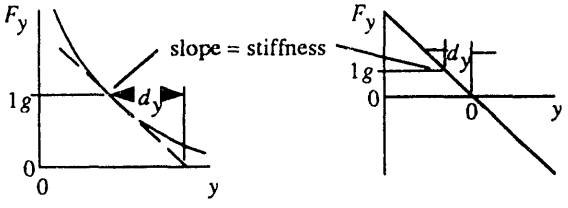

(a) Repulsive force. (b) Shear force.

FIG. 4. TWO TYPES OF STIFFNESS THAT ARE POSSIBLE.

Repulsive force designs, such as the original and new Magneplane and the Japanese MLU series, have a nonlinear force vs. displacement curve, as shown in Fig. 4a, and can not produce a negative force. Most shear force designs that are under development, such as the Japanese sidewall null flux design and our flux canceling design, have a nearly linear force vs. displacement curve, as shown in Fig. 4b, and can produce negative or hold-down forces. Linear shear force designs can be much stiffer for a given clearance between vehicle and guideway, and because of the hold-down force capability are preferable if all other factors are equal.

For all EDS systems the force vs. displacement curve can be linearized and an apparent offset d_y defined as shown in Fig. 4. If F_0 is the equilibrium force, combining (1) and (6) gives

$$\frac{F_0^2}{P_g} = \frac{B_g^2 A_g}{\rho_g} = F_0 \tau_g \frac{1}{L_{vg}}\frac{\partial L_{vg}}{\partial y} = \tau_g \frac{F_0}{d_x}$$

$$\frac{\partial F_y}{\partial y} = \frac{B_g^2 A_g}{\rho_g \tau_g} \quad (10)$$

High efficiency implies high stiffness. High flux density, larger guideway conductors, low resistivity conductors, and low time constant coils all act to increase both efficiency *and* stiffness.

SUSPENSION AND GUIDANCE ALTERNATIVES

There are three basic choices for guideway conductor configuration:

- Continuous sheets;
- Discrete coils, both overlapping or non overlapping;
- Ladders.

All of these have been described in the technical literature, and their important attributes are discussed briefly in the following sections.

Continuous sheet

The original and new Magneplane [2], and other proposed designs [3], use aluminum sheets on the guideway to carry the induced currents that produced the levitation force. The idea, shown in Fig. 5, is to use a relatively thick and wide sheet of conductor under the vehicle suspension magnets. The induced guideway current flows primarily under the vehicle conductors and very near the surface of the conductor.

FIG. 5. CURRENT PATTERN FOR CONTINUOUS SHEET EDS.

The low efficiency of a continuous sheet is due to a skin effect phenomena. The flux density **B** and current density **J** both decay exponentially with depth with characteristic length δ. If the resistivity of the conductor is ρ_g and the frequency of the induced current is f, then

$$\delta = \sqrt{\frac{\rho_g}{\pi f \mu_0}} = \frac{0.0845}{\sqrt{f}}\ \text{(alum., 20°C, } f \text{ in Hz).} \quad (11)$$

For an excitation frequency of 60 Hz the skin depth in aluminum 9.77 mm (0.38 in).

The force density is **J**x**B**, and both fields attenuate with distance at the same rate, so everywhere in the conductor the ratio of force to power is the same. A more detailed derivation shows that the maximum possible ratio of suspension force to guideway power dissipation is

$$\frac{F_y}{P_y} \le \frac{\delta\mu_0}{2\rho} = \sqrt{\frac{\mu_0}{4\pi f \rho}} = \frac{1.88}{\sqrt{f}}\ \text{(alum., 20°C. } f \text{ in Hz).} \quad (12)$$

Equation (12) gives the highest efficiency which is theoretically possible. When end turns, harmonic currents, guidance requirements, and other non ideal attributes are added the efficiency can be still lower. For example, with a 2 meter long magnet the fundamental frequency of induced current is 33.75 Hz at 135 m/s, so the maximum lift efficiency is 0.324 N/w or 30 kW/tonne. In order to achieve this small a loss the sheet must be more than 15 mm thick and in practice the loss will be 40 to 50 kW/tonne.

In summary, an important design objective is to maximize the lift efficiency F_y/P_g, but the continuous levitation strip does not allow independent control of **B** and **J** and the efficiency depends only on material properties and the frequency of the induced current. Stronger vehicle magnets lead to

greater levitation height or more lift per magnet, and wider and thicker levitation strips will allow one to come close to the theoretical limit, but to exceed it we must create a fundamentally different design.

The efficiency limit can be derived with an inductance model, but this model is confused by the distributed nature of the currents. Roughly speaking, there is a high mutual inductance between the vehicle and guideway conductors and a low self inductance of the guideway, so there is no way to achieve a low ratio of guideway current to vehicle current.

The reputation of low efficiency for EDS was one of the reasons the German Maglev project adopted the EMS approach in 1975, and is our principal reason for rejecting continuous sheets. We have rejected continuous sheets for the following additional reasons:

- The low efficiency leads to high drag at low speeds and can cause overheating of the guideway near stations where low speed operation is common.
- The high guideway currents create a strong reaction field which, in turn, creates substantial ac losses in the superconducting magnets when the vehicle is subjected to high speed operation over a realistic guideway that is not perfectly smooth.
- The high drag at low speeds makes it impossible to design a practical system without using wheels at speeds below about 30 m/s (67 mph). Wheels create reliability problems and all sections of the guideway must be capable of supporting the concentrated load a wheel creates.
- The continuous sheet poses difficult mounting problems because of thermal expansion, and it does not appear to lead to lower cost guideways than other designs.
- It is not possible to produce downward directed forces, and the suspension force is substantially nonlinear. These attributes create significant stability and ride quality problems.

Discrete coils

The continuous sheet can be replaced by a sequence of discrete coils, each one connected in a closed loop so as to allow circulating currents. The effect is similar to the continuous sheet except that the current density in the wire is constant and the wire can be located in regions of high field. This type of guideway fits the inductance model very well.

The Japanese MLU guideway used discrete coils and their design is at least as efficient as it would be with sheets except that the mass of conductor is reduced by a substantial factor. But they were not able to take full advantage of stronger vehicle magnets because of the relatively high mutual inductance between vehicle magnets and guideway coils. Also, the discreteness of the coils, as compared to sheets, led to a bumpy ride at low speeds, and also to an attendant high power loss in the cryogenic magnets due to the pulsating fields.

With reference to (6), the lift efficiency is the product of the guideway time constant and the per unit variation of mutual inductance with position. For all practical coil configurations, if the distance between vehicle and guideway coils is c, we find

$$\frac{1}{c} < \frac{1}{L_g}\frac{\partial L_{vg}}{\partial y} < \frac{2}{c} \tag{13}$$

The narrow range indicated by (13) is due to the inverse polynomial behavior of the mutual inductance with distance. Using typical values

$$\text{for c} = 0.14 \text{ m}, \ \frac{L_g}{R_g} = 0.03 \text{ sec}, \ \frac{1}{L_g}\frac{\partial L_{vg}}{\partial y} = \frac{1.5}{c}\text{m}^{-1};$$

$$\frac{F_y}{P_g} = 0.321 \text{ N/W}, \text{ or } P_g = \frac{9.8}{0.321} = 30.5 \text{ kW/tonne} \tag{14}$$

$$\text{at 135 m/s } \frac{F_y}{F_x} = 135 \cdot 0.321 = 43$$

The discrete coil approach offers about a factor of two improvement over a sheet guideway and, most important, there is a possibility for further improvement.

Although there are still limits imposed by practically realizable values of L_g/R_g, the discrete coil design offers more options for increasing lift efficiency than does the continuous strip design. There may be some increase in cost with a discrete coil design, but the extent of the cost increase does not appear to be large. Large air core inductors can be manufactured in an automated factory with labor costs that are small compared to material cost. The coils do not really have to be wound from wire, they only have to create a structure with constant current density and negligible eddy current loss. For example, we can try to emulate the cast aluminum rotor of the squirrel cage induction motor, albeit with much thinner conducting paths. The installation might actually be less expensive than for a continuous strip because there would be no need to use welded connections between large aluminum plates. Another good feature of discrete coils is the fact that frequency does not play as major a role, so shorter vehicle coils could be used and it is easier to use the same vehicle magnets for both suspension and propulsion.

Sidewall Null Flux

The newest Japanese EDS design uses a horizontal gap and the magnetic force is a shear force between vertical surfaces of a *null flux* system. This is a variation of the original null flux system proposed by Danby and Powell in 1966 [1]. This design is more efficient, but not less expensive, than the discrete coil design. A 2-dimensional model is shown in Fig. 6.

The key idea is to increase efficiency by reducing the mutual inductance between the vehicle coils and the guideway coils. This is done by using a Figure-8 coil, and when the coil is symmetrically located with respect to the vehicle coil, there is no flux linking it and no current. There is a very rapid increase of mutual inductance with position, a feature required for high efficiency; see (6).

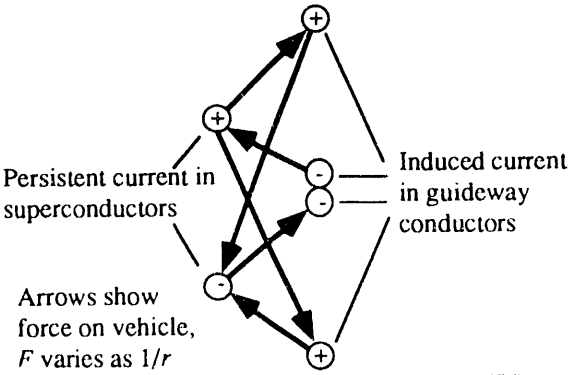

FIG. 6. 2-D MODEL OF SIDEWALL NULL-FLUX EDS.

One virtue of the null flux design is that he current in the coil can be controlled *by design* and we can make almost any tradeoff we like between various parameters, limited only by the theoretical limits discussed earlier. However, this efficiency advantage comes at the expense of using more guideway conductor material and there are more difficult fabrication, mounting and alignment problems. Practical lift power loss is in the range 10 to 20 kW/tonne, or less than half the loss of a simple coil or sheet.

Ladders

Imagine that in the model of Fig. 1 the conductors shown are the *rails* of a ladder and that there are cross connecting conducting *rungs*. This is a cross between a coil and a sheet, and is somewhat analogous to the rotor of a squirrel cage induction motor that has been cut and rolled flat. Unfortunately, unlike the squirrel cage motor, there are high magnetic fields in the aluminum conductors, so the conductor must be constructed in a special way to achieve any advantage over a continuous sheet. The only possible advantage of a solid ladder is the reduced aluminum required as compared with a sheet. However, a laminated ladder can be more efficient than a discrete coil, and can be used with flux canceling suspensions.

FLUX CANCELING EDS

Flux Canceling Suspension

Flux Canceling EDS combines many of the best attributes of other systems with fewer disadvantages. In Fig. 7 the upper and lower rows of magnets on the vehicle create a field that falls off rapidly with distance, but is still on the order of 1 Tesla in the vicinity of the guideway conductors. The suspension conductors on the guideway are arranged as a ladder with the rails providing the vertical lift and the rungs cutting the flux and producing the induced current. The ladder is laminated in a unique way that eliminates skin effect problems.

The result is a system that:

- Produces high efficiency through rapid rate of change of mutual inductance,
- Creates rapid attenuation of fields with distance,
- Makes efficient use of guideway conductors,
- Is susceptible to a range of design compromises,
- Reduces ac losses in vehicle magnets because of reduced guideway currents and mutual inductance,
- Permits a large vertical gap between vehicle and guideway,
- Allows guidance and propulsion using the same vehicle coils.

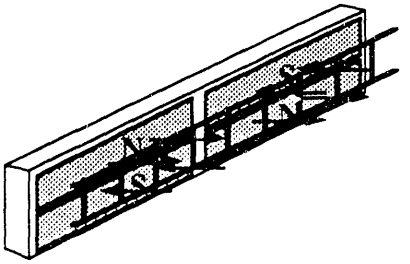

FIG. 7. FLUX CANCELING SUSPENSION.

Most notably there are few disadvantages and improvements are still being made.

Analysis of Flux Canceling Suspension

A two dimensional model is shown in Fig. 8.

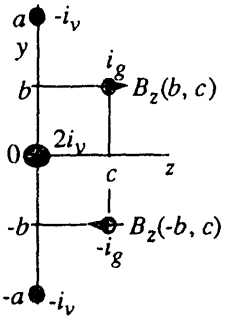

FIG. 8. 2-D MODEL OF FLUX CANCELING SUSPENSION.

The vehicle coils are modeled by three conductors that are long in the x direction, and with current $2i_v$ in the center conductor and $-i_v$ in the upper and lower conductors. The guideway is modeled by two long conductors with current i_g in the upper conductor and $-i_g$ in the lower conductor. The dimensions are given in Fig. 7 and application of Maxwell's Equations allows calculation of the z component of B at the location $y = b$ and $z = c$:

$$B_z = \frac{\mu_0 i_v}{2\pi}\left(\frac{2b}{b^2+c^2} + \frac{a-b}{(a-b)^2+c^2} - \frac{a+b}{(a+b)^2+c^2}\right) \tag{15}$$

The design problem is to determine the vehicle current i_v and the three dimension a, b, and c so as to achieve the highest possible B_z.

The vehicle current is determined by a variety of factors, and for a typical design is 400 kA-turns. This is a compromise between desires for a high field at the guideway but low vehicle magnet weight and low fields in the vehicle.

Assuming the vehicle is displaced vertically from the symmetry position, there will be large currents induced in the guideway conductors by virtue of the motion of the vehicle. In Fig. 8 the induced currents are $+i_g$ and $-i_g$ in the upper and lower guideway rails. The displacement of the vehicle from the symmetry position is so slight that there is no perceptible change in B_z.

We would like to make c as small as possible, but this dimension is constrained by mechanical clearance, cryogenic insulation thickness, and suspension conductor size. The design problem is to pick a and b so as to maximize B_z for a specific choice of c. This optimization can be done analytically leading to

$$a = 2b,\ 9b^4 - 10b^2c^2 - 3c^4 = 0,\ \text{so}\ \frac{b}{c} = 1.1648$$
$$B_z = 1.2182\frac{\mu_0 i_v}{2\pi c} \tag{16}$$

Although there are optimum values of a and b, there is relatively little variation over a wide range of parameters.

Superconducting magnets

The basic vehicle magnet module is the *octapole* of 4 coils shown in Fig. 9. Arrays of these modules provide the field for

a Flux Canceling Suspension. Several modules are placed end-to-end under nearly the whole length of vehicle so as to create a distributed load with a large number of magnetic poles for the LSM.

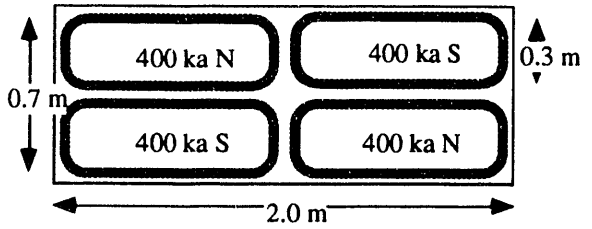

FIG. 9. OCTAPOLE MODULE.

If the only problem were to create a set of magnets with a specified total energy storage, we would use a small number of relatively powerful magnets. Unfortunately, this would lead to a concentrated load on the guideway and a more expensive linear motor. Our compromise is to make every effort to reduce the size and weight of the magnet, and use magnets under most of the vehicle length.

Several octapole modules are physically integrated, end to end, to form a vehicle bogie, and then several bogies are used to provide the primary vehicle suspension. In a typical design the coils are spaced on 1 meter centers. Then a speed range of 50 to 150 m/s implies an electrical frequency of induced currents of 25 to 75 Hz. From theoretical efficiency calculations we know we need on the order of 50 cm^2 suspension area, but for frequencies of 25 to 75 Hz it is difficult to create uniform current density over the entire area due to the skin effect discussed earlier. Thus we resort to either discrete coils constructed from many strands of fine wire, or use laminated conductors with the flux direction parallel to the laminations.

The most effective use of material is achieved with a ladder as shown in Figs. 10. The ladder uses thin aluminum sheets that are bonded together and slit so as to allow the desired currents to flow but with minimum unwanted eddy currents.

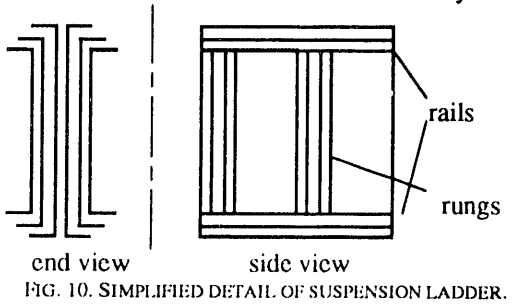

FIG. 10. SIMPLIFIED DETAIL OF SUSPENSION LADDER.

Typical performance

A system concept design was created using flux canceling suspension and guidance and linear synchronous motor propulsion. All guideway conductors were mounted on the upper sides of a box beam guideway [4] and the vehicle had a vertical gap of at least 100 mm The basic suspension module had the characteristics given in Table 2.

The design described in Table 2 led to performance calculations shown in Fig. 12. Over the normal operational speed range the lift loss was less than 10 kW/tonne and the lift to drag ratio was 140 at 120 m/s. This lift loss can be halved by doubling the guideway aluminum mass or by increasing the vehicle coil current by $\sqrt{2}$.

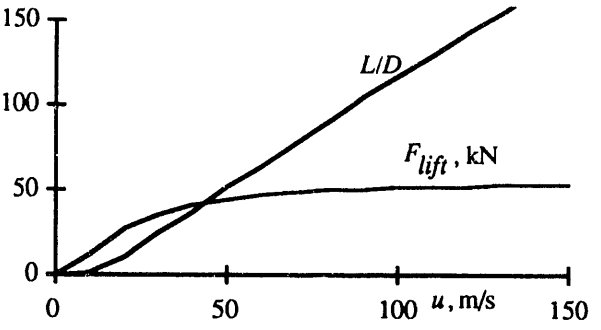

FIG. 12. L/D AND LIFT FOR 8-COIL MODULE.

Table 2. Typical flux canceling design.

Vehicle		
Coils per module	8	4 on each side
Modules per vehicle	12	
Horizontal magnetic gap	145	mm
Horizontal mechanical gap	50	mm
Vertical offset, high speed	15.7	mm
Coil pitch	1	m
Coil length	0.79	m
Coil width	0.3	m
Guideway ladder		
Rungs per meter	6	
Rail width	30	mm
Rung width	50	mm
Thickness	40	mm

The curves in Fig. 12 signify a drag peak at 17 m/s, and at the peak the drag is 20% of the high speed lift. The vehicle is levitated down to 10 m/s by allowing the vehicle to settle up to 8 centimeters below the zero-force position. With high temperature superconductors it will be possible to use superconducting ladders in stations to provide stable levitation at zero speed. In our system concept design we used air bearings for emergency stopping on the guideway, with the intent of providing magnetic suspension down to 0 speed for scheduled stops.

Although the ladder provides the most efficient use of aluminum, it is not necessarily the best approach. We are exploring discrete coil designs that may be less expensive to fabricate and install.

FLUX CANCELING GUIDANCE

The suspension system provides some guidance, but for the design described above the guidance force is only about 10% of the suspension force. It would be possible to design a flux canceling suspension system that produced greater guidance force, but there is a disadvantage of making the guidance force proportional to suspension force. In the interest of increasing efficiency and minimizing interaction between suspension and guidance we developed a separate guidance system.

The guidance system is subject to the same laws that govern the suspension system, we used a flux canceling guidance

system with many of the attributes of the suspension system. The key is to use cross coupling between coils on opposite sides of the guideway so that when the vehicle is centered there is no force and no power loss. This is reminiscent of the guidance system being used in the new Japanese design, except that the guidance is almost totally decoupled from the suspension.

When the vehicle is centered horizontally the voltages induced in the opposite-side coils cancel, so there is no current flow and no lateral force. If the vehicle shifts to one side of the guideway then the induced voltages do not cancel and the resulting current produces a push on one side of the vehicle and a pull on the other side. Within limits the coils can be designed to achieve any desired lateral stiffness, and the stiffness is almost independent of vertical position. The cross coupling achieves high efficiency because there is only power flow when a restoring force is needed. This is in contrast to TR07 which, at high speeds, produces greater power dissipation in the guidance rails than is used for suspension.

A key feature of the design is the relative independence of guidance and suspension forces, so that guidance is effective even if the vehicle is in the zero force position on the suspension ladder. The operation of the guidance can also be explained in terms of the flux pattern shown in Fig. 13. The flux linking the upper and lower coils adds and produces a large voltage when the vehicle is moving. If there is lateral offset, so that current flows in the coils, then the current in the middle legs of the coils interacts with the vertical flux lines to produce a horizontal force.

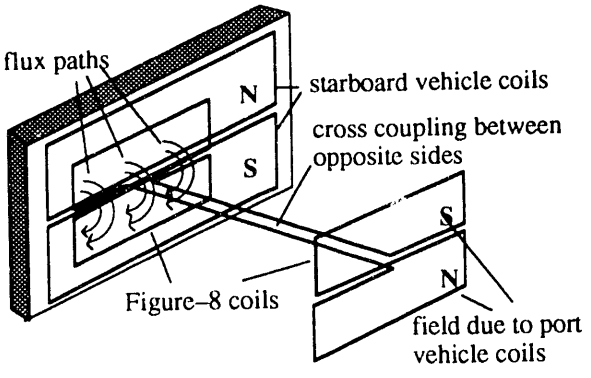

Fig. 13. Flux canceling guidance.

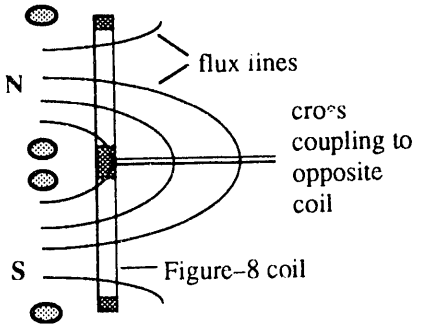

Fig. 14. Guidance coil flux pattern.

ACKNOWLEDGMENT

I wish to thank the many members of the Bechtel System Concept Team that contributed to adapting the flux canceling system to the US1 design. Particular acknowledgment goes to B. Montgomery, R. Thome and R. Pillsbury of the MIT Plasma Fusion Center; S. Phelan of the MIT Civil Engineering Department; G. McAllister, J. Perkowski, and E. Lemcke of Bechtel; and B. Concannon of GM EMD. I appreciate comments from all of the students who contributed in many ways and from more than a dozen MIT staff and faculty from the Electrical Engineering and Computer Science Department and the Laboratory for Electromagnetic and Electronic Systems.

REFERENCES

[1] Powell, J. R. & Danby, G. T., "High speed transport by magnetically suspended trains," presented at the ASME Winter Meeting, N.Y., Tech. Rep. 66-WA/RR-5, Nov. 1966.

[2] Kolm, H. H., & Thornton, R. D., "The magneplane: guided electromagnetic flight," *Proceedings of the 1972 Applied Superconductivity Conference*, May 1-3, 1972.

[3] Atherton, David L., Ed., *Study of Magnetic Levitation and Linear Synchronous Motor Propulsion*, Canadian Institute of Guided Ground Transport, Queens University, Kingston, Ontario, Annual Report for 1972.

[4] R. S. Phelan, "Reduction of guideway residual vibration through strategic vehicle pad spacing arrangements," *These proceedings*, May 19-21, 1993.

Maglev Transportation with Controlled Permanent Magnets and Linear Synchronous Motors

H. Weh, A. Steingröver, H. Hupe
Institut für elektrische Maschinen, Antriebe und Bahnen
Technische Universität Braunschweig,
Postfach 3329, 3300 Braunschweig, Germany

Abstract - This report describes maglev suspension systems in combination with linear drives for maglev transportation of all speed ranges. The function of suspension is separated from the function of propulsion. These special configurations of magnets and motors minimize the force-interactions between the suspension and the propulsion system. The controlled permanent magnet provides inherent stable forces either in the support or in the guidance direction. Demonstration vehicles show the application of controlled permanent magnets and digital gap controls. The linear synchronous motors are directly attached to the levitation system and designed either as a short stator or as a long stator type. A three-dimensional analysis of the magnetic field was carried out to obtain the forces. Computing models reflecting dynamic and nonlinear properties of the magnets and the motors were developed. The dynamic behaviour in various situations was simulated.

I. Introduction

The attractive magnetic forces of electromagnetic suspension systems arise from the Maxwell stress in the air gap of a soft iron core which is split between an exciter on the vehicle and a yoke on the track. A sufficient flux density and hence a resulting force density is generated by a few ampere turns. The levitation magnets are excited solely by an electric current or a controlled permanent magnet as described in [1]. To achieve a stable levitation state the attractive magnetic forces are electronically controlled. The control units necessary for stabilizing the magnets consist of sensors, controllers, inverters and power supplies.

The propulsion forces of linear synchronous machines arise from the interaction of a stator current sheet with an exciting field. The driving or braking forces are generated corresponding to the amplitude of the stator current and the load angle. The vehicle speed corresponds directly to the propagation rate of the travelling wave. The orientation of the field vector necessary for a field-orientated control of the motor is measured by a position sensor. The reactive power can be adjusted by the electric or the permanent magnetic excitation.

The layout of a levitation vehicle is mainly determined by the characteristics of the active components for suspension and propulsion. An improved design of the magnet and the motor according to power demand, magnetic forces, weight and mechanical construction is the aim of this work.

II. Semistable Magnet Configurations

The controlled permanent magnets presented in this paper provide inherent stable forces either in the support or in the guidance direction. The reluctance forces at opposite pole cores in displaced position provide stable force characteristics. With a steep characteristic in the stable direction a position control in this direction is unnecessary and the total amount of control equipments is reduced. The steepness rises with the flux density in the air gap and with the width of the pole cores. A flux density of 1 T and a pole width to air gap ratio of 2 provides sufficient forces for transportation purposes.

A. Magnet with Stable Support Force

A cross-section of a stable magnet arrangement called "magnet with stable support force" is shown in Fig. 1 together with its flux plot. The flux excited by the high-energy permanent magnets (NdFeB) closes its path via the narrow pole edges of the magnets and the double C-shaped rail. A vertical displacement of the

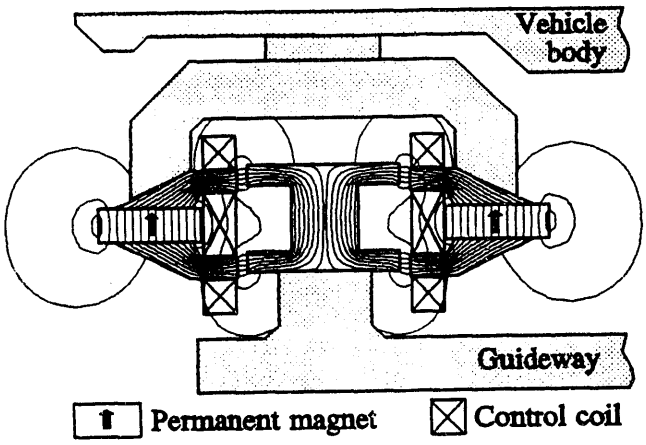

Fig. 1. Magnet with stable support force

magnet produces restoring reluctance forces which first rise proportional to the diplacement and then fall beyond a maximum point. In the stable range the characteristic is analogous to that of a mechanical spring. The magnet responds immediately to track disturbances with restoring forces and has a faster dynamic response than conventional electromagnets, which react with a significant delay caused by the control procedure. Due to the spring characteristic of the support force, the system has to be damped by damper elements in the vehicle bogie which are neccessary anyway.

In a vertical displaced position with increased force the flux is lower than in the centre position, hence the magnet can be designed for large flux densities at the operating point. The flux density is only limited by the saturation of the soft iron parts. Support force to magnet weight ratios of ten are possible.

Horizontally the system has to be stabilized in the same way as conventional attractive levitation systems. An additional excitation with control coils strengthens or weakens the magnetic field to obtain the desired stabilization. The control coils of both sides are connected in series. Only the difference between the normal forces which compensate each other in the symmetrical position results in the guidance force. The magnetic design near the saturation point of iron does not restrict the controlability of the magnets.

A small scale demonstration vehicle built by the IEM shows the possibility of a surface mounted track and the restricted expense of a digital control. The vehicle is levitated by four magnets capable of carrying 75 kg each.

B. Magnet with Stable Guidance Force

The magnetic field of the magnet arrangement shown in Fig. 2 is generated losslessly by the ferrite magnet placed in the centre of the magnet unit [2]. The flux path runs symmetrically through the soft iron poles of the magnet and the L-shaped rails. The flux squeezing configuration increases the flux density in the air gap to a value higher than the remanent flux density of ferrite. The leakage at the flanks of the permanent magnet is small as a result of the large magnet height and the outer downwards shifted air-gaps.

During the process of force dimensioning an overload factor and a control range allowing compensation of disturbances were taken into account. After optimization of the mechanical dimensions a lifting force to magnet weight ratio of ten was achieved. The design is a compromise between the conflicting aims of high forces, small magnet weight, the maximum current density of the control coil and the magnet's dynamic response.

The attractive forces are controlled by an electric current supplied to a control coil. The control current increases or reduces the permanent magnetic flux as required. Energy is consumed only to compensate for track disturbances. At lateral displacements the magnetic forces retract the magnet to the centre position. The inherent stable guidance force amounts to more than 30% of the lift force.

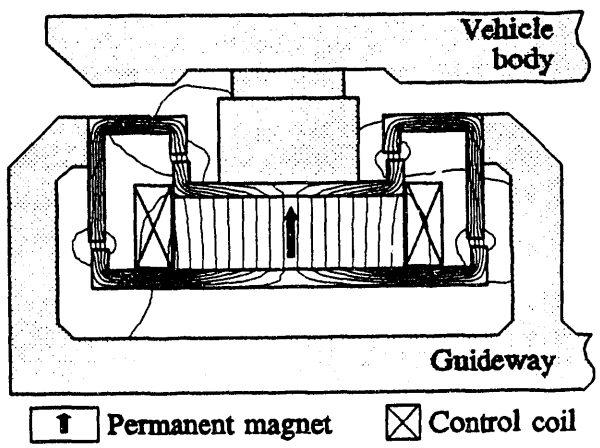

Fig. 2. Magnet with stable guidance force

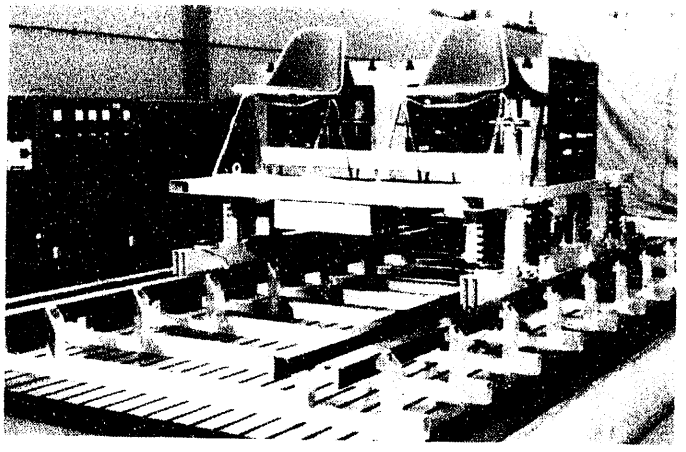

Fig. 3. Demonstration vehicle with four magnets

The ferrite magnet material has an average remanent flux density of 0.4 T. During operation the value of the flux density varies only in the linear range of the B-H-characteristic of ferrite and demagnetization cannot occur. The unipolar configuration of the system allows an additional magnetization in the assembled state to achieve the maximum remanence of the material.

A full-size demonstration vehicle (Fig. 3) was built using "magnets with stable guidance forces." The levitation magnet was developed to provide a lifting force of 7.5 kN for a 3 t vehicle with four magnets which support the vehicle bogie via springs and dampers. The two magnets on each side mechanically form a levitation unit. The vehicle stands on the levitation units and does not embrace the guideway. A mechanical bearing with transverse swinging arms allows the magnets to move only in the vertical direction, although pitching of the levitation units is possible. This degree of freedom is important for the "edge-control concept."

Each magnet is stabilized by its own control unit shown in Fig. 4. The gap between the rail and the magnet is detected by a sensor which provides an input signal for the controller. A digital control algorithm running on a transputer proccesses this gap signal and delivers a control signal to a four-quadrant chopper.

At the nominal operating point the control current is negligible and the total power consumption of the vehicle is mainly determined by the switching losses of the choppers.

The homopolar transverse flux arrangement produces homogeneous flux densities in the longitudinal direction. Minimized force-interactions with the propulsion system allow for combinations with various types of linear drives to form compact units.

C. Simulation Model and Results

A simulation model of the magnets and the vehicle was investigated to examine the behaviour of the vehicle at high speeds and to improve the control methods. The magnet model contains the nonlinear characteristics of the magnetic forces and of the coil inductance. The inhomogeneous flux distribution in the air-gap was taken into consideration in all directions. This includes pitching of the magnets and the unevenness of the rails.

All the most relevant quantities are obtained by a

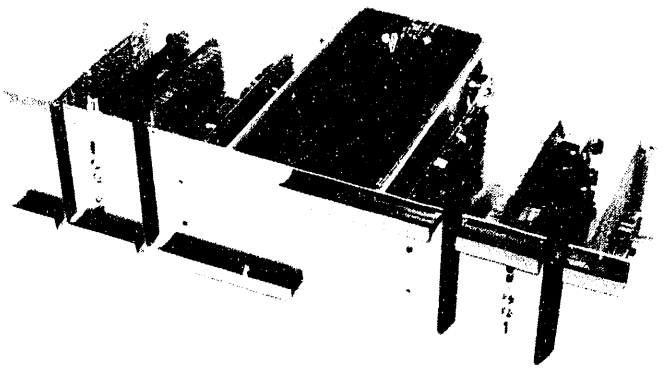

Fig. 4. Control units of the demonstration vehicle

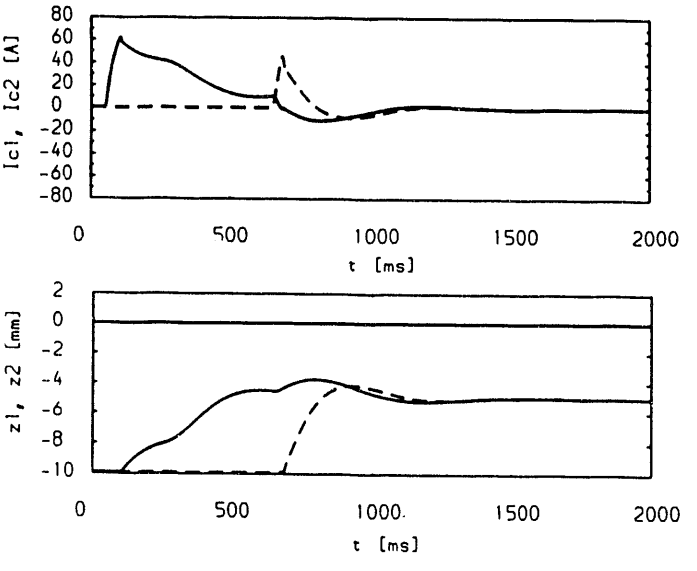

Fig. 5. Simulation results of a start-up procedure

numerical evaluation of the derivatives of the magnetic flux with respect to all the state variables. The introduced state variables are the vertical, the lateral and the rotational positions of the magnet unit, the corresponding velocities and the control currents. They appear in the differential equations with inhomogeneous constants.

The simulation results of a start-up procedure are shown in Fig. 5. The control currents (Ic1, Ic2) and the air-gaps (z1, z2) of a magnet unit were plotted over the time. The magnet 2 (dashed lines) is started, after magnet 1 (solid lines) reached its nominal gap. At this time the magnet unit is pitching and magnet 2 is able to start-up with less current. Only in the start-phase energy is consumed for a short moment. The interactions between the magnets by pitching of the unit are small. A control algorithm with both air-gaps as input values reduces this influence even more.

III. Linear Motor Configurations

The linear synchronous motors presented in this paper provide propulsion forces with negligible normal forces. The motors were developed considering high efficiency, low normal forces and force characteristics adapted to transportation duties. A short-stator type offers advantages for the maglev transportation in the medium speed range with its small power. The small machine power can be installed on the vehicle and the drive energy can be transferred via current collectors to the vehicle. A long-stator type is favourable for the layout of a vehicle in high speed applications which require a higher propulsion power.

A. Transverse Flux Short-Stator Motor

The short-stator motor was developed as propulsion system with a high thrust and a low weight for the medium speed range. The main characteristics of the motor which are advantageous for this application are the small pole pitch of about 0.05 m and the transverse flux arrangement.

In general the thrust of a motor rises with a decreasing pole pitch, if the mechanical power output remains constant. The minimum pole pitch of conventional motors is limited by the leakage and the maximum stator frequency. An air-gap of 0.01 m as usual in electromagnetic levitation systems leads to a optimal pole pitch of about 0.2 m. An additional

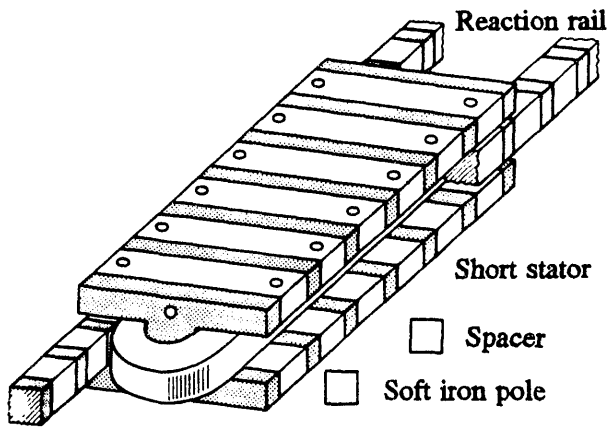

Fig. 6. Transverse flux short-stator motor

increase of the thrust is then only possible with an enlarged layout of the motor.

A transverse flux arrangement enables small pole pitches without disadvantages in the design of the motor. Fig. 6 shows the double C-shaped stator and the passive reaction parts. The reaction parts consist of small iron packets which are mounted on the rails at constant intervalls. The stator consists of a stack of laminated iron packets and nonmagnetic spacers. Several stacks are joined together by the stator coil to form a single-phase module.

The stator current flowing in the longitudinal axis of the motor generates a magnetic flux in the transverse plane (Fig. 7). The leakage in the window and at the heading of the coil is small. So the flux mainly closes its path via the reaction parts according to their longitudinal position (Fig. 8). A movement of the stator modulates the flux and hence the forces.

The motive forces arise by reluctance effects at the

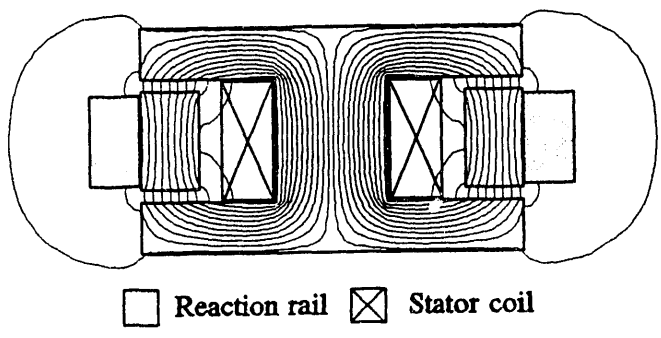

Fig. 7. Flux plot of reluctance motor in cross-section

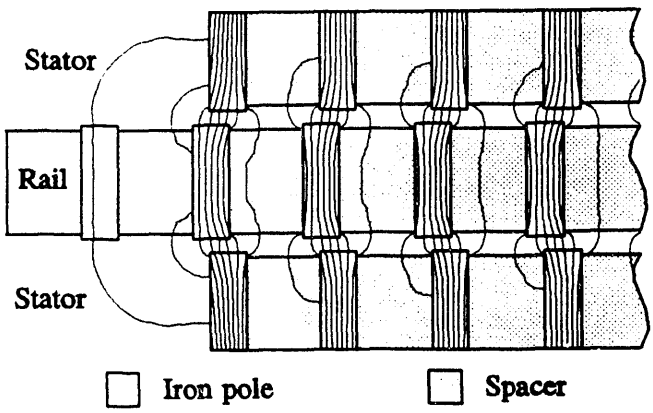

Fig. 8. Flux plot of reluctance motor in longitudinal-section

edges of the marked poles of the stator and the reaction rails. The maximum value of the propulsion force depends on the ratio between the pole pitch and the pole space. For a given air-gap optimal dimensions were found to achieve a minimal weight and a maximal thrust. The absolute ratings were then adjusted by the pole height and the stator's ampere turns. The different planes of the magnetic flux and the electric ampere turns allow an almost independent design of these parts. The thrust of the motor designed for the demonstration vehicle (Fig. 3) reaches about 10 percent of the vehicle weight. The motor weight amounts to 11 percent of the vehicle's weight.

A movement at constant excitation produces an approximatly sinusodial time behaviour of the propulsion force. The negative forces can be suppressed with the stator current set to zero during these time periods. This is achieved by a unipolar rectangular waveform of the current. The magnitude of an in-phase controlled stator current determines the mean value of the driving force. The phase position of the current determines the direction of the motive forces.

A smooth time behaviour of the force can be obtained by superposing of the forces of four modules which are shifted respectively by a half pole pitch. The stator current of each single-phase module is separately controlled according to the phase position of the module. Each module is fed by a two-quadrant chopper.

At higher frequencies which are associated with higher velocities the magnitude of the current pulses are limited by the stator inductance and a phase lag occurs. In this case the mean value of the driving force is reduced. A control method called "pre-commutation" corrects the phase position in the field weakening range. In this way a rise of the thrust can be achieved without increasing the inverter power.

The normal forces in the opposite air-gaps compensate each other in the symmetrical position which is controlled by the suspension system. The remaining influences do not disturb the function of levitation.

B. Permanent Excited Long-Stator Motor

The long-stator concept transfers parts of the on board equipment for the propulsion system to the track. Most maglev trains of the high speed range use an integrated propulsion and support system. In this case the flux of the exciter serves both generation of support forces and excitation of the synchronous motor. The linkage of these function restricts the latitude of the component's design.

The long-stator motor described in this chapter generates forces only in the direction of motion. Fig. 9 shows the configuration of the motor in cross-section. The iron yoke of the stator was cut out to prevent the excitation flux from producing unfavourable normal forces. The excitation is provided by permanent magnets. The flux disperses in longitudinal direction and passes the three-phase winding of the long-stator.

A sufficient flux density is achieved with high-energy permanent magnets (NdFeB) which are mounted on an iron yoke. All components of the magnetic field were calculated for consideration of the inhomogeneous three-dimensional flux distribution of the permanent magnets. An investigation of various magnet forms led

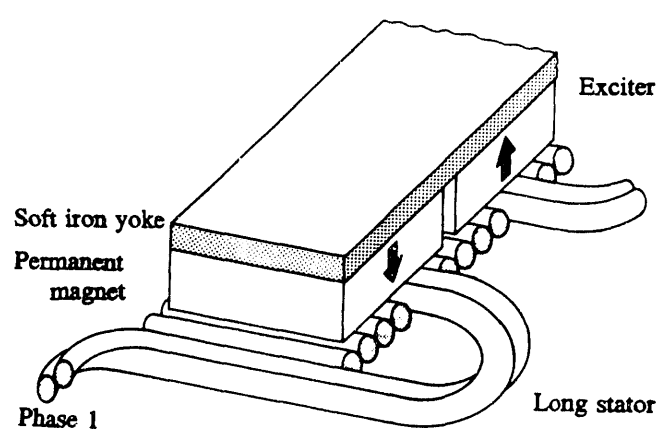

Fig. 9. Permanent excited long-stator motor

to a simple magnet configuration with distances between the permanent magnets.

The values of the propulsion forces were obtained by an integration of the force density over the whole volume of the stator windings. A unique current density in the thick wires was assumed. A thrust of about 9 percent of the vehicle weight is achieved with a winding scheme of the stator, which fills the entire space.

Due to the large distance between the stator and the iron yoke of the exciter the attractive forces are small. Additional force components arise at the coil headings by the leakage flux. The vertical position of the permanent magnetic exciter is controlled by the levitation system. A direct mounting of the permanent magnets beneath the support magnets forms a compact unit.

IV. System Features

The levitation concept with a small magnetic gap offers light levitation magnets and improved vehicle layouts. The selfstable forces of the presented magnets reduce the amount of electronic equipment for stabilizing the magnets. Additionally the energy consumption of the levitation system is reduced using controlled permanent magnets.

The presented linear motors allow a mechanical combination with the levitation magnets. The function of levitation is not impaired by the drives and vice versa. The high efficiency of the synchronous motors reduces the thermal stress of the reactive parts.

The described system components for maglev transportation show the possibility of a simple vehicle and track configuration. Both surface mounted tracks and standing vehicles are advantageous features. Therefore the expense for the infrastructure of a traffic system using magnetic suspension and linear drives can be reduced significantly.

References

[1] H. Weh, H. May, H. Hupe, "High Performance Magnetic Levitation with Controlled Magnets and Magnets with Stable Characteristics," *MAGLEV-Hamburg, Germany*, June 9-10 1988.

[2] H. Weh, A. Steingröver, H. Hupe, "Design and Simulation of a Controlled Permanent Magnet," *International Journal of Applied Electromagnetics in Materials*, 1992.

d:\argn308.shr\ps1-10
dtd Fri05Mar1993(8:49 AM March 9, 1993fnl)

Maglev Transit Technology in Russia

Floyd A Wyczalek
FW Lilly Inc., HSST NA Engineering Division,
Bloomfield Hills, MI 48301 USA

Abstract - There are two well known concepts for achieving magnetic levitation of vehicles: one is based on electromagnetic attraction (EMA); and the second method is based on electrodynamic repulsion (EDR). In turn, each of these concepts have at least two variations. This paper presents a third form of magnetic levitation where the guideway and vehicle coils are superconductive (SC). This configuration is known in Russia as the Magnetic Potential Well (MPW). While the practicality of including SC guideway levitation coils, in addition to SC vehicle coils, may be questionable, test data with this configuration is available for evaluation.

I. Introduction

The specific concept currently under investigation in Russia is a three SC coil concept configured as a sidewall maglev system: where two coils are stationary to form the guideway and the third coil is mounted on the vehicle. Currently, these three SC coils are sized to levitate about one metric ton in a stationary physics laboratory scale experiment [1-6][1].

The scope of this paper is limited to an abbreviated explanation of this concept and to illustrating the experimental characteristics of the magnetic levitation force vs displacement relationships, and linear motor application relationships. This explanation and the accompanying illustrations are based on log records and 35mm color photographs made during a July 1991 visit to the magnetic physics laboratory in the city of Kiev, to observe laboratory demonstrations of the concept. This laboratory is situated at the Academy of Sciences of the newly independent republic of the Ukraine in Kiev.

II. Unites States National Energy Strategy

In the US there is a commitment to the rapid development of maglev technology in general [7-41] because of the newly enacted Intermodal System Transportation Efficiency Act of 1991 (ISTEA), passed by the 102nd Congress and signed by the president in 1991 [42].

ISTEA section 1036(a) declares that it is the policy of the US "to establish in the shortest time practical a US designed and constructed magnetic levitation transportation technology capable of operation along Federal-aid highway rights of way, as part of a national system of the US", see National Maglev Initiative (NMI) [43,44].

III. MPW Magnetic Physics Laboratory Experiment

Fig. 1 shows a schematic of the MPW experimental setup at the Academy of Sciences in Kiev, by Kozoriz [1-5]. It consists of two superconductive SC circuits and their respective cryostats, in a vertical coaxial configuration. The coaxial internal cryostat represents the transit vehicle and it was suspended from a load cell (P) by an adjustable cable. The SC coils include "persistent" thermal switchs to interrupt the SC circuits. The load is varied by adding mass to the pan suspended from the internal cryostat which represents the vehicle.

Displacement (X) is measured with reference to the centerlines (cl) of horizontal symmetry of both SC circuits. Thus, it was possible to obtain magnetic force (P) vs displacement (X) plots to define the levitation and/or repulsion forces under various operating conditions.

Fig. 2 shows a characteristic levitation and repulsion force (P) and SC circuit displacement (X) obtained with the setup shown in fig. 1. In fig. 2, levitation, positive magnetic attraction force +P is defined and plotted in the upward direction, and repulsion force −P is defined and plotted in the vertical downward direction. Levitation gap +X, for a vehicle suspended from a guideway is defined in a rightward X direction.

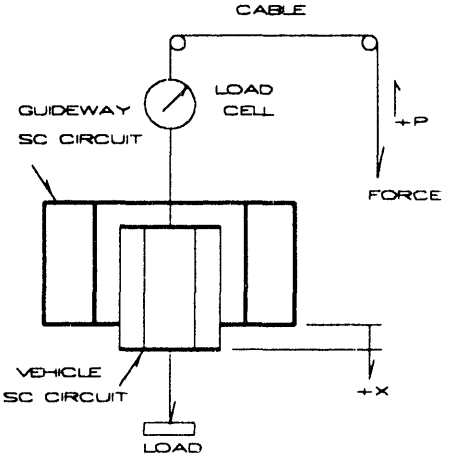

Fig. 1 Schematic sketch of MPW magnetic physics laboratory experimental setup at Academy of Sciences of Ukrainian SSR, Kozoriz [1-5].

1 Numbers in brackets [ ] refer to references at end of paper.

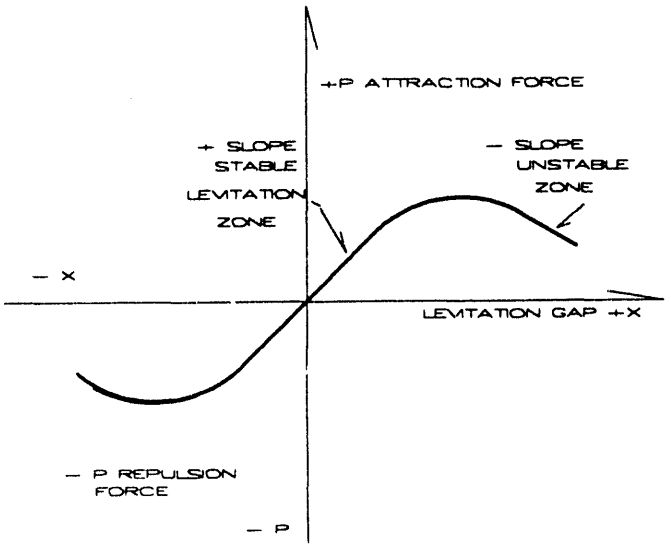

Fig. 2 Definition of positive directions for force +P and displacement +X and MPW characteristic curve of magnetic levitation and/or repulsion force –P vs levitation displacement gap –X obtained with setup fig. 1.

The stable levitation range of this characteristic levitation response curve is the positive slope portion of the +P vs +X plot, where levitation force increases as levitation displacement gap increases. Conversely, the negative slope portion of the curve beyond the maximum force +P is unstable and not useful for levitation, since levitation force decreases as gap increases further.

IV. MPW Linear Motor and Braking Concept

Fig. 3 illustrates the hypothetical vehicle and guideway configuration for the MPW linear motor and regenerative braking system hypothesized by Kozoriz [1-5]. In the MPW linear motor concept, the vehicle SC circuit is accelerated toward two stationary SC circuits, one on each side of the guideway, at instantaneous velocity (V_t), and propelled by the mutually attractive magnetic force +P between the onboard SC and the two stationary guideway SC coils, as defined by Kozoriz.

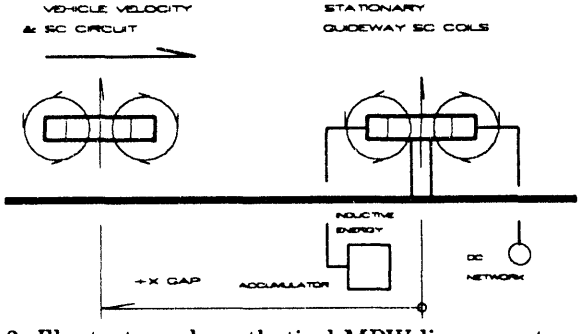

Fig. 3 Illustrates a hypothetical MPW linear motor and guideway configuration concept postulated by Kozoriz [1-5].

Hypothetically, at the instant when X = 0 the guideway SC circuit is opened and SC current flow ceases, it's magnetic field collapses and transfers the magnetic potential energy to the stationary SC inductive energy accumulator. However, in the laboratory, this energy transfer is simulated by energizing the persistent thermal switch to open the SC circuit, this switch also permits the initial charging of the SC coil; and, manually displacing the internal coaxial SC coil with the load cell cable at a small velocity V. Fig. 4a shows the characteristic +P vs +X linear motor curve obtained with this preceding procedure. This conjecture is based on observations during the above laboratory demonstration, but Kozoriz did not confirm this speculation.

Conversely, a braking characteristic curve of –P vs –X beyond the 'cl' mid point line of symmetry of the approaching vehicle SC coil and stationary SC coil, is simulated by opening the current path of the stationary SC coil when $+X \neq 0$, then, closing the SC current path when the vehicle enters $X \leq 0$. This characteristic MPW regenerative braking curve is shown in fig. 4b.

V. SC Magnetic Flux Switch

In the preceding SC linear motor and braking concept described by Kozoriz, thermal switching is too slow to be practical. However, faster switching rates can be obtained with the SC inductive switch concept demonstrated by Spyker and others [48]. An inductive two axis vector switch exhibits submillisecond switching rates and may be more practical.

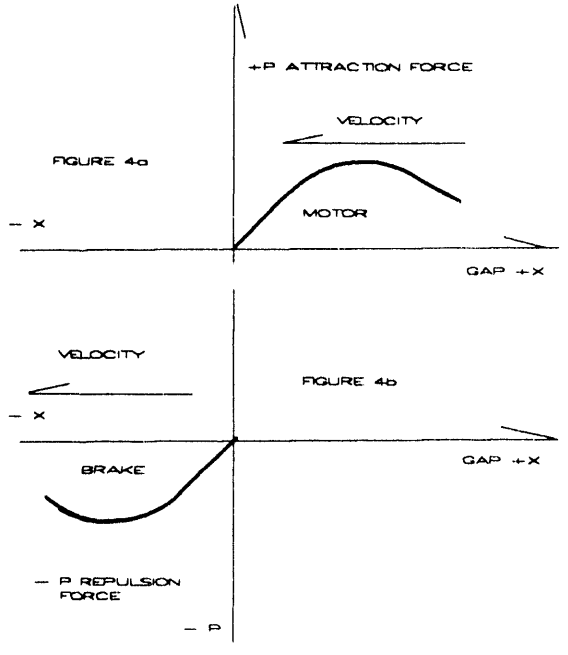

Fig. 4a/4b MPW linear motor +P vs + X characteristic is shown in fig. 4a, while MPW regenerative braking – P vs –X is in fig. 4b, Kozoriz [1-5].

VI. Sidewall Levitation Experiment

Based on the magnetic physics experimental characteristics shown in the preceding paragraphs, Kozoriz [1-5] proposed the hypothetical configuration shown in fig. 5 for a maglev vehicle suspended under a guideway in a gravity field. An example of one of many possible solution sets, the specific design parameters for the stable equilibrium suspension of a free vehicle defined in fig. 5 are shown in Table I.

Fig. 6 shows the MPW experimental setup in a sidewall levitation configuration with three larger SC coils 600mm inside diameter, 100mm in height, and a low ratio between coil thickness and their diameters. A stainless steel frame supports two SC magnets in a sidewall levitation configuration with the vehicle SC magnet levitated between them as shown in fig. 6. The frame also supports a load and displacement measurement system. The space between the two outer SC magnets was adjustable so the gap between the ends of the vehicle and sidewall SC magnets could be varied over a range of 0 to 200mm.

Fig. 7 shows the circular configuration and size of one of these large SC circuits and cryostat assemblies [5]. The coil is off center near the bottom of the cryostat and centered on the off center hole shown in fig. 7, while the helium and nitrogen reservoirs are near the top. The SC magnets were precooled to liquid nitrogen temperatures and then to liquid hydrogen temperatures in a two step process. Detachable input current terminals permit a maximum DC current of 300A which produces a maximum vertical magnetic force of 1200kg.

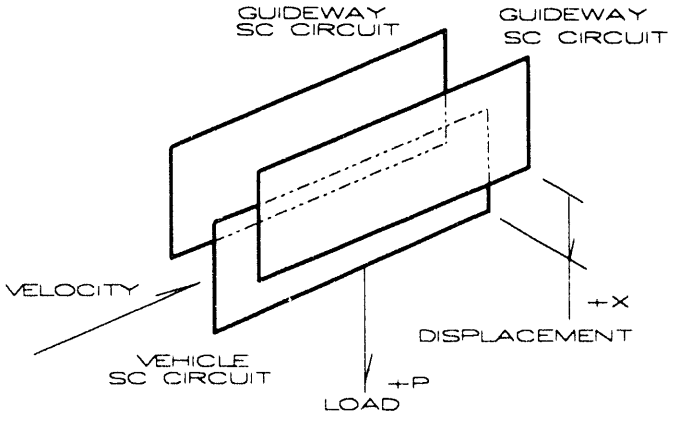

Fig. 5 Coordinate system for the case of a free vehicle with roof mounted rectangular superconducting circuit, magnetically suspended in a gravity field in the equilibrium position, below a sidewall guideway consisting of two SC circuits, Kozoriz [1-5].

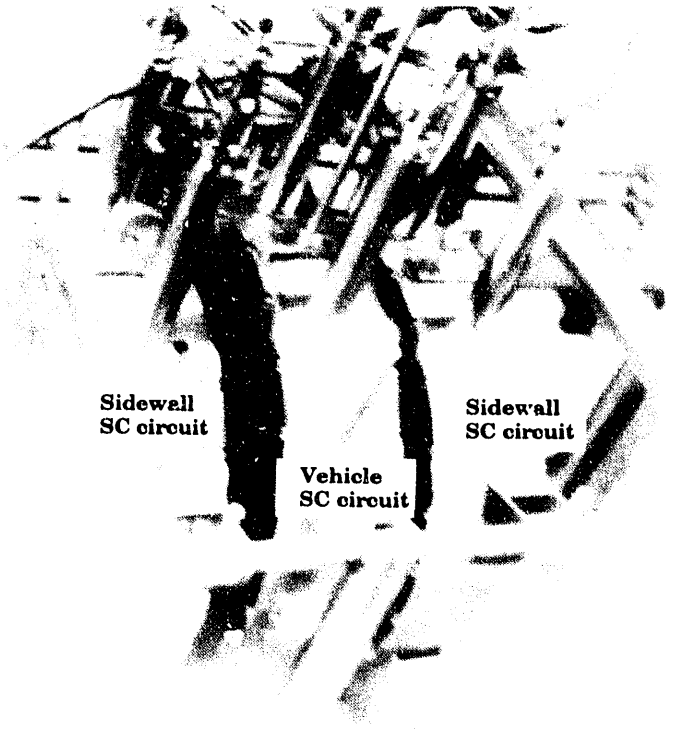

Fig. 6 Configuration of three 600mm OD SC coils in sidewall magnetic levitation experiment viewed from top of the assembled test setup [5].

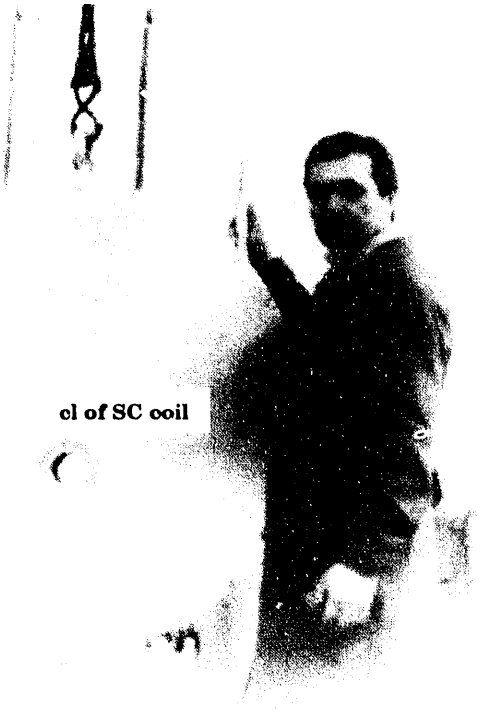

Fig. 7 Side view of typical cryostat encloses one of the 600mm OD SC coils for three coil sidewall magnetic levitation experiments [5].

VII. MPW Maglev Power and Energy Requirements

Evaluation of a hypothetical MPW maglev transit system, based on the mathematical model and transit cycles defined in reference [46], and design parameter assumptions in table I and table II, produced the power requirements, energy consumption, and energy cost results summarized in table III. Energy and power are referenced to the maglev vehicle/guideway. Thus the energy input to the guideway will be larger, depending on a guideway to vehicle percent efficiency assumption.

Table I -MPW parameters for stable equilibrium suspension in gravity field, vehicle with mean effective mass one mton/m car length, one SC coil per meter

Description of Item	Parameters
Mean effective vehicle Mass	$1x10^3$kg/m
Spacing of two-wire dc line	2m
Side of square SC circuit	2m
SC circuits/meter of car length	1 coil/m
Equilibrium levitation gap, static/dynamic	0.5m
Center of mass vehicle-plane SC circuit	2m
Current I_1 in SC circuit	$30x10^3$ A
Current I_2 in two-wire line	$200x10^3$ A
Magnetic linkage Ψ_1SC circuit	0.48 Weber

Table II summarizes MPW maglev vehicle parameters assumed for the power and energy cost models [46] defined in the following paragraphs:

Table II - MPW Maglev Transit Vehicle Design Assumptions to evaluate system performance based on the mathematical model and transit schedules defined in [46]

Description of Item	Parameters
Aerodynamic drag coefficient [47,49] C_d	0.244
Air density, kg/cumeter	1.29 kg/cum
Vehicle frontal area A in sqm	7 sqm
Mean effective vehicle mass, kg/meter	1000 kg/m
Vehicle overall length, meters	25m
Magnetic lift/magnetic drag ratio FL/FD	500
Electric energy cost, $/kW-h	0.1 $/kWh
Efficiency η_1 guideway input to linear motor	0.90
Efficiency η_2 regenerative braking system	0.85

As an example, assuming guideway to vehicle efficiency of 90% for a suburban cycle [46] in table III, aerodynamic and magdrag energy requirements would require a total energy input to the guideway of 1375 kWh, to provide the 1238 kWh, aero 1224 kWh plus magdrag 13.6 kWh, for vehicle cruise at 720 km/h, or 200 m/s. Also, additional energy is necessary for magnetic levitation. This consists of a one time initial energy charge to the SC circuits, plus the continuous power for the refrigeration system to maintain SC coil cryostat equilibrium temperature, which can be sized at about 2 kW/W heat leak rate. The RTRI SC system reports [22,27] a cryostat heat leak rate of 4 Watts/SC circuit, and requires a heat pump rated at 8 kW per SC cryostat.

Table III Energy-power-energy costs for hypothetical MPW maglev transit system, referenced to 25 mton single vehicle

Energy Requirements:			a=4 m/s^2 E1 η_1 = 0.90		
Transit Cycle Type	Total Aero kW-h	Total MagDrag kW-h	Total Accel kW-h	Energy kW-h	Energy Cost $/100km
Urban	30.6	1.36	36.8	76	55.63
Suburban	1224	13.6	170	1565	136.05
Ratios	40	10	5	5	2.5

Power Requirements:					a=4 m/s^2
Transit Cycle Type	Cruise Speed km/h	Cruise Aero Power kW	Cruise MagDrg Power kW	Cruise Total Power kW	Accel Peak Power kW
Urban	360	1102	49	1151	11200
Suburban	720	8813	98	8911	28900
Ratios	2	8	2	8	2.6

Table IV - Energy Recovery with Regenerative Braking

η_2 = 0.85 overall efficiency of regeneration system

Description of Item	Suburban cycle	Urban cycle
E_1 Energy input w/o regeneration, kWh	1565	76
E_2 Regenerated energy returned to guideway, kWh	100	27
Percent energy recovered %	6%	36%

As examples, urban cycle [46] power requirements, at cruising speed 360 km/h, 100 m/s: cruise power of 1102 kW to overcome aerodynamic drag, and 49 kW to overcome magnetic drag. Thus, the total steady state cruise power is 1151 kW, while the peak power needed to accelerate at 4 m/s^2, from standstill to the cruising velocity of 360 km/h, is 11200 kW. For the higher speed suburban cycle [46] power requirements at velocity 720 km/h, 200 m/s are: total steady state power of 8911 kW, and peak acceleration power of 28900 kW.

Table IV compares the energy consumption with and without regeneration [46] and percent energy saved for the transit system, at the assumed 85% regenerative braking efficiency. As an example, in table IV, energy saved over the suburban transit schedule is about 6% with regeneration, and the urban schedule about 36% with regeneration. As expected, regeneration is most effective and essential for a transit schedule with frequent stops and short trips.

The peak acceleration power of 28900 kW in table III suggests a constant acceleration level of 4 m/s^2 from 0 to 200 m/s may be unreasonable. Since maximum guideway tractive force is current limited, more practical guideway power characteristics are: a constant tractive

force of 105000 Newtons from 0 to 100 m/s; and a constant peak power of 14000 kW from 101 to 200 m/s.

Table V shows the acceleration times and acceleration levels obtainable with these assumptions: As examples, acceleration level is about 4 m/s^2 from 0 to 100 m/s vehicle speed, and decreases progressively to about 1 m/s^2 as speed approaches 200 m/s. Furthermore, 0 to 100 m/s acceleration time is still reasonable at 25 seconds and acceleration to 200 m/s is an acceptable 77 s.

Gradeability from standstill on a 30% grade, 30m/100m, capable of accelerating to 100 m/s in 98 s. On a 5% grade, capable of accelerating to 200 m/s in 108 s. On a 5% grade with 50 m/s headwind, capable of accelerating to 200 m/s in 112 s. On a 8% grade with 50 m/s headwind, capable of accelerating to 200 m/s in 181 s. On a 7% grade, accelerates to 200 m/s in 137 s, and on a 8% grade in 167 s.

Table V MPW vehicle acceleration performance as a function of linear traction motor characteristics assumed:
0 to 100m/s tractive force limit = 105 kN, 120 to 200m/s peak power limit = 14000 kW

Speed km/h	Speed m/s	Force kN	Power kW	0%Grade Accel time s	0%Grade Accel m/s^2	7%Grade Accel m/s^2
76	20	105	2100	5	4.2	3.5
216	60	105	6300	15	4.0	3.3
360	100	105	10500	25	3.7	3.1
504	140	100	14000	37	3.1	2.4
576	160	88	14000	45	2.4	1.7
760	200	70	14000	77	1.0	0.3

VIII. Conclusions and Recommendations

1) The MPW maglev concept hypothesized by Kozoriz is a speculation based on the magnetic attraction and repulsion force vs levitation distance characteristics observed experimentally, with a classic magnetic physics laboratory scale apparatus consisting of two superconducting coils in a coaxial configuration, fig. 1.

2) Furthermore, the MPW linear motor acceleration and deceleration concepts were also hypothesized from the magnetic force characteristics obtained experimentally, by manually displacing the internal SC coil at a small velocity V after interrupting the internal SC coil I_1 current path, with a thermal persistent switch, which permitted the SC coil current to be charged at the start of the experiment. As a caveat, this conclusion was inferred from the author's observations of experimental procedures during the MPW experimental demonstration by Kozoriz in Kiev. Kozoriz declined to confirm and/or deny this highly speculative conclusion.

3) This MPW concept consisting of coaxial SC circuits has the unique feature of maintaining magnetic levitation at zero vehicle velocity, and, therefore it does not require a powered acceleration to a lift off velocity, as is the case with the RTRI EDR SC system [22-27]. However, it is not self evident that practical SC circuits configured as shown in fig. 5 will exhibit the same attraction force vs levitation gap characteristics as a coaxial configuration. Although, it appears reasonable to expect that a configuration similar to the RTRI EDR sidewall levitation system reported by Tanaka [27], can levitate at zero velocity when the passive sidewall levitation coils are electrified, instead of relying on electromagnetic induction due to dynamic vehicle motion.

4) Furthermore, the estimate of a low vehicle drag characteristic, and resulting high ratios of (magnetic lift)/(aerodynamic drag plus magnetic drag) is based on the assumption that the maglev vehicle consists of a single car, rather than a series of cars linked together; and also the fact that the MPW magnetic lift does not depend on powered forward vehicle motion. Therefore, the SC MPW concept seems to offer promises that need to be demonstrated by additional tests, aimed at reducing the MPW concept to a more practical form.

5) The future potential of the MPW maglev and LSM propulsion concepts will be determined by the success in transforming this physics laboratory experimental MPW apparatus into more practical maglev and LSM configurations. Furthermore, it is necessary to demonstrate the ability to interrupt the high current levels of a SC circuit with an inductive magnetic flux switch, or some other unspecified method: and inductively transfer the magnetic potential energy to the stationary SC LSM circuits in practical time intervals.

6) As a caveat, convincing experimental evidence has not yet been disclosed to warrant a definitive conclusion that MPW is or is not a candidate as a third maglev concept option, at this point in time.

Acknowledgment

The author acknowledges the contributions made by Dr Tish C Wang, Director of Research and Development, Taiwan Power Company, Taipei ROC, Dr V V Kozoriz, VM Glushkov Inst of Cybernetics, Academy of Sciences of the Ukraine, Kiev; George Korol Ford Motor Company, Troy MI USA; see also Laithwait's Magnetic River [6] referred to our attention by Dr Howard Coffey of Argonne National Lab, Chicago IL USA.

References

[1] VV Kozoriz, *"O Potentsialnoi Yamo Magnetnogo Vzaimodeistviya Idealnykh Tokovykh Konturov"* Dok lAHUSSR, serA1976 n3 pp 248

[2] Kozoriz VV, Mikhalevich VS, *"Stabilizatsiya RavnovesiyaSvobod nogo Tela Magnitnymi Silami"* Problemy Mash chinostroeniya i NadeshchnostiMashchin1990 n6 p12-18.

[3] VV Kozoriz, H Kozoriz, K Gishchak, *'New Principle of Maglev and Traction Underlying Transportation'*, VM Glushkov Inst of Cybernetics, Academy of Sciences of the Ukrainian SAE FTT Conference, SAE #911625, 5-8 Aug 1991, Portland OR.

[4] VS Mikhalevich, VV Kozoriz, VP Shablij, *'Magnetic Levitation Based on: Magnetic Potential Well (MPW) Effect'*, VM Glushkov Inst of Cybernetics, Academy of Sciences of the Ukrainian SSR, SAE FTT Conference, #911626, 5-8 Aug1991, Portland OR.

[5] VV Kozoriz, *'Experimental Studies of MPW levitation Rectangular Coils at 500 to 1500 kg Mass'*, SAE #21588, FTT Conference Costa Mesa CA 10-13Aug1992

[6] ER Laithwaite, *'Transport Without Wheels'*, Pub 1977 USA Westview Press Inc, *'Magnetic River'* sect pp 294-297.

[7] *'National Energy Strategy-Powerful Ideas for America'*, 1st ed 1991/1992, Feb 1991, National Technical Info Service, USDept of Commerce, Washington DC

[8] *'GM Impact Electric Vehicle'*, Impact Techhighlights GM Tech Center, Warren MI, Technical Information Release Dtd 03Jan1990
[9] FA Wyczalek, *'GM Electric Vehicle Technology'*, 24th ISATA-International Symposium on Automotive Technology & Automation, Electric and Hybrid Vehicles, #910605 proceedings pp271-277, Florence Italy 20-24My1991
[10] FA Wyczalek *'GM Electric Vehicle Technology in the 1990's'* IECEC-Intersociety Energy Conversion Engrg Conf#910825 BostonMA4-9Aug1991
[11] Press Release of Technical highlights of Nissan Electric Vehicle Development Aspects of *'1992 Nissan-FEV Future Electric Vehicle, NiCd Battery Electric'*, 29th Tokyo Motor Show, Makuhari Messe Japan 23 Oct-08 Nov 1991.
[12] GE Habercom Jr, *'Tracked Air Cushion Vehicles and Magnetic Levitation-Vol 2, 1976Fe-1979'*, 81 abstracts from the Engineering Index Data Base, Ap1979, 87 p, NTIS.
[13] GE Habercom Jr, *'Tracked Air Cushion Vehicles and Magnetic Levitation-Vol 1, 1970-1975'*, 212 abstracts from the Engineering Index Data Base, Ap1979, 220 p, NTIS.
[14] *'Conceptual Design and Analysis of the Tracked Magnetically Levitated Vehicle Program (TMLV)-Repulsive Scheme: Executive Summary'*, Ford Motor Co, Aeronutronic Div, Feb 1975, Final Report 22p.
[15] *'Tenth and Final Report on High Speed Ground Transportation Act of 1965* FedRailrdAdmOff of R&D, WashDC My1977 400 reports
[16] FA Wyczalek, *'Magnetic Levitation Transporation Strategy Options'*, Proceedings 24th Intersociety Energy Conversion Engineering Conf, Washington DC, 06-11 Aug 1989, #899505 v5 pp2479-83.
[17] FA Wyczalek, *"A National Vision for Maglev Transit in America"*, SAEFTTConf SP-834 901482, pp85-90, San Diego CA, Aug 1990.
[18] FA Wyczalek, *"High Speed Guided Transit Policy in United States of America"*, EVS-10 Int'l Electric Vehicle Symposium, Hong Kong, Proc pp980-988, 03-05 Dec 1990.
[19] FA Wyczalek, *"Maglev Transit in America and US National Energy Strategy* SAEFTT Conf, # 911627, Portland OR, 05-07 Aug 1991.
[20] Gottzein E, Rogg D,*'Status of High Speed Maglev Train Development Federal Republic of Germany'*MechEngrg London 1984 p23-36.
[21] WW Dickhart,III, *'The Transrapid MagLev System'*, Transrapid Inter'nl,SAEFTT Vancouver SP-792 #891714 pp13-22, 7-10Aug1989.
[22] Y Kyotani, T Ohtsuka *'Superconducting Levitated High Speed Ground Transportation In Japan'*RTRIJapanRalwyEngrgv13n4 1972.
[23] H Tanaka *'Present Conditions of Maglev Test in JNR'* Railrd Techogy Res Inst, Japanese Railway Engrg, n96 Dec 1985 p8-11.
[24] H Tanaka, *'Application of SC Magnets to Levitated Vehicles'*, Dep Dir, RTRI, Jr JSME v91 n835 Ju 1988 p36-39 Nihongo.
[25] H Takeda, *'Japanese Superconducting MagLev: Present State and Future Prospects 1989'*, Railroad Tech Res Institute, Japan, SAE FTT Conf Vancouver SP-792 SAE# 891718 pp57 62, 07-10 Aug 1989.
[26] H Takeda,*'Development of Superconducting Maglev in Japan: Present State & Future Perspective'*RTRI SAE FTTConf San Diego SP-834 #901482 pp55-60 13Aug1990.
[27] H Tanaka, *'Japan Railway's Superconductive Maglev System'* RTRI SAE FTT panel, unpublished, Costa Mesa CA 10-13 Aug 1992
[28] A Hayashi, A Ohishi*'HSST MagLev Train at Yokohama Expo'89'* HSST Corp SAEFTT Vancouver SP792 #891715 pp23-32 10Aug1989.
[29] FA Wyczalek, A Ohishi*'HSST Maglev Trains Past, Present and Future'* SAEFTTSanDiegoCA SP-834#901481 pp79-8413-16Aug1990.
[30] FA Wyczalek, A Ohishi,*'Test Demonstration of HSST-100 Maglev Train'*, SAEFTT Portland OR SAE#911623 05-076 Aug 1991.
[31] HT Coffey, LR Johnson, *'Markets for MAGLEV Technology When Integrated into Airport/Airline Operations'*, Center for Transportation Research, Argonne National Lab, SAE FTT Conf Vancouver SP-792 SAE#891717 pp43-55, 06-10 Aug 1989.
[32] *"Benefits of magnetically Levitated High Speed Transportation for the United States"*, Report to the US Senate Committee on Environment and Public Works, Maglev Technology Advisory Comm, Grumman Corp Bethpage NY
[33] R Gran, *'Benefits of Magnetically Levitated High Speed Transportation for the United States'*, Grumman Aerospace Corp, SAE FTT Conf San Diego SP-834 SAE#901475 pp01-10, 13-16 Aug 1990.
[34] M Proise, *'Establishing the Best Magnetically Levitated High Speed Transportation System for the United States'*, Grumman Aerospace Corp, SAE FTT Conf San Diego SP-834 SAE #901476 pp11-20, 13-16 Aug 1990.
[35] T Lynch, *'Energy, Environmental, and Economic Benefits of Florida's High Speed and MagLev Systems Proposals'*, Florida High Speed Rail Commission, SAE FTT Conf San Diego SP-834 SAE# 901477 pp21-54, 13-16 Aug 1990.
[36] RD Thornton, *'MonoRail MagLev'*, Mass Inst of Tech, SAE FTT Conf San Diego SP-834 SAE# 901479 pp00-00, 13-16 Aug 1990.
[37] *'Moving America-New Directions, New Opportunities, A Statement of Natl Transp Policy Strategies for Action'*,US DOT Feb 1990.
[38] *'National Transportation Strategic Planning Study'* US Department of Transportation, Mar 1990.
(39) *Request for Proposal 65P760 for: A Report Identifying New Technology Options for Transit in California with Recommendations for State Initiatives'*, Department of Transportation, Div of Adm Services, 01 Apr 1991.
[40] *'LAX/Palmdale Advanced Technology Demonstration Project'*-Request for Info/Qualifications (RFIQ) LosAngeles Trans Comm (LACTC) 08Mar1991
[41] CALTRANS, *'Transportation Technology Development for California: Program and Policy Review'*, Executive summary report, California Department of Transportation, Office of New Technology and Research Management January 1991, pp1-110.
[42] *'Intermodal Surface Transportation Efficiency Act of 1991 - ISTEA"* Public Law 102-240-18 Dec 1991, 102nd Congress, An Act of.
[43] *'NMI-National Maglev Initiative, Notes'* Transportation bill funds maglev R&D, USDOT, Fed Railroad Adm, USDOE, US Army Corps of Engrs. n2Jan1992 Special Issue.
[44] *'National Maglev Initiative Annual Report 1991'*, Nov 1991, US DOT, US Dept of Commerce printing Office, Washington DC.
[45] FW Sears, MW Zemansky, *'University Physics'*, 2nd ed, Chap33 Magnetic Field Current/Moving Charge pp586-600 AddisonWesleyPb
[46] FA Wyczalek, TC Wang, *'Regenerative Braking Concepts for Electric Vehicles-A Primer'*, 25th ISATA-Int'l Symposium on Automotive Technology & Automation, Zero Emission Vehicles, #920248 Florence Italy 01-05Ju1992
[47] *Marks handbook 4th ed* air viscosity p2-4 Aeronautics p1544 ref NACA TN 614 streamline forms best CD = 0.04 at RN = 10^6 to 10^8 for velocity = 10m/s to 1000m/s at L/D ratio greater than 5 to 1.
[48] RL Spyker, EJ Ruckstadter,*'Reluctance motor employing superconducting magnetic flux switches'*, proceedings 27th Intersociety Energy Conversion Engineering Conf, 929377, San Diego, Aug 1992
[49] T Barrows *'Aerodynamic Forces on Maglev Vehicles'*, Draper Laboratory, Nat'l Maglev Initiative 2nd BAA/SCD symposium, Argonne Nat'l Laboratory, Argonne IL, 7-9 Apr1992.

THE ORGANIC GUIDEWAY CONCEPT

Timothy M. Barrows
Draper Laboratory
Cambridge, Massachusetts 02139

Abstract - A concept is presented for a guideway which can be built in stages. The first stage, for low traffic densities, is a simple concrete structure which avoids the need for propulsion or suspension conductors on the guideway. The cost of this stage is about half that of a typical complete maglev guideway. Later stages add more elements which increase the capacity of the system. In this way the most expensive parts of the guideway are not built unless and until they are needed.

I. Introduction

The organic guideway concept is a system which can start out from very modest beginnings and grow by incremental stages into a full-fledged maglev system. Each incremental stage increases the capacity. In other words, the system can be purchased "by the yard", i.e. an incremental amount of capital can be used to produce an incremental improvement in transportation service.

There is a strong emphasis in this concept on integration with our existing highway network. The stage 1 concept is shown in Figures 1 and 2. These show a vehicle which uses aerodynamic lift at high speeds and ordinary rubber tires at low speeds. Propulsion is by gas turbine, which is capable of either driving a ducted fan or driving the wheels through a transmission. For high speeds, the vehicle must travel in a guideway. At low speeds, however, it can travel in designated lanes of a highway. The general idea is to use the highways for pickup and distribution of passengers over a wide area, and to use the guideway as a high-speed trunk line. The vehicle amounts to little more than an oversize bus. Therefor, minimal changes are required to a highway lane in order to accommodate such vehicles. It would not be necessary to exclude private automobiles from such lanes. The most significant changes would be some widening of on-ramps and off-ramps which have small turn radii.

For levels of traffic between about 1000 and 7500 passengers per hour, stage two would be used. This is shown in Fig. 3. The suspension concept remains unchanged. The gas turbine propulsion system has been replaced with a linear synchronous motor. There is a superconducting magnet on the vehicle which serves as the rotor. The guideway winding is located on a central stem in the middle of the channel. This requires a large capital investment, and provides the benefit of lower operating cost per vehicle. The decision to make the crossover between stage one and two would be made in much the same way that railroads decide to electrify a given line -- it's an economic decision based on the projected price of fuel

Manuscript received March 18, 1993. This work was supported in part by the U.S. Department of Transportation under contract DTFR 53-92-C-00003

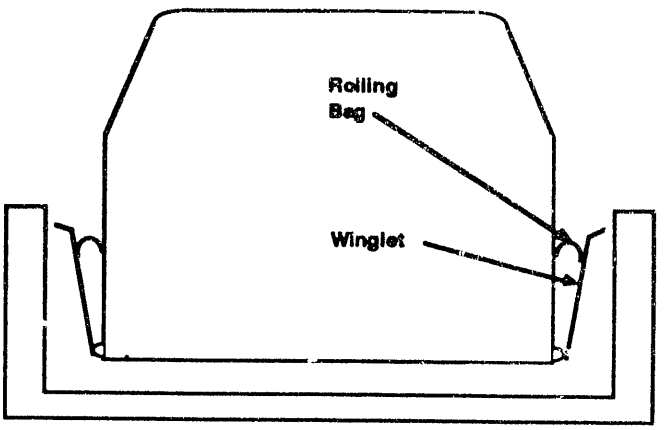

Fig. 1 Stage One Vehicle Cross-section

and whether the traffic is sufficient to justify the investment.

The stage three concept, shown in Fig. 4, is used for traffic above 7500 passengers per hour. It represents the full-fledged maglev system. This traffic level is so high that articulated, multi-car trainsets must be used. Aerodynamic lift is no longer appropriate, for reasons which will be explained below. In order to allow multiple cars in a train, null-flux loops are added to the guidewalls and superconducting lift magnets are added to the vehicles. The central advantage of magnetic lift over aerodynamic lift is that there is no limit to the length of the trainset. For flows of up to 15000 passengers per hour, two-car trainsets would be adequate.

At an early point of development, a network for this organic guideway concept would assume the dendritic structure shown in Fig. 5 (a). Each of the lower stages feeds traffic into the higher stages, thus developing enough traffic to support the overall investment. Stage two guideways feed into the stage three central trunkline, just as the stage one guideways feed the stage two guideways. Existing highways feed into the stage one guideway. The crucial advantage of this concept becomes clear when we examine Fig. 5(b), which shows the same network at a later stage of development. Those parts of the network which have experienced traffic growth would be upgraded to the next higher stage. Thus the network "feels" its way forward, sending out shoots into the traffic market and increasing the capacity of the branch and trunk lines wherever the necessary traffic is found. To go from stage one to stage two it is necessary to add the linear motor windings, substations, and variable frequency wayside inverters. The basic guideway structure remains unchanged. Stage three requires the further addition of null-flux loops, plus some modification of the switches.

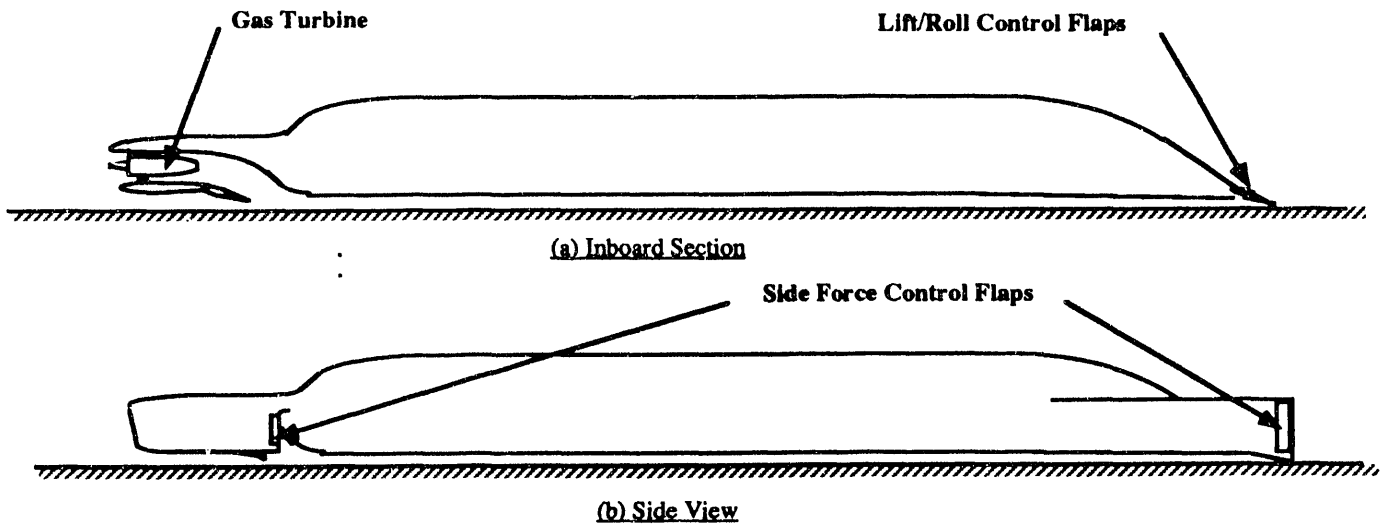

Figure 2 -- Stage one vehicle side views

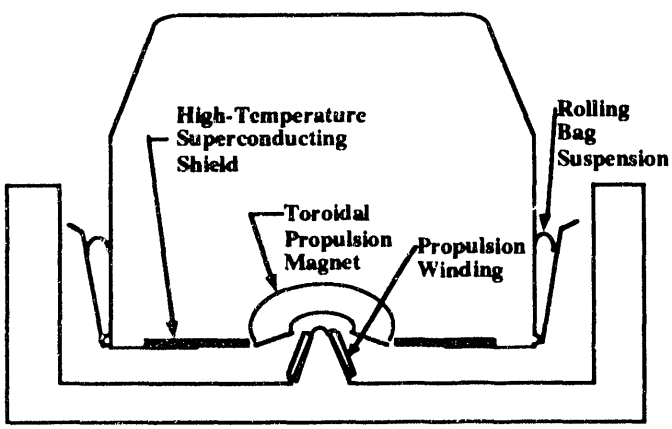

Figure 3 Stage two vehicle cross section

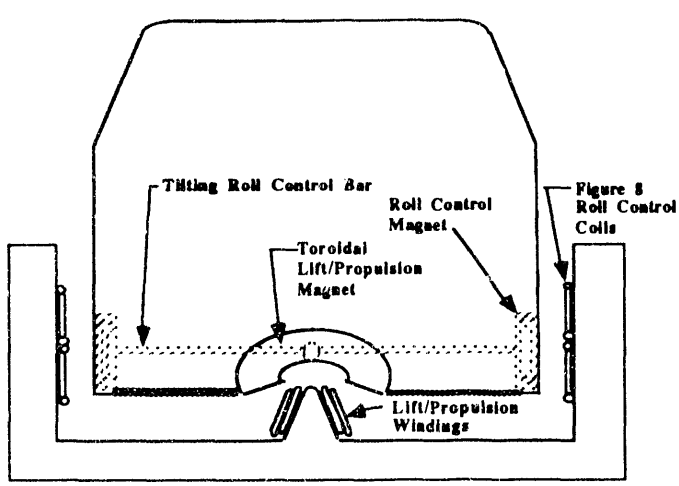

Figure 4 Stage three vehicle cross-section

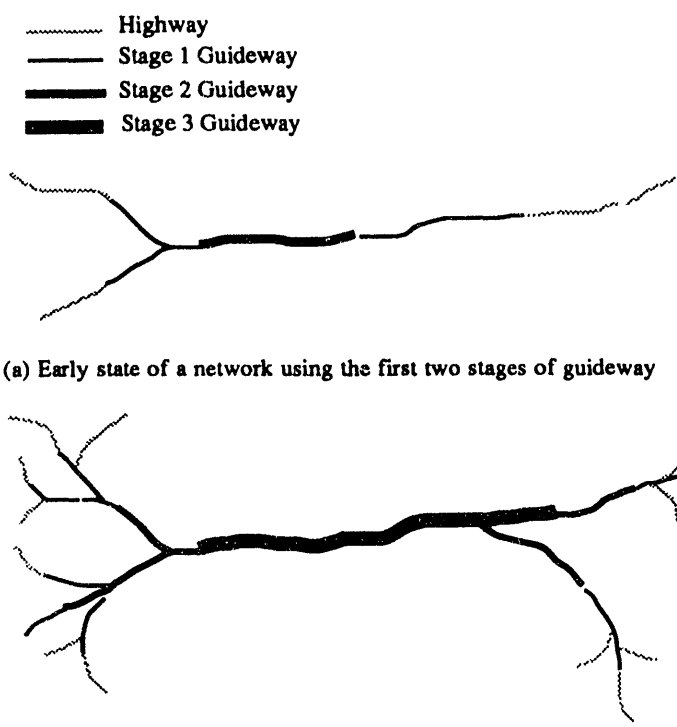

(a) Early state of a network using the first two stages of guideway

(b) Later state showing increased capacity to match increased traffic

Figure 5 Growth Stages of the Network

The rapid transit systems which exist in Europe and to a lesser extent in the U.S. can be cited as examples of such organic growth. In the early part of this century the cities of Europe did not have the large amounts of money which were needed to build such systems. They evolved from trolley lines which became more and more extensive, and as

congestion occurred multi-car trains were used and then the lines were put underground. Indeed, one could say that all existing transportation modes are organic from the standpoint that in their early stages viable systems could be built using relatively small amounts of capital.

The organic guideway concept can result in a truly national system which serves a large range of traffic densities. The emphasis is on building the appropriate system for a given place and time, in such a way that it can evolve as traffic needs change.

II. STAGE ONE DESCRIPTION

In order to begin with the simplest possible guideway, this stage uses aerodynamic suspension and propulsion for operation on the guideway at sufficiently high speeds, and retractable wheels for low speeds. This eliminates the need for some of the most expensive elements: guideway levitation and propulsion windings, substations, and variable frequency wayside inverters. The notion of using aerodynamic lift for suspension of a ground transportation vehicle is fairly well established. In 1974, MITRE Corporation performed a system definition study of the Tracked Ram Air Cushion Vehicle (Ref. 9), which is similar to the present stage one concept. If the flow is confined around the sides of the vehicle, it is not necessary to have wings in order to have an efficient lifting system. Thus in Fig. 1 there is a set of hinged panels, herein called winglets, at the sides of the vehicle whose tips come into close proximity to the guidewalls. These panels partially seal off the pressurized air under the vehicle. Each panel is held in position by a pressurized air bag, which serves as a secondary suspension, in the same way that pressurized air springs are used in most rail passenger cars. The design of these panels is almost identical to that of the French Aerotrain cushions. The major difference is that the French design used air compressors to pressurize both the air bag and the plenum region between the panel and the guideway, whereas the present design uses the dynamic pressure associated with the forward speed of the vehicle, so that no compressors are needed. These lightweight panels only add a negligible amount of weight to the vehicle. There is a similar set of panels under the vehicle which are used in switches (not shown in Fig. 1).

A considerable body of research was conducted at Princeton on the concept of an aerodynamically suspended vehicle traveling in a channel guideway. A theory was developed to predict the forces and moments about all three axes, which led to a detailed model of the longitudinal (heave and pitch) dynamics. Three types of experimental tests were conducted to correlate the theory: wind tunnel tests, tests in which a model was held in a moving carriage, and free-flight tests.

Fig. 2 shows a side view of the vehicle. There is a pair of ducted fans in the front which are each powered by a gas turbine. There are also movable control surfaces in the front and rear of the vehicle which provide control of pitch, yaw, roll, and sway. Table 1 gives a summary of the characteristics of the vehicle. The MITRE vehicle was designed for 100 passengers, whereas the present vehicle carries 75 passengers. Thus some of the numbers in Table 1 were derived by taking the corresponding number of the MITRE vehicle and multiplying them by a reduction factor. This reduction factor was somewhat greater (i.e. less reduction) than the ratio of passengers (75/100 = 75 percent) since some of the vehicle elements do not scale with the number of passengers.

TABLE 1
Data Summary for the Stage One Concept,
Based on the MITRE Tracked Ram Air Cushion Vehicle,
75 Passenger, Fluid Propelled Concept

Dimensions	
Vehicle:	
Length	29 m
Width	3984 mm (between winglet tips)
Height	3 m
Guideway:	
Inside Width	4 m
Height (levitation to surface to top of side wall)	1.5 m
Weight	
Net vehicle weight	23,000 kg
Passengers, crew & baggage	8,000
Fuel	3,000
Gross vehicle weight	34,000
Propulsion Means (Fluid Momentum):	
Two Fans: 1.4 m. dia.	
Prime Mover: aircraft-type turboprop gas turbines, 3000 shp (22.5 MW) each	
Performance	
Cruise speed	134 m/s
Reserve thrust at cruise	5,000 N (1.5% grade)
Maximum static thrust	42,000 N (.135 g's initial acceleration)
Cruise thrust shaft power	3.4 MW
Energy requirement at cruise	2000 Btu/seat mile
Suspension	
Average cushion gap at cruise	38 cm (15 in.)
Average winglet gap at cruise	8 mm (0.3 in.)
Vertical stroke (based on realistic acceleration limits)	±10 cm (4.0 in.)
• Body	±4 mm (0.17 in)
• Winglet	
Noise	
As shown in Figure 2 with a muffled fan and gas turbine	106 db(A) at 50 ft., 300 mph
With maximum acoustic treatment of vehicle and guideway	95 db(a) at 50 ft., 300 mph

There is a large average gap between the vehicle and the guideway, which will greatly alleviate problems of snow and debris Maintenance vehicles are used to periodically clear the guideway of objects which are small enough to be thrown by people or blown by the wind. The large average gap allows the vehicle to pass over such objects unharmed. It is assumed that the majority of guideway will be elevated so that the possibility of larger objects getting onto the guideway is negligible. For those sections of guideway which are not elevated, special provisions must be made to detect or prevent such intrusions.

Switching and banking of the vehicle in turns on the guideway are done in the same manner as described below for the stage two concept.

The question might be raised as to whether it makes sense to have people begin their trip at 55 or 60 mph using stage one vehicles rather than having them use an ordinary bus and change vehicles before getting on the guideway. This question can be answered with another question: "how many people ride to the airport in a bus?" The fact is that almost every ride to an airport takes place in a car or taxi. The 75 people who would ride down the highway in a stage one vehicle represent 75 cars or taxis not causing congestion. From a passenger standpoint the stage one concept is vastly preferable, for several reasons. It avoids the delay of transferring vehicles. With a bus, schedule delays or traffic conditions may mean the intended guideway vehicle is missed, whereas if a passenger is aboard his stage one vehicle at the beginning of the trip this is not a problem. Finally, baggage does not have to be transferred from the bus to the guideway vehicle.

There is a problem with any vehicle which carries fuel in tunnels. This problem can be circumvented by specifying that any portion of the system which requires a major tunnel must have magnetic propulsion (i.e. must be either the stage two or stage three guideway) Since tunnels themselves represent a major capital expense, which is only justified in the case of high traffic densities, it is consistent to go to the more expensive version of the guideway anyway. With shorter tunnels, it should be possible to use stage one vehicles. The safety problems are not markedly different from the situation with vehicular traffic, i.e. certain restrictions and special operating procedures may be required.

III. STAGE TWO DESCRIPTION

The stage two vehicle (Fig. 3) has all the elements of the stage one vehicle except for the gas turbines and the ducted fans, which are replaced by a linear synchronous motor. The vehicle magnets use a toroidal flux path, and there is a double-sided stator winding on a stem in the middle of the guideway. Although it is very tempting to avoid the complication of the guideway stem by having a flat, horizontal winding on the bottom of the guideway, the stem offers four major advantages over the flat stator winding:

(1) The toroidal magnets have a compact and intense flux field which falls off very rapidly with distance so that it is easy to shield the passengers from it. This allows the magnets to be extended for almost the entire length of the vehicle, resulting in much greater propulsive efficiency, since almost all the guideway windings under the vehicle are actively producing thrust.

(2) A flat stator winding is not consistent with the strategy for dealing with debris and snow described for the stage one vehicle. With the stem design, there is a large area at the bottom of the guideway in which debris can sit harmlessly until a maintenance vehicle has a chance to remove it. Snow can accumulate to a depth at which it is easily removed. Many practical problems are foreseen with the flat stator concept, especially under icing conditions.

(3) The stem is the only part of the guideway which experiences high levels of magnetic flux. This allows the use of reinforcing steel at the outside regions of the floor of the guideway, and only requires the use of non-conducting, non-magnetic reinforcement in the immediate vicinity of the stem.

(4) The vehicle can bank relative to the guideway while maintaining a small magnetic airgap for the propulsion system.

In order to obtain a greater insight into the advantage of the toroidal magnet, the reader is referred to Fig. 6, which shows a magnetic field which is enclosed between two conducting sheets. The current flows into the page for the inner sheet and out of the page for the outer sheet. It is possible to arrange the distribution of current so as to prevent any leakage of flux beyond the outer ellipse, i.e. no external field. When the magnetic field is not completely enclosed but has an opening at the bottom as in Fig. 3, some flux leaks out. Fig. 3 shows how the passengers will be shielded from this flux. There is a high-temperature superconducting shield on either side of the toroidal magnet which essentially blocks most of the flux which would otherwise leak around the outside of the torus. This has the added benefit of increasing the flux passing through the stator coils, thus increasing the propulsive efficiency.

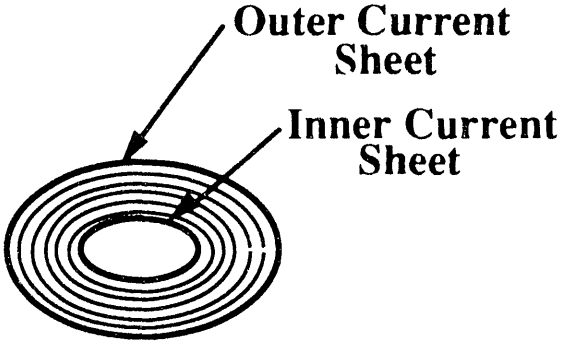

Figure 6 Currents can be distributed around a closed path in such a way as to contain the flux to the interior region

Fig. 7 shows the vehicle at high speed in a banked turn. The vehicle sits higher in the guideway in these curved portions so as to maintain at least a six inch clearance at all points where debris might be found on the guideway. In order to accommodate this extra height, there are short extensions on the guidewalls, and the linear motor stator on the guideway is higher. The vehicle tilts about a point just above the top of the stem so there is no requirement to articulate the toroidal magnets relative to the vehicle.

When the vehicle is stopped or moving slowly the wheels are deployed. In this situation the floor of the vehicle is parallel to the floor of the guideway, so that the maximum unbalanced superelevation is the same as that of the guideway (15 degrees).

Figures 7 illustrates the advantage of having toroidal magnets on the vehicle interacting with a stem on the guideway: the vehicle can tilt and still maintain good magnetic coupling between the vehicle and the guideway. This provides ideal design characteristics. A larger tilt than that shown in the figures is quite possible. Other designs involve some disadvantage. A tilting mechanism, as with the Swedish X-2000, requires an increase in the frontal area of the vehicle plus a heavy mechanism. These drawbacks can be overcome by having a guideway with a rounded bottom, as with the Magneplane design, but this means the vehicle magnets become decoupled from the guideway stator at large tilt angles.

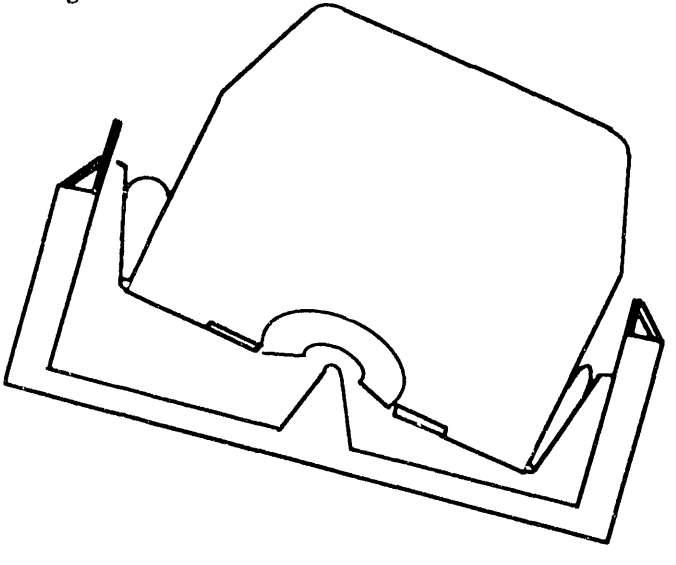

Figure 7 Stage two vehicle at 134 m/s

Low-speed switching is accomplished in the same fashion as is used by conventional wheeled vehicles negotiating a highway off-ramp. The vehicle is simply steered onto the desired branch of the switch. The high speed switching concept is shown in Fig. 8. The entry portions of the switches are covered to prevent debris and snow accumulation and to provide extra protection against crosswinds. There is a set of hinged panels at the bottom of the vehicle (similar to those at the sides of the vehicle) whose tips come into close proximity to the bottom of the guideway. These panels take over the function of sealing off the pressurized air under the vehicle, which is normally done by the hinged panels on the sides. Thus lift can be maintained without the sidewalls. As with the side panels, the bottom panels are held in position by a pressurized air bag, which serves as a secondary suspension, only this time in the vertical direction. The propulsion stem on the guideway must gradually transition into the flattened shape shown. This shape will have a somewhat reduced magnetic coupling which requires thicker stator conductors in the switches in order to maintain the same level of thrust. Fig. 9 shows a view of the switch further down the guideway. The right side of the bottom of the guideway in Fig. 9 is sloped, so that when the vehicle enters the right branch of the switch (the curved branch) it will tilt, thus maintaining passenger comfort in the curve. The lift vector is also tilted, thus helping to pull the vehicle to the right. Once it has started to the right, the vehicle will assume a stable position along the right guidewall as shown in Fig. 9. The overhead covers for the switches are only necessary in the initial portion of the switch, where the average gap is reduced. In these sections, the vehicle may be vulnerable to crosswinds or debris on the guideway (due to the reduced average gap). Once the vehicle is clearly on one path or the other a cover is no longer required.

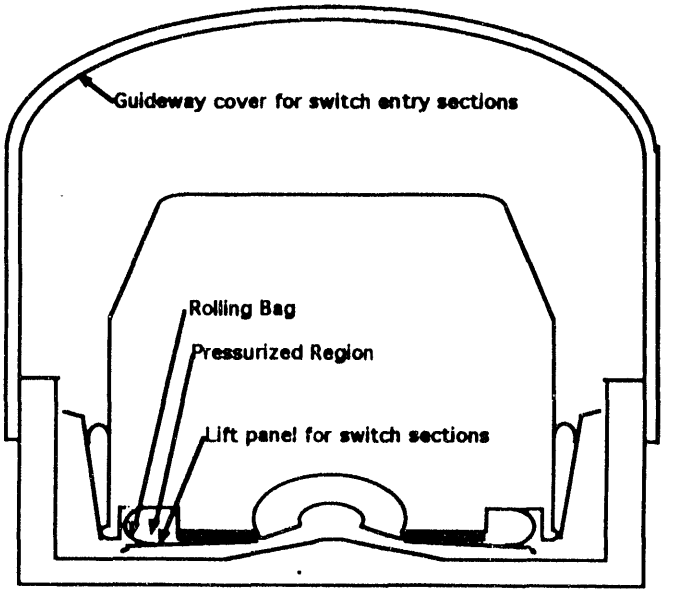

Figure 8 -- Entry section of stage two switch concept

The lateral force necessary to accomplish the actual switching is provided by a pair of deployable speed brakes as shown in Fig. 10. The angle of these speed brake airfoils can be controlled in a symmetric mode or an antisymmetric mode. If they are turned antisymmetrically (i.e. both to the right) they produce a controllable side force. They are turned symmetrically to provide aerodynamic braking. The side force from these deployable airfoils is used to push the vehicle onto the exit branch of the switch (the curved branch,

shown to the right in Fig. 9). It is only necessary to produce a large control force at the front of the vehicle. The vertical flaps at the trailing edge of the vehicle are sufficient to control the position of the aft end, even without the presence of sidewalls. It is not necessary to deploy the airfoils if the vehicle is following the straight path.

There is sufficient average gap between the guideway stator and the superconducting magnet to accommodate mainline curvature. For tighter turns, the guideway stem can be made narrower or lower, as shown in Fig. 9.

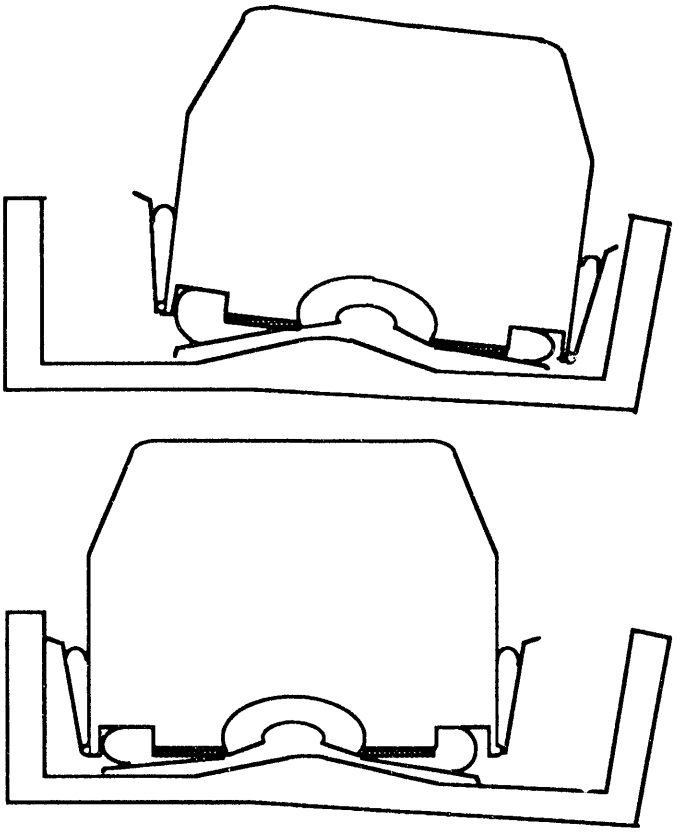

Figure 9 Downstream section of the stage two switch concept

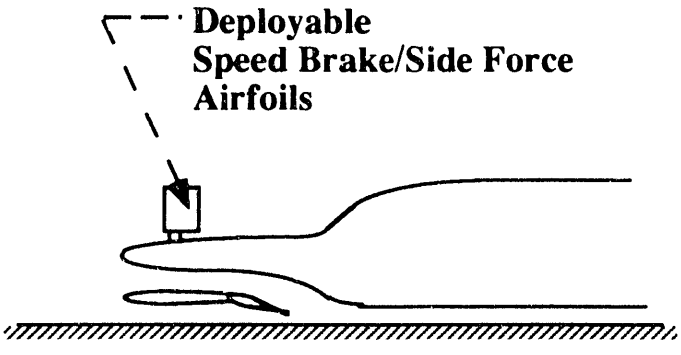

Figure 10 Deployable speed brakes are used to generate guidance forces in switches

IV. STAGE THREE DESCRIPTION

The stage three concept allows multiple-car trainsets. Aerodynamic lift is no longer appropriate, since it is not effective when the length to diameter ratio is greater than about 20. The problem with aerodynamic lift is that for practical reasons the design must allow a small amount of air to leak out between the tips of the winglets and the guideway. There is enough air entering beneath the front of the train for a single car, but not multiple cars. Lift for the stage three vehicle is provided by the addition of levitation coils on the guideway stem (Fig. 4). As with the stage two vehicle, there is a set of toroidal magnets along the centerline of the vehicle, but in the case of stage three they provide lift in addition to propulsion. Because of the fact that the lift acts at the center of the vehicle, it is necessary to add a set of roll control magnets, which interface with null-flux loops on the guidewalls. The null-flux loops have a figure eight configuration, similar to those on the Japanese MLU002 maglev vehicle. There is one pair of roll control magnets at the front of the vehicle and another pair at the rear. Each pair is mounted on a bar which is pivoted at the vehicle centerline. The vehicle can be tilted relative to the bar, thus allowing the vehicle to bank at high speeds in turns. The bar will maintain a fixed position relative to the guideway. The roll control magnets are sufficiently far from the passengers to avoid exposing them to strong fields.

The requirements for guidance forces for this vehicle are small relative to other concepts, due to the protection from crosswinds afforded by the guidewalls. The limited side force which is required can be supplied by a combination of magnetic force from the lift coils and aerodynamic force.

A switch concept for the stage three vehicle has been worked out, but space does not permit a complete description here.

V. SNOW AND ICE REMOVAL

There are drain holes on both sides of the central stem. These take advantage of the heat available from the propulsion windings which can be used to melt ice.

Snow is removed by a combination of low-speed snow removal equipment and special scoops on the passenger vehicles. After the guideway has been idle for some period of time, such as in the early morning, automated snow removal equipment will clear it for the passage of the first vehicle. As more snow falls, it will accumulate in the bottom of the guideway. This does not create any difficulty because of the large average air gap. When there are three or more inches of accumulation, special scoops on the vehicles are deployed. These scoops are small enough to avoid causing excessive drag. The idea is to have each vehicle remove a small portion of the snow and to keep the accumulation below six inches. The scoops have a slip heel which rides on the surface of the snow and thus regulates the depth of snow which is removed. They create a narrow stream which is directed up and over the guidewall.

If there is a period of time during which the number of vehicles per hour is too low to do this effectively, then the

snow removal equipment is again brought in. By limiting the requirement for this equipment in this way, there is minimal disturbance of the high-speed vehicle traffic by the low speed of the snow removal equipment.

VI. FREIGHT TRANSPORTATION

All three stages of the guideway can be used by tractor-trailer trucks during the hours between midnight and 6 am. This concept is shown if Fig. 11. A portion of the resulting savings in delivery cost could be used to help defray the cost of the guideway. This assumes there would be no high-speed passenger vehicles on the line, so the trucks could travel at 60 mph. By taking advantage of the guideway sidewalls, it becomes possible to have several trailers behind one tractor. The tractor-trailer combinations would have to be modified versions of conventional trucks. The tractors would be larger and more powerful. Automatic steering would be used to keep the trucks in the center of the guideway. The trailers would also have provision for automatic steering, and would have solid rubber rollers on the sides in case slippery conditions cause them to slide into the guidewalls. Driver productivity could be increased by a large factor with such long combinations. It is worth noting that the DOT has invested a considerable amount of effort developing automobiles which steer themselves automatically by following a cable buried in the roadway. Automatic vehicle control is one of the long-range goals of the IVHS program. The present concept would be a perfect application of this technology.

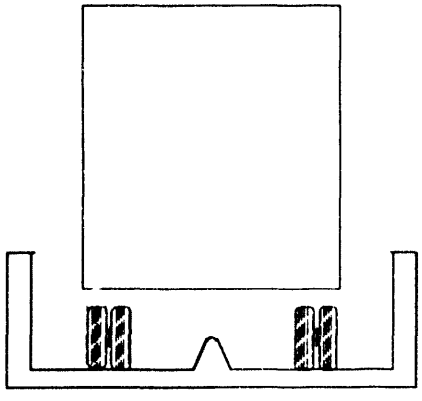

Figure 11 Freight Transportation Concept

VII. GUIDEWAY COSTS

The following cost summary shows that a stage one guideway would cost about half of what a typical maglev system would cost. Costs are $million per mile for a double guideway in flat rural conditions, and do not include sales tax, project management, contingency allowance, or fee, all of which add about 60 percent.

Guideway Structure	12M
Command and Control	1M
Total Stage One Cost	13M
Guideway Propulsion Elements	4M
Levitation/Guidance Coils	3M
Electrification	5M
Total Maglev Guideway Cost	25M

VII. CONCLUSIONS

The conventional view of maglev vehicles is that they represent some kind an advanced, high-speed train. The present concept is quite distinct in that it represents an evolution of our present highway system. It is the most intermodal of all high speed ground transportation concepts. The organic guideway can be seen as a dedicated highway lane for high-productivity trucks and buses. The buses achieve their high productivity in terms of passengers-miles per hour by operating at increased speed. Trucks can achieve higher driver productivity in terms of ton-miles per hour by increasing the amount of tonnage, i.e., by operating longer combinations than are possible on a conventional highway.

REFERENCES

[1]. Aidala, P.V., 'Lateral Stability of a Dynamic Ram Air Cushion Vehicle', U.S. Dept. of Transportation Report No. FRA-ORD&D-75-6, PB236516, 1974.

[2]. Barrows, T.M., 'Fluid, Magnetic, and Mechanical Suspension Concepts for High Speed Ground Transportation', Technology Review, Winter 1975.

[4]. Barrows, T.M., and Widnall, S.E., 'The Aerodynamic of Ram Wing Vehicles for Application to High Speed Ground Transportation', AIAA Paper No. 70-142, Jan. 1970.

[5]. Barrows, T.M., et.al., 'The Use of Aerodynamic Lift for Application to High Speed Ground Transportation', PB 197 242, 1970.

[6]. Boccadoro, Y., 'Towing Tank Tests on a Ram Wing in a Rectangular Guideway', FRA-RT-73-34, (PB 210 743), 1973.

[7]. Curtiss, H.C., and Putman, W.F., 'Experimental Investigation of Aerodynamic Characteristics of a Tracked Ram Air Cushion Vehicle', U.S. Dep't. of Transportation Report No. DOT-TSC-OST-78-1, Jan. 1978.

[8]. Curtiss, H.C., et.al., 'The Aerodynamics of Tracked Ram Air Cushion Vehicles- Effects of Pitch Attitude and Upper Surface Flow', Princeton Univ. MAE Tech. Rept. 1426, also Dep't. of Transportation Report DOT-TSC-RSPA-79-17, 1979.

[9]. Fraize, W.E., and Barrows, T.M., 'The Tracked Ram Air Cushion Vehicle TRACV', MITRE Corp. Report MTR-6554, Nov. 1973. Also FRA-ORD&D-74-27

[[10]. Sweet, L.M., Luhrs, R., and Curtiss, H.C., 'Two-Dimensional Dynamics of Tracked Ram Air Cushion Vehicles with Fixed and Variable Winglets', MAE Dep't., Princeton Univ., 1978-79; and ASME Publication 79-WA/DSC-11.

[11]. Widnall, S.E., and Barrows, T.M., 'An Analytical Solution for Two- and Three- Dimensional Wings in Ground Effect', J. of Fluid Mechanics, vol. 41, p. 769.

Magneplane Vehicle Dynamics Simulation
MAGLEV '93, Argonne National Laboratory, May 19-21, 1993.

Presented by William Aitkenhead, Magneplane International

Abstract

The Magneplane maglev configuration relies upon a trough shaped guideway supporting a vehicle with two saddle shaped arrays of levitation and propulsion magnets. The levitation magnets are tilted 35 deg. with respect to the horizontal plane providing a center of lift in the vehicle above the center of mass.

This paper presents the magnetic and aerodynamic force and moment inputs and disturbance conditions for a 6 degree of freedom vehicle dynamic response model. Ride quality results and control actuator response needs are presented. The vehicle response to a 2" guideway discontinuity is also calculated.

INTRODUCTION

The ongoing discussion of the pros and cons of various configurations for maglev transportation systems seems to center around the cost and benefits for the various methods. While recognizing the importance of estimating system costs and the system utilization that can pay back capital and operational costs, we believe that a more fundamental issue needs to be addressed; that issue being the efficacy of maglev configurations for producing a safe, comfortable ride using achievable construction and assembly methods.

To date the only high speed maglev system to demonstrate a safe and comfortable ride is the German Transrapid. However, the Transrapid does not meet many of the U.S. market imperatives. The capital cost is high; the construction tolerances are high; the allowable guideway deflection is low. The U.S. NMI office sponsored 4 System Concept Definition (SCD) efforts in order to evaluate a number of different schemes vs. the existing Transrapid.

Work sponsored by Army COE contract no. DTFR53-92-C-00006. Dynamics modeling performed by Lincoln Lab. Aerodynamics; James Burnside, Michael Judd, and Charles Haldeman, et al. Magnet analysis by MIT Plasma Fusion Ctr., Bruce Montgomery, Richard Thome, Robert Pillsbury, and Richard Hale, et al. Linear synchronous motor force analysis by Failure Analysis Assoc., Electrical Div., Don Galler, et al.

The US SCD efforts addressed the limitations stated above and have arguably succeeded. However, a clear dynamics discussion of the various maglev configurations is not evident.

A scale Magneplane system was tested in the early 70's demonstrating the critical need for active damping control and the requirement to solve the vehicle dynamics problem in 6 degrees of freedom. For example, the testing program showed a critical coupling between the roll attitude and the propulsion drive that was not solved until the invention of the magnetic keel. Unfortunately model testing at 1/25th scale does not allow proper scaling of the forces acting on the vehicle. In fact, the scale model test was equivalent to operating a full scale vehicle at 1 m/sec.

It is the purpose of this paper to describe the modeling effort that establishes the 6 dimensional behavior of the Magneplane maglev vehicle and shows how this configuration meets the criteria for safe and comfortable ride.

THE MAGNEPLANE CONFIGURATION

The Magneplane maglev configuration relies upon a trough shaped guideway supporting a vehicle with saddle shaped arrays of levitation and propulsion magnets as shown in Fig. 1. The levitation magnets are tilted 35 degrees with respect to the horizontal plane. They provide a center of lift in the vehicle above the center of mass so that the suspension is naturally stable. This configuration also couples lateral and vertical motions.

The Magneplane system uses a .15m (6") levitation gap lowering the natural frequencies for pitch and heave motion to well less than 2 Hz. This suspension has very low natural damping and must be damped by active control of the propulsion system and by aerodynamic control surfaces.

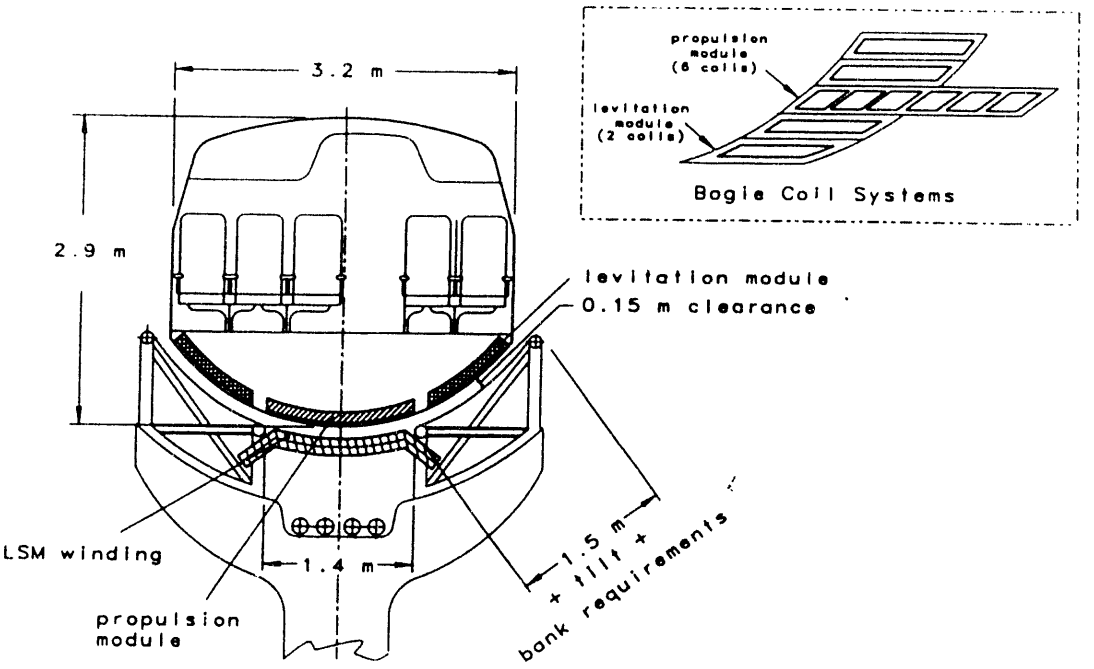

Fig. 1 Vehicle and Guideway Cross Section. Note: typical bogie arrangement.

Because the natural frequencies are low, good damping performance can be demonstrated at control bandwidths that are achievable in these devices. In addition, due to the large gap, the Magneplane suspension is extremely forgiving to large perturbations to the guideway. We have analyzed guideway gaps of up to 2" showing peak accelerations exerted on the vehicle structure of .25g. All of this is accomplished without a secondary suspension. The vehicle natural frequencies are:

TABLE 1
Vehicle Natural Frequencies and Damping

Mode	Frequency (Hz.)	Damping Factor
Heave	1.27	.0077
Pitch	1.46	.025
Sway	0.92	.106
Yaw	1.06	.034
Roll	0.64	.020

Other important properties of the magneplane configuration include:

1. The center of lift is above the center of gravity and is attitude independent. The Magneplane vehicle naturally banks to a coordinated attitude in a curve.
2. Because the Magneplane uses sheet aluminum conductor to generate lift forces, the induced magnetic field generated by the guideway is uniform as the vehicle travels along a span of guideway. Field variations do occur between guideway spans but have been found to have minimal impact on lift and drag.
3. The conductor providing the vehicle support is integrated into the support structure. There is no requirement for lift coil construction, insulation and mounting.

MODEL

The dynamic response and ride-quality simulation is based on the six degree of freedom rigid body equations of motion. The parameters affecting vehicle dynamic response are:

1. Magnetic and aero-dynamic stiffnesses.
2. Active control system characteristics.
3. Mass properties.
4. Magnetic and aero-dynamic passive damping.

The magnetic forces acting on the vehicle are characterized by non-linear springs about equilibrium positions.

Levitation Magnets

For the levitation magnets we write for lift:

$$F_m = F_o\ [h_o/(h_o+h)]^{1.6}$$

where F_m = magnetic lift,
F_o = reference lift force at height h_o and velocity v_o,
h = deviation from h_o.

F_o changes slowly with velocity and is assumed constant for small velocity changes.

The relation for drag is written:

$$D(h,v) = D_o\ [h_o/(h_o+h)]^{1.6} \cdot [v_o/(v_o+v)]^{1/2}$$

where $D(h,v)$ = magnetic drag,
D_o = reference drag at h_o and v_o,
v_o = reference velocity,
v = deviation from v_o.

A lateral force on the levitation magnets vs. proximity to the inner edge of the aluminum sheet is calculated and found to be small with respect to lateral forces acting on the on-board propulsion magnets. The net lateral force on the levitation magnets due to their roll attitude with respect to the guideway is calculated and included in the lateral force state equation.

Propulsion Magnets

The forces on the propulsion magnets include thrust, lift and lateral forces. The thrust is created by the interaction of the propulsion magnets with the LSM windings in the guideway. The magnitude of thrust is a control parameter and varies vs. LSM current and the phase relationship between the LSM current and the on-board propulsion coils.

The LSM current also interacts with the propulsion magnets to produce lift forces. By operating near 0 degree phase angle it is possible to use changes in the phase angle to control the lift with small changes to the thrust.

For both thrust and lift forces a height variation is calculated as:

$$F_m = F_o\ [h_o/(h_o+h)]$$

where F_m = magnetic force,
F_o = reference force,
h_o = reference height,
h = deviation from h_o.

Lateral forces on the propulsion magnets are created by the interaction of the propulsion coils with the LSM and with the edge of the aluminum sheet vs. lateral deviation from center line. These effects have been calculated and modeled as:

$$F_l(y) = Ay^3 + By^2 + Cy$$

where y is the deviation from the center line,
A, B and C are fit to the calculated lateral forces.

Aerodynamic

Other forces acting on the vehicle include aero-dynamic lift and drag on the vehicle body and aero-control surfaces. For the body forces we write:

$$F_{aero}(v) = 1/2\ \rho\ C_d\ S\ (v_o+v)^2$$

where ρ = air density,
C_d = coef of drag or lift, includes induced drag of control surfaces,
S = reference area,
v_o = reference velocity,
v = velocity deviation.

The components of total C_d are: fore body drag, base drag, ground interference, and control surface induced drag.

The aero-dynamic control forces are modelled by lift vs. wind speed and control angle for 5 control axes. We have assumed orthogonal control authority and closed loop controller. Drag forces on control surfaces are assumed to be constant.

Damping

Magnetic and aero-dynamic passive damping factors have been calculated (See Table 1.) and found to be at least an order of magnitude too small to contribute to adequate vehicle damping.

Mass Properties

The mass properties of the vehicle were established using the full layout of the on-board vehicle equipment and passenger load.

Equations of State

The forces acting on the vehicle are written:

F_x = Thrust(vehicle speed, height at each bogie, LSM current and phase angle) - $Drag_{aero}$(vehicle speed, wind gust) - $Drag_{E+M}$(vehicle speed, height at each bogie)

F_z = $Lift_{aero}$(vehicle speed x and z comp., wind gust) + $Lift_{control\ surfaces}$(vehicle speed, control surface angle) + $Lift_{lev.\ magnet}$(height at each bogie) + $Lift_{prop.\ magnet}$(height at each bogie, LSM current and phase angle)

F_y = Side $Force_{aero}$(vehicle side velocity, wind gust) + Side $Force_{control\ surfaces}$(vehicle speed, control surface angle) + Side $Force_{lev.\ mag}$(vehicle attitude, height at each bogie) + Side $Force_{magnetic\ keel}$(height at each bogie, lateral displacement)

Similar expressions are written for the moments. The above equations are supplemented by the relations between the state variables to the center of gravity location and Euler angles and by the kinematic relationships between the individual magnetic gaps and the vehicle position and attitude relative to the guideway. The gap relationships include the effect of guideway misalignments and flexibility.

Control Model

The control method employed for the analysis of the vehicle operation is linear, constant coefficient, full state feedback control using the linear quadratic regulator method. The full non-linear force and moment equations are used to calculate the time varying behavior of the vehicle.

DISTRUBANCES

System excitations and forcing inputs are:

1. Wind gusts and turbulence.
2. Guideway mis-alignments, roughness and flexibility.
3. Virtual forces resulting from accelerations caused by grades and curves.

The gust distribution used is based on the Davenport model:

$nS(n) = 4\ x^2\ u_t^2/(1+x^2)^{4/3}$

where $S(n)$ = gust velocity spectrum,
n = gust frequency,
u_t = friction velocity,
x = $1200\ n/U_{10}$,
U_{10} = 1 hour average wind speed at 10 m,
u' = standard deviation
= $2.5\ u_t$ = $U_{10}/5.7$.

The guideway roughness is treated as filtered white noise with the following spectrum:

$S_{id}(\omega) = A\ u\ /\ \omega^2$

where $S_{id}(\omega)$ = guideway disturbance spectrum,
ω = disturbance angular frequency,
A = 6.1×10^{-8} m (welded rail),
u = vehicle velocity.

The periodic guideway deflection vs. time is modeled as:

$S_d(t) = .5\ a_d \sin(2\ \pi\ u\ t/l_{span})$

where u = vehicle velocity,
a_d = dynamic deflection amplitude of the span,
l_{span} = span length.

The combined guideway disturbance from the above conditions is shown in Fig. 2.

The acceleration demands of following the guideway through various curves and grades have been included in the modeling of the vehicle behavior.

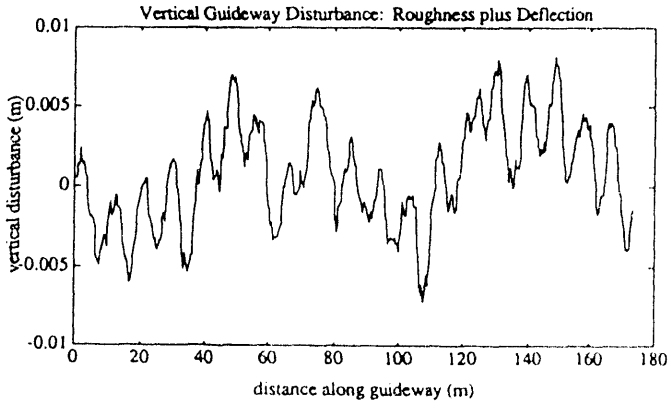

Fig. 2 Combined guideway disturbance.

RESULTS

Summaries of the vehicle response to route segments with the combined disturbances described above are calculated and displayed by the Peplar Index and the 1/3 octave spectral plots. The Peplar ride quality index is shown in Table 2 for various segments of the hypothetical route defined for the SCD study and the required actuator response to achieve the ride quality results. Note that the RMS excursions are well within reasonable limits. Fig. 3 displays the ISO results for a typical segment.

Finally the vehicle response was modeled for a major disruption to the guideway described as a 2" vertical gap in the guideway. The maximum acceleration observed at the vehicle center is .25 g. Accelerations at the ends of the vehicle will be somewhat higher. The large levitation gap enables the vehicle to negotiate a significant guideway disruption with minimum hazard to the passenger.

TABLE 2
Peplar Ride Quality Index and RMS Actuator Values

Severe Seg. Number	1	2	3	4
Ride Quality Index	1.83	1.84	1.82	1.77
LSM Thrust (10^3 N)	34	37	23	3.3
LSM Vert. (10^3 N)	4.0	4.1	3.6	4.5
Aero Vert. (deg.)	9.4	10.2	6.4	1.3
Aero Sway (deg.)	5.1	4.9	5.0	2.6
Aero Pitch (deg.)	10.8	9.8	7.1	3.2
Aero Yaw (deg.)	5.9	5.7	5.8	1.8
Aero Roll (deg.)	10.2	9.1	6.3	3.9

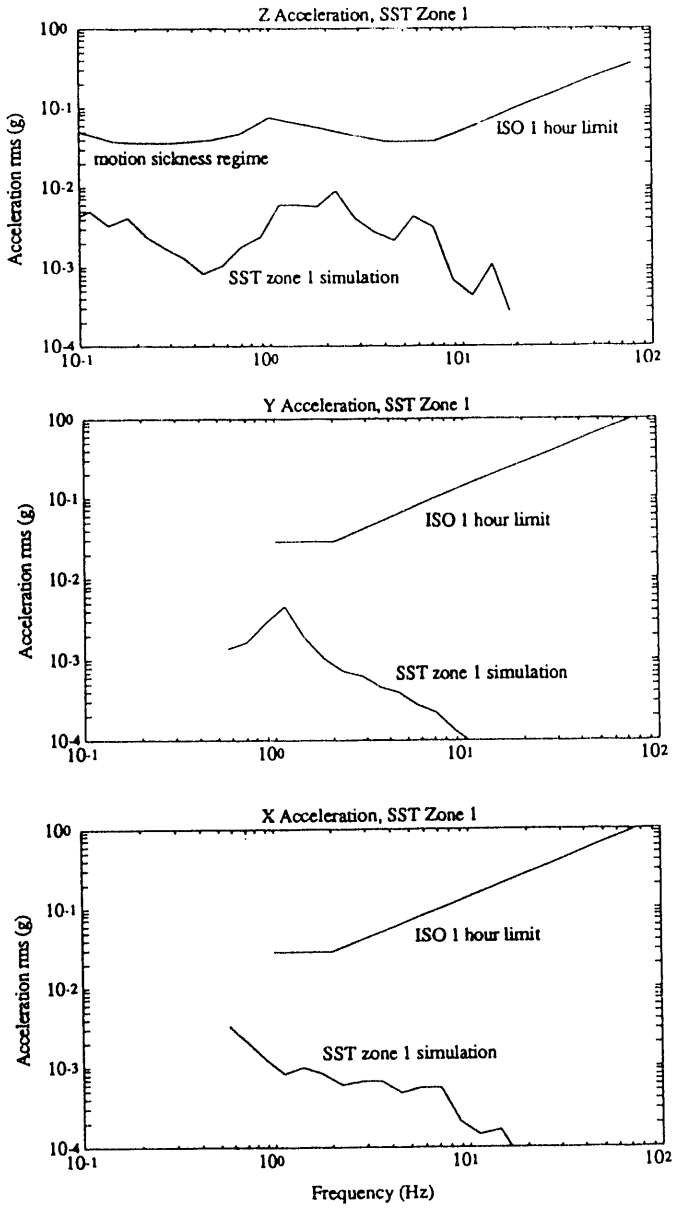

Fig. 3 ISO acceleration plots for segment of hypothetical route.

Technology and Costing Considerations for Full Maglev System Development, As Derived from Bechtel's System Concept Definition Exercise

J. C. Perkowski

Manager, Advanced Civil Systems, Research and Development, Bechtel Corporation
P.O. Box 193965, San Francisco, California
94119-3965

Abstract

The recent NMI-sponsored System Concept Definition exercise provided an opportunity to assess our current design knowledge base and identify technology uncertainties requiring further research during a prototype development stage. Also, through the development of a comprehensive cost estimate of the Bechtel team baseline concept, we were able to determine areas of focus for further work to reduce total systems costs. This presentation will summarize our results in both of these areas (technology and cost estimation) and provide a conceptual approach for how to guide and manage further research efforts as we move towards full prototype development. It will also examine the institutional implications related to cost effective prototype development, with suggestions of alternate approaches to improve chances for successful system implementation.

I. Summary of Bechtel Team Concept

A team of organizations headed by Bechtel completed one of the four maglev System Concept Definition (SCD) exercises recently sponsored by National Maglev Initiative (NMI). Our team concept can be defined as including the following key systems and features:

- A high efficiency electrodynamic suspension system that minimizes energy use and can suspend the vehicle to very low speeds
- A box beam guideway that minimized total structural system cost and environmental impact while providing a high degree of safety and a long service life
- A linear motor propulsion system that provides high acceleration and braking capability and that can also operate effectively at reduced speeds under various possible failure modes
- An automated and fault tolerant control system that allows highly reliable fail-safe operation with short headway and high reliability
- Low speed stop/start capability without requiring a wheel assembly on the vehicle

A typical vehicle/guideway cross section (straight track segment) is shown as Figure 1. Further technical details describing our concept have been presented previously, for example at the January 1993 TRB Annual meeting. Those interested in more information should consult the summary report of the NMI planned for issuance to Congress and the public this spring.

II. Current Concept Cost Estimate

Our overall concept cost estimate is represented in summary form by Table I. This table includes a comparison between our baseline concept costs and costs provided to our team (as well as to the other three System Concept Definition teams) by the NMI staff, based on the document "Maglev Cost Estimation: Capital Cost Elements," January 1992 Interim Report, prepared for the Volpe National Transportation Systems Center. For convenience we have labelled this information as the Government Cost Model, since it was provided as the only Government costing guidelines available during the course of the SCD study. Footnotes to Table I clarify the data and point towards areas requiring further costing study as maglev concepts continue to evolve.

III. Areas of Major Cost Uncertainties

Table II represents our effort at providing a "reduced first cost scenario" for those perceived circumstances where an investor is more interested in minimizing first costs than in any other investment criteria. The single largest line item change is with regards to the guideway electrification subsystem. Although there are few precedents indicating utility interest in assuming the first cost burden for all utility-related components of major transportation installations, it is reasonable to assume that utilities operating in the service region of a maglev system might be induced to join the team during early planning stages and offer a financial arrangement that draws upon their available capital resources rather than that of the maglev system investor. Additional studies are needed to quantify what the possible life-cycle cost premiums would be (if any) from the perspective of the system operator should this arrangement be made. The inclusion of Southern California Edison on the Bechtel team was extremely helpful in identifying and examining at a conceptual level the basis for the proper role of the electric utility in implementing a large infrastructure system of this sort in the real world.

Table II also indicates where less large but still significant improvements might be made in other components of the total system. For example, the Bechtel concept assumed the necessity of including fiberglass

rebar in certain areas of the guideway to minimize magnetic drag penalties and possible rebar degradation that could be associated with the magnetic fields adjacent to the edge of the guideway. Further work during future concept development phases will determine whether this particular cost saving is realistic.

Note that the application of "indirect" costs (comprised, as indicated in Table I, of various management fees, taxes, and contingencies) as a multiplier to "direct" costs means that every dollar saved in the base case estimate actually saves roughly $1.50 from the perspective of the investor. These "indirect" costs have various labels and definitions in the design/construction industry and Table I provides one particular (but not uniformly agreed-upon) means of disaggregating them. However they are defined, there is no doubt that they are real when financial pro-formas are prepared to authorize the design and construction of real systems in the real world. This means that the label of a "$20 million per mile" system is a misnomer if clarification is not provided as to whether indirect charges are included, and could well become a "$30 million per mile" system with the addition of a key footnote. It also means that a "$15 million per mile" system *could* imply a savings of $7.5 million (not $5.0 million) over a "$20 million per mile" system.

IV. Institutional Implications for Prototype Development

The SCD exercise was most useful not only in establishing technical areas of emphasis for prototype work but also in providing us all with a sense of value engineering required at the top-most systems level prior to eventual maglev prototype development. Recall that the SCD was intended as a concept *definition* exercise and that extensive work is programmed as part of the broad ISTEA authorization provisions for further concept *development* prior to construction of a prototype line. This distinction of prototype construction versus concept development versus concept definition is crucial and leads us to suggest the following institutional and administrative procedures that need to be orchestrated now by all of the major players to be involved in further maglev work, in order to optimize in a timely manner the cost-effective implementation of maglev as a prospective major transportation alternative:

- At the most general systems level, a common costing framework with common category labels needs to be established as the mandatory basis for prototype development cost estimation. The framework represented by the data in Table 1 is an adequate starting point since it disaggregates system costs in a meaningful, pragmatic way allowing rapid comparison of key subsystem data.
- Due to the nature of the SCD exercise, it was apparently not possible to provide uniform unit costing data to the SCD teams, and so comparison of SCD costing data between the four SCD teams is not very meaningful. However such unit costing information is essential during the prototype evaluation phase in order to provide a "level playing field" for evaluation of alternate concepts. Common unit costing ranges from the simple (provision of common assumptions for unit material costs) to the complex (provision of piece labor breakdowns for concrete fabrication operations or specialty material operations). It is preferable for the sponsor of further prototype programs to set costing benchmarks in detail and in advance, as far as possible, and allow the contractor to make clearly documented exceptions where appropriate rather than permitting contractors to identify customized procedures claiming elaborate advantages without clearly established comparison to current industry practice.
- True costing of a prototype system must include provision for serving an increased passenger capacity over time, saving first cost investment by not oversizing at the start of operations, provided that further capacity demands can be met through modular additions to the system. For example, as much as one-third of the initial electrification costs of the Bechtel team concept could be avoided by designing initially for a 4,000 passenger-per-hour-per direction system as versus a 12,000 passenger-per-hour-per-direction system. This would be accomplished by downsizing inverter output current, increasing inverter zone length spacing, initially using only a single cable in the DC distribution system and a single transmission line feeder, and reducing the MVA ratings of the transformers and rectifiers.
- It was beyond the scope of the SCD exercise to develop any more than very generic costing for special route segments (bridges et al) that would be a part of any real maglev route (although not necessarily a part of any prototype route). This means that some emphasis must be applied during the concept development phase to indicating whether any special cost penalties apply to a particular technical concept due to its relative inability to adapt to specialized route terrain likely to be found in actual layouts.
- During the upcoming phase of concept development, contractors should be required to analyze the feasibility of implementation of their concepts in the context of a fixed schedule for prototype design and construction. Technical feasibility requires a comparison of less mature versus more mature technological features. Changes required in codes and standard operating procedures need to be clearly identified and examined in detail. Unusual system

aspects such as the extensive software development required for automated control needs special attention. All of these matters taken together represent a risk analysis exercise necessary for full concept development.

- Since ISTEA currently mandates a competitive environment for concept development in the context of a down-select process for prototype construction, proprietary information developed during the concept development phase will have to be effectively shielded until such time as a prototype construction contract is awarded. However, innovations developed by those teams not selected for final prototype construction may have considerable value if applied to the prototype selected. Therefore some means must be found to incorporate those innovations with due compensation to their originators. One suggestion is to mandate a formal review by the winning prototype builder of all other proposed concepts under terms guaranteeing confidentiality and due compensation for techniques and innovations that would add value to the prototype chosen.

In summary, we look forward to examining these and other related institutional implications for maglev system costing that will be essential for successful development of a prototype that in turns leads to full system implementation.

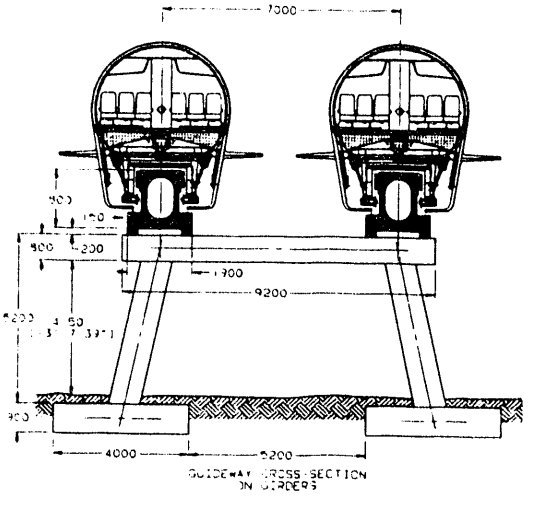

Fig. 1 Vehicle/Guideway Cross Section

Table I

Cost Estimate Summary

Summary Estimate[2]	Gov't Cost Model, $/Mile[9]		Bechtel Team Concept Estimate, $/Mile[5]
■ Structure Only[5]	10,541,977[1]		9,095,744[5]
■ System Guidance Only[1][5]	2,154,240[1]		1,100,000[5]
■ System Propulsion and Levitation[1][5]	Long Stator Core & Hangers[1]	2,323,200	5,600,000[5]
	[1526] DG, Long Stator Winding and Assembly	831,400	
	[1524] Feeder Lines,DG	1,945,000	
	[1525]Motor Switches,DG	960,000	
	Total	6,059,800	
■ Guideway Electrification[7] [1521] Transmission Line Cost [1523] Power Substation & Switching Station Costs			5,100,000[7]
■ C3 costs/mile, DG	[1532]	1,400,000	1,100,000
■ Vehicles, per unit[6]	$5,000,000 to $7,000,000 per unit		4,000,000 per unit
■ Stations and Parking[8]	Site Specific[8]		960,000[8]
■ Maintenance Facilities[8]	N/A[8]		467,200[8]
■ Construction Facilities[8]	N/A[8]		64,000[8]
■ Sales Tax	Not given		6% of all above (direct) costs, except labor
■ Construction Mgmt	Total Project Management Factor is 25%[4]		4% of [direct costs + sales tax]
■ Systems Integration, Engineering, and Design Management	Total Project Management Factor is 25%[4]		10% of [direct costs + sales tax + construction mgmt costs]
■ Procurement and Project Control	Total Project Management Factor is 25%[4]		4% of [direct costs + sales tax + construction mgmt costs]
■ Contingency Allowance[9]	Recommended Ranges from 15-30% (for items other than land)[9][3]		20% of subtotal of all above items, except where noted
■ Fee	Not given		2.5% of all above items (including contingency allowance)

Footnotes to Table I

(1) From Page 6-42 of the Government Cost Model, segment 1213RF, "double elevated in rural flat." The sum of plates and hangers is taken as the equivalent of $4,477,440 for the sum of levitation and guidance and propulsion. The item "long stator iron core and hangers" ($2,323,200) is segregated as dedicated principally to propulsion and levitation, with the item "factory installed vertical guiding steel plates" of $2,154,240 primarily dedicated to the guidance function.

(2) Total system cost per unit length is the sum of (i) all capital costs; (ii) pro-rated vehicle, station, and construction/maintenance facility costs; and (iii) the integrated mutilplier factor for all taxes, contingencies, fees, and service charges.

(3) Taken from page 8-6 of the Government Cost Model document.

(4) Taken from page 8-4 of the Government Cost Model.

(5) We understand that the Government Cost Model data represents a structure that will accommodate 12° girder tilt, zero vehicle tilt, and 0.15g longitude acceleration. Our baseline concept accomodates a 15° girder tilt, a 15° vehicle tilt, and 0.20g longitude acceleration and therefore represents a rather conservative comparison (i.e. our numbers are higher than they would have to be for an exact, "apples-to-apples" comparison) with the Government Cost Model.

Footnotes to Table I (Cont'd)

This point applies to the levitation, propulsion, and guidance elements of the baseline concept as well as to the guideway civil structure, since those elements have had to be defined to accomodate the loads and accelerations of our baseline concept.

(6) See page 6-191, data for category 182 data in the Government Cost Model. Data are rounded.

(7) We have a serious concern regarding comparative costing for Cost Element 1523 of the Government Cost Model, Power Substation and Switching Station Costs. The assumptions used in the Government Cost Model seem very unreasonable for a high-capacity revenue system. If there is only one inverter station every 20 miles, then it must be capable of providing peak power for maximum consist or multi-vehicle loadings in both directions. This in turn would imply at least 30 or 40 MW of peak power required per direction, or about 1.5 to 2 MW per mile of dual guideway. In actual fact the peak power would have to be even higher to allow for reasonable acceleration capability. On the other hand, to accommodate dispatching of multiple single vehicles each carrying between 100 and 200 passengers, the spacing of the power stations would have to be more frequent. In either case, the current data in the Government Cost Model for this item seem too low by a factor of at least five. Further, note that if one assumes a multiple-consist dispatching, then the motor winding must be changed to allow for the higher winding voltages that would be required.

On the basis of the above, we are unable to provide a precise measure of the costs of the "Electrification" line item for the Government Cost Model and make a true comparison with our baseline concept estimate.

(8) The reader is cautioned in particular regarding the station estimate, which is taken from past experience but was not developed beyond the concept definition level. Stations are highly site-specific structures and by definition an exercise of this sort does not yield precise data for estimation. Government Cost Model data cannot be derived sufficiently to yield an accurate comparison.

(9) The Government Cost Model does not include any contingency applied to any individual line items, as orally confirmed by Mr. Todd Greene of DOT/VNTSC on 4-21-92.

Table II

Reduced First Cost Summary

Summary Reduced First Cost	Reduced 1st Cost, $/Mile(1)	Baseline Concept Estimate, $/Mile(1)
■ Structure Only	7,700,000(2)	9,100,000
■ System Guidance Only	900,000(3)	1,100,000
■ System Propulsion and Levitation	4,500,000(3)	5,600,000
■ Guideway Electrification	0(4)	5,100,000
■ C3 costs/mile, DG	1,100,000	1,100,000
■ Vehicles, per unit	$4,000,000 per unit	$4,000,000 per unit

(1) These data represent an executive summary level of analysis and are rounded off.

(2) Assumed savings of $1.1 million per mile if fiberglass is shown to be unnecessary for guideway reinforcement; another 5 percent savings is assumed from a continuous structure design and refinements in automated guideway fabrication techniques.

(3) Guidance, propulsion, and levitation elements are shown reduced in cost by 20 percent from the baseline. Based on discussions with various vendors, it is our view that it will be possible to use numerically controlled wire winding machines and wet epoxy-coated wire to produce structurally rigid coils. This production technique can be used to fabricate the guidance coils and will eliminate the need for the fiberglass frames which represent 40 percent of total guidance coil installed costs. Similarly, this production method could possibly be used to fabricate the levitation ladder. If feasible, the cost of the levitation ladder would in our judgment be significantly reduced. Extensive discussions were required to develop this information with selected vendors on a conceptual basis, and it will require an allocation of next phase effort to develop this alternative further.

(4) For this reduced first cost scenario we assume the electric utility incurs the direct capital cost of all guideway electrification elements, and passes those costs on to the maglev system owner/operator in terms of changed long-term rate structures. This item is not offered as a life-cycle cost savings issue, since its life-cycle cost value would depend upon actual utility rate structures to recapture their first cost investment. It is offered as a suggested means to reduce first cost exposure only for prospective investors in maglev who are concerned about minimizing first exposure as an investment criterion.

System Concept Definition of the Grumman Superconducting Electromagnetic Suspension (EMS) Maglev Design

M. Proise, L. Deutsch, R. Gran, R. Herbermann, S. Kalsi, P. Shaw
Grumman Corporation, Bethpage, New York

Abstract- **Grumman, under contract to the Army Corps of Engineers, has completed a System Concept Definition (SCD) study to design a high-speed 134 m/s (300 m.p.h.) Maglev transportation system. The primary development goals were to design a Maglev that is safe, reliable, environmentally acceptable, and low-cost. The cost issue was a predominant one, since previous studies [1] have shown that an economically viable Maglev system (one that would be attractive to investors for future modes of passenger and/or freight transportation) requires a cost that is about $12.4M/km ($20 Million per mile).**

The design (Fig. 1) is based on the electromagnetic suspension (EMS) system using superconducting iron-core magnets mounted along both sides of the vehicle. The EMS system has several advantages compared to the electrodynamic suspension (EDS) Maglev systems such as, low stray magnetic fields in the passenger cabin and the surrounding areas, uniform load distribution along the full length of the vehicle, and small pole pitch for smoother propulsion and ride comfort. It is also levitated at all speeds and incorporates a wrap- around design for safer operation. The Grumman design has all the advantages of an EMS system identified above, while eliminating (or significantly improving) drawbacks associated with normal magnet powered EMS systems. Improvements include, larger gap clearance, lighter weight, lower number of control servos, and higher off line switching speeds. The design also incorporates vehicle tilt ($\pm 9^0$) for higher coordinated turn and turn out speed capability.

Manuscript received Mach 15, 1993. This work was performed as part of the Maglev System Concept Definition study supported by the U. S. Army Corps of Engineers under contrac No. DTFR53-92-C-000 04.

I. INTRODUCTION

The Grumman Corporation assembled a team of six corporations and one university that were exceptionally qualified to perform the identified SCD study. The Grumman team members and associated responsibilities were:

- *Grumman Corporation* - system analysis and vehicle design
- *Parsons Brinckerhoff* - guideway structure design
- *Intermagnetics General Corp. (IGC)* - superconducting magnet design
- *PSM Technologies* - linear synchronous motor (LSM) propulsion system design
- *Honeywell* - communication, command, and control (C^3) design
- *Battelle* - safety and environmental impact analysis
- *NYSIS* - high temperature superconductor (HTSC) and magnetic shielding analysis.

As a result of the team's efforts, a unique high-speed Maglev system concept (Fig. 1), was identified. If implemented, this design would meet all the goals specified in the abstract and would satisfy U.S. transportation needs well into the 21st century. The design is based on the electromagnetic suspension (EMS or Attractive) system concept using superconducting (SC) iron core magnets mounted along both sides of the vehicle.

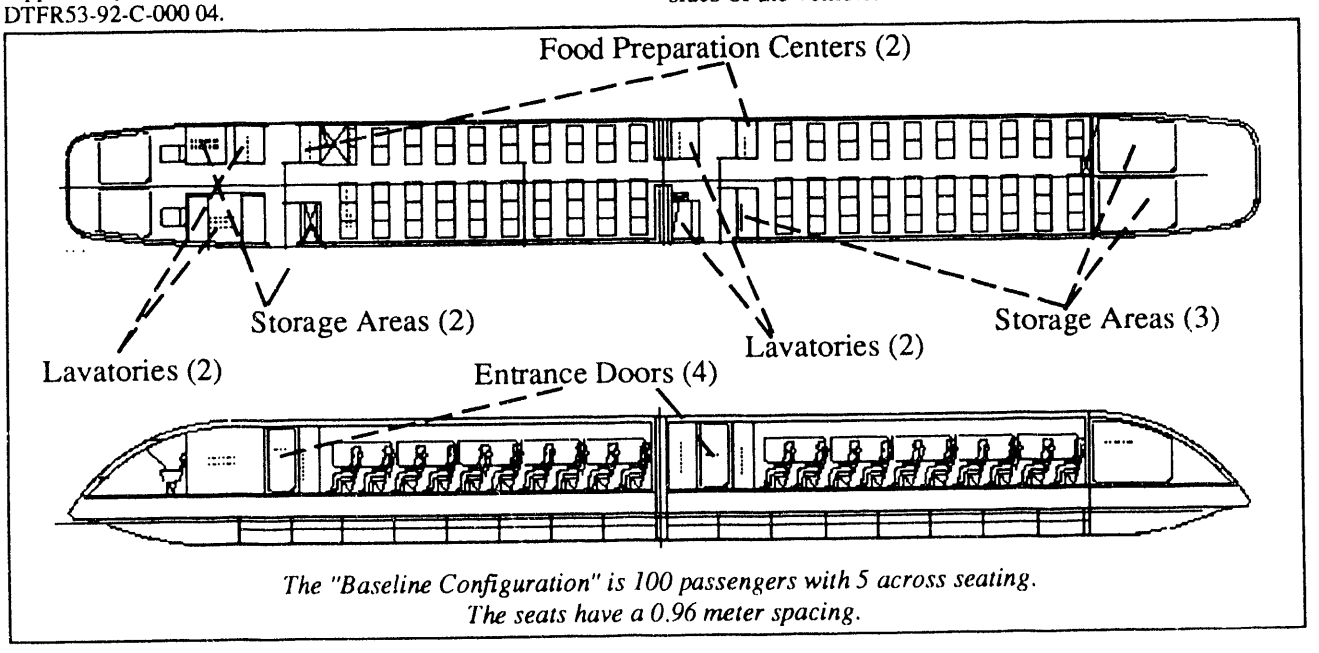

Fig. 1 . Grumman baseline Maglev vehicle configuration

The Grumman team selected an EMS design instead of an electrodynamic suspension (EDS or Repulsive) design because of the following significant advantages that the EMS offers over the EDS system:

- Low magnetic fields in the cabin and surrounding areas (this eliminates or minimizes the need for magnetic shielding and non-metallic rebar in concrete guideways)
- Uniform load distribution along the full length of vehicle (minimizing guideway loads and vibrations in the cabin and contribute to the elinination of a secondary suspension system)
- Small pole pitch (results in smoother propulsion)
- Magnetically levitated at all speeds (needs no supplemental wheel support)
- Wrap-around configuration (safer operation).

EMS systems exist. However, the German Transrapid TR-07 and the Japanese High Speed Surface Transportation (HSST) systems, which use copper wire iron cored magnets instead of SC coils, have a number of basic disadvantages:

- Small gap clearance (1 cm (0.4 in.)), which results in tighter guideway tolerance requirements
- Heavier weight with limited or no tilt capability to perform coordinated turns and maximize average route speed
- Limited off-line switch speed capability (56 m/s maximum)
- Large number of magnets and control servos (≈100 total).

The Grumman team design has retained all of the advantages of an EMS system. At the same time it has succeeded in eliminating, or significantly improving, every aspect of the identified EMS disadvantages. A brief description of our baseline system and how it has accomplished this goal follows.

II. LEVITATION, GUIDANCE & PROPULSION SYSTEM DESIGN

Fig. 2 shows a cross section of the vehicle with the iron core magnets and guideway rail identified in black. The laminated iron core magnets and iron rail are oriented in an inverted "V" configuration with the attractive forces between the magnets and rail acting through the vehicle's center of gravity (cg). Vertical control forces are generated by sensing the gap clearance on the left and right side of the vehicle and adjusting the currents in the control coils to maintain a relatively large 4 cm (1.6 in.) gap between the iron rail and the magnet face. Lateral control is achieved by differential measurements of the gap clearance between the left and right sides of the vehicle magnets. The corresponding magnet control coil currents are differentially driven for lateral guidance control. There are 48 magnets, 24 on each side of a 100 passenger vehicle. In this manner control of the vehicle relative to the rail can be achieved in the vertical, lateral, pitch, and yaw directions. Vehicle speed and roll attitude control are discussed below.

Two magnets combined as shown in Fig. 3 make up what is called a "magnet module." Each magnet in a magnet module is a "C" shaped, laminated iron core with a SC coil wrapped around the center body of the magnet, and two copper control coils wrapped around each leg. Vehicle roll control is achieved by offsetting the magnets by 2 cm (0.8 in.) in a module to the left and right side of a 20 cm (8 in.) wide rail. Control is achieved by sensing the vehicle's roll position relative to the rail and differentially driving the offset control coils to correct for roll errors. The total number of independent control loops required for a complete 100 passenger vehicle control is 26 (1 for each of the 24 modules and 2 for roll control).

The iron rail shown in Fig. 3 (b) also is laminated and contains slots for the installation of a set of 3-phased alternating current (ac) Linear Synchronous Motor (LSM) propulsion coils. The coils are powered with a variable-frequency variable-amplitude current that is synchronized to the vehicle's speed. Speed variations are achieved by increasing or decreasing the frequency of the ac current.

Comprehensive two and three dimensional magnetic analyses [2] have been performed to assure that the magnetic design will simultaneously meet all levitation, guidance and propulsion control requirements identified above, and do it

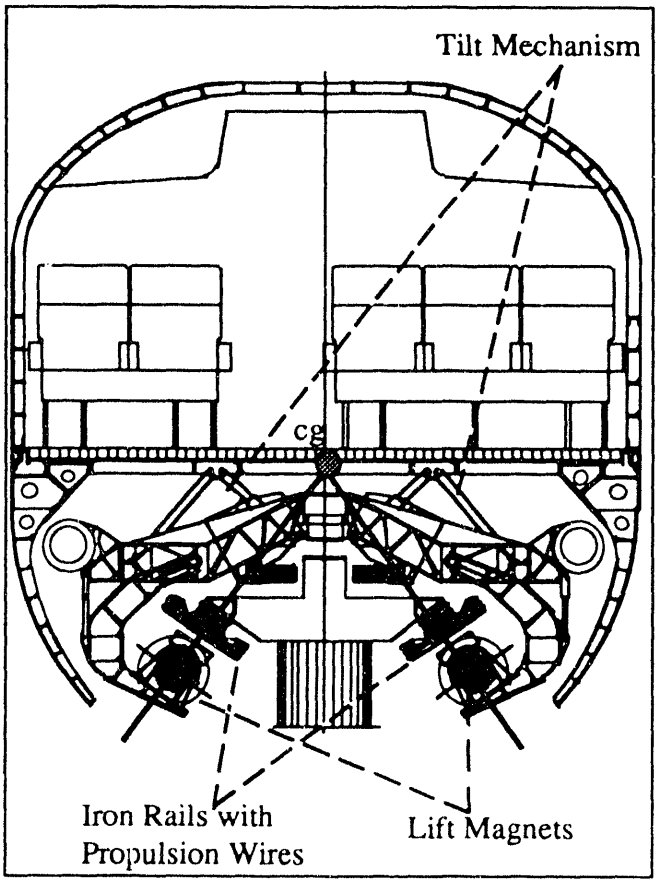

Fig. 2. Cross section of vehicle showing lift magnets, iron rail, guideway and tilt mechanism.

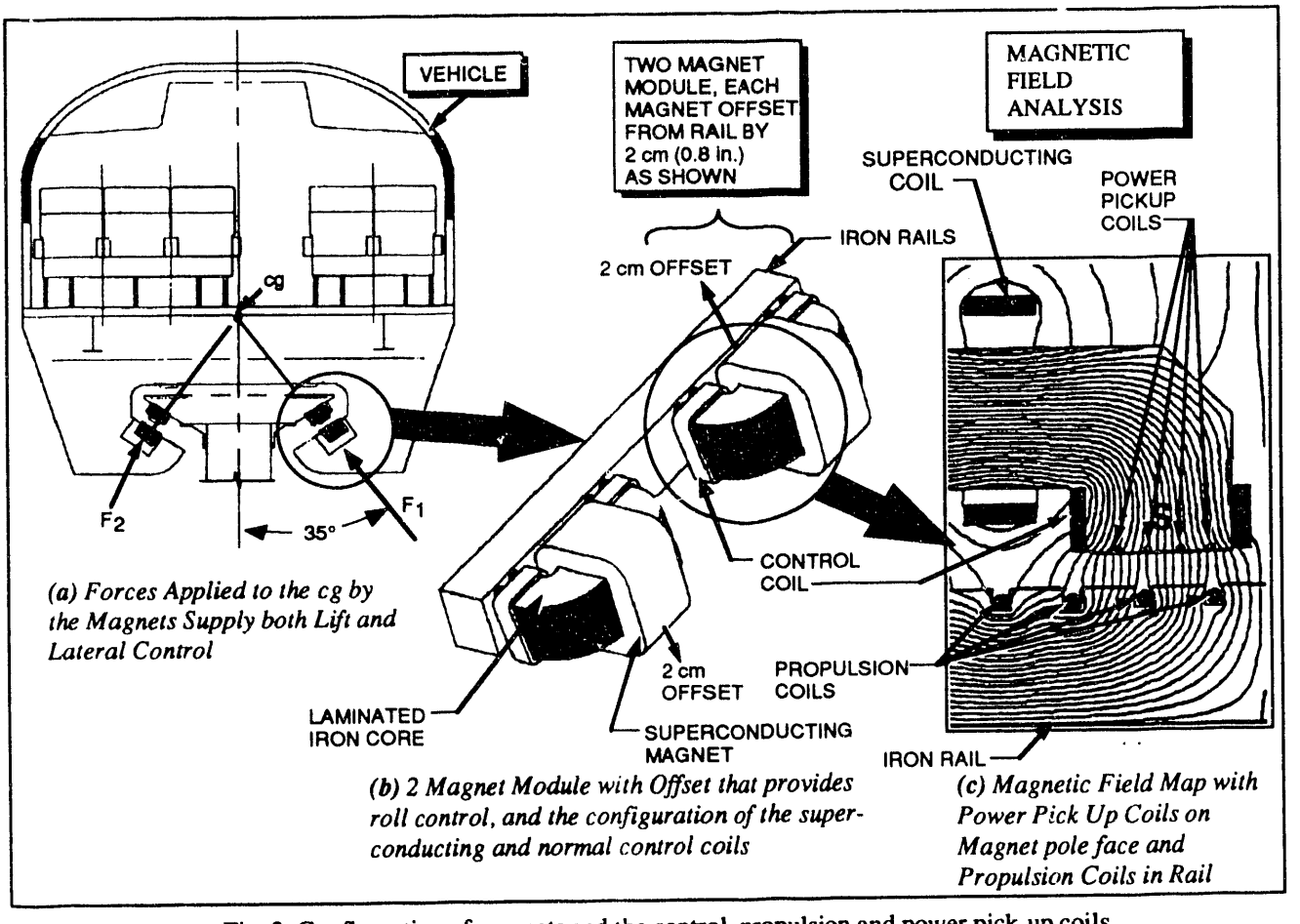

Fig. 3. Configuration of magnets and the control, propulsion and power pick-up coils

without magnetically saturating the iron core. An example of this analysis is shown in Fig. 3 (c).

Power pickup coils are located on each magnet pole face designed to operate at all speed, including standing still, using a unique inductive approach described in [3].

Low magnetic fields in the passenger compartment and surrounding areas represents an important aspect of this design. Fig. 4 identifies constant flux densities in the cabin and station platform that can be expected for the baseline design. Flux density levels above the seat are less than 1 gauss, which is very close to the earth's 0.5 gauss field level. On the platform, magnetic levels, when the vehicle is in the station, do not exceed 5 gauss, which is considered acceptable in hospitals using magnetic resonant imaging (MRI) equipment. The data in Fig. 4 is based on a three-dimensional magnetic analysis program and assumes no shielding. With a modest amount of shielding, these levels could be further reduced should future studies (now under way) indicate a need for lower values. Similarly, ac magnetic fields are anticipated to be within acceptable levels.

Another important aspect of the magnet design is the

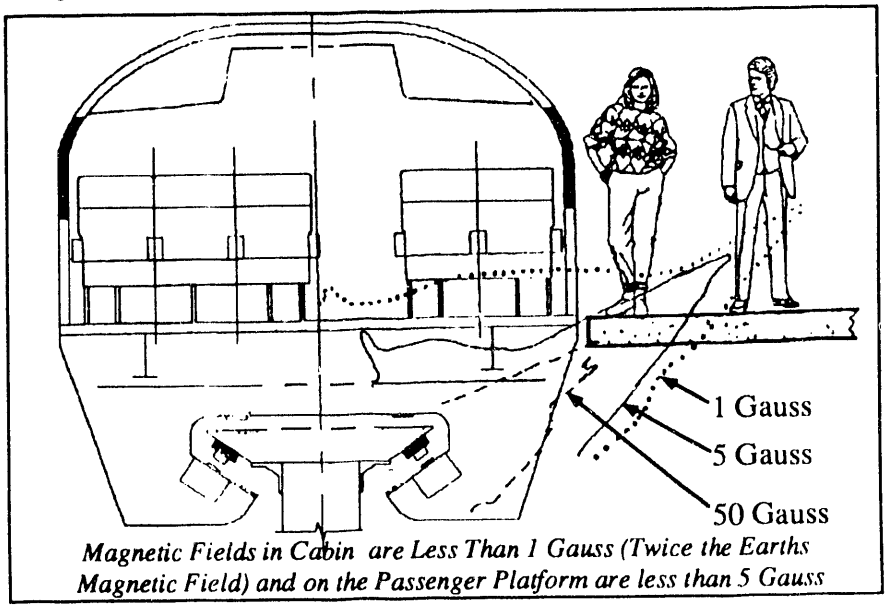

Fig. 4. Magnetic fields in cabin and surrounding area

use of SC wire in place of copper coils used in existing EMS systems. This allows us to operate with a large 4 cm (1.6 in.) gap clearance without paying the heavy weight penalty required if copper coils were used for the same purpose.

The use of an iron core with the SC coil provides an added advantage. The magnetic flux is primarily concentrated in the iron core, not the SC coils as is the case of an EDS system. This reduces the flux density and loads in the SC wire to very low values (<0.35 Tesla and ≈17.5 kPa, respectively). In addition we have implemented a patented constant current loop controller [4] on the SC coil that diminishes rapid current variations on the coil, minimizes the potential of SC coil quenching and allows for the use of state-of-the-art SC wire.

The use of iron-cored SC magnets with their associated low flux density and load levels previously identified affords an additional advantage of our design over an EDS concept. High temperature SC technology has progressed to the point that the field levels these magnets require are achievable with existing High temperature SC wire. It is now reasonable to consider the application of this new emerging technology to this concept. Although we are not baselining the use of high temperature SC for this application (except for its use as lead-in wire to the low temperature SC coil), we are pursuing a one-year development program at this time to manufacture samples of high temperature SC coils of sufficient length and with adequate current carrying density to satisfy our requirements.

In summary, the use of SC iron-core magnets resulted in a significant number of advantages for this concept:

- Large gap size - 4 cm (1.6 in.)
- Low magnetic fields in SC coil - <0.35 T
- Low magnetic fields in passenger cabin - <1.0 gauss dc
- Low load forces in SC coil- ≈17.5 kPa
- State-of-the-art SC wire - 0.65 mm diameter
- Lower weight than copper coil system - ≈80% reduction per magnet
- The potential for near term implementation of high temperature SC wire.

III. VEHICLE DESIGN

A number of important system trade studies were performed to arrive at the baseline vehicle configuration shown in Fig. 1. An example given in Fig. 5 which identifies how the total system cost, which includes the guideway, vehicles, levitation, propulsion, and operating cost, is affected by the number of passenger seats in the vehicle and the number of passengers per hour utilizing the system. Note that minimum cost results between 50 and 150 seats per vehicle. We have chosen 100 passenger seats per vehicle for our baseline configuration.

The 100 passenger baseline systemshown in Fig. 1 lends itself to other single and multi-vehicle (train) configurations that can be developed based on two basic building block modules. The main module consists of a 12.7 m (41.7 ft) long section, which seats 50 passengers with 2 entrance doors (one on each side of the vehicle), 2 lavatories (one designed to accommodate handicapped passengers), multiple overhead and closet storage facilities and a galley area. The forward and aft sections of the vehicle utilize the second module, which consists of a 4.9 m (16 ft) long section that is externally identical, but internally different, depending on its forward or rear location on the vehicle. We have adopted one-way vehicle operation to minimize the impact of weight

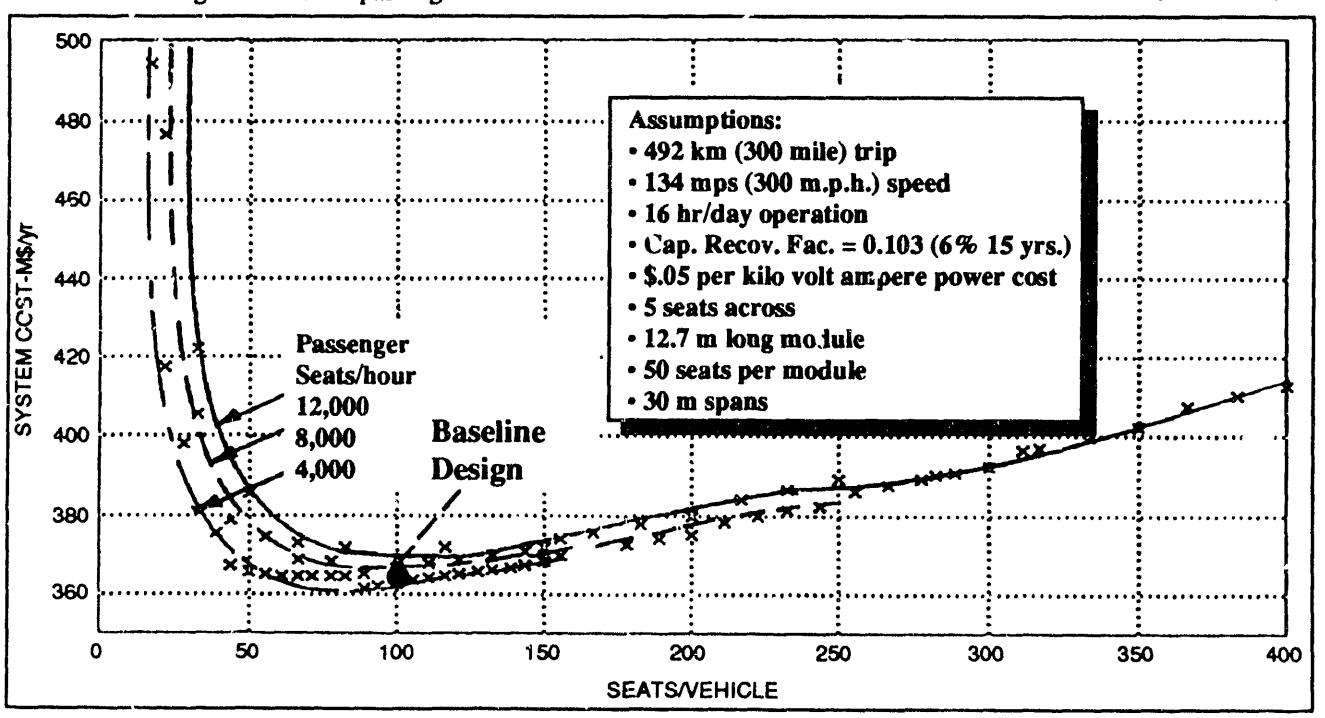

Fig. 5. System cost trade study

for reverse facing seat mechanisms and cost duplicating all the electrical controls and displays on both sides of the vehicle.

We also chose to include business-type aircraft seats with an ample 0.96 m (38 in.) spacing between seats to assure a comfortable seating arrangement for all passengers. Additional detailed vehicle characteristics are given in [5].

Comprehensive two and three-dimensional Navier Stokes computational aerodynamic analyses [6] were also performed on the baseline design to estimate drag and other disturbances acting on the vehicle. Vehicle speeds up to 134 m/s (300 m.p.h.) with 22.3 m/s (50 m.p.h.) crosswinds where investigated.

IV. GUIDEWAY DESIGN

The guideway is an important aspect of our system design because it represents the largest percentage of the total system cost. Fig. 6 shows how system cost distributes between the four major components, i.e., guideway (64.4%); electrical and communication (14.8%); vehicles (13.3%); and the ancillary facilities such as stations, buildings and vehicle parking (7.46%). Details of our system costing procedures is given in [7].

A number of different guideway designs were investigated. Four are shown in Fig. 7 and are identified in terms of increasing cost.

In each case our design mandated that a center platform exist along the full length of the guideway to provide a safe exit for the passengers, in case of an emergency such as a fire or smoke in the cabin. Escape ladders from periodic column locations also were identified.

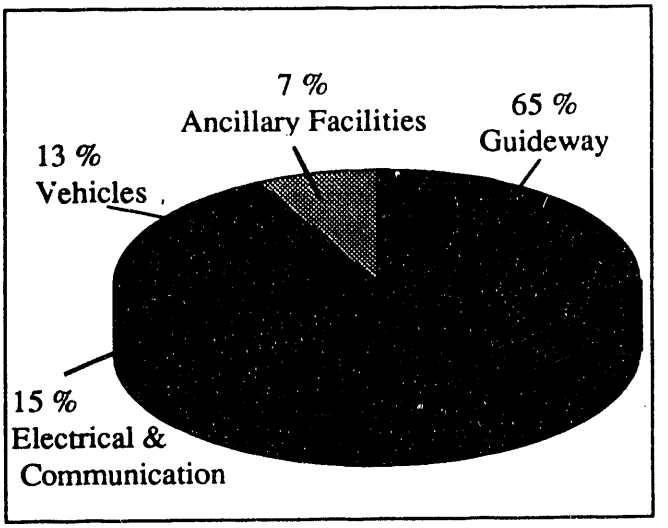

Fig. 6. Distribution of costs across the four major components of the Maglev system

Analysis of the four guideway configurations identified in Fig. 7 showed that the "spine girder" guideway design is not only lowest in cost, but also is relatively insensitive to span length [8]. This has important implications when the

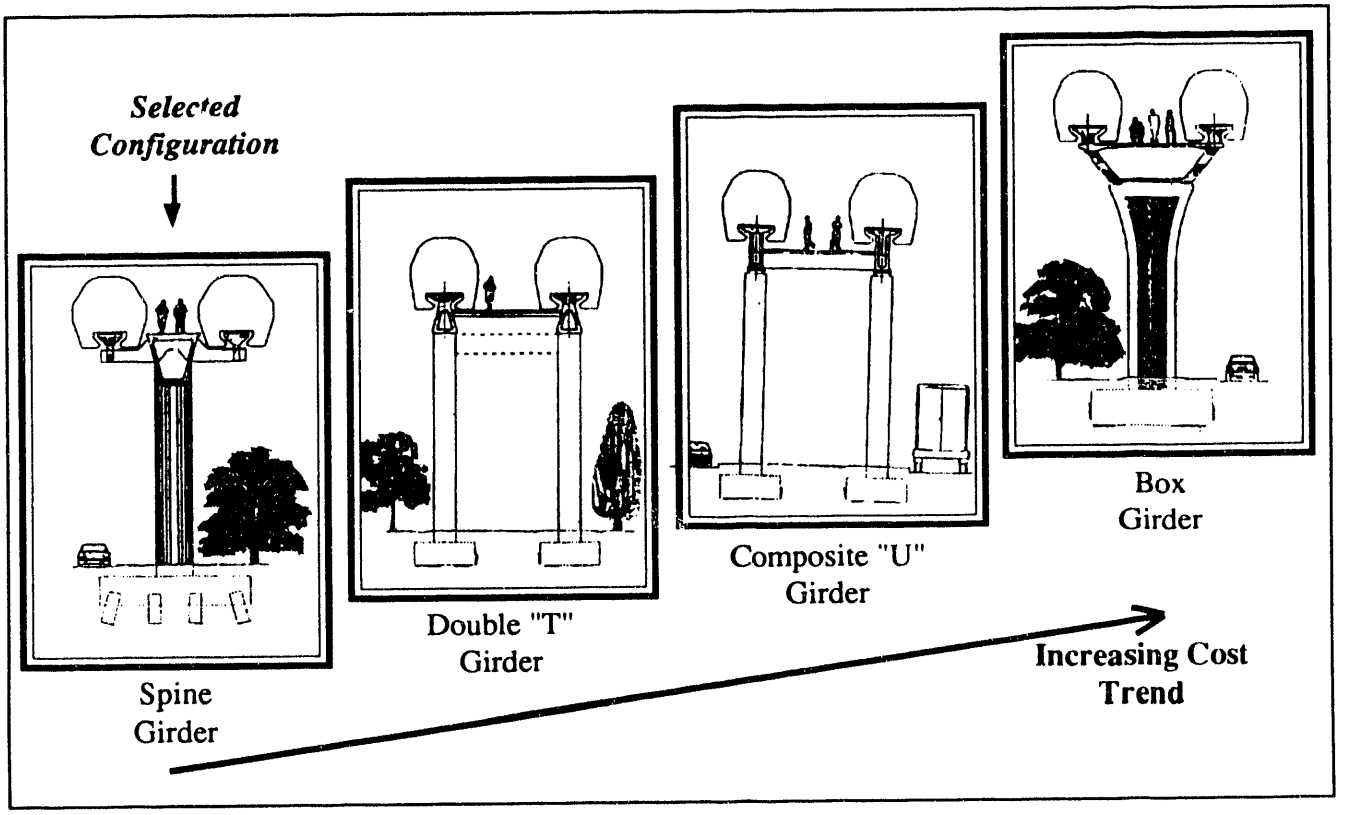

Fig. 7. Alternate guideway structures considered

guideway must be installed in areas such as the U.S. Interstate Highway system, which will require wide ranges in span length depending on local road conditions. In summary, based on this and other considerations, the "spline girder" configuration shown in Fig. 8 was chosen as our baseline for the following reasons:

- Lowest cost dual- guideway ($7.99M/km, for spread footing including iron rail cost)
- Smaller footprint
- Can be more closely designed to suit span variations
- Visually less intrusive because of single column
- Creates less shadow
- Esthetically pleasant.

Detailed descriptions of the baseline guideway and associated cost estimates are given in [9] and [8] respectively. The total system cost, which includes guideway, electrical and communication, vehicles, stations buildings etc. was estimated at $12.4M/km ($20M/mile) [7].

A 5 degree-of-freedom analysis of the interactive effects of the vehicle traveling over a flexible guideway was undertaken [10]. Guideway irregularities resulting from random step changes, camber variations, span misalignment and rail roughness where included in the simulation. Also included where linearized versions of the vehicle levitation and lateral control loops. The results indicated that passenger comfort levels could be maintained without the need for a secondary suspension system.

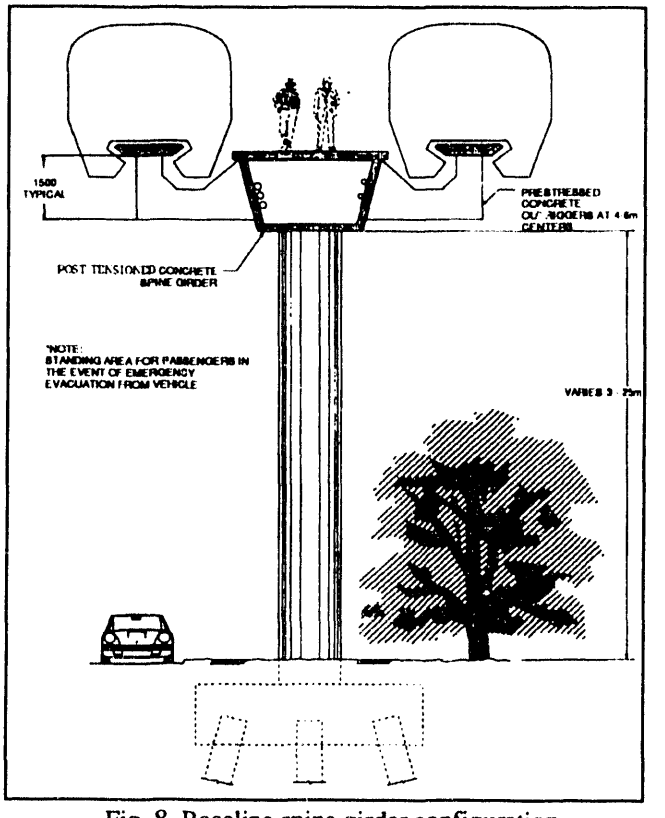

Fig. 8. Baseline spine girder configuration

V. HIGH SPEED OFF-LINE SWITCHING

Another important aspect of our design is the capability of providing high-speed off-line switching. Unlike the German Transrapid, design, which moves one 150 m (492 ft) section of the track laterally 3.61 m (12 ft), we move two sections laterally 3.0 m (10.0 ft) with one actuator motion. The track switching concept is shown in Fig. 9. It identifies the two sections of the track that are moved to accomplish this function. The lower figure shows the through traffic condition for the track switch. The upper figure identifies how the 60 m long switch, A, is flexed to a curved section, while the

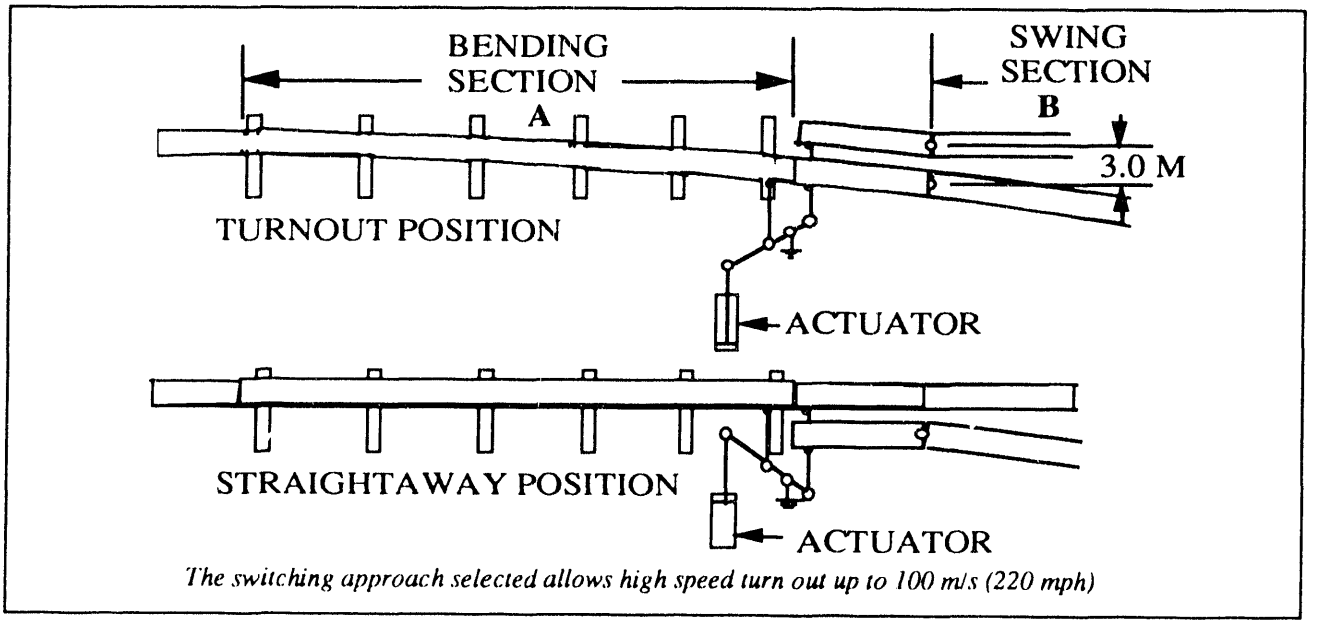

Fig. 9. Off-line switching concept

right hand 60 m long switch, B, is pivoted about the fixed switch points. This combined motion of the two sections (120 m total length) provides a turnout speed of 65 m/s (143 m.p.h.). A 182 m switch length will allow off-line switching at 100 m/s (220 m.p.h.). Transrapid turnout is limited to 56 m/s (123 m.p.h.) with a section length of 150 m.

VI. VEHICLE CABIN TILT DESIGN

Unlike any of the other existing high-speed Maglev designs, such as, the Transrapid TR07 or the Japanese MLU003, we are providing the capability of tilting the vehicle passenger compartment by ±9 degrees relative to the guideway. In this manner, the design, as shown in Fig. 10, will allow for coordinated turns up to ±24 degrees banking (±15 degrees in the guideway and ±9 degrees in the vehicle). This capability will assure that all coordinated turns can be performed at the appropriate tilt angle independent of the speed with which the vehicle is traversing the turn, as well as allowing for high-speed off-line switching.

VII. ECONOMIC ANALYSIS

An economic forecast analysis for a Maglev system was performed as a function of two primary cost drivers: total cost of the major Maglev elements identified in Fig 6, and the passengers per hour utilizing the system. The results of this analysis are presented in Fig. 11 with the assumptions listed below:

- 493 km (300 mile) corridor
- Development and demonstration cost of the Maglev system is not included
- Federal, state and local governments supply right-of-way at no cost
- Ridership is based on 260 days/year, 16 hours/day, 60% capacity
- 20% pre-tax operating margin on ticket price based upon 5 year build, 15 years of operation
- Future interest (8%) & inflation rate (5.4%) following "Data Resources, Inc." (DRI) forecasts.

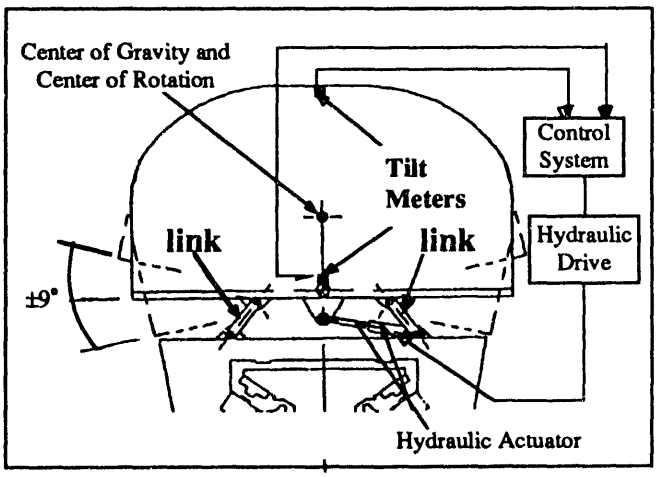

Fig. 10. Tilting mechanism and control system

If we assume a 2,000 passenger per hour usage (typical of high volume routes like Boston/New York/Washington DC) with the previously identified $12.4M/km ($20M/mile) for the baseline system cost the ticket price that would have to be levied is $0.23/km ($0.38/mile); this would still provide a 20% profit margin on the ticket cost for the system operator. Also shown on the figure is the $0.29/km ($0.47/mile)

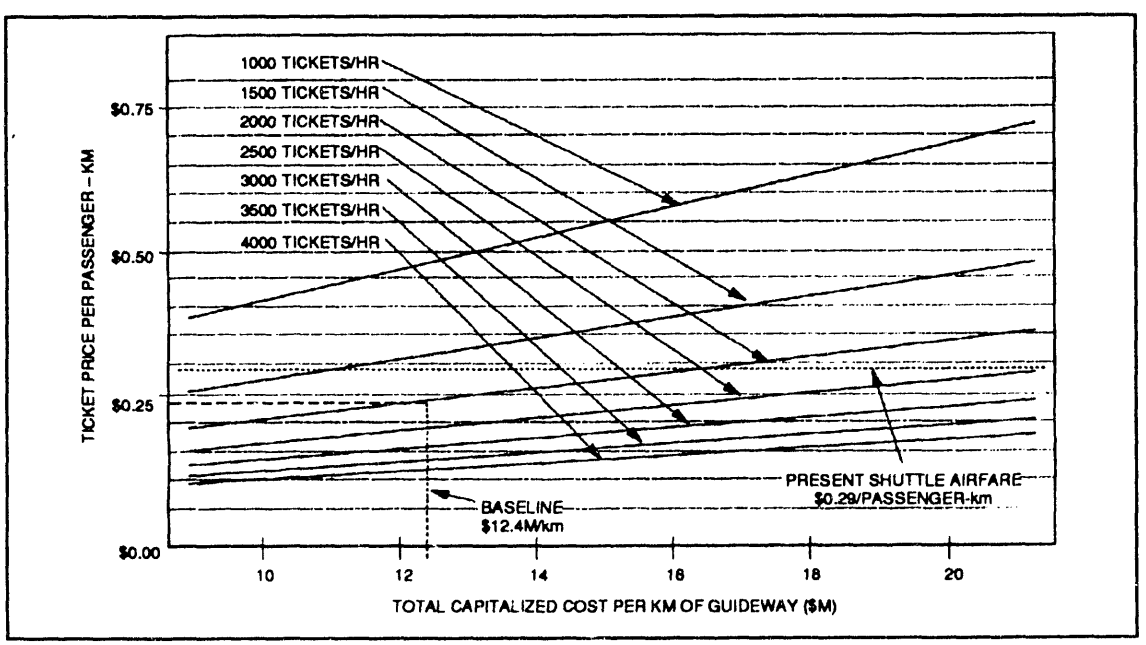

Fig. 11. Economic analysis

present charge for the New York/Washington, DC/Boston corridor. The results indicate that a Maglev system of the type being recommended in this paper can pay for itself during its first 15 years of operation. The implication is that after 15 years, when the capital investments have been fully paid, the proceeds from the high volume traveled routes could be used to support the building and operation of Maglev routes that are located in less densely populated areas. This means that system route miles can double every fifteen years, implying that by the mid twentieth century there could be over 4000 miles of maglev lines in the U.S.

VIII. RECOMMENDATIONS FOR FUTURE STUDY & DEVELOPMENT

Based on the work performed during this study, a number of critical areas have been identified for future evaluation and development:

- Conduct a design, development, and test program to demonstrate the performance of a full scale SC "C" core shaped magnet module
- Perform wind tunnel testing to verify aerodynamic analyses
- Perform additional studies to further reduce the vehicle weight and total system cost through:
  - -Improved magnet design
  - -Lower cost of guideway and iron rail
- Develop and test a guideway integrity and hazard detection system.

IX. CONCLUSION

It is our opinion that the Grumman Team superconducting EMS Maglev concept as described in this paper will provide an effective low cost U. S. Maglev transportation system that can meet all of the goals identified in the abstract and at the same time minimize the negative issues previously discussed. We believe that the Grumman team has performed sufficient analyses in the areas of guideway design, levitation, propulsion and guidance, vehicle structural design, aerodynamics, controllability, dynamic interaction, environmental, safety, and reliability to warrant this optimism.

REFERENCES

[1] R. Gran, "Benefits of Magnetically Levitated High Speed Transportation for the United States," SAE Future Transportation Conference, San Diego, CA, August, 1990, Paper No. 901475

[2] S. Kalsi, R. Herbermann, C. Falkowski, M. Hennessy, A. Bourdillon, "Levitation Magnet Design Optimization for Grumman Maglev Concept," to be presented at the Maglev 93 Conference, Argonne National Laboratory, May 19-21, 1993, Paper No. PS2-7

[3] S. Kalsi, "On-Vehicle Power Generation at all Speeds for Electromagnetic Maglev Concept," to be presented at the Maglev 93 Conference, Argonne National Laboratory, May 19-21, 1993, Paper No. PS5-12

[4] R. Herbermann, "Self Nulling Hybrid Maglev Suspension System," to be presented at the Maglev 93 Conference, Argonne National Laboratory, May 19-21, 1993, Paper No. PS1-7

[5] P. Shaw, "Overview of Maglev Vehicle Structural Design Philosophy, Material Selection and Manufacturing Approach," to be presented at the Maglev 93 Conference, Argonne National Laboratory, May 19-21, 1993, Paper No. PS4-9

[6] R. Ende, M. Siclari, G. Carpenter, "Aerodynamic Analysis of Grumman Maglev Vehicle," to be presented at the Maglev 93 Conference, Argonne National Laboratory, May 19-21, 1993, Paper No. PS5-9

[7] L. Deutsch, "Maglev Cost and Performance Parameters," to be presented at the Maglev 93 Conference, Argonne National Laboratory, May 19-21, 1993, Paper No. OS5-1

[8] B. Bohlke, D. Burg, "Parametric Design and Cost Analysis for EMS Maglev Guideway," to be presented at the Maglev 93 Conference, Argonne National Laboratory, May 19-21, 1993, Paper No. PS3-2

[9] J. Allen, M. Ghali, "Innovative Spine Girder Guideway Design for Superconducting EMS Maglev System," to be presented at the Maglev 93 Conference, Argonne National Laboratory, May 19-21, 1993, Paper No. PS3-1

[10] R. Gran, M. Proise, "Five Degree of Freedom Analysis of the Grumman Superconducting Electromagnetic Maglev Vehicle Control/Guideway Interaction," to be presented at the Maglev 93 Conference, Argonne National Laboratory, May 19-21, 1993, Paper No. PS4-6

Maglev Cost and Performance Parametrics

Lowell Deutsch
Grumman Corp.
Bethpage, NY 11714

Abstract - **A key element in the ultimate viability of Maglev, or any new transportation mode, is the capital and operating cost of the system. An estimate of these cost elements has been made for the Grumman Maglev design produced for the recently completed System Concept Definition Studies conducted for the National Maglev Initiative. Although this design represents one of several possible system designs, it is considered representative of the present state-of-the-art in American Maglev thinking.**

A logical Work Breakdown Structure generated by Parsons Brinckerhoff and the Volpe National Transportation System Center is presented to allow an organized approach to the capital cost estimating process. This WBS is broad enough that it should be applicable to any Maglev system. Costs are presented in a parametric fashion wherever possible to permit extrapolation to systems other than the Grumman design.

The possible cost savings resulting from certain changes in design and operating philosophy were also examined, resulting in a projected decrease in system cost from $12,300/m ($19.8 M/mi) to $10,900/m ($17.5 M/mi.)

I. INTRODUCTION

The activities of the National Maglev Initiative over the past several years have served to reintroduce U.S. interests into the international quest for advanced high speed ground transportation. Four teams of contractors have now completed concept design studies to determine the extent to which improvements can be made to the ongoing German and Japanese Maglev programs. While it seems clear that recent technology advances and incremental improvements in system design can provide a worthwhile "leapfrog" of systems now in development, it is also apparent that the viability of Maglev utilization is not technology dependent.

Manuscript received March 15, 1993. The work was performed as part of the Maglev System Concept Definition study supported by the U.S. Army Corps of Engineers under contract DTFR53-92-C-00004

Few researchers doubt that U.S. industry could successfully build reliable, safe, and effective Maglev systems and transportation companies could operate them. The key to Maglev success, rather, lies with the cost of building and operating the system elements, and the extent to which passengers will use the system. This paper will not address the ridership projections, which are the subject of numerous ongoing studies, but will discuss some of the elements of system cost. In particular, we wish to investigate the more significant cost drivers and mechanisms with which they may be controlled.

The cost data presented here is based on the analysis conducted by Grumman [1] in the recently completed System Concept Definition Study (SCD) sponsored by the National Maglev Initiative. Although there are some differences in cost between the four SCD contractors and between the U.S. studies and Transrapid, and these differences will be important in the final selection of a technology, to a first order the costs are similar at about $12,400/m ($20 M/mi) of dual guideway, exclusive of land cost.

II. WORK BREAKDOWN STRUCTURE

An excellent Maglev Work Breakdown Structure (WBS) was prepared by Parsons Brinckerhoff for their Capital Cost study conducted for the Volpe National Transportation Systems Center [2]. This WBS was adopted without modification and is illustrated in Fig. 1 along with the cost estimates for each element which resulted from the Grumman SCD study.

It is intended to examine the cost elements in this WBS in order to gain a feel for the important cost drivers and to investigate possible means to reduce the total system cost. It is not the goal of this paper to recommend specific changes, but to suggest areas requiring further study with the aim of capital cost reduction. Fig. 2 shows the distribution of capital cost between the four major cost elements; the guideway, the electrical and communication systems, the fixed facilities, and the vehicles.

As may be noted, 2/3 of the total capital cost is involved with the fixed guideway structure. This is obviously where we should concentrate our cost cutting efforts.

LEVEL 1	Est. ($/m)	LEVEL 2	Est. ($/m)	LEVEL 3	Est ($/m)
10 TOTAL CAPITAL COST	12302				
11 REGIONAL COST MULTIPLIER	1				
12 MAINLINE GUIDEWAY COSTS	7934	121 ELEVATED GUIDEWAY	7934	1211 ELEVATED GUIDEWAY CONTINGENCY	
				1212 SINGLE ELEVATED GUIDEWAY	3800
				1213 DUAL ELEVATED GUIDEWAY	7900
				1214 SPECIAL ELEV. GUIDEWAY STRUCT.	
				1215 ELEVATED SWITCHES (HIGH SPEED)	34
		122 AT-GRADE GUIDEWAY	4399	1221 AT-GRADE GUIDEWAY CONTINGENCY	
				1222 SINGLE AT-GRADE GUIDEWAY	
				1223 DUAL AT-GRADE GUIDEWAY	4372
				1224 AT-GRADE SWITCHES (HIGH SPEED)	27
		123 TUNNEL		1231 TUNNEL GUIDEWAY CONTINGENCY	
				1232 DUAL CUT & COVER TUNNEL G'WAY	
				1233 SINGLE MINED/BORED TUN. G'WAY	
				1234 DUAL MINED/BORED TUNNEL G'WAY	
				1235 TUNNEL SWITCHES (HIGH SPEED)	
13 ROW AND OTHER LAND COSTS	0	131 NOT USED			
		132 ROW/LAND CONTINGENCY			
		133 ROW	0	1331 URBAN ROW	
				1332 SURBURBAN ROW	
				1333 RURAL ROW	
				1334 INTERSTATE ROW	
				1335 OTHER ROW COSTS	
				1336 FEE TAKING COSTS	
		134 OTHER LAND	0	1341 STATION LAND	
				1342 MAINTENANCE FACILITY LAND	
				1343 CENTRAL CONTROL STATION LAND	
				1344 SUBSTATION LAND	
				1345 OTHER LAND	
				1346 FEE TAKING COST	
14 CIVIL RECONSTRUCTION & RELOCATION	0	141 CIVIL RECONSTRUCTION CONTINGENCY			
		142 CIVIL RECONSTRUCTION & RELOCATION	0	1421 DEMOLITION	
				1422 HIGHWAY RECONSTR/RELOCATION	
				1423 BRIDGE RECONSTR/RELOCATION	
				1424 SURFACE RECONSTRUCTION	
				1425 UTILITY RELOCATION	
				1426 ENVIRONMENTAL MITIGATION	
15 SYSTEMWIDE ELECTRICAL & COMM	1836	151 ELECTRICAL CONTINGENCY			
		152 GUIDEWAY ELECTRIFICATION	1596	1521 TRANSMISSION LINE	31
				1522 NOT USED	
				1523 POWER SUBSTA/SWITCHING STA	263
				1524 FEEDER LINE	461
				1525 MOTOR SWITCH	115
				1526 LONG STATOR WINDING	726
		153 COMMUNICATION & CONTROL	240	1531 CENTRAL CONTROL FACILITY	20
				1532 GUIDEWAY C-CUBED	220
16 STATIONS	644	161 STATION CONTINGENCY			
		162 STATION BUILDINGS	334	1621 NOT USED	
				1622 MAJOR CITY STATION BUILDINGS	216
				1623 INTERMEDIATE SIZE STATION BLDG.	118
				1624 SMALL STATION BUILDING	
		163 STATION PARKING FACILITIES	8	1631 NOT USED	
				1632 PARKING STRUCTURE	
				1633 PARKING LOT	8
		164 NOT USED			
		165 STATION GUIDEWAY	242	1651 NOT USED	
				1652 OFF-LINE INTER. STA. GUIDEWAY	242
		166 SERVICE & INSPECTION FACILITY	60	1661 SERVICE & INSPECTION FACILITY	60
17 OTHER BUILDING & EQUIPMENT	238	171 OTHER BLDG. & EQPT. CONTINGENCY			
		172 VEHICLE MAINTENANCE FACILITY	189	1721 MAIN MAINTENANCE FACILITY	94
				1722 NOT USED	
				1723 YARD AND VEHICLE STORAGE AREA	95
		174 ROW MAINTENANCE CENTER	34	1741 ROW MAINTENANCE CENTER	34
		175 SPECIAL EQUIPMENT	15	1751 SPECIAL EQUIPMENT	15
18 VEHICLES	1650	181 VEHICLES CONTINGENCY			
		182 VEHICLES	1650	182 VEHICLES	1650
				1821 VEHICLE CARRIAGE, BODY, ETC.	
				1822 INT. FURNISHINGS, HVAC, ETC.	
				1823 LEVITATION AND GUIDANCE	
				1824 ON-BOARD COMM & CONTROL	
				1825 PROPULSION AND BRAKING	
				1826 ON-BOARD POWER SUPPLY	
19 PROGRAM MANAGEMENT	0	191 PROGRAM MANAGEMENT FACTOR			

Fig. 1 Maglev Work Breakdown Structure showing Grumman cost estimates for a typical 1000 km Maglev system. Costs are presented in $ per meter of dual guideway

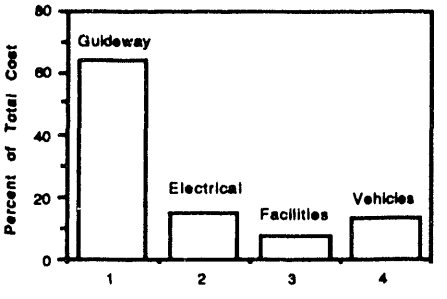

Fig. 2 Maglev capital cost distribution

III. COST ELEMENTS

Guideway The guideway cost estimates are based on the assumption of a dual track, elevated guideway of reinforced concrete construction. This guideway [3][4] was designed by Parsons Brinckerhoff (PB) for the Grumman SCD effort. The construction technique is fairly conventional, and not unlike designs presently in use for elevated highways and other structures. Obviously there will be differences in guideway design required to accommodate other Maglev concepts. However, with so much of the system cost involved with the guideway, we must aim towards the most cost efficient design possible. PB spent considerable effort on investigating alternate designs, and the selected configuration is probably close to optimum. Another factor is that conventional steel reinforced concrete construction is possible with the Grumman EMS Maglev system. The advances in the state-of-the-art required to eliminate the steel, as required by some EDS systems, will not be required.

The estimated cost for the elevated dual guideway is $7900 per meter. Corresponding costs for single elevated and at-grade dual guideways are $3800 and $4372 per meter respectively. These costs include the steel rail required for the EMS system ($2500/m for dual track) but exclude the LSM propulsion components. The elevated track costs are for a design allowing a clearance of 10.7 meters under the lowest part of the structure and a span between support posts of 27 meters on center. Table 1 shows the approximate percentage increases in cost for other heights and spans.

Table 1
Guideway Cost Sensitivity to Height and Span

	Span (m)	27	40	50
	25	17%	19%	33%
Height	20	9%	11%	25%
(m)	15	4%	6%	20%
	10.7	0	2%	16%

Electrical The electrical system consists of the guideway electrification and the communication and control systems. The cost estimates for these elements are $1596/m and $240/m respectively. The distribution of subelement costs in the guideway electrification is shown in Fig. 3.

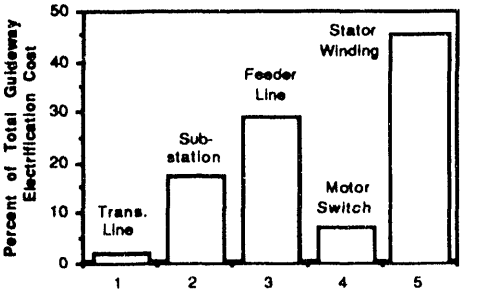

Fig. 3 Distribution of guideway electrification costs

The Transmission line consists of the high voltage lines to interface with the local utility and bring the power to the power substations distributed along the Maglev guideway. The estimate of $31/m was adopted from the PB cost study [2]. The substations include the DC link inverters and transformers required to supply the variable voltage, variable frequency power to the long stator synchronous motor (LSM) which drives the vehicles. The cost of this equipment is essentially proportional to the power required by the vehicle. The actual size of the substations will vary, depending on the local power required. In an area with steep grades or high acceleration requirements, the substation will be larger. They will probably be constructed of basic building blocks, say in the 2 Mw range. It was estimated that the average power requirements for typical routes will be about 8 Mw and this value was used for cost estimating purposes.

Because of the requirement to provide independent speed control to each vehicle, there can be no more than one vehicle on any guideway block served by a single substation. Vehicles typically travel about 10 km apart, therefore an 8 km substation block was selected. There must be two inverters at each substation to serve the dual guideway system. The cost of the dual 8 Mw substation was estimated at $2.1 million, or $263/m for an 8 km spacing. This value may be ratioed up and down in proportion to power level.

It should be noted that three of the four SCD contractors used some variant of the LSM. One design, however, used a locally commutated synchronous motor (LCLSM). This system uses a large number of solid state switches to control the power to each loop in the guideway. This concept is currently under study to see if it can offer any cost or performance advantages.

The feeder line distributes the variable frequency and voltage power to active guideway blocks under the vehicle. Because of the relatively low voltage required by the LSM, these cables, which run the extent of the guideway, are quite expensive. For the Grumman design, six (two tracks times three phases) 1500 MCM aluminum cables were used. The installed cost was estimated at $461/m.

The thyristor motor switches switch power from the feeder cables to the required active LSM blocks. These blocks are estimated to be about 500 m long. The actual length is the result of an optimization on switch cost and LSM efficiency, which drops off with long active blocks. These switches are estimated at $115/m for 500m blocks. This cost will vary inversely with the block length.

The LSM windings represent about 45% of the guideway electrification cost. The EMS configuration represented by these estimates is quite different from the typical EDS system, and therefore these numbers should not be used for the latter systems. The Grumman winding geometry requires 48 m of LSM cable for each meter of dual guideway. Using aluminum conductor with 3 cm^2 cross section and 15 KV insulation, the estimated cost is $726/m. The actual windings will vary in accordance with the local power requirements but this represents an average number.

The communication and control system consists of the automatic train controls (ATC) and associated data and communication systems required to provide a totally automatic, central control. This system was analyzed by Honeywell and, using comparisons with similar systems, the cost was estimated at $240/m, including a Central Control Facility.

Facilities The term facilities in this accounting refers to those fixed stations, maintenance buildings, and parking lots and buildings required for operation of the system. The cost estimates were adopted from the PB study [2] and apportioned to the length of guideway. It was assumed that for a typical 1000 km system there would be one Central Control Facility, two Major City Stations, and five Intermediate Stations with parking lots. The total fixed facilities cost amounts to $963/m.

Vehicles The number of vehicles required is dependent upon the desired passenger capacity. The 4000 passenger (seat) per hour capacity, as specified for a baseline in the SCD studies, is about twice the present plane/train traffic in the Northeast corridor, but less than that in some other parts of the world, such as Japan. With 4000 seats/hr in each direction we will average about one vehicle on each 5 km of guideway. The Grumman vehicle cost estimate is about $8.25 million each, which amounts to $1650 per meter of dual guideway.

IV. POTENTIAL COST SAVINGS

As noted above, with the guideway amounting to 2/3 of the total capital cost, this is the obvious area to search for cost savings. It will be noticed immediately that the at-grade guideway is only 55% of the cost of the elevated guideway. There are very valid arguments why a Maglev guideway should be elevated. These primarily concern the desire to avoid highway grade crossings, where most railroad accidents occur, and the need to prevent objects from falling (through vandalism or natural occurrences) from an overpass onto the guideway. Furthermore, a tenet of the modern Maglev effort in the U.S. is to use the Federal Interstate Highway System in a dual-use mode in order to avoid land acquisition costs. It has been observed that overpasses are encountered on major highways on the order of one per mile [5] and it was assumed that with the vertical g limits on passengers the length of the transition to go from at-grade, over the bridge, and back to at-grade again would also be on the order of one mile.

It was decided to test this assumption by analyzing a typical highway. Using the SCD specified Design Goal comfort requirements of 0.05 g (up) and 0.2 g (down) in the vertical direction, it was calculated that at a typical average speed of 110 m/sec, the transition length would be about 1600 m, or one mile. Examining the 495 mile main line length of the New York State Thruway [6], revealed that there are 362 overpass bridges, or about one each 1.4 miles. It would seem then, that the previous estimates were about right. It was noticed, though, that the bridges occur in clumps around more heavily populated areas.

The Thruway data was analyzed in more detail such that if bridges occurred closer than one mile apart then the guideway could remain elevated. It was found that under these conditions 50% of the guideway could be at-grade. In some instances the guideway was at-grade for only a short distance. A further screening of the data was done with the assumption that if the guideway could not be at-grade for at least one mile then it was left elevated. In this case 41% of the guideway could be at-grade. One might argue that the passengers will not like this repeated vertical motion, but the most conservative comfort levels were used in the analysis. It must be accepted however, that the use of highway rights-of-way will impose considerable motion which must be tolerated if we are to use these low cost alignments. At any rate, turns will probably occur much more frequently than will bridges. These motions, and the comfort considerations which are

implicit are a crucial part of Maglev design and must be given careful study and testing.

If we take the more conservative case of 41% of the guideway at-grade at $4372/m and 59% elevated at $7900/m the average cost will be $6454/m, an 18% reduction in guideway cost. This would drop the system cost to $10,856/m ($17.5 million/mile) from the present estimate of $12,302/m ($19.8 million/mile).

Another area for possible cost savings is in the sidetracks necessary for offline stations. It is accepted that online stations are not consistent with our plans for frequent service from relatively low capacity vehicles. We have generally assumed that we must switch offline at relatively high speeds (e.g. 100 m/sec). This not only drives the switch cost up but requires extensive lengths of side track for deceleration. Using the Design Goal longitudinal acceleration and deceleration values of 0.16 g and switching at 100 m/sec will require a single guideway length of 3187 meters (2 miles) to stop and another 3187 meters to accelerate back to line speed. The switch is estimated to cost $1.7 million and, at $3800/m for single guideway, the deceleration track will cost $12.1 million, seven time the cost of the switch. This also does not consider the possible land cost for the side tracks.

Suppose the vehicles could slow to, say 20 m/sec, prior to switching. The deceleration lane would then be reduced to 127 meters in length. This would save a total of $232/m in system cost or about 1.9%. This savings would be increased somewhat with the redesign of a low speed switch which was not accounted for in this analysis.

The question then is can we safely follow this scenario? To carry 4000 seats/hr in a 100 seat vehicle requires a headway of 90 sec. At 134 m/sec this is a vehicle separation of 12 km. If the leading vehicle brakes to 20 m/sec at 0.16 g the separation distance will close to 7900 m. However at any time the following vehicle can emergency brake at 0.2 g to a stop in a distance of 4600 m. This leaves a safety margin of 3300 m or about 25 sec at full speed. It must be noted though, that this analysis is invalid for higher throughput capacities than 4000 seats/hr. It will also be necessary to have a switch operating time of less than 25 sec.

Although the cost saving predicted for this change in switch philosophy is not great, Maglev switches remain a difficult design challenge, especially for the wraparound EMS systems. It may be preferable to provide the acceleration and deceleration capability to permit a low speed switch to be used.

V. OPERATING COST

A brief examination of system operating and maintenance (O&M) cost was made as a part of the Grumman SCD study. To a first order the O&M costs consist of personnel, material, and energy expenses. The projected values of these costs are listed in Table 2, and total $269 million per year for a typical 1000 km system with a peak capacity of 4000 seats per hour.

Table 2
O&M Cost Summary

Item	Annual Cost ($M)
Personnel	49
Material	48
Energy	172
Total	269

To compare the O&M costs with the annual cost to capitalize the system we may assume a typical capital recovery factor of 0.103 (6% for 15 years). The 1000 km system at $12.3 million per km would cost $12.3 billion and the annual cost of capital would be $1267 million. The projected O&M cost is then 18% of the total annual cost.

In examining the factors which determine the O&M elements, it was found that most of the cost is proportional to the passenger throughput. This includes the personnel, material, and energy costs. To be more precise, it was estimated that 6% of the cost is fixed and 94% is proportional to the throughput (seats/hr).

The energy costs were estimated from a simulation of the 800 km Severe Segment Test (SST) route supplied by the Government for the SCD study. Although it was labeled a Severe Segment Test it seemed to have alignment profiles similar to what might be expected along typical U.S. highway routes. From this analysis it was estimated that 100 passenger vehicles carrying a peak of 4000 seats per hour in each direction and an average of 2000 seats per hour would consume 3.08 billion kwh/yr. Using an energy charge of $0.05/kwh and a demand charge of $7.50/mo per kw, the projected annual energy cost is $172 million.

Much confusion exists over the specific energy consumption of Maglev vehicles and other trains. At a steady state 300 mph cruise the Grumman 100 passenger vehicle consumes 5.072 Mw at the utility interface. This translates to a specific energy of 379 Joules/passenger-meter. If we were to use a train consist of 10-fifty passenger modules the total aerodynamic drag would increase by only 63%. The specific energy would drop to 124 Joules/passenger-meter because of the five-fold increase in the seating capacity. This scenario would drop the annual energy cost to $56 million. However, the train, which now

weighs five times as much, will require a stronger elevated guideway and a more powerful electrical system to achieve the same performance. Our studies show that the optimum (from a total cost standpoint) configuration is in the vicinity of 100 passengers.

REFERENCES

[1] Michael Proise, et. al., "System Concept Definition of the Grumman Superconducting Electromagnetic Suspension (EMS) Maglev Design," Unpublished, to be presented at the Maglev 93 Conference, Argonne National Laboratory, May 19-21, 1993, Paper No.OS4-4

[2] J.A. Harrison, et. al., Parsons Brinckerhoff Quade & Douglas, "Maglev Cost Estimation: Capital Cost Elements," Unpublished, Volpe National Transportation Systems Center, Cambridge, MA 02140

[3] B. Bohlke, D. Burg, "Parametric Design and Cost Analysis for EMS Guideway,"Unpublished, to be presented at the Maglev 93 Conference, Argonne National Laboratory, May 19-21, 1993, Paper No. PS3-2

[4] J. Allen, M. Ghali, "Innovative Spine Girder Guideway Design for Superconducting EMS Maglev System," Unpublished, to be presented at the Maglev 93 Conference, Argonne National Laboratory, May 19-21, 1993, Paper No. PS3-1

[5] The Maglev Technology Advisory Committee, Reporting to the United States Senate Committee on Environment and Public Works, "Benefits of Magnetically Levitated High Speed Transportation for the United States, Vol. 2 - Technical Report," March 1992

[6] Willard H. Ristau, New York State Thruway Authority, Private communication

ANALYSIS OF MAGLEV CORRIDORS

George R. White
Transportation Systems Research Center, School of Engineering
University of Pittsburgh, Pittsburgh, Pennsylvania 15261

Abstract - **The most critical question facing the U.S. with respect to MAGLEV may not be "how", but rather "why". Unless some defining picture exists of where MAGLEV lines might operate, and how MAGLEV services might interact with existing air and auto transportation, national concurrence is apt to be wanting on assuming the costs and uncertainties attending its technical development. The 1990 US Census Bureau data on the 281 Metropolitan Statistical Areas (populations and personal incomes) can be combined with US Geological Survey position data (latitudes and longitudes) to enable a Figure of Merit assessment of all plausible MAGLEV trips (40 < miles < 600) on all plausible corridors in the United States. Results are mildly surprising. Although as expected the Boston-Washington Standalone Corridor is the most valuable, by a factor 3x over the nextmost, that nextmost is not the Sacramento-San Diego Standalone Corridor (found to be fourth), but two extension corridors continuing beyond Washington to Pittsburgh-Cleveland-Detroit in the Midwest, and to Richmond-Norfolk in the Midsouth. An hierarchical sequence of the LEVEL I Route (Boston to/from Washington) through LEVEL IV Routes (Atlanta to/from East Coast and Midwest; Phoenix-Tucson to/from San Diego) is quantitively defined by the TOP 75 CSMA cities along the route (traffic decrease by a factor of two per LEVEL). Several early contenders for federal sponsorship score at a low disfavored LEVEL V (Texas, Florida, Las Vegas). The resulting overall picture of MAGLEV possibilites is thought to be quite comprehensive, involving 77.6% of US population, and quite stable, shifting only with the slow rate changes of demographics. An aggregate 25 of the Lower 48 States have population in the Metropolitan Areas which would be served through LEVEL IV, so substantial definition and justification for MAGLEV may appear from this work.**

I. INTRODUCTION

The national interest in High Speed Rail and Magnetic Levitation Transportation has been markedly stimulated by the December 1991 enactment of the federal Intermodal Surface Transportation Efficiency Act. A prototype MAGLEV system at least 19 miles long may be funded with $750 million. While such demonstration may illuminate some technical issues, the larger questions of where MAGLEV corridors should be located, for what values-added, will be unresolved by any such single short-span operation.

Manuscript received March 15, 1993. This paper has been issued with more detailed tables and maps as Transportation Systems Research Center Report 93-1a (January 1993).

Analysis of MAGLEV corridors between all possible cities can establish their potential for Relative Value in Rider-Miles versus Route Miles, in so far as determined by the underlying factors of population, personal income, and distance. While nothing in the analysis establishes absolute level of demand, the interpretation of relative value has integrity for prioritizing potential MAGLEV corridors, and for resolving among varying alternatives for route stops.

The definition of priority for explicit MAGLEV corridors allows logical sequential strategy for plans and implementation, when and if resolution of issues increasingly favors MAGLEV prospects. The role for an ISTEA MAGLEV prototype then is more useful in clarifying relevant economic, social, and political factors than in merely demonstrating technology.

The U.S. Census Bureau has identified a total of 281 Metropolitan Statistical Areas, Primary Metropolitan Statistical Areas, and Consolidated Metropolitan Statistical Areas. All trips may be considered to link Metropolitan Statistical Area pairs, of which there are N(N-1)/2 or 39,340. Thus there is a large but tractable data base for analysis of MAGLEV prospects.

II. POSSIBLE NICHE

The Crucial Question is why should the U.S., with already the world best auto/interstate and jet/airport transport systems spanning the whole country, expect value from new transport which is neither as flexible as autos nor as fast as jets. There are two reasons why such may be the case.

(1) Autos have a two-dimensional capability, linking any point in one area to any point in another with facility. Jets have only a zero-dimensional capability, linking one point to but one other point. A MAGLEV line can provide the intervening one-dimensional capability, linking points on-line to other points on-line with ease.

(2) Subjective judgement is that autos average 55 mph, with little wasted time. Statistical regression of airline schedules versus great circle distances shows

that jets average 520 mph as point to point cruise, but with 45 minutes of wasted air and ground delay each flight segment. MAGLEV market position could be proportionally between at 180 mph average speed, three times that of cars and one-third that of planes, with little wasted time delay.

III. Data and Analysis

The 1990 Census [1] provides full population and personal income data for all 281 Metropolitan Areas. The US Geological Survey Atlas [2] provides latitude and longitude to 0.1 minute (about 600 feet), from which any of the 39,340 city pair great circle distances are computed as needed, by spherical trigonometry,

$$TrueMilesAB = 69.09 \cdot \arccos[\sin(LatA)\sin(LatB) + \cos(LatA)\cos(LatB)\cos(LongA - LongB)] \quad (1)$$

with arccos expressed in degrees. RidershipScoreAB is taken as proportional to traffic potential for the AB pair:

$$RidershipScoreAB = \frac{PopA \cdot PopB \cdot \$A \cdot \$B \cdot 10^{-16}}{TrueMilesAB} \quad (2)$$

with 1990 Census values for each Metropolitan Area used for population (PopA) and average personal income ($A).

Once actual RouteAB is chosen, RidershipScoreAB is lowered by the ratio TrueMilesAB/RouteMilesAB. This corrected traffic potential times the RouteMilesAB is thus proportional to the total potential for passenger miles of the city pair. The ratio (TrueMilesAB/RouteMilesAB) is applied as final adjustment, to represent subjectively the displeasure with circuitous routes. The resulting quantity

$$Rider\text{-}MilePotentialAB = RidershipScoreAB \cdot \frac{TrueMilesAB^2}{RouteMilesAB} \quad (3)$$

is the relative contribution each city pair along a route makes to total traffic on the route. The cumulative Rider-MilePotential for all city pairs along a route is taken as proportional to the total values-added (i.e. revenue or public service equivalent) by travel on the route. The cumulative RouteMiles is taken as proportional to the fiscal cost of the route. The Figure of Merit for each MAGLEV corridor

$$Merit = \frac{\Sigma Rider\text{-}MilePotential}{\Sigma RouteMiles} \quad (4)$$

places that corridor in an hierarchy of profitability (or public service value) against all other possible corridors.

The Census pays special attention to the Top 75 Metropolitan Areas of the total 281. This group contains 60.5% of the total U.S. population, and dominates potential travel. Initial analysis is therefore concentrated on Top 75 MSAs, to establish the dominant themes of plausible routes.

Specific attention must be paid to the jet and auto competition. Two cutoff limits are adopted. Subjective judgement is that trips below 40 RouteMiles should be given zero as RidershipScoreAB, representing irresistible preference for auto flexibility. More objectively, trips beyond 600 RouteMiles have zero as RidershipScoreAB, representing pre-emption by jet travel. Below this distance MAGLEV can be advantageous.

Specifically, nonstop MAGLEV express time between two major cities 600 miles apart is 2.0 hours, while nonstop flight schedule between their airports is 1.9 hours (45 minutes + 600/520mph), with airport access time more than taking up the difference. The MAGLEV advantage between secondary cities is equally clear. Such air trips now require hub-and-spoke connection, with two 45 minute flight segment overheads added to the hub connection interval (about another 45 minutes). Thus, the all-stops MAGLEV at 180 mph average speed takes 3 hours 20 minutes to connect two secondary cities 600 miles apart, while hub-and-spoke air takes 3 hours 24 minutes (3 x 45 minutes + 600/520mph).

Both autos and jets are more able to follow great circles than MAGLEV, so schedules for the latter must minimize stops along circuitous routes to compensate. The number of stops affecting the dominant city pair on circuitous routes (e.g. - Cleveland to New York via Washington) is curtailed so that average speed over the True Mileage (not Route Mileage) meets the 180 mph competitive objective.

IV. Levels of Priority

The tables and maps of this report are then classified as to their national priority, given by their hierarchical Figure of Merit. The Northeast Corridor stands alone as Level I, having a Merit Figure of nearly 50,000 Rider-Mile Potential/Route Mile (Tab. 1).

Consequently, whether a national program makes sense hinges on the next most valuable, the Level II standalone California Corridor Sacramento to San Diego, having a Merit Figure of 13,000 Rider-Mile Potential/Route Mile (Tab. 2). If costs and appeal don't validate this California prospect, no other routes in the U.S. are sound. Likely, MAGLEV use only along the East Coast would receive neither votes nor funds enough for implementation.

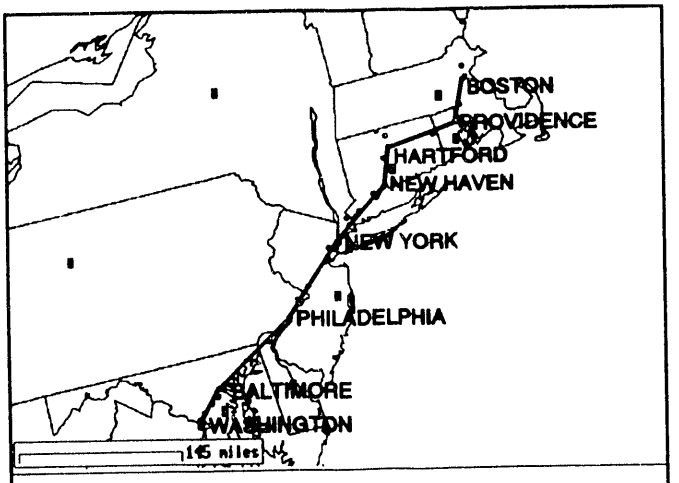

TABLE 1. LEVEL I CORRIDOR

Boston/Washington Corridor	415 Miles	8/Top 75	Merit 48,680

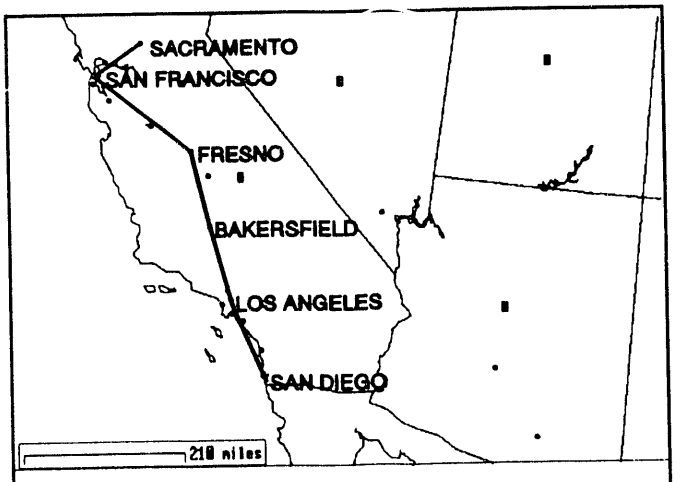

TABLE 2. LEVEL II CORRIDOR

Sacramento/San Diego Corridor	549 Miles	6/Top 75	Merit 13,395

However, if Merit Figures of Level II (say, greater than 10,000) are valid for implementation, other Routes open up as continuing extensions of the Northeast Corridor (Tab. 3). First among these, in fact with Merit of 16,000 (higher than California), is the extension of MAGLEV from the Washington to Pittsburgh, Cleveland, and Detroit. Upon reflection, it is not surprising that linking the nation's Sixth, Thirteenth, and Nineteenth MSA populations with its First, Fifth, Seventh, and Eighteenth should have substantial value. Of some surprise is the outcome that a second Level II corridor extension is valid from Washington to Richmond and Norfolk. This route as yet has not been featured in MAGLEV speculation and advocacy.

Additional Level II Extensions are found to be valid (Merit greater than 10,000) branching off at Toledo to Chicago, and continuing to Milwaukee. Similarly, the Extension from Richmond to the North Carolina Piedmont (Raleigh-Durham, Greensboro, and Charlotte) meets the Level II criterion.

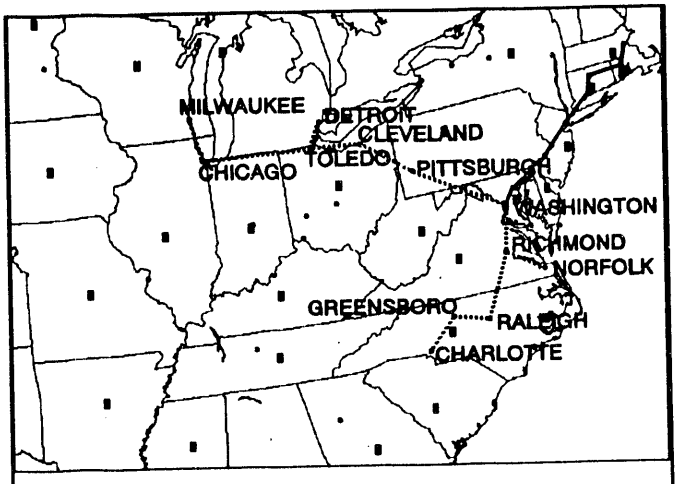

TABLE 3. LEVEL II EXTENSIONS

Washington/Detroit Extension	455 Miles	+4/Top 75	Merit 16,572
Washington/Norfolk Extension	176 Miles	+2/Top 75	Merit 15,914
Toledo/Chicago Extension	212 Miles	+1/Top 75	Merit 12,251
Richmond/Charlotte Extension	290 Miles	+3/Top 75	Merit 11,076
Chicago/Milwaukee Extension	82 Miles	+1/Top 75	Merit 10,324

In all cases, the higher priority predecessor is assumed to exist and provide extension traffic. Thus Detroit to Chicago journeys are crucial for the Toledo extension, and Midwest to Tidewater trips for the Virginia routes.

V. SEQUENTIAL STRATEGY

One need not build MAGLEV lines in the hierarchical sequence of priority, provided the conditional dependency is fully understood. In particular, the Boston/Washington Corridor may be the most costly and difficult to plan, with the challenge of MAGLEV crossing the Hudson River through New York City being well deferred for a decade or more, especially since AMTRAK does provide interim mid-speed Washington connections. Similarly, San Francisco Bay may compel deferral of service to East Bay cities and connection to Sacramento.

However, a second aspect of sequential strategy requires explicit attention. By factor of two, one may define a

lower Level III (Merit greater than 5,000). Level III would extend via Albany from both New York and New England to Syracuse, Rochester, Buffalo, Erie, Cleveland, Columbus, Dayton, and Cincinnati; the Chicago to Saint Louis route also qualifies at Level III (Tab. 4).

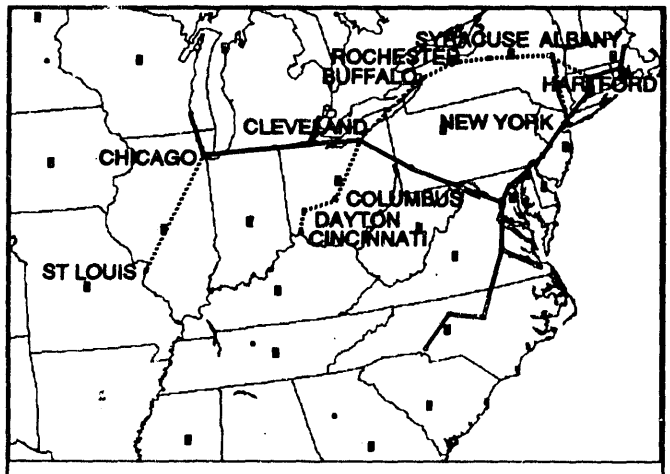

TABLE 4. LEVEL III EXTENSIONS

New York/Hartford/Buffalo Ext	480 Miles	+4/Top 75	Merit: 8,271
Buffalo/Cleveland/Cinci Ext	412 Miles	+3/Top 75	Merit: 6,226
Chicago/Saint Louis Extension	262 Miles	+1/Top 75	Merit: 5,050

Similarly, Level IV (Merit greater than 2,500) Corridors merits subsequent commitment if and when the overall success of MAGLEV has become even more certain and more rewarding. In Level IV, the East Coast extension to Atlanta is matched by Midwest ties from Minneapolis to Chicago, continuing South with feeds from Detroit and from Cleveland as well to reach Nashville and Atlanta (Tab. 5). The first California Corridor extension emerges at Level IV, San Diego to Phoenix and Tucson (Tab. 6).

Relegated to the disfavored category are the remaining Level V corridors with Merit below 2,500 (Tab. 7). Note that not only are the early clamorous contenders Texas, Florida, and Las Vegas in Level V category, but also that Florida connection (Orlando and Jacksonville to Atlanta) scores at this low Merit. No plausible connection to Texas even emerges for consideration.

VI. REFINEMENTS TO LEVELS I & II

The initial determinants of Level I & II MAGLEV corridors are the populations, personal incomes, and distances among 25 of the Top 75 MSA cities. To complete the roster of MAGLEV stations, six further determinants may be added. Plausible choices are

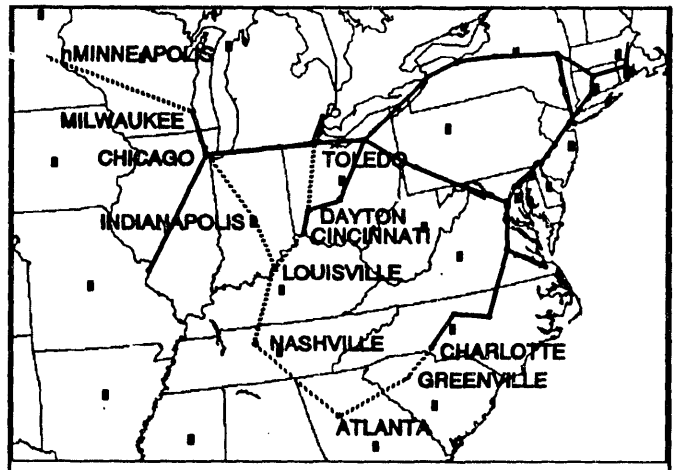

TABLE 5. LEVEL IV EXTENSIONS

Toledo/Cinci/Louisville Ext.	225 Miles	+1/Top 75	Merit: 4,293
Chicago/Louisville/Nashville Ext.	427 Miles	+2/Top 75	Merit: 3,128
Milwaukee/Minneapolis Ext.	298 Miles	+1/Top 75	Merit: 2,865
Charlotte/Atlanta Extension	229 Miles	+2/Top 75	Merit: 2,794
Nashville/Atlanta Extension	214 Miles	+1/Top 75	Merit: 2,506

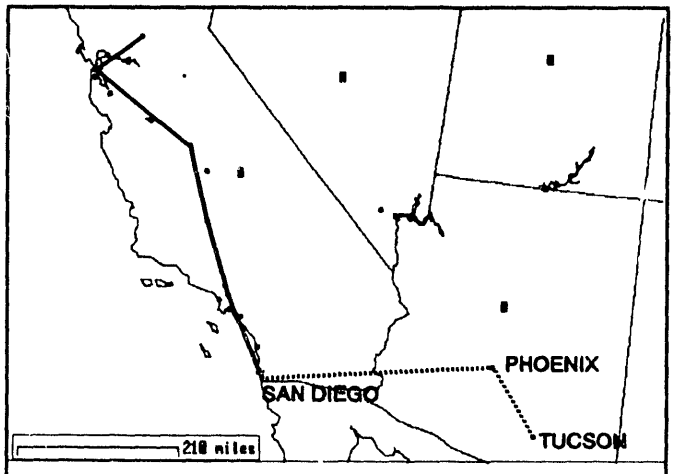

TABLE 6. LEVEL IV EXTENSIONS

San Diego/Phoenix Extension	299 Miles	+1/Top 75	Merit: 3,455
Phoenix/Tucson Extension	107 Miles	+1/Top 75	Merit: 2,757

TABLE 7. LEVEL V (DISFAVORED)

Los Angeles/Las Vegas Exten.	228 Miles	+1/Top 75	Merit: 2,312
St Louis/Kansas City Extension	238 Miles	+1/Top 75	Merit: 2,143
Dallas/Houston/San Antonio Y	394 Miles	4/Top 75	Merit: 1,848
Tampa/Orlando/Miami Trunk	294 Miles	4/Top 75	Merit: 1,693
Atlanta/Orlando Connection	410 Miles	+1/Top 75	Merit: 1,622
Los Angeles/Las Vegas Trunk	228 Miles	2/Top 75	Merit: 1,518

advanced in each of the six categories in order to illustrate fully developed LEVEL I & II characteristics.

First: Consolidation of Bi-State MSA Cities appears reasonable where the Census Bureau has not joined two immediately adjacent metropolitan areas on opposite sides of a state line (presumably for political distinction). The largest such pair is Hartford CT/Springfield MA, which would rank 24th as a single MSA. Indeed their common airport, Bradley Field, is a plausible joint MAGLEV stop. The Providence RI/Bristol County MA pairing connotes that all of Bristol County MA lies as close to a downtown Providence MAGLEV station as do many parts of Rhode Island included in the Providence MSA area; the joint population would rank 28th as a single MSA. The Youngstown OH/Sharon PA pair would rank 67th as a single MSA.

#	Rank	Description	Population	$/Capita
26	'24'	Bradley Intl Airport	1,726,556	19,662
-	'28'	Prvidnce RI/Brstl Cty MA	1,422,595	17,118
27	'67'	Yngstwn-Wrrn OH/Sharn PA	613,622	14,249

Analytical complexity lies in determining objectively which Nearby-Pair cities within a certain distance should be treated as single MAGLEV stops, and by what criteria.

Second: Bottom 76-281 MSA Cities contain the next 17.1% of U.S. population (MSAs #1-281 total 77.6% of US). Of course, if one of these cities lies directly along a TOP 75 MSA route, it is to be included as a MAGLEV stop. For even modest deviation, the Figure of Merit must be recomputed for the whole route, to assure that major city pair impairments from extra Route Miles do not exceed the gain from new-stop passengers. If a MSA #76-281 City lies beyond a TOP 75 CMSA terminus, a Figure of Merit of 10,000 (the LEVEL II criterion) for its extension justifies lengthening the MAGLEV Route.

The minimum list of MSA #76-281 Cities for addition is:

#	Rank	Description	Population	$/Capita
27	'67'	Yngstwn-Wrrn OH/Sharn PA	613,622	14,249
28	106	Prtsmth-Dovr-Rochestr NH	350,078	19,284
29	119	Vsalia-Tlare-Prtrvlle CA	311,921	12,898
30	138	South Bend-Mishawaka IN	247,052	15,748
31	183	Elkhart-Goshen IN	156,198	15,736
32	254	Burlington NC	108,213	15,649
33	259	Cumberland MD	101,643	12,529

Third: Major Airports are accessible by only minor deviations from the LEVEL I & II routes. Inclusion of 16 such airports is obvious. For the four largest metropolitan areas, the location of additional airports having substantial airline service can be taken as proof that additional sites need MAGLEV service (New York City: JFK, Laguardia, MacArthur; Los Angeles: Ontario, Burbank, Long Beach; Chicago: Midway; San Francisco: Oakland, San Jose).

#	MSA	Sixteen Major Airports	Population
34	1	Newark International (New York)	17,953,372
35	2	Los Angeles International	14,531,529
36	3	Chicago O'Hare International	8,065,633
37	4	San Francisco International	6,253,311
38	5	Philadelphia International	5,899,345
39	6	Detroit Metropolitan	4,665,236
40	7	Washington National	3,923,574
41	7	Dulles International (Washington)	3,923,574
42	9	Logan International (Boston)	3,783,817
43	13	Cleveland Hopkins International	2,759,823
44	15	Lindbergh Field (San Diego Intl)	2,498,016
45	18	Baltimore-Washington International	2,382,172
46	19	Pittsburgh International	2,242,798
26*	'24'	Bradley Intl (Hartford/Sprngfield)	1,726,556
47	34	Charlotte/Douglas International	1,162,093
48	55	Raleigh/Durham International	735,480

#	MSA	Additional Airports Needing MAGLEV Service
49	1	JFK International (New York)
50	1	LaGuardia (New York)
51	1	Long Island/MacArthur (New York)
52	2	Ontario International
53	2	Long Beach
54	2	Hollywood-Burbank
55	3	Chicago Midway
56	4	Oakland International
57	4	San Jose International

Fourth: Turnpike & Interstate Park-N-Rides need selection, but require no deviation of LEVEL I&II routes.

#	MSA	Expressway/Intersection
58	9	I-95/MA128/US1 Peabody MA
59	75	I-95/I-495 Attleboro MA
60	-	I-395/US6 Danielson CT
61	35	I-84/CT72 New Britain CT
62	1	Merritt Pkwy/CT8/CT25 Bridgeport CT
63	1	I-95/US1/CT104/CT106 Stamford CT
64	1	Htch Riv Pwy/I-287/I-684 White Plains NY
65	1	GS Pwy/NJ Tpk/I-287 Perth Amboy NJ
66	5	I-295/US1/US206 Trenton/Princeton NJ
67	5	I-95/PA Tpk/US1 Langhorne PA
68	5	I-95/I-295/I-495/US40 Wilmington DE
69	18	I-95/I-695/US1/US40 Overlea MD
70	18	I-95/I-295/US1/MD32 Savage MD
71	7	I-95/I-495/US1 College Park MD
72	-	I-81/US11/WV51 Martinsburg/Winchester WV/VA
73	19	I-70/PA Tpke/US119 New Stanton PA
74	13	I-480/I-271/USALT422 Bedford Hts OH
75	-	Ohio Tpke/US250 Milan OH
76	-	I-69/Indiana Tpk Fremont IN
77	3	I-65/I-94/Indiana Tpk Gary IN
78	3	I-57/I-94/D Ryan Expy L Calumet IL
79	3	I-94/I-294 TriState Tlwy "Wye" Northbrook IL
80	24	I-94/US41/WI20 Racine WI
81	-	I-95/US1/US17/VA3 Fredericksburg VA
82	28	I-64/VA238 Yorktown/Newport News VA
83	49	I-85/I-95/US1/US460 Petersburg VA
85	-	I-95/US58/US301 Emporia VA
86	-	I-85/USI/US158/NC39 Henderson NC
87	34	I-85/US29/US52/US70 Salisbury NC
88	4	I-80/I/780 Vallejo CA
89	213	I-5/CA152 Los Banos CA
90	2	I-5/I-210/I-405 San Fernando CA
91	2	I-5/I-405 Irvine CA
92	15	I-5/CA78 Oceanside CA

Their location can be wherever MAGLEV routes determined by other factors cross an appropriate highway, due to high auto mobility aiong expressways. Clearly, MAGLEV must make exit/entry (e.g. Beltway) stops at

every major metropolitan area, for maximum interception of autos (note that airport stops may qualify).

Fifth: Economic Redevelopment Priorities are high for those areas with large obsolete residential and commercial establishments, whose basic industries have permanently disappeared. Southeastern MA (Attleboro) missed the "Massachusetts Miracle". Bridgeport light manufacturing center factories have evaporated. As ex-Mayor Kenneth Gibson said, "I don't know where the cities of America are going, but Newark is going to get there first". Cumberland is the threshold of the benighted soft coal fields. The Mon Valley (McKeesport) must find new competitive advantage, or continue irreversible decline. Youngstown and Gary replicate the decay of the steel industry. These citations substitute for analysis, but witness the truth that political science is as potent as economic science.

#	MSA	Description
59	9	I-95/I-495 Intersection Attleboro MA
62	1	Meritt Pwy/CT8/CT25 Intrsction Bridgeport CT
34	1	Newark Airport (New York)
33	259	Cumberland MD
93	19	McKeesport PA
27	67	Youngstown-Warren OH/Sharon PA
77	3	I-65/I-94/Indiana Tpk Intersection Gary IN

Any major national transportation program in the Northeast must pay its dues in redevelopment of economic decline, by adding transportation competitive advantage.

Sixth: Limitation on Stops is the final refinement to LEVEL I & II routes. Each route has dominant city pairs, with heaviest Rider-Mile Potential. For such pairs, the specification is that MAGLEV provide service speed averaging 180 mph over the true (great circle) distance. Intervening stops "cost" 2.03 minutes more than uninterrupted cruise; this time serves for 0.15g deceleration to stop, 30 seconds nominal platform dwell time, and 0.15g acceleration back to 300 mph cruise speed. Thus N gives the maximum number of stops allowed for

$$2\,(\text{min/}stop)\cdot N(No.\ stopsAB) = \frac{TrueMilesAB}{3\,(miles/\text{min})} - \frac{RouteMilesAB}{5\,(miles/\text{min})} \qquad (5)$$

a MAGLEV going 5 mi/min along the route to average 3 mi/min over the true distance between the city pair.

Express and Local Trains are one consequence of this strategy on stops. Such trains will certainly be required along the East Coast LEVEL I Corridor. New York to Washington is nearly direct (205 true miles, 207 route miles). The formula allows 13 stops. Yet the Cleveland-New York route (403 true miles/513 route miles, N = 16) or the Norfolk-New York route (296 true miles/383 route miles, N = 11) are circuitous compared to auto/jet alternatives between these dominant city pairs. With minimum stops on the Midwest and Midsouth Extensions, the Cleveland and Norfolk MAGLEV schedules still must bypass some East Coast stops (say 7 Local Stops) and serve only the more important ones (say 6 Express Stops). The balances (10 stops Cleveland /Washington, 5 stops Norfolk/Washington) allow Extension Route stops every 35 miles or so. Many more Local trains per day will be required to service the Washington/New York traffic (50,000 Merit) than through trains for the Cleveland or Norfolk traffic (16.000 Merit), so the system offers good balance.

The Roster of 93 Stops is listed for Levels I & II, adding all of the elements specified above to the original 25 Top 75 CSMA/MSA cities. Levels I & II promise economic, social, and political vitality, with major service in the Northeast, Midwest, Midsouth, and California:

Description	Population	Miles
Portsmouth to Washington (15.4% US)	38,245,728	539
Washington to Detroit (4.4% US)	10,997,250	477
Toledo to Chicago/Milwaukee (4.1% US)	10,076,066	321
Washington to Norfolk (0.9% US)	2,261,747	186
Richmond to Charlotte (1.5% US)	3,813,517	301
Sacramento to San Diego (10.6% US)	26,286,846	616
Grand Total, LEVEL I&II (36.9% US)	91,681,154	2,440

a premier portion of the nation. Of the Top 75 CMSA cities, 26 are served by the 93 stops and the 2,440 route miles of MAGLEV Levels I & II, while 8 more will be added if the 1,154 route miles of Level III are justified, and 7 more will be added if the 1,800 route miles of Level IV are also authorized. Of the Lower 48 States, a total of 25 have population in the metropolitan areas served at Levels I, II, III, and IV.

VII. Conclusion

The possibilities for MAGLEV depend more on economic, social, and political questions than on technical issues. "Of course we can, but should we?" The population, wealth, and distribution in the U.S. may well provide a context rewarding to MAGLEV, but only if plans and actions are guided by accuracy rather than mere enthusiasm. This paper endeavors to provide assistance in clarifying where MAGLEV may fit, and where almost certainly it will not.

References

[1] U.S. Bureau of the Census. *State and Metropolitan Area Data Book, 1991*. Washington, 1991.

[2] U.S. Geological Survey. *The National Atlas of the United States of America*. Washington, 1970.

Market and Energy Demand Analysis of a U.S. Maglev System

Anant D. Vyas and Donald M. Rote
Center for Transportation Research, Argonne National Laboratory
Argonne, Illinois 60439 USA

Abstract - **High-speed magnetically levitated (maglev) vehicles can provide an alternative mode of transportation for intercity travel, particularly for short- and medium-distance trips between 100 to 600 mi (160 and 960 km). The patterns of growth and the underlying factors affecting that growth in the year 2010 are evaluated to determine the magnitude of U.S. intercity travel that would become the basis for maglev demand. A methodology that is sensitive to the travelers' socioeconomic attributes was developed to forecast intercity travel. Travel between 78 major metropolitan areas by air and highway modes is projected, and 12 high-density travel corridors are identified and selected. The potential for a maglev system to substitute for part of that travel is calculated by using a model that estimates the extent of diversion from highway and air to maglev. Energy demand is estimated on the basis of energy usage during acceleration and cruise phases for each corridor and corridor connections.**

I. INTRODUCTION

Intercity travel, involving trips longer than 100 mi (160 km), in the United States by highway and air modes has shown consistent increases. Travel by urban and rural interstate highways increased at annual rates of 5.6% and 3.2%, respectively, during 1971-1989 [1,2]. Travel by commercial airlines, in terms of domestic enplanements, increased at an annual rate of 5.6% during the same period [3,4]. Intercity travel will continue to grow, requiring considerable enhancement of highway and air capacity. Travel by highways will increase by 1.3% per year during 1989-2010 [5] and air enplanements will increase by 3.8% per year through 2002 [4].

The projected 50% increase in air travel would worsen the air traffic congestion and spread delays to all major airports. Several ideas have been advanced to handle the projected increase in air travel, including approach procedure improvements, new terminal airspace procedures, new runways, and the development of new technologies to close the gap between visual flight rules and instrument flight rules. The Federal Aviation Administration (FAA) projects that new airports will be required beyond the year 2000 to maintain the quality of service available today [6]. Since new airport construction is an expensive, time-consuming, and politically sensitive option, other options need to be investigated. One viable option is to divert some of the intercity travel to an alternative mode.

Short-haul aircraft operations represent an area where alternative travel modes could help alleviate air traffic congestion and allow airlines to concentrate on mid- and long-haul operations. Such alternative modes should provide service comparable with that of airlines at a similar price. Magnetically levitated (maglev) vehicles are expected to travel at speeds up to 300 mi/h (480 km/h) and have the potential to provide service comparable to airlines for trip lengths of 100-600 mi (160-960 km).

Manuscript received April 30, 1993. This work was supported by the U.S. Department of Energy under Contract W-31-109-Eng-38, the Electric Power Research Institute under contract RP3025-03, the U.S. Department of Transportation, and the U.S. Army Corps of Engineers.

II. METHODOLOGY

The methodology employed for this research consisted of several sequential steps. A baseline scenario was developed, and future demographic, economic, energy price, and technological data were compiled. A set of 78 metropolitan statistical areas (MSA) from the 48 contiguous states was selected for analysis. This set contained all metropolitan areas with populations over one million, all airline hubs, areas that formed one end of the top 50 air traffic routes under 600 mi (960 km), and metropolitan areas identified as potential maglev cities by an earlier ANL study [7]. A trip generation methodology was developed to project highway and air travel. Both air and highway trips were distributed by using the Fratar model. The top 100 metropolitan area pairs involving distances of 600 mi (960 km) or less were analyzed, and 12 corridors of high density travel were identified. Highway and air travel times and cost estimates were developed by using data from a related project, while maglev time and cost estimates were generated specifically for this analysis. A diversion model was applied to assess the extent of diversion from highway and air to maglev. Energy consumption estimates were developed by using maglev vehicle characteristics from published and unpublished data. The resulting energy demands were computed and analyzed for each high-density travel corridor.

A. Travel Demand Projection

Intercity trips are generated by using a methodology that applies travel rates by demographic groups. The methodology assumes the propensity to travel is a function of the traveler's socioeconomic attributes. The travel rates have not reached saturation and would change as economic output, fuel prices, personal income, and household work force configuration

change. Travel is also a function of mode maturity. As all travelers who could use a particular intercity travel mode use it and become familiar with it, that mode is assumed to have reached maturity. The methodology treats the highway mode as a mature mode, while the air mode has an opportunity to attract more travelers. Surveys by U.S. Travel Data Center (USTDC), along with data from the FAA, the Federal Highway Administration, and the Bureau of the Census were used to develop the travel rates.

Trip productions are dependent on three demographic attributes: household income, traveler age, and traveler employment status. Three trip production models, identical in structure, are applied, and a weighted sum of production is developed for each metropolitan area for each trip type,

$$P(i,t) = \Sigma_j W^j * T_p^j(i,t) \quad (1)$$

$$T_p^j(i,t) = \Sigma_k N^j_k(i) * R^j_k(t), \quad (2)$$

where P(i,t) represents productions from zone i for trip type t, W^j is the weight assigned to socioeconomic attribute j, and $T_p^j(i,t)$ is the productions for socioeconomic attribute j for the same zone and trip type combination from (2). $N^j_k(i)$ represents the number of units in subcategory k of attribute j for zone i, and $R^j_k(t)$ is the travel rate for the same combination.

Trip attractions are a function of four variables: households with income less than $20K, households with income greater than or equal to $20K, high-travel potential employment, and entertainment attractiveness. Professional, managerial, technical, and lower-level managerial employment are classified as having high travel potential. Each zone is assigned a code reflecting its entertainment attractiveness. Attractions, A(i,t) for zone i for trip type t, are the sum of trips attracted by each attribute times an entertainment factor plus a constant, with entertainment factor and the constant term dependent on the above mentioned code.

$$A(i,t) = \Sigma_j T_a^j(i,t) + F(k,t) \quad (3)$$

$$T_a^j(i,t) = N^j(i) * R^j(t) * EF(k,t), \quad (4)$$

where EF is the entertainment factor, F is a constant, and both are dependent on entertainment attractiveness code k. Values N and R represent zonal socioeconomic attributes and associated attraction rates as explained before.

Since the travel rates have not reached saturation, procedures to compute future travel rates were developed. The highway mode was considered mature, and all changes in trip rates were captured by tracking the changes in household income and number of workers per household. Past surveys by the U.S. Travel Data Center were used develop the following equation.

$$V_h = -15.454 + 0.193 * Y_h + 15.63 * W_h, \quad (5)$$

where V_h represents vehicle trips per household, Y_h is the average personal income per household in thousands of 1982 dollars, and W_h is the number of workers per household.

The changes in demographic composition of the nation's population are accounted for in the structure of the trip-generation model. The production component of the model allows for five classes of income (in 1988 dollars): <$20K, $20-25K, $25-35K, $35-50K, and >$50K; five classes of age: <18, 18-24, 25-44, 45-64, and >64; and four classes of employment status: high-travel potential employment, low-travel potential employment, retired, and not working. Future highway trips will be influenced by movement of population between the classes of these demographic attributes and also by changes in travel habits.

Changes in nationwide intercity travel were projected by applying the regression model to the U.S. Department of Commerce demographic projections [8]. The trip-generation model was also run using the state-level data for the years 2000, 2010, 2020, and 2030, while keeping the 1988 travel rates constant. This provided measures of changes caused by the movement of population among the demographic classes and geographical areas. The difference between the regression model and constant trip rate estimates provided a measure of the change in travel rates.

A different procedure was followed to estimate future year trip rates for the air mode. The air mode has the potential to attract more travelers as a greater and greater fraction of the population begins using it. A Gallup survey for the Air Transportation Association of America (ATA) [9] shows the incidence of flying (persons who used the air mode once) rising from 49% in 1971 to 74% in 1990. A model that projects enplanements per capita was developed as follows:

$$E_c = -1.7 + 0.154 * G_c - 0.0055 * C_c + 0.019 * IF, \quad (6)$$

where E_c represents enplanements per capita, G_c is gross national product per capita in thousands of 1982 dollars, C_c is airline revenue per enplanement in 1982 dollars, and IF is incidence of flying (as percent ever flown).

The above equation requires projection of revenue per enplanement and incidence of flying for future years for which procedures were developed. A logistic model was used to project incidence of flying. This variable, representing maturity of the air mode, is dependent on time. The following model was developed using the 1975-1988 data from ATA [9]:

$$IF = 1 - 0.42 * e^{-0.0343 * (t - 1975)}, \quad (7)$$

where t represents the forecast year.

A model for projecting airline revenue per enplanement, C_c, was developed using data published by Aerospace Industries

[3] and U.S. Department of Transportation [10]. This variable is dependent on fuel price and productivity improvements in air-carrier operations. The productivity variable is rather difficult to quantify, but it can be represented by time. The following relationship was established for any year beyond 1988:

$$C_c = 60.33 + 0.26 * J_p + (2030 - t)^2 / 101.2, \quad (8)$$

where J_p represents jet fuel price in 1982 dollars per 100 gallons and t is the year of interest.

The Fratar model was used to distribute both highway and air trips. The model adjusts an existing origin-destination trip matrix to match a set of growth factors for trip productions and attractions. Use of the model thus requires a base-year trip matrix. A base-year air-trip matrix was constructed using the 1988 10% ticket sample file from the U.S. Department of Transportation [11]. Next, the total trip matrix was subdivided into business and nonbusiness trip matrices by using the 1988 trip production and attraction shares provided by the trip-generation model. The Fratar model was then applied to produce a set of trip matrices for the year 2010. Production/attraction growth factors provided by the trip-generation model were used.

Since a comprehensive database for intercity highway travel between metropolitan areas does not exist, a step-wise procedure was employed to construct a base year highway-trip matrix. First, two MSA to MSA highway-trip matrices, one for business and the other for nonbusiness travel, were constructed by using distance based air trip to highway trip ratios. The ratios reflect an intercity mode preference pattern in which the highway mode carries several times the number of passengers as the air mode when the trip distance is short. Next, these matrices were revised to reflect the trip estimates from surveys conducted by states or other agencies. Data from Northeast corridor, New York state corridor, Pennsylvania corridor, Ohio High Speed Rail Study, Illinois-Michigan Study, Illinois-Wisconsin-Minnesota (Tristate) Study, Texas Triangle Study, and Florida High Speed Rail Study were incorporated. Finally, the Fratar model was applied to project year 2010 highway trip interchanges. Trip productions and attractions from the trip-generation methodology described above were used to compute these growth factors.

In our modeling effort, we found that intercity travel is strongly influenced by four major factors: population, number of households, employment, and income. The U.S. population is expected to continue to grow in absolute numbers, but the rate is expected to decline between 2000 and 2010. A likely strong influence on travel behavior is the percent of the population over 65, which increases significantly after 2010. Accompanying this trend is an increase in the number of households, which continues rapidly even out to 2030, but the current tendency towards smaller households is expected to continue -- helped along by the growing over-65 population. This has an important implication for highway travel (and, in turn, for the potential for maglev travel), because the vehicle occupancy for nonbusiness trips would be expected to decline as the household size shrinks. Thus the per-person cost of travel would increase, making travel by common carrier (air or maglev) more attractive.

Air travel is forecast to continue to increase, but at rates lower than historical rates. The number of air trips increased at an annual rate of 5.2% during 1970-90. The projected rate of growth for the next 20 years is 3.1% annually. The annual rate of growth during the last decade of this century is projected to be 3.3%. The demand for air travel will increase from 294.2 million trips in 1988 to 581.8 million trips in 2010. The air mode will be close to maturity in 2010, when a projected 87% of the population will have flown at least once as compared with 73% in 1988.

Since maglev is a common-carrier mode, a majority of its trips will be diverted from air, the existing high-speed common carrier mode. Also, as maglev technology develops, it will be tested first in select places before introducing it in a network of connected corridors. Air trip interchanges in the year 2010 were analyzed, and the top 100 MSA pairs involving distances of 600 mi (960 km) or less were tabulated. Twelve corridors were selected from the analysis of these trips and from the list of corridor studies conducted by states and federal agencies. Table 1 lists the selected corridors.

Thirty one metropolitan areas, out of 78, are part of the twelve selected corridors, representing 930 interchanges. Many of these are not feasible to traverse by maglev alone, given the selected maglev corridors. For example, Los Angeles to New York City or Dallas to Chicago trips cannot be made by maglev alone. When such infeasible interchanges were removed, and interchanges involving less than 500 annual trips were eliminated, a total of 400 interchanges remained for trip diversion and energy demand analysis.

TABLE 1 HIGH DENSITY TRAVEL CORRIDORS

1.	Northeast Corridor: Washington (DC), Baltimore, Philadelphia, New York City, Hartford, Boston
2.	New York State Corridor: New York City, Albany, Syracuse, Rochester, Buffalo
3.	California Corridor: San Francisco, Los Angeles, San Diego
4.	California-Las Vegas Corridor: Los Angeles, Las Vegas
5.	Florida Corridor: Miami, Orlando, Tampa
6.	Texas #1 Dallas-Houston Corridor: Dallas, Houston
7.	Texas #2 Dallas-San Antonio Corridor: Dallas, Austin, San Antonio
8.	Texas #3 Houston-San Antonio Corridor: Houston, Austin, San Antonio
9.	Illinois-Michigan Corridor: Chicago, Detroit
10.	Quad-State Corridor: St. Louis, Springfield (IL), Chicago, Milwaukee, Madison, Minneapolis-St. Paul
11.	Pennsylvania Corridor: Philadelphia, Harrisburg, Pittsburgh
12.	Michigan-Pennsylvania Corridor: Detroit, Toledo, Cleveland, Pittsburgh

B. Modal Characteristics Development

Travel time and cost characteristics were developed for air, highway, and maglev. Procedures to estimate travel time and cost components for air and highway modes were developed by using data from several sources while maglev components were derived based on published operating criteria, discussions among ANL staff, and technical judgement.

Air characteristics are subdivided as MSA level and MSA pair specific. The MSA level characteristics include access/egress time and cost, time spent in an airport before the aircraft doors are closed, time between aircraft door closing and being airborne, time between touching ground and aircraft doors opening, and time spent in an airport between aircraft door opening and boarding ground transportation.

The access and egress time values were computed using average distance from the most populated place in each county of the MSA and weighting them by county population. We obtained the county-level population forecasts from each state and used them to compute average distance. MSAs were classified by their population as extra-large (more than 5 million), large (3-5 million), medium (1-3 million), and small (less than 1 million) for the assignment of average speeds. The speeds represent average values for all approach modes, including coach and public transit where applicable.

Wait time and in-airport time were estimated using data from a ground-access study [12]. Base-year (1988) taxi, queue, and take-off times, as well as landing, taxi, and idle times, were estimated using an earlier study [13]. The values in the study were updated by using the percent of operations delayed by 15 minutes or more as published by the FAA [6]. The queue subcomponent will increase exponentially with the increase in aircraft operations if airport capacities are not expanded. We assume periodic capacity expansion by various means to cause a linear relationship between air travel demand and queuing time. The practice of not allowing an aircraft to take-off for a destination airport that is experiencing delays is assumed to continue in the future. Thus, average landing times are expected to increase very little.

Airport access costs are computed separately for business and nonbusiness purposes by using average distance and airport-specific access mode shares. Access modes include 1) drive and park or use of rental car, 2) taxi or limousine, 3) coach/airport bus, 4) mass transit, and 5) courtesy vehicle. A sixth mode, driven by friend/relative, was allowed for nonbusiness travel only. Cost components include fuel and nonfuel operating costs, parking fees, labor costs, tolls, and fares, which vary depending on the access mode.

Linehaul time and fare are two MSA pair specific components. Linehaul times were computed using a regression equation. Average fares were also computed using a regression equation that accounted for the effect of hubs, fuel prices, and productivity improvements. These fares do not account for increases in capital cost, which are likely to be substantial.

The highway mode characteristics were compiled for intercity passenger trips by assuming that all the trips were made by automobiles. A vehicle trip was subdivided into three parts: travel within the origin MSA, travel between MSAs, and travel in the destination MSA. Highway travel times and costs depend on such parameters as distance, intercity highway speed limits and miles driven per day, lodging cost per night, fuel economy and fuel prices, nonfuel automobile operating cost per mile, duration of stops for fuel and rest during highway travel, and time and distance traveled within origin and destination MSAs. A value of 700 mi (1120 km) was selected as the distance driven per day. A 50 mi (80 km) allowance is automatically made to allow a traveler to complete the trip without incurring lodging cost.

The automobile cost component consists of fuel and other operating costs. It does not contain depreciation, registration, and insurance. Both fuel and other operating costs are computed as dollars per mile using energy price and fuel economy data. Nonfuel auto operating costs include lubrication, tires, and maintenance [14].

Maglev time and cost information was developed using highway distance and some allowance for circuity. The resulting total distance for each origin-destination pair is subdivided by speed class, and the linehaul time is computed on the basis of the number of miles in each speed class, the number of stops, and the number of transfers. The speed classes are 165 mph (265 kmph), 200 mph (320 kmph), 250 mph (400 kmph), and 300 mph (480 kmph). All MSAs with populations over 3 million, and those in the Northeast corridor, are assumed to require travel at reduced speed for some distance within the metropolitan area (5 to 15 mi). All other distances for each speed regime were determined by technical judgment based on the individual corridor.

Direct travel is considered feasible between all large MSAs with stops at major intermediate points. For example, a trip from New York to Chicago does not require any transfers, but requires stops in Philadelphia, Pittsburgh, and Detroit. In addition, each major metropolitan area may have more than one stop (i.e., downtown, suburban, airport) and each stop is assumed to have a duration of 2.5 minutes. Travel to or from a smaller MSA can involve a transfer at a major hub (or half a transfer if some direct service is possible), with an average transfer delay of 30 minutes.

Maglev out-of-vehicle times (access/egress and waiting times) were obtained by multiplying the air out-of-vehicle times by a factor of 0.75. This factor accounts for the fact that metropolitan areas will probably have more than one maglev station, so that the average distance to a station will be less than the average distance to an airport. Maglev access costs were assumed to be 90% of those for air. The factor for access costs is higher than that for out-of-vehicle times because access cost is influenced less by distance than access

time. Maglev fares were assumed to be 80% of the air fare to account for the lower linehaul travel speed.

C. Estimation of Diversion to Maglev

A diversion model was selected to estimate trip diversion from highway and air modes to the new mode. The model includes such logical parameters as waiting time, linehaul time, and cost [15]. Rail trips were added to the diversion estimates by using constant diversion rates. The model requires total travel cost, in-vehicle travel time, and out-of-vehicle travel time for highway, air, and the new mode. Business out-of-vehicle travel times were computed as 20 minutes less than nonbusiness out-of-vehicle travel time if the nonbusiness out-of-vehicle time for an origin-destination pair was greater than 100 minutes; as 15 minutes less if the nonbusiness out-of-vehicle time was in the range 80-100 minutes, and as 10 minutes less for all other values.

The trip diversion model multiplies the out-of-vehicle time by a factor less than 1. This reduction was not considered appropriate for the highway mode since it makes the common-carrier mode more attractive (by reducing the effect of access/egress time and waiting time). Also, the maglev mode has constant terms for each purpose and mode combination. Since the diversion model was developed for trips shorter than 500 mi (800 km), highway business diversion for longer distances may not be predicted properly. A value of −0.8 was added for distances of 600-900 mi (960-1440 km), and an additional −0.8 was added for longer distances. Even after these additions, the model tended to predict high shares (80-95% for longer trips). Thus, the diversion from business highway trips was restricted to 66% for distances of 500-750 mi (800-1200 km), assumed not to require any lodging cost, and restricted to 50% for longer distances.

Rail trip estimates were compiled from various origin-destination counts obtained from the Federal Railroad Administration. The rail trips were subdivided as business and nonbusiness equally. Fixed diversion rates of 85% for business and 70% for nonbusiness were applied for maglev.

D. Energy Calculations

Electric utilities are likely to view the loads generated by the maglev system as less than ideal because its demand is unsteady due to accelerations and because peak maglev demands tend to coincide with peak loads in the rest of the utility system (midmorning and late-afternoon). Maglev could operate either with long trains or in smaller units of one or two vehicles. When operating with one or two vehicles, the acceleration energy requirements of each individual unit would decrease, which would help smooth out the electrical demand oscillations of a maglev system.

Large-scale off-board energy storage facilities could be used to reduce the peak loads for maglev systems. These facilities could be distributed along the maglev corridor and charged from base-load power plants at night or from spinning reserve. Spinning reserve is the margin that utilities are required to maintain in order to handle unforeseen situations, such as a sudden shutdown of a power plant or a large unexpected load. The requirement is about 10% in excess of the current demand, and storage devices could be charged from this spinning reserve since the charging could be interrupted at any time.

Maglev vehicles travelling at cruising speeds require energy to overcome aerodynamic drag, which increases sharply with speed, and magnetic drag, which is highest at low speeds. In addition, hotel energy, which is independent of speed, is required for use on-board the vehicle (about 300 kW). During acceleration energy is also required to bring the vehicle up to speed. A 150-seat electrodynamic maglev vehicle was characterized by using data from various sources (most of which are unpublished).

The magnetic drag force (computed as 780 divided by speed in meters per second for speeds above 50, or 30.25 kN otherwise) and energy requirements to overcome magnetic and aerodynamic drag are given in Table 2 for various speeds.

The actual electric energy demand required from the power plant was computed by considering the efficiency of the linear synchronous motor mounted on the guideway (90%), the efficiency of the power conditioning unit at the wayside station (85%), and the electricity transmission efficiency (95%). These combine to give an overall efficiency of about 72.7% for maglev. The electric generation efficiency is not included.

TABLE 2 AERODYNAMIC AND MAGNETIC DRAG ENERGY

Speed (km/h)	Magnetic Drag Force (kN)	Drag Energy (kWh/km)		
		Magnetic	Aerodynamic	Total
200	13.96	3.88	1.56	5.44
266	10.58	2.94	2.72	5.66
322	8.73	2.42	4.00	6.42
402	6.98	1.94	6.24	8.18
483	5.82	1.62	8.99	10.61

III. RESULTS

Table 3 summarizes the most important ridership and energy results for each corridor. The table includes passenger demand, passenger miles traveled, energy intensity, and total energy demand. The individual corridor totals do not include trips that traverse that corridor but have either the origin or destination (or both) outside the corridor. However, those trips are accounted for in the "corridor connections" totals. The individual corridor totals for ridership and energy would increase if any corridor is connected to any other corridor, but

since the values depend on the exact extent of the entire network, those projections cannot be made at this time. Travel demand will also increase if connections are provided at the airports involving high volumes of connecting trips. An air traveler could transfer to maglev for a part of the trip that either originates or terminates at a point outside the connected corridors. Estimates of such diversion will require more detailed analysis. We carried out a simple analysis of trips involving origin or destination in Albany, Syracuse, Rochester, and Buffalo with a maglev airport connection that showed potential increases in the range of 5-15%, depending upon airline cooperation.

The estimated total energy demand for the 12 corridors is 5.26 trillion watt-hours. Aside from energy demand, the power demand profile will influence utility planning and load management. A 150-seat maglev vehicle will require approximately 20 MW of power at startup (accelerating at 0.16 g or 1.57 m/s^2) and 5.4 MW while cruising at 300 mph (480 kmph).

TABLE 3 MAGLEV TRAVEL AND ENERGY DEMAND IN 2010

Corridor & Connections	Demand 10^3	PMT 10^6	EI Wh/PMT	Energy 10^6 kWh
Northeast Corridor	23,456	5,344	201	1,073
New York State Corridor	5,173	1,335	249	333
NE/NYS Connection	476	233	231	54
California Corridor	12,603	4,545	223	1,014
CA - Las Vegas Corridor	6,137	2,027	231	468
Florida Corridor	6,858	1,688	265	448
Dallas-Houston Corridor	3,069	773	255	197
DFW-Austin-S Antonio	2,487	560	255	143
HST-Austin-S Antonio	1,770	373	252	94
Chicago-Detroit Corridor	1,658	478	247	118
Quad-State (STL-MSP)	4,124	1,253	252	316
Midwest Connection	569	338	250	84
Pennsylvania Corridor	1,503	356	253	90
NE-Penn Connection	1,268	562	232	130
NYS-Penn Connection	30	18	246	4
Detroit - Pitt Corridor	419	89	256	23
Other Connections	3,596	2,720	245	665
System Total	75,197	22,691	232	5,255

A. Profile of Electricity Demand

The profile of potential electricity demand was analyzed by selecting two sections of the future maglev lines: 1) Boston to New York City and 2) Los Angeles to San Francisco. All trips that will use the selected sections were identified and summed. For example, the Boston to New York City section will be used by trips originating from or ending in Boston and having the other end in New York City or maglev cities beyond New York City, as well as trips originating from or ending in Hartford and having the other end in New York City and maglev cities beyond New York City.

In this analysis, we assumed the number of vehicles travelling daily between terminal cities to be distributed in the same way as the aircraft flights are. We computed the number of vehicles required to serve the demand by assuming a 60% load factor and uniformly distributed demand through the year. We also used the average energy intensity for the section. The number of vehicles en route at any specific time of day is computed from travel time and average headway. The power demand for maglev is computed by using 20 MW for accelerating vehicles and 5.4 MW for cruising vehicles. The actual power demand will be influenced by route geometry, location and number of stops, maximum speed, and demand charges.

TABLE 4 ELECTRICITY DEMAND PROFILE FOR THE BOSTON-NEW YORK CITY SECTION

Travel Distance (mi)	249			
Travel Time (min)	85			
Passengers per Year in each Direction (10^6)	4.86			
Average Passengers per Day in each Direction	13,310			
Vehicle Tips per Day in Both Directions	296			
Profile (both directions) by Time of Day	6-10 AM	10 AM-2 PM	2-6 PM	6-10 PM
Vehicle Trips	74	72	88	62
Avg. Headway	6.5	6.7	5.5	7.7
Vehicles en route	26-28	24-26	30-32	20-22
Potential Annual GWh Demand	124	121	149	104
Power MW[1]	265-285	244-265	306-326	204-224
Power MW[2]	329-354	304-329	380-405	253-278

[1] Assuming 33% of the vehicles accelerating at a time.
[2] Assuming 50% of the vehicles accelerating at a time.

TABLE 5 ELECTRICITY DEMAND PROFILE FOR THE LOS ANGELES-SAN FRANCISCO SECTION

Travel Distance (mi)	395			
Travel Time (min)	122			
Passengers per Year in each Direction (10^6)	5.31			
Average Passengers per Day in each Direction	14,560			
Vehicle Trips per Day in Both Directions	324			
Profile (both directions) by Time of Day	6-10 AM	10 AM-2 PM	2-6 PM	6-10 PM
Vehicle Trips	86	74	90	74
Avg. Headway	5.6	6.5	5.3	6.5
Vehicles en route	42-44	36-38	44-46	36-38
Potential Annual GWh Demand	254	220	268	220
Power MW[1]	428-448	367-387	448-469	367-387
Power MW[2]	531-557	455-481	557-582	455-481

[1] Assuming 33% of the vehicles accelerating at a time.
[2] Assuming 50% of the vehicles accelerating at a time.

IV. REFERENCES

[1] Federal Highway Administration, *Highway Statistics: Summary to 1985*, U.S. Department of Transportation, Washington, D.C. (1987).

[2] Federal Highway Administration, *Highway Statistics 1988 and 1990*, U.S. Department of Transportation, FHWA-PL-89-003 and FHWA-PL-90-003, Washington, D.C. (1989-91).

[3] Aerospace Industries Association of America, *Aerospace Facts and Figures 1981/82*, Washington, D.C. (July 1981).

[4] Federal Aviation Administration, *FAA Aviation Forecasts: Fiscal Years 1991-2002*, U.S. Department of Transportation Report FAA-APO-91-1, Washington, D.C. (March 1991).

[5] Energy Information Administration, *Annual Energy Outlook*, U.S. Department of Energy Report DOE/EIA-0383(90), Washington, D.C. (Jan. 1990).

[6] Federal Aviation Administration, *1990-91 Aviation System Capacity Plan*, DOT-FAA-SC-90-1, U.S. Department of Transportation, Washington, D.C. (Sep. 1990).

[7] Johnson, L.R., et al., *Maglev Vehicles and Superconductor Technology: Integration of High-Speed Ground Transportation into the Air Travel System*, Argonne National Laboratory Report ANL/CNSV-67, Argonne, Illinois (April 1989).

[8] Bureau of Economic Analysis, *1985 OBERS BEA Regional Projections: Volume 2 - Metropolitan Statistical Area Projections to 2035*, U.S. Department of Commerce, Washington, D.C. (1985).

[9] *Air Travel Survey 1990*, Produced for the Air Transport Association of America by The Gallup Organization, Inc., Princeton, NJ (1990).

[10] Volpe National Transportation Systems Center, *National Transportation Statistics*, Research and Special Programs Administration, U.S. Department of Transportation, Cambridge, MA (1983-1990).

[11] Research and Special Projects Administration, *O&D City Pair Summary (Data Bank 6)*, U.S. Department of Transportation, Washington, D.C. (1990).

[12] City of Chicago, *The 1989 Ground Access Study*, Department of Aviation, Unpublished Data, Chicago, Illinois (1990).

[13] Yamartino, R.J. and D.M. Rote, *Updated Model Assessment of Pollution at Major U.S. Airports*, Proceedings of Air Quality and Aviation: An International Conference, Federal Aviation Administration Report FAA-EE-78-26, U.S. Department of Transportation, Washington, D.C. (Nov. 1978).

[14] Motor Vehicle Manufacturers Association, *MVMA Motor Vehicle Facts & Figures '88*, Detroit, Michigan (1988).

[15] Brand, D., et al., *Forecasting High-Speed Rail Ridership*, Transportation Research Record 1341, pp. 12-18, Transportation Research Board, Washington, D.C. (1992).

Reducing Magnetic Fields from Maglev Guideways to Reasonable Levels

J. P. Blanchard
Research and Development Advanced Civil Systems Group,
Bechtel Corporation, San Francisco, CA 94119-3965

Abstract - **Magnetic fields required by magnetically levitated high speed trains must be sufficient to lift, guide, and propel the passenger or freight vehicle at speeds of up to three hundred miles an hour. This implies a need for locally high field intensities to create forces sufficient to do these jobs. At the same time a number of limiting factors require the fields to be carefully restricted elsewhere: they may not interfere with wayside or vehicle based electronic guidance and control equipment, they must not detract from the structural integrity of the guideway, and they must not be biologically significant to either the passengers or people in the vicinity of the system. This presentation will explore the expected field patterns from the Bechtel team's National Maglev Initiative System Concept Definition design and how the design accommodates each of the limiting issues identified above.**

I. INTRODUCTION

Bechtel recently lead one of four teams in the National Maglev Initiative System Concept Definition study. The results of this effort provided a series of designs expected to form a basis for future maglev concept development that will ultimately offer the United States a mass transit alternative to meet the needs of the twenty first century. Central to the Bechtel team effort was the design of a levitation, propulsion, and guidance system that uses magnetic fields sufficient to sustain adequate speed, safety, and ride comfort at speeds up to 300 miles per hour. The basis of this system is a linear synchronous motor consisting of a number of vehicle based superconducting magnets that create a constant magnetic field and a guideway propulsion winding that creates a traveling magnetic field. The interaction of these two fields produces the propulsive force[1]. The same superconducting magnets are used for levitation and guidance, with additional guideway equipment providing the necessary fields for these functions.

This paper considers the anticipated impact of the magnetic fields associated with the Bechtel team maglev design on people and maglev system components outside of the levitation, propulsion, and guidance packages. Additional technical details about the levitation, propulsion, and guidance systems will be presented in other sessions at this conference[2,3]. Far field calculations of magnetic fields associated with the general design discussed here are described in greater detail elsewhere[1]. In light of the preliminary stage of design of this system, any conclusions drawn here must be considered preliminary yet valuable because they begin to frame the possible concerns, allowing future design work to accommodate refinements as needed to mitigate fields in strategic areas.

II. HOW IS "REASONABLE LEVELS" DEFINED?

A. *Source Characteristics*

It is generally recognized that the nature and extent of interaction of a magnetic field depends on its intensity, frequency, and orientation with respect to other objects, as well as its spatial and temporal duration. In this paper we examine three distinct forms of magnetic fields: a static, or dc, field; a periodic or sinusoidally varying ac field; and impulse or anomalous fields. Actual field patterns encountered will likely be a combination of these three types.

This work was supported in part by the U.S. Department of Transportation under contract no. DTTFR 53-92-C00003.

The source of each type of field will depend on the observer's reference frame. If on-board the vehicle, a static field will be seen from the superconducting magnet on the vehicle and the guideway based currents will be seen as periodic ac or impulses depending on whether they are from anomalous or regularly spaced sources. Anomalous sources might be, for example, unexpected irregularities in the guideway, or some local misalignment of the magnet system. By contrast, the wayside based observer is generally less likely to encounter significant dc fields unless positioned near an inverter station, but will see an impulse or periodic ac field every time a vehicle passes, sometimes accompanied by switching transients.

Each of these field types interacts differently with conducting loops in external systems. The static field cannot induce currents in such loops but will exert a force on established current loops in accordance with Ampere's Law. By contrast, the ac fields can not only create forces, but also induce currents in conducting loops. Those arising from regular, sinusoidally varying fields are maintained (or continuously refreshed) by the external field while those from impulses decay away, generally in the form of resistive heat losses.

B. Exposure Concerns

A "reasonable level" may be defined as one that does not produce an adverse effect. Consequently, there will be different "reasonable levels" for different components of the system that are exposed to the magnetic fields from the maglev system. In this paper we focus on three key components that could be adversely influenced by the system's magnetic fields: the command/control/communication (C3) system; the structural supports; and people onboard or in the vicinity of the maglev system. These components are not specific to the Bechtel design but would exist in any maglev project. However, the mitigation section below will examine general mitigation concepts then concentrate on the Bechtel team's approach to reducing the likelihood of adverse effects arising as a result of its magnet system.

1) Command/Control/Communications

Electromagnetic interference arising from stray fields is a potentially significant concern. Ac fields, particularly those that generate impulse currents, are expected to be of generally greater concern here than dc fields because of their ability to induce spurious currents on conducting lines. As a limit, any field induced currents should not corrupt existing data communications, result in significant power losses, or interfere with normal suspension, levitation, and guidance forces to unbalance the vehicle or hinder its intended motion.

2) Tolerance Limit of Structural Members

Most systems will use concrete, a magnetically inert material, for the majority of structural components. However, the mild steel reinforcement typically found in concrete structures is expected to be extremely sensitive to the magnetic fields in its vicinity. In particular, the ac fields may induce currents in the connected sections of reinforcement, the dissipation of which will deposit some heat in the structure. Whether this is significant will depend on the magnitude of the heat generated and where it is deposited in the structure. Both the ac and the dc fields will create forces within the structure if there is any remnant magnetic field in the structural steel. Again, the significance of these forces depends on their magnitude, which in turn depends on the strength of the field seen by the reinforcing steel as well as the magnitude of the remnant field, if any, in the steel. Over the expected fifty year lifetime of the structural support system, the cumulative effect of these forces and heat depositions must not significantly weaken the structure.

3) Physiological Limitations

Existing research suggests that electromagnetic fields, under some circumstances, can interact with the human body to produce biological effects. While clear delineation of hazardous levels, if such exist, remains generally elusive at this time there is general agreement that limits on solely static fields should be higher than for ac fields. Nevertheless, the steady (dc) and time varying (ac) fields arising from the maglev system should not pose a physiological hazard to train passengers or people in the vicinity of the system and should conform to human exposure standards where they exist.

Presently the most stringent known dc magnetic field limit for people is 10 mG, beyond which signs should be posted warning people with implanted cardiac pacemakers of higher fields. Ac field limits vary by jurisdiction from no limit in most areas to as low as a suggested 2 mG near some school areas.

Limits on impulse fields have been suggested in the scientific literature but none has, to date, been implemented. While these are limits only on the magnitude of fields, some research suggests that biological effects may also depend on the magnetic field's frequency, spatial orientation with respect to the body, temporal duration, and may in fact involve a complex interaction between a variety of field parameters.

III. DESIGN AND MITIGATION

A. General Mitigation Concepts

There are a number of ways to mitigate the effects of magnetic fields on the various systems described above. Notice that mitigation generally, but not always, consists in a reduction of the field magnitude. In some cases, mitigation may also require a change in operating frequency or duty cycle.

First, it is well known that the magnitude of magnetic fields declines in value with distance from source depending on the nature of the source. The field reduction will generally be at least as rapid as the inverse of the distance from the source, and in some cases will be proportional to the square or cube of the inverse of the distance. This allows a field reduction simply by increasing the distance between the source and the observer where possible. Note that while it is possible to reposition people and communications equipment away from magnetic field sources to reduce their exposure, the structural system, including mounting brackets for the guideway based levitation, propulsion, and guidance equipment, cannot be moved away from the sources.

Where distance between source and observer is not possible, shielding can sometimes be used to reduce fields within a specified volume. However, there is almost always a penalty of higher fields elsewhere as a result. Shielding can be passive, using a materials with a high relative magnetic permeability such as mu metal, or active, with bucking coils creating a field that cancels the original field in a defined area.

In some cases, the best form of mitigation is to use material that is magnetically inert to do the job originally performed by a conducting or magnetically active material. Examples include the use of fiber optics in command/control/communications systems and fiber reinforced plastic reinforcement in structural systems.

B. Design Specific Field Reductions

Beyond these general suggestions for mitigating the effects of magnetic fields, the Bechtel team identified several design specific methods for altering the magnetic field as needed to accommodate the diverse requirements placed on the system. Because the vehicle based superconducting magnets are expected to be the largest single source of magnetic fields experienced either onboard the vehicle or in the wayside, much of this work concentrated on those magnets. Note that the fields from these magnets will be experienced as dc fields on board the vehicle and as ac fields by wayside based people and equipment as the vehicle passes by.

Thornton et al.[1] suggest several distinct ways to mitigate the fields arising from the vehicle's magnets. Each of these involves a trade-off with other system parameters.

First, increasing the length of the vehicle magnet arrays reduces the far field component of the magnetic field substantially. If this is combined with tapering the field strength of the end magnets, the overall maximum field is decreased by a factor of up to about three with only a minimal reduction in motor thrust.

Second, reducing the pole pitch of the vehicle based magnets reduces the far field but requires higher frequencies for the propulsion system. This in turn leads to higher eddy current losses and a requirement for more turns in the magnets or a closer spacing between the vehicle and guideway magnet systems. Nevertheless, if research in biological effects of magnetic fields indicates a complex relation between effects and the frequency and relative magnitude of ac and dc fields, as some studies suggest, this may become a critical set of tradeoffs.

Third, the use of proprietary flux cancelling designs in the magnet systems can reduce fields by a factor of two or better. Although there may be penalties in terms of weight and cost for such systems, the benefits appear to compensate for these.

Finally, active shielding can be used to reduce fields in specific areas as noted earlier. Thornton et

al. suggest this should only be included after implementing other field reduction techniques because of the weight and power requirements for this kind of shielding.

In addition to these methods that focus attention on the vehicle based magnets, there are a few guideway based field mitigation options. A more efficient suspension system, for example, will make better use of the fields from the vehicle magnets, thereby reducing the need for extra capacity in the vehicle magnets while minimizing ac losses in the suspension system. The proprietary Bechtel team design for the suspension system contains significant improvements in the efficiency of this system. Also, since the fundamental frequency of the guideway current depends directly on the vehicle speed relative to the pole pitch of the vehicle magnets, there is inherently some flexibility in the field frequencies experienced on the wayside as a result of guideway based equipment if warranted. Since variations in frequency can also be expected to change a variety of other operational characteristics of the system and must be carefully considered in terms of their influence on overall system performance.

IV. CONCLUSIONS AND FUTURE WORK

We identified in this paper source characteristics and exposure concerns related to maglev system magnetic field effects on equipment and people outside of the levitation, propulsion, and guidance systems where those fields are primarily used. General magnetic field mitigation options were reviewed and design specific options were noted for field mitigation within the context of the Bechtel team National Maglev Initiative system concept.

The Bechtel team design provides the basis for additional concept development. There is additional work to be done in refining all elements of the concept including the magnet systems. Additional work is anticipated to further identify the critical tradeoffs required with guideway reinforcement concepts to balance cost, strength, and power losses. In addition, more work is needed to verify the robustness of communication systems under all anticipated operating conditions. Finally there is a vital need to clarify the key parameters of magnetic field interaction with biological systems in order to clearly understand the most appropriate forms of magnetic field mitigation for people onboard and in the vicinity of the maglev system.

ACKNOWLEDGMENT

The author thanks Professor Richard D. Thornton for useful discussions and acknowledges his extensive work on the maglev systems described here.

REFERENCES

[1] R. D. Thornton, D. Perreault, and T. Clark, "Linear Synchronous Motors For Maglev," DOT/FRA/NMI-92/13, January 1993, available through National Technical Information Service, Springfield, VA 22161.

[2] R. Thornton, "Flux Cancelling Maglev," poster presentation PS1-8, Maglev '93, Argonne National Laboratory, Argonne, IL, 19-21 May 1993.

[3] R. Thornton, "Linear Synchronous Motor Design," oral presentation OS6/7-1, Maglev '93, Argonne National Laboratory, Argonne, IL, 19-21 May 1993.

Loss and Guideway Interaction Force Measurements on a Superconducting Magnet for Maglev Applications

Charles R. Dauwalter
Charles Stark Draper Laboratory, Inc., Cambridge, MA

Abstract

Accurate knowledge of losses in superconducting magnets is an important requirement for the design of levitation, guidance and propulsion systems for electrodynamic maglev vehicles. An experiment in preparation is described to measure ac fields due to guideway currents, and magnetic forces and force gradients, which will provide the basis for subsequent measurements of superconducting coils for maglev suspensions. The experimental apparatus can test full-size maglev components at velocities approaching expected maximum speeds. The initial experiment, the apparatus to be used and its advantages for experimentally addressing maglev design issues, and current status are described.

Introduction

Accurate knowledge of losses in superconducting magnets is an important requirement for the design of levitation, guidance and propulsion magnets for maglev vehicles; the designs must provide thermal margins adequate to prevent accidental quenching. Sources of loss include AC fields caused by the varying currents induced in the guideway and the mechanical movement of conductors and cryostat internal structure caused by both the magnetic forces and magnet accelerations in response to those forces. Knowledge of these losses will be crucial for the proper design of superconducting magnets and the cryostats and refrigeration systems which support them, and will thus influence the cost of these subsystems as well. Significant sources of loss in superconducting magnets include hysteresis and eddy current losses in the wires making up the magnet windings, mechanical losses in the windings and supporting structures, and mechanical and eddy current losses in the shields which will be required to reduce the strength of ac fields arising from currents induced in the guideway conductors by passage of the superconducting magnets on the vehicle.

Manuscript received March 15, 1993. This work is supported by Draper Laboratory Independent Research and Development funding.

Tinkham[1] concluded that ac losses in maglev levitation, guidance and propulsion magnets could be substantial, conceivably exceeding the heat leak of the cryogenic system. Further, the most serious ac loss problem in a real vehicle would be associated with the low frequency vehicle motions near the natural frequency of the primary suspension system. Subsequently, Hunt[2] developed a simple model which showed that by assuming full flux penetration of the superconducting wire, Tinkham's calculations overestimated the ac losses. It should be noted that in Hunt's experiments, a coil fabricated with multicore wire showed a decrease of persistent current magnitude following exposures to high ac field levels.

Mechanical effects in superconducting coils and shields will also be a significant factor in the proper design of suspension magnets and cryogenic systems for maglev systems. It is well known that relative motions between conductors in a supercondicting magnet can initiate quenches; these usually occur with increasing current when energizing the magnet. Maglev suspensions employing variants of the null-flux configuration are generally stiffer than those of the image flux variety and usually require a secondary suspension to maintain satisfactory ride quality. The combination of higher stiffness and secondary suspensions results in higher acceleration levels of the superconducting magnets than is usually the case

in image flux systems. Iwasa[3] noted that the racetrack magnets used in maglev, which cannot use the proven floating-coil technique that virtually guarantees freedom from premature quench in, e.g. NMR solenoids, will still be affected by mechanical disturbances. Consequently, the effect of losses from such disturbances must be considered in magnet design and qualification. While numerous measurements have been made of such effects, e.g.[4] [5], none are known to the author which combine these with application of ac fields.

Experience with superconducting generators has shown that mechanical resonances of shields can induce significant ac losses in the superconductors when excited by the ac fields they were intended to attenuate[6], and such resonances can be excited as well by mechanical vibrations of the magnet system caused by vehicle interaction with guideway imperfections and response to wind gusts.

The combination of ac magnetic fields and mechanical vibrations is expected in maglev systems and their effects must be understood quantitatively to design a satisfactory system immune not only to unexpected quenches, but to possible decay of magnet persistent currents. One of the objectives of the work described here is to develop a facility enabling such experiments on full-scale or near full-scale sized components.

Initial Experiment

An experiment is being prepared to prove-out the experimental arrangement and procedures for measurements on superconducting magnets, and to verify predicted ac field levels due to guideway currents and levitation average and ripple forces. A representative maglev suspension arrangement, approximating that of the Japanese ML002 vehicle studied by Brown[7] is being used. The initial experiment will be conducted using a conventional copper coil excited by a dc current supply to simulate the superconducting coil. Calculations using the parameters of a similar coil[8] indicate that the thermal limit is an excitation ≈1/35 of the nominal ampere-turns of the superconducting coil, producing a guideway ac field proportionately smaller. The levitation force will thus be smaller by a factor of ≈1,400, giving a lift force of ≈22N(≈5 lbs.), a value which should be readily measurable, although probably not with high accuracy.

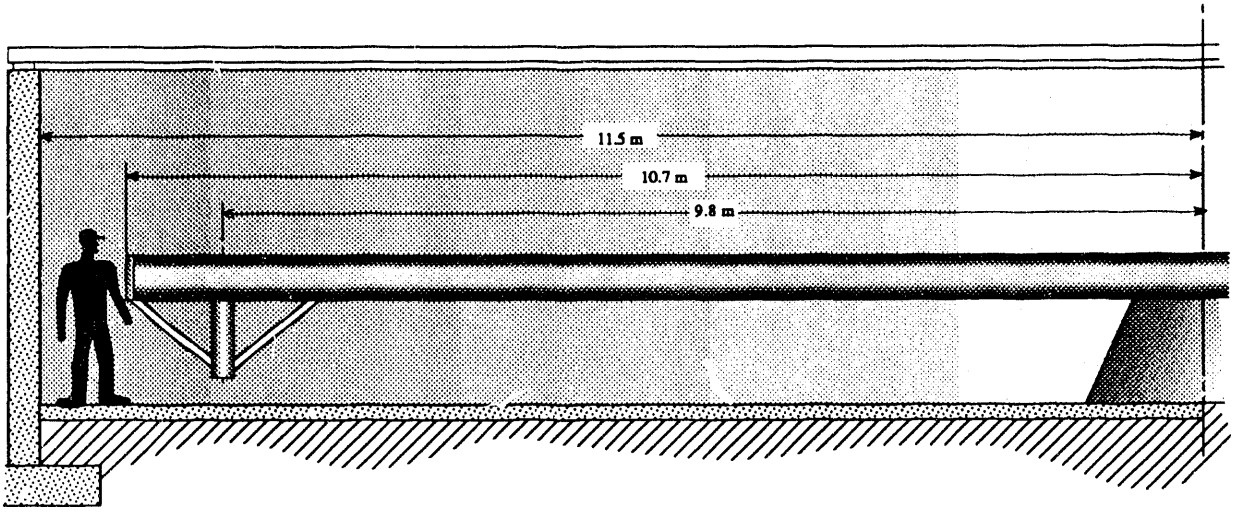

Figure 1. Centrifuge elevation

Equipment

The experiment will be conducted using a large centrifuge at Draper's environmental test facility. This machine was constructed to

perform high acceleration exposure testing of inertial guidance systems and components and for calibration and error evaluation of high precision accelerometers. The centrifuge arm is asymmetric with respect to the center of rotation; the long end is shown in elevation in Fig. 1, and the short end in plan view in Fig. 2.

The length of the long and short ends of the arm are 10.7m (35 ft.) and 6.6m (21.7 ft.), respectively; the interior concrete wall of the building has a radius of 11.6m (38 ft.). The centrifuge was designed to operate safely at an acceleration level of 200 g, measured at the test location at 9.73m,(32 ft.) radius, and has been routinely operated at a maximum acceleration of 100g, which corresponds to a tip velocity at the long end of the arm of 102.3 m/s (335.7 ft/s), about 76% of the 134 m/s expected maglev vehicle maximum speed. Currently, the machine capability is limited by its primary power source (a diesel-electric generator set) to a maximum acceleration of 35 g, corresponding to a tip velocity at the long end of 60.5 m/s (198.6 ft/s).

This machine has a number of attributes that suit it well for testing maglev system components, particularly suspension and propulsion magnetics, and suspension subsystems:

- ability to accept full scale components, important for magnetics which do not scale well
- high speed, ≈75% of projected maximum maglev speeds
- capability for continuous operation
- little or no component curvature required, due to large radius of curvature (10.7m(35 ft.))
- relatively low centrifugal acceleration at high speeds due large radius of curvature (10.7m(35 ft.))
- large load capacity, ≈3.5Mg(7,500 lbs.)
- ≈150 slip rings, some with high current (≥50A) capability
- ability to readily simulate the effect of low frequency suspension motions (0.9×n Hz at 60 m/s; n=integer), by adjustable guideway deformations
- hydrostatic oil bearings for low mechani-

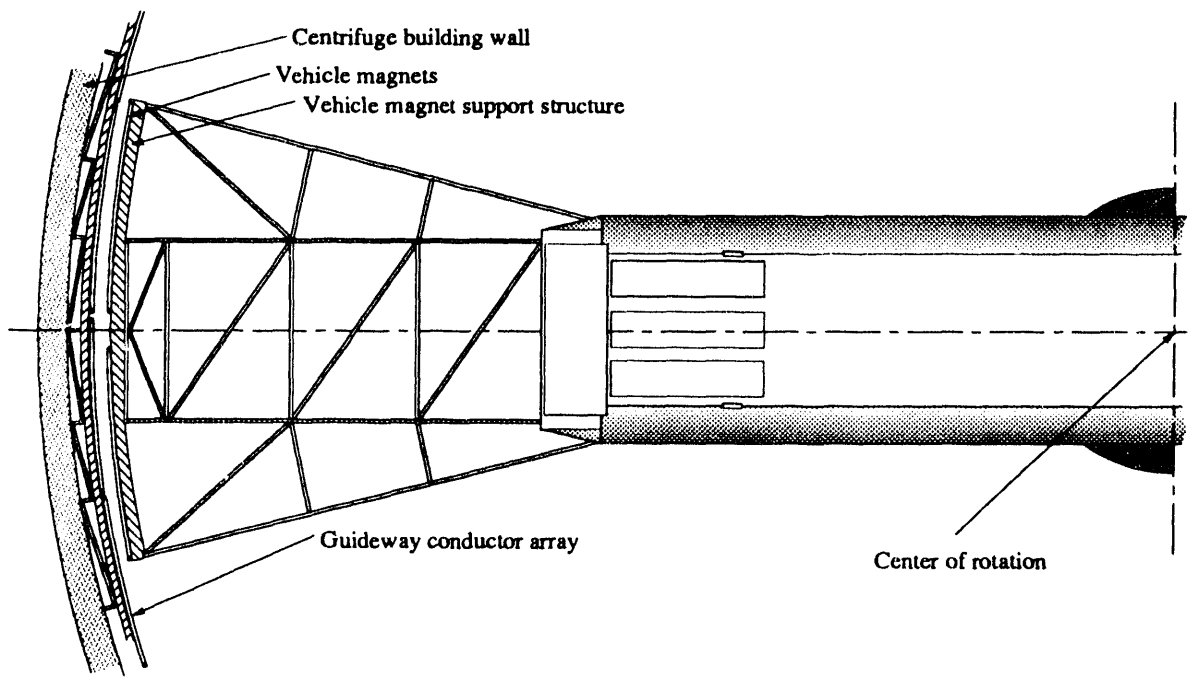

Figure 2.
Centrifuge plan view, magnet and guideway installed

cal noise
- stable and accurate speed control

Potential disadvantages include the centrifugal force that the magnet/cryostat system must withstand and the necessity for a complete array of guideway conductors around the periphery if the most realistic simulation is required (the initial experiment uses only a short section of simulated guideway, and entrance and exit effects are likely to be significant, particularly with respect to ac losses). The centrifugal forces generally should not pose a severe problem for magnets; at 100 m/s tip velocity they are approximately an order of magnitude smaller than the internal magnetic forces of the coil and approximately of the same order as the levitation forces.

Fig. 2 shows the simulated superconducting magnet mounted on the short end of the centrifuge arm; the magnet is supported ≈4 m (≈13 ft.) away from the nearest steel structure of the arm to prevent distortion of the magnet field. The support structure is shown as a space frame for illustration purposes, but will be made from welded aluminum plates and pipe for the necessary rigidity. The coil and its mechanical support is attached to the arm by means of strain gage instrumented members for measurement of forces.

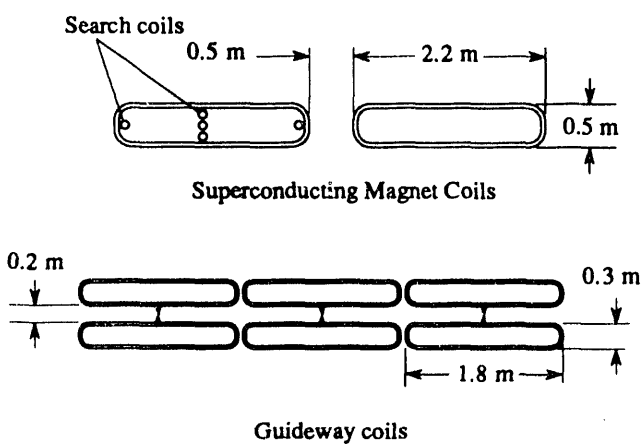

Figure 3. Coil configurations

Details of the coils are shown in Figure 3, which also shows a number of calibrated search coils provided for measurement of ac fields due to guideway currents; each search coil is buffered by a preamplifier before the signals pass through the slip rings. The magnet coils are excited by a constant current DC supply in an adjacent control room through high current slip rings on the arm.

Attachment of the guideway conductor array to the building is by means of adjustable supports to allow precise alignment (or intentional misalignment) with respect to the magnet path. Low value current sampling resistors are provided for measurement of the guideway coil currents.

Status

The detailed design of the centrifuge modifications necessary to adapt it for maglev component testing is in process and should be sufficiently complete to initiate construction by early summer 1993.

References

[1] M. Tinkham, "ac losses in superconducting magnet suspensions for high-speed transportation," J. Appl. Phys, vol. 44, No. 5, pp. 2385-90, May 1973

[2] T. K. Hunt, "ac losses in superconducting magnets at low excitation levels," J. Appl. Phys. Vol. 45, No. 2, pp. 907-13, Feb. 1974.

[3] Y. Iwasa, "Mechanical disturbances in superconducting magnets-a review," IEEE Trans. Mag., Vol. 28, No. 1, pp. 113-29, Jan 1992.

[4] T. Takao and O. Tsukamoto, "Stability against the frictional motion of conductor in superconducting windings," IEEE Trans. Mag., Vol. 27, No. 2, pp. 2147-50, March 1991.

[5] T. Ogitsu and K. Tsuchiya, "Investigation of wire motion in superconducting magnets," IEEE Trans. Mag., Vol. 27, No. 2, pp. 2132-35, March 1991.

[6] Prof. Joseph L. Smith, Jr., private communication.

[7] W. S. Brown, C. R. Dauwalter, F. Heger and M. Weinberg, "Comparison of major parameters in electrodynamic and electromagnetic levitation transport systems," DOT/FRA/NMI-92-15, pp.

3-12 et seq., Sept. 92, National Technical Information Service, Springfield, VA 22161

[8] J. C. Perkowski, et al., "Maglev system concept definition, Bechtel Team (Final Report)," Federal Railroad Administration Contract DTFR53-92-00003, pp. D1-1, Sept. 1992, in press.

Magnetic Fields From a Maglev Linear Synchronous Motor

1993 Maglev Conference

D. Galler, W. J. Greenberg

Abstract - This paper presents the analysis of magnetic fields from air core Linear Synchronous Motor (LSM) windings found in certain kinds of maglev systems. The exposure of passengers and passers-by to the magnetic field of the LSM winding is of particular concern in these systems.

In the maglev air core LSM, passengers are subjected to a magnetic field which is synchronized with the vehicle and is therefore perceived as a dc field. Outside the vehicle all other (stationary) personnel and equipment experience an ac field similar to that generated by an ac utility transmission line. The ac field is usually experienced at distances beyond a few meters from the LSM winding in the maglev guideway. It is this "far field" that is the subject of this paper.

Magnetic field analysis of a 3-phase LSM winding is presented. Numerical procedures used to compute the fields are also presented. For these procedures the LSM winding is modeled as a series of current sticks in space. The procedures can compute the field from any winding configuration represented this way as long as the surrounding space does not contain magnetic material. The results are presented in normalized fashion with winding current as a parameter, and are compared to results for typical utility distribution and transmission line configurations. The results are compared to limits which have been adopted by some states in the U.S. for transmission line magnetic fields.

I. Introduction

No study to date has demonstrated that low level ac magnetic field exposure adversely affects humans. Several studies have shown that magnetic field exposure can produce changes in cells and in laboratory animals' behavior, enzyme and hormone levels, and bone healing rate. Other studies have attempted to correlate human cancer rates with magnetic field exposure levels in the presence of other uncontrolled factors. A summary of the studies and field levels adopted by scientific agencies is presented in [1]. A good example of the popular literature on the health effects is [2].

Manuscript received March 22, 1993. This work was supported in part by the U.S. Army Corp of Engineers under Contract DTFR-53-92-C-00006.

The results of many of the studies are generally considered inconclusive by the scientific community. Nonetheless, advanced transportation systems must address the magnetic field issue on two levels. First, the system should be designed to minimize magnetic field exposure since the adverse effects of long term exposure have not been conclusively disproven. Second, there is a widespread perception by the public that magnetic fields may be harmful. If these advanced systems are to gain public acceptance, low stray fields must be achieved.

Most states in the U.S. have not adopted magnetic or electric field requirements. The guidelines adopted by some states for utility transmission line fields are summarized in Table I.

TABLE I
ALLOWABLE MAGNETIC FIELD STRENGTH AT THE EDGE OF A TRANSMISSION LINES RIGHT-OF-WAY

Florida	
500 kV (Single Circuit)	200 mG
500 kV (Double Circuit)	250 mG
230 kV and below	150 mG
New York (Interim)	
100 kV and above	200 mG
New Jersey (Considering)	
Not specified	200 mG

From this data it appears that a 200 mG level at the edge of the right-of-way would be a typical acceptable level.

In the remainder of this paper we will describe how a maglev system generates ac far fields that appear at the edge of a typical right-of-way. These fields will be computed and compared to those of transmission and distribution line geometries.

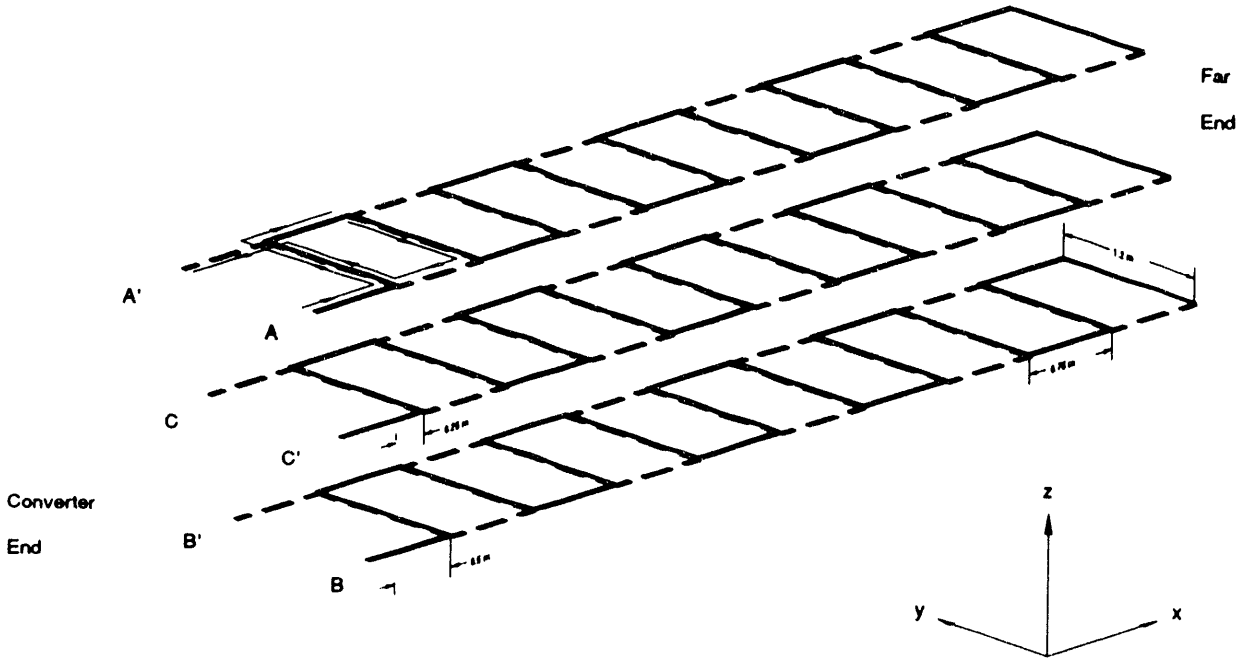

Fig. 1. Exploded View of Magneplane LSM Winding

II. Maglev Propulsion

A brief description of a maglev system is presented in this discussion to illustrate how the ac fields are generated. The data and examples are based on the configuration of the system proposed by Magneplane International [3] although similar results may be obtained on other systems. The discussion starts with a description of the propulsion system, which uses an air-core linear synchronous motor (LSM).

Fig. 1 is a diagram of a 3-phase LSM winding in which the phases have been separated for clarity. Each phase consists of two rectangular patterns which are connected together at the far end. The electrical connections for each phase are at the near end where they will be connected to a wayside power converter. The two patterns in each phase winding are mirror images of each other. Each phase of the winding is identical but is offset in the x direction by 1/3 of a pole pitch from the preceding phase. The winding is 1.2 m wide and has a pole pitch of 0.75 m.

The propulsion field is generated by the conductors which are parallel to the y axis - the transverse conductors. These conductors generate a magnetic field with x and z components only. To see how the travelling wave is produced consider 3-phase power at an instant in time when the A phase current is at a peak value of I. At this instant the other two phases carry currents of -I/2 since the sum of the phase currents must be zero. Proceeding in the x direction the sequence of currents in the transverse conductors is I, I/2, -I/2, -I, -I/2, I/2, I. This sequence produces a quasi-sinusoidal magnetic field above the winding. At heights of 0.2 to 0.3 m the field is a virtual sine wave because of the diffusion of the field from all the conductors. As the currents advance in time the field advances in space down the maglev guideway in the positive x direction.

In the Magneplane system the LSM winding is mounted at the bottom of a guideway whose cross section is roughly a semicircle. On each side of the winding the guideway walls are composed of aluminum levitation sheets. At normal operating speeds the vehicle is levitated by eddy current repulsion which occurs between the levitation sheets and superconducting levitation coils carried by the vehicle. Thrust is produced by the z-axis component of the LSM travelling field interacting with superconducting propulsion coils carried by the vehicle.

In most maglev systems the LSM winding is constructed in sections called blocks. When a vehicle approaches a block that block is energized and remains energized until the vehicle has completed the transition into the next block. Only one

vehicle can be in a block at a time. In the Magneplane system the blocks can be up to 2 km long.

Except for fields from the vehicle as it passes, the LSM winding radiates an ac field whenever a vehicle is in that block. This is the source of the ac far field evaluated in this paper.

Additional parameters of a maglev system that relate to LSM ac fields are:

1. propulsion current
2. frequency range of propulsion current in the LSM
3. percentage of time a given block is energized while the system is in operation
4. number of hours per day the system is in operation

III. Magnetic Field Calculation

Since the propulsion system described here is essentially an air-core LSM the magnetic field can be computed as if the winding were a series of current sticks in free space. This is also the case for utility lines since they radiate primarily in air. The following discussion describes a numerical procedure which is used to compute the fields from the LSM winding and generate comparison cases based on utility transmission and distribution line geometries.

There is a closed form solution for the magnetic field at a point in space due to a current stick of finite length. The problem is generally arranged as shown in Fig. 2 where the stick lies on the z-axis in a 3-dimensional cartesian coordinate system.

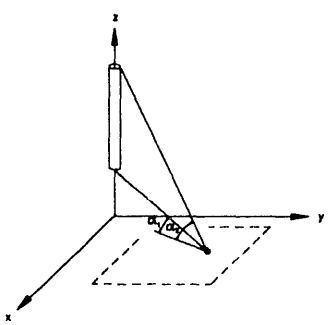

Fig. 2. Geometry of Current Stick and Point in Space Where Magnetic Field is Desired

The solution is usually written as [4]

$$|\beta| = \frac{\mu_0 I}{4\pi R} (\sin \alpha_2 - \sin \alpha_1) \quad (1)$$

where R is the distance from the point to the z axis. α_1 is the angle between the measurement point and the bottom of the stick. α_2 is the angle between the measurement point and the top of the stick.

The point is defined by the coordinates x_p, y_p, z_p.

The magnetic field at the point can only have x- and y-axis components. These are expressed as

$$\beta_x = \sin \phi |\beta| = \frac{-Y_p}{R} \cdot |\beta| \quad (2)$$

$$\beta_y = \cos \phi \, |\beta| = \frac{X_p}{R} \cdot |\beta| \quad (3)$$

These equations are basically the solution of the problem in a specific local coordinate system. The three components at a point from a stick in any orientation can be found by performing a linear transformation from global coordinates into this local coordinate system. A computer program has been developed which performs this procedure and is used to generate the results presented in the remainder of this paper. The steps of the procedure are summarized in Appendix A.

IV. Basis of Calculation

The magnetic field strengths for the LSM winding described above and two utility line configurations were computed for comparison. The fields were calculated in a y-z plane located in the center of 200 meter spans for each of the three cases.

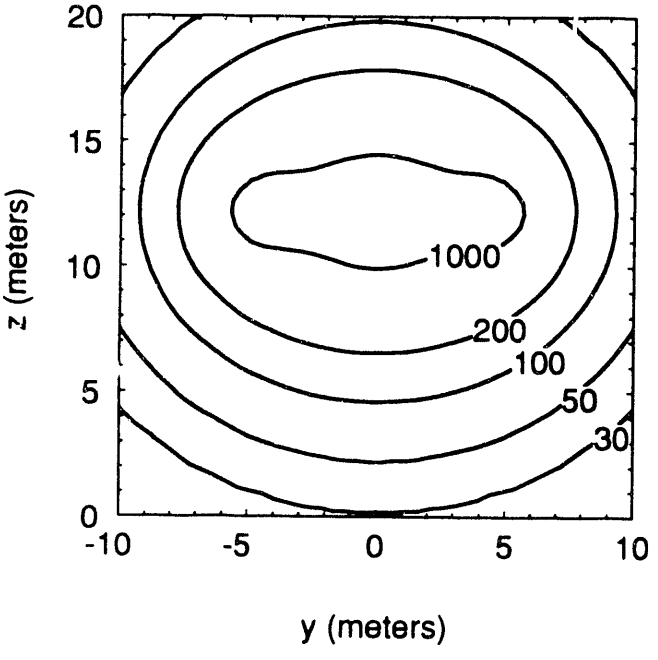

Fig. 3. Magnetic Field From a Transmission Line in mG

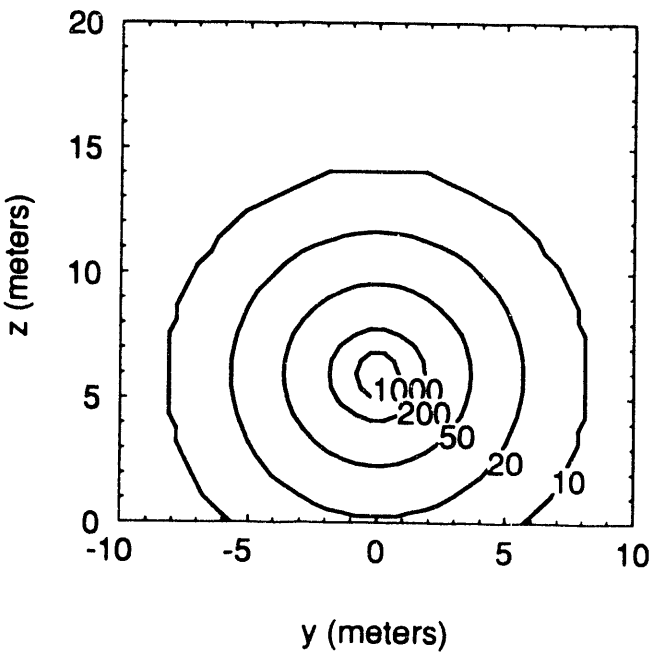

Fig. 4. Magnetic Field From a Distribution Line in mG

Span lengths for the transmission and distribution line cases could be set arbitrarily. However, LSM lengths were set for computational convenience since a 200 m model has about 3200 current sticks. Additional test cases were run to verify that LSM length did not affect the results. The results presented are the same as those for infinitely long spans.

The current for each configuration was 1000 A rms. However, the calculations are based on the currents carried by the conductors at one instant in time. For reference we have chosen to use an instant when the central conductor of the distribution and transmission configurations is at peak current. From this discussion it should be noted that the fields shown are instantaneous field values and not the rms ac field values. The instantaneous fields are somewhat more instructive in terms of field effects and are useful for the comparisons made here.

V. Results

Fig. 3 shows the fields from a typical three-conductor transmission line where the conductors lie in a plane. The conductors are 4.6 m apart and 12.2 m above the ground. This arrangement is typical for 115 to 161 kV [5]. The conductors can usually carry about 1000 A. The field pattern has a maximum value at ground level of about 30 mG.

Fig. 4 shows a configuration used for distribution called spacer cable. The three conductors are strung on an insulating spacer which controls their separation. The outer conductors are 0.3 m apart and 6.1 m above the ground. The center conductor is 0.23 m below the outer conductors. The field is much more restricted than the transmission line configuration because the conductors are more closely spaced. This allows a greater degree of field cancellation at the same distance below the lines. The maximum field is about 20 mG at ground level.

Fig. 5 shows the magnetic field results for the LSM winding described earlier in this paper. The winding is 1.2 m wide and 6.5 m above the ground. The fields at ground level are well below 1 mG when the winding carries 1000 A. Under certain conditions the same general winding arrangement can carry up to three times this current. The fields would still be no higher than about 3 mG, well below those of the transmission and distribution lines at 1000 A.

The low ac far field has to do with several specific features of the winding geometry. First, the pitch of the winding was selected to optimize the propulsion field at a distance of about 0.25 m from the winding. The field drops off rapidly beyond that due to cancellation of the many transverse conductors. Second, the end turns are tightly coupled. The conductors on each side carry opposing sinusoidal current patterns. This again causes a high degree of cancellation at relatively small distances.

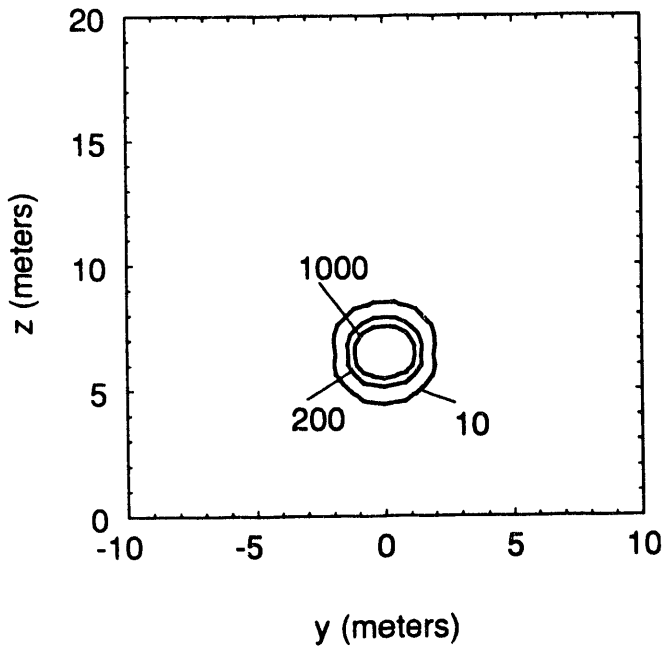

Fig. 5. Magnetic Field From LSM Winding in mG

TABLE II
SUMMARY OF RESULTS

Maximum Field Magnitude at Ground Level in mG	
Transmission	30
Distribution	20
Maglev	1

IV. SUMMARY AND CONCLUSION

The magnitude of ac far fields from transmission and distribution line configurations have been compared to a maglev LSM winding. The results are summarized in Table II and show that the LSM winding has much lower far fields than either the transmission or distribution lines. The geometry of the LSM winding is such that it carries many small segments of current which cause substantial cancellation beyond 1 m from the winding.

The close coupling of the phases and transverse conductor spacing are critical factors in achieving low far field levels. These factors should be considered in designing LSM windings to meet low radiated field requirements.

The ac far fields from the type of LSM winding analyzed in this paper are much lower than typical transmission and distribution lines currently used by utilities. In addition, the fields are much lower than present utility standards for transmission lines. The results should satisfy the general public perception of health risks from low level exposure caused by maglev LSM windings of the general geometry presented here.

APPENDIX A

3-D Magnetic Field Calculation Procedure

The entire procedure is summarized below. We start out with the measurement point at X_p, Y_p, Z_p and the current stick with a starting point X_1, Y_1, Z_1, ending point X_2, Y_2, Z_2, and carrying the current Z.

Notation

Variables in global coordinates are in upper case while local coordinate variables are in lower case.

1. Translate the stick to the local coordinates.

$$x_1 = 0 \quad x_2 = X_2 - X_1$$
$$y_1 = 0 \quad y_2 = Y_2 - Y_1$$
$$z_1 = 0 \quad z_2 = Z_2 - Z_1$$

2. Compute the rotation angles.

$$\sin \varphi = \frac{y_2}{\sqrt{y_2^2 + z_2^2}}$$
$$\cos \varphi = \frac{z^2}{\sqrt{y_2^2 + z_2^2}}$$

$$\hat{z} = \sin \varphi \, y_2 + \cos \varphi \, z_2$$

$$\sin \theta = \frac{-x_2}{\sqrt{x_2^2 + \hat{z}^2}}$$

$$\cos \theta = \frac{\hat{z}}{\sqrt{x_2^2 + \hat{z}^2}}$$

3. Translate the point from global to local coordinates.

$$x_p = X_p - X_1$$
$$y_p = Y_p - Y_1$$
$$z_p = Z_p - Z_1$$

4. Rotate the point to align with the stick rotation.

$$\begin{bmatrix} x_p \\ y_p \\ z_p \end{bmatrix} = \begin{bmatrix} \cos\theta & \sin\theta\sin\varphi & \sin\theta\cos\varphi \\ 0 & \cos\varphi & -\sin\varphi \\ -\sin\varphi & \cos\theta\sin\varphi & \cos\theta\cos\varphi \end{bmatrix} \begin{bmatrix} x_p \\ y_p \\ z_p \end{bmatrix}$$

5. Compute the end point of the stick along the z axis.

$$z_2 = \sqrt{x_2^2 + y_2^2 + z_2^2}$$
$$x_2 = 0$$
$$y_2 = 0$$

6. Compute the distance from the point to the z axis.

$$R = \sqrt{x_p^2 + y_p^2}$$

7. Compute the magnitude of the field.

$$|\beta| = \frac{\mu_0 I}{4\pi R}\left[\frac{Z_2 - Z_p}{\sqrt{(Z_2 - Z_p)^2 + R^2}} + \frac{Z_p}{\sqrt{Z_p^2 + R^2}}\right]$$

8. Compute the x and y components in the local coordinate system.

$$b_x = \frac{-y_p}{R}|\beta|$$
$$b_y = \frac{x_p}{R}|\beta|$$

9. Rotate the field components back to the global coordinate system.

$$\begin{bmatrix} \beta_x \\ \beta_y \\ \beta_z \end{bmatrix} = \begin{bmatrix} \cos\theta & 0 & -\sin\varphi \\ \sin\theta\sin\varphi & \cos\varphi & \cos\theta\sin\varphi \\ \cos\theta\sin\varphi & -\sin\varphi & \cos\theta\cos\varphi \end{bmatrix} \begin{bmatrix} b_x \\ b_y \\ 0 \end{bmatrix}$$

10. Compute the magnitude of the field as

$$|\beta| = \sqrt{\beta_x^2 + \beta_y^2 + \beta_z^2}$$

Acknowledgments

The authors would like to thank Dr. R.J. Thome of the MIT Plasma Fusion Center for his support and guidance during the Magneplane Concept Definition Study. The authors would also like to thank Helen M. Martin for her work in preparing the manuscript.

References

[1] Electromagnetic Fields: the jury's still out. IEEE Spectrum. August 1990. Fitzgerald, Morgan, and Nair.

[2] Currents of Death. Paul Brodeur, 1989, Simon and Schuster.

[3] Magneplane Concept Definition Study, Final Report. September 1993. Contract No. DTFR-53-92-C-00006.

[4] Engineering Electromagnetics. W.H. Hayt. 1974, McGraw-Hill, New York.

[5] The Lineman's and Cableman's Handbook. 7th Edition. E.B. Kurtz, T.M. Shoemaker. 1986, McGraw-Hill, New York.

Magnet Design Optimization for Grumman Maglev Concept

S. Kalsi and R. Herbermann
Grumman Corporation, Bethpage, New York

C. Falkowski and M. Hennessy
Intermagnetics General Corporation., Guilderland, New York

A.Bourdillon
State University of New York at Stony Brook

*Abstract**- The Grumman baseline Electromagnetic Suspension (EMS) Maglev system consists of superconducting C-iron cored magnets on the vehicle. They are attracted to iron rails mounted on the underside of the guideway. The magnets and rails are oriented in an inverted 'V' configuration in such a manner that the attractive force vectors between the magnets and the rails act through the center of gravity of the vehicle. These magnets simultaneously perform functions of vehicle levitation and propulsion. They are powered by NbTi superconducting coils operating at 4.2K. An electromagnet consists of a C-core, a superconducting (SC) coil on the back leg of the C-core and a normal control coil on each leg of the C-core. The SC coil provides the nominal lifting capability and the normal coils handle rapid variations in load with respect to the nominal value.

The baseline magnet configuration was selected on the basis of extensive 2-D and 3-D magnetic analyses to meet the levitation and propulsion requirements. The selected magnetic system design employs 48 magnets, 24 on each side of a 100 passenger vehicle. The polepitch is 750 mm and the gap between the magnet poles and the rail is 40 mm. The NbTi SC coil has a modest ampere-turns (50,000 AT) requirement, experiences a peak field of ~0.5 T and operates at 4.5K. High temperature SC leads are specified for minimizing the helium boiloff. Because of the iron core the SC winding experiences little magnetic loads. The magnet is cooled with pool boiling liquid helium which is contained within the helium vessel of the coil. No helium refrigeration equipment is carried on-board on the vehicle. Instead the boiled-off helium gas is compressed into a nitrogen cooled storage tank. Sufficient quantity of liquid helium is carried on-board for an uninterrupted 24 hour operation. At the end of a day, the gaseous helium is discharged at a central location for reliquification and the liquid helium supply in the magnets is replenished.

*Manuscript received March 15, 1993. The work was performed as part of the EMS Maglev System Concept Definition study supported by the U. S. Army Corps of Engineers under contract DTFR53-92-C-000 04.

I. INTRODUCTION

The important aspect of the Grumman Electromagnetic Suspension (EMS) system design [1] is the ability to levitate the vehicle, with a wide airgap 40 mm (1.6 inch), using iron cored SC magnets located along both sides of the vehicle's length. The magnetic field in the gap is also utilized to propel the vehicle at speeds up to 134 m/s using 3-phase propulsion coils embedded in the iron rail slots. The ability to accomplish this levitation and propulsion under a wide range of maneuvers, guideway irregularities and aero disturbances without saturating the iron is a complex task requiring extensive magnetic and control system analysis.

Figure 1 shows the baseline EMS magnet system consisting of an iron-cored magnet and a guideway iron rail. The laminated, iron-cored magnets and iron rails are oriented in an inverted "V" configuration (see [1] for details) with the attractive force between the magnets and rails acting through the vehicle's center of gravity (cg).

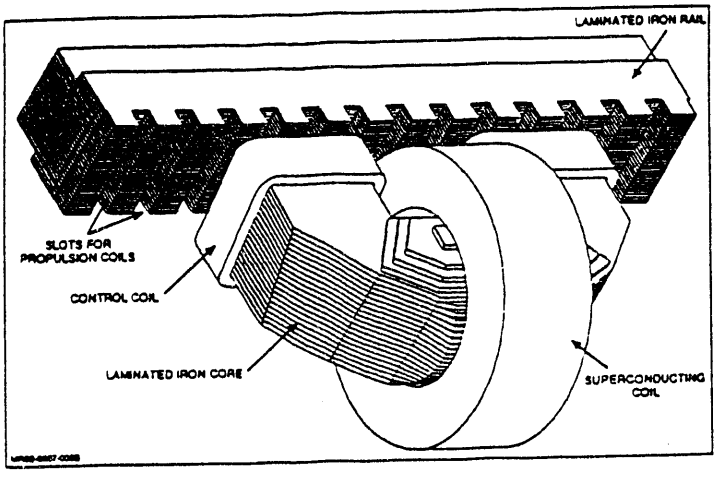

Fig. 1. EMS Levitation and Propulsion Systems

The vertical control forces are generated by sensing the average gap clearance on the left and right side of the vehicle and adjusting the current in the control coils mounted on the magnet poles to maintain a constant 40 mm (1.6") gap. Lateral control is achieved by differential measurement of the gap clearance between the left and right sides of the vehicle. The corresponding magnet control currents are differentially driven for lateral control. In this manner, control of the vehicle relative to the rail is achieved in the vertical, lateral, pitch, and yaw directions. For roll control, the C-magnet assemblies are alternately off-set with respect to the rail width by 20 mm. With this arrangement if the vehicle deviates from the nominal operating position, the lateral forces generated between the poles and the rails are such that they drives the system back to the equilibrium state. This process is further helped by sensing the vehicle's roll position relative to the rail and differentially driving the offset control coils to correct for roll errors. The iron rail on the guideway is laminated and carries 3-phase propulsion winding powered by a variable frequency ac source synchronized to the vehicle speed. Vehicle housekeeping power is inductively induced into coils mounted on the pole faces of each magnet.

II. REQUIREMENTS

The total weight of a 100 passenger fully-loaded vehicle is 60,000 Kg. The force generated by the magnet system must be 90% larger to provide lateral guidance in the inverted "V" configuration. The total baseline levitation and guidance force to be provided by the magnet system is 115,000 Kg. A load variation of +/- 45,000 Kg is required about the baseline value for rapid gap control. These and other baseline requirements are summarized in Table 1. The vehicle has 18 m length available for accommodating the SC magnets and an airgap of 40 mm must be maintained between the levitation magnet pole faces and the rail. By reacting with 3-phase AC windings housed in the rails, these levitation magnets also generate a propulsion force of 6,000 Kg for nominal operation and 10,000Kg for extended operation. The extended operation includes the requirements for accelerating on uphill grades, against head-wind, etc.

TABLE I
MAGLEV VEHICLE REQUIREMENTS

PARAMETER	UNIT	VALUE
Baseline levitation per vehicle	Kg	115,000
Load variation	Kg	45,000
Vehicle magnetic length	m	18
Airgap between poles and rail	mm	40
Propulsion force - nominal	Kg	6,000
- extended	Kg	10,000
Maximum vehicle speed	m/s	134

The levitation magnets must also generate sufficient lateral force to counter roll moments. Furthermore, the SC magnets must be designed for reliable operation and for easy maintenance.

III BASELINE DESCRIPTION

A. *Pole Configuration*

The baseline C-magnet and rail configuration is shown in Fig. 2. The key parameters of the baseline magnet system are summarized in Table II. Each C-magnet assembly consists of a C-shaped iron core, a SC magnet located around the back leg of the iron core, and normal control coils around each pole of the iron core.

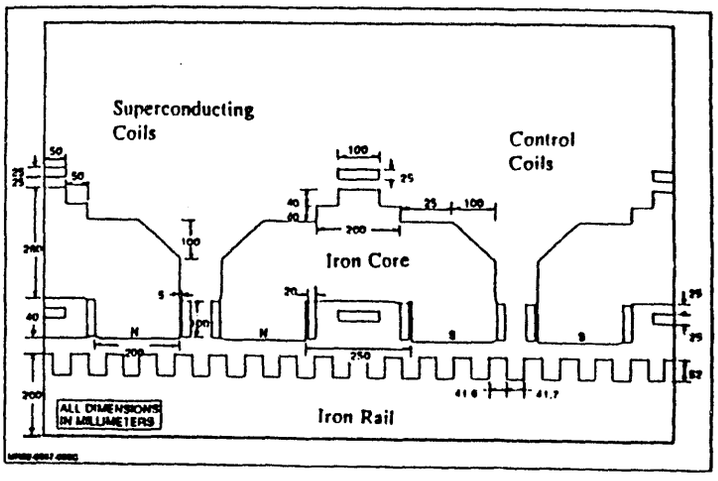

Fig. 2. Baseline Pole and Rail Geometry

TABLE II
Baseline Levitation Magnet and Rail Parameters

PARAMETER	UNIT	VALUE
Lift capability per pole	Kg	2,400
Variation in lift capability	Kg	940
Pole pitch	mm	750
Number of poles		48
Airgap length	mm	40
Peak of sinusoidal field component in airgap	T	0.9
Operating frequency at rated speed	Hz	89
Nominal lift-to-weight ratio		6.4
Rail width	mm	200
Rail thickness	mm	200
Number of slots/pole in the rail		9

As shown in Fig. 2, the C-magnet assemblies are arranged such that the polarity of the poles of adjacent C-magnets are

identical. Thus a pole (N or S) is formed by two legs of adjacent C-magnet assemblies. This arrangement of poles is the same as that accomplished with a continuous row of magnet poles on a single magnet core assembly. The baseline pole pitch is 750 mm.

Each pole face also has five slots (as shown in Fig. 3) for accommodating coils for inductive power generation on-board the vehicle for operating equipment and housekeeping services. These coils generate power at zero and low speeds by high frequency transformer action, and from airgap flux pulsations at high speeds. This power generation concept is described in [2]. The poles are skewed (Fig. 3) to minimize the effect of traction winding space-harmonics on the traction force.

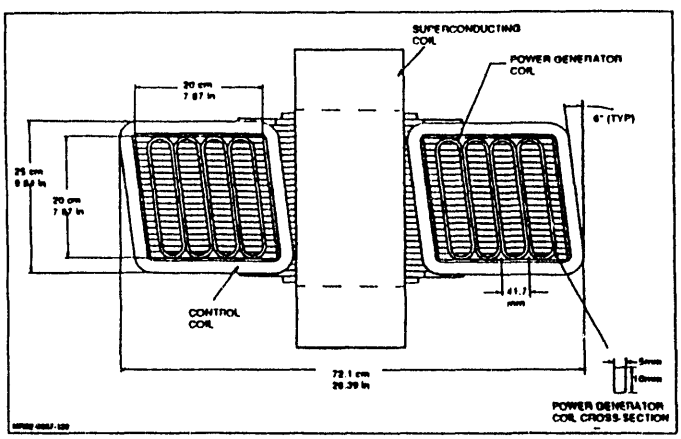

Figure 3: Skewed Magnet Poles with Power Generator Coils

B. Principle of magnet system operation

The SC magnet on a C-core operates in a quasi-steady state. During operation, any change in the size of the airgap tends to change the flux in the gap and in the core. However because the normal control and SC coils are part of the magnetic circuit, they prevent any change in the flux linking their bores. Both coils generate currents of appropriate polarities to maintain constant flux linkages through their bore. The gap control system shown in Fig. 4 circumvents this problem as explained below.

For reasons of SC coil stability and heat loads, the SC coil is supplied from a constant current source that has built-in capability to prevent current changes occurring faster than ~ 1 Hz. On the other hand, the airgap is expected to change at frequencies up to 10 Hz. The normal control coils develop self currents in response to these oscillations of gap length with an intent to restore the gap to its nominal value. If a steady change in the gap is noticed (due to

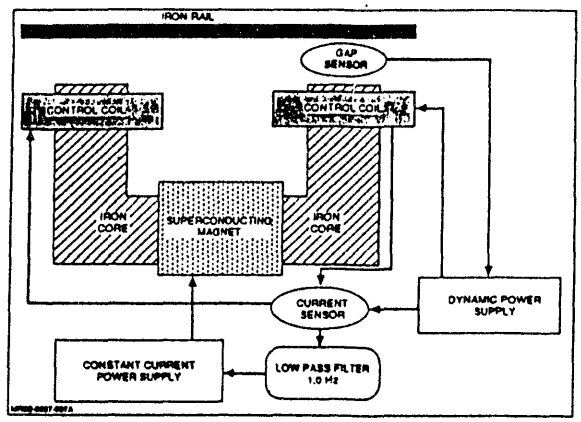

Figure 4: Magnet Control System

increased or decreased load), then the current in the SC coils is allowed to change so as to drive long-term currents in the normal coils to zero. It is possible to achieve a certain degree of damping with the shorted coils. But in a practical system, it is essential to dynamically control these coils to respond to gap variations resulting from passenger load changes, maneuvering around curves or during grade changes of a given route. For this purpose, the airgap is constantly monitored and current of appropriate polarity is supplied to each normal coil for maintaining the nominal gap. This concept is described in more details in [3].

C. Effect of Normal Control Coils on the Levitation Force

The normal control coils are provided to compensate for fast changes in the required levitation capability. A set of calculations were performed to estimate the effect of control coil ampere-turns on the levitation force as a function of airgap length. Because of very high field levels in the iron core, it was decided to perform these calculations with 3-D codes (both TOSCA and ANSYS were used). Fig. 5 shows the combined lift and guidance force as a function of control coil current for constant gap lengths. The same data is

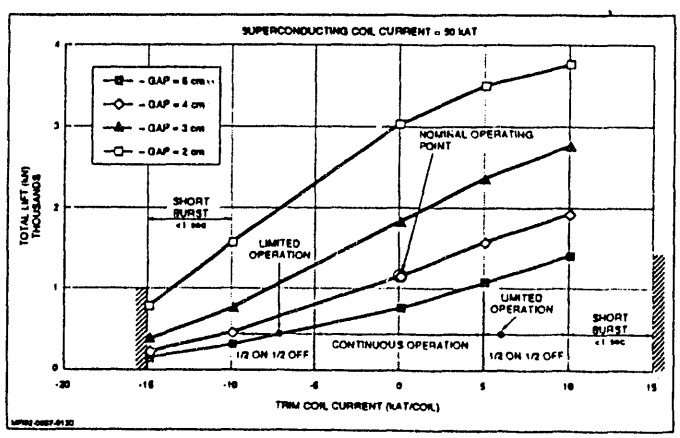

Figure 5: Levitation vs Control Coil Current for Constant Airgap Lengths

presented in Fig. 6 but as function of gap length for constant values of control coil currents. In both figures, the magnet is nearly a linear function of gap length and control coil current around the nominal operating point of 40 mm gap and zero control coil current. When the core saturation increases, the relationship becomes non-linear. However, the important factor is to generate a sufficient amount of levitating force variation to maintain controllability of the vehicle and this objective has been achieved [4].

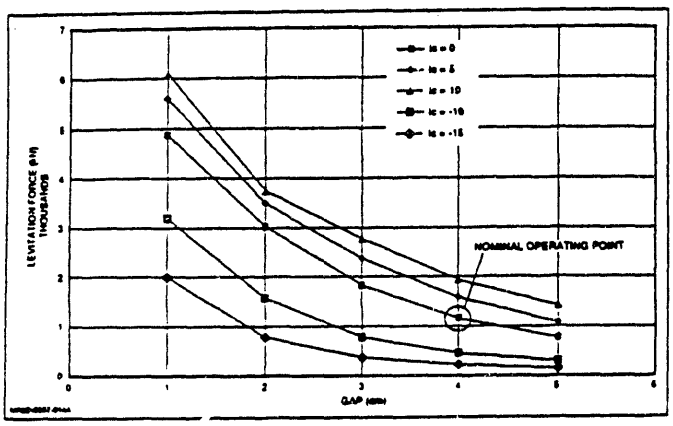

Figure 6: Levitation vs Airgap Length for Constant Control Coil Current

D. Roll Control

The EMS Maglev concept proposed here is inherently stable against roll rotation. This is achieved by off-setting C-magnet poles with respect to the rail. Two C-magnet assemblies are carried as a module. Alternate magnet modules are shifted laterally with respect to the rail by about 20 mm. As a result of this shift, a lateral force is generated between the poles and the rail. The total forces on all poles sum to zero during normal operation. During a transient condition, if all poles move to one side with respect to the rail, the force decreases on poles that are getting aligned with the rail and the force increases for poles that are getting more misaligned. The net force always tends to return the system to the equilibrium state.

An estimate of the lateral restoring force was made with a 2-D finite element analysis. The lateral force as a function of misalignment is shown in Fig. 7. The permanent misalignment between the poles and rails is initially fixed at 20 mm. The restoring force for this misalignment is 890 N/pole; this is about 4% of the nominal levitation force and is considered adequate for most operating scenarios.

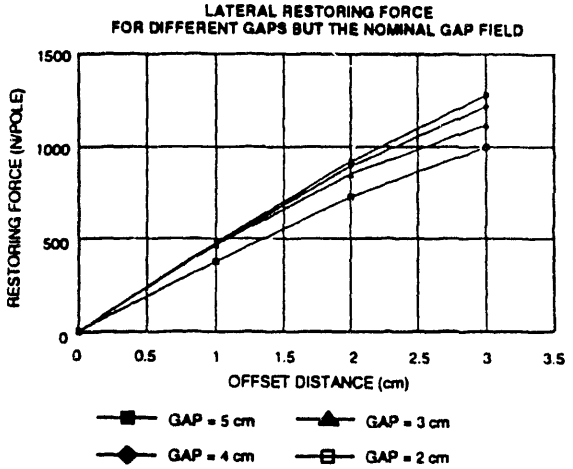

Figure 7: Lateral Restoring Force

E. Stray Magnetic Field Level

3-D magnetic field calculations were performed to estimate stray field in the passenger compartment and the surrounding areas. The flux density levels below the seat are less than 1 G, which is very close to the ambient earth's field (0.5 G). On the platform, magnetic field levels do not exceed 5 G, which is considered acceptable in hospitals using magnetic resonant imaging (MRI) equipment. These results were obtained without any shielding. With a modest amount of shielding, these field levels could be further reduced should future studies indicate a need for lower values.

IV. ESTABLISHING POLEPITCH

The sizing of both the depth of the rail guideway magnetic core and the core depth of the vehicle magnets are directly proportional to the polepitch. Thus the polepitch is the key factor in establishing overall system weight and steel materials cost.

The C-magnet and rail configuration of Fig. 2 was utilized for performing a parametric study to select an optimum polepitch that minimizes the overall cost of a Maglev system consisting of a double 300 mile track with 100 cars operating at any given time. The study was performed to satisfy requirements of Table I. The results of the study are summarized in Fig.8. As can be seen , the cost of the system continually increases with polepitch because a larger polepitch requires a deeper (thicker) rail to carry the magnetic field. A certain level of airgap field is required for the levitation capability, but it is not proportional to the polepitch because increasing the polepitch also improves the levitation efficiency of the magnet (large poleface to airgap length ratio). The lowest polepitch of 750 mm was selected

on basis of a volumetric constraint to accommodate the SC coil, its cryostat and the two normal control coils.

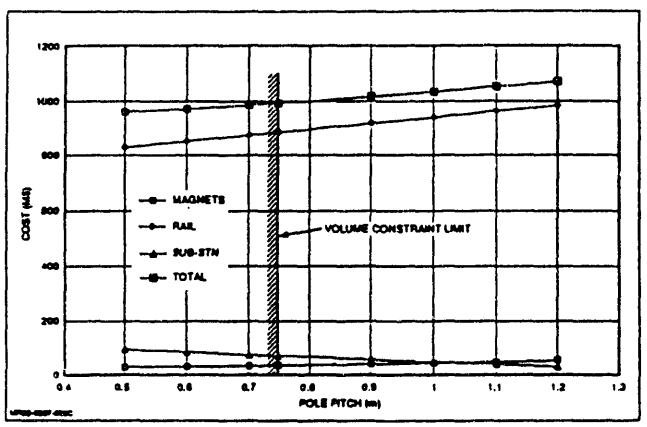

Figure 8: Maglev Levitation System Cost vs Polepitch

V. ESTABLISHING NUMBER OF MAGNETS REQUIRED

The 3-phase traction winding in the rail requires that the field produced by the excitation poles on the car (iron cored DC magnets) be sinusoidal in shape and its harmonic components be as small as possible for minimizing their deleterious effect on the traction force and eddy-current losses. The suspension magnets provide the key functions of levitation and propulsion simultaneously in the EMS system. Because of this constraint, a minimum number of poles are required for a given airgap magnetic field strength to accomplish the tasks of levitating and propelling the vehicle.

The analysis to determine the minimum number of poles follows. The levitation force generated by a sinusoidal field is given as:

$$F_l = 0.5\, w\, \tau\, \{B_m^2/(2\mu_o)\}\, N_p \qquad (1)$$

where F_l = levitation force (N)
B_m = peak of the sinusoidal field (T)
w = width of the rail (m)
τ = polepitch (m)
μ_o = permeability of air = $4\pi 10^{-7}$
N_p = number of pole on a vehicle

Similarly the total traction force (N) per pole is:

$$F_t = 1.5\, B_m\, I_m\, q\, w\, \eta K_d\, N_p \qquad (2)$$

where I_m = Peak of the sinusoidal current in traction winding (A)
q = slots per pole per phase in the rail
η = Efficiency of traction motor ~ 99%
K_d = Distribution for the traction winding

After eliminating B_m between (1) and (2), the equation for the number of poles is:

$$N_p = \{F_t^2/F_l\}\, \{\tau/(I_m^2\, q^2\, 9\, \mu_o\, w)\}/(\eta^2\, K_d^2) \qquad (3)$$

The baseline values for various variables are:

- F_t = 60 kN
- F_l = 1,150 kN
- τ = 0.75 m
- I_m = 1,900 A
- q = 3
- w = 0.2 m
- η = 0.99
- K_d = 0.96

With these values, the number of poles determined from Eq. (3) is 36. The baseline is fixed with 48 poles to provide redundancy.

VI. MAGNET DESIGN

A. Magnetic Analysis

Initially majority of calculations were performed with 2-D code (EMP, a commercial version of POISSON code) assuming a M43 iron core material. Fig. 9 shows field distribution calculated with the 2-D code in the airgap, pole and rail iron.

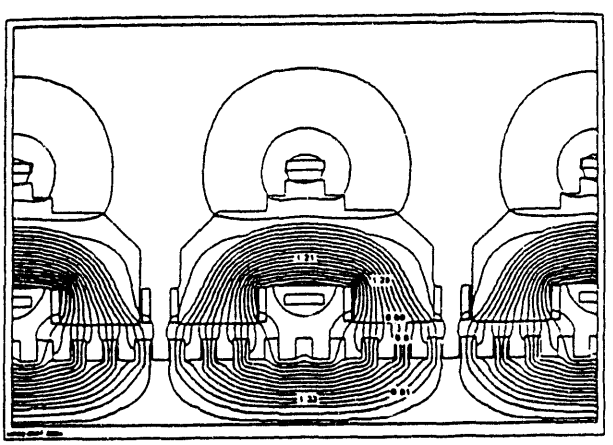

Figure 9: Baseline Magnetic Field Calculations with 2-D Code (Permendur Iron)

Fig.10 shows field distribution calculated with a 3-D code (TOSCA). The field distribution calculated by the two codes for the airgap is similar, but the 3-D calculation given in Table IV shows a much higher degree of saturation of the pole-iron (in the vicinity of the SC coil). To reduce this saturation to a reasonable value, a permendur iron (2% vanadium, 49% iron, and 49% cobalt) was specified in place

of the M43 material. Table IV also compares the resulting field values for the M43 iron and the baseline permendur pole iron. The SC coil provides 54 kA-turns. Locations of field comparison is marked in Fig. 9.

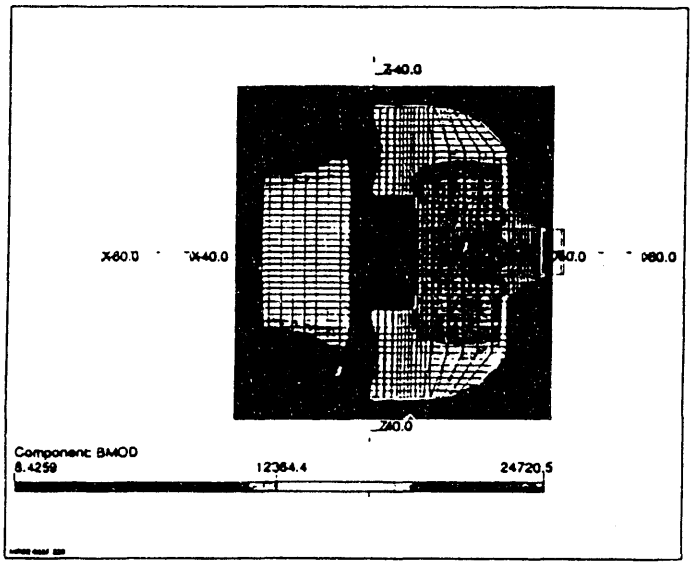

Figure 10: Baseline Magnetic Field Calculations with 3-D Code (Permendur Iron)

TABLE IV
COMPARISON OF FIELD VALUES CALCULATED WITH 2-D AND 3-D CODES FOR THE BASELINE

LOCATION (SEE FIG. 9)	2-D FIELD (T) M43 IRON	3-D FIELD (T) M43 IRON	3-D FIELD (T) Permendur
A	1.21	2.45	2.47
B	0.89	1.73	1.2
C	0.8	0.87	0.88
D	1.33	1.52	1.45

The penalty of selecting a permendur iron for the poles instead of M43 is approximately 7% of the vehicle cost.

B. Sizing of SC coil and cryoplant

A cylindrical SC coil and cryostat were selected for each C-magnet assembly since they are easier to fabricate and are lighter in weight than non-cylindrical shapes. For this reason, the iron core cross-section under the magnet is made circular. The iron is built from 0.050 inch thick laminations (Permendur).

The SC coil carries 54 kA-turns to produce the required field to simultaneously meet requirements of levitation and propulsion. The SC coil is designed by using a 0.65 mm diameter NbTi wire that has been developed by Brookhaven National Laboratory for their Relativistic Heavy Ion Collider (RHIC) dipole magnets. The key parameters for the SC coil are summarized in Table V.

TABLE V
SC COIL PARAMETERS

Parameter	Unit	Value
Ampere-turn rating of SC coil	kA-turn	54,000
Peak field at the SC coil	T	0.5
Operating current	A	53
Operating temperature	K	4.5
Number of turns		1,020
NbTi wire diameter - bare	mm	0.6477
Copper-to-superconductor ratio		2.2
Ratio of Operating to critical current		0.09
Temperature margin to current sharing	K	3.69

The SC coil has 1,020 turns, each turn carries 53 A to produce required 54 kA-turns. These turns are accommodated in a coil pack of 4 layers with 255 turns in each layer. The coil pack is epoxy impregnated to produce a monolith structure. No separate quench protection system is required because the energy stored in the magnet is very small. In event of a quench, the magnet is disconnected from the supply and is shorted at its terminals.

The total heat load for the magnets on each car is 8 W. The weight and the cost of a cryogenic refrigeration plant would be 2,540 Kg and $110,000 respectively. It also will be necessary to supply ~16 kW of power to run the refrigerator plant. To mitigate the weight and operating power penalty a decision was made to employ a cryogenic storage system. The liquid helium cryogenic storage system consists of a small compressor operating at 350 psi that takes the gaseous helium boiloff and compresses it into a storage tank held at liquid nitroger temperature. Sufficient helium inventory is carried in the magnet for a 24-hour continuous operation. The gaseous helium storage system is sized to accommodate helium boiloff over a 24-hour period. At the end of the 24-hour period, the gaseous helium is discharged at a central location and liquid helium is replenished in the magnets. Two cryogenic storage systems are provided for each 50 passenger module. The weight of each cryogenic system is 580 Kg which includes 180 Kg for a compressor and 400 Kg for the gaseous helium storage tank.

C. Potential of Using High Temperature Superconductors

The iron cored SC magnets of the Grumman concept are in the best position to take advantage of the new High Temperature Superconductor (HTS) technology. While the peak field in the iron is greater than 2 T, but in the SC winding region it is less than 0.35 T. The superconductor is

also required to supply a modest 54 kA-turns to generate the required field for vehicle levitation and propulsion. Because of very small fields and forces experienced by the SC coil and recognizing rapidly advancing state-of-the-art of the HTS technology [5], Grumman considers that this Maglev concept is in a best position (relative to all other SC magnet Maglev concepts) to take advantage of the HTS technology. The following are the attractive features of the HTS magnet:

- Operation at liquid nitrogen temperature (77 K)
- No need for liquid helium compressor or storage tanks
- Simpler and lighter cryostat
- Lower weight and capital cost
- Lower manufacturing cost
- Lower operating and maintenance cost

VI. CONCLUSIONS

The Grumman developed EMS Maglev system has the following key characteristics:

- A large operating airgap - 40 mm
- Low magnetic field at the SC coil - <0.5 T
- Low magnetic field in passenger cabin ~ 1 G
- Low forces on the SC coil
- Employs state-of-the-art NbTi wire
- No need for an active magnet quench protection system
- Lower weight than a magnet system with copper coils

The EMS Maglev described in this paper does not require development of any new technologies. The system could be built with the existing SC magnet technology. The future work is planned to improve the design to minimize high magnetic fields in the iron core and to consider the possibility of replacing the helium cooled NbTi SC coils with nitrogen cooled High Temperature Superconductors.

REFERENCES

[1] M. Proise, et al. "System Concept Definition of the Grumman Superconducting Electromagnetic Suspension (EMS) Maglev Design", presented at the Maglev '93 Conference, Argonne National Laboratory, May 19-21, 1993.

[2] S. Kalsi, "On-vehicle Power Generation at all Speeds for Electromagnetic Maglev Concept", presented at the Maglev '93 Conference, Argonne National Laboratory, May 19-21, 1993.

[3] R. Hurbermann,"Self Nulling Hybrid Maglev Suspension System", presented at the Maglev '93 Conference, Argonne National Laboratory, May 19-21, 1993.

[4] R. Gran and M. Proise,"Five Degree of Freedom Analysis of the Grumman SC Maglev Vehicle Control/Guideway Interaction", presented at the Maglev '93 Conference, Argonne National Laboratory, May 19-21, 1993.

[5] P. Halder and L. Motowildo, "Recent Development in the Processing of High Jc Silver Clad Mono- and Multi-Filament (Bi, Pb)2Sr2Ca2Cu3O10 Wires and Tapes,"Journal of Metals, October 1992.

Superconducting magnet and refrigeration system for Maglev vehicle

Hiroshi Nakashima
Maglev System Development Division, Railway Technical Research Institute,
1 - 24 - 1 Nishishinjuku, Shinjuku - ku Tokyo

Motoaki Terai
Linear Express Development Division, Central Japan Railway Company,
1 - 6 - 6 Yaesu, Chuo - ku, Tokyo

Masayuki Shibata
Hitachi Research Laboratory, Hitachi Ltd.
7 - 1 - 1 Ohmika - cho, Hitachi City, Ibaraki

Mutsuhiko Yamaji
Toshiba Corp.
1 banchi Toshiba - cho Fuchu City, Tokyo

Yoshihiro Jizo
Manager Magnetic Levitated Train Project Group,
Maglev System Design section, Mitsubishi Electric Corp.
1 - 1 Tsukaguchi - Honmachi 8 - chome, Amagasaki City, Hyogo

Abstract - The development of the JR (Japanese Railways) superconducting magnetic levitation (JR Maglev) system was started in 1972. Many running tests have been carried out at Miyazaki test track to set up a speed record of 517km/h on Dec.1979. New test line to confirm the probability of commercial operation is under construction in Yamanashi Prefecture which is located about 100km west of Tokyo.

The superconducting magnet is one of the most important parts for the Maglev system. These superconducting magnets should be designed to satisfy severe weight and heat leak restriction. Furthermore, they have to stand both mechanical and electro-magnetic disturbances on running conditions.

Here the outline of the superconducting magnets designed as prototype for Yamanashi test line and the way of improvement of coil stabilization will be discussed.

I. Introduction

The superconducting magnet is one of the most important parts for Maglev system. Recently, there are many applications of superconducting magnets under development, such as MRI, energy storage, Synchrotron Radiation ring, MHD ship propulsion, electric motors or generators, high energy testing facilities, and so on. Among these applications, we can say, the superconducting magnet for the Maglev system is rather a special one, because this superconducting magnet is used in rather different environments from others. So they have to be designed to stand these severe environments.

Here tests results about the superconducting magnets and the refrigeration system for Yamanashi test vehicle is discussed.

II. Superconducting magnet

A. Basic structure

Figure 1,2 shows the outside view and the illustration of the superconducting magnet. Table 1 shows the basic characteristics of the super-conducting magnet, made as one of the models for the Yamanashi test vehicle.

This superconducting magnet is composed of four superconducting coils, thermal insulating supports, thermal radiation shield, liquid helium tank, liquid nitrogen tank and vacuum vessel.

The on - board refrigerator which re - liquefy the evaporated gas helium is mounted on this LHe tank. The compressor for this refrigerator is also installed on the bogies.

Figure 3 shows the image of the superconducting coil. About 4km length of the NbTi multi-filament superconducting wire is used for one superconducting coil. The wound up coil is

Table 1 Basic characteristics of the superconducting magnet.

Items	Specifications
Dimension of SCM	5.32m(L) × 1.17m(H)
Weight of SCM	less than 1200kg
Volume of LHe tank	60 litres
Volume of LN_2 tank	44 litres
Superconducting coil	
Magnetmotive force	700kA (1167 turns)
Shape of SC coil	race track
Copper ratio of SC wire	1.0
Dimension of SC wire	1.16 × 2.06mm
Heat leakage to inner vessel	3W
Levitative force per magnet	98 kN
On-board refrigerator	built-in type
Refrigeration capacity	more than 5W at 4.4K

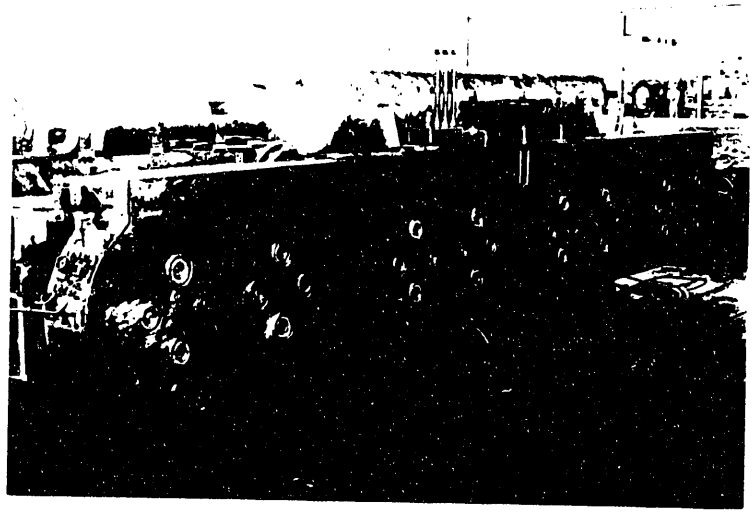

Fig. 1 Outside view of the superconducting magnet

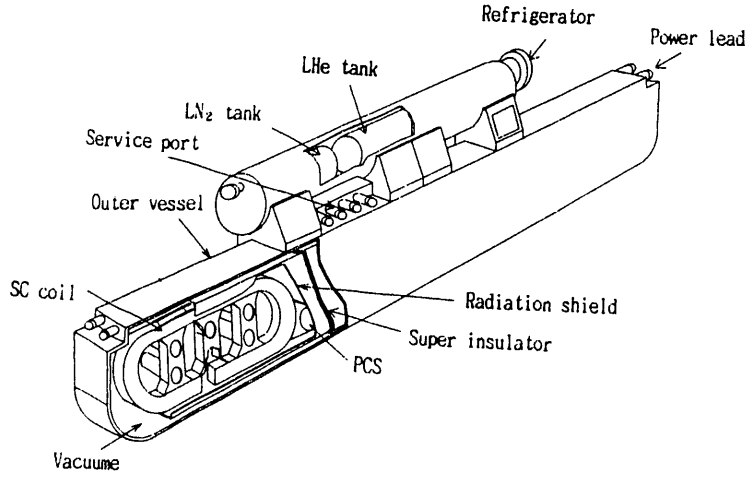

Fig. 2 Illustration of the superconducting magnet

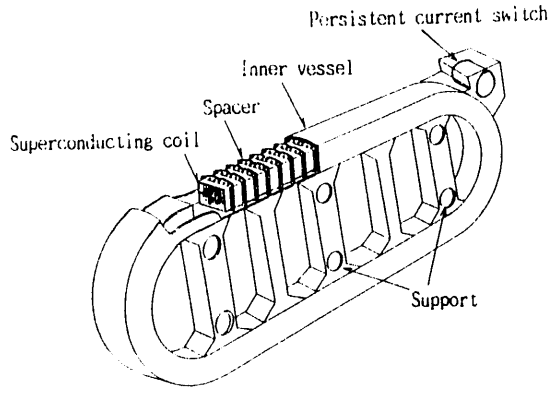

Fig. 3 Illustration of the superconducting coil

impregnated with epoxy resin to suppress the micro movement of the superconducting wire. The impregnated superconducting coil is fixed in the inner vessel made of stainless steel. Many spacers along the coil axis keep a distance between the inner vessel and superconducting coil. Liquid helium supplied from the upper tank is delivered to the narrow channel between spacers keeping the coil temperature at 4.2 to 4.3K.

All forces for levitation, propulsion and guidunce of the vehicle are transmitted from the superconducting coils to the room temperature structure passing through the thermal insulating supports.

The superconducting magnets are used on-board. For this reason, next things arise as the subjects of development.

a. The total weight of the magnet should be as light as possible.
b. The heat leak to the cryogenic temperature region, has to be made as small as possible.
c. It should have enough reliability under the severe condition of getting mechanical and electro - dynamic disturbances.

B. Disturbances under the running condition

The superconducting magnets are exposed to much disturbances from outside. Main disturbances are the magnetic field fluctuation

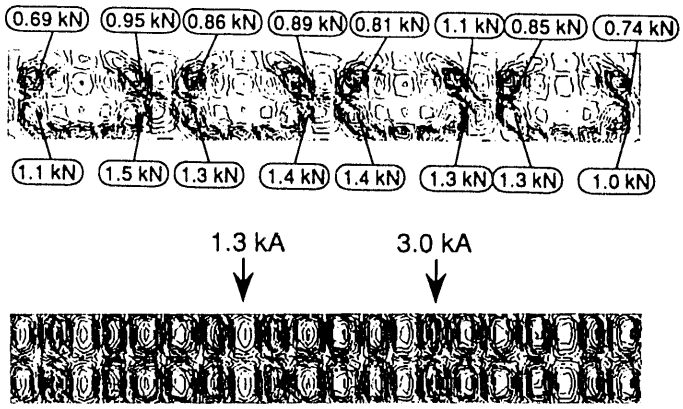

Fig. 4 Eddy current and force distribution at vacuum vessel

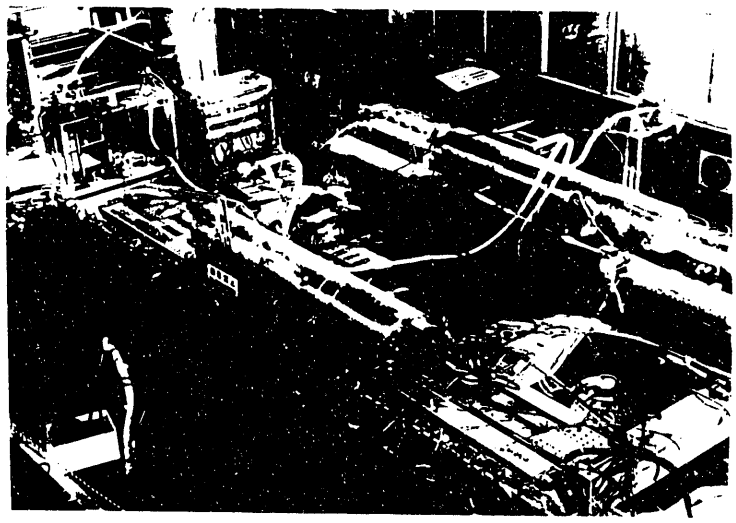

Fig. 5 Outside view of electro-magnetic disturbance simulator for the superconducting magnet

which arises from the ground coils (both for levitation and propulsion) and the mechanical vibration.

Figure 4 shows the calculated distributions of the eddy currents and the force on the vacuum vessel when the superconducting magnet receives the magnetic field fluctuation. These complex distribution changes also at high frequency decided by the runing speed of the vehicle.

The superconducting coil (inner element of the super-conducting magnet) receives the influence of both the magnetic field fluctuation and the mechanical vibration transmitted from the outer vessel. As the results, the superconducting coil vibrates intensively especially at the resonance frequency. Sometimes this vibration bring on the deformation of the coil, which makes a mechanical sliding inside resulting as the local heating. Further more the relative movement between the superconducting coil and the thermal radiation shield plate makes the magnetic field fluctuation inside again, causing eddy current losses at the inner vessel of the superconducting coil.

To estimate the influence of the magnetic field fluctuation on the superconducting magnet, a simulating facility was constructed. Fig.5 shows an outside view of this facility. The simulating ground coils are set opposed to the super-conducting magnets. The VVVF inverter is connected to these coils, submitting the magnetic fluctuation to a simulated running condition. The currents and the frequency from this inverter can be changed widely to simulate the condition up to the speed of 550km/h.

The influence is estimated by measuring the increase of mass flow rate of the evaporated gas helium, which means the heat load increase within the liquid helium temperature region.

III. Superconducting coil stability

The most important matter for the super-conducting coil is to keep stable the rated magneto - motive force.

The performance confirmation of the super-conducting coils for the Maglev system have been done by over-energization of the coil before installing the cryogenic vessel. Namely, the superconducting coils which are used with a magnetomotive force of 700kA were confirmed that it never experiences any quenching until 800kA. Even though the superconducting coils mounted on test vehicle MLU002 has caused many troubles of quenching, which happened mid-running tests. This proved that the static way of testing the coil performance was insufficient.

In order to make clear the influence of the mechanical vibration on the superconducting coil, two kinds of dynamic test facilities were provided.

A. Electro-magnetically vibrating coil test

Figure 6 shows an image of this test facility. The plural number of normal-conducting coils are set opposed to a superconducting coil to make the magnetic flux fluctuation. This magnetic flux can cause a bending or twisting force to the energized superconducting coil. Electric powers to the normal coils are controlled both in currents and in frequency.

On this test facility, the supplied current is

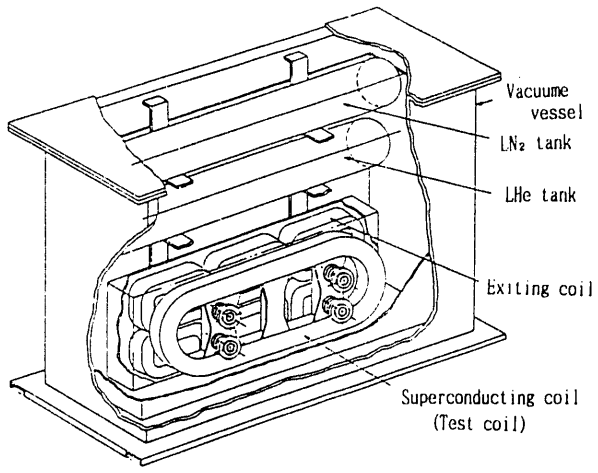

Fig. 6 Electro-magnetical coil vibrating test facility

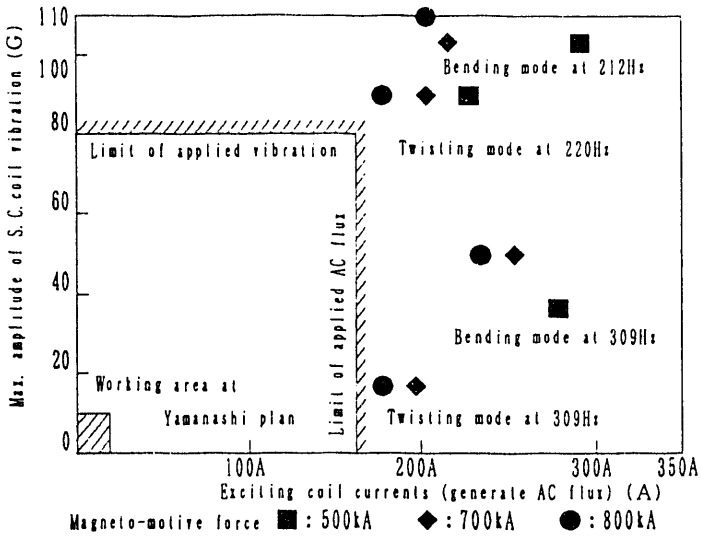

Fig. 7 Typical result of electromagnetic coil vibrating tests

increased until the coil quenches. The current when the superconducting coil quenched, served as a stability barometer of this superconducting coil.

Figure 7 shows a typical test results gained by this test facility. The horizontal line shows the current supplied to the normal conducting coil, and the longitudinal line shows the measured maximum amplitude of superconducting coil vibration.

As is shown, coil quenching occurred when the current is greater than about 170A even if the amplitude of superconducting coil vibration is at small value. The cause of this quenching is supposed to be the joule heating by the eddy current at the inner vessel, which means the limitation of this testing method.

The test results also show that the super-conducting coil has enough margin of stability compared with the shaded potion of supposed working area at Yamanashi plan shown in the figure.

B. Mechanical vibration test.

Figure 8 shows another test facility. This test facility is designed to check the characteristics of the superconducting coil when it is mechanically bent or twisted. Three or four rods are connected to the superconducting coil. One or two rods are oscillated by an oil pressure servo actuator.

This test facility is used not only for confirming the quenching characteristics but also for measuring the heat generation caused by mechanical deformation of the coil.

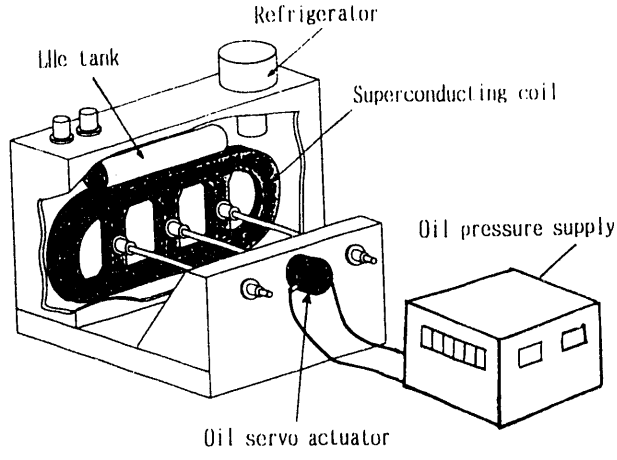

Fig. 8 Mechanical coil vibrating test facility

IV. Cooling system

The features of the on-board cooling system of the superconducting magnet are listed as follows.

(1) It has to keep the cryogenic temperature continuously without any consumption of the gas helium.
(2) The dependency on the ground cryogenic systems should be reduced.
(3) Gas helium system should be kept closed on board, even if the energization or de-energization of the magnet is done every day.
(4) The refrigerator should have enough reliability. It will be continuously operated in

long times in the revenue operation system in future.

(5) The system can be handled as simply as possible and should be compact light weighted and high efficiency.

For the on-board refrigeration system, the energization or de-energization of the magnet is the largest heat load disturbances. The heat load comes to much larger than the cooling capacity of each on-board refrigerator.

When the superconducting magnet is energized, the excess gas evaporated from the LHe reservoir will be stored into an on-board buffer tank temporarily by the compressor of the refrigerator. The stored gas helium will be re-liquefied by the on-board refrigerator taking several hours.

Three types of on-board 4K refrigerator with Joule-Thomson cycle has been developed for maglev system. These are Claude cycle refrigerator (with reciprocating pistons), Stirling cycle refrigerator and Gifford-Mcmahon(GM) cycle refrigerator.

Stirling cycle refrigerator is now keeping the most high efficiency compared with other types, even though it has some difficulties in the layout arrangement on the bogies.

For Claude cycle refrigerator, much efforts have made on a development of new valve mechanisms and heat exchanger. Even though, the reliability of this refrigerator has not reached to satisfied level.

Until recently, GM cycle has been evaluated as a low efficiency cycle refrigerator. Nevertheless, the needs of maglev system extremely promoted the improvements of GM refrigerator in recent few years on large capacity and high efficiency mainly on the rason of the employment of regenerator with new materials. Now the developed GM refrigerator has shown high effeiciency of figure of merit (FOM) less than 1000 and large refrigeration capacity of more over 8W, surpassing in the each of Claude cycle refrigerator.

As is well known, GM cycle refrigerator has a big merit that its mechanism is very simple, and so many refrigerators were produced mainly for the cryopomp system. For this reason, the reliability of this refrigerator is outstandingly superior to other cycles.

So, it is planned to concentrate the development on GM cycle and Stirling cycle refrigerator for Yamanashi test vehicle.

V. Concluding remarks

The superconducting magnets for the Maglev system are used in more severe environments than in other applications. For this reason the stability of the superconducting coil is one of the most important problems.

On the test vehicle MLU002 we experienced many coil quenching troubles. After that many improvements were done to increase the stability.

They are practically implemented in the designing of the superconducting magnets for Yamanashi new test line under construction.

The remaining main problem to be solved is the confirmation of the reliability of the total system. This will be one of the important roles to be accompleshed by the new test line.

The development of the superconducting magnets for Maglev system was subsidized by the Ministry of Transportation of Japan.

References

(1) H.Nakashima, T.Herai : THE CRYOGENIC SYSTEM FOR MAGNETIC LEVITATION VEHICLES, 11th International Conference on Magnetically Levitated System Linear Drive, 1989, p235-239

(2) H.Tsuchishima, T.Herai : SUPERCONDUCTING MAGNET AND ONBORD REFRIGERATION SYSTEM ON JAPANESE MAGLEV VEHICLE, Applied Superconductivity Conference, 1990.9

(3) E.Suzuki, H.Tsuchishima, T.Herai, A.Kishikawa : CONSTRUCTION AND EXPERIMENTAL RESULTS OF THE NEW TYPE SUPERCONDUCTING MAGNET, Applied Superconductivity Conference, 1992.8

(4) J.Fujie : Current Status of Superconducting Maglev System, Advances in Superconductibity Ⅲ, 1990.11, p1263-1268

(5) H.Tsuruga : Superconducting Maglev System on the Yamanashi Maglev Test Line, Future Transportation Technology Conference and Exposition, Costa Nesa, California, August 1992

(6) T.Hanai, T.Tokumasu, J.Ohmori, M.Terai : Analysis of eddy current in the cryostat of superconducting magnets on a MAGLEV vehicle, International Symposium on Nonlinear Phenomena in Electromagnetic Fields, Nagoya, January 1992

(7) M.Shibata, S.Hasegawa, N.Maki, T.Saitoh, T.Kobayashi, M.Terai, Ohishi : 48-th Meeting on Cryogenic and Superconductivity, Preprint, p29,1992(in Japanese)

(8) M.Yamaji, H.Nakashima : Superconducting magnet for Magnetically Levitated Vehicle, 1st International Symposium on Superconductivity (ISS'88)

Comparison of Magnetic Lift and Drag Forces For Two EDS Maglev Topologies

J. R. Hale, D. B. Montgomery, R. D. Pillsbury, Jr., R. J. Thome, J. Feng, A. Radovinsky

Plasma Fusion Center, Massachusetts Institute of Technology, Cambridge, Massachusetts 02139

***Abstract* - Results of magnetic lift and drag force calculations for two EDS maglev topologies are compared and contrasted. Dependencies of thee forces upon vehicle coil and guideway geometries are quantified, and the reuslting impact upon design decisions that affect other aspects of a maglev system design are discussed.**

I. INTRODUCTION

For the purposes of this paper, electrodynamic maglev systems will be categorized into either of two general topologies. In one of these, the magnetic force that supports the vehicle is generated more-or-less parallel to the planes of both the vehicle coils and the guideway coils. The guideway coils can be either pairs of cross-connected loops [1],[2], or repeating single loop or ladder elements. We will refer to this topology hereinafter as Type I. The so-called "null-flux" geometries are one example of this topology, while "flux-canceling" geometries represent another.

In systems configured with the second topology, the vehicle is supported by magnetic force generated perpendicular to the plane of both the vehicle coils and the guideway conducting elements. With this topology, the guideway conducting elements can be repeating single loops or ladders, or continuous sheets or plates of conducting material. We will refer to this topology hereinafter as Type II.

Designers of a maglev system based on either topology must confront a complex web of competing performance specifications. All must make choices, utilizing a combination of objective engineering, economic analysis, and design philosophy. All must accept whatever less favorable features their particular system design yields, in exchange for the more favorable features that they have judged to be most vital to the success of their concept.

The Fusion Technology and Engineering Division of the MIT Plasma Fusion Center has collaborated with two National Maglev Initiative (NMI) Systems Concept Definition (SCD) teams, Bechtel and Magneplane, carrying out design and analysis of superconducting vehicle magnets, guideway conductor optimization, and field and force calculations. The Bechtel system is representative of a flux-canceling Type I topology, while the Magneplane system is representative of a Type II topology.

We emphasize that the following discussion is based on *conceptual designs*, and both can be expected to evolve and improve with further development. Moreover, we selected these two concept systems as examples because of our first-hand participation in their development. There are a number of alternative embodiments of both topologies under development around the world, but it is not our purpose here to attempt a comprehensive review. Hence, a Type I system, or a Type II system, in the context of this paper, should be taken in most instances to refer to the specific concept designs we have chosen as examples, rather than to their respective generic topologies.

II. METHODS OF CALCULATION

We analyzed the magnetic forces exerted on a coil carrying a constant current moving at constant speed near a conducting medium utilizing three distinct computational tools. These tools can be characterized by the approximations used in modelling the currents induced in the passive conductors. They are: (1) a flat sheet of finite thickness and infinite extent; (2) a "thin" sheet of finite extent; and (3) a filamentary model of precisely defined geometry

Manuscript received April 15, 1993. This work supported in part by Magneplane International, under contract MIT-C-00006, and by Bechtel Corp., under contract 21705-TSC-3.

with unspecified current magnitudes. The first two tools solve for the magnitudes, directions and locations of the eddy currents induced in the conducting elements. These two are useful for analysis of the sheet levitation topology. The third method defines (or assumes) the pattern of the eddy currents but not their magnitudes, and is useful for analyzing guideway elements made of coils.

The first method is based on the approach of Reitz and Davis [3]. The infinite extent of the sheet allows the problem to be solved with quasi-analytic techniques. The second algorithm uses a "thin" shell finite element program, EDDYCUFF [4]. The primary assumptions are that there is no current flow in the direction perpendicular to the sheet midplane and that the conducting media has a thickness that is small relative to a skin depth. That is, the current density through the thickness is uniform. The third technique uses the approach of Hoppie, et al. [5]. It takes advantage of the periodicity of the guideway elements to achieve computational efficiency. The inductances of the loop or ladder conducting elements are calculated by defining them as current filaments with a specified distribution and unknown current magnitudes.

We have cross-checked these three independently created computational tools against one another by running identical sample cases; good agreement among them underlies our confidence in all three.

III. BASELINE GEOMETRIES

Designers commonly devise a "figure of merit" -- a raw number calculated from parameter values combined in such a way as to guide the designers in their approach to optimization of the device or system in question. Such figures of merit can be applied legitimately in comparisons among several variants, if they all have the same generic character or basis. In the following discussion, the ratio of magnetic lift to magnetic drag (L/D) to the mass of aluminum per unit length of guideway has proven useful as an objective figure of merit in comparing different guideway geometries for each of the two topologies separately. But to invoke this ratio as a figure of merit in comparing one topology with another is too simplistic, and does not account for the complex web of trade-offs that must be made.

One of the first tasks leading to the definition of a baseline geometry for both topologies was the selection of the respective vehicle coil configurations. For the representative Type I system, the baseline vehicle coil configuration chosen by the Bechtel SCD team is a longitudinal series of octupoles, with a total of 96 coils, 48 on each side of the vehicle. These vehicle coils are utilized for both levitation and propulsion. For the representative Type II system, the Magneplane SCD team chose coil pairs energized as quadrupoles as the baseline lift system, with a total of eight coils per vehicle, four in each of two bogies. For propulsion, the Magneplane utilizes a separate six-coil module in each of the two bogies.

We carried out a series of analyses in order to optimize the guideway electromagnetic configurations for each topology separately. For the Type I system, a decreet loop guideway yielded a 9% higher magnetic lift to drag ratio than did a ladder geometry, but at the expense of a larger mass of aluminum per unit length of guideway. The incorporation of the ratio of L/D to mass of aluminum per unit length of guideway, along with other parameters, into a figure of merit, was useful in evaluating comparisons among the dozens of variations within this topology. This tradeoff analysis led to the selection of a ladder geometry guideway as the baseline.

Guideway optimization analysis for the Type II system compared magnetic L/D for discreet loops, ladders, and continuous conducting sheet geometries. The sheet guideway produced the highest L/D ratio, and this was chosen as the baseline, despite the fact that a figure of merit based on the ratio of L/D to mass of aluminum per unit length was 45% larger for the optimal ladder configurations than for the sheet. In this case, other design trade-offs outweighed the influence of this particular figure of merit.

Further tradeoff studies and design iterations for both topologies led to the following values for the baseline relative position of the vehicle with respect to the guideway. For the representative Type I SCD (@ 134 m/s):

o Lateral clearance (m)	0.05
o Vertical offset (m)	0.016

For the representative Type II SCD system (@150 m/s):

o Clearance (m)	0.15

In both of these systems, designers have made tradeoff decisions, accepting some penalties in performance or cost or both, in exchange for one or more benefits judged to be vital to the success of the overall concept, including success in the marketplace.

IV. RESULTS

Figs. 1 and 2 show the calculated magnetic lift to drag ratio, and the vertical position at constant lift, as a function of speed, for the Type I and Type II systems, respectively. The 'vertical position' is defined differently for the two topologies. For Type I, the term 'vertical offset' refers to the difference between the horizontal plane of symmetry of the guideway ladders, and the horizontal plane of symmetry between pairs of vehicle magnets. ('Vertical offset' is one of the parameters that determine the electromagnetic interaction between vehicle coils and guideway conductors; the vertical clearance between this vehicle's undercarriage and the top of its guideway structure is on the order of 0.25 m.) In the case of Type II, 'vertical clearance' is the separation between the top surface of the guideway sheet and the underside of the vehicle magnet cryostats, which are flush with the fuselage. In the figures, note that the vertical scales on the two plots are identical. Neither of these figures represents an actual operating scenario, for in both cases, some mechanical means of support would limit, and in fact, define the vertical position during take-off and landing. Implementation of this low-speed vertical position control by mechanical means, prior to magnetic lift-off, is expected to be easier for the flux-canceling Type I system because of its lower magnetic drag characteristics.

The first obvious contrast evident from these figures is that the Type I vehicle has a higher L/D ratio, ranging from a factor of about 3.4 at 50 m/s to as much as 4.5 higher at 150 m/s. Inasmuch as the total magnetic drag is simply the quotient of vehicle weight and L/D, this higher ratio means that, even if it had a somewhat greater gross weight, the Type I vehicle would require less propulsive power to overcome magnetic drag.

But total drag has a second component, aerodynamic drag, that increases with the square of the speed, and tends to dominate the total drag at high speed. If the aerodynamic drag coefficients were comparable for vehicles of these two topologies (including their respective guideway proximity effects), the corresponding drag force would be proportional to the respective frontal areas. For example, if the Type I implementation were to incorporate a secondary suspension system that increased its net effective frontal area by a factor as large as two, then the sum of magnetic and aerodynamic drag for that vehicle could exceed the total drag for the Type II vehicle at some velocity within the normal operating range, despite the larger magnetic drag of the Type II vehicle. In this hypothetical case, the lower magnetic drag of the Type I vehicle could be an advantage, in terms of total drag losses, lower speed take-off and landing, and on route profiles dominated by frequent stops and modest average speeds. On high speed, inter-city routes, however, the lower aerodynamic drag losses characteristic of the Type II vehicle would be an advantage.

Electric power cost for operation is one important economic factor intimately connected with L/D, and LSM gap. In addition, the designers' tradeoff choices of gaps and coil geometries have an economic impact on other facets of system procurement and operation, among which, for example, are costs associated with procurement of power conversion and distribution equipment. These costs would likely be lower for this Type I SCD system, with its small-gap LSM, and lower magnetic drag characteristics.

In the interest of simplification, we have chosen to plot magnetic L/D in Figs. 1 and 2 with no factor included to indicate the aluminum requirements in the guideway. Calculations of magnetic L/D for the Type I vehicle included only the guideway components from which lift is derived, the vertical ladder structure. For the Type II vehicle, the corresponding guideway components are the aluminum sheets. The mass of aluminum per unit length of guideway for the Type I *levitation ladders* is less than that required for the Type II system's sheets by a factor of about 0.54.

However, in the Type II SCD, those sheets participate by providing not only lift, but also lateral guidance, interacting with both the levitation magnets and the LSM magnets to generate restoring force in the event of an off-centerline excursions, which in turn can add to magnetic drag. For a comparison across topologies, then, one needs to include any additional mass of aluminum that the Type I system requires for lateral guidance force. Attempts to combine magnetic lift, drag, and guidance forces with total aluminum procurement and fabrication, and installation costs, into a practical figure of merit, are beyond the scope of this paper.

V. OTHER DESIGN AND OPERATION IMPACTS

The selection of topology, a particular embodiment of that topology, and the subsequent design optimizations that are carried out by designers of a maglev system, yield differences in other features besides lift to drag ratios. In order to achieve high magnetic L/D, combined with comparatively

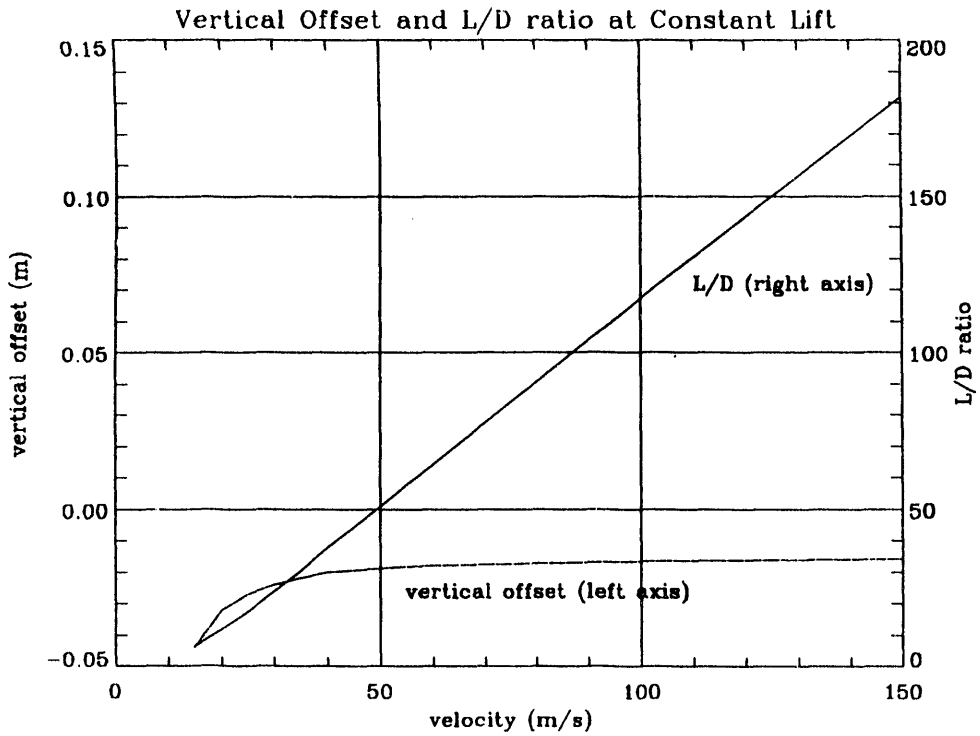

Fig. 1 - Plot of magnetic lift to drag ratio, L/D, (solid curve, right-side vertical scale), and vertical offset (dashed curve, left-side vertical scale), as a function of speed, at constant lift, for the Type I concept vehicle. Horizontal clearance, 0.145 m. Vertical offset is measured relative to horizontal plane of symmetry of guideway ladder.

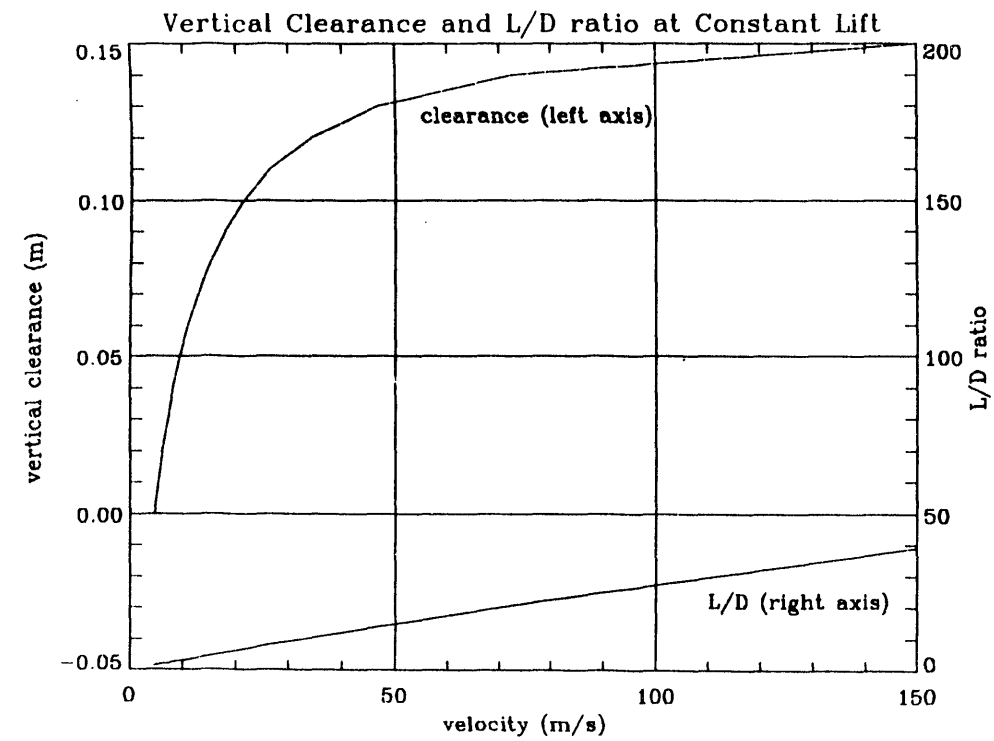

Fig. 2 - Plot of magnetic lift to drag ratio, L/D, (solid curve, right-side vertical scale), and vertical offset (dashed curve, left-side vertical scale), as a function of speed, at constant lift, for the Type II concept vehicle. Vertical clearance, 0.15 m, measured from sheet guideway surface to vehicle bottom surface.

low guideway conductor volume per unit length, designers of the Type I concept chose a comparatively small horizontal clearance between the vehicle and the vertical guideway surface. This proximity has an additional advantage for this topology in that it reduces the gap in the LSM. But as in any tradeoff, there are other consequences of small clearance that can be viewed as potential liabilities, or at least as features that require mitigation. There are of course design tradeoffs in the Type II, large gap topology, too, that yield superiority in some features, at the expense of other less favorable characteristics that require mitigation.

The following itemization briefly describes some of these trade-off considerations for both topologies. The range of choices inherent in overall system design is, of course, vastly more complex than this brief summary can convey.

o The flux-canceling topology yields low magnetic drag because comparatively modest eddy currents are induced in the guideway, for only an equivalent flux *difference* must be generated. But, inasmuch as the eddy currents are modest, the attendant fields that interact with the vehicle coil currents to produce lift are also modest. The magnetic drag in a sheet levitation geometry, by contrast is larger, because the induced guideway eddy currents must generate the equivalent of the entire linked flux produced by the vehicle coils.

o A low magnetic drag system of the Type I topology is thus, by virtue of the comparatively small vehicle coil-to-guideway ladder spacing, magnetically stiff. A secondary suspension system may be utilized in such cases. In addition, if active controls were incorporated, there would be higher response and performance requirements demanded for circuits and mechanical actuators. The small gap is not inherent in Type I topologies, but rather is selected on the basis of tradeoffs, some of which have already been mentioned.

o Among many other trade-off choices, the designers of the Type II system elected to implement their topology with a comparatively large gap, thereby taking advantage of the following favorable consequences, among others: less critical tolerances for guideway alignment and mid-span deflection, which could be expected to reduce the cost and maintenance of the guideway; lower magnetic stiffness and lower vehicle oscillation frequencies, which could be expected to facilitate active damping.

o For the Type I system concept vehicle, the ratio of total magnet system mass to vehicle mass is about 0.18. The magnet system comprises 96 identical coils, distributed among 12 bogies. These magnets serve multiple functions -- levitation, propulsion, and guidance. The corresponding ratio for the Type II system is about 0.11. This magnet system comprises 8 identical levitation magnets and 12 propulsion magnets, distributed between two bogies. In this vehicle, too, the magnets perform multiple functions: the 'levitation magnets' provide some guidance force as well, and the 'propulsion magnets' provide some levitation and guidance forces in addition to propulsion.

o By distributing the required ampere-turns among many comparatively small alternating polarity magnets, the Type I design achieves an order of magnitude smaller stray magnetic field in the passenger cabin, compared to the Type II design. Reducing the stray fields in the Type II vehicle to acceptable levels, while achievable, requires more on-board weight, and additional on-board power.

o In addition to the lift, drag, and guidance reaction forces that either guideway will experience, in the implementation of the Type I topology under discussion, the guideway levitation ladder experiences bursts of forces and torques as each vehicle passes.

o The vehicle magnets in the Type II vehicle may experience more a.c. losses arising as a result of low frequency (< 5 Hz) variations in gap between guideway and vehicle, induced, for example by guideway span flexure. Such changes in gap imply changes in flux linkage, and hence, corresponding variations in vehicle coil current.

o Because of the discreet nature of the guideway elements in the Type I SCD, the leading and trailing edges of the vehicle superconducting magnets will experience a superimposed a.c. field. The magnitude will, however, be attenuated by the aluminum cryostat walls, so a.c. losses in the superconductor from this source are expected to be small. In fact, vehicle magnets in both systems are likely to be immune from high frequency a.c. losses from external sources.

o Upon encountering a +0.01 m vertical step in guideway alignment at cruising speed (> 100 m/s), the Type I vehicle bow magnets would experience a lift force impulse equal to 62% of their normal vertical load. A +0.01 m step in the sheet guideway would produce a force impulse

about 11% higher than the normal cruise load in the Type II vehicle front bogie magnets.

VI. CONCLUSIONS

We have endeavored to present, in an objective context, a few of the most prominent differences between two SCD maglev vehicles that are based on different levitation topologies. In so doing, we hope to have demonstrated that comparing figures of merit of one sort or another during design iteration of a given system can be helpful in the selection of an optimal configuration. But the application of a figure of merit devised as an optimization tool for one topology, to a system of different topology, can turn out to be misleading. The art of trade-off analyses becomes increasingly complex, the further the design progresses, and the art of creating figures-of-merit must somehow mix the practicality and economics of technology with the economics of the marketplace.

REFERENCES

[1] S. Fujiwara, and T. Fujimoto, "Characteristics of the combined levitation and guidance system using ground coils on the side wall of the guideway, " *11th International Conf. on Magnetically Levitated Systems and Linear Drives,* July 7-11, 1989, p.241,244.

[2] T. Saitoh, K. Miyashita, and H. Kiwaki, "Study for harmonic ripple of electromagnetic force in superconducting magnetically levitated vehicle with non-rectangular ground coils, " *11th International Conf. on Magnetically Levitated Systems and Linear Drives,* July 7-11, 1989, p.245,250.

[3] J. Reitz and L. Davis, "Force on a rectangular coil moving above a conducting slab," *J. Appl. Physics.,* Vol 43, No. 4, April 1972.

[4] *EDDYCOFF (version 9) User's Manual,* copyright 1992, Mitsubishi Atomic Power Industries, Inc., translated and edited by MIT Plasma Fusion Center staff, 1992.

[5] L. Hoppie, F. Chilton, H. Coffey, and R. Singleton, "Electromagnetic lift and drag forces on a superconducting magnet propelled along a guideway composed of metallic loops," Applied Superconductivity Conference, Annapolis, Md. 1972.

TRANSRAPID TR-07 MAGLEV-SPECTRUM MAGNETIC FIELD EFFECTS ON DAILY PINEAL INDOLEAMINE METABOLIC RHYTHMS IN RODENTS

Kenneth R. Groh
Center for Mechanistic Biology and Biotechnology
Argonne National Laboratory
Argonne, Illinois 60439

Abstract. This study examined the effects on pineal function of magnetic field (MF) exposures (ac and dc components) similar to those produced by the TransRapid TR-07 and other electromagnetic maglev systems (EMS). Rats (6/group.) were entrained to a 14:10 light-dark cycle and then exposed to a continuous, or to an inverted, intermittent (on = 45 s, off = 15 s, induced current = 267 G/s) simulated multifrequency ac (0-2 kHz) and dc magnetic field (MF) at 1 or 7 times the TR-07 maglev vehicle MF intensity for 2 hr. Other groups of rats were exposed to only the ac or the dc-component of the maglev MF. For comparison, one group was exposed to an inverted, intermittent 60-Hz MF. At the end of the exposure, each group was sacrificed and compared to an unexposed group of rats for changes in pineal melatonin and serotonin-*N*-acetyltransferase (NAT). MF exposures at an intensity equivalent to that produced by the TR-07 vehicle (1X; 0.1-50 mG, 1.6 kHz-10 Hz; 250 mG dc) had no effect on melatonin or NAT compared with sham-exposed animals under any of the conditions examined. However, 7X TR-07-level continuous 2-h MF exposures significantly depressed pineal NAT by 45% ($p < 0.03$) compared to controls. Pineal melatonin was also depressed 33-43% by a continuous 7X TR-07 MF exposure and 28% by an intermittent 60-Hz 850-mG MF, but the results were not statistically significant. This study demonstrates that intermittent, combined ac and dc MFs similar to those produced by the TR-07 EMS maglev vehicle alter the normal circadian rhythm of pineal indoleamine metabolism. The pineal regulatory enzyme NAT was more sensitive to MF exposure than melatonin and may be a more desirable measure of the biological effects of MF exposure.

INTRODUCTION

Maglev promises to be an efficient mode of transportation which could complement short airplane commuter flights in the range of 1000 km [1] and, traveling at speeds up to 500 km/h, these vehicles could provide excellent service between cities and major airport hubs. The possibility of using magnetically levitated vehicles for high-speed ground transportation has been examined since the early 1970s. Germany and Japan have each spent in excess of one billion dollars to develop and test prototype maglev systems, the German TransRapid TR-07 maglev system using conventional magnet levitation and propulsion and the Japanese using superconducting magnets. The Japanese expect to demonstrate one of their designs by the mid-1990s, and final plans are underway to install a 22-km TR-07 maglev system in Orlando, Florida, in the same time frame. A National Maglev Initiative, led by the Federal Railroad Administration and supported by the Army Corps of Engineers and the Department of Energy, was established in 1990 by the federal government to explore the options available for using this technology in the United States.

In the last 25 years nonionizing electromagnetic field (emf) exposure has come under scrutiny as another potentially harmful environmental agent. Both electric and magnetic fields in the extremely low frequency range (3-3000 Hz), as well as static magnetic fields have produced biological effects in cellular and animal investigations.

Extensive animal studies have demonstrated the most significant and repeatable emf effects in the areas of emf perception, behavior, and neuroendocrine effects [2]. Wilson et al. [3] demonstrated depression of greater than 50% in the pineal melatonin rhythm in rats by continuous exposure to a 100-kV/m 60-Hz electric field for three weeks. However, the rhythm returned after the field exposure ceased. In later studies with 60-Hz electric field exposures as low as 1.7 kV/m, Wilson showed the same depression in melatonin and in serotonin-*N*-acetyltransferase (NAT), the regulatory enzyme in the metabolic pathway from serotonin to melatonin in the pineal. A phase delay of approximately 2 h in the melatonin rhythm was also produced by the emf exposure [4].

Vasquez et al. [5] continued to add to the neuroendocrine effects observed as a result of emf exposure. Rats exposed to 39-kV/m, 60-Hz electric fields showed phase shifts of up to 4 h in the circadian rhythms of the neurotransmitters norepinephrine, dopamine, and the serotonin metabolite 5-hydroxyindoleacetic acid (HIAA) in the hypothalamus, striatum, and hippocampus.

Not only have environmental-level magnetic fields produced depression in circadian neurotransmitter rhythms, but rapidly changing magnetic fields of low, ambient intensity have shown similar neurotransmitter effects. Lerchl et al. [6, 7] showed that intermittent, 1-hour, earth-strength, dc MFs depress normal melatonin and NAT rhythms in the rat pineal. This suggests that transient fields that produce induced

currents may contribute to biological response to emf exposure.

Electromagnetic fields produced by maglev and other electrified rail systems have not been well characterized, with the exception of a recent Federal Railway Administration (FRA)-sponsored study of the German TransRapid TR-07 maglev vehicle [8, 9]. Currently, the FRA is measuring the electric and magnetic fields produced by a number of electric-powered transportation systems, and detailed emf exposure information will soon be available.

From the information that is available about the electromagnetic fields produced by maglev and electric-powered vehicles, the majority of magnetic fields are dc and in the ELF range. The intensities vary and depend upon the specific transportation system characteristics. In superconducting vehicles, dc fields could reach upwards of 150 G, with ac field magnitudes in the range of 1.0 G in the passenger compartment [10, 11]. In addition, it is likely that time-varying dc, power frequency (50-60 Hz), and transient ELF magnetic field components will be encountered.

Which parts of this very complicated emf spectrum will prove to be most important in assessing the presence or absence of a potential health hazard is unclear at this time, but these transportation systems do have emf field emissions in the frequency and intensity ranges which have demonstrated to have biological effects in cell, animal, and human studies. No significant effects have been identified in the few studies that have examined transportation system passengers or workers for biological responses to emf exposure [10].

The purpose of this study was to begin examining the complex-spectra, time-varying emf fields produced by maglev transportation systems that use conventional EMS (TR-07) or superconducting magnet technology. Maglev MFs were simulated using the TransRapid TR-07 maglev spectra measured by Electric Research and Management, Inc. (ERM) [8, 9]. Using rats, MF exposures were used that are likely to be encountered by passengers and system workers, as well as MF conditions that have produced repeatable biological effects using power frequency or static dc fields.

MATERIALS AND METHODS

A pair of Helmholtz coils (r = 0.5 m) were oriented with the diameter perpendicular to the north-south ambient field. A bipolar power supply (Kepco, Flushing, NY, Model BOP 50-2M, 50 V, 0-2 A) was used to energize the Helmholtz coil system. The simulated maglev magnetic field (MF) (dc and multi frequency ac) spectrum was generated using a 286 AT personal computer and LabWindows Data Acquisition and Analysis software (National Instruments, Austin Texas). The program developed is capable of producing a dc- and/or multifrequency ac signal to the bipolar power supply (of up to 10 individual frequency and intensity components) in the range of 0-2 G (dc) and 0-2 kHz (ac). The ramp rate of the signal can be varied over a wide range (microseconds to seconds) to vary dB/dt, producing an induced voltage in the Helmholtz coil and subsequent eddy currents.

Maglev magnetic field exposures were simulated from spectra collected inside the moving (168 km/h) passenger compartment of the TR-07 prototype vehicle, as measured by ERM in August 1990 [9]. Fig. 1 depicts the actual and simulated complex ac spectrum of this prototype maglev vehicle. The dc component of the TR-07 was 250 mG above ambient.

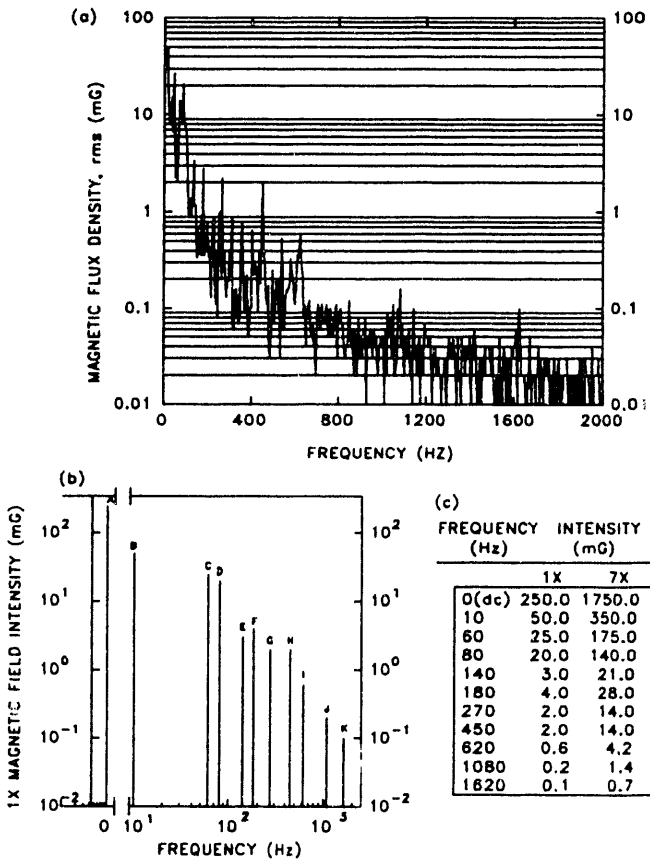

Fig 1. TR-07 Magnetic Field Spectrum. (a) Actual measurement recorded August 1990 by Electric Research and Management [9], at a velocity of 168 km/h. The dc component was 250 mG above the ambient field. Simulated TR-07 MF (b). The prominent frequencies (Hz) and their respective intensities, including a 250-mG dc component, were delivered simultaneously by computer to the Helmholtz coil. The entire spectrum was increased 7 fold for the 7X exposures (c).

Although the ac and dc MF intensities, and especially the transient profiles, are uniquely different, EMS maglev

vehicles are expected to produce similar magnetic field profiles quite different from the dc, 60-Hz, and other magnetic field exposures that have previously been used in biological exposure experiments.

Male Sprague-Dawley (Cobb strain) rats (*Rattus norvegicus*), 44-47 d old, 100-120 g were entrained for two weeks to a 14:10 light-dark (LD) cycle (dark period [D] = 0500-1500), with dim red light present during the dark portion of the cycle. Food and water was available *ad libitum*. Conditions were constant at 22 °C and 50% RH. For every exposure group, six similarly treated animals served as controls.

Daily for 7 d, groups of six animals were placed into two cages that were modified with plastic barriers to allow individual containment and exposure of three rats per cage in the central area of the Helmholtz coils. MF exposures occurred during dark for 2 h, ending at 6 or 9 h after dark onset, when pineal melatonin and NAT are at maximum levels. Another group of six animals were exposed for similar lengths of time, ending 5 h after light onset (minimum melatonin and NAT).

The magnetic field exposures were physically presented in several different ways:

1. Exposure length: 1, 2, or 4 h

2. Continuous MF exposure or intermittent exposures (repeating pattern of 45 s on, 15 s off) were quickly ramped, producing a dc-component-induced current of 37 (1X TR-07) or 267 (7X) G/s. Rapid application of an intermittent, inverted earth-strength static MF has been shown to significantly decrease pineal melatonin and NAT [6, 7].
3. Exposure to horizontal MF components or parallel to the inclination of the ambient magnetic fields (55°).

4. Exposure in the same direction as or opposite to ("inverted") ambient magnetic field.

Immediately after an exposure, the exposed and control rats were alternately sacrificed, and the pineal was removed and frozen (-60 °C, dry ice, average time 30 s) until assay. Melatonin was determined by radioimmunoassay [7, 12], and serotonin-*N*-acetyltransferase activity (NAT; EC 2.3.1.5) was determined by radioenzymatic assay [13]. Differences between control and exposed groups of animals were compared using the Student t-test.

RESULTS

Simulated TR-07 MF Exposures (1X)

No significant changes in pineal melatonin levels occurred as a result of simulated TR-07 MF exposure under a number of MF delivery protocols (Fig. 2). Continuous MF exposure during dark (maximum melatonin) for 1, 2, or 4 h in two

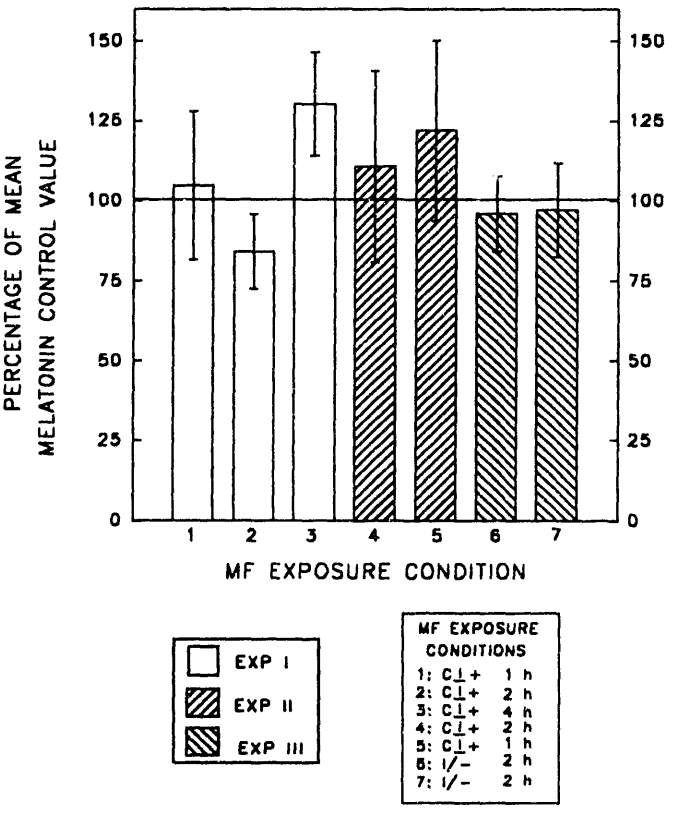

Fig 2. Pineal Melatonin Response to 1X TR-07 MF Exposure. During the nighttime (dark) peak in pineal melatonin, rats were subjected to TR-07 frequency and intensity MF exposure in three separate experiments. The exposures in Experiment I were continuous, in the same direction as the ambient MF, and varied in length (1, 2, or 4 h). MF-exposures in experiment II were a repeat of those in experiment I. Exposures in Experiment III were inverted to the ambient field, intermittent (45 s on/15 s off), and turned on rapidly to produce induced (eddy) currents. The unexposed control group mean between MF exposure experiments differed in the absolute amount of melatonin per pineal, so the exposed melatonin/pineal response was calculated as percentage of control response within experiments (control = 100%). Bars are standard error.

experiments did not depress pineal melatonin below control levels. Intermittent, inverted TR-07-level (1X) maglev MF

exposures (net MF = +150 mG, dB/dt = 37 G/s) for 2 h also had no effect on maximum (dark) melatonin levels.

TR-07 Maglev (7X) and AC- and DC-Component MF Exposures

Together, the results of three experiments (with all animals exposed to MFs when melatonin reached maximum levels in the pineal considered as one group, 4.5-8.5 hours after dark onset), showed that only 2-h inverted, intermittent 7X TR-07 dc exposures (net MF = -1.3 G, dB/dt= 267 G/s) produced a significant 46% decrease in NAT (Fig. 3,"D7", $p < .03$,). The animals exposed to the 1X, 7X, or 7X ac component intermittent maglev fields did not differ in pineal NAT from

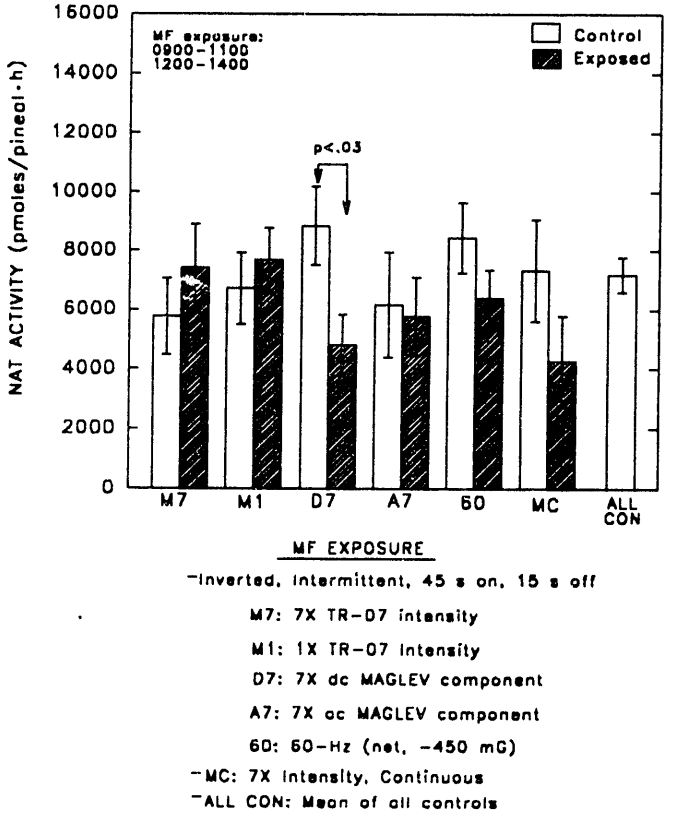

Fig 3. Nighttime MF Exposure and NAT Response. Animals (six per group) were entrained for two weeks (14:10 LD; D = 0500-1500) and then exposed to MFs. Exposures were either at 0900-1100 or 1200-1400, and were combined (n = 12). Following exposure, the animals (and controls) were sacrificed and the pineals were removed, frozen (-60 °C), and assayed for amount of pineal NAT per animal. Bars are standard error.

unexposed controls sacrificed at the same time, but 60-Hz and continuous maglev exposed NAT levels were decreased 28% and 42%, respectively, although these decreases were not statistically significant. During this same period of maximum melatonin in the pineal, none of the MF exposure conditions resulted in a significant change in pineal melatonin (Fig. 4), although a 2 h continuous 7X maglev

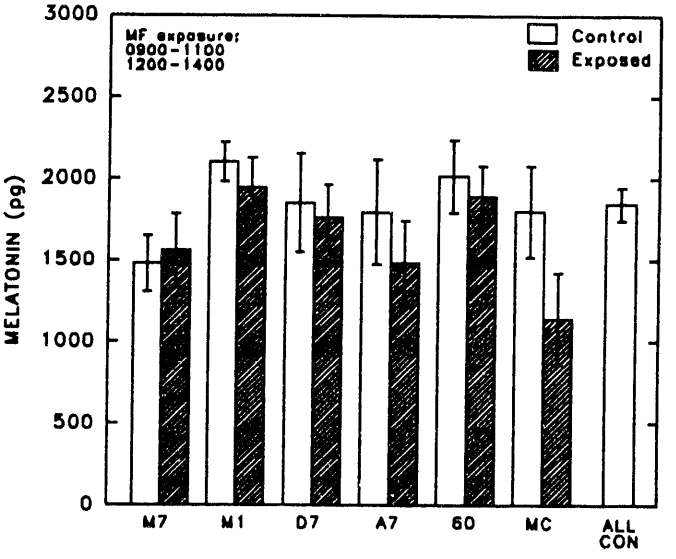

Fig 4. Nighttime MF Exposure and Melatonin Response. Animals (six per group) were entrained for two weeks (14:10 LD; D = 0500-1500), and then exposed to MFs. Exposures were either at 0900-1100 or 1200-1400, and were combined (n = 12). Following exposure, the animals (and controls) were sacrificed, and the pineals were removed, frozen (-60 °C), and assayed for the amount of pineal melatonin per animal. Bars are standard error.

exposure ("MC") depressed pineal melatonin 37%. The directionality (whether a MF horizontal to or parallel to the ambient field was used to expose groups of animals) also did not produce changes in pineal melatonin.

DISCUSSION

This study demonstrates that MF exposure at intensities produced by the German TransRapid maglev EMS vehicle does not produce changes (depression) in pineal melatonin and NAT levels, which have been used as a sensitive, reproducible, indicators of biological response to emf exposure [14-19]. However, when the dc component of the TR-07 MF was increased 7-fold (1-2 G), and delivered intermittently to produce induced eddy currents, pineal NAT was significantly reduced (50-60%) compared to control, unexposed animals ($p < 0.03$). MFs at this strength have been measured or are expected for EMS and EDS maglev vehicles.

In addition, a number of MF exposure conditions did reduce melatonin and NAT changes as much as 50%, but the declines were not statistically significant. Continuous 7X TR-07 maglev exposures decreased NAT 40-47% (Fig. 3). Melatonin was also decreased 37% by continuous 7X maglev exposures (Fig. 4). These MF exposures consisted of TR-07

ac MF components which would produce induced (eddy) currents similar to the intermittent dc MF exposures found to significantly reduce pineal indoleamine metabolism in this study and by Lerchl et al. [6,7].

Although the percentage decrease was large (in the range of 50%), small group sizes (n = 6), individual animal differences in entrainment, and individual sensitivity to MF exposure may have combined to dilute the group pineal melatonin and NAT differences between MF-exposed and control animals. The amount of group variation was large, and the same in both control and exposed animal groups.

Individual animals vary in their entrainability to most endogenous and exogenous agents [20], and Rosenberg et al. [21] has shown that up to 20% of rats show no change in perception of electric fields as great as 100 kV/m, measured by changes of activity, Variations in individual animal entrainment by as small as 1 h in pineal melatonin and NAT entrainment rhythms could have resulted in a large pineal melatonin and NAT group differences in response to MF exposure, as was seen in this study. Increased group size and optimal MF-exposure times identified in future studies will more successfully test the ability of these weak, non-ionizing MF exposure conditions to alter pineal rhythms.

Since melatonin has been shown to inhibit the growth of breast tumor cell lines *in vitro* [22], emf depression of pineal melatonin has been proposed as a possible mechanism to explain the growing human epidemiological evidence which suggests that emf exposure increases brain tumors and leukemia [4]. The plausibility of melatonin depression and the emf epidemiological link to cancer in humans has been strengthened by Wilson et al. [23], who, in a pilot study, found a decrease in the urinary melatonin metabolite 6-hydroxy melatonin sulfate (6-OHMS) at night in human subjects who used high-current electric blankets (relative to subjects using low-current electric blankets).

Whether decreased in pineal indoleamine metabolism does contribute to increases in carcinogenesis remains to be more solidly demonstrated, and any contributions from transportation system MF exposures will help to resolve this presently perplexing controversy.

ACKNOWLEDGMENT

This work was supported by an interagency agreement between the Department of Transportation/Federal Railway Administration and the Department of Energy.

REFERENCES

[1] L. Johnson, D. M. Rote, J. R. Hull, H. T. Coffey, J. G. Daley, and R. F. Giese, "Maglev vehicles and superconductor technology: integration of high-speed ground transportation into the air travel system," *Argonne National Laboratory Report ANL/CNSV-67*, Argonne, IL, 1989.

[2] I. Nair, M. G. Morgan, and W. K. Florig, "Biological effects of power frequency electric and magnetic fields -- background paper," *Office of Technology Assessment Report OTA-BP-E-53*, Washington, D. C.: U. S. Govt. Printing Office, 1989.

[3] B. W. Wilson, L. E. Anderson, D. I. Hilton, and R. D. Phillips, "Chronic exposure to 60-Hz electric fields: effects on pineal function in the rat," *Bioelectromagnetics*, vol. 2, pp. 371-380, 1981.

[4] B. Wilson, and L. E. Anderson, "ELF electromagnetic field effects on the pineal gland," in *Extremely Low Frequency Electromagnetic Fields: The Question of Cancer*, B. W. Wilson, R. G. Stevens, and L. E. Anderson, Eds. Columbus, OH: Battelle Press, 1990, pp. 159-186.

[5] B. J. Vasquez, L. E. Anderson, C. I. Lowery, and W. R. Adey, "Diurnal patterns in brain biogenic amines of rats exposed to 60-Hz electric fields," *Bioelectromagnetics*, vol. 9, pp. 229-236, 1988.

[6] A. Lerchl, D. O. Nonaka, and R. J. Reiter, "Marked rapid alterations in nocturnal pineal serotonin metabolism in mice and rats exposed to weak intermittent magnetic fields," *Biochem. Biophys. Res. Commun.*, vol. 169, pp. 102-108, 1990.

[7] A. Lerchl, D. O. Nonaka, and R. J. Reiter, "Pineal gland: its apparent 'magnetosensitivity' to static magnetic fields is a consequence of induced electric currents (eddy currents)," *J. Pineal Res.*, vol. 10, pp. 109-116, 1991.

[8] F. Dietrich and W. E. Feero, "Safety of high speed magnetic levitation transportation systems: magnetic field testing of the TR07 maglev vehicle and system," vol. I (analysis), U.S. *Department of Transportation Report DOT-VNTSC-FRA-92-6.1*, 1992.

[9] F. Dietrich, D. Robertson, and G. Steiner, "Safety of high speed magnetic levitation transportation systems: magnetic field testing of the TR07 maglev vehicle and system," vol. II (appendices), U.S. *Department of Transportation Report DOT-VNTSC-FRA-92-6.2*, 1992.

[10] W. A. Creasey, D. Phil, and R.B. Goldberg, "Health effects of low frequency electromagnetic fields due to maglev and rail systems," *Department of Transportation Report*, in press.

[11] M. Nakagawa and T. Koana, "EMF issues with maglev in Japan," *Proceedings of the First World Congress for Electricity and Magnetism in Biology and Medicine* (June 14-19, 1992, Lake Buena Vista, Florida), San Francisco, CA: San Francisco Press, in press.

[12] G. E. Webley, H. Mehl, and K. P. Willey, "Validation of a sensitive direct assay for melatonin for investigation of circadian rhythms in different species," *J. Endocrin.*, vol. 106, pp. 387-394, 1985.

[13] T. Deguchi and J. Axelrod, "Sensitive assay for serotonin N-acetyltransferase activity in rat pineal," *Anal. Biochem.*, vol. 50, pp. 174-179, 1972.

[14] B. W. Wilson, E. K. Chess, and L. E. Anderson, "60-Hz electric-field effects on pineal melatonin rhythms: time course for onset and recovery," *Bioelectromagnetics*, vol. 7, pp. 239-242, 1986.

[15] J. Olcese, S. Reuss, J. Stehle, S. Steinlechner, and L. Vollrath, "Responses of the mammalian retina to experimental alteration of the ambient magnetic field," *Brain Res.*, vol. 448, pp. 325-30, 1988.

[16] J. Olcese, S. Reuss, and L. Vollrath, "Evidence for the involvement of the visual system in mediating magnetic field effects on pineal melatonin synthesis in the rat," *Brain Res.*, vol. 333, pp. 382-84, 1985.

[17] J. Olcese and S. Reuss, "Magnetic field effects on pineal gland melatonin synthesis: comparative studies on albino and pigmented rodents," *Brain Res.*, vol. 369, pp.365-68, 1986.

[18] P. Semm, "Neurobiological investigations on the magnetic sensitivity of the pineal gland in rodents and pigeons," *Comp. Biochem. Physiol.*, vol. 76A, pp. 683-689, 1983.

[19] R. J. Reiter, L. E. Anderson, R. L. Buschbom, and B. W. Wilson, "Reduction of the nocturnal rise in pineal melatonin levels in rats exposed to 60-Hz electric fields in utero and for 23 days after birth," *Life Sci.*, vol. 42, pp. 2203-2206, 1988.

[20] M. C. Moore-Ede, F. M. Sulzman, and C. A. Fuller, *The Clocks That Time Us*, Cambridge, MA: Harvard University Press, 1982.

[21] R. S. Rosenberg, P. H. Duffy, G. A. Sacher, and C. F. Ehret, "Relationship between field strength and arousal response in mice exposed to 60-Hz electric fields," *Bioelectromagnetics*, vol. 4, pp. 181-191, 1983.

[22] D. Blask, "The emerging role of the pineal gland and melatonin in oncogenesis," in *Extremely Low Frequency Electromagnetic Fields: The Question of Cancer*, B.W. Wilson, R.G. Stevens, and L.E. Anderson, Eds. Columbus, OH: Battelle Press, 1990, pp. 319-335.

[23] B. W. Wilson, C. W. Wright, J. E. Morris, R. L. Buschbom, D. P. Brown, D. L. Miller, R. Sommers-Flannigan, and L. E. Anderson, "Evidence for an effect of ELF electromagnetic fields on human pineal gland function," *J. Pineal Res.*, vol. 9, pp. 259-69, 1990.

INNOVATIVE SPINE GIRDER GUIDEWAY DESIGN FOR SUPERCONDUCTING EMS MAGLEV SYSTEM

John B. Allen, P.E.
Parsons Brinckerhoff Quade & Douglas, Inc.
Tampa, Florida 33607

Morad G. Ghali, P.E.
Parsons Brinckerhoff Quade & Douglas, Inc.
Tampa, Florida 33607

ABSTRACT: To ensure the economic feasibility of full capacity Maglev systems, guideway designs need to be low cost yet structurally rigid and durable. A spine girder design was developed using precast segmental concrete technology and the resulting guideway structure appears applicable to any Maglev vehicle. A spine girder is composed of a central box girder and two tracks supported on outriggers. This results in an efficient guideway system which will meet all requirements for Maglev loads and allowable construction tolerances. This paper summarizes the basic development process for the spine girder and illustrates the potential application of the concept to other Maglev systems.

1. INTRODUCTION

As part of the Grumman Team in the Maglev System Concept Definition Study (SCD) #4, Parsons Brinckerhoff was responsible for developing a twin track guideway structure to accommodate the Grumman EMS Maglev vehicle.

2. OBJECTIVES

For any design development process, it is important at the outset to list out the main objectives to be attained. For the guideway structure, seven primary, but interlinked, objectives were established.

A. Operational Layout

The guideway must be capable of safely supporting the design vehicles with allowance for operating clearances, track centers and other dimensional constraints.

B. Structural Stiffness

The structure has to be sufficiently rigid to ensure that static and dynamic movements of the structure under vehicle loads and differential temperature do not exceed the magnetic air gap clearances and that ride quality criteria are achieved.

A stiffness constraint is rarely of major significance for a highway or even a conventional transit structure. However, for Maglev operations with vehicles operating at up to 300 mph it is a major factor. With a theoretical air gap of 40 mm, it is necessary to limit structural distortions from all causes to a maximum of ±15mm from the mean position.

C. Cost

For any Maglev system, the cost of the fixed guideway structure will substantially exceed 50% of the total system implementation cost, if land costs are excluded.

To protect the viability of the system, it is imperative that the guideway design permits construction costs to be held to a minimum.

D. Speed of Construction

Guideway construction will usually represent the critical path for system completion. As well, it is to be expected that any Maglev route will cross terrain which varies significantly. Construction of the guideway must therefore be able to proceed rapidly and under variable conditions.

E. Emergency Passenger Evacuation

A Maglev route may extend hundreds of miles and it is therefore possible that vehicles will become disabled in remote areas. Provision should be made for emergency egress of passengers from a vehicle, anywhere along the guideway.

F. Maintenance

The fixed guideway needs to be a reliable structure

with a capability to operate in the widest range of weather conditions which are known to occur along the route.

Although all structures benefit from maintenance, it should be as maintenance free as possible so that passenger schedules are not routinely disrupted and to keep operational costs under control.

G. Appearance

A Maglev guideway will be highly visible to pedestrians, motorists and residents. At a minimum, the appearance of the guideway needs to be visually tolerable. Desirably it should have a pleasing appearance.

Beyond these seven primary objectives, other issues need to be considered in assessing the overall suitability of any scheme. Such issues include size and frequency of supports; potential for noise transmission; the ability to be constructed in crowded urban areas and/or environmentally sensitive areas; and the ability to accommodate curved track alignments.

3. ASSUMPTIONS

A number of engineering assumptions were made as the basis for the development and comparison of the guideway concepts. Some key assumptions are outlined below. Environmental factors are necessarily 'average', reflecting the non-site specific nature of the S.C.D.

3.1 Vehicle Loadings

The worst effects of either of the 1, 2 or 3 car vehicles defined in Figure 1. Impact was taken as 20% for the main guideway girder and 50% for track support members.

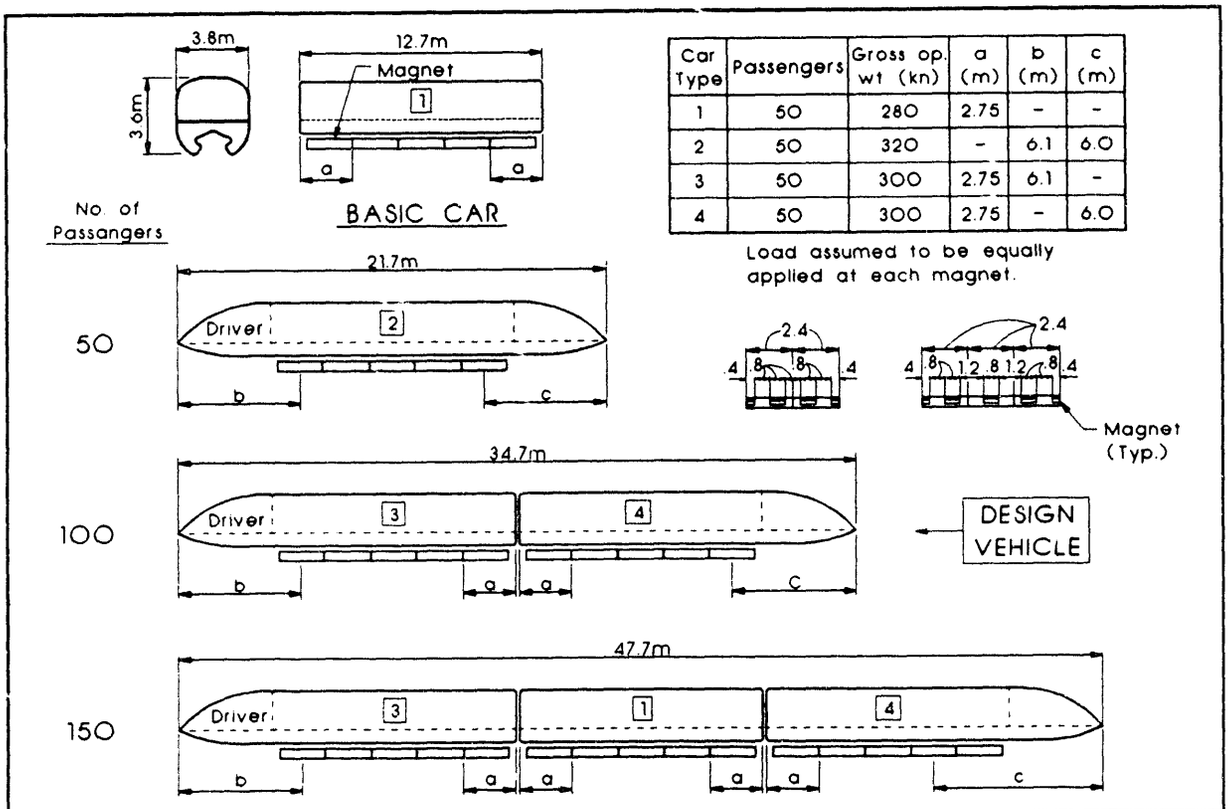

Car Type	Passengers	Gross op. wt (kn)	a (m)	b (m)	c (m)
1	50	280	2.75	-	-
2	50	320	-	6.1	6.0
3	50	300	2.75	6.1	-
4	50	300	2.75	-	6.0

PARSONS BRINCKERHOFF	SIMPLIFIED VEHICLE LAYOUTS AND LOADINGS	FIGURE 1

Vehicles were assumed to be operating with a 150m (500 ft.) minimum clearance. To avoid excessive aerodynamic buffeting forces, tracks were spaced at a minimum of 7.5 m (24.5').

Longitudinal braking/acceleration forces were taken as 125 kN (28 kips) per vehicle.

Detailed dynamic analysis to assess ride quality effects were part of the concept development work and are described elsewhere. Sufficient to note here that computed dynamic magnifications were less than the 20% assumed above.

3.2 Design Method

In line with forthcoming revisions to the national bridge design specifications, the load factor design was used to compute the necessary strengths of all elements, including foundation caps and piles. For the concept designs, the load combinations were limited to the following:

Group I	=	1.3(DL+1.25*(LL+I)+0.3*LF)
Group II	=	1.3(DL+W)
Group III	=	1.3(DL+(LL+I)+LF)
Group IV	=	1.25(DL+(LL+I)+W)
Group V	=	1.0(DL+EQ)

3.3 Seismic

The guideway designs were examined under seismic zone 2A Normalized Response Spectra for soil type 2.

3.4 Differential Temperature

A very significant component of structural distortion which needs to be allowed for. The guideway 'top slabs' were taken to vary in temperature in accordance with the profiles defined in the 1989 AASHTO guide specification assuming top hot conditions of 45°F and top cold of 23°F.

3.5 Snow and Ice

For nonoperational conditions, 1.45 kPa (30 psf) was assumed on horizontally projected areas. For operational conditions, 2.9 kPa (60 psf) on areas away from the tracks.

4. CONCEPT DEVELOPMENT

For the twin track guideway a number of structural options were examined. Initially both steel and prestressed concrete structures were considered, but it soon became apparent that the steel options had real difficulty in being cost competitive with concrete when the stiffness limitations were applied. As a result, steel options were not considered in later development stages. Spans in the range 25-30 m were found to give the best balance of construction cost versus reduction of piers.

Fig. 2 illustrates the essential stages and tradeoffs of the development process (all structures prestressed concrete).

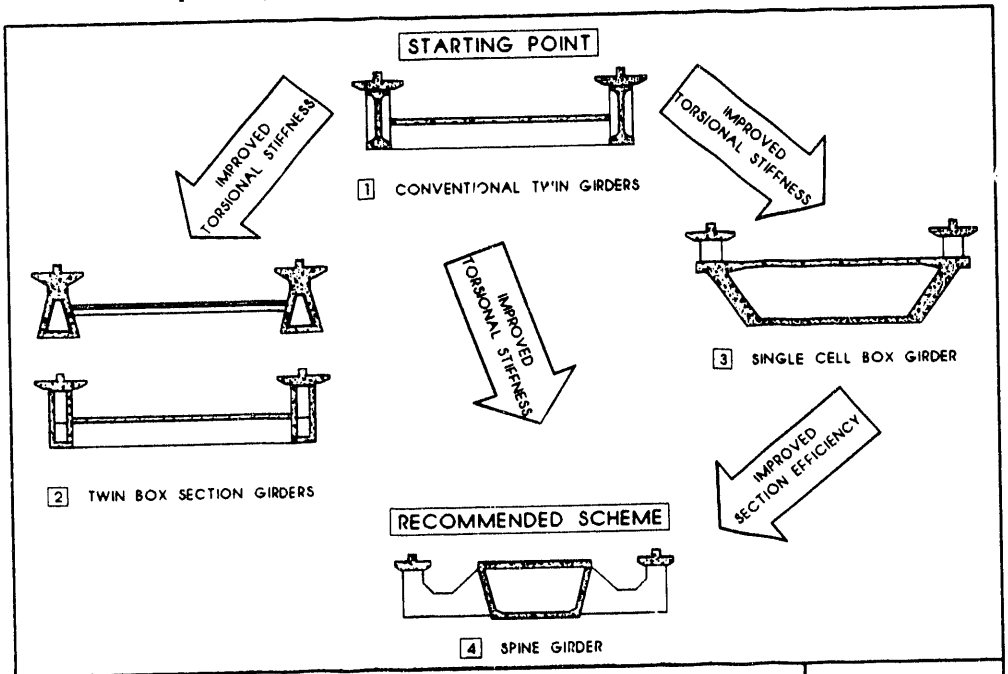

PARSONS BRINCKERHOFF | GUIDEWAY GIRDER DEVELOPMENT | FIGURE 2

Conventional twin I girders (1) were the starting point. Although they have been used on low speed guideways, the girders have poor torsional stiffness which makes them unsuitable for curved track. As well, it is difficult to integrate the emergency evacuation slab into the section.

Twin box section girders (2) were then examined. They provide much improved torsional stiffness. However, the overall costs are still high since the emergency slab, which is a substantial load, is not significantly contributing to the flexural capacity of the guideway.

A single cell box girder (3) is an alternative and still quite conventional from a design sense. Torsional stiffness is higher than for the box beams and the emergency slab does useful work as the top flange of the box section. However with 7.5 m track centers, the wide flanges are more than necessary from a structural viewpoint. This causes costs to be higher than desired.

If the section is developed further to a narrower spine girder (4) with the tracks supported on discrete cantilever outriggers, the box section becomes more efficient. The width to depth ratio reduces and with less concrete the flexural stiffness can be increased and the prestressing quantities reduced. Since the top flange of the spine box can move up relative to the track level, any girder depth increase does not force the structure to be higher. As well the single box girder solution can readily be supported on a single column substructure.

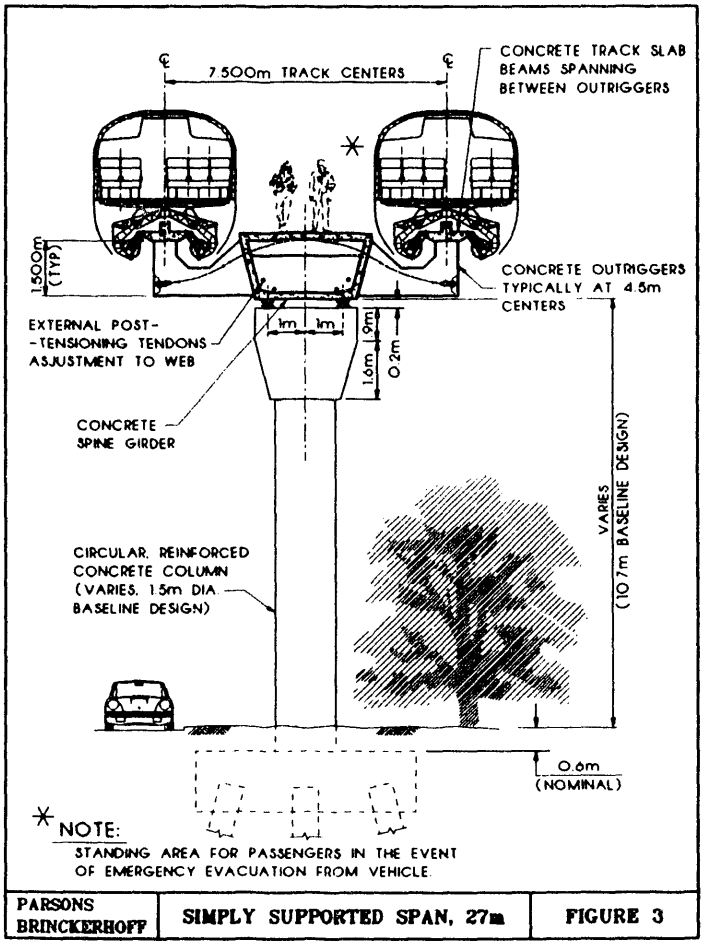

The outcome of the process described briefly above, was that the spine girder structure was developed further and, following a construction analysis, became the recommended 'baseline' guideway design for the SCD (Figure 3).

5. FURTHER FEATURES OF THE CONCEPT

For a 27 m simply supported span, a 1.5 m deep spine girder provides enough strength and rigidity to support two operational tracks. This basic system can be extended to 40-50 m spans by increasing the spine depth and/or using variable depth spans.

As initially developed the longitudinal post tensioning is contained within the spine but external to the concrete (Figure 4). This represents a system which is geared to rapid span erection. In active seismic zones, the option exists to relocate some of the tendons into the webs to improve ductility.

The external tendons provide a means for actively correcting camber errors which may occur in some spans over time. Fig. 4 shows conceptual views of the hardware that would be needed.

For curved sections of track, the single column may be canted (constructed off vertical) to reduce the net effects of centrifugal loads on the foundations. Alternatively 'A' frame piers may be used for curved track or tall piers.

Simply supported span have been adopted to keep the construction process simple. There is no advantage in a Maglev guideway to eliminate expansion joints - in fact more, smaller, joints are preferable to fewer, larger, joints from the electrical distribution viewpoint. However, it is recognized that a continuous guideway would offer some stiffness and material saving advantages. Whether these factors would outweigh the operational and construction benefits of simple spans needs to be examined in more detail. Experience to date suggests that there will be little if any overall advantage with continuous spans.

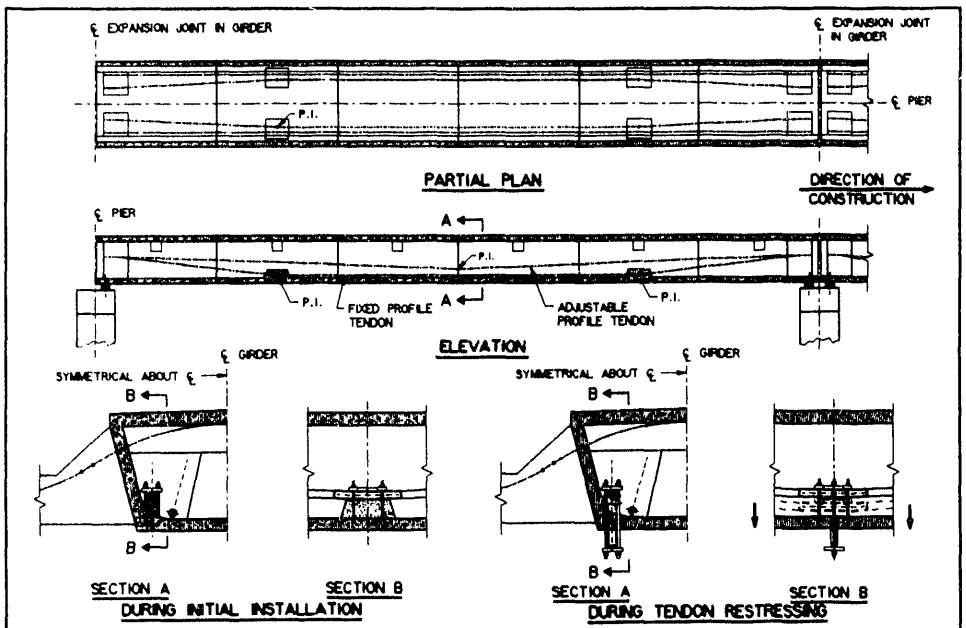

PARSONS BRINCKERHOFF	SPINE GIRDER PRE-STRESSING	FIGURE 4

6. CONSTRUCTION ISSUES

It is possible to construct a spine girder structure using a variety of techniques but it is believed that precast segmental construction offers the better solution for the majority of any Maglev route. In coming to this conclusion, a range of construction options was investigated including:

(a) cast in place construction of whole spans (27 m long)
(b) precast construction of whole spans (27 m long)
(c) precast segmental construction (4.5 m segments)

In method (a), the whole span is cast in place on supporting formwork. Guideway construction is slow unless massive investments are made in formwork and falsework. Construction is more affected by weather and site conditions and the need to transport all labor and materials to (remote) site locations also causes costs to rise.

Method (b) does allow centralized precasting plants to be set up with the associated production efficiencies. However except where the plants are close to the guideway, transport and erection equipment for the heavy girders would be expensive.

Method (c) also allows centralized precasting but the shorter, lighter, segments could be delivered to site and lifted into place with smaller and less expensive equipment. During erection the segments for each span, with one pair of outriggers attached to each segment, are assembled on a temporary steel truss (spanning between piers) and then post-tensioned together to make them self supporting. This

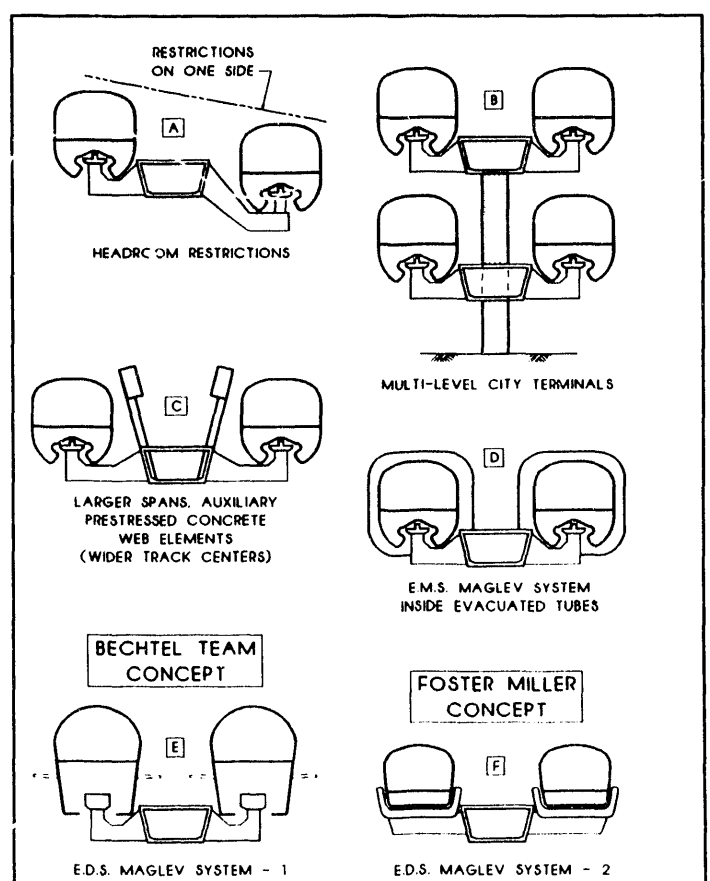

PARSONS BRINCKERHOFF	DEVELOPMENT OF THE CONCEPT	FIGURE 5

method can more readily accommodate span length variations by changing the number of segments used in the span.

Further, the construction of this system can be engineered to minimize/eliminate ground level activities during the erection of the segmental guideway.

Trusses can be made self-launching and segments delivered over the previously erected guideway.

Other gantries, supported off the spine, can be used to erect track slab and rail sections in a follow-up process.

This approach reduces impacts on existing rights-of-way which may either be in heavy use or sensitive to disturbance (forest, wetlands, etc.).

Experience in the highway bridge construction industry supports the selection of method (c) for Maglev guideway construction. For such large scale projects, investments in precasting plant and other equipment can be economically written off over the project.

7. SUMMARY OF THE ADVANTAGES OF THE SPINE GIRDER CONCEPT

a. Based on our construction cost estimates, the spine girder provides the most economical twin track guideway concept. The cost per line-meter is about $5,400, excluding the steel rail track.

b. The durability of the spine concept will be high due to the fact that practically the entire concrete spine box will be compressed by the post-tensioning system. As a result, cracking and fatigue problems are controlled, the service life increased, and maintenance efforts reduced.

c. The spine layout greatly enhances the ability to perform maintenance operations on the guideway slab and magnetic rail. The top of the spine can effectively be used as a service road to provide access to the guideway rails and/or disabled vehicles. It will also serve as an emergency evacuation platform for passengers.

d. The relation between the depth of the box and the height of the column is aesthetically pleasing. The single column reduces size of the guideway 'footprint' at ground level.

e. In case of fire in a vehicle, the spine box will not be subject to intense heat. Effectively, the only elements which will be subject to heat damage are the track slab sections.

f. With the use of segmental spine construction and the potential for further use of precast sections for the track slab beams and the columns, a significant part of the work can be done off-site. This should reduce overall impacts on traffic and the route environment.

g. For a project of this magnitude, segmental construction can result in a saving in time as has been demonstrated on similar scale highway projects.

h. Maglev utility and communication lines can be contained within the spine and accessed through the top or bottom slabs.

8. FURTHER DEVELOPMENT

The spine girder guideway design, as developed for SCD #4, has the potential to be extended to accommodate the special span cases which will inevitably arise during the design of a real route. Such cases include:

- longer spans
- varying vertical alignments between the 2 guideways
- skew spans

Some of the techniques available are illustrated in Fig. 5 (a)-(c).

Beyond this, the guideway could also be used for different Maglev vehicles or other hybrid high speed transport systems Fig. 5 (d)-(f).

9. CONCLUSION

The selection of spine girder satisfies the goals of the project. It provides for both an efficient design and economical construction; combined with an aesthetically pleasing guideway.

10. ACKNOWLEDGEMENTS

The majority of the work described in this paper was carried out as part of the National Maglev Initiative funded by the Federal Railroad Administration.

The authors gratefully acknowledge the assistance of Parsons Brinckerhoff in providing the resources to produce this paper and of Grumman Aerospace who were receptive at all stages to the introduction of new ideas.

Parametric Design and Cost Analysis for an EMS Maglev Guideway

by Brenda Myers Bohlke (1) and Douglas B. Burg (2)

(1) *Parsons Brinckerhoff Quade & Douglas, Inc.*
460 Spring Park Place
Herndon, Virginia 22070

(2) *Parsons Brinckerhoff Quade & Douglas, Inc.*
4200 West Cypress Street
Tampa, Florida 33607

Introduction

The Federal Railroad Administration and the Army Corps of Engineers through the auspices of the National Maglev Initiative, awarded four teams contracts to design new conceptual level maglev systems. Of the four concepts proposed, three are based on a superconducting electrodynamic suspension (EDS) system. The fourth team, led by Grumman Aerospace Corporation, proposed a maglev system based on superconducting electromagnetic suspension and propulsion (SEMS). Parsons Brinckerhoff's principal responsibility as a member of this team was to design an innovative and cost-effective guideway as the backbone of the system. This paper presents the alternative guideway configurations considered and the evaluation and ranking used in the selection of a baseline design.

The SEMS concept imposed some constraints on the guideway design, such as the capability to support a continuous laminated iron rail and provide for tight alignment and realignment; a nominal air gap of 40 mm that affects the total allowable deflection; emergency braking surfaces; and dynamic loading imposed by the high speed vehicle. Other demands for adaptability in construction were evaluated, such as constructing elevated structure within existing right -of- way with minimal impact on the existing facility users facility, and erection efficiency

Guideway Alternatives Screening

Nine twin guideway concepts were identified and evaluated during the initial screening. Each configuration was ranked in each of the following categories: stiffness, structural efficiency on tangent and curved sections, cost, durability, maintainability, and aesthetics. Other considerations were given to operational considerations and emergency egress. Only simply supported spans were considered for the baseline selection. The guideway concepts and their respective designations are listed in Table 1 with the comments from the initial screening.

Five of the original nine configurations passed the initial screening by ranking highest in the criteria categories listed above. These five are shown in Figure 1.

Structural Evaluation

The five guideway configurations that passed the initial screening were analyzed to determine strength and stiffness performance and to determine quantities to estimate the comparative construction costs. The structural analyses included the following:

- Baseline vehicle loading (100 passenger vehicle)
- Vertical deflection criteria not to exceed $\pm$ 25 mm (1 in)
- Loading combinations to account for dead load, live loads (single vehicle and passing vehicles), wind loads, and seismic zone 2
- Parametric analyses of varying span lengths
- Pile and spread footing foundation support
- Varying layout of column supports
- Varying column heights

The baseline configuration for all alternatives was defined as having a span length of 27 m (100 ft), dual guideway, and vertical clearance of 10.7 m (35 ft) to the base of the superstructure. Based on the structural analyses, the spine girder (S4) affords the best performance in terms of strength and stiffness.

Use of a central spine with secondary track beams requires only one load-carrying member, compared with two main members where each members

supports one track. A single, deeper girder is more efficient than two shallow girders. The S4 concept can accommodate a deeper girder without increasing the track height by using the space between the tracks. None of the other concepts have this capability.

Table 1. Structure types and evaluation comments

Structure Type	Ref.	Evaluation Comments
Twin Triangular Concrete Box Beams	S1	Passed initial screening
Twin rectangular concrete box beams	S2	Passed initial screening
Single concrete box girder	S3	Passed initial screening
Single concrete spine girder	S4	Passed initial screening
Stiffened concrete slab	S5	Passed initial screening
Twin concrete I girder	S6	Low torsion strength; low stiffness; poor aesthetics
Twin trapezoidal concrete box beams	S7	Wide top flange creates support of track slab awkward
Twin steel box girders	S8	More expensive to construct; more intensive maintenance
Multiple steel plate girders	S9	Low torsional strength; low stiffness; more expensive to construct; higher maintenance costs

The spine girder also provides more advantages over the others including: construction flexibility, alignment and realignment after construction, tolerances, low torsion and adequate strength, a central platform to be used for maintenance access or emergency egress, and adaptability for switching.

Cost Comparison

To assist in the selection of a baseline guideway structure, cost estimates[1] were prepared for each of the five twin-track concepts identified for a range of span lengths (18, 27, 36, 45 and 49.5 meters). An example of the breakdown of the quantities and format used in the cost estimate is shown in Table 2. For clarity, the costs were divided into costs associated with the superstructure, and the substructure, as outlined below.

Superstructure: Structural steel; concrete, reinforcing steel, pre-stressing, bearings and seismic isolation systems.

Substructure: Column concrete or steel, reinforcement, earthworks; footings and piles

So as not to bias one element, a 10% mobilization and demobilization costs was assigned to each set. Other assumptions are documented at the top of the page. No allowance was made for contingencies or for site-specific items such as clearing, fencing, access roads, traffic control and the like, as these items are common to all concepts and do not affect the cost comparisons.

For the baseline configuration, the cost of construction of the concrete spine box girder was estimated to be $7.99 M/km ($12.9 M/mile) including the cost of the iron rail. The estimate of the capital costs for the total system was $12.4 M/km ($20 M/mile). Figure 2 shows the results of the parametric analysis of the guideway costs versus span length for each of the five structural types. The concrete box spine girder (S4) consistently has the lowest costs and is less sensitive to changes in span length that may be required. A composite of the cost curves for the substructure costs, superstructure costs and total costs for the baseline spine box girder is shown in Figure 3.

As a result of these comparison of the structural and cost analyses, the concrete box spine girder (S4) was selected as the baseline for the superconducting electromagnetic suspension Maglev system. Figure 4 is an isometric showing the box girder outrigger-layout and post-tensioning cables. An artist's rendering of the spine girder guideway system, illustrating the concept of the track slab supported on the outriggers, is shown in Figure 5. Details of the design are presented in a companion paper entitled "Innovative spine girder guideway design for a Superconducting Electromagnetic Suspension Maglev System".

[1]These estimates were consistent with the format for Maglev Cost Estimation: Capital Cost Elements prepared by Volpe National Transportation System Center.

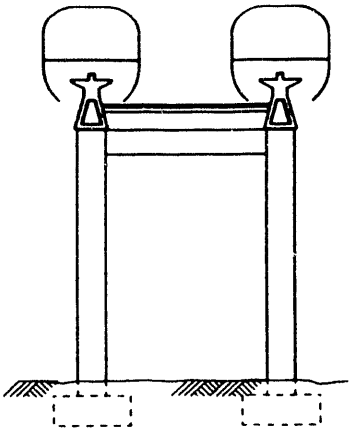

ALTERNATE S1
TRIANGULAR CONCRETE BOX BEAMS

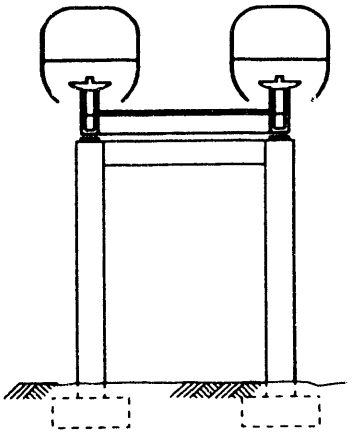

ALTERNATE S2
RECTANGULAR CONCRETE BOX BEAMS

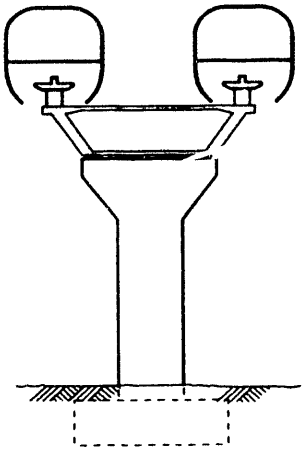

ALTERNATE S3
SINGLE CONCRETE BOX GIRDER

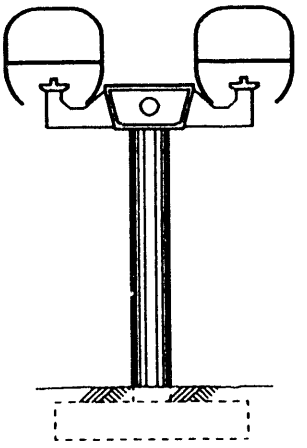

ALTERNATE S4
SINGLE CONCRETE SPINE GIRDER

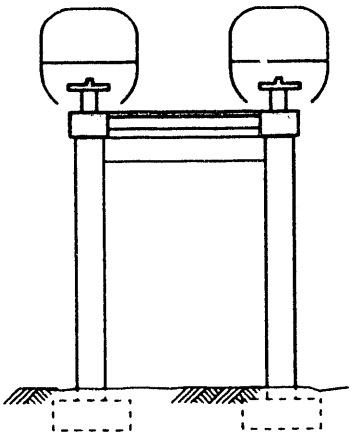

ALTERNATE S5
STIFFENED CONCRETE SLAB

PARSONS BRINCKERHOFF	STRUCTURAL ALTERNATES FOR COST COMPARISON	FIGURE 1

MAR 93 13.57.10

CADD:[MAGLEVGG.ARGONPAP.FG]CSTALT01.FGB;1 13-MAR-93-09.0·

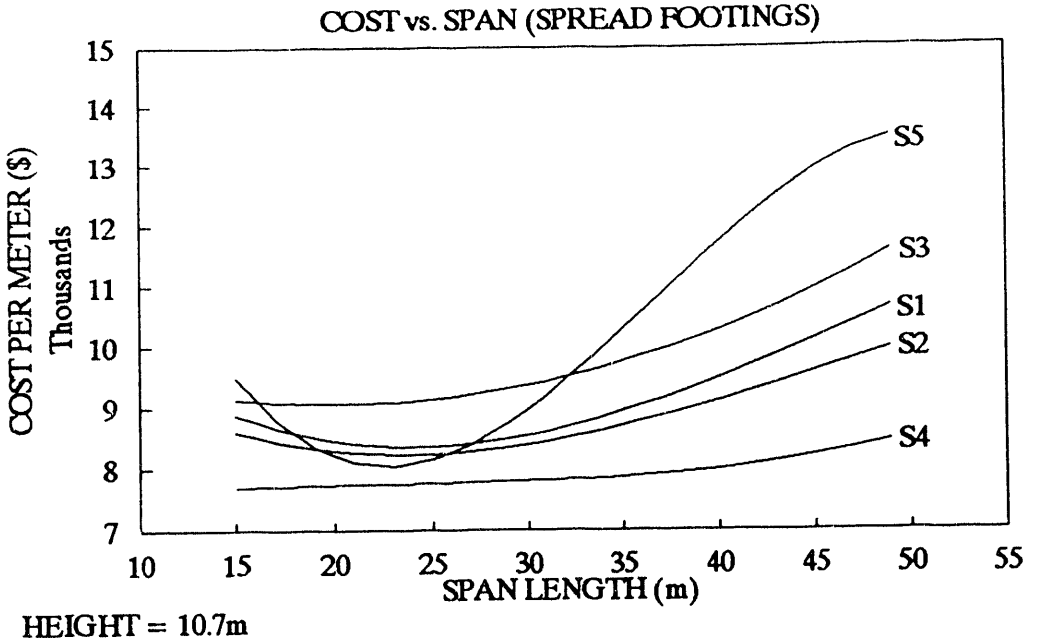

Figure 2. Results of the parametric cost analysis for the guideway

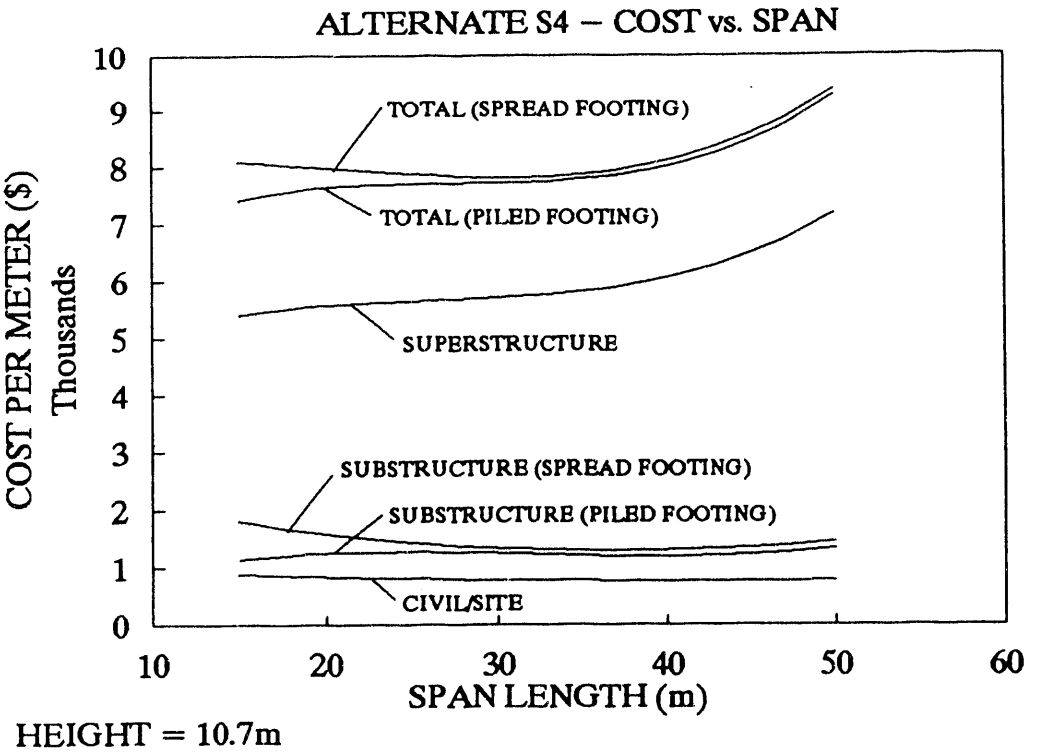

Figure 3. Spine box girder component and total costs as a function of span length

S4 - Spine Beam - Piled Foundation - Dual Guideway				
Span				
Spine Beam Length	:	26.3 Meters		
Type	:	Simply Supported		
Cent. to Cent. Column	:	27 Meters		
Superstructure				
Depth	:	1.8 Meters		
X-Sectional Area	:	3.013 Meters^2		
Ground Clearance	:	10.7 Meters		
Column				
Height	:	11.3 Meters		
Diameter	:	1.524 Meters		
Driven Pile				
Length	:	19 Meters		
Quantity	:	4		
Total Preliminary Cost		$7,833/M		
Description	**Unit**	**Quantity (Per KM)**	**Rate ($)**	**Cost (Per KM)**
Superstructure				
Structural Steel	kg	47,477	1.75	$83,084
Precast Concrete	m^3	3,013.3	530.00	1,597,035
Cast-in-Place Concrete	m^3	150.7	625.00	94,165
Reinforcement	kg	270,746	1.65	446,730
Prestressing Strands	kg	104,520	4.75	496,470
Rail	kg	1,173,732	2.10	2,464,837
Bearings & Seismic Isolation System	Each	148.1	750.00	111,111
Mobilization/Demobilization	%	8		423,475
Subtotal Superstructure				$5,716,907
Substructure				
Column Concrete (Precast)	m^3	-	400.00	$0
Column Concrete (Cast-in-Place)	m^3	935.4	400.00	374,176
Column Reinforcement	kg	110,148	1.32	145,395
Footing Excavation (Earth)	m^3	523.7	5.00	2,618
Footing Excavation (Rock)	m^3	-	25.00	0
Footing Concrete	m^3	317.0	260.00	82,413
Footing Reinforcement	kg	49,765	1.32	65,690
Driven Piles	m	2,814.8	200.00	562,963
Mobilization/Demobilization	%	8		98,660
Subtotal Substructure				$1,331,916
Civil/Site (Indicative - Specific Site Costs Will Vary)				
Clearing & Grubbing	m^2	3,520.0	0.90	$3,168
Earth Excavation, Cut & Fill, Haul	m^3	8,430.0	9.57	80,702
Rock Excavation, Removal & Haul	m^3	920.0	119.01	109,489
Surveying	m.d.	37	300.00	11,187
Column Protection	Each	37.0	2,460.00	91,111
Testing & Calibration	m.d.	6	2,200.00	13,673
Vegetation Control	m	1,000.0	6.50	6,500
Mobilization/Demobilization	%	8		25,266
Maintenance of Traffic	%	6		$443,395
Subtotal Civil/Site				$784,492
TOTAL				$7,833,315

Table 2 Guideway cost break down for spine beam with pile foundation

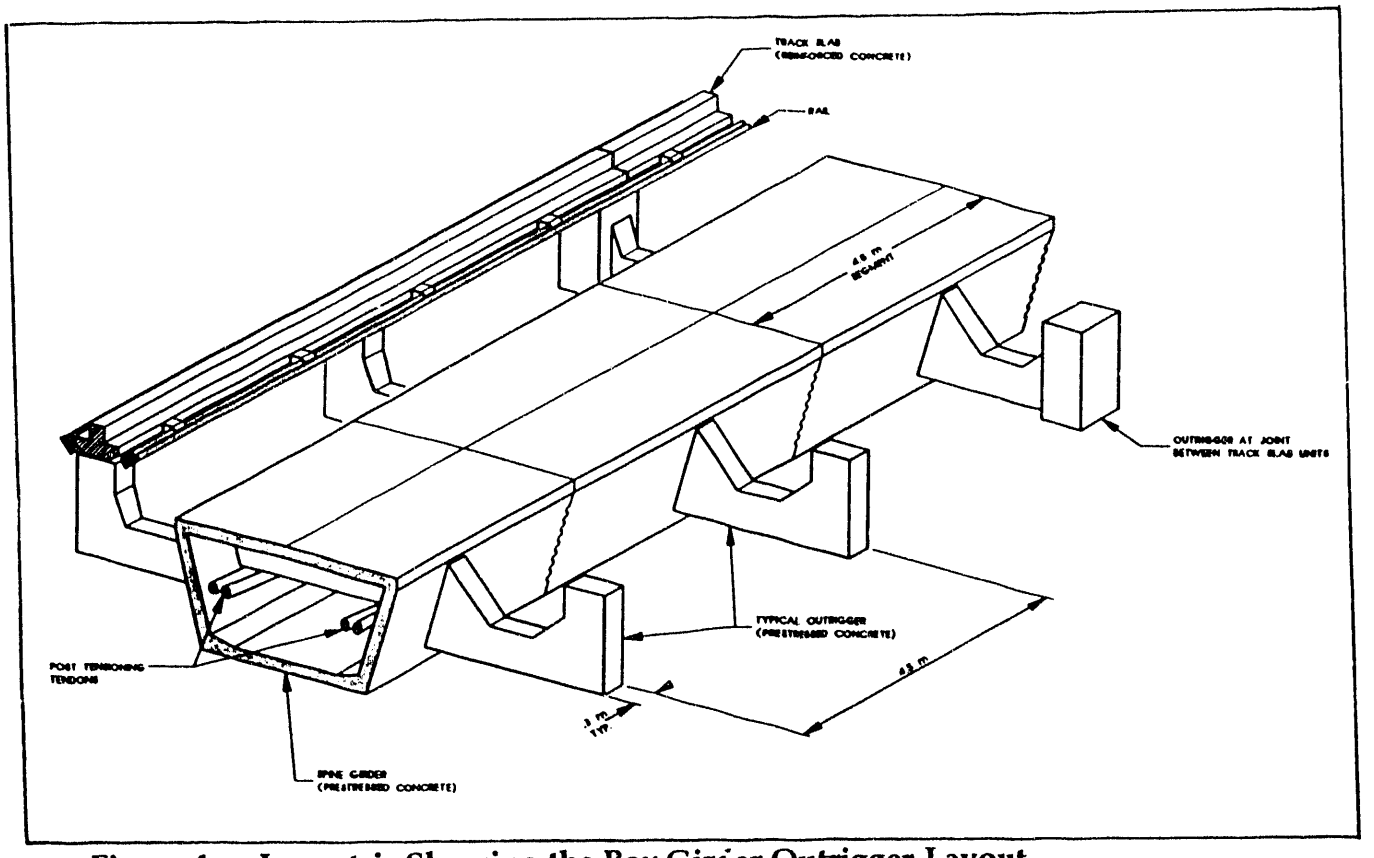

Figure 4. **Isometric Showing the Box Girder Outrigger-Layout and Post-tensioning Cables**

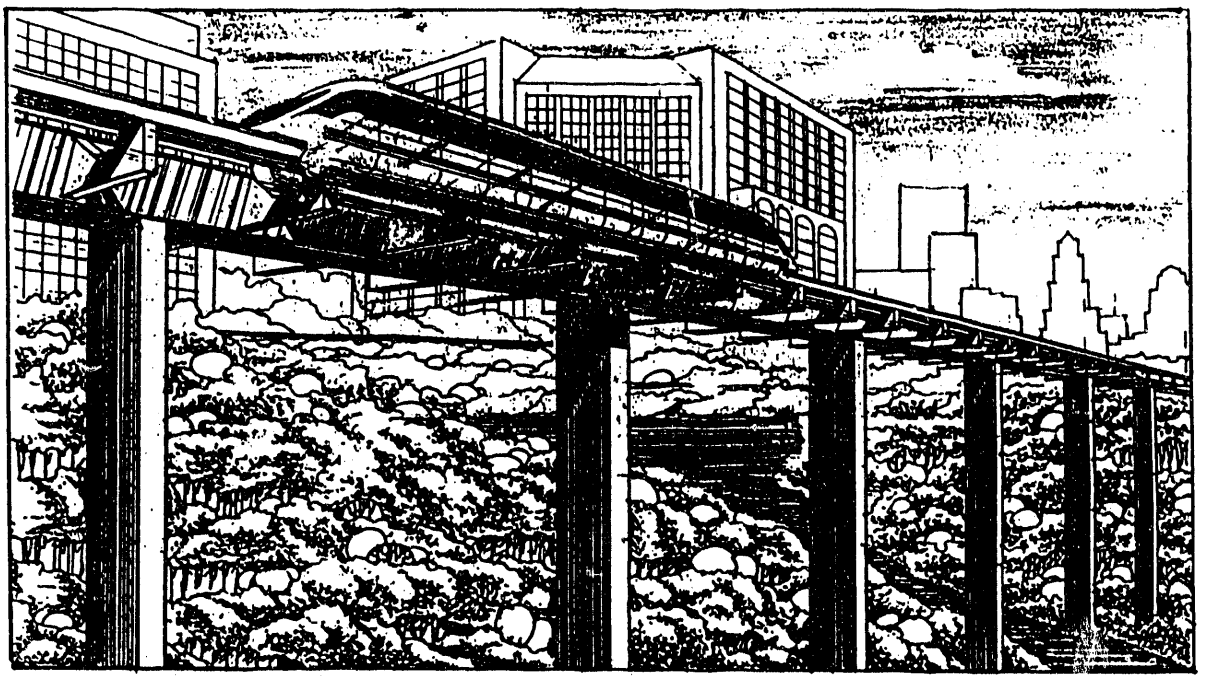

Figure 5. **An artist rendering showing relationship of track slab and outriggers to the central concrete box girder guideway.**

Guideway and Infrastructure in JR Maglev

Katuya OKADA
General Manager of Civil Engineering Department,
Maglev System Development Division,
Railway Technical Research Institute

Akira TAKANO
Deputy Director, Planning Department
Japan Railway Construction Public Corporation

Mikio YAMAZAKI
Senior Engineer, Linear Express Development Division,
Central Japan Railway Company

<Introduction>

We are now newly constructing a test line in Yamanashi Prefecture for ascertaining the practical use of the superconducting magnetically levitated train, which is expected to be an epoch-making, ultra-highspeed mass-transportation system in the 21st century.

The fundamental research and development for this JR-type Maglev were started by Japan National Railways (JNR) at the beginning of 1960's. And they have fairly advanced. For example, in 1979, an unmanned vehicle attained a maximum speed of 517km/h on Miyazaki Test Line. And a manned vehicle attained a speed of 400km/h in 1987.

With the division and privatization of JNR in 1987, Railway Technical Research Institute (RTRI) took over JNR's business and continues running tests of vehicles on Miyazaki Test Line. However, Miyazaki Test Line is not suitable for testing the practical use of JR Maglev, because it is only 7km in length with a single track and it includes no tunnel section. So a new test line which has an overall length of some 40km or so has been needed.

In 1990, under guidance of Minister of Transport and with a state subsidy, RTRI, Central Japan Railway Company and Japan Railway Construction Public Corporation formed a consortium and started the construction of the new test line. The Yamanashi Test Line has a length of 42.8km including double track sections and about 35km of tunnel sections. On the new test line, we intend to confirm the stable running at 550km/h and others to establish the actual service at 500km/h.

In this JR Maglev, the guideway and the infrastructure have to support reliably and guide safely vehicles which run at ultra-high speed, and have to give passengers a comfortable riding quality. We researched and developed the design of its structure, the precision of coil arrangement and the method of its construction with all our might. We obtained good results from our rich experiences in the construction and maintenance of Shinkansen.

This paper gives an introduction to these technical points.

1.Role and Structure of Guideway

(1)Role of Guideway

The guideway of JR Maglev consists of Propulsion Coils, Levitation and Guidance Coils and Wheel Paths(for support and for guidance). The section of guideway is U-shape. Three types of guideway are shown in Fig.1.

Propulsion Coils and Super-Conducting Magnet(SCM) on board compose a Linear Synchronous Motor(LSM), which propels the vehicle by its electro-magnetic power. So the precise arrangement of Propulsion Coils is very important in order to maintain a harmonious propulsion power.

Levitation and Guidance Coils levitate and guide the vehicle owing to the attraction and repulsion acting between the induced current on the coils and magnetic force of SCM on board. So the precision of their alignment has direct influence on the lateral and vertical vibrations of vehicle, that is riding quality.

(2)Structure and Size of Guideway (Fig.2)

The guideway has a width of 3.3m and a height of about 1.4m, in accordance with the size of vehicle.

The maximum speed(550km/h), costs of construction and operation, riding quality - all things considered, we set the standard of Yamanashi Test Line as follows;

*the maximum radius of curvature	8,000m
*the steepest slope	40‰
*the maximum cant	10deg.
*the distance between the centers of tracks	more than 5.8m

The steeper slope contributes to shortening the length of tunnel sections and to reducing the cost of construction,

but it increases the propulsion power and energy consumption to operate vehicles. So there is a limit to its contribution. The minimum radius of curvature was determined in order to restrict the lateral acceleration acting on passengers below an allowable value in a run at a speed of 500km/h on a curve with cant 10degrees.

2.Types of Guideway

We have three types of guideway. They are classified in terms of structure and construction of the side-wall on which coils are arranged.

(1)Beam-type Guideway

Its basic concept is as follows;

- prestressed concrete beams are made at a beam product yard.
- coils are attached on the side surface of beam at a coil attaching yard.
- and beams with coils are carried up to the site on beam-carrier and are fixed to the floor slab by a beam-setter.
- beam's standard length (=guideway unit) of 12.6m is determined in consideration of the coil size and the facility of construction.

(2)Panel-type Guideway

- concrete panels (a littleprestressed to prevent cracks) are made at a panel product yard.
- coils are attached on the surface of panel at a coil attaching yard.
- and panels with coils are carried up to the site and fixed to the surface of concrete side-wall built beforehand (using a panel carrier-setter).
- panel has a standard length of 12.6m, the same as the beam.

(3)Direct-Attaching-type Guideway

- concrete side-walls are built on the site.
- coils are attached directly on the surface of side-wall.

Each type has its characteristics concerning the assurance of precision, the facility of work, cost of construction and facility of maintenance. We arranged them properly in Yamanashi New Test Line in order to adapt them to the conditions of site and infrastructure.

3.Assurance of Precise Setting of Guideway

(1)In the Direction of Track

Propulsion coils have to be set precisely at intervals of 1.8m. An imprecise setting causes a phase lag between coil pitch and SCM pitch on board, which decreases the propulsion power of linear-synchronous motor.

So coils and guideway units are set according to the Real Distance which is obtained by correcting the errors in plans due to slope of track, height of site above sea level and distortion in projected map.

(2)In the Lateral Direction

Levitation and Guidance Coils have to be set precisely on both side-walls of guideway maintaining a fixed distance(3.3m) and a fixed level. An imprecise setting causes vehicle vibrations (lateral and vertical direction), namely uncomfortable riding quality for passengers.

At ultra-highspeed of 500km/h, a track irregularity (especially of long wave) influences more greatly the riding quality than in the case of conventional railway. In Yamanashi Test Line, we determined the precision of setting in order to maintain the riding quality as good as that of Tokaido Shinkansen. The allowable amplitude of irregularity is as small as less than 1cm in the vertical and lateral waves shorter than 150m.

(3)How to Assure the Precision

In order to get a high-precision guideway, we performed a high-precision skeleton-survey before the construction of infrastructure. After the construction, we shall repeat the high-precision survey on the infrastructure to reset the planned center line on the floor slab. And we set the basic points on the track center of floor slab at intervals of 12.6m (equal to guideway unit's length).

Thus we can build side-walls or fix beams and panels very precisely referring to these basic points.

4.Characteristics in Plan and Design of Infrastructure

In plan and design of infrastructure, we have to consider sufficiently JR Maglev's characteristics (its ultra-highspeed, magnetic drag, etc.), unlike the case of conventional railway.

(1)Allowable Deflection of Bridge

We determined the limit of bridge's vertical deflection by vehicle's load in order to maintain good riding quality.

After a dynamic response analysis of vehicle models operated on a vertically deflected curve of bridge, we obtained the calculated vertical acceleration acting on the passenger seat. The limit was determined such that the vertical acceleration might be less than the allowable value. It is about half the value in the case of Shinkansen, reflecting the difference of speed.

(2)Allowable Unequal Displacement of Structures

A displaced block or a bent-angle of structure causes not only an uncomfortable riding but also threaten the safety of running, especially in the case of a big displacement.

In order to restrain the acceleration of a vehicle and to maintain the clearance between guideway and vehicle, we determined its limit. Especially, the limit for bent-angle is fairly less than in the case of Shinkansen.

(3)Use of Low Magnetic Steel

In a guideway or infrastructure, normal steel placed near SCM on board not only causes the levitation force to drop due to attraction, but also causes a magnetic drag to be generated due to eddy current or loop current.

In the construction of reinforced concrete slabs of guideway and reinforced concrete bridges or tunnels, because the magnetic drag fairly decreases inversely to the distance from SCM, we intend to use a low- magnetic steel (iron bar) in the region 1.5m away from SCM's element coil (shown in Fig.3).

(4)Tunnel Cross Section

The tunnel cross section is shown in Fig.4. It is about 20% larger than that of Shinkansen. We designed it in consideration of the structural gauge, the space for maintenance and several things as follows;

- *decrease of the pressure fluctuation which is caused by ultra-highspeed running at 500km/h in tunnel (to maintain the strength and air-tightness of vehicle)
- *the smaller the tunnel cross section and in consequence the larger the aerodynamic drag in the tunnel, the more expensive becomes the operation
- *decrease of the micro-pressure waves radiated from the tunnel mouth when a train advances into the tunnel at a speed of 500km/h.
- *cost of tunnel construction

We studied all these things and determined the area ratio of vehicle and tunnel section as 0.12 (the effective area of interior is 74m^2)

(5)Electrical Equipment in Tunnel

The ultra-highspeed running in tunnel generates a very big wind load and a large pressure fluctuation.

So we fix the electric lamps and cables in dents of concrete lining, and prevent lids of cable-duct from floating up by negative pressure.

5.Turnout

As regards the turnout, a high-speed turnout for intermediate station and a lower-speed turnout for terminal or depot are needed.

For high-speed turnout, we developed a U-shaped traverse type which had already been tested in Miyazaki Test Line, as shown in Fig.5. We set bogies under the movable U-shaped beams (7 units, about 90m long) to move guideway and turnout track by hydraulic pressure jacks or an electric motor.

The radius of curvature of 800m and the transition curve length of about 19m are determined to hold the acceleration below the allowable value at a 70km/h running over curves.

6.Machines for Carrying and Setting Beams and Panels

A speedup of working is very important for the construction of a commercial line hundreds kilometers long. We developed the machines for speedy carrying and setting of beams and panels attached with coils.

In the case of Beam-type Guideway, the beam carrier carries two beams with coils at the same time (one beam with coils weighs about 20tons) up to the work site from the yard, and then the beam-setter(shown in Fig.6) sets them on the floor slab with highprecision.

In the case of Panel-type Guideway, we use a machine shown in Fig.7, which carries two panels at the same time (one panel with coils weighs about 14tons) and sets them on the side-wall with highprecision.

<Conclusions>

We described briefly the features in design and construction of the guideway and infrastructure of JR Maglev.

They have been built up on the broad technical base of railway construction and maintenance in Japan, and they'll become more refined through the construction of Yamanashi Test Line and the test runs on it.

We hope that the excellence of JR Maglev as a highspeed, mass transportation system will be proved objectively through the tests in Yamanashi and a big stride will be taken toward its commercialization.

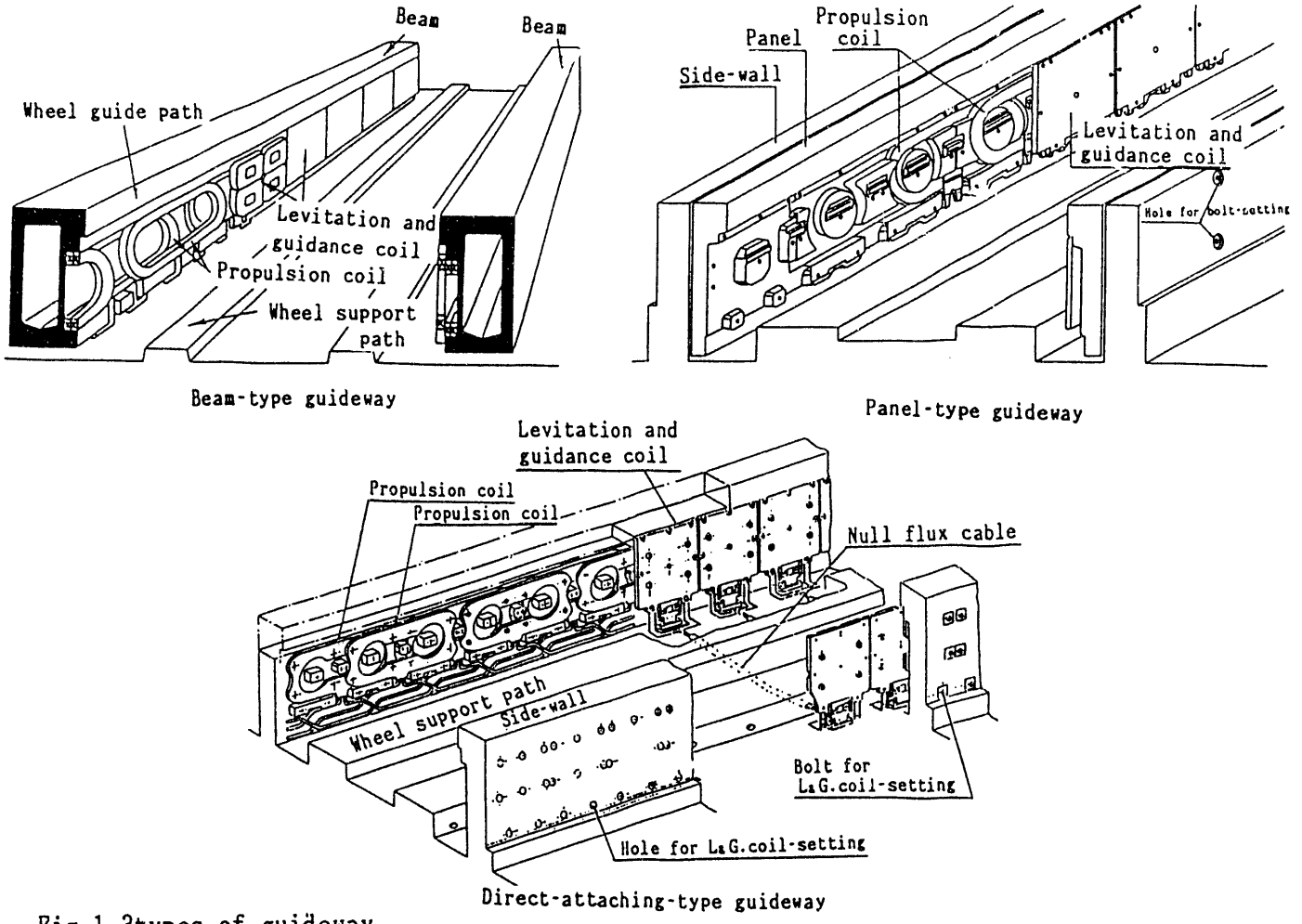

Fig.1 3types of guideway

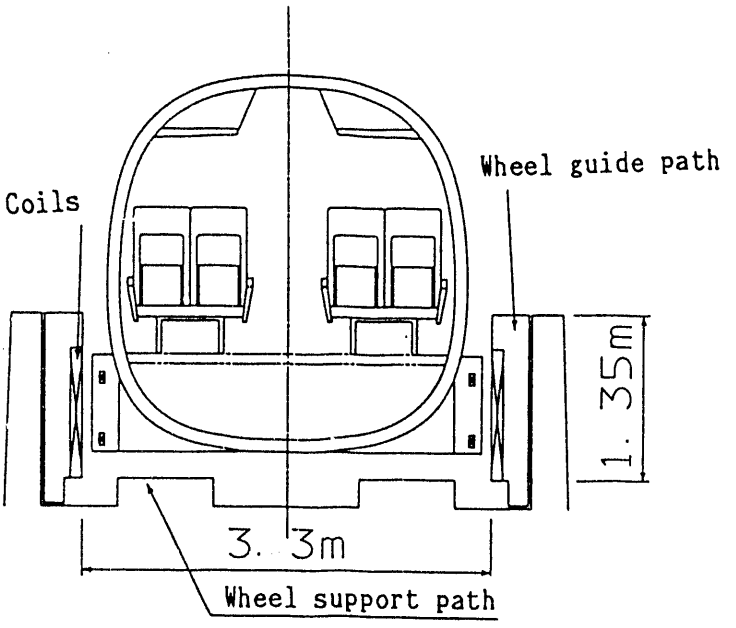

Fig.2 Size of guideway

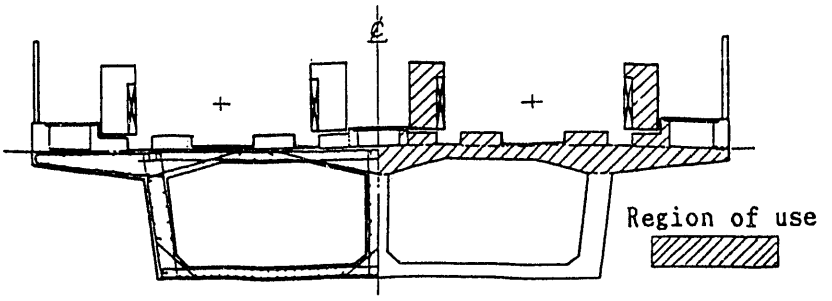

Fig.3 Region of use of low magnetic steel

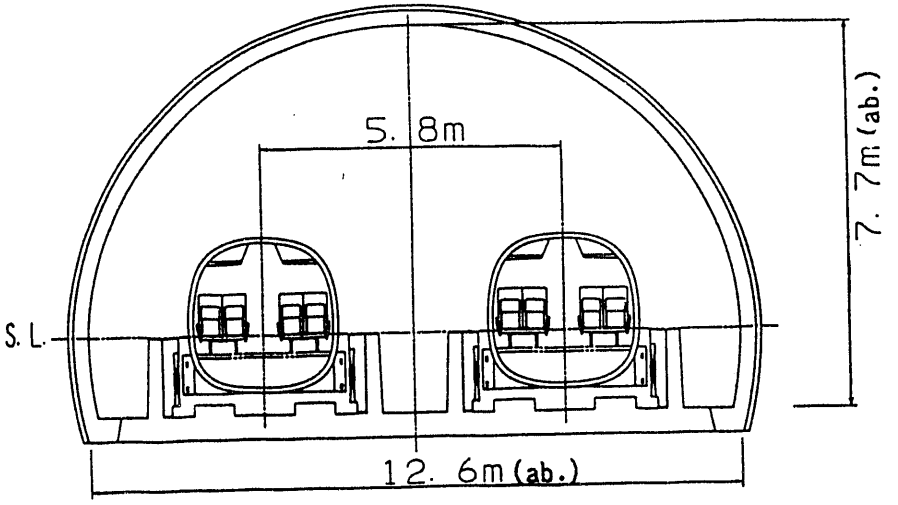

Fig.4 Tunnel cross section

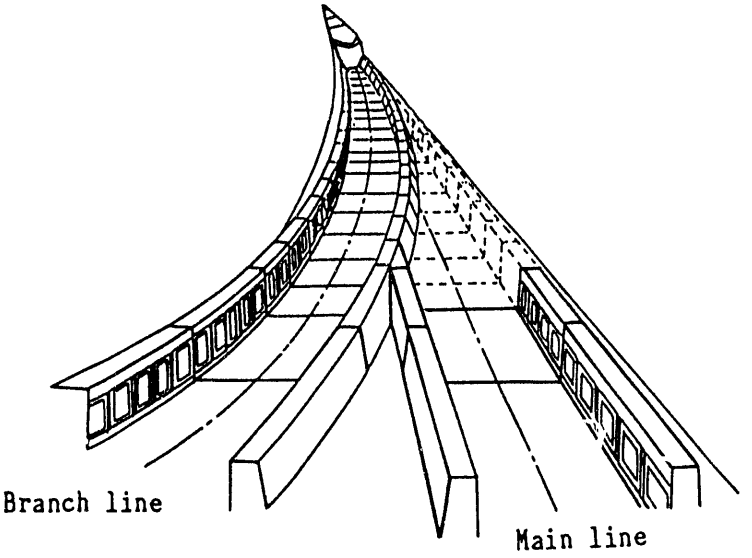

Fig. 5 Turnout of a traverse type

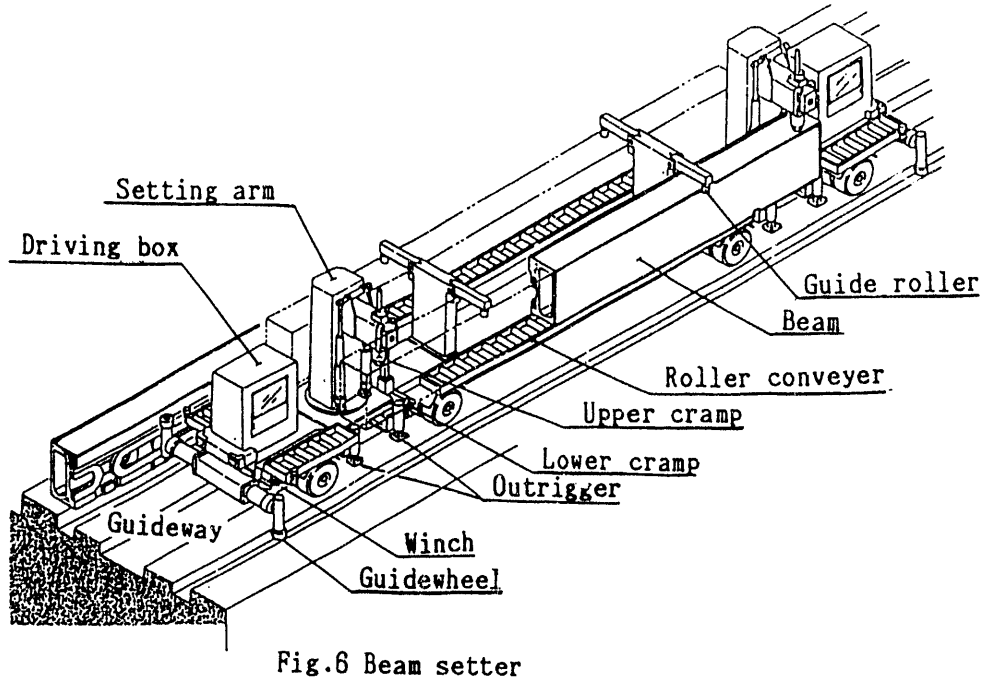

Fig.6 Beam setter

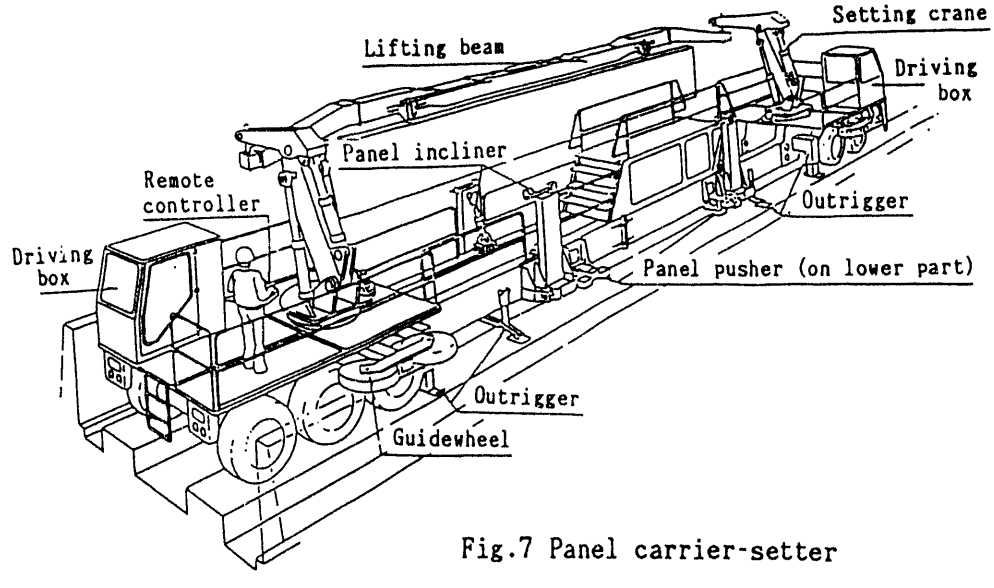

Fig.7 Panel carrier-setter

Reduction of Guideway Residual Vibration through Strategic Vehicle Pad Spacing Arrangements

R. Scott Phelan
J. Muller International
San Diego, California 92123 USA

Abstract - **This paper focuses on the dynamic analysis of guideway beam behavior during high speed vertical maglev vehicle loading. In addition to peak dynamic *positive* (i.e. downward) beam deflection, the dynamic analyses of this paper focus on peak *negative* (i.e. upward), and *residual* (i.e. free) beam vibration response. Equations are presented which predict the exact speeds a vehicle—having a particular loading pad configuration—can travel over a given beam and yet produce no residual vibration in the beam! These *convergent* vehicle velocities are shown to be determined by both beam properties and vehicle loading configurations. The two beam properties which determine convergent velocities are fundamental frequency f_1, and span length L. For vehicles having a fully distributed loading configuration, the vehicle length L_v determines additional convergent velocities. Similarly, for vehicles having discretely spaced loading pads, additional convergent velocities are determined based on a) the number of pads n_p, b) loading pad length L_p, and c) the spacing between loading pad centroids S_p (see Figure 6). Only the force of the traveling vehicle (i.e. not the mass), on a simply-supported, undamped, straight guideway beam is considered.**

I. INTRODUCTION

When a maglev vehicle travels over a supporting guideway beam element, the dynamic beam response normally results in three maximum deflections critical to guideway structural design. The three are maximum downward, upward, and residual (i.e. free) beam deflections. Concentrated vehicle loads relatively distant from one another generally produce high positive and negative beam deflections—which are not desirable—on elevated guideway spans of 20 m or more. In contrast, more closely spaced (i.e. distributed) vehicle loads result in less severe positive and negative beam deflections. Beam deflections during residual vibration are not directly influenced by the extent of vehicle load distribution. This paper shows, however, that design for complete cancellation of beam residual vibration at specific vehicle speeds is possible using strategic vehicle loading pad spacing arrangements

Since non-magnetic concrete reinforcing material is expected to be required in superconducting maglev guideways [1], it is desirable to minimize negative and residual beam vibrations in order to reduce the need for this type of reinforcement. In addition to resulting reduced material costs, reduction of residual beam vibrations decreases guideway fatigue loadings, which leads to longer predicted guideway lifespan.

Manuscript received March 15, 1993. This work was supported in part by the U.S. Department of Transportation under contract DTFR53-91-C-00076. Additional support from the Bechtel Corporation, Advanced Civil Division is gratefully acknowledged.

II. GOVERNING EQUATIONS

A. Forced Beam Response under a Traveling Load

Transverse forced deflection response for an undamped beam having uniform mass and stiffness when subjected to a traveling point load is given by the following equation [2].

$$u(x,t)=\frac{2P}{mL}\sum_{n=1}^{\infty}\frac{\sin\frac{n\pi x}{L}}{\left(\frac{n\pi v}{L}\right)^2-\omega_n^2}\left\{\frac{n\pi v}{L\omega_n}\sin\omega_n t-\sin\frac{n\pi v t}{L}\right\}$$

$$n=1,2,3,\ldots,\infty;\ 0\le t\le L/v \quad (1)$$

where

- $u(x,t)$: transverse displacement at a distance x along a beam of length L and uniform unit mass m at time t (downward deflection is positive)
- P : force of the load
- v : velocity of the traveling load
- ω_n : nth mode beam angular frequency (rad/sec)

Equation (1) considers all beam vibration modes. It is valid when $n\pi v/L \neq \omega_n$ and for the time period that the single concentrated load is on the beam, i.e. when $0 \le t \le L/v$. The following notation is helpful in representing beam transverse response.

$$\Delta=\frac{\pi x}{L};\quad \partial=\frac{2P}{mL};\quad \beta=\frac{\pi v}{L};\quad \mu_n=(n\beta)^2-\omega_n^2 \quad (2)$$

$$\begin{bmatrix}u_n(t)\\ \dot{u}_n(t)\\ \ddot{u}_n(t)\end{bmatrix}=\left(\frac{\partial}{\mu_n}\right)n\beta\begin{bmatrix}\omega_n^{-1}\sin\omega_n t-(n\beta)^{-1}\sin n\beta t\\ \cos\omega_n t-\cos n\beta t\\ -\omega_n\sin\omega_n t+n\beta\sin n\beta t\end{bmatrix} \quad (3)$$

Using the notation in (2) and (3), the transverse deflection $u(x,t)$, velocity $\dot{u}(x,t)$, and acceleration $\ddot{u}(x,t)$, of the beam at time t and distance x along the beam due to a single point load during forced vibration can be represented as shown in the following equation.

$$\boxed{\begin{bmatrix}u(x,t)\\ \dot{u}(x,t)\\ \ddot{u}(x,t)\end{bmatrix}=\sum_{n=1}^{\infty}\begin{bmatrix}u_n(t)\\ \dot{u}_n(t)\\ \ddot{u}_n(t)\end{bmatrix}\sin n\Delta} \quad (4)$$

B. Residual (Free) Beam Response due to a Traveling Load

Because linearly elastic beam behavior is assumed, a distributed load can be modeled as a series of closely spaced point loads using superposition. To completely model a distributed load, the beam free vibration response is needed. Free (i.e. residual) vibration initial conditions due to a single point load traveling across the beam are equal to the beam deflection and velocity at the time the load leaves the

guideway, (i.e. when $t = L/v$). The following notation is used to describe these free vibration initial conditions.

$$|u_n| = u_n(L/v); \quad |\dot{u}_n| = \dot{u}_n(L/v) \tag{5}$$

Time during beam residual vibration response is denoted by T, where $T = t - L/v$. By definition, T is zero when $t = L/v$. Also, by definition, residual vibration equations for a single given point load are valid only when T is greater than zero for the given point load.

Beam residual vibration response equations are presented without derivation. The equations are based on a modal beam analysis. Equation (6) indicates the free (or residual) transverse deflection $u(x,T)$, velocity $\dot{u}(x,T)$, and acceleration $\ddot{u}(x,T)$, of the guideway beam at time T and distance x along the beam for an undamped, simply-supported beam having uniform mass and stiffness [1].

$$\begin{bmatrix} u(x,T) \\ \dot{u}(x,T) \\ \ddot{u}(x,T) \end{bmatrix} = \sum_{n=1}^{\infty} \begin{bmatrix} 1 & 0 & 0 \\ 0 & \omega_n & 0 \\ 0 & 0 & \omega_n^2 \end{bmatrix} \begin{bmatrix} C_n & S_n \\ -S_n & C_n \\ -C_n & -S_n \end{bmatrix} \begin{bmatrix} |u_n| \\ \omega_n^{-1}|\dot{u}_n| \end{bmatrix} \sin n\Delta \tag{6}$$

where $C_n = \cos \omega_n T$; $S_n = \sin \omega_n T$

III. CONCENTRATED VS. DISTRIBUTED LOADINGS

A. Two-Point Concentrated Vehicle Load

Figure 1 represents a 30 m maglev vehicle traveling at 125 m/s. The mass of the vehicle is 2.0 tonne/m and is transferred to the guideway by two 294.2 kN concentrated loads located at each end of the vehicle. For this example, the vehicle travels over a beam 25 m in length with a fundamental frequency, f_1 of 6.67 Hz, and a vertical bending stiffness, EI, of 1.9952×10^{10} N•m^2.

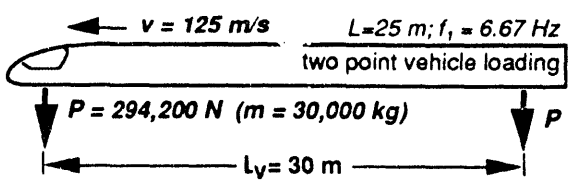

Figure 1. Two Point Vehicle Loading

Figure 2 shows the dynamic response of the beam midspan when it is subjected to the moving two-point concentrated vehicle load shown in Figure 1.

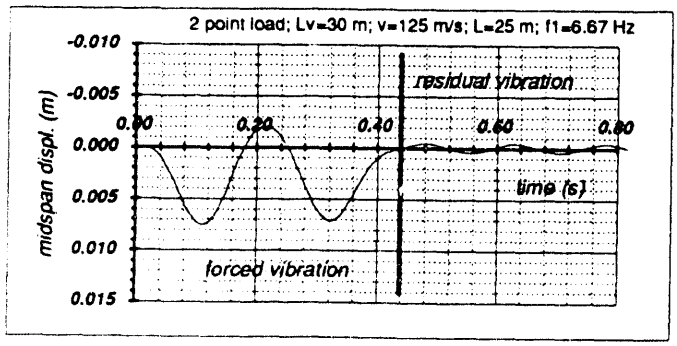

Figure 2. Beam Response (Two Point Load, v=125m/s)

The beam has a peak positive (i.e. downward) midspan deflection of 7.5 mm at $t = 0.11$ s during forced vibration response. The peak negative (i.e. upward) deflection during forced response occurs at $t = 0.22$ s, and is equal to 2.1 mm. In Figure 2, the bold vertical line shown at $t = 0.44$ s represents the time when the trailing edge of the vehicle exits the guideway beam. At this time, the beam shifts from forced to residual vibration response. The maximum residual deflection of the beam in this example is 0.44 mm.

The positive dynamic amplification factor, DAF, is the ratio of the maximum positive beam deflection under dynamic loading to the maximum static beam deflection under a fully distributed load, as indicated in (7).

$$DAF = \frac{\Delta_{dyn.pos}}{\Delta_{stat.pos}} \tag{7}$$

where

$\Delta_{dyn.pos}$: maximum positive (i.e. upward) dynamic beam deflection

$\Delta_{stat.pos}$: maximum static beam deflection under a fully distributed load

For the 60 tonne, 30 m maglev vehicle shown in Figure 1, an equivalent fully distributed load, w_v, is 19.6 kN/m (see Figure 3). Thus, for this example, $\Delta_{stat.pos}$ is equal to 5 mm (i.e. $5w_vL^4/384EI$), and the DAF is 1.51. Both the time it takes for a vehicle to cross a beam span and the fundamental beam frequency play significant roles in determining the DAF for a beam subjected to a passing vehicle.

Also important in maglev guideway design are two additional dynamic amplification measures. The maximum negative dynamic amplification factor $NDAF$ is the ratio of maximum upward, or "springback", beam deflection to maximum static deflection. Similarly, the maximum residual vibration factor $RDAF$ is the ratio of maximum beam deflection in residual, or free, vibration to $\Delta_{stat.pos}$. These two amplification factors are represented in (8). For the two point loading case shown in Figure 2, the NDAF and RDAF are equal to 0.41 and 0.09, respectively.

$$NDAF = \frac{\Delta_{dyn.neg}}{\Delta_{stat.pos}}; \quad RDAF = \frac{\Delta_{dyn.res}}{\Delta_{stat.pos}} \tag{8}$$

where

$\Delta_{dyn.neg}$: maximum negative (i.e. upward) dynamic beam deflection

$\Delta_{dyn.res}$: maximum beam deflection during residual vibration

B. Fully Distributed Vehicle Load

Both positive and negative dynamic amplification factors, DAF and NDAF respectively, can be reduced considerably using a distributed vehicle loading. Figure 3 shows a fully distributed vehicle loading, where a 2 tonne/m vehicle mass produces a 19,613 N/m fully distributed force traveling across a 25 m, 6⅔ Hz beam. Figure 4 shows the dynamic beam response when it is subjected to this fully distributed vehicle load at 125 m/s. The maximum dynamic midspan deflection of 5.40 mm occurs at $t = 0.18$ s. Thus, the maximum DAF for the fully distributed load case is 1.08. In this case, the maximum negative beam deflection of 0.78 mm is equal to the maximum residual vibration. The NDAF and the RDAF in this example are both equal to 0.16.

Thus, by fully distributing the vehicle load, the DAF is reduced by 28% (i.e. from 1.51 to 1.08) and the NDAF is reduced 61% (i.e. from 0.41 to 0.16). Though not true generally, in this example the RDAF actually increases with a

fully distributed vehicle load. Dynamic amplification factors for a range of loading distributions are shown in Figure 5. As indicated in Figure 5, the NDAF is significant for vehicles having large gaps between loading pads. As the gap between loading pads decreases, the maximum negative beam deflection occurs during residual vibration. Thus, for closely spaced vehicle loading pads, NDAF is equal to RDAF.

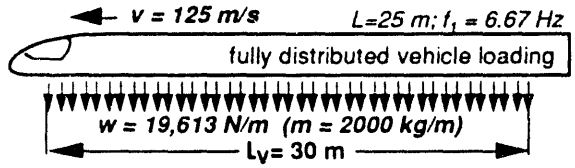

Figure 3. Fully Distributed Vehicle Loading

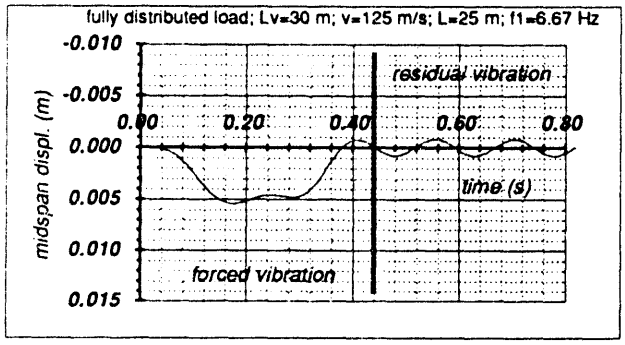

Figure 4. Beam Response (Fully Distributed Load)

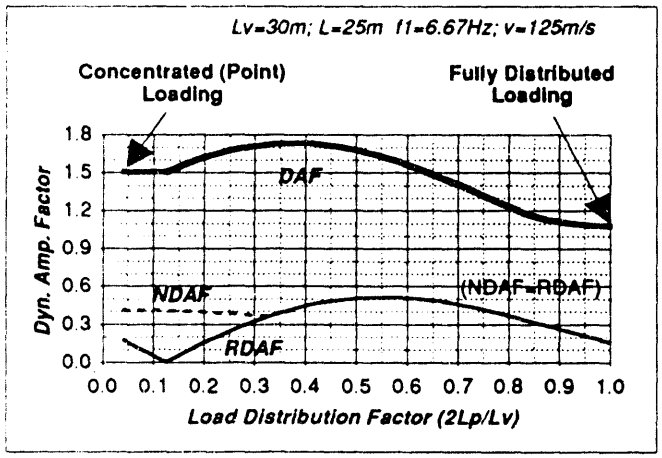

Figure 5. Dynamic Amp. Factor: Point vs. Dist. Loadings

IV. CONVERGENT VELOCITY EQUATIONS

In order to reduce guideway fatigue and the amount of non-magnetic reinforcement required, it is helpful to cancel both negative and residual vibrations when possible. As indicated in Figures 2 and 4, negative beam deflections can occur during forced and/or residual vibration response. Adequate vehicle load distribution can essentially eliminate negative deflections during forced vibration response.

Residual vibrations are dependent on 1) beam frequency, 2) beam length, 3) vehicle loading configuration, and 4) vehicle speed. Vehicle speeds at which beam residual vibrations are completely canceled, termed *convergent* velocities v^*, are determined according to the following four equations derived in closed form by the author [1].

1. Beam Length (all vehicles)

$$v_L^* = \frac{2Lf_1}{2\lambda + 1} \quad (\lambda = 1,2,3,\ldots) \tag{9}$$

2. Vehicle Length (fully distributed vehicle loads)

$$v_{L_v}^* = \frac{L_v f_1}{\lambda} \quad (\lambda = 1,2,3,\ldots) \tag{10}$$

3. Pad Length (vehicle pads)

$$v_{L_p}^* = \frac{L_p f_1}{\lambda} \quad (\lambda = 1,2,3,\ldots) \tag{11}$$

4. Pad Spacing (vehicle pads)

Near-zero cancellation occurs at velocities according to (12) for vehicles having equally spaced loading pads of equal length. Complete beam residual vibration cancellation occurs at mode n when $n^2 \neq in_p$ where $i = 1,2,3,\ldots$.

$$v_{S_p}^* = \frac{n_p S_p f_1}{\lambda} \quad (\lambda = 1,2,3,\ldots \text{ and } \lambda \neq in_p;\ i = 1,2,3,\ldots) \tag{12}$$

V. VEHICLE PAD DISTRIBUTION EXAMPLE

Figure 6 shows a vehicle with three 5 m loading pads each separated by 7.5 m. The distance between pad centroids, S_p, is 12.5 m. The fundamental vertical bending frequency of the beam is 6.67 Hz. Using (12), the set of convergent vehicle spacings for a 90 m/s vehicle speed, is: $S_p^* = \lambda(4.5\,\text{m})$, where $\lambda = 1,2,4,5,7,\ldots$, or 4.5 m, 9 m, 18 m, 22.5 m, 31.5 m, etc. Any of these pad spacings will result in near-zero beam residual vibrations. The 12.5 m vehicle pad spacing in Figure 6, however, does not match any of these 90 m/s convergent pad spacings. As expected, Figure 7 shows convergence is not reached as the maximum midspan deflection in residual vibration is over 50% of $\Delta_{dyn.pas}$.

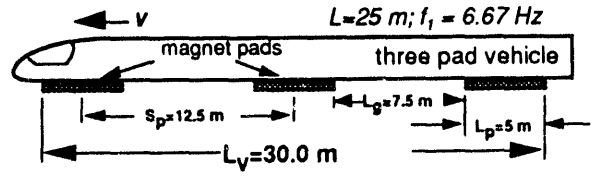

Figure 6. Three Pad Vehicle, Sp = 12.5 m (Lv= 30 m)

When the same vehicle travels at 125 m/s, convergent pad spacings are: $S_p^* = \lambda(6.25\,\text{m})$, where $\lambda = 1,2,4,5,7,\ldots$, or 6.25 m, 12.5 m, 25 m, 31.25 m, 43.75 m, etc. Since the S_p of the vehicle is equal to one of these convergent spacings, no beam residual vibration is expected at 125 m/s. This expectation is confirmed in Figure 8, where the beam residual deflection response to the given vehicle load traveling at 125 m/s is shown to be completely canceled!

In addition to analyzing beam response at any given vehicle velocity, it is instructive to determine beam response for a particular vehicle at all expected vehicle velocities. Figure 9 shows results of a sensitivity analysis which considers a guideway beam subjected to the three vehicle loading configurations (i.e. Figures 1, 3, and 6) for all speeds up to 160 m/s. The figure indicates the positive, negative, and

residual dynamic amplification factors (i.e. the DAF, NDAF, and RDAF, respectively) for the given speed range. Velocities for which zero RDAF values occur, correspond to predicted convergent velocities found by using (9) thru (12).

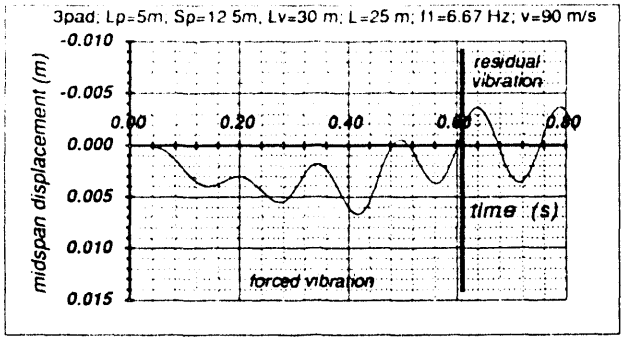

Figure 7. Beam Response for Sp =12.5 m (v=90 m/s)

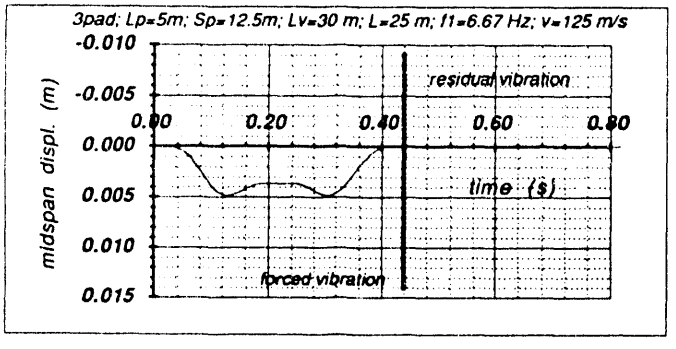

Figure 8. Beam Response for Sp =12.5 m (v=125 m/s)

Beam response due to the two-point vehicle load is shown in Figure 9a. For most of the vehicle speeds (e.g. 100 m/s), NDAF is equal to RDAF. This indicates the maximum negative deflection during forced vibration is equal to or less than the maximum residual deflection. For velocities where NDAF is greater than RDAF (e.g. 125 m/s), the beam experiences higher negative deflection during forced response than during residual response (see also Figure 2). In such situations, though the beam experiences less fatigue loading, sufficient compressive reinforcement is required to resist peak negative bending moments. In general, loading pad spacing reduction eliminates this effect.

Figure 9b shows the beam response to the fully distributed vehicle loading at all speeds less than 160 m/s. When compared with Figure 9a, Figure 9b shows beam behavior under the fully distributed vehicle to be much more stable across the speed range. The DAF remains less than 1.30 at all speeds for the distributed vehicle. Similarly, both NDAF and RDAF remain less than 0.45 at all speeds.

Figure 9c shows the beam dynamic behavior when subjected to the three pad vehicle of Figure 6 for all speeds up to 160 m/s. Under this loading, the DAF behavior of the beam is actually superior to that observed for the fully distributed vehicle case for speeds greater than 110 m/s. Additionally, the high speed range at which near-zero residual vibrations occur shifts from a 100 to 111 m/s range for the fully distributed vehicle load, to a 111 to 125 m/s range for the three pad vehicle. The "cost" for this high speed beam response improvement is the resonant behavior that occurs in the 67 to 111 m/s speed range shown in Figure 9c.

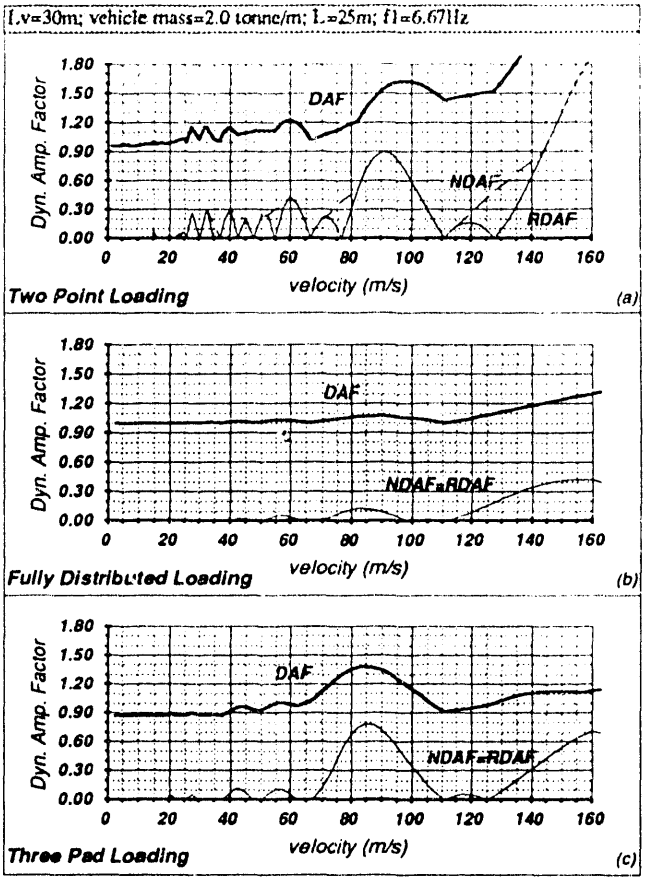

Figure 9. Beam Response and Conv. Velocities (3 cases)

VI. GUIDEWAY RESIDUAL VIBRATION REDUCTION

The following three sensitivity analyses illustrate the benefits of matching vehicle loading configurations with guideway dynamic beam behavior.

A. Fully distributed vehicle

Figure 10 shows the effect that changes in fully distributed vehicle length have on the DAF for expected maglev vehicle velocities. The fully distributed vehicle length L_v varies from 37.5 m to 62.5 m. The surface curve in Figure 10 shows essentially no change in DAF for the beam as the length of the vehicle varies. This plot agrees with earlier studies on high speed vehicle/guideway interactions [3].

In contrast to the stability of the DAF to changes in vehicle length, Figure 11 shows the dramatic effect these changes in length have on the RDAF for the same speed range. As shown in Figure 11, each vehicle length produces a different set of convergent and resonant velocities. All convergent velocities shown in Figure 11 are predicted by (9) and (10). None of the vehicle length cases produce either zero or near-zero residual vibrations for **all** speeds in the range. However, with maglev vehicle speeds expected to range from 0 to 150 m/s, the 45 m vehicle appears to offer the best compromise of vehicle lengths for all speeds in this range.

For all speeds less than 150 m/s, the RDAF for the 45 m vehicle remains less than 0.20.

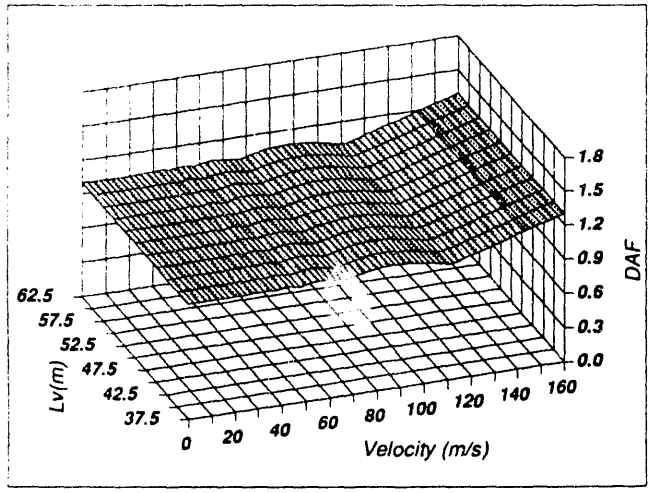

Figure 10. Fully Distributed Vehicle Length (DAF)

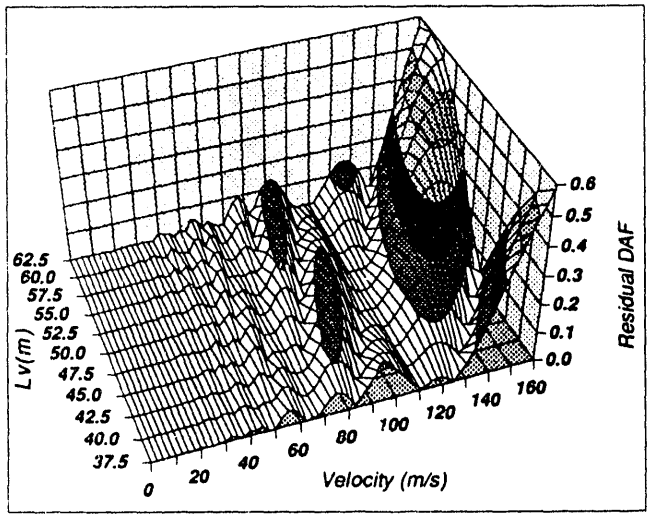

Figure 11. Fully Distributed Vehicle Length (RDAF)

B. Two pad vehicle

To evaluate the influence of vehicle pad length and spacing on dynamic guideway beam behavior, sensitivity analyses were performed for a variety of vehicle pad loading configurations. Figures 12 and 13 illustrate a two pad, 52.5 m vehicle analysis. The two vehicle loading pads are positioned at each end of the vehicle, with a gap length, L_g, between the two pads. Spacing between the centroids of the pads, S_p, is equal to $L_p + L_g$. Thus, the 0.0 m L_g represents a fully distributed 52.5 m vehicle. The DAF shown in Figure 12 remains below 1.50 in the speed range for gap lengths less than 5 m. In contrast to changes in fully distributed vehicle lengths, Figure 12 shows that changes in loading pad configurations do indeed influence the DAF of the beam.

Figure 13 shows beam RDAF for the 52.5 m, two pad vehicles. All convergent velocities shown in Figure 13 are predicted by (9), (11), and (12). None of the gap length cases result in a beam RDAF less than 0.20 for all speeds in the range. Superior high speed beam behavior, however, occurs using a 5 to 7.5 m gap vehicle, as shown in Figure 13. The resonant beam behavior at mid-range speeds with this vehicle is unfortunate, but not overly restrictive. Because maglev operation is expected to occur at higher vehicle speeds, the 5 to 7.5 m gap vehicle is desirable. Operation at mid-range speeds with such a vehicle, however, should be minimized.

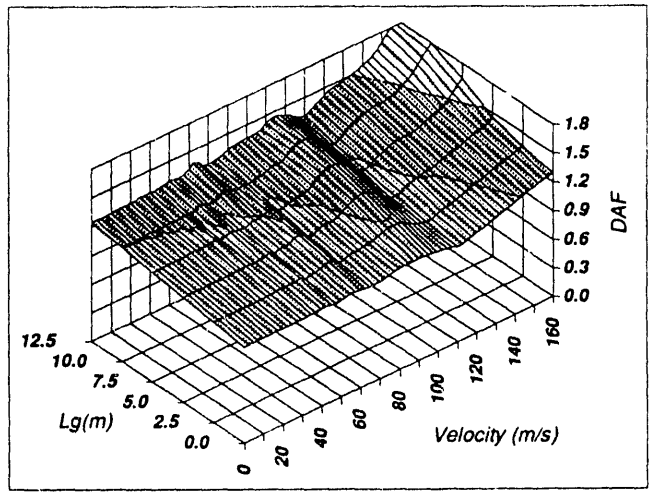

Figure 12. Vehicle Loading Pad Length (DAF)

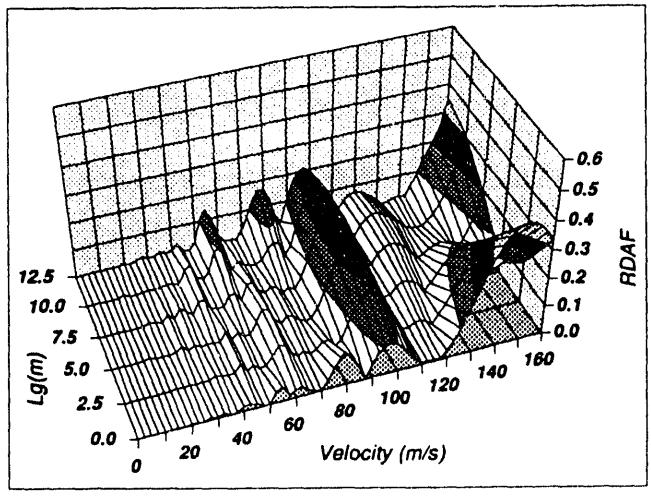

Figure 13. Vehicle Loading Pad Length (RDAF)

C. Six pad vehicle

The third and final dynamic beam behavior sensitivity analysis performed in this section is shown in Figures 14 and 15. The vehicle is modeled to represent the six pad, 29 m vehicle proposed by the Bechtel/MIT maglev team for the U.S. National Maglev Initiative's system concept definition study [4]. The Bechtel/MIT vehicle has six 4 m pads, each separated by a 1 m gap. Beam behavior caused by the traveling vehicle for a number of beam lengths and frequencies is analyzed.

As shown in Figure 14, the DAF is less than 1.20 for speeds less than approximately 150 m/s when beam length is 25 m and less. However, Figure 15 shows that the RDAF behavior for the 25 m beam is extreme at high speeds. In contrast, the RDAF for a 20 m beam is less than 0.20 for all

speeds in the given range. Thus, this 29 m vehicle appears well suited for the 20 m beam span, but not for the other spans.

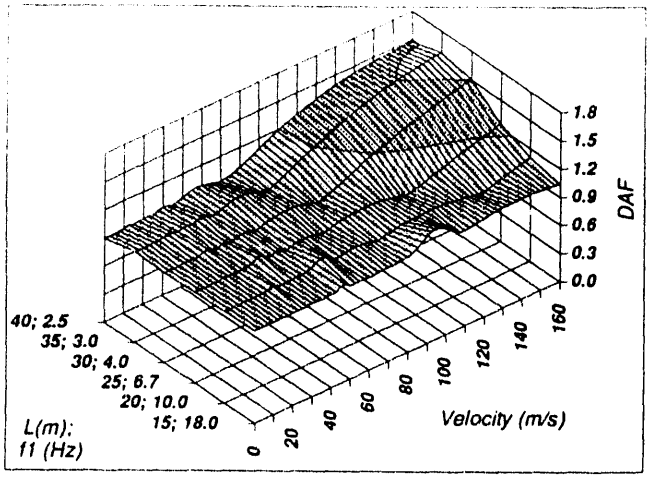

Figure 14. Beam Length and Frequency (DAF)

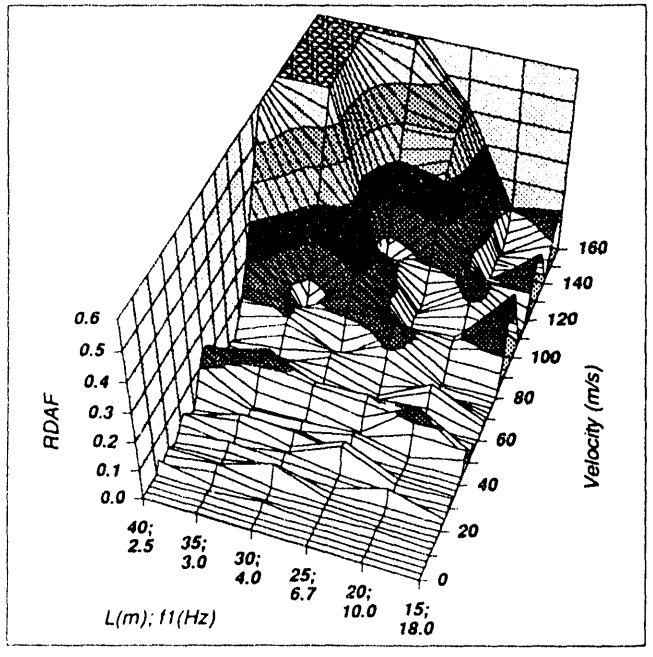

Figure 15. Beam Length and Frequency (RDAF)

These three analyses demonstrate that the guideway beam dynamic behavior is highly sensitive to vehicle loading configuration and to vehicle speed. All three analyses have particular design implications. The first example shows that though changes in fully distributed vehicle lengths have little effect on the DAF of a beam, the RDAF is highly sensitive to such changes. One difficult design issue is that no single vehicle length performs satisfactorily on a given beam for all expected maglev vehicle speeds. The second example shows that though the DAF increases with increased vehicle gap length and with the use of discrete loading pads, the RDAF of the beam becomes more controllable under such conditions. Figure 13 indicates that specific vehicle loading configurations can be designed to complement beam dynamic behavior at particular operating speed ranges. The third example demonstrates that individual beam segments can be designed to match a particular vehicle loading configuration for a given speed range at specific locations along the guideway corridor.

VII. CONCLUSIONS

It is shown that a vehicle length and loading pad configuration can be adjusted for a particular beam to produce *convergent* conditions—whereby all beam residual vibration is canceled—at desired vehicle speed ranges! This ability to cancel beam residual response is remarkable and potentially has a number of important maglev design implications including benefits such as a) increased guideway lifespan, b) reduced non-magnetic concrete reinforcement requirements, and c) potentially shorter operational vehicle headway allowances.

This paper presents equations describing the transverse vibrations of a simply-supported beam due to a traveling load during both forced and residual vibration modes—(4) and (6). Equations representing convergent velocity conditions, solved in closed form by the author, are also shown—(9) thru (12). These convergent velocity equations will assist in ensuring future compatible maglev guideway beam and vehicle loading configuration designs.

ACKNOWLEDGMENTS

The author wishes to thank Richard Thornton, Jerome Connor, Thanasis Triantafillou, and Jeroen Timmermans of the Massachusetts Institute of Technology for their comments, suggestions, and help during the course of this work. Thanks also goes to Mike Silver of the National Maglev Initiative for his insights and assistance.

REFERENCES

[1] Phelan, R.S., *High Performance Maglev Guideway Design*, Doctoral Dissertation, MIT Department of Civil and Environmental Engineering, February 1993.

[2] Humar, J.L., *Dynamics of Structures*, Prentice Hall, 1990, pp. 668-671.

[3] Richardson, H.H. and D.N. Wormley, "Transportation Vehicle/Beam-Elevated Guideway Dynamic Interactions: A State-of-the-Art Review", *Journal of Dynamic Systems, Measurement, and Control*, 74-Aut-P, ASME, pp. 1-11, 1974.

[4] *Maglev System Concept Definition*, Final Report—Volume 1, prepared by Bechtel Corp., Hughes Aircraft, General Motors Electromotive, Massachusetts Institute of Technology, and Draper Laboratories for the U.S. Department of Transportation Federal Railroad Administration, September, 1992.

Alignment and Surveying of Magnetic Levitation Train Guideways

Hans–Jürgen Marx
Weißensteinstr. 70, 4200 Oberhausen 11, Federal Republic of Germany

Robert Stoeckl
Thyssen Industrie AG Henschel, Anzinger Str. 11, 8000 München 80, Federal Republic of Germany

Abstract – This report will detail the steps required for the alignment and surveying of a Transrapid application route. The system parameters which need to be considered during the planning of the route are listed and innovative solutions are presented to accomplish the stringend requirements of the surveying process.

I. Introduction

All of the activites involved in the geometric processing of a Transrapid guideway are summarized under the heading, alignment and surveying.

The essential requirement of the alignment is to create an ecologically and economically balanced route for the Transrapid system. The non–contact magnetic levitation technology allows an extremely economical choice of alignment parameters, and therefore opens up the possibility of a route choice which well matches the topographical features of the landscape.

Through the use of computer–aided manufacturing processes in the fabrication of the guideway beams, e.g. numerically controlled cutting equipment for the steel components, robotic fit–up and finish welding of the steel beams, adjustable beam forms for the concrete beams, and highly automated equipping of the beams with stator packs, the guideway beam costs are not influenced by the alignment. The alignment engineer therefore has a maximum amount of creative freedom in laying out the basic route.

In accordance with the current planning legal conditions valid for the Federal Republic of Germany, the planning, alignment, and surveying activities can be divided into three general phases. These are shown in Fig. 1.

II. Rough Alignment

Based on the traffic volume prognoses, the general boundary conditions for a Transrapid application route can be determined. The number of tracks, the revenue speed, and the location of the stops are of importance here.

The first activity for the rough alignment is the selection of the corridor. Using small scale maps (topographical overview 1:100 000), the possible corridors between the stop points are defined. Using value analysis, the optimal corridor can be determined. The appropriate state development programs and state planning laws can already be accounted for in this phase. Globally applied to all route decisions, as already mentioned, are the consideration of the ecological and economical aspects.

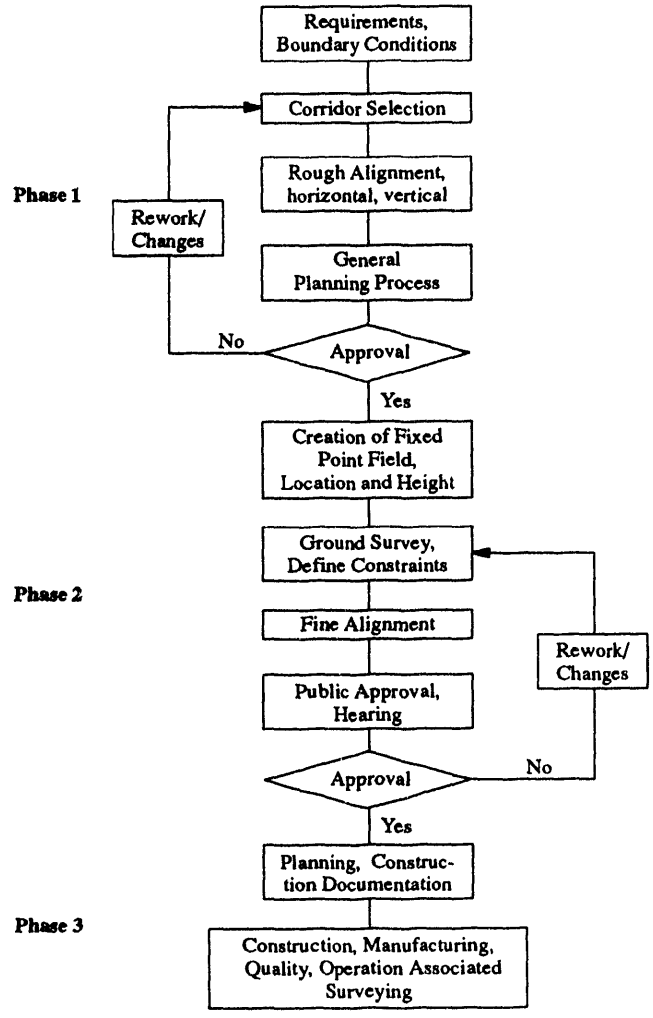

Fig. 1. Planning, Alignment and Surveying Activities

In the next activity, the plan and elevation views of the rough alignment are executed. The basis for these are scale 1:25 000 topographical maps. In this phase of the planning, the following objectives are of particular importance:

– colocation with existing traffic routes, within limits of the

alignment parameters (see Table I)
- accounting for ecological restrictions, possibly by detouring around problem areas
- avoidance of separating effects on the existing infrastructure
- fitting into or adapting to the landscape

The alignment calculation will be carried out in this phase in accordance with the guideway alignment data shown in the Table I, but to simplify the situation, only the straight and pure circular elements are taking into account. The initial constraint diagnosis, cost, and trip time calculations can be made. Through fulltime data processing support of this process, different variations can be investigated without great expense.

Furthermore, the environmental compatibility check would occur in this phase.

During the subsequent public approval process, the authorities will examine the route and if problems arise, an additional iteration in the corridor or rough alignment determination will be carried out. With this approval, the rough alignment will be released for the next planning phase.

TABLE I

Guideway Alignment Data

Lateral Acceleration	≤ 1.5	m/s^2
Vertical Acceleration		
– Crest	≤ 0.6	m/s^2
– Trough	≤ 1.2	m/s^2
Omnidirectional Jerk		
– Normal track	≤ 1.0	m/s^3
– Singular points	≤ 2.0	m/s^3
Lateral Inclination	≤ 16	°
Torsion (change of cant)	≤ 0.1	°/m
Longitudinal Inclination	≤ 10	%
Horizontal Curvature		
Minimum	350	m
200 km/h	705	m
300 km/h	1,590	m
400 km/h	2,825	m
500 km/h	4,415	m

The sinusoidal transition curves and superelevation ramps are of equal length.

Vertical Curvature	Crest [m]	Trough [m]
Minimum	500	500
200 km/h	5,145	2,575
300 km/h	11,575	5,790
400 km/h	20,575	10,290
500 km/h	32,150	16,075

III. Fine Alignment

To form the basis for the fine alignment, exact planning materials are required along the approximate route. A local position and height fixed point field will be established for this and used for the polygon generation along the route. The exact location determination of the fixed point field can be accomplished using one of two methods, the traditional surveying with angle and distance measurement (polygon method) or using satellite location equipment (GPS: global positioning system).

The main differences between these two methods are shown in Table II. The GPS method is favored today in heavily populated areas and in wilderness areas due to its enormous advantages.

The vertical determination of the fixed point field is accomplished using precision levelling. The fixed height points are normally attached to the existing fixed location points since they are robustly built and firmly anchored in the ground.

Based on this location and height fixed surveying network, the topographical documentation of the landscape near the route can occur. Well-known terrestrial and also photogrammetric surveying methods are available to accomplish this. The constraint points with their X, Y, and Z coordinates will also be cataloged during this landscape mapping.

The digitally collected landscape data can then be assembled into a digital landscape model.

The plan representations can subsequently be made in scale 1:1 000. Based on these planning materials, the fine alignment can be calculated in plan and elevation views according to the alignment parameters shown in Table I. The progression of the alignment through space, which results from a combination of the plan and elevation parameters, will be exactly determined mathematically.

TABLE II

Comparison of the Traditional Surveying Process (Polygon Method) with Global Positioning System (GPS)

Activities	**Polygon Method**	**GPS**
Reconnaissance of long traverse leg points with sighting of neighboring fixed points	Yes	No
Clearance of sight lines	Yes	No
Procurement of reference points for the determination of the compressed polygon and for determination of constrained points	No	Yes
Execution of the angle and distance measurement	Yes	No

The specially developed computer program used to generate this space alignment, also has the ability to generate the sinusoidal forms for the transition elements in the planview and the clothoidal forms for the elevation view, and thereby produce an exact geometric 3–D space alignment. Another important aspect of this calculation is the examination of the allowed overlapping of the alignment parameters in the plan and elevation views, in order to evaluate whether the allowed acceleration values have been maintained.

The progression of the guideway functional surfaces (stator pack, guidance rail, glide plane) in space are a result of this fine alignment. The data will be digitally processed for subsequent use in the guideway activities, in particular for the beam fabrication and equipping.

The detailed representation of the route forms the basis for the subsequent public planning approval process. In this process, the chosen alignment will be publicly displayed, in order to allow the affected citizens the possibility to comment. Eventual objections from the examining authorities or the citizens may lead to another iteration in the fine alignment process. At the end of this public approval process, the certification for the realization of the chosen maglev route will be given.

IV. Construction Site Activities and Surveying

The construction site materials will be created according to the alignment materials. The technical surveying calculations required to transfer the guideway to the actual topography are based on these construction materials.

The next step in the local surveying work, is to expand on the fixed point field described in section 3, i.e. fixed points need to be added inbetween the existing ones. The experience at the Transrapid Test Facility in Emsland has shown that point intervals of approximately 200 m are appropriate.

The surveying work associated with the erection of an elevated guideway requires in addition to the rough marking of the construction road, a maximum of four operating steps:

Step 1: Marking the locations of the substructure foundations
Step 2: Marking the locations of the support piers
Step 3: Marking the locations on the pier caps of the required recesses and bearing fixtures
Step 4: Fine positioning of the guideway beams on the substructure piers

According to the construction specifications, step 1 has to be achieved with a tolerance of ± 30 mm, step 2 with a tolerance of ± 10 mm, and step 3 with a tolerance of ± 5 mm.

The tolerances are not to be considered in the geodetic sense, rather they represent absolute error limits. To confirm that the tolerances have been maintained for the polar measured and marked points, the points will be polar surveyed a second time from an independent standpoint and a design value / actual value comparison carried out.

After the rough positioning of the beams on the substructure piers, the beams have to be positioned as in step 4, i.e. referenced to the space curve. The fine positioning accuracy is specified with the following tolerances:

X–direction ± 2.0 mm
Y–direction ± 0.5 mm
Z–direction ± 0.3 mm

Here too, the specified tolerances are to be regarded as limits, though not as absolute values against a general reference point (polygon point), rather relative to the relevant reference points of the neighbouring beams.

A concept has been worked out for the fine positioning which makes it possible to set the displacement dimensions for achieving the design position directly on the support– and guidance components.

To establish the reference for the alignment space curve in the immediate neighbourhood of the beams to be positioned, adapter bolts are mounted onto the foundation plates and their exact location and vertical position determined.

This specially developed surveying method for the fine positioning, consists of three geodetic surveys:

- polygonization of the adapter points on the foundation (measured from the fixed bearing locations)
- execution of an alignment using the adapter points on the foundations
- double polar point determination, whereby the adapter points are over–determined

All surveying results are electronically stored, evaluated, and computed in coordinates. The points can be assessed in relation to their neighbouring points through the use of error ellipses produced by a compensating calculation.

The beams are positioned for height and cant using suspended invar steel bands attached magnetically to defined positions on the stator packs. Immediately prior to the fine positioning operation, the adapter bolts on the foundation plates are measured from the vertical fixed point field using precision levelling techniques.

Lead screws or hydraulic presses are temporarily intalled on the supports for the physical positioning of the beams on the piers.

Special templates, precision plumb–lines, and a portable computer are used to generate the displacement values for the erection personnel in order to fine position the beams longitudinally and laterally. A precision leveler with deflecting prism is used for the plumb measurements, which eliminates the need for the centering required with conventional optical plumb measurements. The horizontal and vertical positioning of the beam has to take into account the longitudinal thermal expansion of the beam.

A single–span beam is first positioned at the fixed bearing,

then at the loose bearing. A double–span beam is positioned at the fixed middle bearing, then at the two loose end bearings. The beam is positioned in the area of the loose bearings, using special templates attached to the beam at the fixed bearing point. After the fine positioning of the beam, the measurements are repeated and the displacements recalculated to check the position of the beam. The tolerance limits specified are approximately 0.5 mm for the horizontal position and 0.3 mm for the height. If these values are exceeded, then repositioning is necessary. Only then is the beam released for grouting of the bearings.

Since the surveying procedure and the beam erection work are not decoupled, dependencies occur in the course of the work. A concept to separate these activities is being worked on as part of the current development program.

V. Measurement Activities during Beam Production

Depending on their application and the height of the guideway above the ground, beams can be produced from steel, concrete, or composite (steel + concrete) for the following situations:

- at–grade
- low lying
- elevated
- at–grade in a tunnel
- bridge / special construction

At the Transrapid Test Facility in Emsland (TVE), the guideway includes at–grade and elevated sections of both steel and concrete beams for testing and demonstration purposes. The solution used for the at–grade guideway at Emsland involves substructure piers resting on individual foundations with fixed and loose bearings.

From the statics viewpoint, two different types of beam exist at the TVE:

- single–span with one fixed and one loose bearing
- double–span with one fixed and two loose bearings

In parallel to the construction associated surveying activities described in the previous sections, manufacturing associated measurement activites also occur. These concentrate themselves on the fabrication of the beams and their equipment with the stator packs for the longstator propulsion system.

A. Steel Beams

The alignment and measurement work required for the steel beam manufacture is described below.

The calculation and production of the steel guideway beams, due to the integration of the lateral guidance rails and the glide surface into the welded construction, is derived directly from the alignment space curve geometry. The individual structural components of the steel beam are of sheet metal and their geometric shape must correspond directly to the specified space curve geometry. An integrated data flow is accomplished using computers to transform the space curve geometry into the data required for cutting the individual steel sheets. For the calculation of the components cut with NC controlled machines (e.g. the deck plates), the transformation of the spatially curved plates (3–D space) into a plane (2–D space) has to be taken into account.

Beam fabrication assembly fixtures will be constructed in the various factories for the fit–up of the components to be welded. The required set–up values for the fixtures as a function of the space curve geometry, are also calculated and transferred using computers. Included in these data calculations is structural information, such as beam camber.

After its fabrication, the beam must be equipped with the longstator propulsion components. During this stage, the approximately one meter long stator pack is assembled with high precision to the underside of the beam according to the predetermined space curve geometry. This is accomplished using stationary, NC controlled machining and assembly equipment in a temperature stabilized plant.

The set–up of the beam on the machining equipment is accomplished by using the technical measurement concept of "actual position determination". In the machining program are specific beam reference points. The machine will then be manually (or semi–automatically) taught these points (actual position). On the basis of these reference points, the original machining program in the NC controller will be transformed to correspond to the current beam position.

This concept allows the rows of stator packs to be assemblied with high precision to the beam, which contributes significantly to the excellent ride comfort of the Transrapid system.

B. Concrete Beams

The geometries of the concrete beams are calculated according to their structural requirements by their manufacturers, largely independant of the space curve geometry. The concrete beam is equipped with the support and guidance components (guidance rails, stator packs) generally at a later stage. Only the attachment points for the support and guidance components have to be according to the requirements from the alignment space curve geometry. This information is calculated and transferred to the production equipment at the appropriate stage. The mounting of the guidance rails is accomplished using a special assembly fixture. The machining and assembly of the stator packs proceeds in a fashion similar to the steel beam.

VI. Quality Assurance

As part of the quality assurance program, geodetic surveys will be performed during all phases of the guideway manufacture. The results of these measurements together with the construction materials and the specific tolerances allowed, form the design / actual comparison. Using this method, the adherence to the required geometric quality can be guaranteed.

The geometric quality assurance focuses on the three essen-

tial functional levels of the guideway:

- geometric progression of the underside of the stator packs
- geometric progression of the lateral guidance rail surfaces
- geometric progression of the emergency glide plane (deck plate of the beam)

After completion of the guideway, as the first step, an operation associated reference measurement will be performed. Measurements are taken at definite points on the structures and these are used primarily as a reference to monitor the long term changes in the guideway (deformation, settling).

Periodic guideway inspections are included in the operation plans for a magnetic levitation train route and among other things, the geodetic inspection of the points contained in the reference measurement is performed.

The comparison between the actual measurements and the reference measurement allows conclusions about the geometric changes occurring in the Transrapid guideway.

The results of the Transrapid Test Facility in Emsland lead to the conclusion that due to the guideway design, such changes seldom occur or only within tolerably small ranges. The respective survey intervals are oriented on the geologic conditions present and are only performed at long time intervals.

VII. Summary

Through the system specific advantages of the magnetic levitation train Transrapid, alignments which are extremely flexible and well integrated into the topographical situation are possible. In comparison with traditional track–guided traffic systems, the alignment parameters have been greatly improved, especially when the allowed guideway cant (superelevation) of 16° and the maximum gradient of 10% are considered.

Through the computer–based data flow in the alignment process and guideway beam manufacturing process, the type of guideway has become virtually cost neutral. That means that a straight steel guideway beam costs virtually the same as a curved steel beam. The alignment engineer therefore has a maximum amount of creative freedom in laying out the guideway route.

The new surveying processes specially created for the magnetic levitation train guideway and perfected at the Transrapid Test Facility in Emsland, guarantee that the specified tolerances can be maintained with a minimum expenditure.

VIII. References

[1] H.–J. Marx and R. Stoeckl, "Guideway Alignment and Surveying", TRANSRAPID MAGLEV SYSTEM, Hestra–Verlag, ISBN 3–7771–0208–3.

[2] P. Mnich, H.–J. Marx and R. Stoeckl, "System – Specific Problems and Basic Data of TRANSRAPID Route Alignment", ZEV Glasers Annalen, ISSN 0941–0589, Heft 11/12 1992.

[3] O. Breitenbach, R. Stoeckl and M. Wcislo, "The Guideway Equipment", TRANSRAPID MAGLEV SYSTEM, Hestra–Verlag, ISBN 3–7771–0208–3.

[4] R. Stoeckl and G. Schwindt, "Manufacturing Process and Assembling Line of Guideway and its components on the TRANSRAPID MAGLEV SYSTEM", International Conference on MAGLEV & Linear Drives May 19–21, 1987, Las Vegas.

Aerodynamic Drag of Maglev Vehicles

Frank A. Balow III † and Kenneth R. Sivier *

Department of Aeronautical and Astronautical Engineering
University of Illinois at Urbana-Champaign
Urbana, IL 61820

Abstract

This paper presents an approach for making a preliminary estimate of the aerodynamic drag of Maglev vehicles. The method involves combining traditional methods of drag estimation for aircraft at subsonic speeds with estimates based on data reported in literature for the drag breakdown of Maglev-type vehicles. An example is presented for a generic, single car Maglev vehicle with an operational speed of 500 km/hr.

I. Introduction

A. *Nomenclature*

C_f	skin friction coefficient
C_{Df}	skin friction drag coefficient
C_{dp}	form drag coefficient
d	hydraulic diameter
D_f	skin friction drag force
L	characteristic dimension, overall length
M	Mach number
q	dynamic pressure
Re	Reynolds Number
S	cross-sectional reference area
V	fluid velocity
ρ	fluid density
μ	fluid viscosity
λ	hydraulic skin friction coefficient

B. *Problem Definition*

As the operational speeds of high-speed rail and Maglev vehicles are increased, a larger and larger percentage of the vehicles' total traction power is needed to overcome the aerodynamic drag. At speeds in excess of 400 km/hr, the aerodynamic drag of a high-speed rail car can require 80% of the traction power [1]. With the absence of wheel/rail drag, Maglev vehicles require a proportionately higher percentage of this power to balance the aerodynamic retarding force.

There are few first order approaches to estimating the drag of Maglev vehicles. Most traditional methods are based on wind tunnel or field testing of multi-car wheel/rail trains. Current Maglev design, however, focuses on single car configurations. This makes many of the previous approaches inapplicable for proper evaluation of the important aerodynamic features of current and future systems.

It is clear, then, that there is a need for a quick and relatively accurate method for estimating the drag of Maglev vehicles during the design process. It is important that this be a generalized method that relates the effect of each vehicle component to the result. This paper presents such a method. This method builds the total answer by summing the drag of the individual components. This is done by using traditional estimation methods from the aerospace industry combined with experimental data from Maglev testing. In this way, a first-order estimate of the aerodynamic drag and its components can be produced.

C. *Literature Review and Discussion*

Although there is a considerable amount of literature on the aerodynamics of trains (trains passing, train-in-tunnel effect, etc.), there are very few published methods for determining the aerodynamic drag of Maglev vehicles. However, extensive experimental work has been done on the problem by both the Japanese and the Germans. General papers reporting on this work form part of the basis for the method presented here.

Matsunuma, Nagayama, and Kobayashi [2] of the West Japan Railway Company, address many aerodynamic aspects of the Maglev problem. Unfortunately, they touch only briefly on the subject of aerodynamic drag and present a drag coefficient estimating procedure in the form of (1) below.

$$C_D = C_{dp} + \frac{\lambda L}{d} \qquad (1)$$

Manuscript submitted March 15, 1993 to Maglev '93 Conference. This work was supported by the General Motors Electro-Motive Division under Research Agreement No. 92-PRI-S-0378 as part of the National Maglev Initiative.

† Graduate Research Assistant
* Associate Professor

where $d = 2\left(\frac{S}{\pi}\right)^2$

Their study is of the Series 100N Shinkansen, a multi-car vehicle. Therefore their analysis is only partially applicable to present single-car designs. Matsunuma et. al. do make one important point: when increasing the internal volume of a slender vehicle, less drag is generated by increasing the cross-sectional area than by increasing the length.

A paper by Barrows [3] gives general guidelines for developing a streamlined shape for Maglev vehicles. Barrows, who has worked on many such ground based transportation systems, does not present a formula for calculating drag. He instead looks at present multi-car designs and modifies the drag coefficient as if the vehicle were a single car configuration. He does this by first using (1) to predict the drag of a single vehicle of the same length as the multi-car operational vehicle, and then scaling that value to the length of the vehicle under consideration.

There are, at the present time, no commercially operational single car Maglev vehicles. The closest configurations are the Transrapid TR06 and TR07. The TR06 has open bogies while the TR07 has its magnets enclosed. Thus, the TR07 is a better test subject for the fully enclosed systems under consideration. According to [3], the reported value for the total C_D for the TR07 is 0.45. Using the procedure described above, Barrows arrives at a C_D value of 0.3 for a single car of about half the length of the TR07.

Peters [1] provides no method for calculating the drag of Maglev vehicles, but does give a component by component breakdown of the total aerodynamic drag for several operational systems. Peters divides the aerodynamic drag into four major categories: bogie drag, skin friction drag, roof equipment drag, and pressure drag. These breakdowns are given in Table I.

Bogie drag is the sum total of both the bogie aerodynamic drag and the associated guideway interference drag. Guideway interference drag is caused by the turbulent flow between the guideway and the vehicle. Skin friction drag is the retarding force resulting from viscous shearing stresses over the wetted area of the vehicle. Roof equipment drag includes the drag from air conditioners, generators and pantographs that appear unfaired (i.e. unblended) anywhere on the surface of the vehicle (excluding surfaces in close proximity to the guideway). Pressure drag is due mainly to contributions from the shape of the nose and tail.

TABLE I
Percentage Component Drag Breakdown of Several Existing Maglev Systems

Drag Component	Percentage of Total Aerodynamic Drag
Bogie(s)	38 - 66
Skin Friction	27 - 30
Roof Equipment *	8 - 20
Pressure Drag †	8 - 13

* Includes pantograph
† Nose and tail effects

D. Adjustment of Empirical Drag Percentages

Table I above presents experimentally determined drag data for existing Maglev systems. However, current designs differ from these vehicles primarily in that they:

- are single car configurations
- lack pantograph equipment
- have greater operational velocities

Clearly, then, the values from Table I must be adjusted in order to represent the systems under consideration.

The most obvious change that must be made is the deletion of the roof equipment term. All guidance controls and power pick-ups are taken care of by on-board systems. Secondly, Peters [1] reports that up to 2/3 of the total aerodynamic drag of Maglev vehicles may be caused by bogie drag. This would indicate that the lower bound of the bogie drag should be increased.

Taking these two adjustments into account, a redistribution of drag percentages is done using bogie drag as the independent variant. This is done because bogie drag is felt to have the largest contribution to overall drag. By keeping the skin friction and roof equipment drag values (not percentages) constant, four example scenarios listed in Table II are generated.

TABLE II
Various Adjusted Percentage Component Drag Breakdowns for Current Maglev System Designs

Drag Component	Percentage of Total Aerodynamic Drag			
Bogie(s)	51	55	60	66
Skin Friction	35	32	28	24
Roof Equipment	0	0	0	0
Pressure Drag †	14	13	12	10

† Nose and tail effects

The first and last scenarios represent a lower and upper bound for the calculations. The cases in Table II with bogie drag totaling 50-60% of the total

aerodynamic drag are felt to be the most accurate based on current literature.

II. Discussion of Drag Components

The method presented below for estimating the components of aerodynamic drag for Maglev vehicles assumes that the Maglev vehicle in question is a single, semi-ellipsoidal car. The single car assumption permits the use of documented methods to predict aircraft fuselage drag. The second assumption precludes vortex-shedding corners along the vehicle's length.

B. Skin Friction Drag

Skin friction drag can be estimated from the vehicle geometry, the operating speed, and the type of vehicle boundary layer (i.e. laminar or turbulent). The boundary layer type depends on the Reynolds Number characteristics of the vehicle.

1) Reynolds Number: Reynolds Number is a ratio of the dynamic and viscous forces in a fluid and is defined as

$$Re = \frac{\rho V L}{\mu} \quad . \qquad (2)$$

Transition from laminar to turbulent flow usually occurs at Reynolds Numbers from 2×10^5 to 2×10^6. The boundary layer type is thus dependent upon the characteristic dimension of the vehicle and the operating speed.

The skin friction coefficient (not to be confused with the skin friction drag coefficient) is determined from either (3) or (4) depending on whether the flow is laminar or turbulent, respectively.

$$C_f = \frac{1.328}{\sqrt{Re}} \qquad (3)$$

$$C_f = \frac{0.455}{(\log_{10}Re)^{2.58}(1+0.144M^2)^{0.65}} \qquad (4)$$

2) Skin Friction Drag Coefficient: Two different methods are used to predict the skin friction drag coefficient. The first is from Raymer [4]. This method allows for a wide variation of fuselage parameters including a choice of laminar, turbulent, or mixed boundary layer flow. The second method is from Roskam [5]. It is less flexible in its range of parameters and allows for only turbulent flow on the body. As a check of the compatibility of the methods, the analysis from Raymer was run for a fully turbulent flow. The values calculated for the skin friction drag coefficient compared well (within 1%) with those calculated from Roskam's approach for an equivalent vehicle.

The skin friction drag coefficient is related to the drag force by (4).

$$D_f = qSC_{D_f} \qquad (4)$$

C. Pressure Drag

The pressure drag of a cylindrical body (such as an aircraft fuselage or Maglev vehicle) is mainly due to the shape of the nose and tail. The nose geometry is the smaller of the two contributors. A properly shaped nose will contribute almost no pressure drag to the total. For example, Ref. [3] shows very little difference in drag between a large variety of slender nose shapes. The key requirement is that vortex-shedding surfaces be avoided. If this is done, the contribution of the nose to the pressure drag term may be neglected.

The tail, however, is a potential source of large pressure drag. If the base is simply cutoff as in Fig. 1a, a large amount of bluff-body vortex shedding will occur. This will cause a significant increase in pressure drag. Tapering the tail can produce two different results. Figure 1b shows the effect of tapering the base too quickly. The result of this is, again, boundary layer separation and a large pressure drag. Figure 1c shows a base that is tapered so gradually that the flow remains attached, but the increase in skin friction drag (due to the large base wetted area) is larger than the decrease in pressure drag.

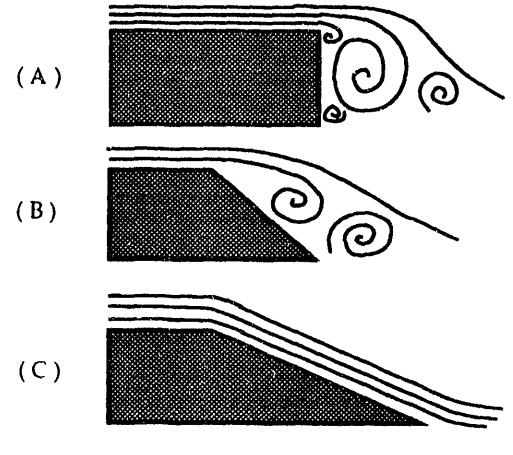

Fig. 1. The Effect of Base Tapering on Separation

A compromise to the mutually exclusive problems in 1b and 1c is reached by finding the minimum for a set constrained by both skin friction and

pressure drag. The solution to this is shown graphically in Fig. 2. The figure was generated from material in [6]. Notice that the optimum answer occurs at a fineness ratio of approximately 5.0. Fineness ratio is defined as the body length divided by the body diameter. As Matsunuma et. al. [2] show, making a body wider will cause less drag than making it longer. This applies, of course, only for fineness ratios greater than the fineness ratio for the minimum drag coefficient. This fact then may be used to evaluate the savings in total aerodynamic drag that may be achieved by proper base boat-tailing.

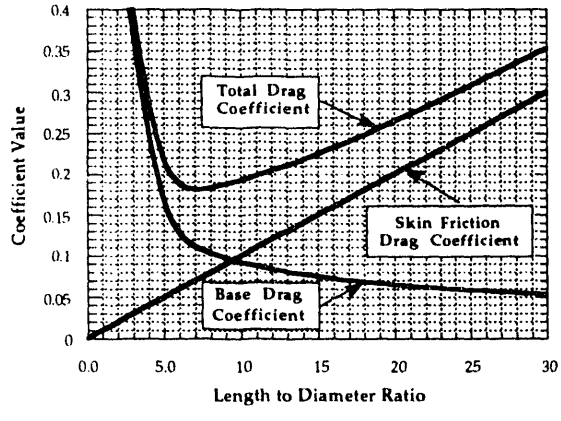

Fig. 2. Base, Skin Friction, and Total Drag as a Function of Length-to-Diameter Ratio

D. Guideway Interaction Drag

The effect of the interaction between the bogies and the guideway is a large part of the overall aerodynamics of Maglev vehicles. Unfortunately, there is no simple way to estimate this effect from fundamental principles. Therefore, to select a percentage range from Table II, a guideway interaction scaling factor was derived.

This factor is basically an area scaled value taken from existing designs. By first calculating the drag of the vehicle without the presence of the guideway (i.e. as if it were flying through the air) and then subtracting this value from the measured value of the system with the guideway, a value for the combined bogie/interference drag can be estimated. This area based ΔC_D turns out to be about 8.4×10^{-4} per square meter. The generality of this value should not be overestimated. This scaling factor is dependent on some nominal separation distance between the guideway and the vehicle plus a generic cross section. For this analysis, the separation was 0.1 m and the cross-section was 15 m^2. Also, this value may only be used for vehicle operating in the 500 km/hr range.

III. Example Application of the Method

A. Outline of Steps

1. Determine the relevant physical parameters of the system.
2. Determine the Reynolds Number and therefore the boundary layer type.
3. Calculate the skin friction drag coefficient.
4. Calculate the bogie/interference drag coefficient using an appropriate scaling factor.
5. With this figure, determine the proper drag percentage breakdown.
6. Determine if the pressure drag of the base has been optimized and modify if necessary.
7. Sum the pressure, bogie and skin friction drag coefficients.
8. Add 10% of the of the pressure and skin friction drag to the total to account for leakage and protuberance drag. [4]

B. Geometry

The example configuration shown in Fig. 3 is a single, streamlined system with physical parameters listed in Table III. All of the bogies are externally faired and there is no equipment on any exposed surface. The undercarriage adjacent to the guideway is typically irregular and assumed to be subject to turbulent interaction.

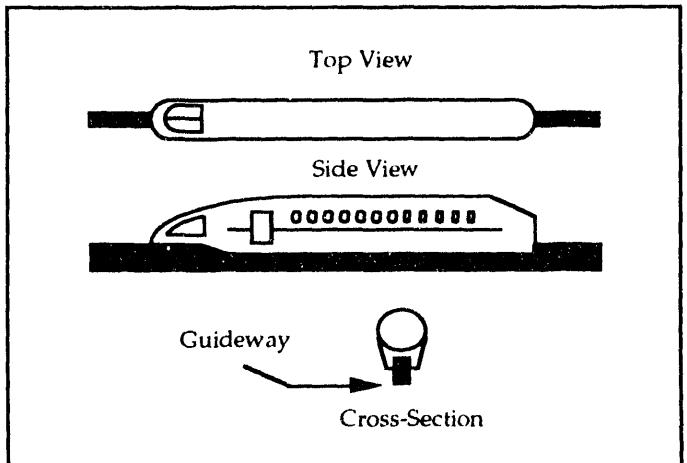

Fig. 3. Schematic of Example Maglev System

TABLE III
Relevant Physical Parameters for Example Maglev System

Physical Parameter	Value
Overall Length	34.78 m
Operational Speed	134 m/s
Cross-Sectional Area†	14.7 m^2
Wetted Area†	503 m^2
Base Taper Angle	22° *
Guideway Separation**	0.1 m

† Wetted and cross-sectional area conventions are shown in Figure 4
* 22° taper recommended by [7]
** Included for bogie/guideway interaction scaling factor

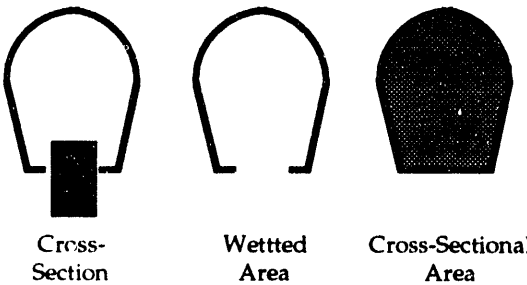

Fig. 4. Wetted and Cross-Sectional Area Convention

B. Evaluation of Reynolds Number and Skin Friction Drag Coefficient

For the skin friction drag calculations, it is important, to determine how much (if any) of the fuselage is in laminar flow. Obviously the more wetted area that has laminar flow over it, the lower the skin friction drag. For this vehicle, the effect of laminar flow on the skin friction drag coefficient can be seen in Figure 5.

The Reynolds Number for this vehicle, at operational speeds, is on the order of 10^8. The Reynolds Number of 25% of the overall length is on the order of 10^7, an order of magnitude greater than the maximum transition Reynolds Number. This would indicate that even though [5] predicts that up to 30% of an aircraft fuselage may be in laminar flow, this is not the case here. A fully turbulent boundary layer is assumed here. From (3) then, the skin friction coefficient is found to be 0.001789. Following the method outlined in [4], the skin friction drag coefficient is found to be 0.057.

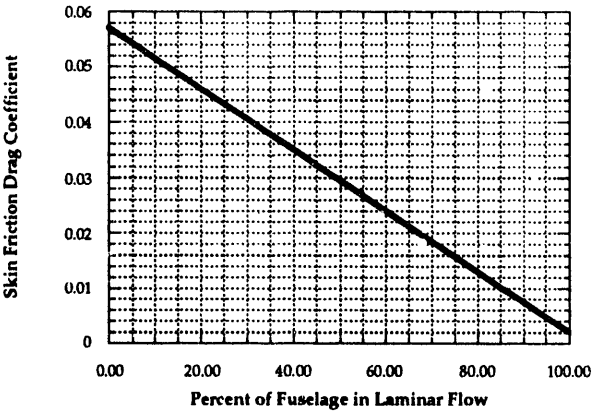

Fig. 5. Effect of Laminar Flow on Skin Friction Drag Coefficient

C. Evaluation of Pressure Drag Coefficient

To see the effects of a properly shaped tail, the data in Table IV are presented. Also note the drag reduction possible with an optimized tail shape. Note that the vehicle being analyzed does not have an efficient base. It would be possible to lower the total aerodynamic drag of the base to 50% the drag of the present design.

TABLE IV
Base Drag Coefficient Comparison

Base Geometry	Base Drag Coefficient
Blunt	.1609
22° Taper*	.0537
Optimized	.0277

* Base is tapered and then cut as shown in Fig. 3.

D. Evaluation of Guideway Interaction Drag

The total undercarriage area adjacent to the guideway is approximately 170m^2. Using the scaling factor from Section 2.D above, this gives a bogie drag coefficient of 0.143. With this value, one can select a range of values from Table II which seem most accurate. A bogie drag coefficient of 0.143 would correspond (for this vehicle) to a bogie drag component of about 52% for this base geometry and about 63% for an optimized base.

E. Summary of Example

Table V gives final values for this configuration and the results for an optimized base configuration. Notice that the optimized base results in an almost 8% savings in total aerodynamic drag

TABLE V
Summary of Example Drag Coefficients

Drag Component	Percentage of total Aerodynamic Drag/Value			
	Present Design		Optimized Design	
Bogie(s) Drag	52	.143	63	.143
Skin Friction Drag	21	.057	27	.057
Pressure Drag	27	.053	10	.028
L and P Drag	+10†	.0253	+10†	..009
Total Drag Coefficient		.264		.237

† of the skin friction and pressure drag

IV. Comparison of Results

A comparison of the drag example vehicle's drag coefficient (as estimated by the above component buildup method) with estimates using the methods of [2] and [3], is presented in Table VI. The result, using (1) from [2], is 8.9% greater than the component buildup result. The Barrows result, which is for a single-car version of the TR07, is 5.7% greater than the component buildup result.

TABLE VI
Summary of Results from Various Methods

Method	Total C_D for Example Vehicle
Component Buildup	0.278
Matsunuma et. al.	0.290
Barrows	0.280
Average	0.282

Two comments can be made about the results presented in Table VI. First, the major weakness of the component buildup method is the uncertainty in the bogie and the bogie/guideway interaction drag. It is also the largest of the three components. Second, the uncertainties of the results based on [2] and [3] are unknown and hence a comparison cannot be used to validate the component buildup method.

V. Conclusions

The component buildup method was formulated to provide a quick, reliable approach to estimating the drag of Maglev vehicles. It includes procedures, commonly used in subsonic aircraft studies, to estimate skin friction and pressure drag. It also includes, however, estimates for the bogie/guideway interaction drag that are based on empirical data that do not reflect design details. The overall results appear reasonable when compared with the results of other reported methods.

The advantages of the component buildup method are:

1. It provides reliable methods for estimating both skin friction and pressure drag. The methods explicitly reflect the configuration and operational characteristics of the vehicle.

2. It demonstrates that the bogie/guideway interaction produces the largest drag component. Since this is the least well understood component, the method identifies this as the area where the greatest effort is required to (a) establish a reliable method of drag estimation and (b) to control, through design, the total vehicle aerodynamic drag.

3. It shows the potential reduction in drag that can be obtained through proper design of the vehicle tail. It also shows that through proper design, the vehicles nose pressure drag is negligible.

VI. References

[1] J.L. Peters, " Aerodynamics of very high speed trains and Maglev vehicles: State of the Art and Future Potential ", *Int. J. of Vehicle Design*, Technological Advances in Vehicle Design Series, SP3, *Impact of Aerodynamics on Vehicle Design*, 1983.

[2] S. Matsunuma, Y. Nagayama, S. Kobayashi, " A Study on the Characteristics of the Aerodynamics of the Magnetically Levitated Transportation System ", West Japan Railway Co., Osaka, Japan, 1989.

[3] T. Barrows, " Vehicle Aerodynamic Drag ", unpublished.

[4] D.P. Raymer, *Aircraft Design: A Conceptual Approach*.. AIAA Education Series, Washington, D.C., 1989.

[5] J. Roskam, *Airplane Design: Part VI*. Roskam Aviation and Engineering Corp., Lawrence, KS, 1990.

[6] A.C. Hammit, The Aerodynamics of High Speed Ground Transportation, Western Periodicals Co., CA,1973.

[7] W.A. Mair, " Reduction of Base Drag by Boat-tailed Afterbodies in Low-Speed Flow ", *The Aeronautical Quarterly*, Vol. XX, 1969.

MAGLEV SECONDARY SUSPENSION USING ELECTROACTIVE FLUIDS

Dilip K. Bhadra and C. Ross Harder
General Atomics, San Diego, California 92186-9784
and
George Mansfield
San Diego State University, San Diego, California 92121

Abstract - The feasibility of a semi-active secondary suspension for a Maglev has been studied in the context of electrorheological fluids (ER-fluids) providing the necessary performance. Such fluids exhibit enhanced shear-stress-bearing capacity in the presence of an external electric field and such response is fast and reversible.

Analytical models have been developed to study the dynamics of Maglev vehicles both in two-degree-of-freedom and multiple-degree-of-freedom configurations together with appropriate modeling of ER-fluids under the dynamic conditions relevant for vehicle performance. The question of ride-comfort has been addressed in the presence of both periodic and stochastic disturbances. Our studies indicate that a semi-active system for the secondary suspension with switching between passive and active algorithms based on sensing frequency and acceleration may be optimal for the range of frequencies appropriate to ride comfort. Results from a computer-controlled subscale experiment carried out on a motion control device using ER-fluid indicate both significant enhancement of forces generated in the device as electric field is turned on together with fast response time of the fluid. Such a device may provide the basis for an innovative and rather inexpensive design for high-performance secondary suspension for a Maglev.

I. INTRODUCTION

For most transportation systems, a major part of system capital cost is for guideway construction. This is particularly true for Maglev with its high speeds and vehicle/guideway interactive propulsion and levitation. Thus, improvements in vehicle suspension performance which allow increased speed, increased construction tolerances and reduced guideway maintenance can have a significant impact upon transportation system economic feasibility. It is not clear whether passive suspension systems, which have been employed in the past for the majority of ground transport vehicles, will be adequate for high-speed Maglev vehicles of the future. Active suspension systems, which may use continuous or intermittent power from an external source, are able to provide improved isolation of the passenger and freight compartment from external force and guideway disturbances.

The major disadvantages of such active suspensions are their need for an external power source, their increased complexity, decreased reliability, increased maintenance level and finally, relatively high cost.

A semi-active suspension system, for example, one using an electrically-controlled fluid (electrorheological fluid or ERF) as discussed in this paper, may provide the necessary control forces under ride environment conditions for a high speed vehicle (like Maglev) without involving the level of complexity and cost of a fully active suspension system.

The purpose of the secondary suspension study of Maglev application is to explore the feasibility of using electroactive fluids as a means of vibration control so as to satisfy the ride comfort criteria for a variety of input disturbances.

A. Passive Systems

A typical passive system provides relatively good control at low frequencies. However, in order to limit resonant peaks in acceleration with high damping a price is paid in terms of high transmissibility and harshness at higher frequencies. This could be dealt with by sensing velocity (and implicitly guide deflection input frequency) and varying damping open loop as vehicle speed changes. The required profile of damping versus frequency will vary depending on basic system parameters such as natural frequencies and mass ratios. Reference [1] has plots for the anticipated situations for maglev periodic inputs and resonances. Examination of these show the feasibility of a speed scheduled damper scheme to meet ride comfort standards. Of course, for transient or random inputs, a single damping would be the only design solution and this has compromise non-optimum results.

B. Active Systems

As opposed to passive systems, active suspensions are

Manuscript submitted March 15, 1993. This work was primarily supported by U.S.D.O.T. under contract #DTFR53-91-C-00063.

able to add energy to the system as required to reduce net vehicle acceleration and/or suspension displacement. When optimal schemes in the form of a "linear quadratic" performance criterion have been applied to SDOF systems for random guideway disturbances, the resulting control law is that of "skyhook" damping, i.e., proportional to the velocity of the sprung mass only.

C. *Semiactive Systems*

"Semiactive" schemes are those in which complex control laws are employed but no "energy adding" hardware is allowed. The result is a sort of "intelligent passive" controller. These arrangements are ideal applications for electrically controllable, ER-fluid, passive dampers. Two examples of semiactive control laws are:

1) Pseudo skyhook or semiactive damping: the damper is not allowed to add energy to (i.e. accelerate) car body mass:

$\dot{Z}_2(\dot{Z}_2 - \dot{Z}_1) > 0$: high damping on car mass

$\dot{Z}_2(\dot{Z}_2 - \dot{Z}_1) \leq 0$: low or zero damping on car mass

where the subscripts 1 and 2 refer to primary and secondary masses, respectively.

2) Relative control: the damper force is set to cancel the spring force at those times when suspension relative displacement and relative velocity act in opposition to each other:

$$F_D = -K(Z_2 - Z_1) \text{ when } (\dot{Z}_2 - \dot{Z}_1) \leq 0$$
$$= 0, \text{ or near } 0, \text{ when } (Z_2 - Z_1)(\dot{Z}_2 \dot{Z}\ 1) > 0$$

D. *Adaptive Systems*

These are special "real time" versions of active or semiactive controllers. Here the suspension parameters are continuously varied ("adapted") in time to provide optimum performance irrespective of inputs or changes in system character, such as change in vehicle payload. The most popular adaptive scheme is the "model reference adaptive control" or MRAC [2].

In the following sections, we first discuss the necessary properties of ER-fluids, and then the dynamical models for a multiple-degree-of-freedom system and the results from the scale-model experiment on ER-fluid dampers.

II. Basic Properties of ER Fluids

ER-fluids are basically combinations of electrically polarizable solids in a non-conducting oil-like medium (e.g., corn starch in silicone oil or lithium polymethacrylate in paraffin oil). In the presence of an external electric field, such fluids exhibit non-Newtonian behavior in the sense that it can withstand a significant amount of shear $\geq$ 1 psi) even under static conditions.

For the most part, ER-fluids have been considered for applications involving shear loading conditions. The typical constitutive behavior of an ER material in shear is shown in Figure 1(a), ER material behavior can be divided into pre-yield and post-yield regions, with these regions defined as those in which the material is strained below and above a critical yield strain (the value of this critical strain is about 1%, in general, for many ER formulations). In the post-yield state, the actual viscosity of the material μ, remains relatively constant as the applied electric field is varied while the property that changed is T_y, the yield stress of the Bingham plastic-like suspension. This idealized behavior is shown in Figure 1(b) and, if one assumes that the shear stress exceeds the yield stress of the material, then the ER material behavior can be represented by the equation:

$$T = T_y + \mu\dot{y}$$

where

T_y = dynamic yield stress
μ = absolute viscosity
$\dot{y}$ = shear rate

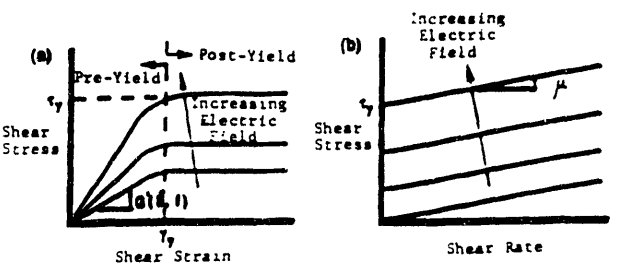

Fig. 1. Typical rheological behavior of an ER material denoting the pre- and post-yield material behavior.

At near zero shear rates the static yield stress dictates behavior. Typically, static yield stress is greater than dynamic yield stress. For the design of devices incorporating ER material in the post-yield state, the principal material properties of interest are the idealized Bingham plastic or dynamic yield stress, the static yield stress and the viscosity. The dynamic yield stress is a strong function of electric field as obtained from experimental results for various fluids.

III. Vehicle and Guideway Dynamic Models

The secondary suspension approach studied here is employed in a two-degree-of-freedom (TDOF) model and

also a multiple-degree-of-freedom model (MDOF), the excitations for each of which are provided by random and periodic inputs representing guideway irregularities.

A. Guideway Model

For the TDOF model the only inputs are guideway deflections and irregularities. The guideway deflections are periodic due to the weight of the constant speed vehicle loading the guideway at and between supports over time. Guideway roughness input Z_0 is assumed stochastic with the power spectral density (PSD) of Z_0 given by

$$\phi(\omega) = \frac{Av}{\omega^2},$$

where

A = roughness parameter
V = vehicle velocity (m/sec)
ω = frequency (rad/sec)

B. Vehicle Model

The lumped-parameter, linear, "quarter-car" model of Fig. 2 is employed for linear analysis and nonlinear computer simulation. A MDOF model, as shown in Figure 3, was selected both for MDOF analysis and simulations of the heave, pitch and roll modes. We assume a 4-corner, point mass bogie setup. Neglecting sway and yaw motions on the ground that they are relatively decoupled from other modes, one can write bogie and car body equations based on the parameters shown in Fig. 3. In terms of degrees of freedom, the MDOF model includes vertical motion of individual bogies and of the car body plus pitch and roll of the car body. Pitch inputs are via heave input with longitudinal eccentricity of car CG and/or front to rear time difference in suspension heave inputs. In order to simulate the actual ER-fluid damping characteristics of the secondary suspension, damping ratios used now become function of the electric field strength and relative velocity.

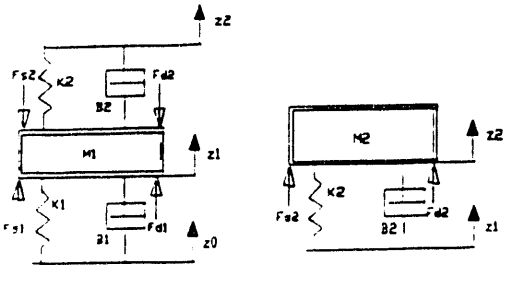

a. Bogie mass free body b. Car mass free body

Fig. 2. Free body diagrams for (a) bogie mass and (b) car body mass in bounce mode (gravitational effects cancelled by initial spring forces).

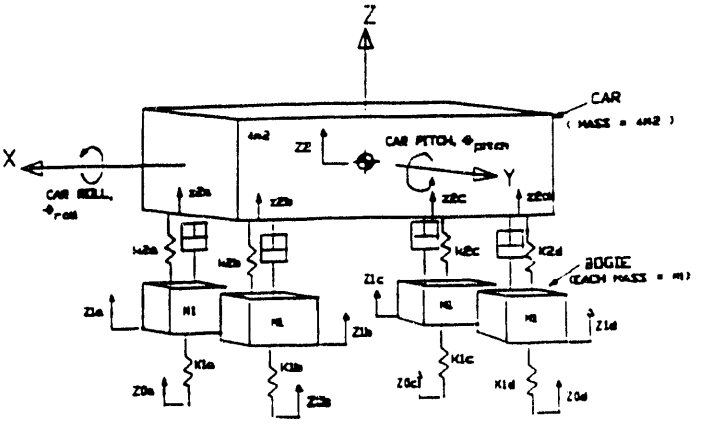

NOTES:

1. CAR MASS = 4 = M2
2. K2a,b,c,d ALL EQUAL
3. K1a,b,c,d ALL EQUAL
4. ALL DAMPERS EQUAL
5. ALL SPRINGS, DAMPERS AT EACH CORNER ARE COLINEAR.

Fig. 3. Final MDOF model of rigid body maglev suspension system.

C. Numerical Modeling

A multipurpose TDOF computer model was developed using TUTSIM software [3]. This software was selected for its compact code, ease of parameter input, multi-variable plotting and built-in optimization routines. In this software, the approach is very similar to analog computer simulations of the past.

III. Results from Analysis

A. Periodic Disturbance

For deterministic periodic inputs due to guideway deflections under load, the secondary suspension must effectively damp resonances and maintain accelerations below comfort standard limits (e.g., ISO standards). Results have been obtained for three types of primary suspensions (viz., sheet guideway and null-flux system and EMS system) with various damping settings and a wide range of disturbance input frequencies for passive, active and semi-active secondary suspensions. Figure 4 shows a typical case for the acceleration response of a null-flux primary suspension system. An ISO 1 hour reduced-comfort limit normalized for the maximum disturbance amplitude of Z_0 = 1 cm was superimposed over the actual acceleration plots. For this amplitude of disturbance, none of the dampers totally satisfied the ISO standard. On balance, in the critical 2 to 7 Hz band, the semiactive system produced the best vibration isolation when compared to the passive system. Low frequency amplitudes of all the three schemes were relatively equal whereas the high frequency "harshness" was lowest for the active case and highest for the passive case.

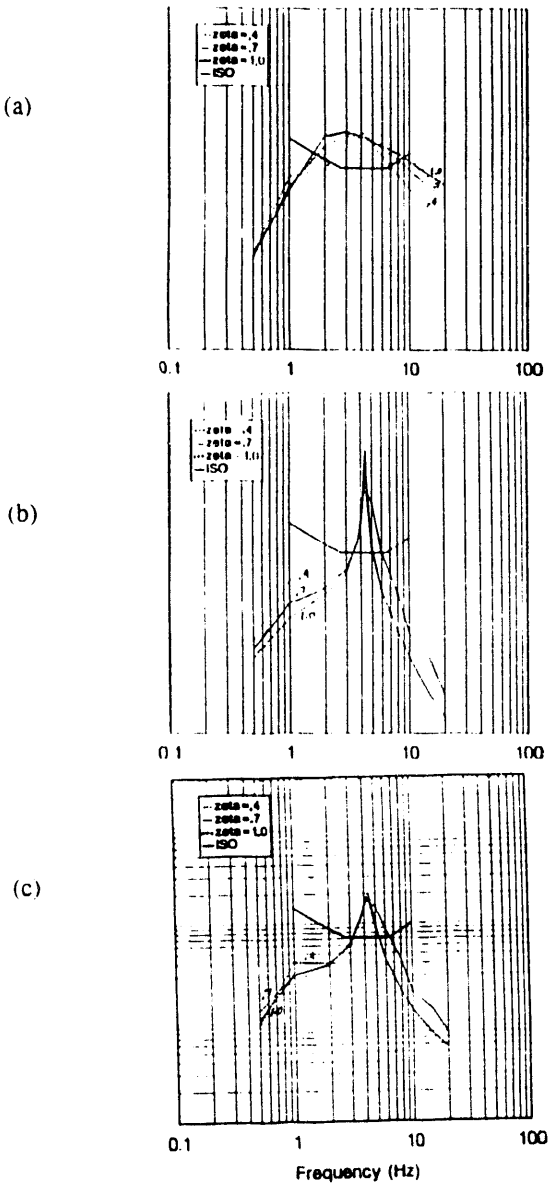

Fig. 4. Null flux guideway disturbance - acceleration response for a. passive damping, b. active damping c. semiactive damping. ISO standard is normalized for an assumed 2.0 cm peak to peak guideway input amplitude.

The quantity ζ_2 denotes the non-dimensional damping coefficient for the secondary suspension.

B. Stochastic Disturbance

The PSD for the acceleration of the secondary mass can be shown to be given by:

$$G(\omega) = \omega^4 \phi(\omega)\, T(\omega)\, T^*(\omega),$$

where T(w) is the displacement transfer function for the

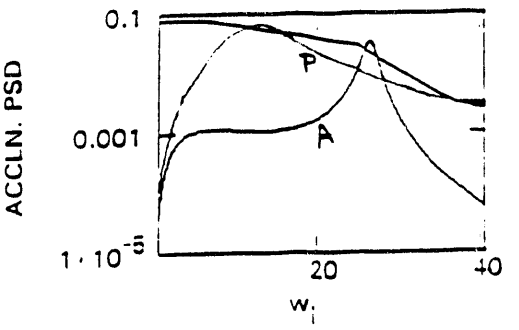

Fig. 5. Acceleration PSD for the secondary mass (for an EDS system with Null-flux guideway) ζ_2 = 1.2 and A - 10^6 m. (UTACV standard and active response Aa) and passive response (P)

TDOF system. Results were obtained for a variety of secondary damping settings and the roughness parameter A for all three primary suspension systems. Figure 5 presents a typical example for a null-flux system and compares the ride quality in terms of the USDOT Urban Tracked Air Cushion Vehicle standards. The active system response stays well below the UTACV limit except around the primary suspension frequency of ~ 4 Hz while the passive system exhibits marginal behavior.

As an example of the MDOF modeling results, Fig. 6 presents comparative response to a pulse, simultaneously at all four bogies, for CG displacement (Z_2) and accelerations $\ddot{Z}_2$, plus $L_s\ddot{\theta}_p$, $W_s\ddot{\theta}_r$, which are the linear contributions to pitch and roll accelerations at the sides and ends of the car. Here, the semi-active damping damps $\ddot{Z}_2$ very well but $L_s\ddot{\theta}_p$ has some sharp spikes prior to settling. A pulse input, in addition to being a classic "transfer function identifier", roughly simulates guideway disturbances such as foreign

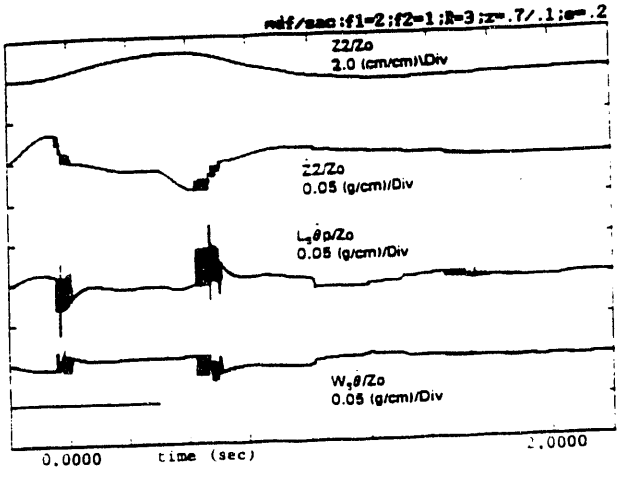

Fig. 6. Guideway pulse input response for semiactively damped, sheet guideway system. Plots of CG displacement and acceleration plus pitch and roll acceleration contributions. CG eccentricities = 20% (x and y).

object build-up, guideway distortion, etc. This particular example does not consider the time difference of front/rear bogie inputs. However, we have studied the effect of such time differences in the more realistic sinusoidal guideway disturbance simulations.

IV. A Subscale Experiment

The subscale test device is illustrated in Figure 7. The device consists of two masses m_1 and m_2 (where $m_2 > m_1$) arranged in a coaxial configuration allowing for one degree of freedom in bounce mode. The mass m_1 (hereafter called assembly #1 or driven mass) is attached to a Ling Dynamics model 411 vibration generator. The mass m_2 (or sprung mass) is attached to assembly 1 with a suitable spring and a cylindrical ER-fluid damper. Each mass assembly is fitted with sensors for acceleration, velocity and displacement sensing. The signals received from each sensor are routed to a computer via A/D converter channels.

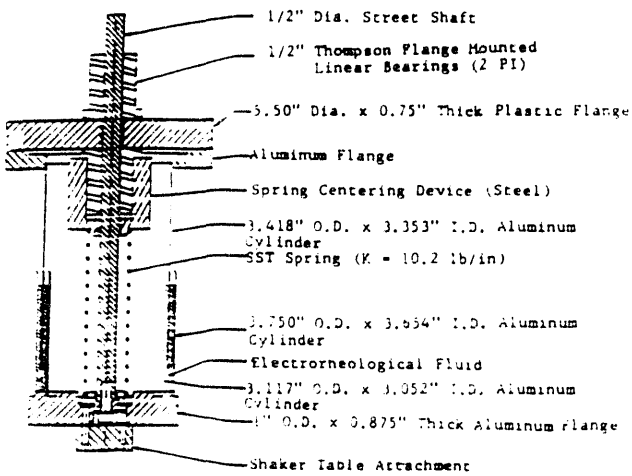

Fig. 7. Engineering drawing of the subscale test device.

The dynamic ER fluid damper tests consisted of the following experiments:

(i) Vibration tests with ER fluid loaded in the gap without voltage applied.

(ii) Vibration tests with the ER fluid energized at a constant voltage.

(iii) Vibration tests with an active control algorithm imposed as discussed earlier (two algorithms were tested which vary the applied electric field).

According to the semi-active scheme employed, the damping force generated during the proper phase of the oscillation is proportional to the absolute velocity of the upper mass, i.e., $F_1 \propto V_2$. In an ER-fluid system, the shearing force developed is proportional to some power of the electric field E:

$$F_1 \propto E^n$$

where $n \sim 1$ (for electric fields in the range of 1-2 kV/mm). To generate a damping force proportional to V_2, one then adjusts the electric field proportional to V_2, the coefficient of proportionality being determined by the maximum electric field strength to be superimposed on the system. The results of these data runs are illustrated in Figure 8 along with data sets representing soft passive damping (no ER voltage applied) and stiff passive damping (constant ER voltage applied). The soft passive damping example is of course the baseline which illustrates the system resonance. The stiff passive damping example indicates good attenuation of the resonance peak, but poor attenuation of higher frequency inputs.

The semiactive control algorithm allows the damper to act as a force generator when the relative velocities are such that the desired force dissipates energy. Under all other conditions, the voltage command is zero and the system behaves in a soft passive mode. As illustrated in the figure, the use of this control algorithm allows for excellent attenuation of the resonant peak and somewhat improved performance at high frequency inputs.

The relative control algorithm was tested in a similar fashion except the voltage command was scaled to the relative displacement of the driven and sprung masses. Data runs were conducted over the same frequency range after a baseline was established. The results are illustrated in Figure 9.

As illustrated in the figure, the relative control algorithm is less effective in attenuating the system resonance but demonstrates improved performance at high frequencies when compared to the semiactive damping algorithm.

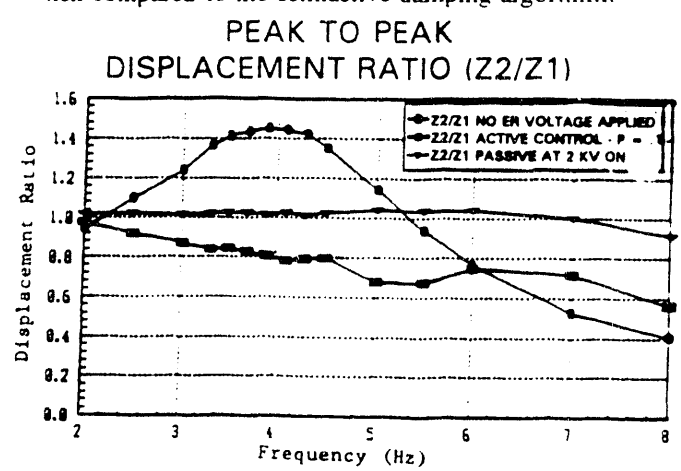

Fig. 8. Experimental transmissibility curves for soft and stiff passive and semiactive control concepts using ER fluids.

A. *Simulation of Semiactive Damper*

The effect of increased yield stress due to an applied field

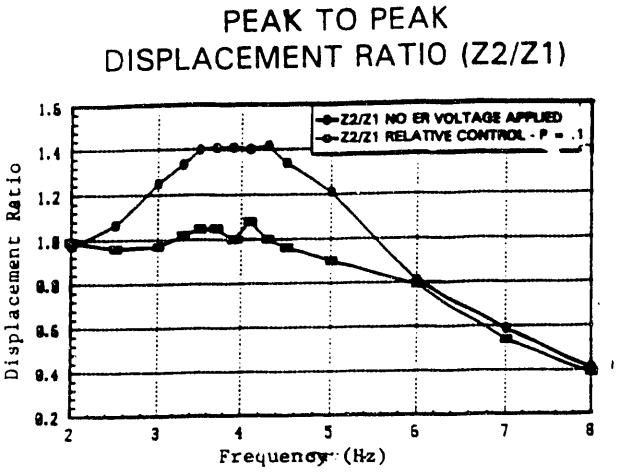

Fig. 9. Experimental transmissibility curves for soft passive and relative damping control algorithm.

was included via a model were for the ER effect. This is given by

$$F_E = K_2 E^n$$

for $E = K_1 \dot{Z}_2$. In the "damper" on state:

$$F_E = K_2 (K_1 \dot{Z}_2)^n = K_E (\dot{Z}_2)^n$$

where $K_E = K_1^n K_2 = 0.7$, $n = 2.0$.

Figure 10 shows the best TUTSIM fit for this model of semiactive damping. The TUTSIM model is not as "harsh" at high frequencies as the physical model. One possible explanation for this is that when the field is turned off (zero ER effect), a residual yield stress in the fluid produces incremental shear transmissibility from Z_1 to Z_2 via the relative velocity Z_1 - Z_2. The test data suggests that an effective solution for the real maglev suspensions is to design the semiactive algorithm to be frequency-dependent, reverting to deenergized, passive damping at high frequencies. This might be achieved by real time spectrum analysis of car

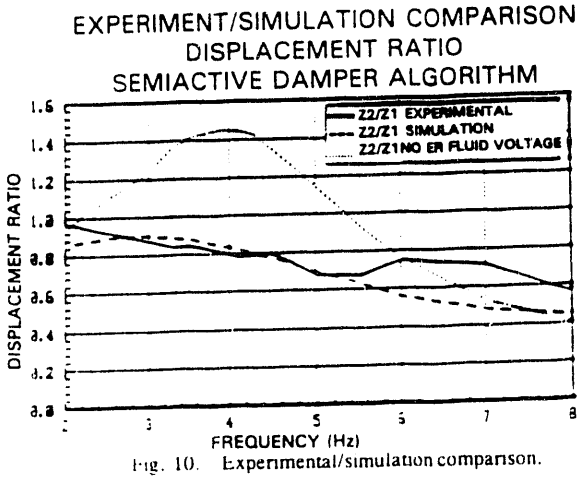

Fig. 10. Experimental/simulation comparison.

acceleration data. This can be implemented inexpensively using state-of-the-art computer hardware and software.

V. Conclusions

The feasibility of a semi-active secondary suspension for maglev vehicles in consideration of passenger ride comfort has been studied, centered on the exploring the utility of electrorheological fluids in a suspension to provide the necessary performance. Some significant conclusions are:

(i) In general, an active or a semi-active system is superior to a passive system, except in some narrow frequency domains.
(ii) A semi-active system with the capability of switching between passive and semi-active control algorithms based on frequency sensing and acceleration may be optimal for the range of frequencies relevant to ride comfort.
(iii) With its fast fluid response time, the ER-fluid, in combination with computer-controlled power amplifiers, exhibits the possibility of its usage in a variety of "adjustable passive" and semi-active control schemes.

The potential benefits for such a secondary suspension for maglev application are:

(i) Provide the necessary ride-comfort with a "rougher" guideway without the complications and expense of a fully active system
(ii) Derive overall savings in system cost as a result of reduced guideway construction costs.

NOTE: Detailed results related to this paper is in Ref. [4].

References

[1] D. N. Wormley et al., "Magnetic Levitation Vehicle-Suspension Guideway Interaction", Technical Memorandum, FRA Contract DIFR53-91-C0062, 1992.
[2] V. V. Chalam, "Adaptive Control Systems", Marcel Dekker (1987).
[3] W. Reynolds and J. Wolf, "TUTSIM Block Diagram Simulation Language", TUTSIM Products, Palo Alto, CA, 1991.
[4] D. K. Bhadra et al., "Adaptive Suspension using ER-Fluid Dampers", General Atomics Report #GA-C21052 prepared under DOT Contract DTFR53-91-C-0063.

Maglev Vehicle Dynamic Interaction With Aerial Guideways[1]

Laurence E. Daniels
Parsons Brinckerhoff Quade & Douglas
Herndon, Virginia 22070

Donald R. Ahlbeck
Battelle
Columbus, Ohio 43201-2693

***Abstract* - This paper presents dynamic interactions between vehicles and aerial structures under high speed operations. The results focus on important design parameters for aerial structures under high speed operations.**

I. Introduction

Many maglev concepts have design operating speeds in excess of 200 km/h which is the current upper limit of US. engineering experience. The lack of experience above 200 km/h is reflected by restrictions in US. structural design codes and guidelines for railroad and transit aerial structures and bridges to operating speeds less than 200 km/h. A comparison of impact factors for speeds less than 160 km/h (Figure 1) shows a wide range of values reflecting the industry's uncertainty concerning impact factors even at moderate speeds.

Since the late 1960s, investigators have explored the dynamic implications of high speed vehicle-guideway interactions [2] through [12]. These studies identify the mass ratio and the crossing frequency ratio as parameters that relate dynamic response to beam properties.

These studies suggest that live load dynamic amplification will be negligible for the following criteria:

- mass ratios less than 0.30
- Crossing frequency ratios less than 0.20 [11] or 0.25 [4]

However, the validity of these values and the relation of these ratios to a design impact factor remain to be established for specific types of systems. Many of the cited studies do not address maglev suspensions and are limited by ignoring one or more of the load elements (aerodynamic effects, etc.) that contribute to an impact factor. The results in this paper include the important load influences for the maglev configurations currently available.

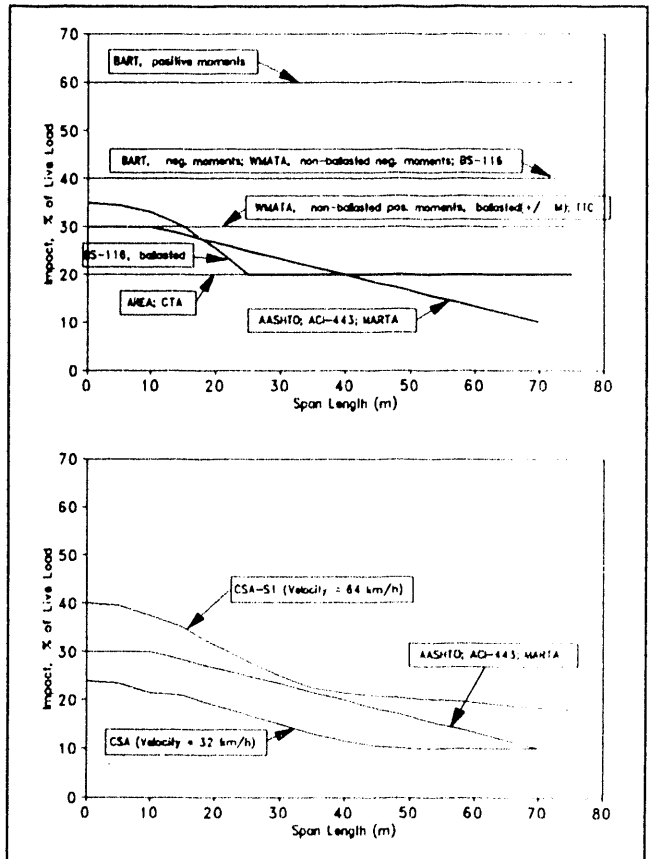

Fig. 1. Comparison of Impact Factors. AASHTO = American Association of State Highway and Transportation Officials; ACI-443 = American Concrete Institute Committee 443; AREA = American Railroad Engineering Association; BART = Bay Area Rapid Transit; BS-116 = British Standards Institute; CSA-S1 = Canadian Standards Association; CTA = Chicago Transit Association; MARTA = Metropolitan Atlanta Rapid Transit Authority; TTC = Toronto Transit Commission; WMATA = Washington Metropolitan Area Transit Authority.[1]

II. Approach

The approach develops 5 guideway designs with provide a representative range of beam parameters that properties representative of maglev structural designs. The approach includes the structural parameters of the steel V-shaped guideway by Transrapid as a reference. The beam designs are to US structural codes andguidelines (except the German Transrapid guideway) for several reasons:

[1]Manuscript received March 15, 1993. The original study [13] was supported by the U.S. Federal Railroad Administration and the New York State Energy Research & Development Administration.

- The designs and the parameters that come from the designs are credible reflections of current practice;
- The structures have a common base of comparison to structures that are designed for contemporary rail transportation;
- The analysis will illustrate the dynamic performance of beams that are designed to US standards and practices;
- The analysis will illustrate the dynamic performance differences between foreign and US standards;
- The maglev system (Vehicle, propulsion, controls) used in this country could be a foreign design, but it must operate on a guideway conforming to US standards.

The study team accepted the following criteria for the development of the beam designs:

- Maximum mid-span deflection of the beam is less than the span length divided by 1000.
- The Impact Factor is 30% of the live load (i.e. of the vehicle weight).

Representative span lengths are chosen as 21 m and 39 m.

All analysis is conducted using one vehicle configuration for both EMS- and EDS-type vehicles. The vehicle parameters are based on capacity requirements, vehicle structural requirements, clearance requirements and on-board equipment housing requirements[13]. The primary vehicle parameters are:

- Vehicle weight (full capacity): 45,360 kg
- Overall length: 18 m
- Body width: 3.5 m
- Body natural frequency: 8 Hz

The guideways were chosen to provide practical designs over a range of materials and guideway properties. The beams selected are illustrated in figure 2. The maglev types are the electromagnetic system (EMS), or "attractive" type, and the electrodynamic system (EDS), or "repulsive" type. The guideway choices accommodate either type.

III. Analysis

The dynamic analysis entailed development of computer models for each of the maglev types including the parameters for multi-vehicle trains, and multiple spans

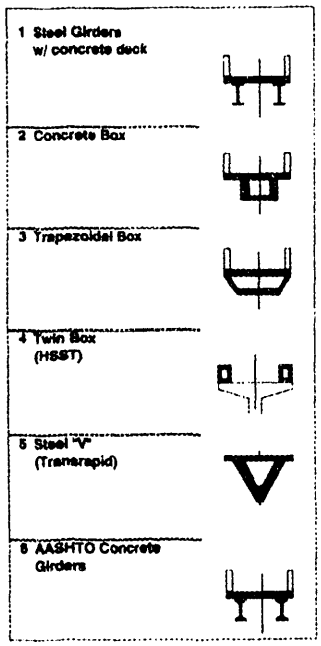

Fig. 2. Selected Guideway Structures

(simple or continuous), in each of the three principle planes of motion. The EMS vehicle model has 22 degrees of freedom and the EDS vehicle model is represented by 14 degrees of freedom. These models are shown schematically in Figure 3.

The different vehicle/guideway structure combinations were evaluated by three basic criteria:

- Passenger ride comfort
- Loads and bending moments on the beam.
- Peak acceleration response of the beam.

Ride comfort limits were based on the International Standards Organization (ISO 2681) one-hour reduced comfort limits in the most sensitive frequency range. These are summarized as:

- Vertical -- 0.036 g rms (4 to 8 Hz)
- Lateral -- 0.025 g rms (1 to 2 Hz)

These values refer to one-third octave band rms values of random vibration. If the response is relatively discrete sinusoids, as it indeed appears to be, it is reasonable to increase these levels to the following peak values:

- Vertical -- 0.051 g peak (4 to 8 HZ)
- Lateral -- 0.036 g peak (1 to 2 Hz)

[Reference [13] fully describes the vehicle, the guideway and the analysis.]

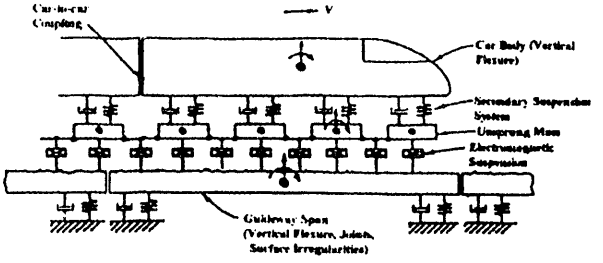

Model of EMS-Type Vehicle on Guideway

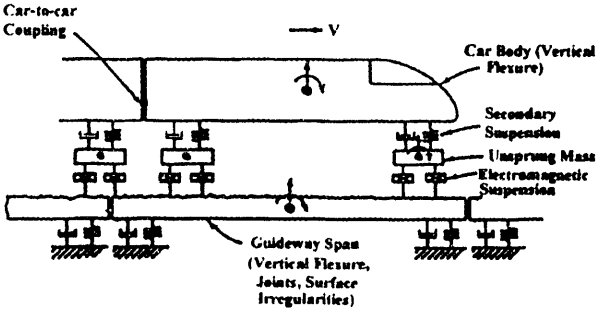

Model of EDS-Type Vehicle on Guideway

Figure 3. Maglev Vehicle Models

IV. RESULTS

A. Comparison of EMS and EDS Maglev Dynamic Responses

The two fundamental maglev system approaches, EMS and EDS, have completely different suspension geometries as well as suspension characteristics. The EMS guideway gap is smaller than the EDS gap which produces a much higher electromagnetic suspension stiffness, resulting in much closer dynamic coupling than the EDS approach.. The EMS design approximates a uniform suspension along the full vehicle length to achieve levitation, while the EDS design is closer to discrete load points on the quideway similar to conventional rail wheel loading.

These differences in configuration and in coupling stiffness produce quite different vehicle and guideway interactive responses between the two different maglev systems. Ride quality of the two vehicle types is compared in Figures 4 through 12; guideway accelerations are compared in Figures 13 through 19.

1) Car Body Accelerations

a) Simply Supported Spans, 21 m Span Length: On the more standard guideway designs (Guideways 1, 2, 3, and 6), the ride of the EDS-type vehicle has a vertical characteristic resonance between 200 and 300 km/h with amplitudes higher than the one-hour ride comfort limit of 0.51g peak. In contrast, the EMS-type vehicle remains below the desired ride comfort limit up to about 400 km/h, above which the acceleration levels increase monotonically with speed.

On the two light-weight Guideways 4 and 5, Figures 6 and 7, the 200 to 300 km/h vertical acceleration resonance is evident for Guideway 4 in the EDS system but more than twice the desired comfort amplitude, while Guideway 5's response is broader and at higher speed, peaking at 350 km/h and slightly exceeding the comfort limit at the peak resonance. On both Guideways 4 and 5 (particularly Guideway 5), the EMS-type vehicle generates vertical acceleration levels well above the desired limit over the whole speed range of 200 to 600 km/h.

The comparison highlights two separate responses between EMS and EDS system dynamics for all guideways: The EDS system produces a resonance in the 200 to 400 km/h speed range but has generally much lower response outside the resonance range; the EMS system responds with increasing accelerations with increasing speeds, but largely without the EDS 200 - 400 km/h resonance. The slope of the curves steepens at a speed between 400 and 500 km/h for the EMS-type vehicle depending on the configuration.

b) Simply Supported Spans, 40 m Span Length: Figure 9 shows similar results for longer span lengths, except the maximum acceleration levels are higher than the shorter span lengths and the resonance conditions occur at significantly lower speeds.

c) Two-Span Continuous Structures: Continuous spans reduce the car body accelerations considerably, illustrated in Figures 10 and 11. The resonance speed shifts slightly for the EDS system; the increase in EMS slopes at speeds above 400 km/h is mitigated from simple spans. While not all configurations are analyzed, it is expected that the continuous span approach to design provides favorable dynamic performance over simple span treatments.

2) Beam Accelerations

a) Simply Supported Spans, 21 m Span Length: As for the carbody response, the mid-span beam response to the EDS-type vehicle is typified by a pronounced resonance in the 250 to 400 km/h speed range. For standard guideway configurations (Figure 12, Guideway 1; Figure 13, Guideway 2, which is representative of Guideway 3, also; Figure 16, Guideway 6), peak accelerations of 0.5 to

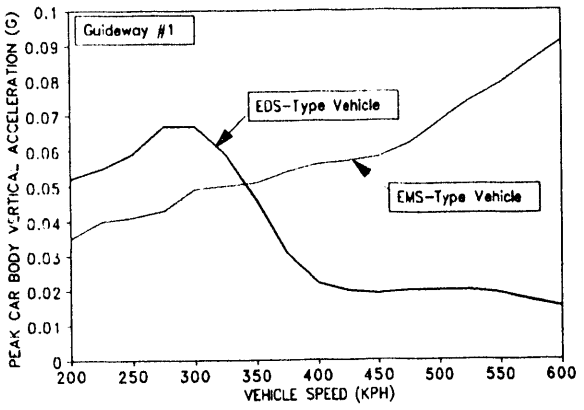

Figure 4. Steel Girder with Concrete Deck, 21 m Span, Carbody Vertical Accelerations

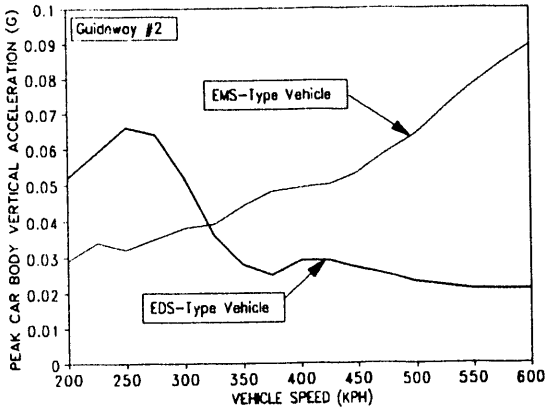

Figure 5. Concrete Box Guideway, 21 m Span, Carbody Vertical Accelerations

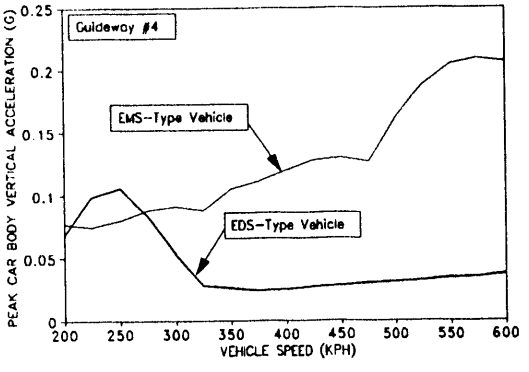

Figure 6. Twin Box Beam (HSST), 21 m Span, Carbody Vertical Acceleration

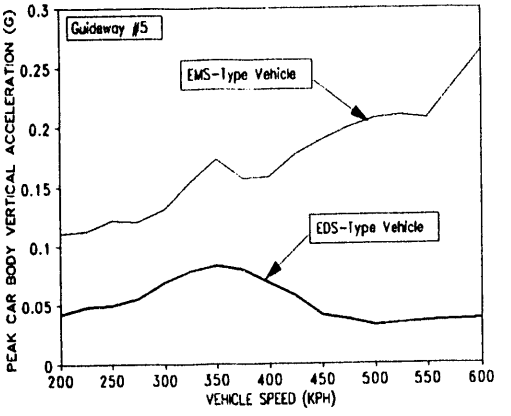

Figure 7. Steel "V" Guideway (Transrapid)21 m Span, Carbody Vertical Accelerations

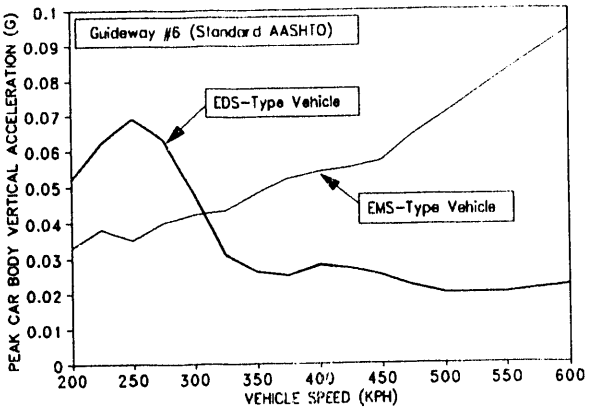

Figure 8. AASHTO Concrete Girders. 21 m Span, Carbody Vertical Accelerations

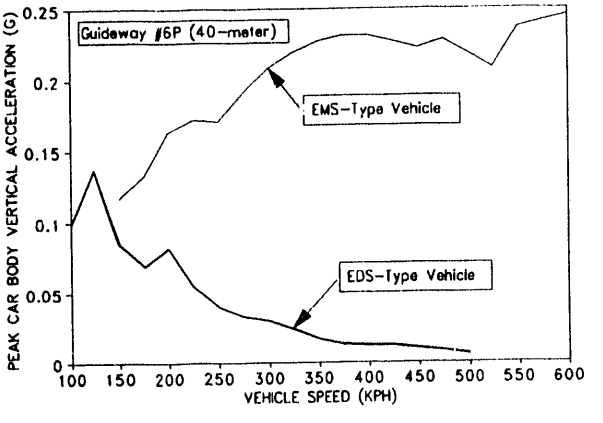

Figure 9. AASHTO Concrete Girders, 40 m Span, Carbody Vertical Accelerations

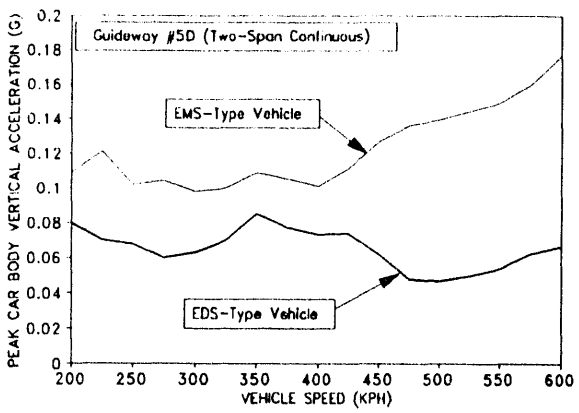

Figure 10. Steel "V" Guideway (Transrapid), Two-Span Continuous Guideway, Carbody Vertical Accelerations

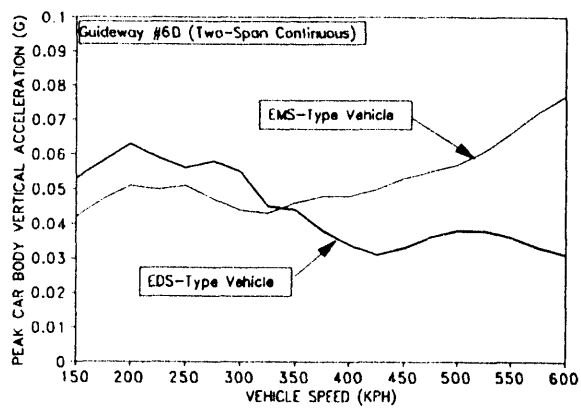

igure 11. AASHTO Concrete Girders, Two-Span Continuous Guideway, Carbody Vertical Accelerations

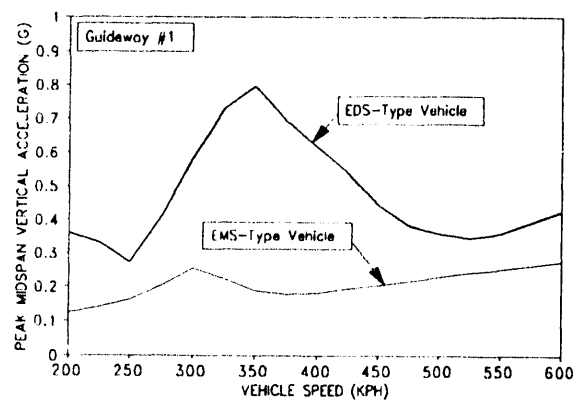

Figure 12. Steel Girder Beams with Concrete Deck, 21 m Span, Mid-Span Vertical Beam Accelerations

0.8 are developed at those resonant speeds. The light-weight guideways (Guideway 4 and 5) are simply overwhelmed by the more massive vehicle, and peak mid span acceleration levels over 1 g (Figure 14, Guideway 4) and over 2 g (Figure 15, Guideway 5) are predicted.

The EMS-type vehicle, with its distributed load, produces much lower levels of guideway vertical acceleration. In general, the mid span response remains at or below the desired impact factor levels for the EMS-type vehicle.

b) Simply Supported Spans, 40 m Span Length: The response of the longer (40 meter) simply-supported beam, Guideway 6P, is shown in Figure 17. Here the response for both vehicles remains within normal impact factor limits of 0.3g up to 400 km/h. Above this speed, the EMS-type vehicle generates progressively higher response levels. It must be noted, however, that higher modal resonsances of the beam not included in the current model (4^{th} bending mode and higher) may come into play at these higher speeds.

c) Two-Span Continuous Structures: The effects of two-span continuous beams (a 43-meter beam with a center column support) on guideway beam response are shown in Figures 18 and 19 for Guideways 5D and 6D. In both cases, reductions in response level are achieved over the simply-supported spans. On light-weight Guideway 5D, the EDS-type vehicle develops mid-span acceleration levels well above the desired 0.3g limit. The beam accelerations for the EMS-type vehicle increases with speed while staying below the 0.3g limit up to about 450 km/h. On Guideway 6D, both vehicles stay below the limit, although the EDS-type vehicle again produces generally higher response levels and the EMS vehicle demonstrates increased accelerations above 450 km/h.

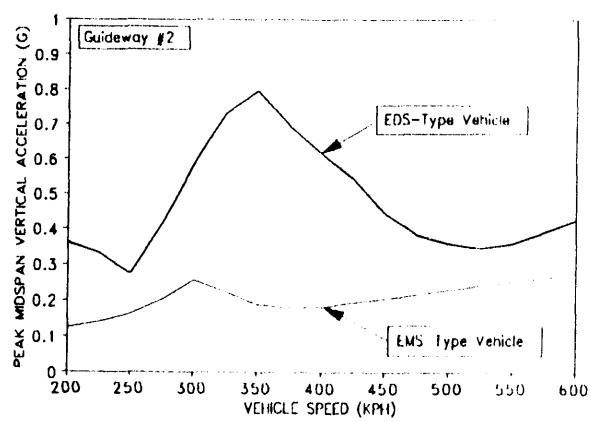

Figure 13. Concrete Box Guideway, 21 m Span, Mid-span Vertical Beam Accelerations

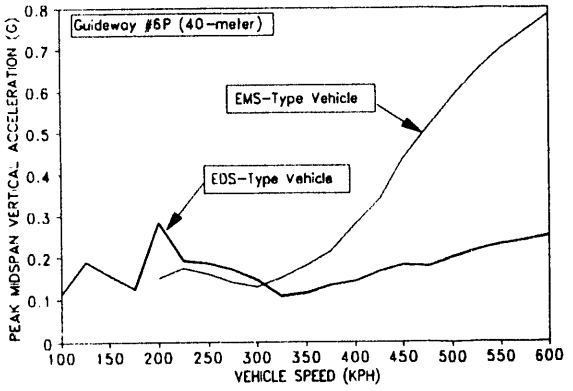

Figure 14. AASHTO Concrete Girders, 40 m Span, Mid-Span Vertical Beam Accelerations

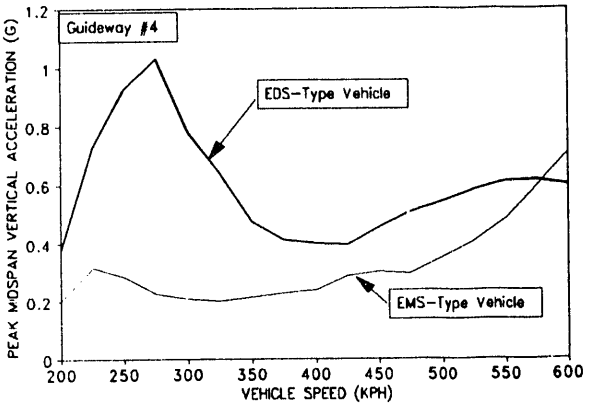

Figure 15. Twin Concrete Box Beam Guideway (HSST), 21 m Span, Mid-Span Vertical Beam Accelerations

V. Discussion

The results show the trade-off between the two maglev system types where the stiffer suspension of the EMS-type levitation creates a more severe ride quality but a benign beam dynamic response. In contrast, the "softer" EDS-type levitation suspension produces generally acceptable ride quality at the expense of severe, and in some cases unacceptable, beam responses.

The figures in the foregoing plots indicate there may be two types of dynamic responses: The first is a resonance that peaks between speeds of 100 km/h and 400 km/h, with significantly lower responses at

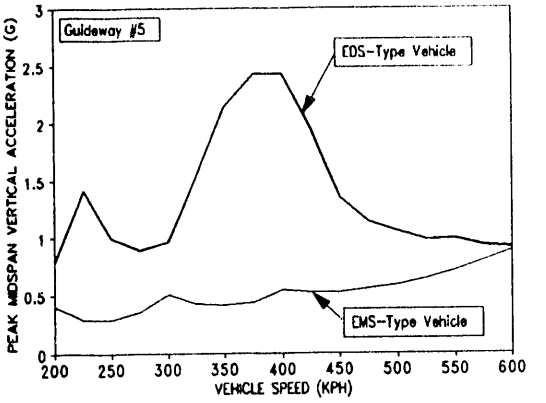

Figure 16. Steel "V" Guideway (Transrapid), 21 m Span, Mid-Span Vertical Beam Accelerations

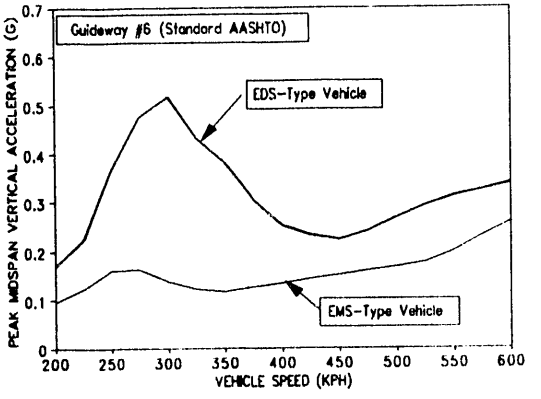

Figure 17. AASHTO Concrete Girder, 21 m Span, Mid span Vertical Beam Accelerations

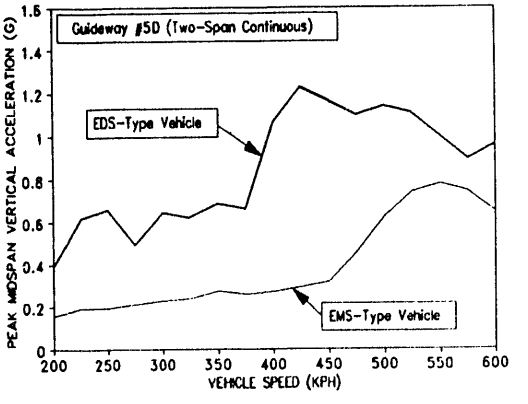

Figure 18. Steel "V" Guideway (Transrapid), Two-Span Continuous Guideway, Mid-Span Vertical Beam Accelerations.

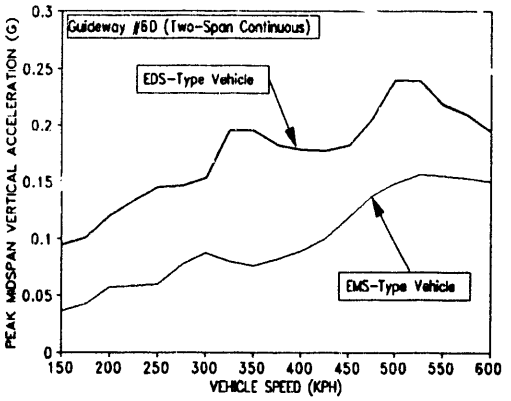

Figure 19. AASHTO Concrete Girders, Two-Span Continuous Guideway, Mid-Span Vertical Beam Accelerations

other speeds; the second is an increase in response with speed that appears to have a critical change in acceleration/speed slope around 450 km/h for many of the configurations analyzed.

The indicator for the resonance between 100 and 400 km/h is the mass ratio, R_{mass}, of the vehicle, $m_{Vehicle}$, and the guideway beam, m_{Beam}:

$$R_{mass} = \frac{m_{Vehicle}}{m_{Beam}} \qquad [1]$$

The indicator for the general increased response with increasing speed is the crossing frequency ratio, *CFR*, using the span's fundamental natural frequency, f_{beam}, speed, V, and span length, $length_{span}$:

$$CFR = \frac{\frac{V}{length_{span}}}{f_{beam}} \qquad [2]$$

Table A (Appendix) provides the simple-span mass ratio for each of the beams used in this study where the vehicle mass is the sprung mass and the beam mass is the mass of the span excluding its support (piers, etc.). The table lists the maximum acceleration between 100 to 400 km/h for each configuration, assuming the resonance in this range is associated with the mass ratio parameter. The maximum beam accelerations in Table A generally increase with mass ratio, illustrated in Figure 20. and the impact ratio must be stated separately for the different maglev suspension types. Acceptable beam designs and vehicle configurations are those systems producing guideway accelerations below the desired value of 0.3g (for these beam designs).

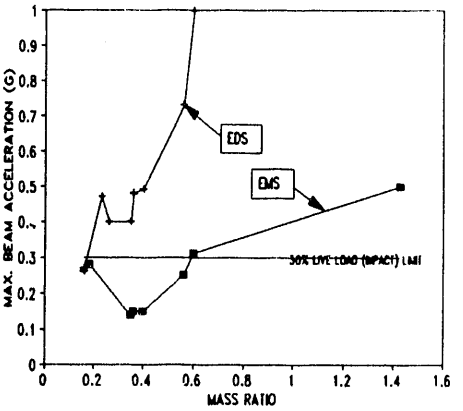

Figure 20. Maximum Accelerations vs. Mass Ratio for Responses between 100 to 400 km/h

The crossing frequency ratio (*CFR*) states that beam deflections increase with the coincidence of speed, span length and beam natural frequency. Wormley, in several papers, suggests that deflection amplitudes increase as CFR approaches a value of 1, but the peak amplitudes may not necessarily occur at that value, rather the peak deflections occur between *CFR* = 1.2 and 1.4.

Table B (Appendix) lists the values of CFR at the allowable impact factor, 0.3g, and the speed at which that value of CFR occurs. The purpose of this table is to determine if there are designs which create an excessive acceleration due to crossing frequency resonance. The results in Table B show that the CFR at 0.3g beam acceleration are above a value of one, generally confirming Wormley's statements, and the crossing frequency resonance increased significantly above speeds of 450 km/h. For all beams except beam design 5, it appears that the designer may use beam designs that have a *CFR* equal or less than 1 if the mass ratio is below an appropriate value for impact factor criteria.

For the configurations analyzed in this work, the design parameters for an Impact Factor of 1.3 (30% of sprung mass) are:

- *CFR* equal to or less than 1
- Mass Ratios less than the Table C values

Table C
Mass Ratio Limits for 30% Impact Factor

Span Length (m)	Maglev System Type	
	EMS (Mass Ratio)	EDS (Mass Ratio)
21	0.60	0.30 [Note 1]
39	0.30 [Note 2]	0.18

Notes for Table C:

1. The maximum mass ratio value available in the study is 0.26 and did not generate 0.3g accelerations below CFR = 1.0
2. The minimum mass ratio value available in the study is 0.35 with all beams including the one with a 0.35 value exceeded the 0.3g acceleration limit. Therefore some lower value is needed than 0.35.

VI. Conclusions

Based on analysis of 6 guideway beams and two separate levitation methods, two general types of resonance occur at the speeds contemplated for maglev operations. These two resonance types are related to (1) the mass ratio of the vehicle and the guideway, and (2) the crossing frequency ratio. The paper discusses how these resonance mechanics may be associated with the design criteria for guideway structural design. The paper offers candidate parameter values for these ratios, based on the configurations studied.

References

[1] R.A. Dorton, H.N. Grouni, "Review of guideway design criteria in existing transit system codes," *ACI Journal*, April 1978, pp. 134 - 144.

[2] W.S. Chiu, D.N. Wormley, R.C. Smith, H.H. Richardson, "Coupled dynamic Interactions between high speed ground transport vehicles and discretely supported guideways," U.S. DOT, Report PB 199 136, 7/70, 117 pgs.

[3] W.S. Chiu, R,G. Smith, D.N. Wormley, "Influence of vehicle and distributed guideway parameters on high speed vehicle-guideway dynamic interactions," *ASME Journal of Dynamic Systems, Measurement and Control*, March 1971, pp. 25-34.

[4] H.H. Richardson, D.N. Wormley, "Coupled dynamics of transportation vehicles and beam-type elevated guideways," *AMD Vol. 5, American Society of Mechanical Engineers, NY*, 1973, pp 1-30.

[5] H.H. Richardson, D.N. Wormley, "Transportation vehicle/beam-elevated guideway dynamics interactions: A state-of-the-art review," *ASME Journal of Dynamic Systems and Control*, June 1974, pp. 169-179.

[6] C.C. Smith, et al, "Multiple continuous span elevated guideway - vehicle dynamic performance," *ASME Journal of Dynamic Systems, Measurement, and Control*, March 1975, pp 30-40.

[7] D.N. Wormley, C.C. Smith, A.J. Gilchrist, "Multispan elevated guideway design for passenger transport vehicles," U.S. DOT, two volumes: Report PB 253 008 (Volume I) and Report PB 253 009 (Volume II), April 1975.

[8] J.K. Hedrick, R.J. Ravera, J.R. Anderes, "The effect of elevated guideway construction tolerances on vehicle ride quality," *ASME Journal of Dynamic Systems, Measurements, and Control*, December, 1975, pp. 408-416.

[9] D.N. Wormley, J.K. Hedrick, et al, "Elevated guideway cost-ride quality studies," *Proceedings, ASCE Specialty Conference on Advances in Civil Engineering*, Raleigh, N.C., 5/19/77, ASCE NY 1977, pp 150-154.

[10] D.N. Wormley, M.L. Naqurka, G. Isaacs, "Rail transit train/elevated structure dynamic interactions," December 1981, prepared for UMTA/DOT (report number not available), 98 pgs.

[11] D.U. Maotoh, "Investigation of structural design criteria for automated transit aerial guideways," U.S. DOT/UMTA Report UMTA-IT-06-0311-84-1, April, 1984 (available through NTIS as report number PB 4196419).

[12] J.F. Wilson, "Optimum design methodology for elevated transit structures," October 1981 (publication information unknown).

[13] L.E. Daniels, D.R. Ahlbeck, Z.J. Stekly, G.M. Gregorek, "Influence of guideway flexibility on maglev vehicle/guideway dynamic forces," U.S. Department of Transportation, Federal Railroad Administration, National Maglev Initiative, Report DOT/FRA/NMI-92/09, July 1992.

APPENDIX

TABLE A
MASS RATIO vs. MAXIMUM BEAM ACCELERATION

Guideway Description	Span Length (m)	Guideway Mass per Span (kg)	Mass Ratio (m_v/m_b)	Maximum Beam Accelerations EMS (g)	EDS (g)
1 Steel Girders	21	63,500	0.56	0.25	0.73
w/ concrete deck	39	136,208	0.26	*	0.40
2 Concrete Box	21	101,918	0.35	0.14	0.40
	39	218,760	0.16	NA	0.26
3 Trapezoidal Box	21	88,583	0.40	0.15	0.49
	39	199,891	0.18	0.47	NA
4 Twin Box	21	59,056	0.60	0.31	1.00
(HSST)	39	153,309	0.23	NA	0.47
5 Steel "V" (Transrapid)	24	25,001	1.43	0.50	NR
6 AASHTO Concrete	21	98,107	0.36	0.15	0.48
Girders	39	218,760	0.16	*	0.27

NA = Not Analyzed
NR = Not Relevant
* = Not meaningful, no significant resonant peak between 100 and 400 km/h.
Vehicle Sprung Mass for mass ratio = 35,700 kg

Table B
CROSSING FREQUENCY RATIOS
at Beam Accelerations of 0.3g and Speeds over 400 km/h

Guideway Description	Span Length (m)	Span Natural Frequency (hz)	CFR & Speed at which 0.3g exceeded EMS Speed (km/h)	EMS CFR	EDS Speed (km/h)	EDS CFR
1. Steel Girder	21	7.4	600	1.07	550	0.98
	39	2.9	440	1.08	500	1.22
2. Concrete Box	21	6.8	600	1.17	550	1.07
	39	3	NA		500	1.19
3. Trapezoidal	21	7.2	600	1.1	550	1.01
Box	39	3.1	NA		500	1.15
4. Twin Box	21	5.3	475	1.18	550	1.37
(HSST)	39	2.2	NA		500	1.62
5. Steel "V" (Transrapid)	24	7	250	0.41	NA	
6. AASHTO	21	6.4	600	1.24	550	1.14
Girder	39	2.5	420	1.2	500	1.42

NA = Not Analyzed

Modeling and Control of Maglev Vehicles with Aerodynamic and Guideway Disturbances

K. Flueckiger, S. Mark, and D. McCallum
The Charles Stark Draper Laboratory, Inc.
555 Technology Square
Cambridge, MA 02139-3563

Abstract – A modeling, analysis, and control design methodology is presented for maglev vehicle ride quality performance improvement as measured by the Pepler Index. Ride quality enhancement is considered through active control of secondary suspension elements and active aerodynamic surfaces mounted on the train.

To analyze and quantify the benefits of active control, the authors have developed a 6 degree-of-freedom lumped parameter model suitable for describing a large class of maglev vehicles, including both channel and box-beam guideway configurations. Elements of this modeling capability have been recently employed in studies sponsored by the U.S. Department of Transportation (DOT).

A perturbation analysis about an operating point, defined by vehicle and average crosswind velocities, yields a suitable linearized state space model for multivariable control system analysis and synthesis. Neglecting passenger compartment noise, the ride quality as quantified by the Pepler Index is readily computed from the system states. A statistical analysis is performed by modeling the crosswind disturbances and guideway variations as filtered white noise, whereby the Pepler Index is established in closed form through the solution to a matrix Lyapunov equation. Data is presented which indicates the anticipated ride quality achieved through various control arrangements.

1. Introduction

A maglev vehicle's suspension system is required to maintain the primary suspension air gap while minimizing passenger compartment vibrations in the presence of guideway irregularities and aerodynamic disturbances. It must meet these requirements while: (1) minimizing the size of the required air gap so that more efficient lift magnets can be employed; (2) minimizing the stroke length of the secondary suspension so that vehicle frontal area and drag are as small as possible; (3) minimizing the size, weight, and required power of active suspension elements. Unfortunately, these design goals conflict with the desire to increase the allowable guideway roughness (to reduce guideway cost) and maximize the crosswind disturbance rejection. Active control offers great potential to improve suspension performance. Constructing a maglev transportation system, or even a short test section, is a very expensive venture. Therefore, it is cost effective to develop analytic tools that can predict trade-offs between the various conflicting system requirements and performance metrics. This allows design alternatives to be examined before building either an actual system or scale model. Unfortunately, the scaling properties associated with magnetic systems precludes construction of accurate maglev vehicle scale models.

Manuscript received 18 March 1993. This work was supported in part by Draper Independent Research and Development project #463.

In this paper we describe a modeling, analysis, and control design methodology specifically for ride quality improvement as measured by the Pepler Index. We consider a generic EDS type of maglev vehicle having a null flux primary suspension and bogies. This is a variation of the vehicle proposed by the Bechtel consortium's System Concept Definition study [1]. The model incorporates front and rear bogies, each having roll but no pitch or yaw dynamics. The guideway disturbance is modeled in three directions (vertical, lateral, and roll) as linear systems driven by white noise. A crosswind disturbance, which acts against the side of the vehicle, is also modeled in this fashion. We consider control authority produced by an active secondary suspension consisting of actively controlled elements (hydraulic or electro-mechanical actuators) that exert forces between the vehicle and its suspension bogies. We also analyze the potential benefits of actively controlled aerodynamic surfaces implemented in conjunction with the conventional secondary suspension. The aerodynamic control surfaces considered here are winglets that exert forces directly on the vehicle body, which, due to high vehicle operating speeds, can produce reasonably large forces when modestly sized. Aerodynamic control surfaces have the advantage of exerting forces directly on the vehicle without reaction forces on the bogies.

Wormley and Young developed a heave and pitch model of a vehicle subjected to simultaneous guideway and external (such as wind) disturbances [2]. A methodology for optimizing the performance of passive suspension in the presence of these simultaneous disturbances was derived and the results evaluated. Guenther and Leonides developed a multiple degree-of-freedom model for a maglev vehicle that includes front and rear bogies, with a time-delayed guideway disturbance to the rear bogie [3]. A control system was developed based on the solution to the stochastic optimal control problem. Gottzein, Lange, and Franzes developed a secondary suspension model with an active control system for a Transrapid type EMS vehicle [4]. A Linear Quadratic Gaussian (LQG) controller was developed for the vertical direction.

The research presented here is a natural extension of the works cited above to provide an incorporated 6 degree-of-

freedom model that includes guideway irregularities and aerodynamic effects. The remainder of this paper is organized as follows: §2 contains an overview of the model employed in our analysis; §3 hosts a discussion of the control system analysis and design methodology employed by the authors to obtain results given in §4; §5 concludes with summary remarks about and consequences of our findings.

2. Analysis Model Overview

Key elements of the analytic model developed for ride quality analysis and control system synthesis are presented within this section. Assumptions imbued in the modeling process are stated explicitly. However, for the sake of brevity, a rigorous treatment of vehicle dynamics is not developed here. The interested reader is referred to [1] and [5] for a more lengthy discussion.

A depiction of the maglev system under discussion is given in Fig. 1, which shows the vehicle body suspended on two bogies. The bogies contain superconducting magnets required for the primary suspension that suspends the bogies relative to the guideway. The secondary suspension is composed of passive spring and damper elements as well as active components that exert forces between the bogies and the vehicle body. We assume that the primary and secondary suspension elements exert forces in the vertical and lateral directions, as well as roll torque. Additional control authority is provided by six active aerosurfaces mounted on the train.

Disturbances to the system are guideway irregularities and aerodynamic forces due to crosswinds. The guideway is assumed to be perfectly rigid, but with an irregular surface that can be described by three sets of independent statistics: one each for vertical, lateral, and roll disturbances. For analysis purposes, we assume a worst case scenario where crosswind disturbances act in the lateral direction.

We assume that the vehicle forward velocity, V, is constant and that there is no coupling between the magnetic propulsion and levitation systems. The vehicle body and bogies are permitted to move in the vertical and lateral directions, and also to roll. The vehicle body has the additional freedom to yaw and pitch. Variations about the vehicle's forward velocity are not included in the model. The allowable directions of motion are sketched in Figures 2 and 3, where: the variable y represents the lateral direction, z vertical, ϕ roll, θ pitch, and ψ yaw. The lack of bogie yaw and pitch dynamics is not seen to be a major analytic deficiency. The torque on the vehicle body due to bogie yawing is expected to be small compared to the torque on the vehicle due to the lateral displacement of the bogie. This is due to the significantly larger moment arm about the vehicle body's center of gravity (CG). A similar argument applies to bogie pitch. In conjunction with this restriction, there is no finite magnet length filtering of the guideway disturbances, as might be the case for an actual vehicle. The following additional assumptions are made: the CGs of the vehicle body and bogies are in the geometric center of the respective bodies, both laterally and longitudinally; the vehicle body and bogies are completely rigid; the passengers and their baggage are fixed to the vehicle body; both bogies have identical dimensions, mass properties, and primary suspension stiffnesses; small angle approximations are valid throughout the linear suspension model whenever relating linear to angular displacements.

The maglev vehicle's physical parameter values in our analyses are similar to a box-beam guideway design developed by the Bechtel consortium for the U.S. Department of Transportation [1]. Representative gross physical properties are summarized in Table 1. The remainder of this section consists of a brief overview of the suspension force models followed by a discussion of the active aerodynamic surfaces considered. The section is concluded with a description of the guideway and crosswind disturbance models employed.

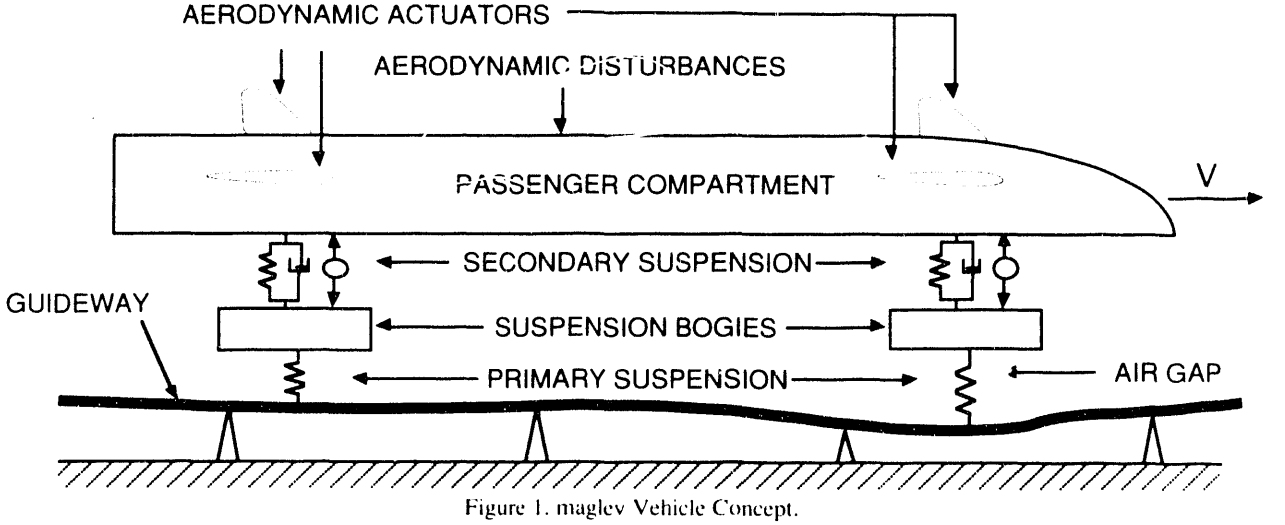

Figure 1. maglev Vehicle Concept.

A. Suspension Forces

To obtain a suitable linear system description, we model the system in a lumped mass fashion. All suspension elements are modeled as massless generalized springs. For example, the suspension force, **F**, due to the displacement between the front bogie and the guideway is determined by the relationship below:

$$\mathbf{F} = \mathbf{K}\mathbf{r} + \mathbf{D}\dot{\mathbf{r}} \qquad (1)$$

where **K** is the spring stiffness matrix, **D** is the damping, and **r** is the equilibrium displacement vector. The spring constants for the primary suspension system are dependent upon forward velocity; representative values are given in Table 2. Damping for this type of magnetic suspension is believed to be very low [6] and therefore is assumed zero for modeling purposes. Passive secondary suspension spring constants and damping ratios are selected to improve ride quality while simultaneously preventing touchdown and limiting the active secondary suspension stroke. This procedure is discussed in §3.

It is assumed that all suspension forces act in equal and opposite directions across the gap between the elements under consideration. For simplicity, we model these forces as being applied to fixed points relative to the guideway's, bogies', and passenger compartment's centers of gravity.

B. Aerodynamic Actuation

Six active aerodynamic surfaces, as shown in Figure 1, are available to the control system for improving ride quality. We assume that these actuators operate in "free-stream" and are modeled as winglets with one degree of freedom. Four winglets are mounted on the sides of the train and produce vertical forces at the surfaces' centers of pressure: two in front on opposite sides, and two in back on opposite sides. Two winglets are mounted on the top of the train (in "rudder-like" arrangements) to provide lateral forces.

The lift force for a flap in free-stream is given by:

$$F_L = \frac{1}{2}\rho |V_{air}|^2 A C_L(\alpha) \qquad (2)$$

where ρ is air density, A is area, V_{air} is the velocity of the air mass relative to the winglet, and α represents angle of attack. We consider only the lift component of the flap forces. The induced drag of the flaps is calculated to determine the drawbacks of aerodynamic control in [5], but its effect on ride quality is not considered here. Since induced drag acts parallel to the velocity vector, drag forces lie in a direction not included in our model. The lift coefficient is obtained from conventional aerodynamic theory [7] and is nearly linear for small angles of attack. A linear equation for $C_L(\alpha)$ results: $C_L(\alpha) = C_{L\alpha}$, where $C_{L\alpha} = 0.0264/°$. We assume that V_{air} in (2) is equal to the train's velocity and ignore the effects of crosswind and vehicle rotation. Also, we use a

TABLE 1
Representative Physical Dimensions

Parameter	Value
Vehicle Height	4.9m
Vehicle Length	36.1m
Vehicle Width	3.7m
Total Mass	64400kg
Passenger Compartment Mass	40830kg
Distance Between Bogies	17.1m
Bogie Height	0.75m
Bogie Width	1.5m
Guideway Width	1.2m
Top Winglet CP to Train CG (vertical)	2.3m
Side Winglet CP to Train CG (horizontal)	-1.0m

TABLE 2
Primary Suspension Stiffness

Vehicle Speed	Lateral Stiffness	Vertical Stiffness
50.0Km/s	-2.73e6 N/m	-8.06e6 N/m
100.0Km/s	-3.11e6 N/m	-9.61e6 N/m
134.0Km/s	-3.38e6 N/m	-9.93e6 N/m
150.0Km/s	-3.24e6 N/m	-10.0e6 N/m

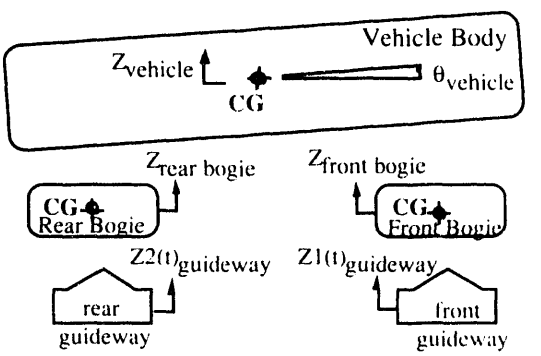

Figure 2. Degrees of Freedom: Side View.

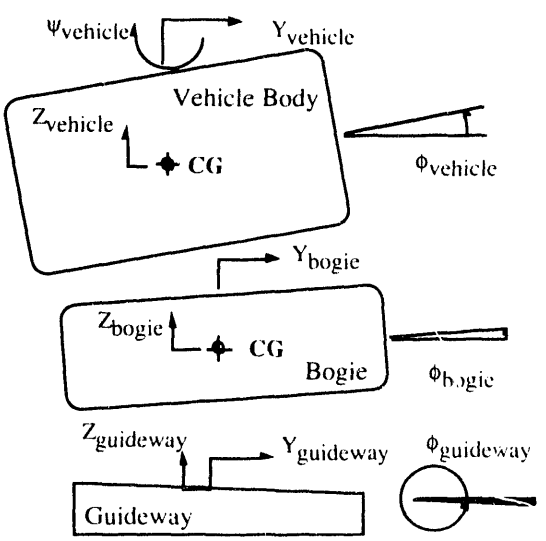

Figure 3. Degrees of Freedom: Front View.

small angle approximation for α to model the lift force as perpendicular to the undeflected winglet surface.

In theory, a very large aerodynamic force can be obtained for relatively low aero-actuator torque. Since the flaps rotate about their centers of pressure, the aerodynamic torques across flap rotation joints are small when compared to the forces generated by the flaps. However, the actual force required in a hydraulic system that drives a winglet can still be large, due to physical constraints and practical considerations. The dynamics of the closed-loop system may dictate a high actuator bandwidth resulting in large actuator power requirements.

C. System Disturbances

Guideway irregularities are captured by the stochastic model:

$$\Phi_{\text{guideway}}(\omega) = \frac{A_r V}{\omega^2} \tag{3}$$

where Φ_{guideway} is the guideway Power Spectral Density (PSD), A_r is the Roughness Parameter, and V is the train's forward velocity. A roughness parameter, A_r, corresponding to welded steel rail (gage 4-6) is used to define the guideway PSD, which is then used to form a linear system driven by white noise to describe the guideway position variations. While a typical guideway will not be welded steel rail, its roughness as seen by the train will be dominated by the alignment of guideway coils. Roughness parameters are given in Table 3.

The crosswind description used in our analysis consists of the sum of two terms: a constant, steady-state mean value and a time variant random process. The mean crosswind velocity is equal to half of the peak crosswind velocity, assuming a maximum three sigma variation from the mean. In our analysis we assume 26.8Km/s (60mph) crosswind peak. The PSD of the time varying crosswind component is given by:

$$\Phi_{\text{wind}}(\omega) = \frac{2\sigma_w^2 \nu}{\omega^2 + \nu^2} \tag{4}$$

where the break frequency, ν, is 1.0 rad/sec. Φ_{wind} is implemented by a linear system driven by white noise. We assume that the crosswind is perpendicular to the guideway. This maximizes vehicle sideslip, effectively softening the lateral suspension stiffness and thereby degrading system performance.

TABLE 3
Guideway Roughness Parameters

Parameter	Value
A_r (vertical)	1.2e-5 rad^2/s
A_r (lateral)	1.2e-5 rad^2/s
A_r (roll)	5.7e-6 rad^3/m-s

3. Analysis

Analysis of the system model begins with choosing the passive secondary suspension's stiffness and damping parameters. The function of the secondary suspension system is to improve ride quality while simultaneously preventing vehicle contact (touchdown) on the guideway. The active secondary suspension stroke must also be kept within practical limits. Typically, the passive suspension parameters cannot be selected to optimize all of these criteria simultaneously, and hence, the parameters are determined through trade-off analyses. Once the suspension elements have been defined, a force balance condition is exploited to determine nominal operating equilibrium values for the vehicle's center of pressure and sideslip angle, given forward and average crosswind velocities. Finally, the linear perturbation model is assembled and a candidate control law synthesized. The resulting closed-loop system is analyzed in a statistical framework. The remainder of this section presents further details of these procedures.

A. Secondary Suspension Parameter Optimization

The primary suspension design involves an inherent conflict between ride quality and guideway tracking. A stiff primary suspension provides improved guideway tracking at the expense of significant guideway and wind disturbance transmission to the passenger compartment. Additionally, a stiff magnetic suspension generally exhibits efficient power consumption. Power considerations, rather than ride quality factors, generally dictate primary suspension design. With the primary suspension parameters assumed given, the secondary suspension parameters are chosen to address the trade-off between the system performance measures of interest, with the overall goal of achieving the best ride quality.

System performance can be evaluated with the root mean squared (RMS) values of relevant quantities in our model. RMS acceleration levels can be used to compute the Pepler index. The primary air gap and secondary suspension stroke requirements can also be estimated from the RMS variations of these variables, which provides a method of specifying the primary and secondary suspension stroke limits through stochastic control techniques. The motivation behind this treatment stems from the guideway and wind disturbances being characterized by linear systems driven by white noise, whereby it is natural to determine the system outputs for analysis in a similar form.

TABLE 4
Passive Secondary Suspension Parameters

Vertical Natural Frequency	0.8 Hz
Vertical Damping Ratio	0.10
Lateral Natural Frequency	1.5 Hz
Lateral Damping Ratio	0.5
Roll Stiffness	0.0 N-m/rad
Roll Damping	2.0e6 N-m-s/rad

Details of the trade-off studies used for characterizing the passive secondary suspension system are beyond the scope of this paper, but can be found in [1] and [5],. The design parameter values are listed in Table 4.

B. Operating Point Force Balance

To obtain a linear state space perturbation analysis model, we need to determine vehicle steady-state sideslip angle, β, and the location of the center of pressure (CP) relative to the CG. This is performed through a force balance analysis, where forces and moments arising from the constant component of crosswind velocity are canceled by the primary and passive suspension systems (Equation (1)). Crosswind forces on the train are modeled as a side force acting perpendicular to forward velocity at the CP. The aerodynamic side force is given by:

$$\left[F_y\right]_{aero} = \frac{1}{2}\rho|V_{air}|^2 A_t C_y(\beta) \qquad (5)$$

where A_t is the train's cross-sectional area and $C_y(\beta)$ is the coefficient of side force. The air-relative train velocity, V_{air}, is the vector sum of the train's earth-relative and crosswind velocities. The aerodynamic coefficient, $C_y(\beta)$, is non-linearly dependent on the sideslip angle and is described by a third order polynomial fit to data generated in [5].

Thus, given forward vehicle velocity and steady-state crosswind speed, the aerodynamic forces on the vehicle are computed as a function of β and CP location via (5). A set of nonlinear equations is solved numerically to determine β and CP by balancing $[F_y]_{aero}$ against the nonaerodynamic forces contained in the model, where all time-varying zero mean disturbances and actuator displacements are nulled. For the data presented in §4, the vehicle and mean wind velocities are 134km/s (300mph) and 13.4Km/s (30mph) respectively. The resulting steady-state sideslip, β, is 0.102rad (5.73°), which corresponds to a 0.0023rad (0.134°) vehicle yaw angle, ψ.

C. Covariance analysis

To construct our linear perturbation model, we further assume that the passenger compartment and bogie angular rotation rates are small, and we neglect nonlinear coupling terms due to Coriolis accelerations and gyroscopic effects. The resulting linear equations of motion are placed in state space form, $\dot{\mathbf{x}} = \mathbf{Ax} + \mathbf{Bu} + \mathbf{Fw}$, where: the system state, $\mathbf{x}$, contains train and bogie positions and velocities, and guideway positions (constrained to appropriate degrees of freedom); the system actuator input vector, $\mathbf{u}$, contains active secondary suspension force and aerosurface deflection commands; and the disturbance input vector, $\mathbf{d}$, is (Gaussian) white noise.

A measure of ride quality are commonly used for maglev vehicles is the Pepler ride quality criteria [8]. Although both measures are dependent on train accelerations, the Pepler Index also includes the effects of roll and noise. The Pepler ride quality index, P.I., is given by:

$$P.I. = 1.0 + 0.5\sigma_{\dot{\phi}} + 17\sigma_{\ddot{z}} + 17\sigma_{\ddot{y}} + 0.1(dB(N) - 65) \qquad (6)$$

where $\sigma_{\dot{\phi}}$ is the passenger RMS roll rate, $\sigma_{\ddot{z}}$ is the passenger RMS vertical acceleration, $\sigma_{\ddot{y}}$ is the passenger RMS lateral acceleration, and dB(N) is the passenger compartment noise level (decibels). In our analysis, we ignore the compartment noise level. Hence, P.I. is a scalar sum of system statistics, which can be denoted $\mathbf{z} = \mathbf{Cx} + \mathbf{Du}$ (ignoring the constant term, 1.0). By defining our analysis variables in this manner, we proceed to design a controller using Linear Quadratic Regulator (LQR) theory, which synthesizes a state feedback control law of form: $\mathbf{u} = -\mathbf{Gx}$. The gain matrix, $\mathbf{G}$, is selected to minimize a quadratic cost functional that includes weighted terms containing performance variables of interest and control energy required. The cost functional, J, provides an optimal trade-off between actuator effort and closed-loop system performance:

$$J = \lim_{T\to\infty} E\left\{\int_0^T \left(\mathbf{z}(t)^T \mathbf{Q}\,\mathbf{z}(t) + \mathbf{u}(t)^T \mathbf{R}\,\mathbf{u}(t)\right)dt\right\} \qquad (7)$$

The matrices $\mathbf{Q}$ and $\mathbf{R}$ are used to vary the relative importance of the system outputs and control effort respectively (E denotes the expectation operator). The gain matrix $\mathbf{G}$ minimizing this cost functional is given by:

$$\mathbf{G} = \mathbf{R}^{-1}\left[\mathbf{D}^T\mathbf{QC} + \mathbf{B}^T\mathbf{K}\right] \qquad (8)$$

where $\mathbf{K}$ is the solution to an algebraic Riccati equation [9]:

$$\mathbf{KA} + \mathbf{A}^T\mathbf{K} + \mathbf{C}^T\mathbf{QC} - [\mathbf{KB} + \mathbf{C}^T\mathbf{QD}]\mathbf{R}^{-1}[\mathbf{B}^T\mathbf{K} + \mathbf{D}^T\mathbf{QC}] = \mathbf{0} \qquad (9)$$

We calculate the closed-loop system steady-state state covariances analytically. If $\mathbf{A}_{cl}$ is the closed-loop system matrix ($\mathbf{A}_{cl} \equiv \mathbf{A} - \mathbf{BG}$), then the state covariance matrix steady-state solution, Σ_{xx}, is the solution to the Lyapunov equation [10]:

$$\mathbf{A}_{cl}\Sigma_{xx} + \Sigma_{xx}\,\mathbf{A}_{cl}^T + \mathbf{FF}^T = \mathbf{0} \qquad (10)$$

A system output for analysis, denoted $\mathbf{y}$, is defined as a linear combination of system states: $\mathbf{y} = \mathbf{C}_{out}\mathbf{x}$. The output covariance matrix, Σ_{yy}, is given by:

$$\Sigma_{yy} = \mathbf{C}_{out}\,\Sigma_{xx}\,\mathbf{C}_{out}^T \qquad (11)$$

The RMS component of the output vector, $\mathbf{y}$, is the square-root of the terms along the diagonal of Σ_{yy}. This analysis methodology permits us to compute analytically the statistics of important system properties, such as the Pepler

Index, bogie displacements, and actuator commands, without having to resort to Monte Carlo schemes.

4. Results

Results obtained using the analysis model described in §2 are presented here. We assume a forward vehicle velocity of 134Km/s (300mph) and a peak crosswind (three-sigma) velocity of 26.8Km/s (60mph). Control algorithms are developed and the resulting closed-loop systems analyzed as per §3. We select the weighting matrices, **Q** and **R** in (7), to provide good ride quality while maintaining strict (plus or minus three-sigma) suspension gap requirements defined in [1]. Table 5 provides data indicating basic system performance for three candidate control strategies: (1) no active control (open-loop); (2) active secondary suspension control only; (3) active secondary suspension and aerosurfaces. The Pepler index is computed for passengers located at the rear, center, and front of the train. Lateral and vertical primary suspension gap RMS variation values are also tabulated.

Note that the active secondary suspension system significantly reduces the Pepler Index. However, air gap variations increase considerably in the vertical direction. The inclusion of aero-actuation reduces the Pepler index further (recall, P.I. has minimum value 1.0) while also reducing the primary suspension gap variation, albeit not to the level of the strictly passive case.

5. Concluding Remarks

To analyze and quantify the benefits of active control, the authors have developed a six degree-of-freedom lumped parameter modeling capability suitable for a broad class of maglev vehicle and guideway configurations. Perturbation analyses about an operating point defined by train and average cross-wind velocities yield linearized state-space descriptions of the maglev system for multivariable control system analysis and synthesis. Results presented in §4 indicate that the use of active aerodynamic control surfaces, in coordination with the active secondary suspension system, provides significant improvement to the passenger ride quality while ameliorating primary suspension gap requirements. Similar results by the authors [1][5] for alternative system configurations support this conclusion.

Our analysis and design methodology permits us to alter physical properties, actuation (and potentially, sensing) elements, and disturbance inputs contained within the linear model description. This can be exploited to ascertain optimal system design parameters through parametric trade-off analyses. (We appreciate that specific performance predictions generated by linear analyses should ultimately be verified through high fidelity nonlinear simulation.) A natural extension to our work includes appending additional modeling capabilities, *e.g.*: curved and rolling guideways, vehicle bending modes, actuator and sensor dynamics and noise, and, of course, more sophisticated control techniques.

References

[1] *Maglev System Concept Definition*, contract DTFR 53-92-C-00003, prepared by Bechtel/Draper/MIT/Hughes/General Motors for U.S. Department of Transportation: Federal Railroad Administration.

[2] Wormley, D.N., Young, J.W., "Optimization of Linear Vehicle Suspensions Subjected to Simultaneous Guideway and External Force Disturbances," Journal of Dynamic Systems, Measurement, and Control: Transactions of the ASME, Paper No. 73-Aut-H, March 16,1973.

[3] Guenther, Christian R., Leonides, Cornelius T., "Synthesis of a High-Speed Tracked Vehicle Suspension System - Part I: Problem Statement, Suspension Structure, and Decomposition" IEEE Transactions on Automatic Control, vol. AC-22, No. 2, April 1977.

[4] Gottzein, E.; Lange, B., Ossenberg-Franzes, F., "Control System Concept for a Passenger Carrying maglev Vehicle," High Speed Ground Transportation Journal, Vol 9, No. 1, 1975, pp 435-447.

[5] Barrows, T., McCallum, D, Mark, S, and Castellino, R. C, *Aerodynamic Forces on Magelv Vehicles*, contract DOT/FRA/NMI-92/21, prepared by C.S. Draper Lab. for U.S Department of Transportation: Federal Railroad Administration.

[6] Thornton, Richard D., "Magnetic Levitation and Propulsion, 1975," IEEE Transactions on Magnetics, Vol. Mag-11, No. 4, July 1975.

[7] Borst, H.V.; Hoerner, S.F., "Fluid-Dynamic Lift," published by Mrs Liselotte Hoerner, Bricktown, NJ, 1975.

[8] Dunlap and Associates, Inc., *Development of Techniques and Data for Evaluating Ride Quality Volume II: Ride Quality Research*, Report No. DOT-TSC-RSPD-77-1. II for U.S. Dept. of Transportation, February, 1978.

[9] Kwakernaak, H., and Sivan, R., *Linear Optimal Control Systems*. New York: Wiley-Interscience, 1972.

[10] Jazwinski, A., *Stochastic Processes and Filtering Theory*. New York: Academic Press, Inc., 1970.

TABLE 5
System Performance

Active Actuators	Pepler Index			RMS Primary Suspension Gap Variation			
	Front	Rear	Center	Lateral Front	Lateral Rear	Vertical Front	Vertical Rear
None	5.6	4.5	4.4	1.2cm	0.50cm	0.64cm	0.65cm
Active Secondary	2.0	1.9	1.7	1.2cm	0.48cm	1.5cm	1.5cm
Active Secondary and Aero	1.6	1.5	1.5	1.1cm	0.31cm	0.94cm	0.89cm

Rail Irregularity and Module Response in HSST-100 System

Mituru Iwaya
Engineering Department, HSST Corporation

Abstract - **This paper shows the relation between rail irregularities and magnet responses on rolling stock. The chosen irregularities can cover almost all the modes which can arise during practical operation of the vehicle. The test run data are also confirmed by theoretical study.**

I. Introduction

The test run of the HSST-100 system in Nagoya was almost completed in 1992 [1]. Among others, we have accumlated a lot of data with regard to the relation between guideway displacement and vehicle behaviour from August to September last year.

As for maglev vehicles, magnet levitation height gives decisive weight to the overall design. Magnet gap fluctuation comes mainly from the guideway rail irregularity. The guideway side claims large tolerance on rail accuracy, on the other hand, the vehicle side demands precisely aligned rail profile. The balance between them can be obtained from repetitive experiments.

II. Test Facility

The test data aquisition was made on the 800m area from Ooe station, where steel tie bars are installed[1],[2]. Various rail displacements were intentionally incorporated by moving tie bars. The offered vehicle is the HSST-100 type with full cabin load. It ran on the subject guideway in various speed and the measured data are the magnet gap, car body acceleration and others.

The guideway disturbance can be represented by ramp input and step input. Other types of disturbance can be artificially synthesized with these. Therefore, I would like to make a close inquiry on these items at first.

III. Behaviour against Girder Deflection

The standard span length in the test site is 20m. Assuming a deflection ratio of 1/1500, we put down the midspan of the girders as far as 13mm (Fig.1). Therefore,when the vehicle comes to the pier position, the attack angle between the two adjacent girders comes equal to that of 1/1500 deflection ratio. It means that the girder deflection ratio comes to nearly 1/1100 when the vehicle is running on the middle of the girder. This fact necessitates our attention especially when we evaluate vehicle body acceleration.

Fig.2 left shows average gap fluctuation of the magnets in this test. It can be noted that the gap fluctuation value increases in accordance with vehicle speed.The maximum gap deviation occurs at the girder conjunction point. Therefore, it can be easily presumed that the value can be reduced with some modification of the rail profile at the both extreme of the girder. Fig.2 right shows the result of this modification which is about 20 to 30 percent reduction in magnet gap fluctuation. Our calculation predicted 50 percent reduction in this case. The difference may be caused by other irregularities originally incorporated in the rail system. The allowable fluctuation is ±4mm in HSST-100 system. Such a slight modification is desirable in this meaning.

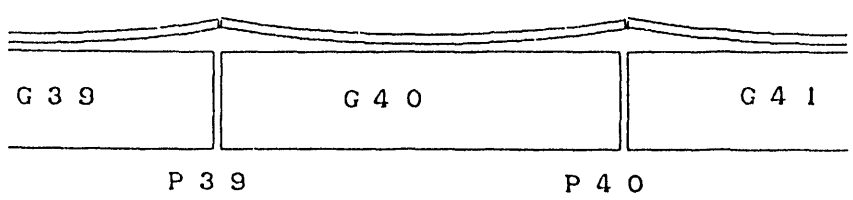

Fig.1 Rail Profile in Girder Deflection Test

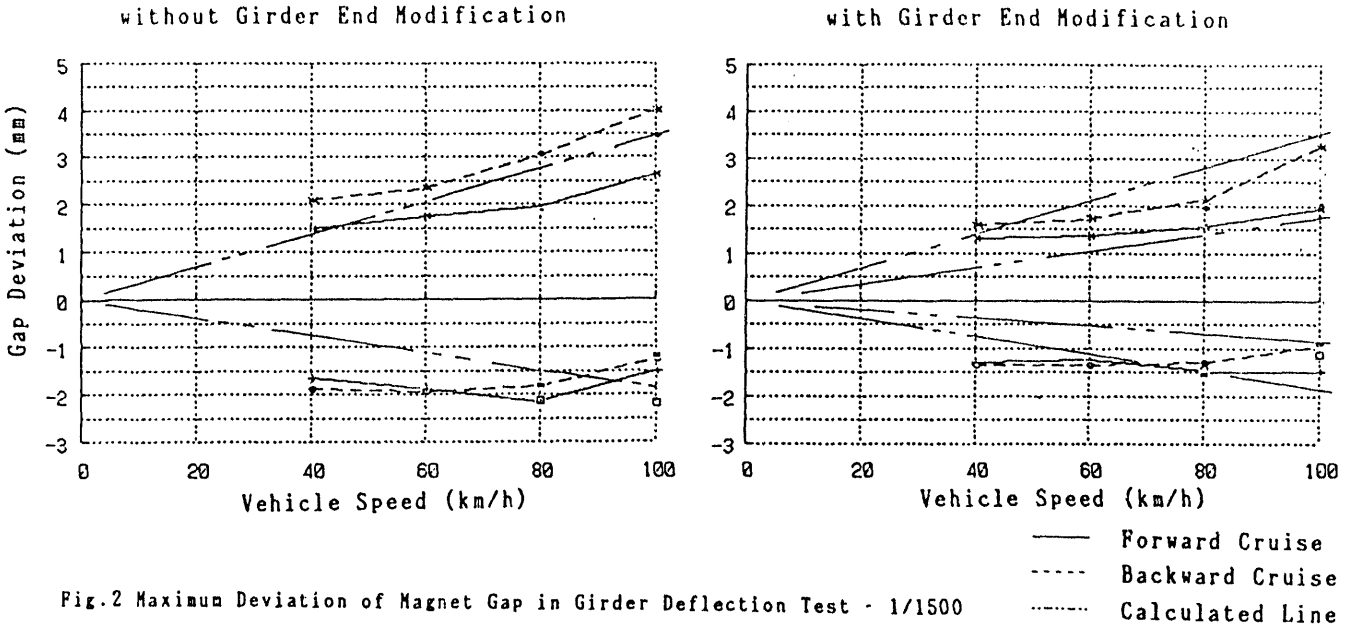

Fig.2 Maximum Deviation of Magnet Gap in Girder Deflection Test - 1/1500

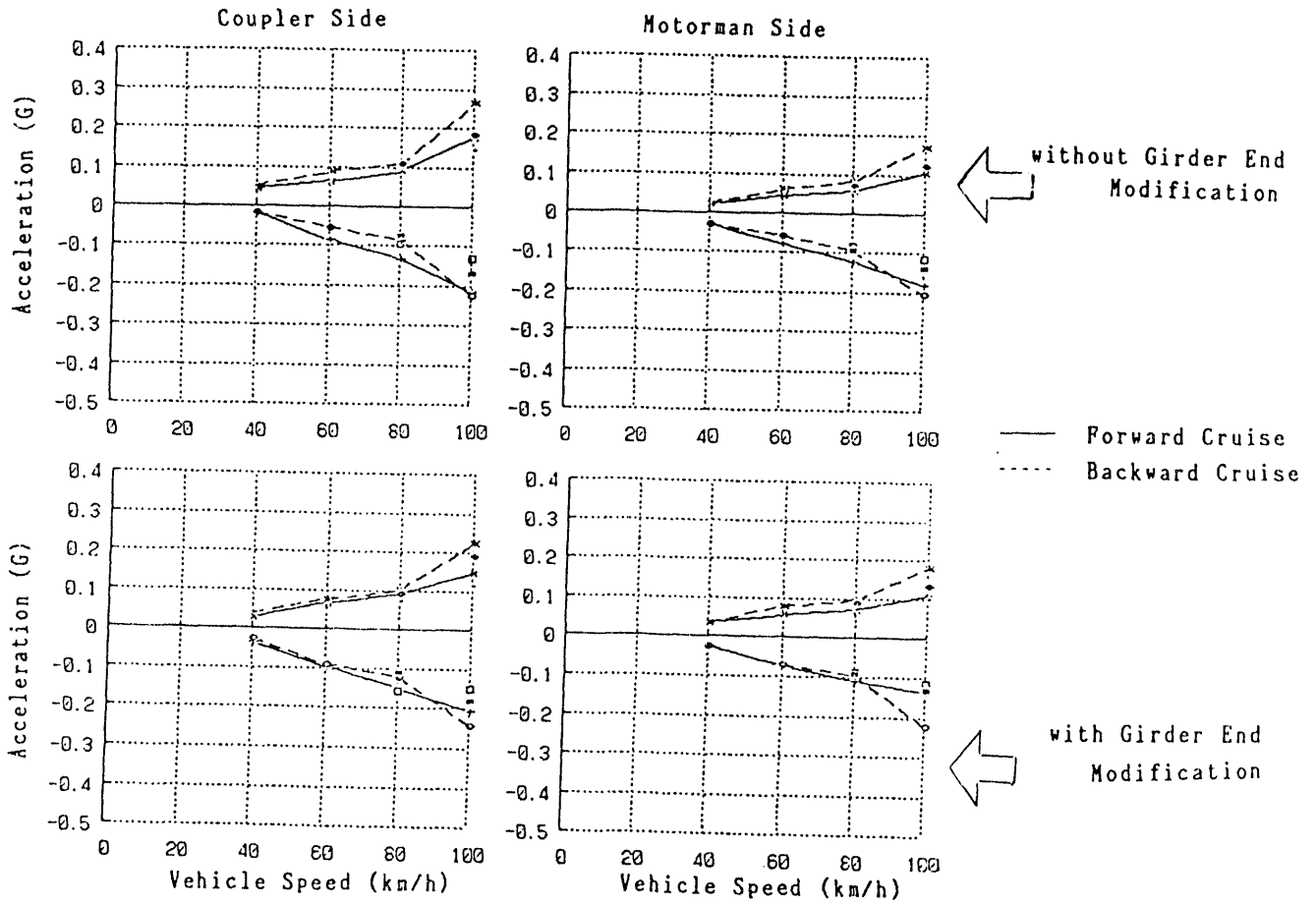

Fig.3 Maximum Acceleration of Car Body in Girder Deflection Test

The same analysis is made on vehicle body acceleration as shown in Fig.3. The coupler side acceleration seems to exceed 0.2G, however, this value must be undercut by nearly 30% for the reason stated above. The motorman side value can be considered to be showing right acceleration on 1/1500 girder. In any case, the rail profile modification on girder ends will give an improvement also in this case.

Same test was carried out on 40m span girder which deflection ratio is designed and confirmed as 1/1300. Both magnet gap fluctuation and car body acceleration indicated no particular increase compared with that of the standard 20m girder of 1/2800 up to the running speed of 100km/h.

IV. Module Responce against Rail Step

Another fundamental response is that in step disturbance. The running test was carried out on rail step of 1.5mm and 2.0mm as in Fig.4. The result of magnet gap fluctuation with 2mm step is shown in Fig.5. The calculated result is also shown on the same figure. Those two lines deviate from each other in the higher speed range. It is assumably caused by other rail irregularities originally incorporated in the system.

The calculated gap fluctuation is based on one dimensional model. Therefore, the value has simple relation with vehicle speed. Actually, the vehicle has three dimensional expanse, which causes rather complicated response with regard to vehicle speed. Such a complexity is omitted here.

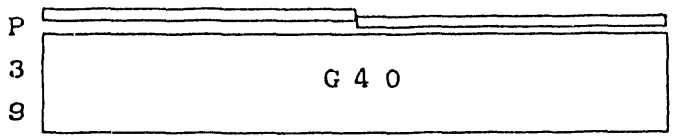

Fig.4 Rail Profile in Vertical Step Test

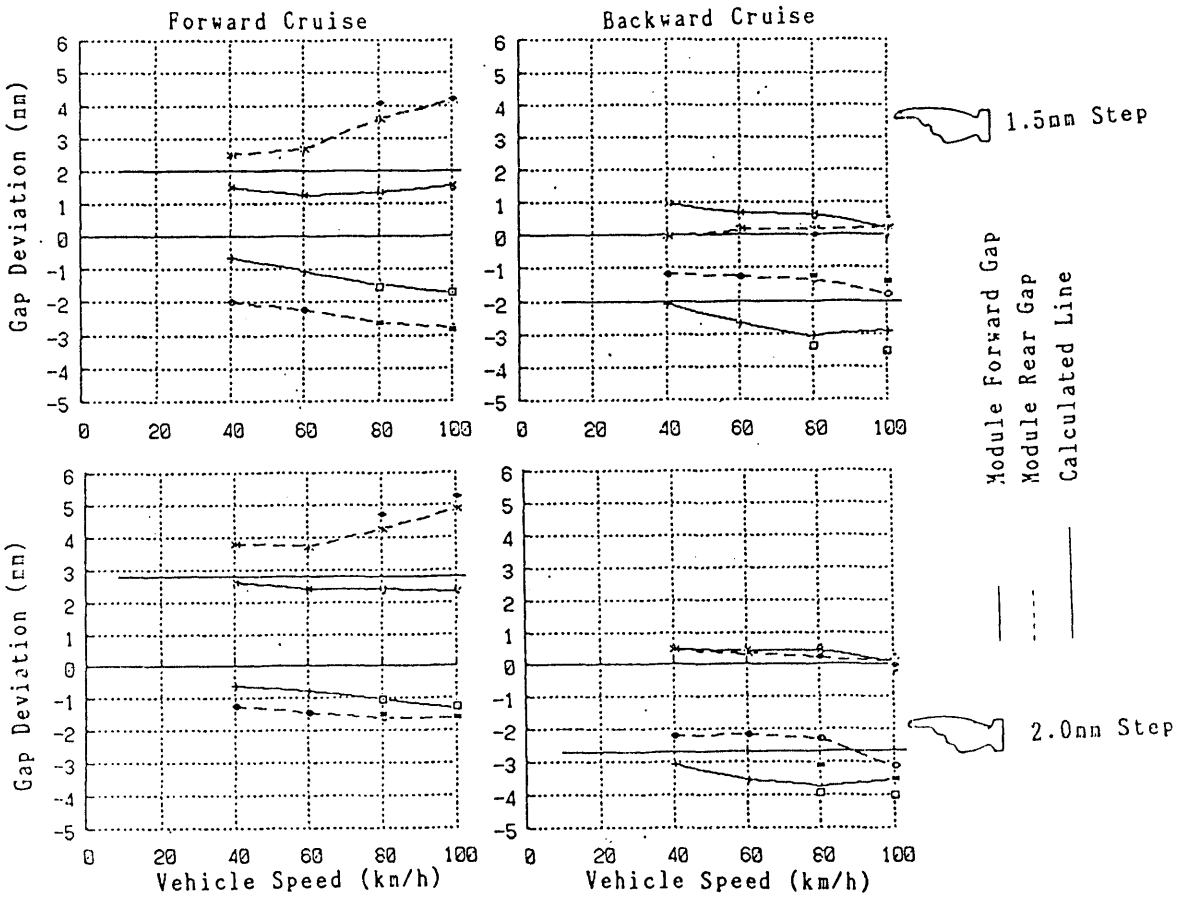

Fig.5 Maximum Deviation of Magnet Gap in Vertical Step Test

V. Collation with Theiretical Analysis

Every rail profile can be expressed in Fourier series. For example, ramp shape y such as girder deflection is a function of dimension x as;

$$y = \frac{\cos x}{1^2} + \frac{\cos 3x}{3^2} + \frac{\cos 5x}{5^2} + \cdots \quad (1)$$

Here, the dimensional parameter of x can be replaced by time parameter t as;

$$y = \frac{\cos vt}{1^2} + \frac{\cos 3vt}{3^2} + \frac{\cos 5vt}{5^2} + \cdots \quad (2)$$

When the vehicle speed comes up by twice, then the equation becomes;

$$y = \frac{\cos 2vt}{1^2} + \frac{\cos 6vt}{3^2} + \frac{\cos 10vt}{5^2} + \cdots \quad (3)$$

Comparing equation (3) with equation (2), we can confirm that twice the speed we get twice the frequency. Originally, from equation (1) or (2), twice the frequency we will get 1/4 of the amplitude. This means that the amplitude becoms 4 times higer than that of the original. On the other hand, spectral density becomes half in (3). In this way we can conclude that the external disturbance becomes twice when a car passes ramp conjunction point with twice the speed.

Same discussion is valid when a car passes step disturbance point where;

$$y = \frac{\sin x}{1} + \frac{\sin 3x}{3} + \frac{\sin 5x}{5} + \cdots$$

In this case, we can conclude that twice the speed a car gets the *same* disturbance as in the original.

Above stated is the discussion which was made in drawing the calculated line in Fig.2 and Fig.5. It is generally said that random irregularity usually found in a rail alignment has a spectrum of $\sum \sin kx/k\sqrt{k}$. In this case, twice the speed we get square root twice of disturbance from the rail[2].

VI. Conclusion

We have also conducted other irregularity test such as rail level, lateral step, guage, tilt and so on. In these cases we could hardly find any evil effect on vehicle behaviour. Thus we are convinced that the major attention lies on rail vertical alignment and the influence of its defect appears less than that of a ramp disturbance.

The results and data obtained here will believably help us much when we consider a design of guideway and vehicle in future.

VII. Additional Note

Note 1. Girder End Modification(Fig.2)

The girder bends down with active load. When the rails are installed on the girder in a straight line, two adjacent rails make an attack angle of 4.2mrad with 1/1500 of girder deflection. When the rails are installed on the girder previously with 2.1mrad of inverse attack angle, then the arising angles with girder deflection are distributed to two positions and the absolute values are reduced into half. Such a girder end modification can be easily obtained by moving the end tie bars a little downward. This modification gives an advantage in magnet gap fluctuation, and also car body acceleration decreases are confirmed with various test data.

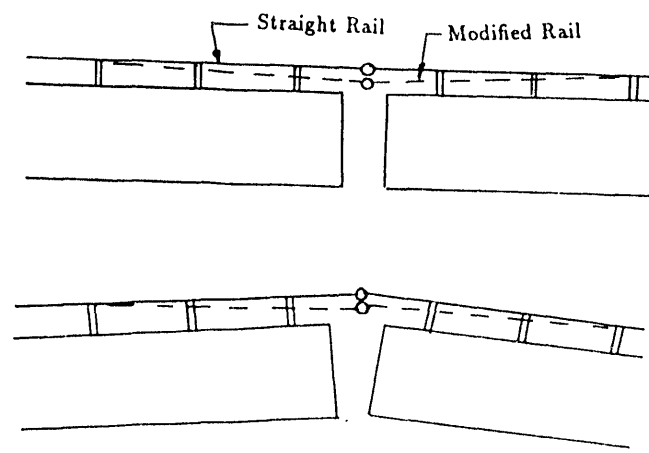

Note 2. Dynamic Difference between Motorman Side and Coupler Side(Fig.3)

Fig.3 shows obvious difference in the acceleration measured at the motorman side and coupler side. The test train consists of two cars. When the coupler side comes to the midpoint of the girder, the deflection reachs its climax (shown as d1). On the other hand, when the motorman side comes to the midpoint, the girder springs back in a considerable amount(shown as d2). As the results, the coupler side car body vibrates with the amplitude of d1, while the motorman side car body does with the amplitude of d2. That results in 30% difference.

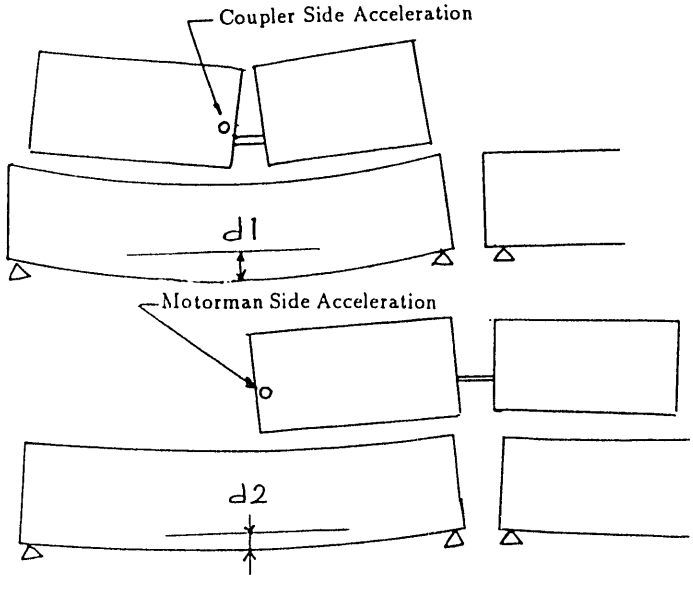

Note 3. Step Response of the Magnet(Fig.5)

The calculated response with rail 1.5mm step upward is shown below. In this case, the magnet deviation from the rail reachs its climax(-2mm) when the after side passes the step point. Here the minus value means lowering of the magnet. The plus value does not represent its climax and, therefore, is omitted from Fig.5. In this figure, forward cruise means downward step, and backward cruise means upward step. The measured lines show both maximum plus value and maximum minus value.

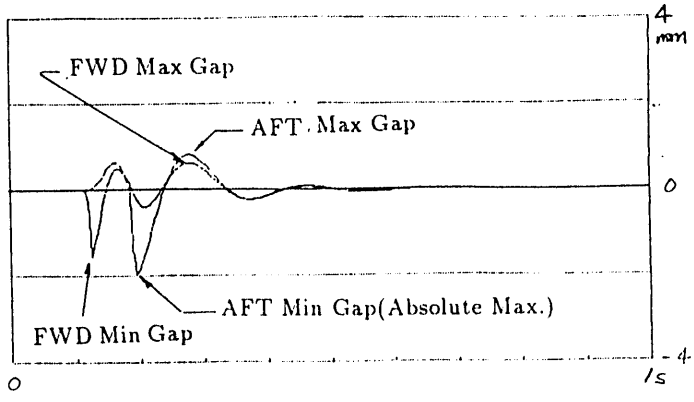

REFERENCES

[1] M. Iwaya, HSST-100 SYSTEM EXPERIMENTS IN NAGOYA TEST SITE, WCTR 1992, Lyon

[2] M. Fujino, OUTLINE OF HSST-100 AND TEST LINE IN NAGOYA, Maglev Conference 1993, Argonne

Five Degree of Freedom Analysis of the Grumman Superconducting Electromagnetic Maglev Vehicle, Control and Guideway Interaction

Dr. Richard J. Gran
Director, Advanced Concepts, Grumman Corporation, Bethpage, NY 11714

Michael Proise
Maglev Program Manager, Grumman Aerospace and Electronics Group

Abstract **- This paper describes the control system and the five degree of freedom (5 DOF - heave, sway, pitch, yaw, and roll) model of the Grumman Maglev Vehicle described in [1]. The simulation model has 12 magnet modules (4 magnets per module) mounted along the vehicle canted at the appropriate angle to give both lateral and lift forces acting through the vehicle's center of gravity (cg). The model also includes the effect of the distributed forces that are created as a consequence of the magnet geometry. Because the control system at each magnet module is a third order system, the complete 5 DOF model has 42 coupled differential equations (3 each for the magnet modules times 12 modules plus 2 each for pitch, yaw, and roll). The model that we developed is linear in the magnet servos, but the results were compared to a nonlinear single magnet control simulation and we are confident that the linear model predicts the behavior of the nonlinear system.**

The guideway was modeled as a simple pinned beam in both bending and torsion to determine the guideway motions as a consequence of the vehicle moving over the beam. This motion is combined with stochastic models for the guideway camber, step and ramp discontinuity created by the pillar height variations, and the irregularities caused by the random roughness of the rail. The combined effect of all of these motions was used to excite the 5 DOF vehicle simulation model.

The model was also used to compare the effect of various suspension systems. The first assumed a four point force suspension at each corner of the vehicle using a conventional spring/damper system, the second was a similar four point suspension using magnetic forces such as would be used in an electrodynamic suspension (EDS) system and the third was uniformly distributed load along both sides of the vehicle as in an electromagnet suspension (EMS) system. The comparison of these three different suspensions allows an understanding of those aspects of the Grumman EMS design [1] that permits the elimination of a secondary suspension system.

It was also determined that a uniformly distributed load significantly alters the guideway deflections, and the rule of thumb of using twice the static deflection to determine the dynamic deflection is not valid.

Manuscript received Mach 15, 1993. This work was performed in part for the Maglev System Concept Definition study supported by the U. S. Army Corps of Engineers under contract No. DTFR53-92-C-000 04.

I. FIVE DEGREE OF FREEDOM MODEL

A. Servo Model

The starting point for this analysis is the Grumman supeconducting EMS concept described in [1]. Additional information on the magnet designs is described in [2] and the levitation and guidance control servo is discussed in [3]. The linear model of the servo is shown in the block diagram of Fig. 1. The differential equation that describes this model are also shown in the figure. The forces that are applied to the magnet module are added at the summing junction denoted Sum1 in the diagram. The forces at the sum are those created by linearizing the magnet force. The magnet is nonlinear in both the current and the position. The force needed to balance the weight of the vehicle is assumed to be provided continuously, and the perturbations around that operating point define the linear model shown. The perturbation force caused by the motion of the magnet is denoted by K1. K1 is really the partial of the magnet force due to guideway gap error around the nominal gap clearance c. 4 cm (1.6 in). It is fed back with a positive sign which is representative of the unstable characteristics of the magnets being attracted towards the iron rail. For the simulation, K1 was 281,000 pounds per foot. The other force at Sum1 is caused by changes in force due to current variations in the magnet coils. For the simulation this term, denoted by dfdi, is 933.3 pounds per kilo-ampere turn. Since each of these force terms were developed by assuming that a single magnet servo was lifting the entire vehicle, dividing the force over the 12 independent modules of four magnets each, requires that these constants be divided by 12. This is also true of the mass – for the analysis the mass is assumed to be 1/12 of the complete vehicle mass which is 61 kN (4192 slugs).

The control system uses gap error, vehicle rate and acceleration as feedback controls. The rate is determined by integration of the accelerometer. The gains for the acceleration are also used (with Kf) to set the servo bandwidth and damping.

The feedback control gain in the forward loop is denoted by Kf. The servo design selects this gain, the gain on the accelerometer, and the gain on the rate feedback so that the root

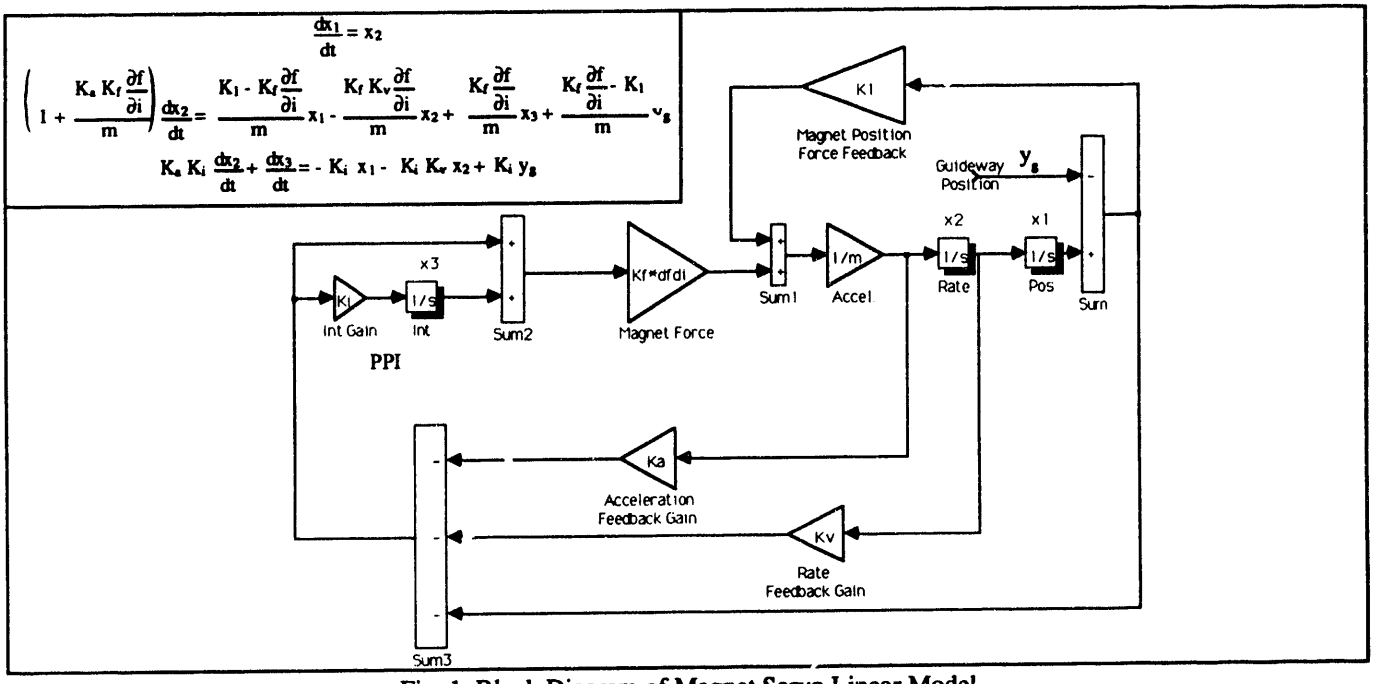

Fig. 1. Block Diagram of Magnet Servo Linear Model

locus shown in Fig. 2 results. The rate, and accelerometer gains (with Kf) are selected to give a closed loop bandwidth (ω_{cl}) of 10 Hz., and a damping (ζ) of .707. The value of Kf that achieves this is 3650.3 kilo-ampere turns per unit input (note in the figure that the formula for Kf is denoted by "Gain").

The proportional plus integral (PPI) control that precedes Sum2, is included to cause the system to have zero steady state error to steps (without this feature, guideway step irregularities would always result in a steady state error). The gain Ki in the integral compensation is selected to place the closed loop zero introduced by the compensator on top of the open loop left half plane pole caused by the positive force feedback K1. With this strategy, the resulting closed loop system is second order. Note that the unstable plant poles are at ±28.36 rad/sec for the nominal design, so the integral gain is selected to be 28.36.

To simplify the complexity of the model twelve independent magnet modules where assumed in the design analyzed, but the base-line design [1] actually will have 24 modules of two magnets each. In this base-line configuration, up to twelve magnets (5 modules) may fail with enough lifting power still remaining to support the entire vehicle. Thus the combination of redundant magnet modules and magnets that are inherent in this design make the overall control system innately robust to failures and extremely reliable.

A. Effect of Distributed Forces

Since the magnet modules are distributed along the bottom of the vehicle, the forces applied to the guideway gap variations are also distributed. To show the effect of the

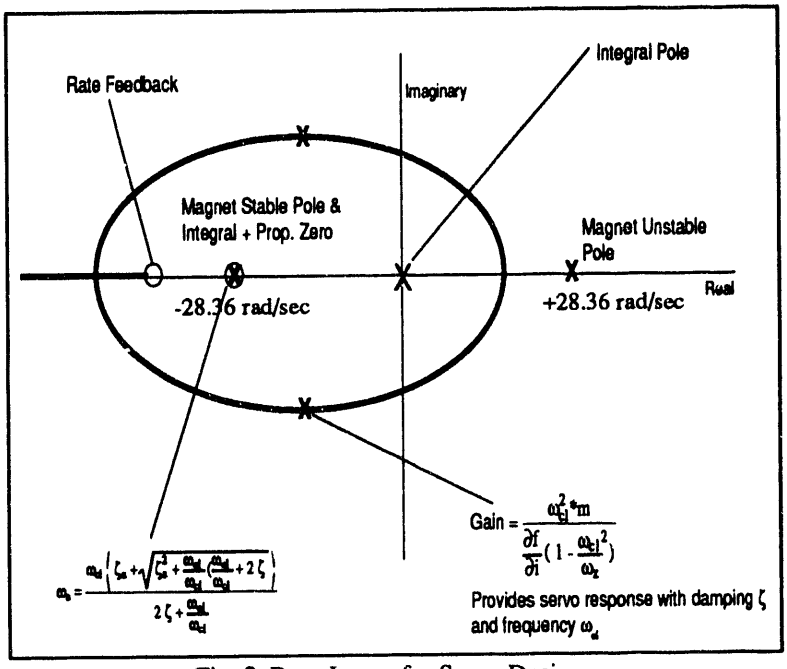

Fig. 2. Root Locus for Servo Design

distributed forces and measurements, a frequency response analysis was developed that assumes that the guideway is a single sine wave with wavelength λ. Thus the input to the control system gap sensor is sin $(2\pi v t/\lambda)$ where v is the vehicle speed. Since the sensors and control forces are distributed over the module mean that the displacement used to control the position of the magnet module is given (to a first approximation) by:

$$y(t) = \frac{1}{t_m}\int_{t-\frac{t_m}{2}}^{t+\frac{t_m}{2}} \sin(\frac{2\pi v t}{\lambda})\, dt \qquad (1)$$

where: t_m=the time it takes to traverse a module (i.e. $t_m = l_m/v$; l_m is the module length).

The integral is easily computed, and the result is that the gap input y(t) becomes:

$$y(t)=\frac{\lambda}{\pi l_m}\sin(\frac{\pi l_m}{\lambda})\sin(\frac{2\pi v}{\lambda}t) \qquad (2)$$

This expression shows exactly how the amplitude of a sinusoidal input is reduced as a consequence of the averaging over the time t_m in (1). The amplitude reduction in the temporal frequency domain can be obtained from the fact that $2\pi v/\lambda = \omega$

When this is substituted into (2) the Frequency (temporal) response is given by:

$$H(\omega)=\sin(\omega l_m/2v)/(\omega l_m/2v) \qquad (3)$$

which is a sin x/x curve in the frequency domain. The final transfer function for the gap error with a sinusoidal guideway input is the product of (3) and the transfer function for the gap servo. The resulting transfer function is given by:

$$\frac{\text{Gap Error}}{\text{Guideway Temporal Motion}}(\omega) = -\frac{j\omega(j\omega+23.5)(j\omega+89.68)}{(j\omega+42.42+j42.42)(j\omega+42.2-j42.2)(j\omega+28.36)} \qquad (4)$$

The transfer function (4) has the magnitude and phase plot shown in Fig. 3. As can be seen, the magnitude of the frequency response is damped to .707 and the bandwidth of the servo is 10 Hz (62.8 rad/sec). These are the design parameters we used for the servo design previously discussed. The result of combining the servo transfer function with the frequency response from (3) is shown in Fig. 4. These figures include the effect of the sin x/x curve (from (3)) and the effect of the location of the magnet modules. There are 6 magnet modules on each side of the vehicle and each module is 5.8 m (19.2 feet) long. The forces that are applied by these magnets are delayed in time by t_m as defined above. The effect of this time delay is to alter the phase of the transfer function at each of the module locations by ωt_m. Thus the phase is different for the different speeds and different locations, as shown in Fig. 4, but the magnitude curves are the same at each of the magnet locations. Note that no attempt was made to subtract 360 degrees from these phase curves so that the phase angles become very large in the plots.

C. Dynamic Model

Each of the magnets along the bottom of the vehicle cause a force to be applied to the vehicle at a particular location. These forces cause both translation and rotational motions that depend upon the location and the fact that the magnets are canted at an angle β with respect to the vertical. The angle β=35 degrees is chosen so as to apply all of the combined forces through the vehicle cg. The nomenclature that is used for these forces, and the way in which the various forces enter into the system are shown in Figure 5. Note that a sign appears before l1 through l3 to indicate the direction of the resulting moment, with a negative sign indicating that the moment is negative. When the equations of motion are developed these three moment arms are converted into 12 different values so that the moments can be obtained by a

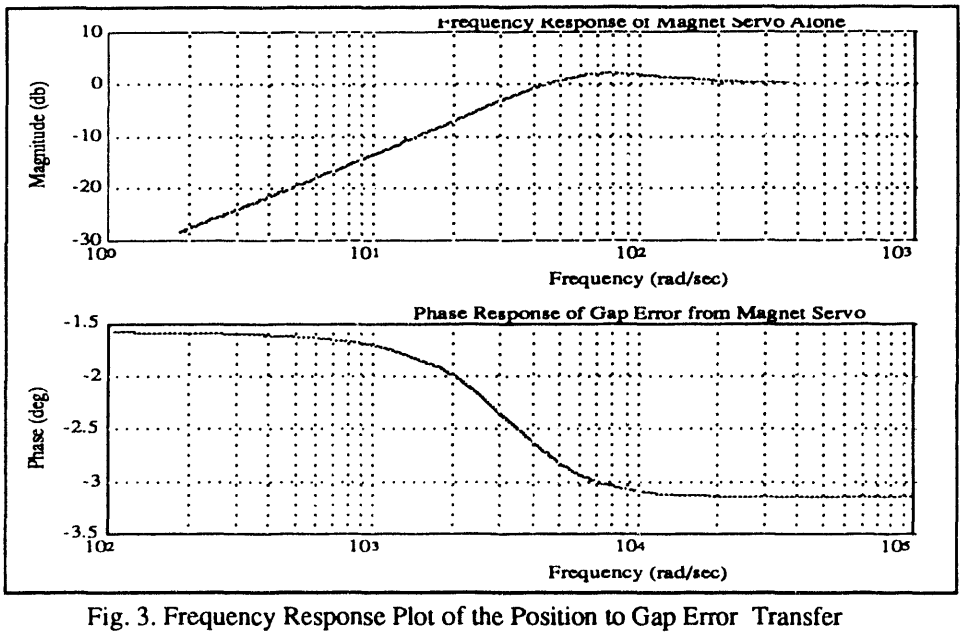

Fig. 3. Frequency Response Plot of the Position to Gap Error Transfer Function for the Magnet Servo

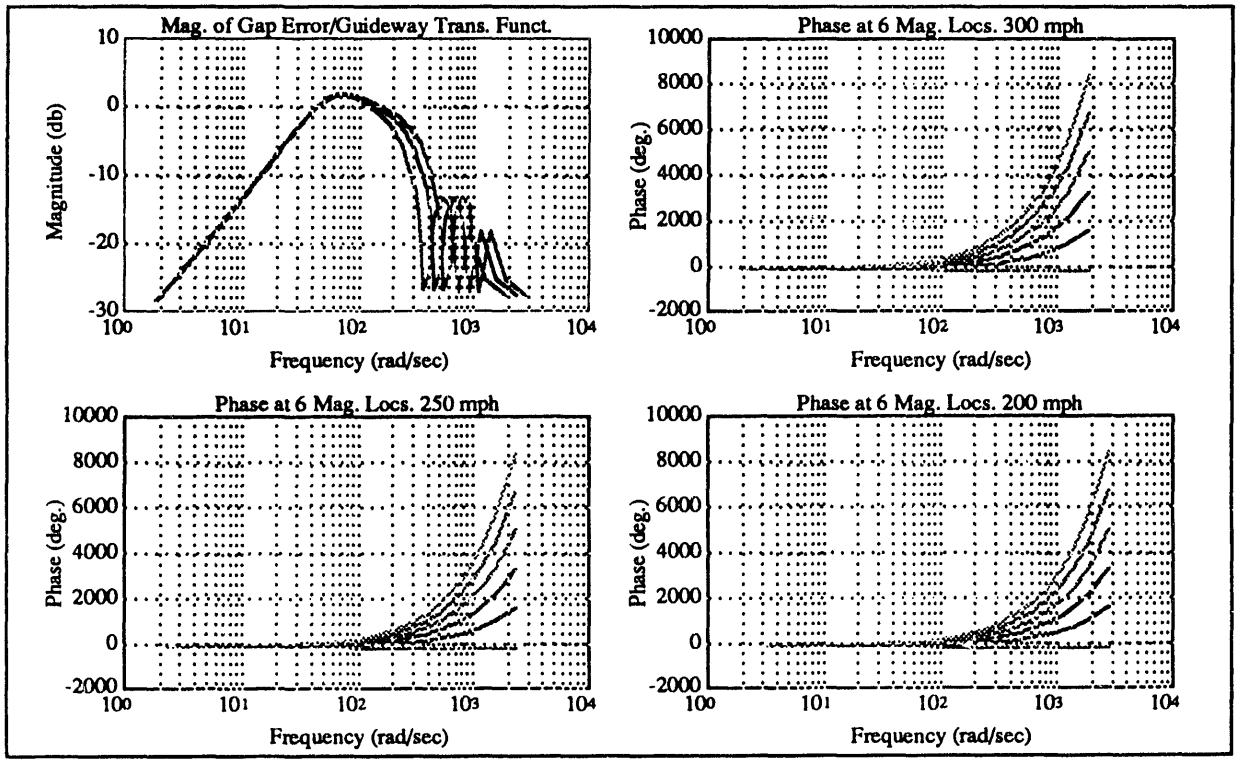

Fig. 4. Transfer Functions for Different Speeds and Magnet Module Locations

summation over the magnets 1 through 12. Thus the 12 moment arms are defined as follows:

$$\lambda_1 = -13,\ \lambda_2 = -13,\ \lambda_3 = -12,\ \lambda_4 = -12,\ \lambda_5 = -11,\ \lambda_6 = -11$$
$$\lambda_7 = 11,\ \lambda_8 = 11,\ \lambda_9 = 12,\ \lambda_{10} = 12,\ \lambda_{11} = 13,\ \lambda_{12} = 13 \quad (5)$$

Notice that with these definitions, all of the moment arms match the forces as defined in the figure, and furthermore the odd numbers are associated with forces on the right and the even numbers with forces on the left side of the vehicle. The

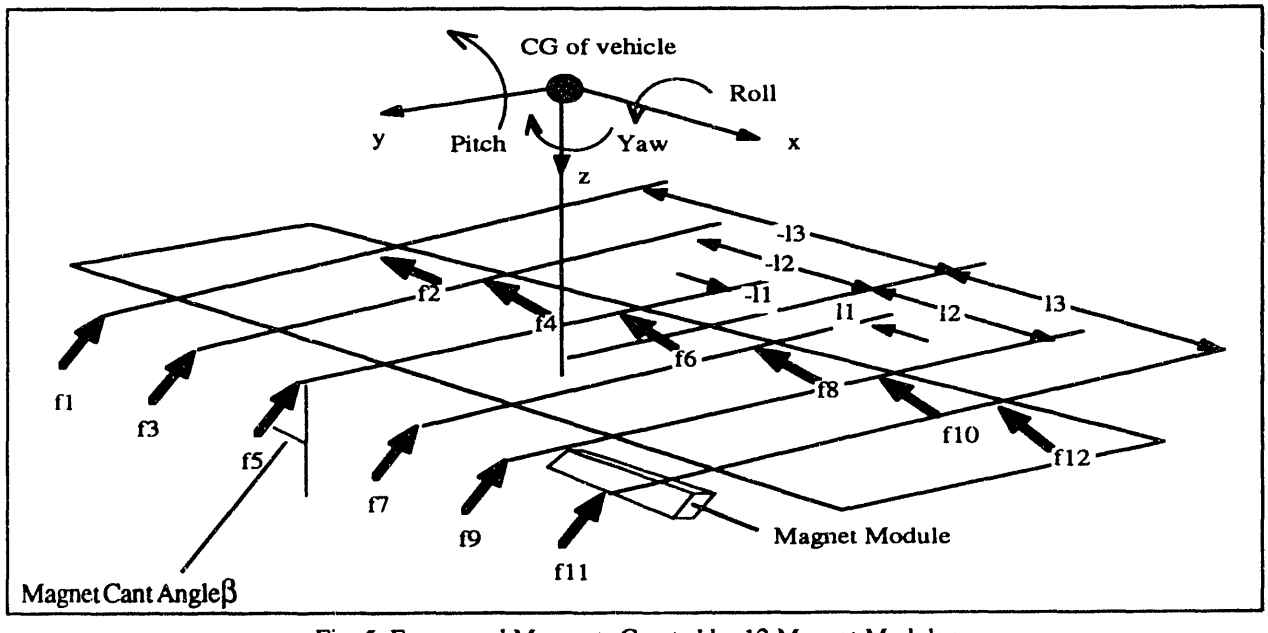

Fig. 5. Forces and Moments Created by 12 Magnet Modules

nominal values for l1, l2, and l3 are 5.76 m (18.9 ft.), 11.52 m (37.8 ft.), and 17.29m (56.7 ft.) respectively.

With these definitions, the forces and moments created are as follows:

Heave: $\cos(\beta)\ \Sigma f_i$; where the summation is over all i
Lateral: $\sin(\beta)\ \{\Sigma f_i$ (over even i) - Σf_i (over odd i)$\}$
Pitch: $\cos(\beta)\ \Sigma \lambda_i f_i$; where the summation is over all i
Yaw: $\sin(\beta)\ \Sigma \lambda_i f_i$; where the summation is over all
Roll: cgshift $\{\Sigma f_i$ (over even i) - Σf_i (over odd i)$\}$ (6)

In the roll expression, "cgshift" denotes the shift in the cg along the y and z axes from the nominal position. This cg shift is the only way that roll disturbances are induced since the nominal force vectors of all of the magnets is through the cg.

The state equations are created using a state vector (of size 40x1) that is defined by:

$$x = [\ \theta\ \ d\theta/dt\ \ \psi\ \ d\psi/dt\ \ x_1\ \ x_2\ \ \dots\ \ x_{12}\ ]^T \qquad (7)$$

where: $x_1, x_2 \dots x_{12}$ = the 12 different magnet servos all modeled with the mass and other terms divided by 12 as was discussed previously. If we use the subscript i to denote the i^{th} magnet module, the forces and moments in (6) can be determined from the acceleration of each module. Since the acceleration is the 2nd element in the state vector $\dot{x}$, the force from the i^{th} module is given by $[0\ m\ 0]\dot{x}$ which is written in a consise form by using the fact that $\dot{x} = Ax + bu$. The resulting state space model of the complete coupled dynamics is given by (8) below. In (8), the vector **u** is the guideway motions at the 12 magnet locations, $s = [0\ m\ 0]A$ and $\alpha = [0\ m\ 0]\mathbf{b}$. The inputs u are calculated as averaged motions that are shifted in time by d/v where d is the magnet location with respect to the front of the vehicle, and v is the train speed. With these definitions, the matrix B is simply the concatenation of the magnet state equations and terms that cause the pitch and yaw motions from guideway motions. Thus B is the 40 by 12 matrix given by (9).

$$B = \begin{bmatrix} 0 & 0 & \dots 0 \\ \lambda_1 \alpha \cos\beta & \lambda_2 \alpha \cos\beta & \dots \lambda_{12} \alpha \cos\beta \\ 0 & 0 & \dots 0 \\ \lambda_1 \alpha \sin\beta & \lambda_2 \alpha \sin\beta & \dots \lambda_{12} \alpha \sin\beta \\ \mathbf{b} & 0 & \dots 0 \\ \vdots & \vdots & \vdots \\ 0 & 0 & \dots \mathbf{b} \end{bmatrix} \qquad (9)$$

The full five DOF simulation uses (8) and (9) to calculate the combined heave, sway, pitch and yaw. The roll uses (6) to determine the torques applied about the z axis, combined with the equation $I_z d^2\phi/dt^2 =$ torques applied - $K_\phi \phi$. The constant K_ϕ is the effective restoring spring force in roll caused by the staggered geometry of the magnets in each module. This spring constant with a rate feedback term in roll provides the required roll damping and restoring force.

The results of the simulation with these equations of motion are discussed in section IV. The next two sections are devoted to describing the inputs **u** that are caused by the guideway vibration and the guideway irregularities. Each of these cause an effective temporal variation in the gap that is a function of the speed of the vehicle and the spatial distribution of the guideway displacements.

II - GUIDEWAY VIBRATION

Details of the baseline "spline girder" guideway design

$$\dot{x} = \begin{bmatrix} 0 & 1 & 0 & 0 & [0\,0\,0] & \dots & [0\,0\,0] \\ -\sum_{i=1}^{12} \frac{\alpha \lambda_i^2}{I_y} & 0 & -\sum_{i=1}^{12} \frac{\alpha \lambda_i^2 \cos\beta}{I_y} & 0 & \frac{\lambda_1 \cos\beta}{I_y} s^T & \dots & \frac{\lambda_{12} \cos\beta}{I_y} s^T \\ 0 & 0 & 0 & 1 & [0\,0\,0] & \dots & [0\,0\,0] \\ -\sum_{i=1}^{12} \frac{\alpha \lambda_i^2 \tan\beta}{I_z} & 0 & -\sum_{i=1}^{12} \frac{\alpha \lambda_i^2}{I_z} & 0 & \frac{\lambda_1 \sin\beta}{I_z} s^T & \dots & \frac{\lambda_{12} \sin\beta}{I_z} s^T \\ -\frac{b\lambda_1}{\cos\beta} \begin{bmatrix}0\\0\\0\end{bmatrix} & & -\frac{b\lambda_1}{\sin\beta} \begin{bmatrix}0\\0\\0\end{bmatrix} & & A & [0]_3 [0]_3 \dots [0]_3 \\ -\frac{b\lambda_2}{\cos\beta} \begin{bmatrix}0\\0\\0\end{bmatrix} & & -\frac{b\lambda_2}{\sin\beta} \begin{bmatrix}0\\0\\0\end{bmatrix} & & [0]_3 & A\ [0]_3 \dots [0]_3 \\ \vdots & \vdots & \vdots & \vdots & \vdots & \vdots & \vdots \\ -\frac{b\lambda_{12}}{\cos\beta} \begin{bmatrix}0\\0\\0\end{bmatrix} & & -\frac{b\lambda_{12}}{\sin\beta} \begin{bmatrix}0\\0\\0\end{bmatrix} & & [0]_3 & [0]_3 [0]_3 \dots A \end{bmatrix} x + Bu \qquad (8)$$

identified for the Grumman design is given in [4]. The vibration of the guideway is broken into two independent parts: heave and torsion. The model used to simulate the guideway dynamics is a simple beam that is pinned at each of the support pillars. The pillars are assumed to be rigid, and there are no interactions between the guideway and the pilings, and soil.

A. Bending Dynamics

The underlying equation of motion that describes a simple pinned beam (the Bernoulli-Euler beam) is:

$$E I_y \frac{\partial^4 z(x,t)}{\partial x^4} + c \frac{\partial z(x,t)}{\partial t} + \rho a \frac{\partial^2 z(x,t)}{\partial t^2} = f(x,t) \qquad (10)$$

where: z(x,t) =vertical displacement as a function of time (t) and distance along the beam (x) with z(0,t) = 0 and z(guideway length, t) = 0 (i.e. there is no motion at the beam ends)

E =modulus of elasticity of the beam material

I = cross sectional inertia of the beam about the axis of bending (pitch)

ρa =mass density times the cross sectional area of the beam - i.e. the mass per unit length of the beam

f(x,t) =loading (force) on the beam as a function of time and distance

c =viscous damping coefficient.

To determine the solution of (10), we assume that the displacement z is the product of a function of time and a function of distance. Thus:

$$z(x,t) = \sum_{i=1}^{n} A_n(t)\ \phi_n(x). \qquad (11)$$

When (11) is substituted into (10), the mode shapes $\phi_n(x)$ are the solutions of the differential equation:

$$\frac{d^4\phi_n(x)}{dx^4} - \frac{m\,\omega_n^2}{EI}\phi_n(x) = 0 \qquad (12)$$

which, with the initial conditions given in (10), has a solution given by:

$$\phi_n(x) = \sin\left(\frac{n\pi x}{\text{guideway length}}\right) \qquad (13)$$

The solutions for $\phi_n(x)$ are called the mode shapes of the beam. In (12) the frequency ω_n^2 is given by:

$$\omega_n^2 = \left(\frac{n\pi}{\text{guideway length}}\right)^4 \frac{E I}{\rho a} \qquad (14)$$

The resulting differential equation (15) for the time varying modal amplitudes q, is obtained by substituting (11) into (10) and then multiplying by $\phi_n(x)$ and integrating from x=0 to x=guideway length. Where the forcing function $f(x_n,t)$ is developed as follows. When the vehicle moves across the guideway, the force applied is distributed over the magnet modules. We have assumed that this force is continuous over the length of the vehicle, so that f(x,t) has the form shown in Fig. 6. In the simulation the guideway is divided into 100 grid elements (so that Δx is 0.27 m), and the time grid and space grid are made consistent by assuming that Δt = Δx/speed. With this assumption, the vehicle moves one Δx in one time Δt. The simulation is for 1 second, so that at the nominal speed of 134 m/s (300 mph) Δt is 0.002 seconds. With these quantizations, and the assumption that only the first 5 modes are significant, the discrete force is a 100 by 500 matrix. In this form the first 5 modes are modeled using (15), where the state vector q is the mode amplitudes and their derivatives, and the matrix $\Phi_n(x_n)$ is a 5 by 100 matrix

$$\dot{q} = \begin{bmatrix} \dot{A}_1 \\ \ddot{A}_1 \\ \vdots \end{bmatrix} = \begin{bmatrix} 0 & 1 & \cdots 0 & 0 \\ -\omega_1^2 & -2\zeta\omega_1 & \cdots 0 & 0 \\ \vdots & \vdots & & \vdots \\ 0 & 0 & \cdots -\omega_5^2 & -2\zeta\omega_5 \end{bmatrix} q + \begin{bmatrix} 0 & \cdots & 0 \\ \omega_1^2 & & 0 \\ \vdots & & \vdots \\ 0 & \cdots & 0 \\ 0 & & \omega_5^2 \end{bmatrix} \Phi(x_n)\, f(x_n,t) \qquad (15)$$

$$\Phi(x_n) = \begin{bmatrix} \sin(0) & \sin\left(\frac{\pi\,\Delta x}{\text{guideway length}}\right) & \cdots \sin\left(\frac{\pi\,100\,\Delta x}{\text{guideway length}}\right) \\ \vdots & & \\ \sin(0) & \sin\left(\frac{\pi\,\Delta x}{\text{guideway length}}\right) & \cdots \sin\left(\frac{\pi\,100\,\Delta x}{\text{guideway length}}\right) \end{bmatrix} \qquad (16)$$

created from the mode shapes as follows:

A structural damping ratio ζ = 0.02 was assumed for all of the modes.

The simulation of the guideway motion from (15) results in the individual mode amplitudes, and the actual displacements of the guideway are obtained from q by using equation (11). Since this equation can be viewed as a matrix product, the physical motions may be written as:

$$z(x,t) = \Phi(x_n)^T \begin{bmatrix} 1\,0 & 0\,0 & \cdots 0\,0 \\ 0\,0 & 1\,0 & \cdots 0\,0 \\ \vdots & \vdots & \vdots \\ 0\,0 & 0\,0 & \cdots 1\,0 \end{bmatrix} q \qquad (17)$$

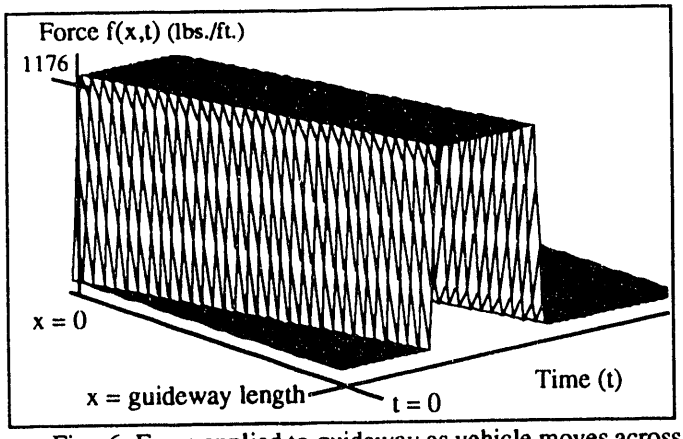

Fig. 6. Force applied to guideway as vehicle moves across

The resulting z(x,t) is a matrix with 100 rows representing the physical location along the guideway at increments Δx, and 500 columns representing time at the interval Δt. A plot of this displacement is shown in Fig. 7 (a).

B. Torsional Vibration Dynamics

The torsional vibration is modeled in the same way as bending. The torsion model is the "Saint-Venant" equation given by:

$$\rho I_x \frac{\partial^2\phi(x,t)}{\partial t^2} + b\frac{\partial\phi(x,t)}{\partial t} + G J \frac{\partial^2\phi(x,t)}{\partial x^2} = m(x,t) \quad (18)$$

where: $\phi(x,t)$ = angle of twist per unit length

ρI_x = product of the mass density and the cross-sectional inertia

$G J$ = torsional stiffness where G is the shear modulus, and for an isotropic material is equal to $E/2(1+\nu)$ and J is the polar moment of inertia -ν is the Poisson ratio for the material and E is Young's modulus

$m(x,t)$ =twisting moment applied to the guideway by the vehicle

b =viscous damping coefficient in torsion

Equation (18) is solved in exactly the same way as the bending equations. The mode shapes are slightly different since (18) is second order in x whereas the bending equation is fourth order.

The modes are: $\sqrt{2}\sin\left(\frac{n\pi x}{\text{guideway length}}\right)$ and the mode frequencies are: $\omega_n^2 = = \frac{n\pi}{\text{guideway length}}\sqrt{\frac{GJ}{\rho I_x}}$.

The resulting torsional vibrations multiplied by the lever arm from the guideway beam center line to the center of the

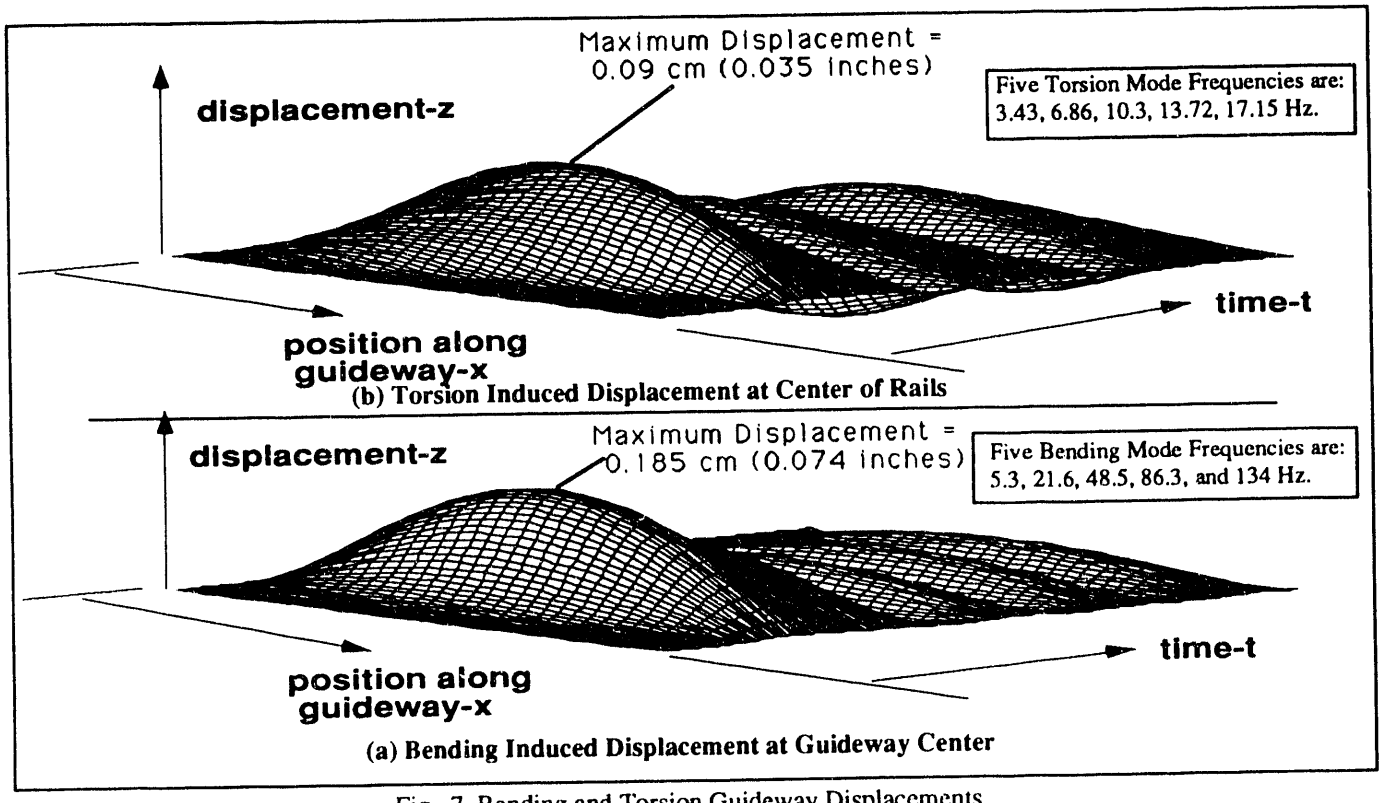

Fig. 7. Bending and Torsion Guideway Displacements Functions of Distance Along the Guideway and Time

rail (to give heave motion) is shown in Fig. 7 (b).

III. GUIDEWAY IRREGULARITIES

The guideway irregularities are caused by the pier height variations, the variations created by the mounting of the rails to the guideway structure, by variations in the camber that is added to the guideway to account for the vehicle loading, and surface irregularities in the steel that makes up the rails. Each of these is modeled as a simple stochastic process where the independent variable is the location along the guideway (x). These spatial variation are then converted into functions of time for the vehicle simulation by using the change of variable t = x/v (where v is the speed of the vehicle).

A. Rail and Span Offsets (or Steps)

The steps in the rail from section to section are a consequence of the vertical offsets due to the installation of the rails on the guideway, and the manufacturing and installation tolerances of the pilings, the guideway support columns, and the guideway elements. In addition, environmental effects such as frost, temperature, and settling affect the column heights. We have modeled these effects as a random step discontinuity in the rail at each column. The assumption is made that the right and left rails are affected independently, so that each rail has a discontinuity given by:

$$\text{step left} = s_1$$
$$\text{step right} = s_2 \qquad (19)$$

where: s_1 is a Gaussian random variable with mean zero and variance of 0.15 cm (0.06 inches).

The Gaussian assumption means that most of the time the variation will be around 0.15 cm (0.06 inches), and with probability .99 the value will be less than 0.5 cm (0.2 inches). Note that this variation can be positive or negative, so these step irregularities are around the nominal guideway position.

In the simulation, typically 8 guideway sections were modeled with independent sets of left and right steps at each section. The resulting temporal variations seen by the vehicle when its speed is 134 m/s (300 mph) are shown in Fig. 8.

B. Rail and Span Angular Misalignment (or Ramps)

The ramps in the rail and guideway are also a consequence of column height differences. This effect is modelled as follows:

$$\text{ramp} = s_3(i-1) + (s_3(i) - s_3(i-1))\ x/(\text{guideway length}) \qquad (20)$$

where: $s_3(i)$ = the height variation at the ith column and it is a Gaussian random variable with mean zero and variance of 0.25 cm (0.1 inches)
x = the distance along the guideway segment with x going from 0 to guideway length.

This variation is assumed to be the same for the left and right rail, and is also shown in Fig. 8.

C. Variations in the Camber in the Guideway

Post tensioning of the guideway is used to counteract the loading that is applied to the guideway. However the nominal prestress camber that is applied may change as a consequence of variations in the prestress, sagging due to creep and long term loading effects. The model for camber errors is:

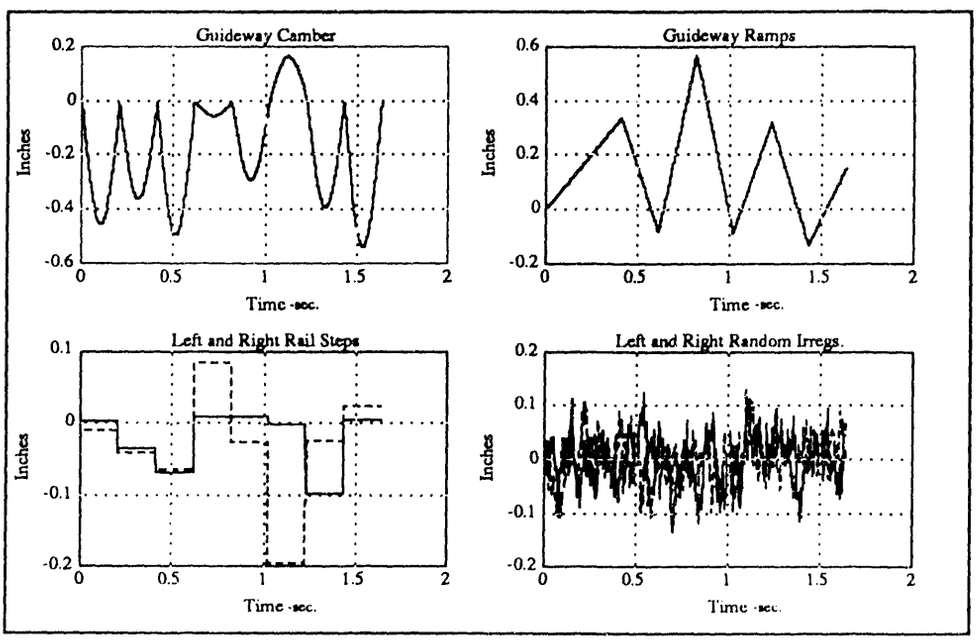

Fig. 8. Guideway Irregularities - Camber, Ramps, Steps and Random

$$y = s_4 \left| \sin\left(\frac{\pi x}{\text{guideway length}} \right) \right| \qquad (21)$$

where: s_4 = Gaussian with zero mean and a variance of 0..25 cm

Figure 8 shows a typical set of camber variations modeled using (21).

D. Random Roughness Irregularities

The random roughness is a consequence of the manufacturing process for the rails. The guideway roughness is an "exponentially correlated" random process that is modeled with the differential equation:

$$\frac{dy}{dx} = -\gamma y + \sqrt{2\gamma}\ \sigma \text{ white noise} \qquad (22)$$

In this equation, σ is the desired variance of the process y, and γ is 1/(correlation length). The correlation length is the distance over which y is related to its previous values (correlated). Beyond 3 times the correlation length, these irregularities are independent. Since the rail in our design is pinned to the guideway at each out-rigger, and at points half-way between the out-rigger, the correlation length must be 2.3 m (7.5 feet) - the distance between the mounting brackets. In the model we have used this length so that γ becomes 1/7.5. The resulting rail roughness is different for the right and left rail, as is shown in Fig. 6. The variance in (22) is 0.1 cm (0.043 inches).

IV. SIMULATION RESULTS

The 5 DOF simulation was exercised with the inputs described above to determine the response in heave, sway, pitch, yaw, and independently in roll. The combined guideway irregularities shown in Fig. 8 and vibration induced motions shown in Fig. 7, are averaged over a magnet module. This averaged motion becomes the input to the magnet module – which accounts for the fact that the forces applied by the magnet are distributed over the length of the module. Figure 9 shows the effect of this averaging. In Fig. 9 (a), the combined left and right rail irregularities (combining the steps, ramps, camber, and roughness) are plotted vs. time (corresponding to a vehicle speed of 134 m/s). As can be seen, the maximum deflection of the rails is about 1.5 cm (0.6 inches). In Fig. 9 (b), the guideway vibration seen at each of the servo locations is plotted. To obtain this motion from the guideway vibration shown in Fig. 7, the bending and torsion induced vibrations are added together, and to determine the motion at each of the servo locations the combined motions as a function of x and t are converted into a function of t alone using the fact that $x = x_0 + v\,t$ where v is the speed of the vehicle and x_0 is the location of the magnet module. Since the quantization in z and in t were made consistent with the velocity v, the actual procedure for doing this is simply reading the matrix z(x,t) along the diagonal beginning at $x = x_0$. One last observation about Fig. 9 (b) is that the vibration shown is due to eight guideway segments. This is achieved by duplicating the bending and torsion response of the single section that was simulated. Figure 9 (c), shows the combined motions from (a) and (b) when they are averaged over the module length. The dramatic reduction in amplitude from a maximum of about 1.75 cm (0.7 inches) to a maximum of 0.125 cm (.05 inches) is a consequence of the distribution of the loads over the magnet module length. It is this feature - combined with the large gap size - that allows us to have good ride quality without a secondary suspension.

As a comparison, we were able to use the same dynamic analysis to compare our design with one that uses a four point suspension and a conventional spring, mass, damper suspension (such as would be the case were the vehicle a wheeled system) and a four point suspension using magnets (such as would be the case for an electrodynamic suspension). These results are shown in Fig. 10. As can be seen, the accelerations for the four point suspensions (without secondary suspensions) are almost an order of magnitude bigger than the accelerations in our design.

The heave acceleration power density spectrum (PSD) results shown in Fig. 10 where plotted on a 1/3 octave frequency band and compared to the one

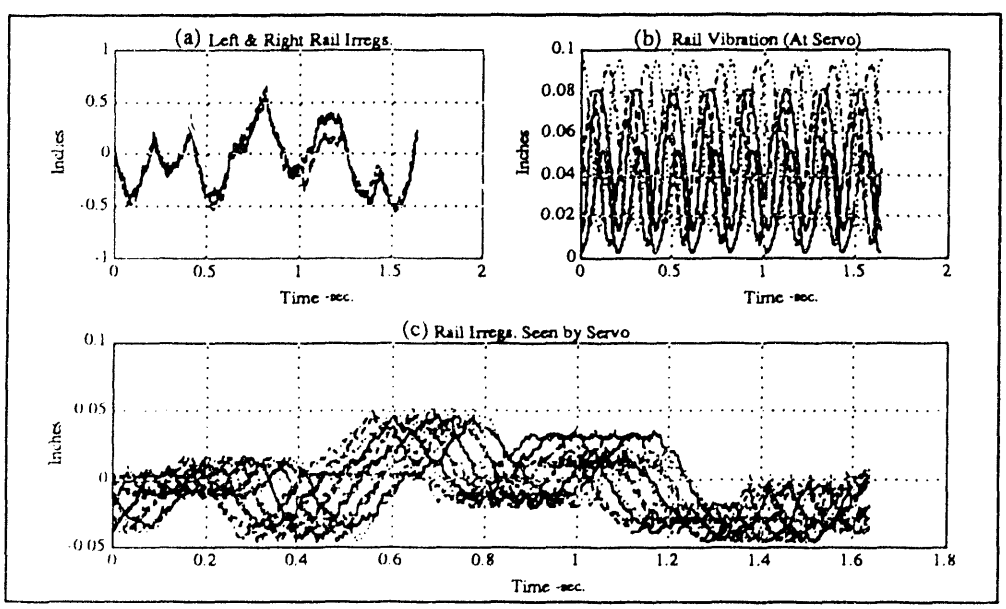

Fig. 9. Guideway Irregularities and Bending/Torsion Induced Motions at the Rails and as Seen by the 12 Magnet Servos

hour vertical ISO comfort limits established for the SCD study. The results indicate that the vibration levels which the passengers will experience will be significantly below the ISO standards. The conclusion therefore is that the only way the four point suspension can achieve the ride quality requirements is with a secondary suspension, whereas we have achieved better then required ride quality without a secondary suspension.

Clearly, the ability to achieve the superb levels of acceleration is a consequence of; 1) the large gap size we have in our design, 2) the controllability using acceleration feedback, and 3) the distributed loading on the vehicle and guideway. The gap size is important because we do not have to follow irregularities that are as big a 1.25 cm (0.5 inches) since we have the "headroom" to allow this gap error to be ignored. In the Transrapid design, with a much smaller gap this is not true.

Wide gap step errors (up to 3 cm) where also investigated using this program and compared to results from a single axis non-linear simulation [3]. The two simulations confirmed that rapped changes in gap can be accommodate within control authority limits of the servo.

V. CONCLUSIONS

The simulation of the vehicle motion demonstrates that the use of a distributed force with a large gap allows an inherently smooth ride quality. This feature has allowed a design that does not require a secondary suspension system, with a significant concomitant weight savings. This weight savings directly translates into reduced guideway cost. In addition, the guideway stiffness does no have to be large in order to handle the dynamic loading because the load is distributed. These two consequences of a distributed large gap design makes the overall Grumman concept a very promising development system

.

REFERENCES

[1] M. Proise et al., "System Concept Definition of the Grumman Superconducting Electromagnetic Suspension (EMS) Maglev Design," to be presented at the Maglev 93 Conference, Argonne National Laboratory, May 19-21, 1993, Paper No. OS4-4

[2] S. Kalsi, R. Herbermann, C. Falkowski, M. Hennessy, A. Bourdillon, "Levitation Magnet Design Optimization for Grumman Maglev Concept," to be presented at the Maglev 93 Conference, Argonne National Laboratory, May 19-21, 1993, Paper No. PS2-7

[3] R. Herbermann, "Self Nulling Hybrid Maglev Suspension System," to be presented at the Maglev 93 Conference, Argonne National Laboratory, May 19-21, 1993, Paper No. PS1-7

[4] J. Allen, M. Ghali, "Innovative Spine Girder Guideway Design for Superconducting EMS Maglev System," to be presented at the Maglev 93 Conference, Argonne National Laboratory, May 19-21, 1993, Paper No. PS3-1

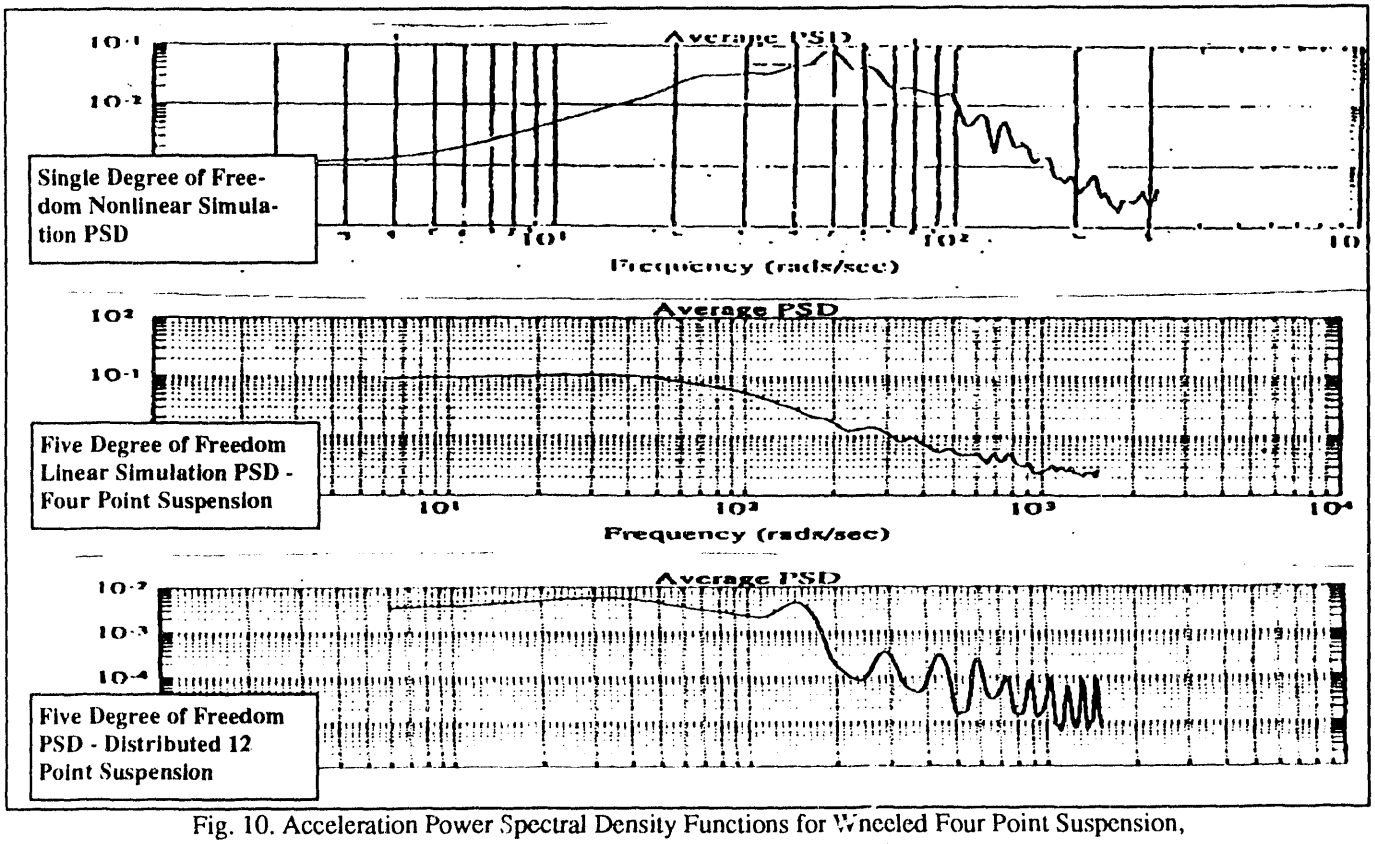

Fig. 10. Acceleration Power Spectral Density Functions for Wheeled Four Point Suspension, Magnet Four Point Suspension and Distributed Suspension

Vehicles for Superconducting Maglev System on Yamanashi Test Line (Except Linear Synchronous Motors)

Kikuo TAKAO
Vehicle Engineering Department, Maglev System Development Division, Railway Technical Research Institute, Kokubunji-shi, Tokyo 185

Noriyuki SHIRAKUNI
Linear Express Research and Development Division, Central Japan Railway Co.Ltd., Chuo-ku, Tokyo 103

Abstract - A superconductive magnetic levitation (Maglev) system in Japan has been developed to the extent that basic technology is established on Miyazaki Maglev Test Track and now for the purpose of practical technology development the construction of Yamanashi Test Line is underway. This paper describes the lightweight bodies, lightened bogies with elastic support of superconducting magnets (SCM) for vehicles of Yamanashi Test line.

I. Introduction

Development of a superconductive magnetic levitation (Maglev) system in Japan was started in 1962 by Japanese National Railways (J.N.R.). That was two years before Tokaido Shinkansen Line between Tokyo and Osaka went into a revenue service.

We decided at once that the next new high-speed train should be Maglev System. Then we began to study Maglev System and at the same time to design vehicles for Maglev System.

In 1972 an experimental vehicle ML100 of superconductive Maglev system succeeded for the first time in a levitated running on the Experimental Short Test Track. In 1975 ML100A succeeded in a perfect non-contact run by SCM.

In 1977 the test run of ML500 took place on Miyazaki Test Track of 7 km length. ML500 attained a maximum speed record of 517 km/h in 1979.

We have made many experiments since 1979 on Miyazaki Test Track by several different types of vehicles, which were ML500, ML500R, MLU001 and MLU002.

And over 10,000 people including general persons tried a ride on the Maglev Vehicles MLU001 and MLU002. The experimental and trial run of manned vehicles proved the safety of Maglev System and Vehicles.

On the basis of those experimental results we have developed and designed Maglev Vehicles for Yamanashi Test Line since 1990.

Right now we have already decided configurations of Vehicles on the Yamanashi Test Line. We started a detailed design of vehicles and soon we shall fabricate new vehicles.

Here are outlined the Vehicles for Maglev on Yamanashi Test Line and details of development of the experimental vehicles for Maglev on Miyazaki Test Track.

This Yamanashi Test Line Construction Project is receiving financial support of the Government.

II. Details of Development of the Vehicles for Maglev System

A. ML100

ML100 which was the first experimental small vehicle for superconducting Maglev system debuted in 1972 (Fig.1). It had 4 seats. In 1972 ML100 succeeded in levitated running at a speed of 60 km/h on the Experimental Short Test Track in J.N.R.'s Kunitachi Laboratory. In 1975 ML100A succeeded in levitated perfect non-conducted running.

The results of repeated experiments by ML100 series made us confident of the possibility of 500 km/h running.

That was the first step in Maglev system.

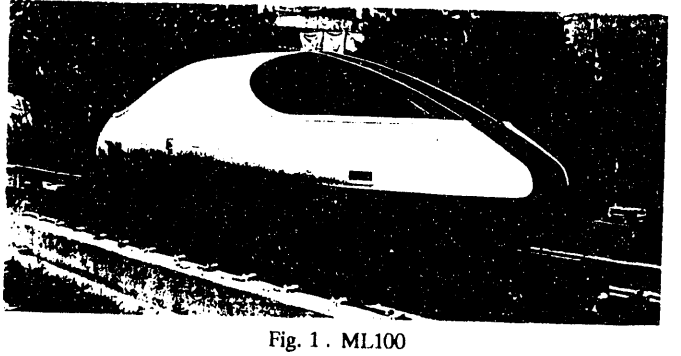

Fig. 1 . ML100

B. ML500

In 1975 we constructed Miyazaki Test Track with a length of 7 km.

In 1977 ML500 was fabricated for the new test track with inverted-T shaped guideway (Fig.2).

ML500 attained a maximum speed record of 517 km/h run on 21 December 1979. We could succeed in the experimental

500 km/h running only in 7 years after taking the first step.

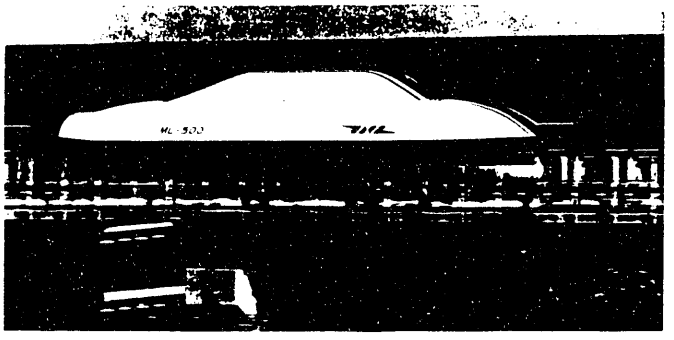

Fig. 2. ML500

C. MLU001

In 1980 Miyazaki Test Track was reconstructed. The invert-T shaped guideway was transformed into U-shaped.

From 1980 to 1982 the manned vehicle MLU001 was fabricated for the U-shaped guideway. MLU001 is a 3-car unit (Fig.3).

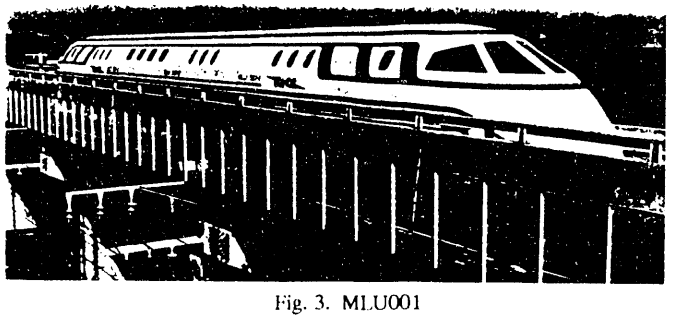

Fig. 3. MLU001

In 1986 MLU001 of 3-car unit attained a speed of 352.4 km/h. In 1987 MLU001 of 2-car unit a maximum speed of 405.3 km/h run unmanned and attained a speed of 400.8 km/h run manned. The trial ride on MLU001 carried about 1,200 people in total.

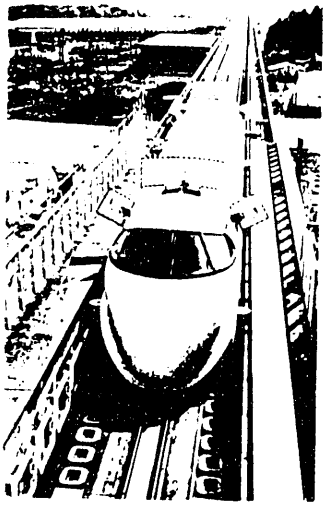

Fig. 4. Experiment of aerodynamic brake on MLU001

MLU001 also had an experiment of an aerodynamic brake system which we had developed to secure a reliable emergency braking at a speed of over 350 km/h. The brake works by aerodynamic drag of aerodynamic panels which are parts of the outside plates of the body, which are designed to be lifted by a hydraulic system. The experimental results proved that its braking force is effective enough for running at speeds higher than 350 km/h (Fig.4).

D. MLU002

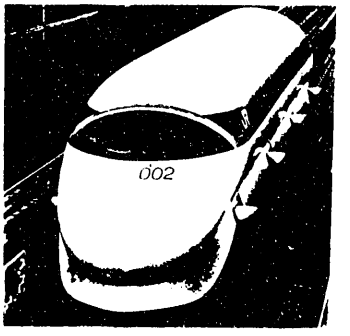

Fig. 5. MLU002

In March 1987 the construction of MLU002 was finished just before J.N.R. was privatized and divided (Fig.5).

The coil distribution was changed to a concentration style from a dispersion style.

In December 1989 MLU002 attained a speed of 394 km/h run.

It had 44 seats for passengers. About 9,500 people tried a ride on MLU002. The number of trial riders of MLU001 and MLU002 including general people amounted to over 10,000 persons. This testified to the safety of the vehicle for Maglev system.

But unfortunately we lost MLU002 by a fire accident on 3 October 1991.

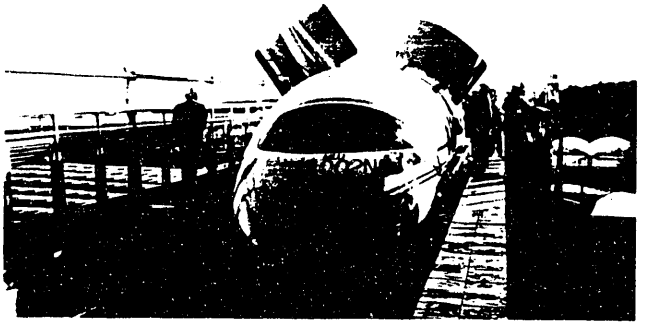

Fig. 6. MLU002N

E. MLU002N

In December 1992 the latest vehicle named MLU002N debuted on Miyazaki Test Track (Fig.6).

We designed it taking lessons from the fire accident. We chose kinds of material, structure of body and, bogie and equipment for fire-protection. For example, all-aluminum body instead of FRP'use, non-combustible material in the body, new aluminum wheels without using magnesium alloy, safety tires, use of fire-resistant hydraulic oil, fire extinguishing appliances, fire warning systems, and so on.

MLU002N newly has a pair of aerodynamic brakes as emergency brake system and 12 seats for passengers.

To provide the magnetic cushion and the better riding comfort, each bogie has two different types of elastic support of SCM , one system which uses air spring and some links connecting a bogie and SCM (called "Link" system), and the other system which uses an intermediate bogie frame connected to the body and the other bogie frame is coupled to SCM

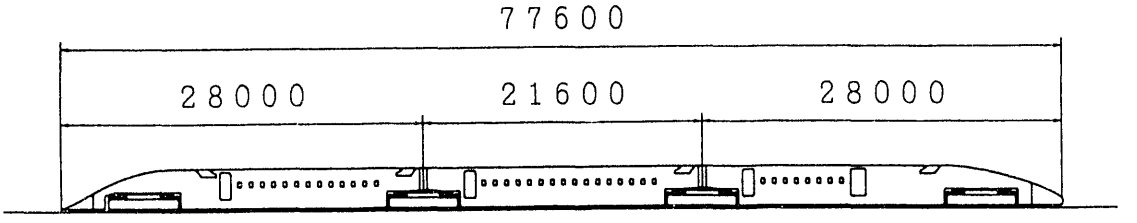

Fig. 7. Outline of Yamanashi Maglev Vehicles

directly (called "Double Bogie Frame" system).
MLU002N's test runs started in January 1993.

III. Vehicles for superconducting Maglev system on Yamanashi Test Line

A. Outline of Vehicles

Yamanashi Test Line is the last stage for making sure the possibility of commercialization of Maglev system. Therefore we have to bear the revenue service in mind in designing new vehicles. For example, seating capacity, service equipment, high riding comfort, etc.

There are two train sets which will run at a speed of over 500 km/h (maximum speed of 550 km/h) on Yamanashi Test Line, one of which is a 3-car unit and the other a 5-car unit. Each train consists of articulated bogies (Fig.7).

B. Lightweight Bodies

The bodies must have their weight reduced as much as possible and at the same time must have enough rigidity and air-tightness for the riding comfort. The total weight of each body including all equipment is limited to less than 13 tons for a middle-car or 17 tons for an end-car.

We have already developed 4 types of lightweight bodies since 1989. Here is the present status of R&D.

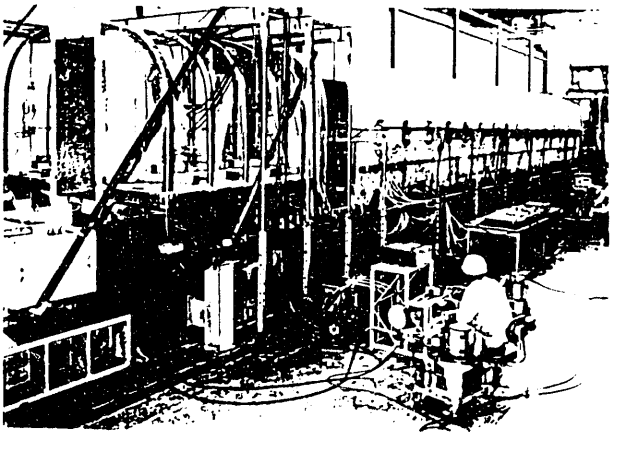

Fig. 8. The experiment of H1-body

1) H1 type body: In 1989 H1 type body named H1-body was fabricated, the length of which was 21.0 meters (Fig.8).

It was the first trial body for the commercialized Maglev vehicle. It is made of aluminum and steel. The main part of body is constituted of aluminum. Outside shell is made of aluminum shapes. And frames are made of machined aluminum plates. They are joined by spot-welding or riveting. Both ends of body are constituted of steel, because it is effective for shielding magnetic influence of SCM. The main body and the end body are joined by special riveting.

The cross section shape of H1-body is little different from other 3 types of trial bodies.

H1-body was put to many experiments which gave many useful results. Experiments of H1-body included static load tests; vertical load test, compressive load test from both ends, air-tight load test, back and forth load test between body and bogies, and so on.

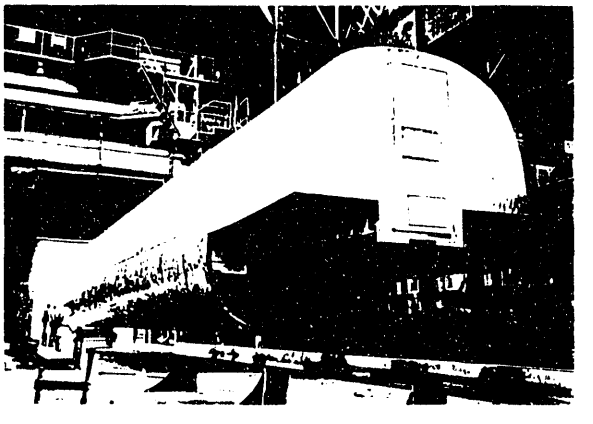

Gig. 9. H2-body

2) H2 type body: H1-body was still in the experimental stage of developing a lightweight body. In 1990 H2 type body named H2-body was fabricated, the length of which was 23.7 meters, that is 2.7 meters longer than H1-body. It is called "long-body", which was the first trial long-body of Maglev vehicle (Fig.9).

It is made of aluminum and steel, the same as H1-body. The main part of body is constituted of aluminum plates. Outside shells are thin aluminum plates. Stringers and frames are machined aluminum plates. They are joined by all spot-welding. Both ends of body are constituted of steel for the same reason as H1-body. The main body and the end body are joined by special riveting. It is a kind of semi-monocoque structure.

The cross section of H2-body is a successive conical curve

instead of circular curve.

H2-body have been put as many experiments under the static load as H1-body. Additionally it has been put to an experiment for fatigue strength to prove its durability under repeated air-tight load.

3) H3 type body: In 1991 H3 type body named H3-body was fabricated, length of which was as long as "long-body" (Fig.10).

It is made of duralumin used in airplane and steel. The main part of body is constituted of duralumin. Outside shells are thin duralumin plates. Stringers and frames are machined duralumin plates. They are joined by all riveting. Both ends of body are constituted of steel and partly duralumin. The main body and the end body are joined by special riveting. It is a kind of semi-monocoque structure.

The cross section of H3-body is a successive conical curve, the same as H2-body.

H3-body was put to as many experiments under the static load as H1-body and H2-body. And it had an experiment for fatigue strength, the same as H2-body.

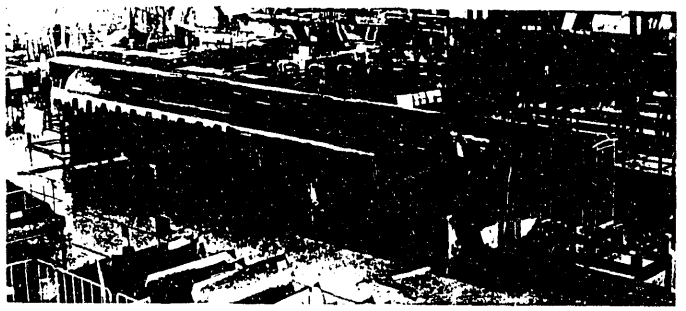

Fig.10. H3-body

4) H4 type body: In 1992 H4 type body named H4-body was fabricated, the same as "long-body"(Fig.11).

It is made of brazed aluminum honeycomb panels and steel. The main part of body is constituted of all brazed aluminum honeycomb panels. Outside shells are the built-in aluminum honeycomb panels with aluminum frames. Therefore not any stringers and frames are seen inside. They are joined by welding. Both ends of body are constituted of steel. The main body and the end body are joined by special riveting. It is rather a semi-monocoque structure.

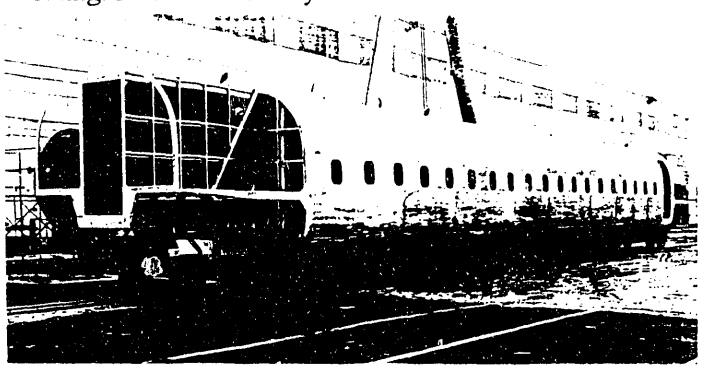

Fig.11. H4-body

The cross section of H4-body is a successive circular curve almost the same as conical curves for H3-body.

H4-body was tested the static load as many times as other bodies. And it is now undergoing on fatigue strength under air-tight load.

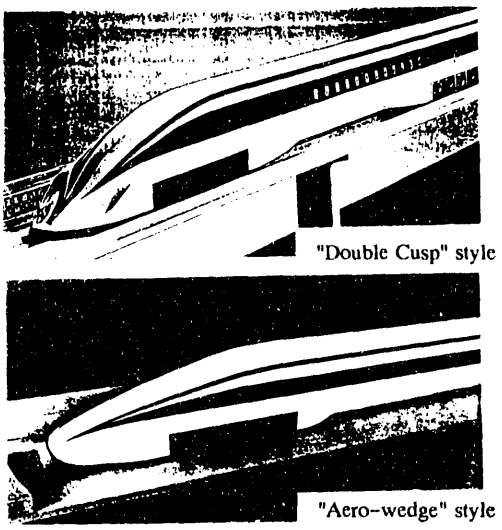

Fig.12. Nose-shape of head cars

C. Nose-shape of Head Car

Vehicles for superconducting Maglev on Yamanashi Test Line have two types of nose-shape (Fig.12). One type is called "Double Cusp" style and the other is called "Aero-wedge" style. Both of them are superior in aerodynamic performance, especially in aerodynamic drag, aerodynamic noise and micro-pressure waves of tunnel. We designed them based on the results of CFD analysis and some experiments in the wind tunnel.

D. Bogies

The bogies are also lightened. Additionally one type of them has to suspend the SCM elastically by air-springs for riding comfort.

If the SCM is quenched, the rubber tires must be able to run long distance at high speeds. So we need tough and safe tires.

The on-board contact-free power-collection utilizes the electromagnetic inductance between the SCM aboard the vehicle and the levitation coils on ground.

Under such conditions we are developing the new Maglev bogies.

1) Elastic Support of SCM: The bogies for Yamanashi Vehicles will have the elastic support system of SCM to provide the magnetic cushion and the riding comfort.

The conventional bogie frame consisted of cross-beams and

side-beams connected with SCM directly and rigidly (Fig.13).

The elastic support of SCM called "Double Bogie Frame" system uses two different frames, one of which is intermediate bogie frame connecting the body to 2 air-springs, and the other is SCM supporting frame connecting the intermediate bogie frame to another 4 air-suspension (Fig.14).

We are going to design Double Bogie Frame referring to the experimental result at Miyazaki Test Track using MLU002N.

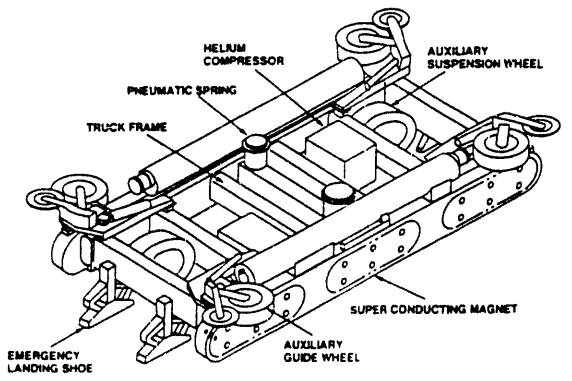

Fig.13. Conventional Bogie (MLU002)

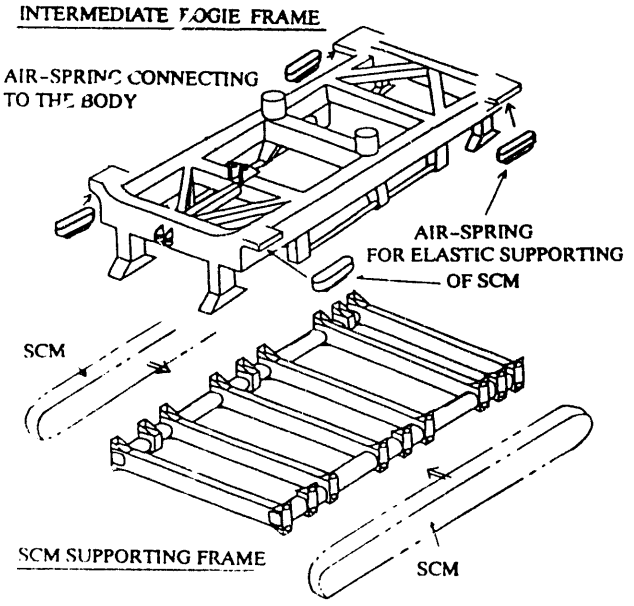

Fig.14. Bogie of elastic support of SCM ("Double Bogie Frame" system)

2) Lightweight Bogie Frame: The total weight of each bogie is limited to less than 6.5 tons including SCM and all equipment. But it is difficult to reduce the weight of bogie frame, because the structure of bogie frame is so simple that there is no room for further reduction.

We have already designed lightweight bogie frame and fabricated some new trial bogie frames.

The conventional bogie frame was made of aluminum plates and shapes. We have made R&D about material and constitution of frame, whose candidates are all FRP shapes, aluminum honeycomb panels, all riveting structure without welding, and so on.

In 1991 we tried fabricating SCM supporting frame made of brazed aluminum honeycomb panels. The side-beams of the frame are welded box girders whose sides are brazed aluminum honeycomb panels. The SCM frame was much lighter in weight than the conventional frame of aluminum plates and shapes. And its strength and rigidity were enough.

We are going to start a detailed design of bogies for Yamanashi Vehicles.

E. Other Components

There are many special components of the vehicles for superconducting Maglev on Yamanashi Test Line. For example, aerodynamic brake and wheel disk brake system, suspension mechanism, auxiliary pneumatic tire wheels, guide wheels, inductive power collection system, interior accommodation, fire warning and extinguish system, and so on.

But we omitted many things on account of limited space all over here though we would like to introduce a lot of equipment that we have developed.

Under such conditions we are developing the new Maglev Vehicles.

IV. Closing Remarks

We gave on outline of vehicles for Maglev system on Miyazaki Test Track and Yamanashi Test Line.

We expect to succeed in Maglev system.

REFERENCES

[1] Kan-ichiro KAMINISHI, "The Development of Superconducting Maglev System," QR of RTRI, Vol.33, No.4, Nov.'92, pp.230-234

[2] Shohiko MIYATA, "Status Quo of Research and Development of Superconductive Magnetically Levitated Train," pp.1-8

[3] Koichiro OKUTO,etc, "The Development of SCM Aluminum Frame," SUMITOMO LIGHT METAL TECHNICAL REPORTS, Vol.32, No.2, APR.1991, pp.43-48

Overview of Maglev Vehicle Structural Design Philosophy, Material Selection and Manufacturing Approach

Paul Shaw
Grumman Corporation, Bethpage, New York

Abstract - **The basic purpose of this study was to obtain a cost effective, manufacturable, technically efficient baseline vehicle structural design.**

The philosophy used in the study was based on a pragmatic vehicle building block approach employing an elemental 50 passenger module. The module when fitted with a nose and tail can stand alone and be used during low volume traffic periods, saving energy and operating cost. Two connected modules are suitable for intermediate traffic volume. Additional modules, in increments of 50 passenger blocks, can be attached to the 100 passenger vehicle to build a train that will serve high volume markets.

The initial conceptual design was based on a preliminary vehicle design specification that included load and stiffness criteria, cabin size and shape, and provisions of the Americans With Disabilities Act.

The size and general shape of the passenger cabins was largely driven by anthropometric requirements, seating comfort needs, aisle width, cabin facilities, window arrangement and primary suspension envelope. Based on these considerations, a cabin area for the basic 50 passenger module was defined. The nose and tail compartments were aerodynamically designed to minimize drag and downward forces.

As an initial effort to achieve the necessary balance between design drivers, such as, weight, cost and structural integrity, aluminum and composite conceptual structural designs and manufacturing approaches for the cabin primary structure were developed.

In light of the similarity between the aluminum and composite structural weights and the fact that aluminum shows a stiffer structural design for the same weight, aluminum structure has been selected for our baseline design. As usual, however, the final design will be a balance of cost, weight and manufacturability.

I. Introduction

The basic purpose of this effort was to obtain a cost effective, manufacturable, technically efficient baseline vehicle structural design.

The philosophy used in this study is based on a pragmatic vehicle building block approach employing an elemental 50 passenger module. The module when fitted with a nose and tail can stand alone and be used during low volume traffic periods, saving energy and operating cost. Two modules connected together comprise the baseline 100 passenger conceptual design configuration that is suitable for intermediate traffic volume. Additional modules, in increments of 50 passenger blocks, can be attached to the 100 passenger vehicle to build a train that will serve high volume markets.

The conceptual structural design performed considered such parameters as vehicle design specification, size, shape and material application. The preliminary design specification developed served as a design starting point (Table I). It was based on data described in the RFP, DTFR53-91-R-00021 [1], and federal report, DOT-FR-40024 [2], and industry practice. The specification was upgraded as the vehicle design evolved and load and moment data became available.

II. Passenger Cabin Definition

Details of the 50/100 passenger cabins for the conceptual configuration are given in Fig. 1. The size and general shape was largely driven by anthropometric requirements, seating comfort needs, aisle width, cabin facilities, window arrangement and primary suspension envelope. Passenger physical measurements for sizing cabin height and seat size were based on a 98 percentile data base for U.S. men or aviators (typically the group with the largest measurements) [3]. Table 2 shows a comparison of selected anthropometric measurements and an example of how the measurements were taken and a pictorial representation. Fig. 2 depicts application of the anthropometric analysis with respect to cabin layout and inside dimensions.

Seating comfort needs were established based on a review of airline seating format [4]. Seat comfort depends on three factors; seat pitch, which determines your leg room and the space you have for reading or working, seat width describe the space you have to sit in, and seat configuration tells how seats are grouped within each row and affects comfort because it determines the proportion of middle seats. A score of 100 represents the minimum seating dimensions that were judged comfortable for all passengers in a full vehicle: 0.91 m (36 in.) pitch, 0.56 m (22 in.) width, and a 2x2 configuration. The width selected for our design, 0.61 m (24 in.) and seat pitch 0.97 m (38 in.) augment the ranking while the 2x3 configuration offset some portion of this enhancement resulting in an overall comfort score equal to or slightly greater than 100. We expect from this analysis that the ride

Manuscript received March 15, 1993. The work was performed as part of the EMS Maglev System Concept Definition study supported by the U. S. Army Corps of Engineers under contract DTFR53-92-C-000 04

TABLE I
CONCEPTUAL VEHICLE DESIGN SPECIFICATION

• Load Criteria	
Floor:	Nominal - 1436 N/m2 (30 lb/ft2)
	Maximum - 4790 N/m2 (100 lb/ft2)
	Maximum Deflection - 0.38 cm (0.15 in.)
Exterior Panel:	Pressures are low - it is anticipated that criteria such as damage resistance and tolerance will be the design drivers for the gross acreage of the vehicle body
Roof:	4790 N/m2 (100 lb/ft2)
	(Assume a 2 g vertical acceleration of vehicle for adverse conditions induces the maximum compressive stress in the roof and maximum tensile stress along the bottom)
Aerodynamic:	Tip - 1.33 x 104 N/m2 (1.9 psi)
	Body -2.66 x 104 N/m2 (-3.8 psi)
Crash:	5 mph bumper impact
	Seat restraint - 16 g
• Stiffness Criteria:	Fundamental vehicle bending frequency > 6.5 Hz.
• Tilt Capability	±9 degrees
• Temperature Range	-73°C to +94°C (-100 °F to +200 °F)
• Weight Target (100 passenger vehicle)	
Empty	51,863 kg (114.1 klb)
Payload	9,500 kg (20.9 klb) [100 passengers, average weight including luggage = 93.2 kg (205 lb) + 2-3 crew/attendants = 181.8 kg (400 lb)]
• Seat Definition	Configuration- 2x3
	Width - 0.61 m (24 in.)
	Pitch - 0.97 m (38 in.)
	Aisle - 0.56 m (22 in.)
• Americans With Disabilities	Space to store folded wheelchair, and provisions for restroom - satisfy requirements of the Americans With Disabilities Act
• Doors - 2/Side	Width/door - 0.81 m (32 in.)[100 passenger vehicle]
• Service Facilities	Similar to a 737-500 aircraft
• Storage	Overhead compartments, vestibule closets and tail section
• Subsystems	Located in chassis below passenger and crew compartments
• Primary Suspension System	(100 passenger vehicle)
	No. magnets - 48
	Pole pitch - 0.75 m (29.6 in.)

comfort produced with this seating design would be acceptable to all passengers. Selection of the 2x3 configuration was initially based on prior studies that showed that vehicle structural weight is minimized with a 5 or 6 seat configuration [5].

A review of train and commercial aircraft seats was performed and led to selection of a large seat equivalent to a 767 aircraft business class seat. The seat is designed to meet static and safety requirements listed in Boeing Document D6T10782-1, and 14 Code of Federal Regulations (CFR) Part 25 Amendment No. 25-64. A special focus of the seating considerations was accommodation for the anthropometric dimensions of current and future passenger population. Toward this end, estimates based on population data were made of anthropometric seating data. It was seen in this review that the neck and head of the passengers (corresponding to a 1992 98th-percentile male buttock-to-knee length) is above a point where the seatback will provide support. Extension of the seat by 5 inches would appear to afford support for even very large passengers (e.g., 2012 98th-percentile male). This is depicted in Fig. 2 and requires that the selected seat be modified so it may be used in this design.

Entrance doorway, aisle, and vestibule area width dimensions and service facilities were developed by review of Federal Aviation Regulation (FAR) 25.815, 49 CFR parts 27, 37, and 38, and examination of 737-500 aircraft cabin (108 seats) drawings. The various design widths selected for our vehicle meet (or exceed) the passenger loading/unloading and movement provisions of competitive short-haul aircraft service. Entryway and aisle widths leading to the first row of seats has also been sized for wheelchair bound passengers and readily facilitates boarding and seat access. The first row of seats (5) has been designed with a 1.1 m (42 in.) pitch to provide additional space and to accommodate disabled per-

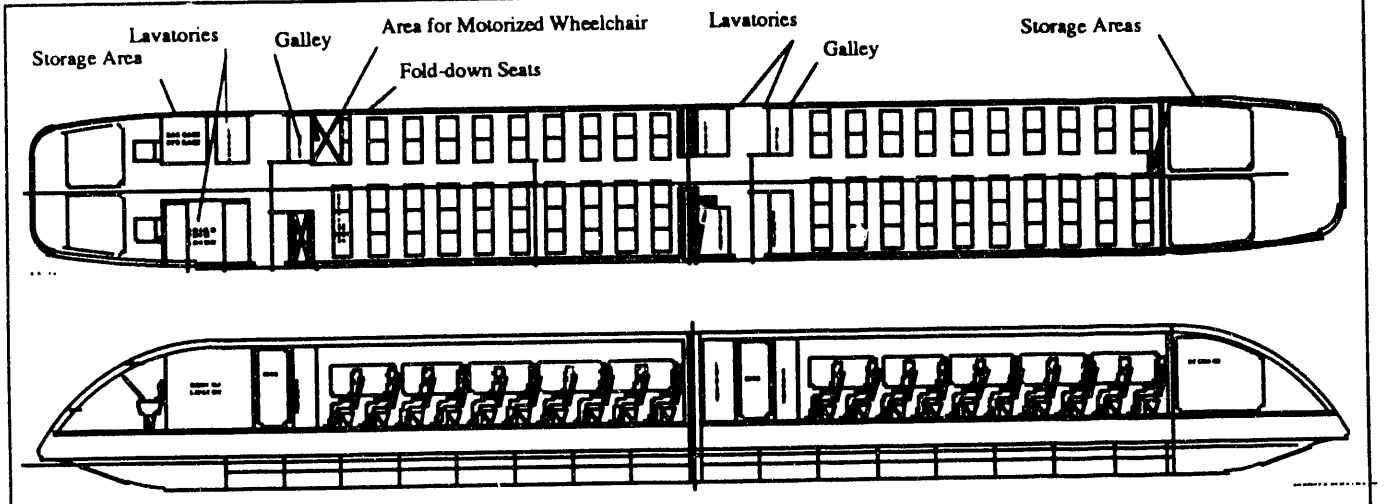

Fig. 1. Baseline configuration showing size and general shape of vehicle, seating arrangements, cabin facilities, and location of doors and windows.

sons that chose to remain in their wheelchair or transfer to a seat and fold/store their wheelchair/mobility aid. Clearance space is made available with fold-down seats that may be used when not occupied by a wheelchair or mobility aid user. The general public service facilities are similar in size and number to those on a 737-500 aircraft. An accessible restroom, with the required clearance envelope, has also been provided for disabled persons. These features are shown in Fig. 1.

A number of window arrangements were studied but only two configurations, two and five equal size windows appeared to provide unobstructed passenger viewing. Other window representations produced partially obstructed viewing. Based on preliminary structural analysis considerations, a window frame bulkhead approximately every 1.83 m (72 in.) was specified, defining a five window configuration for the baseline design.

Based on the above considerations, a cabin area for the basic 50 passenger module has been defined (see [6], Fig. 2). The internal dimensions are: height (head room) - 2.05 m (81 in.), width - 3.66 m (12.0 ft), and cabin length - 12.71 m (41.7 ft). The aisle width, 0.56 m (22 in.) and head room are equivalent to or exceed those of a 737-500 aircraft. Seat pitches of 0.97 m (38 in.) typical and 1.1 m (42 in.) handicapped are used to ensure adequate leg room. The service area length is 2.6 m (8.7 ft) and includes a lavatory, galley, storage areas and two doors - one on each side of the module, 0.81 m (32 in.) in width. The doors are operated by an exterior sliding mechanism. When closed the outer surface of the door is flush with the exterior surface of the vehicle.

III. Nose and Tail Definition

The nose (crew compartment) and tail (large baggage storage area) are 4.9 m (16 ft) in length and have been aerodynamically designed to minimize drag and downward forces. Aerodynamic analysis dictated a design that brought the nose leading edge closer to the guideway reducing the air scoop effect of a raised nose. The tail compartment configuration is identical in size and shape to the nose. No meaningful aerodynamic penalty was created by having a common configuration. This approach offered the benefit of simplifying design and manufacturing operations. As a by-product of the nose design, additional space was created behind the engineer's compartment and in the tail section and is available for baggage storage. A 100-passenger vehicle, composed of two 50-passenger blocks and crew and tail compartments would be 35.4 m (116.2 ft) in length. For a 50-passenger low traffic volume vehicle, the length would be 19.71 m (64.7 ft).

IV. Material Selection/Manufacturing Approach

Composite Cabin – The principal concerns associated with the selection of a baseline design concept for vehicle construction are weight, cost, and structural integrity. As an initial effort to achieve the necessary balance between the above noted design drivers, a conceptual structural design for the vehicle primary structure was developed for subsequent evaluation. The cabin concept was designed as a foam-filled sandwich structure, with internal frames and longerons at

TABLE II
COMPARISON OF SELECTED ANTHROPOMETRIC MEASUREMENTS

Dimension name: Sitting height
Subject sits erect, his head in the frankfort plane, and his feet resting on a surface adjusted so that his knees are bent at about right angles with the anthropometer arm firmly touching the scalp, measure vertically from the sitting surface to the top of the head.

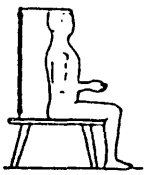

Group	Survey Year	Percentiles				
		3	5	50	95	98
USAF flying personnel	1967	34.44	34.70	36.65	38.80	39.31
U.S. adult - men	1960-62	33.45	33.66	36.06	38.35	38.76
U.S. adult -women	1960-62	31.26	31.46	33.82	36.37	36.37
U.S. Army women	1977	30.74	31.11	33.53	35.76	36.23
U.S. Army aviators	1970	33.41	33.73	35.79	37.91	38.46

discrete locations along the length of the vehicle and foam filled bulkheads at each end. All structural members utilize advanced composites as the primary materials of construction, predominantly glass/epoxy with selective use of graphite/epoxy or hybridized with the graphite for those locations which may require additional stiffness. Usage of low density phenolic or polyimide foam as the sandwich core material efficiently provides the structural characteristics of overall rigidity, facesheet stability, and shear continuity. In addition, the natural thermal insulating and acoustic absorption properties of the foam should preclude the necessity of adding secondary systems to accomplish those requirements. Acoustic analysis will assure that noise in the car will not exceed the noise standards contained in 49 CFR, Appendix A to part 210 [7].

The plastic cabin has been designed to maximize the use of adhesive bonding for assembly, thereby eliminating the cost associated with hole drilling and fastener installation. As currently defined, all composite details would be precured, bonded as a subassembly (preferably using a quick curing automotive type adhesive), with subsequent "blow" foaming of all internal cavities to complete the assembly. An alternative method of manufacture would use rigid foam, precured frames and longerons, adhesive and uncured facesheets assembled in a single cocure operation.

Aluminum Cabin – To compare the effectiveness of the composite design, a conceptual all aluminum structural design for the vehicle primary structure was also developed for subsequent evaluation. The cabin concept presented is designed as a built-up sheet and stringer, mechanically fastened structure with internal frames and longerons, at discrete locations along the length of the vehicle and bonded honeycomb sandwich panels for the floor. All structural members utilize either 2000, 5000, 6000 or 7000 series aluminum alloys as the primary materials of construction;

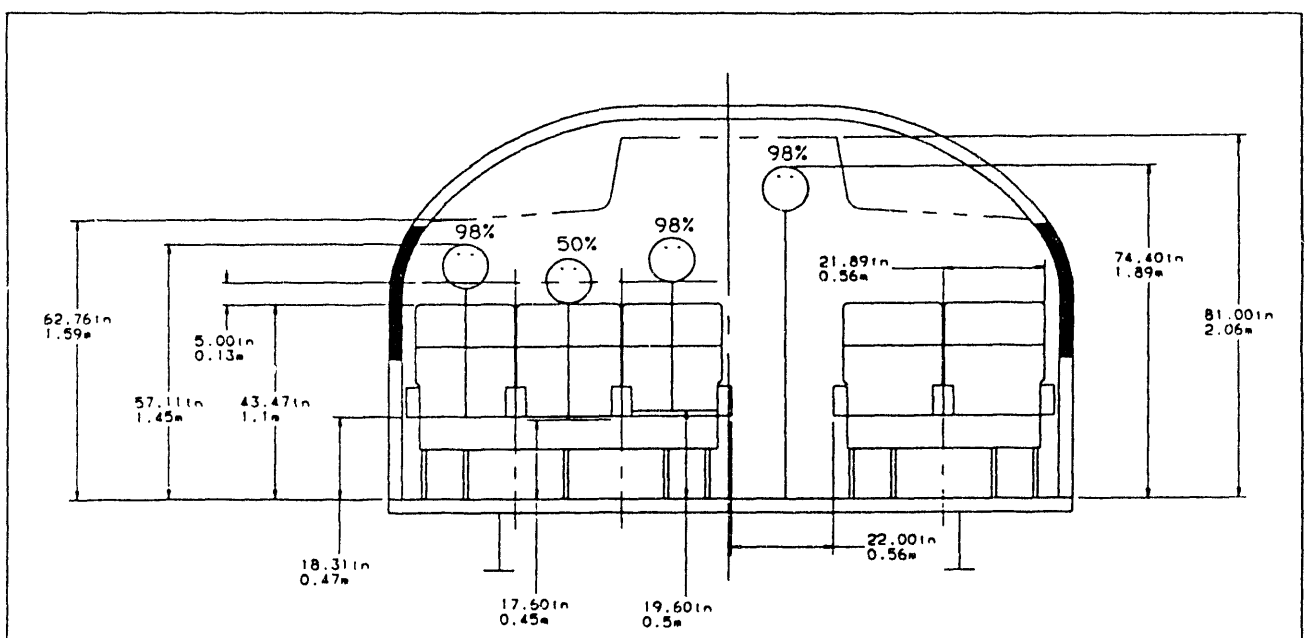

Fig. 2 Anthropometric profile

predominantly low cost 6013 material is used for both flat and formed sheet applications with selective use of alloy 7150 for those locations that require additional strength, e.g., undercarriage beams, webs, etc. Because the aluminum built-up structure does not have the natural thermal insulating and acoustic absorption properties of the foam, secondary systems must be included in the detail design to meet the noise standards contained in 49 CFR, Appendix A to part 210 [7].

The metallic cabin as currently defined has been designed to maximize the use of automated drilling and mechanical fastening for assembly, thereby eliminating the cost associated with composite lay-up and curing. As an alternative method of manufacture, because 6013 is weldable, some sheet structure may be design to be joined by welding, saving weight, and then mechanically fastened to the 7150 primary structural members.

Nose & Tail, Fairings & Panels - For the composite designs, the upper nose and tail skin structures are fabricated from glass structure with either nomex honeycomb (phenolic resin bonded aramid fiber) or low density phenolic or polyimide foam as the sandwich core material. All details would be precured, bonded as a sub-assembly with subsequent, if required, "blow" foaming of all internal cavities to complete the assembly. An alternative method of manufacture would use nomex honeycomb core or rigid foam, precured frames and longerons, adhesive and uncured facesheets assembled in a single cocure operation. For the aluminum design, these details would be fabricated from easily formed alloy 6013 and the sections built-up by sheet and stringer construction. For both designs, the assemblies are bonded/bolted to the floor frame and to the cylindrical section of the passenger module.

The primary material for the lower removable nose and tail sections, fairings, and suspension system side panels are low density integrally stiffened glass laminates. Details would be precured and bonded as a sub-assembly, or as an alternative fabrication approach, uncured and assembled in a single cocure operation. An alternative design and manufacturing approach for the side panels would use low cost, easily fabricated aluminum alloy 6013 in built-up sheet/stiffener construction.

V. Other Design Considerations

Materials selected must meet acceptance requirements concerning fire and toxicity resistance that, at a minimum, comply with NFPA 130, "Fixed Guideway Transit Systems" [8]. In addition, vehicle lightning protection would be provided by incorporating the requirements of NFPA 130 [8], as applicable, into the design, and by bonding copper or aluminum mesh to non-metallic external surfaces to serve as a high conductivity electrical path to dissipate a lightning strike. Glazing and nose compartment materials must meet, at a minimum, the requirements of the 49 CFR, part 223 [7], in order to protect passengers and crew from injury as a result of objects, e.g., birds, projectile, etc., striking the windows or leading surfaces of the vehicle. Existing CFR regulations are oriented toward relatively large object impacts. The high Maglev vehicle speed introduces windshield and lead surface vulnerability to impact damage from small objects, like birds and these impacts may be more analogous to an aircraft than a train. Federal Aviation Administration aircraft glazing requirements [9] need to be considered in modifying existing regulations for high speed Maglev systems.

VI. Weight Breakout

A preliminary structural analysis of the non-metallic composite and aluminum sheet/stringer vehicle superstructure and aluminum underfloor structure was performed to obtain a weight estimate. The results are presented in Table III. The weight of the two designs are close to each other for several reasons. One reason is the starting point chosen for each; the composite design has a hat section frame whereas the aluminum design has a Z section frame that is somewhat smaller. The final selection will have to be integrated with the final design and will include such considerations as running cable and retaining windows in place. Another reason is the choice of materials for each application: graphite/epoxy would have been lighter than aluminum for the floor facesheets but probably not be as wear resistant as fiberglass. Likewise, the shell sandwich skins would have been lighter if made from graphite/epoxy but a lot more expensive than aluminum or fiberglass. As usual, the final design will be a balance of cost, weight and manufacturability.

VII. Stiffness

Since the vehicle structure is lightly loaded, stiffness considerations become (other than in impact dominated zones) the primary design constraint. To simplify the vehicle dynamic control problem, the fundamental natural frequencies of the vehicle structure should be higher than the guideway's first structural bending frequency of 5.4 Hz [10].

TABLE III
Comparison of Estimated Structural Weight

Structural Element	Composite Design Weight		Aluminum Design Weight	
	Kg	(lb)	Kg	(lb)
Superstructure	3061	(6734)	3103	(6827)
Substructure	2795	(6149)	2795	(6149)
Secondary Structure	2305	(5070)	2305	(5070)
Total	8161	(17,953)	8203	(18,046)

A value of 10 Hz or larger would be desirable for the vehicle structure. Calculations based on the assumption that the vehicle could be represented by a uniform free-free beam supported at six locations along the vehicle length (denoting the six pairs of magnet suspension units), determined a range of vehicle bending stiffness and fundamental bending frequencies. These values are presented in Fig. 3.

Comparison of these EI values with calculated values of 676 MN-m^2 (2.36×10^{11} lb-$in.^2$) for the composite vehicle design and 1713 MN-m^2 (5.98×10^{11} lb-$in.^2$) for the aluminum vehicle design, indicates that the composite design would be marginal with ~8 Hz; the aluminum design acceptable with ~12 HZ. However, to allow for the preliminary nature of the calculations and provide a larger margin, particular for the composite design, the EI can be increased by selectively reinforcing the roof with additional plies of unidirectional graphite/epoxy, or for the aluminum design adding stiffeners or a thicker outer skin, or simply for either design, by increasing the stiffness of the substructure longerons and floor support beams. These design changes would result in a relatively small weight penalty which is accounted for in the contingency factor.

VIII. Summary

The basic purpose of this study was to obtain a cost effective, manufacturable, technically efficient baseline vehicle structural design.

The philosophy used in the study was based on a pragmatic vehicle building block approach employing an elemental 50 passenger module. The module when fitted with a nose and tail can stand alone and be used during low volume traffic periods, saving energy and operating cost. Two connected modules are suitable for intermediate traffic volume. Additional modules, in increments of 50 passenger blocks, can be attached to the 100 passenger vehicle to build a train that will serve high volume markets.

The size and general shape of the passenger cabins was largely driven by anthropometric requirements, seating comfort needs, aisle width, cabin facilities, window arrangement and primary suspension envelope. Based on these considerations, a cabin area for the basic 50 passenger module was defined. The nose and tail compartments were aerodynamically designed to minimize drag and downward forces.

As an initial effort to achieve the necessary balance between design drivers, such as, weight, cost and structural integrity, aluminum and composite conceptual structural designs and manufacturing approaches for the cabin primary structure were developed.

In light of the similarity between the aluminum and composite structural weights and the fact that aluminum shows a stiffer structural design for the same weight, aluminum structure was selected for our baseline design. As usual, however, the final design will be a balance of cost, weight and manufacturability.

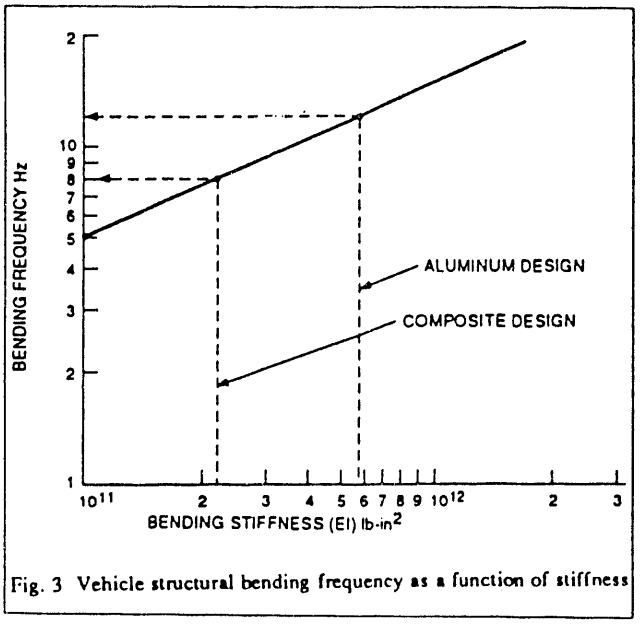

Fig. 3 Vehicle structural bending frequency as a function of stiffness

Acknowledgment

The author is grateful to Mr. Ron Sternberg, Mr. Burt Dawkins, and Mr. Warren Egensteiner all of Grumman Corporation for their assistance in this study. He also wishes to thank Mr. Michael Proise, also of Grumman Corporation and Program Manager of the study, for his advice and for making time for many important discussions.

References

[1] U.S. Department of Transportation, Federal Railroad Administration, RFP No. DTFR53-91-R-00021.

[2] "Conceptual Design and analysis of the Tracked Magnetically Levitated Vehicle Technology Program (TMLV) - Repulsion Scheme," Volume I, Technical Studies, Philco-Ford Corporation, DOT-FR-40024, February 1975.

[3] "A Comparison of Selected International Anthropometric Measurements," Grumman Aerospace Corporation, Report No. EG-SDAI-78-51, June 27, 1978.

[4] The Airline Seat Squeeze, Consumer Reports, Travel Letter, August 1989.

[5] New York State Technical & Economic Maglev Evaluation, Grumman Space and Electronics Division, Prepared for New York State Energy Research and Development Authority and Thruway Authority, Energy Authority Report 91-5, June 1991.

[6] System Concept Definition of the Grumman Superconducting Electromagnetic Suspension (EMS) Maglev Design, M. Proise, L. Deutsch, R. Herbermann, S. Kalsi, P. Shaw, In press-Maglev '93 Conference, Argonne National Laboratory, May 19-21, 1993.

[7] Code of Federal Regulations, Volume 49, parts 200 to 399, Revised October 1, 1991.

[8] National Fire Protection Association, NFPA 130, "Standard for Fixed Guideway Transit Systems," 1990 edition.

[9] Federal Aviation Administration, FAR 25.63

[10] Innovative Spine Guider Guideway Design for Superconducting EMS Maglev Systems, J.Allen and M. Ghaili, In press-Maglev '93 Conference, Argonne National Laboratory, May 19-21, 1993.

Aerodynamic Analysis of the Grumman Maglev Vehicle

Michael J. Siclari*, Gilbert Carpenter* & Robert Ende+
Grumman Aerospace & Electronics Group
Bethpage, New York 11714

Abstract - **The revival of interest in the U.S. in high-speed rail technology has necessitated an increase in attention to the aerodynamics of high-speed ground vehicles. Maglev vehicles, in particular, present several unique aerodynamic problems due to their very high speeds (~300 mph) and close proximity to a stationary rail or guideway. In conjunction with its System Concept Definition (SCD) study for the National Maglev Initiative (NMI), the Grumman Corporation has undertaken a three-dimensional Navier-Stokes analysis in an attempt to better understand the aerodynamic phenomena peculiar to such a Maglev design.**

I. INTRODUCTION

Grumman's concept for the Maglev SCD study is an EMS design incorporating a V-shaped guideway, superconducting magnets, and a modular design approach (see Fig. 1). The design cruising speed is 300 mph (134 m/s), which corresponds to a Mach number of 0.4 at sea level. The basic aerodynamics analysis for the design study involved developing an efficient vehicle shape and calculating the aerodynamic loads and pressure distributions on the vehicle, as well as looking at additional phenomena such as vehicle passing interactions, tunnels, and aero-acoustic noise. A full 3-D Navier-Stokes analysis also was carried out in conjunction with the basic aerodynamics engineering analysis. Navier-Stokes computations include the effects of viscosity, compressibility, and turbulence. This paper concentrates on the details and results of this preliminary computational study.

II. COMPUTATIONAL METHOD

The computation of the Navier-Stokes flow over a Maglev vehicle was undertaken using an in-house finite volume code whose solution module was originally developed by Prof. Jameson of Princeton [1, 2] and modified by Grumman [3] to include general geometries.

The basic solution algorithm is a vertex-based multi-stage, Runge-Kutta explicit time integration scheme with local time stepping and implicit residual smoothing to accelerate convergence. A multi-grid scheme also is implemented in the code to accelerate convergence. Without multi-grid, the computational time required for one Navier-Stokes computation on a 500,000-point grid would be on the order of ten to twenty hours on a Cray Y-MP supercomputer. The multi-grid scheme reduces the required computational time by an order of magnitude, and reasonably converged solutions (i.e., three to four orders of magnitude) can be achieved in one to two hours of CPU time.

An algebraic Baldwin-Lomax turbulence model is used to account for turbulence in the flow. Unlike other methods that include only viscous terms normal to the surface, the current Navier-Stokes solver includes all viscous terms in the governing equations. Future work will include studying the implementation of a more accurate turbulence model for this type of flow.

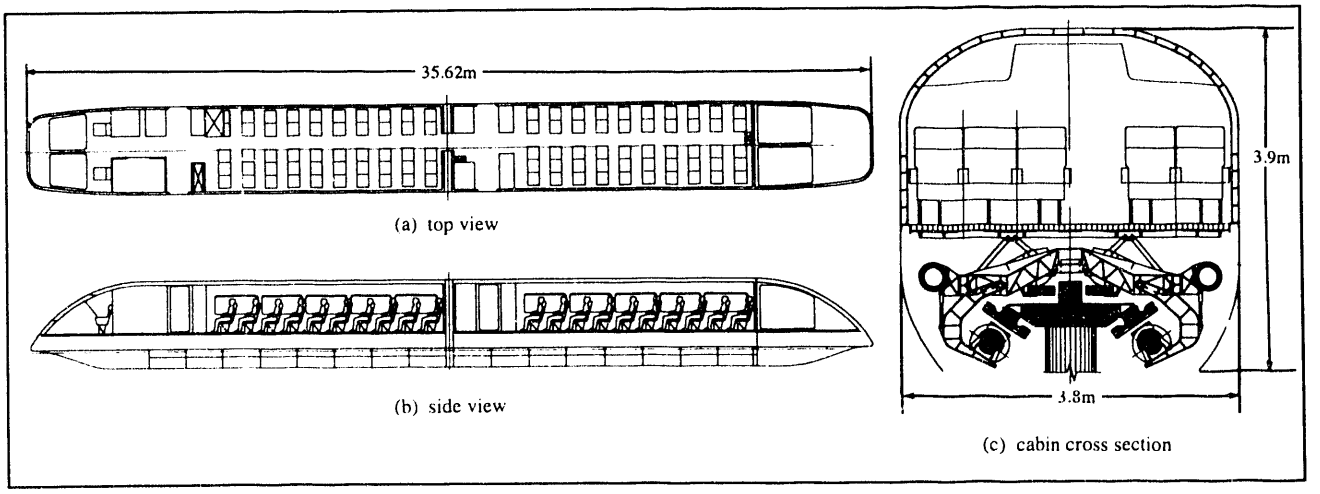

Fig. 1. Illustration of Grumman Maglev concept.

Manuscript received March 15, 1993.

* Corporate Research Center
+ Flight Sciences Directorate, Engineering

III. GEOMETRICAL CONFIGURATIONS

In the study, two geometrical configurations were considered. The first model used the simplified geometry shown in front view in Fig. 2. This consisted of a flat-bottomed vehicle (representative of an Electro-Dynamic Maglev) with a small gap over a moving ground plane. The ground plane was assumed to be infinite in extent relative to the vehicle. The lower cross-sectional shape of the simplified model was basically a rectangle or a square with a sharp corner. The vehicle is symmetric fore and aft, with the nose and tail turned up slightly. (The nose and tail shape may by seen in Fig. 9.)

The second, more advanced Maglev model, representative of the Grumman design, is shown in Fig. 3. The advanced configuration is elevated on a rail with the underside of the vehicle wrapping around the rail. The advanced model has no sharp corners in its cross-sectional shape. This model is also symmetric fore and aft and employs a "drooped" nose and tail shape (See Fig. 10 for the nose and tail shape relative to the rail.)

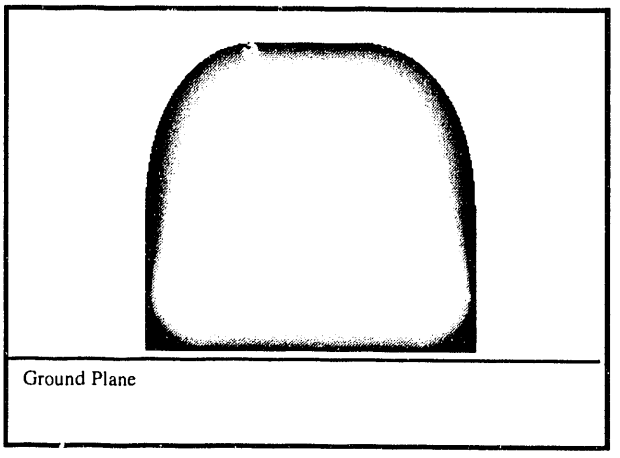

Fig. 2. Front view of simplified maglev geometry.

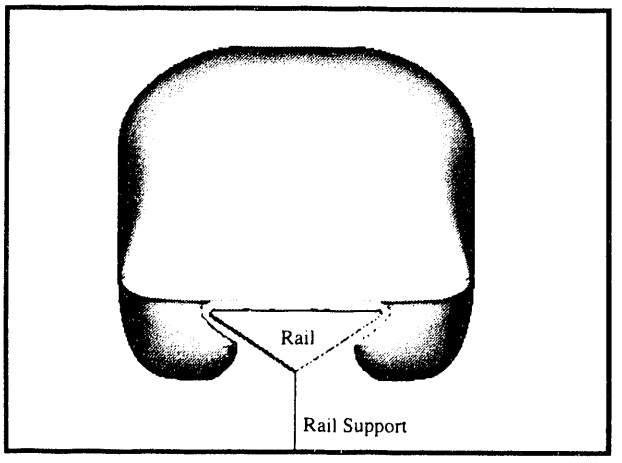

Fig. 3. Front view of advanced maglev geometry.

IV. COMPUTATIONAL GRIDS

The computational grids were created using the GRIDGEN software on a Cray Y-MP supercomputer and a Silicon Graphics IRIS workstation [4]. Both models used similar grid resolutions. No attempt was made to model the magnets on either configuration. A cross-sectional grid for the simplified model near the mid-section of the vehicle is shown in Fig. 4. A similar mid-section cross-flow plane grid used for the more advanced model is shown in Fig. 5. Both of the half-plane computational grids used 468,149 points, with 121 points wrapping circumferentially around the vehicle, 73 points axially and 53 points radially. The advanced model was elevated on a rail, as shown in Fig. 6. It was extremely challenging to develop a grid for the advanced configuration.

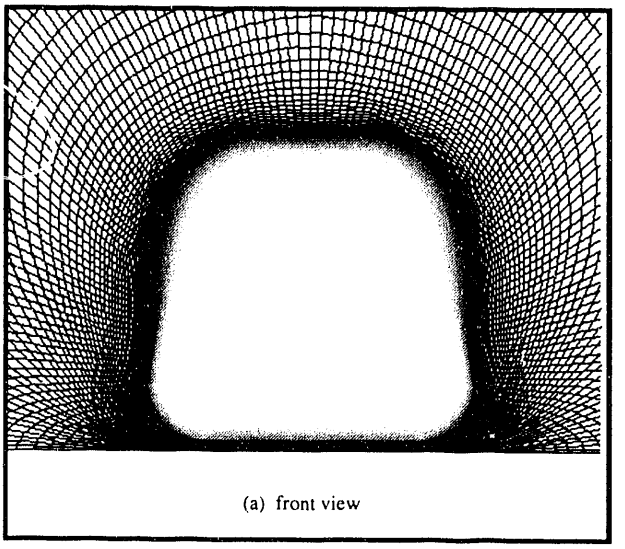

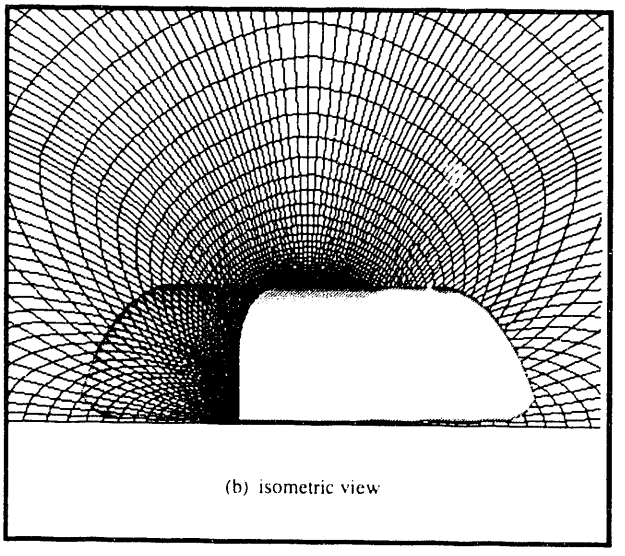

Fig. 4. Computational grid at mid-section of simplified model.

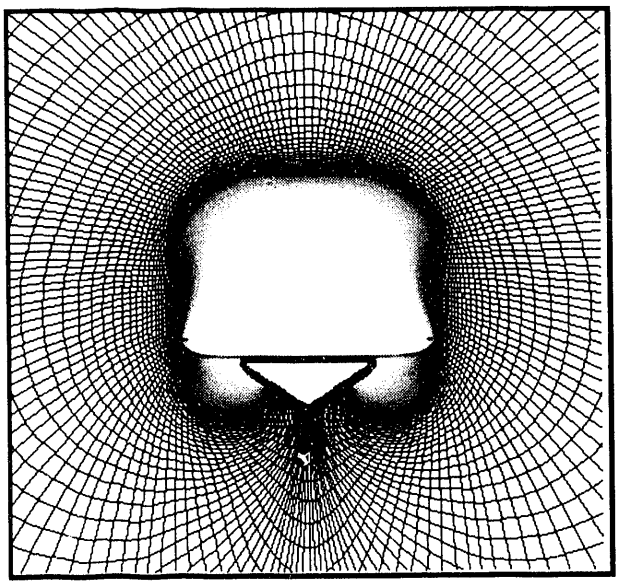

(a) front view

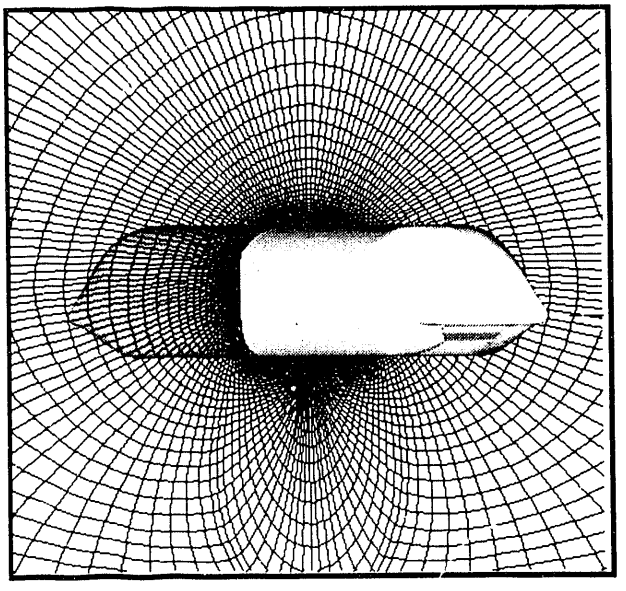

(b) isometric view

Fig. 5. Computational grid at mid-section of advanced model.

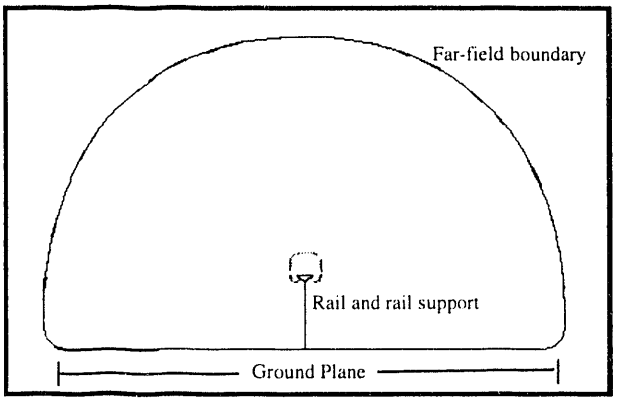

Fig. 6. Outer boundary of computational grid for advanced model.

V. BOUNDARY CONDITIONS

The computation of the Navier-Stokes flow over a Maglev vehicle is distinguished by the ground effect due to the small distance between the vehicle and the ground plane or rail upon which it rides. Both the air and the ground are stationary, and the vehicle is moving. As is typical in most CFD computations, the vehicle is stationary with the air moving relative to the vehicle. For the ground effect problem, the typical (hard surface) no-slip surface boundary conditions cannot be applied to the ground or rail upon which the vehicle rides. The ground or the rail also must move at a speed corresponding to the freestream velocity. Hence, boundary conditions of freestream velocity are prescribed on the ground plane or the rail.

To accommodate this mixture of boundary conditions, the outer boundary circumferential grid line (shown in Fig. 6) was divided into two regions. For the simplified model, the part of the outer boundary grid beneath the vehicle and extending laterally outboard used prescribed freestream axial velocity as the boundary condition. The remaining portion of the outer boundary grid used characteristic-based inflow/outflow boundary conditions typical of a subsonic flow computation. In the advanced model grid, the rail, the rail support, and the portion of the outer grid corresponding to the ground (see Fig. 6) were prescribed to move at the freestream axial velocity, with the two other components of velocity set to zero.

Note that the rail support was continuous and assumed to be infinitely thin; thus, the rail support coincided with the symmetry plane. Setting the two other velocity components to zero is consistent with the symmetry plane condition.

VI. RESULTS

Navier-Stokes computations were carried out for both the simplified and the advanced configurations. In each case, the freestream Mach number was prescribed to be 0.40, corresponding to approximately 300 mph at sea level.

A. Simplified Model

Fig. 7 shows several views of the computed flow pattern about the simplified model. The flow is characterized by a vortex shed by the rather blunt nose of the vehicle. This vortex is caused by flow separation around the nose of the vehicle and is shed axially, running along the side of the vehicle. There also is significant flow spillage from the underside of the vehicle. The flow pattern along the side of the vehicle is quite complex and is illustrated in Fig. 7a by velocity vectors at an axial station cutting through the mid-section of the vehicle. Actually, there are

two vortices present. The outer vortex is caused by the flow separating as it tries to turn around the nose of the vehicle. The second, inner vortex is caused by the flow separating as it spills or emerges from the underside of the vehicle and encounters the sharp underside corner of the vehicle's geometry. Fig. 7b shows the streamline pattern looking from directly behind the vehicle, and Fig. 7c shows a rear isometric view of the streamline pattern. Two large counter-rotating vortices develop behind the vehicle, which is typical of any bluff body flow. The nose vortices and underside vortices all merge into the rearward shed vortices behind the vehicle.

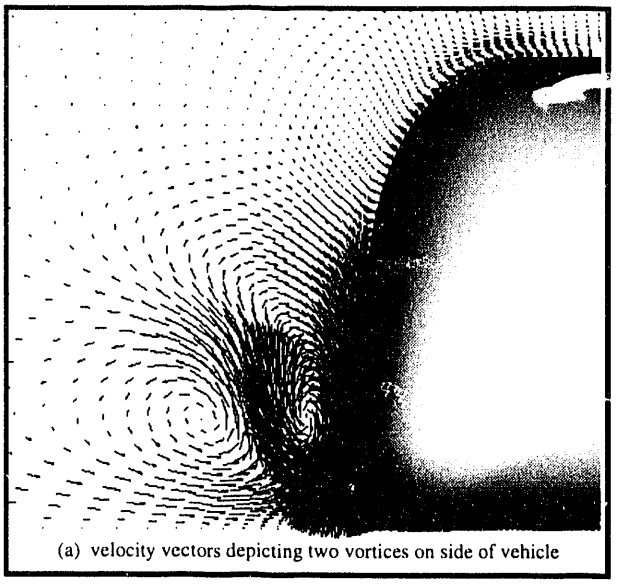

(a) velocity vectors depicting two vortices on side of vehicle

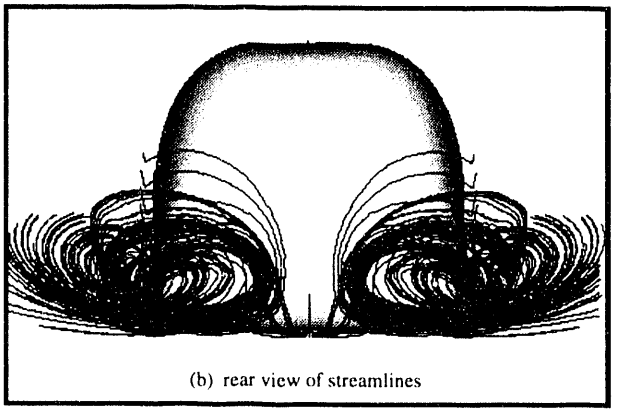

(b) rear view of streamlines

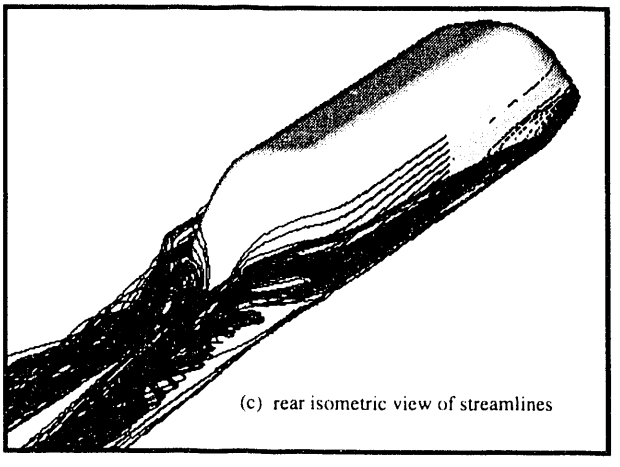

(c) rear isometric view of streamlines

Fig. 7. Flow pattern computed about simplified model.

B. Advanced Model

Fig. 8 shows the flow pattern computed for the advanced configuration. Once again, the flow separates around the nose of the vehicle, and the vortex is then carried downstream along the side of the vehicle. However, spillage from the underside of the vehicle is not apparent for this configuration. Fig. 8a shows velocity vectors at the mid-section of the vehicle, while Fig. 8b, c, and d show various views of the streamline pattern. The flow pattern is somewhat different from the one previously shown for the simplified vehicle. Only one vortex, from flow separation around the nose, is apparent on the side of the vehicle. Flow separation does not occur due to flow spillage from underneath the vehicle. There are two reasons for this. First, the underside of the advanced vehicle wraps around the rail and, hence, creates a natural channel for the flow. It is possible that this characteristic of the advanced configuration might lead to the generation of a larger normal force (greater positive lift). In addition, the geometry of the advanced vehicle does not contain the sharp underside corners of the simplified model. As a result, secondary separation due to spillage from the underside of the vehicle does not occur.

C. Recirculating Flow Regions

The flow behind the simplified model exhibits flow separation and a significant amount of recirculating flow. Air flowing over the aft end of the simplified model actually gets sucked forward underneath the vehicle (i.e., reverse flow) and eventually gets turned back as it flows out laterally. This is due in part to the curvature in the geometry of the underside of the simplified vehicle. Fig. 9 and 10 compare the extent of recirculating or reverse flow in the centerline plane for the two configurations. Contours of negative axial velocity are plotted just behind the aft ends of the vehicles and in the symmetry planes. The dark regions on the figures depict reverse flow or an upstream flow direction. These regions are usually referred to as recirculating flow regions. Fig. 9 shows the extent of the reverse flow for the simplified model. A significant region of reverse flow occurs below the aft end of the vehicle. Fig. 10 shows a similar plot for the advanced configuration. Here, the reverse flow is concentrated in a small region on the upper half of the configuration, while reverse flow below the vehicle is not apparent. This indicates less flow separation at the aft end, which should result in

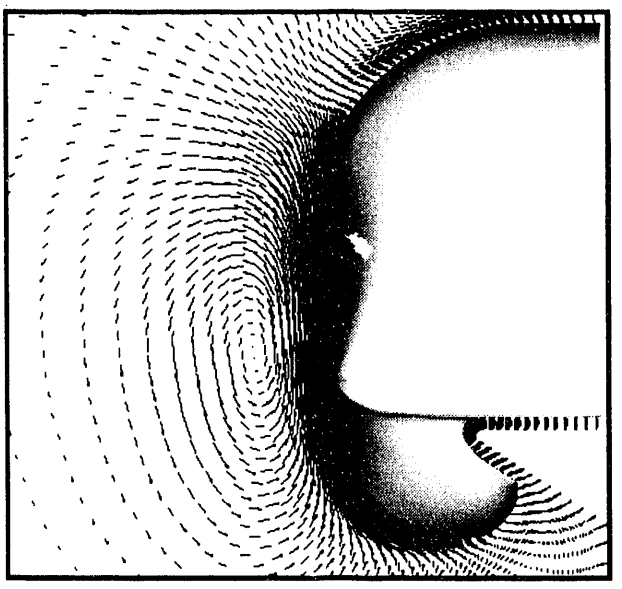

(a) velocity vectors depicting single vortex on side of vehicle

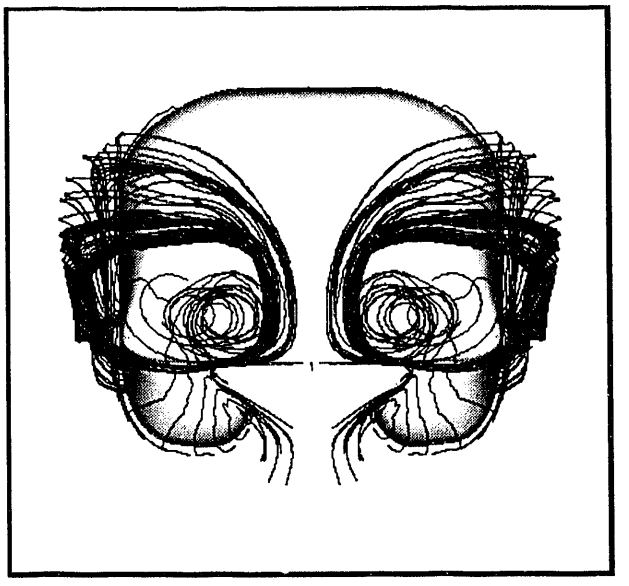

(b) rear view of streamlines

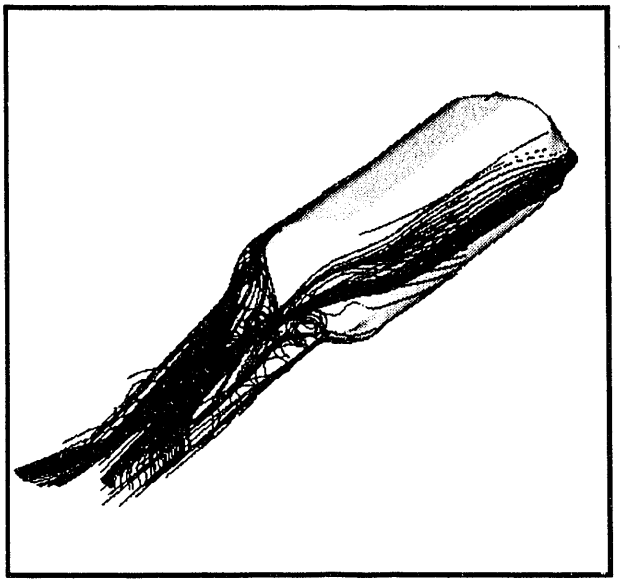

(c) rear isometric view of streamlines

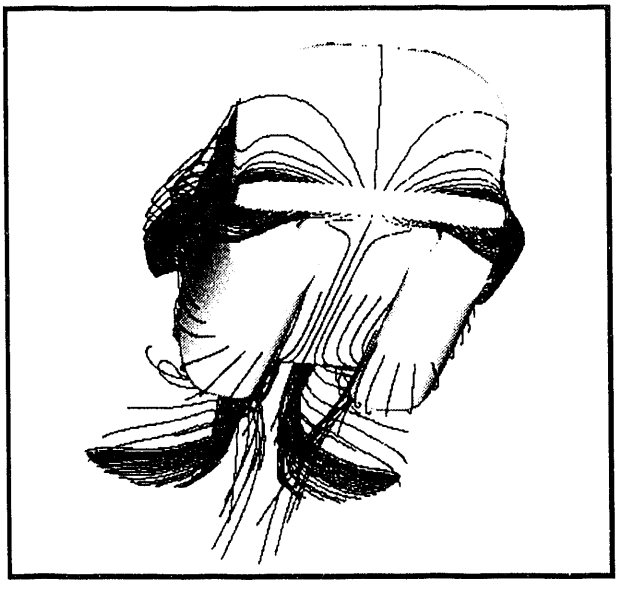

(d) underside view of streamlines

Fig. 8. Flow pattern computed about advanced model.

lower pressure drag for the advanced configuration. It should be noted that the reverse flow regions are complicated three-dimensional volumes, and only centerline cuts of these regions have been depicted by Fig. 9 and 10.

VII. SUMMARY

The Navier-Stokes computations have served to illustrate several important aspects that should be considered in the design of a high-speed Maglev vehicle. The shape of the nose is very important in retaining attached flow conditions on the front portion of the vehicle. Flow separation near the nose, as has been demonstrated by these computations, causes a vortex to be shed running along the side of the entire length of the vehicle. This vortex could lead to additional drag, as well as undesirable noise levels for the occupants. The characteristics of the flow also are very sensitive to the cross-sectional shape of the vehicle. The simplified model indicated the development of a second vortex from the flow spillage and separation around the sharp underside corners of the cross-sectional shape. On the other hand, the wrap-around rail configuration apparently eliminates flow spillage from the underside of the vehicle since it creates a natural channel for the air trapped by the underside of the vehicle.

The amount of flow separation occurring on the aft end of a Maglev vehicle also is dictated by the geometry of the vehicle. The design of a vehicle

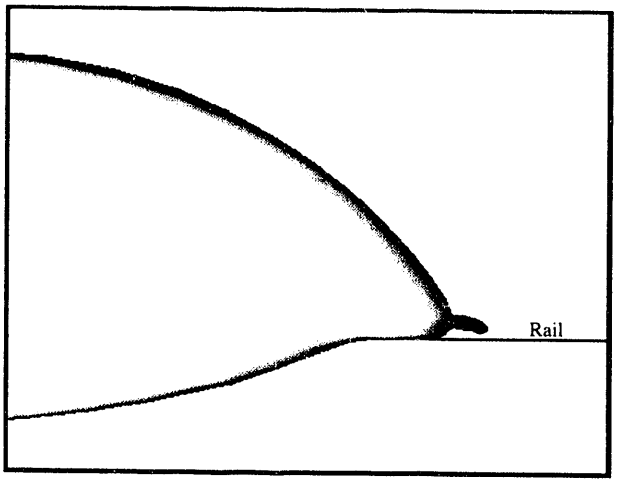

Fig. 10. Centerline reverse flow region at aft end of advanced model.

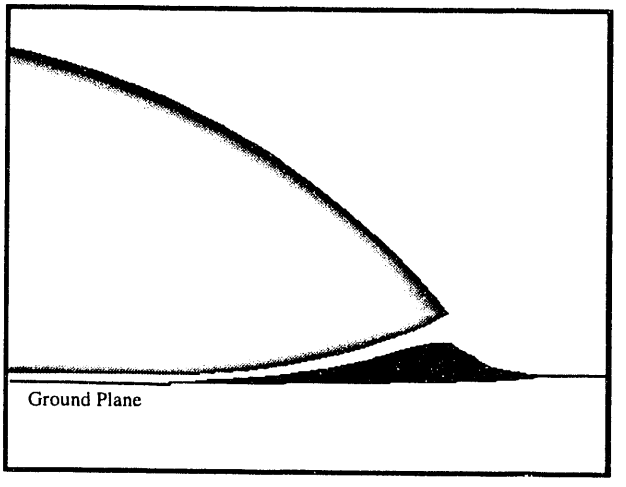

Fig. 9. Reverse flow region at aft end of simplified model.

with minimum flow separation over the aft end is desirable, as the degree of separation will have an effect on the drag of the vehicle and its ultimate efficiency.

VIII. FUTURE WORK

Future work will focus on several aspects of the aerodynamic analysis. The computational method will be verified through correlation with experimental results. A more accurate turbulence model will be added to better calculate flow separation. Finally, unsteady calculations will be made to examine phenomena such as tunnel entrance/exit and passing interactions.

REFERENCES

[1] Jameson, A., "A Vertex Based Multigrid Algorithm for Three-Dimensional Compressible Flow Calculations," *Numerical Methods for Compressible Flows*, edited by T.E. Tezduar & T.J.R. Hughes, AMD78, published by A.S.M.E. 1986, pp 45-73.

[2] Martinelli, L., Jameson, A., and Malfa, E., "Numerical Simulation of Three-Dimensional Vortex Flows over Delta Wing Configurations," presented at the International Conference on Numerical Methods in Fluid Dynamics, Rome, Italy, 1992.

[3] Volpe, G., Siclari, M.J., and Jameson, A., "A New Multigrid Euler Method for Fighter - Type Configurations," AIAA Paper No. 87-1160-CP, presented at the AIAA 8th Computational Fluid Dynamics Conference, Honolulu, Hawaii, June 1987.

[4] Steinbrenner, J.P., Chawner, J.R., and Fouts, C.L., "The GRIDGEN 3D, Multiple Block Grid Generation System," WRDC-TR-90-3022, Vols. I & II, Wright Patterson Air Force Base, 1990.

Dynamics, Stability, and Control of Maglev Systems

Y. Cai, S. S. Chen, S. Zhu, T. M. Mulcahy, D. M. Rote, and H. T. Coffey
Argonne National Laboratory, Argonne, Illinois 60439

Abstract - **This paper presents an overview of the work on dynamics of maglev systems completed at Argonne during the last two years. Specifically, vehicle/guideway interaction and ride quality, active and semiactive suspension control, and stability analysis are summarized.**

I. Introduction

The dynamic response of maglev systems is important in several respects: safety and ride quality, guideway design, and system costs. Dynamic response of vehicles is the key element in the determination of ride quality, and vehicle stability is an important element relative to safety. To design a proper guideway that provides acceptable ride quality in the stable region, vehicle dynamics must be understood. Furthermore, the trade-off between guideway smoothness and the levitation and control systems must be considered if maglev systems are to be economically feasible. The link between the guideway and the other maglev components is vehicle dynamics. For a commercial maglev system, vehicle dynamics must be analyzed and tested in detail [1].

This paper is a summary of our previous work on dynamics, stability, and control of maglev systems [2-8]. First, the importance of vehicle/guideway dynamics in maglev systems is discussed. Emphasis is placed on modeling the vehicle/guideway interactions with a multicar or multiload vehicle traveling on a single- or double-span flexible guideway. Coupled effects of vehicle/guideway interactions in a wide range of vehicle speeds and with various vehicle and guideway parameters are investigated [2-5].

Second, the alternative control designs of maglev vehicle suspension systems are investigated to achieve safe, stable operation; in addition, acceptable ride comfort requires some form of vehicle motion control. Active and semiactive control law designs are introduced into primary and secondary suspensions of vehicles [4,8].

Finally, the paper discusses the stability of maglev systems based on experimental data, scoping calculations, and simple mathematical models. Divergence and flutter are obtained for coupled vibration of a three-degree-of-freedom maglev vehicle on a guideway consisting of double L-shaped aluminum segments. The theory and analysis developed in this study provides the basic stability characteristics and identifies the future research needs for maglev systems [6,7].

Manuscript received April 23, 1993. This work was partially funded by the Illinois Dept. of Commerce and Community Affairs, the U.S. Army Corps of Engineers, and the Federal Railroad Administration through interagency agreements with the U.S. Department of Energy.

II. Dynamic Interactions of Maglev Vehicle/Guideway Systems

To simplify the vehicle model, only vertical motions of the vehicle are considered, based on the assumption that vertical motion is dominant and that other motions can be ignored when vertical motion is evaluated [2,4,9].

For a flexible guideway, elastic deformation must be considered. Attention is focused on vertical guideway deflection when analyzing vehicle/ guideway interactions. The classical Bernoulli-Euler beam equation is used to model guideway characteristics in virtually all recent analyses of vehicle/guideway interactions.

A multicar, multiload vehicle traveling along a flexible guideway at a velocity v, as shown in Fig. 1, is considered in our mathematical model for dynamic analysis of vehicle/guideway interactions. The car body is rigid and has a uniform mass. The center of mass is consistent with that of the moment of inertia. Each car is supported by certain numbers of magnets (or bogies) with linear springs and dampings, which form the primary and secondary suspensions of the vehicle.

Simulations on the dynamics of a multicar vehicle are completed by using the model given in Fig. 1. Fig. 2 shows midspan beam deflections when multicar vehicles travel at 100 m/s. In the parameter range considered in this study, no matter how many cars are included in the vehicle, the maximum beam deflection remains the same, but the duration of deflections increases as car number increases. Fig. 3 shows maximum displacements of the guideway midspan when the multicar vehicle travels at various speeds. Again, results for 1, 2, 3, and 4 cars are the same. As in previous studies on the concentrated-load single-car vehicle, maximum guideway displacements tend to increase as vehicle speed increases [2,3]. Fig. 4 shows the Urban Tracked Air Cushion Vehicle (UTACV) ride comfort specification (ranging from 0-10 Hz) for multicar vehicles traveling at 100 m/s. Power spectral densities (PSDs) of multicar vehicle accelerations satisfy the ride comfort criterion.

III. Control Designs of Maglev Suspension

To achieve quick response and a high-quality ride over a less-expensive guideway, control designs must be exploited in suspension systems. Moreover, with the assistance of suspension controls, a rougher guideway surface could be used, and the overall investment cost of the guideway could be reduced.

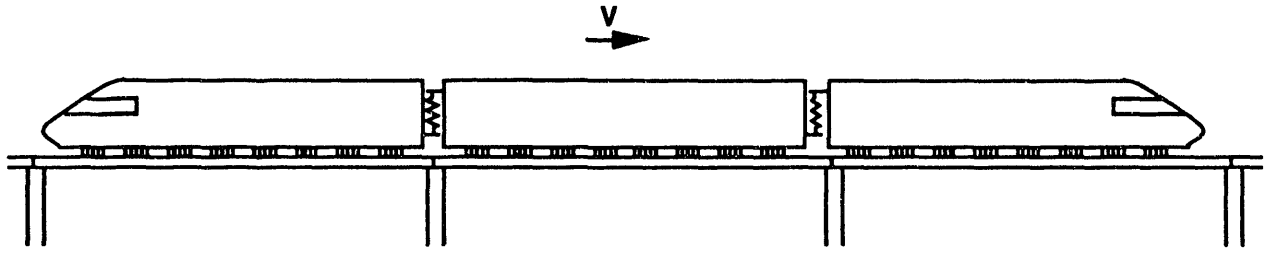

Fig. 1. Model of multicar, multiload maglev vehicle traveling along a guideway.

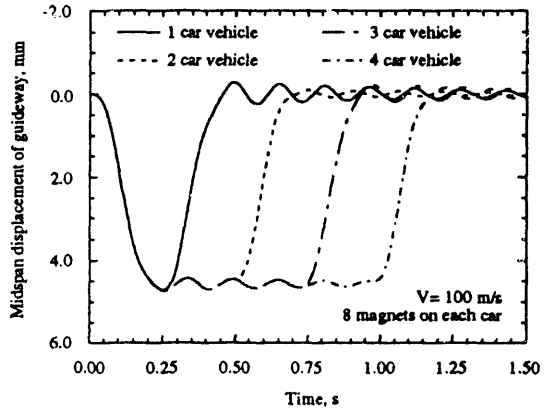

Fig. 2. Midspan displacements of guideway for multicar vehicles with eight magnets on each car and traveling along the guideway at 100 m/s.

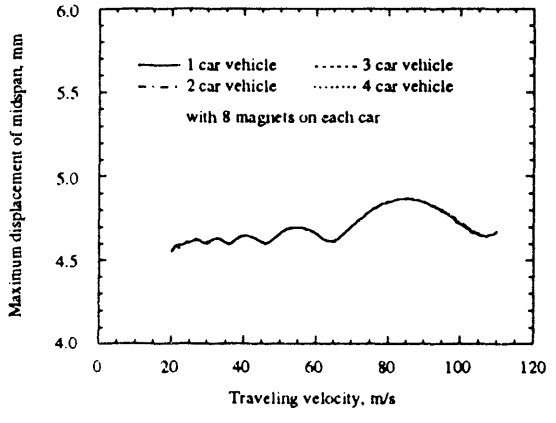

Fig. 3. Maximum midspan displacements of guideway when multicar vehicles with eight magnets on each car travel along the guideway at various speeds.

To investigate the improvement of the dynamic response and ride comfort of maglev systems, different control designs (active and semiactive) are examined in this study. For most control-law synthesis, it is desirable to work with linear dynamic models of low order. A low-order maglev vehicle model, which may be selected as a two-degree-of-freedom quarter-vehicle model representing primary and secondary suspensions, is necessary in control design to formulate a low-order controller.

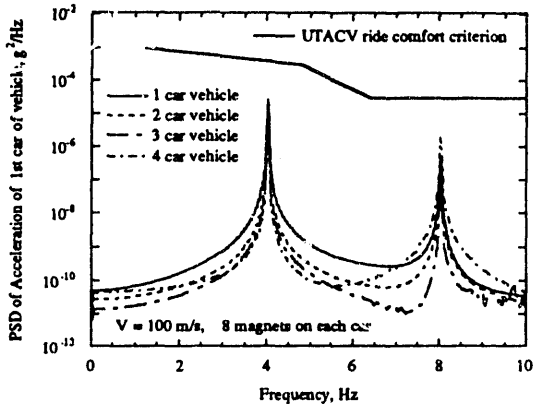

Fig. 4. PSD of car body accelerations when multicar vehicles with eight magnets on each car travel along the guideway at 100 m/s.

A one-dimensional vehicle model with two degrees of freedom (Fig. 5) and consisting of two lumped masses m_p and m_s, two linear springs k_p and k_s, and two viscous dampings c_p and c_s, representing primary and secondary suspensions, respectively, is used in the control synthesis of maglev systems. The passive parameters of the German Transrapid Maglev System TR06 are utilized for analysis in this study because no other Transrapid data are available in the literature [10-13].

An active primary suspension system is suitable for maglev vehicles [14]. Such a system provides continuous or discrete variation in effective spring constants and damping coefficients, according to some control law that may be designed in software rather than hardware. In the approach used here, the force element can be realized with a linear electrohydraulic actuator that connects magnet and bogie in the primary suspension (see Fig. 6). A position sensor detects the air gap between magnet and guideway, and an accelerometer, mounted on the bogie, detects bogie motion. The resulting signals are processed by the controller according to designed control law in software, in turn causing the actuator to ensure that the air gap does not exceed specific tolerances within the safety margin and that the acceleration PSD of the suspension remains as low as possible in the specified frequency ranges in order to guarantee good ride comfort.

In this study, an active feedback control path is applied to the simplified vehicle model, providing a less complicated control model. A lag-lead regulator is designed in the inner feedback path for the primary suspension (see Fig. 7).

It is noted that the active primary suspension system does not damp the excessive overshoots of the secondary suspension in the transient response and the frequency response. To achieve the desirable limits of the overshoots and the settling time, a semiactive control is introduced into the secondary suspension.

Semiactive suspension controls using a "skyhook" damper (Fig. 8) offer a considerable advantage in terms of transmissibility control. It can be constructed, without the need for an inertial reference, with an active element under feedback control. This can be done by a proportional control law involving the absolute velocity of the mass. It was proved that semiactive control with the skyhook configuration can increase the damping factor and that the resonant peak is suppressed while high-frequency transmission is simultaneously reduced [15].

Based on the principle of semiactive control of the secondary suspension, a feedback control path $K_s s$ (active damping) is added to the secondary suspension (see Fig. 7).

The detailed parameters are given in [4]. The PSD of vehicle acceleration with both primary and secondary feedback control is shown in Fig. 9. Ride comfort is much improved.

Figs. 10 and 11 show the transient responses of the primary and secondary suspensions with a unit-step input of guideway disturbance. Figs. 10 and 11 show that active and semiactive control designs indeed improve vehicle response and provide acceptable ride comfort.

IV. Dynamic Stability of Maglev Systems

For safety, maglev systems must be stable. Magnetic forces are basically position-dependent, although some are also velocity-dependent. These motion-dependent magnetic

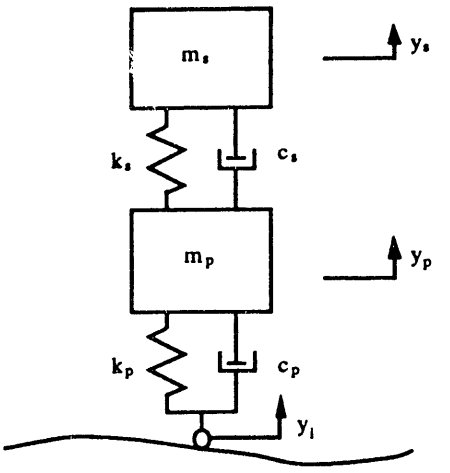

Fig. 5. One-dimensional two-degree-of-freedom vehicle model with primary and secondary suspensions for maglev systems.

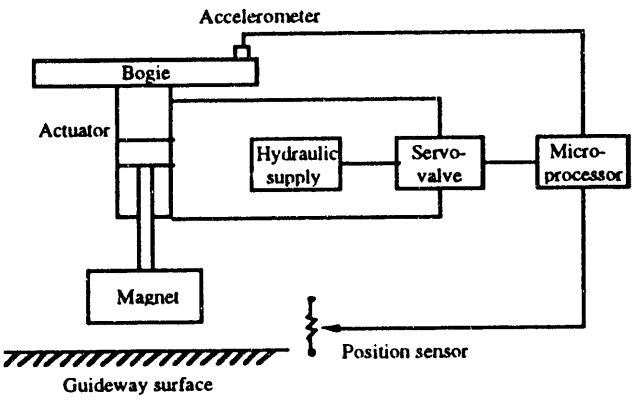

Fig. 6. Active electro-hydraulic system.

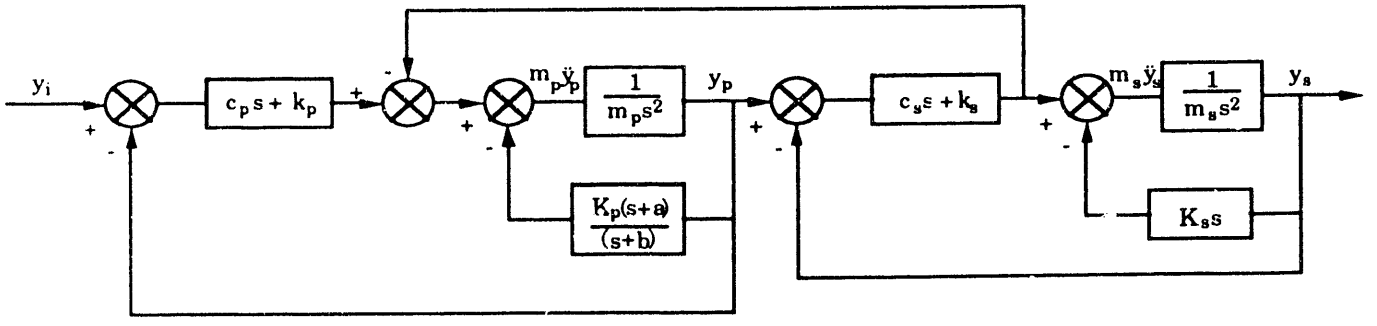

Fig. 7. Block diagram for two-degree-of-freedom vehicle model of maglev system with primary and secondary suspension feedback controls.

forces can induce various types of instability. Moreover, the periodic structure of the motion-dependent magnetic forces may in some cases induce parametric and combination resonances [6,7,16]. This study considers the stability of maglev systems and is based on experimental data, scoping calculations, and simple mathematical models. The objective is to provide some basic stability characteristics and to identify future research needs.

Different vehicles are considered [6], in order to provide an understanding of stability characteristics. Fig. 12 shows a cross section of a generic vehicle on a double L-shaped aluminum sheet guideway. A vehicle-guideway structure similar to this was used by Coffey et al. [14]. Assume that the vehicle travels at a constant velocity along x direction. Two permanent magnets are attached to the bottom of vehicle and provide lift and guidance force F_{L_1}, F_{L_2}, F_{G_1}, and F_{G_2}. Assume at the initial state that $h_1 = h_2 = h_0$ and $g_1 = g_2 = g_0$.

Based on magnetic forces and stiffnesses measured by the experiments [6], the eigenvalues and eigenvectors of a maglev vehicle on a double L-shaped guideway were calculated with the theoretical model developed in this section. Some very interesting results were obtained from those calculations.

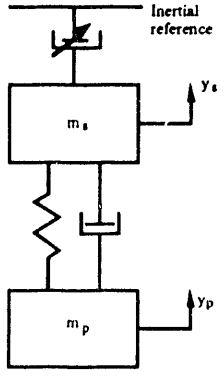

Fig. 8. Skyhook damper for secondary suspensions.

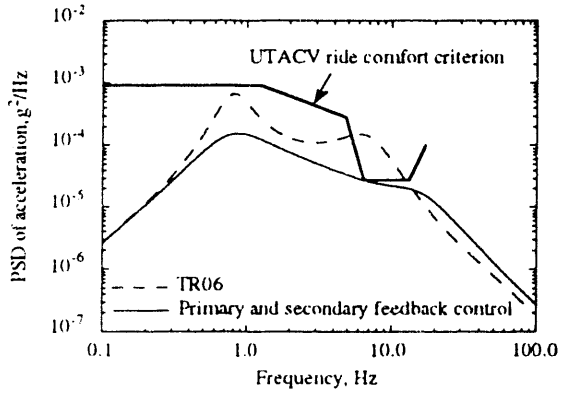

Fig. 9. PSD of vehicle acceleration using active and semiactive feedback controls in primary and secondary suspensions, with vehicle speed V = 100 m/s and guideway roughness amplitude A = 10^{-6} m.

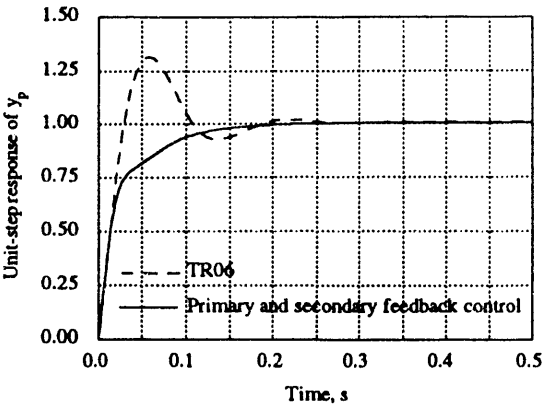

Fig. 10. Comparison of transient response y_p of primary suspension with unit-step input of guideway perturbation for TR06 and a new system using active and semiactive feedback controls in primary and secondary suspensions.

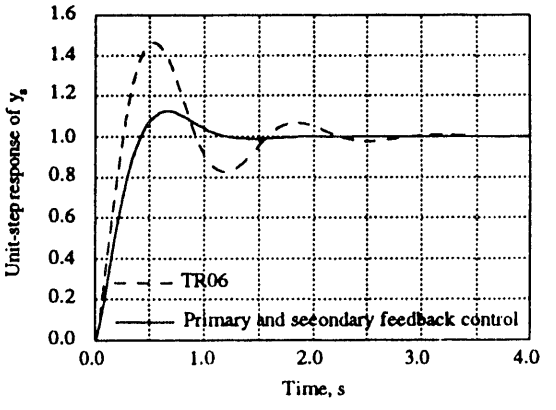

Fig. 11. Comparison of transient response y_s of secondary suspension with unit-step input of guideway perturbation for TR06 and a new system using active and semiactive feedback controls in primary and secondary suspensions.

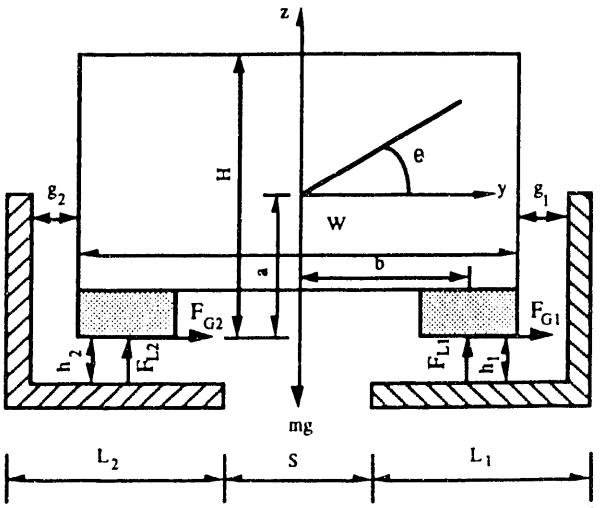

Fig. 12. Maglev system with a vehicle operating on double L-shaped aluminum sheet guideway.

Fig. 13 shows that eigenvalues of vehicle motion versus levitation height vary when guidance gaps are fixed ($g_1 = g_2 = Y^* = 12.7$ mm). The first mode ω_1 shows an uncoupled heave motion; the imaginary part of the eigenvalue is zero, while the second and third modes are coupled roll-sway motions. Within the range of height h = 19.0 to 35 mm, the imaginary parts of the eigenvalues are not zero. This indicates that within this range, flutter does exist for these coupled roll-sway vibrations.

Figure 14 shows eigenvalues of vehicle motion versus lateral location of vehicle when $g_1 = g_2 = g_0 = 25$ mm and levitation heights h = 12.7 mm. Notice that for the third mode, which presents the transversal motion of vehicle, the real part is zero and the imaginary part is not zero within a certain region. This indicates that the lateral motion of the vehicle is subjected to a divergence, given those vehicle and guideway parameters.

It should be pointed out that the measured and calculated data for motion-dependent magnetic forces and force coefficients are limited and that damping effects were not considered in the above analysis. Even though divergence and flutter appear in the eigenvalue results, we still have difficulty in completely predicting the dynamic instability of this three-degree-of-freedom maglev vehicle model because of the lack of knowledge of possible motion-dependent magnetic forces and aerodynamic forces. Further experimental and modeling research is needed to gain a more complete understanding of dynamic instability in maglev systems.

V. Closing Remarks

(1) The dynamic interaction model of a maglev system with a multicar, multiload vehicle traveling along a flexible guideway was developed in this study. It was verified that this model is suitable for analyses of vehicle/guideway interactions in maglev systems.

(2) Active and semiactive feedback control designs in primary and secondary suspensions can be realized through electro-hydraulic systems. The conceptual designs of hydraulic controllers will be taken into account in our future work.

(3) Instabilities of maglev-system models have been observed experimentally at several institutions [16]. An integrated experimental/analytical study of stability characteristics is an important aspect of maglev research. Motion-dependent magnetic forces may also be important elements in modeling and understanding dynamic instabilities of maglev systems. At this time, it appears that very limited data are available for motion-dependent magnetic forces. Efforts will be made to compile analytical results and experimental data for motion-dependent magnetic forces. When this work is completed, recommendations will be presented on research needs on magnetic forces. In addition, specific methods to obtain motion-dependent magnetic forces will be described in detail.

(4) Maglev may become a major transportation mode in the 21st century. Because the cost for a commercial maglev system is still very high, it is wise to consider dynamic control systems before completing the guideway design so that overall system cost can be reduced.

References

[1] S. S. Chen, D. M. Rote, and H. T. Coffey, "A review of vehicle/guideway interaction in maglev systems," ASME Publication PVP-vol. 231, pp. 81-95, 1992.

[2] Y. Cai, S. S. Chen, and D. M. Rote, "Vehicle/guideway interaction of maglev systems," Argonne National Laboratory Report ANL-92/19, March 1992.

[3] Y. Cai, S. S. Chen, D. M. Rote, and H. T. Coffey, "Vehicle/guideway interaction for high-speed vehicles on a flexible guideway," *Proc. CSME Forum 1992 "Transport 1992+"*, June 1-4, 1992, Montreal, Canada, Vol. III, pp. 750-757.

[4] Y. Cai, S. S. Chen, and D. M. Rote, "Dynamics and controls of maglev systems," Argonne National Laboratory Report ANL-92/43, September 1992.

[5] Y. Cai, S. S. Chen and D. M. Rote, "Vehicle/guideway interaction and ride comfort of maglev systems," accepted for presentation at Int. Conf. on Speedup Technology for Railway and Maglev Vehicle, November 22-26, 1993, Yokohama, Japan.

[6] Y. Cai, S. S. Chen, T. M. Mulcahy, and D. M. Rote, "Dynamic stability of maglev systems," Argonne National Laboratory Report ANL-92/21, April 1992.

[7] Y. Cai, S. S. Chen, T. M. Mulcahy, and D. M. Rote, "Dynamic stability of maglev systems," *Proc. 63rd Shock and Vibration Symposium*, 27-29 October 1992, Las Cruces, NM, pp. 533-543.

[8] Y. Cai, S. Zhu, S. S. Chen, and D. M. Rote, "Control of maglev suspension systems," accepted for presentation at Active and Passive Damping Symposium, 1993 ASME Pressure Vessels and Piping Conference, July 25-29, 1993, Denver, Colo.

[9] H. H. Richardson, and D. N. Wormley, "Transportation vehicle/beam-elevated guideway dynamic interactions: a state-of-the-art review," *ASME Trans., J. Dynamic Systems, Measurement, and Control*, vol. 96, pp. 169-179, 1974.

[10] G. Bohn, and H. Alscher, "The magnetic train Transrapid 06," *Proc. Int. Conf. Maglev and Linear Drives*, May 14-16, 1986, Vancouver, B.C., Canada, Publ. by IEEE, 86CH2276-4, pp. 233-242, 1986.

[11] G. Bohn and G. Steinmetz, "The electromagnetic suspension system of the magnetic train 'TRANSRAPID,'" *Proc. Int. Conf. Maglev Transport '85*, Sept. 17-19, 1985, Keidanren Kaikan, Tokyo, Japan, Publ. by IEEE, Japan, pp. 107-114.

[12] I. Faye, W. Kortum, and W. Schwartz, "Modeling, control design, and performance evaluation of high speed ground vehicle dynamics," *Mech. Struct. & Mach.*, vol. 17(2), pp. 259-281, 1989.

[13] W. Kortum, W. Schwartz, and I. Faye, "Dynamic modeling of high speed ground transportation vehicles for control design and performance evaluation," *Dynamics of Controlled Mechanical Systems*, IUTAM/IFAC Symposium, Zurich, Switzerland, 1988, pp. 336-350.

[14] Coffey, H. T., et al., "An evaluation of the dynamics of a magnetically levitated vehicle," Prepared by SRI for U.S. Dept. of Transportation, Federal Railway Administration, Report FRA-ORD&D-74-41, March 1974.

[15] R. Stanway, J. L. Sproston, and X. Wu, "Variable suspension damping using electro-rheological fluids," *IMechE C382/034*, pp. 547-558, 1989.

[16] D. Chu, and F. C. Moon, "Dynamic instabilities in magnetically levitated models," *J. Appl. Phys.*, vol. 54(3), pp. 1619-1625, 1983.

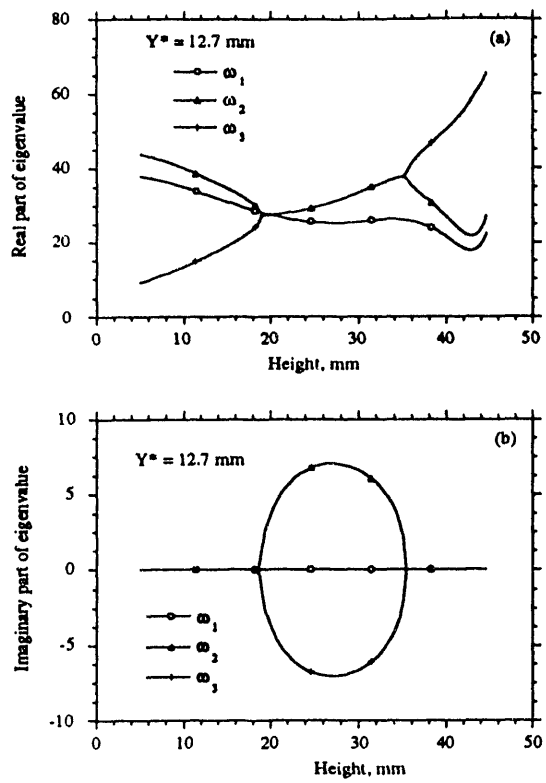

Figure 13. Maglev-system eigenvalues vs. vehicle levitation height, with $Y^* = 12.7$ mm.

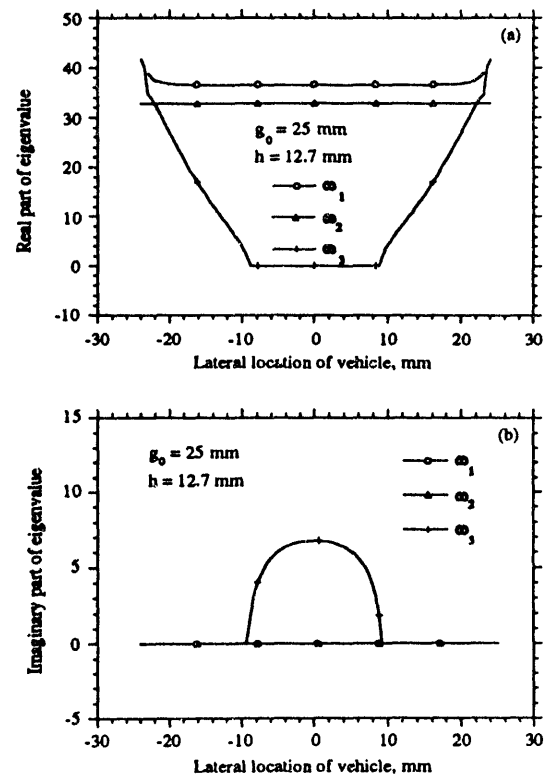

Figure 14. Maglev-system eigenvalues vs. lateral location of vehicle, with $h = 12.7$ mm and $g_0 = 25$ mm.

Linear Synchronous Motor Design

Richard D. Thornton
Department of Electrical Engineering and Computer Science, MIT, Cambridge, Mass. 02139

Abstract - **This paper discusses the major issues that are involved in the design of a maglev Linear Synchronous Motor propulsion system. It is a short version of a more detailed report [11], except that discussion of power electronics, position sensing, and control are covered in companion papers in these Proceedings [12, 13]. Examples are taken from current designs for U.S. application.**

INTRODUCTION

A linear synchronous motor is a complex system and its design requires an integration of skills from many disciplines. The capital and operating costs of the LSM are significant parameters in the cost of a complete maglev system, and it is imperative to treat the LSM design as an integral part of the complete system. It is not possible to discuss the design except in the context of other aspects of the system, so this paper makes frequent reference to existing systems and the recently completed System Concepts developed by 4 U.S. maglev design teams.

BASIC CONCEPTS

Types of linear motors

The Linear Induction Motor (LIM) and the Linear Synchronous Motor (LSM) are both suitable for maglev. The LIM is not usually suitable for wide gap EDS because it has unavoidable high losses and weight, so this report focuses on the LSM.

Multiphase electric power can be supplied to windings on the guideway, called "active guideway" or "long primary" or "long stator". The power can also be supplied to windings on the vehicle, called "active vehicle" or "short primary" and sometimes called "short stator," but since it isn't stationary, stator is an inappropriate term.

The unpowered portion of a LSM is called the field and consists of an array of magnets with constant field strength. These magnets can be conventional electromagnets, superconducting coils or permanent magnets. Unfavorable scaling laws make permanent magnets inappropriate at the power levels required for high speed transportation. An electromagnetic field can be used if the air gap is less than about 10 mm, but for wider gaps there are very large power dissipation in the field magnet windings because of basic material properties and limitations. Virtually all Electro Dynamic Suspension (EDS) and wide gap Electro Magnetic Suspension (EMS) designs use superconducting field magnets and an active guideway linear synchronous motor. The German Transrapid TR07 uses electromagnetic field magnets with the guideway winding embedded in slots in the laminated steel rails on the guideway. A System Concept proposed by the Grumman Team uses a novel EMS design in which superconductors carry the main field current, but normal conductors carry ac currents and are controlled by sensors that maintain the air gap constant.

Manuscript received March 15, 1993. This work was supported in part by the U.S. Department of Transportation under contract DTFR53-91-C-00070. Support from the MIT EECS Department and Laboratory for Electromagnetic and Electronic Systems is also gratefully acknowledged.

This report focuses on the long primary LSM with an emphasis on EDS, but with some discussion of EMS issues. Many designs for EMS and EDS use the magnets that create lift to also create the field for the LSM. This implies that there are two motors, which will be designated the port and starboard motors.

The currents in the guideway winding are controlled so as to make the vehicle move at the same speed as the traveling magnetic field, and hence the term *synchronous* motor. A synchronous motor system includes:

- Windings in the guideway which produce a traveling magnetic field;
- A motor power distribution system that connects electronic power controllers to motor windings in the blocks in which the vehicles are located;
- Electronic power controllers that convert fixed voltage and frequency utility power into variable voltage and frequency power that is applied to the windings;
- A utility power distribution system that accepts utility generated power and distributes it to electronic power converters located at regular intervals along the guideway;
- A control system that provides the correct current waveforms in the guideway windings according to vehicle force and speed requirements, and also provides various protection and failure monitoring facilities.

Propulsion differences between EDS and EMS

For an EMS system there is a limited area in the slots of the iron core that carries the magnetic flux, and the cost of increasing this area is quite high. Thus particular attention must be paid to the space limitations on the conductors and their insulation. The winding resistance and inductance are necessarily larger than for EDS, because of the limited area and proximity to high permeability material. The block lengths of the EMS guideway must be reduced to limit the winding resistance and inductance. This creates a requirement for feeder cables and wayside switching components.

For an EDS system the magnetic field produced by the vehicle is assumed to be created by superconducting magnets with no iron in the magnetic path. Thus there are less severe limits on the size of the motor winding, and the area of the conductors can be tailored to the need. For example, we can use larger area windings where more motor thrust is required. The penalties for too large a winding area are a reduced field for the portions of the winding more distant from the field source and a higher cost for the winding.

Another important difference is the electrical excitation frequency. EMS designs have a shorter pole length and thus a higher frequency. Examples are the Transrapid design with a pole pitch of 0.258 meters and the Grumman Team design with a pole pitch of 0.6 meters. For comparison, the Japanese EDS design uses a 2 meter pole pitch, the Bechtel Team's US1 design uses a 1 meter pole pitch, and the New Magneplane design uses a 0.75 meter pole pitch. The electrical frequency for EMS can be several times larger than the frequency for EDS and this increases the impact of winding inductance and affects other system design parameters.

Not only does EMS require a higher frequency, but the presence of iron near the winding increases the inductance of

the winding, and this aggravates the impact of the higher frequency. One should not expect that an LSM design that is optimized for EMS will also be optimum for EDS.

VEHICLE ATTRIBUTES

In a maglev system people and freight are carried in a vehicle or train of vehicles that are coupled into a single unit that is aerodynamically streamlined. In this paper the term vehicle is used to mean either a single rigid structure or a tightly coupled set of cars that are not intended to be decoupled. System design concepts for U.S. applications are based on point-to-point travel with off-line loading; this leads to vehicles the size of a narrow body commercial jet aircraft with between 100 and 200 passengers. Systems being developed in Germany and Japan are based on the use of longer vehicles that carry 600 to 1000 passengers. The focus of this paper is on designs with smaller vehicles that operate with short headway.

We assume a maximum safe operating speed requirement of 150 m/s (336 mph) and a maximum normal operating speed of 120 to 135 m/s (268 to 302 mph). For these speeds we can estimate the vehicle propulsion requirements for different sizes of vehicles for level travel. The following table gives probable values for minimum and maximum size US-style vehicles as well as for TR07.

TABLE 1. TYPICAL VEHICLE ATTRIBUTES.

Parameter	US min	US max	TR07	units
length	26	51	51	m
width	3.0	4.1	3.7	m
height	4.0	4.1	4.1	m
sections	1	3	2	
coach seats	72	216	180	
empty mass	30	60	90	tonnes
loaded mass	38	82	105	tonnes
Fm @135m/s	18	48	53	kN

The numerical values are based on ranges of parameters in some of the recently completed System Concept Designs and on published values for TR07 with some adjustment to make the comparisons comparable. F_m is the motor thrust requirement for level travel. The motor force is proportional to the motor current and to the length of the magnet assembly which provides the field for the motor. Some vehicle designs, such as the EDS designs proposed by the Japanese and the Foster-Miller Team have superconducting propulsion field magnets over only about 25% of the vehicle length. Other designs, such as Transrapid and those proposed by the Grumman, Magneplane and Bechtel Teams, assume the propulsion magnets run nearly the full length of the vehicle. The motor design requirement is very different for these two cases.

MOTOR ATTRIBUTES

Design alternatives

The power is specified by the mechanical requirements, but there are possible tradeoffs between voltage, current, number of phases, electrical frequency, and method of winding. This tailoring is constrained by a number of practical realities:

- The motor winding can have almost any number of phases. Most designs use 3 phases, but there are very good reasons to consider the use of more phases for an EDS design.
- The lower limit on motor voltage is determined by the length of the propulsion field magnets, the motor width, and the average magnetic field. In EMS designs it appears that voltage constraints limit the choice to 1 conductor per slot, and with long vehicles even then the phase voltages can be over 10 kV. Problems of insulation suggest that for EMS the instantaneous voltage from a winding to earth ground should not exceed about 15 kV. For EDS there is no iron so for short vehicles there are more options; the equivalent of 2 or more turns per slot is possible.
- With separate port and starboard motors it is possible to use two inverters, or the windings may be connected in series or parallel so as to use only a single inverter.
- In a guideway turn it is necessary to increase the pole pitch on the outside of the turn and decrease the pole pitch on the inside of the turn. This change in pole pitch can limit the radius of turn that is acceptable.

Motor performance limits

The motor performance is conveniently described by showing various limiting constraints on a plot of motor force F vs. vehicle velocity u., shown in Fig. 1 for a typical EDS design. The force for level cruise is minimum near u = 50 m/s; for lower speeds the suspension drag dominates while for higher speeds the aerodynamic drag dominates. In order to provide acceleration the force must be increased substantially, as shown by the curve for a 0.1 g acceleration. Fig. 4 is based on the following assumptions: vehicle mass = 63.4 tonnes; aerodynamic drag = 39 kN at 135 m/s and proportional to the speed squared; EDS suspension drag = 10 kW/tonne, miscellaneous eddy current power loss = 150 kW at 135 m/s and proportional to speed squared.

The plot of Fig. 1 can also be interpreted as a plot of motor current vs. voltage, with the scaling constants determined by the motor design. To simplify the analysis, measure the motor current and voltage as the dc input to the power inverters. Then, for example, if a design requires a dc motor current of 1000 amperes to achieve a force of 100 kN, conservation of energy requires that the motor induced voltage be 100 volts for every 1 m/s of vehicle speed. We can then relate limitations on motor current, voltage and power to limits on motor output thrust, speed, and power; these limits are shown by three curves in Fig. 1. The motor current limit determines the maximum thrust, the motor voltage limit determines the maximum speed with a slope determined by winding resistance, and the power converter power output limit (if there is one) creates a limit on motor output power.

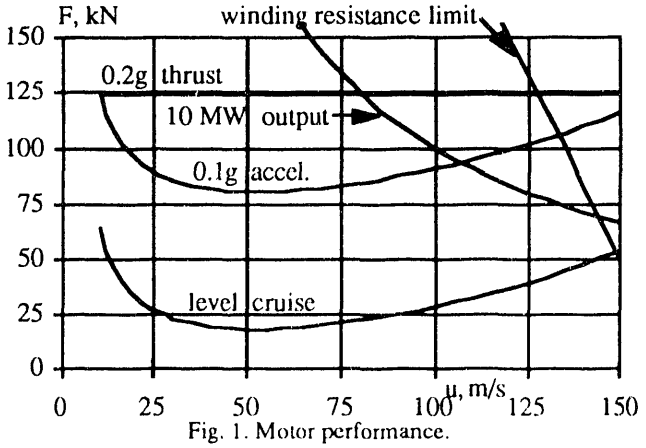

Fig. 1. Motor performance.

Motor winding

The guideway has several phases of propulsion windings, each carrying the same frequency current, but with currents phased such that there is a traveling magnetic field that moves at the same speed as the vehicle. A simplified winding diagram for a 3-phase motor is shown in Fig. 2. The wavelength λ is the distance between equivalent points in the periodic magnetic wave, and is equal to twice the pole pitch, which is the distance between successive magnetic poles. The three phase currents are i_1, i_2 and i_3; the control of these currents is the key to controlling the propulsive force for the vehicle. The force is proportional to the active width w, the average vertical magnetic field in the transverse portions of the winding, and the number of magnetic poles on the vehicle.

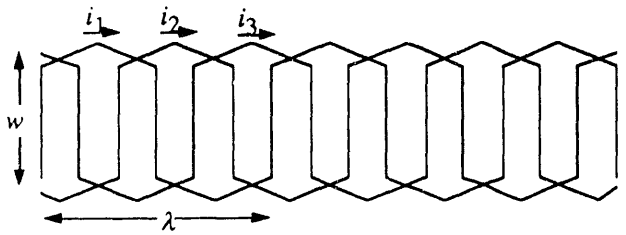

Fig. 2. One conductor per slot, 3-phase meander winding.

For optimum motor efficiency, the current waveform should have the same shape as the waveform of the induced voltage in the propulsion winding, and this shape depends on many details of the motor design. In most designs the induced voltage is very nearly a sine wave, but for some EDS designs there can be up to 15% third harmonic voltage, and this harmonic voltage actually reduces the peak motor voltage. By providing a third harmonic component in the current the performance of the motor is enhanced. Note that the winding must be constructed from many insulated strands in order to avoid excessive eddy current loss. For most applications the winding will be less expensive if constructed from aluminum wire. A typical design requires about 100 tonnes of aluminum per km of guideway and can operate at 90% efficiency with a block length of 2 km.

Helical windings

Most rotating superconducting machine designers have found that a *helical* winding is preferable to a conventional meander winding of the type shown in Fig. 2 [10]. To envision a helical winding, imagine that a wire is wound in a helical fashion around a cylindrical form. After the winding is finished, the form is removed and the winding flattened. A multi-phase helical winding is wound by winding several interspersed helices. The result is a winding with substantially lower inductance and, for most designs, lower resistance for given conductor mass and field intensity. We believe that the helical winding will be the winding of choice for most EDS maglev systems. Unfortunately, it does not work well when the winding must be embedded in slots in a laminated steel core, as in an EMS system.

With a helical winding it is possible to create a winding with an inductance to resistance ratio of 2 to 4 ms. If L/R can be kept low, the electronic inverters will be less expensive and more efficient [12].

Motor field

For an EDS design the motor field is usually produced by a nonferromagnetic structure with superconducting coils. The shape of the field in the plane of the winding controls the forces acting on the vehicle. With proper design it is possible for the propulsion system to produce forces for ride quality control as well as for propulsion [7]. For a typical design the average magnetic field in the plane of the propulsion winding is in the range 0.5 to 1 Tesla.

The motor field can create strong fields at significant distances from the superconducting coils, and this field can create a number of problems. The best way to reduce these external fields is to use the smallest coil size possible and to use a long array of equally spaced, alternating polarity poles; the field then falls off exponentially with distance. In order to achieve the full impact of this field reduction, it is necessary to taper the field strength in the coils at the end of the array [11].

Acceleration and deceleration

Acceleration is limited by the thrust available from the linear motor, but it is also limited by requirements of providing passenger comfort. For U.S. applications it is expected that some sections of the guideway will follow Interstate Highway Rights of Way, and vehicles will thus be subject to relatively frequent speed changes in order to negotiate turns with acceptable banking angles. This makes it necessary to limit vehicle acceleration to values that are compatible with passengers standing and walking. There is some debate as to how high this can be, but a value of 0.2 to 0.3 g appears to be acceptable and even higher values have been proposed. Although still higher acceleration is possible with seated and belted passengers, the frequency of speed changes makes this impractical except at special places, such as when stopping at a station. The cost of the propulsion system may also pose acceleration limits.

Fig. 3 shows typical acceleration and deceleration as a function of the motor thrust. Note that for a wide range of speeds the vehicle drag is on the order of 0.03 to 0.05 g, so quick estimates can be made by assuming the net propulsive force for acceleration is 0.04 g less than the motor thrust. At the higher speeds the motor thrust is primarily used to overcome aerodynamic drag.

Under normal conditions the desire to achieve high ride quality imposes both deceleration and acceleration limits, and these two limits are usually equal in magnitude. Normal braking can be regenerative with most of the vehicle's kinetic energy being converted to electric power that is made available

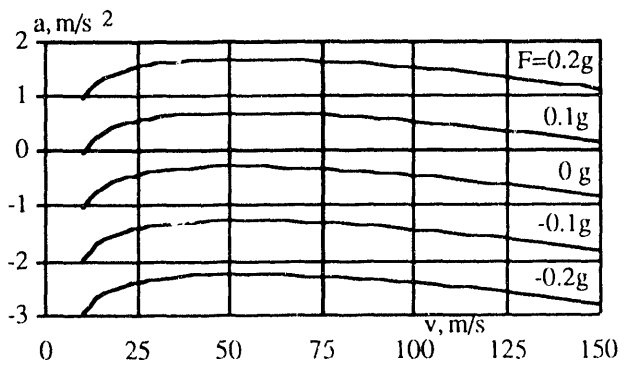

Fig. 3. Acceleration vs. speed for different motor thrusts.

for propulsion of nearby vehicles or, with some designs, inserted back into the utility grid. A companion paper [12] discusses the design of the power electronic system, including methods for achieving regenerative braking.

Unscheduled braking

Unscheduled braking will occur when the vehicle is required to stop unexpectedly because of a fault condition, but the fault condition is within design limits. For example, if a vehicle switches off the main line but the switch then fails, all trailing vehicles must slow down more rapidly than normal. Since the headway has been chosen to allow for this type of failure, normal regenerative braking would be employed and the electronic inverter would provide speed control. For this mode the linear motor should be capable of providing at least 0.25 g reverse thrust and, when the aerodynamic and magnetic drag are added, the total deceleration will be on the order of 0.3 g. Where possible the passengers would be given a few seconds warning before being subjected to this level of deceleration, but 0.3 g deceleration is commonly experienced in other travel modes and is assumed to be acceptable where necessary to avoid accidents. For this scenario, and assuming typical aerodynamic and magnetic drag, the vehicle can be stopped in about 3 kilometers.

For severe and very rare events, such as an unexpected and major earthquake, braking rates in excess of 0.5 g may be desirable. The active guideway LSM offers *dynamic braking* as an option that should be carefully considered by system designers. Dynamic braking is created by connecting passive resistors across the motor winding. Then the voltage generated by the moving vehicle creates current and hence power loss in these resistors. This induced current does not have to flow through the inverter or any power limiting component so very high braking forces are possible. The major limits on braking force are the resistance and inductance of the winding and the mechanical strength of the winding and guideway structural members. This mode can be made fail safe because it does not require active control or a source of power. The power resistors and winding must not overheat during the deceleration, but this is a one time process so there is time for these components to cool down after the braking event.

A typical plot of dynamic braking force vs. vehicle velocity is shown in Fig. 4 and given by

$$F_{db} = \frac{F_{max}\left(u / u_{dp}\right)}{1+\left(u / u_{dp}\right)^2}, \quad u_{dp} = \frac{\lambda R}{2\pi L}.$$

The maximum force, F_{max}, depends on several design parameters and for a typical EDS design is between 0.25 and 0.5 g. The velocity at the drag peak, u_{dp}, depends on wavelength , phase resistance R, and phase inductance L, as given in (1). Ideally an unexcited block would be shunted with a resistor value chosen to provide minimum stopping distance with no other action by the controller. For a vehicle with typical drag coefficients and mass, dynamic braking can stop the vehicle in less than 2 km.

The plots in Fig. 4 are for a typical design with a maximum braking force of 0.4 g at a speed of 40 m/s (89 mph). By adding a series resistor with resistance equal to the winding resistance (R=2 in Fig. 4), the velocity of the drag peak is doubled but the magnitude of peak drag force is not changed.

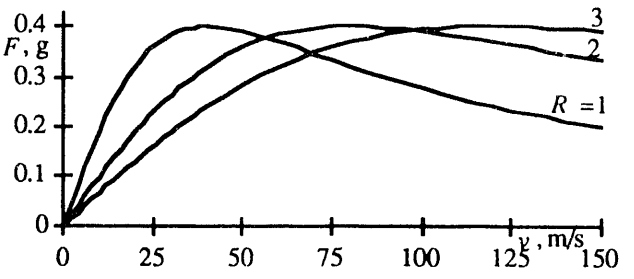

Fig. 4. Typical dynamic braking force vs. velocity for different R

An LSM for an EMS system has too high an inductance to provide rapid braking, so other mechanisms must be used. TR07 uses eddy current brakes which induce currents in solid steel guidance rails. These eddy current brakes are used for most deceleration greater than about 0.05 g.

System designers must reconcile the merits of rapid braking versus the cost of building a stronger guideway and the risk of a faulty control system producing unnecessary rapid braking. An unnecessary application of dynamic braking could, itself, cause accidents! I believe that dynamic braking is desirable, but only if it is well designed and incorporated into the system planning.

Fault tolerance

For any high speed guided transportation system it is imperative that the system have a high degree of fault tolerance. This means:

- In the event of a minor failure it should be possible to operate almost indefinitely with, at most, some modest reduction in power. For example, a multi-phase motor can be operated with some phases disabled.
- More serious failures should be extremely rare, and it should be possible for a person or team of people to effect the repair in a very short time.
- More common failures that can not be avoided by good design should have redundancy or automatic repair capabilities so that the system can operate at nearly full capacity in spite of a failure.
- No failure that can be reasonably expected should be allowed to compromise the safety of operation.
- Some components can be expected to fail after several years of service. For these components there should be automatic monitoring to try and anticipate the failure, and replacement should be relatively rapid.

Other issues

Redundancy is related to fault tolerance, but not all systems with redundancy are fault tolerant, and vice versa. A requirement for redundancy need not be very expensive. For example, it is unnecessarily expensive to install complete spare inverters; a modular design can allow a complete set of spare parts to be built for a small fraction of the cost of a complete inverter.

All new transportation systems tend to change in their early years as their strengths and weaknesses become more apparent. A maglev propulsion system should be designed with a view to allowing larger vehicles and closer headway when demand warrants. It should also embody a modular design so that weaknesses can be corrected without total reconstruction.

BLOCK SWITCHING AND POWER DISTRIBUTION

Motor winding excitation control

A generic block switching scheme is shown in Fig. 5. The guideway is divided into zones with one or more inverter modules for each zone and for each direction of travel. The zone is then divided into blocks which are excited in sequence as the vehicle moves down the guideway. Switching devices, either mechanical or solid state, are used to connect the inverter to the appropriate block as the vehicle moves along the guideway. Feeder cables are used to transfer power from an inverter to an active block.

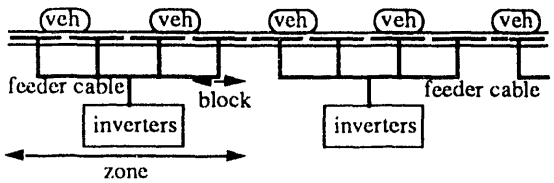

Fig. 5. Zone control system.

The zone length is determined by the minimum vehicle headway and the assumption that there will be an upper limit to the number of vehicles per zone. The zone is then divided into blocks with the restriction that no more than one vehicle may be in a block at a given time. There must be at least one inverter, or inverter pair in the case of a dual motor system, for each vehicle in a zone at any time.

The block length is determined by a number of factors. For an EMS system the winding resistance and inductance would be excessive for block lengths greater than about 0.5 km, and this implies the use of several blocks for each zone. For EDS it is possible to use block lengths of 2 to 3 km so one could make the zone length equal to the switching block length. For a high capacity system this may be a good design, but with today's estimated traffic and for most U.S. locations, the headway requirement will be greater than 4 km. Thus the block length is usually less than a full zone, and some sort of block switching is required.

Designers of the TR07 system envision headways on the order of 20 km, so they have used many blocks per zone and long feeder cables. Our proposal for U.S. applications is to use a zone length of 3 to 4 km with inverters feeding power either upstream or downstream to adjacent 1.5 to 2 km blocks. This method eliminates the need for any feeder cables, although some switching circuitry is required.

In addition to block switching, there must be a way to effect the gradual transfer of a vehicle from one block to the next. Some designs have used *leap frog* designs in which one inverter powers one block and a different inverter powers the next block. Other designs have used a *staggered* arrangement in which a port motor is used to transfer the vehicle across a gap in the starboard motor, and vice versa. Our proposal is to use a system analogous to a ship's lock in a canal, with solid state switching used to control the passage of the vehicle through the electronic lock. This way there is no need for extra inverters. Whatever the method, it is imperative that ride quality is not degraded by having discontinuities in propulsive force at a block boundary.

The determination of optimum block length is an important system design decision and many factors must be considered. For example, one reason to have short block length is to allow for short vehicle headway distances when the vehicles are operating at reduced speed. There will be occasions when some malfunction or weather condition requires vehicles to proceed at lower than normal speed along a portion of the guideway. If the vehicle spacing is forced to be more than about 2 km, then the guideway capacity will be reduced at speeds below about 100 m/s, and the entire guideway system will be disrupted by a slowdown in a small section of guideway. A preferred mode is to allow reduced speed operation with vehicles spaced as close as 2 km. This can be done by using the port motor for one block and the starboard motor for an adjacent block; at low speeds only one of these motors is needed for efficient propulsion of a single vehicle.

Utility power distribution

The utility power distribution will normally have the form shown in Fig. 6. Substations every 20 to 50 km convert 3-phase, high voltage utility power to lower voltages suitable for distribution. The power distribution can be either dc or 3 phase ac with line to ground voltages in the 15 to 25 kV range. Power is distributed along the guideway to wayside inverters which generate variable voltage, variable frequency power for the LSM. This power system is similar to ones used for conventional electrified rail and does not pose any problems that have not been addressed in that context. However, we believe that the alternative of dc distribution deserves serious consideration. It greatly simplifies the implementation of regenerative braking and leads to lower cost underground cables.

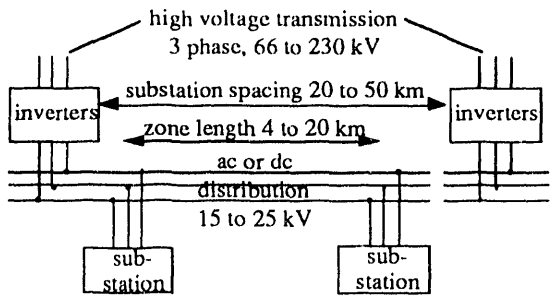

Fig. 6. Typical power distribution.

The choice of transmission line voltage is based on availability and power requirements. Lower voltages will lead to lower cost, but voltages less than 66 kV will not have enough capacity for a high speed maglev system, and even 66 kV systems may be inadequate. Voltages over 230 kV will lead to very high substation cost and should be avoided unless the maglev substation can share facilities with other power users.

The choice of line-to-ground distribution voltage is based on power levels and distribution distances. Most high speed rail systems use 25 kV the exception being the German ICE which uses 15 kV. The German Transrapid maglev design is based on a 17.3 kV, 3 phase distribution system that is common in Germany. Studies have also arrived at line to ground voltages in the 15 to 25 kV range as the best choice for U.S. maglev. The substations contain transformers and equipment for protection and control. For dc distribution the substations also include a rectifier. There are options as to whether regenerated power can be fed back into the transmission line system and whether there is a voltage control capability for the distribution circuit.

The required power levels depend upon speed. A fully loaded maglev vehicle averaging 125 m/s will require about 100 Wh per seat-km. If the guideway capacity is 12,000 passengers per hour, then the power demand is 100 x 12,000 = 1.2 MW per km for each direction of travel, or 2.4 MW/km for a dual guideway. The power system size is more closely related to guideway capacity than to any other parameter.

Other utility issues

Utilities are very concerned about the potential impact of maglev on their power system. The principal concerns are flicker, harmonic generation, and power flow-through. Flicker is caused by rapid and large changes in power demand and is undesirable because it causes disturbing flicker in electric lighting. Harmonic generation must be mitigated by proper power circuit design and with filtering. The power flow-through issue must be addressed by preventing power from flowing from one transmission line to another via the power distribution system.

In 1991 energy costs for large consumers varied from 3.3 to 10.8 ¢/kWh, depending on the state [11]. In the areas that are most likely candidates for a maglev system, the cost is in the range of 5 to 8 ¢/kWh, or less than 10% of the vehicle operating cost. But the capital cost of the maglev system is strongly dependent on the energy consumption, so power usage is more important than is sometimes assumed. Note that the energy cost is strongly dependent on whether the maglev operator or the utility owns and operates the power distribution system; with the former option the energy cost might be 30% less than the values given above.

ACKNOWLEDGMENT

I wish to thank Ray Wlodyka, Frank Raposa and other staff of the National Maglev Initiative for their comments and suggestions. Thanks are also due to Dave Perreault, Tracy Clark, Jim Kirtley, John Kassakian and Marty Schlecht of the MIT Laboratory for Electromagnetic and Electronic Systems and several staff of the MIT Plasma Fusion Center.

REFERENCES

[1] J. R. Powell, G. T. Danby, "The linear synchronous motor and high speed ground transport," 6th Intersoc. Energy Conversion Eng'g Conf., Boston, Mass., 1971.

[2] D. L. Atherton, *Study of Magnetic Levitation and Linear Synchronous Motor Propulsion*, Canadian Institute of Guided Ground Transport, Queens University, Kingston, Ontario, Annual Report for 1972.

[3] H. H. Kolm, R. D. Thornton, "The magneplane: guided electromagnetic flight," *Proceedings of the 1972 Applied Superconductivity Conference*, May 1-3, 1972.

[4] G. Danby, J. Powell, "Integrated systems for magnetic suspension and propulsion of vehicles," pp. 120-126, *Proceedings of the 1972 Applied Superconductivity Conference*, May 1-3, 1972.

[5] R. D. Thornton, "Design principles for magnetic levitation," *Proc. IEEE*, vol. 61, no. 5, May 1973, pp. 586-598.

[6] G. R. Slemon, R. A. Turton, P. E. Burke, S. B. Dewan , "Analysis and control of a linear synchronous motor for high-speed ground transport," *Linear Electric Machines*, Proceedings of Conference at London, England, Oct. 21-23, 1974, pp. 143-148.

[7] R. D. Thornton, "The magneplane linear synchronous motor propulsion system," *Linear Electric Machines*, Proceedings of Conference at London, England, Oct. 21-23, 1974, pp. 230-235.

[8] I. Boldea, S. A. Nasar, *Linear Motion Electromagnetic Systems*, John Wiley & Sons, New York, 1985.

[9] K. Heinrich, R. Kretzschmar, editors, *Transrapid Maglev System*, Hestra-Verlag Darmstadt, 1989.

[10] J. L. Kirtley, "Air-Core armature shape: a comparison of helical and straight-with-end-turns windings," *Proceedings of SM100*, Zurich, Switzerland, August 27-29, 1991.

[11] R. D. Thornton, D. Perreault, T. Clark, *Linear Synchronous Motors for Maglev*, Report for National Maglev Initiative, NTIS, January, 1993.

[12] D. Perreault, *Power Electronics for Linear Synchronous Motor Propulsion Systems*, these proceedings, May 19-21, 1993.

[13] T. Clark, *Position Sensing and Control*, these proceedings, May 19-20, 1993.

Improvements of the Attractive Force Levitation Concept

H. Weh, H. May, H. Hupe, A. Steingröver
Institut für elektrische Maschinen, Antriebe und Bahnen
Technische Universität Braunschweig,
Postfach 3329, 3300 Braunschweig, Germany

Abstract - This paper deals with the use of controlled permanent magnets for suspension as a step to decrease the losses of the control coils. At nominal air gap these magnets are controlled with negligible ampere-turns. Therefore the thermal stress of the control coils and the electronics will be reduced.

Maintaining the TRANSRAPID[1] guideway the powerless permanent magnetic excitation enables operations at larger mechanical air gaps up to 20 mm.

A new concept of an inertial gap control no longer requires to employ the constant gap control scheme with its implications. The mechanical vibrations transferred from the magnet to the cabin will be reduced. Results of a simulation show a considerable improvement of riding quality, even without intermediate spring frame.

I. Introduction

Contactless transportation with electromagnets is determined by attractive magnetic forces. They influence to a great extent the construction of the vehicle as well as the arrangement of the tracks. To utilize these unstable forces for contactless transportation, control and power electronics have to be installed on the vehicle. The tracks have to be mounted on pillars in a raised position as these forces can act only from underneath [1]. This also means that the tracks inevitably bend under the weight of the vehicle because of their limited stiffness [2]. Additional disturbances of the track of range of the mechanical air-gap can also be caused by sunken pillars on weak sub-soil or by distortion e.g. due to warming up caused by sunlight.

To maintain the quality of magnetic levitation under deteriorated track conditions an increase of the effective air gap length becomes necessary. As the air gap length has a significant influence on the participating power components, the dimensions of magnets, power electronics and batteries have to be increased as well. To avoid also an additional increase of the vehicle weight, special measures have to be taken. This can be realized by means of an excitation of the magnets without losses and the application of control techniques which effectively suppress vibrations.

II. Scaling Guidelines

The weight of the magnet which consists of the iron weight and the copper weight depends on various quantities. With a given vehicle mass and a given pole surface area determined by the long stator, the flux density in the air gap has to be held constant when the air gap size varies.

The ampere-turns varies proportional to the air gap size. However the resulting quadratic increase in the ohmic losses in the control coil also demands an enlarge of the copper cross-section in the magnet. In order to maintain a constant current density, this copper mass must increase in proportion to the air gap size. The influence of the leakage flux also increases proportionally. Therefore, to avoid an extra thermal load of the magnet, the coil surface areas have to be increased appropriately, or additional cooling measures have to be taken.

The iron volume has to be adjusted only to provide space for the larger coil, and to make sure that the yoke of the magnet is not saturated at all operating points due to the increased leakage flux.

[1] The German High Speed Maglev Train

III. Energetical Considerations of the Electromagnetic Supporting Techniques

The magnetic energy stored in the air gap volume of the vehicle is an approximate measure of the required technical expenditure. It must be provided by the energy supply and must be handled by the inverters and converters. Additionally recharging the magnetic energy in the air gap must be feasible, because at electrically excited magnets losses are always existent and can not be avoided. In the EMS (electromagnetic suspension) technology this is, beside the control function, an additional task for magnets, inverters and batteries.

Also in the EDS (electrodynamic suspension) technology the energy stored in the magnetic field determines the size of the required aggregates such as superconducting coils, batteries and cooling devices which compensate for thermal insulation losses.

With a given air gap flux density $B_{\delta\,max}$ of an EMS system, the maximum support force $F_{z\,max}$ determines the required pole surface area A_{pole}. This relationship results from the idealized MAXWELL force equation:

$$F_z = A_{pole} \frac{B_\delta^2}{2\,\mu_0} \qquad (1)$$

The total magnetic energy W_{mag} is determined by the gap volume and the air gap flux density (the energy stored in the iron and in the leakage paths are neglected). Under consideration of (1) the following relationship for the air gap energy can be derived:

$$W_{mag} = F_{z\,max} \cdot \delta_0 \qquad (2)$$

For example: to carry a vehicle of 100 t (air gap $\delta_0 = 10\,mm$) applying the EMS technology, an energy of 9.8 kJ is necessary to magnetize the air gap. Comparing the magnetized volume and the flux density of EDS to that of EMS levitation systems, the required magnetic energies in the air gap are significant higher. E.g. in the Japanese EDS vehicle MLU-002 approximately 8700 kJ of magnetizing energy is stored in the superconducting coils [3].

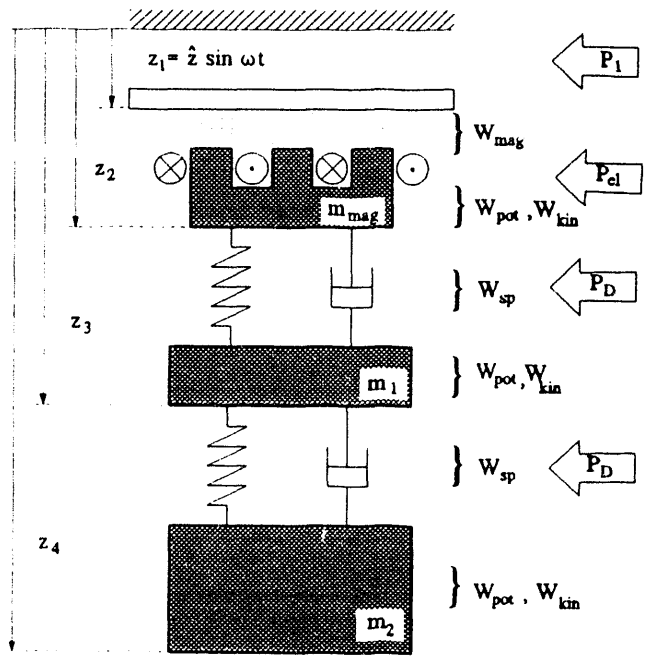

Fig. 1: Energy balance of an electromagnetic support system

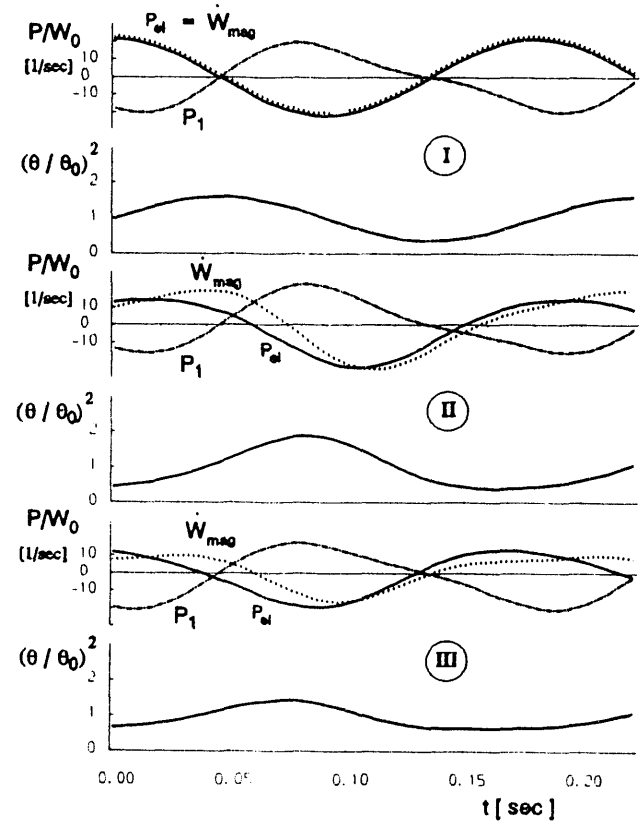

Fig. 2: Time behavior of the energy exchange at a sinusoidal track disturbance

Before an evaluation can be made about the components whose size depends on their power, the complete energy exchange under dynamic load conditions of the levitation system must be investigated. The following simplifications were made:

1. The track is supported by pillars and the girders are bent sinusoidally.
2. The levitation system is approximated by a first order low pass lag with a given cut-off frequency ω_{mag}.
3. The vehicle mass is decoupled from the levitation magnet by a well damped spring-damper system.
4. The investigation is confined to the one dimensional case.

The following kinds of energy are involved in the energy exchange: the magnetizing energy (W_{mag}) in the air gap volume and the kinetic (W_{kin}) and the potential energy (W_{pot}) of the levitation magnets and of the vehicle (Fig. 1). Input quantities of the system are the electrical power P_{el} which is fed into the control coils and the mechanical power P_1 which is, in the one dimensional energy model, transferred to the system by the oscillating tracks. In the real vehicle this is equivalent to the interaction with the energy of propulsion. From the balance of power:

$$W_{mag} + W_{kin} + W_{pot} = \int P_{el}\,dt + \int P_1\,dt \qquad (3)$$

significant characteristics of the system can be determined.

Without detailed knowledge about the electromagnetic characteristics of the levitation magnet, but with the masses, the cut-off frequency of the levitation system ω_{mag} and the natural frequency $\omega_{vehicle}$ and damping $D_{vehicle}$ of the magnetic suspension, it is possible to determine the supplied electrical power as a function of time as depicted in Fig. 2. An additional power component due to the ohmic losses and a reactive power component due to the magnetization of the leakage inductance must be considered.

Curve I depicts the results assuming the air gap to be held absolutely constant. Both, the mass of the magnet and that of the vehicle act as one unique body. The supplied electrical power directly equals the variation of the magnetizing energy. In curve II the dynamic lag of the control system is taken into account. Although the magnitude of the ampere-turns is increased the magnitude of the required reactive power is reduced. The resulting direct component of the electrical power corresponds to the direct component of the supplied mechanical power P_1. In the case of decoupling the vehicle mass from the magnet by a spring-damper system (curve III), the major difference to curve II lies in the reduced ohmic power losses ($\sim \theta^2$) which is caused by smaller dynamic force amplitudes.

On real tracks the excitation consists not only of the basic frequency but also of frequencies of higher order which have to be considered in the power calculations proportional to ω^3.

Fig. 3 depicts the maximum and minimum values of the electrical apparent power as a function of the natural frequency of the control loop. In the frequency range lower than 10 Hz the energy exchange with the battery increases whereas the ohmic losses reduce in proportion to the natural frequency. With an inertial control ("platform riding", natural frequency = 0 Hz) only the ohmic losses and the reactive power for the magnetization of the leakage inductance have to be provided. The dotted lines show the same quantities for a heavy magnet (33 % of the vehicle weight). Therefore the application of permanent magnets is appropriate to

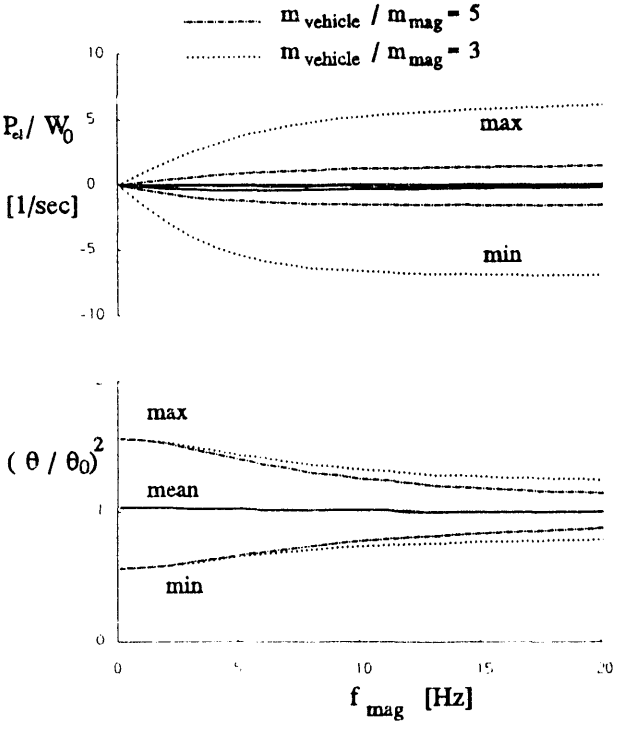

Fig. 3: Influence of the cut-off frequency to the energy exchange

reduce the losses in the resistances which depend on the magnitude of the ampere-turns.

IV. Permanently Excited Levitation Magnets

The significant ohmic power losses at large air gap sizes can be reduced by permanent magnetic excitation of the levitation magnets [4]. In this case the required amount of permanent magnet material can be evaluated by an investigation of the energies.

Contrary to the electrical excitation the permanent magnet has an internal magnetic resistance. This is equivalent to the statement that at most 50% of the "free energy" provided by the permanent magnet can be transferred to the air gap volume. The theoretical maximum value of the relation between the mass of the magnet and the mass of the vehicle is given by:

$$\left(\frac{m_{PM}}{m_{vehicle}}\right)_{theor} = 2 \cdot \frac{\delta_0 \cdot g \cdot \rho_{PM}}{(B \cdot H)_{max}} \qquad (4)$$

$$g = 9.81 \frac{m}{sec^2}$$

Considering also the leakage flux of the permanent magnet with a leakage constant of $b_\sigma = 0.03m$ the relation between the masses must be reduced by a factor depending on the design of the magnet.

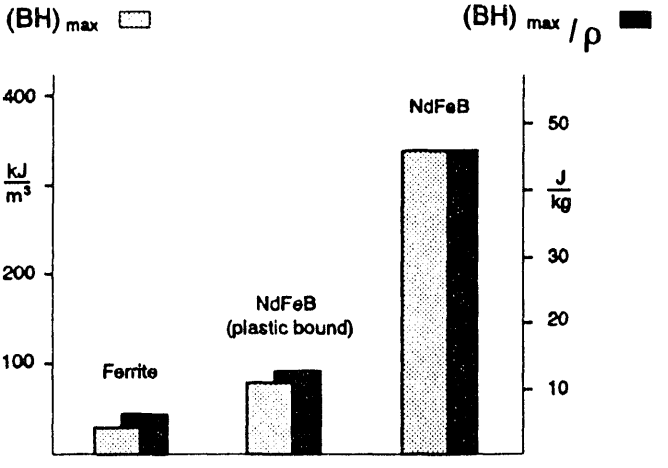

Fig. 4: Energy density of permanent magnetic materials

$$\frac{m_{PM}}{m_{vehicle}} = \left(\frac{m_{PM}}{m_{vehicle}}\right)_{theor} \cdot \left(1 + \sqrt{1 + 8 \cdot b_\sigma \cdot (B \cdot H)_{max} \cdot \frac{l_{vehicle}}{m_{vehicle} \cdot g} \cdot \frac{B_\delta}{B_r}}\right)^2 \qquad (5)$$

Advanced high energy magnets (NdFeB) provide an energy density of up to $340\,kJ/m^3$ and an energy to weight ratio of $(B \cdot H)_{max} / \sigma_{PM} = 45\,J/kg$ (Fig. 4). Assuming a vehicle mass of 2 t/m and an air gap of

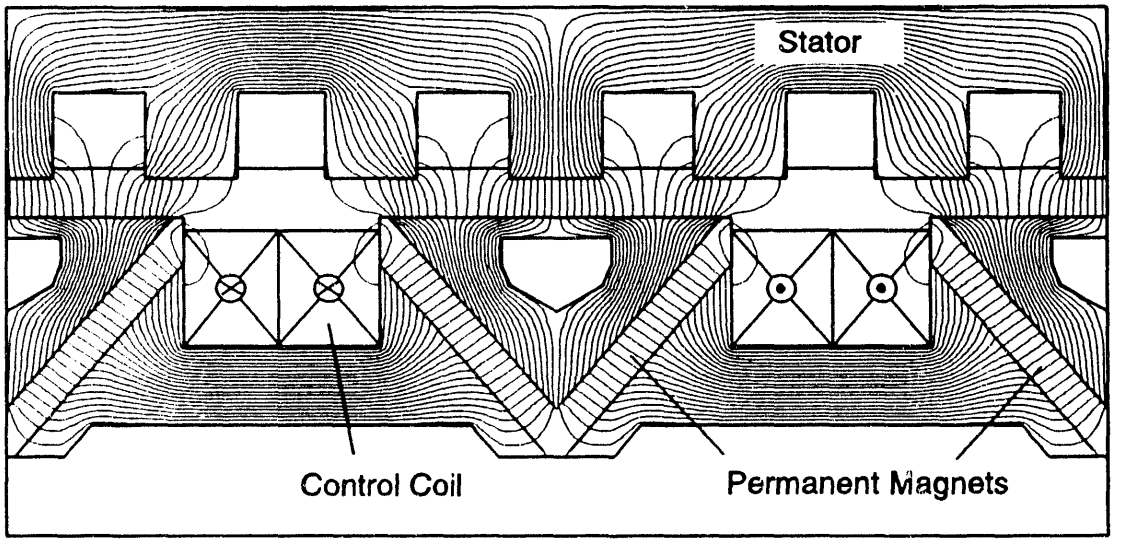

Fig. 5: Permanent magnetic excited suspension system (longitudinal section)

Table 1: Data of the controlled permanent magnet

air-gap	16	18	mm
height of the PM	15	17	mm
ampere-turns	2.5	2.8	kA
F_{pol}	3.3	3.3	kN
mass of the PM	1.65	1.85	%
losses per pole	58	73	W

2 cm, only 1.8 % of the vehicle mass is required for the mass of the permanent magnets.

Permanent excited magnets offer the possibility of increasing the air gap length up to 2 cm because of their lossless excitation. Fig. 5 shows the flux plot of the combined levitation and propulsion technology. The permanent magnets are arranged in a V-shape to reduce the leakage flux at the back of the magnets. The data for the magnets are given in Table 1.

To maintain the safety of operation the support magnet should be divided into several independent control units. Permanent magnets achieve the same reliability as electrically excited magnets by a modification of the inverter and by adding extra independent de-excitation equipment.

V. Inertial Control

As shown in sections I. and II. an increase of the air gap length results in an significant increase of the weight of the levitation magnets. Therefore it becomes more suitable for the control, from the energy point of view, to aim for an average air gap level instead of following the periodic oscillations of the track (Fig.1). The energy exchange of an inertial control is similar to that of a control with a low natural frequency as shown in Fig. 3.

However the control system must still be able to compensate for transient disturbances of the track (e.g. on slopes), and the levitation magnet has to follow these deviations almost immediately. For this reason suppressing the exciting frequencies by a band elimination filter or a "soft" control setup is not suitable, hence a "hard" inertial control scheme should be used to avoid inadmissible gap values.

The control structure shown in Fig. 6 is based on a state control concept which is supplied with a variable air gap request. The frequency and magnitude of this request equal the periodic oscillations of the tracks. A disturbance detection system calculates and adapts this request by means of an analysis of the acceleration of the magnet. The supervising logic observes the air gap

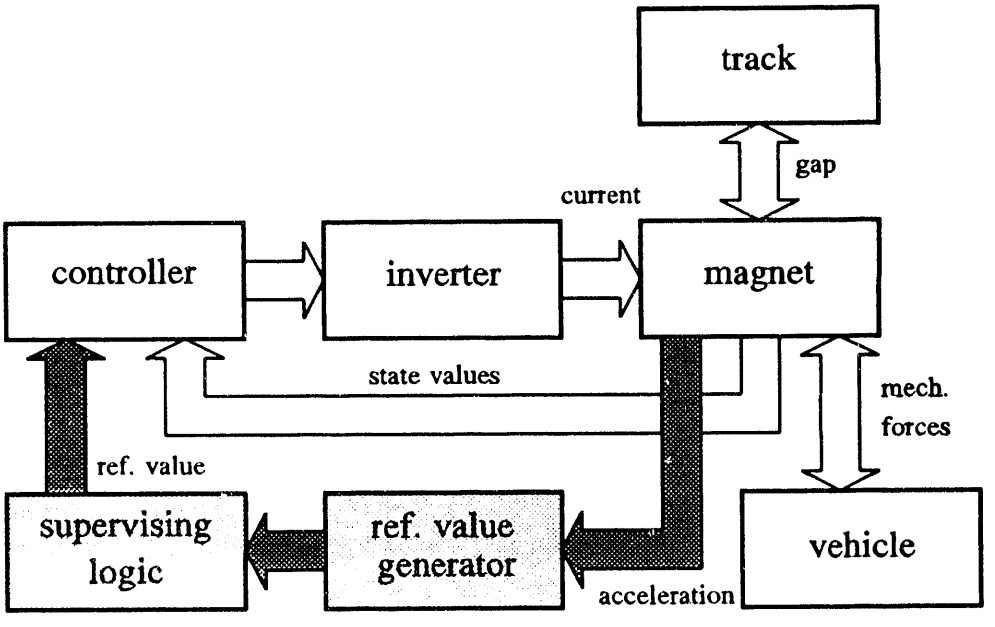

Fig. 6. Block diagram of the inertial gap control

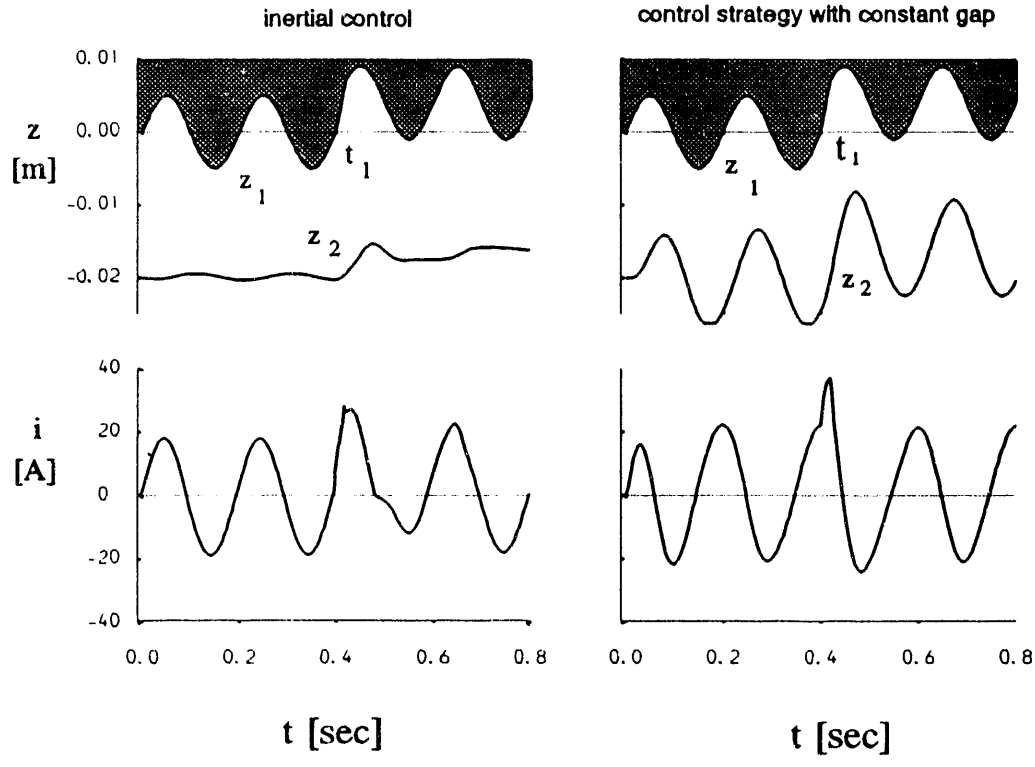

Fig. 7: Simulated behavior of the inertial gap control

length, and when the control error exceeds specific limits, the reference input can be switched.

The curves depicted in Fig. 7 are the results of a simulation. A sinusoidal 5 Hz oscillation was applied to simulate the periodic disturbances of the track, and at time t_1 an additional ramp disturbance was superimposed. The positive characteristics of the inertial control not only determine the energetic behavior of the magnet but also significantly reduce the tendency of the vehicle body to follow the unevenness of the track.

VI. Practical Aspects

As shown in chapter II with the air-gap the mass of the magnet increases both the electronics and the battery power. A 2 cm air-gap length demands a magnet to vehicle mass ratio up to 0.3. By the use of a permanent magnet the excitation supply can be reduced.

Only the inertial control strategy hinders the increased demand on power and energy. Furthermore this strategy leads to an improved riding quality with non vibrating magnets. Therefore the magnets can be connected to the cabin without the additional spring frame which is normally used for isolating the cabin frame from mechanical vibrations. Design and construction of the guideway are less determined by comfort requirements yielding reduced track costs.

VII. References

[1] H. Weh, "MAGLEV Levitation Technology and its Development Potential," *MAGLEV-Yokohama, Japan, July 7-11 1989.*

[2] J. Meins, W. Ruoss, "Analyse der Fahrversuche zur Dynamik des Trag-Führsystems des Fahrzeugs Transrapid 06/1", *VDI-Berichte 635, 1987*

[3] Y. Jizo, S. Fujiwara, K. Nemoto, "Superconducting Magnets of New Test Vehicle 'MLU002' on Japanese EDS System" *MAGLEV-Hamburg, Germany, June 9-10 1988.*

[4] H. Weh, H. May, H. Hupe, "High Performance Magnetic Levitation with Controlled Magnets and Magnets with Stable Characteristics," *MAGLEV-Hamburg, Germany, June 9-10 1988.*

Technical Assessment of Maglev System Concepts

James H. Lever
U.S. Army Cold Region: Research and Engineering Laboratory
Hanover, New Hampshire 03755

Abstract - This paper presents an overview of the methods and results of the Government Maglev System Assessment. As part of the National Maglev Initiative, we examined the technical characteristics of the NMI's four contracted system concepts, the French TGV high-speed train and the German TR07 maglev prototype. In general, the U.S. concepts offer a potential for higher performance at similar cost compared with TR07. All five maglev concepts offer a large performance advantage over TGV.

I. INTRODUCTION

The Federal Government organized the National Maglev Initiative (NMI) to determine whether it should actively encourage maglev investment. As part of this effort, the NMI awarded four System Concept Definition (SCD) contracts to teams led by Bechtel Corp., Foster-Miller, Inc., Grumman Aerospace Corp. and Magneplane International, Inc. These $2M, 10-month contracts resulted in very thorough descriptions and analyses of four different maglev concepts.

The NMI's Government Maglev System Assessment (GMSA) team consisted of scientists and engineers from the U.S. Army Corps of Engineers (USACE), the U.S. Department of Transportation (USDOT) and USDOE's Argonne National Laboratory (ANL), plus contracted transportation specialists. The GMSA team assessed the technical viability of the four SCD concepts, the German TR07 maglev prototype, and the French TGV high-speed train. The author coordinated this effort.

The GMSA team will publish its final report later this year [1]. This paper summarizes the concepts studied, our assessment methods and a selection of our primary findings.

II. OVERVIEW OF SYSTEM CONCEPTS

Table 1 lists physical characteristics of the six high-speed ground transportation (HSGT) concepts studied.

TGV-Atlantique

TGV-A is a steel-wheel-on-rail technology optimized for high-speed operation (83 m/s). It uses fixed-consist, non-tilting trainsets powered by a.c. synchronous rotary traction motors. Roof-mounted pantographs collect power from an overhead catenary. Braking is by a combination of rheostatic brakes and axle-mounted disc brakes. The track consists of continuous-welded rail on concrete/steel ties with elastic fasteners supported on a specially engineered base. Its high-speed switch is a conventional swing-nose turnout.

Transrapid 07

TR07 is an electromagnetic system (EMS) using separate sets of conventional iron-core magnets to generate vehicle lift and guidance. The non-tilting vehicle wraps around a T-shaped guideway. Propulsion is by a long-stator linear synchronous motor (LSM). Attraction to edge-mounted guideway rails provides guidance; attraction to the stator pack beneath the guideway generates lift. Control systems regulate levitation and guidance forces to maintain small (8-10 mm) air gaps. TR07 has demonstrated safe operation at 120 m/s at a test facility in Germany and is capable of 134-m/s cruising speeds. The TR07 guideway uses steel or concrete beams constructed and erected to very tight tolerances. Its switch is a bendable steel guideway beam.

Bechtel SCD

The Bechtel concept is a flux-canceling electrodynamic system (EDS). The vehicle contains six sets of eight superconducting magnets per side and straddles a concrete box-beam guideway. Interaction between these magnets and an aluminum ladder on each sidewall generates lift; similar interaction with null-flux coils provides guidance. Propulsion is by a sidewall-mounted LSM. The single-car vehicle has an inner tilting shell and uses aerodynamic control surfaces to improve ride quality. To avoid magnetic interactions, the upper portion of the guideway contains non-magnetic, fiber-reinforced plastic (FRP) reinforcing rods. The concept's switch is a bendable beam constructed entirely of FRP.

Foster-Miller SCD

The Foster-Miller concept is an EDS similar to Japan's MLU002. Superconducting vehicle magnets generate lift by interacting with null-flux coils located in the sidewalls of a U-shaped guideway; similar interaction with series-coupled propulsion coils provides null-flux guidance. Its innovative locally commutated linear synchronous motor (LCLSM) sequentially energizes individual propulsion coils in sync with the vehicle. The vehicle consists of passenger modules with end bogies containing four magnets per side. The U-shaped guideway has two parallel, post-tensioned concrete beams joined transversely by precast concrete diaphragms. To avoid magnetic interactions, the upper post-tensioning rods are FRP. The high-speed switch uses switched null-flux coils to guide the vehicle through a vertical turn-out; it requires no moving structural members.

Grumman SCD

The Grumman concept is an EMS with similarities to TR07. However, Grumman's vehicle wraps around a Y-shaped guideway and uses just one set of magnets and rails for levitation, guidance and propulsion. The magnets are superconducting coils around horseshoe-shaped iron cores. Normal coils on each iron-core leg modulate levitation and guidance forces to maintain a large (40-mm) air gap. Propulsion is by conventional LSM. Vehicles have tilt capability and may be single- or multi-car consists. Magnets are located along the full vehicle length. An innovative spine girder supports two Y-shaped guideway sections. Switching is with a TR07-style bending guideway beam.

Magneplane SCD

The Magneplane concept is a single-vehicle EDS using a trough-shaped aluminum guideway for sheet levitation and guidance. Centrifugal forces tilt the "Magplanes" into coordinated turns. Front and rear bogies contain superconducting levitation and propulsion magnets. Centerline magnets interact with LSM windings for propulsion and also generate electromagnetic guidance forces. Side magnets react against the aluminum guideway sheets to provide levitation. Magneplane uses aerodynamic control surfaces and LSM-phase control to dampen vehicle motions. The guideway sheets form the tops of two structural aluminum box beams supported directly on piers. The high-speed switch uses switched null-flux coils to guide the vehicle through a turn-out; it requires no moving structural members.

III. Steps in Assessment Process

Our process to assess maglev's technical viability consisted of four main steps. This section briefly describes the rationale and methods for each step.

A. Verification Of Subsystem Performance

Team members developed numerical models to verify the performance of key high-risk or high-cost subsystems: guideway structures, magnetic suspensions and stray fields, motor and power systems, and vehicle/guideway interaction.

These models employed fairly standard engineering approaches. J. Ray (USACE) used large, 3-d beam- and solid-element finite element models together with hand calculations to analyze guideway structural performance. H. Coffey, J. He & Z. Wang (ANL) used dynamic circuit theory and 2-d and 3-d finite element models to calculate suspension characteristics and stray magnetic fields. F. Raposa (consultant to USDOT) developed an equivalent circuit

TABLE 1 General Physical Characteristics of Concepts Studied

Parameter	TGV-Atlantique	TR07	Bechtel	Foster-Miller	Grumman	Magne-plane
Basic Concept	steel wheel-on-rail	EMS, separate lift & guidance	EDS, ladder levitation	EDS, sidewall null-flux	EMS, common lift & guidance	EDS, sheet levitation
Vehicles/Consist	1-10-1	2	1	2	2	1
Seats/Consist	485	156	106	150	100	140
Gross Mass (10^3 kg)	490	106	63	73	61	48
Floor Area/Seat (m^2)	1.2	0.83	0.80	0.74	0.93	0.58
Cruise Speed (m/s)	83	134	134	134	134	134
Total Bank Angle (°)	7	12	30	28	24	35
Primary Suspension	passive	active	passive	passive	active	semi-active
Secondary Suspension	passive	passive	active	passive	none	none
Critical Air Gap (mm)	N/A	8	50	75	40	150
Low-Speed Support	N/A	maglev	air bearings	wheels	maglev	air bearings
Normal Braking (g)	0.045	0.12	0.20	0.16	0.16	0.16
Emergency Braking (g)	0.10	0.30	0.25	0.25	0.20	0.50
Cryogenic System	N/A	none	isochoric	recompress.	recompress.	refrigerator
Onboard Power (kW)	9,000	460	190	220	170	190
Guideway Type	ballasted rail	T-shaped	box beam	sidewall	Y-shaped	trough
Switch Concept	swing-nose rails	bendable steel beam	bendable FRP beam	vertical elect.-mag.	bendable steel beam	horizontal elect.-mag.

model to analyze both air-core and iron-core LSMs; he separately estimated the performance of power-conditioning equipment. D. Tyrell (USDOT) employed a multiple degree-of-freedom dynamic model to model vehicle/guideway interaction, including control system behavior.

These analyses generally yielded good agreement with published data for TGV and TR07 (collected primarily by C. Boon, Canadian Institute of Guided Ground Transport, and R. Armstrong & R. Hasse, USACE). When applied to the SCDs, they produced performance data and identified areas of concern generally comparable to the contractors' results.

B. Verification of System Performance

To compare concept performance at the system level, team members developed two additional models. G. Anagnostopoulos (USDOT) simulated the performance of each concept along an 800-km hypothetical route containing hills, sharp turns, stops and long straight segments. This Severe Segment Test (SST) simulated vehicle performance subject to route, technological and ride-comfort constraints. The results helped us to resolve issues such as the suitability of each concept to use along interstate rights-of-way. The model also yielded realistic trip times and energy consumption for each concept.

Using standardized procedures, R. Suever & J. Potter (USACE) estimated guideway capital costs for each concept. These costs predominate for HSGT systems; thus, they were critical to our assessment of the relative advantages of each concept. Standardization allowed us to reduce variability in cost estimates due to different physical assumptions (e.g. column height) and different definitions of subcomponents. It also allowed independent verification of contractors' cost estimates.

C. Application of SCD System Criteria

The NMI targeted inter-city transportation as maglev's primary mission. Its SCD request-for-proposals (DTFR53-91-R-00021) included a set of system criteria to guide concept development towards that mission. We thus adopted these criteria to assess each concept's mission suitability.

For each criterion, we developed qualitative and quantitative cross-checks on the performance of each concept. These cross-checks included checking data sources, analyses used and the consistency of related characteristics. In many cases, these criteria also directed our modeling efforts. We rated each concept's performance against the SCD criteria.

D. Application of Other Criteria

Characteristics other than the SCD criteria may affect maglev's technical viability in the U.S. We therefore developed additional assessment criteria and applied them to each concept in a way similar to the SCD system criteria. Several of these other criteria (particularly mission flexibility, aerodynamics, and energy efficiency) became focal points of analysis and debate. We again rated each concept against these other criteria and added the results to those for the SCD criteria to complete our mission suitability assessment.

IV. SPECIFIC ASSESSMENT RESULTS

This section presents two assessment results to illustrate how the overall process worked. In addition, Table 2 summarizes several important evaluation parameters for each concept. To separate design preferences from technological attributes, we defined a "standard passenger (SP)" as 0.80 m^2 of floor area (including galleys and lavatories) and used this as a normalizing parameter. This is roughly the average space allotment for the six concepts studied, and it approximates business-class airline seating.

A. Energy Efficiency

Assessment of energy efficiency illustrates how we combined model results with external data. We compared energy intensity (EI, Joules/seat-meter) for all concepts with that of short-haul air travel. We used the number of standard passengers for the number of seats. For the HSGT systems, we computed energy consumption along the SST and at steady cruise (calculated at the electrical supply point). Table 2 presents the resulting EI values. Note that TGV cannot climb the SST grades. However, Table 2 shows that its cruise EI (projected for 134 m/s) is slightly less than the best maglev concepts primarily due to its long consist length.

We selected the Boeing 737-300 for our comparison baseline. This aircraft is among the most fuel efficient in the U.S. short-haul fleet (with an EI about 75% of fleet average). By the time maglev travel becomes significant, fleet-averaged energy intensity will likely approach that of the 737-300 [2].

Airlines file data on fuel consumption with the USDOT for all flights. We used these data for 737-300 aircraft for the period ending June, 1991, and conducted a regression analysis to obtain average fuel consumption per flight as a function of trip length. We then converted jet-fuel volume to its energy equivalent (1.42×10^8 J/gal.).

The 737-300 allocates 0.54 m^2 of cabin floor area per seat for its 140-seat arrangement. This is slightly less than the Magneplane vehicle (the least spacious of the HSGT systems). Conversion to standard passengers gives this airplane 96 seats.

Figure 1 compares the resulting base energy intensities of the maglev concepts with that of a 737-300 as a function of trip length. For energy consumed at the system connection (i.e., airport or electrical supply) average maglev energy intensities range from about 1/5 to 1/4 that of a 737-300 for 200- to 1,000-km trips. Thus, using energy prices forecast for the year 2010 ($0.89/gal., $0.065/kWh [2]) maglev would realize energy-cost savings compared with air travel of roughly 60% to 30% for this trip range.

Supplying energy to a transportation system also consumes energy. We accounted for this by applying

TABLE 2 EVALUATION PARAMETERS FOR EACH CONCEPT (values reflect GMSA analyses unless noted)

Parameter	TGV-A	TR07	Bechtel	Foster-Miller	Grumman	Magne-plane
Standard Passengers/Consist (SP)	700	160	110	140	120	100
Gross Mass/SP (kg)	700	650	600	520	530	470
Max. Low-Speed Accel. (g)	0.05	0.096	0.14	0.15	0.097	0.17
Reserve Accel. @ 134 m/s (g)	N/A	0.01	0.12	0.05	0.05	0.04
3.5% Grade Speed (m/s)	30	120	140	140	140	140
10% Grade Speed (m/s)	N/A	10	140	110	5	90
0-134 m/s Time (s)	N/A	320	75	120	180	99
Minimum Radius[1] (m)	*6,000*	5,800	2,600	2,800	3,300	2,200
Prop. Efficiency[2] @ 134 m/s *[83 m/s]*	*[0.78]*	0.83	0.87	0.91	0.78	0.84
Power Factor[2] @ 134 m/s *[83 m/s]*	*[0.94]*	0.74	0.98	0.97	0.98	0.99
Aero. Drag/SP @ 134 m/s (N)	220	360	430	280	240	170
Total Drag/SP @ 134 m/s (N)	240	390	500	320	270	380
Energy Intensity @ 134 m/s (J/SP-m)	310	450	590	340	360	450
SST Energy Intensity (J/SP-m)	N/A	690	620	440	420	650
SST Trip Time (min.)	N/A	150	120	120	130	130
Guideway Tolerances: Safety (mm)		5	6	25	30	50
: Ride-Comfort (mm)	1-3	2	3	12	5	20
Consist Cost[3]/SP ($k)	41	58	39	93	71	200
Dual Elevated Cost: SCD[3] ($M/km)		9.7	17	9.3	7.8	13
: GMSA ($M/km)	14	12	14	20	9.9	15

[1]TGV 83 m/s, 0.05 g unbalanced lateral accel.; maglev 134 m/s, 0.10 g unbalanced lateral accel.
[2]Propulsion efficiency and power factor calculated at utility connection for steady cruise.
[3]Cost directly from SCD, TGV or TR07 reports; variations compared with GMSA costs are primarily due to differences in unit costs, subcomponent groupings and guideway heights used.

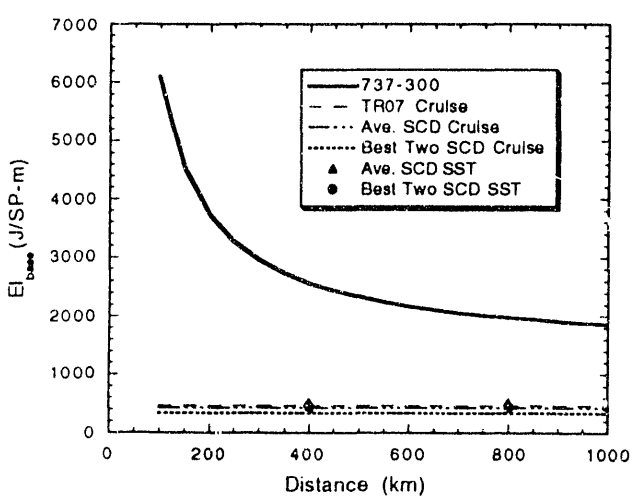

Fig. 1. Base energy intensity at system connection (airport or electrical supply)

thermodynamic efficiency factors to the energy delivered to each system. However, this approach implies that jet fuel saved in air travel is burned to produce electricity for maglev. *It completely ignores the flexibility of electrical power production.* Natural gas, coal, hydro, nuclear, solar, wind, and trash are electrical power sources that simply cannot fuel commercial aircraft. Essentially, maglev will decouple intercity travel from dependence on refined petroleum, and simple efficiency factors do not capture this distinction.

Nevertheless, we applied efficiency factors for energy supplied to aircraft and maglev. For jet fuel, Johnson et al. [3] applied an efficiency of about 90% to account for transportation, refining, and distribution losses. We adopted this value as the only correction applicable for air travel. For electrical power generation and transmission, Johnson et al. used efficiencies of 35% and 95%, respectively. We also used a 95% factor for transmission efficiency. However, modern fossil-fuel plants are much more efficient than 35%.

Modern natural gas- and oil-fired combined-cycle plants (gas turbine with steam-turbine bottoming cycle) commonly achieve base-load efficiencies of 47-48% [4-5]. Modern coal-fired plants are also approaching these efficiencies [6-7]. These power plants have lower capital cost per unit capacity than older technologies, and they produce very low emissions. Indeed, reference [2] forecasts that from 1990 to 2010 combined-cycle generating capability will grow at about 20 times the total growth rate of electrical-generating

capability. Furthermore, utilities will add modern, efficient equipment to meet new demands beyond current forecasts, such as for a major maglev network. We thus selected an electrical-generation efficiency of 47%. Combined with a 95% transmission efficiency, this yields an electrical supply efficiency of 45% for maglev.

Figure 2 shows resulting net energy intensities for air and maglev as functions of trip length. Electrical supply efficiencies bring the energy intensities closer, but the results still overwhelmingly favor maglev. For 200- to 1,000-km trips, maglev energy intensities range from about 1/4 to 1/2 that of a 737-300. And as noted, this comparison ignores the flexibility of power-plant fuel afforded by maglev's electrical propulsion. In terms of energy consumption and flexibility, maglev is clearly superior to short-haul air travel.

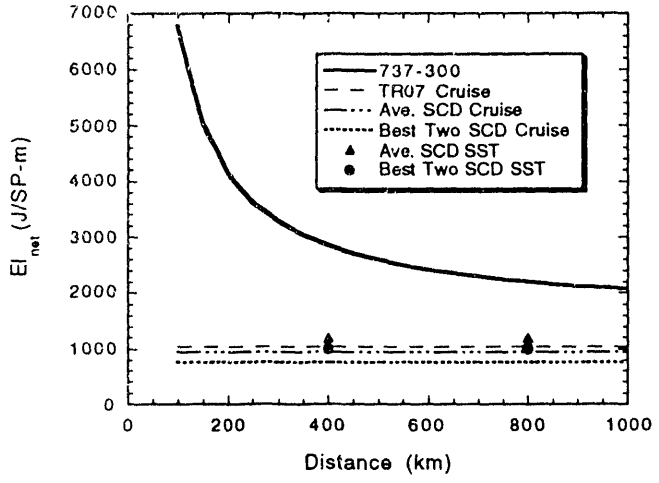

Fig. 2. Net energy intensities including energy supply efficiencies (90% jet fuel, 45% electricity)

B. Speed

The SCD-RFP listed 134 m/s (300 mph) as a design goal for system speed. Table 3 summarizes our findings on this criterion. As for many criteria, assessment of system speed required data from our motor, guideway, magnetic-suspension and vehicle-dynamics models.

V. Overall Technical Assessment

Presented below are several of the team's main findings. Reference [1] provides more thorough descriptions of these and other findings.

A. Long-Term Potential of Maglev compared with HSR

Speed/Trip Time

TGV-A offers 83 m/s commercial service, and has demonstrated a peak speed of 143 m/s. Thus, steel-wheel-on-rail technology is directionally stable at maglev's design-goal

TABLE 3. Assessment Results for System Speed

TGV-A: doesn't meet criterion - 83 m/s service speed, tested at 133 m/s (143 m/s downhill) - 64 m/s along turnouts - speed through curves limited by non-tilting body and 7.15° superelevation of track - cannot achieve 134 m/s presently - motor and brakes not designed for 134 m/s - significant power transfer and maintenance issues must be resolved to achieve 134 m/s commercial service - significant additional investment needed to meet criterion	*TR07: meets criterion* - demonstrated 121 m/s on test track - motor analyses indicate that concept can achieve 134 m/s - structural analyses: guideway is capable of 134-m/s loads - vehicle-dynamics model confirms that vehicle can meet ride-comfort criteria and can safely maintain gap at 134 m/s - demonstrated switch turn-out speed of 56 m/s, through-speed probably full speed - speed through curve limited by non-tilting body and 12° guideway tilt
Bechtel: exceeds criterion - motor analysis: sufficient power and thrust for > 134 m/s - thrust capability enables steady 134 m/s on 10% grade - structural analyses show guideway to be strong enough, but FRP reinforcing is unproven - vehicle dynamics not verified due to insufficient detail on active suspension in final report - primary suspension has required lift and guidance forces	*Foster-Miller: exceeds criterion* - motor analysis: sufficient power and thrust for > 134 m/s - thrust capability enables steady 105 m/s on 10% grade - LCLSM is unproven and must work as intended - structural analyses show guideway to be strong enough, but FRP post-tensioning tendons are unproven and must work - vehicle-dynamics: passive secondary needs tuning - primary suspension has required lift and guidance forces
Grumman: meets criterion - motor analysis: sufficient power and thrust for > 134 m/s - thrust capability of 60-kN baseline motor limits operation on 10% grade to very low speeds (about 5 m/s) - structural analyses show guideway to be strong enough, steel reinforcing adequate - control of primary suspension may not capitalize on large gap, but vehicle should meet ride-comfort and safety requirements at 134 m/s - lift, lateral-guidance and roll forces are adequate	*Magneplane: exceeds criterion* - motor analysis: sufficient power and thrust for > 134 m/s - thrust capability enables steady 90 m/s on 10% grade - need to correct power factor - structural analyses show guideway to be strong enough - vehicle suspension relies on active aerodynamic control, requires significant engineering research for implementation (actuators, control software, etc.) - lift & guidance forces are probably adequate (unable to verify magnetic keel effect, but it seems reasonable)

speed of 134 m/s. For reasons primarily related to life-cycle costs, however, TGV does not currently operate at 134 m/s; it will require further improvements to do so. Such improvements will entail significant capital investment and development effort.

Power transfer by pantograph/catenary may be HSR's most immediate speed-limiting issue. Observers noted nearly continuous arcing during TGV's 143 m/s run. Even with steady contact, pantograph/catenary wear will increase with speed. Both of these problems require R & D effort to solve.

By comparison, high speed potential is essentially an inherent characteristic of maglev. Guidance and propulsion occur without physical contact. Magnetic elements and guideway structures can achieve the guidance forces necessary for very high speed. Furthermore, a long-stator LSM requires no power transfer. In essence, maglev comes "out of the box" ready for 134 m/s service, and higher-speed service is well within the technology.

Other features combine to shorten maglev's trip times relative to HSR. Maglev's maximum acceleration is 2-3 times TGV's. Additionally, all SCD concepts can maintain 140 m/s on a 3.5% grade compared with 30 m/s for TGV. Also, lack of vehicle tilting limits TGV's curving speed. Although tilting HSR systems exist, they require further development to reach even 83 m/s service.

Maglev can offer trip times comparable to air travel for trips shorter than about 800 km. HSR's longer trip times yield lower ridership and revenues relative to maglev. Such lower revenues can offset HSR's capital cost advantage and yield lower profitability.

Safety, Availability & Cost

HSR systems in both Europe and Japan have exemplary safety records. However, the technology requires sophisticated preventative maintenance (inspections and adjustments) to achieve such safety. Maglev possesses characteristics that should permit equivalent safety under more extreme conditions and with less maintenance.

Several maglev concepts employ vehicles that wrap around their guideways; others have guideways that partially wrap around their vehicles. These approaches can provide more than 1-g "derailment" containment in the event of extreme environmental disturbances or component failures.

Large-gap maglev systems are much more tolerant of ground displacements caused by earthquakes than is HSR. These displacements can be larger for maglev before triggering ride-comfort-, safety- or wear-related maintenance. Greater tolerance also provides an added margin for bringing high-speed vehicles safely to rest during earthquakes.

Maglev's non-contact propulsion and braking render it less susceptible to snow, ice and rain than HSR. Also, maglev concepts with wrap-around guideways offer some protection from cross-winds. These features offer maglev an availability advantage in adverse weather for safety comparable to HSR.

Maglev should achieve HSR's outstanding safety record. Its greater tolerance to earthquakes and adverse weather may be decisive availability and cost advantages in the demanding U.S. environment.

B. Potential of U.S. Maglev compared with TR07

Performance Efficiency

Comparisons of performance and cost of TR07 and SCDs revealed two important findings: U.S. maglev can offer slightly better performance than TR07 at much lower cost (especially for at-grade sections); U.S. maglev can offer much better performance than TR07 at similar cost.

Compared with TR07, the Grumman system offers a 10% lower SST trip time for about 20% lower guideway cost (40% lower at-grade). Similarly, the Bechtel concept offers a 20% SST trip-time savings for about 10% higher guideway cost (or 10% lower at-grade). While these are specific SCD concepts, they illustrate the performance/cost advantages likely to result from a U.S. maglev development effort.

Suitability to Existing Rights-of-Way

The SCD concepts are much better suited than TR07 to deployment along existing rights-of-way. Generally, they require about half the curve radius of TR07 at 134 m/s, climb 5-times steeper grades at full speed, and reach 134 m/s in about half the time. These characteristics mean that a U.S. maglev system will achieve much shorter trip times along existing, lower-speed rights-of-way.

In principle, Transrapid could upgrade TR07 with a tilting vehicle body and a larger LSM. However, the former would involve a major redesign of the vehicle, an increase in roll stiffness of the magnetic suspension, and strengthened curved guideway beams. Upgrading the LSM may prove more difficult because stator slot width limits the diameter (and hence the current capacity) of the stator windings. While these improvements are possible, they would not occur without significant R & D time and costs.

C. Key Innovations: Benefits and Risks

The SCD concepts contain numerous innovations in maglev technology. Here we summarize some innovations, their potential benefits and risks.

Active Vehicle Suspensions

Three of the four SCDs utilize active vehicle suspensions. Coupled with a large gap, an active suspension can maintain a smooth ride over very flexible and rough guideways. This allows use of, respectively, less structural material and less stringent construction tolerances, reducing guideway costs.

Maglev's large magnetic forces make active control of the primary suspension an attractive option; Grumman selected this approach. Active control of aerodynamic surfaces is also an option, although unsteady air flow may complicate its implementation.

The main risks with active suspensions are their added weight, cost and reliability penalties compared with passive suspensions. A reasonable R & D effort should minimize these risks. Small-scale testing of active magnetic suspensions should quickly demonstrate their feasibility. Similarly, wind-tunnel testing and computational fluid modeling should establish the feasibility of active aerodynamic control.

LCLSM

Foster-Miller's LCLSM could become a significant innovation in vehicle propulsion. Its advantages include high overall efficiency (91% as seen at electrical supply), significant degraded mode capability, and use for power transfer.

Its principal risk is that solid-state inverters are at present too expensive for the LCLSM to be economical. Foster-Miller has argued that the large number of inverters needed (about 2,400/km) will enable mass production to reduce their cost by a factor of 10. This is difficult to prove until mass production actually occurs.

Vehicle control with a LCLSM is also unproven. Issues include the LCLSM's ability to control acceleration and speed, and to maintain adequate lateral stability. However, reduced-scale testing can address these issues in a reasonably short period.

Large-Gap EMS

A major concern about TR07's suitability for the U.S. environment is its small, 8-mm suspension gap. To achieve adequate ride comfort and safety margin, TR07's guideway must be very stiff and well aligned. These requirements increase the guideway's cost and its susceptibility to foundation settlement, earthquake movement, thermal expansion, and ice accretion.

Grumman utilizes iron-core, superconducting magnets to increase the suspension gap of its EMS concept to 40 mm. It actively controls this gap with normal electromagnets. The vehicle requires no secondary suspension, and it maintains adequate ride comfort and safety over irregularities many times larger than TR07's limits. This suspension also simplifies hardware requirements by utilizing the same magnets and reaction rails to provide all lift and guidance forces. Overall, these improvements offer to simplify guideway design and construction, lower guideway costs, and reduce susceptibility to environmental disturbances.

The main risks with this approach are with its implementation. The control coils must deliver adequate forces to ensure stability and safety under all conditions. Control currents must not induce excess losses in the superconducting magnets. Furthermore, the control algorithm must take advantage of the hardware's capabilities. These issues may initially be addressed through laboratory testing of a complete magnet/control system; eventually verification will require complete-vehicle tests at either full or reduced scale.

VI. CONCLUSIONS

The GMSA's main goal was to assess the technical viability of maglev in the U.S. We examined in detail the NMI's four contracted SCD concepts and compared their performance potential with that of TGV and TR07.

All maglev concepts studied are potentially technically feasible. Verification of the feasibility and practicality of some features clearly requires further work.

All five maglev concepts studied offer much greater performance potential than TGV. Maglev offers higher speed, better acceleration and curving capabilities, and potentially lower maintenance and higher availability for comparable safety. The four U.S. concepts also offer a performance advantage over TR07, and they could do so for similar or lower cost. Note that further development will likely improve the performance of both TGV and TR07. However, a comparison of the costs of such improvements with the costs to develop U.S. maglev was beyond the scope of our study.

ACKNOWLEDGMENTS

The author gratefully acknowledges the significant contributions to the GMSA effort of the other primary team members: J. Ballard, K. Shaver (USACE); M. Coltman, J, Milner (USDOT). I also thank D. Bushnell (NASA) for his timely review of the SCD aerodynamic analyses, J. Harding (USDOT) for his energy consumption data, and C. Boon, H. Coffey, J. Lacombe and J. Potter for their helpful reviews of this paper. The GMSA final report lists many more contributors than is possible here; their help was sincerely appreciated throughout our work.

REFERENCES

[1] *Technical Assessment of Maglev System Concepts - final report of the Government Maglev System Assessment team* (J. H. Lever, ed.) in press.

[2] *Annual Energy Outlook 1993 with Projections to 2010,* 1993. Report no. DOE/EIA-0383(93).

[3] Johnson, L.R. D.M. Rote, J.R. Hull, H.T. Coffey, J.G. Daley and R.F. Giese, 1989. Maglev vehicles and superconductor technology: integration of high-speed ground transportation into the air travel system. ANL/CNSV-67, Argonne National Laboratory.

[4] Farmer, R., 1992. Combined cycle power: delivering new levels of net plant efficiency. Gas Turbine World, Sept.-Oct., pp. 20-34.

[5] *Gas Turbine World - The 1992-93 Handbook*, 1992. Pequot Publishing, Fairfield, Connecticut.

[6] Bajura, R.A. and Webb, H.A., 1991. The marriage of gas turbines and coal. Mechanical Engineering, American Society of Mechanical Engineers, New York, pp. 58-63. Also, H.A. Webb, personal communications.

[7] *Assumptions for the Annual Energy Outlook 1993,* 1993, Report no. DOE/EIA-0527(93).

MAGLEV PERFORMANCE SIMULATION

George Anagnostopoulos
Volpe National Transportation Systems Center

J. Edward Anderson
J.E. Anderson Associates

Frank L. Raposa
F.L. Raposa Services

Abstract - This paper summarizes the results of the development of a maglev simulation program for the performance evaluation of ground guided vehicles operating over a complex route such as a freeway. The program as developed has been tailored to evaluate maglev vehicles on a route termed the Severe Segment Test route developed by the National Maglev Initiative program. The simulation is capable of being extended to any arbitrary route as well as to the evaluation of any guided ground transport system.

I. Introduction

The development of a maglev system requires rational selection of specific system characteristics based on the design, performance and operation of different alternatives. These alternatives include the extent to which a system can bank, the extent to which the maglev guideway can be allowed to depart from the desired right-of-way and the maximum thrust and speed capability of the propulsion system. The Maglev Performance Simulator (MPS) was developed to enable the evaluation of different system concepts studied for the National Maglev Initiative program. It is a discrete-event simulation program which describes the kinematics of vehicles subject to guideway and ride quality constraints, and determines the power and energy required to propel vehicles against physical resistances. The simulation performs 3-dimensional horizontal and vertical turns while the vehicle is proceeding along a longitudinal path. Linear synchronous motor models are an integral part of the simulation.

Manuscript received March 15, 1993. This work was supported in part by the U.S. Department of Transportation under contracts DTRS-92-P-81-250 and DTRS-57-88-C-00041.

II. Maglev Performance Simulator Program

A. Description

MPS is a suite of 8 programs which permits analysis of the performance of either individual or fleets of maglev vehicles with curved guideways and on-line or off-line stations in an arbitrary configured network. Guideway geometry, ride comfort criteria, and technology specific characteristics such as propulsion, mechanical resistance and tilt capabilities are input data. MPS outputs trip time, average speed and energy based on three-dimensional curved maglev flight. MPS converts predefined route data into a completely defined path and determines the kinematics of the vehicle as it is constrained by ride quality criteria, banking capability propulsion limitations. Its objective is to minimize trip time.

The MPS program models are shown in Fig. 1. Route data which is generally described by horizontal and vertical profiles is inputted to MPS through the HORZDAT and VERTDAT program modules. Each profile describes the distance between points of intersection along tangents, the change of angle or azimuth at each point of intersection and the radius of curvature at each point of intersection. The HORZCHNG and VERTCHNG modules allow modification of input conditions.

For given comfort limits of acceleration and jerk, these modules calculate both the length of the curves along its tangents and along the arc. Also calculated are the speed limits for each curve considering the distance available to accelerate or decelerate. Inputs to HORZDAT are line speed limits (V_L), superelevation angle plus tilt angle plus comfort angle (A_m/g), comfort horizontal jerk (J_m), distance from the last horizontal path change between intersections of tangents to the

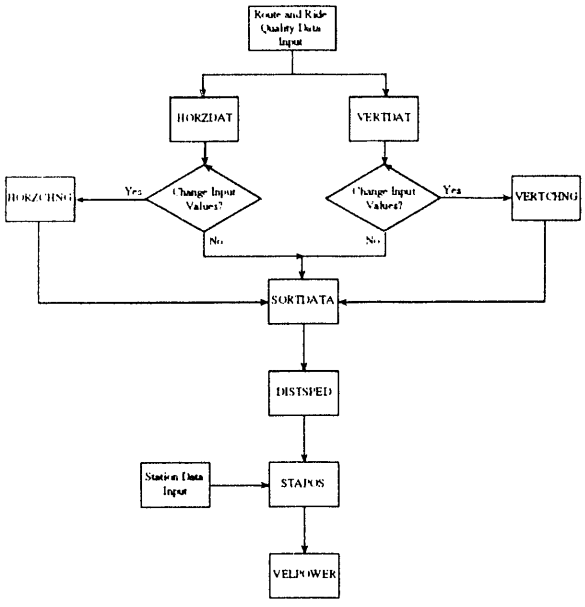

Fig. 1. MPS Program Flow Diagram

curve (DS), minimum radius of curvature (R), and change in azimuthal direction (dA). MPS determines the distance (S) traveled along the path, the maximum allowable speed of the vehicle in the curve (V), the azimuth relative to the origin, the straight line length from the beginning of the spiral to the midpoint of the curve (X_s) measured along the tangent, the arc length of the guideway in the horizontal curve (ArcL), and the length of constant curvature section (LCC).

Inputs to VERTDAT are line speed limits (V_L), comfort upward vertical acceleration (A_{mu}), comfort downward vertical acceleration (A_{md}), comfort horizontal jerk (J_m), station distance relative to the origin (Sta), elevation at Sta, and the length of vertical curve at each station with no spiral section. VERTDAT calculates the grade, change in grade, radius of curvature, the speed through the vertical curve based on comfort acceleration, the X_s distance to the midpoint of the vertical curve, the arc length of the guideway in the vertical curve (ArcL), and the length of constant curvature section (LCC).

The module HORZCHNG permits a change of acceleration and jerk parameters and corresponding V, X_s, and ArcL. VERTCHNG permits similar changes to vertical parameters. The SORTDATA module combines the horizontal and vertical data from HORZDAT or HORZCHNG with that of VERTDAT or VERTCHNG.

DISTSPED uses the results of the SORTDATA module to determine the station distance along the tangent to the curve, the length of path along the curved guideway, the minimum speed through each curve along the guideway (or speed gate), the grade at each station, the length of guideway in the curve, and the transverse acceleration. STAPOS uses the output from the DISTSPED module to insert zero speed points at each station as well as station dwell time. The output from STAPOS is then a complete set of speed gates.

The VELPOWER program module determines the performance of the system using the output of the STAPOS module and two parameter files for each system being analyzed. These parameter files define the physical characteristics and the LSM characteristics of the system being analyzed. In VELPOWER, upon passing a minimum speed gate, the vehicle is accelerated at either the maximum comfort limit or the maximum motor thrust limit, whichever is the most restrictive. At each computation step the braking profile is calculated to determine the last possible point at which to brake in order to reach the next speed gate. In this way the maximum possible speed is achieved and the next speed is reached in minimum time.

VELPOWER thus computes the minimum time-power and comfort-limited speed profiles. It also determines the power and energy required to perform these speed profiles. VELPOWER outputs time, length of path along the guideway, speed, acceleration and jerk, thrust, power and energy. Electrical characteristics such as voltage, current, power factor and overall efficiency are also outputs.

III. Theory of the Maglev Performance Simulator

The guideway of a maglev system is a curved path in space defined by three types of data: geometric data, system data, and ride-comfort data. The geometric data is a set of points in space at the intersection points (apexes) of tangents to adjacent segments of the curve, and the largest acceptable radius of curvature at each point. Apexes of the path are first set in a horizontal plane and then, along the horizontal projection of the path, the elevations of apexes that define the changes in direction in the vertical plane are superimposed to give a composite of horizontal and vertical turns. The pertinent system data are the permissible superelevation angle of the guideway, and the possibility and degree of tilt of the vehicles with respect to the guideway in turns. The ride-comfort data are the tolerable values of acceleration and jerk in the longitudinal, lateral, and normal directions, and the tolerable value of roll rate.

A. The Maximum Tilt Angle

The relationship between the sum of the superelevation angle and tilt angle ϕ_t, the lateral comfort acceleration a_l, and the normal comfort acceleration a_n are shown in Fig. 2, from which the comfort angle is defined by

$$\phi_c = \tan^{-1}\frac{a_l}{a_n}. \tag{1}$$

The radius of curvature in a horizontal turn R is V^2/a_H, in which a_H is the horizontal component of acceleration, given from Fig. 2 by

$$a_H = g\tan(\phi_c + \phi_t). \tag{2}$$

The maximum allowable value of a_H is restricted by the comfort values of acceleration according to the equation

$$a_H^2 = a_l^2 + a_n^2 - g^2. \tag{3}$$

Substituting equations (1) and (3) into equation (2), the maximum allowable tilt angle is

$$\phi_{t_{max}} = \tan^{-1}\sqrt{\left(\frac{a_l}{g}\right)^2 + \left(\frac{a_n}{g}\right)^2 - 1} - \tan^{-1}\frac{a_l}{a_n}. \tag{4}$$

B. Theory of Spiral Curves

Through a series of programs, MPS accepts first the geometric data and then the superelevation angle, tilt angle and ride-comfort data. Using the theory of plane spiral curves[1], the necessary properties of the curve are derived as follows: The normal component of acceleration is given by the well-known formula

$$a_n = V\dot{\theta} = V^2\frac{d\theta}{ds} = \frac{V^2}{R} \tag{5}$$

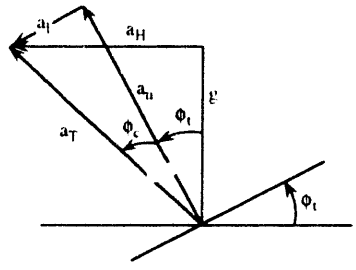

Fig. 2. Acceleration Vectors

in which s is the arc length and $V = ds/dt$. The less-well-known formula for the normal component of jerk is

$$J_n = V\ddot{\theta} + 2\dot{V}\dot{\theta} = V^2\frac{d}{ds}V\frac{d\theta}{ds} + 2V^2\frac{dV}{ds}\frac{d\theta}{ds} = \frac{d}{ds}V^3\frac{d\theta}{ds} \tag{6}$$

The curve length is minimized if J_n is taken as constant at the maximum comfort value. Then, starting a curve at zero curvature, the curvature at any point along the curve if found by integrating equation (6). Thus

$$\frac{d\theta}{ds} = \frac{J_n s}{V^3} = \frac{1}{R} = \frac{a_n}{V^2} \tag{7}$$

which shows that, if R is given, the speed must be restricted according to

$$V \le \sqrt{a_n R} \tag{8}$$

and the maximum length of a spiral arc is

$$s_{max} = V\frac{a_n}{J_n}. \tag{9}$$

But, maximum roll rate is given by

$$\dot{\phi}_{max} = V\frac{d\phi_{max}}{ds} \tag{10}$$

in which ϕ_{max} is the sum of the superelevation angle and the tilt angle. If the guideway rolls up at a constant rate of twist

$$\phi_{max} = \frac{d\phi_{max}}{ds}s_{max} = \frac{\dot{\phi}_{max}}{V}s_{max}$$

$$or \quad s_{max} = V\frac{\phi_{max}}{\dot{\phi}_{max}}. \tag{11}$$

If the maximum comfort values are used in all cases, equations (9) and (11) don't in general give the same maximum arc length. The longer value must be chosen and there is no disadvantage to adjusting the other by reducing either the normal jerk or the roll rate, since the length of the twisted spiral is the same in both cases.

If we take the velocity to be constant, equation (7) can be integrated to give the change in the angle of the curve throughout the spiral. Thus

$$\theta = \frac{J_n s^2}{2V^3}. \qquad (12)$$

The objective of MPS is to find the maximum average speed between any two points. The maximum speed through a curve is attained if the vehicle need only slow to a minimum at one point: the center of the curve. This condition is obtained if the curve increases curvature continuously to its center and then decreases curvature to zero, i.e., there is no section of constant maximum curvature in the curve, only one point of maximum curvature. In this case, if, in equation (12), s/V is the larger of the values given by equations (9) and (11), angle θ is half the given total change in direction, Θ. Then, from equation (12),

$$V \le \frac{J_n}{\Theta} Max\left\{\left(\frac{a_n}{J_n}\right)^2, \left(\frac{\phi_{max}}{\dot{\phi}_{max}}\right)^2\right\} \qquad (13)$$

The selected V must be the smaller of the values given by equation (8) and (13). If the guideway curve is described with respect to orthoginal coordinates x and y, where x is in the direction of the velocity vector at the beginning of the spiral transition curve, the differential equations of the spiral-shaped guideway are

$$\frac{dy}{ds} = \sin\theta, \quad \frac{dx}{ds} = \cos\theta \qquad (14)$$

To integrate for the coordinates of the transition, it is sufficient to expand the trigonometric functions in equations (14) to the second term. Then, substituting equation (12) and integrating, the results can be expressed in the form

$$y = \frac{J_n s^3}{6V^3}\left(1 - \frac{\theta^2}{14}\right)$$
$$x = s\left(1 - \frac{\theta^2}{6}\right). \qquad (15)$$

The spiral transition curve is shown in Fig. 3. The required properties of the curve are: 1) the distance X_a along the tangent to the curve from its beginning to the apex; 2) the offset distance d_o from the center of the curve to the apex; and 3) the curve length.

If x_c, y_c, and θ_c relate to the centerpoint of the curve, the above quantities are given by the equations

$$X_a = x_c + y_c \tan\theta_c$$
$$d_o = y_c \sec\theta_c \qquad (16)$$
$$Curve\ Length = 2s_{max}.$$

C. The Velocity Profile

Based on the foregoing analysis of the curves, a set of speed gates is determined at the positions of the apexes along the path of the vehicle. At these apexes, the speed of the maglev vehicle must reduce to the value specified, and, in between, the vehicle tries to accelerate to as high a speed as possible. As shown in Fig. 4, the velocity profile has three parts: In part (1), the speed that can be attained depends on the comfort levels of longitudinal acceleration and jerk. In part (2), the speed is limited by power, which is usually expressed as a limit on current and MVA. In part (3), the vehicle is braked at a specified rate to reach the speed specified at the next speed gate. At each computation point, as the computation of the acceleration profile progresses, the speed that would be reached at the next speed gate if braking is initiated at that point is calculated. When the correct gate speed is calculated, the vehicle switches to the braking mode.

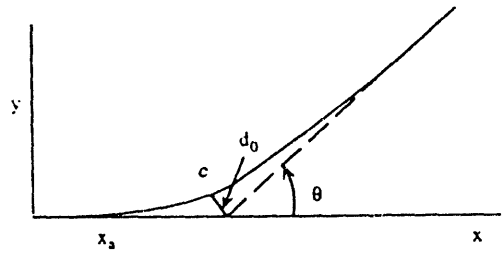

Fig. 3. The Spiral Transition

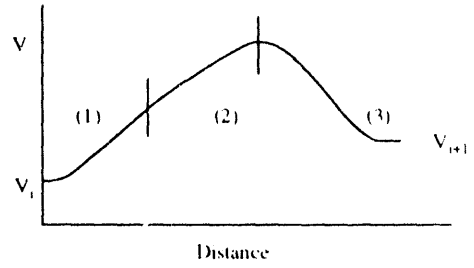

Fig. 4. The Velocity Profile

IV. Linear Synchronous Motors

A. Summary of Operation

The linear synchronous motor (LSM) consists of two electromagnetic members, the armature and the field. In long stator LSM systems the armature, commonly called the stator, is located on the guideway and the field is on the vehicle.

Electromagnetic suspension systems (EMS) typically make use of iron core structures for both the field and the stator. The flux density saturation of the iron limits the magnitude of the flux density in the air gap. EMS are small air gap systems where typical air gaps are of the order of 0.01 to 0.04 m. Electrodynamic suspension systems (EDS) use air core structures for both the field and the stator. Superconducting field windings on the vehicle are required to achieve the large flux densities required for operating EDS systems. These air gaps typically operate at 0.10 to 0.20 m spacings between the stator and field.

LSMs are controlled to produce orthogonal forces. Many maglev systems make use of LSMs to achieve either the lift and propulsion forces, or the guidance and propulsion forces. The LSM used in the Transrapid TR07 for example, provides both propulsive as well as levitation forces.[2] The LSM is similar to its rotary counterpart which for a machine of fixed dimensions and materials can only produce a finite total force. This total force is then apportioned to its orthogonal components by appropriate control of the LSM field. For example, the force produced by the LSM can be oriented to be an all longitudinal force or it can be oriented to be all vertical force or any combination of the two.

B. Equivalent Circuit Model

The approach taken here is an extension of the graphical technique developed by Fitzgerald for the analysis of salient pole machines.[3] An equivalent circuit model for an LSM is shown in Fig. 5. It is a generalized circuit for synchronous machines and is shown on a per phase basis. Its use, in conjunction with the assumption of sinusoidal behavior of the LSM, is quite accurate for estimating motor performance. The left side of the circuit shows the motor's electrical parameters and the right side its mechanical parameters. The parameters are stator voltage and current V_1 and I_1, counter EMF (CEMF) E_1, and stator resistance and reactance R_1 and jX_q. The mechanical parameters are the thrust developed at the

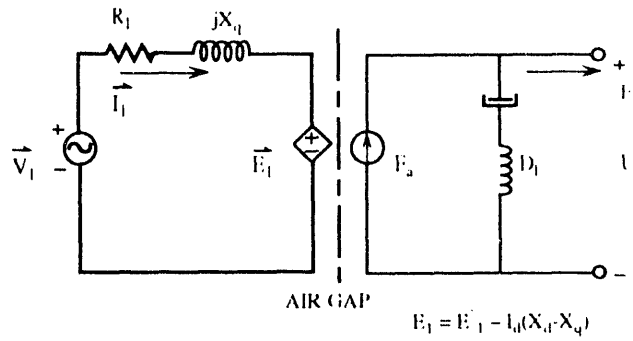

Fig. 5. Equivalent Circuit Model for the Linear Synchronous Motor

air gap F_a, the mechanical losses D_1 and the output thrust F_x.

The resistance R_1 and reactance jX_q, can be determined from the LSM layout geometry and materials used. The resistance R_1 consists of the ohmic resistance and induced eddy current losses. The reactance term jX_q represents inductive elements of the LSM. Its component parts are different for iron core LSMs than they are for air core LSMs. In iron core LSMs, the jX term accounts for the leakage reactance of the stator winding and the magnetizing reactance of the stator core. In air core LSMs, the jX term accounts for the self inductance of the stator as well as the mutual inductance of the stator and field windings.

Fig. 6 is the phasor description for Fig. 5. The angles γ_o and δ are referred to as the internal power factor and power angle, respectively. The current I_1 has been resolved into its components, I_d and I_q. The CEMF magnitude is given by $E_1 = \dot{E}_1 - I_d \cdot (X_d - X_q)$.

C. LSM Modeling Equations

At the air gap of the machine, the electrical power is equal to the mechanical power. From Fig. 5:

$$N_p \cdot E_1 \cdot I_1 \cdot \cos(\gamma_o) = F_a \cdot u_s \qquad (17)$$

where γ_o is the angle between E_1 and I_1, u_s is the vehicle velocity and the other terms are as defined above. The term N_p is the number of phases of the particular LSM being analyzed. For example, $N_p = 3$ represents a 3-phase LSM. Vehicle magnetic drag and other loss components are generally combined with vehicle aerodynamic drag and given as a vehicle total resistance. We will adopt the same convention and set $F_a = F_x$. The force F_x includes all mechanical load and loss components.

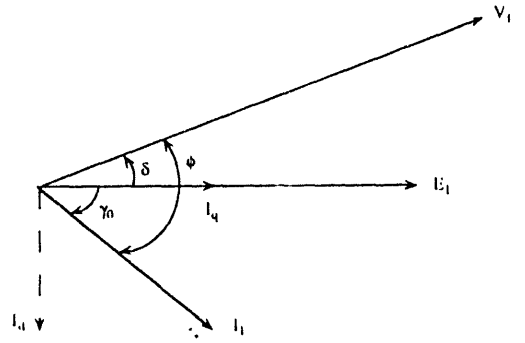

Fig. 6. Phasor Diagram for the Curcuit of Fig. 5

Counter EMF and Flux Density. The CEMF of the LSM is related to the air gap flux density. From the theory of synchronous machines:

$$E_1=\sqrt{2}\cdot l\cdot p\cdot N\cdot B_1 u_s \qquad (18)$$

where B_1 is the air gap flux density, N is the number of parallel conductors per pole/per slot, *l* the transverse width of the stator winding, p the number of pole pairs of the LSM field. The CEMF is $E_1 = (w\cdot M\cdot I_f)/\sqrt{2}$, where M is the mutual inductance with the field winding present, I_f the field current in ampere-turns and $\omega=2\pi f_1$ where f_1 is the operating frequency. In evaluating the steady state performance of LSMs, it is usual to assume that air gap flux density is kept constant, which results in the ratio $E_1/f_1=$constant. The frequency in terms of vehicle velocity and pole pitch τ_p is $f_1=u_s/(2\cdot\tau_p)$.

Longitudinal Thrust. From equations (17) and (18), the thrust F_x is:

$$F_x=N_p\sqrt{2}\cdot l\cdot p\cdot N\cdot B_1 I_1\cos(\gamma o) \qquad (19)$$

which shows that the thrust of the LSM is proportional to its stator current I_1, for constant air gap flux density B_1 and for a machine of given construction.

LSM Power Input and Efficiency. The power input to the LSM, its power factor and efficiency for a 3-phase system ($N_p=3$) are given by:

$$P=3\cdot V_1\cdot I_1\cdot\cos(\phi) \qquad (20)$$
$$Q=3\cdot V_1\cdot I_1\cdot\sin(\phi) \qquad (21)$$
$$S=3\cdot V_1\cdot I_1 \qquad (22)$$
$$PF=\cos(\phi) \qquad (23)$$
$$\eta=(F_x\cdot u_s)/(3\cdot V_1\cdot I_1\cdot\cos(\phi)) \qquad (24)$$

where P, Q and S are the real, reactive and complex components of power. The angle ϕ is the angle between V_1 and I_1. Q will be negative for leading power factor and it will be positive for lagging power conditions.

D. Voltage and Current Equations for LSMs

The Iron Core LSM. Iron core LSMs are built with projecting poles and concentrated windings. The reluctance along the polar (direct) axis is appreciably less than the reluctance along the interpolar (quadrature) axis. The magnetizing reactance has two components, the direct-axis X_{dm}, and quadrature-axis X_{qm}. These reactances, when combined with the leakage reactance X_1, form the LSM reactance. The direct-axis reactance is $X_d=X_{dm}+X_1$, and the quadrature-axis reactance is $X_q=X_{qm}+X_1$.

Phasor diagrams for the iron core LSM are shown in Fig. 7 the case for lagging power factor, and Fig. 8 the case for leading power factor. The LSM stator current is resolved into its components. The in-phase component is I_q, where $I_q = I_1\cos(\gamma_o)$, and the out-of-phase component is I_d where $I_d=I_1\cdot\sin(\gamma_o)$. The voltage components for the resistor R_1 are I_dR_1 and I_qR_1, and voltage components for the direct and quadrature axis reactances, jI_dX_d and jI_qX_q. The sign of the angle γo must be taken into account. Positive angles are taken in the counterclockwise direction and negative angles in the clockwise direction. As previously discussed, the sign of I_d is negative for lagging power factor and is positive for leading power factor.

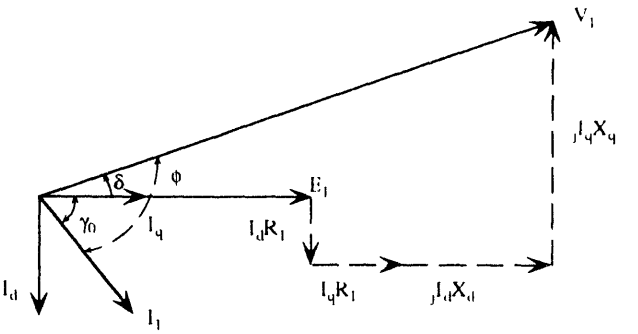

Fig. 7. Iron Core LSM Phasor Diagram for Lagging Power Factor

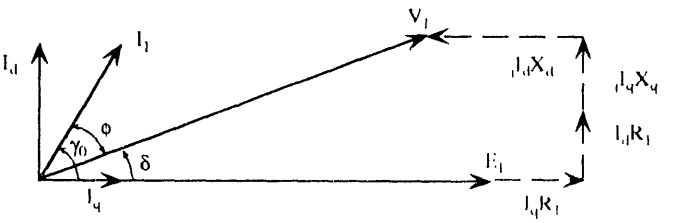

Fig. 8 Iron Core Phasor Diagram for Leading Power Factor

Summing all of the in-phase components results in:

$$V_h = E_1 + (I_q \cdot R_1) - (I_d \cdot X_d) \quad (25)$$

$$V_v = (I_q \cdot X_q) + (I_d \cdot R_1) \quad (26)$$

$$V_1 = \sqrt{(V_v^2 + V_h^2)} \quad (27)$$

$$\delta = \tan^{-1}(V_v / V_h) \quad (28)$$

The iron core LSM, like its rotary counterpart, can exhibit leading or lagging power factor independent of load power factor. A normally excited field results in power factor being determined by the load which is lagging for the LSM. An overexcited field exhibits capacitive characteristics and makes the LSM have a leading power factor.

The Air Core LSM. For the air core LSM, the above equations have the magnetizing reactances $X_{dm}=0$ and $X_{qm}=0$. From Fig. 5 this results in $X_q=X_1$, and the phasor components are:

$$V_h = E_1 + R_1 \cdot I_1 \cdot \cos(\gamma_o) - X_1 \cdot I_1 \cdot \sin(\gamma_o) \quad (29)$$

$$V_v = R_1 \cdot I_1 \cdot \cos(\gamma_o) + X_1 \cdot I_1 \cdot \sin(\gamma_o) \quad (30)$$

where V_h is the sum of all components in phase with E_1, and V_v is the sum of all components in quadrature with E_1. Solving for the magnitude and phase for V_1 results in equations identical in form to equations (25) and (26) above.

E. Electrical Power Distribution to the LSM

The model description to this point is valid for the condition where the LSM field windings cover the entire LSM stator length. In most cases, stators of block length LSMs are significantly longer than a vehicle length, typical block lengths being 300 to 1000 m with vehicle lengths of 12 to 40 m. This requires that the portion of the LSM stator not covered by vehicle field windings be considered as part of the distribution system. Figs. 9 and 10 show the output from the frequency converter station to the guideway, where the LSM stator has a block length L. The feeder cable from the output of the converter to the LSM block is represented by resistance R_f and reactance jX_f. The magnetic length of the vehicle l_v is the total length of the LSM field windings on the vehicle. The active portion of the LSM stator is that section directly under field windings, and this section moves down the LSM block as the vehicle moves along the guideway.

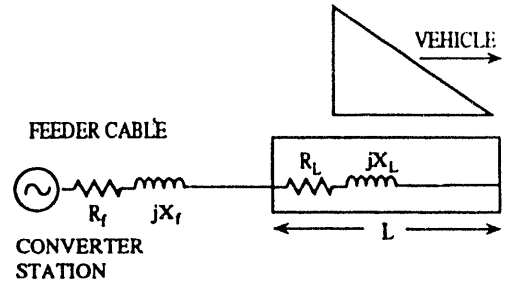

Fig. 9. Schematic of Power Supply to an LSM Block

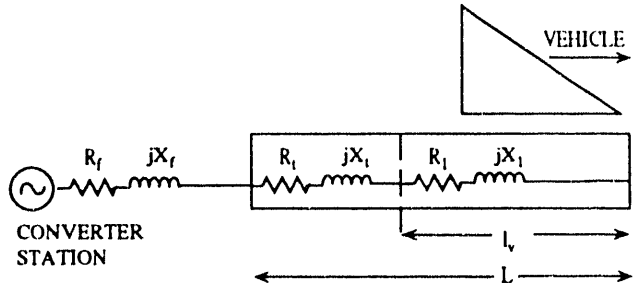

Fig. 10. Electrical Model for Fig. 9

Fig. 10 shows the circuit element details for modeling the active and inactive portions of the LSM block length, as well as the feeder cables from the converter station. From Fig. 10, the inactive portion of the LSM block is modeled as an extension to the feeder cable distribution with values $R_t = R_L(L-l_v)/L$ and $X_t = X_L(L-l_v)/L$. We will define R_L and jX_L as the resistance and reactance of entire LSM block length where jX_L is the reactance of the block length without the LSM field winding, that is with no vehicle present. These values, when combined with the feeder resistance and reactance R_f and X_f, form the equivalent series resistance $R_s = R_f + R_t$, and reactance $X_s = (X_f + X_t)$. The resistance for the active portion of the LSM is the R_1 element of Fig. 5 for both iron core and air core LSMs is given by:

$$R_1 = R_L \cdot (l_v / L) \quad (31)$$

For the iron core LSM, the X_d and X_q terms are given by:

$$X_d = X_{dm} + X_L \cdot (l_v / L) \quad (32)$$

$$X_q = X_{qm} + X_L \cdot (l_v / L) \quad (33)$$

For the air core LSM, the reactance for the active portion of the LSM is given by $X_1 = X_L \cdot (l_v/L) + X_m$.

X_m is the reactance resulting from the mutual coupling of the air core LSM with its field windings.

V. Results

MPS may be used to analyze many different system characteristics. For example, the difference between speed and distance for two different vehicle technologies (V1 and V2) is shown in Fig. 11. V1 has a more powerful LSM than V2, and also has 18 degrees greater tilt capability. Both technologies are using the same ride quality constraints. In this case longitudinal acceleration and braking are equal to 0.16 g's. Fig. 11 shows that the vehicles start out from a station and progress through five curves which necessitate lowering the speed of both vehicles. Between the initial station and the first curve at 9000 m, the added power of the LSM allows V1 to achieve a speed of 120 m/s before the vehicle must brake to reach its minimum or gate speed through the curve. V2 only achieves a speed of 80 m/s.

Because of the tilt capability V1 is able to negotiate the curve at a higher speed. Therefore, the initial speed out of the turn is higher and the vehicle requires less time and distance to accelerate to line speed. This is evident at the third turn where V1 achieves line speed (134 m/s) and V2 reaches 100 m/s, but takes more distance to achieve this speed. The average speed of V1 is greater than V2 and therefore, its trip time is less. Although two parameters were varied simultaneously in this case, MPS can be used to vary one parameter at a time to determine the effects of different system characteristics.

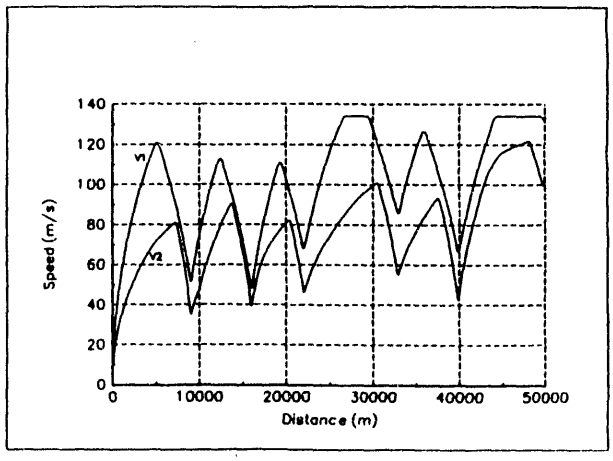

Fig. 11. Maglev Performance Vehicle

VI. Conclusions

MPS has successfully achieved the integration of guideway curving design, vehicle kinematics and linear motor performance analysis into a single program. The program has demonstrated that a vehicle can be controlled and it performance constrained by either maximum comfort limits or the maximum propulsion motor limits whichever are most restrictive. MPS has shown that geometric, system, and ride-comfort data can be brought together to describe the layout of guideway curves including transition spirals.

The linear synchronous motor model used in MPS has been shown to be applicable to both iron core and air core machines. With suitable selection of parameters, the LSM model accurately describes the performance of either type of machine. The model structure also enables the capabiltiy of operating the LSMs over a wide range of power factor including leading as well as lagging power factor operation.

The results produced by MPS compare quite favorably to the limited maglev performance results available in the literature. MPS results also compare quite closely with the results produced by the recently completed four SCD studies conducted for the National Maglev Initiative program.

References

1. Transit Systems Theory, J. E. Anderson, Lexington Books, D.C. Heath, Lexington, Mass, 1978.

2. Transrapid Maglev System, Heinrich and Kretzschmar, Hestra-Verlag, Darmstadt, 1989, p. 50-59.

3. Electric Machinery, Third Edition, Fitzgerald, Kingsley and Kusko, Mc-Graw Hill, New York, 1971, p. 312-319.

Noise from High Speed Maglev Trains

Carl E. Hanson
Harris Miller Miller & Hanson Inc.
429 Marrett Road
Lexington, Massachusetts 02173

Abstract - **Noise has been identified as a potential source of concern associated with the introduction of high speed maglev trains in the existing transportation system in the United States. The first operational maglev systems have been shown to generate high noise levels at high speeds, with noise levels over 100 dBA at 25 meters typical for the maximum cruising speeds. At speeds greater than 250 km/hr, the dominant noise source is of aerodynamic origin. Although there has been only a limited amount of research devoted to noise control of maglev systems, there are many reasons to believe that the noise level can be brought to acceptable levels with advanced design techniques.**

This paper describes the findings of a study of noise generated by maglev systems including recommendations for further research to develop a better understanding of the sources of sound generation associated with high speed maglev operations [1].

I. Introduction

Noise from high speed magnetically levitated trains (maglev) has not been considered a potential environmental problem. It is commonly believed that if a vehicle is suspended above a rigid guideway, then the only noise is the "sound of the wind." Available data from maglev development programs reveal that noise levels at low speeds tend to confirm public expectations of quiet operations. However, the data also show that the noise levels from high speed maglev may be high enough to cause environmental impact in residential areas. Consequently, mitigation of adverse noise effects must be taken into consideration early in the planning and development of maglev. Research on this exciting mode is still in its early stages and as development moves forward, the noise control effort will continue to yield improvements.

Manuscript received March 15, 1993. This work was supported by the U.S. Department of Transportation, Federal Railroad Administration, under Contract No. DTFR-53-91-C-00074, as part of the National Maglev Initiative Program.

II. Noise Sources

Maglev noise is dominated by three sources: propulsion and auxiliary equipment, mechanical/structural radiation and airflow moving past the train. The sources differ in where they occur on the system as shown in Fig. 1. Following is an overview of noise sources occurring on maglev trains.

A. *Propulsion noise.*

Maglev trains are electrically powered; the propulsion noise sources are those from electromagnets, control units and associated cooling fans. Noise from the magnets is a result of induced vibration from magnetic forces, such as oscillating magnetostriction. Another magnet-related sound occurs at the pole passing frequency. Pole passing sound is caused by interaction between magnets on the moving vehicle and those on the stationary guideway at a uniform spacing. Location of these forces is at the magnet gaps between the vehicle and the guideway. Radiation can come from there as well as from larger structures (vehicle panels, guideway, etc.) caused to vibrate in response to such forces. Cooling fans can be a significant source which shows up in the noise spectrum in frequency bands near 1000 Hz independent of maglev speed.

B. *Mechanical/structural noise.*

Mechanical/structural noise is caused by guideway vibrations and vehicle body vibrations which tend to radiate sounds at the low end of the audible frequency range.

Noise from guideway vibrations is caused by: (1) wheels rolling on guideway support surfaces at low speeds for electrodynamic levitated systems (this type of maglev requires forward motion before lift can occur), (2) magnetic pole passing, and (3) load forces on the guideway structure as a train passes over each span.

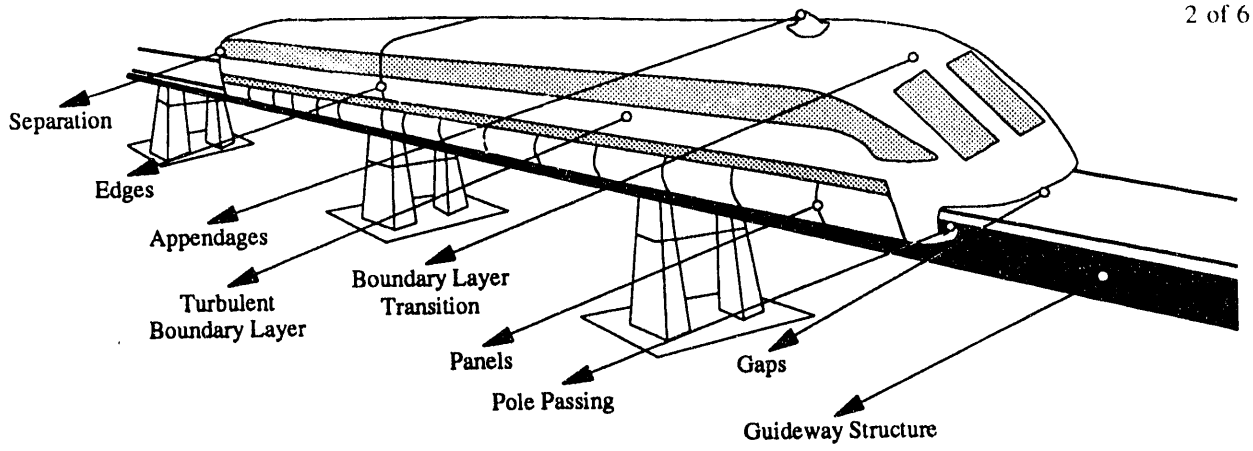

Fig. 1. Noise Sources on a Maglev System

Rolling noise from tires tends to be a broadband sound, while pole passing noise is tonal. Fundamental resonance frequencies of guideway support beams are generally below the audible range at 10 Hz or less, although radiation from steel box beam panels can occur up to about 80 Hz. The vehicle body also responds to dynamic forces, resulting in vibration and sound radiation.

C. *Aeroacoustic noise.*

Noise from airflow over a maglev vehicle is generated by flow separation and reattachment at the front, turbulent boundary layer over the entire surface of the vehicle, flow interactions with edges and appendages, and flow interactions between moving and stationary components of the system. Aeroacoustic noise increases with speed ranging from 60 to 80 times the logarithm of train speed and generally dominates noise levels from all high speed trains at speeds of 250 Km/hr or greater.

III. Noise Characteristics

A. *Noise Levels*

Maximum noise levels (Lmax) of the current generation electromagnetic levitated vehicle undergoing tests at the Emsland Test Track in Germany are plotted in Fig. 2 [2]. Lmax measured at a single point is the result of contributions of many sound generating mechanisms, some of which can result in similar noise characteristics. Hypotheses concerning dominant sources over various speed ranges are based on empirical evidence and theories of aerodynamic sound generation. Fig. 2 illustrates actual measured data from TR07, superimposed on models of noise generation over three important speed ranges. At speeds below 225 km/hr, noise from guideway structures and other mechanical sources has been found to depend on velocity to the third power (labeled A). Aeroacoustic sources make their presence known at speeds above about 225 km/hr. At speeds between 225 km/hr and 350 km/hr, noise from vortex shedding and vehicle body radiation is expected to increase as velocity to the sixth power (labeled B); and at speeds greater than about 350 km/hr turbulent boundary layer noise has a strong speed dependency, -- velocity to the eighth power (labeled C).

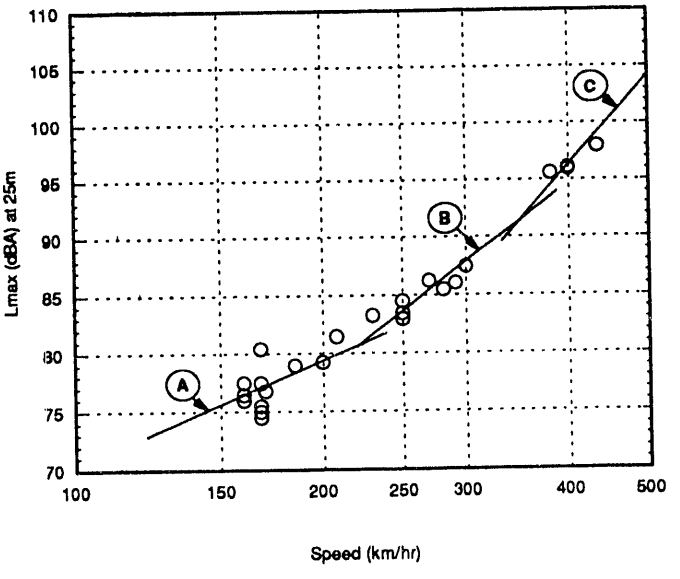

Fig. 2. Measured Noise of TR07 Compared With Estimates A = 30 log speed; B = 60 log speed; C = 80 log speed

B. Noise Spectra

An example of the difference in sound spectra for a maglev train at three speeds is shown in Fig. 3. One-third octave band spectra for the TR 07 are shown for the speeds of 160 km/hr, 250 km/hr and 435 km/hr. The mid-frequency portion of the spectra from 160 Hz to 1250 Hz fills in as speed increases; spectra levels increase roughly according to 30 log speed from 160 km/hr to 250 km/hr, and 60 log speed from 250 km/hr to 435 km/hr. The major differences show up in the frequency bands below 160 Hz. At 160 km/hr, tonal components are evident in the one-third octave bands centered at 160 Hz and 500 Hz. These correspond to the pole-passing frequency (172 Hz) and the slot-passing frequency (516 Hz) at that speed. The slot-passing frequency continues to be evident at the higher speeds, moving to the 800 Hz and 1600 Hz bands for the 250 km/hr and 435 km/hr speeds, respectively.

The spectra in Fig. 3 show that passbys of a maglev can be characterized as a relatively low frequency sound, with considerable sound energy in the frequency range where the human hearing system is most sensitive (1000 Hz to 2000 Hz). Sound levels at frequencies above 2000 Hz drop off rather rapidly.

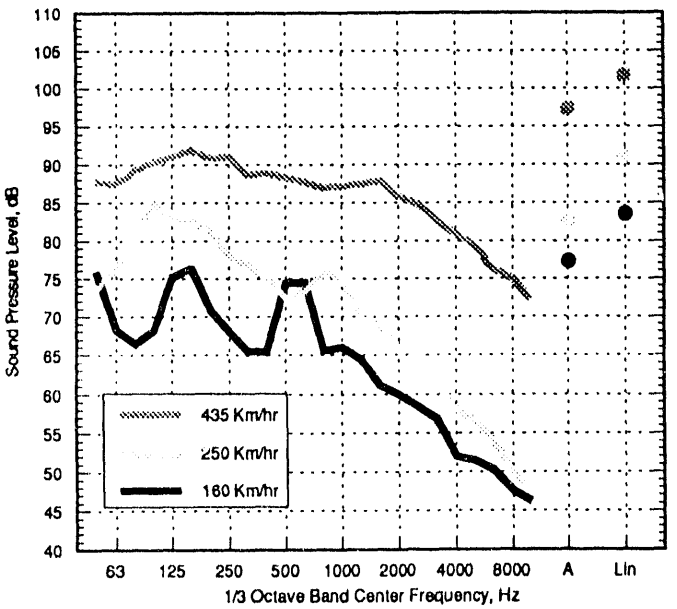

Fig. 3. Noise Spectra from Maglev Passbys

B. *Sound Exposure Level*

The sound exposure level (SEL) of a single passby, defined as the total sound energy of the event normalized to a one-second time period, is the basic unit for calculating a vehicle's contribution to environmental noise impact. Because a train is made up of several vehicles, the SEL for the entire train is determined approximately by:

$$SEL_{train} = SEL_{veh} + 10 \log N$$

where N = number of vehicles in the train. This expression is only approximate because the first and last vehicles may actually radiate more aeroacoustic energy at high speeds than the vehicles in-between due to special flow characteristics at the nose and the tail. Measured SEL's from the Transrapid TR07, normalized with respect to a single vehicle length of 25 meters, are shown in Fig. 4.

C. *Onset Rate*

The onset rate refers to the rapid increase of sound level, expressed in decibels per second, associated with an approaching maglev train. Researchers have determined that onset rates greater than about 15 dB/sec are likely to cause startle. Measured onset rates from maglev passbys show a direct dependency on speed and an inverse dependency on distance from the guideway.

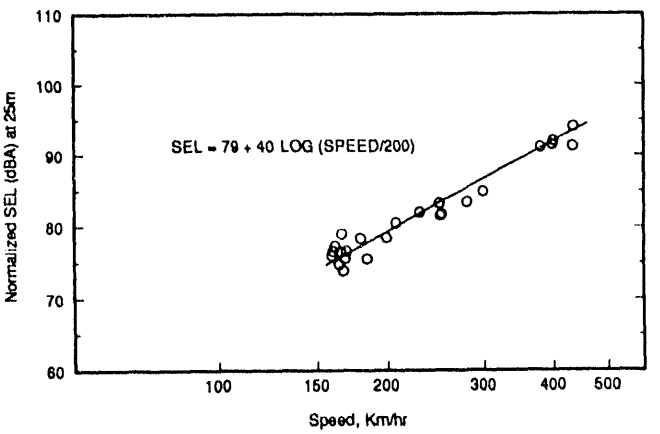

Fig. 4. SEL of TR07 Normalized to Single Vehicle

IV. Development of Noise Criteria

The introduction of a new transportation system into a community generates concerns about the change in the noise environment brought about by the new source. When the new source has unique features, as does maglev, or when the community has not had prior exposure to a particular source, as will happen with a maglev system, the concerns are heightened. The unknown community reaction to such a potentially significant new development is not an acceptable risk for the builders and financiers during these times of environmental awareness. It is important to have a means of rating the noise created by maglev in terms of the disturbance it creates, in order to gauge the community response and to avoid unacceptable installations. A review of existing environmental noise criteria and research on annoyance due to rapid onset rates resulted in recommendations for maglev noise impact criteria.

A. *Environmental Noise Criteria*

Assessment of the impact of a new noise source in the community has been covered extensively by the U.S. Environmental Protection Agency (EPA). Research sponsored by the EPA in the 1970's provided the basis for the development of noise descriptors and criteria by other federal agencies including various modal administrations of the Department of Transportation. Among the key findings of EPA research is that the day night sound level (Ldn) is the suitable noise descriptor for comparing the noise impact of a new noise source with that of other noise sources in a residential community. Ldn is a measure of a receiver's cumulative A-weighted sound exposure from all events over a full 24 hours, with all nighttime events between the hours of 10 pm and 7 am given a 10 dB penalty. As opposed to the maximum level from a single event (as shown in Fig. 2), Ldn is used to describe the noise "climate" in a neighborhood and has been found to correlate well with the results of attitudinal surveys of residential noise impact [3].

Recent noise criteria developed by Federal Transit Administration can be applied to assessment of the noise impact from maglev operations [4]. The noise impact criteria shown in Fig. 5 take into account the existing ambient noise level, expressed in terms of Ldn, as well as the noise from the proposed project, also expressed in terms of Ldn. When applied to maglev, the single difference is that an "onset-rate adjusted L_{dn}" is used (defined in next sub-section).

The noise criteria and descriptors depend on land use, designated either Category 1, Category 2 or Category 3:

Category 1 includes tracts of land where quiet is an essential element in their intended purpose, such as nationally significant historic sites or outdoor concert pavilion.

Category 2 includes residences and buildings where people sleep,

Category 3 includes institutional land uses with primarily daytime and evening use such as schools, churches and active parks.

For Category 2 land use where nighttime sensitivity is a factor, the noise criteria use L_{dn}. For Category 1 and 3 land uses involving primarily daytime activities, the impact is evaluated in terms of the L_{eq} for the noisiest hour of maglev-related activity during which human activities occur at a noise-sensitive location. The latter is referred to as "peak-hour L_{eq}." Because the L_{dn} and daytime peak-hour L_{eq} have similar values for typical noise environments, they are used interchangeably to evaluate noise impact for Category 1 and Category 2 sites. However, because Category 3 sites are less sensitive, the criteria allow the maglev noise to be 5 decibels greater than for Category 1 and Category 2 sites.

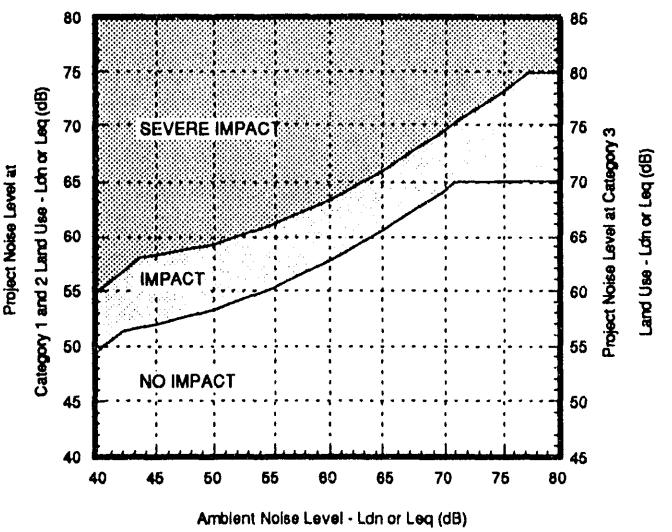

Fig. 5. Proposed Noise Impact Criteria

The noise impact criteria are defined by two curves which allow increasing project noise levels as ambient noise increases up to a point, beyond which impact is determined based on maglev noise alone. Below the lower curve in Fig. 5 , a maglev system is considered to have no noise impact since, on the average, the introduction of the system will result in an insignificant increase in the number of people highly annoyed by the new noise. The curve defining the onset of noise impact stops increasing at 65 dB for Category 1 and 2 land use, a standard limit for an acceptable living environment defined by a number of Federal agencies. Maglev noise above the upper curve is considered to cause Severe Impact since a significant percentage of people would be highly annoyed by the new noise. This curve flattens out at 75 dB for Category 1 and 2 land use, a level associated with an unacceptable living environment. As indicated by the right-hand scale on Fig. 5, the project noise criteria are 5 decibels higher for Category 3 land use.

Between the two curves the proposed project is judged to have an impact, though not severe. The change in the cumulative noise level is noticeable to most people, but may not be sufficient to cause strong, adverse reactions from the community. In this transitional area, other project-specific factors must be considered to determine the magnitude of the impact and the need for mitigation.

B. *Onset Rate Adjustment for Ldn*

As discussed in Section III C, there is evidence that an adjustment may be required for sound signatures with rapid onset rates. Based on the foregoing discussion of L_{dn} and the need for an adjustment to account for onset rate, it is recommended that an "onset-rate adjusted day-night sound level" be used to assess noise impact from maglev operations. This unit is the L_{dn} contribution from maglev operations as computed from the SELs of individual passbys, except that an adjustment is made to the SELs for passbys with rapid onset rates. A simple adjustment is proposed for ease in application and for purposes of being conservative: add 5 dB to the SEL where onset rates are 15 dB per second or more.

Fig. 6 shows the relationship of speed and distance to define locations where the onset rate exceeds 15 dB per second for a maglev train. This curve was determined using a synthesis of noise from a single maglev vehicle passby, accounting for divergence, directivity, convective augmentation, ground effect, atmospheric absorption and emission level (spectra) as a function of speed. TR07 data measured by TUV Rheinland and HMMH were used to obtain the relationship shown in Fig. 6 [2].

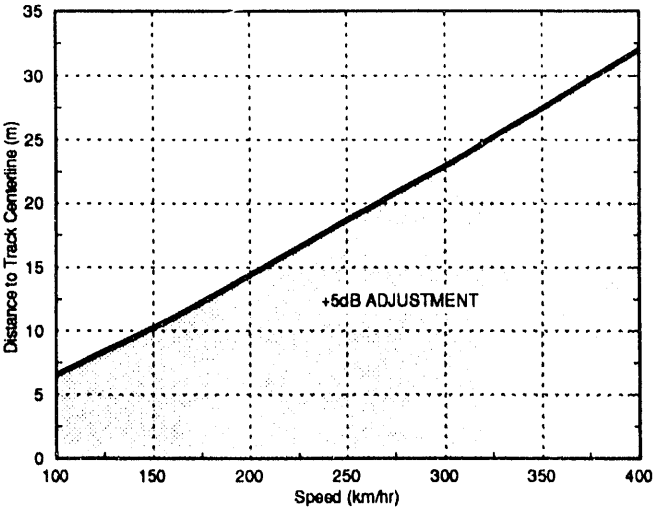

Fig. 6. Onset Rate Adjustment to Maglev SEL

V. Assessment of Noise Impact

The procedure for assessing impact is to determine the pre-project ambient noise level and the predicted maglev noise level at a given site, in terms of either Ldn or Leq as appropriate, and to plot these levels on Fig. 5. The location of the plotted point in the three impact ranges is an indication of the severity of the impact.

A. *Example of Application of Criteria*

For our example of noise impact from the introduction of maglev as it exists without noise mitigation, we will look at the replacement of existing passenger train service in the Northeast Corridor between Boston and New York. In the route through a suburb of Boston, the closest residences are located between 10 and 30 m from existing tracks. Without trains, the typical existing ambient Ldn is 60 dBA [5]. For that existing ambient, the proposed criteria show that Ldn's of 58 dBA and 63 dBA from a new source would cause "impact" and "severe impact," respectively (Fig. 5).

Current Northeast Corridor service has a total of 16 day and 6 night trains passing through the suburbs of Boston. Assuming a similar level of service could be provided by 10 - car maglev trains with the same schedule, the normalized SEL from Fig. 4 is converted to SEL for a 10-car train using the SEL equation in Section III.C. Two speeds are considered; an upper bound of 400 km/hr and a lower bound of 250 km/hr. The "onset rate adjustment" is obtained for the appropriate speed from Fig. 6.

The results shown in Fig. 7 illustrate the distances from the guideway that would considered to be impacted using the proposed criteria. Severe impact would result for any residence within 40 m at the upper speed of 400 km/hr and would drop to 18 m for 250 km/hr. The method can be employed in reverse to determine the speed at which no impact will occur for a residential area. For example, if the nearest house was 30 m, the speed would have to be reduced to 267 Km/hr to fall into the "no impact" zone of Fig. 7. This example shows that without additional mitigation measures, noise from a current generation high speed maglev system could cause severe noise impacts in residential neighborhoods near the guideway. Negative public reaction could result in restrictions of speed or locating new maglev rights-of-way.

VI. Unresolved Noise Issues

Because maglev has a great potential to serve as an alternative to aircraft as a short haul carrier between cities, the mode will of necessity be placed in densely populated areas. Consequently, noise control will be a major part of the design/development process for maglev. Before design guidelines for noise control can be developed with confidence for a new maglev system, the following design issues should be resolved through an acoustic test program.

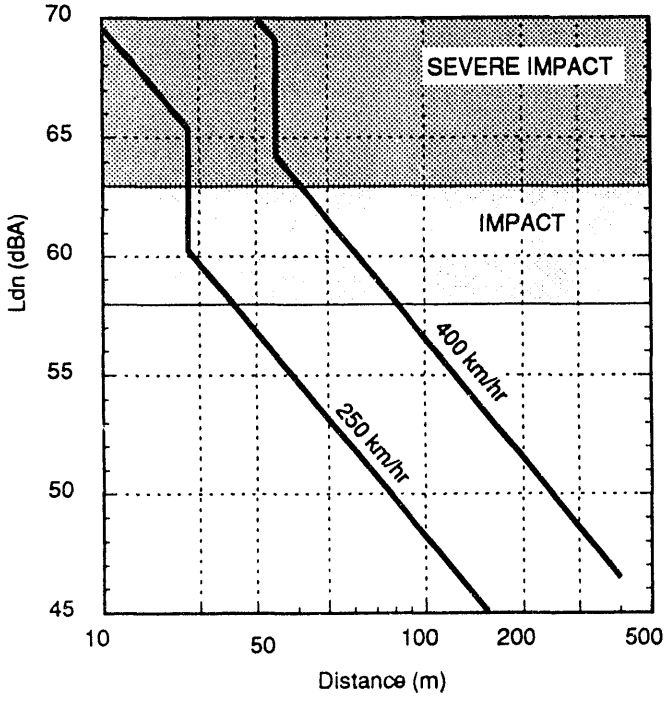

Fig. 7. Noise Impact Assessment Example

- What are the key aeroacoustic sources for each speed range?
- How much of the sound radiation generated by the boundary layer can be attributed to vehicle structure?
- How effective are boundary layer control methods in reducing noise?
- How much noise is generated by the vehicle flow interaction with guideway structure?
- How much sound is radiated from the guideway structure?
- How much noise will be generated by lifting surfaces if they are employed for guidance purposes?

A research program to resolve these and other noise issues should be undertaken during the design phase of a new maglev system. Mechanical/structural noise tests are best performed on full scale facilities, but there are two approaches to conducting research on aeroacoustic problems: model testing in wind tunnels, and full- or nearly full-scale testing on a test track. The choice revolves around the extent to which structural re-radiation is found to be important. Model testing gives scale measurement of the direct radiation component and provides a convenient method for sorting out the various aeroacoustic mechanisms. However, if structural radiation is found to be important, then testing will be required on a larger scale prototype.

References

[1] C. Hanson, P. Abbot, I. Dyer, "Noise from High Speed Maglev Systems," U.S. Department of Transportation Report No. DOT/FRA/NMI - 92/18, Washington, D.C., March 1993.

[2] TUV Rheinland, "Gerauschmessungen an der Magnetschnellbahn TR07 und an anderen Verkehrssystemen im Vergleich," Institut fur Energietechnik und Umweltschutz, Bericht-Nr. 933/329005/05-06, 4 July 1990.

[3] S. Fidell, D.S. Barber, T.J. Schultz, "Updating a dosage-effect relationship for the prevalence of annoyance due to general transportation noise," J. Acous. Soc. Am., vol. 89, January 1991.

[4] U.S. Department of Transportation, Federal Transit Administration,"DRAFT: Guidance Manual for Transit Noise and Vibration Impact Assessment," Report No. UMTA-DC-08-9091-90-1, July 1990.

[5] Harris Miller Miller & Hanson Inc. measurements for Northeast Corridor Electrification Program.

Corroboration of Magnetic Forces in U.S. Maglev Designs

Howard Coffey, Jianliang He, and Zian Wang
Argonne National Laboratory
Argonne, Illinois 60439

Abstract - Four System Concept Definition (SCD) contractors to the National Maglev Initiative (NMI) developed conceptual designs of maglev systems in 1991-1992. The objective of the work reported here was to perform independent calculations of the magnetic forces and fields of these four systems to assess the "reasonableness" of the results presented to the government. Commercial computer software was used for computing forces in the system employing nonlinear ferromagnetic materials and for some calculations of induced eddy current effects in finite-sized systems. Other cases required the use of models developed at ANL and verified by experiment, or in a few cases, new computer programs that have not been validated by experiment. The magnetic forces calculated by the contractors were found to be credible in every case evaluated. The stray fields were also found to be in reasonable agreement with those calculated by the contractors, but, for lack of space, are not reported here.

Introduction

Since the four conceptual maglev systems designed under the NMI program were developed analytically without the benefit of experience with operational systems, a government team was established to independently analyze the proposed concepts[1]. These designs included three electrodynamic (EDS) and one electromagnetic (EMS) system. One EDS concept used coils, another a conducting ladder, and the third a conducting sheet in the guideway. The EMS concept used iron-cored superconducting magnets aboard the vehicle. Null-flux coils were used in two guidance systems. No single method of analysis was adequate for calculating the electromagnetic fields and forces of all the systems proposed.

Foster-Miller

The Foster-Miller concept uses "racetrack-shaped" superconducting magnets on the vehicle, which interact with sidewall-mounted null-flux coils to produce levitation and a portion of the guidance forces. Propulsion, and the primary guidance, are provided by a single set of coils, which are connected across the guideway and powered in parallel from the wayside. The baseline 150-passenger, 73-metric-ton, 2-car train is levitated on three bogies. Each bogie contains eight magnets and must levitate 24.3 metric tons. Each magnet has a mean winding width of 0.5 m, a mean length of 1.0 m, and 1800 kA-T of current. The null-flux coils in the guideway are 0.74 m long, 0.90 m high and 0.04 m x 0.04 m in cross section.

The levitation forces were analyzed using a Dynamic Circuit Theory model [2,3] developed by J.L. He et al. of Argonne National Laboratory. This model uses numerical techniques to calculate the dynamic time-dependent forces of coil-type suspension systems.

The magnets aboard the vehicle and the null-flux coils in the guideway must be displaced from their symmetrical positions to generate levitation or guidance forces. The computed levitation forces are shown in Figure 1 as functions of the vertical displacement (at 134 m/s) and velocity (with a 0.035 m offset). The weight of the vehicle is about 240 kN/bogie. At the operational speed of 134 m/s, this basic levitation requirement is met with a vertical offset of about 0.035 m, and a lift-to-drag ratio of about 180 results. The maximum lift is approximately 640 kN at this speed and occurs with a vertical displacement of 14 cm, providing a maximum-to-nominal lift ratio of 2.65, which is in good agreement with the value of 2.6 calculated by Foster-Miller.

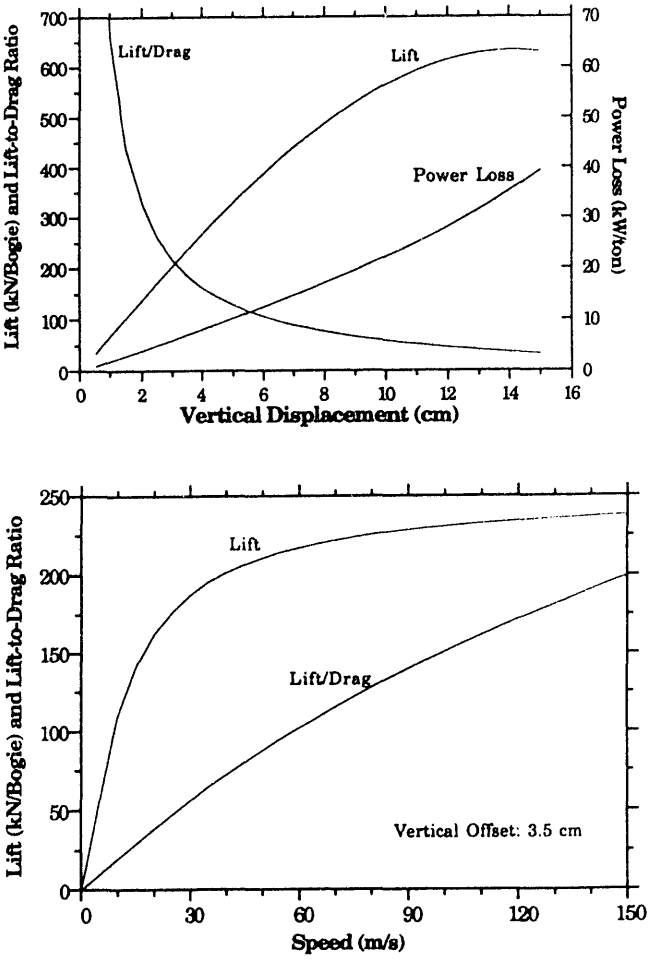

Figure 1. Suspension force vs vertical offset at 134 m/s (top) and vs speed with 0.035 m offset (bottom). Gap = 0.275 m, Velocity = 34 m/s, Current = 1800 kA-T, Conductor cross-section = 16 cm^2.

Extra lift is required at operational speeds in turns, in gusty winds, and to provide a margin of safety. As shown in the figures, the lift force develops progressively as the speed increases, and although the lift might appear excessively conservative at high speeds, this performance is needed to achieve levitation at lower speeds. The power dissipation of 7.5 kW/ton under nominal operational conditions compares with a value of 6 kW/ton calculated by Foster-Miller.

It should be noted that the displacements at takeoff (50 m/s) and landing (20 m/s) will be greater than the 0.035 m discussed here, and the marginal lift force will be reduced. Since the coils can be wound with multiple turns, the conductors can be thinner than the skin depth, and an increase in drag due to the skin effect is not a concern. The calculations assume copper conductors in the guideway, with the cross-sectional area indicated.

The primary guidance forces in this system are those resulting from the interaction with the cross-connected propulsion coils. Our calculated guidance forces resulting from the interaction of the superconducting magnets with the propulsion coils (for one pair of magnets) as functions of lateral displacements of the vehicle are shown in Figure 2. The guidance force depends on the air gap assumed between the superconducting magnets and the propulsion/guidance coils as shown. These forces are lower than Foster-Miller's by about 15%. Additional lateral forces will occur as a result of the propulsion current in these coils.

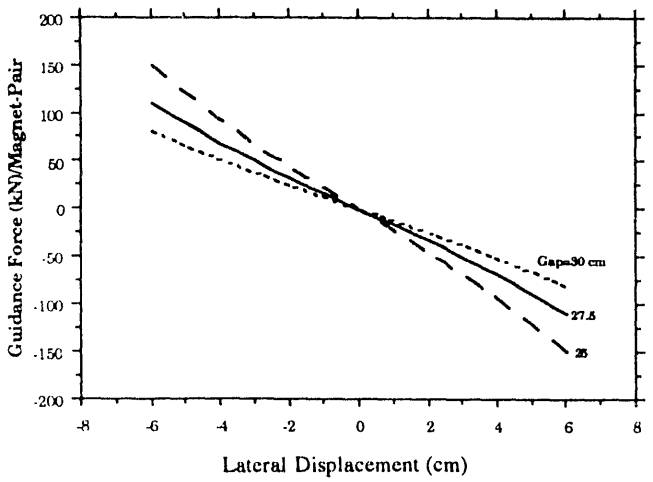

Figure 2. Guidance Force vs Lateral Displacement with Air Gap as Parameter.

Bechtel

The Bechtel design uses a "ladder"-type guideway and an array of on-board magnets with alternating polarities to effectively achieve a "null-flux" configuration. When the on-board magnets are symmetrically located with respect to the center line of the ladder track, no net flux is experienced by the ladder track and no currents or forces result. The equilibrium operating position of the magnets is a few centimeters below this centerline.

Ninety-six superconducting magnets on the vehicle are contained in six modules of eight magnets on each side of the vehicle, the 1-m-long and 0.3-m-wide magnets being positioned with their planes in the vertical direction. The modules are spaced 1 m apart along the length of the vehicle, and the magnets are arranged so that each magnet is adjacent to other magnets with different polarities. The modules are 4 m long and 0.6 m wide.

To analyze the lift and drag forces in this design, the dynamic circuit theory model was modified to include a LSM waveform approximated as a continuous sine wave extending the length of the vehicle. This approach is analogous to that used in conventional motor theory and is an approximation in that higher-order harmonics, eddy currents in the coils, and end effects resulting from the finite lengths of the magnets are not included. Nevertheless, the model approximates Bechtel's results and indicates the "reasonableness" of their computations.

A steady-state circuit approach was used in the model and provides closed-form analytic solutions that are well-suited for the analysis of coil-type EDS systems.

The results of the lift force calculations are shown in Figure 3 in which the forces are normalized in the same manner as those presented by Bechtel (Figure 4).

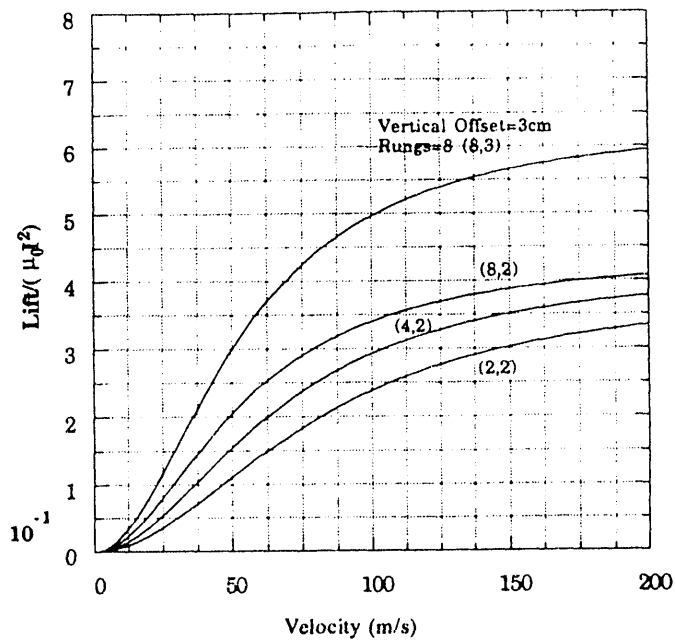

Figure 3. Normalized Lift vs Speed with Number of Rungs and Vertical Offset as Parameters (ANL). See text for parameters.

These calculations are for an array of four coils for comparison with the corresponding calculations made by Bechtel. The notations 8,3 etc., refer first to the number of rungs per meter in the ladder guideway and second to the displacement in centimeters of the vehicle-mounted magnets

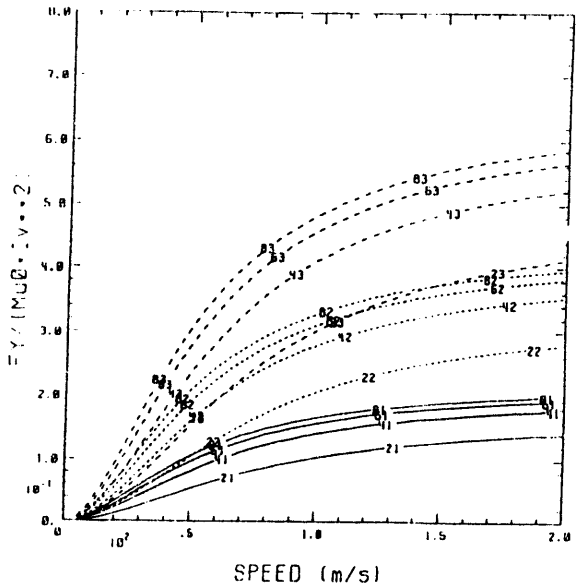

Figure 4. Normalized Lift vs Speed with Number of Rungs and Vertical Offset as Parameters. (Bechtel)

below the centerline of the ladder. The upper and lower horizontal rails of the ladder are 0.030 m high and 0.020 m thick, while the rungs, or vertical members of the ladder, are 0.01 m wide and 0.020 m thick. Our calculations ignore the skin effect, which will be appropriate if Bechtel uses a laminated structure. Further, only the first harmonic of the waveform is considered. To obtain the agreement shown, the effective resistance was arbitrarily adjusted, but it remains within a factor of two of the expected value. The Bechtel calculation is more conservative than ours. The drag forces were also calculated and are similarly in agreement. The number of rungs per meter has a significant effect on the lift and drag forces and is an important design parameter.

The lift and drag forces, lift-to-drag ratio, and the ladder-interaction guidance force resulting from one of the six bogies composed of two magnet modules, one on each side of the vehicle (16 magnets per bogie), are shown in Figure 5 as functions of the vertical offset of the magnets from the centerline of the ladder track. During cruising, the vertical displacement will be about 0.030 m. The offset will be greater at lower speeds. The lift-to-drag ratio calculated with the model is 140 at 134 m/s. Bechtel calculated two power losses in the coils, leading to lift-to-drag ratios of 130 if eddy currents are disregarded and 110 if they are included.

Guidance in this system derives from interactions of the on-board "octopole magnets" with: 1) null-flux guidance coils, 2) the levitation ladder, and 3) the propulsion motor. The dominant interaction is that between the magnets and the figure-eight-shaped null-flux coils in the guideway. Corresponding coils on opposite sides of the guideway are connected in series across the guideway.

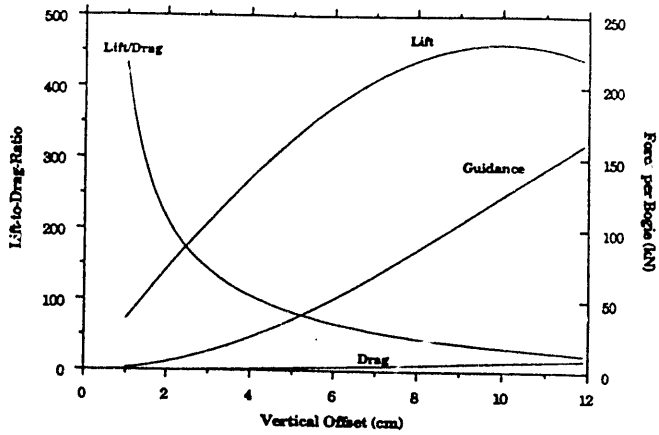

Figure 5. Magnetic Forces vs Vertical Displacements at 134 m/s. 8 rungs/meter; 0.20-m gap; 400 kA-T current; 16 magnets/bogie (ANL)

The primary guidance force from the null-flux coil interaction is shown in Figure 6 as a function of the lateral displacement. The "Bechtel" curve is the sum of the separate forces on the two sides of the bogie. The cross-sectional area and conductivity of the conductor were not reported and have been adjusted within physically permissible limits to achieve the agreement shown. A value of 0.1 on the scale shown corresponds to 20 kN for an eight-magnet bogie, resulting in a total restoring force of 240 kN for the entire vehicle when it slips to the side by 0.02 m.

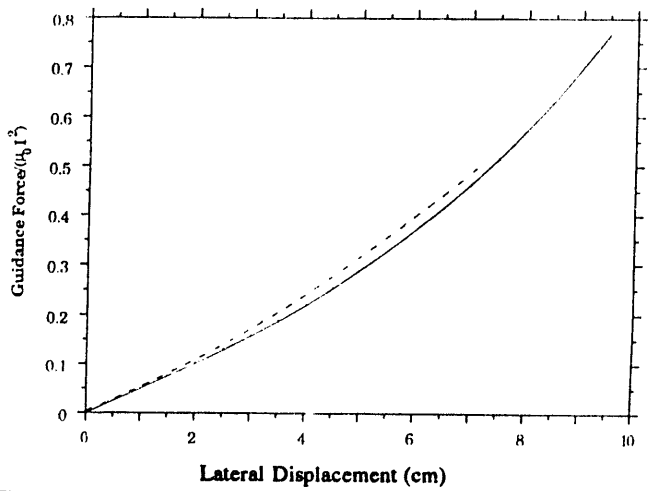

Figure 6. Normalized Guidance Force vs Lateral Displacement (cm). Four Magnets Each Side. Solid Curve (ANL); Broken Curve (Bechtel).

Grumman

The Grumman conceptual maglev design is an EMS system using constant-current superconducting magnets to generate the magnetomotive force for the iron poles of the on-board magnets. Dynamic control of the magnetic field is provided by separate trim coils near the pole faces of the magnet. The gap between the iron poles and the LSM stator is 40 mm. One set of magnets acting against a single

reaction plate (the stator of the LSM) provides both lift and guidance forces. The stator is mounted at a 35° angle from horizontal in the guideway (Figure 7). The lift and guidance forces are components of the force normal to the faces of the poles, and this normal force is the important design force. This concept requires that control be provided when the magnets are displaced sideways on the rail. The baseline vehicle carries 100 passengers and weighs 61.4 metric tons.

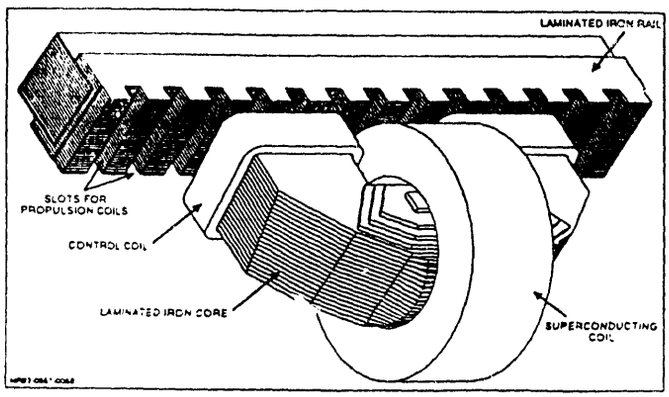

Figure 7. Electromagnetic Suspension System (Grumman), Showing Superconducting Coil for Bias and Control Coils for Dynamic Control.

Since the gap in this system is 40 mm, and the fringe fields were expected to be relatively large, the computer code TOSCA®[4] was used for the analysis of this system. The pole faces are square with sides of 0.200 m and react against a square-cross-section rail also having sides of 0.200 m. Forty-eight magnets (24 on each side of the vehicle) of this type are used. The magnets are staggered (Figure 8) to provide control as the magnet moves to the side of the rail. Each pole extends to the side of the rail by 0.020 m. Only the limits of the static fields produced by the combination of the superconducting and the control coils were computed.

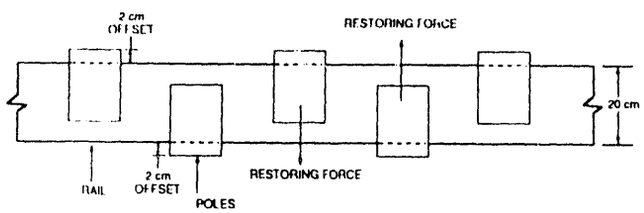

Figure 8. Position of Magnet Poles on Guideway Rail (LSM Stator) to Provide Stability Against Lateral Motion. (Grumman)

Due to the high magnetic intensities in the poles and guideway, Vanadium-Permendur and M43 steel are proposed by Grumman for use in the poles and rails, respectively. In our calculations, only M43 steel was used.

The forces normal to the faces of the poles calculated by Grumman and ANL are shown in Figure 9 as functions of the current in the trim coils with the baseline current of 50 kA-T in the superconducting magnet. The trim coil current shown is the sum of the currents in both trim coils on a single core. The vertical lift force on the vehicle is the sum of these normal forces on each magnet multiplied by $\cos 35^0$. At the nominal operating point shown, the vertical force is about 940 kN, while the vehicle weighs about 630 kN, providing a 50% margin in lift for cornering, wind, and safety factors. The guidance force is the difference between the forces on magnets on opposing sides of the vehicle multiplied by $\sin 35^0$.

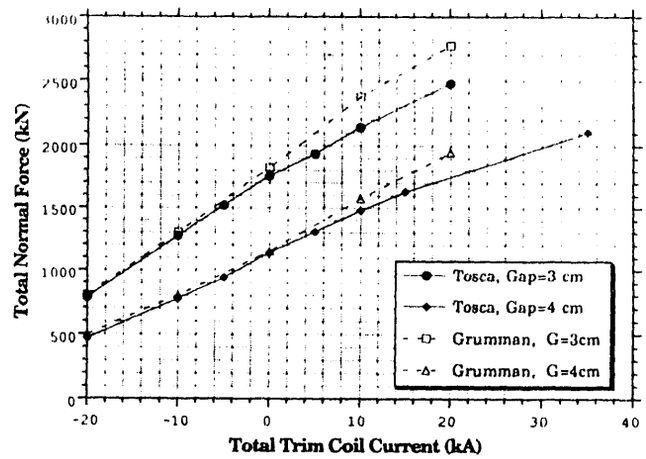

Figure 9. Total Force Normal to Face of Magnets. Current in Superconducting Magnets = 50 kA-T. Total Current in Both Trim Coils as Variable. (ANL/Grumman)

As the magnets are displaced laterally (see Figure 8), some magnets move onto and others off of the rail, resulting in a force that tends to restore the magnets to their equilibrium positions. The restoring force shown in Figure 10 was calculated for the case in which the magnetic field in the gap is constant. Since the capability of specifying a constant-gap field is not contained in TOSCA, the current was varied to approximate this condition, and the forces were scaled to the appropriate values using a B^2 scaling to obtain the results shown. This approach approximates a condition in which the normal force is constant. The restoring force is stabilizing with all the gap spacings evaluated. Our results (using M43) indicate a somewhat greater variation with the gap dimension than do the Grumman data. Similar calculations (not shown) were made for the case of constant magnet current.

Magneplane-International

The Magneplane system is a continuous-sheet EDS system in which eight magnets aboard the vehicle induce currents in aluminum sheets in the guideway as the vehicle passes by. These currents interact with the magnets to produce the repulsive forces that levitate and guide the vehicle. The guideway, shaped as a trough, permits the vehicle to roll in a turn, avoiding the use of a separate tilt mechanism.

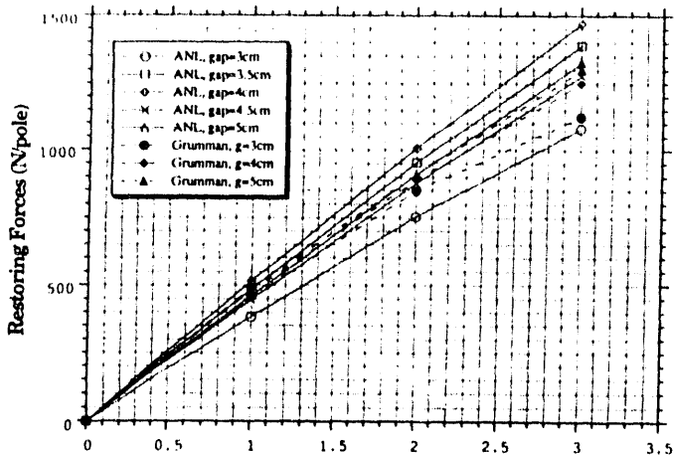

Figure 10. Lateral Restoring Force vs Displacement (cm) (ANL).

Continuous-sheet guideways, unlike those using discrete coils, provide a non-pulsating interaction with the superconducting magnets, simplifying the achievement of ride comfort and reducing the ac losses in the cryostat and magnet. Stabilization of the system in the roll direction is by means of the interaction of the propulsion coils with the edge of the guideway and by airfoils. Propulsion of the system is analogous to that of the other EDS systems, except that the 12 magnets used for propulsion are separate from those used for levitation, and the LSM windings are under the vehicle. The dimensions, currents, and layout of the magnets are shown in Figure 11.

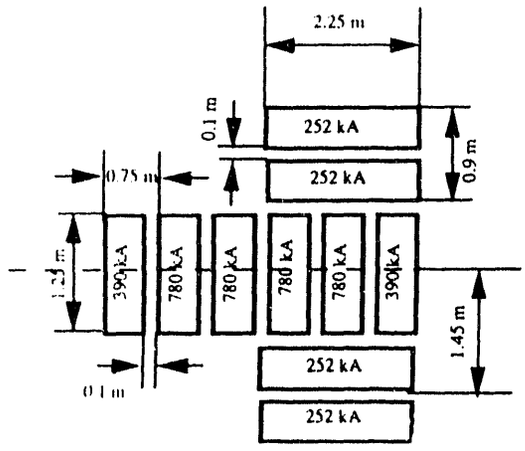

Figure 11. Dimensions, Configuration, and Currents of Magnets used at one end of Magneplane 140-Passenger Vehicle. A Mirror Image of these Magnets is Used at the Opposite End of the Vehicle.(Magneplane)

Analytic models are available for calculating the magnetic lift and drag forces on magnets moving above an infinitely wide conducting ground plane. Analyses for single magnets have been given by Chilton and Coffey[5] and Reitz and Davis[6]. A similar analysis, by Lee and Menendez[7], accounts for multiple magnets. The latter formulation was programmed and used for this analysis. Values for a single magnet calculated using this formulation compare well with those from a previous program, based on [6] and [7], which has been validated by numerous experiments. The guideway is sufficiently wide that the lift forces calculated are expected to be affected only marginally by its finite width.

The lift and drag forces for a single bogie composed of two sets of two magnets for the baseline 45-passenger vehicle (180 kA-T) are shown in Figures 12 and 13. Since the baseline force demanded of this bogie is 76 kN, it is seen that considerable marginal support exists above that required for levitation of the vehicle.

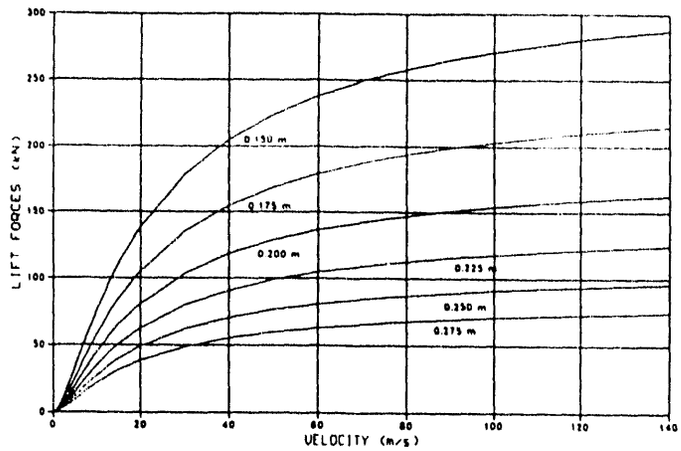

Figure 12. Lift Forces Calculated for Two Sets of Two Magnets on a Single Bogie of the Baseline 45-Passenger Vehicle. Magnets 2.25 m long, 0.4 m wide, 0.1 m spacing. (ANL)

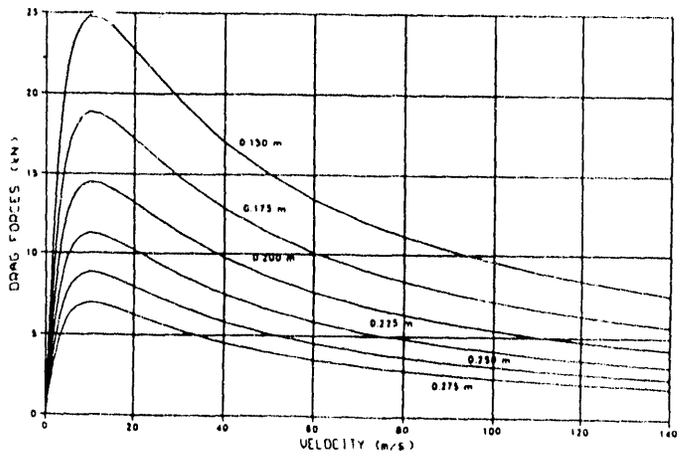

Figure 13. Drag Forces Calculated for Two Sets of Two Magnets on a Single Bogie of the Baseline 45-Passenger Vehicle. (ANL)

Electrodynamic interactions of magnets with the edges of finite conductors as encountered in the keel stabilization of the Magneplane require calculations using 3D-finite element computations. ELEKTRA®, a commercial computer code

capable, in principle, of calculating the forces of moving magnets interacting with a finite-width conducting guideway, was used for the analysis. Requirements for nodes on which the fields were to be computed, however, exceeded the capabilities of the Sun Station used in these analyses, limiting our considerations to reduced sizes and very low velocities. By arbitrarily reducing the size of both the vehicle and the current by a factor of 16, the eddy current patterns of Figure 14 were obtained at a velocity of 6 m/s. (The Magneplane system uses six propulsion magnets rather than the four modeled here.) Eddy currents induced by the combined propulsion and levitation magnets are shown.

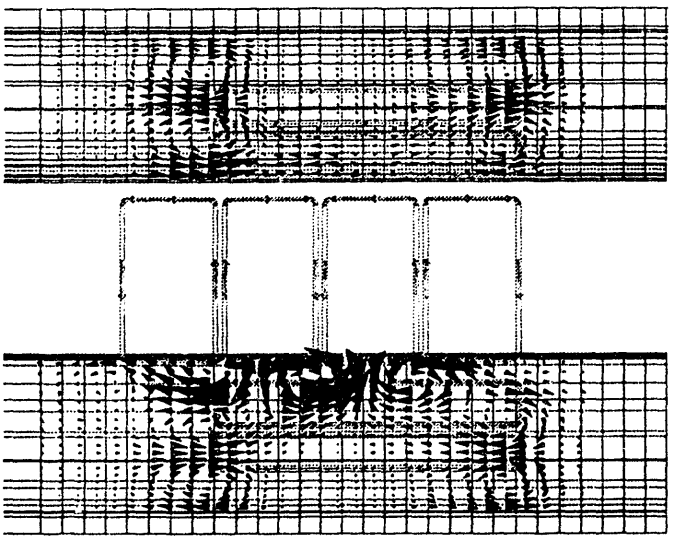

Figure 14. Eddy Current Pattern Induced in Guideway by Magneplane-Type System, with Levitation Magnets but only Four Propulsion Coils.

The resulting force tends to restore the vehicle to its neutral position upon displacement laterally, but no attempt was made to extrapolate this force to a full-scale system. These results were not considered to be sufficient for evaluating the details of this interaction.

This mechanism provides stability against roll and also provides some guidance of the vehicle. Additional guidance is achieved by allowing the vehicle to rotate in the trough-shaped guideway. Separate guidance magnets are not used.

Conclusions

To the extent that the suspension systems proposed by the System Concept Definition contractors were analyzed in this task, the work reported here corroborates (with minor differences) the calculations of magnetic forces by the contractors for their respective maglev designs. No assessment was made of the viability of the superconducting magnets or the cryogenics as they are proposed, and the systems proposed by the contractors were not altered. Further improvements in the systems proposed might or might not be possible. The individual contractors retain proprietary rights in their respective system designs.

The analysis of the Magneplane International system is more limited than are those for the other systems, for the reasons discussed above.

Acknowledgements

This work was supported by the U.S. Army Corps of Engineers and the Federal Railroad Administration through interagency agreements E8691R001 and DTFR53-93-X-00047, respectively, with the U.S. Department of Energy.

References

1. Government Maglev Systems Assessment Team results.

2. He, J.L., D.M. Rote, and H.T.Coffey, *Computation of Magnetic Suspension of Maglev Systems using Dynamic Circuit Theory*, Proc. International Symp. on Magnetic Suspension Technology, sponsored by National Aeronautics and Space Administration (NASA) Langley Research Center, Hampton, Va. (Aug. 1991).

3. T.M. Mulcahy, J.L. He, D.M. Rote, and T.D. Rossing, *Forces on a Magnet Moving past Figure-Eight Coils*, International Magnetics, 1993 Conference, Stockholm, Sweden, April 13-16, 1993.

4. TOSCA and ELEKTRA are trademarks of Vector Fields, Inc., Aurora, Ill. and Oxford, England.

5. Chilton, F., and H.T. Coffey, *Magnetic Levitation, Tomorrow's Transportation*, The Helium Society, Washington, D.C., 1971, p. 288. See also, Coffey, H.T., F. Chilton, and L.O. Hoppie, *The Feasibility of Magnetically Levitating High Speed Ground Vehicles*, Feb. 1972, National Technical Information Center, Alexandria, Va PB 210505, and Coffey, H.T., J.D. Colton and K.D. Maher, *Study of a Magnetically Levitated Vehicle*, February, 1973, National Technical Information Center, Alexandria, Va, PB221696.

6. Davis, L.C., and J.R. Reitz, *Eddy Currents in Finite Conducting Sheets*, J. Appl. Phys, 42, 4119-4127, 1972, and Reitz, J.R., *Forces on Moving Magnets due to Eddy Currents*, J. Appl. Phys., 41, pp 2067-2071, 1970.

7. Lee, Shung-Wu, and Ronald C. Menendez, *Force on Current Coils Moving over a Conducting Sheet with Application to Magnetic Levitation*, Proc. IEEE, 62, 567-577, 1974.

CONTROL STRATEGIES OF A LSM DRIVE FOR EDS-MAGLEV SYSTEMS

F.Albicini, M.Andriollo, G.Martinelli and A.Morini
Department of Electrical Engineering - University of Padova
Via Gradenigo 6/a - 35131 PADOVA (Italy)

Abstract - In the paper an inverter-fed linear synchronous motor for EDS-MAGLEV systems is analyzed in order to evaluate the harmonic contents of the armature current as well as of the mechanical power. Some control strategies for improving the drive performance are discussed.

I. INTRODUCTION

The drive of a magnetically levitated train with electrodynamic suspension (EDS-MAGLEV) usually consists of a PWM inverter feeding an air-cored long-stator linear synchronous motor (LSM) with on-board superconducting field coils.

The drive performance may be analyzed by means of an equivalent circuit and with reference to the generic harmonic of the applied voltage, counter e.m.f. and current. Differently from [1], in this paper the equivalent circuit is defined by means of general expressions taking into account also the arrangement in which the field coils are grouped in opposite polarity pairs and the armature coils arranged in two overlapped layers [2]. The latter implies a different harmonic content of the LSM c.e.m.f., with the presence - in addition to the fundamental component pulsating at ω_r - of harmonics pulsating at $k\omega_r/2$ ($k=1,3,4..$).

The developed model allows to analyze the steady-state behavior of the PWM inverter- LSM drive by means of the evaluation - as a function of the speed - of the instantaneous values of the applied voltage, current and mechanical power, given the harmonic content of the c.e.m.f., the frequency, amplitude and phase of the triangular carrier wave and the waveform of the modulating wave. The model also allows to calculate the ohmic losses, the converter apparent power and the power factor.

Two control strategies are proposed in order to optimize the drive performance with respect to the armature ohmic losses and to the LSM power ripple. Such performances are obtained by impressing suitable current harmonics by means of the control of the harmonic content of the applied voltage. The obtained results are compared with the case of sinusoidal current.

As an example, a proposed EDS-MAGLEV train is considered [2] and the results obtained by applying the proposed control strategies are given.

Manuscript received March 15, 1993. This work was supported by the Progetto Finalizzato CNR Trasporti 2.

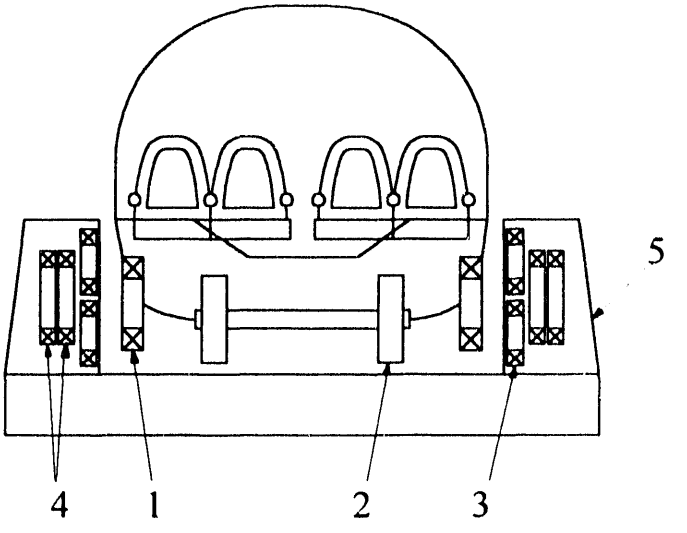

Fig.1 - *Schematic cross section of an* EDS-MAGLEV *vehicle.* [**1**: *on-board* SC *coils;* **2**: *auxiliary suspension*; **3**: *ground levitation coils*; **4**: *two-layer armature coils*; **5**: *guideway*]

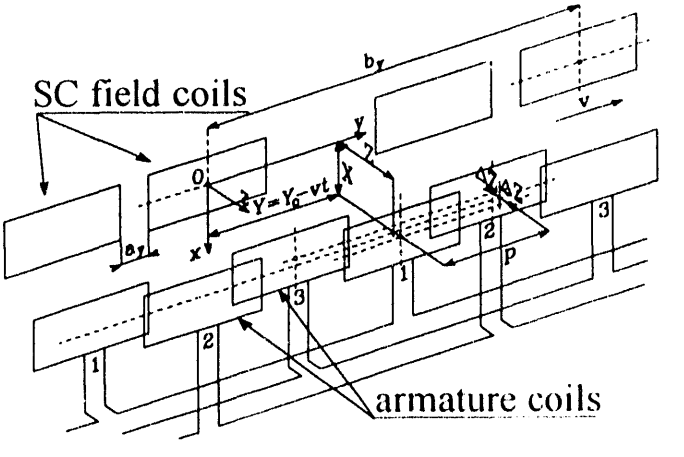

Fig.2 - *Field and armature coils of the* LSM. [b_Y: *polar pitch*; a_Y: *distance between the field coils of a pair*; p: *pitch of the armature coils*; **1,2,3**: *phases*; $X, Y = Y_0 - v_0 t, Z \pm \Delta Z$: *coordinates of a generic armature coil*; $2\Delta Z$: *distance between the armature layers*; v_0: *train speed*]

II. COILS ARRANGEMENT

Fig.1 shows a typical coil arrangement of the LSM of an EDS-MAGLEV train. The windings may be represented by series of rectangular-shaped coils: Fig.2 shows the

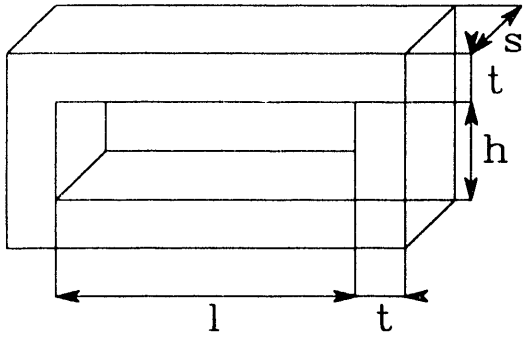

Fig.3 - *Reference dimensions of armature and field coils, with number of turns respectively* N_t *and* N_s.

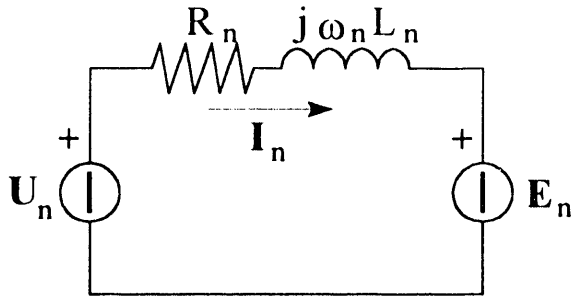

Fig.4 - *Single-phase equivalent circuit related to one section of the armature winding.*

field and armature coils with reference to one side of the train. For the sake of clearness the coils are represented as filiform, even if the developed expressions take into account the actual coil thicknesses (Fig.3). The field and armature coils are on vertical parallel planes: the former are grouped into opposite polarity pairs and the latter into three phases and two layers.

III. LSM EQUIVALENT CIRCUIT

With reference to one section of the armature winding and to the n-th harmonic, Fig.4 gives the LSM single-phase equivalent circuit. It is:

E_n LSM counter e.m.f.
R_n, L_n armature resistance and inductance (included the series impedance of the connections)
U_n converter applied voltage
I_n armature current

A. Counter e.m.f. E_n

Given a reference system (x,y,z) fixed to the field coils, $X, Y = Y_0 - vt, Z \pm \Delta Z$ are the coordinates of a generic armature coil (Fig.2). The mutual inductance per polar pitch between the field winding and the i-th armature phase (i=1,2,3) is given by [3]:

$$M_{is} = k \sum_{\substack{n=j\,k/2 \\ j=1}}^{\infty} \mathfrak{M}_{tsn}(X,Z) \sin\left[n\frac{2\pi(Y+b)}{b_y} - \frac{2\pi(i-1)j}{3}\right] \quad (1)$$

with k armature coils per phase and polar pitch. The coefficients $\mathfrak{M}_{tsn}(X,Z)$ and b depend on the system geometry (parameters l,h,t,s,b_y,a_y,ΔZ of Figs.2 and 3) as well as on the number of turns N_s and N_t; their complete expressions are given in [3].
With the positions $Y_0 = -b$ and:

$$\omega_r = k\frac{2\pi}{b_y} v \quad (2)$$

the mutual inductance as a function of time and then the e.m.f. induced in the i-th phase can be obtained from (1). It results, with reference to the sign convention of Fig.4 [4]:

$$e_{is}(t) = N_p I_s \frac{\partial M_{is}}{\partial t} = \sum_{j=1}^{\infty} \sqrt{2}\, E_j \cos\left[\frac{j\omega_r}{2}t + \frac{2\pi(i-1)j}{3}\right] \quad (3)$$

$$E_j = -j\, k^2 N_p v I_s \frac{\pi}{b_y\sqrt{2}} \mathfrak{M}_{tsn}(X,Z) \qquad n = j\frac{k}{2} \quad (4)$$

with I_s field current and N_p polar pairs per section.
The LSM c.e.m.f. contains the fundamental pulsating at ω_r (related to the speed v by means of (2)), and harmonics pulsating at $j\omega_r/2$ (j=1,3,4,..); the phasor E_j represents in module and phase the j-th harmonic of the c.e.m.f..

B. Resistance R_n *and inductance* L_n

In order to evaluate the series inductance of the circuit of Fig.4, the phase self and mutual inductances must be determined.
The mutual inductance between a coil of the phase i and a coil of the phase j is given by [5]:

$$M_{ij} = \sum_{0}^{\infty}{}_n \mathcal{L}_{tn} \cos\left(n\frac{2\pi Y_{ij}}{b_y}\right) \quad (5)$$

with Y_{ij} distance between the coils. The coefficient $\mathcal{L}_{tn}$ depends on the geometrical parameters of the armature winding as well as on the number of turns N_t; its complete expression is given in [5].
For $Y_{ij}=0$ and $Y_{ij}=\pm b_y/3$ respectively, the coil self and mutual inductance L and M can be obtained from (5).
Bearing in mind that the sides of the armature winding are in parallel [1], the phase inductance L_{an} and resistance R_a are, with reference to the n-th harmonic:

$$L_{an} = N(L - M)/2 \qquad n \neq 3k \quad (k=1,2,3,..) \quad (6)$$

$$L_{an} = N(L + 2M)/2 \qquad n = 3k \quad (k=1,2,3,..) \quad (7)$$

$$R_a = NR/2 \quad (8)$$

with N armature coils connected in series per phase and section and R resistance of a coil.
Finally, the parameters of the circuit of Fig.4 are:

$$L_n = L_{an} + L_f \qquad R_n = R_a + R_f \qquad n \neq 3k \quad (k=1,2,3,..) \qquad (9)$$

$$L_n = L_{an} + L_f + 3\,L_{neut} \qquad R_n = R_a + R_f + 3\,R_{neut} \qquad n=3k \quad (k=1,2,3,..) \qquad (10)$$

where L_f and R_f are the inductance and resistance of the series connections and L_{neut} and R_{neut} those of the neutral connection.

C. Converter voltage U_n

If the converter is operating so that it can supply a voltage containing the fundamental and harmonics pulsating at $n\omega_r/2$ $(n=1,3,4,..)$, the phase currents can be generally expressed in the following way:

$$i_i(t) = \sum_{n=1}^{\infty} \sqrt{2}\, I_n \cos\left[\frac{n\omega_r}{2}t - \gamma_n + \frac{2\pi(i-1)n}{3}\right] \qquad (11)$$

With the phasor $\mathbf{I}_n$ representing in module and phase the n-th current harmonic, the equation:

$$\mathbf{U}_n = \mathbf{E}_n + (R_n + j\frac{n\omega_r}{2} L_n)\,\mathbf{I}_n = \mathbf{E}_n + \mathbf{Z}_n\mathbf{I}_n \qquad (12)$$

gives the phasor $\mathbf{U}_n$, representing in module and phase the n-th converter voltage harmonic (Fig.4).
In order to obtain a desired drive performance, the armature currents are requested to have a suitable harmonic content, represented by h^* phasors $\{\mathbf{I}_{d1}, \mathbf{I}_{d2}, .., \mathbf{I}_{dh^*}\}$: by means of (12), the desired harmonic content of the converter voltage $\{U_{d1}, U_{d2}, .., U_{dh^*}\}$ is then defined. The voltage spectrum is actually obtained by means of a PWM technique, in which the carrier frequency f_c is limited by the converter switching capability. Given $\{U_{d1}, U_{d2}, .., U_{dh^*}\}$ and the frequency, amplitude and phase of the carrier wave, the switching instants $\{t_1, t_2, .., t_\mu\}$ are determined and then the actual spectra of voltage $\{U_1, U_2, .., U_{h^*}, U_{h^*+1}, ..\}$ and current $\{I_1, I_2, .., I_{h^*}, I_{h^*+1}, ..\}$ are evaluated. They differ from the desired ones essentialy due to harmonics with frequencies near f_c and multiples.

IV. MECHANICAL POWER

With reference to the currents (11) and according to the developments given in [3] and [4], the mean value and the harmonics of the propulsion force per polar pitch F_y acting on the train can be determined. The LSM mechanical power $P_{em} = N_p F_y v$ immediately follows. It is:

- mean value (see (4)):

$$\langle P_{em} \rangle = -k^2 N_p v I_s \frac{\pi 3\sqrt{2}}{b_y} \sum_{h=1}^{\infty} I_h \mathcal{M}_{ls(hk/2)}(X,Z)\cos(\gamma_h) = 3\sum_{h=1}^{\infty} E_h I_h \cos(\gamma_h) \qquad (13)$$

- generic harmonic (the complete expressions of $a_{\mu h} = -\mathcal{A}_{\mu h}/N_p v$ and $b_{\mu h} = -\mathcal{B}_{\mu h}/N_p v$ are given in [4]):

$$p_{em\mu}(t) = P_{em\mu}\cos\left(\frac{3}{2}\mu\omega t - \varphi_\mu\right) \qquad (14)$$

$$P^2_{em\mu} = \left\{\sum_{h=1}^{\infty}\left[\mathcal{A}_{\mu h} I_h \cos(\gamma_h)\right]\right\}^2 + \left\{\sum_{h=1}^{\infty}\left[\mathcal{B}_{\mu h} I_h \sin(\gamma_h)\right]\right\}^2 \qquad (15)$$

$$\mathrm{tg}(\varphi_\mu) = \sum_{h=1}^{\infty} \mathcal{B}_{\mu h} I_h \sin(\gamma_h) \Big/ \sum_{h=1}^{\infty} \mathcal{A}_{\mu h} I_h \cos(\gamma_h) \qquad (16)$$

The instantaneous mechanical power contains, in addition to the mean value, harmonics pulsating at $3\mu\omega/2$ $(\mu=1,2,3,..)$. The mean value is contributed by the current components $I_h\cos(\gamma_h)$, while the components $I_h\sin(\gamma_h)$ contribute the harmonic content.

V. CONVERTER CONTROL STRATEGIES

Three converter control strategies are discussed, in order to obtain different drive performances:
A: sinusoidal currents pulsating at $\omega_r = 2\pi k v/b_y$
B: current spectrum to minimize the ohmic losses in the armature windings
C: current spectrum to minimize the power ripple.

A. Sinusoidal armature currents

Once imposed $\langle P_{em} \rangle$, the desired current spectrum is $\{I_{d1}=0, I_{d2}\neq 0, .., I_{dh^*}=0\}$, with I_{d2} given by (13). Correspondently, the desired voltage spectrum $\{U_{d1}, U_{d2}, .., U_{dh^*}\}$ is given by (see (12)):

$$U_{dn} = E_n \quad (n\neq 2) \qquad U_{d2} = E_2 + Z_2 I_{d2} \quad (n=2) \qquad (17)$$

Once determined the actual voltage spectrum $\{U_1, U_2, .., U_{h^*}, U_{h^*+1}, ..\}$, the actual current spectrum $\{I_1, I_2, .., I_{h^*}, I_{h^*+1}, ..\}$ is evaluated.

B. Minimization of the ohmic losses

The second strategy is aimed at operating the converter so that - for the mean power $\langle P_{em} \rangle$ imposed by the desired motion conditions - the current spectrum $\{I_{d1}, I_{d2}, .., I_{dh^*}\}$ produce the minimum ohmic losses in the armature windings and series resistances.
The ohmic losses can be expressed in the following way:

$$P_{dJ} = 3\sum_{n=1}^{h^*} R_n I_{dn}^2 \qquad (18)$$

The minimum value of P_{dJ} is obtained in correspondence to h^* currents:

$$I_{di} = \frac{\langle P_{em} \rangle}{3 \sum_{n=1}^{h^*} \frac{E_n^2 \cos^2(\gamma_n)}{R_n}} \cdot \frac{E_i \cos(\gamma_i)}{R_i} \qquad i = 1,..,h^* \quad (19)$$

Once determined the spectra $\{U_1, U_2, .., U_{h^*}, U_{h^*+1}, ..\}$ and $\{I_1, I_2, .., I_{h^*}, I_{h^*+1}, ..\}$, the actual ohmic losses are given by:

$$P_J = 3 \sum_{n=1}^{\infty} R_n I_n^2 \quad (20)$$

C. Minimization of the power ripple

The method developed in [1] allows to cancel a desired harmonic of the mechanical power: as it doesn't take into account sub-harmonics, it is not applicable to armature windings arranged in two layers.
In this paper and with reference to [4], the method is generalized in order to obtain the minimization of the whole harmonic content of the power, whatever the spectrum of the c.e.m.f. and with a moderate increase of the r.m.s. value of the armature current.
Bearing in mind (13)÷(15), the relative harmonic content of the power can be expressed as:

$$R = \frac{\sqrt{\sum_{\mu=1}^{\mu^*} P_{em\mu}^2}}{\langle P_{em} \rangle} = \sqrt{\sum_{\mu=1}^{\mu^*} \left[\frac{P_{em\mu}}{\langle P_{em} \rangle} \right]^2} \quad (21)$$

where μ^* is the number of harmonics considered in the series expansion of the power. In order to minimize R, it is convenient that the current quadrature components are zero, that is $\gamma_h = 0$ or $\gamma_h = \pi$. Assumed such values for γ_h and with reference to h^* harmonics considered in the current series expansion, (15) and (13) become:

$$P_{em\mu} = \sum_{h=1}^{h^*} \mathcal{A}_{\mu h} \mathcal{I}_h \qquad \mu = 1,2,..,\mu^* \quad (22)$$

$$\langle P_{em} \rangle = 3 \sum_{h=1}^{h^*} E_h \mathcal{I}_h = \sum_{h=1}^{h^*} \mathcal{A}_{0h} \mathcal{I}_h \quad (23)$$

with $\mathcal{I}_h = \pm I_h$ depending on $\gamma_h = 0$ or $\gamma_h = \pi$.
By assuming as base power the desired value $\langle P_{em} \rangle$ of the mean power and as base current the quantity $\langle P_{em} \rangle / \mathcal{A}_{02}$ (that is the r.m.s. value of the current which gives such mean power if the current is supposed sinusoidal), (21)÷(23) can be expressed as follows:

$$R^2 = \sum_{\mu=1}^{\mu^*} p_{em\mu}^2 \qquad p_{em\mu} = \sum_{h=1}^{h^*} a_{\mu h} i_h \qquad 1 = \sum_{h=1}^{h^*} a_{0h} i_h \quad (24)$$

$$p_{em\mu} = \frac{P_{em\mu}}{\langle P_{em} \rangle} \qquad i_h = \frac{\mathcal{I}_h \mathcal{A}_{02}}{\langle P_{em} \rangle} \qquad a_{\mu h} = \frac{\mathcal{A}_{\mu h}}{\mathcal{A}_{02}} \quad (25)$$

Combining the first and second of (24) and using matrix notation, the following is obtained:

$$R^2 = [\,i\,]^t [\,b\,] [\,i\,] \quad (26)$$

$$[\,a_0\,]^t \cdot [\,i\,] = 1 \quad (27)$$

$$[a_0] = \begin{bmatrix} a_{01} \\ a_{02} \\ \dots \\ a_{0h^*} \end{bmatrix} \qquad [a] = \begin{bmatrix} a_{11} & \dots & a_{1h^*} \\ a_{21} & \dots & a_{2h^*} \\ \dots & \dots & \dots \\ a_{\mu^* 1} & \dots & a_{\mu^* h^*} \end{bmatrix} \qquad [i] = \begin{bmatrix} i_1 \\ i_2 \\ \dots \\ i_{h^*} \end{bmatrix}$$

with $[b] = [a]^t [a]$. The minimum value of (26) with the constraint (27), is obtained in correspondence to:

$$[\,i\,] = \frac{[\,b\,]^{-1} [\,a_0\,]}{[\,a_0\,]^t [\,b\,]^{-1} [\,a_0\,]} \quad (28)$$

and then:

$$R = \sqrt{[\,i\,]^t [\,b\,] [\,i\,]} = \frac{1}{\sqrt{[\,a_0\,]^t [\,b\,]^{-1} [\,a_0\,]}} \quad (29)$$

VI. EXAMPLE OF APPLICATION

With reference to the proposed control strategies, the developed model has been utilized to analyze voltage, current and power in an EDS-MAGLEV system with the arrangement of Fig.2 and the data of Tab.I. The train is made up by 14 vehicles, is about 120 m long and its mass is about 306 tons [2]. Tab.II gives the values of vertical displacement X and total force $F_{tot} = N_p \langle F_y \rangle$ used in calculations.
The inertial force F_{in} has been assumed equal to 150 kN and corresponds to an acceleration of about 0.05 g ($\cong$ 0.49 m/s^2). The aerodynamic drag has been evaluated on the basis of $F_{aer} = (\rho g c_w A v^2)/2$, with $\rho \cong 1.225$ kg/m^3 (air density), $g \cong 9.81$ m/s^2, $c_M = 0.35$ (penetration coefficient) and $A = 8.9$ m^2 (train frontal section). The vertical displacement X and the electromagnetic drag $\langle F_{drag} \rangle$ have been calculated with reference to [6].
The impedance of the connections has been neglected and, according to the inverter configuration proposed in [7], the neutral connection and then the presence of homopolar currents have been taken into account. The series expansions of voltage, current and power have been termined at the 202-th harmonic, starting from the sub-harmonic at $\omega_r/2 = \pi k v / b_y$.

Tab.I - *Parameters of a system with the coil arrangement of Figs. 2 and 3 (s: field; t: armature).*

$l_s = 2.15$ m	$h_s = 0.45$ m	$t_s = 0.05$ m	$s_s = 0.08$ m
$N_s = 1000$	$I_s = 700$ A	$a_y = 0.45$ m	$b_y = 21.6$ m
$l_t = 2.49$ m	$h_t = 0.53$ m	$t_t = 0.07$ m	$s_t = 0.08$ m
$N_t = 15$	$k = 4$	$N = 74$	$N_p = 30$
$Z = 0.245$ m	$\Delta Z = 0.04$ m		
$R = 20.8$ mΩ	$L = 0.89$ mH	$M = 0.30$ mH	

Tab.II - *Vertical displacement* X *and forces acting on the train* (kN) *as a function of speed* v.

v [km/h]	X [mm]	$<F_{drag}>$	F_{aer}	F_{in}	F_{tot}
100	46.4	89.7	1.3	150	241.0
150	34.1	43.5	2.8	150	196.3
200	29.6	28.2	5.0	150	183.2
250	27.4	20.9	7.8	150	178.7
300	26.2	16.6	11.2	150	177.8
350	25.4	13.8	15.3	150	179.1
400	24.9	11.6	20.0	150	181.6
450	24.5	10.3	25.3	150	185.6
500	24.3	9.2	31.2	150	190.4

Fig.5 shows the LSM c.e.m.f. for the steady-state running at speed v=500 km/h; the frequency of the fundamental component is f_r=25.72 Hz, while the sub-harmonic at $f_r/2$ is relevant, due to the coil arrangement in two layers. The waveform also contains relevant high harmonics.

With reference to the current and power waveforms and for v=500 km/h, the diagrams of Fig.6 and 7 compare the results of the converter control strategies. Fig.6a and 7a give the results referred to an ideal converter (that is an inverter which exactly supplies the desired spectrum); Fig.6b and 7b give those referred to the actual PWM inverter. In the latter case, as the carrier frequency f_c is assumed to be 90 times the frequency f_r of the fundamental of the modulating wave, high harmonics near f_c and multiples are present. In the simulation of the proposed strategies, the spectrum of the currents has been controlled impressing h^*=22 harmonics and sub-harmonics.

As regards the current waveform, the limitation of the frequency f_c has a non-relevant effect. The strategy C implies a peak-value greater than strategies A and B, while the strategies B and C imply a relevant harmonic content, the sub-harmonic at $\omega_r/2$ being predominant.

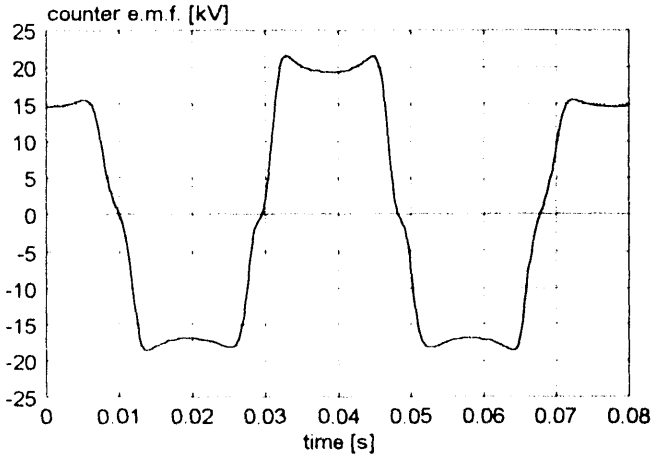

Fig.5 - *Instantaneous c.e.m.f. at* 500 km/h.

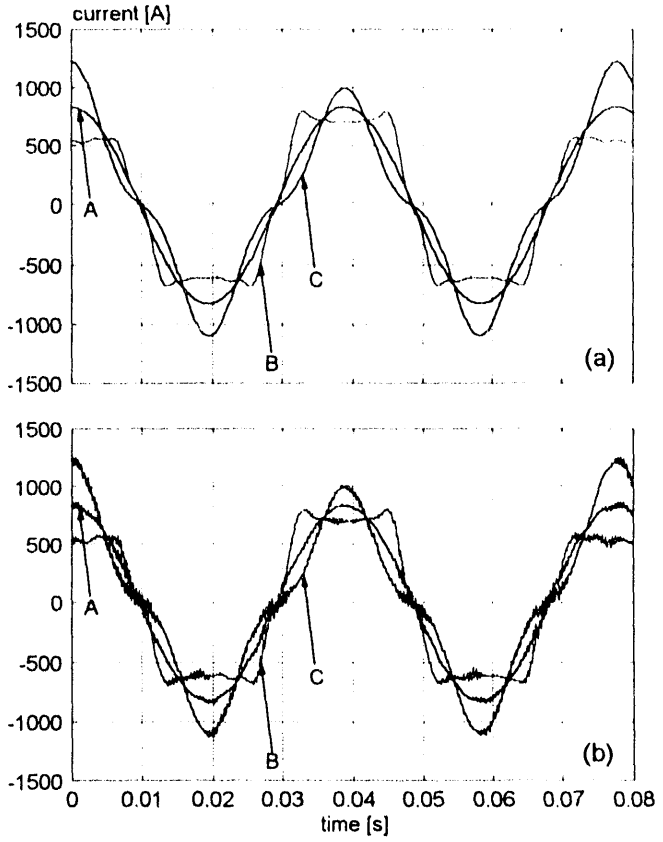

Fig.6 - *Current vs. time for the three proposed strategies in the case of ideal* (a) *and actual* (b) *inverter.*

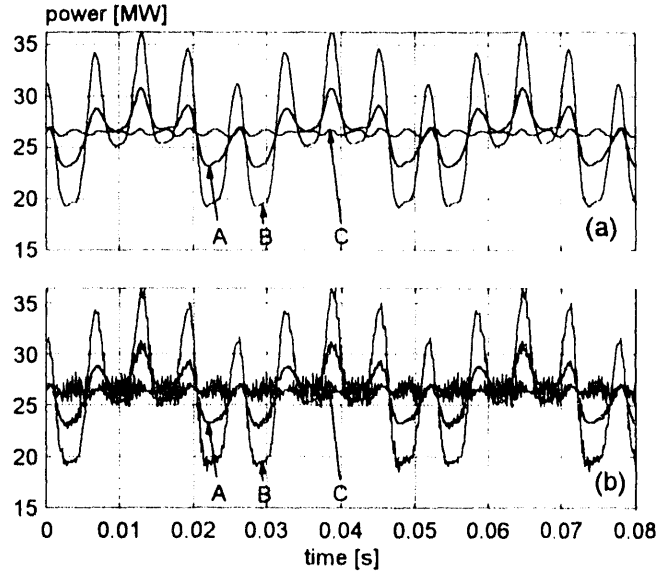

Fig.7 - *Power vs. time for the three proposed strategies in the case of ideal* (a) *and actual* (b) *inverter.*

As regards the power waveform, the results obtained with the actual and ideal converter are similar for the strategies A and B, quite different for the strategy C. A and B imply the presence of a relevant component at $3\omega_r/2$ in addition to the desired mean value $<P_{em}>$

With reference to the proposed strategies and versus ϑ, Fig.8÷10 compare r.m.s. current, inverter apparent power and power factor. Fig.8 shows that, even at speed lower than 500 km/h, B implies the lowest r.m.s. current, while C implies the highest. Fig.9 shows that the strategy C implies the highest value of apparent power, while A the lowest. In fact B, in spite of the lowest r.m.s. current, implies r.m.s. voltage and then apparent power higher than A. Finally, Fig.10 gives the power factor, as the ratio between inverter active and apparent power: the power factor increases with the speed, being the highest in A and the lowest in C.

The results of the simulations allow the following considerations:

- as regards the current r.m.s. value and the apparent power, A and B are the best strategies: B, however, also implies a relevant power ripple. The power ripple implies non-relevant speed ripple, due to the high inertia of the train, but may be the cause of disturbances on the supply network.
- as regards the power ripple, C is the best strategy, provided one can accept that at 500 km/h the current r.m.s. value increases of 11% and the apparent power and ohmic losses increase of 22%.

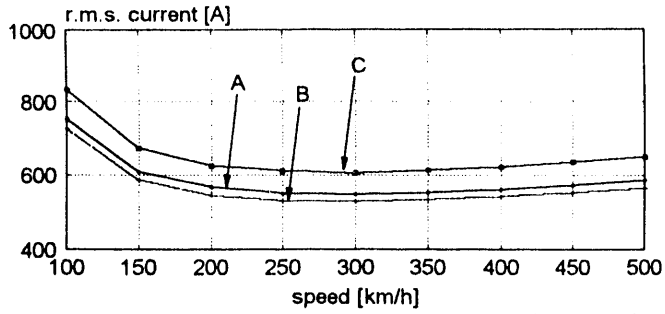

Fig.8 - *Current r.m.s. value versus speed for the three proposed strategies.*

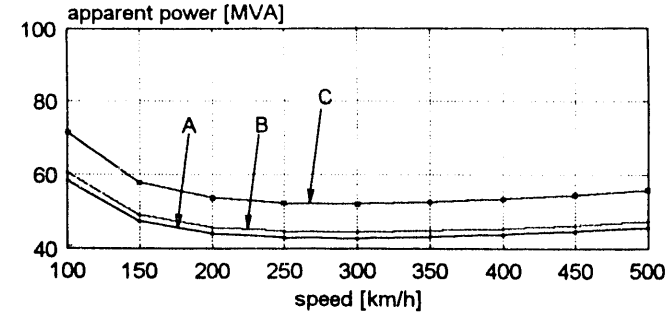

Fig.9 - *Apparent power versus speed for the three proposed strategies.*

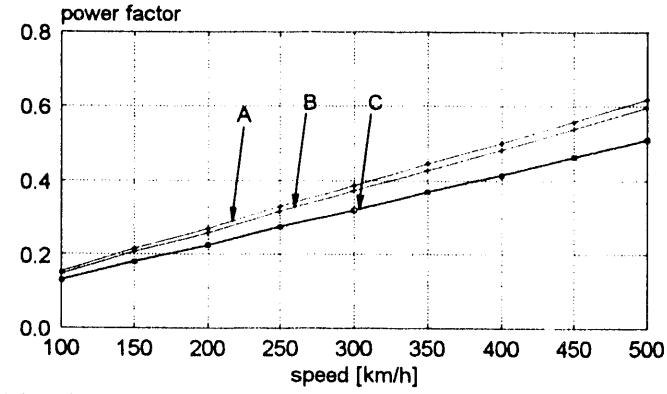

Fig.10 - *Power factor versus speed for the three proposed strategies.*

VII. CONCLUSIONS

The paper generalizes previous developments related to simplified arrangements of the propulsion system of EDS-MAGLEV trains and describes a model of the PWM inverter-LSM drive which allows the evaluation of voltage, current and power in the following conditions:

- LSM field coils grouped in opposite polarity pairs;
- LSM armature coils arranged in two overlapped layers;
- different inverter control strategies in order to obtain the desired drive performances;
- actual voltage and current spectra due to the PWM technique.

The diagrams of the application example show the effects of the proposed control strategies.

REFERENCES

[1] F.Albicini, S.Bolognani, G.Martinelli, A.Morini, "Harmonic analysis of LSM drives for EDS-MAGLEV systems", *Intern. Conf. on Electrical Machines*, Cambridge (USA), August 13÷15, 1990.

[2] H.Tanaka, "JR Group probes MAGLEV frontiers", *Railway Gazette International*, July 1990.

[3] F.Albicini,M.Andriollo,G.Martinelli,A.Morini, "General expressions of propulsion force in EDS-MAGLEV systems with superconducting coils", *Applied Superconductivity Conf.*,Chicago (USA), Aug. 23÷28, 1992.

[4] F.Albicini,M.Andriollo,G.Martinelli,A.Morini, "Metodo analitico di calcolo e criterio di ottimizzazione della forza di propulsione in sistemi MAGLEV-EDS", Internal Report UPdie 92/03, Nov.1992.

[5] M.Andriollo, G.Martinelli, A.Morini, A.Scuttari, "Calcolo delle correnti indotte negli avvolgimenti di sospensione in sistemi MAGLEV di tipo EDS", Internal Report UPdie 92/01, April 1992.

[6] M.Andriollo, G.Martinelli, A.Morini, "General expressions for forces acting in EDS-MAGLEV systems driven by linear synchronous motors", *Intern. Aegean Conf. on Electrical Machines and Power Electronics*, Kuşadasi (Turkey), May 27÷29, 1992.

[7] S.Tadakuma, S.Tanaka, H.Inoguchi, Y.Tanoue, H.Ikeda, S.Kaga, "Consideration on large capacity]PWM inverter for LSM drives", 2nd *Intern. Power Electronics Conf.*, Tokyo (Japan), April 1990.

Longstator Linear Synchronous Motor Modeling for Simulation and Control System Design

Jeffrey A. Britton
Dr. Ronald L. Klein

Department of Electrical and Computer Engineering
West Virginia University
Morgantown, West Virginia
(304) 293-6371

Abstract - This paper develops a state space model for the longstator linear synchronous motor (LLSM). The motor form considered consists of a three phase armature winding mounted on the guideway and a field winding mounted on the translator (vehicle) with no damper windings on the translator. The parameters of the state space model are expressed directly in terms of the machine geometry and airgap. With this explicit representation of the airgap, responses to various load disturbances may be directly simulated for different airgap widths.

I. Introduction

The basic geometric configuration of the LLSM considered is shown below in Figure 1.

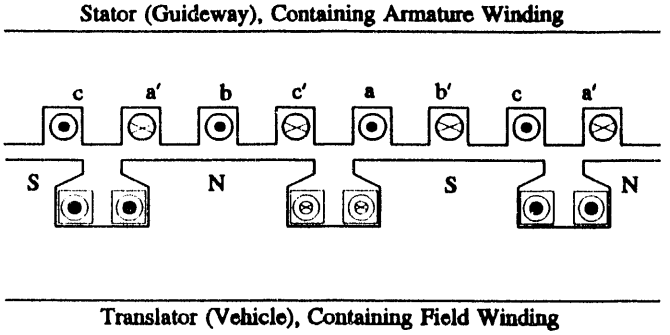

Figure 1. Geometric Configuration of the LLSM Considered

As in all salient pole synchronous machines the stator winding self inductances and stator inter-winding mutual inductances vary at twice the electrical speed of the translator (rotor in a conventional rotating machine) due to the time varying airgap seen by the stator mmf as the translator traverses the guideway. In a similar manner, the stator winding to translator (field) winding mutual inductances vary at the electrical speed of the translator. The standard practice of assuming sinusoidal variation of these inductances is used here so that Park's transformation to the rotor reference frame may be used to eliminate the periodic time variation of these inductances [1].

Our approach to develop the voltage equations in rotor reference frame variables follows the method outlined by P. C. Krause for the rotating synchronous machine [2]. The state space model is developed and presented for the rotating synchronous machine. The necessary modifications are introduced to convert the rotating machine variables to linear machine variables.

II. Rotating Machine Voltage Equations

In the rotor reference frame, the q-axis, d-axis, zero sequence and field voltage equations which describe the LLSM shown in Figure 1 are developed. These equations are:

$$v_{qs} = i_{qs} r_s + \omega_r \lambda_{ds} + p\lambda_{qs} \quad (1)$$

$$v_{ds} = i_{ds} r_s - \omega_r \lambda_{qs} + p\lambda_{ds} \quad (2)$$

$$v_{os} = r_s i_{os} + p\lambda_{os} \quad (3)$$

$$v_{fd} = i_{fd} r_{fd} + p\lambda_{fd} \quad (4)$$

where,

v_{qs}, v_{ds}, and v_{os} = q-axis, d-axis and zero sequence *applied* voltages (V),

v_{fd} = applied field voltage referred to the stator (V),

i_q, i_d, and i_o = q-axis, d-axis and zero sequence currents (A),

i_{fd} = field current referred to the stator (A),

λ_{qs}, λ_{ds} and λ_{os} = q-axis, d-axis and zero sequence flux linkages (Wb-t),

λ_{fd} = field flux linkages referred to the stator (Wb-t),

r_s = per phase armature winding resistance (Ω),

r_{fd} = field resistance referred to the stator (Ω) and

$p \equiv d/dt$.

The flux linkages appearing in (1)-(4) are given by:

$$\lambda_{qs} = i_{qs}(L_{ls} + L_{mq}) \quad (5)$$

$$\lambda_{ds} = i_{ds}(L_{ls} + L_{md}) + i_{fd} L_{md} \quad (6)$$

$$\lambda_{os} = i_{os} L_{os} \quad (7)$$

$$\lambda_{fd} = i_{fd}(L_{lfd} + L_{md}) + i_{ds} L_{md} \quad (8)$$

where,

L_{ls} = the leakage component of the total q and d-axis inductances (H),

L_{mq} = the magnetizing component of the q-axis inductance (H),

L_{md} = the magnetizing component of the d-axis inductance (H) and

L_{lfd} = the field leakage inductance referred to the stator (H).

The equivalent q-axis, d-axis and zero sequence circuits implied by (1)-(4) are shown in Figure 2.

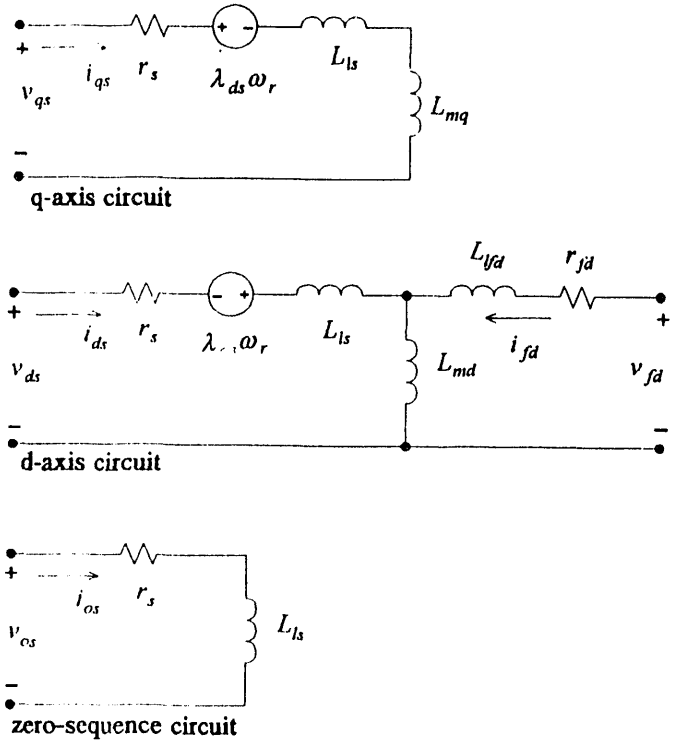

Figure 2. Equivalent Circuit of the LLSM With the Reference Frame Fixed in the Rotor

To obtain the state equations we re-express (1)-(4) in terms of flux linkages per second (ψ), replacing flux linkages (λ). This modification allows the currents i_q, i_d, i_o and i_{fd} to be expressed in terms of flux linkages per second and reactances (rather than inductances). The flux linkages per second linking a winding are defined as $\psi = \omega_b \lambda$ (Wb-t/sec), where ω_b is the base electrical radian frequency used to calculate the machine reactances. With these changes, (1)-(4) become:

$$v_{qs} = i_{qs} r_s + \frac{\omega_r}{\omega_b}\psi_{ds} + \frac{p}{\omega_b}\psi_{qs} \quad (9)$$

$$v_{ds} = i_{ds} r_s - \frac{\omega_r}{\omega_b}\psi_{qs} + \frac{p}{\omega_b}\psi_{ds} \quad (10)$$

$$v_{os} = i_{os} r_s + \frac{p}{\omega_b}\psi_{os} \quad (11)$$

$$v_{fd} = i_{fd} r_{fd} + \frac{p}{\omega_b}\psi_{fd} \quad (12)$$

The flux linkages per second may now be expressed in terms of inductive reactances instead of inductances. The flux linkages per second appearing in (9)-(12) are given as:

$$\psi_{qs} = i_{qs}(X_{ls} + X_{mq}) \quad (13)$$

$$\psi_{ds} = i_{ds}(X_{ls} + X_{md}) + i_{fd} X_{md} \quad (14)$$

$$\psi_{os} = i_{os} X_{ls} \quad (15)$$

$$\psi_{fd} = i_{fd}(X_{lfd} + X_{md}) + i_{ds} X_{md} \quad (16)$$

where,

$$X_{ls} = \omega_b L_{ls} \quad (17)$$

$$X_{mq} = \omega_b L_{mq} \quad (18)$$

$$X_{md} = \omega_b L_{md} \quad (19)$$

$$X_{lfd} = \omega_b L_{lfd}. \quad (20)$$

III. Rotary Machine State Space Model

Equations (9)-(12) may be put into state space form by solving for the $p\psi$ terms, and eliminating the currents by expressing them in terms of flux linkages and reactances. The voltage terms are retained as inputs. Using (13)-(16), the currents may be expressed as:

$$i_{qs} = \frac{\psi_{qs}}{(X_{ls} + X_{mq})} \quad (21)$$

$$i_{ds} = \left(\frac{X_{fd}}{X_{fd}X_d - X_{md}^2}\right)\psi_{ds} - \left(\frac{X_{md}}{X_{fd}X_d - X_{md}^2}\right)\psi_{fd} \quad (22)$$

$$i_{os} = \frac{\psi_{os}}{X_{ls}} \quad (23)$$

$$i_{fd} = \left(\frac{X_d}{X_{fd}X_d - X_{md}^2}\right)\psi_{fd} - \left(\frac{X_{md}}{X_{fd}X_d - X_{md}^2}\right)\psi_{ds} \quad (24)$$

defining,

$$X_q = X_{ls} + X_{mq}$$

$$X_d = X_{ls} + X_{md}$$

$$X_{fd} = X_{lfd} + X_{md}.$$

Substituting (21)-(24) into (9)-(12) and solving for the $p\psi$ terms:

$$p\psi_{qs} = \omega_b v_{qs} + (\frac{-r_s \omega_b}{X_q}) \psi_{qs} + (-\omega_r) \psi ds \quad (25)$$

$$p\psi_{ds} = \omega_b v_{ds} - (\frac{X_{fd} r_s \omega_b}{X_{fd} X_d - X_{md}^2}) \psi_{ds} + (\frac{X_{md} r_s \omega_b}{X_{fd} X_d - X_{md}^2}) \psi_{fd} + \omega_r \psi_{qs} \quad (26)$$

$$p\psi_{os} = \omega_b + (\frac{-r_s \omega_b}{X_{ls}}) \psi_{os} \quad (27)$$

$$p\psi_{fd} = \omega_b v_{fd} - (\frac{X_d r_{fd} \omega_b}{X_{fd} X_d - X_{md}^2}) \psi_{fd} + (\frac{X_{md} r_{fd} \omega_b}{X_{fd} X_d - X_{md}^2}) \psi_{ds} \quad (28)$$

Equations (25)-(28) are the flux linkage state equations for the rotating synchronous motor.

To complete the model, an equation of motion is needed to express the angular acceleration of the rotor in terms of the total mechanical inertia and the accelerating torque. This relationship is:

$$T_e = -J(\frac{2}{P}) p\omega_r + T_l \quad (29)$$

where,

P = number of field poles on the rotor

J = mechanical inertia of the rotor and load (kg-m^2)

T_e = electromagnetic torque (N-m)

T_l = load torque (N-m).

The corresponding state space equation is:

$$p\omega_r = (\frac{-P}{2J}) T_e + (\frac{P}{2J}) T_l \quad (30)$$

To put (30) into final state space form, T_e must be expressed in terms of the state variables. For the model developed here, the electromagnetic torque may be expressed as:

$$T_e = (\frac{3P}{4})[\frac{\psi_{ds} i_{qs}}{\omega_b} - \frac{\psi_{qs} i_{ds}}{\omega_b}] \quad (31)$$

Substituting the expressions for i_{qs} and i_{ds} from (21) and (22) into (31), T_e may be expressed as:

$$T_e = \frac{3P}{4}[(\frac{1}{\omega_b X_q} - \frac{X_{fd}}{\omega_b (X_{fd} X_d - X_{md}^2)}) \psi_{ds} \psi_{qs} + (\frac{X_{md}}{\omega_b (X_{fd} X_d - X_{md}^2)}) \psi_{qs} \psi_{fd}] \quad (32)$$

Substituting (32) into (30) for T_e, the following fifth state equation is obtained:

$$p\omega_r = [\frac{-3P^2}{8J}(\frac{1}{\omega_b X_q} - \frac{X_{fd}}{\omega_b (X_{fd} X_d - X_{md}^2)})] \psi_{ds} \psi_{qs} + [\frac{-3P^2}{8J}(\frac{X_{md}}{\omega_b (X_{fd} X_d - X_{md}^2)})] \psi_{qs} \psi_{fd} + (\frac{P}{2J}) T_l \quad (33)$$

The position of the rotor with respect to the synchronously rotating stator field is generally of interest when simulating the response to a load disturbance, although this position is not an essential state variable. With δ_r being defined as the angular difference between the rotor and the synchronously rotating stator field, a sixth state equation for δ_r is written in terms of ω_r (rad/sec) (the rotor electrical speed) and ω_e (rad/sec) (the electrical speed of the synchronously rotating reference frame).

$$p\delta_r = \omega_r - \omega_e \quad (34)$$

Although δ_r is now included as the sixth state variable in the machine model, it is important to note that the dimension of the system is only five. Equations (25)-(28) and (33) represent the complete state space model for the rotating synchronous machine. Equation (34) is included so that the position of the rotor may be viewed as an output.

IV. Conversion to *Linear* Motor Equations

The conversion to the linear machine equations is accomplished through a simple substitution of all rotating machine variables by linear machine variables. Specifically, all angular velocities (rad/sec) are replaced with linear velocities (m/s), all angular positions (rad) are replaced by linear positions (m), and all torques (N-m) are replaced by linear forces (N). Thus the complete state space model for the LLSM is given below, wherein all rotating machine variables have been replaced by their linear counterparts:

$$p\psi_{qs} = (\frac{\pi v_b}{\tau}) v_{qs} + (\frac{-r_s \pi v_b}{\tau X_q}) \psi_{qs} + (\frac{-\pi v_r}{\tau}) \psi_{ds} \quad (35)$$

$$p\psi_{ds} = (\frac{\pi v_b}{\tau}) v_{ds} - (\frac{X_{fd} r_s \pi v_b}{\tau (X_{fd} X_d - X_{md}^2)}) \psi_{ds}$$

$$+\left(\frac{X_{md} r_s \pi v_b}{\tau(X_{fd} X_d - X_{md}^2)}\right)\psi_{fd} + \left(\frac{\pi v_b}{\tau}\right)\psi_{qs} \quad (36)$$

$$p\psi_{os} = \left(\frac{\pi v_b}{\tau}\right)v_{os} + \left(\frac{-r_s \pi v_b}{\tau X_{ls}}\right)\psi_{os} \quad (37)$$

$$p\psi_{fd} = \left(\frac{\pi v_b}{\tau}\right)v_{fd} - \left(\frac{X_d r_{fd} \pi v_b}{\tau(X_{fd} X_d - X_{md}^2)}\right)\psi_{fd}$$
$$+\left(\frac{X_{md} r_{fd} \pi v_b}{\tau(X_{fd} X_d - X_{md}^2)}\right)\psi_{ds} \quad (38)$$

$$pv_r = \left[\frac{-3P^2\tau^2}{8\pi^2 J}\left(\frac{1}{v_b X_q} - \frac{X_{fd}}{v_b(X_{fd} X_d - X_{md}^2)}\right)\right]\psi_{ds}\psi_{qs}$$
$$+\left[\frac{-3P^2\tau^2}{8\pi J}\left(\frac{X_{md}}{v_b(X_{fd} X_d - X_{md}^2)}\right)\right]\psi_{qs}\psi_{fd}$$
$$+\left(\frac{P\tau^2}{2J\pi^2}\right)F_l \quad (39)$$

$$pd_r = v_r - v_e \quad (40)$$

where,

v_b = base vehicle speed = $\left(\frac{\tau}{\pi}\right)\omega_b$ (m/s)

v_r = actual vehicle speed = $\left(\frac{\tau}{\pi}\right)\omega_r$ (m/s)

v_e = mech. synchronous speed = $\left(\frac{\tau}{\pi}\right)\omega_e$ (m/s)

F_l = load force = $\left(\frac{\pi}{\tau}\right)T_l$ (N).

V. Circuit Parameters in Terms of Motor Geometry and Airgap

Work by I. Boldea and S. A. Nasar has generated a detailed set of relations which may be used to express the reactances appearing in the above state space model in terms of the motor geometry and the width of the air gap [3], [4], [5].

The magnetizing reactance along the d-axis, X_{dm}, models the induced voltage in the d-axis circuit due to all flux that crosses the airgap along the direct field winding axis and is expressed analytically as follows:

$$X_{md} = \frac{6\mu_0 \omega_b l_e \tau}{2\pi^2 g K_c} P K_{md} \quad (41)$$

where,

μ_0 = permeability of a vacuum = $4\pi \cdot 10^{-7}$ (H/m)

ω_b = base electrical frequency = $2\pi f_b$ (rad/sec)

l_e = motor width in transverse direction (m)

τ = motor pole pitch (m)

g = airgap width under pole shoes neglecting armature slotting (m)

P = number of field poles on the translator

K_c = Carter's Coefficient for armature slotting

$$K_{md} = 4\int_0^{\tau_p/\tau} \cos^2\left(\frac{\pi x}{\tau}\right) d\left(\frac{x}{\tau}\right)$$

where, τ_p = pole shoe length (m).

The magnetizing reactance along the q-axis, X_{mq}, models the induced voltage in the q-axis circuit due to flux that crosses the airgap along the quadrature axis, and is analytically expressed as:

$$X_{mq} = X_{md}\frac{K_{mq}}{K_{md}} \quad (42)$$

where,

$$K_{mq} = 4\int_0^{\tau_p/\tau} \sin^2\left(\frac{\pi x}{\tau}\right) d\left(\frac{x}{\tau}\right).$$

More details on the calculation of K_c, K_{md} and K_{mq} are given in [3] and [4].

The leakage reactance, X_{ls}, of the LLSM may be viewed as being composed of three components [3].

$$X_{ls} = X_a + X_{as} + X_e \quad (43)$$

The first of these components, X_a, is the armature reaction reactance, and is directly analogous to the armature reaction reactance in a rotating synchronous machine. The stator currents in the machine will produce a magnetic field of their own which interacts with the main flux field produced by the field magnets. X_a models the change in induced voltage as the net flux density under the field poles changes due to armature current. X_a may be expressed as:

$$X_a = \mu_0 \omega_b [(\beta_c + \beta_d) l_e + \beta_e(\tau + 0.06)] P \quad (44)$$

where, β_c = slot leakage specific permeance

$$= \frac{h_s}{3w_s} + \frac{h_{s1}}{w_s}$$

β_d = differential leakage specific permeance

$$= \frac{5g/w_s}{5 + (4g/w_s)}$$

β_e = end connection specific permeance

≈ 0.6 for typical LLSM construction

where, w_s = slot width (m)

h_s = winding height in each slot (m)

h_{sl} = total slot height minus h_s (m).

The physical definitions of w_s, h_s and h_{sl} are shown in Figure 3.

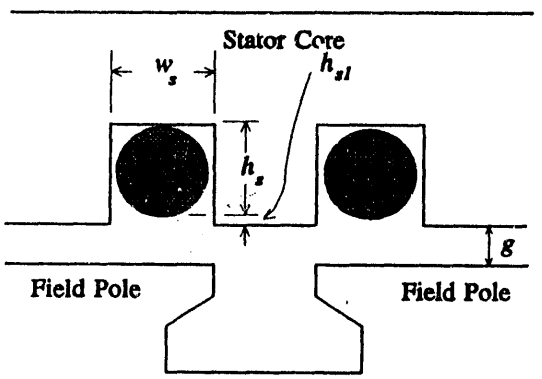

Figure 3. Definition of Dimensions for Calculation of Specific Permeances

More information on calculation of the specific permeances is available in [5].

The second of these components, X_{as}, represents the leakage reactance due to slots and end turns where the translator is not present, and may be expressed as:

$$X_{as} = \mu_0 \omega_b [\beta_c l_e + \beta_e (\tau - 0.06)](P' - P) \quad (45)$$

where, P' = number of energized stator poles per guideway segment.

The third component, X_e, represents leakage flux paths below the guideway where the translator is not present, and may be expressed as:

$$X_e = \frac{6\mu_0 \omega_b l_e \tau}{2\pi^2 (\tau/\pi)} (P' - P) \quad (46)$$

It is worth noting that (46) is very similar in form to (41). Equation (46) gives the reactance due to all of the stator poles ($(P' - P)$ in number) whose mmf does not have a closed magnetic circuit through the field poles. Also note that the g term in (41) is replaced by τ/π in (46), where τ/π is the equivalent airgap seen by the LLSM armature coils when the translator is not present.

The total leakage reactance of the armature windings plays a much greater role in the LLSM than in a rotating synchronous motor. The long length of energized guideway extending beyond and before the translator causes the X_{as} and X_e terms to dominate the LLSM leakage reactance. This model assumes that the leakage reactance of the field winding, X_{lfd}, is negligible. However an expression could easily be developed to analytically express X_{lfd} if it was inappropriate to neglect it in a particular design.

The resistance r_s appearing in (35)-(37) is analytically expressed as:

$$r_s \approx \frac{\rho(\tau + l_e + 0.06)P'}{A} (\Omega) \quad (47)$$

where,

ρ = conductivity of the armature conductor material (Ω/ m),

A = cross-sectional area of the armature conductors (m^2)

The resistance of the field winding referred to the stator is expressed in a similar manner:

$$r_{fd} = \frac{\rho_{fd} l_{fd}}{N_{fd}^2 A_{fd}} (\Omega) \quad (48)$$

where,

ρ_{fd} = conductivity of the field conductor material (Ω/ m),

l_{fd} = total length of the field conductor (m),

A_{fd} = cross-sectional area of the field conductors (m^2),

N_{fd} = number of field winding turns.

It is important to note that all of the parameter expressions given in this section assume only one turn per stator pole.

VI. Conclusion

A general dynamical model for an LLSM is needed in order to analytically represent and simulate an LLSM of many specific designs. Such an analytical state space model has been developed in this paper. The approach used has been to begin with a rotor referenced rotary machine model in which time varying inductances (reactances) become time invariant, and to write rotary machine equations in applied voltages, currents and flux linkage per second. This representation has been transformed to state space form. From state space form the rotary machine equations have been transformed to linear

machine form. Finally the equation reactance and resistance parameters have been related directly to the linear motor geometric parameters, including the airgap explicitly.

This model provides a convenient LLSM dynamical model which can represent many specific design configurations. The state space equations may be per unitized to any convenient voltage and MVA base to facilitate digital computer simulation for any size LLSM. It can also be utilized to analyze airgap variations including both deterministic and stochastic airgap disturbances. Finally, it can form the basis of control analysis and design for the LLSM.

References

[1] R. H. Park, "Two Reaction Theory of Synchronous Machines - Generalized Method of Analysis - Part I," *AIEE Trans.*, Vol. 48, July 1929, pp. 716 - 727.

[2] P. C. Krause, *Analysis of Electric Machinery*, McGraw-Hill, 1986, pp. 133 - 160.

[3] I. Boldea and S. A. Nasar, *Linear Motion Electromagnetic Systems*, John Wiley and Sons, 1985, pp. 307 - 331.

[4] S. A. Nasar, *Handbook of Electric Machines*, McGraw-Hill, 1987, pp. 7.28 - 7.38.

[5] S. A. Nasar and I. Boldea, *Linear Electric Motors - Theory, Design, and Practical Applications*, Prentice - Hall, 1987, pp. 91 - 108.

Maglev Position Sensing and Control

Tracy M. Clark
Massachusetts Institute of Technology
Laboratory for Electromagnetic and Electronic Systems
Cambridge, MA 02139 USA

Abstract - **This paper describes techniques and an architecture that may be suitable for use in controlling the propulsion motor of a magnetically levitated vehicle system. The control system utilizes an observer to estimate the electrical position of the vehicle, based on both back EMF measurements and an alternative scheme that is capable of reliable operation at slow vehicle speeds.**

I. Introduction

The propulsion system described is based on a linear synchronous motor with a multi-phase stator winding located within the guideway and a constant rotor field excitation (which may be implemented as a set of superconducting coils) located within the vehicle [9]. A chopper and a set of inverters drive the stationary windings of the motor with variable frequency, variable magnitude waveforms [8]. This stator drive produces a magnetic field pattern that moves along the guideway as a travelling wave. The velocity and position of the travelling wave are determined by the frequency and phase of the currents driven through the motor windings. The interaction of the travelling magnetic field pattern produced by the windings (the stator field) and the field produced by the permanent magnets located in the vehicle (the rotor field) results in a propulsive and/or a lifting force on the vehicle [1].

The control architecture described in section II is hierarchical in nature, and assumes that wayside electronics control the LSM (*i.e.* the vehicle is 'passive'). The guideway is divided into a large number of zones, each of which contains the power electronics, sensing system, and control hardware necessary to propel a vehicle along the guideway with the desired velocity profile. A communication bus connecting each zone controller with its nearest neighbors is necessary to facilitate a coordinated passing of vehicle control from one zone controller to the next as the vehicle crosses a zone boundary. An additional communication network links a number of zone controllers with a central controller. Each zone controller is responsible for the control of only a single vehicle. The central controller coordinates the movements of many vehicles, and provides to each zone controller the proper velocity profile for the vehicle within its zone boundaries.

The hardware used to implement a zone controller is described in section III. The vehicle position sensing system is made up of several layers of sensing mechanisms, including optical and/or Hall effect sensors, sensing the back EMF induced in the stator windings by the moving rotor (vehicle) field, and a novel scheme employing a vehicle-mounted driver that induces position dependent signals in the stator windings. The zone control algorithms are implemented digitally with a microprocessor. An observer based control architecture is utilized to provide a robust and flexible controller. This architecture could also be extended to provide adaptive control strategies as well as condition and fault monitoring capabilities [2].

II. Control Architecture

A hierarchical control architecture is depicted in the block diagram of Fig. 1. The central controller is the top-level controller for a region of guideway, and this computer-based controller's function is to coordinate the global movement of all vehicles within the region. The central controller computes the desired velocity profile for all vehicles within its jurisdiction based on status information received from the zone controllers, other central controllers, weather reports, scheduling reports, track condition reports, etc... The velocity profile commands for each vehicle are sent to the appropriate zone controller.

Zone Controller

The zone controller implements the low-level control functions necessary to operate the propulsion motor. Each zone controller is responsible for sensing the position and velocity of a vehicle within its zone boundaries, and computing the stator drive necessary to force the vehicle to follow a defined velocity profile. The zone controller must communicate with neighboring zone controllers to facilitate a coordinated pass-off of control as a vehicle crosses a zone boundary. Each zone controller sends status information to and receives instructions from a central controller.

Manuscript received March 15, 1993. This work was supported by the National Maglev Initiative, the Department of Electrical Engineering at MIT, and the Laboratory for Electromagnetic and Electronic Systems at MIT.

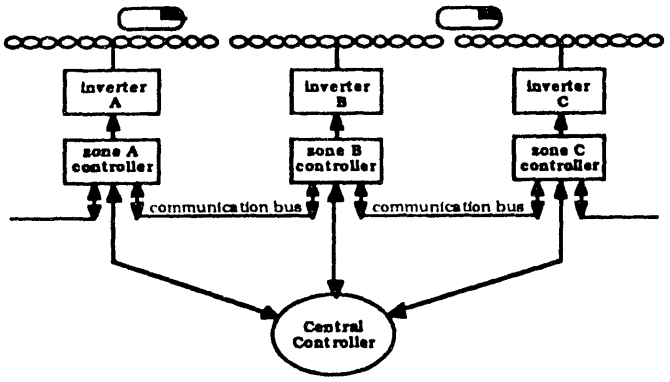

Fig. 1 Hierarchical control architecture

Velocity Control Loop

The zone controller's velocity control loop is shown as a block diagram in Fig. 2. The P-I compensator, the observer, the commutation algorithm, and a portion of the position sensing calculation are all implemented digitally. (A demonstration system has been developed using a Motorola 68HC16 micro-controller.) The digital implementation provides a flexible platform that can be extended to allow sophisticated features such as adaptive control, parameter estimation, or condition monitoring [2].

The controller utilizes a linear state observer to compute the vehicle velocity based on position measurements [3]. Discrete-time filter techniques could be used instead of an observer to derive velocity information. There are, however, some disadvantages associated with the filter technique. Substantial low-pass filtering is necessary to reject position sensor noise, and the dynamics of the low-pass filter degrade the performance of the velocity control loop. In addition, the filter design is complicated by the nonlinear, periodic nature of the sensed position. (The electrical position has a discontinuity, or wrap-around, at a position of 2π.)

The desired velocity profile Vref is a function of position to allow speed changes for hills, turns, stations, etc..., as well as weather or traffic conditions. Specification of the appropriate velocity profile is the responsibility of the central controller.

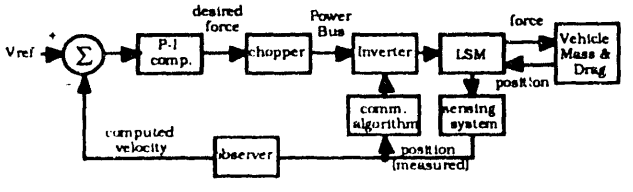

Fig. 2 Block diagram of velocity control loop

III. Position Sensing

A synchronous motor produces a constant force only when the stator and rotor fields are stationary with respect to one another (*i.e.* the stator field is synchronized with the rotor field). The dynamics of the 'hunting transient' associated with small perturbations from synchronous operation can be extremely underdamped or even unstable [4]. Either damper windings or a feedback controller may be used to stabilize the dynamics of the hunting transient. The use of damper windings precludes operation of the motor at the most efficient (maximum torque per amp) torque angle [1]. For this reason a feedback controller is employed, and it requires motor position and velocity information. A sensing system is necessary to measure the position of the rotor. (Some systems also use a rotor velocity sensor, others derive velocity information from repeated sensing of position.) Rotary synchronous motors often utilize optical shaft encoders or hall-effect sensors to determine the rotor position. The cost associated with placing optical or hall-effect position sensors along the entire length of the MagLev guideway would be prohibitive. Several 'sensorless' position sensing schemes have been proposed for use in rotary machines [5,6], these schemes rely upon sensing the amount of back EMF induced in the stator windings by the moving magnetic field of the rotor. The back EMFs are substantial when the rotor velocity is large, and reliable sensing is possible. However, when the rotor is moving slowly (or stationary) the back EMFs are small (or non-existent), and reliable sensing via back EMF information is not possible.

An alternative position sensing mechanism that will operate reliably at slow vehicle speeds is required. The proposed system works in the following manner. An inductor located on the vehicle is driven with a sinusoidal current. The flux through this inductor links with the stator windings in the guideway, the amount of mutual coupling between the inductor and each of the stator phases is a function of the vehicle position. The position of the vehicle is determined by measuring the amount of signal energy coupled into each of the stator phases. This sensing scheme will work at any vehicle speed since it does not rely on movement of the rotor field to link a time-varying magnetic field with the stator windings.

Electrical Position and Mechanical Position

For the MagLev linear motor, the electrical (or relative) position of the rotor is expressed as an angle (in radians or degrees), and is used to control the commutation of phase voltages or currents. The mechanical (or absolute) position of the rotor is expressed as a distance (in meters or kilometers), and is used to determine the velocity profile of

the vehicle and to coordinate the 'hand-off' of the vehicle from one section of track to another. The relationship between electrical and mechanical position is shown in Fig. 3. The period of an electrical cycle corresponds to a one wavelength change in the mechanical position.

The mechanical position is deduced by counting the number of periods of electrical position from a mechanical position reference. Mechanical position references are obtained by using Hall-effect or optical position sensors placed at regular intervals along the guideway (at zone boundaries). The mechanical position counter is reset when the vehicle passes by a mechanical position reference sensor.

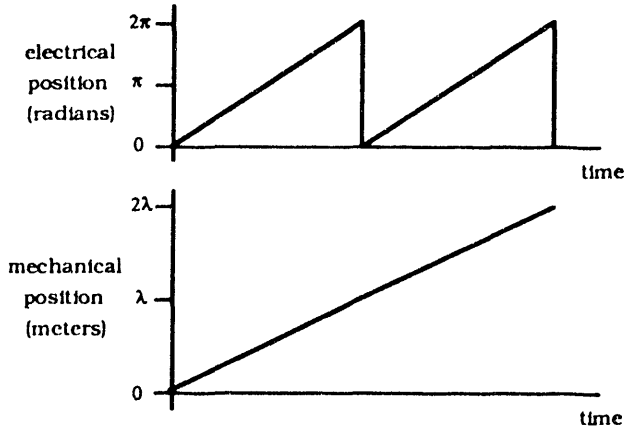

Fig. 3 Comparison of electrical and mechanical position

Back EMF Sensing

This form of position sensing is often referred to as 'sensorless' in the literature, and has been successfully employed in the control of rotary machines [5,6]. The concept is briefly presented here to demonstrate how it might be incorporated into a MagLev system.

The flux from the permanent magnets in the vehicle links with the stator windings, thus movement of the vehicle induces a voltage in the stator windings. This induced voltage is often referred to as a 'back EMF' or a 'speed voltage'. The back EMF is periodic and has a waveshape, $\mathcal{G}(\theta)$, that depends on many details of the motor design geometry (pole shape and pitch, winding shape, etc...). $\mathcal{G}(\theta)$ can be determined experimentally, computed using finite-element methods, or estimated using approximate calculations [7]. $\mathcal{G}(\theta)$ is often represented as a Fourier series, and the fundamental component of the series usually dominates. The magnitude of the back EMF is proportional to the vehicle speed. The back EMF induced in each phase is of the form:

$$\begin{aligned} E_{phaseA} &= \mathcal{G}(\theta)\cdot\mathcal{K}_v\cdot v \\ E_{phaseB} &= \mathcal{G}(\theta-2\pi/3)\cdot\mathcal{K}_v\cdot v \\ E_{phaseC} &= \mathcal{G}(\theta+2\pi/3)\cdot\mathcal{K}_v\cdot v. \end{aligned} \quad (1)$$

The induced back EMF cannot be measured directly due to the voltage drops associated with the stator current flowing through the resistance and inductance of the stator windings. However, by measuring both the stator voltage and stator current, the induced back EMF can be determined:

$$\mathbf{e} = \mathbf{v} - (s\mathbf{L} + \mathbf{R})\cdot\mathbf{i}. \quad (2)$$

where **e** is the vector of induced EMFs, **v** is the vector of phase voltages, **i** is the vector of phase currents, **L** is the motor inductance matrix, and **R** is the motor resistance matrix.

Normalization to remove the velocity-dependent magnitude of **e** is accomplished via division by $\mathcal{K}_v$ and the (estimated) velocity. The position measurement is the value of θ that best fits the measured data:

$$\begin{aligned} \theta &= \mathcal{G}^{-1}(E_{phaseA}/(\mathcal{K}_v\cdot v)) \\ \theta &= \mathcal{G}^{-1}(E_{phaseB}/(\mathcal{K}_v\cdot v)) + 2\pi/3 \\ \theta &= \mathcal{G}^{-1}(E_{phaseC}/(\mathcal{K}_v\cdot v)) - 2\pi/3. \end{aligned} \quad (3)$$

Finding the best fit value θ^* is somewhat complicated since the function $\mathcal{G}^{-1}$ is both nonlinear and multiple-valued. The algorithm implemented in a laboratory test system solves for θ^* by first calculating both possible values of θ for each of the three equations in (3). ($\mathcal{G}^{-1}$ is two-valued for the laboratory test motor.) Eight sets of θ values are formed by grouping one of the two θ values from each of the three equations in (3). The average of each set is calculated, resulting in eight candidate values for θ^*. The candidate θ^* associated with the set that has the smallest variance is chosen as the best fit value θ^*.

Alternative Position Sensor

An alternative (electrical) position sensing concept is pictured in Fig. 4. The inductor and its driver are located in the vehicle. The inductor is driven with a current $I_L = I_O \mathrm{Sin}\,\omega_C t$, which links a flux $\Phi_L = \Phi_O \mathrm{Sin}\,\omega_C t$ with the phases of the stator winding located in the guideway.

The amount of flux linked by each of the stator phases varies as a function of vehicle position, $\mathcal{F}(\theta)$. The function $\mathcal{F}(\theta)$ is periodic, and is similar to the waveshape $\mathcal{G}(\theta)$ associated with the back EMF. $\mathcal{F}(\theta)$ can be determined either analytically or experimentally.

Fig. 4 is drawn with the vehicle in the position that links the maximum possible amount of flux with stator phase A. We will define this position as having a value $\theta = 0°$. The voltage induced in each of the stator phases by the time-varying flux Φ_L is therefore (The $\mathcal{F}'(\theta)\cdot\mathrm{Sin}\omega_C t$ terms are neglected since $\omega_C >> \omega_{motor}$.) :

$$\begin{aligned} V_{phaseA} &= V_A\cdot\mathrm{Cos}\omega_C t = V_o\cdot\mathcal{F}(\theta)\cdot\mathrm{Cos}\omega_C t \\ V_{phaseB} &= V_B\cdot\mathrm{Cos}\omega_C t = V_o\cdot\mathcal{F}(\theta-2\pi/3)\cdot\mathrm{Cos}\omega_C t \\ V_{phaseC} &= V_C\cdot\mathrm{Cos}\omega_C t = V_o\cdot\mathcal{F}(\theta+2\pi/3)\cdot\mathrm{Cos}\omega_C t. \end{aligned} \quad (4)$$

Each of the phase voltages represents a signal at the carrier frequency ω_C amplitude modulated by the function $\mathcal{F}(\theta)$ (or $\mathcal{F}$ of θ shifted by a constant). The frequency of the carrier is chosen to be much higher than the fastest possible electrical frequency of the motor. Fig. 5 shows a plot of V_{phaseA} for a vehicle accelerating from a stationary position at $\theta = 0$. (For clarity, the modulating frequency ω_C has been reduced to a value of 10 Hz, instead of 25 kHz. The function $\mathcal{F}(\theta)$ is assumed to have only a fundamental component, *i.e.* $\mathcal{F}(\theta) = \mathrm{Cos}(\theta)$.) Fig. 6 shows the modulating signal V_A for the same vehicle run, note that V_A is the 'envelope' of the modulated waveform V_{phaseA}.

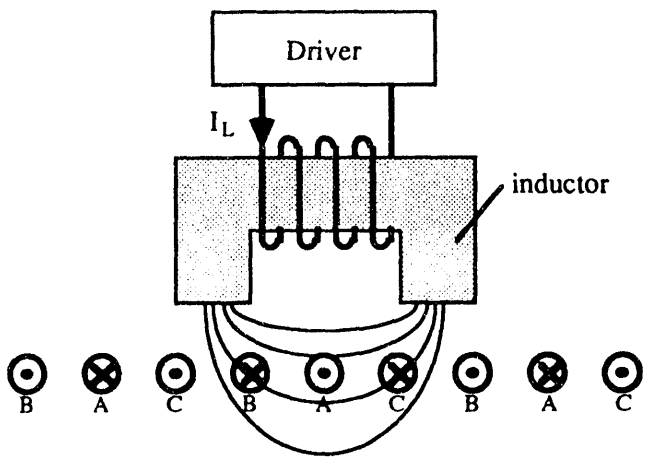

Fig. 4 Position Sensing Pictorial

Demodulating Hardware

A block diagram of the system to extract the position information from the modulated carriers present on the stator phase windings is shown in Fig. 7. Each phase voltage is first sent through a band-pass filter centered at the carrier frequency to reject signals other than the position information. A synchronous demodulator extracts the envelope waveform from each modulated carrier, and an A/D converter digitizes the envelopes. An algorithm implemented in a microprocessor determines the position of the vehicle by finding the value of θ that best solves the nonlinear system of equations:

$$\begin{aligned} \mathcal{F}(\theta) &= a \\ \mathcal{F}(\theta-2\pi/3) &= b \\ \mathcal{F}(\theta+2\pi/3) &= c. \end{aligned} \quad (5)$$

The best fit value θ^* is found in the same manner used with the position sensing system based on back EMF measurements.

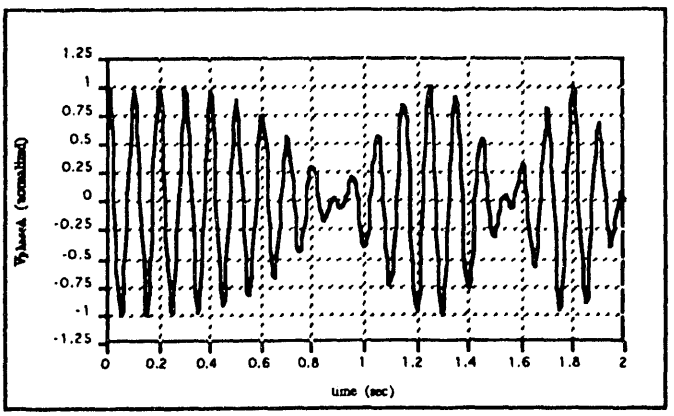

Fig. 5 Modulated carrier for accelerating vehicle

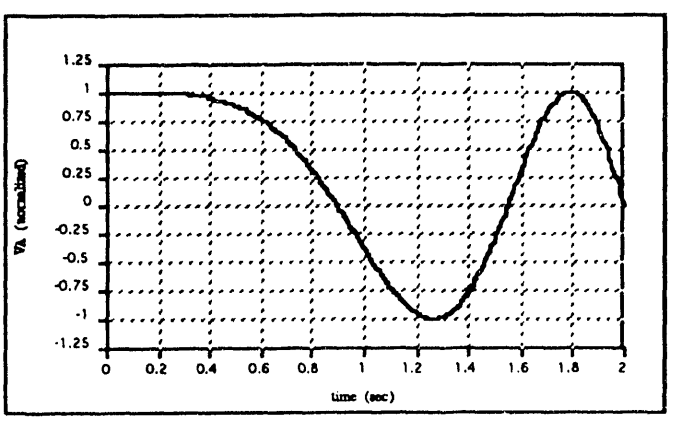

Fig. 6 Modulating signal for accelerating vehicle

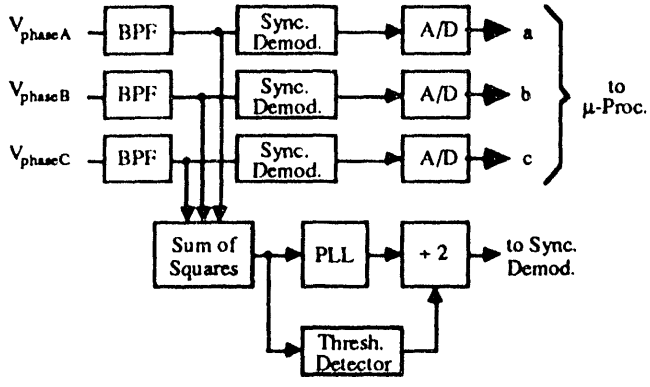

Fig. 7 Block diagram of demodulator circuitry

The synchronous demodulators must be clocked at the carrier frequency. Since an unmodulated carrier is not explicitly available, the carrier frequency must be reconstructed from information contained in the modulated carriers. This reconstruction is accomplished by phase locking an oscillator to the sum of the squares of the modulated carriers. The oscillator frequency is divided by two to obtain the reconstructed carrier. The reconstructed carrier may be either in phase or π radians out of phase with the original carrier. This half-cycle uncertainty is not resolvable without additional information from the modulating circuitry. A simple method of providing this additional information may be realized by occasionally blanking the carrier for exactly one cycle. The carrier would be as shown in Fig. 8. The demodulating circuitry detects the blank carrier cycle with a threshold detector and resets the ÷2 circuit, thus ensuring the proper phase relationship between the actual and reconstructed carriers.

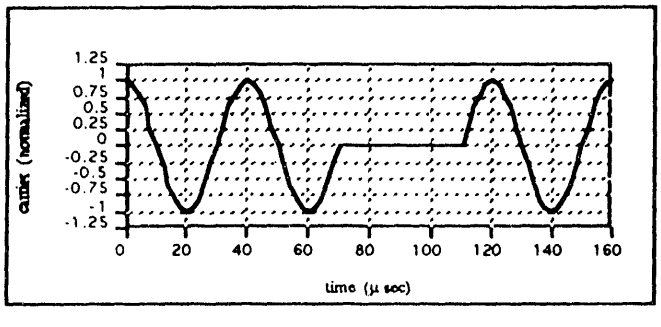

Fig. 8 25 kHz carrier with blank cycle

IV. Summary

A laboratory model of a vehicle system propelled by a LSM employing the control architecture and position sensing techniques outlined in this paper has been constructed, and initial test results are quite promising. The position sensing system is very robust and operates over vehicle speeds ranging from stationary to over 1.5 times the scale maximum design speed. The control loop can be configured either as a velocity servo (the normal cruising mode for a vehicle system), or as a positional servo (a mode which could be useful for stopping the vehicle at the proper location in a terminal). The accuracy of the sensed position is limited primarily by the slightly irregular spacing of the (hand-wound) stator windings, to an uncertainty of approximately 0.8mm (1/32 inch, or 7.5 electrical degrees). A new version of the LSM with a more precise (helically machine-wound) stator winding is currently under construction.

Acknowledgments

I would like to thank Prof. Richard Thornton and Dave Perreault of MIT for many suggestions and discussions pertaining to the material in this report and the development of the test system, Victor Liau of MIT for a lot of microcode programming in the test system, and the contract monitors from NMI, Ray Wlodyka and Frank Raposa.

References

[1] W.S. Brown, "A 1/25 Scale Magneplane", PhD Thesis, Oct. 1975, MIT Dept. of Elec. Eng., Cambridge, MA

[2] R.B. Sepe and J.H. Lang, "Real-Time Adaptive Control of the Permanent-Magnet Synchronous Motor", IEEE Trans. on Industry Applications, vol. 27 #4, 1991

[3] D.G. Luenberger, "Introduction to Dynamic Systems", John Wiley & Sons, 1979

[4] G.C. Verghese, J.H. Lang, and L.F. Casey, "Analysis of Instability in Electrical Machines", IEEE Trans. on Industry Applications, vol IA-22, #5, 1986

[5] A. Lumsdaine and J. Lang, "State Observers for Variable Reluctance Motors", IEEE Trans. on Industrial Electronics, vol. 37 #2, 1990

[6] L.A. Jones and J. Lang, "A State Observer for the Permanent-Magnet Synchronous Motor", IEEE Trans. on Industrial Electronics, vol. 36 #3, 1989

[7] R.D. Thornton, D. Perreault, and T. Clark, "Linear Synchronous Motors for MagLev", DOT/FRA/NMI-92/13, Jan. 1993

[8] D.J. Perreault and R.D. Thornton, "Power Electronics for Linear Synchronous Motor Propulsion Systems", Maglev '93, in press

[9] R.D. Thornton, "Linear Synchronous Motor Design", Maglev '93, in press

Methanol Reforming PEM Fuel Cells as an Onboard Power Source for Maglev Vehicles

Brian T. Concannon
Electro-Motive Division, General Motors Corporation, LaGrange, IL 60525

Abstract - **The application of a proton exchange membrane fuel cell and an integral methanol reformaer is considered in this paper with regard to the maglev vehicle design of the Bechtel system concept definition (SCD). A companion paper [2] describes many different ways of producing electrical power for a maglev vehicle's onboard electrical power requirements. The power being discussed is not that which propels the maglev vehicle but merely runs its onboard loads such as lights, galleys, heating, air conditioning, hydraulics, air compressors, and so on. The evaluations of the various alternatives is presented in [2], but the detailed desription of the fuel cell alternative is contained herein.**

Some of the discussion and the design requirements mentioned in this paper are based on the Bechtel SCD only.

1. Introduction

Fuel cells operate by electrochemically bonding hydrogen and oxygen, which creates electricity with water as a by-product. However, it is not necessary to use hydrogen directly. The proposed system begins with methanol as its fuel, uses steam to crack small volumes of it at any one time into hydrogen gas, and then combines the hydrogen with oxygen from the air to create electricity and water. This has the advantage of not having to carry hydrogen and/or oxygen tanks on-board. Instead, the much less volatile methanol can be used. Although hydrogen can also be used as a fuel directly, we feel that overcoming the ubiquitous though probably unjustified public perception of hydrogen as a "dangerous" fuel is a battle that we do not want to fight in this particular effort.

General Motors Corporation will deliver a 10 kw fuel cell system to the Department of Energy, Electric and Hybrid Propulsion Division, Office of Transportation Technologies, under contract DE-AC02-90CH10435 approximately in March, 1992. The prime contractor is Allison Gas Turbine Division of GM ("AGT"), with participation by General Motors Research Laboratories, AC-Rochester Division of GM, Los Alamos National Laboratory, Dow Chemical Company, and Ballard Power Systems. Dr. Howard Creveling is the program manager at AGT, and the COTR (Contracting Officer's Technical Representative) at the DOT is Dr. Pandit G. Patil.

The subject fuel cell is actually a "stack" of individual cells. To achieve the 186 kw needed for the maglev vehicle's auxiliary power, a stack of 36 of these cells would be needed. A series connected arrangement of cells would give a 756 volt, 250 amp DC power source. By slightly chopping down the voltage and passing the power through a set of inverters, the fuel cells would supply the main 440 volt vehicle AC lines. This can be done with readily available commercial equipment. Our implementation is actually to use two independent fuel cell systems, following our philosophy to use dual systems where weight is not increased much by doing so. Should one fuel cell system fail, the remaining fuel cell can run continuously at 30 percent overload (though at not-so--desirable fuel efficiency) to power all of the vehicle loads, though at slightly reduced capacity. This is a distinct advantage for this approach. A boost converter would be part of the inverter so that the 440 volt bus can be powered from half the normal dc input voltage.

The fuels cells operate at 80 degrees Celsius. This is a very manageable temperature, unlike the case of more primitive fuel cells which require temperatures of up to 1000 degrees Celsius. The warm-up time for the fuel cells is only a few seconds, more than fast enough for use aboard the maglev vehicle. The only instance in which a fuel cell has a longer warm-up time is when it is starting cold. This added delay comes from heating the water into steam which is used to crack the methanol into hydrogen. The fuel cell design team is confident that they will be able to obtain a seven second delay from cold start to full output. However, on a maglev vehicle the only "cold" period will be when the vehicle is first starting out for a day's service, so a slightly longer delay will not cause a problem.

2. Size/weight considerations

The projected system, which includes the fuel cell and the methanol processor, has a density of 556 kg/m^3. This is broken down as follows:

- Volume: 0.003684 m^3/kw (271 kw/m^3)
- Mass: 2.05 kg/kw

These numbers are optimistic for the present day fuel cell. The fuel cell which is the subject of the DOT contract

mentioned above may miss the above design goals by about 33 percent, but with the development time available for a maglev system, the design goals would almost certainly be reached, according to the program manager at AGT.

With the subject fuel cells, it is possible to obtain better efficiency by running the cells at less than their full load. A 70% load is very efficient for the proposed system. At 70% of the continuous load capacity the fuel cell runs at 51% thermal efficiency, much better that the 34% efficiency tuypical of state of the art spark ignition engines. At fully rated load the fuel cell runs at 38% thermal efficiency, increasing the fuel cost per kwh by 34%. This, together with the fact that it is beneficial in some situations to have a 30% load capability cushion, caused us to decide to run the fuel cells at 70% of their load capacity at 186 kw onboard power demand. Running at this 70% load, to create 186 kw the system will have a mass of

- 186 kw x 2.05 kg/kw ÷ 70% = 545 kg

and require

- 186 kw x 0.003684 m^3/kw ÷ 70% = 0.979 m^3.

At a 70% load, the fuel cells consume .409 kg/kwh. The following chart shows the weight the fuel adds (+10% fuel tank weight) based on the recharge period. The density of methanol is 797 kg/m^3. If the fuel is only changed once a day, then the recharge amount would be equivalent to 16 operating hours out of each 24 hour day. However, all that is required to recharge the system is to refill the methanol tank. It may then prove economical to have a shorter recharge interval. Recharging would then be done at end stations after passengers unboard the vehicle.

The price of methanol is difficult to establish. We have obtained estimates ranging from 30 cents per gallon (in California, where the price is regulated) to $1.48 per gallon. (Sorry for the nonmetric units...) If we assume a price of $1.00 per gallon ($0.33 per kilogram), the daily fuel cost works out to be 1344*$0.33 = $443/day. The cost of providing the power via the linear synchronous motor, at 100 percent transfer/conversion efficiency, would be 186 kw times 16 hours/day times $0.085/kwh or $253 per day, or a difference of at most $190/day. We use the term "at most" to remind the reader that the 186 kw load is for extreme weather conditions and the highest speed, so the usual power system load will be only about 110 kw. The difference in operating cost then gets to be in the neighborhood of only $112 per day.

Recharge Period	Mass of Fuel and Tank
2 hours	168 kg
4 hours	336 kg
8 hours	672 kg
16 hours	1344 kg

The total mass for a fuel cell/fuel supply system with an eight hour recharge period would be 1217 kg. This is a low weight system for the power that is being created. In addition, if fuel cells are used, most of the emergency batteries that had been planned for can be removed to save even more on weight. Fuel cells would also be more useful in an emergency situation than the emergency batteries as they would allow full power to be maintained, whereas the emergency batteries would only have the power capacity to maintain 5 kw of selected emergency loads for just one hour. Clearly, this is a major advantage of the fuel cell approach and actually is a factor that provides a safer vehicle in non threatening stopped emergency conditions. With batteries only supplying emergency power, passenger evacuation would be a likely event in many cases, and evacuation itself can lead to injuries. Keeping the passengers comfortable within the vehicle and not evacuating them is safer.

3. Further safety considerations

The fly in the ointment regarding selection of a fuel cell system for onboard vehicle power is the fact that methanol fueling the fuel cell must be stored on board, increasing the possibility of a fire. This consideration is inescapable. Methanol is less likely to ignite than gasoline, diesel fuel, or jet fuel, but still it will burn if lit accidentally, even though it burns slower and cooler than the other fuels mentioned. Precautions would be taken to provide accident-resistant double or triple-walled storage tanks located sensibly and distributed in multiple locations with check valves in the lines to reduce the amount of fuel provided to any fire. Of course, the lines themselves and their associated fittings are sources of fuel leaks, so a tradeoff study would involve this leak consideration as well.

If there were a simple way to change the methanol or impregnate it into some carrier to make it less flammable or even inflammable, then the electric vehicle program would have incorporated such technology, but such is not the case. The methanol tanks on our vehicle are located between the fuel cell proper and the spherical hydrogen dewar in the fore equipment compartment, providing protection from puncture in a collision. The nose of the vehicle will also be engineered to collapse in a vehicle collision and absorb crash energy, further reducing the probability of puncture of the tank. Of course, total commitment to crash avoidance via a properly engineered and operated control

system would be the major line of defense against collision-induced fires, but total reliance upon crash avoidance would not be a wise engineering approach.

The fire hazard problem must be approached from several directions:

- Resistance of the storage tanks to puncture
- Location/distribution of the storage tanks to minimize the fire hazard
- Resistance of the lines and fitting to leaks
- Provision of check valves to avoid "gushing" spills to a fire
- Keep the leaks/spills away from the passenger compartment
- Provide moats and drains with sensors to detect leaks or spills
- Provide a water-flushing system to dilute spills and leaks
- Provide a video camera in the fore equipment compartment for visual inspection
- Provide an automated, tamper-resistant, spill-resistant filling system
- Provide fire extinguishing equipment of the proper type, reliability, number, and location
- Refill the methanol tanks at more frequent intervals in order to reduce the amount of fuel on board.
- Include methanol fire considerations in the vehicle evacuation plan

The Bechtel team is not burying its head in the sand about this safety issue, but feels that overall, when all the considerations are taken into account, the safety hazard is small enough that it does not overshadow the previously discussed advantages of the fuel cell approach. By highlighting this issue here, and openly discussing the fire hazard issue, we hope that our decision to put a flammable liquid on board our vehicle will be met with understanding. Automobiles, aircraft, diesel locomotives, power boats and lawn mowers carry flammable liquids too, and the associated hazards have become accepted parts of everyday life. Were they not, automobiles and aircraft and locomotives and power boats and lawn mowers would differ greatly from their present embodiments. Our emphasis on crash avoidance via the control system will greatly reduce the safety impact of onboard fuel.

References:

1. Bechtel Corporation, Maglev SCD Final Report, September 30, 1992, Volume I, pages C-1 to C-121.

2. B.T. Concannon, "Onboard Power Source Alternatives for Maglev Vehicles", 12th International Conference on Magnetically Levitated Systems and Linear Drives, Argonne National Laboratory, May 19-21, 1993 (companion paper)

Onboard Power Source Alternatives for Maglev Vehicles

Brian T. Concannon
Electro-Motive Division, General Motors Corporation, LaGrange, IL 60525

Abstract - **This paper describes several different ways of producing electrical power for a maglev vehicle's onboard electrical power requirements. The power being discussed is not that which propels the maglev vehicle but merely runs its onboard loads such as lights, galleys, heating, air conditioning, hydraulics, air compressors, and so on. The evaluations contained herein relate to a 186 kilowatt onboard power system for the maglev vehicle of the Bechtel System Concept Definition, or any maglev vehicle with a similar power requirement. The choice of a three phase, 440 volt ac onboard power system for that particular vehicle concept does not significantly influence the selection of the power source type.**

Arriving at the final selection required weighing several alternative methods and selecting the best alternative. Substantial information is presented about the alternatives in [3] and is summarized in this paper.

Some of the discussion and design requirements mentioned in this paper are based on the Bechtel SCD only.

Introduction

Some options for providing onboard power for a maglev vehicle include the following:

1 Energy storage
2 Power cable link
3 Sliding electrical contact
4 Linear generator
5 Linear transformer/inductive pickup
6 Wind turbine
7 Engine generator set
8 Fuel cells

Each option has both benefits and drawbacks. These options, with their respective benefits and drawbacks, are discussed below. Please note that the fuel cell option has been selected for our baseline vehicle design, and all information about the alternative choices is presented in order to document our work and to put our choice of fuel cells in the proper perspective.

1. Energy Storage

A number of possible approaches which have been considered but quickly eliminated from consideration rely upon their initial energy content to provide continuous onboard power over a three hour period without energy transfer from the guideway. The approaches include inductive energy storage (SMES), capacitive storage, battery storage, mechanical storage (springs, flywheels), thermal energy storage, and compressed/liquefied air. None of these technologies provide the required energy storage capacity within reasonable weight or volume limitations. The stored energy required to meet the needs of one maglev trip is formidable. The following calculation shows how the energy requirement for a three hour trip is established:

186 kw x 1000 watts/kw x 3 hours x 3600 sec/hr = 2.008E+9 joules per trip, or 2 gigajoules / trip

Fuel-based power sources are not included in this stored-energy category of onboard power sources even though stored chemical energy might be considered to fall into this category; fuel-based onboard power systems of several types are considered in upcoming paragraphs.

Table 1 shows the masses derived from reference 1 for several of the stored energy systems that were considered. The numbers apply to energy storage and conversion systems for in-field military applications. Alternatives other than those listed in reference 1 were considered as well. Rough calculations give the results in table 2 for three additional alternatives:

Incidentally, fuel cell parameters in ref[1] imply an onboard power system with a mass of 2000 kg and a

TABLE 1
ESTIMATES PER REF [1]

Description	Mass, kg	Volume, m^3
Flywheel in vacuum chamber	20,000.	5.
Magnetic/Inductive (SMES type)	200,000.	20.
Capacitive	4,000,000.	2,000,000,000.
Batteries	20,000.	N/A

TABLE 2
ESTIMATES FOR ADDITIONAL ENERGY SOURCE TYPES

Description	Mass, kg	Volume, m^3
Compressed/Liquefied Air	45,000.	485.
Springs	506,000,000.	64,516
Thermal Energy (Heated H_2O)	31,000.	8.

volume of 2 cubic meters. Advances in cell technology since [1] was written in 1989 have changed the picture for fuel cells. The fuel cell system that was eventually selected for our maglev vehicle has a mass of 1210 kg and a volume of 1.74 cubic meters.

2. Power cable link

Another approach to generating onboard power would be to utilize magnetic fields from the high voltage +/-15 kvdc power cables that run from one inverter to another. The present plan is to bury these cables or run them beneath the guideway beam, but we did consider running them on top of the guideway beam (protected, of course) in order to create an onboard power source. Obviously it is tricky to mount 15 kv equipment on the beam The cables forming this power cable link could alternatively be specialized, extra dc cables at very low voltage whose sole function is to create onboard power. Such a dedicated arrangement would effectively be a weak "inductive pickup" system.

The cables would be located in the magnetically neutral plane in the center of guideway. The cables would crisscross every quarter meter (0.25 m) as illustrated in Fig. 1. The calculations for the power cable link that are found in the appendix to [3] are generous approximations and simplifications for calculating the field and induced voltage in the coils. Many refinements could be made; however, the computations give a good indication of the unfeasibility of this concept.

The calculated voltage per turn (84 millivolts) on the vehicle pickup coil is a weak voltage level. The resulting projected mass of the vehicle coils is 29,110 kg. Not only is this too heavy, but the space required for this much copper wire simply is not available. And all this is at the vehicle speed of 150 m/s; lower speed operation gives proportional reductions in capacity. For these reasons we dropped consideration of the power cable link approach to onboard power generation.

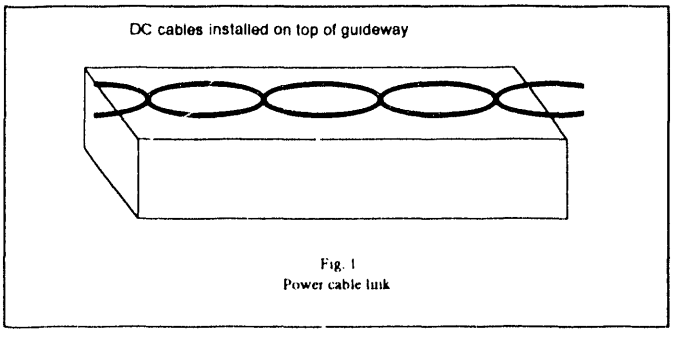

Fig. 1
Power cable link

3. Sliding Electrical Contacts

It would be possible to transfer auxiliary electrical power into the maglev vehicle via a third rail, catenary, or other frictional sliding arrangement. Though ugly to behold, these approaches are commonly used for transferring propulsion power to transit cars and electric passenger locomotives, so the mere 186 kw power requirement is not a limitation on such an approach. There are several other obvious factors that take precedence, as follows:

- Transferring power at the full vehicle speed of 500 kph makes the approach different from its present applications. It would be expected that at such a high speed, the pickup equipment on the vehicle and the guideway would wear out quickly.

- At 500 kph, maintaining contact between vehicle and guideway halves of the pickup would be difficult. If occasional bouncing of the pickup could be tolerated, then the associated wear problems are aggravated, and electromagnetic interference (EMI) problems become more severe.
- Safety concerns of such an approach are heightened. One way to mitigate this is to choose as low a voltage as possible, placing more emphasis on the current collection design of the pickup equipment as opposed to the voltage design factors.
- The cost of this approach is high because pickup equipment must be provided on virtually the entire guideway length.

Some of these concerns could be lessened if the vehicle were not required to pickup power at full speed, but only up to some fraction of full speed instead. For the sake of discussion, let us assume that the sliding contact approach is used up to 350 kph, and above that speed the pickup mechanism on the vehicle is lifted or otherwise physically disconnected from its guideway counterpart. Most likely batteries would be employed to run the onboard power system above 350 kph, which does have merit in the case of a system which closely follows an interstate highway and therefore goes up and down in speed often in order to go around the many associated curves. The resulting dependence upon batteries would increase vehicle weight and thereby further increase system cost. In addition, the amount of power transfer must necessarily increase, and the batteries must be able to take a very, very fast charge during the power transfer times. This approach cannot be entirely discounted without in-depth study of hybrid systems, but we regard this approach as unviable due to the many obvious technical headaches associated with it.

4. Linear Generator

The linear generator in the context of this paper is a device which uses the currents induced in the levitation ladder rungs on the guideway for producing onboard power. In concept, the currents in the stationary ladder rungs produce a varying magnetic field with respect to the moving vehicle, due both to the variations in the current with time and the changes in the rung-to-generator-coil proximity as the vehicle moves past the ladder. This magnetic field is linked by simple nonrotating coils of copper wire on the linear generator mounted on the maglev vehicle. As the magnetic field varyies with currents in the ladder rungs and by the varyiation of distance of the coils from the rungs, changing flux linkages induce voltage in the pickup coils of the linear generator. This voltage would be fed into a rectifier/inverter for use on the vehicle.

No additional equipment would be required on the guideway or on the ground; the present ladder arrangement would provide the onboard power, almost for free. There is no such thing as "free power", though. The onboard power would be derived indirectly from the linear synchronous motor which would have to overcome the increased drag due to the linear generators; however, this would be an extremely economical way to pickup the onboard power because the LSM power only costs 8.5 cents per kilowatt hour in this SCD.

It is envisioned that there will be one linear generator in each space between each pair of bogies for a total of ten units as shown if Fig. 2. The dimensions for each unit, containing many power pickup coils each, would be 90 cm high, 60 cm wide, and 9 cm thick. An individual pickup coil was sized at 30 cm high by 9 cm deep. These dimensions were chosen based upon the physical space available between the bogies, the size of the levitation ladder and the desire to have the linear generator as close as possible to the ladder.

An analysis was performed by calculating the pickup coil flux linkages at many positions along the ladder. The rung currents were assumed to be varying per the results of a dynamic circuit analysis of the magnets and ladders as the pickup coil and vehicle positions changed. This required a substantial amount of work in order to include the effects of both time variation of current and position variation of the pickup coil simultaneously. The average pickup coil voltage was predicted to be about 1 mv per turn, showing that the extraction of sufficient power from the levitation ladder would be difficult at best.

Fig. 2
Side view of Linear Generator Location

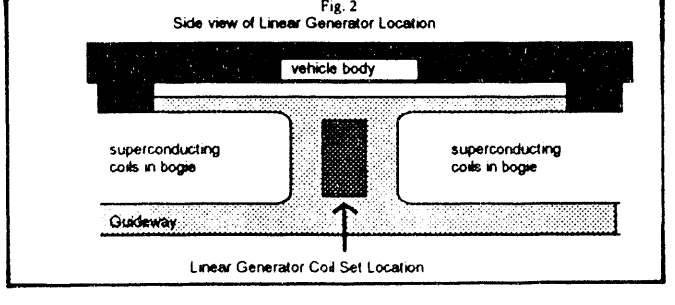

5. Linear Transformer

A transformer in its commonest, stationary form transfers power from one side of an electrical circuit ("the primary side") to another side of an electrical circuit ("the secondary side"), with an associated and desired change of voltage taking place as well. The linear transformer for maglev applications would be employed not so much because a transformer can change voltage levels, but because it transfers power from one place to another. The linear transformer for maglev would have its primary circuit laid out along the entire guideway, being fed power by wayside inverters specially built for the onboard power requirement alone. The secondary circuit would be mounted on the vehicle very close to the primary circuit on the guideway. Physical contact between the two transformer halves is not necessary or desirable; magnetic fields working at a small distance are responsible for the power transfer.

There are several ways to arrange coils and cores to effect a linear transformer capable of transferring 186 kw of power. Engineering judgment was invoked to justify the configuration shown in Fig. 3. The ferrite core is molded into a rather flat channel. The cutout in the channel provides space for turns on the winding. Each primary turn runs completely down the channel for 25 meters (one concrete beam length), then returns along one of the outside edges. The width of the secondary core is closely allied to the width of the primary core, though its depth can be greater. Each secondary turn wraps around the 0.8 m long secondary core in a similar fashion to the primary winding. The secondary halves must be guided by a hydraulic or aerodynamic mechanism on the vehicle to maintain the small air gap between the primary and secondary halves.

Wherever the linear transformer would be located, it will not be pretty. We do keep the appearance of the guideway in mind, and placing electrical equipment on it will never improve its apperance. The appearance considerations are indirectly manifested in reliability issues in the sense that adding kilometer after kilometer of electrical equipment is more likely to have associated reliability and cost penalties, so one is well advised to keep the appearance issue in mind, whether artist or engineer or otherwise.

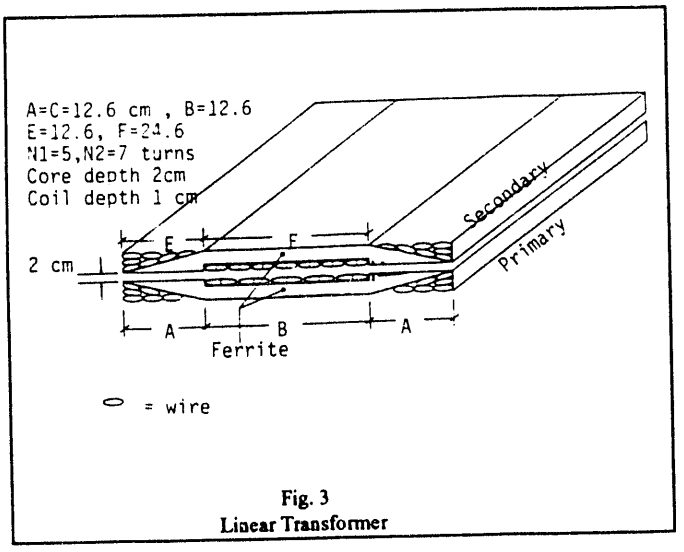

Fig. 3
Linear Transformer

A computer program was written to optimize the transformer parameters and dimensions. The optimization was done in a manner that maximized a figure-of-merit function based on power factor, cost, and output voltage. Cost was computed by multiplying raw material costs by a factor of four. Material costs were $3.31/kg for copper Litz wire for the windings and $7.00/kg for ferrite core materials. Not all design parameters and dimensions were allowed to vary during the optimization process. The air gap was fixed at 2 centimeters after realizing that the design was hopeless at the nominal 5 centimeter clearance used at all other places between the vehicle and the guideway. The final optimized design is shown in Fig 3, and the numerical listing of its performance parameters is:

- Cost per km $1.2 million
- Frequency 5862 Hz
- primary voltage 1528 volts
- primary amps 681
- primary power factor 0.24
- core dimensions: see Fig. 3

Its performance is poor due to the unavoidably large amount of leakage reactance. Leakage reactance is proportional to the length of the core, and the 25 meter length is so vast that the little can be done to reduce the leakage reactance. Using a shallow, wide cutout in the channel helps. So would using shorter core lengths, but this is impractical since the secondaries always span a total length of 24 meters and have to couple to active primary cores.

As it is, the vehicle would span two primary cores most of the time, so two primary sections always have to be energized. As the vehicle moves along, the proper primary cores would have to be switched in and out of the connection circuit to the inverters. This would severely and detrimentally impact the cost and reliability of the linear transformer system.

A most important result is the cost per km of the transformer itself. If we double the cost to include the inverter supplies and connection circuit costs, the result is 2.4 million dollars per kilometer, or almost 4 million dollars per mile. Clearly this is a cost prohibitive approach.

The inductive pickup approach is different from a linear transformer approach. The inductive pickup nomenclature implies a magnetic coupling of coils on the vehicle to dc magnets on the guideway. Relative motion of the vehicle's coils through the dc fields induces voltage in the vehicle that can provide for its onboard power. Although the operating principles are much different from those of the linear transformer, the type and amount of materials and labor to provide and inductive pickup system are probably quite similar. In the absence of the time required to do a conceptual design of an inductive pickup system, and with a myriad of configuration possibilites to be evaluated, we deferred to the design of the linear transformer and simply assumed that the costs would be (in the light of hindsight) similarly unacceptable. It should be noted that an inductive pickup system has a low speed power capacity problem, as the voltage induced in the vehicle coils is proportional to the vehicle speed.

6. Wind Turbine

When the maglev vehicle is traveling at a high enough velocity, it is possible to guide air to one or more wind turbine generators to provide onboard power for the vehicle. Our concept for this alternative power source would be to provide two streamlined ducts in the nose of the vehicle to feed a pair of wind turbines located in the fore equipment compartment. The low velocity ("spent") exhaust air would be ducted downward or sidewards to the exterior of the vehicle. Each turbine would have its own control subsystem to regulate its voltage and frequency (+/- 5 percent) via variable pitch blades. We would expect each generator driven by the turbines probably to be a lightweight synchronous generator.

The power indirectly must be supplied through the linear synchronous motor on the guideway. As a matter of fact, the wind turbine efficiency would only be about 62 percent. When combined with the generator efficiency of 0.9, the increase in linear synchronous motor power turns out to be 344 kw.

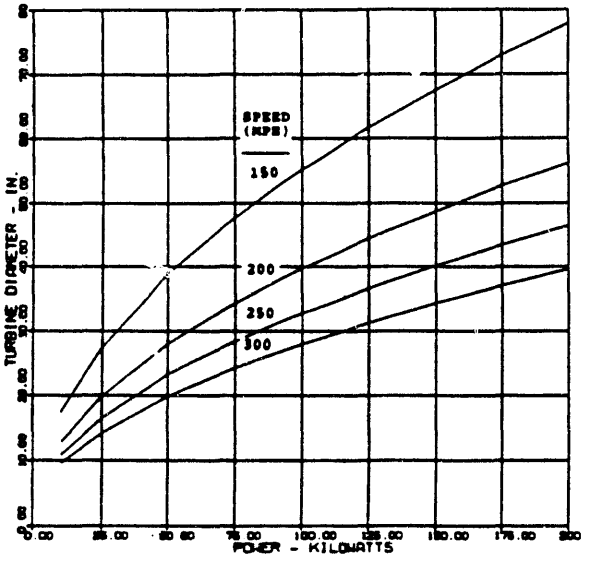

Fig. 4
Turbine diameter (in.) vs. Power and Air Speed

Estimates of turbine size and weight were provided by subcontractors at the University of Illinois via, the Sunstrand Corporation, a commercial supplier of ram air turbines. Sunstrand has provided a graph (see Fig. 4) of turbine size versus power and airspeed for two-bladed turbines. At 500 kph, a four bladed turbine would be more desirable and would reduce this diameter by 23 percent. In any event, the curve shows that at 93 kw each, the turbines would be 0.94 meters in diameter. Regarding the mass of each turbine, additional information from Sunstrand gives the following rules:

- Mass (kg) of turbine and strut=diameter in inches
- Mass (kg) of generator=power (kw)

The projected combined turbine/generator mass becomes .94*39.4+93=130 kg per unit. Clearly this is the smallest projected power source mass of any of the alternatives so far (and upcoming as well) and is a distinct advantage for this alternative.

The disadvantage of wind turbine generators is obvious: they lack power capacity at low vehicle speeds because the low air speed will not drive the turbines at full capacity. This requires the onboard batteries to be larger. In an emergency power situation where a maglev vehicle is stopped, the wind turbines are totally useless.

7. Engine Generator Set

Obvious options for an engine in an engine/generator set include:

- diesel internal combustion engine
- gasoline internal combustion engine
- jet-fueled aviation turbine
- other less common fuels driving either engine type

Each would have a 400 Hz three phase generator mated to it. Most likely, as with so many other systems in this SCD, two half-sized systems would be provided in order to provide redundancy and fault tolerance. No inverter would be required in such an approach because the rotating generator would provide the required power type directly at its terminals.

The aircraft turbine would be the lightest of these options. All would require a fuel tank for operation, as well as significant ancillary equipment. Although muffled, all would be noisy and would emit undesirable exhaust gases. These are major drawbacks to using engine/generator sets for the onboard power source. The great advantages of this option are the simplicity, absence of inverters, low cost, and the availability of full power at any vehicle speed.

8. Baseline Choice: Fuel Cells

Recent technological developments have made fuel cells a very attractive and practical power source alternative. While fuel cells have long been considered too bulky and costly for many practical uses, recent research by General Motors into fuel cell application on hybrid electric automobiles has made tremendous advances. The type of fuel cells proposed for maglev onboard use has been developed and tested in a GM test facility and is a viable application of present day, or at least foreseeable future, technology. This methanol-reforming PEM fuel cell is described in a companion paper [4].

9. Comparison of alternatives

Table 3 condenses some of the information from the foregoing text and the companion paper. The inclusion of a cost column in table 3 and the exclusion of a safety column does not imply anything about our emphasis, but instead merely shows that cost is more easily quantified than safety.

One of the advantages that has been somewhat of a "sleeper" is the emergency power capability. The ability of a power source to operate continuously in the event of total failure of the guideway electrical systems tempts one to speculate about driving the vehicle with one or more deployable dc motor-driven crawler devices if somehow the vehicle does not coast to a preferred stopping point.

The choice we made for our baseline maglev concept is the fuel cell, based on the advantages and disadvantages of all of the alternatives described in the text of this paper. Although a fuel cell of the type proposed has not been developed at the 186 kw level, we expect the development of this technology over the next few years, in parallel with a maglev system development effort, to achieve the projected weight, volume, and performance levels quoted in this paper. The presen performance of this fuel cell is not far from those levels, and development of the technology is already under way at GM relative to electric automobiles. If the safety issues of this fuel cell turn out to be addressable relative to automobiles, then they should certainly be addressable relative to maglev vehicles as well.

References:

1. Palmer, David N., "Downsized Superconducting Magnetic Energy Storage Systems, Proc. IECEC, Vol. 1, August 7-11, 1989, Table 6, page 456

2. J.L.He, D.M.Rote, and H.T.Coffey, "Computation of Magnetic Suspension of Maglev Systems Using Dynamic Circuit Theory", International Symposium on Magnetic Suspension Technology, NASA Langley Research Center, Hampton, VA, August 19-23, 1991

3. Bechtel Corporation, Maglev SCD Final Report, September 30, 1992, Volume I, pages C-1 to C-121.

4. B.T. Concannon, "Methanol Reforming PEM Fuel Cells as an Onboard Power Source for Maglev Vehicles", 12th International Conference on Magnetically Levitated Systems and Linear Drives, Argonne National Laboratory, May 19-21, 1993 (companion paper)

TABLE 3
COMPARISON OF ALTERNATIVE POWER SOURCES

Description	Advantages	Disadvantages	Capital Cost	Rating
Storage Approaches	No transfer mechanism required	Impractical	Various	last
Power Cable Link	Uses cables to meet more than one need	Insufficient power at lower speeds, dependence upon cable current level	High	7
Sliding Contacts	High capacity at any speed	Wearout, EMI, safety, appearance	High	6
Linear Generator	Low capital cost, reliable	Insufficient power at lower speeds	Low	5
Inductive Pickup	High capacity	Low capacity at low speed, appearance, unknown reliability	Very high	4
Linear Transformer	High capacity	Unknown reliability, appearance	Very high	4
Wind Turbine	Very lightweight, no inverter required	Low speed capacity	Low	3
Engine/ Generator	Simple, reliable, no inverter required	Fuel onboard, high operating cost, noise, vibration, pollution, weight	Low	2
Methanol-Reforming PEM Fuel Cells	Lightweight, noiseless, nonpolluting, overload capacity	Fuel onboard, higher operating cost	Low	first

Comparative Analysis of EDS and EMS Maglev Systems

Antonino Di Gerlando, Ivo Vistoli
Dipartimento di Elettrotecnica - Politecnico di Milano
Piazza Leonardo da Vinci, 32 - 20133 Milano, Italy

Marino Galasso
Ansaldo Trasporti
Viale Sarca, 336 - 20126 Milano, Italy

Abstract - In the present paper some elements of analysis of transportation MAGLEV systems driven by long stator linear synchronous motors are proposed.

Some basic comparative evaluations are performed, about active material quantities necessary for the armature (conductive, insulating materials) and energetic performances.

I. INTRODUCTION

The MAGLEV systems here examined are the EDS types, with repulsive levitation, equipped with superconducting (SC) field windings, and the EMS types, with attractive levitation, characterized by conventional field windings.

Aim of the paper is to perform a comparative analysis between the two systems, in order to evaluate, where possible in quantitative terms, the main structural and functional parameters: to this purpose, the peculiar features of the systems are briefly described.

In the EDS type, the structure includes, as known, a "U" shaped track fixed to the ground: at the sides of the track, the armature three-phase windings are disposed; in the Miyazaki test-track the levitation windings are arranged horizontally [1], while the levitation windings of the Yamanashi experimental track [2] are in lateral positions and have a "8" shape. The EDS vehicle is equipped with SC magnets, faced to the track windings; their functions are: linear synchronous motor (LSM) excitation, levitation and lateral guidance. As regards the last two functions, it is important to point out that the behavior of the EDS system is intrinsically stable: given any perturbation of the operation trim, the system reacts, by automatically generating suitable forces that restore the stable equilibrium. The distances between vehicle and track are of the order of hundreds of mm, both in vertical and horizontal direction: these distances, together with the intrinsic stability, are important elements for the system safety.

In the EDS vehicle, a linear synchronous generator (LSG) feeds both a battery and the on board loads, through some converters: the LSG armature conductors exploit the harmonic m.m.f.s generated by the stator armature or the levitation windings.

Also the basic structure of the EMS system includes a track fixed to the ground, but with shape and composition considerably different from the previous one, mainly for the arrangement of three-phase armature windings within a slotted ferromagnetic structure [3].

Manuscript received March 31, 1993.
Work supported by the Italian Research National Council (CNR) PFT2 Project; Contract N°92.01972.PF74.

The EMS type vehicle is equipped with electromagnets for the field excitation and for the lateral guidance: the field electromagnets are employed also for levitation, based on the electromagnetic attractive effect. Considering the intrinsic instability of this kind of levitation, a great importance is assumed by the feeding systems and active control of these electromagnets, also considering that in the EMS system the air-gaps are significantly lower than those of the EDS case, of the order of ten millimeters, both in vertical and horizontal direction.

The feeding of the on board loads is assured by a linear synchronous generator, whose armature conductors are arranged in the pole-pieces of the excitation-levitation system disposed on the vehicle; a feeding scheme similar to that of the EDS system can be adopted, connected at the LSG output terminals.

II. COMPARISON CRITERIA BETWEEN MAGLEV SYSTEMS

The considerable differences between EDS and EMS systems make difficult to find univocal criteria suitable to perform this comparison: the adopted methodology employs simplified models and partially refers to data of constructed (or being constructed) prototypes (Miyazaki [1], Yamanashi [2,4,5], Emsland [3]). In order to operate a homogeneous comparison, it is necessary to assume the equality of the following quantities:

- route length of the track;
- maximum speed;
- number of carried voyagers/(hour·direction);
- armature insulation class.

In general, these quantities are not the same in the mentioned systems: actually, only their basic features have been assumed, applying to them suitable variations for a homogeneous comparison.

For a better effectiveness, the comparison will employ p.u. quantities: as much as possible, all the quantities considered during the analysis will be expressed as ratios in which the values of the EDS system are referred to the corresponding values of the EMS system. Generally, the subscript "d" will mark the quantities of the EDS system, while the subscript "m" will be used for quantities of the EMS system; where necessary, the subscripts "d1", "d2", "dy" will mark quantities of the MLU001 and MLU002 Miyazaki prototypes and of the Linear express Yamanashi project respectively.

Among the parameters employed for the comparison, there are the following quantities:

- ratio between the flux density values:

$$K_B = \frac{B_d}{B_m} \quad ; \qquad (1)$$

- ratio between the rated thrusts:

$$K_F = \frac{F_d}{F_m} \quad ; \tag{2}$$

- ratio between the LSM polar pitches:

$$K_p = \frac{\tau_d}{\tau_m} \ . \tag{3}$$

The flux density values considered in (1) are spatial average values, calculated within the plane of the armature winding.
As known, in the EDS case the field near the SC coils is considerably higher than that in the proximity of the armature (B_d), because of the appreciable reciprocal distance and because the magnetic field develops totally in the air. Vice versa, in the EMS system the small air gap allows to simply refer to flux density, without further specifications.

As regards the ratio K_F between the thrusts, it is known that the drag force applied to the vehicle at high speeds (300÷500 km/h), is due to the air mainly, and depends on the vehicle front section, length and speed squared. This means that (being equal speed, shape and steady state running operation in plane) the vehicles should be thrust by the same propulsion force. On the other hand, the armature electric power input is converted not only into mechanical power, but also in electric power for the on board LSGs.
In the EDS system, the LSGs feed the cryogenic system and the on board auxiliary services only. Vice versa, in the EMS system the LSGs must feed also the field, levitation and guidance conventional coils.
Moreover, the EMS type train has a higher mass per unit length, due to the on board ferromagnetic material and the higher rating of the generation-conversion on board units: this requires a higher propulsive force along the track sections not in plane.
In conclusion, in the EMS system the LSM mechanical power must be higher than that of the EDS system and, correspondingly, the EMS rated thrust must be higher.

As regards the ratio K_p, it is directly linked to the different maximum frequencies for the feeding of the armature.

III. CHARACTERIZATION OF THE ARMATURE

In the following, some expressions involving the quantities of armature active materials of the different systems and their energetic quantities are obtained and analyzed.
It is clear the importance of this analysis: the characteristics of the armature, arranged all along the track, give a considerable contribution to the construction cost of the infrastructure and greatly affect the choices regarding the feeding devices and the system efficiency.

A. Armature conductive material

Let consider the armature phase winding of a generic MAGLEV system; the following quantities are defined:
- u: number of conductors per slot;
- ℓ: active length of every single conductor;
- q: number of slots per pole per phase;
- Γ_t: total length of the track;
- L_c: total length of the phase wire;
- a: number of parallel paths of each phase.

The length L_c of the phase armature wire of each MAGLEV system equals:

$$L_{cd} = \frac{u_d}{a_d} \cdot q_d \cdot \frac{\Gamma_t}{\tau_d} \cdot (\ell_d + \tau_d) \ ;$$
$$L_{cm} = \frac{u_m}{a_m} \cdot q_m \cdot \frac{\Gamma_t}{\tau_m} \cdot (\ell_m + \tau_m) \ . \tag{4}$$

Defined

$$K_s = \frac{\ell_d}{\ell_m} \ , \tag{5}$$

the ratio between the wire lengths becomes:

$$\frac{L_{cd}}{L_{cm}} = \frac{a_m}{a_d} \cdot \frac{q_d}{q_m} \cdot \frac{u_d}{u_m} \cdot \frac{K_s \cdot \ell_m + K_p \cdot \tau_m}{\ell_m + \tau_m} \cdot \frac{1}{K_p} \ . \tag{6}$$

Then, denoted with:
- p the total number of armature poles;
- U the total number of conductors in series per phase (for all the track length),

we have:

$$u = \frac{U \cdot a}{c/3} \ ; \quad \Gamma_t = \tau \cdot p \ ; \quad c = 3 \cdot p \cdot q. \tag{7}$$

Considering that:

$$\Gamma_t = p_m \cdot \tau_m = p_d \cdot \tau_d \ , \tag{8}$$

from (7) one obtains:

$$\frac{u_d}{u_m} = \frac{U_d}{U_m} \cdot \frac{a_d \cdot q_m}{a_m \cdot q_d} \cdot K_p \ . \tag{9}$$

By substituting (9) in (6) we have:

$$\frac{L_{cd}}{L_{cm}} = \frac{U_d}{U_m} \cdot \frac{K_s \cdot \ell_m + K_p \cdot \tau_m}{\ell_m + \tau_m} \ . \tag{10}$$

As known, on the basis of a power balance equation, the LSM thrust can be expressed in the following manner:

$$F = 3 \cdot E \cdot I \cdot \cos(\gamma) / v \ , \tag{11}$$

where:
- E and I are the e.m.f. and the current of one armature phase;
- γ is the angle between the phasors $\bar{I}$ and $\bar{E}$;
- $v = 2 \cdot f \cdot \tau$ is the vehicle speed.

Considering that:

$$E = \frac{\pi}{\sqrt{2}} \cdot f \cdot \Phi \cdot U_i \cdot k_w \ , \tag{12}$$

where k_w is the winding factor, U_i the number of conductors in series per phase faced to the inductor and $\Phi = B \cdot \tau \cdot \ell$ the flux of one pole, (11) becomes:

$$F = \frac{3 \cdot \pi}{2 \cdot \sqrt{2}} \cdot B \cdot I \cdot \cos(\gamma) \cdot \ell \cdot k_w \cdot U_i \ . \tag{13}$$

On the other hand, indicated with L_i the length of the track portion faced to the p_i inductor poles placed on the train, we have:

$$L_i = p_i \cdot \tau = \Gamma_t \cdot (U_i / U) \ . \tag{14}$$

By the ratio between the thrusts (13) of the two systems (with U_i expressed by means of (14)), one obtains the following expression of the ratio between the armature currents:

$$\frac{I_d}{I_m} = \frac{U_m}{U_d} \cdot \frac{K_F}{K_D} \cdot \frac{\ell_m}{\ell_d} \cdot \frac{\cos(\gamma_m)}{\cos(\gamma_d)} \cdot \frac{L_{im}}{L_{id}} \cdot \frac{k_{wm}}{k_{wd}} \ . \tag{15}$$

If we consider the same type of conductive material and an equal global thermal exchange coefficient, from the equality of the armature winding temperature rises one obtains:

$$S_m \cdot \Delta_m = S_d \cdot \Delta_d \ , \tag{16}$$

being S and Δ the superficial and linear current density respectively. Considering that Δ can be expressed as follows:

$$\Delta = \frac{3 \cdot U \cdot I}{\Gamma t} \quad , \tag{17}$$

the ratio between the densities S becomes:

$$\frac{Sd}{Sm} = \frac{\Delta m}{\Delta d} \cdot \frac{Um \cdot Im}{Ud \cdot Id} \quad . \tag{18}$$

By expressing the ratio of the wire sections Ac of every parallel path in the following manner:

$$\frac{Acd}{Acm} = \frac{Id}{Im} \cdot \frac{am}{ad} \cdot \frac{Sm}{Sd} \quad , \tag{19}$$

on the basis of (15) and (18) we obtain:

$$\frac{Acd}{Acm} = \left(\frac{KF}{KB} \cdot \frac{\cos(\gamma m)}{\cos(\gamma d)} \cdot \frac{\ell m}{\ell d} \cdot \frac{Llm}{Lld} \cdot \frac{Um}{Ud} \cdot \frac{kwm}{kwd} \right)^2 \cdot \frac{am}{ad} \cdot \frac{Ud}{Um} . \tag{20}$$

By inserting (10) and (20) in the expression of the ratio $\dot{Q}c$ between the volumes Qcd and Qcm of conductive material:

$$\dot{Q}c = \frac{Qcd}{Qcm} = \frac{ad}{am} \cdot \frac{Lcd}{Lcm} \cdot \frac{Acd}{Acm} \quad , \tag{21}$$

one obtains:

$$\dot{Q}c = \frac{Ks \cdot \ell m + Kp \cdot \tau m}{\ell m + \tau m} \cdot \left(\frac{KF}{KB} \cdot \frac{\cos\gamma m}{\cos\gamma d} \cdot \frac{\ell m}{\ell d} \cdot \frac{Llm}{Lld} \cdot \frac{kwm}{kwd} \right)^2 . \tag{22}$$

Eq.(22) can be simplified, by observing that:
- the two systems have approximately the same length ℓd and ℓm of the active conductors:

$$Ks = \ell d / \ell m \approx 1; \tag{23}$$

- by adopting the same control strategy of the LSMs, one can assume that:

$$\cos(\gamma d) \approx \cos(\gamma m) \; ; \tag{24}$$

- from the study of the levitation of the EMS system, it follows that:

$$\ell m \approx \tau m \; ; \tag{25}$$

- about the winding factors, we can assume:

$$kwd / kwm \approx 1 \; . \tag{26}$$

Given these hypotheses, eq.(22) becomes:

$$\dot{Q}c = \frac{Qcd}{Qcm} \approx \frac{1 + Kp}{2} \cdot \left(\frac{Llm}{Lld} \cdot \frac{KF}{KB} \right)^2 \quad . \tag{27}$$

In order to perform the quantitative analysis of (27), for now the following ratios are assumed:

$$KB = Bd/Bm \approx 1.2/0.6 = 2 \; ; \quad KF = Fd/Fm \approx 0.9 \; . \tag{28}$$

As regards the maximum output frequency of the converters, taking the experimental data as a starting point, we have:

Transrapid 06 (EMS, Emsland): 215 Hz
MLU001 (EDS, Miyazaki): 27 Hz
MLU002 (EDS, Miyazaki): 28 Hz
Linear express (EDS, Yamanashi [4,5]): 56.6Hz.

Therefore, we have the following Kp values:

$$Kp1 = \tau d1/\tau m = fm/fd1 = 215/27 = 7.96$$
$$Kp2 = \tau d2/\tau m = fm/fd2 = 215/28 = 7.68 \tag{29}$$
$$Kpy = \tau dy/\tau m = fm/fdy = 215/56.6 = 3.80 \quad .$$

The ratio between the inductor lengths (Lld/Llm) is an important parameter, as shown by its quadratic influence in (27): it has been considerably modified during the historical evolution of the MAGLEV systems. As a matter of fact, in the EMS system the presence of a ferromagnetic circuit allows the disposition of the field electromagnets all along the train, while the high values of the flux density in air in the EDS system obliged, in the subsequent projects, to concentrate the SC coils within the extreme positions of each coach [2], in order to extend the usable passenger zone immune from the fields.
Then, the following ratios can be assumed:

$$\text{MLU001: } Lld1/Llm = 1$$
$$\text{MLU002: } Lld2/Llm = 0.75 \tag{30}$$
$$\text{Linear express: } Lldy/Llm = 0.25 \; .$$

On the basis of (28), (29), (30), the values of the ratio $\dot{Q}c$ between the quantities of conductive materials, evaluated by (27), are:

$$\text{MLU001: } Qcd1/Qcm = 0.91$$
$$\text{MLU002: } Qcd2/Qcm = 1.56 \tag{31}$$
$$\text{Linear express: } Qcdy/Qcm = 7.78 \quad .$$

It must be noted again that the values given by (31) do not correspond completely to the experimental conditions, because only partial reference to the real parameters has been made for the homogeneous comparison.
Adopting again the first eq. of (28), fig.1 shows the ratio $\dot{Q}c$, for the three considered EDS systems, as a function of the ratio Kp.
It is evident the dramatic increase of the quantity of conductive material necessary when passing from a train of the Miyazaki type to that with an inductor of the Yamanashi type.
Moreover, the following remarks must be made:
- in case of a MLU001 train type, the quantity of conductive material is lower than that of the EMS system, for all the Kp values included in the utilizable range;
- in case of a MLU002 train type, the quantity of conductive material is lower than that of the EMS system for $Kp < 4.5$, that is for a frequency $fd > 47$ Hz (with $fm = 215$ Hz);
- in case of a train having the same ratio Lld/Llm of the Linear express, the quantity of the armature conductive material is always higher than that of the EMS system;

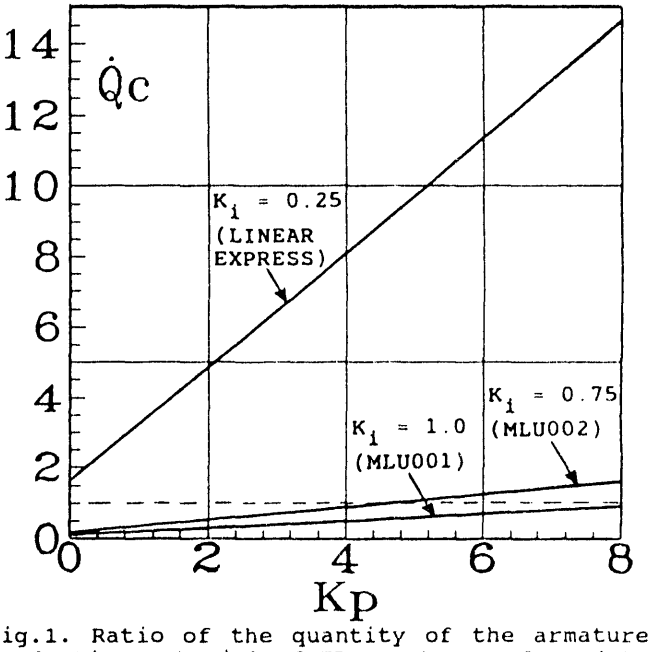

Fig.1. Ratio of the quantity of the armature conductive material of EDS systems referred to that of the EMS system ($\dot{Q}c = Qcd/Qcm$), as a function of the ratio between the corresponding polar pitches ($Kp = \tau d/\tau m$); parameter: $Ki = Lld/Llm$, ratio between the inductor lengths.

- by adopting for the EDS system the same maximum frequency of the EMS system (K_p=1), the values of the ratio $\dot{Q}_c$ are:

$$\dot{Q}_{c1} = 0.20; \quad \dot{Q}_{c2} = 0.36; \quad \dot{Q}_{cy} = 3.24 \ . \qquad (32)$$

Fig.2 shows, for MLU002 and Linear express type trains, how the ratio $\dot{Q}_c$ is modified when the flux density B_d increases (that is $K_B = B_d/B_m$ increases), being unvaried the other conditions of (28)÷(31).
The rise of the flux density can be obtained by one or more of the following ways:
- variation of the shape of the SC coils;
- increase of the SC current;
- reciprocal approaching between SC coils and armature windings.

Fig.2 shows that the rise of the flux density always implies a reduction of $\dot{Q}_c$. The amount of this reduction is higher in the Linear express type system; in case of K_p=1 (f_d =215 Hz) the condition $\dot{Q}_c$ = 1 occurs with K_B = 3.6 .

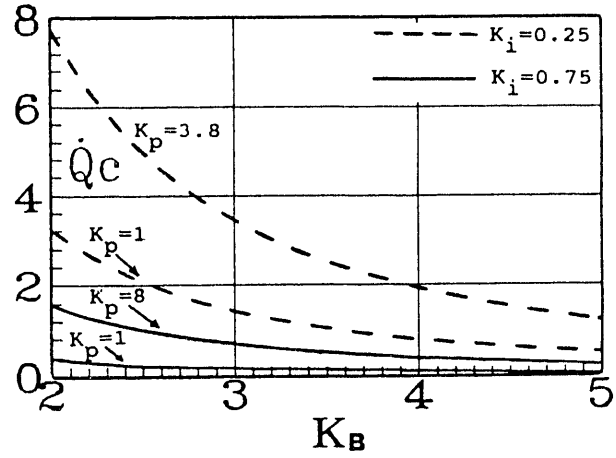

Fig.2. Ratio between the quantities of conductive material ($\dot{Q}_c=Q_{cd}/Q_{cm}$) as a function of the ratio between the average flux density within the armature plane ($K_B=B_d/B_m$); parameters: polar pitch ratio ($K_p=\tau_d/\tau_m$) and ratio between the inductor lengths ($K_l=L_{id}/L_{im}$).

B. Armature insulating material

Assuming that the insulating width of the wire is approximately proportional to the maximum feeding voltage (V_M), the ratio between the quantities of insulating material equals:

$$\dot{Q}_i = \frac{Q_{id}}{Q_{im}} = \frac{V_{Md}}{V_{Mm}} \cdot \frac{\mathcal{P}_d}{\mathcal{P}_m} \cdot \frac{L_{cd}}{L_{cm}} \ , \qquad (33)$$

where $\mathcal{P}$ is the perimeter of the single wire.

If we assume the same shape for the wire sections of the two systems, the perimeter ratio depends on the section ratio as follows:

$$\frac{\mathcal{P}_d}{\mathcal{P}_m} = \sqrt{\frac{A_{cd}}{A_{cm}}} \ . \qquad (34)$$

Thanks to (20) and (23)÷(26), eq.(34) becomes:

$$\frac{\mathcal{P}_d}{\mathcal{P}_m} = \frac{K_F}{K_B} \cdot \frac{L_{im}}{L_{id}} \cdot \sqrt{\frac{U_m \cdot a_m}{U_d \cdot a_d}} \ . \qquad (35)$$

As a first approximation one can assume:

$$\frac{V_{Md}}{V_{Mm}} \approx K_B \cdot \frac{U_d}{U_m} \ . \qquad (36)$$

Finally, on the basis of (10) and (35) and taking into account (36), eq.(33) becomes:

$$\dot{Q}_i \approx K_F \cdot \frac{L_{im}}{L_{id}} \cdot \frac{1 + K_p}{2} \cdot \left(\frac{K_V}{K_B}\right)^{3/2} \cdot \sqrt{\frac{a_d}{a_m}} \ , \qquad (37)$$

having put:

$$K_V = V_{Md}/V_{Mm} \ . \qquad (38)$$

A complete quantitative analysis of (37) would require to know the values of $K_V = V_{Md}/V_{Mm}$ and a_d/a_m. For the mentioned cases, the ratio K_V could be deduced from literature data (V_{Mm}=4.25kV; V_{Md1}=3kV; V_{Md2}=5.8kV; V_{Mdy}=29kV), while it would be difficult to deduce the values of the ratio between the number of parallel paths. But, in any case these values are not meaningful, because they belong to systems having different ratings, thus not suitable to a homogeneous comparison.
Considering that both these ratios represent, within certain limits, arbitrary design choices, for the analysis of (37) K_V will be assumed as a parameter and a_d/a_m will be supposed equal to unity. In these hypotheses, and assuming again the (28)÷(31), the ratio $\dot{Q}_i$ equals:

EDS type :	MLU001	MLU002	Linear express
$\dot{Q}_i/K_V^{3/2}$:	1.43	1.84	3.06

These values show that also the ratio of the quantities of insulating material is unfavorably affected by the reduction of the ratio L_{id}/L_{im}.
Figs.3.a,b show, for a Linear express type EDS system, how the ratio $\dot{Q}_i=Q_{id}/Q_{im}$ decreases when the ratio $K_B=B_d/B_m$ increases, considering $K_V=V_{Md}/V_{Mm}$ as a varying parameter, for two different values of the ratio $K_p=\tau_d/\tau_m$.

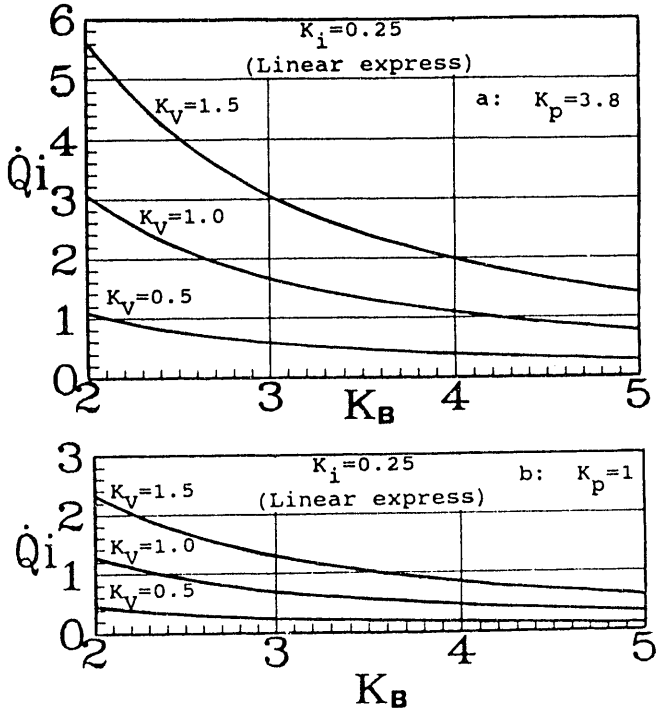

Fig.3. Ratio between the quantities of armature insulating material ($\dot{Q}_i=Q_{id}/Q_{im}$) as a function of the ratio between the average flux densities in the armature plane (K_B= B_d/B_m); parameter: ratio between maximum feeding voltages ($K_V=V_{Md}/V_{Mm}$); a: K_p=3.8; b: K_p=1.

By examining fig.3 one concludes that:
- an increase of K_B allows a discrete reduction of the insulating material quantity, at least in the first rising range of K_B;
- the reduction of K_P (associated to an increment of the maximum output frequency of the feeding converter) implies favorable effects on the reduction of the ratio Q_I;
- the increase of the ratio K_V implies a considerable increase of the ratio Q_I.

C. Armature magnetic material

The comparison between the two types of system is not homogeneous and it cannot be performed in quantitative terms: actually, the presence of SC field windings in the EDS case makes unnecessary the use of a ferromagnetic core, both with regard to armature and vehicle, while it is necessary to employ a ferromagnetic core in the EMS system.

On the other hand, the EDS system is characterized by the presence of some elements, that are absent in the EMS system:
- levitation coils, all along the track;
- suitable magnetic shields, disposed on the train for protection from fields.

D. Energetic characterization

A significant index of the system energetics is the armature efficiency: in the present analysis, all the power electromagnetically transferred from armature to vehicle is assumed to be useful power; therefore we have:

$$\eta = \frac{\text{Useful power}}{\text{Useful power + Armature losses}} \quad . \tag{39}$$

As regards the armature losses, only the armature wire Joule losses will be considered: doing so, there is a lack in the losses evaluation for both the types of system:
- in the EMS case, because the losses in the ferromagnetic material are not calculated;
- in the EDS case, because the losses in the levitation coils disposed all along the track are not considered.

On the other hand, in both the cases, these losses are practically concentrated along the track portion engaged by the train.
The calculation of the armature Joule losses must be performed with reference to the track sectors really fed: subdivided the total track length into a suitable number of adjacent sections, each having length Γ_s, the track segment really fed usually consists of two adjacent sections, the first of them being partially engaged by the train; then we have:

$$\Gamma_{ad} = 2\cdot\Gamma_{sd} \quad , \qquad \Gamma_{am} = 2\cdot\Gamma_{sm} \quad , \tag{40}$$

where:
- Γ_{sd} and Γ_{sm} are the length of each section, for the EDS and EMS systems respectively;
- Γ_{ad} and Γ_{am} are the corresponding fed segments of the track.

For each system, the length of the phase wire corresponding to the fed segments of the track can be expressed as follows (see (4)):

$$\begin{aligned} L_{ad} &= \frac{\Gamma_{ad}}{\Gamma_t}\cdot\frac{u_d}{a_d}\cdot q_d\cdot\frac{\Gamma_t}{\tau_d}\cdot(\ell_d + \tau_d) = \frac{\Gamma_{ad}}{\Gamma_t}\cdot L_{cd} \\ L_{am} &= \frac{\Gamma_{am}}{\Gamma_t}\cdot\frac{u_m}{a_m}\cdot q_m\cdot\frac{\Gamma_t}{\tau_m}\cdot(\ell_m + \tau_m) = \frac{\Gamma_{am}}{\Gamma_t}\cdot L_{cm} \end{aligned} \quad . \tag{41}$$

Therefore, indicated with

$$K_L = \Gamma_{ad}/\Gamma_{am} \tag{42}$$

the ratio between the fed segments of the track, the following relation is obtained:

$$\frac{L_{ad}}{L_{am}} = K_L\cdot\frac{L_{cd}}{L_{cm}} \quad . \tag{43}$$

Thus, on the basis of (10), (20), (42) and considering (23)÷(26), the ratio between the corresponding phase resistances equals:

$$\frac{R_d}{R_m} = \frac{L_{ad}}{L_{am}}\cdot\frac{a_m}{a_d}\cdot\frac{A_{cm}}{A_{cd}} \approx K_L\cdot\frac{1 + K_P}{2}\cdot\left(\frac{L_{id}}{L_{im}}\cdot\frac{K_B}{K_F}\cdot\frac{U_d}{U_m}\right)^2 \quad . \tag{44}$$

Finally, on the basis of (15), again considering (23)÷(26), the ratio between the armature Joule losses becomes:

$$\dot{P}_J = \frac{P_{Jd}}{P_{Jm}} = \frac{R_d}{R_m}\cdot\left(\frac{I_d}{I_m}\right)^2 \approx K_L\cdot\frac{1 + K_P}{2} \quad . \tag{45}$$

Eq.(45) shows that the ratio between the armature Joule losses depends on the ratio between the polar pitches (K_P) and on the ratio between the fed segments of the track (K_L).

Indicated with P_u the total useful power given by the LSM and with P_a the input power absorbed by the fed armature segments, we have:

$$P_a = P_u + P_J \quad . \tag{46}$$

Therefore, the efficiency of the EDS armature can be written as follows:

$$\eta_d = 1 - \frac{P_{Jd}}{P_{ad}} = 1 - \frac{1 + K_P}{2}\cdot K_L\cdot\frac{P_{Jm}}{P_{ad}} \quad . \tag{47}$$

Moreover, considering the following relations:

$$P_{ad} = \frac{P_{ud}}{\eta_d} \quad , \quad \frac{P_{ud}}{P_{um}} = K_F \quad , \quad P_{um} = \eta_m\cdot P_{am} \quad , \tag{48}$$

one can write:

$$P_{ad} = P_{am}\cdot\frac{\eta_m}{\eta_d}\cdot K_F \quad , \tag{49}$$

from which, by insertion in (47), one obtains:

$$\eta_d = 1 - \frac{1 + K_P}{2}\cdot\frac{K_L}{K_F}\cdot\frac{\eta_d\cdot P_{Jm}}{\eta_m\cdot P_{am}} \quad . \tag{50}$$

By observing that:

$$\frac{P_{Jm}}{P_{am}} = 1 - \eta_m \tag{51}$$

and solving (50) with respect to η_d, we have:

$$\frac{\eta_d}{\eta_m} \approx \frac{1}{\eta_m + \frac{K_L}{K_F}\cdot\frac{1 + K_P}{2}\cdot(1 - \eta_m)} \quad . \tag{52}$$

It is interesting to find the parametric conditions for which the different energetic quantities assume the same value in the two types of systems.

By imposing in (45) the equality of the armature Joule losses, one obtains:

$$\dot{P}_J = 1 \quad \Rightarrow \quad K_L = \frac{2}{1 + K_P} \quad . \tag{53}$$

Vice versa, the condition of equality between efficiencies, imposed in (52), gives:

$$\eta_d = \eta_m \quad \Rightarrow \quad K_L = \frac{2}{1 + K_P}\cdot K_F \quad . \tag{54}$$

Finally, by imposing the equality of the absorbed power in (49) and taking into account (52), we obtain:

$$P_{Jd} = P_{Jm} \quad \Rightarrow \quad K_L = \frac{2}{1 + K_p} \cdot \frac{1 - K_F \cdot \eta_m}{1 - \eta_m} \quad . \qquad (55)$$

Eq.(53) shows that, in case of adopting the same polar pitch in the two types of system (K_p=1), the equality of the armature Joule losses occur with K_L=1.
In case of a value K_p=3.8 (situation of the Linear express), the equality of the armature losses would occur with a value K_L=0.42; vice versa, the hypothesis of K_L=1 would lead, in this case, to P_J=2.4 .

Fig.4 shows the dependence of the efficiency ratio η_d/η_m on the efficiency η_m of the EMS system: one can observe that, being equal K_L, the adoption of a value K_p=1 implies η_d/η_m values that are indeed more favorable than those corresponding to K_p=3.8: moreover, with K_p=1, it is sufficient to adopt K_L=0.9 in order to obtain η_d=η_m.
Vice versa, with K_p=3.8 the efficiency η_d appears quite lower, approaching the η_m values for K_L values that are considerably lower then the previous ones (η_d=η_m occurs for K_L=0.375).

Similar remarks about the reduction of K_p and/or of K_L can be made referring to (55).

The previous analysis shows the need, in the EDS case with K_p>1, of adopting, for the length of the fed sections, a value lower than that of the EMS case, with the aim not to worsen the efficiency excessively.

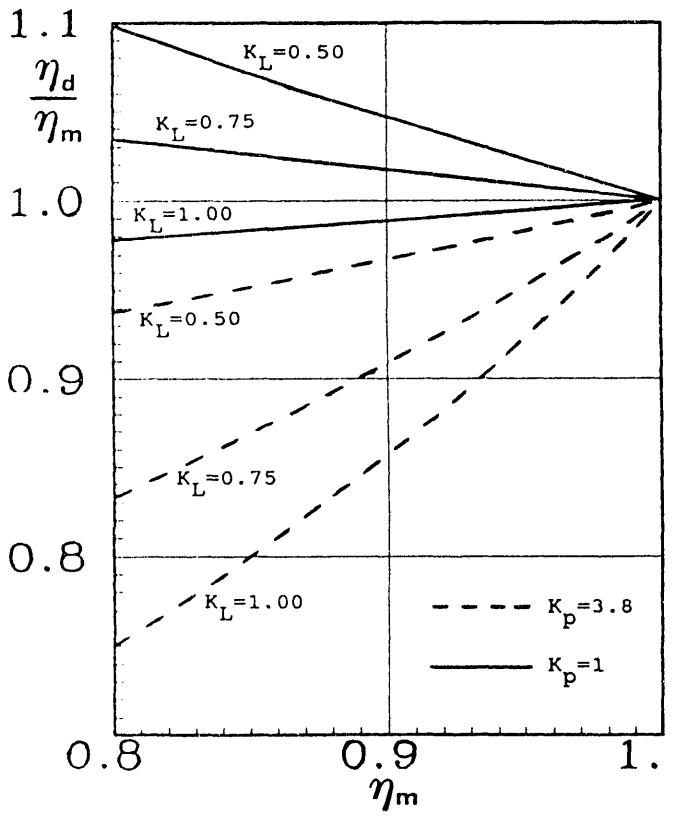

Fig.4. Ratio between the armature efficiencies of the EDS and EMS systems (η_d/η_m) as a function of the armature efficiency that can be attributed to the system EMS; parameters: ratio between the polar pitches ($K_p=\tau_d/\tau_m$) and ratio between the lengths of the fed segments of the track ($K_L=L_{ad}/L_{am}$).

This condition can result not compatible with a regular and reliable operation of the system: as a matter of fact, too much short sections can make more critical the correct feeding sequence of the sections themselves. In any case, the reduction of the length of each section implies a rise of the number of three-phase switches (proportional to $1/K_L$). Therefore the length of the armature sections must be chosen on the basis of a compromise between the need of an acceptable efficiency and the need to maintain a reliable operation and to limit the number of switches.

IV. CONCLUSIONS

In the present paper some parameters have been analyzed for the comparison between EDS and EMS type MAGLEV systems, with reference to the problems of general design and energetics: this comparison, far away to allow a final judgment about the superiority of one system with respect to the other one, allows a good (even if partial) evaluation of their characteristics.

The adopted methodology has shown the dependence of the quantities of active material (conductive and insulating materials) and of the energetic quantities (armature efficiency, input power and losses) on the functional parameters (flux density, thrust, voltage) and on the constructional parameters (polar pitch, ratio between fed segments of the track, ratio between the inductor lengths of the vehicles).

The studies have shown the advantages, in case of the EDS system, in reducing the polar pitch and increasing the average flux density in the plane of the armature, with the aim to compensate the negative effects of the concentration of the superconducting windings at the extremes of the coaches only.

The analysis will continue, both as regard the extension of the comparison to other components of the MAGLEV systems, such as the conversion-feeding devices, and in the perspective of a comparison in economic terms.

REFERENCES

[1] Kyotani Y., "Magnetic Transport System Development in Japan", 9th International Conference on Magnet Technology, Zurich (Switzerland), September 1985.

[2] Tanaka H., "JR Group Probes MAGLEV Frontiers", Railway Gazette International, July 1990.

[3] Mayer W.J., Meins J., Miller L., "The high Speed MAGLEV Transportation System Transrapid". IEEE Trans. on Magnetics, Vol.24 N°2, March 1988.

[4] Tadakuma S., Tanaka S., Inoguchi H., Tanoue Y., Ikeda H., Kaga S., "Consideration on Large Capacity PWM Inverter for LSM Drives", Int. Power Electron. Conf. Rec., Vol.1, pp.413-420, April 1990.

[5] Masada E., Ohsaki H., Seki A., "A Study on the Power Supply System for The Superconducting MAGLEV Transport", EPE Conference, Firenze (Italy), September 1991.

[6] Di Gerlando A., Galasso M., "Feeding Problems in MAGLEV Systems", Proceedings of the Italian National Workshop on Electric Drives with Linear Motors, Milano (Italy), April 1992 (in Italian).

Design Problems of Linear on Board Generators in EMS MAGLEV Transportation Systems

Antonino Di Gerlando , Ivo Vistoli
Dipartimento di Elettrotecnica - Politecnico di Milano
Piazza Leonardo da Vinci 32, 20133 Milano, Italy

Abstract - The power needed for feeding the on board apparatus in the EMS MAGLEV systems is obtained by linear synchronous generators arranged in the field poles of the LSM.

In the present paper some operation aspects of these machines are studied, with the aim to analyze their design criteria: different topics are examined, in particular the interaction with the LSM operation, the winding configurations and a possible modular arrangement of the generation-conversion units.

I. INTRODUCTION

In the EMS Maglev vehicles equipped with long stator linear synchronous motor (LSM), the feeding of the excitation and guidance windings, together with that of the auxiliary services, requires an adequate level of the on board available power, that must be generated during the motion of the vehicle.
Among the different possibilities, till now only the solution consisting of a linear synchronous generator (LSG) has been studied and experimented: it is an electrical machine capable to obtain A.C. energy from the harmonic magnetic fields produced by the currents circulating in the LSM armature windings. This energy, suitably converted, is subsequently used for recharging the batteries and feeding the on board loads.

II. CALCULATION OF THE ELEMENTARY E.M.F.

The LSG, arranged in the LSM pole-pieces, is obtained by inserting suitable windings, sensitive to the harmonic m.m.f.s produced by the LSM armature currents. For studying the LSG, some simplifying hypotheses are assumed, that allow a handy design oriented analysis:
- the LSG armature currents are considered perfectly sinusoidal;
- the effects of the harmonic m.m.f.s are studied neglecting the presence of the teeth, except for the use of Carter's factors;
- the Fourier series of the m.m.f. waveforms is operated by assuming periodic shapes;
- the end effects are neglected.

In the following, all the quantities concerning the LSG construction and operation will be marked with the superscript '.

Named v the synchronous speed, the speeds of the LSM armature harmonic m.m.f.s (measured in an armature reference frame) equal:

$$v_n = v/n = 2\cdot f\cdot\tau/n = 2\cdot f\cdot\tau_n \ , \qquad (1)$$

with n harmonic order, f feeding frequency, τ_n polar pitch of the n-th harmonic m.m.f..

Considerations regarding manufacture and operation aspects lead to construct a LSM armature winding characterized by unity values both of the N° q of slots per pole per phase and of the N° u of conductors in the slot; then all the harmonic m.m.f.s are tooth harmonics and their winding factors equal unity.
The harmonic orders of the LSM m.m.f.s equal:

$$n = 1 + 6\cdot k \ , \qquad k = \pm1, \pm2, \pm3, \ldots; \qquad (2)$$

from eq.(2), the positive values of n (7, 13, 19,...) correspond to harmonic m.m.f.s running in the same direction of the fundamental m.m.f., while the negative values (-5, -11, -17,...) correspond to harmonic m.m.f.s running in the opposite direction.
From (1), (2), the speed of the n-th m.m.f., measured with respect to the vehicle, equal:

$$v'_n = \frac{v}{n} - v = v\cdot\left(\frac{1-n}{n}\right) \ ; \qquad (3)$$

then the frequencies of the e.m.f.s induced in the armature of the LSG are given by:

$$f'_n = \left|\frac{v'_n}{2\cdot\tau_n}\right| = f\cdot|1-n| = 6\cdot f\cdot|k| \ . \qquad (4)$$

Eq.(4) shows the interesting result that the LSG "sees" the harmonic m.m.f.s, two by two, with the same frequency, multiple of a factor |1-n| with respect to LSM feeding frequency. In particular, both the 5-th and the 7-th harmonic m.m.f.s induce e.m.f.s with frequency $f' = f'_5 = f'_7 = 6\cdot f$; the 11-th and 13-th harmonic m.m.f.s produce $f'_{11} = f'_{13} = 12\cdot f = 2\cdot f'$, and similarly for the higher harmonics.
Neglecting the presence of the teeth, the amplitude of the flux density due to the n-th harmonic m.m.f. is given by:

$$B_{nM} = \mu_o\cdot\frac{M_{nM}}{\delta} = \frac{\mu_o}{\delta}\ \frac{3\cdot\sqrt{2}}{\pi}\cdot\frac{I}{|n|} \ , \qquad (5)$$

and the corresponding flux per pole equals:

$$\Phi_n = \frac{2}{\pi}\cdot B_{nM}\cdot\tau_n\cdot\ell_e = \mu_o\cdot\frac{6\cdot\sqrt{2}}{\pi^2}\cdot\frac{\tau\cdot\ell_e}{\delta}\cdot\frac{I}{n^2} \ , \qquad (6)$$

with ℓ_e transversal width of the LSM (1 side).
Lastly, the e.m.f. induced in each of the 2 conductors forming a full pitch turn equals:

$$e'_n = \frac{\pi}{\sqrt{2}}\cdot f'_n\cdot\Phi_n = \frac{6\cdot\mu_o}{\pi}\cdot\frac{\tau\cdot\ell_e}{\delta}\cdot f\cdot I\cdot\frac{|1-n|}{n^2} \ . \qquad (7)$$

Observing eq.s (4) and (7), one can conclude that it is sufficient to study the LSG operation and design referring to the 5-th and 7-th harmonic m.m.f.s only.

Generally the phase harmonic e.m.f. equals:

$$E'_n = k'_{wn}\cdot U'\cdot e'_n \ , \qquad (8)$$

where k'_{wn} and U' are the winding factor and the number of conductors in series per phase.
From eq.(7), given the LSM and its operating conditions, the e.m.f. e'_n is determined: then, the choices regarding the LSG can affect the value of the other factors of eq.(8) only.

Manuscript received March 6, 1993.
Work supported by the Italian Research National Council (CNR) PFT2 Project; Contract N°92.01972.PF74.

III. CHOICE PROBLEMS OF LSG WINDINGS

A very important choice concerns the value of the coil pitch τ': to show its influence let consider fig.1. Named β the electrical angle between the magnetic axes of LSM inductor and armature, fig.1 refers to two particular operating conditions:
- alignment between magnetic axes of LSM inductor and armature (corresponding to $\beta=0$);
- time instant in which the current in the phase A of the LSM has the maximum value.

The 1-st condition will be removed in the following, showing the effects of angles $\beta\neq0$.
The 2-nd condition allows to represent easily the air-gap m.m.f. diagram and its fundamental, 5-th and 7-th harmonics: in any case the conclusions drawn for the e.m.f.s e'_5 and e'_7 have general validity, because these e.m.f.s have constant amplitude and same frequency.
The presence of only one turn having pitch τ', in symmetric position with respect to the field pole axis, allows to easily show the phasor composition of the two elementary e.m.f.s (e'_n) to give the turn e.m.f. (E'_{tn}).
Observing in fig.1 the disposition of the 5-th and 7-th harmonic m.m.f.s with respect to the LSG turn, one can deduce that the harmonic turn e.m.f.s (E'_{t5} and E'_{t7}) are two phasors opposed each other (the central halfwaves of the corresponding m.m.f.s are opposed).
The amplitude of each turn harmonic e.m.f. E'_{tn} depends on the value of τ': if we adopt a value τ' equal to the polar pitch τ_n of the n-th harmonic m.m.f., the turn e.m.f. equals the scalar sum of the e.m.f.s e'_n, because these e.m.f.s are in phase; of course, the choice of exploiting both the harmonics leads to adopt a coil pitch τ' within these limits:

$$\tau_7 < \tau' < \tau_5 \quad . \tag{9}$$

From this, one obtains the phasor diagrams of fig.2: the phase angles γ_5 and γ_7 of the figure can be calculated by means of the following expression, for n=-5 and n=7:

$$\gamma_n = \pi \cdot \frac{n}{|n|} \cdot \left(\frac{\tau' - \tau_n}{\tau_n} \right) \quad . \tag{10}$$

By calculating the polar pitch factors ($k'_{\tau n}=E'_{tn}/(2\cdot e'_n)$), some particular values can be obtained, shown in Table I:

Table I
Polar pitch factor $k'_{\tau n}$ as a function of τ'/τ

τ'/τ	1/7	1/5	2/7
$k'_{\tau 5}$	0.901	1	0.782
$k'_{\tau 7}$	1	0.809	0

From Table I one can observe that:
- a coil pitch τ' equal to the polar pitch of the 7-th harmonic m.m.f. produces the maximum 7-th harmonic turn e.m.f. and reduces the 5-th harmonic e.m.f., and vice-versa;
- a pitch τ' equal to the double of the 7-th harmonic polar pitch cancels the corresponding e.m.f., heavily reducing also the 5-th harmonic e.m.f..

Considering the same configuration of fig.1 for $\beta>0$, one can realize that the 5-th and 7-th harmonic e.m.f.s are not opposed each other any more: this fact because, during the variation of β, the displacement angle β_n of the two harmonic m.m.f.s is different:

$$\beta_n = |n| \cdot \beta \quad . \tag{11}$$

Then, the phase displacement between the 5-th and 7-th harmonic e.m.f.s equals:

$$\Delta\beta = \pi + \beta_7 - \beta_5 = \pi + 2\cdot\beta \quad , \tag{12}$$

as shown in the phasor diagram of fig.3.
It is worth to notice that in fig.3 E'_5 and E'_7 indicate the winding e.m.f.s of one phase, considering that the angle β produces the same displacement both on the turn e.m.f. (E'_{tn}) and on the winding e.m.f. (E'_n).
From fig.3 one obtains the following expression for the amplitude of the winding e.m.f. E', resultant of the e.m.f.s E'_5 and E'_7:

$$E'=\sqrt{(E'_5)^2+(E'_7)^2+2\cdot(E'_5)\cdot(E'_7)\cdot\cos(\Delta\beta)} \, . \tag{13}$$

Before analyzing the different winding structures, it is worth to do some remarks regarding the choice between three-phase or single-phase armature winding:
- considering that there are no loads directly connected to the LSG terminals, the number of phases is not a constraint a priori;
- a three-phase generator produces, at the D.C. side of the rectifier, a harmonic pollution level that is lower compared with that of a single-phase generator;

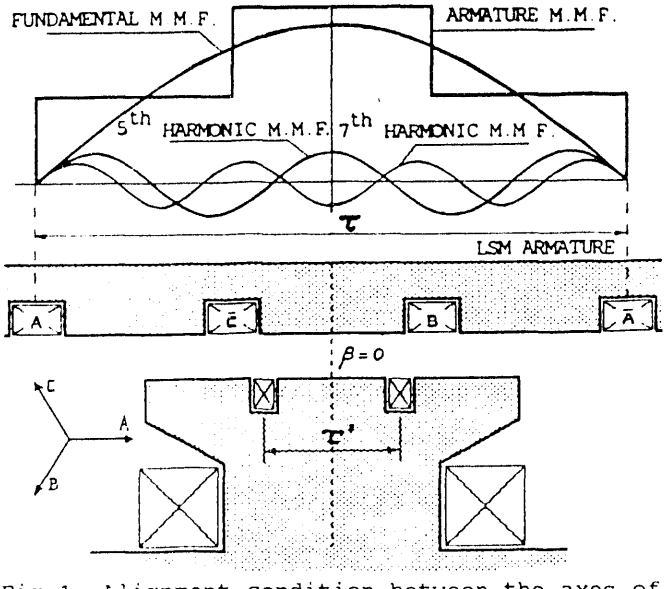

Fig.1. Alignment condition between the axes of the LSM armature m.m.f. and 1 LSG coil ($\beta=0$).

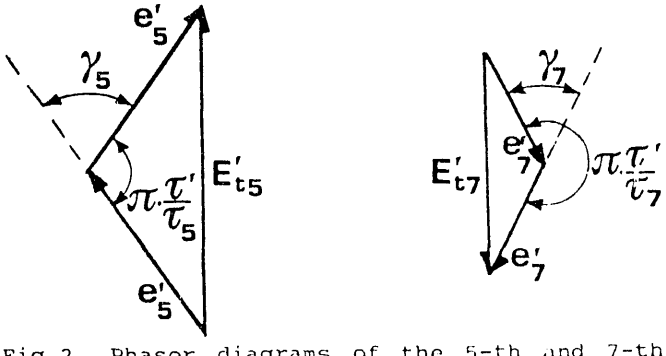

Fig.2. Phasor diagrams of the 5-th and 7-th harmonic e.m.f.s induced in the turn of fig.1.

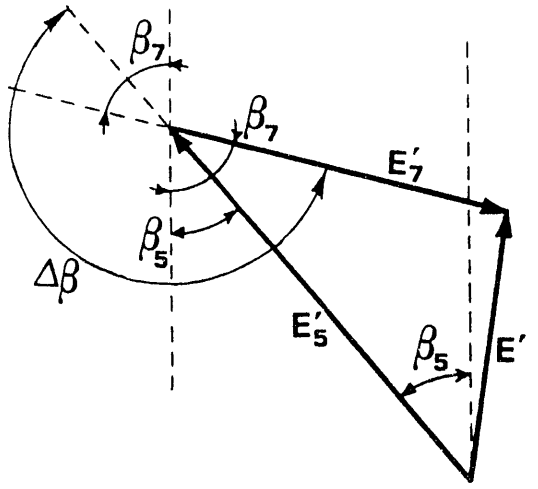

Fig.3. Sum of 5-th and 7-th harmonic e.m.f.s.

- on the other hand, the room requested by a three-phase winding is higher than that of a single-phase winding, and it can be difficult to arrange it in the LSM pole-pieces.

Moreover, in case of a three-phase LSG the two terns of e.m.f.s (due to the 5-th and 7-th harmonic m.m.f.s, running in opposite directions) have opposite cyclic sequence: then, in the harmonic composition there is an effect similar to that shown in fig.4.
The dissymmetry level depends on the ratio between the 7-th and 5-th harmonic e.m.f.s amplitudes and on the angle β (see eq.(12)).
In the choice of the coil pitch τ' for 3-phase LSG windings it is necessary to consider that:
- a value of τ' within the limits of eq.(9) is not acceptable for the dissimmetry: as a matter of fact, even if the LSG does not feed any 3-phase load, it would transfer the dissimmetry to the D.C. side of the rectifiers, producing there high levels of harmonics which are non-characteristic and, what is more, depend on the operating conditions;
- a pitch τ' that cancels the 7-th harmonic e.m.f. eliminates the dissimmetry, but implies a severe reduction of the 5-th harmonic e.m.f. (see 3-rd column of Table I).

In any case, the possible compromise choice, consisting in allowing a limited level of dissimmetry, does not eliminate the construction difficulties, due also to the problems of end winding crossings.

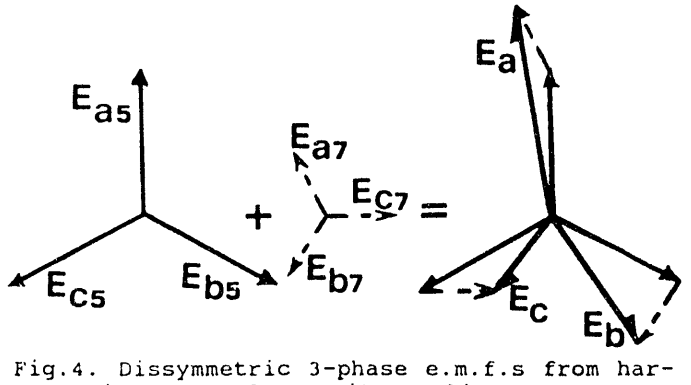

Fig.4. Dissymmetric 3-phase e.m.f.s from harmonic terns of opposite cyclic sequence.

IV. ANALYSIS OF SINGLE-PHASE WINDINGS

In the following the analysis of single-phase windings will be performed: these windings are intrinsecally easier to be constructed compared with three-phase windings.

The LSG is characterized by the presence of some active conductors, distributed along the air-gap surface of the LSM field poles: the choices of the number of these conductors, of their disposition in each field pole and of their series and parallel connections are conditioned by several elements:
- phase e.m.f. amplitude and its sensitiveness to the LSM operating conditions;
- construction problems of the windings;
- number of converters necessary for a good operation of the system, both in normal conditions and in case of partial failure (problem of the reserve);
- harmonic pollution of the rectified voltage.

The amplitude of the phase e.m.f. constitutes an important element for the choice: nevertheless, being equal the induced e.m.f., the configurations that better satisfy also the other exigences are to be preferred.
Given a single-phase winding with p' poles, q' slot per pole, u' conductors per slot, U' conductors connected in series ($U'=u'\cdot q'\cdot p'$), the winding factor (k'_{wn}) that appears in eq.(8) can be expressed as a product between a distribution factor (k'_{dn}) multiplied by a polar pitch factor ($k'_{\tau n}$).
For a structure uniformly toothed, the two factors have the following expressions:

$$k'_{dn}=\frac{\sin\left(\frac{\pi}{2}\cdot\frac{\tau'}{\tau_n}\right)}{q'\cdot\sin\left(\frac{\pi}{2\cdot q'}\cdot\frac{\tau'}{\tau_n}\right)} \quad ; \quad k'_{\tau n}=\frac{\sin\left(p'\cdot\frac{\gamma_n}{2}\right)}{p'\cdot\sin\left(\frac{\gamma_n}{2}\right)} \quad , \qquad (14)$$

with γ_n given again by eq.(10).
As regards the expressions for the harmonic elementary e.m.f.s (e'_n), the phase e.m.f.s (E'_n), the phase displacement between the harmonics ($\Delta\beta$) and their resultant (E'), eq.s (7), (8), (12), (13) are still valid.

In order to perform a homogeneous analysis of the different winding configurations, the following comparison conditions are considered:
- reference is made to the theoretical no-load values of the rectified voltage (E'_{od}) instead of the RMS values of the phase e.m.f. (E'); as known, for single-phase rectifiers we have:

$$E'_{od} = \frac{2\cdot\sqrt{2}}{\pi}\cdot E' \quad ; \qquad (15)$$

- the same total number of conductors U', disposed in each field pole, is adopted.

The first hypothesis allows to extend the comparison also to those cases in which there are more than one winding portions within each field pole, and the series connection of these portions is made at the D.C. side of the rectifiers; the second condition allows a comparison being equal the number of active conductors, and it is intended in a generalized sense, even in case of more than one winding portion disposed within each LSM field pole.
The only elements that can be modified in order to obtain different values of E'_{od} are the following:
- the subdivision of the winding;

- the winding factor, by the choice of p', q', τ'.

The maximum allowed N° of poles of the LSG winding is limited by the length of the field pole (roughly equal to $2 \cdot \tau/3$): the analysis showed that it is practically impossible to adopt a p' value more than 4, also in order not to reduce the pitch τ' excessively.

By observing the 1-st eq. of (14), one can realize that the highest values of the winding factor can be obtained for q'=1, because the distribution factor becomes unity.

By studying different kinds of windings the following general characteristics have been deduced:

- in the range of practical interest of the LSM angle β ($60° \leq \beta \leq 120°$), during the increasing of the coil pitch τ', at first the function $E_{od}(\beta,\tau')$ increases, then decreases, with a maximum occurring for a τ' value depending on the winding type;
- the voltage E'_{od} is an even function, with respect to the position $\beta=\pi/2$ (equal to the angle for which the maximum occurs).

In order to estimate the characteristics of the different winding types, it is necessary to make reference to the data of a real EMS MAGLEV system. To this end, starting from some constructed prototypes (e.g. the Transrapid 06, studied in Emsland, Germany), a general design of the LSM has been performed: to the corresponding main data, shown in Table II, the subsequent results will be referred.

Table II

General data of the LSM considered for the study of the LSG of an EMS MAGLEV system

Operation data:	
maximum speed	v = 415 km/h
maximum inverter frequency	f = 225 Hz
maximum thrust	Fx = 40 kN
rated armature current	I = 635 A RMS
air gap flux density	B_f = 0.63 T
Construction data:	
mass of the vehicle	M= $1.2 \cdot 10^5$ kg
Total N° of poles (per side)	p = 102
N° of poles of each magnetic unit	p_u = 6
air gap	δ = 10 mm
field pole transversal length	ℓ_e = 220 mm
polar pitch	τ = 255 mm

In fig.5 the schemes of some studied windings are shown, together with their synthetic description: an analysis of their characteristics helps to conveniently choose one of the types. For now, just the winding disposed within one LSM field pole will be considered.

In fig.6 the amplitudes of the no-load rectified voltage E'_{od} are shown, as a function of the angle β, for the 6 cases of fig.5; in Table III the values of the ratio τ'/τ are shown, corresponding (for $\beta=\pi/2$) to the maximum of the rectified voltage, together with the value of this maximum ($E'_{od(max)}$).

Table III

Values of the ratio τ'/τ corresponding to the maximum of the no-load rectified voltage E'_{od}, for $\beta = \pi/2$ and for the 6 cases of fig.s 5, 6 (Total number of conductors: U'=8).

CASE N°	1	2	3	4	5	6
τ'/τ	.167	.173	.173	.127	.155	.171
$E'_{od(max)}$ [V]	3.07	4.23	4.19	3.47	4.30	4.82

TYPE OF SINGLE-PHASE WINDING	WINDING SCHEME
CASE 1 SINGLE EXTENDED WINDING p'=4 ; q'=2 ; u'=1 ONE RECTIFIER	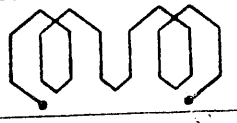
CASE 2 SINGLE EXTENDED WINDING p'=4 ; q'=1 ; u'=2 ONE RECTIFIER	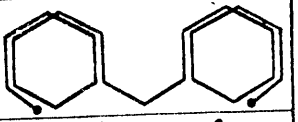
CASE 3 DOUBLE EXTENDED WINDING 2 x (p'=4 ; q'=1 ; u'=1) TWO RECTIFIERS	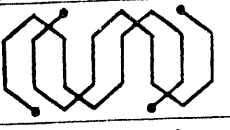
CASE 4 DOUBLE WINDING WITH 2 COILS 2 x (p'=2 ; q'=2 ; u'=1) TWO RECTIFIERS	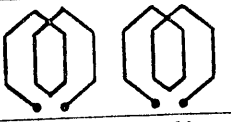
CASE 5 DOUBLE WINDING WITH 2 COILS 2 x (p'=2 ; q'=1 ; u'=2) TWO RECTIFIERS	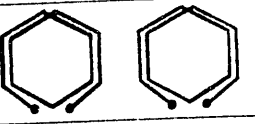
CASE 6 CROSSED DOUBLE WINDING 2 x (p'=2 ; q'=1 ; u'=2) TWO RECTIFIERS	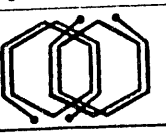

Fig.5. Synthetic description and schemes of some LSG single-phase windings (U'=8).

1st Case: single extended winding with p'=4; q'=2; u'=1.

It is a winding with slots uniformly distributed along the LSM field pole.

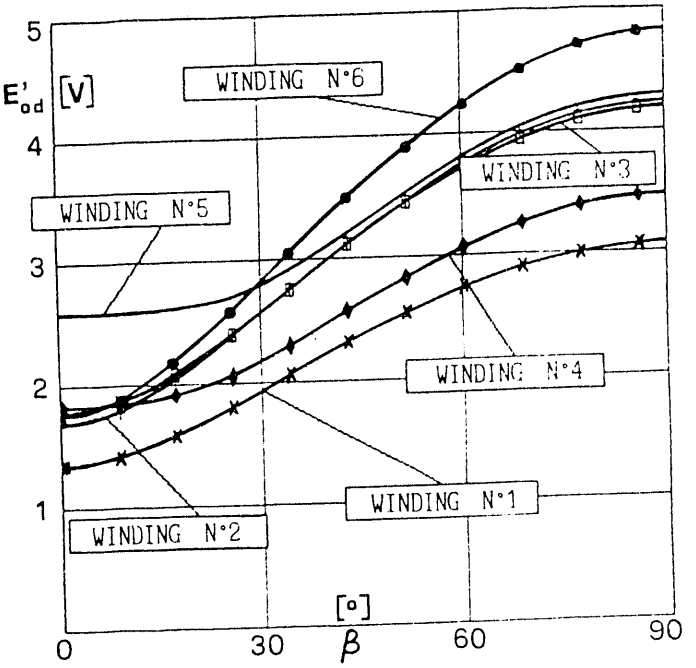

Fig.6. No-load rectified voltages E'_{od} of the 6 windings of fig.5, as a function of β.

An interesting remark concerns the value of the coil pitch τ' for which the maximum of E'_{od} occurs: it is exactly the intermediate value between the polar pitch of the 5-th and the 7-th harmonic m.m.f.s.
The low value of the rectified voltage (the lowest among the 6 shown cases), together with the constructional complications of two end winding crossings, suggest that the adoption of the structure N° 1 is not convenient.

2^{nd} Case: single extended winding with $p'=4;\ q'=1;\ u'=2$.

It is a winding having a number of slots halved compared with those of case 1, again uniformly distributed: in confirmation of what already observed as regards the distribution factor (k'_{dn}), concentrating the active sides of one pole in the same slot leads to increase the value of the rectified voltage.
Another element in favour of this winding is the absence of end winding crossings.

3^{rd} Case: double extended winding with $2\cdot(p'=4;q'=1;\ u'=1)$.

The conductors are arranged in the same slot structure of case 1, but they are connected in such a way to form 2 distinct windings, whose voltages are separately rectified and added at the D.C. side of the rectifiers.
This subdivision partially reduces the negative effect of the phase displacement between the elementary e.m.f.s: then an improvement occurs, compared with case 1, with an increase of the voltage $E'_{od(max)}$; nevertheless, this voltage remains lower than that of case 2; moreover, it requires the doubling of the N° of the rectifiers and, above all, implies a high N° of end winding crossings, with the corresponding constructional complications.

4^{th} Case: double coil winding with $2\cdot(p'=2;q'=2;u'=1)$.

It shows a different connection among the conductors, arranged in the same structure of case 1, from which it is evident the origin, based on a simple central separation.
In this case the increase of the rectified voltage, pursued by the subdivision of the winding into two portions, implies the halving of the number of end winding crossings of case 3, but the amplitude of $E'_{od(max)}$, compared with that of case 2, makes this solution not particularly interesting.

5^{th} Case: double coil winding with $2\cdot(p'=2;q'=1;u'=2)$.

This structure represents the natural evolution of case 2, from which it is obtained by subdividing the winding in the central zone: similarly to case 2, it has the advantage of the absence of crossings.
In case of coil active sides arranged in uniformly distributed slots, the rectified voltage value is slightly higher compared with that of case 2, but with respect to this case, the number of necessary rectifiers is double.

6^{th} Case: crossed double winding with $2\cdot(p'=2;q'=1;u'=2)$.

This disposition can be considered derived from the previous one, by approaching and intersecting the two coils, up to obtaining a sequence of uniformly distributed active sides: this transformation leads to an important increase of the rectified voltage amplitude (it is the highest among the 6 cases).

On the other hand, this kind of winding implies serious constructional difficulties: here, the problem of the end winding crossings, considered important for some of the previous cases, is much more worsened by the simultaneous crossing of four end windings for each field pole front.

The previous analysis leads to recognize that the configurations of cases 2 and 5 are globally more valid, both in operational and in constructional terms: however the disposition of case 5 allows further improvement opportunities.
As a matter of fact, applying to the configuration of case 5 the idea of approaching the two coils, without reaching their crossing, it is possible to obtain the disposition represented in fig.7: the winding has the same winding data of case 5, but the two coils have the adjacent sides arranged in the same central slot. This slot has a double width compared with that of the slots at the opposite extremes of the LSM field pole.
The winding represented in fig.7 can be called "double winding with adjacent coils".

For a correct evaluation of this winding it is opportune to take into account the effective room requested by the active sides, as shown in fig.7: then, told b'_c the width of the slots in the extreme positions of the pole (for the central slot, b'_c is the distance between the axes of two adjacent active sides), the middle of the coils is at a distance

$$y = 0.5\cdot(\tau'+b'_c)$$

from the polar axis of the field pole.
Modifying the b'_c value (to be defined during the LSG design) changes the position of the coils and varies the rectified voltage; the values of $E'_{od(max)}$ are shown in Table IV for 3 possible values of b'_c (and for $\beta=\pi/2$): in all the cases, the coil pitch τ' corresponding to the maximum value of E'_{od} is equal to 1/6 of the polar pitch τ.

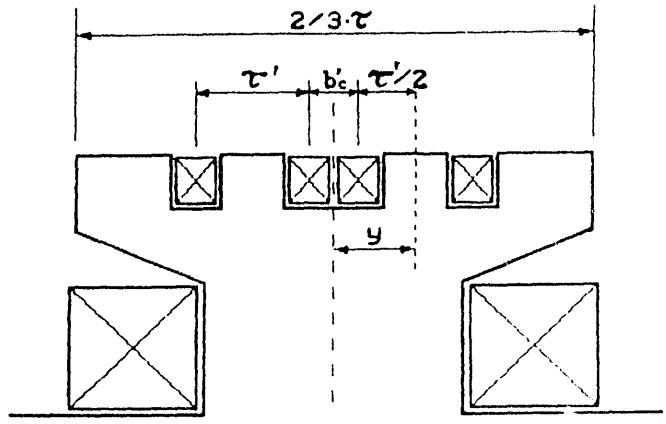

Fig.7. Double single-phase winding with adjacent coils arranged in three slots.

Table IV

Maximum values of the rectified voltage $E'_{od(max)}$ of a double winding with adjacent coils, as a function of the slot width b'_c; coil pitch: $\tau' = 42.5$ mm $= \tau/6$.

b'_c	[mm]	10	20	30
$E'_{od(max)}$	[V]	4.63	4.53	4.43

From the previous analysis one can conclude that:
- the double winding with adjacent coils can generate values of rectified voltage having interesting levels, of the order of those obtainable with the double winding with crossed coils (case 6);
- quite wide variations of slot width b'_c implies low variations of E'_{od};
- the winding is easy to be manufactured.

In conclusion, this winding seems to be the best one among the different examined single-phase windings.
As regard the dependence on the LSM operation quantities (β, f, I), the following expression is valid:

$$E'_{od} = K_e(\beta) \cdot f \cdot I \quad . \qquad (16)$$

Chosen the traction diagram, consisting of a first part with constant thrust and a second part with constant power, it follows that E'_{od} linearly grows in the first part (up to 50 m/s roughly), and then it remains practically constant in the other part; moreover, the study shows that β affects quite weakly the voltage E'_{od}.
This behaviour is favourable to the dimensioning of the battery and of the on board generator system.

V. THE GENERATION-CONVERSION MODULES OF THE LSG SYSTEMS

A suitable configuration of the LSG system implies the use of several modules in parallel, each of the kind represented in fig.8; the characteristics of the module are the following:
- every electrical unit G contains all the fore (or hinder) series connected coils of each magnetic unit;
- among all the units G of one module, those equipped with fore coils are paralleled to the input of one rectifier, while the units with hinder coils are paralleled to the input of the other rectifier;
- the outputs of the two rectifiers of each module are series connected and sent to a step-up chopper.

This modular structure allows:
- operation in case of failure of one module;
- reduction of the D.C. side harmonic pollution, thanks to the series connection of the rectifiers;
- decoupling of the voltage level of the high voltage D.C. bar from the level of the units.

VI. CONCLUSIONS

In this paper some design problems regarding the linear on board generators of the EMS MAGLEV systems have been discussed. The analysis concerned:

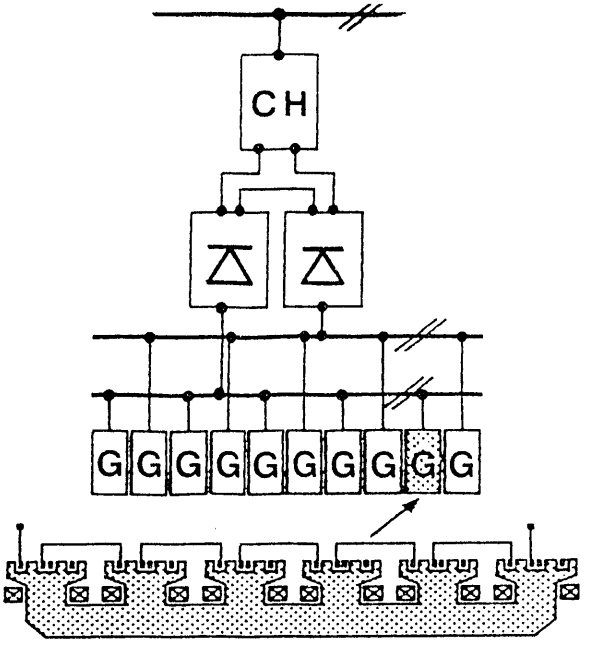

Fig. 8. Scheme of one LSG generation-conversion module (G) and detail of one magnetic unit equipped with fore series connected coils.

- the characteristics of the LSM harmonic m.m.f.s;
- the LSG elementary and winding e.m.f. amplitudes and phases;
- the choice between three-phase or single-phase windings;
- the distribution and connection of the LSG active sides;
- the structure of the generation-conversion modules.

The studies will go on, according to different research lines:
- winding configurations of the LSG;
- improvement of the model for studying the operation;
- choices regarding the conversion devices.

REFERENCES

[1] I. Boldea, S.A. Nasar, "Linear electric motors: theory, design, practical applications", Prentice-Hall, 1987.
[2] I. Boldea, S.A. Nasar, "Linear motion electromagnetic system", Wiley Interscience, New York, 1985.
[3] W.J. Mayer, J. Meins, L. Miller, "The high speed Maglev trasportation system Transrapid", IEEE Trans. on Magnetics, vol.24, N°2, March 1988.
[4] G. Bohn, G. Steinmetz, "The electromagnetic levitation and guidance technology of the "Transrapid" test facility Emsland", IEEE on Mag., vol.Mag-20, N°5, Sept. 1984.
[5] G.W. McLean, "Review of recent progress in linear motors", IEE Proc.-B, vol.135, N°6, November 1988.
[6] G. Carnelli, S. Mariani, "Linear on board generator for EMS MAGLEV transportation systems", graduation thesis, Politecnico di Milano, (in Italian), 1992.

On-vehicle Power Generation at all Speeds for Electromagnetic Maglev Concept

S. Kalsi
Grumman Corporation, Bethpage, New York

*Abstract** The electromagnetic suspension (EMS) maglev utilizes attraction force between two electromagnets for generating levitating force. The Grumman EMS maglev levitation magnets [1] are iron-cored superconductive type. A significant amount of power (~150 kW) is needed on vehicle for powering superconducting magnets and their cooling system, for airconditioning and heating systems, and for lighting. This power must be transferred to vehicle magnetically because it is difficult to employ mechanical sliding contacts at high speeds 134 m/s (~300 mph). Grumman has adopted a power generation concept which is a hybrid of the following two techniques. The first technique takes advantage of magnetic field variations in the airgap between the levitation magnet poles and the rail. The airgap field variations are caused by the slots in the rail. These field variations induce power into coils located in the face of each levitation pole. The power generation coils are designed such as to generate the required amount of power when the vehicle is travelling at the full rated speed. This generated power is a strong function of vehicle speed and it drops as the vehicle slows down. However, the power is required on vehicle at all speeds including standing still and for this reason the second technique for power generation is utilized. In this technique, the rail windings are supplied with a single phase high-frequency (600 Hz) current. This current creates a stationary magnetic field (with respect to rail) that pulsates at 600 Hz. This pulsating field induces power into the power generation coils. Because this power generation scheme is primarily dependent on the transformer action it is possible to generate the needed amount of power at all speeds (from standstill to full-speed). The drawback of this scheme is that the high frequency current (500 A) imposes additional heat load in the traction windings. To alleviate this problem, it is proposed that the power be generated at low speeds with the high frequency excitation of traction windings, and at high speeds with the airgap field variations due to the rail slots. This hybrid power generation approach provides required power at all speeds and it eliminates a need to carry batteries on-board on the vehicle to complement the generated power at low speeds.

I. INTRODUCTION

In conventional rotating machinery, slot harmonics of the 3-phase stator windings are utilized for generating power on the rotor for the field excitation. Because of a large airgap length in the Grumman maglev systems and its relatively small stator winding current, it is difficult to pick up sufficient power with this approach. Total power of 150 kW is required on a Grumman maglev car under all operating conditions. This power can be generated from the single phase field pulsations at all speeds (from zero to full-rated speed) as discussed above in the abstract. In the event of a power system failure and loss of power on the rail, a small amount of battery power is still required to keep the vehicle levitated, to coast it to a safe station, and to brake it. These batteries are single use high power density type.

II. POWER GENERATION WITH SLOT HARMONICS

The harmonic contents of the field profile at the pole surface are given in Table I. The 19th harmonic has a significant value that is used for power generation. The 19th harmonic flux pulsations are caused by the airgap permeance changes caused by the rail slots.

TABLE I
FIELD HARMONICS AT THE POLE SURFACE AT 134 m/s

Harmonic Order	Peak Field (G)
1st	8,884
5th	- 884
7th	- 150
11th	627
13th	106
17th	- 361
19th	1,593

The pole-pitch of the 19th harmonic is 41.7 mm which is equal to the pitch of the rail slots. It is possible to accommodate four concentric coils in a 200 mm wide poleface. Each pole face has five slots (three slots 10x15 mm and two slots 5x15 mm). The concentric coils have a bore width of 32 mm and a cross-section of 5x15 mm. The arrangement of coils in the poleface is shown in Fig.1. The performance of the power generation coils is summarized in Table II. Total power that can be generated is 4.2 kW/pole or 200 kW for the whole vehicle with a 40 mm gap clearance.

The power generated on the vehicle is linear function of speed and therefore, the generated power is proportionally low at lower speeds. One possible alternative is to reduce the airgap at low speeds thereby increasing the harmonic

*Manuscript received March 15, 1993. The work was performed as part of the EMS Maglev System Concept Definition study supported by the U. S. Army Corps of Engineers under contract DTFR53-92-C-000 04.

TABLE II
CHARACTERISTICS OF ON-VEHICLE POWER GENERATION BY SLOT HARMONICS

Parameter	Unit	Value
Slot harmonic		19
Pole pitch for the harmonic	mm	41.7
Coils per poleface		4
Amplitude of harmonic field	T	0.1593
Flux linkages per coil	Wb	0.0012
Time required to travel one polepitch at full-speed	ms	0.31
Induce voltage- all coils in series	V (rms)	9.18
Coil current (single turn/coil)	A	478
Coil current density	A/mm^2	6.37
Slot size (width x depth)	mm	10 x15
Coil cross-section (width x depth)	mm	5 x 15
Leakage inductance	mH	0.67
Terminal voltage - all coils in series	V (rms)	8.85
Power factor		1
Power generated	kW	203

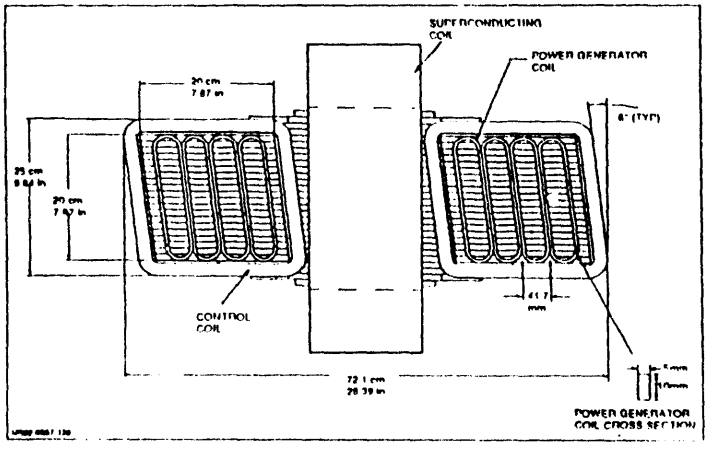

Fig. 1. Coils for Power Generator Mounted on to the Pole Iron

field amplitude at the poleface. This does not work well. For example at 20 mm gap, the levitation force increases for the same excitation level in the poles. Because the levitation force level must remain unchanged, it is necessary to reduce the excitation proportionally which in turn reduces the airgap harmonic field. After adjustment of excitation for the desired levitation force level, the 19th harmonic amplitude is comparable to the value for the nominal operation. Thus reducing the airgap to generate more power will not work. If the power is desired at all speeds then it would be necessary to use alternate techniques.

III. POWER GENERATION WITH HIGH FREQUENCY EXCITATION OF TRACTION WINDING

The high frequency power generation approach is based on excitation of the traction windings of the Linear Synchronous Motor (LSM) with a high frequency (600 Hz), single phase current. The high frequency excitation approach can generate power at all speeds (from zero to full-rated speed). The main advantage of this approach is the minimizing the need for storage betteries on the car. These batteries represent additional weight which requires more powerful levitation magnets for levitating themselves and the batteries. The single-phase current in the traction winding creates an additional I^2R loss in the traction winding. To circumvent this problem, it is proposed to generate only a fraction of power by high frequency (transformer action) to complement the power generated with the slot harmonics at speeds lower than the full nominal speed. At lower speeds, the traction force requirement may also be less which inturn requires lower traction winding current than when operating at the full rated speed. Thus at lower speeds, more high frequency current could be carried in the traction winding without imposing additional heat load on the traction winding.

Description of the high-frequency power generator

The traction winding is supplied from an inverter with a variable frequency current. The circuit diagram used for this is shown in Fig. 2. The ac power drawn from the power grid is first converted to dc in the rectifier section of Fig. 2. The inverter section generates ac for supplying current to the traction winding at desired frequency. Capacitors at the output of the inverter are incorporated for over-voltage control . Three phase traction windings are connected to the output of the inverter.

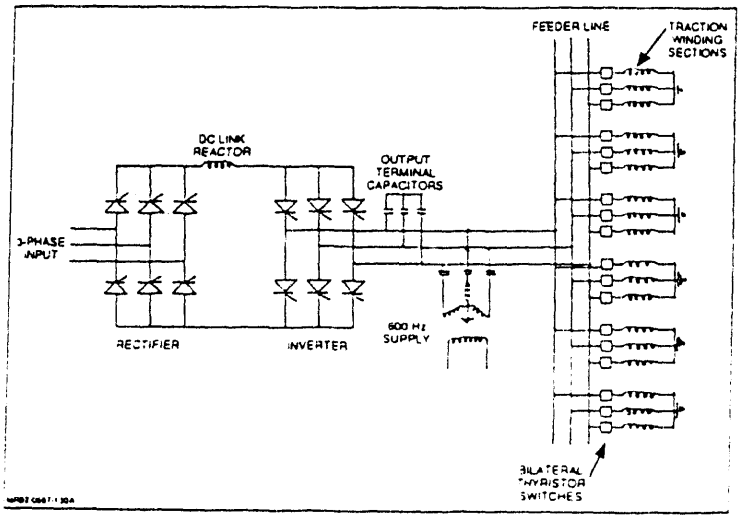

Fig. 2. 600 Hz Current Supply for Traction Windings

For power generation on a maglev vehicle, a single phase AC is supplied through transformers shown in Fig. 2. The frequency of this power is selected as 600 Hz to minimize its effect on the levitation and propulsion force components. The 600 Hz power is supplied through the single phase transformers. The capacitors in the 600 Hz supply circuit of Fig. 2 are for blocking flow of low frequency currents of the traction windings through the 600 Hz transformer.

The power is induced into four coils located in each poleface (Fig. 1). Mechanism of power generation with this technique is discussed below. If a single phase current is supplied to all phases, the resultant space harmonic waveform is that shown in Fig. 3. The harmonic components of this wave are summarized in Table III. Only the fundamental and the 3rd harmonic are the dominant components of the waveform and are also included in Fig. 3. Because these harmonics are generated by a single phase current in the rail winding, they are static with respect to the rail but pulsate at the supply frequency (600 Hz).

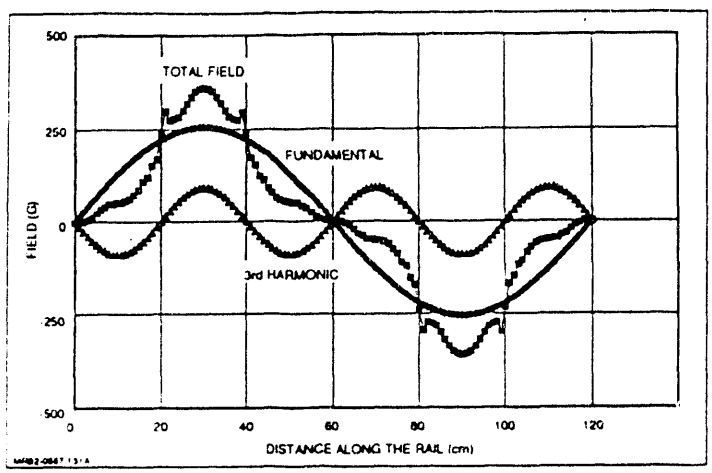

Fig. 3 Field Produced by 600 Hz Rail Current at the Poleface

TABLE III

FIELD HARMONICS GENERATED BY 500 HZ SINGLE PHASE CURRENT IN TRACTION WINDINGS

Harmonic Number	Value (G)
1	255
3	-90
5	17
7	11
9	8
11	-11
13	8
15	8
17	1/2
19	7

Voltages are induced in the power generation coils both by transformer action and by relative motion between the rail and the power generation coils. The voltage induced in each power generation coil by the transformer action is given by the Eqn. (1) below.

$$V_t = (dB_n/dt)\, l\, (2\tau/(n\pi))\, \mathrm{Sin}\{(n\pi/\tau)(vt + a/2)\} \mathrm{Sin}\{(n\pi/\tau)(a/2)\} \quad (1)$$

$$dB_n/dt = \omega B_n$$

where B_n = Peak field component of n^{th} harmonic from Table-III (T)

V_t = Voltage induced by transformer action in a power generation coil (V)

τ = Pole pitch (m)

n = Harmonic number

v = Linear velocity of maglev car (m/s)

a = Coil bore width (m)

l = Coil length - perpendicular to the plane of paper (m)

t = Time (s)

ω = Angular frequency (rad/s)

The high frequency traction winding currents also induce speed dependent voltages in the power generation coils. The voltage induced in each coil is given by the Eq. (2) below:

$$V_s = 2\, B_n\, l\, v\, \mathrm{Cos}\{(n\pi/\tau)(vt + a/2)\}\, \mathrm{Sin}\{(n\pi/\tau)(a/2)\} \quad (2)$$

The Eq. (2) can also be used for calculating voltages induced by the field due to slot harmonics (make τ equal to the slot pitch). The various voltage components are summarized in Table IV.

The traction winding must carry 500 A of high frequency current to induce 5 V in each poleface coil. By mixing contributions of both high frequency and slot harmonics it is possible to generate the required power at all speed. Fig. 4 shows a plausible combination of the two schemes. In this approach, at standstill the whole power is generated by high frequency and at full speed the whole power is generated by the slot harmonics. This way the total increase in the traction winding I^2R losses could be minimized.

TABLE IV

VOLTAGE INDUCED IN THE POWER GENERATOR COILS

Harmonic	Transformer Voltage (V/turn)	Speed Voltage at 134 m/s (V/turn)	Space Harmonic Order
High Frequency	2.66	0.5	1
	2.57	0.48	3
Slot Harmonic		1.6	19

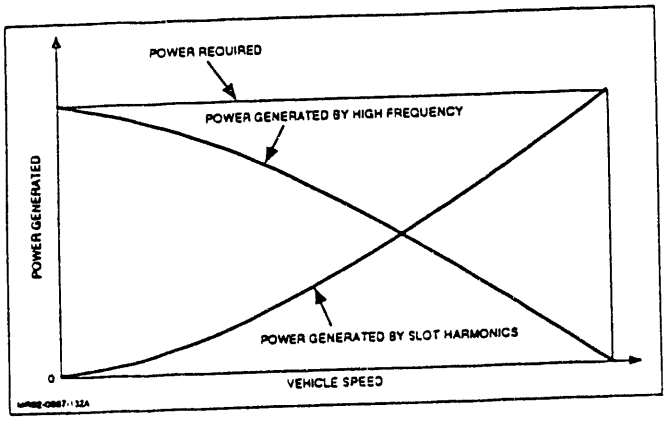

Fig. 4. Control of Power Generation as a Function of Vehicle Speed

IV. CONCLUSIONS

The power generation scheme discussed in this paper provides power at all speeds for use on a maglev vehicle. In future work, mockups of the traction winding and power conditioning equipment will be developed to demonstrate feasibility of the high frequency power generation concept. It is possible to extend this concept to Electrodynamic Suspension (EDS) maglev vehicles.

REFERENCES

[1] M. Proise, et al. "System Concept Definition of the Grumman Superconducting Electromagnetic Suspension (EMS) Maglev Design", presented at the Maglev '93 Conference, Argonne National Laboratory, May 19-21, 1993.

Present State of Development of Synchronous Long-Stator Propulsion System for TRANSRAPID Maglev Trains

Dr.-Ing. habil. Uwe Henning
Siemens AG, Transportation Systems Group,
Erlangen, Germany

Abstract - The synchronous long-stator motor for the TRANSRAPID maglev vehicle is a propulsion system with proven service maturity. The overall concept is described and new technology prototypes are presented for the various subsystems and components. The main focus is on the converter and drive control systems.
The converter system used features inverters equipped with GTO thyristors. The results obtained with a test converter system are discussed. The concept of the digital drive control system is also described along with the experience gained at the TRANSRAPID test facility (TVE) in Emsland in Northern Germany.

1. Propulsion system featuring neutral-point-clamped inverters with GTO thyristors

1.1 Task definition

The synchronous long-stator propulsion system for the TRANSRAPID has proven its operational reliability at the TVE test facility in Emsland in Northern Germany. The concept has been systematically refined for service maturity. The propulsion system envisaged for revenue service is based on the staggered arrangement of motor windings. The motor stator sections on the left- and right-hand sides of the guideway are offset (staggered) relative to each other in the direction of travel. They are fed by separate feeder cable systems which are supplied at both ends from converters in the adjacent substations. The converter system used features state-of-the-art GTO thyristors.

1.2 Power section of the converter

A study of various concepts featuring 4.5 kV, 3 kA GTO thyristors culminated in a design solution based on neutral-point-clamped inverters and output transformers. Fig. 1 shows the block diagram of the converter system which is to be used in future revenue service and produces output voltages of variable magnitude and frequencies of up to 270 Hz. The motor voltage is max. 10 kV (phase-to-phase), and the output per converter is 15 MVA.
The input converter is fed by rectifier transformers and consists of four 3-phase bridges connected in 12-pulse sequence control. In addition to smoothing reactors and back-up capacitors, the DC link circuit features braking choppers and resistors to absorb the energy generated in braking mode.
Each neutral-point-clamped inverter supplied with two DC link part-voltages essentially comprises four GTO thyristors and six diodes per phase. The output voltage is adjusted by variation of the DC link voltages, while the inverters are operated in the lowest frequency range under pulse control. Between 0 and 32 Hz, the primary winding of the output transformer serves as a current dividing reactor for parallel connection of the inverters. In the 32 to 270 Hz range, the transformer increases the inverter output voltage to the required motor voltage of 10 kV.

1.3 Test results

To verify the operational reliability of a converter featuring a neutral-point-clamped inverter, a test converter system was set up and tested under simulated revenue service conditions. The results obtained provide the necessary basic data and knowledge concerning the response and operation of the system [1].
In order to reduce the fundamental frequency of reactive power, the two voltage sources needed for the neutral-point-clamped inverter each comprise two fully controlled rectifier bridges. Fig. 2 shows the control angle curve a_a for the outer rectifier bridges, as well as the control angle curve a_i for the inner bridges as a function of output voltage U_{st} of the current controller. The rectifier bridges always operate in set pairs, i.e. the two outer rectifier bridges are always controlled together while the two inner bridges remain at their maximum control limits, and vice versa.
For sequence control of the rectifier bridges, the fundamental frequency of reactive power curve was calculated for the conditions of the test converter as a

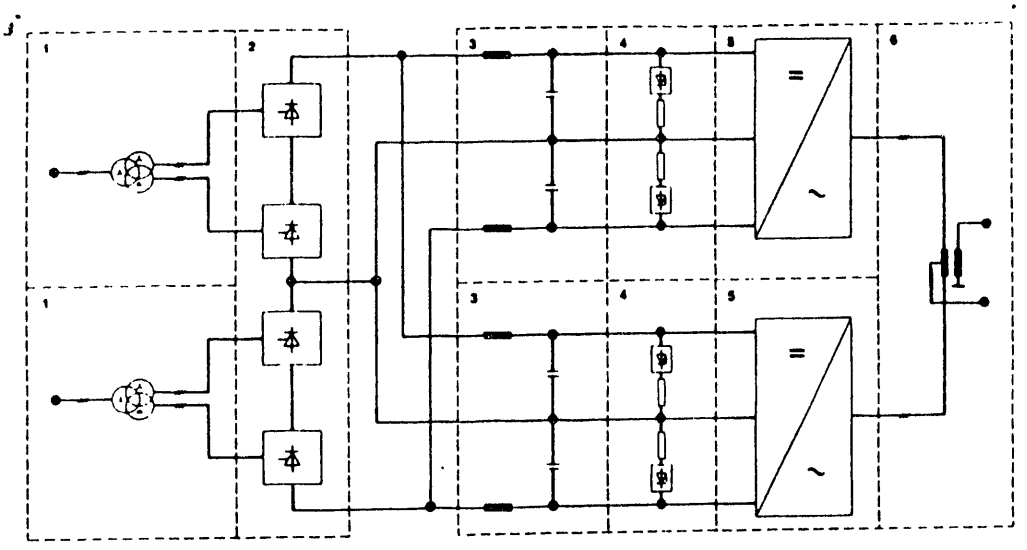

Fig. 1. Block diagram of converter system .

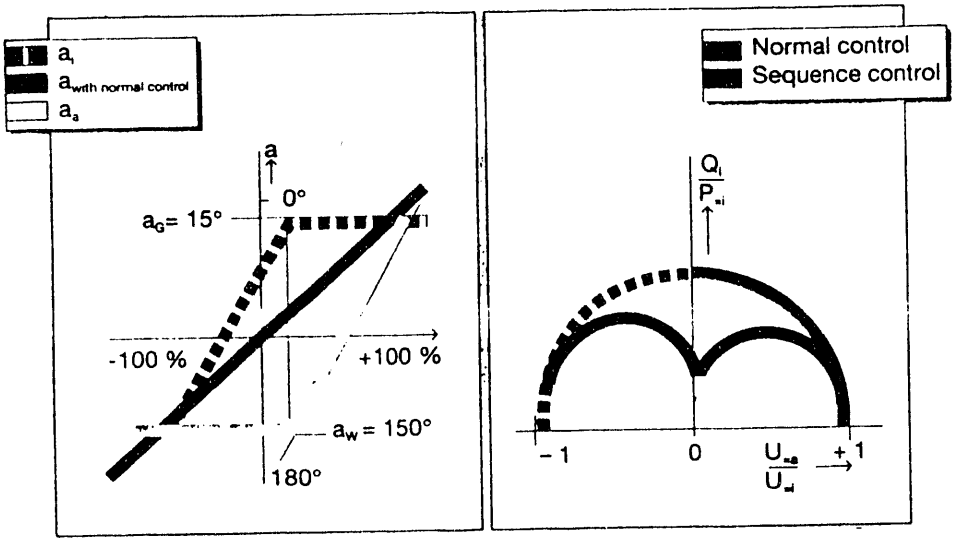

Fig. 2. Control curve and fundamental frequency of reactive power for sequence control of rectifier bridges

function of limiting control angle (Fig. 2). The comparison with normal control shows a considerable reduction during the rectifier mode (first quadrant), particularly in the low-voltage range.

On the output side, during operation of the neutral-point-clamped inverters on the common output transformer, the phase angles of both inverter voltages are adjusted so that, when the voltages are added up in the output transformer, a motor voltage is obtained with minimum harmonics.

This is necessary to limit resonant currents in the cable system of the long-stator motor. A method was developed so that once the resonant frequencies of the individual feeder sections are established, the phase-shift angle can always be controlled to minimize the magnitude of the resonance-exciting harmonics (Fig. 3).

2. Digital drive control

2.1 *Overview*

The digital drive control system (DDC) developed by Siemens in 1989 has proven itself at the TVE test facility in Emsland [1]. The main functions are (Fig. 4): Vehicle position detection, speed control, current

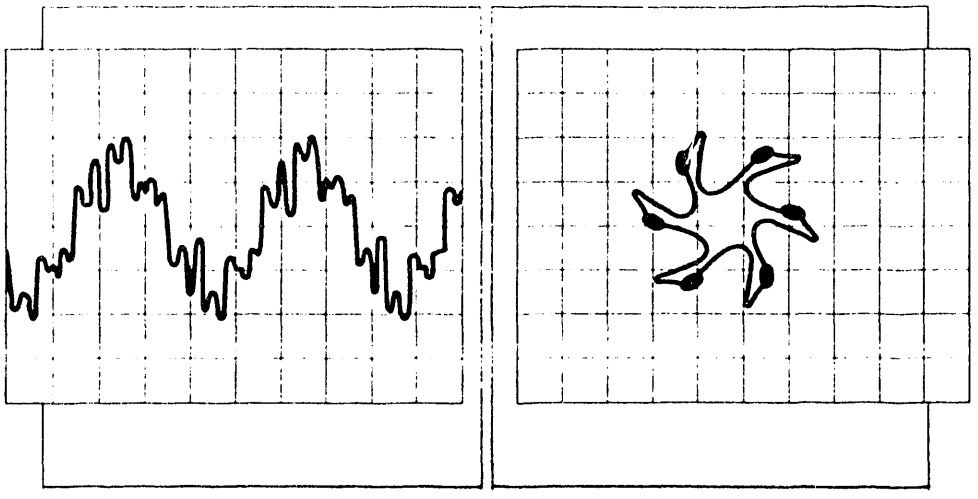

Fig. 3. Inverter current at $\gamma = 18.7°$, $f_1 = 240$ Hz, $f_{Bas} = 1680$ Hz, $U_d = 2x200$ V, (20 A/T, 1ms/T)

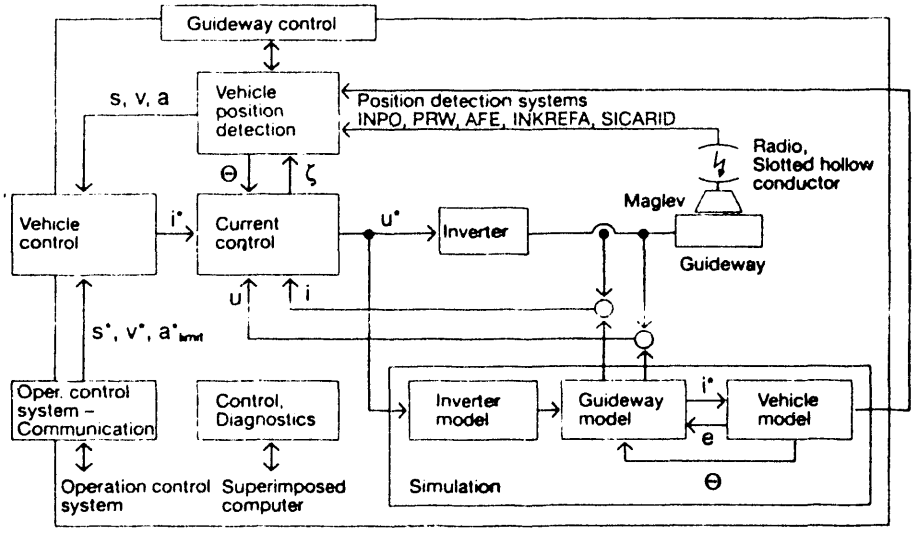

Fig. 4. Block diagram of digital drive control

control, serial data communication with BLT II operations control system, target braking with reference value generator and constant distance control.

DDC is based on the components of the SIMADYN D multi-microcomputer system. The processor modules are designed to perform general open-loop and closed-loop functions. High-speed current and voltage measurement, current control and setpoint output to the inverter, processing of all vehicle position detection data, as well as phase-angle control and maglev simulation - all these functions are implemented by a special signal processor module.

Processor sampling times were selected to meet function requirements. For example, since resonant frequencies of the distributed system (with output transformer, feeder cable and switch section winding) are at approx. 1.5 kHz, a sampling time of 100 µs is needed for current and voltage measurement purposes.

The DDC has an enhanced test capability thanks to more accurate inverter simulation, to the inclusion of all switch section parameters, and to the creation of a digital vehicle model including all vehicle position detection and location systems.

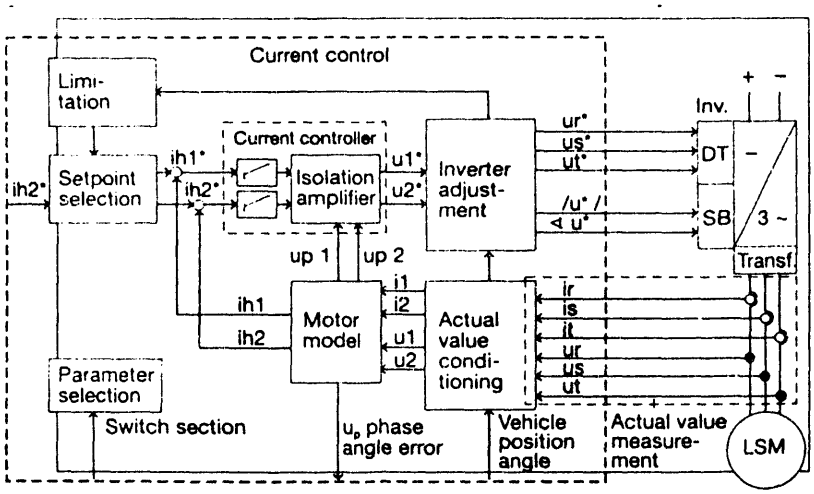

Fig. 5. Block diagram of digital current control

2.2 *Current control*

The current control operates according to the Transvector control principle, which means that the stator current components are adjusted in parallel (thrust current) and vertically (magnetizing current) to the magnetic flux in the motor air gar according to the speed control (vehicle control) setpoints (Fig. 5).

2.3 *Vehicle position detection*

Vehicle position detection comprises the functions of phase-angle control, absolute position detection, and load force sensing (with a controlled vehicle model).
The current control system is based on the principle of field-oriented closed-loop control. To be able to break the currents and voltages down as required into components that are parallel and vertical to field orientation, it is necessary to know the angle between motor excitation and the stator (in this case, rotor excitation = the magnetic levitation field of the vehicle).
Phase-angle control determines this geometrical, periodic load angle with the aid of a number of measurement methods and also establishes the actual vehicle speed.

2.4 *Vehicle control*

Vehicle control encompasses the target brake, reference variable generator, and distance-speed control functions.
The target brake constitutes the most significant additional function in the new digital drive control system. It enables the maglev to travel over the guideway according to a specified route-speed profile (which makes due allowance for the momentary vehicle status, the position-related and speed-related braking capability of the propulsion system, and the ride quality conditions) and to come safely to a halt at a preappointed destination [2].
The position-speed message issued by the operations control system to digital drive control defines the sections of the route, each section with its own start position and target position, limit speed, as well as permissible acceleration and deceleration rates. The first section of the route begins with the same start position as the direction-of-travel message, which serves to prepare the vehicle for entry of the actual start position and relevant vehicle direction and direction of travel. The speed permitted in each route section is dictated by the limit speed, the permissible speed at every target position is always zero. This automatic zero position speed can be cancelled by the transmission of a new position-speed message having a start position identical to the destination of the preceding route section.
This system makes it possible to determine a route-speed profile over the entire dedicated guideway, from start position to final destination (Fig. 6).
The resulting route-speed profile defines the dedicated, technically secured operation curve. The drive command message can be used to select any speed setpoint within this operation curve. If the setpoint exceeds the limit speed of the particular section, digital drive control restricts the drive command message to the speed limit.
The reference variable generator provides the link between target braking and setpoint selection according to the drive command message, on the one

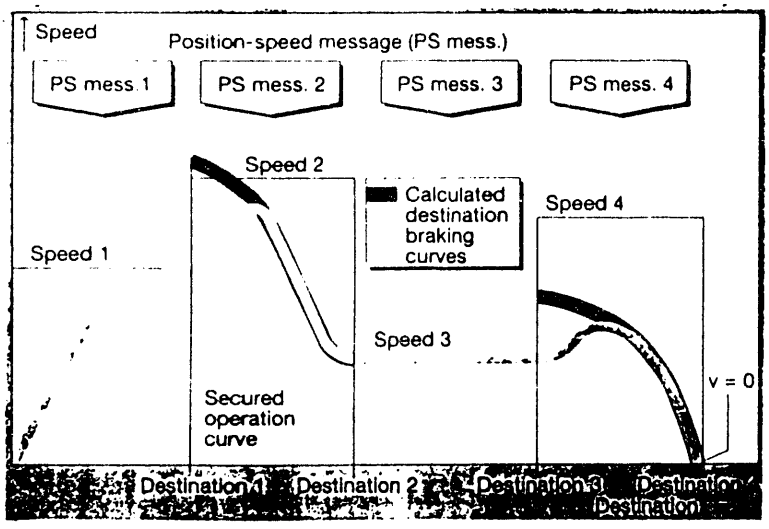

Fig. 6. Route-speed profile, target brake curves

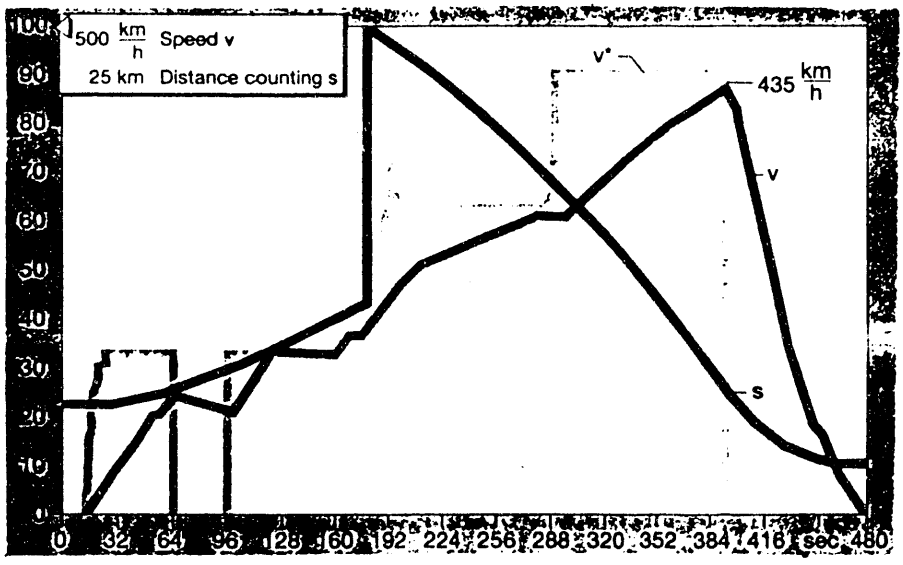

Fig. 7. Record run of December 18, 1989

hand, and the distance and speed control system, on the other. It continually processes the data from the internal route-speed profile and calculated target braking curve and compares this data with the specified speed setpoint. It selects the variables currently needed and determines reference variables without overshoot for distance-speed control and for acceleration precontrol in accordance with ride quality standards (acceleration/deceleration limit value 1.5 m/s^2, jerk limit value 0.5 m/s^3).

2.5 Field experience

The functions of the DDC system were demonstrated in high-speed trial runs in mid-December 1989, when record speeds of up to 435 km/h were reached (Fig. 7). To demonstrate and test the staggered arrangement of motor windings, the DDC system was configured to permit operation of switch sections 4 to 7 alternatively using the staggered motor-winding method or the leap-frog feeder circuit arrangement. The trial runs verified the principle operating reliablility of the staggered arrangement of motor windings.

The test runs performed with target braking control showed that the vehicle can be controlled according

the setpoints issued by the supervisory level and that preselected destinations can be approached in almost optimum time.
The performance of the DDC system at the TRANSRAPID test facility demonstrates that it is possible and expedient to use a digitally based drive control system for maglev vehicles, as well as the current control system for fundamental frequencies of up to approx. 270 Hz tested with that control system. It has also been proved that, on the basis of the existing configuration, no major problems are to be expected for future applications.

3. Outlook

The synchronous long-stator propulsion system for TRANSRAPID has sufficient maturity for revenue service. From a technical point of view, the basic criteria for the realization of a reference passenger-service line have been satisfied.

REFERENCES

[1] Henning, U.; Friedrich, R.; Hochleitner, J.; Laber, H.; Weller, A.; Eikermann, J. and Ruppel, J.: Entwicklungsstand des Langstatorsynchronmotor-Antriebssystems des TRANSRAPID
Statusseminar Schnellbahnen, Fulda, November 1991 (pp. 18.1...18.23).

[2] Henning, U.; Knigge, R.; Freitag, V.: Propulsion and Control System for High-speed Maglev Trains.
6th World Conference on Transport Research, Lyon, June 1992, SS 03 (pp.1100.1...1100.12)

Power Supply System for Superconducting Magnetic Levitation System

Haruo Ikeda, Hisao Ohtsuki
MAGLEV System Development Division, Railway Technical Research Institute, Tokyo, Japan

Jun-ichi Kitano, Yutaka Osada
Linear Express Development Division, Central Japan Railway Company, Tokyo, Japan

Nobuo Katoh
Toshiba Corp., Tokyo, Japan

Naoki Morishima
Mitsubishi Electric Corp., Hyogo, Japan

Hidetoshi Aizawa
Hitachi Ltd., Ibaraki, Japan

Abstract - **A development for the superconducting magnetic levitation system as a new high speed transportation has been progressing in Japan. Many kinds of running tests have been carried out at the test track with 7 km length in Miyazaki Prefecture since 1977. Now, a new test track is under construction in Yamanashi Prefecture.**

The driving system for the new test track employs a linear synchronous motor (LSM) with primary side on ground which consists of the superconducting magnets aboard the vehicle and the armature coils on the ground. The 3-phase ac current with variable frequency and variable amplitude, which synchronizes with the vehicle speed, is supplied to the armature coils. The power converter installed at the power conversion station feeds the driving power to the armature coils, and the vehicle speed is controlled by the amplitude of ac current. The circulating current type cycloconverters with a rating of 16 MVA have been used as the driving power source for LSM at Miyazaki test track. This type cycloconverters have great influence on the utility power system. Then, it is decided to adopt PWM (Pulse Width Modulation) inverter at Yamanashi test track. Therefore, PWM inverter with a rating of 10 MVA was installed and some experimentations have been carried out at Miyazaki test track.

The driving power is fed to the armature coils through change-over switchgears and power cable which represents a three-twisted cable combined with a neutral wire. The change-over switchgears connect this power cable to the armature coils which are electrically divided into some sections of a fixed distance. Moreover, these change-over switchgears need to be operated many times without maintenance.

This paper describes not only the new power supply system but also the function, configuration, and characteristics of each component for the LSM with primary side on ground in the superconducting magnetic levitation system.

Manuscript received March 15, 1993. This development has been financially supported by the Japanese Government.

I. INTRODUCTION

In Japan, a new test track for MAGLEV, which employs LSM (Linear Synchronous Motor) with the superconducting magnets aboard the vehicle and the primary armature coils on the ground, is now under construction in Yamanashi Prefecture. Feasibility tests for MAGLEV will be carried out at the new test track.

The feeding system with three power converters shown in Fig.1 is adopted at the new test track. The adoption of this system enables a vehicle to run even if one of the three power converters does not operate.

The devices for power supply used in the new test track are being manufactured at the factories of the specified makers, and some of them have been completed.

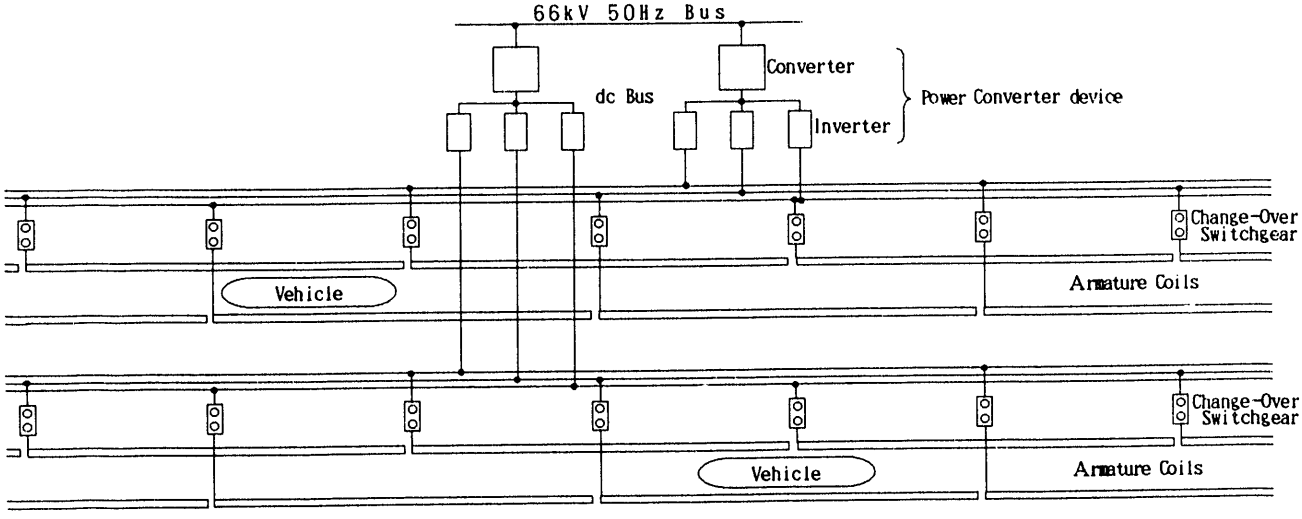

Fig.1 Power Supply System at the New Test Track

The prototypes of power converter and power feeding cable were tested at Miyazaki test track. And 4 prototypes of change-over switchgear were produced on trial basis, and a life test of more than 300,000 switchings has been carried out at the factories. The result of these experimentations shows that this type devices for power supply can be employed at the new test track.

This paper gives an outline of these devices for power supply which have been already manufactured to be employed at the new test track, and reports on the results of the experimentation which has been carried out at Miyazaki test track and the factories of the specified makers.

II. POWER CONVERTER

The power converters with large capacity, which supply the driving power to the LSM, are required for MAGLEV system. In the LSM system, 3-phase ac current with variable frequency and variable amplitude, which synchronizes with the vehicle speed, needs to be supplied to the armature coils. The power converter installed at the power conversion station feeds the driving power to the armature coils, and the vehicle speed is controlled by the amplitude of ac current. Therefore, the power converter for driving LSM is required to have the following capabilities;

(1) Changing the output frequency from dc to high frequency (around commercial frequency).

(2) Supplying necessary 3-phase currents even if an electromotive force of high voltage is present. The circulating current type cycloconverters with a rating of 16MVA have been used as the driving power source for LSM at Miyazaki test track. This type cycloconverter has great influence on the utility power system. Then, it is decided to adopt GTO (Gate Turn-Off Thyristor) inverters with PWM (Pulse Width Modulation) control at the new test track.

1. Power Converters for the New Test Track

At the new test track, 2 groups of power converter are required, because 2 vehicles are operated at the same time according to the test plan. Each group of power converters consists of 1 converter and 3 inverters. A GTO inverter with PWM control is employed in both groups. However 2 different type converters are employed in each group. One is a common (reverse blocking triode) thyristor converter with firing phase-angle control. The other is a GTO converter with PWM control. Table 1 shows the specifications of power converters for the new test track. The main frames of converter and inverter have been manufactured, and are ready for installation at the new test track. The external appearances of the converter and the inverter are shown in Fig.2.

2. Prototype Inverter Installed at Miyazaki Test Track

In the actual use of PWM inverter, some problems need to be solved such as changing the main circuit constitution of inverter between low speed and high speed circuit, suppression of magnetic saturation in transformer and reduction of high

TABLE 1 SPECIFICATION OF POWER CONVERTER FOR THE NEW TEST TRACK

		For North Line	For South Line
Converter	Type of control	Firing phase-angle control	PWM control
	Capacity	69 (MVA)	33 (MVA)
	Input voltage	66 (kV)	66 (kV)
	Input frequency	50 (Hz)	50 (Hz)
	Output voltage	±3,450 (V) dc	±2,625 (V) dc
Inverter	Number of phases	3	3
	Capacity	38 (MVA)	20 (MVA)
	Output current	960 (A) sinusoidal wave	1,015 (A) sinusoidal wave
	Output phase voltage	3,530 x 4 (V)	2,300 x 3 (V)
	Output frequency	0 ~ 56.6 (Hz)	0 ~ 46.3 (Hz)
	Carrier frequency	500 (Hz)	300 (Hz)
	Element	GTO thyristor 4,500V - 3,000 A	GTO thyristor 4,500V - 4,000 A
	Element composition	4S - 1P - 4A / full bridge	3S - 1P - 4A / full bridge
	Cooling type	Water cooling	Water cooling

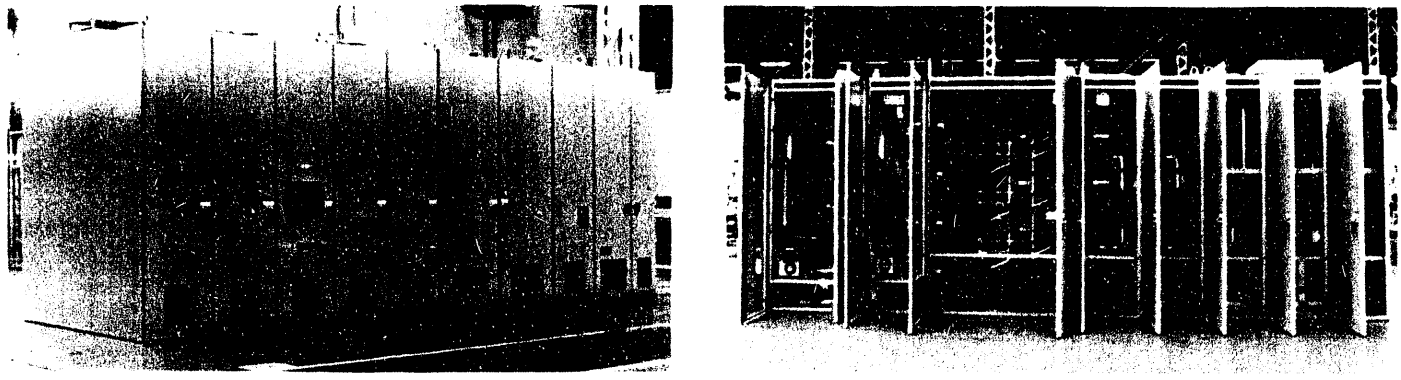

Fig. 2 External appearance of inverter for the new test track

harmonics caused by PWM control. In order to confirm the effectiveness of methods which solve these problems, a PWM inverter with a rating of 10MVA produced on trial basis was installed at Miyazaki test track, and the performance and characteristics of the inverter were confirmed by running tests.

2.1 Constitution of Inverter

A. Main Circuit Constitution

Fig.3 shows a diagram of the main circuit (bridge connection) and Table 2 shows the specification of the inverter. In order to realize high output voltage with less harmonics, the inverter consists of 2 unit inverters with an output transformer, and it is designed such that the output voltage can be summed up by cascade connection of the transformer, as shown in Fig.3. However, in case of low speed, since the output frequency of the inverter is low, it is impossible for the inverter to supply the necessary voltage from the output transformer. Therefore, at the low output frequency, an inverter constitution which has not the output transformer is needed.

In the system shown in Fig.3, when the output frequency is low, one of the two unit inverters functions as a half-bridge (HB) inverter which does not need the output transformer, and the other unit inverter functions as a full-bridge (FB) inverter.

When the inverter is not operated at change-over sections, the switching from the main circuit for low speed to the one for high speed is done by opening and closing the switches (SWL, SWH) shown in Fig.3. The frequency at which the main circuit for low speed is switched to the one for high speed depends on the maximum output voltage of the main circuit for low speed and the capacity of the output transformer. In practical use, the switching frequency is from 6 to 8 Hz because of change-over sections.

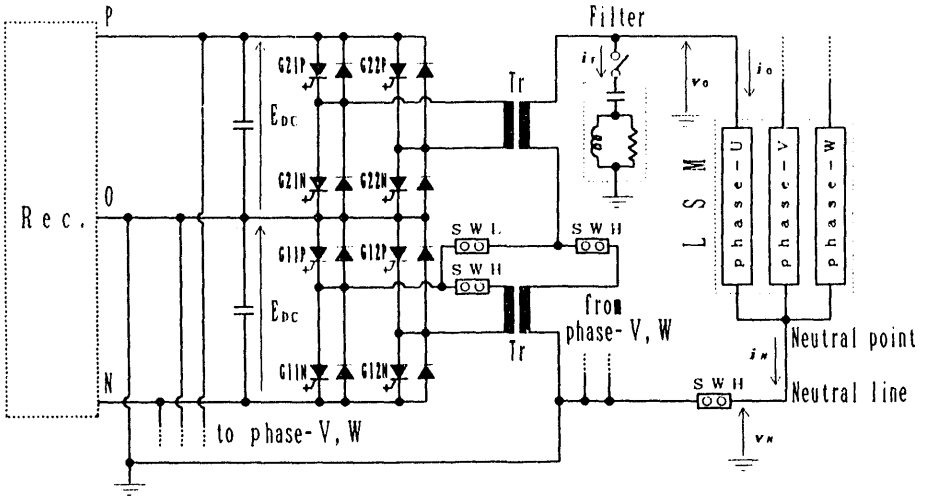

Fig. 3 Main circuit of PWM inverter for Miyazaki test track

TABLE 2 SPECIFICATION OF INVERTER FOR MIYAZAKI TEST TRACK

Performance (one phase)	DC input voltage	O-P, N-O DC3,450V (DC3,650V)
	Capacity	3,024kVA (3,195kVA)
	Output voltage	AC1,680V x 2 (1,780V x 2)
	Output current	AC900A
	Output frequency	0 - 30Hz
	Carrier frequency	500Hz
Type, Structure	Conversion type	Asynchronous PWM typed inverter
	Cooling type	Water cooling
	Element	GTO thyrister 4,500V-3,000A
	Element composition	2S-1P-4A/full-bridge

B. Output Transformer

The output transformer for LSM drive, which is different from the ordinary transformer used at the commercial frequency, is used at a very low frequency and under an unbalance between positive and negative output voltage caused by asynchronous PWM control. Then saturation or asymmetrical magnetization tends to arise in the iron core of the transformer. In order to supply stable power to LSM under this situation, it is necessary to so design the iron core of the transformer as not to cause saturation or asymmetrical magnetization. Since the maximum flux density of the transformer has been designed for about 1.4 times the rated value, the flux does not attain the saturation area in the rated operation. Moreover, the transformer does not produce output voltage under 2 Hz, and the time required for current rise at starting operation or current fall at stopping operation is set at integral multiples of output frequency so that any residual flux does not remain in the iron core of the transformer.

C. Filter

Many harmonics caused by PWM controller are contained in the output voltage of PWM inverter. To reduce the harmonics content, a filter is installed at the output of inverter as shown in Fig.3. The filter serves to suppress harmonics resonance occurring in feeding circuit in addition to reducing the harmonics.

2.2 Output Control

A. Output Current Control

In order to supply an output current to LSM corresponding to the output current reference given from the speed controller, the 3-phase output currents are totally controlled on d-q coordinates and also the zero-phase component is individually controlled to make the neutral line current zero. On the other hand, in case of low speed main circuit where zero-phase component does not exist, the d-q control without zero-phase control is used.

B. Output Voltage Assignment Control

In order to prevent the magnetic saturation of output transformer in the main circuit for low speed, the rate of the output voltage from FB and HB is controlled. The output voltage is wholly assigned to HB under 2 Hz. On the other hand, when the frequency is more than 2 Hz, the output voltage from HB is supplied depending on the V/f characteristics of output transformer. In the main circuit for high speed, 2 FB are assigned

each to supply half the necessary output voltage.

C. Asymmetrical Magnetization Suppression Control

The magnetic saturation of output transformer can be basically avoided by large magnetic flux density in the iron core of output transformer. However, very low output frequency or dc component contained in the output voltage, which is induced by positive and negative output voltage irregularities caused by PWM control, tends to asymmetrically magnetize the iron core in the output transformer and finally leads to magnetic saturation. Therefore, it is necessary by controlling the output voltage of the inverter to prevent the output transformer from being asymmetrically magnetized. When the exciting current exceeds a specified magnitude, the asymmetrical magnetization suppression controller detects the occurrence of asymmetrical magnetization and prevents the iron core of output transformer from being asymmetrically magnetized with the imposition of a voltage for canceling the asymmetrical magnetization on the output voltage control signal being given from the output voltage assignment controller.

2.3 Results of the Experimentation

In order to confirm the basic performance of the inverter in a trial, running tests with and without vehicles were carried out. The results are summarized as follows;

(1) PWM inverter is available for the power conversion device in LSM drive to supply stable power.

(2) Switching from the main circuit constitution for low speed to the one for high speed can be done while the operation is suspended at the change-over sections.

(3) Even in the area of low frequency, under the asymmetrical magnetization suppression controller, the output transformer is available.

(4) The harmonics in output voltage caused by PWM controller and the harmonic resonance caused by feeding circuit can be reduced, if the filter is inserted at the output of inverter.

III. Feeding Circuit Facilities

The main parts of feeding circuit are change-over switchgears and a power feeding cable in MAGLEV system. Most of the change-over switchgears to be used at the new test track were manufactured. A prototype of power feeding cable, whose specification had been already completed, was experimented at Miyazaki test track.

1. Change-Over Switchgear

The change-over switchgears connect the power feeding cable to the armature coils which are electrically divided into some sections with a fixed distance, and open or close according to the position of vehicle. Therefore, it is necessary that the change-over switchgears can be operated many times with quick movements. Vacuum switches are employed as the main contacts of the change-over switchgear for the following reasons;

(1) The size of devices can be small.

(2) Repeated operation can be done.

(3) High speed operation can be done.

(4) Total cost including maintenance cost is low.

Table 3 shows the specification of the change-over switchgear used at the new test track. The switchgear contains a disconnector and a switch of earth, which are used for maintenance of ground armature coils. The tanks of switchgear are filled with insulation gas for the purpose of reducing the insulating distance.

Four prototypes of change-over switchgear were produced on trial basis, and a life test of more than 3 00,000 switchings has been carried out at the factories of the makers. The results of these experimentations show that in the change-over switchgears no wear was detected after the life test.

The external appearance of the change-over switchgear used at the new test track is shown in Fig.4.

2. Power Feeding Cable

At the new test track, a cross-linked polyethylene insulation power cable (X-cable), which represents a three-twisted cable combined with a neutral cable, is employed as the power feeding cable, for the following reasons;

(1) The space for laying is small. (Particularly, this is im-

TABLE 3 Specification of Change-over Switchgear

	For North Line	For South Line
Voltage (kV)	24 (7.2)	12 (7.2)
Current (A)	960 (150)	1,015 (150)
Frequency (Hz)	0 ~ 60	0 ~ 60
Number of phases	4 (including neutral)	4 (including neutral)
Closing hour (ms)	Less than 300	Less than 300
Opening hour (ms)	Less than 300	Less than 300
Life of switching	More than 300,000	More than 300,000

( ): For neutral

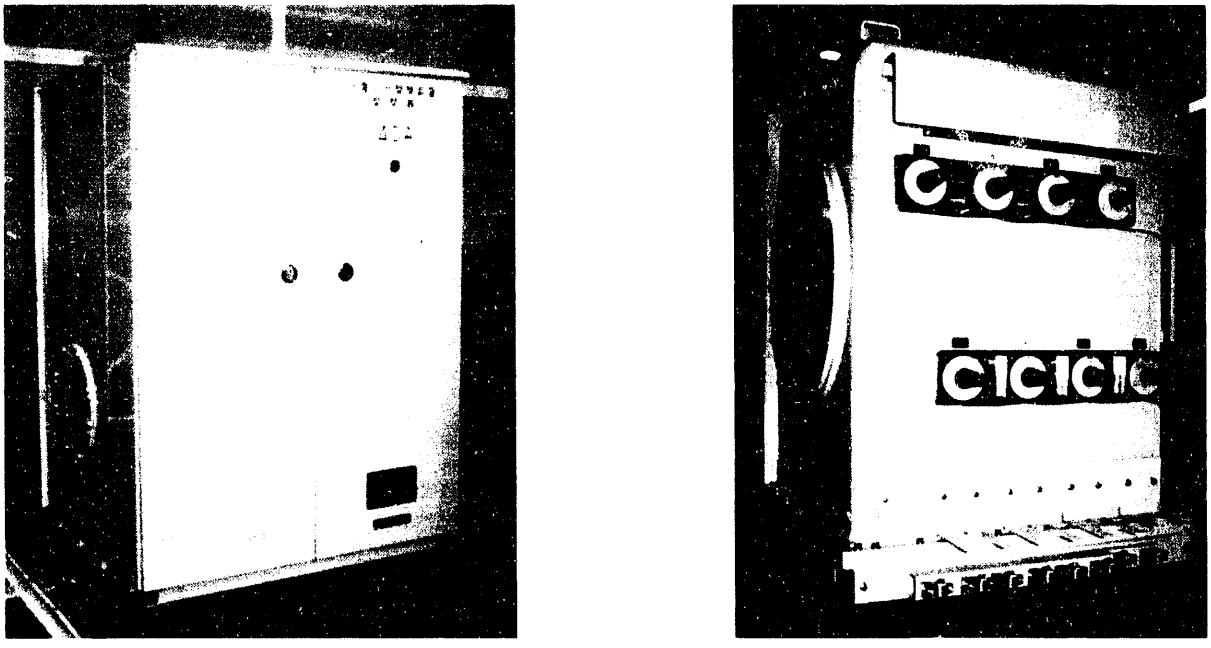

(1) Front view

(2) Rear view

Fig. 4 External appearance of change-over switchgear

portant at tunnels.)

(2) The cost for laying is low, because the cable can be mechanically laid.

(3) The influence on other facilities such as inductive interference can be reduced. The cross section of the power feeding cable is shown in Fig.5.

In the output voltage of PWM inverter, many harmonics caused by PWM controller are contained. The influence of the harmonics upon the insulation life of X -cable has not yet been clarified. Therefore, a long -term-deterioration test is carried out on X-cable. As the stressing voltage, a harmonic voltage (2 kHz) is applied in addition to the fundamental voltage (50 Hz).

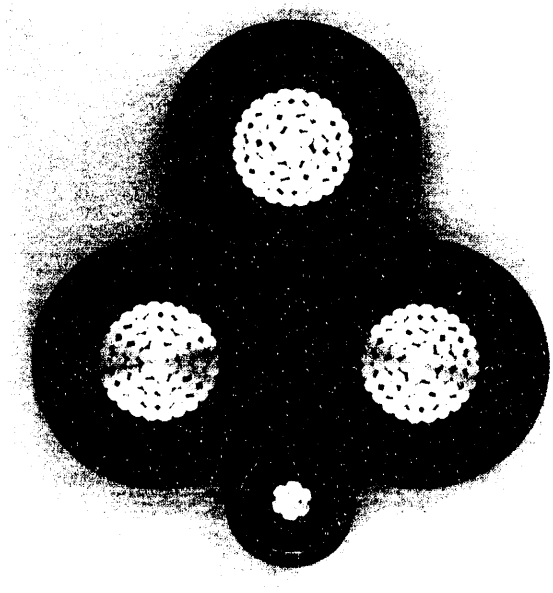

Fig. 5 Cross section of the power feeding cable

REFERENCES

[1] S.Kaga, S.Fukada, A.Okui, and H.Ikeda, "Development of PWM Inverter for Driving LSM", RTRI REPORT, Vol.5, No.12, pp.29-39, Dec., 1991

[2] Y.Nakamichi, A.Okui, S.Kaga, and H.Ikeda, "Characteristics of PWM inverter with large capacity for driving LSM", Proceedings of Symposium on Power Electronics, Electrical Drives, Advanced Electrical Motors, pp193-198, Positano, Italy, May 1992

[3] A.Seki, Y.Hosokawa, J.Kitano, H.Ikeda, S.Kaga, et al., "A 20MVA VVVF PWM inverter for the Yamanashi Maglev Test Line", Proceedings of 1992 National Convention Record I.E.E. Japan, Industry Applications Society, pp.11-14, Nagoya, Japan, Aug., 1992

[4] H.Ikeda, S.Kaga, K.Iwashige, J.Kitano, H.Kikuchi, et al., "A 38MVA PWM inverter for Yamanashi Test Track", Proceedings of 1993 National Convention Record I.E.E. Japan, March, 1993

[5] Y.Nakamichi, H.Toda, K.Ajiki, H.Ohtsuki, and R.Suzuki, "Development of Apparatus for Applied Voltage Tests Containing Harmonics", Proceedings of 1991 National Convention Record I.E.E. Japan, No.12, pp.53, Apr., 1991

Current control for Thrust Force Controlling Inverter of HSST

Ichiro Miyashita Youichi Ohmori
Technical Research Lavoratory, Toyo Electric Mfg. Co., Ltd.
Yamato, Kanagawa, 242 Japan

Abstract — This paper discusses the current control systems of the thrust force controlling inverter of HSST, which improves the feeling of accoustic noise genarated from Linear Induction Motors (LIM). Since the maximum allowable frequency of the inverter is limitted within a small value, due to the switching capability of GTO, any other method is needed to suppress the noise, without increasing inverter switching frequency. Some newly developed PWM and current control methods are compared from the viewpoint of the perception of electromagnetic noise and the current controllability, using some running test data.

1 INTRODUCTION

The mechanical noise of HSST is very low, because HSST is a Maglev car, and it doesn't have any mechanical noise generating components, such as gears, tortional shafts, or drives wheels to transmit the power from motor to the vehicle body. Since the electromagnetic noise generated from LIM is greater than mechanical noise, especially at low speed,it is required that electromagnetic noise be suppressed to a level lower than that of conventional electric motor coaches. The capacity of the cooling system for GTO inverter was severely restricted in order to make the body light. In consequence, the upper limit of switching frequency of GTOs was limitted to about 200Hz, while 400Hz is allowable in normal electric motor coaches. Therefore, a way to improve the feeling of noise was chosen, instead of attempting to lower the absolute quantity of noise, by reconstructing the current control loop. The current control systems of three types of experimental HSST car, such as series 04, 05, and 100, are evaluated from the viewpoint of both acoustic noise and current controllability, using actual running test data.

2 OUTLINE OF HSST

Table 1 shows the principal specifications of thrust force controlling inverters. HSST-04 and -05 series were tested in transporting of visitors, at '88 Saitama Exhibition and '89 Yokohama Exotic Showcase. Both series were designed for 200km/h service with 1500V input voltage, however, their operating speed were restricted only by 60 km/h with 750V, a half of rated voltage ; because the tracks were too short to run at a faster speed than that, in both exhibitions. On the contrary, HSST-100 series was desiged for 100km/h operation, with 1500V rated voltage. It is composed of two motor cars. Each of them have a driver's cab and 6 modules of 3 phase LIM coils. One inverter mounted on one car leeds the 12 modules of LIM, in all. HSST-100 recorded 110km/h in the test track.

Fig.1 shows the main circuit diagram of HSST-100. The main circuit of HSST-05 is fundamentally same as Fig.1, but in each car of HSST-05 has its own inverter and 8 modules of LIM fed by the inverter.

Table 1: INVERTER SPECIFICATION

		HSST-04	HSST-05	HSST-100
Input voltage	[V]	750	750	1500
Output voltage	[V]	550	550	1100
Output current	[A]	800	800	800
Capacity/car	[kW]	740	740	330
Slip frequency	[Hz]	17.5	12.5	12.0
Switching freq.	[Hz]		max 210	

3 THE RESTRICTION FOR THRUST FORCE CONTROL

A LIM module of HSST is composed of three phased L'M coil and a pair of levitation magnet coils. Though each coil system is electrically independent, the normal force of LIM which acts across the air gap between magnetic cores and reaction plates interferes with the levitation force. Fig.2 shows the characteristic curve of thrust force and normal force vs. slip frequency of LIM. The thrust force reaches its maximum value when slip frequency equals to 5Hz. But the normal force at that slip frequency still takes a large negative value. The normal force gets to zero when slip frequency is 17.5Hz, while the thrust force considerablly goes past its maximum value. In HSST-04, the slip frequency was fixed at 17.5Hz to keep the normal force zero. In HSST-05 it was changed to 12.5Hz to improve the thrust force characteristics of LIM.

4 THRUST FORCE CONTROL

The fundamental equations of voltage, current, and thrust force of LIM are shown by equation (1) and (2), as similar to rotary induction motor with cage rotor.

$$\begin{bmatrix} v_1 \\ 0 \end{bmatrix} = \begin{bmatrix} R_1 + pL_1 & pM \\ (p - j\omega_m)M & R_2 + (p - j\omega_m)L_2 \end{bmatrix} \begin{bmatrix} i_1 \\ i_2 \end{bmatrix} \quad (1)$$

$$F = (\pi/Z_p) \cdot M i_1 \times i_2 \quad \ldots\ldots\ldots\ldots\ldots\ldots\ldots\ldots\ldots\ldots (2)$$

Here,

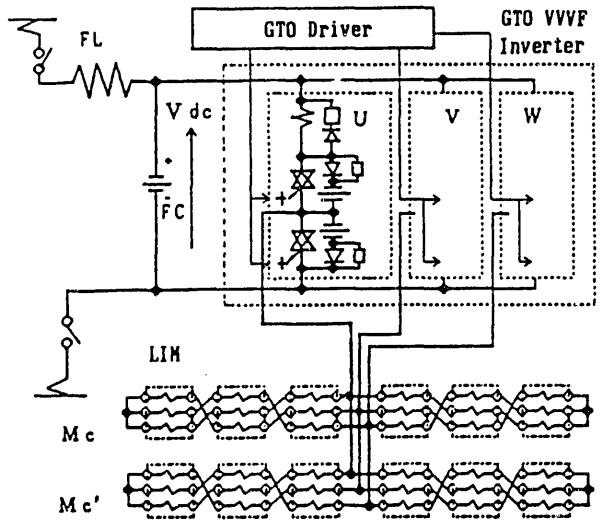

Fig.1 Main Circuit Connection Diagram

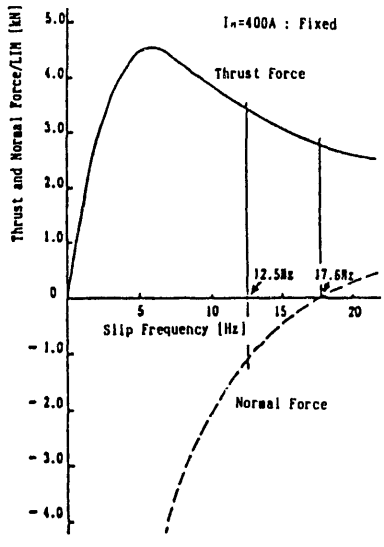

Fig.2 Thrust and Normal Force of LIM

R_1: Primary resistance R_2: Secondary resistance
L_1: Primary inductance L_2: Secondary inductance
M: Mutual inductance Z_p: Pole pitch
ω_1: Primary angular frequency
($\omega_1 = 2\pi f_1$, f_1: Inverter frequency)
ω_m: Motor angular frequency
($\omega_m = 2\pi f_m$, $\omega_s = \omega_1 - \omega_m$)
ω_s: Slip angular frequency
($\omega_s = 2\pi f_s$, f_s: slip frequency)
i_1: Primary current vector i_2: Secondary current vector
F: Thrust force

The spatial vector of primary current i_1 is defined equation is as follows.

$$i_1 = \sqrt{\frac{2}{3}}(i_u + i_v e^{-j\frac{2\pi}{3}} + i_w e^{-j\frac{4\pi}{3}}) \quad \cdots\cdots(3)$$

Here, i_u, i_v, i_w are the detected LIM input currents. The current components in d-q coordinates i_d, i_q are expressed by equation (4), using equation (3).

$$\begin{bmatrix} i_d \\ i_q \end{bmatrix} = \sqrt{\frac{2}{3}} \begin{bmatrix} 1 & -\frac{1}{2} & -\frac{1}{2} \\ 0 & \frac{\sqrt{3}}{2} & -\frac{\sqrt{3}}{2} \end{bmatrix} \begin{bmatrix} i_u \\ i_v \\ i_w \end{bmatrix} \quad \cdots\cdots(4)$$

The voltage spatial vector is also defined by the same form as equation(1) replacing i by v. Using the relation $i_u + i_v + i_w = 0$, the components of spatial vector are simplified as euations (5),(6).

$$v_d = \sqrt{\frac{3}{2}} v_u \quad \cdots\cdots(5)$$

$$v_q = \frac{v_u + 2v_v}{\sqrt{2}} \quad \cdots\cdots(6)$$

The magnitude of spatial vector of current i_1 is expressed by equation (7).

$$I^2 = 2(i_u^2 + i_u i_v + i_v^2) \quad \cdots\cdots(7)$$

The steady state voltage equation is obtained as (8) from (1), substituting p as $j\omega$,and using the relation $\omega_s = \omega_1 - \omega_m$.

$$\begin{bmatrix} v_1 \\ 0 \end{bmatrix} = \begin{bmatrix} R_1 + j\omega_1 L_1 & j\omega_1 M \\ j\omega_s M & R_2 + j\omega_s L_2 \end{bmatrix} \begin{bmatrix} i_1 \\ i_2 \end{bmatrix} \quad \cdots\cdots(8)$$

By eliminating i_2 from equation (2) and (8), thrust force can be expresseed by equation (9), using the magnitude of spatial vector I of primary current.

$$F = \frac{\pi}{Z_p} \cdot \frac{\omega_s R_2 M^2}{R_2^2 + \omega_s^2 L_2^2} I^2 \quad \cdots\cdots(9)$$

The magnitude of spatial current vector I given by equation (7). As the slip angular frequency ω_s is fixed at a constant value, the current vector I must be adjusted to control thrust force F.

The secondary flux interlinkage Ψ_2 is defined by equation (10).

$$\Psi_2 = M i_1 + L_2 i_2 \quad \cdots\cdots(10)$$

Eliminating from the second column of equation (8), and (10), Ψ_2 is expressed by equation (11), using ω_s and i_1 . And using the magnitude of Ψ_2 obtained from (11), and thrust force is rewritten as equation (12).

$$\Psi_2 = \frac{R_2 M}{R_2 + j\omega_s L_2} i_1 \quad \cdots\cdots(11)$$

$$F = \frac{\pi}{Z_p} \cdot \frac{\omega_s}{R_2} \Psi_2 \quad \cdots\cdots(12)$$

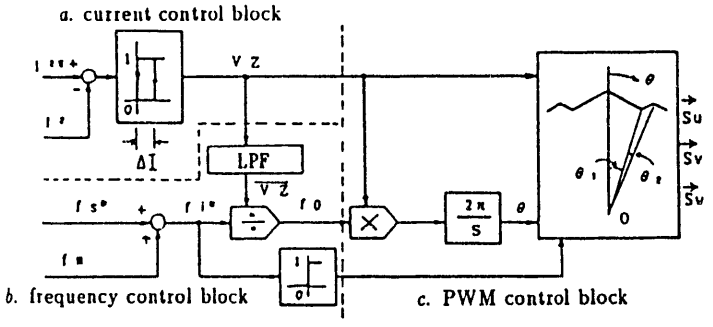

(a)HSST-04

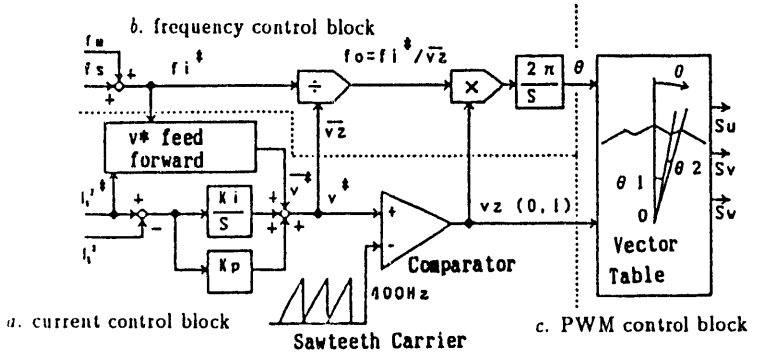

(b) HSST-05

Fig.3 Control Block Diagram

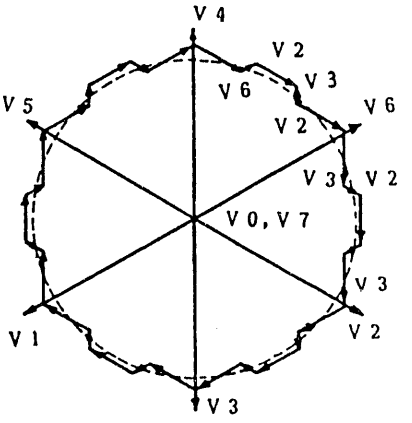

Fig.4 Quasi-Circular Voltage Locus

This means that the thrust force is controlled by adjusting the secondary flux Ψ_2 with fixed slip angular frequency ω_s, while torque is controlled by adjusting the slip angular frequency with the secondary flux kept constant in usual vector control of induction motors.

5 CURRENT CONTROL METHOD

5.1 The current control of HSST-04 and -05

The thrust force can be controlled by adjusting primary current I, with fixed slip ω_s, as mentioned above. The command of the square of current I^2 is made by solving the equation (9) for I^2. Actual I^2 is calculated from detected LIM current i_u and i_v by equation (7). Fig.3 show the block diagrams of I^2 control system. (a) and (b) are the control systems of HSST-04 and -05, respectively. Both systems have many common parts. They are divided into three parts:

a. current control block
b. frequency control block
c. PWM control block

Fig.4 shows a quasi-circular vector locus obtained by connecting 6 output voltage vectors of inverter, alternately with appropriate timing. The flux vector is expressed as a point on this locus, because flux of LIM equals to the time integral of the inverter output voltage. The length of each side on this locus is the product of the magnitude of output voltage vector and its output time. If the output of inverter is controlled so that the flux vector traces along with this locus, with a certain frequency f_0, the lower f_0 is, the larger the radius becomes. The tracing speed can be decreased, without changing the radius of the locus, by output of zero voltage vector on this locus with appropriate timing. The trace is interrupted when zero vector is output, and restarted when it removed. Thus the average tracing speed can be controlled. Fundamental behavier of each part of current control system is as follows.

a. Current control block

The fundamental difference between (a) and (b), in Fig.3, is how to treat the error signal of current squared I^2. In (a) method, error signal is directly transformed into an zero vector command VZ, by hysteresis comparator, while in (b) method,it is indirectly transformed, by comparing with triangular carrier wave, through the average voltage command v^* by PI amplifier. In both system, zero vector command decides the actual zero vector output timing. In VZ=0, zero vector is output, and VZ=1, zero vector is removed.

The average output frequency of zero vector is adjusted to be 400Hz, from the limmit of GTO switching capability.

The perception of electromagnetic noise seems to be concerned deeply with the zero vector generating pattern. The method using instantaneous control, as shown in (a), generates noise of a random nature, while the one using constant frequency carrier, as in (b),

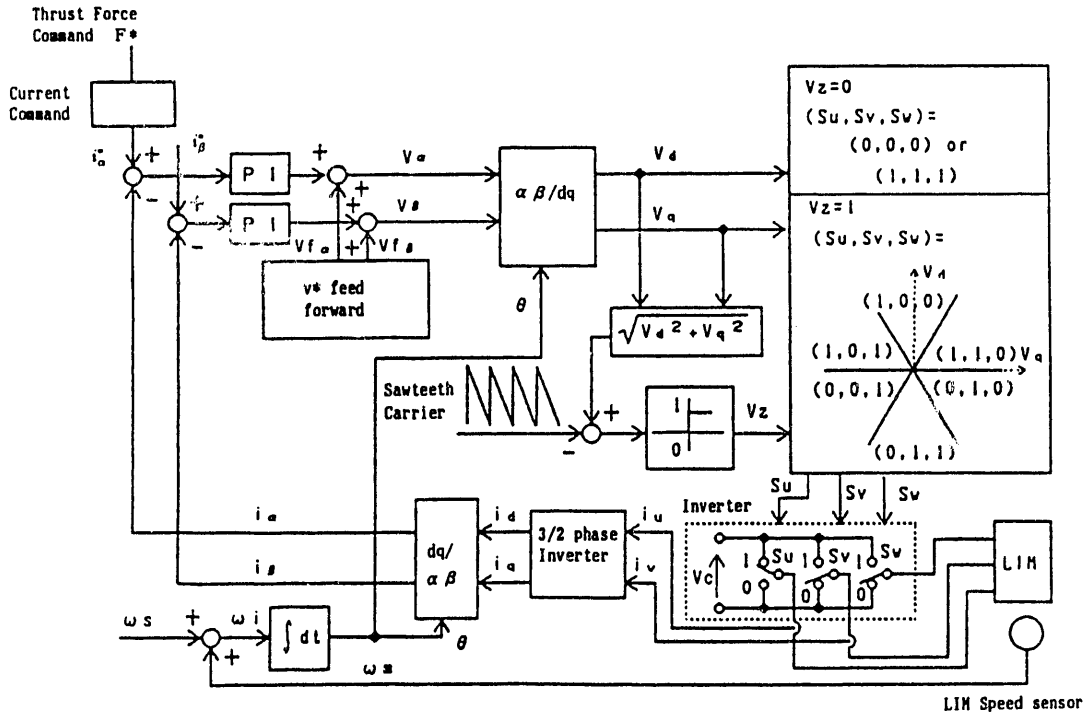

Fig.5 HSST-100 Control Block Diagram

produces noise with a monotonous feeling.

b. Frequency control block

Adding slip frequency command f_s^* to LIM frequency f_m, inverter frequency command f_1^* is obtained, shown as equation (13).

$$f_1^* = f_m + f_s^* \quad \cdots\cdots(13)$$

f_1^* corresponds to the average tracing speed of vector locus in Fig.4. Note that the instantaneous inverter frequency f_0 is equivalent to the instantaneous tracing speed, and the average tracing speed decreases to $f_0 \cdot \overline{VZ}$, because it will be stopping while zero vector is applied. Here, $\overline{VZ}$ is the time ratio of zero vector. Therefore, the instantaneous inverter frequency f_0 is obtained by dividing the given average frequency command f_1^* by the time ratio $\overline{VZ}$, as shown in equation (14).

$$f_0 = f_1^* / \overline{VZ} \quad \cdots\cdots(14)$$

By judging the polarity of frequency command f_1^*, the rotating direction controlling signal is generated.

c. PWM control block

This block decides which voltage vector is suitable for inverter voltage phase angle θ, from six non-zero vector $V_1 \sim V_6$. θ is calculated by integration of frequency f_0 , in the period while VZ=1. When VZ=0, zero vector V_0 or V_7, which can be reached by fewer switching numbers is selected. The voltage vector is output for this block, expressed by inverter switching state variables (Su,Sv,Sw). Here, Su,Sv,Sw=1, when inverter output is switched to positive bus, and Su,Sv,Sw=0, when switched to negative bus.

The phase angles θ_1, θ_2 in Fig.4, are gradually decreased to zero, as $\overline{VZ}$ increases to 1. At first only θ_1 decreases. After θ_1 gets to 0, θ_2 begins to decrease. Finally, when $\overline{VZ}$ reaches 1, $\theta_1 = \theta_2 = 0$. This corresponds to 1 pulse mode.

5.2 A feedforward of voltage command

The voltage command operating block, in Fig.3(b), oparates the voltage command V*, using equaton (15). This signal is fed forward to the output of current PI controller. Effective stabilization of current control loop can be obtained by this feedforward signal, even if with approximate operation. In fact, by this feedforward signal, P gain of current controller. Because it supplies almost all signal which the PI controller must generate by amplifing error signal. This method is applied to HSST-100.

$$v^* = (2\pi f_1^* A + R_1 \frac{B}{A}) \sqrt{\frac{3}{2}} \frac{I^*}{V_{dc}} \quad \cdots\cdots(15)$$

$$A = \sqrt{B^2 + C^2} \quad \cdots\cdots(16)$$

$$B = \frac{\omega_s R_2 M^2}{R_2^2 + \omega_s^2 L_2^2} \quad \cdots\cdots(17)$$

$$C = L_1 - \frac{\omega_s^2 + L_2 M^2}{R_2^2 + \omega_s^2 L_2^2} \quad \cdots\cdots(18)$$

5.3 Current control system for HSST-100

The line voltage for Series HSST-100 is raised up to the rated 1500V. It becomes more difficult to suppress electromagnetic noise and stabilize the current control system, than in 750V line voltage. Therefore, current magnitude control was divided into two axis

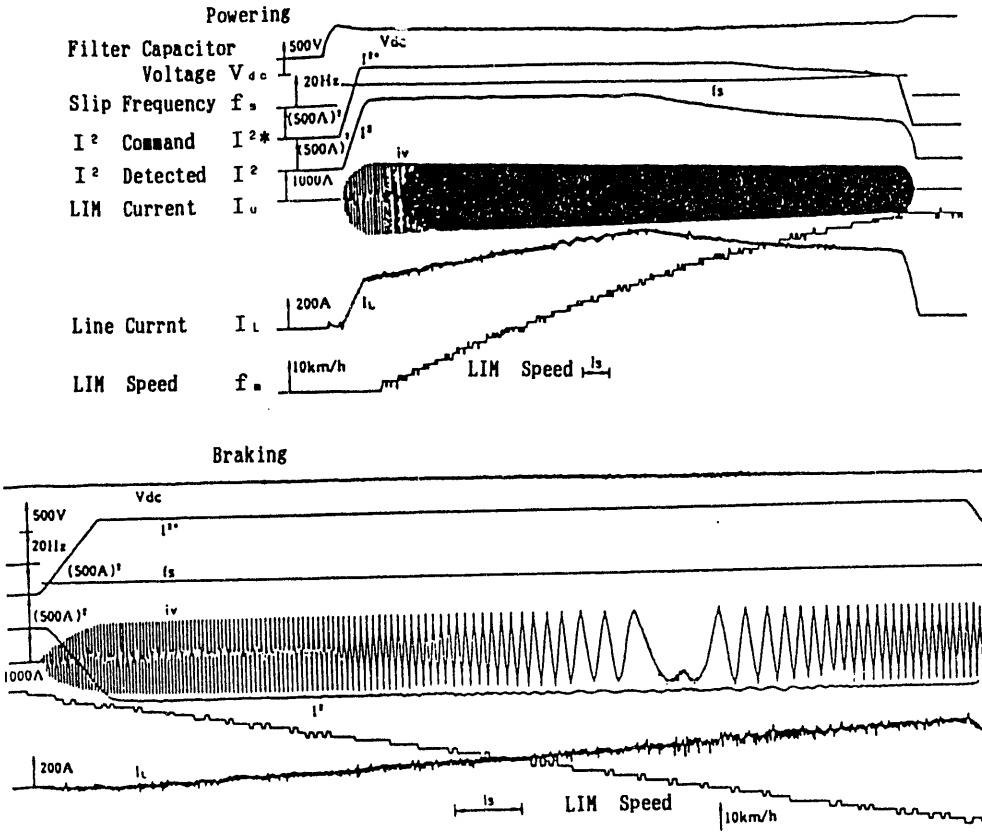

(a) HSST-05

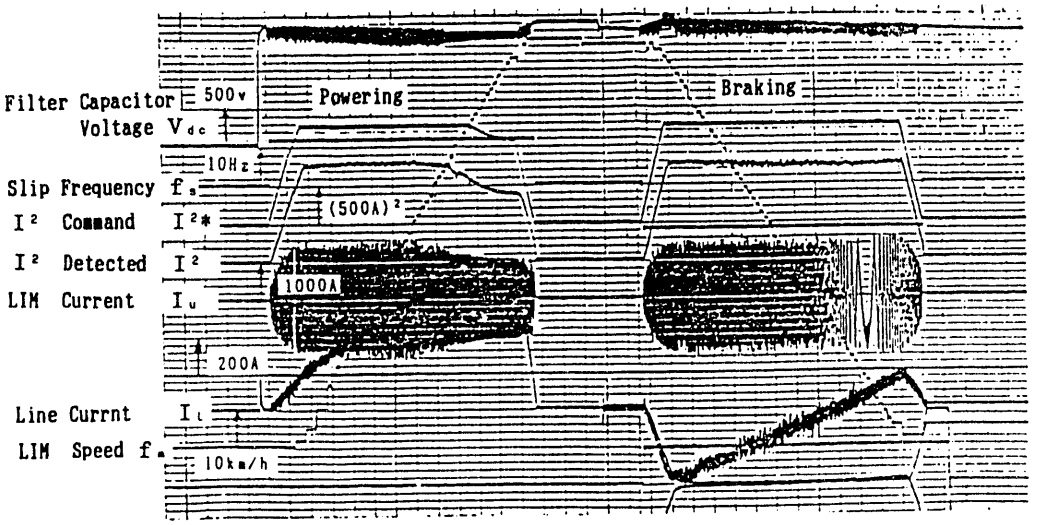

(b) HSST-100

Fig.6 Oscillogram of Running Test

components, and controlled independently, in order to improve the stability of control system.

Fig.5 shows the control block diagram. A direct voltage vector selection method was applied instead of the qasi-circular locus control method in HSST-05. An appropriate voltage vector is instantaneously selected by judging in which segment does the voltage phase angle θ exist; the segment given by dividing a cicle into six equal ones. This method increase the freedom of voltage vector selection than quasi-circular locus method, which especially improves the stability of current control near zero frequency. Zero vectors are controlled using constant frequency carrier signal. This zero vector control method is as same one as HSST-05, which had comparatively good reputation as for acoustic noise feeling. The electromagnetic noise from LIM has monotonous like the one from chopper controlled DC motor. Uncomfortable stepwise tone change of noise, raised by the step down of carrier frequency, in convevtional subharmonic PWM method with synchronized carrier signals, in acceleration and deceleration. In Fig.5, current control is done by making i_α and i_β follow the curren command i_α^* and i_β^*, respectively. Here, i_α and i_β are the α-axis ar d β-axis components of $\alpha-\beta$ coordinates rotating with the inverter frequency f_i^*. And current commands i_α^* and i_β^* are given by equations (19) and (20). i_α^* is given by solving equation (9) for current I, while i_β^* is kept zero at any instant. By keeping β-axis component zero, current control system can be simple.

$$i_\alpha^* = \sqrt{\frac{Z_p}{\pi} \cdot \frac{R_2^2 + (2\pi f_s)^2 L_2^2}{2\pi f_s R_2 M^2} F} \quad \cdots\cdots (19)$$

$$i_\beta^* = 0 \quad \cdots\cdots (20)$$

The detected LIM input current i_u and i_v are transformed to i_d and i_q in a stationary $d-q$ coordinates by coodinates transformation block, as shown in equation (5),(6).

And i_d and i_q are further transformed to i_α and i_β in a rotationary $\alpha-\beta$ coordinate using equation (21).

$$\begin{bmatrix} i_\alpha \\ i_\beta \end{bmatrix} = \begin{bmatrix} cos\theta & sin\theta \\ -sin\theta & cos\theta \end{bmatrix} \begin{bmatrix} i_d \\ i_q \end{bmatrix} \quad \cdots\cdots (21)$$

The current error signals $(i_\alpha^* - i_\alpha)$ and $(i_\beta^* - i_\beta)$ are independently amplified by each PI controllers. The outputs of PI controllers impressed to the inverse transfomation block. At that time, the feedforward signal of voltage command is added to the output of PI controller. Here, θ can be obtained by integrating the inverter frequency f_i^*. The output of inverse transformation block are given to PWM block,as final voltage commands v_d^* and v_q^* in stationery $d-q$ coordinates. One voltage vector is specified to every segment, mentioned above.

$$\begin{bmatrix} v_d^* \\ v_q^* \end{bmatrix} = \begin{bmatrix} cos\theta & -sin\theta \\ sin\theta & cos\theta \end{bmatrix} \begin{bmatrix} v_\alpha \\ v_\alpha \end{bmatrix} \quad \cdots\cdots (22)$$

The zero vector command VZ is obtained by comparing the magnitude of voltage vector with · arrier signal. If the voltage command is greater than the carrier, then VZ=1. Otherwise, VZ=0. PWM control block outputs zero vector, if VZ=0. And it outputs the specified voltage vector of the segment to which the angle θ belongs, if VZ=1.

6 RESULTS OF RUNNING TESTS

Fig.6 shows the oscillograms of running test. (a), (b) are of HSST-05, HSST-100, respectively. A common feature to both is that no stepwise change can be admitted in current waveforms, caused by pulse mode change. In fact, step change in acoustic noise from LIM could not be heard. The different points between (a) and (b) are ; 1)instantaneous ripple of current amplitude in (a) is smaller than in (b), because in (a), the output voltage vectors are programmed in regular order ; 2) the current waveform, especially at zero frequency in braking mode, is smoother in (b) than in (a). This is because the degree of freedom in selecting suitable voltage vector is higher, in (b) than in (a).

7 CONCLUSION

New current control systems for HSST are discussed from the view points of noise perception and current controllability. The electromagnetic noise from LIM strongly depends upon the zero vector control method. Zero vector control method by carrier signal with constant frequency seems to have good perception of noise, because it doesn't generate the stepwise tone changes in noise, which has been one of the defects of conventional synchronized subharmonic PWM method. The instantaneous voltage vector control method using 6 equally divided segments of a circle, has good current controllability.

Although the current control system of HSST-100 has the excellent features of both method, further improvement and reduction of electromagnetic noise should be done.

Acknowledgment

The authers would like to their thanks to the members of CHSST Co., Ltd., and Prof. Isao Takahashi of Nagaoka University of Technology.

References

[1] I. Miyashita and Y. Ohmori: "*New modulation method for VVVF Inverter for HSST-05* ", 11th International Conference on Maglev, July, 1989, pp.185-190

[2] T. Koseki and E. Masada: "*Lateral motion of a short-stator type magnet wheel with electromagnetic suspension system* ", 10th International Conference on Maglev, June, 1988, pp.101-110

A Novel Maglev System Driven by Air-Cored, Linear Induction Motors

E. Levi, Z. Zabar, L. Birenbaum, and S. Y. Yoo
Polytechnic University
333 Jay Street, Brooklyn, NY 11201

Abstract - The propulsion, suspension, and guidance system, presented here, consists of two principal parts. The first is a horizontal linear co-axial array of coils energized in polyphase fashion. The second is an exterior conducting sleeve with a longitudinal cut along the bottom to provide an opening for mechanical support of the coils. The paper presents some encouraging results of a preliminary study.

I. INTRODUCTION

Today's major competitors in the field of magnetic levitation for high-speed ground transportation are Germany and Japan, despite the early lead that the United States had acquired in the 70's. Both the German and the Japanese systems employ linear synchronous motors which are energized by the wayside. The difference is that, while the German motor utilizes iron cores to carry the magnetic flux, the Japanese one lets the flux be carried by air [1,2]. The main disadvantage of iron-cored motors is the need to maintain an air-gap clearance between the two parts in relative motion not exceeding 1 cm. At high speed this is difficult to achieve and implies high track-maintenance costs. The main disadvantage of the air-cored motors is the need for superconducting magnets which, with today's technology, are impractical, and expose personnel and passengers to high magnetic fields. Moreover, operation in the synchronous mode with energization by the wayside necessitates the maintenance of a perfect match between the vehicle's speed and the frequency of the energy supply system, which requires expensive power conditioning apparatus extending over the whole length of the track. In both the German and the Japanese systems the air gap through which energy is transferred from one winding to the other is planar, and only a fraction of the current-carrying conductors contributes to the generation of useful forces.

II. DESCRIPTION

The air-cored, induction, magnetic levitation system which is the subject of this paper bypasses all of the above difficulties. Since it is air-cored, it allows an air-gap clearance of a few inches; since it is operated in the induction mode, it allows energization by means of constant, industrial-frequency supplies. Moreover, its special topology with cylindrical air gap develops force components which are strong enough to provide suspension and guidance, as well as propulsion, and to which the conductors contribute over their whole length. The special topology and the presence of a massive secondary sleeve also may solve the problems of high compliance and low damping which plague the other Maglev systems [3].

A schematic representation of the proposed system is shown in Figs. 1 and 2 for energization by the wayside and on board the vehicle, respectively. The energized part of the motor or primary consists of an array of coaxial circular coils or of a helically wound cylindrical solenoid.

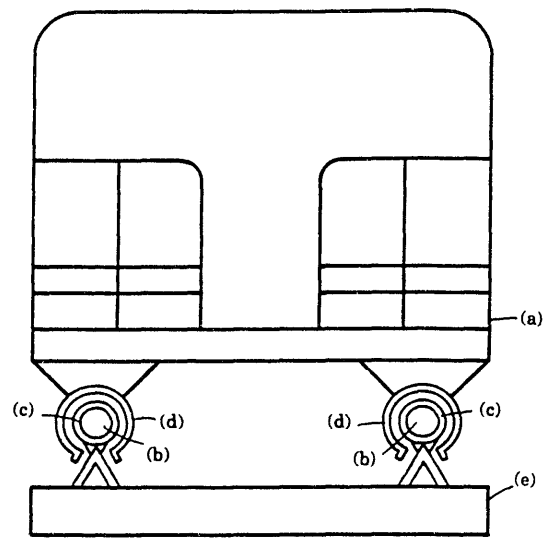

Fig. 1: Proposed Maglev System with energization from the wayside.
(a) vehicle, (b) air-cored linear induction motor, (c) energized motor primary: array of circular coils, (d) motor secondary: passive conducting cut cylinder, and (e) vehicle support.

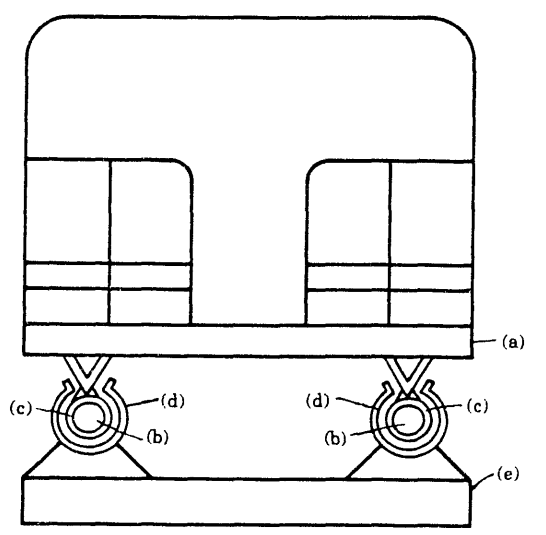

Fig. 2: Proposed Maglev System with energization on board the vehicle.
(a) vehicle, (b) air-cored linear induction motor, (c) energized motor primary: array of circular coils, (d) motor secondary: passive conducting cut cylinder, and (e) vehicle support.

Manuscript received March 15, 1993.

The primary is divided into sections which are energized sequentially by a polyphase system of alternating currents, thereby producing a traveling wave of magnetic flux density. This flux is coupled to the passive part of the motor or secondary, which ideally would consist of a cylindrical sleeve made of conducting material, such as aluminum, located concentric and exterior to the primary.

The relative motion, or slip between the wave (traveling along the primary) and the secondary would induce purely azimuthal currents in the secondary sleeve. The interaction between the primary and secondary currents would create a longitudinal force component used for propulsion and a strong radial centering force component used for levitation and guidance. However, in order to allow for mechanical support of the interior primary, the exterior cylindrical secondary sleeve must be cut longitudinally. In this case the currents induced in the secondary maintain their azimuthal direction over most of the cylindrical surface and turn longitudinal in the proximity of the cut to close along its two edges (See Fig. 3). The ribs which line the edges provide a low-resistance longitudinal path for closure of the azimuthal currents, and also provide mechanical strength. The currents which flow in the cylindrical portion of the sleeve in the azimuthal direction are denoted (Fig. 3b) by roman numerals I and III. The currents which flow in the rib in the axial direction are denoted by roman numeral II.

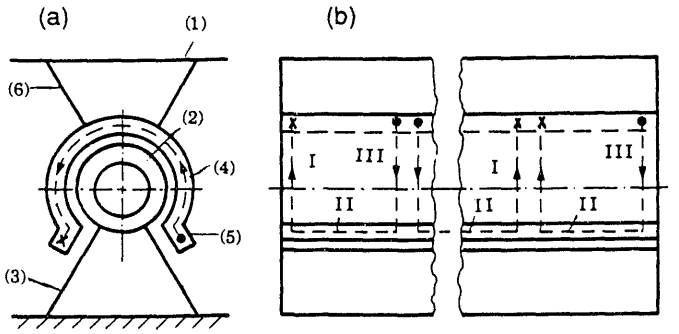

Fig. 3: Current path in motor: (a) front view; (b) side view. (1) vehicle, (2) primary drive coils, (3) primary support, (4) motor secondary: passive conducting cut cylinder, (5) edge, and (6) support for the secondary part.

These longitudinal portions of the secondary currents, being in opposite directions along the two edges, and having no counterpart in the primary, produce no appreciable force and, therefore, degrade only minimally the performance of the ideal motor in its propulsion, levitation, and guidance functions.

A main feature of the concentric location of the primary and secondary is the confinement of the magnetic flux that is carried by the inner core of the primary and that closes mainly in the cylindrical air gap between the primary and the secondary. This makes it unnecessary to use iron cores to reduce the magnitude of the magnetization-current needed to establish the magnetic field, and to reduce the exposure of personnel and passengers to the magnetic fields.

Another feature deriving from the cylindrical symmetry of the primary and secondary is that all portions of the current-carrying conductors contribute to the generation of useful forces. This tends to increase efficiency and tends to minimize material stresses, size, and cost of the apparatus.

The decision on whether to locate the energized primary by the wayside or on board the vehicle depends on economic considerations. Energization from the wayside is advantageous when the density of traffic is high. The primary is then energized in blocks of about 5 miles length for the sake of efficiency and in order to allow for emergency braking by means of phase reversal. In this case, the vehicle carries only the passive secondary and is, therefore, cheaper and somewhat lighter. When, instead, the energized primary is carried by the vehicle and the passive secondary lies along the road way, the track is cheaper. However, energization on board the vehicle implies the need for either current collection by catenary or third rail or the need for prime energy store and conversion apparatus located on board the vehicle. Tests conducted by the Office of Research and Development, Federal Railroad Administration, U. S. Department of Transportation in the early 70's have shown that properly designed distribution and collection systems can transfer the required electric power to vehicles traveling at speeds in excess of 300 mph (134 m/s) [4].

III. Approach to the Design

This novel Maglev System is a spin-off of an ongoing effort for the development of coil-gun-type electromagnetic launchers. The approach to the design will follow parallel lines. Determination of the dimensions of an electrical motor and optimization of the design are of necessity iteration processes that can be best performed using the simplest mathematical model. Significant simplification can be obtained by limiting considerations to the steady state. On the other hand the physical dimensions must be selected by making sure that the maximum allowable values of the electrical, mechanical, and thermal stresses are not exceeded. These local stresses can be determined only by using a field approach. To facilitate the analysis, one must simplify the geometry.

An approach that has been successfully tested reduces the primary and secondary windings to current sheets at equivalent radii and proceeds to the analysis of the cylindrical geometry by way of two intermediate-step approximations, the planar and modified planar ones [5]. This procedure leads to the determination of the parameters for the equivalent circuit of Fig. 4 and, as an example, to the dimensions listed in Appendix 1. In the figure, the 'Coupled' part represents the energized part of the primary that is coupled to the secondary sleeve. The 'Uncoupled' part represents the energized part of the primary that is not coupled to the sleeve. A special problem that was not contemplated in the previous work and that has been addressed by numerical computation, arises because of the loss in the symmetry of revolution caused by the cut in the exterior secondary sleeve. This will be dealt with in the next section.

Once the optimal physical dimensions have been determined, one can proceed to predictions of the transient performance. In linear induction motors, this involves edge and end effects. Whereas in the Maglev system described here the edge effects are limited only to one part of the motor, the passive sleeve, the end effect is particularly

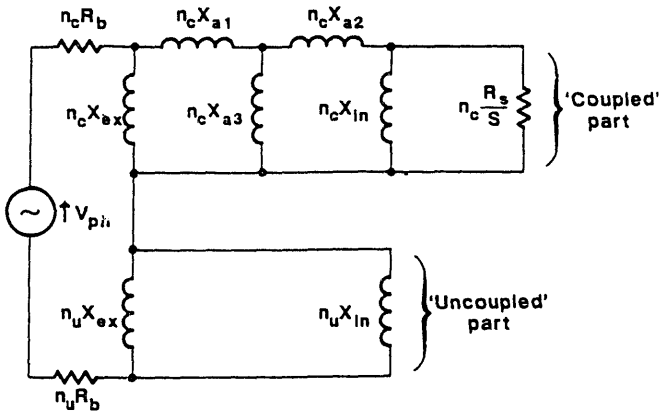

Fig. 4: Single-phase equivalent circuit of an air-cored, linear induction motor.
V_{ph} - phase voltage, R_b - primary resistance, R_s - secondary resistance, S - slip, x_{ex} - reactance of the exterior open space, x_{in} - interior open space reactance, x_{a1}, x_{a2}, x_{a3} - air gap reactances, n_c and n_u denote the number of coils-per-phase coupled and uncoupled to the sleeve.

troublesome with "short stators." When the energized primary is located on board the vehicle, the passive reaction rail finds itself suddenly exposed to a magnetic field, as it slides under the leading edge of the energized structure. When the cruising speed of the train is higher than the velocity with which the electromagnetic field diffuses through the conductor, the voltage induced by transformer action predominates over the motion-induced voltage. The resultant currents oppose the inducing magnetic fields, thereby causing a considerable reduction in the attainable thrust. An analytical treatment of this phenomenon and a bibliography on the subject are presented in Ref. 1. The transient performance is being handled using a computer simulation code based on the mesh-matrix approach [6]. This has been successfully applied to electromagnetic launchers [7], albeit in a case without edge effects.

IV. Edge Effects

The longitudinal cut in the passive sleeve which constitutes the secondary of the new Maglev motor destroys the cylindrical symmetry of the structure. Such a symmetry, however, is violated also in the case of an electromagnetic launcher, when the projectile sleeve is not exactly centered within the barrel. In order to ascertain the in-bore dynamics of the projectile in the barrel, a special computer simulation code was formulated [8]. This program sums up the contributions of all the current elements in the sleeve according to Biot-Savart's law of force and, since the computation is not symmetry dependent, it applies also to the Maglev case. Studies of the Maglev dynamics have not been performed. Only the steady-state performance has been analyzed. As could be expected the cut in the sleeve causes a loss in propelling force which is roughly proportional to the loss in the sleeve area facing the primary. More complex is the effect of the cut in the sleeve on the transverse force which provides suspension and guidance. Figure 5 shows the normalized net force f_s on the sleeve as a function of the normalized displacement d between the axes of the energized coils and of the passive sleeve, with the angle α of opening in the sleeve cut as a parameter. The sketches in Fig. 5 show the case of suspension with energization by the wayside. That is the situation in which the driver coils are fixed to the ground and the sleeve is attached to the vehicle. The sketch on the upper left-side assumes that the vehicle with the sleeve is lowered with a displacement d. The sketch on the lower right-side assumes that the vehicle is elevated.

Starting with the ideal case of a fully cylindrical sleeve, $\alpha = 0°$, it appears that the net force on the sleeve opposes the upward and downward displacements equally. The net transverse force is then a restoring one. As the angle α of the sleeve opening is increased to 15° and 30°, the force continues to be directed upwards when the sleeve axis is below the driver coils axis, as shown on the left hand side of Fig. 5. For a given displacement, the force increases as α increases because the downward component of force, that would have been produced by the missing section of the sleeve, is absent. The net force thus opposes the displacement that would be produced by gravity and provides suspension. In contrast, in the situation depicted on the right side, that is, in which the vehicle and with it the sleeve have bounced upward, the net force is still upwards for a relatively small value of d, but changes its sign for sufficiently large displacements. As before, the reason is that the cut eliminates those sleeve currents which would provide a restoring force.

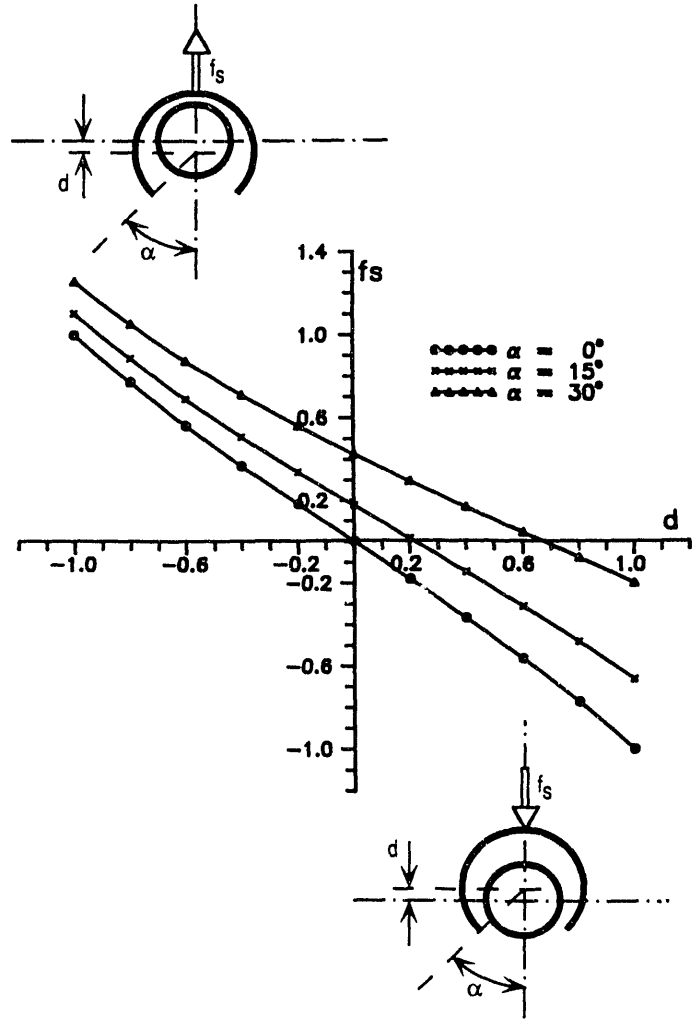

Fig. 5: Transverse force vs displacement between axes with sleeve opening-angle as a parameter.

V. CONCLUSIONS

The paper describes a new relatively simple Maglev system driven by air-cored, linear induction motors. The motors provide the necessary guidance and levitation forces as well as the propulsion force. The concept itself, the principle of operation, behavior of azimuthal currents induced in the secondary passive part, and some basic relations of the transverse forces acting inside the motor's air-gap are presented. In conclusion, this preliminary investigation has confirmed the potential of the novel Maglev system, but it has brought to light the complexity of the forces which govern its dynamics.

REFERENCES

[1] E. Levi, *"Linear Propulsion,"* Sec. 23, pp. 103-120, Standard Handbook for Electrical Engineers, 12th Edition, McGraw-Hill, 1987.

[2] J.L. He, D.M. Rote and H.T. Coffey, *"Survey of Foreign MAGLEV Systems,"* Report No. ANL/ESD-17, Argonne National Lab., Center for Transportation Research, July 1992.

[3] E. Levi and Z. Zabar, *"Air-Cored, Linear Induction Motor for Magnetically Levitated Systems"*, patent application No. 07/974,177, dated 11/10/92.

[4] M. Guarino, Jr., *"Development of Linear Motors in the U.S.A., Past, Present and Future,"* Proceedings Status Seminar Magnetobahn 1978, Willingen, Germany, April 24-28, 1978 (in German).

[5] J. L. He, E. Levi, Z. Zabar, and L. Birenbaum, *"Equivalent Circuits and Parameters for Induction Type Electromagnetic Launcers,"* IEEE Trans. on Magnetics, Vol. 29, No. 1, pp. 667-674, January 1993.

[6] D. G. Elliot, *"Mesh-Matrix Method for Electromagnetic Launchers,"* IEEE Trans. on Magnetics, Vol. 25, No. 1, pp. 164-169, January 1989.

[7] J. L. He, Z. Zabar, El Levi, and L. Birenbaum, *"Transient Performance of Linear Induction Launchers Fed by Generators and by Capacitors Banks,"* IEEE Trans. on Magnetics, Vol. 27, No. 1, pp. 585-590, January 1991.

[8] K.B. Kim, Z. Zabar, E. Levi, and L. Birenbaum, *"Projectile Stability in the Barrel of a Linear Induction Launcher,"* to be presented at the 9th IEEE Pulsed Power Conf., Albuquerque, NM; June 21-23, 1993.

APPENDIX 1

Example of Preliminary Design

The following example of a single-vehicle MAGLEV system gives an idea of the dimensions of the new configuration presented here.

Performance Specifications

Cruising speed.....v = 400 miles/h = 179 m/s
Vehicle weight.....W = 50 tonnes = 4.9×10^5 N
Power.....P = 65 MW
Traction force.....$F = \frac{P}{v} = 3.65 \times 10^5$ N
Clearance.....c = 2" = 0.051 m

Application of the procedure outlined in Ref. 5 , once for a system energized by the wayside and once for a system energized on board the vehicle, yields the following dimensions:

[A] Energization by the wayside at 60 Hz

Coils .....OD_c = 8" = 0.2 m;
ID_c = 5½" = 0.14 m; N_c = 1
Material.....aluminum
Weight.....$W_c = 2 \times 43$ kg/m $= 2 \times 70$ tonnes/mile
Passive Armature....ID_a = 12" = 0.3 m;
$OD_a = 14\,^{13}/_{32}$" = 0.36 m
Length.....$l_a = 4 \times 3.57$ m
Material.....aluminum
Weight.....$W_a = 4 \times 300$ kg.

[B] Energization on board vehicle

Coils .....OD_c = 8" = 0.2 m;
ID_c = 5½" = 0.14 m; N_c = 1
Length.....$l_c = 4 \times 3.57$ m
Material.....aluminum
Weight.....$W_c = 4 \times 153$ kg.
Passive Armature....ID_a = 12" = 0.3 m;
$OD_a = 14\,^{13}/_{32}$" = 0.36 m
Material.....aluminum
Weight $W_a = 2 \times 84$ kg/m $= 2 \times 135$ tonnes/mile

Power Electronics for Linear Synchronous Motor Propulsion Systems

David J. Perreault and Richard D. Thornton
Massachusetts Institute of Technology
Laboratory for Electromagnetic and Electronic Systems
Cambridge, MA 02139 USA

Abstract - **Drive requirements for linear synchronous motor propulsion systems are described, and the potential converter architectures for this application compared. A series connection of current source converters is proposed which makes it feasible to take power directly from a medium dc voltage distribution bus through a chopper, reducing transformer and distribution line costs. Design tradeoffs for series connected converters are also discussed. Finally, a brief discussion of the economics of converter design is presented.**

INTRODUCTION

Linear synchronous motor propulsion systems represent a challenging application for power conversion technology. Drives for this application must be designed to handle the transition of vehicles between blocks of the LSM [1]. If a load-commutated drive is used, such as the cycloconverter system at Miyazaki, the system must be designed to only deliver power when a back emf is present for commutation [2]. Even if the system is force-commutated, such as the German designs and the newer Japanese design [3], [4], the converter must be able to handle the rapid load changes which occur. Fault-tolerance is also a critical issue for any commercially viable propulsion system. Power converters for this application must be designed to survive at least a single point failure in any device or winding and remain operable to provide high availability. The special nature of the load thus places stringent requirements on the power conditioning equipment.

PROPULSION POWER REQUIREMENTS

The LSM requires power electronics for converting fixed voltage, fixed frequency power from the utilities to variable frequency power for exciting the N-phase motor windings. The power converters must have independent control over the magnitude, frequency and phase of the currents induced in the windings. Depending on the motor design, the back emf (and the desired current waveform) may not even be sinusoidal.

The fundamental output frequency the power converter must synthesize is determined by the vehicle speed and the pole pitch of the motor (1).

$$f = \frac{V}{2P} \tag{1}$$

Manuscript received March 15, 1993. This work was supported in part by the U.S. Department of Transportation under contract DTFR53-91-C-00070. Support from the Massachusetts Institute of Technology Department of Electrical Engineering and Computer Science and the Laboratory for Electromagnetic and Electronic Systems is also gratefully acknowledged.

Typical pole pitches for EDS suspension maglev systems are on the order of half a meter or more, yielding maximum output frequencies below 150 Hz. EMS systems typically have a shorter pole length, and thus a higher maximum output frequency. For comparison, the Japanese EDS design has a pole pitch of 2 meters, while Transrapid uses a pole pitch of 0.258 meters.

Table 1 gives a rough idea for the power requirements for level travel at different speeds for a maglev vehicle capable of carrying about 120 passengers. This table assumes aerodynamic drag power varies as the cube of speed, eddy current loss is proportional to speed, power loss in the magnetic suspension is constant, and the linear motor losses are proportional to the square of thrust [5]. These calculations are in line with the 200 passenger TR07 maglev vehicle, which is estimated to consume 4.2 MW on a level guideway at 111 m/s, as well as other power analyses [6]. For a maximum speed of 135 m/s, the inverter must be able to provide about 6.6 MW for level cruise. However, while a typical maglev vehicle requires around 40-50 kN of thrust for level cruise at these speeds, peak thrusts on the order of 120 kN are necessary to accommodate acceleration requirements [5]. Thus, the inverter should be sized for almost three times the power required for level travel at the maximum operating speed. If the guideway is level and straight, a reduction in acceleration may be acceptable, but we will assume that the power converter should produce peak power on the order of 10-20 MW.

While the power required is specified by the mechanical requirements, there are possible tradeoffs between voltage, current and number of phases. Most practical designs use between 3 and 6 phases for the motor. The motor voltage is determined by the length of the propulsion magnets, the motor width, the average magnetic field, and the number of turns per "slot" (1 or 2 being most common in today's designs). Voltages which result vary from a thousand volts to over 10 kV. This tradeoff has a major impact on the design of the power converters.

Other parameters of major importance in the design of the power converters are the inductance and resistance of the motor windings. Motor reactance per unit length is determined by the materials and geometry of the motor windings (along with the effects of any magnetic materials), and determines the practical limit on block lengths [7]. Typical winding inductances can range from below a millihenry to over twenty millihenries per phase, with typical per phase resistances on the order of an Ohm [3], [4], and [5].

TABLE I
BASELINE POWER REQUIREMENTS FOR LEVEL TRAVEL FOR A TYPICAL 120 PASSENGER MAGLEV VEHICLE

Speed	m/s	30	60	90	120	135	150
Power	MW	0.86	1.23	2.45	4.86	6.65	8.91

CONVERTER ARCHITECTURES

Converter architectures for this application can be broadly classified into 3 basic types: those that convert directly from ac to ac, those that convert a controlled dc voltage to ac, and those that convert a controlled dc current to ac [8], [9]. Direct ac/ac conversion requires an ac distribution bus, while the dc link of the other methods may be created from either ac or dc distribution using either rectifiers or choppers, as required.

Cycloconverter

Cycloconverters use bridges of switches to directly synthesize an ac output waveform from ac line voltages, without any intermediate energy storage (Fig. 1). This type of structure was employed in the MLU002 Japanese maglev system to generate power at up to 34 Hz [2]. Despite the large number of switches required, the elimination of energy storage elements makes this converter an economic solution at high powers if natural commutation is employed. However, the lack of energy storage also leads to some serious drawbacks. The output voltage and the input line current both have significant harmonics which vary with the output frequency and load, making them hard to filter. Furthermore, the converter fundamentally operates with less than unity power factor, and the power factor degrades as the output voltage is lowered. These drawbacks, along with a limited output frequency, make this converter an unlikely candidate for a commercial propulsion system.

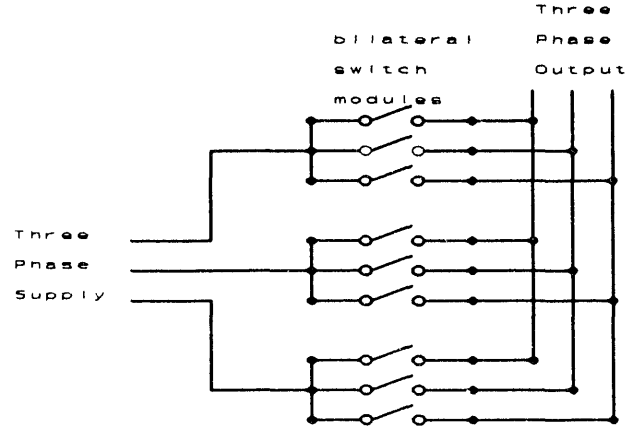

Fig. 1 A Cycloconverter structure.

Voltage-Source Inverter

The Voltage-Source Inverter (VSI) is the most widely used power inverter up to the low megawatt range (Fig. 2). Sinusoidal output currents are obtained using sinusoidal or programmed Pulse Width Modulation (PWM), or hysteretic current control [10],[11],[12]. This converter has the advantages of a wide output frequency range, limited only by switching losses or thyristor commutation, and frequencies of over 200 Hz are easily achieved at the megawatt level. Input and output harmonics are well defined, and both harmonics and output voltage can be controlled via the PWM scheme. Also, VSIs may be paralleled to increase power rating, with the potential to improve waveform quality and fault tolerance. Paralleled VSIs are the basis of the German and newer Japanese designs [3], [13]. It may be preferable to use an ac power distribution scheme with VSIs to allow the distribution voltages to be easily converted to the lower dc link levels. However, if regeneration is desired, two quadrant input rectifiers are needed. Furthermore, the number and size of the transformers required for this approach is significant. Some designs, such as Transrapid, even need additional transformers to boost the inverter output voltage for high-speed operation.

Current-Source Inverter

Current-Source Inverters (CSIs) function by switching a dc current link to generate an ac output current waveform, and are often used at the megawatt level. Two approaches are widely used for current-source inverters. The first approach is to generate quasi-square current waveforms using pulse-commutated SCRs, as outlined in [14], [15]. The single-phase ASCI Inverter of Fig. 3 is of this type, with the capacitors serving to both commutate the SCRs and absorb the reactive energy stored in the out-going motor phase. The second approach is the use of fully controlled switches (such as GTO's) and a separate capacitive filter network, shown in Fig. 4 for a single phase and described in [16], [17] for three-phase bridges. The switches are controlled to generate a PWM waveform in the filter/load circuit, yielding quasi-sinusoidal currents in the load.

The relatively high inductance of the motor windings poses a major problem for the design of the inverter. The peak output frequency of both types of CSIs is limited by the need to commutate the link current between phases of the motor, with typical maximum frequencies on the order of 60 - 120 Hz. The peak output voltages of a CSI are also determined by the winding inductance. If the winding inductance is too high, a CSI is probably not a good choice. As a rough measure, assume the waveforms are sinusoidal, and compare the voltage across the winding inductance to the magnitude of the motor back voltage. If the inductive voltage is less than half the motor voltage, then a CSI may be a good choice. Otherwise, a voltage source inverter is probably preferable.

An advantage of CSIs for this application is the ease with which they can be connected in series [18], [19], [20]. For example, assuming that there are dual 3 phase motors, or a 6 phase motor, we can construct the circuit with two three

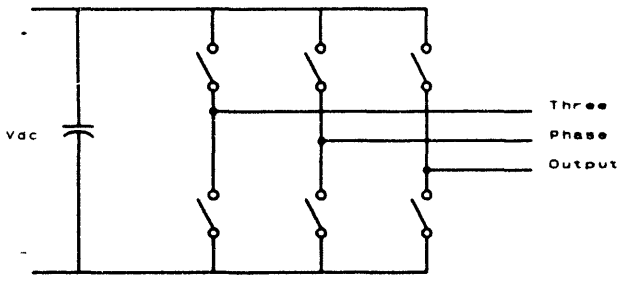

Fig. 2 A three-phase Voltage Source Inverter.

phase bridges in series, as described in [20]. We can carry the series converter idea one step further by using a separate H-bridge for each phase, and putting all the phases in series. A series-connected design makes it feasible to take power directly from a medium voltage dc distribution bus through a chopper, reducing transformer and distribution line costs. A degree of fault tolerance may also be obtained by this approach. For LSM designs where the maximum frequency not too high and reasonable care has been taken to reduce the winding inductance, the advantage of the series-connected CSI may be quite significant.

Other Alternatives

In soft-switched architectures, switching losses are decreased by using a resonant or quasi-resonant auxiliary circuit to obtain a zero-voltage and/or zero current switching opportunity for the main devices [21],[22]. The reduced switching losses which result can be used to improve efficiency or waveform quality, or reduce converter size, at the expense of complexity. Unless one of these benefits becomes an overriding criteria in a design, these architectures probably offer no advantage for this application.

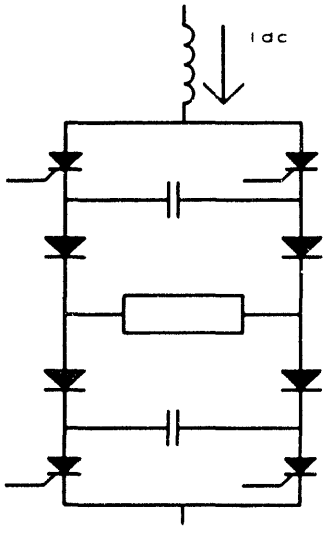

Fig. 3 The ASCI quasi-square wave CSI.

SERIES-CONNECTED CURRENT SOURCE INVERTER

As previously discussed, a series-connected current source inverter (SCCSI) can be advantageous if the required output frequency is not too high, and the winding inductance is sufficiently low. The ability to drive the series-connected converter directly from distribution level voltages eliminates the transformers that would otherwise be necessary. Furthermore, if bypass and breakout is provided for each series-connected converter, it is possible to achieve a degree of tolerance to single point failures in the converters or motor windings.

The selection of a SCCSI design approach depends heavily on the load parameters, including back voltage, current, winding inductance and number of phases. Design selections include the choice between quasi-square wave (QSW) and PWM architectures, use of three phase or separate h-bridge converters, and which quadrant is used to provide regeneration.

Quasi-square wave vs. PWM architectures

The selection of a CSI architecture for a given design is driven by the devices available and the parameters of the load. One major concern when designing these converters is the sizing of the filter and commutation elements, which must be tailored to the load parameters.

For quasi-square wave architectures, the fundamental limitation comes from commutation time requirements and the need to absorb all of the energy in the motor phase. Consider the single phase ASCI inverter of Fig. 3. The capacitor size is selected as large as possible, while still meeting commutation time limits at the highest frequency of operation [10]. Unless a separate clamp circuit is used, the capacitor has to absorb all the energy in the load, and will charge to a peak voltage roughly proportional as:

$$V_p \propto I\sqrt{\frac{L}{C}} \tag{2}$$

which determines the ratings of the switches and capacitors in the circuit. Thus, as the inductance and/or maximum current increase, the device ratings grow in size, and eventually make the approach impractical.

For the PWM circuit of fig 4, the limitations are somewhat different. The capacitive filter should be sized such that a quasi-sinusoidal current passes through the load, while the switching harmonics are shunted through the filter. For a simple capacitive filter then, the capacitance should be chosen by the criteria of (3), while remaining large enough such that the peak capacitor voltages are limited. The capacitor voltage limitation implies that as the load inductance and

$$f_{out} << \frac{1}{2\pi\sqrt{LC}} << f_{pwm} \tag{3}$$

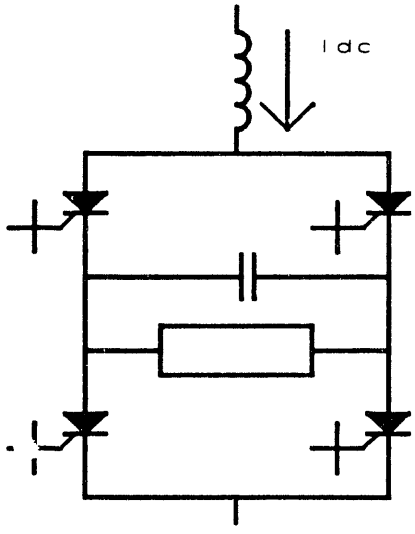

Fig. 4 A PWM Current Source Inverter

current increase, so does the switching frequency.

In many situations, either converter structure is practical from a design standpoint, and selection is based on economics and performance characteristics. PWM converters typically have smaller capacitors and link inductors than QSW converters, but require fully controlled switches such as GTOs. Furthermore, the waveforms available with the PWM converter are essentially sinusoidal, while QSW converters generate stepped waveforms, either of which may be preferable depending on the motor design. Finally, the dynamic response of the PWM converter is faster, but is more sensitive to transients and requires a more complex control system.

The simulated waveforms for the QSW CSI of Fig. 3 are shown in Fig. 5, for a motor with L_{phase} = 1 mH and a peak back voltage of 1500 V running at 80 Hz. The simulation assumes 130 μF commutation capacitors, and the 150° conduction patterns employed in [19]. The simulated waveforms of the PWM converter of Fig. 4 are shown in Fig. 6 for the same motor parameters, a 60 μF filter capacitor, and an average switching frequency of 720 Hz. Equations for simulating these circuits can be found in [19] and [5]. The simulations illustrate the trade-offs between the converters. For this motor design, the QSW converter requires far more capacitive energy storage than the PWM converter, and also requires higher device ratings. However, if the back voltage was trapezoidal, this converter could transfer nearly 30% more power than the PWM topology. The PWM converter can generate an accurate sinusoidal phase currents using relatively small filter elements, at the expense of fully controlled switches and a high switching frequency.

Single phase vs. three phase bridges

Most long-stator LSM propulsion systems designed to date have used 3 phase stator windings, connected in a wye configuration [23]. Depending on the space available for the windings and voltage limits, it may be possible to wind the LSM with separate single phase windings. In this case, one has the option of driving each phase separately with an H-bridge, and series connecting the bridges.

The major criteria for selecting between a series connection of single or three phase bridges is how the total voltage compares with the distribution level voltage. It is instructive to compare the two options, however, since the distribution voltage itself is a design parameter.

The primary advantage of the three-phase bridge is that it requires only half as many switches (and gate drives, snubbers, etc.) as an equivalent set of single phase converters. Comparing the device ratings of single phase converters to a three phase bridge driving a Wye connected load, we find that the voltage ratings in the single phase converter are $1/\sqrt{3}$ as large [19]. The penalty for using a single phase setup is therefore not as severe as it would appear.

The filtering requirements are also different for the two topologies. In general, because of the flexibility in switching, the link inductance does not have to absorb as large a volt-second integral in the single phase connection, and thus the inductor can be made smaller. In one design, it was found that the link inductance could be reduced 30-35% for the same current ripple [19]. For QSW converters, the same total energy storage is required in the capacitors. However, the increased commutation flexibility in the single phase circuit allows larger capacitors to be used at a lower voltage, reducing the device ratings in the circuit even further [19]. Thus, while the single phase circuit requires more switches, the reduction of switch ratings and link inductor size help offset this cost.

The reduction in switches also implies that the three-phase converter cannot generate waveforms with triplen harmonics. This is desirable for sinusoidal back voltages, but may not be optimal otherwise. Many linear motor designs have back voltages that are substantially nonsinusoidal, and may have third harmonics as large as 20% of the fundamental. For LSMs with significant third harmonic terms, a series connection of single phase QSW converters allows power to be transferred via the third harmonic, increasing the thrust for the same peak voltages and link current. Furthermore, the use of single phase bridges increases the flexibility available in generating PWM waveforms [18].

In the final analysis, a series connection of single phase converters may be more expensive than a three phase connection. However, it offers flexibility in control, a higher stacked voltage, and the opportunity to use the independence of motor phases for fault tolerance.

Input converter design options

One advantage of series-stacked current source inverters is that they can be driven directly from a medium voltage distribution bus. If a three-phase AC bus is used, then a phase-controlled converter (either 6 or 12 pulse) can be used. If allowed, regeneration can be provided by running the

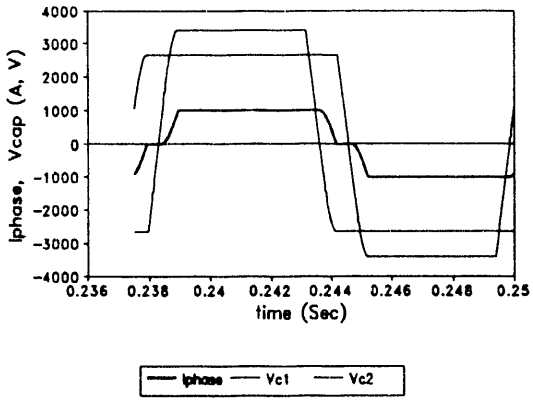

Fig. 5 Simulated behavior of the QSW CSI of Fig. 3

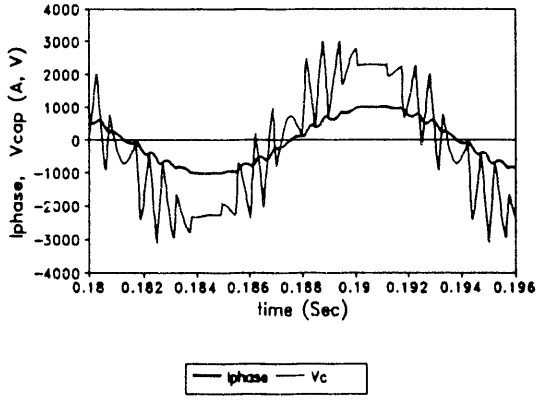

Fig. 6 Simulated behavior of the PWM CSI of Fig. 4

converter in the inversion region, while maintaining a positive link current.

Alternatively, the series-stacked CSI architecture can be driven through a chopper from a dc distribution bus, with an attending reduction in transformer and distribution costs. The dc bus can be used for transmitting regenerated power from a braking vehicle to one which needs the power. By using a 30 kV bus, it is possible to transmit power at least 30 km, so the probability of finding a vehicle to absorb the power is relatively high. The 30 kV bus could be created using separate +15 kV and -15 kV voltages, halving the maximum voltage to ground.

Regeneration can be provided in one of two manners with this type of system. One method is to use a chopper which can generate positive or negative output voltage, while maintaining a unidirectional output current. One possible implementation of this approach is shown in Fig. 7. The disadvantage of this method is that the chopper devices have to be rated for the full 30 kV bus voltage. Alternatively, a converter can be used which provides a positive output voltage, but can reverse the link current to regenerate power. This technique allows the simpler chopper implementation of Fig. 8, but requires bidirectional switch implementations in the inverter. The selection between these two approaches is fundamentally an economic one. In either case, fault tolerance and performance of the chopper can be improved using interleaving of multiple converters [7],[24].

ECONOMIC ISSUES

Consider the pricing of industrial variable speed drives. Typically, companies manufacture standard "off the shelf" drives up through the 400-600 Horsepower range, while drives above this range are usually made to order. Most standard lower power units are of the PWM voltage-source type, employing various devices from transistor arrays to GTO's. Higher power drives (1000-10000 HP) are typically of the current-source type, either of the classic ASCI QSW type or the recent GTO-based PWM variety. (One exception to this is in the transportation industry, where weight and volume are often important.) Information from high power drives manufacturers indicate that a value of ~75-125 $/kVA is a reasonable figure for industrial power inverters at the few megawatt level. Below a few hundred kVA, the price to power ratio increases due to fixed costs, and may increase above the 10 MVA level as well due to the lack of a large market.

An important observation is that the power switching devices often contribute to only about 5 or 10% of the total cost. Three-phase transformers alone are estimated to cost on the order of $20/kVA, and may therefore be a sizeable fraction of the cost of an inverter station. Energy storage elements, control, heat removal equipment, and skilled labor can also represent a sizeable fraction of the cost. Thus, while it is considered that a factor of 2 to 3 reduction in cost may be possible via economies of scale, it is not clear that a factor of 10 reduction is possible.

CONCLUSION

Drive requirements for linear synchronous motor propulsion systems have been described, and the potential converter architectures for this application have been compared. A series connection of current source converters has been proposed, which makes it feasible to take power directly from a medium dc voltage distribution bus through a chopper, reducing transformer and distribution line costs. Design tradeoffs for SCCSIs have also been discussed, including the selection between single and three-phase topologies, QSW or PWM converters, and appropriate input converters. Finally, a brief discussion of the economics of converter design has been presented.

ACKNOWLEDGEMENT

The authors wish to thank Ray Wlodyka and Frank Raposa of the National Maglev Initiative for their comments and

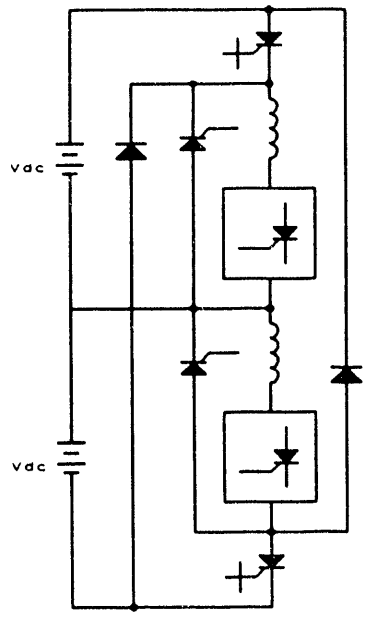

Fig. 7 A chopper with unidirectional I, bidirectional V.

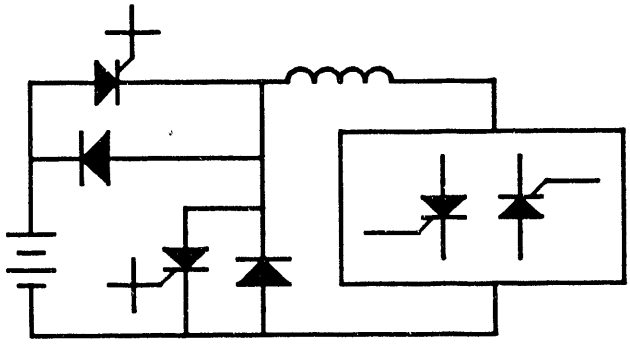

Fig. 8 A chopper with unidirectional V and bidirectional I.

suggestions during the course of this work. Thanks are also due to Tracy Clark, John Kassakian and Marty Schlecht of LEES for the insights they provided.

REFERENCES

[1] T. Clark, "Maglev Position Sensing and Control", *12th International Conference on Magnetically Levitated Systems and Linear Drives*, May 1993, (in press).

[2] S. Saijo, S. Kioke, and S. Tadakuma, "Characteristics of Linear Synchronous Motor Drive Cycloconvertor for Maglev Vehicle ML-500 at Miyazaki Test Track", *IEEE Trans. IAS*, Vol. IA-17, No. 5, Sept/Oct 1981.

[3] R. Friedrich, K. Dreimann, and R. Leistikow, "The Power Supply and the Propulsion System of the Transrapid 06 Vehicle - Result of Trials", *IEEE International Conference on Maglev and Linear Drives*, Vancouver Canada, May 1986, pp. 243-249.

[4] S. Tadakuma, S. Tanaka, H. Inoguchi, Y. Tanoue, H. Ikeda, and S. Kaga, "Consideration on Large Capacity PWM Inverter for LSM Drives", *Int. Power Electron. Conf. (IPEC) Record*, Vol. 1, April 1990, pp. 413-420.

[5] R.D. Thornton, D.J. Perreault, and T. Clark, "Linear Synchronous Motors for Maglev", *National Maglev Initiative BAA Final Report DOT/FRA/NMI-92/13*, January, 1993.

[6] E. Abel, J.L. Mahtani, R.G. Rhodes, "Linear Machine Power Requirements and System Comparisons", *IEEE Trans. Magn.*, Vol. MAG-14, No. 5, September 1978, pp. 918-920.

[7] R.D. Thornton, "Linear Synchronous Motor Design", *12th International Conference on Magnetically Levitated Systems and Linear Drives*, May 1993, (in press).

[8] B.K. Bose, "Adjustable Speed AC Drives - A Technology Status Review", *Proc. IEEE*, Vol. 70, No. 2, February 1982, pp.116-135.

[9] B.L. Jones and J.E. Brown, "Electrical variable-speed drives", *IEE Proceedings*, Vol. 131 Pt. A, No. 7, September 1984, pp. 516-558.

[10] B.K. Bose, Power Electronics and AC Drives, Prentice-Hall 1986

[11] P.N. Enjeti, P.D. Ziogas, and J.F. Lindsay, "Programmed PWM Techniques to Eliminate Harmonics: A Critical Evaluation", *IEEE 1988 Industry Applications Society Annual Meeting*, 1988, pp. 418-430.

[12] D.M. Brod and D.W. Novotny, "Current Control of VSI-PWM Inverters", *IEEE 1984 Industry Applications Society Annual Meeting*, 1984, pp. 418-425.

[13] S. Tadakuma, S. Tanaka, K. Miura, S. Inokuchi, and H. Ikeda, "Fundamental Approaches to PWM Control Based GTO Inverters for Linear Synchronous Motor Drives", *IEEE 1991 Industry Applications Society Annual Meeting*, 1991, pp. 847-853.

[14] D. Dewan, S. Rosenberg, N. Nicholson, "Comparison of Single Phase Current Source Inverter Configurations", *IEEE 1975 Industry Applications Society Annual Meeting*, 1975, pp. 783-789.

[15] M. Showleh, W. Maslowskim and V. Stefanovic, "An Exact Modeling and Design of Current-Source Inverters", *IEEE 1979 Industry Applications Society Annual Meeting*, 1979, pp. 439-457.

[16] M. Hombu, S. Ueda, and A. Ueda, "A Current Source GTO Inverter with Sinusoidal Inputs and Outputs," *IEEE Trans. IAS*, Vol. IA-23, No. 2, March/April 1987, pp. 247-255.

[17] S. Nonaka, and Y. Neba, "A PWM GTO Current Source Converter-Inverter System with Sinusoidal Inputs and Outputs," *IEEE Trans. IAS*, Vol. IA-25, No. 1, Jan/Feb 1989, pp. 76-85.

[18] S. Biswas, B. Basak, S. Sathiakumar, and J. Vithayathil, "A New Three-Phase Current Source Inverter with Flexible PWM Capability," *IEEE Trans. IAS*, Vol. IA-23, No. 5, Sept./Oct. 1987, pp. 921-926

[19] S. Bowes, and R. Bullough, "Novel PWM Controlled series-connected current-source inverter drive", *IEE Proceedings*, Vol. 136, Pt. B, No. 2, March 1989, pp. 69-82.

[20] T. Lipo, and L. Walker, "Design and Control Techniques for Extending High Frequency Operation of a CSI Induction Motor Drive", *IEEE Trans. IAS*, IA-19, No. 5, Sep/Oct 1983, pp.744-753.

[21] R.W.A. DeDoncker, D.M. Divan, and T. A. Lipo, "High Power Soft Switching Inverters", *IEEE PESC 91 Tutorial*, Boston, MA, 1991.

[22] S. Bhowmik and R. Spee, "A Guide to the Application-Oriented Selection of AC/AC Converter Topologies", *IEEE Applied Power Electronics Conference*, Boston, MA, 1992, pp. 571-578.

[23] G.W. McLean, "Review of recent progress in linear motors", *IEE Proceedings*, Vol. 135, Pt. B, No. 6, Nov. 1988, pp. 380-416.

[24] B. Miwa, "Interleaved Conversion Techniques for High Density Power Supplies", *M.I.T. Ph.D. Thesis*, May, 1992.

Analytical evaluation of the influence of the armature coils distribution on the thrust of linear synchronous motor for Maglev

Marco Trapanese
Centro Ricerche sui Sistemi Elettrici di Potenza - Consiglio Nazionale delle Ricerche
c/o Dipartimento di Ingegneria Elettrica - v.le delle Scienze 90128, Palermo, Italy.

Abstract - The paper deals with the role of the armature structure on the thrust of a superconducting linear synchronous motor for EDS (ElectroDynamic Suspension) Maglev. All the coils of the motor have been analitically modelled as filiform square shaped coils. Double and single layer armature structures can be described by the model and have been examined. It is shown that the thrust of the single layer structure is smoother than the thrust of the double layer structure. The role of the spatial distribution of the coils is also examined. It is shown that exists a critical dimension, which is derived, that states the maximum dimension of the allowed irregularities on the armature coils position. Irregularities, which are larger than this critical dimension, are shown to affect seriously the average thrust.

I. INTRODUCTION

The thrust of superconducting synchronous linear motor has unavoidable oscillation even if the time dependence of the armature current is perfectly sinusoidal. These modulations are generated by various causes: the spatial localisation of the armature coils, the imperfectly assembly, the structure of the secondary etc. Such modulations have been widely investigated with numerical techniques [1-3], but there is still a lack of analytical investigation, which could allow to focus the role of each machine parameters on this phenomenon. In this paper an analytical model of linear synchronous motor for EDS (ElectroDynamic Suspension) Maglev system is introduced. Such a model allows to estimate the thrust oscillations and to get some insights on the influence of the armature coils distribution on the above mentioned oscillations.

II. SIMPLIFIED MODEL OF SYNCHRONOUS MOTOR FOR MAGLEV

The fundamental structure of the superconducting linear synchronous motor for EDS system is shown in Fig. 1. In the motor the field coils and the armature coils have race track configuration. It can be seen that the armature coils are vertically installed on the side walls and that the superconducting field coils are vertically placed on the moving train. The armature coils are supplied by a three phase current system. The superconducting magnets are used both to levitate and to set the excitation field. Thanks to the presence of the superconducting magnets the motor is an ironless core type and this implies a lighter vehicle. Moreover, it must be noted that the most recent design requires a double layer structure for the armature coils.

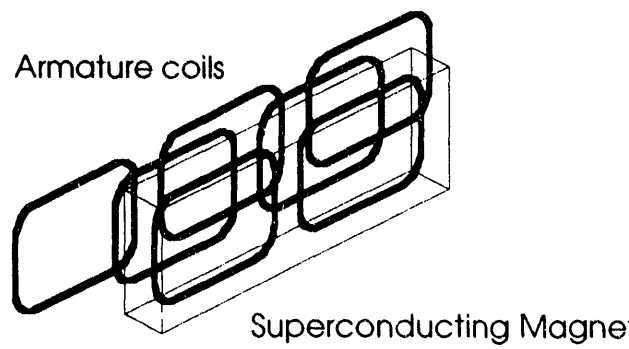

Fig. 1. Structure of a superconducting synchronous motor.

Under the hypotheses to substitute the objective structure of the coils with square shaped coils it is possible to develop an analytical model of the motor which takes into account the finite thickness of the coils [4]. This model can be further on simplified if one wishes to investigate only the propulsion force, because it has been shown [4] that the finite thickness of the coils slighly affects the field calculation. Moreover in order to calculate the propulsion force only the field produced by the vertical sides of a race track coil must be taken into account. From these considerations it follows that the model shown in Fig. 2 will be used to describe the real motor. In this figure the series of coils of finite thickness has been replaced by a series of filiform coils. The coils are supposed to be supplied by a three phase system of sinusoidal current. The side AB is the vertical side of an armature coil and is long L. The pole pitch is 3d and each coil is supposed to be 3d horizontally long. From Fig. 3 it can be also seen

Manuscript received March 22, 1991.This work was supported in part by MURST.

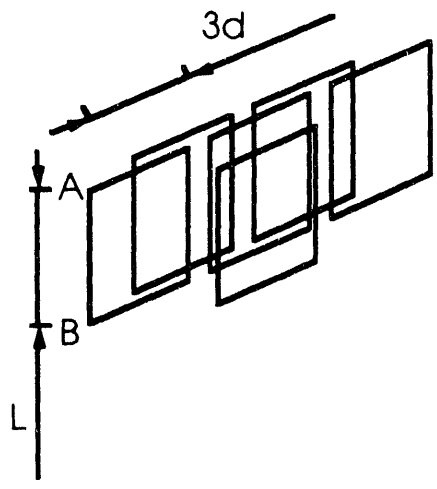

Fig. 2. Simplified model of synchronous motor for Maglev.

that the armature is supposed to be infinitely long and that the moving magnet consists of one coil.

III. THE MAGNETIC FIELD GENERATED BY THE ARMATURE COILS.

In order to calculate the propulsion force from Laplace's law the x component of the flux density generated by the vertical sides of the coil must be calculated. In Fig.3 a cross section of the armature coils arrangement of Fig.2 is shown. The field generated by one vertical side of the generic phase coil can be obtained with the usual expression for the field generated by a filiform conductor of finite length:

$$\mathbf{B}(x,y,z,x_0,y_0)=\frac{\mu_0}{4\pi}\frac{I}{\sqrt{(x-x_0)^2+(y-y_0)^2}}\times$$

$$\times\left(\frac{L/2+z}{\sqrt{(x-x_0)^2+(y-y_0)^2+(L/2+z)^2}}+\right.$$

$$\left.+\frac{L/2-z}{\sqrt{(x-x_0)^2+(y-y_0)^2+(L/2-z)^2}}\right) \qquad (1)$$

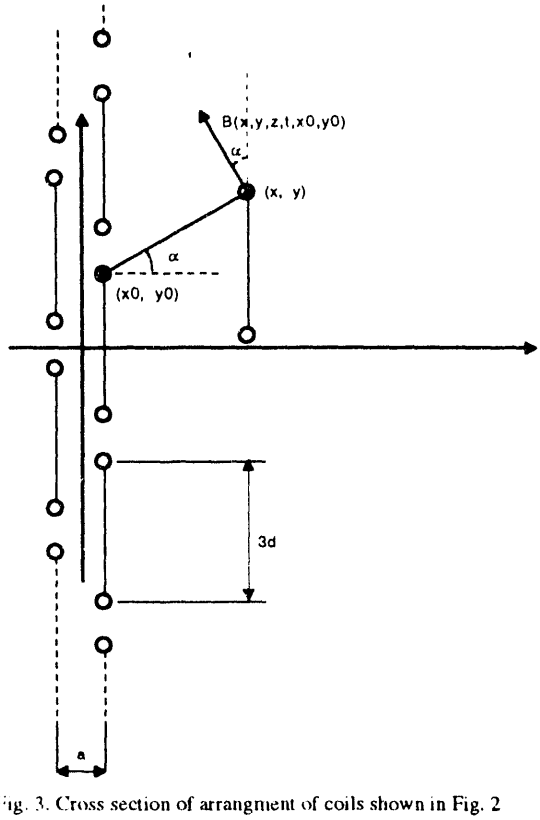

Fig. 3. Cross section of arrangment of coils shown in Fig. 2

where the coordinates of the middle point of the vertical side are $x = x_0$, $y = y_0$ and $z = 0$. L is the length of the vertical side of the armature , μ_0 the vacuum permeability, x,y and z are the coordinates of the point where the field is calculated. The direction of the field is orthogonal to the plane identified by the vertical side and the vector which connects its middle point and the point (x,y,z). I is the peak value of the sinusoidal current which flows in the generic phase. The equation (1) can be specialised to a particular phase specifying to which phase the conductor belongs: that is equivalent to specify the coordinate xo,yo and the current phase angle ϕ . The y coordinate of the vertical side of the i-th coil can be expressed as:

$$y_{ief} = y_{oef} + 6di \qquad (2).$$

Where i indicates the number of coil and can span from $-\infty$ to $+\infty$, e can be equal to +1 or -1 and indicates respectively the front and back vertical side, f indicates the phase and can span from 1 to 3.
In table 1 the coordinates of the 0-th coil and the phase angle of each phase are shown.

TABLE I

Coordinates of 0-th Armature coil and current phase angle			
Phase	X_0	Y_{01}, Y_{0-1}	Φ
V f=1	a/2	1.5d, -1.5d	0
U f=2	-a/2	3.5d, 0.5d	$-2\pi/3$
W f=3	-a/2	-0.5d, -3.5d	$2\pi/3$

The Yo column gives the coordinate of the front and the back end of the armature coils. In the phase column the indexes which identify each phase in the mathematical expression are explicitly given.

It must be noted that in order to take into account the double layer structure of the armature the Xo coordinate of the i-th coils is given by:

$$x_{fi} = x_{0f}(-1)^i \qquad (3).$$

Moreover, it is important to note that the expression into brackets in (1) represents the correction introduced from the fact that the vertical side has a finite length. To obtain the x component (which is the component needed to calculate the propulsion force) of the field produced in a generic point x,y by a single armature coil, the superposition principle can be used. It must be stressed that the current is positive on one side of the coil and negative on the other. Fig. 3 shows a geometrical sketch of the coils location. It follows that the x component can be expressed as:

$$B_{xfi}(x,y,z) = \sum_{e=-1}^{1} -e\ B(x,y,z,x_{if},y_{ief}) \frac{y - y_{ief}}{\sqrt{(x - x_{if})^2 + (y - y_{ief})^2}} \qquad (4)$$

where all symbols have been already defined. The multiplication by e in (4) takes into account the fact that the sign of current in the front side is opposite to that one in the back side. The radio that multiplies the magnetic field represents the sin of angle α, which is seen in Fig.3

The x component of the field which is generated by all coils of the three phase system can be derived summing (4) over all coils and all phases. It is convenient also to insert the time dependence of the current. Then the x component of the field is:

$$B_x(x,y,z,t) = \sum_{e=-1;i=-\infty;f=1}^{e=1;i=\infty;f=3} -e\ B(x,y,z,x_{if},y_{ief}) \times \times \frac{y - y_{ief}}{\sqrt{(x - x_{if})^2 + (y - y_{ief})^2}} \sin(\omega t + \varphi_u) \qquad (5)$$

where the sin factor takes into account the time dependence of the field and is generated by the time dependence of the three phase current system. ω is the supply frequency. t is the time variable.

III. THE PROPULSION FORCE

Supposing that the superconducting magnet is travelling at synchronous speed, the y coordinate of the front end vertical side can be expressed as:

$$y = y_s + v_s t \qquad (6)$$

where y_s is the position at t=0 and v_s is the synchronous speed. The x coordinate is assumed to be

$$x = x_s \qquad (7).$$

The propulsion force can be calculated substituting (6) and (7) into (5) and using Laplace's law, which in the case under study assumes the following form:

$$F_y(x,y,t) = \int_{-L_s/2}^{L_s/2} B_x(x,y,z,t)\ i_s\, dz \qquad (8)$$

where i_s is the current in the superconducting coil and L_s is the length of the vertical side of the superconducting coil. B_x is given at (5). Inserting (5) into (8) and exchanging the sum with the integrals it follows:

$$F_x(x,y,t) = \sum_{e=-1;i=-\infty;f=1}^{e=1;i=\infty;f=3} -e \frac{y - y_{ief}}{\sqrt{(x - x_{if})^2 + (y - y_{ief})^2}}\ i_s \times \times 2 \int_{-L_s/2}^{L_s/2} B(x,y,z,x_{if},y_{ief})dz \cdot \sin(\omega t + \varphi_u) \qquad (9)$$

where the factor two describes the fact that the front and the back end of the superconducting coil give a contribution to the total propulsion force

Each integral contained in (9) presents the following form:

$$C = \int_{-L_s}^{L_s} \frac{\mu_0}{4\pi} \frac{I}{\sqrt{(x-x_0)^2 + (y-y_0)^2}} \times \times \left(\frac{I/2 + z}{\sqrt{(x-x_0)^2 + (y-y_0)^2 + (I/2+z)^2}} + \frac{I/2 - z}{\sqrt{(x-x_0)^2 + (y-y_0)^2 + (I/2-z)^2}} \right) dz \qquad (10).$$

Such an integral can be easily performed and the result is:

$$C = 2\left(\sqrt{(x - x_{if})^2 + (y - y_{ief})^2 + (L/2 + L_s/2)^2} + \right.$$
$$\left. - \sqrt{(x - x_{if})^2 + (y - y_{ief})^2 + (L/2 - L_s/2)^2}\right) \qquad (11)$$

Notice that (11) becomes simply equal to L_s in the case of infinite length of vertical sides of the armature coils. Substituting (11), (6) and (7) in (9) one finds that the propulsion is:

$$F_x(x,y,t) =$$

$$= \frac{\mu_0}{4\pi} i_s I \sum_{e=-1;i=-\infty;f=1}^{e=1;i=\infty;f=3} -2e \frac{y_s + v_s t - y_{ief}}{(x_s - x_{if})^2 + (y_s + v_s t - y_{ief})^2} \times$$

$$\times C \cdot \sin(\omega t + \varphi_u) \qquad (12)$$

Equation (12) can be used to compare the time dependence of the propulsion force in the single and double layered structure. Fig. 4 shows the time dependence in the case of a single layer structure. Fig.5 refers to double layered structure is adopted. The parameter used to obtain the numerical results are shown in table II. It can be seen that the double layered structure presents stronger thrust oscillation.

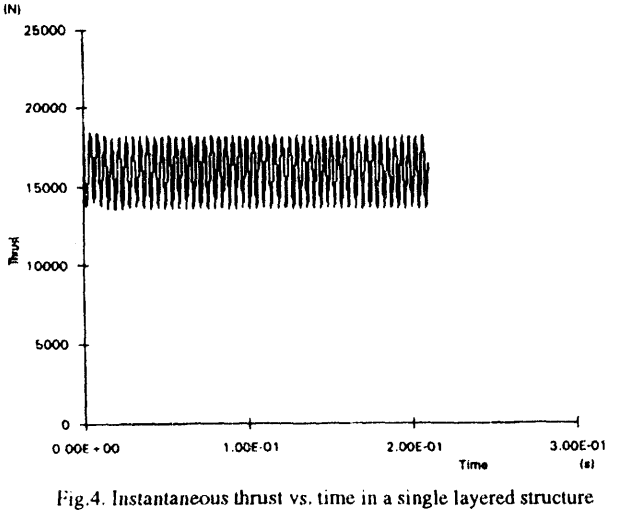

Fig.4. Instantaneous thrust vs. time in a single layered structure

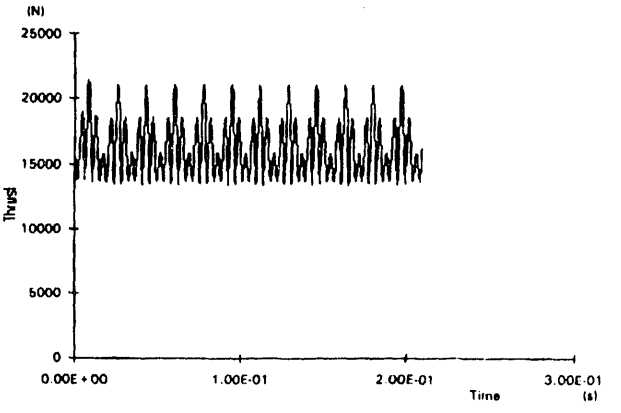

Fig. 5. Instantaneous thrust vs. time in a double layered structure

TABLE II

NUMERICAL PARAMETERS USED TO OBTAIN NUMERICAL RESULTS	
Armature coils	Superconducting coil
d = 0.43m vel = 100 m/s L = 0.6m I = 48kAt a = 0.05 m (in the double layer case)	Yo = 0.0 x_s =0.2m L_s= 0.5m Is = 700 kAt

IV. THE INFLUENCE OF ARMATURE COILS DISTRIBUTION ON THRUST

A. The average thrust

In order to get the role of armature coils distribution on thrust, it is useful to calculate the average thrust that can be defined as:

$$\bar{F} = \lim_{T \to \infty} \frac{1}{T} \int_{-T}^{T} F(x,y,t)\, dt \qquad (13)$$

To simplify the integration it is possible to assume

$$L >> L_s \qquad (14).$$

With this assumption (12) becomes:

$$F_x(x,y,t) = \frac{\mu_0}{\pi} i_s I L_s \times$$

$$\times \sum_{e=-1;i=-\infty;f=1}^{e=1;i=\infty;f=3} \left[-e \frac{y_s + v_s t - y_{ief}}{(x_s - x_{if})^2 + (y_s + v_s t - y_{ief})^2} \sin(\omega t + \varphi_f)\right] \qquad (15)$$

It can be seen from (13) that to have a non null average thrust the integral of F(x,y,z,t) on t must be proportional to T (i.e. divergent when T goes to infinity). As a result it is interesting to study the integrals in (13) and it can be easily shown that result is [5]

$$\int_{-\infty}^{+\infty} F_X(x,y,t)\,dt = \frac{\mu_0}{\pi} i_S H_{\delta} \times$$

$$\times \sum_{\substack{e=-1;i=-\infty;f=1 \\ e=1;i=\infty;f=3}} \left[-e \cdot \frac{1}{v_s} \cos\left(\varphi_f - \frac{\omega}{v_s}(y_s - y_{ief})\right)\right] \qquad (16).$$

The summation on e can be performed in (16) and it gives:

$$\int_{-\infty}^{+\infty} F_X(x,y,t)\,dt = \frac{\mu_0}{\pi} i_S H_{\delta} \times$$

$$\times \sum_{\substack{i=-\infty;f=1 \\ i=\infty;f=3}} \frac{2}{v_s} \sin\left(\frac{\omega}{2v_s}(y_{01f} - y_{0-1f})\right) \times$$

$$\times \mathrm{Im}\left(\exp\left(j\left(\varphi_u - \frac{\omega}{v_s} y_s + \frac{\omega}{v_s}\delta di + \frac{\omega}{v_s}(y_{01f} + y_{0-1f})\right)\right)\right) \qquad (17)$$

Equation (17) can be rewritten as:

$$\int_{-\infty}^{+\infty} F_X(x,y,t)\,dt = \frac{\mu_0}{\pi} i_S H_{\delta} \sum_{f=1}^{f=3} \frac{2}{v_s} \sin\left(\frac{\omega}{2v_s}(y_{01f} - y_{0-1f})\right) \times$$

$$\times \mathrm{Im}\left(\exp\left(j\left(\varphi_f - \frac{\omega}{v_s} y_s + \frac{\omega}{v_s}(y_{01f} + y_{0-1f})\right)\right) \times\right.$$

$$\left. \times \sum_{i=-\infty}^{i=+\infty} \left(\exp\left(j\,\frac{\omega}{v_s}\delta di\right)\right)\right) \qquad (18)$$

where the dependence on i has been separated from that on f.

Equation (18) gives the average thrust but in order to get more information on the role of the coils distribution some more manipulation on the sum on i is needed. Moreover, the only way to get an average thrust different from zero is to make infinite the sum on i in (18). Under the assumption that the pole pitch is perfectly constant and equal to 3d, it means to have:

$$v_s = \frac{3\omega d}{\pi} \qquad (19)$$

which is the usual synchronism condition. When the pole pitch is not constant the sum on i in (18) must be carefully examined. This term can be expressed in this way:

$$\sum_{i=-\infty}^{i=+\infty} \left(\exp\left(j\,\frac{\omega}{v_s}\delta di\right)\right) =$$

$$= \sum_{i=-\infty}^{i=+\infty} \int_{-\infty}^{\infty} \delta(\delta di - y)\left(\exp\left(j\,\frac{\omega}{v_s} y\right)\right) dy =$$

$$= \int_{-\infty}^{\infty} \sum_{i=-\infty}^{i=+\infty} \delta(\delta di - y)\left(\exp\left(j\,\frac{\omega}{v_s} y\right)\right) dy \qquad (20)$$

where the δs are Dirac's functions. Their sum is the density of the probability of the position of the coils when the ideal set of coil positions is obtained in the assembly phase. Such an interpretation allow to model any deviation of the coil position replacing the ideal distribution (which consists of a set of Dirac's functions) with a distribution density suitable to describe the real situation.

B. Some examples of the role of armature coils distribution on thrust.

The equation (18) is suitable to analyse the role of armature coils distribution on thrust. In real systems the armature coils distribution can presents many kinds of defects:

(i) localised deviation of the coil from the ideal position because of errors in the assembly stage, temperature effects, weather effects and so on;

(ii) long range alteration of the pole pitch due to assembly errors.

A localised deviation from the ideal position can be modelled assuming that the distribution of the position of the i-th coils is a gaussian distribution which has δdi as average and σ as standard deviation. This means that in order to calculate the average thrust the following expression must be considered

$$\sum_{i=-\infty}^{i=+\infty} A \int_{-\infty}^{\infty} \exp\left(\frac{\delta di - y}{\sigma_0}\right)^2 \left(\exp\left(j\,\frac{\omega}{v_s} y\right)\right) dy \qquad (21)$$

(A is the normalisation constant) instead of the one expressed in (20). Equation (21) can be easily calculated and gives:

$$\sum_{i=-\infty}^{i=+\infty} A \int_{-\infty}^{+\infty} \exp\left(\frac{6di-y}{\sigma_0}\right)^2 (\exp(j\frac{\omega}{v_s}y))\,dy=$$

$$= \sum_{i=-\infty}^{i=+\infty} \exp\left(\frac{j\omega 6d}{v_s}i\right) \exp\left(-\frac{\omega}{4v_s}\sigma\right) \qquad (22).$$

The equation (22) gives the same result of (20) multiplied by an exponential factor. The exponential factor in (22) when:

$$\frac{\omega}{4v_s}\sigma >> 1 \Rightarrow \sigma >> \frac{4\,v_s}{\omega} = \frac{2}{\pi} 6d \qquad (23)$$

can seriously reduce the average thrust. Moreover, it is important to note the right hand side of (22) is a length almost equal to the pole pitch. It can be also said that if the position of the ith coil is described by a density function whose standard deviation is smaller than the pole pitch the thrust is not greatly affected.

A long range irregularity can be described assuming a gaussian function where the average position of the coil depend on i. In this case the (22) is still valid but d must replaced by d(i). It can be easily understood as the sum on i in (17) can be seriously affected (and therefore the average thrust can become null) because all the complex exponential factors will be have uncorrelated exponents giving a null sum.

VI. CONCLUSION

In this work a simplified model of a synchronous linear motor for Maglev has been introduced. It consists of an infinite long series of filiform armature coils and a short primary formed by one single filiform coil. As regards the instant force of this model it is found that:

-the thrust oscillation of the double layered armature are bigger than the ones of the single layer structure;

-the results of such a simplified model qualitatively agrees with numerical and experimental analyses from other authors; this implies that the model can be used to understand the various aspects of the working condition of the synchronous motor;

As regards the role of the distribution of the armature coils:

-it has been shown that short range irregularities do not affect the average thrust;

-it has been derived that the length that can be used to define the short range is the pole pitch;

-it has been shown that long range irregularities strongly reduce the thrust.

REFERENCES

[1] H.Osaki, S. Torii, H. Deguchi, M. Tamura and E. Masada, "Study of superconducting linear drives from electromagnetic and electromechanical points of view", in *Proceedings of EPE - Firenze 1991*, pp. 487-492, vol.1, 1991.

[2] F.Albicini, S. Bolognani, G.Martinelli, A.Morini, "Harmonic analysis of LSM drives for EDS-MAGLEV Systems", in *Proceedings of ICEM - Cambridge* (Massachusetts) 1990, pp. 440-447, 1990.

[3] S.Fujiwara, "Influence of the distribution irregularity in the coils of linear synchronous motor for Maglev", in *Proceedings of EPE - Firenze 1991*, pp. 111-114, vol.1, 1991.

[4] F.Albicini, M.Andriollo, G.Martinelli, A.Morini, A.Scuttari, "Calcolo del campo magnetico e delle mutue induttanze in sistemi di trasporto Maglev di tipo EDS azionati da motori lineari sincroni", in *Proceedings of national workshop 'Azionamenti Elettrici con motori lineari'*, pp. 3.1-3.30, Milano, 1992.

[5] I.S.Gradstheyn, I.M. Ryzhik, *Table of Integrals ,Series and Products*, Academic Press, New York, p.407

STATUS OF THE SAFETY CERTIFICATION PROCESS OF THE TRANSRAPID SYSTEM

Dipl.-Ing. Joachim Blomerius
TÜV Rheinland Sicherheit und Umweltschutz GmbH
Bahn-, Steuerungs- und Softwaretechnik
Postfach 91 09 51
W-5000 Köln 91
Germany

Abstract - On the threshold of the first maglev demonstration project TÜV's safety experts have successfully completed in the recent years the safety assessment of relevant subsystems and components which may be regarded as prototypes for a revenue application of TRANSRAPID. Safety and reliability of the specific maglev properties such as contact-free levitation, guidance, propulsion, and braking (key functions of maglev technology) have been successfully approved.

During test operation on TVE problems due to the stator mountings became obvious which could affect the guideway safety. The way to face the problems and to re-establish the operational safety of the guideway is shown.

1. INTRODUCTION

In Germany, each transportation system must be examined and certified prior to operation by an independent organization in order to get release by the competent supervisory authorities.

TÜV Rheinland - together with TÜV Hannover - is the responsible organization for safety certification of the TRANSRAPID maglev system operating at the TVE test facility. The process applied by TÜV Rheinland when achieving the overall TVE safety is called PASC (Program Accompanying Safety Certification).

TÜV Rheinland's work comprises study and approval of safety proofs submitted by the developers/manufacturers or operator of TVE, completed by acceptance tests on laboratory and/or manufacturers' plant level and/or TVE level.

Since more than a decade, TÜV Rheinland is involved in the safety certification of maglev technology of the TRANSRAPID type. In a series of reports addressing high speed maglev safety [1, 2, 3] this report addresses the work of the safety experts within the past four years on the threshold of the first maglev demonstration project. In the same time safety requirement goals covering specific maglev system properties were established that must be met by the maglev system developer [4].

Manuscript received March 15, 1993. This work was supported in part by the German Federal Ministry of Research and Technology under Grant No. TV 9106.

2. SAFETY ASSESSMENT OF RELEVANT SUBSYSTEMS AND COMPONENTS

In the past four years TÜV's experts have successfully completed the safety assessment of relevant TVE subsystems and components which - on the threshold of the first maglev demonstration project - may be regarded as prototypes for a revenue application of maglev.

These items comprise a complete new vehicle (two-car trainset), the TR 07, the OCS (Operational Control System) to operate the TR 07, guideway components and the operational safety of the entire system.

2.1 The Maglev Vehicle TR 07 (Fig. 1)

Of course the vehicle was and is in the centre of attention of all development and safety assessment activities as the levitation and guidance system may be looked upon as the "heart" or "key" component of maglev technology.

Following the safety goals met with the vehicle TR 06 the vehicle TR 07 should provide passengers and employees with the highest practical level of safety. This means that in an emergency the TR 07 will no more stop at any spot along the guideway (like TR 06), but is required to reach a station or designated stopping place.

This approach leads to fundamental system requirements concerning a maglev vehicle with regard to the rescue strategy; the resulting properties are

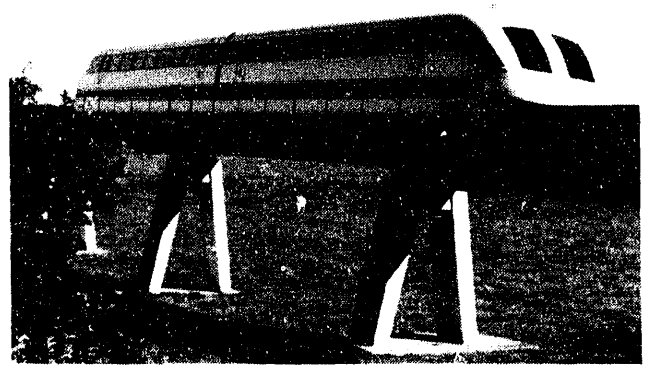

Fig.1 TRANSRAPID 07 on TVE elevated guideway

- safe hovering
- programmed braking
- fire protection.

Before discussing the requirements on system level and how they are met, the requirements on the maglev vehicle component level shall be discussed in detail.

2.1.1 Vehicle Components

The following items of the vehicle were identified to be safety relevant, and were reviewed on behalf of the safety assessment:

1) Car Body (strength analysis; side/end doors; vehicle couplers; interior materials (fire performance); glazing materials (car end))

2) Secondary Suspension (load assumptions; strength analysis)

3) Levitation/Guidance System
   - Mechanics (load assumptions; strength analysis; supporting skids)
   - Electrical/Electronic Equipment (safety devices in the magnet control circuit; eddy current brake)

4) On-Board Energy System (batteries; outside power feed; linear generator feed; electrical safety; energy distribution; wiring)

5) On-Board Control System (on-board control inclusive door and levitation/guidance control; hinge point control)

The main results of the safety assessment are outlined briefly.

1) Car Body:
   The requirements of the stresses in the structural parts under all loading conditions and abnormal operations (e. g. emergency braking), of the end doors to function as fire walls are met.
   The requirements of the side doors and their control in accordance with the requirements of ICE-doors, of the glazing materials (car end) in accordance with DB requirements for high speed trains are met.

   Requirements of fittings and linings in the passenger compartment:

   Due to a revenue application - oriented rescue strategy the criterion for the assessment of fire behaviour with regard to
   - avoidance of corrosive and toxic decomposition products
   - increased resp. additional requirements of density and composition of smoke gases and of heat release

   have been increased.

   The guidelines for material selection are the recently established fire protection requirements of passenger or crew compartments for aircraft.

   As to the TR 07 the requirements are met.

2) Secondary Suspension:
   (connection of car body to the levitation frames)
   The requirements of the stresses in all mechanical and pneumatic parts to control the vertical, lateral, and roll motions of the vehicle under all loading conditions are met.

3) Levitation/Guidance System:
   - Mechanics
     The magnets are connected to the levitation frames by means of primary suspension and links. Especially the levitation magnets are connected together like a chain with hinged supports; at these hinge points the skids and the pneumatic springs of the secondary suspension are allocated.
     In each car of TR 07 two opposite guidance magnets are replaced by the eddy current brake magnets.
     The requirements of the stresses in all structural parts under all loading conditions and abnormal operations are met.

   - Electrical/Electronic Equipment
     o Magnet or Gap Control Circuit (basic unit of the modular-oriented design of the levitation/guidance system)
       There was an extensive testing on the components of the gap control circuit as their proper function and behaviour under all normal and abnormal operations determine predominantly the safety of vehicle and passengers.
       Among the components of the gap control circuit - chopper with safety properties, controller, gap sensor system, limitation of magnetic forces versus gap, magnet with coils - the chopper, the gap sensor and the magnetic force limitation device must meet special safety requirements to ensure contact - free operation especially between levitation magnets and the stator packs of the guideway with the exception of rare events with permissible loads.
       To ensure safe hovering, the levitation/guidance function can be safeguarded by a large number of the aforementioned autonomous, decentralized units (64 levitation and 48 guidance gap control circuits). Considering the maximum conceivable number of failed units (due to faulty units, loss of some power supply) the overall levitation/guidance function will be maintained (see Fig. 2).
       The requirements of ensuring contact - free operation by the single unit and of the system property "safe hovering" are met as well.

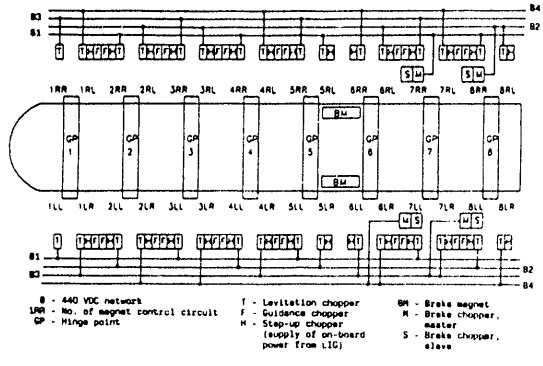

Fig. 2 TR 07, allocation (schematic, one car) of magnet control circuits with levitation choppers and power networks

o Eddy Current Brake
The TR 06 skid brake system turned out to be unsuitable for a revenue application, so for the TR 07 a maglev adequate, no - contact secondary (emergency) brake system with safety properties was designed and realized, which acts on the lateral guidance rail.
This brake decelerates the vehicle safely from highest speeds below a pre-set threshold velocity (about 120 - 110 km/h), then there is a transition to a skid brake system up to standstill of the vehicle. This is due to loss of effectiveness of the eddy current brake at low speeds.
As to a revenue application vehicle the skid brake system will be activated at 10 km/h.
The eddy current brake consists of eight autonomous, decentralized braking circuits with regard to activation and connection to the on-board power supply. The brake must be activated safely, if there is a failure in the primary (propulsion) brake system. In a wide speed range deceleration rates similar to the propulsion brake must be achieved (about 1 m/s^2, see Fig. 3).
The single brake circuit must be specially qualified and reliable. In the event of a failure there is no preferred direction. To realize the overall safety properties of the eddy current brake the principles of redundancy and failure-tolerant behaviour must be applied. The eddy current brake has properties of an active system.
Six out of eight circuits (loss of two redundancies) determine the safety relevant braking distance.
The eddy current brake is directly controlled by the OCS. After extensive testing it can be stated that the requirements of a maglev adequate secondary brake system are met.

4) On-Board Energy System:
There was an extensive testing as well, because on the one hand high fire protection requirements, on the other hand functional requirements with due regard to safe hovering and supply of safety relevant sinks had to be met.
For this purpose, the TR 07 has eight battery-buffered 440 VDC-networks and eight battery-buffered 24 VDC-networks for safety relevant sinks (four per car). The networks are mutually independent, electrically/ mechanically safely separated, and allocated in the car body underneath the passenger compartment.

Electrical connections in critical areas and in areas with key functions are executed in ground fault - and short circuit-proof cabling.
The cables and lines are halogen-free and flame-resistant. Preservation of function under a 3-hour flame effect is given. The maximum voltage for operating equipment in the passenger and crew compartment is 24 VDC.
The requirements of the on-board energy system with due regard to safe hovering and fire protection are met.

5) On-Board Control System:
The on-board control mainly serves to control and monitor the levitation/guidance system and the doors. It receives all commands from the vehicle-based safety computer (see later on, OCS) where all safety-relevant functions of the TR 07 are concentrated.
The on-board control transmits the levitation and set-down commands to the levitation/guidance system. To avoid set-down commands untimely or due to a failure during running operation at high speed, the set-down command is interlocked in each gap control unit unless vehicle speed is below a pre-set threshold velocity (see also eddy current brake, transition to skid brake). The speed signal is generated independently in each gap control unit.
The hinge point control disables partly the pneumatic spring over the hinge point in case of failure of one adjacent gap control unit. Should both adjacent units fail, then the spring is completely disabled. In this case, skid-to-guideway contact of individual skids is possible at any speed. However, this is a permissible abnormal operation.
The requirements of the on-board control system with due regard to safe hovering are met.

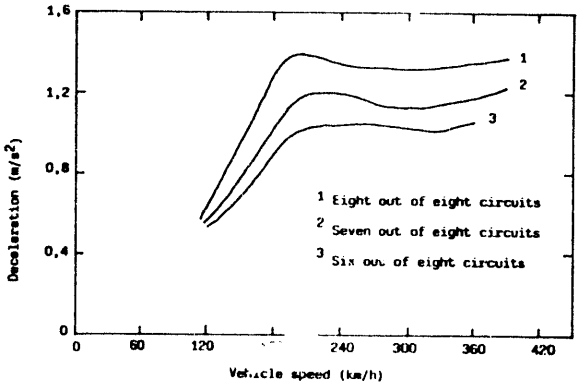

Fig.3 Braking characteristics of TR 07 eddy current brake (result of TÜV acceptance tests)

2.1.2 System Properties

Remarkable features of a revenue application-oriented rescue strategy for high speed maglev vehicles are

- increased fire protection requirements and
- ability of programmed braking (emergency stop no more possible at any spot of the guideway),

because vehicles will operate on guideway sections without safety areas. The necessary technical prerequisite is "safe hovering" - the property that defines the system and has consequences for almost all subsystems.
"Safe hovering" characterizes the property of the high-speed maglev train of being able to maintain its levitation function even in the event of the maximum conceivable breakdown and/or emergency at least to such an extent that limited and short-term continued operation is possible to reach the next station or designated stopping place.
Thus, the levitation function must have a safe life, since there is no reliable failure direction for this as a whole.
This safe hovering is achieved by the so-called active vehicle subsystems levitation/guidance and on-board energy supply with a structure of autonomous, decentralized and redundant units with failure-tolerant behaviour; energy needs are

covered from vehicle motion-starting at a speed of about 100 km/h-by way of linear generators. This ensures safe hovering even without active propulsion, i. e. with sufficient motion energy. In addition, interlocking of the set-down command in each gap control unit (see above) contributes to safe hovering.
The increased fire protection requirements are met by appropriate material selection for the interior of the compartment and by the energy supply safety measures. The compartment does not contribute to fire propagation; one car is considered a fire segment. In an emergency, passengers must move to the adjacent car. The end doors (escape route) have an approval of at least 30-minute fire barrier so that there is enough time for rescue. The occurrence of a system-inherent fire in the car body underneath the passenger compartment is unlikely.
TRANSRAPID vehicles are provided with two braking systems of different principle which are controlled by the OCS. This ensures programmed braking with both types of brakes. Under normal conditions braking will first act on the propulsion (thrust reversal); if a failure occurs or under abnormal operations the eddy current brake must provide the necessary deceleration.

The fire protection and programmed braking requirements with due regard to the successfully achieved property "safe hovering" have been met.

2.1.3 Summery TR 07

Based on its design, concept and the submitted safety proofs the TR 07 has got release for operation on TVE. The operational safety is ensured up to maximum speed on TVE (up to now 436 km/h). It can be stated that safety and reliability of the specific properties such as contact-free levitation, guidance, propulsion and braking ("key" functions of maglev technology) have been successfully approved. In addition, TÜV Rheinland's experts continue safety certification through an ongoing test program on the TVE test facility.

2.2 Guideway components

There is made a distinction between the structural parts (guideway girders etc.) of the guideway and the guideway equipment (stator packs and their mountings etc.). The structural parts must meet the local construction code, whereas the equipment is considered maglev specific.

For the new double-span concrete and steel prototype girders in the channel track a new type of stator pack mountings was designed (due to problems with guideway integrity chapter 3 gives attention to the stator mountings).
The property of these mountings is a design that does not threaten overall operation in the event of failure of one component. The solution is "cold redundancy" where the load is supported by one of two branches. If the first (operational) branch fails the load is supported by the second (redundant) branch for continuous safe but limited operation (see Fig. 4).

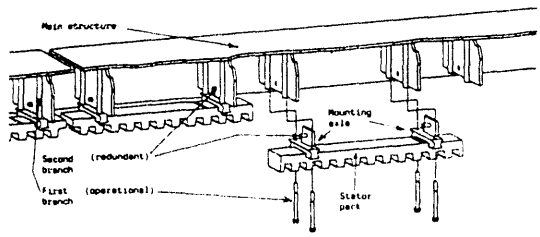

Fig. 4 Stator mountings for the double-span steel prototype girder (cold redundancy, schematic)

Upon failure of the first branch there is a vertical drop of the stator of max. 2 mm. This deviation of the stator functional surface is permissible for the levitation function, but measures for detection are required.
For this purpose an on-board measuring system to monitor the stator pack functional surface integrity has been developed, based on the principle of gap sensoring of the levitation system. Data of the guideway as projected are collected and stored in the measuring system as reference data. With the existing measuring system there is an off-line comparison between reference data and measured data collected during a test run with TR 07 (e.g. at the end of daily operation).
There is an online measuring system underway which allows the aforementioned comparison during each test run. Basic requirement is the reliable detection of a surface failure; a system malfunction shall be detected safely.

It can be stated that the requirements of a safely operable guideway can be met by means of redundant, failure-tolerant stator mountings together with a stator surface measuring system.

2.3 Operational Control System (OCS)

Though the actual OCS to run the TR 07 on TVE is a subset of a future maglev revenue application OCS (one power substation, one trainset, single-track guideway), it has been designed as a complete system. The use of modular vehicle - and wayside-based components in hard- and software technology of future OCS's is a common concern; standard safety computers of the wheel-on-rail technology are applied.
To make use of the efficiency of maglev, speed and location informations must be generated to ensure best utilization of speed and brake profiles. Due to the guideway-oriented propulsion system the components must be split up in mobile (vehicle -based) and stationary (wayside-based) components for purposes of vehicle control and safety. There is a need for safe data links to and from the vehicle; the OCS utilizes a 40 GHz radio link system (see Fig. 5).
The basic safety objectives of TVE OCS are to provide a safe switch travel when running through the northern and southern loop, to supervise the speed profile, to provide programmed braking (either with the propulsion or the vehicle brake system), and safe propulsion shut-off when the vehicle brake is activated.

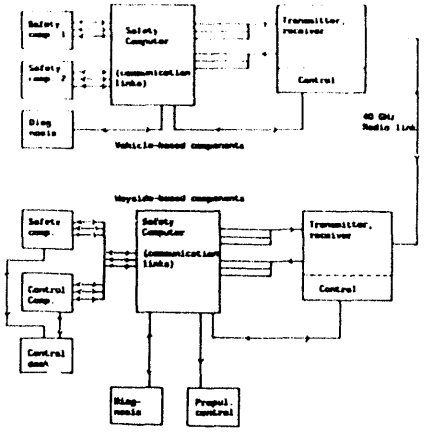

Fig. 5 TVE operational control system (schematic)

TÜV Rheinland's part is certification of the TVE OCS safety properties. Key component is a 2 x 3 standard computer of railway signalling systems to provide vehicle, wayside, and communication links safety.
The following items are in the process of certification:

1) Vehicle - based systems (safety computer specification; hardware configuration, maglev-specific hardware; location; eddy current brake control; supply of OCS components; source code (application software); executable code)
2) Wayside - based systems (safety computer specification; hardware configuration; propulsion shut-off and switch control; source code (application software); executable code; input equipment (central operator's desk))
3) Communication links (safety computer specification; hardware configuration, maglev-specific hardware; source code (application software); executable code; safe data links procedure)

As to the status of certification process the safety proofs have been submitted and studied. Adequate hardware and software validation and verification procedures are utilized. The check of the source code versus the specification serves to prove the correctness of the code. By checking the specification versus the computer environment and TVE system requirements the validity is proved. It is emphasized that the computer specifications are powerful documents within the safety proof.
Further steps within the safety proof are the OCS acceptance tests on system level (scheduled in spring 1993) and a half year safety test operation with minimum requirements of daily OCS test rides and covered distance; safety critical failures are not admitted.
If all steps of the safety proof have been successfully achieved, there will be release for operation of TR 07 under full control of the OCS (scheduled in autumn 1993).

3. GUIDEWAY INTEGRITY

In the recent years the guideway turned out to be of major concern; not the structural parts, but the elements for connecting the stator packs to the guideway girders (stator mountings).

In the following outline the significance of the stator packs will be highlighted:

- they react with the levitation magnets, their bottom surface is the functional surface for the gap control circuit
- they produce the travelling magnetic field for the propulsion, and provide vehicle power through induction for the linear generators
- by way of four fastening points per stator pack all loads generated by the vehicle are introduced into the structural parts of the guideway.

The latter elements are vertically allocated, prestressed screw bolts.

These elements are the deciding factor for the positional safety of the stator packs (that means guideway geometry) and - as far as the failure tolerance of the vehicle against vertical deviations of stator packs has not been approved - of high safety concern (see Fig. 6).

Experiences gained with the design of the stator mountings in the recent years showed the following:

- due to the big number of stator packs (TVE: about 2000 per km) material and mounting defects cannot be reliably excluded
- the design with due regard to the stator packs and to the guideway structure is similar to a rigid frame
- stress values in the bolts gained by testing show dynamic portions of about 30 % of the static or mean value; the frequency is determined by the levitation magnet - even pole - division and the vehicle speed
- due to the rigidness of design there are distinctive eigenvalues due to vehicle speed (e. g. northern guideway loop type concrete: about 200 km/h; see Fig. 7, TR 07 test run).
- the stresses are more unfavourable than the load assumptions the original design was submitted to (number of load cycles; amplitudes in case of resonance frequency)

The result is that the planned behaviour of the stator pack mountings is not maintained, as critical deviations of stator packs due to failure of one mounting axle cannot be excluded.

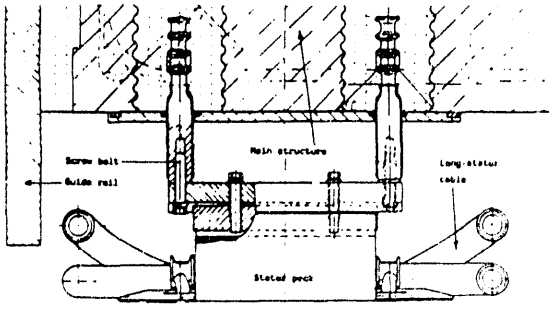

Fig. 6 Stator mountings TVE concrete guideway northern loop (one mounting axle)

These facts led to permanent guideway inspections, to closing of guideway sections up to change of mounting elements in guideway sections. Therefore the operable guideway and the chance of test and visitor rides were subject to considerable restrictions.

To solve the problems intensive r&d effort is made for new design concepts. Two methods are pursued:

1) Wayside-based modification of the mountings so that a critical vertical deviation of a stator pack can be excluded (a critical deviation could lead to a collision with a levitation magnet)
This solution is called "cold redundancy with on-board failure detection" and has been undertaken on the double-span prototype girders (see 2.2, Guideway Components).
The requirements of construction due to the small deviation gap are still considerable (e.g. maintenance procedures).

2) - Vehicle-based modification to ensure collision-tolerance of the maglev vehicle. This is - in terms of safety - the vehicle property that a collision between a levitation magnet and a critical deviated stator pack does not endanger passengers in the vehicle and other persons outside near the guideway; material damage of the vehicle and the guideway is permissible.
- Wayside-based modification of the mountings so that critical deviations of the stator packs are limited to an extend that collision occurs within the slopes provided at both ends of the magnets.
- The on-board failure detection may within this approach no more considered safety-relevant. Its effect is increase of availability, as collision probability decreases.

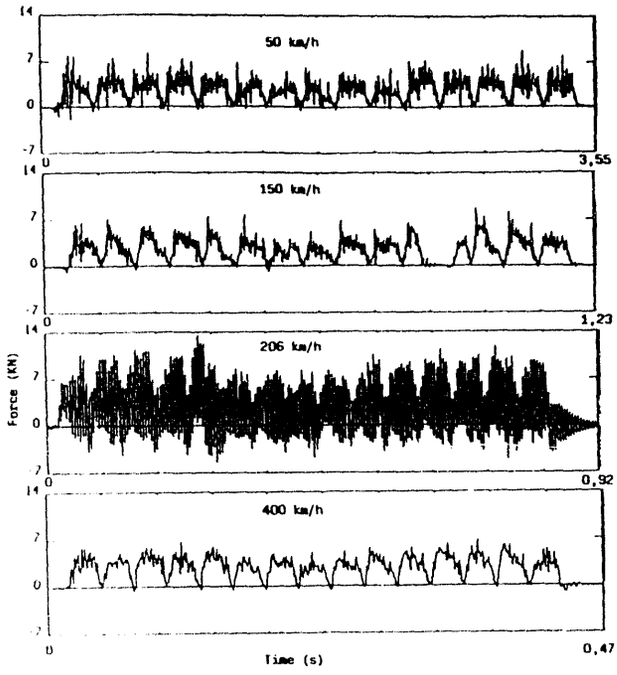

Fig. 7 Typical vertical stress in one of the four bolts (TVE concrete guideway northern loop)

The two methods provide advantages in the safety assessment of stator mountings; due to the aforementioned procedures they are no more safety relevant; failures are permissible. Requirements of mounting elements are shifted from safety to reliability requirements.

According to method 2), the strategy to achieve a safely operable guideway is based on the following three pillars:

- collision-tolerant vehicle
- limitation of stator deviation with additional mountings ("simple" or "quick" redundancy) to a maximum critical value (about 15 mm)
- on-board failure detection to monitor the stator geometry

This strategy will be implemented in a guideway section in spring 1993 and is in this moment reviewed by the safety experts, precondition to operate TVE guideway as a whole.

4. COOPERATION TÜV - FRA

Totally independent from the aforementioned safety experts' activities procedures for release of maglev systems with electromagnetic suspension (EMS) in the U.S. were developed within the cooperation TÜV-FRA. In Germany, these activities are sponsored by the Ministry of R&T.

As a result of the cooperation, the German safety requirements for high speed maglev (EMS) trains have been translated in English language. During the next conference there will be a report about the cooperation and the requirements of high speed maglev trains.

REFERENCES

[1] H. Jansen and P. Mnich, "Safety Aspects of the Maglev Test Site TRANSRAPID Versuchsanlage Emsland ", in the proceedings of the 7th International Conference on Maglev Transport '85, September 17-19 1985, Tokyo

[2] J. Blomerius, "Safety and Licensing Aspects of TRANSRAPID and Maglev Systems", in the proceedings of the 9th International Conference on Maglev and Linear Drives, May 19-21 1987, Las Vegas

[3] H. Jansen, "Safety Requirements for Maglev Systems in Germany-Review and Forecast", in the proceedings of the 5th World Conference on Transport, July 10-14 1989, Yokohama

[4] High-Speed Maglev Trains; German Safety Requirements, Report No. DOT/FRA/ORD-92/01, Translation of: Magnetschnellbahnen, Sicherheitstechnische Anforderungen (RW MSB),
TÜV Rheinland, Köln, Ausgabe 1, März 1991

VERTICAL DYNAMICS OF A SUPERCONDUCTING SUSPENSION SYSTEM

D. Casadei - U. Reggiani - G. Serra - A. Tani

Università degli Studi di Bologna - Facoltà di Ingegneria - Istituto di Elettrotecnica
Viale Risorgimento, 2 - 40136 BOLOGNA - ITALY

Abstract - This paper deals with the analysis of the vertical dynamics of an electrodynamic levitation system using superconducting coils and a passive damping system.

The vertical dynamics of the levitation system is described by the motion equation and the electromagnetic transient equations. The operation both in constant current mode and in constant flux mode is considered.

The results show that the levitation system behaviour is different in the two operating modes and the effectiveness of the damping system depends on its distance from the levitation coil and its resistivity.

The analysis can be also utilised in the design of an active control which allows the levitation system damping characteristics to be improved.

I. Introduction

In magnetically levitated transport systems with electrodynamic suspensions (EDS-MAGLEV systems) the repulsive levitation is achieved by means of a magnetic force between a high magnetic field generated by superconducting coils on the vehicle and a magnetic field due to currents induced in normal conductors or coils on the track, when the vehicle travels over it [1], [2], [3].

Electrodynamic suspension systems provide a stable force of repulsion, but have not intrinsic damping characteristics. As persistent vertical oscillations are unacceptable in vehicle suspension systems, some form of damping needs to be introduced. Apart from using a conventional spring-damper secondary suspension system, the main damping methods are the passive damping and the active damping [4], [5], [6]. In this paper the former method is studied.

In the passive method an aluminium or copper plate acting as a shield is placed between the magnet and the track, the shield being rigidly attached to the superconducting magnet. Whenever there is a vertical movement, the change in the magnetic field induces eddy currents in the shield which in turn introduces some damping force in the levitation system.

This paper presents a study of the vertical dynamics of a simple electrodynamic levitation system using superconducting coils and a passive damping system. The vertical dynamics of this suspension system is described by the vertical motion equation and the equations that represent the electromagnetic phenomena due to the resulting action of the superconducting coils, the track and the damping system.

Two mathematical models of this problem, which differ in the approach used for describing the electromagnetic transient, are considered. One of the two models is based on the partial differential equation of the time-varying electromagnetic field, which is generated when a perturbation in vertical direction occurs. This equation can be solved numerically by a two-dimensional, finite-element analysis in the space dimension and by a time-stepping procedure in the time dimension. In the other model the electromagnetic phenomena are represented by lumped parameter circuit equations. The self- and mutual inductances of the circuits are calculated as functions of the levitation height by a finite-element analysis of stationary magnetic fields. In both the models the vertical motion equation is solved by a time-stepping procedure. The lift force per unit length, which has to be introduced at each step in the motion equation, is calculated by Maxwell stresses in the former model and in terms of currents and directional derivatives of mutual inductances in the latter.

As regards the superconducting coil, the operation both in constant current mode and in constant flux mode is studied. Considering a perturbation in vertical direction, the responses of a levitation system without damping are compared with the responses of the same system when a damping system is incorporated. The results show that the levitation system behaviour is sensibly different according to the superconducting coil operating mode. Furthermore, the effectiveness of a passive damping system depends on its distance from the levitation coil and its resistivity.

Manuscript received March 15, 1993. This work was supported by the Italian PF T2 Project.

II. MODELS

A cross-section of a simple levitation system, normal to the longitudinal motion direction, is shown in Fig. 1. In the analysis the conductors on the track are regarded as a conducting sheet.

In this paper we study the case of high-speed vehicles, where the conducting sheet may be assumed to behave as a perfect diamagnetic, so that the magnetic field does not penetrate the track.

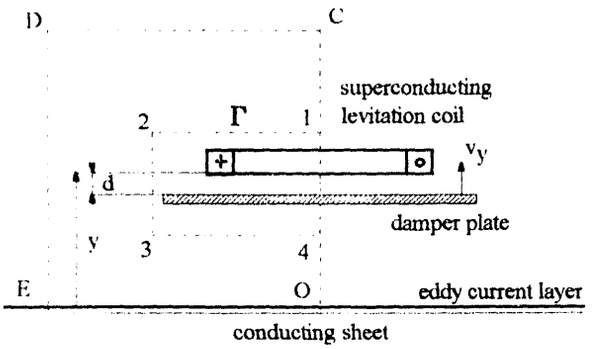

Fig. 1 - Cross-section of the levitation system

Under the above-mentioned assumptions the boundary represented by the line OCDEO in Fig. 1 is an equipotential line of the magnetic vector potential.

The vertical motion equation may be written as

$$m\frac{dv_y}{dt} = F_y - mg \tag{1}$$

$$\frac{dy}{dt} = v_y \tag{2}$$

where m and F_y are the total mass and the lift force per unit length respectively, and y is the levitation height.

Two different models for describing the electromagnetic transient are considered.

A. Field Model

This model is described by the partial differential equation of the electromagnetic field. When a two-dimensional, finite-element analysis is used for solving the field equation, the lift force Fy calculated by Maxwell stresses may be expressed as

$$F_y = \frac{1}{\mu_0} \mathbf{A}_\Gamma^T \mathbf{W} \mathbf{A}_\Gamma \tag{3}$$

In Eq. 3 $\mathbf{A}_\Gamma$ is a column vector of nodal values of the z-directed component A, of the magnetic vector potential. Vector $\mathbf{A}_\Gamma$ is related to the nodes of the triangles that lie on the line 1234 denoted with Γ in Fig. 1. $\mathbf{A}_\Gamma^T$ is the transpose of $\mathbf{A}_\Gamma$ and $\mathbf{W}$ is a square matrix [7].

The nodal values of A, the current density J in the superconducting coil and the flux Φ linking the superconducting coil must satisfy the following equations obtained by the same procedure illustrated in [7], [8]

$$\left(\mathbf{S} + v_y \mathbf{G}_p\right) \mathbf{A} + \mathbf{U}_p \frac{\partial \mathbf{A}_p}{\partial t} - \mathbf{T}_c \mathbf{J} = 0 \tag{4}$$

$$\mathbf{Q}_c \mathbf{A}_c = \Phi \tag{5}$$

where the subscripts c and p indicate the coil and the plate, respectively. The elements of the matrices in Eqs. 4 and 5 are functions of the levitation height y and, consequently, of time t.

Eq. 4 is the finite-element field equation and Eq. 5 gives the total flux linking the superconducting coil.

When the operation in constant current mode is considered, the coil current density has a specified constant value, $J=J_0$=const. , and in Eqs. 4 and 5 **A** and Φ are unknown. In constant flux mode it is $\Phi=\Phi_0$=const., where Φ_0 is given. In this case **A** and J are the unknowns which have to be determined.

In conclusion, for a fixed operating mode, when the levitation height y_t, the vertical speed $v_{y,t}$, the vector $\mathbf{A}_t$ are known at time t, the quantities $v_{y,t+\Delta t}$, $y_{t+\Delta t}$, $\mathbf{A}_{t+\Delta t}$ and $\Phi_{t+\Delta t}$ (or $J_{t+\Delta t}$) at time $t+\Delta t$ are given by Eqs. 1-5 and can be calculated with a step-by-step procedure. The elements of vector $\mathbf{A}_t$ are related to the nodes of the mesh defined at time $t+\Delta t$ and are obtained by linear interpolation of the known values of A in the nodes of the mesh defined at time t.

When the damper plate is not used, Eq. 4 becomes

$$\mathbf{S} \mathbf{A} - \mathbf{T}_c \mathbf{J} = 0 \tag{6}$$

B. Circuit Model

The damper plate is replaced by N_d short-circuited coils having cross-section sizes so that the current density can be assumed uniformly distributed. This circuit technique is particularly useful when active damping systems which use a control coil are studied. In this way the levitation system is described by a set of (N_d+1) coupled circuits.

By the principle of conservation of energy it can be

shown that the lift force, in matrix form, is given by

$$F_y = \frac{1}{2}\, \mathbf{i}^T \frac{d\mathbf{M}}{dy}\, \mathbf{i} \qquad (7)$$

In Eq. 7 **i** is the column vector of the circuit currents at time t and **M** is the self- and mutual inductance matrix. The elements of matrix **M** are functions of the levitation height y. These elements are obtained by cubic splines interpolation of the self- and mutual inductance values calculated, for different levitation heights, by a two-dimensional, finite-element analysis.

The electromagnetic dynamics is described by a system of circuit equations which may be expressed, in matrix form, as follows

$$\mathbf{v} = \mathbf{R}\,\mathbf{i} + \mathbf{M}\frac{d\mathbf{i}}{dt} + \frac{d\mathbf{M}}{dy} v_y\, \mathbf{i} \qquad (8)$$

In Eq. 8 the voltage vector **v** and the resistance matrix **R** are given by

$$\mathbf{v} = \begin{vmatrix} 0 \\ 0 \\ \cdot \\ \cdot \\ 0 \\ \frac{d\Phi}{dt} \end{vmatrix} \quad ; \quad \mathbf{R} = \begin{vmatrix} R_1 & 0 & \cdot & \cdot & \cdot & 0 \\ 0 & R_2 & \cdot & \cdot & \cdot & \cdot \\ \cdot & \cdot & \cdot & \cdot & \cdot & \cdot \\ \cdot & \cdot & \cdot & \cdot & \cdot & \cdot \\ \cdot & \cdot & \cdot & \cdot & R_{N_d} & \cdot \\ 0 & \cdot & \cdot & \cdot & \cdot & 0 \end{vmatrix} \qquad (9)$$

where Φ is the flux linking the superconducting coil.

With reference to the operation in constant current mode the unknowns of Eq. 8 are the linked flux and the currents in the damping circuits, whereas in constant flux mode the currents in all the $(N_d + 1)$ circuits are unknown.

Vertical dynamics can be analysed by solving Eqs. 1, 2, 7 and 8 with a step-by-step procedure.

C. *Inductance Matrix Calculation*

The self- and mutual inductances required in the circuit model are calculated by a two-dimensional, finite-element analysis. Reference is made to the geometry shown in Fig. 2 where the damper plate is replaced by N_d=4 short-circuited coils. For a given levitation height y and distance d between the levitation coil and the damping coils, the vector potential distribution is determined supplying one circuit at a time by a stationary current.

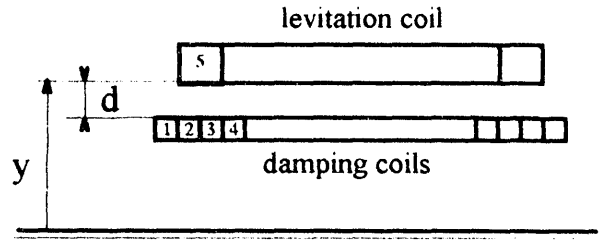

Fig. 2 - Cross-section of the levitation system with damping coils.

Fig. 3 shows a plot of the flux distribution due to the superconducting coil current.

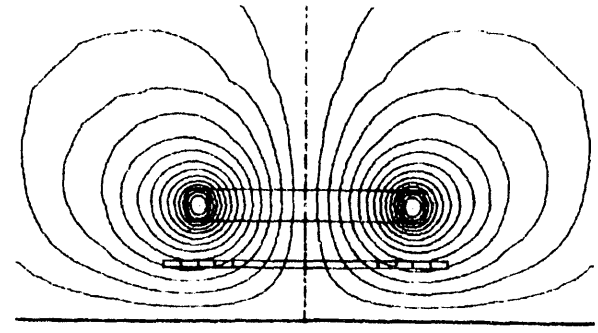

Fig. 3 - Plot of the flux distribution due to the superconducting coil, y = 0.25 m, d=0.10 m.

The self-inductance per unit length of the jth circuit is given by

$$M_{jj} = \frac{1}{i_j}\,\frac{N_j}{S_j}\int_{S_j} A_j\, dS_j \qquad (10)$$

and the mutual inductance per unit length between the jth circuit and the kth circuit is expressed by

$$M_{kj} = \frac{1}{i_j}\,\frac{N_k}{S_k}\int_{S_k} A_j\, dS_k \qquad (11)$$

where A_j is the z-directed component of the vector potential due to the only current i_j, N_j and S_j (or N_k and S_k) are the number of turns and the cross-section of the jth (or kth) coil, respectively. In this way, the inductance array can be viewed as a 3-dimensional array M_{kjh}. The subscripts k and j identify the coupled circuits, whereas

h identifies the discrete value of the levitation height. In order to reduce the number of elements of the inductance array, the calculation should be performed for few values of the levitation height. However, the calculated values can be opportunely interpolated to obtain continuous functions.

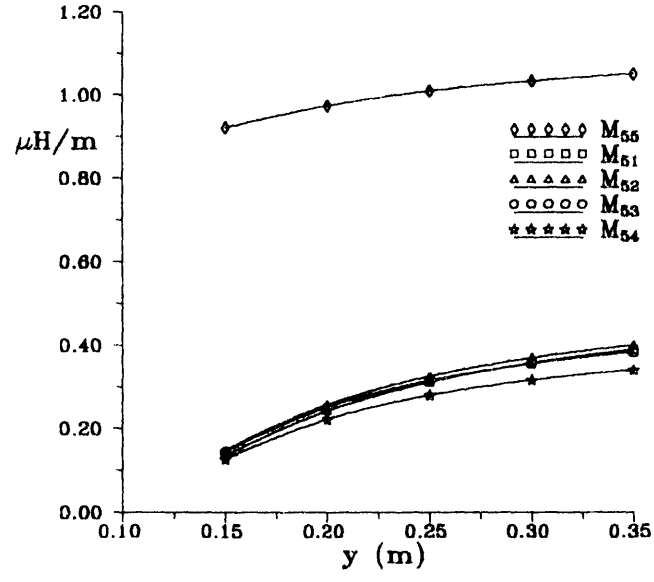

Fig. 4 - Self- and mutual inductances (for 1 turn) M_{55} , M_{51} , M_{52} , M_{53} , M_{54} versus levitation height.

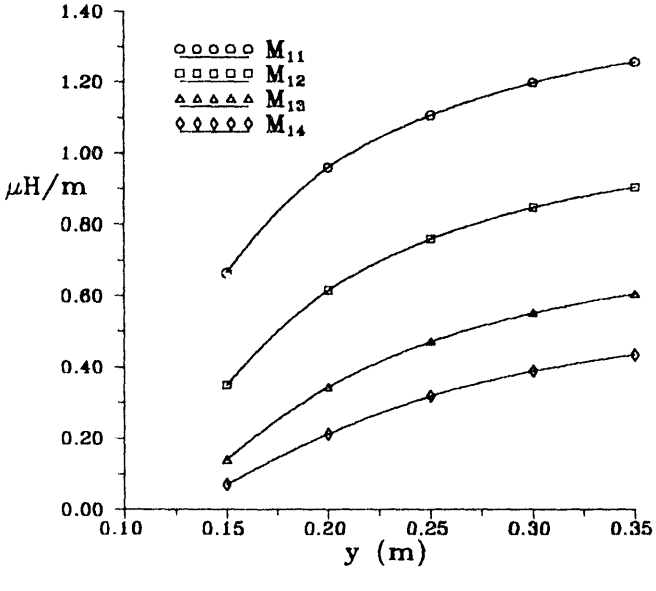

Fig. 5 - Self- and mutual inductances (for 1 turn) M_{11} , M_{12}, M_{13} , M_{14} versus levitation height.

With reference to a suspension system having the characteristics reported in Table I, Fig. 4 shows the self-inductance of the superconducting coil (coil 5) and the mutual inductances between this coil and the damping coils (coils 1, 2, 3, 4), versus the levitation height. The plotted values are related to coils with 1 turn. Fig. 5 shows the self-inductance of the damping coil 1 and the mutual inductances between this coil and the other damping coils.

III. Numerical Solutions and Results

The characteristics of the levitation system studied are listed in Table I.

TABLE I

Superconducting coil		
Width	=	0.45 m
Cross-section	=	50 mm x 80 mm (w x h)
Rated Mmf	=	600 kA
Rated levitation height	=	0.25 m
Damping Coils		
Number of coils	=	4
Cross-section of a coil	=	40 mm x 20 mm (w x h)
Distance d	=	0.10 m
Total mass per unit length	=	10.000 Kg/m

The numerical results shown below have been obtained employing the circuit model. The numerical solution of the field model is very expensive and requires large computational time, because the system geometry varies with time. On the other hand the linearity of the system and the use of short-circuited coils as damping system, allows the circuit model to be properly employed, resulting in low computational time.

In the analysis the operation both in constant current mode and in constant flux mode is considered. The static lift force as function of the levitation height, for the two operating modes, is represented in Fig. 6. The force-height curve corresponding to constant flux mode shows higher values of stiffness.

To analyse the vertical dynamics, a step of 0.05 m has been placed in the track, so that the levitation height is reduced from 0.25 to 0.20 m.

Fig. 7 shows the resulting responses for the operation both in constant current mode and in constant flux mode, without passive damping system. As a consequence of this perturbation, the frequency of the undamped oscillations is around 1.39 Hz for constant current mode and 1.48 Hz for constant flux mode.

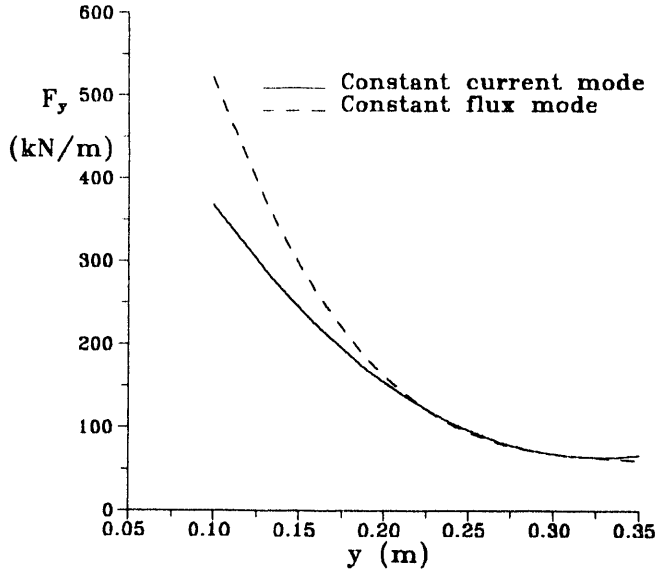

Fig. 6 - Static force-height characteristic.

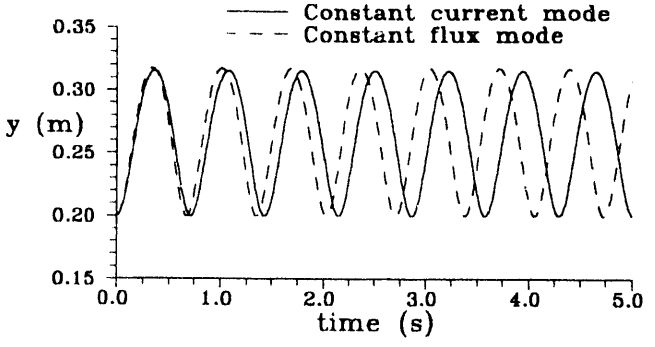

Fig. 7 - Undamped response for a vertical perturbation.

Fig. 8 shows the step response for the same perturbation when copper damping coils are placed at a distance d = 0.10 m. As it is possible to see, the operation in constant current mode results in a lower settling time.

The copper losses E_j (j=1,2,3,4) in the damping coils, during the transient in constant current mode, have been determined and the corresponding per cent distribution is given by

$$E_1 = 28\% \quad , \quad E_2 = 27\% \quad , \quad E_3 = 24\% \quad , \quad E_4 = 21\%$$

Nearly equal values have been obtained in constant flux mode.

Fig. 9 shows the step response in the case of aluminium damping coils operating in the same conditions as in Fig. 8.

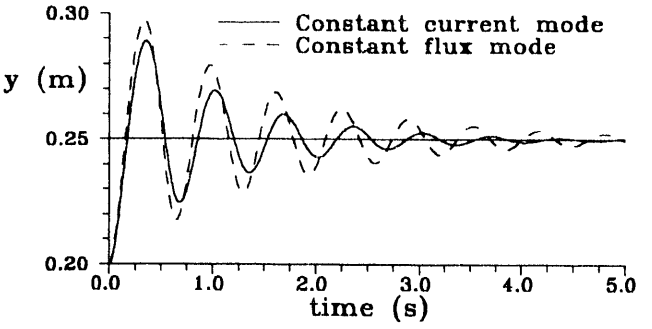

Fig. 8 - Step response with copper damping coils d = 0.10 m.

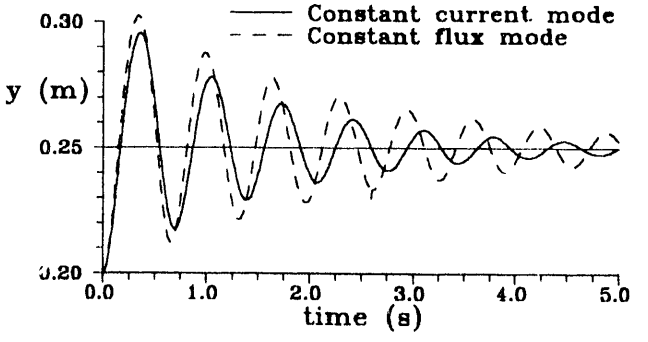

Fig. 9 - Step response with aluminium damping coils d = 0.10 m .

By the comparison of Figs. 8 and 9 it appears that the settling time increases considering higher values of the damping coils resistivity. In order to show the influence of the resistivity on the step response, we have considered a performance index which represents the time integral of the levitation height square error (ISE).

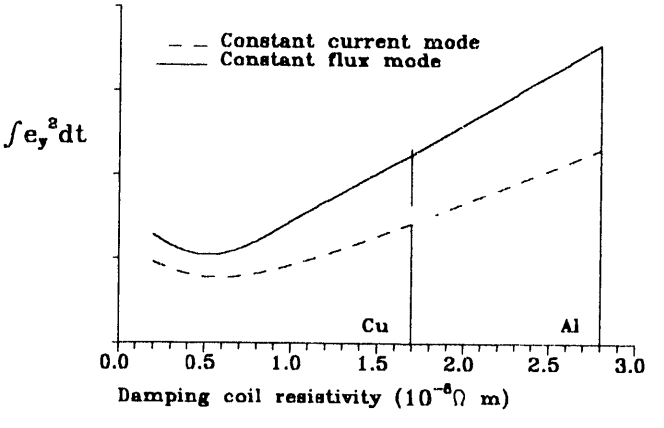

Fig. 10 - Performance index versus damping coil resistivity.

Fig. 10 shows the performance index as function of the resistivity. The curves assume a minimum for an ideal value which is about one third of the copper resistivity. This result suggests that a similar analysis could be carried out in order to determine the damping coil cross-section which minimises the performance index.

Finally, the influence of the distance d between the levitation coil and the damping coils has been investigated. The step response in the case of copper damping coils, placed at a distance of 0.05 m, is shown in Fig. 11. The analysis of Figs. 8 and 11 clearly shows that a lower damping effect is obtained when the distance d is reduced. A larger damping effect could be achieved increasing d over the value of 0.10 m. However, it is clear that the increase of d determines an equal decrease in the clearance.

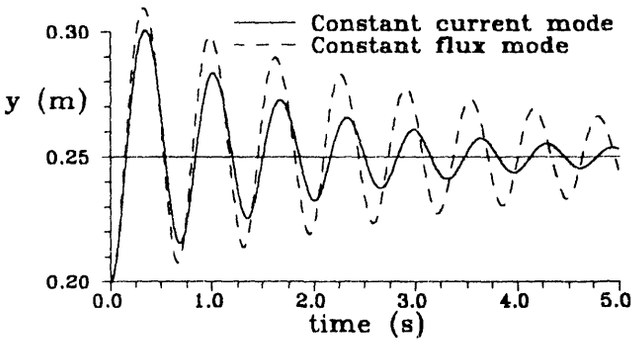

Fig. 11 - Step response with copper damping coils d = 0.05 m .

In order to attain a good ride quality, the damping effect on the mechanical oscillation of the vehicle could be improved by using an additional active damping system. This could be obtained by an active control of the current in one of the coils of the damping system.

CONCLUSIONS

In this paper two mathematical models for studying the vertical dynamics of EDS-MAGLEV systems have been presented. The field model is suitable for the analysis of levitation systems which employ a damper plate. The circuit model has been adopted in this paper to investigate the effectiveness of a passive damping system which uses short-circuited coils. The levitation system performance has been analysed both in constant current mode and in constant flux mode.

Although the static lift force characteristic presents higher values of stiffness in constant flux mode, the results obtained for a step vertical perturbation show that the passive damping system is more effective in constant current mode. The analysis has also demonstrated that the levitation system performance improves as the distance between the levitation coil and the damping coils increases. Furthermore, the advantages of using copper damping coils rather than aluminium damping coils have been emphasised. The results obtained show that an interesting investigation could be carried out with reference to the cross-section optimum value of the damping coils. A detailed study concerning this aspect and the possibility of using a coil of the damping system as control coil will be the subject of a future work.

REFERENCES

[1] P. K. SINHA: Electromagnetic suspension: Dynamics and Control. London,UK, Peregrinus, 1987.

[2] T. SAKAMOTO: A. R. EASTHAM, G. E. DAWSON: Induced currents and forces for the split-guideway electrodynamic levitation system. IEEE Transactions on Mafgnetics, Vol. 27, NO. 6, November 1991.

[3] N. CARBONARI, G. MARTINELLI, A. MORINI: Calculation of levitation, drag and lateral forces in EDS-MAGLEV transport systems. Archiv fur Elektrotechnik, vol. 17, 1988, pp. 139-148.

[4] T. YAMADA, M. IWAMATO, T. ITO: Magnetic damping force in magnetically levitated high speed trains. Trans. I.E.E.J. Vol. 94-B, No. 11,49-54, Jan. 1974

[5] M. NAGAI, S. TANAKA: Study on the dynamic stability of repulsive magnetic levitation systems. JSME International Journal Series III, Vol. 35, No. I, 1992, pp.102-108.

[6] S. FUJIWARA: Damping characteristics of Maglev using inductive power collection. MAGLEV '88, June 9-10, 1988, Hamburg, Germany, pp. 337-344.

[7] B. BRUNELLI, D. CASADEI, U. REGGIANI, G. SERRA: Finite- element analysis of a sector-motor transient. Symposium on Electrical Machines for Special Purposes, Bologna (Italy) September 9-11, 1981, proceedings pp. 47-59.

[8] B. BRUNELLI, D. CASADEI, U. REGGIANI, G. SERRA: Transient and steady-state behaviour of solid rotor induction machines. IEEE Transactions on Magnetics, vol. MAG-19 n. 6, November 1983, pp. 2650-2654.

Maglev Command, Control and Communications System Design Requirements Analysis and Safety-Critical Architecture

James W. Lewis
Rex Y. Yee
Advanced System Design Department

Command and Control Division, Systems Sector
Hughes Aircraft Company, Fullerton, CA 92634

Abstract- The development of a control system for a maglev application can largely be based on existing control systems for fully automated rail based systems. However, various aspects, unique to maglev, will require new solutions. Foremost among these is the greatly increased speed. This, coupled with the desire for very frequent service, are requirements that go well beyond the capabilities of many existing systems. Another difference, with similarly significant effects on operational control system design, is the use of a linear synchronous motor located on the guideway. This greatly changes the design approach needed for maintaining adequate levels of propulsion or motor control. In this paper, those operational control system requirements unique to maglev will be discussed along with the appropriate architectural and technological responses.

I. Introduction

The hierarchical command and control structure will be reflected in the developed architecture with three levels of command and control functions. In this paper we shall examine the requirements in four areas (physical, functional, performance, and safety) then shall synthesize these requirements into a control system architecture. The highest level of control will provide centralized supervisory function for the management of the flow of vehicles(e.g., the handling of anomalies, diversions, delays, and emergencies). The second tier at the protection level will assess the integrity of the route and control the speed of the vehicles. The lowest level controls the operation of the propulsion, levitation, and guidance systems to maintain the required ride dynamics. This hierarchical approach puts the responsibility for control at the point of need and at the point which will limit the span of control. An infrastructure of multiple communication modes will provide operational knowledge of all vehicle locations at all times and provide the necessary human communications as well. In addition, the architecture will reflect the need for responsiveness and availability in the careful partitioning of centralized, decentralized, and distributed data, processes, and control.

II. System Architecture Requirements

The maglev command and control system must be designed around the realities of the physical components of the system. Each of these components will include computers and software which all together will form the command and control subsystem. Functionality and performance must be allocated to each component of the system to ensure that all requirements are met, including passenger capacity and throughput, reliability of revenue service and absolute safety. Each of these component will be inter-connected as an integral part of an integrated system to achieve the defined objective of a fully automated, fail-safe, fault-tolerant high speed ground transportation system.

These components are: 1. Vehicle: the moving component, it includes all the hardware and software devices, the communication and controls equipment for levitation, guidance and suspension subsystems; 2. Zone/Block: a section of the guideway with a single wayside controller which includes all the supporting structure, the wayside power equipment, and all sensors, and communications equipment; 3. Switch: a moving section of the guideway that changes the route of the vehicle; 4. Station: a prime interface between the passengers and the system which interacts with one or more zones to move vehicles into or through the station and includes communications equipment and controls and monitor station services such as ticketing, reservations and station facilities; 5. Central(CCF): the top level element of the maglev system which consists of data processing equipment, displays, and terminals for operators to monitor normal operations and alert them to abnormal situations, and gives them the ability to override the automatic operation of the system.

As the functions of the system are defined, they must be allocated to these system components. A variety of global

Manuscript received March 15, 1993. Work supported in part by National Maglev Initiative Program under contract DTFR 53-92-C-00003.

goals, both traditional and system specific, need to be satisfied in a meaningful way to achieve system objectives. Among the more important objectives are:

- Fully automated operation, that is, no real-time operator intervention, at the vehicle, zone, station, or central, is required for normal operations
- Allocating functions to the most local level at which they can safely and reasonably be performed to simplify the cognitive overhead needed to produce a given element, enhance its reliability, and reduce the span of control so that malicious failure modes are constrained
- Accommodate future expandability, both in the extent of the system and in ability to interface with adjacent maglev systems, and to accept future enhancements in technology and functionality
- Provide redundancy and back-up paths to achieve extremely high levels of availability

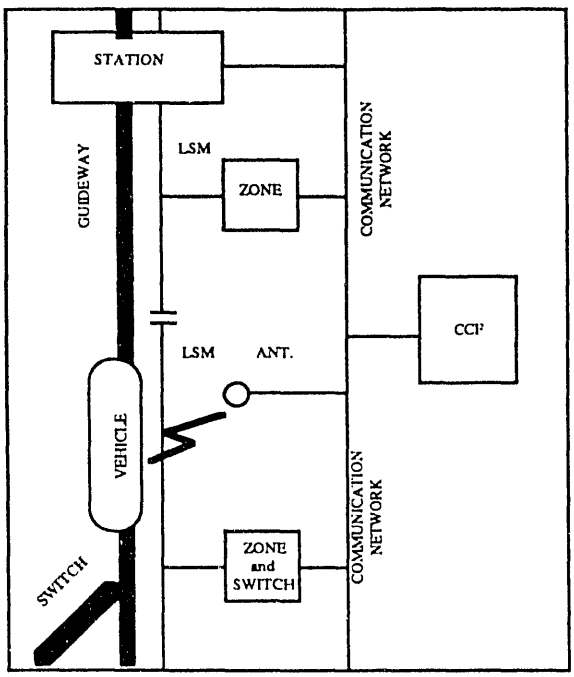

Maglev System Components Diagram

III. Control Function Requirements

Control system functions are traditionally divided into three areas: operation, protection, and supervision. The operation function regulates the movement of the vehicles by directly interfacing with the motor. The protection function prevents vehicle collisions. The supervision function allows human operators to monitor and intervene in the operation of the system. To these three, we have added a communications function to tie the system together. Although the functional characteristics of each area can be largely derived from existing automatic rail systems, Maglev technologies do introduce some new requirements and certainly change the allocation of functions to the system's physical components.

(a) Operation Functions:

This set of functions concern monitoring and control of components on the vehicle, along the guideway, and in the stations. The most notable difference from common rail base systems is that the motor, a linear synchronous motor, now is part of and runs the length of the guideway. The length of motor sections is a trade-off between the cost of the control element, the efficiency of the section (related to length), and the desired minimum separation between vehicles. The length of these motor sections has obvious impacts on the safe separation strategy to be employed. On-board functions to control the cryogenics and the tilt mechanism are also new. Some maglev approaches may not include any tilt capability, but our simulation studies have shown significant speed improvement on alignments where tight curves must be accommodated. Finally, some level of automatic sensing of the environment seems necessary for any system being operated automatically while vulnerable to weather and seismic effects.

- Vehicle State Monitoring - reporting position and velocity
- Cryogenic Control - maintain superconductors temperature
- Propulsion/Braking/Levitation Control - control velocity, levitation gap and braking requirements
- Secondary Suspension Control - control ride comfort
- Switch Control - switch actuation and status reporting
- Vehicle Systems Control - monitor on-board systems
- Environment Monitoring - monitor local and regional weather and seismic conditions
- Station Control - monitor and control station subsystems

(b) Protection Functions:

These functions must provide a fail-safe mode of operation. Therefore, they can override the actions of the control or supervision functions to ensure a vehicle always remains in a safe state. The protection functions must operate independently from the other functions. A function which will assume greater importance with a maglev system (because of its greater speed and decreased crash worthiness) is that of ensuring guideway integrity and the absence of any obstruction. Also, emergency braking control will be different than for light or heavy rail systems since the braking mechanisms are different.

- Vehicle Separation Control - maintain separation between vehicles at least sufficient for a safe stop
- Vehicle Position and Identification - maintain absolute knowledge of location and identification of all vehicles
- Route Integrity Control - detect any obstruction
- Emergency Braking Control - control emergency braking systems on vehicle or on guideway
- Emergency Speed Control - speed control in the event of a motor failure
- Emergency Response Management - ensure transition to a safe state in the event of any failure

(c) Supervision Functions

The supervision functions are characterized by either requiring operator interaction or requiring global information. They must not be required for safety and are not critical for maintaining short term operations. But provision for operator intervention is required to optimize long-term operations. Schedules might have to accommodate on-line and off-line stations and express and local service. Data recording and analysis should allow feed-back of operational problems into the route planning function and should allow full characterization of system anomalies for subsequent resolution. Finally, the operator should be offered guidance in the resolution of any system problem. This will require functions designed around all possible failure modes of the system.

- Performance Monitoring - monitor and display to the operator the performance of the entire system
- Alarm and Malfunction Reporting - alert the operator and detect any malfunction
- Control and Override Automated Subsystems - allow the operator to safely control any part of the system, including the automated functions
- Failure Management - manage the response to an incident to maintain safety and restore service
- Data Collection and Analysis– record and analyze data on the entire system
- Route Planning and Dynamic Scheduling - off-line develop the timetable and on-line detect schedule interruptions and control schedule recovery
- Initiation and Termination Service - start and stop operation of any vehicle or the entire system
- Station and Passenger Interface Control - provide information to the passengers and monitor the movement of passengers at all times

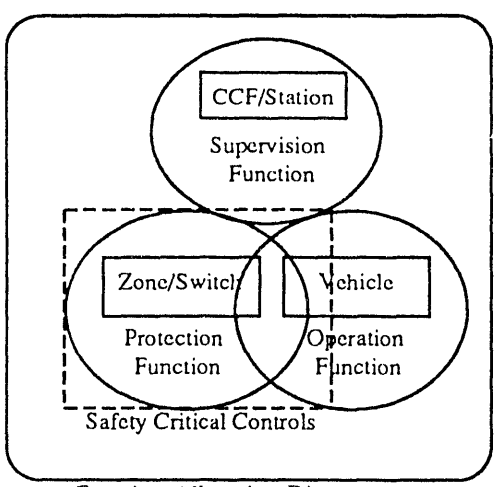

Function Allocation Diagram

(d) Communications

The communications subsystem must provide a transparent and error-free transfer of information (voice and data) to and between all other subsystems in a fully automated and fail-safe manner and with sufficient reliability to meet the overall system availability goals. Two major factors will direct the selection of a communications architecture and its components. The first is the need to accommodate both mobile and fixed point users. The other is the need to provide both primary and back-up communications links.

- Vehicle Communications: In general, since radio frequency bandwidth is limited, it will be desirable to keep the vehicle communications to a minimum. The vehicle only needs to report its status, position, speed and acceleration. It may request a speed reduction (or a stop) based on unacceptable ride comfort or an emergency situation. The vehicle will receive route and schedule information such as station arrival time or a route deviation for local verification and validation.

- Zone Communications: The zone is the primary point of vehicle propulsion control as well as the primary collection point for vehicle location and detection functions. It will be in contact with adjacent zones for vehicle hand-off. It will exchange data with central on vehicle movement. The zone may also act as the initial relay point for all vehicle communications with other system elements and with external elements.

- Station and Switch Communications: Stations and switches, although different elements, have the same type of requirement to communicate with the immediate and adjacent zones to ensure safe operation with respect to vehicle movements. Switches may receive control signals from the zone or from central. Stations, in addition, will communicate passenger related information to and from central and will have to provide information to external agencies such as inter-modal transportation services.

- Central Control Facility Communications: The Central Control Facility, with its responsibilities for controlling region wide vehicle flow, for monitoring and for emergency and failure response, and for passenger handling, will require relatively wide bandwidth communications with all other elements of the system. In addition, emergency back-up communications links, probable with significantly less bandwidth, must be provided to most, if not all, other elements.

IV. Performance Requirements

(a) Operational Headway Control:

The principle for headway control during normal operations is to enforce a pre-determined vehicle separation strategy which meets the system's requirement to provide the highest level of safety along with maximum throughput. The Operational Headway is the headway between vehicles at

which the system is able to operate continuously and still maintain schedules without vehicle bunching as a result of normal disturbances and normal passenger induced delays. The three most analyzed headway control strategies are: constant-time headway control, constant-distance headway control, and constant-safety factor headway control.

• A constant-time headway control algorithm maintains a constant time slot (e.g., 40 seconds) between vehicles at any command speed. The command speed is dictated by the supervision function. The maximum speed of a following vehicle will be adjusted to maintain as a minimum a constant time slot between it and the leading vehicle.

• A constant-distance headway control algorithm maintains a constant distance between vehicles at any command speed. A similar approach as the constant time strategy is applied except the distance between vehicles is the determining factor. In this approach, the speed of a following vehicle is adjusted to maintain as a minimum a constant distance slot between it and the leading vehicle.

• A constant-safety factor control algorithm provides the most conservative approach to maintaining the separation between vehicles. It ensures that the minimum time or distance to a leading vehicle is maintained based upon the braking system capability. The algorithm follows the same command speed profile as the other algorithms, but then assess the speed of both the leading and the following vehicle to use the most conservative measure (either constant-time or constant-distance) to maintain the separation between the vehicles.

Another factor has to be considered in developing the headway control algorithm. One of the characteristics of an LSM is to require synchronous movement of the vehicle with respect to the guideway based on the frequency generated by the guideway. This allows only one vehicle to be present in each block (motor section) at a time. Thus the selection of block length will create a minimum separation between vehicles at any speed and will limit the total number of vehicles moving around the system.

(b) Operational Headway and Capacity Analysis

The general remarks are concluded as follows: 1. All three headway control strategies are able to meet the initial system requirements; 2. the system capacity is based on off-line stations; 3. the current capacity may be doubled through multi-vehicles concept; 4. the constant distance strategy provides the least system capacity; 5. the headway control and the capacity requirements will be factors to determine the size and the number of vehicles. Following are parametric tables which illustrate the maximum system capacity for the three headway control strategies with system speeds from 100 to 500 kmph. This study was done for a hypothetical route which featured many sharp turns. The constant parameters used are: 1. Route distance: 800 km; 2. Normal braking rate: 1.5 m/sec^2; 3. Vehicle Capacity: 120 passengers.

The following performance was achieved by a single vehicle:

Trip time(hrs)	8.0	4.0	2.6	2.0	1.6
Speed(kmph)	100	200	300	400	500
Speed(m/s)	28	56	83	111	139
Stop Time (sec)	19	37	56	74	93
Stop Dist.(m)	365	1164	2478	4306	6649

The strategies yielded the following results:

Case I: Safety/brick wall stop

Block(m)	2000	2000	4000	8000	8000
H/W(sec)*1	72	36	48	72	58
Vehicles/hr	50	100	75	50	63
Pphpd*2	6000	12000	9000	6000	7500

Case II: Constant distance >= 4000 meters

Block(m)	4000	4000	4000	8000	8000
H/W(sec)*1	144	72	48	72	58
Vehicles/hr	25	50	75	50	63
Pphpd*2	3000	6000	9000	6000	7500

Case III: Constant time >= 40 sec

Block(m)	2000	2000	4000	8000	8000
H/W(sec)*1	72	40	48	72	58
Vehicles/hr	50	90	75	50	63
Pphpd*2	6000	10800	9000	6000	7500

Notes:

1. Headway, that is the time to cross the block at the average speed.
2. Peak system capacity in Passenger per Hour per Direction.

V. Safety and Certification Issues

(a) Safety Requirements:

The high speed of the maglev vehicle, lack of physical contact with the guideway, coupled with the need for the vehicle to levitate and the cost of the guideway infrastructure, impose significant weight, and therefore structural limitations on the vehicle. It imposes different and more stringent, safety requirements. However, designing vehicles for reduced weight requires compromises in the ability of the vehicle to survive collisions without major vehicle damage and without serious passenger injury. The probability of low speed vehicle to vehicle or vehicle to fixed object collisions must be as small as that allowed for higher speed collisions. The allowable probability for collisions needs to equal or improve on the risk levels normally associated with aircraft if public acceptance is to be gained.

The reduced headway between vehicles imposed by the increased system throughput envisioned for some maglev routes imposes further safety requirements. When compared to existing light and heavy rail systems, maglev vehicles could run closer together in time. Allowing high levels of stopping force is unattractive except to avoid imminent collision due to the potential for injury to passengers. Thus, either the allowable stopping force which can be applied to the vehicle must be increased or the C^3 system design must

include sufficient sensors and rapidity of control to allow faster reaction to "brick wall" stopping situations.

Since the maglev system employs a tightly coupled drive system, failures in the on-board magnetic and the guideway mounted windings must be extremely rare due to the catastrophic result of vehicle to guideway touchdown when the vehicle is in motion. The reliability of the wayside power and control is also critical and has a major safety impact. Thus, the C^3 system must be designed to ensure that the span of control of any one motor segment along the guideway is minimized. However, since wayside power and control must be provided for each guideway section, and the costs of the circuitry to provide needed functionality is high, system cost conflicts directly with the safety needs of the system. The final maglev C^3 architecture must provide cost effective command and control while ensuring that system and passenger safety is not compromised at any point in the system design and operation.

(b) Certification Requirements:

Certifying the maglev C^3 system with responsible government agencies prior to system use in revenue service is crucial for public acceptance. Certification may be required by the Federal Railroad Administration (FRA) and is likely to be required by each of the public utility commissions (PUCs) in the states where a maglev system is planned for use. While the requirements for certification have not been developed, the aircraft industry - which uses vehicles at similar speeds and with similar crash avoidance needs - can provide some guidance. The Federal Aviation Administration (FAA) currently requires that aircraft systems be "designed so that the occurrence of any failure condition which would prevent the continued safe flight and landing of the airplane is extremely improbable". It appears that the FRA and the state PUCs will adopt requirements which are at least as stringent for maglev failures which put at risk the lives of multiple passengers.

Probabilities as small as 10^{-9} (some FAA requirements) per operating hour are not verifiable through testing. Verification through analysis is possible, and is commonly used in certifying aircraft systems. The system to be certified must be designed so that multiple independent events must occur prior to the catastrophic event occurring. If the initiating events are independent, the probability of the catastrophic event occurring is then the product of the probabilities of the individual events. However, the independence of the multiple events must be carefully proven.

For a C^3 system, showing independence between system elements requires a system partitioning which is carefully architected to allow certification. The layers of command and control must be able to either continue safe, albeit with reduced functionality, operation or must be able to bring the maglev system to a safe state under all conditions of failure, including complete loss of functionality from one or more layers. The ability of analysis techniques to provide accurate certification of probabilities as low as 10^{-3} for software intensive C^3 systems has been questionable.

However, the last several years have brought advances in the ability of the safety and reliability engineering disciplines to predict software reliability, model the impact of software reliability and hardware and software fault coverage, and perform detailed analysis of software safety characteristics. Absolute certification of software safety is not yet possible, however, progress has been made. When recently developed analysis methods such as software fault trees, backward threading techniques and software Failure Modes and Effects Analysis, used to assess each of the independent initiating events for a hazardous condition, are combined with a rigorous and carefully designed test program, a level of safety assurance sufficient to allow revenue service can result.

VI. C^3 System Architecture

The development of the maglev command and control system involves the allocation of the three categories of function (operation, protection, and supervision) onto the five available system components (vehicle, zone, switch, station, Central Control Facility) into an architecture which can meet the performance and safety requirements. The structure of the system also must accommodate the hierarchy required for safety (in which safety critical control functions should be located close to the mechanism being controlled and with a limited span of control) and the hierarchy required for efficient operation (in which functions are located at the lowest level where all the required data is available).

The operation functions deal with a number of the listed components and in general will be allocated to embedded processors within those components in keeping with the desire to reduce communications requirements and to limit the span of control. For instance, with vehicle control functions located in each vehicle, failure of these functions will only incapacitate one vehicle, as long as the vehicle can be moved out of the way.

Protection functions will be mostly allocated to the zones along the guideway. The distributed nature of the guideway subsystem, with each zone only comprising 4 km. of the guideway or less, will limit the span of control of any individual control element. Thus a failure in any one zone would only affect that zone. If the zones are designed to be short enough to allow un-powered passage of normal vehicle movements, zone failures would only degrade, not stop, revenue service.

With the exception of displays and sensors for passenger control at the stations, all supervision functions will be allocated to the Central Control Facility. This must be done because these functions either require operator interaction or because they require access to a global range of information. Although supervision functions are not safety critical, they are necessary to maintaining an expeditious flow of vehicles (and therefore passengers). Since failure at the CCF could affect expeditious traffic flow, some back-up to the CCF, at least for its automatic flow control functions, should be provided. A good candidate for this back-up capability is the station.

(a) Command and Control System Architecture:

As the allocation questions are answered, it is important to look at each processing component to understand the architectural nature of each component and its relationship to other components. This can be done by looking at the control, processes, and data handling requirements of the component and the resulting information transfer needs. The following table shows those relationships:

Function	Supervision	Protection	Operation
Control	Hierarchical	Master/Slave	Single Point
Process	Heterogeneous Network	Heterogeneous Network	Multiprocessor
Data	Database Management System	Replicated Distributed Files	Local Files
Approach	Centralized System Function	Distributed Protection Function	Decentralized Operational Function
Comm	WAN/LAN	Redundancy Point-to-Point	Embedded
Element	Central/Station	Zone/Block	Vehicle

System Architectural Diagram

The control responsibilities of the supervision functions are hierarchical in nature where these functions are controlling the actions of subordinate components. The network of components so controlled consists of a wide variety of types, including stations, zones, switches, and vehicles. To exercise effective control, supervision functions need a global view of the system, with access to information covering all components. A database management system will likely be included in the implementation of the supervision functions.

The nature of the control exercised by the protection functions must be local, affecting only a segment of the guideway and the vehicles within that segment, and must be absolute, capable of overriding commands from the supervision function and stopping control actions of the operation function. The processes of protection are distributed into many small zones, each of which must be aware of the activity and status of adjacent zones but only capable of controlling the movement of vehicles within the local zone. Database needs of the protection functions are considerably less than for supervision functions. Further, each zone will have the same range of information needs. Communications paths (both primary and back-up) must exist to some number of nearby zones (not just to directly adjacent zones) and to vehicles within those zones.

The span of control exercised by the operation functions is strictly local and independent of other components of the system. Each vehicle, for instance, does not require any knowledge of any other vehicle to carry out its operations functions. To increase availability, operation functions will be implemented with redundant computers. The database needs of most operation functions are modest and complex database management systems are not required. While specific command and control logic in the fully implemented networked system will have much in common, there may be parameter differences at each location (e.g., with respect to specific route data or environmental data, etc.), or locations will be configured slightly differently (e.g., a zone controller at a station may have increased power ratings to handle the initial movement of maglev vehicles).

(b) Communications System Architecture:

There will be a need for both data and voice communications within the maglev system. The communications paths to and from the vehicle will be implemented with radio frequency technologies since contact between the vehicle and the guideway is not allowed. As with all use of radio paths, data transfer requirements must be kept to a minimum, the communications protocols must allow for temporary interruption, and multiple paths must be provided. Communications will be based on area network topologies where the network provides intrinsic message path management. This is a standard network methodology whereby the network message integrity is inherently fault tolerant providing both self-healing and self-optimization for capacity requirements..

VII. Summary

Some of the command, control and communication system requirements related to the functional partitioning and allocation for a maglev system can be found in existing fully automated rail systems. However, new technologies, unique to maglev, new performance requirements, required for public acceptance, and the continuing application of modern control and communication technology to safety-critical subsystems are all critical to the future implementations of the maglev system. In all of these areas, the implications are becoming clearer through the on-going research efforts.

It is also clear that much work remains, both in the determination of the complete set of requirements, and the new technologies in designing a responsive control system architecture to fulfill the needs for a convenience of access and the speed of service.

It is recognized that if the maglev technology is to grow it must be treated as part of a national intermodal transportation complex. As such, a command, control and communications architecture must anticipate a complex network control problem. If a network concept is assumed from the beginning, interoperability can become more viable. The global assets management and scheduling concerns will necessitate a network of real-time data base management system utilizing the Artificial Intelligence(AI) and Neural Network capability as the key element in the development of a new phase of the high-speed ground transportation systems.

Acknowledgments

Much of the substance of this paper was developed as part of Hughes Aircraft Company's effort for the Maglev System Concept Definition program of the Federal Railroad Administration. In addition to the authors, those that contributed to this effort include Peter Goddard in safety analysis, Cam De Pierre in communications design, and Laurel Rudzik and Doris Tamanaha in system engineering. Gail Nagle, of Draper Laboratory, also contributed in the area of fault-tolerant design.

References

[1] US DOT/FRA NMI SCD Report, "Communication and Controls Concept", Bechtel Consortium, V.1, Book 2 of 2, pp. C4.1 - C4.45, September, 1992

[2] E. Schnieder, K.H. Kraft, H. Guckel, "Automated Operations Control System For High-Speed Maglev Transportation", Proceedings of International Conference on Maglev and Linear Drives, pp. 181-188, May, 1987

[3] E. Schnieder, "The Operations Control for Super Speed Magnetic Trains", HESTRA-VERLAG Darmstadt, "Transrapid Maglev System", pp. 61-64, 1989

[4] Joachim Blomerius, "Safety and Licensing Aspects of Transrapid and Maglev Systems", Proceedings of International Conference on Maglev and Linear Drives, pp. 205-210, May, 1987

[5] M.P. Mariani, Editor, "Distributed Data Processing, Technology and Critical Issues", TRW Series of Software Technology 4, TRW - Defense Systems Group, 1984

[6] Friedman, M.A., Tran, P.Y., and Goddard, P.L., "Reliability Techniques For Combined Hardware And Software Systems", RL-TR92-15, 1992.

[7] Goddard, P. L., "Reliability Modeling Of Hardware/Software Systems To Support Architectural Trade-Offs", Proceedings of the second annual International Symposium of the National Council On Systems Engineering, July 1992.

[8] Leveson, N. G., Cha, S. S., and Shimeall, T. J., "Safety Verification of Ada Programs Using Software Fault Trees", University of California, Irvine, February 1991.

[9] Goddard, P. L., "Validating The Safety Of Embedded Real-Time Control Systems Using FMEA", Proceedings of the Annual Reliability and Maintainability Symposium, January 1993.

Aerodynamic Braking Systems for Maglev Vehicles

James J. Guglielmo*, Thomas J. Zych*, and Kenneth R. Sivier**

Department of Aeronautical and Astronautical Engineering, University of Illinois at Urbana-Champaign, Urbana, Illinois 61801

ABSTRACT

This paper summarizes the results of a study of speed brake and drag chute deceleration systems for Maglev vehicles. These systems offer practical solutions to the need for additional braking in both routine and emergency decelerations. Three types of drag brakes are discussed: vehicle surface brakes, (both forward and aft opening), and plug brakes. From the points-of-view of storage and operational simplicity, the plug-type brakes appear most feasible. Based on incremental deceleration requirements of 0.2g, a total exposed brake area of 11.6 m^2 is needed. Various types of drag chute designs, materials, and deployment methods are also discussed. Drag chute systems are sized for decelerations of 0.2g and 0.8g, resulting in requirements for 4.65 m and 9.30 m diameter canopies, respectively.

NOMENCLATURE

a	deceleration rate (m/sec^2)
C_D	coefficient of drag
$(C_DS)_o$	system steady state drag area (m^2)
D	drag force (N)
D_o	nominal diameter of canopy (m)
F_{decel}	deceleration force (N)
F_{max}	maximum opening shock force (N)
F_s	steady-state drag force (N)
F_{snatch}	lines-taut snatch force (N)
g	gravitational acceleration (m/sec^2)
n	permeability constant
S	instantaneous inflated canopy area and speed brake frontal area (m^2)
S_{ref}	reference area (m^2)
t	time (sec)
t_i	inflation time (sec)
t_f	filling time (sec)
v	velocity (m/sec)
v_o	velocity at time of drag chute deployment (m/sec)
W	weight (N)
x_i	instantaneous shock factor
ρ	density of air (kg/m^3)

Subscripts:

sb	speed-brake
veh	Maglev vehicle

Manuscript submitted March 15, 1993 to Maglev '93 Conference. This work was supported by the General Motors Electro-Motive Division under Research Agreement No. 92-PRI-S-0378 as part of the National Maglev Initiative.

* Graduate Research Assistant.
** Associate Professor.

INTRODUCTION

With the application of superconducting magnets, the Magnetic Levitation (Maglev) vehicle has become a promising new transportation system. While this new technology has made high-speed trains both practical and economical, it has also introduced certain design problems that did not arise for traditional, low-speed rail systems. For example, the superconducting magnets and mechanical guideway brakes can provide a limited amount of braking force, but they are inadequate in emergency situations. In order to supplement the standard mechanical brakes on the Maglev vehicle, aerodynamic brakes offer a relatively simple and effective solution.

Two of the most common aerodynamic deceleration systems are speed brakes and drag chutes. Speed brakes have the advantage of controlling the amount of braking desired by varying the amount of flat-plate area exposed to the flow, thus making them practical for routine braking as well as emergency situations. To reduce the required size of speed-brakes for emergency decelerations, drag chutes are a viable compliment.

For the purpose of demonstrating practical applications of these aerodynamic braking systems, representative Maglev vehicle characteristics have been assumed and are listed in Table I.

TABLE I
MAGLEV VEHICLE CHARACTERISTICS

Cruise Velocity = 500 kph (139 m/sec)
Mass of Maglev Vehicle = 82,000 kg
$C_{D_{veh}} = 0.24$ (Ref. 1)
$(C_DS_{ref})_{veh} = 3.5\ m^2$
Standard Sea Level Conditions

SPEED BRAKES

Speed Brake Sizing

The sizing of speed brakes is dependent upon drag coefficients for flat plates mounted on a surface. According to [2], dive-brakes mounted perpendicular to a fuselage result in a coefficient of drag of about 1.17, based on the projected frontal area of the brake. However, if guide vanes are inserted in the flat plate to turn the flow outward and the brakes are swept forward at an angle of 45°, the value of C_D is increased to about 1.48. Reference [3] suggests using a value of D/q ≈ 1.0 times the flat plate frontal area. These three values of the speed brake drag coefficient are selected for the initial analysis in the design study.

The sizing of the speed brakes is based on balancing the speed brake aerodynamic drag force and the required deceleration force. The following relationship results:

$$S_{sb} = \frac{1}{C_{D_{sb}}}\left[\frac{2a(W/g)}{\rho v^2}\right] \qquad (1)$$

where the deceleration force is defined as

$$F_{decel} = ma = \left(\frac{W}{g}\right)a \qquad (2)$$

Table II presents the results of the required speed brake areas for various deceleration rates and the three coefficients of drag. These deceleration rates are due to the speed brakes only.

TABLE II
VARIATION IN SPEED BRAKE SIZE

	Speed Brake Area (m^2)		
Initial Deceleration Rates	C_D = 1.00	C_D = 1.17	C_D = 1.48
.6g	40.8	34.9	27.5
.5g	34.0	29.1	23.0
.4g	27.2	23.3	18.4
.3g	20.4	17.4	13.8
2g	13.6	11.6	9.19
.15g	10.2	8.72	6.89

Speed Brake Design

Several different types of speed brakes for Maglev vehicles have been investigated. The three types which are discussed here are plates forming part of the outer surface of the vehicle (both forward and aft opening), and plug-type plates that are stored internally and deployed perpendicular to the outer surface of the vehicle. An examination of the perceived advantages and disadvantages of each of the three configurations is presented.

For all three types, the assumed configuration consists of eight plates, one bank of four arranged radially forward of the passenger cabin and a second bank of four similarly arranged aft of the passenger cabin. It has been assumed that the effectiveness of the aft plates is not affected by the flow around the forward plates. The dimensions of each plate are 1.35 x 1.07 m, for a total speed brake frontal area of 11.6 m^2. The plate sizing is based on two constraints: first, the plates in each bank do not overlap and, second, when two vehicles pass each other, both with plates fully deployed, safety clearances are maintained under all conditions, as shown in Fig. 1.

1) Surface plates opening aft: This configuration consists of curved plates which, when closed, form part of the outer surface of the Maglev vehicle. They are hinged at the rear and open aft, using a system of hydraulic pistons or wormgear motors to control the motion of the plate. The proposed layout is shown in Fig. 2.

Advantages: This system can be rapidly deployed by using the vehicle's dynamic pressure to aid in opening the plates and requires only a small motor to close the plates once the vehicle has stopped. Alternatively, hydraulic pistons can provide both damping during deployment as well as the closing force. In case of total hydraulic failure, the plates can still be deployed by using springs to push the edge of the plate far enough into the slipstream to be fully opened by the dynamic pressure. Variable braking power is achieved by partial deployment of the plates.

Disadvantages: High stress concentrations at the hinge will require a structural buildup in that area to carry the load. In the case of opening restraint system failure, the plates may

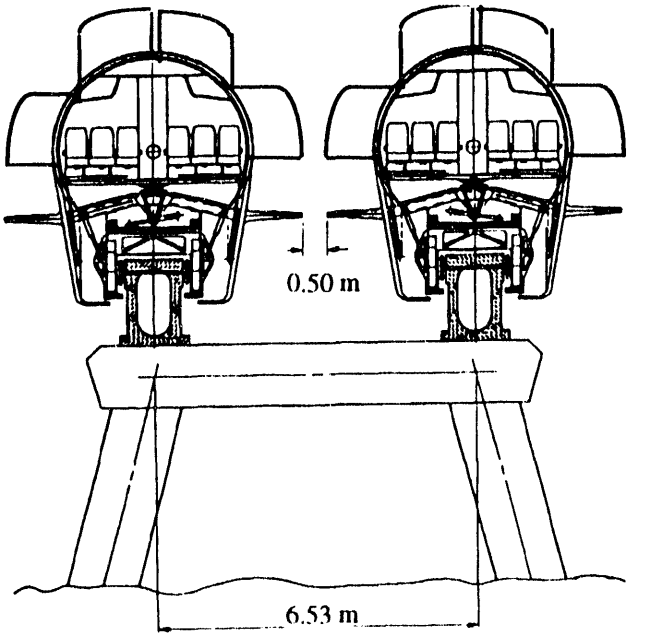

Fig. 1. Speed brake placement and clearances.

be torn off by the resulting forces. These disadvantages can be reduced by using internal hinging systems.

2) Surface plates opening forward: This system is similar to the previous system depicted in Fig. 2 with the following exceptions: the plates are hinged at the front and the springs are removed.

Advantages: Variable braking power is achieved by deployment of the plates at less than 90° incidence to the flow.

Disadvantages: Motor size or hydraulic system capacity depends on the desired opening speed. The plate surfaces facing the flow are convex, resulting in a drag coefficient less than the value for a flat or concave surface, and thus requiring an increase in speed brake size. Preliminary estimates [2] indicate an increase in required area on the order of 50%. Finally, unpowered deployment of this system is not possible.

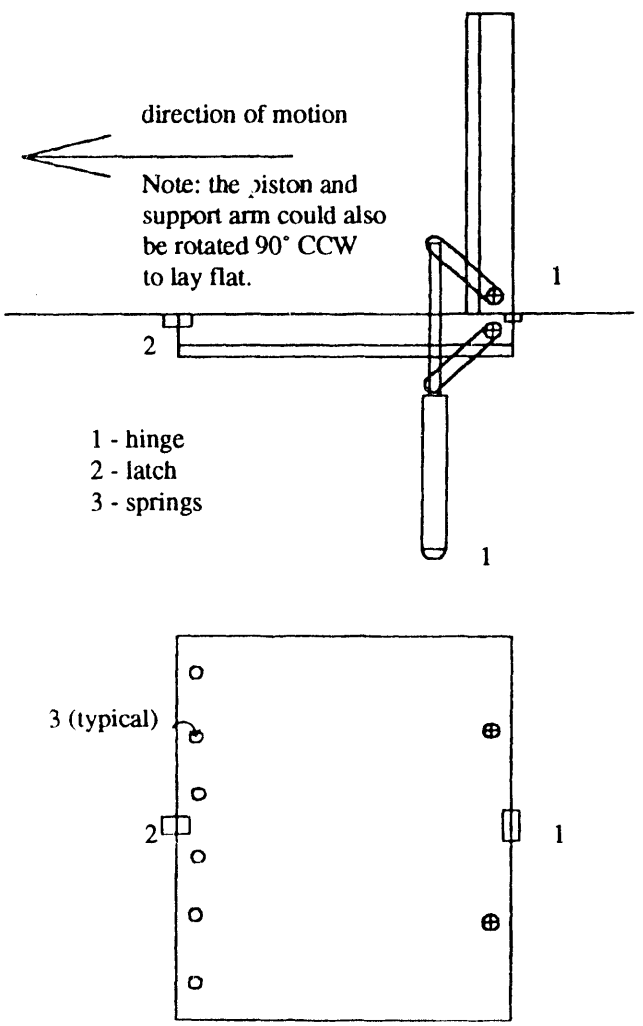

Fig. 2. Surface plates opening aft.

3) Plug-type plates: These are flat plates that are stored entirely inside the Maglev vehicle and deployed perpendicular to the direction of motion. Deployment and retraction are by hydraulic piston or wormgear motor. The proposed layout is shown in Fig. 3.

Advantages: A relatively simple and robust mechanical system. Variable braking can be achieved easily by partial deployment of the plates. A simple spring-loaded emergency power-loss deployment scheme appears feasible.

Disadvantages: This system may be relatively slow to deploy. It also appears to be the most demanding system in terms of internal volume requirements, as each pair of plates (two pairs forward and two aft) requires a 20-25 cm 'slice' of the vehicle for stowage, structural, and deployment considerations.

On the basis of the above analysis and the constraints from the Maglev vehicle's general dimensions and passing clearances, the effective speed-brake area is of primary importance. This consideration eliminates the forward opening configuration, as it would require significantly more area than the other two designs due to its lower coefficient of drag.

The plug-type system is selected over the aft-opening surface-plate configuration due to its simple storage and deployment scheme and better potential for accommodating

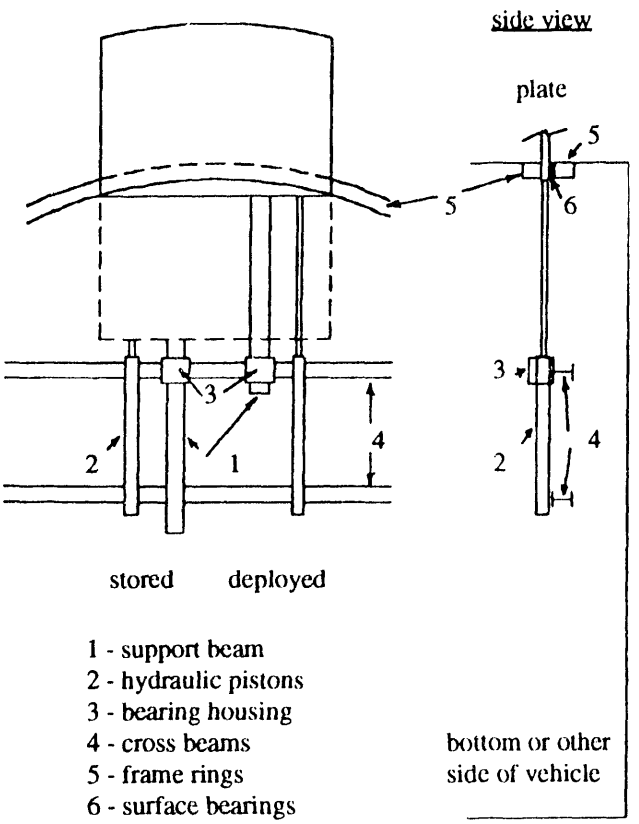

Fig. 3. Plug-type plates.

the aerodynamic loads. It is felt that these factors outweigh the disadvantage of the increased internal storage requirements.

Speed Brake Structural Considerations

For a maximum braking load of 160 kN, and assuming that this load is equally distributed between the eight plates, the maximum load on each plate is estimated at 20 kN. The plate thickness and construction are based on this loading. The criterion used in sizing the plate thickness is a tip deflection of 20 mm at maximum loading. A reduction in the allowable tip deflection would, of course, increase both the thickness and mass of the plates.

Both steel and aluminum have been investigated (assuming a solid plate) as possible speed brake materials. As expected, the steel plate is a good deal thinner (22 mm vs. 32 mm for Al) but has nearly twice the mass (246 kg vs. 128 kg for Al). Taking the greater susceptibility of steel to environmental damage into account as well, aluminum is clearly the material of choice.

A significant reduction in weight is achieved through a built-up aluminum plate arrangement consisting of five C-channels sandwiched between two face plates. For example, a 55% decrease in mass is attained for only a 16% increase in thickness when compared to the solid aluminum plate. For this large decrease in mass, it is felt that the small increase in thickness and complexity is more than justified. However, this is only one possible solution, and may not be optimal. In addition, composite materials may provide similar performance at lower mass and/or thickness, and should be investigated.

The internal vehicle structure must be able to carry the aerodynamic forces and moments acting on the plates. This can be accomplished by locating a fuselage frame ring directly behind the plates and by supports, parallel to the hydraulic pistons, attached to a support beam via a bearing housing. Details of this arrangement are presented in Fig. 3. In order to balance both the force and moment on a single plate, preliminary estimates indicate forces on the order of 30 kN at the frame ring and 10 kN at the support beam.

Drag Chutes

Drag Chute Design

Parachutes (or drag chutes) can be broken down into three classifications: solid textile, slotted textile, and gliding parachute canopies. Of these three subsets, only the solid and slotted textile canopies are logical choices for use as an emergency deceleration system for the Maglev vehicle. The solid textile canopy is typically used for personnel and cargo recovery, but has poor stability characteristics and high opening forces. Slotted parachutes, such as the cross canopy and ribbon canopy [4], are commonly used for the deceleration of ground vehicles and aircraft, and exhibit excellent stability, good drag characteristics, and low opening shock forces. The cross canopy design is dropped from further consideration because of its tendency to rotate about its axis of symmetry. The ribbon canopy drag chute remains as a potential deceleration device. This type of chute is commonly used for vehicle and aircraft decelerations at dynamic pressures up to around 273 kN/m^2, which at standard sea level atmospheric conditions corresponds to a velocity of 668 m/sec.

The canopy deployment process, which can be divided into distinct stages, is depicted in Fig. 4. The initial stage begins at the time of drag chute deployment and ends at the instant the suspension lines become fully stretched. At this latter time, the local maximum force, known as the lines-taut snatch force, occurs. The inflation time is defined as the time interval between the occurrence of the snatch force and the maximum opening shock force. At this instant, the maximum force for the whole system (Maglev and drag chute) occurs as the canopy inflates radially. During the final stage, the interactive forces between the drag chute and the Maglev vehicle return to their steady-state value. The filling time, t_f, is defined as the time interval from the occurrence of the snatch force to the instant the canopy first reaches its steady-state diameter.

The estimations of the maximum shock force, steady-state force, and the inflation time after initial deployment are based on the method presented in [5]. Since the Maglev vehicle's mass is around 82,000 kg, the infinite mass assumption is valid when analyzing the drag chute opening shock forces. The analysis method is outlined in (3)-(6). The total filling time is calculated from

$$t_f = \frac{nD_o}{v} \tag{3}$$

where, according to [5], the permeability constant, n, for ribbon chutes is equal to 14. According to Fig. 5, the shock factor,

$$x_i = \frac{F_{max}}{F_s} = \frac{C_D S}{(C_D S)_o} \tag{4}$$

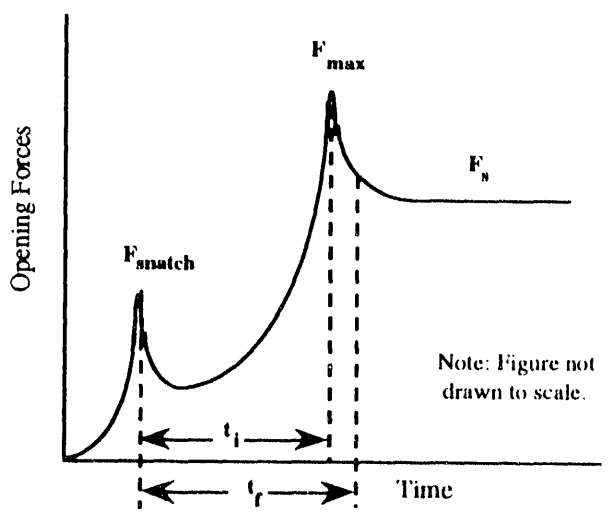

Fig. 4. Opening forces during deployment of parachute for infinite mass assumption.

is approximately 1.05 to 1.10 for the infinite mass case, where the steady-state force is defined as:

$$F_s = \frac{1}{2}\rho v^2 (C_D S)_o \qquad (5)$$

The variation of velocity with time after deployment of the speed brakes is calculated from the following relationship.

$$v(t) = v_o \left[\frac{1}{2}\rho\,(C_{D_{sb}} S_{sb})(g/W)\, t v_o + 1\right]^{-1} \qquad (6)$$

The effects of several specified deceleration rates on parachute size, deployment forces, filling time, and suspension line length are presented in Table III. The results are based on a typical drag coefficient for ribbon parachutes of 0.80 [4]. To achieve this drag coefficient, it is suggested [6] that the suspension line length be approximately three times the parachute nominal diameter.

TABLE III
RIBBON CHUTE SIZING RESULTS; $C_D = 0.8$

Initial Deceleration Rate	0.8g	0.6g	0.2g
Steady-State Force (kN)	644	483	160
Required Chute Area (m^2)	68.0	51.0	17.0
Diameter of Canopy (m)	9.30	8.06	4.65
Suspension Line Length (m)	27.9	24.2	14.0
Inflation Time (sec)	0.94	0.81	0.47
Max. Shock Force (kN)			
$F_{max} = 1.05F_s$	676	507	169
$F_{max} = 1.1F_s$	708	531	177

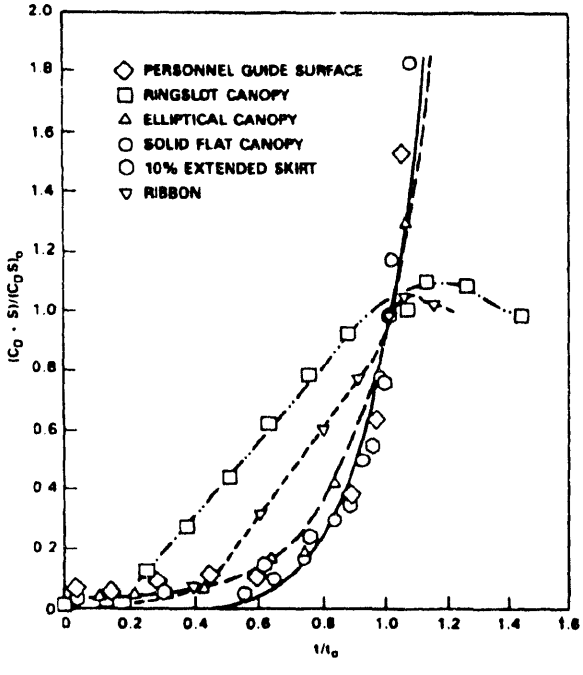

Fig. 5. Drag-area ratio versus dimensionless filling time (Ref. 5).

Figures 6 and 7 present the velocity and distance traveled by the Maglev vehicle after drag chute deployment for both the 0.2g and the 0.8g emergency braking requirements. Both figures include the aerodynamic drag contributions of the Maglev vehicle, but the speed brakes are assumed to be retracted.

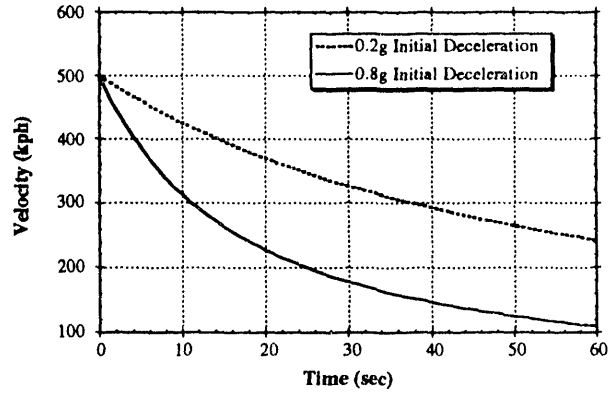

Fig. 6. Velocity of Maglev vehicle after drag chute deployment.

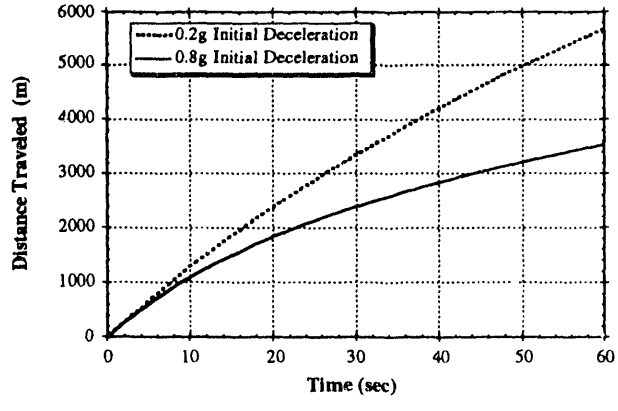

Fig. 7. Distance traveled by Maglev vehicle after drag chute deployment.

Drag Chute Materials

Both nylon and Kevlar materials have been investigated for use in the drag chute system of the Maglev vehicle. The main differences between the two materials are summarized in Table IV. Kevlar materials, while more expensive, have less than one-half the weight and one-third the bulk of nylon materials. For the specified 0.2g deceleration from the drag chute system, an all-Kevlar design results in a mass of approximately 10 kg and a packed volume of 0.03 m^3, including suspension lines. Table V represents typical weight savings compared to an all nylon construction for parachutes incorporating Kevlar materials [7].

TABLE IV
PROPERTIES OF NYLON AND KEVLAR MATERIALS

	Nylon 66	Kevlar 29
Elongation	16-28 %	4-5 %
Ult. Tensile Strength (kN/m^2)	5.59×10^3	19.2×10^3
Strength-to-Weight Ratio	1.00	2.70

TABLE V
WEIGHT SAVINGS OF KEVLAR MATERIALS

Modification	Weight Savings
Kevlar Suspension Lines on Existing Nylon Parachute	20-25%
Reinforced Nylon Canopy with Kevlar Radials and Suspension Lines	30%
All-Kevlar Parachute	50%

Drag Chute Deployment

Due to the region of separated and highly turbulent flow at the back end of the Maglev vehicle, some method is needed to eject the drag chute into a region of undisturbed air during deployment. One solution is to utilize a deployment mortar [8]. A typical mortar depicted in Fig. 8 has a mass of 36 kg and a usable volume of 0.05 m^3, which is more volume than is required for the 0.2g drag chute design proposed above. Assuming the mass of the mortar varies as the square root of the volume results in a mortar mass of about 30 kg.

Table III indicates a force of 169 kN must be carried into the structure from the parachute suspension line bundle. Reference [9] lists the ultimate tensile strength of Kevlar at 19.2×10^3 kN/m^2. Taking into account a safety factor of 1.5, this results in a bundle cross-sectional area of 125 cm^2. This load will be carried by an arrangement of frame rings and crosspieces similar to that suggested for the plug-type speed brakes.

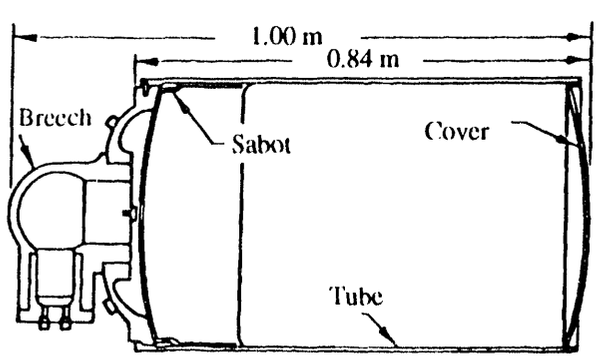

Fig. 8. Parachute deployment mortar (Ref. 8).

For a 0.8g emergency deceleration, the resulting 9.30 m diameter for a single drag chute is impractical due to the clearance requirements previously discussed. Two 6.58 m diameter drag chutes would produce the required deceleration force. This would require two mortars, resulting in significant mass and volume penalties. In addition, the drag chutes must be deployed one above the other to maintain safety clearances between passing vehicles, resulting in a more complicated suspension line arrangement.

CONCLUSION

Speed brakes and drag chutes have both been shown to be useful aerodynamic braking systems for Maglev vehicles. Speed brakes provide an effective method of decelerating a Maglev vehicle in both ordinary as well as emergency situations, while a drag chute is useful for providing additional emergency braking power at only a small cost in mass and volume. It is expected that Maglev vehicles will utilize both of these systems in order to provide reliable, efficient, and safe braking characteristics.

REFERENCES

[1] Balow, F.A. and Sivier, K.R., "Aerodynamic Drag of Maglev Vehicles," unpublished, to be presented at Maglev '93 conference.

[2] Hoerner, Sighard F., *Fluid-Dynamic Drag*, Hoerner Fluid Dynamics: Vancouver, WA, 1965.

[3] Raymer, Daniel P., *Aircraft Design: A Conceptual Approach*, AIAA: Washington D.C., 1989.

[4] Cockrell, D.J., "The Aerodynamics of Parachutes," AGARDograph No.295, 1987.

[5] Ludtke, W.P., "Notes on a Generic Parachute Opening Force Analysis," Naval Surface Weapons Center, Silver Spring, Maryland, AIAA-86-2440.

[6] Purvis, J.W., "Parachute Drag and Radial Force," AIAA-86-2461, AIAA 10th Aerodynamic Decelerator and Balloon Technology Conference, 1986.

[7] Peterson, C.W., and Johnson, D.W., "Parachute Materials," Sandia National Laboratories, Albuquerque, New Mexico, June 1987.

[8] Ewing, E.G., Bixby, H.W., and Knacke, T.W., "Recovery Systems Design Guide," AFFDL-TR-78-151, 1978.

[9] Peterson, C.W., et al., "Kevlar Parachute Design and Performance," Sandia National Laboratories, New Mexico, 1984.

Signaling System of Maglevetype HSST

Fumio Hashimoto
Railway Signal Devision, Kyosan Electric Mfg. Co., Ltd.,
Yokohama,Japan

I . Introduction

The normal-conduction, maglevetype linear motor railway system HSST was commercially operated in the Yokohama Exposition held in Yokohama, Japan, from March 25 to October 1, 1989, using Model HSST-05 as the YES'89 Line (YOKOHAMA EXOTIC SHOWCASE). It was the first maglevetype railway system in Japan, and it accepted for railway business and was operated commercially for 6 months. Model HSST-04 of the system was demonstrated in the "Saitama Exposition" held in the city of Kumagaya, Saitama Prefecture, in March 1988. Based on the experience and knowhow acquired throughout these events, the development of an urban-traffic-oriented maglevetype linear motor system was launched toward a goal of practical applications. In the meantime, a test system of 1.5 km in length was constructed in Nagoya in May 1991, and the system has been tested to operate a train at a maximum speed of about 110 km/h.

This brochure describes an overview of the operation control system and its test results, which system is equipped in the test lines, with a particular emphasis on the railway-signaling system and the automatic operation system, among other numerous subsystems.

II . Alterations of the Operation Control Systems for the HSST

The first operation control system used for the HSST was intended for shuttling each train in a single track in the Expositions. It was then developed into practical systems capable of operating several trains at high speed and density, by incorporating various options in operation mode. Among practical magleve lines, there is an example with two single tracks arranged parallel to connect an airport satellite and a terminal, which is operated in unman mode. This is a typical application example for transportation between two stations, like the HSST systems operated in the Saitama and Yokohama Expositions, in an extension distance of about 600 m. These systems were automatic operation systems provided with an overrun-protective function. In the Yokohama Exposition, the system achieved a zero-problem record of operation throughout the period of 6 months, and it was proved that this type of operation system could be applied practically. On the other hand, fundamental requirements as an urban-oriented system include a maximum speed of about 100 km/h in minimum operation intervals of about 100 seconds each. Therefore the railway signaling equipment must be a cab-signal type with an ATO system backed up by ATP.

From this point of view, the function has been developed stepwise using a special test line. At first, the overrun-protective function in a point-control system using transponders, as operated in the Yokohama Exposition, was incorporated. It was then modified to a continuous-control system using a pattern belt and, at present, testing has been continued using the fixed-pattern-type ATP. In addition, the entire system has been developed into a moving block system that can follow the location of a preceding train and the state of switches and controls of following trains. Verification experiments for the latest system have been accumulated in the test line, satisfactorily demonstrating system robustness for practical applications.

III . Configuration of the System

Objectives of the testing using the test line include the verification of safety, economic performance, and practical efficiency of the system as an urban-oriented traffic system at a traveling speed of 100 km/h. The operation control system has been constructed aiming at smooth and safe backup of these tests and capability of applying to next-generation systems in terms of operation control.

The test line consists of a single main track from the Ohye Station to the Higashi-Nagoya-Ko Station via an intermediate branch location, and another route from an intermediate location to the shunting track via a turnout; in the former, a train is shuttled for testing at a speed of 100 km/h, while testing in the shunt route is for operating trains in a curved branch track of 25 m in a minimum radius of curvature. In these tests, trains are operated in either manual or automatic modes. In the automatic mode, test runs for long-term durability testing are applicable. The configuration of the system for these operations is shown in Fig. 1.

The system is classified into the following subsystems.

(1) Signaling system
   a) ATP equipment using transponders (emergency braking)
   b) Pattern-type ATP equipment (normal braking)
   c) Speed-detection equipment
   d) Continuous-detection-type check-in, check-out train-detection equipment

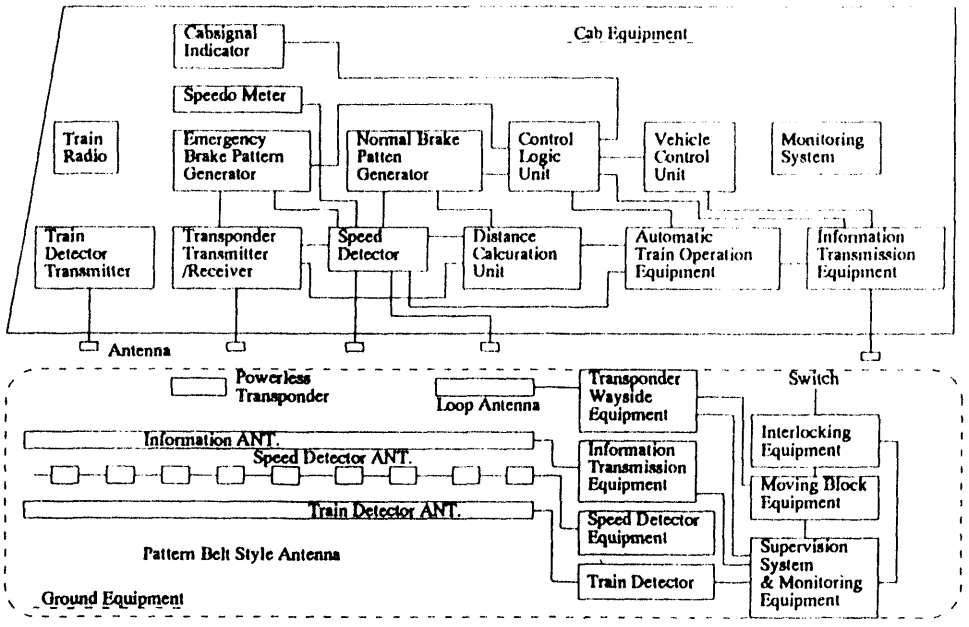

Fig. 1 Configuration of the system

e) Interlocking equipment

(2) Operation system
- a) Program train operation (PTO) equipment
- b) Manual train operation (MTO) equipment
- c) Operation monitor equipment
- e) Car monitor equipment

(3) Information transmission system
- a) Wayside-cab information transmission equipment

(4) Supervision system
- a) Wayside-cab supervision equipment

IV. Overview of the Major Systems

A. Signaling Control

For signaling control, two systems of the control equipment are provided for the test track. The ATP equipment using transponders was used in the signaling control systems for the Saitama and Yokohama Expositions, aiming mainly at overrun protection at both terminals in shuttling transportation. With this equipment, a system can be constructed by mainly using wayside transponders without requiring power supplies on the ground where a train is operated in a simple mode such as shuttling between two terminals. Consequently, simple and economic signaling control can be applied without sacrificing safety. However, with an urban-traffic type system in which a number of trains are operated in a high density, it is mandatory to incorporate a conventional continuous-detection, continuous-control system. Particularly where an automatic operation or unman operation is intended, a point-detection, point-control system will not be satisfactory. The concept of a conventional continuous-control system is not free from fixed blocking, in which the position of a train is detected in each block section so that a permissible speed is set for each section in order to control train operation. Consequently, the train-detection equipment and the hardware of the ATP equipment must be constructed in each section. Particularly in the case where trains are operated densely, a block section must be divided into many subsections, requiring high construction cost. Hence the continuous-pattern-type ATP equipment has been introduced presently as a novel signaling control system, because only one train is operated at the test track, and the system has been operated for demonstration testing. This continuous-pattern-type ATP equipment is constructed with the consideration that it will be improved into a moving block system in the future. With the system, operation of trains is controlled by receiving information on the location and speed of trains through the wayside-cab information transmission equipment.

For detecting the speed of a train in the maglevetype railway, the system that operated successfully in the Saitama and Yokohama Exhibitions is employed. Using train-speed pulses, the system provides information on an absolute, fail-safe distance for the continuous-pattern-type ATP. In addition to the detection of such information on absolute distance, a conventional continuous-detection-type check-in, check-out train-detection equipment, as used in new traffic systems which vehicles run with the rubber tire, is also incorporated for a trial. Although the latter technology has already been established, it has been installed in order to check noise immunity of the system, in particular.

An overview on the major equipment and apparatuses is described in the following.

1) ATP Equipment

The ATP equipment performs blocking controls for intermediate sections, and in addition it also carries out overrun-protective controls at the same time by using a pattern-type speed monitoring, so that a train can enter the station section at as high a speed as possible, because the overrun-allowance distance from a regular stop point to the dead end is only about 10 m.

Fig. 2 shows the protective patterns at the overrun-protection-initiating points, for the transponder-type and the continuous-pattern-type ATP control systems.

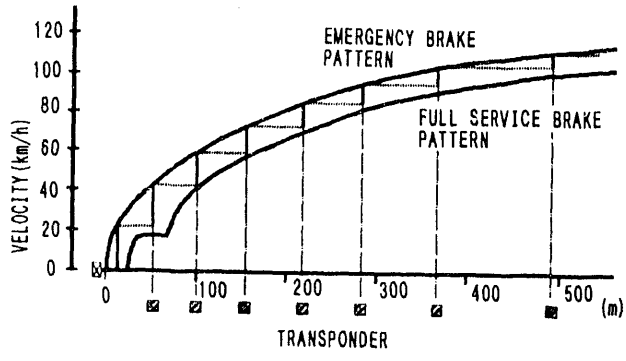

Fig. 2 ATP braking pattern

The final overrun-protective curve in Fig. 2 relates to the transponder type, which was provided for backing up the continuous pattern-type ATP and the moving block type train control, which was first introduced in the present field testing. According to an ordinary speed limit pattern of the transponder type, the normal braking limit curve is dominant in priority, and normally the final overrun-protective curve will not be in effect. Therefore the transponder-type equipment will not be needed where a continuous-pattern-control-type ATP or a moving block type is applied practically. Fig. 3 depicts the operation status of emergency braking where the transponder-type ATP equipment is used independently.

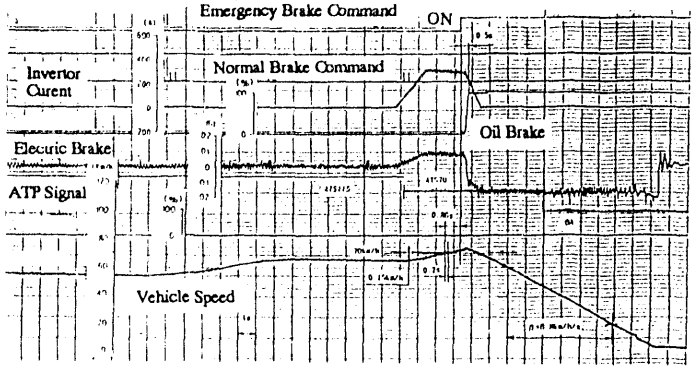

Fig. 3 Emergency-braking response characteristics of the transponder-type ATP

With this example, a train receives ATP information on a permissible speed of 115 km/h from an outside transponder, and the train stores this instruction and the location of a transponder that will receive a next instruction; and, when the train travels at 70 km/h, it receives an instruction of ATP 70 from the next transponder. Fig. 3 illustrates a state in which an ATP is effected when the actual speed of the train exceeds 70 km/h.

Fig. 4 shows an operation state of normal braking with the continuous-pattern-type ATP equipment during running of a train in the field.

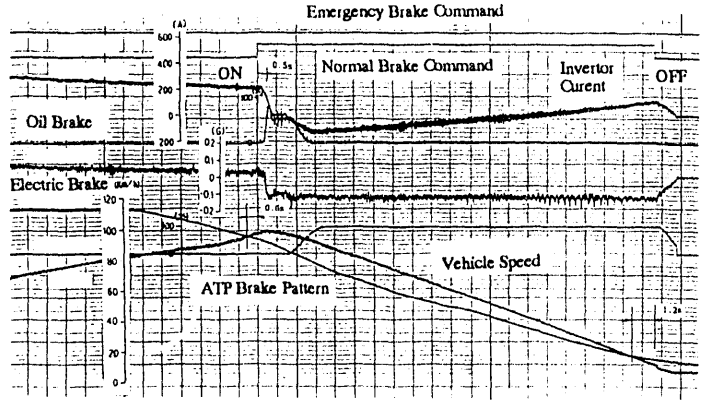

Fig. 4 Continuous-pattern-type normal braking response characteristics

This example denotes a state where a service braking pattern (SBP pattern) is effected at 110 km/h; where a train follows the pattern at an actual speed of about 60 km/h. The minimum range resolution of the SBP pattern is 60 cm in terms of absolute distance vs. permissible speed. The idle time of braking is a total of 1.1 seconds, including about 0.6 seconds for monitoring the speed and 0.5 seconds to the time of effecting normal braking. Delay time of releasing of braking is about 1.2 seconds.

According to the continuous-pattern-type ATP control, an ever-changing permissible speed must be immediately and clearly indicated to the operator. Therefore a speed meter with a speed-indication pattern, shown in Fig. 5, is provided in the operator's cabin. The outermost, fine graduations show the permissible speed SBP pattern, in which the width of a band indication increases or decreases in 2-km/h graduation units as displayed in fine bands. A wide-band indication inside the SBP pattern shows an actual speed; like the SBP pattern, an actual speed is indicated in a bar that extends and contracts in 2 km/h units. The operator can easily operate the train at a speed lower than an instruction given in the SBP pattern while comparing it with the SBP indication. Specific interfacing between man and machine is one of the most important themes during designing of the equipment. An actual speed is also digitally indicated on a center part, besides a bar

indication. The minimum graduation of the digital indication is 1 km/h.

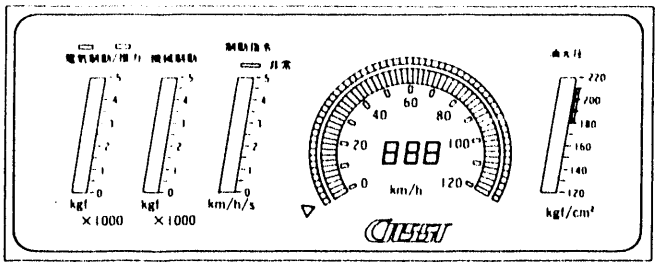

Fig. 5 Indication of SBP pattern and speed

2) Speed-Detection Equipment and Absolute Distance Detection Equipment

Both speed-detection equipment and absolute-distance-detection equipment use a pattern belt having openings in 30-cm intervals and a cab antenna having 3 coils in 20-cm spacings. The configuration is shown in Fig. 6. This system has been transferred from those used in the Saitama and Yokohama Expositions. Charts for showing signal receiving and pulse detecting are shown in Fig. 7. For speed detection, three ranges of speed are defined for constructing a detection logic. As a result, a stabilized accuracy of detection is realized. The minimum detection speed in effect is 0.5 km/h. In a range of 0.5 km/h to 1.2 km/h, pulses of a 10-cm width each are used. In other ranges of 1.2 km/h to 3.6 km/h, and over 3.6 km/h, pulses of 20 cm and 60 cm in width, respectively, are employed for speed detection. In addition, phases of the 3 antenna systems on the cab are compared with each other to confirm the robustness of the fail-safe logic and for detecting back-traveling of a train. The cab antennas are installed distributedly at two locations of a car, in order to prevent missing of signals in the turnout unit and to improve reliability of the entire system. Thus the system is configured into a dual system. The relationship of speed vs. pulse frequency is shown by the following equation.

$$F = K * V \text{ [Hz]} \quad \text{(Where K: 2.778, V: speed [km/h])}$$

The absolute-distance-detection equipment accumulates these pulses through a fail-safe process, which pulses are used as distance information for the continuous-pattern-type ATP and moving block systems. Once the system is applied practically and a train passes a turnout, interference between trains traveling in the main track and the shunt track may possibly cause a distance-measurement error or missing of information. To prevent the occurrence of these circumstances, measurement distance is compensated by the transponders referring to a point of departure and so on.

The accuracy of this speed-detection equipment was tested in the presence of the officers from the Traffic Safety Department, Traffic Safety & Public Nuisance Research Institute of the Ministry of Transport. Measurement results were satisfactory.

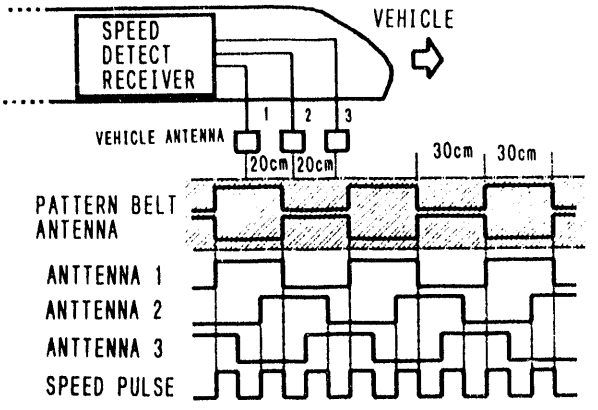

Fig. 6 Speed-detection pattern and output logic

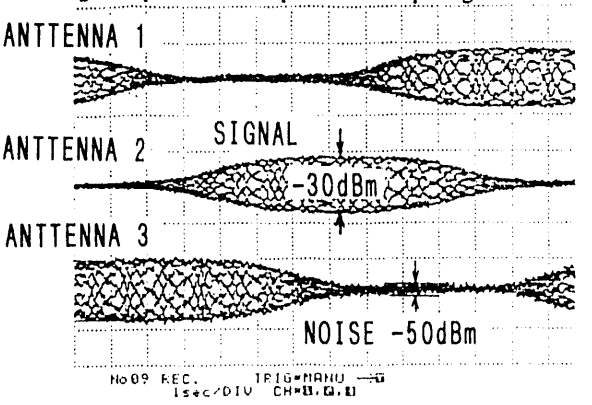

Fig. 7 Speed signal receiving level

B. Operation System

The operation system includes a series of controls, i.e. levitation control, departure control, inter-station constant-speed traveling control, fixed-location stop control, and landing control. The automatic operation system in use is substantially the same as those satisfactorily operated in the Saitama and Yokohama Expositions, except for a feature of the present system; the step-control-type ATP has been replaced with a pattern-type ATP, for backing up. Fig. 8 depicts an example operation pattern in actual traveling.

Fig. 8 shows part of traveling from departure to arriving at the terminal station. The train departs from the right end and accelerates after passing through a 100R curve-speed-limit section of 50 km/h. And a permissible speed changes from time to time according to a normal-braking pattern from 100 km/h for the prevention of overrun at the terminal. Under these restrictive conditions, train speed is controlled by the ATO. Because of a limited length of the chart, the

curve does not extend to fixed-location stopping. However, since the maximum overrun allowance is only about 10 m, the final TASC(Train Automatic Stopping Control) pattern is based on a fixed-location stop control to be effected from about 10 km/h. The accuracy of fixed-location stopping is about ±20 cm.

Fig. 8 Automatic operation following the normal-braking pattern

C. *Information Transmission Equipment*

The information transmission equipment functions as an induction-radio-type poling-selecting system; information from a number of trains is transmitted and received in one wayside station. Major roles of the equipment include sequential receiving of various information signals, including traveling speed of a car, absolute distance range of traveling, and operation status of the car, from the wayside system, for each train; and an operation curve is displayed on the wayside operation control equipment, while operation records are stored into a log file during the test. Only one train travels normally at present. Therefore the train can only respond to sequential poling. However in considering a moving block test to be performed in the future, the equipment is designed so that numerous trains can be controlled. Fig. 9 shows an answer from a car in response to poling from the wayside equipment.

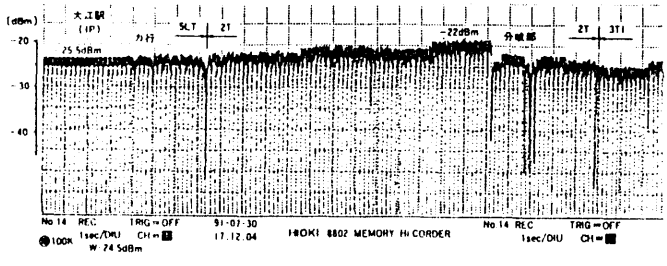

Fig. 9 Receiving level in the wayside equipment for transmitted information

V. Noise Characteristics

Interference-noise characteristics of a magleve-type railway system to other signal telecommunication systems are one of the most important matters to be examined. Sources of interference noise include the levitation coil on the cab, the linear motor in the VVVF control, the SIV or the like for supplying devices on the car with electric power, which emit radiation noise, the feeder that carries a current transmitted from a substation, and the return bus for transmitting a return current from cars. Noise from these sources interferes with the system via antennas and pattern belts for signal transmission. Consequently their positional relationship is a dominant factor. Fig.10 Shows the relative position between cab antenna and driveng system in YES'89 line.

Once the system is applied practically, the location of electric feeders must be changed because of different girder structures, for instance. Additionally, feeder voltages in use include DC 750 V and DC 1,500 V. Therefore it was also verified what effect might result from these factors. In the test system, the electric power systems were installed on the other side of the telecommunication and control systems, separately on both sides of the girder located at the center. Furthermore, signal transmission channels were provided at a location satisfactorily apart from electric devices mounted on a car. Fig. 11 illustrates an example of adverse effect given to the cab equipment in terms of receiving levels of the speed-detection equipment, typically for a frequency band of 10 kHz to 100 kHz which was used in the instruments for measuring interference noise. Fig. 11 relates to an accelerating state in which a maximum of car current of about 500 A created a maximum noise-receiving level of about -40 dBm. It resulted in a minimum of C/N of 20 dB. Therefore absolutely no problems occurred in the related equipment and apparatuses. Fig. 12 shows an example of noise-receiving levels via a wayside pattern belt, with the information transmission equipment. In this case, too, a satisfactory C/N of a maximum noise level of about -44 dBm is assured.

On the other hand, in the test track as shown in Fig. 13, feeder voltage is set at DC 1,500 V with the positive and negative feeders installed separately on both sides of the girder. As a result, the pattern belt for transmission use was constructed in a center part of the girder. Since the distance between devices in the car and the pattern belt was made extremely close and it was feared that direct noise from a power system on the car might interfere, then noise-immunity characteristics of the cab antennas, wayside pattern belt, transponders, etc., were surveyed. Fig. 14 shows measurement results of the speed-detection equipment on the car, which is considered less immune to noise. Obviously, the maximum noise level was less than -40 dBm, which results in a similar C/N level to that of the Yokohama Exposition. Therefore no practical problems were acknowledged. Although the occurrence of an adverse effect on the wayside pattern belt was originally expected, a satisfactory C/N level with a maximum noise level of less than -50 dBm was obtained.

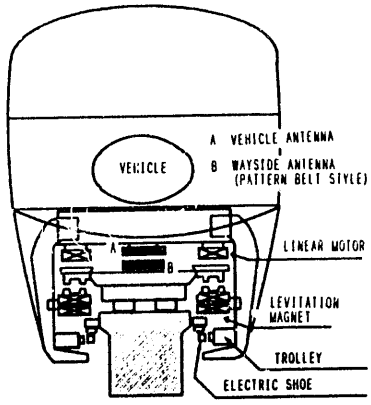

Fig.10 Layout of the girder structure and the signal systems in the Yokohama Exposition

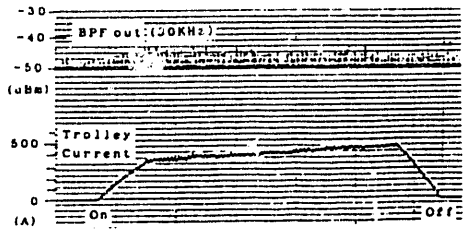

Fig. 11 Noise level on the car (Yokohama Exposition)

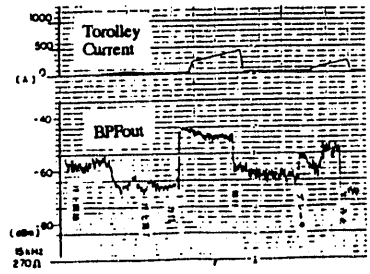

Fig. 12 Wayside noise level (Yokohama Exposition)

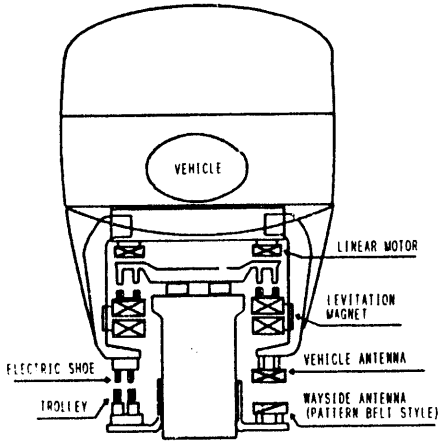

Fig. 13 Layout of the girder structure and the signal systems in the test track

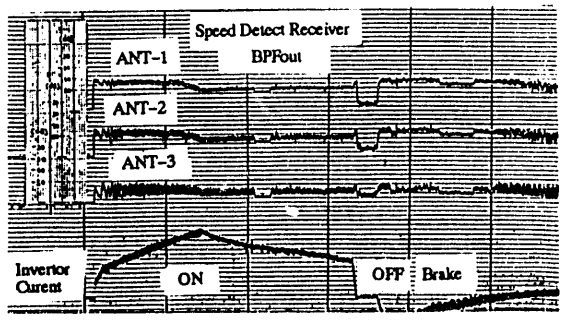

Fig. 14 Noise level in the test track

VI. Conclusions

With the present test track, various experiments were carried out according to the test and study items proposed by the Committee as described at the beginning of the text. Throughout the test period, various data, such as functions and safety as an urban-oriented traffic system, were acquired, and the robustness of the system for practical applications was proved. Based on these technologies, a practical system with high safety and economic performance can be built according to local conditions.

REFERENCES

[1] F. Hashimoto, "Signal and Communication of HSST-05", Institution of Electrical Engineering of JAPAN, IEEJ 1989.

[2] F. Hashimoto and T. Endo, "Operation System of HSST-05", Japan Railway Cybernetics Conference, Vol. 25 .

[3] F. Hashimoto, "Signalling and Communication System of Magleve type HSST", The Institution of Railway Signal Engineers, Aspect91, 1991 .

Siemens Operations Control System for Maglev Trains

Harald Eilers
System Engineering, Siemens AG, Transportation Systems Group,
Braunschweig, Germany

Verena Freitag
System Engineering, Siemens AG, Transportation Systems Group,
Braunschweig, Germany

Rainer Knigge
Maglev Group Leader, Siemens AG, Transportation Systems Group,
Braunschweig, Germany

Abstract - The maglev train operation is safeguarded and controlled by an operations control system which has been developed to full advantage by Siemens. For reasons of safety and economic efficiency, it is necessary to automate this system's functions - with manual intervention only being required, if at all, to overcome disturbances. A multitude of interconnecting functions are neccesary to carry out the tasks of an operations control system. These functions are grouped according to three main task areas and effected as subsystems - central, decentral and mobile. During the course of several research projects, these subsystems have been further developed for maximum efficiency.

0 Introduction

When a traffic system is compared with a living organism, the operations control can be likened to the brain and nervous system. Only by means of an "intelligent" operations control can the technical and operational possibilities of a maglev system be fully exhausted.
However long the line or however many branchings it may have, our operations control system can be used for electrodynamic or electromagnetic systems of levitation. The technical means for implementing maglev operation – as regards vehicles, propulsion, guideway and switches – are fundamentally different from those employed in conventional railway systems [1].

1 Functions of the Operations Control System

By operations control is meant all the functions and equipment which serve to protect, control and manage train movements as well as the intercommunication between these functions.
In order to fully utilize the advantages of a maglev system, operations control is subdivided into three functional groups [2]:

- *Central functions*
  Managerial tasks which are carried out centrally.
- *Decentral functions*
  Tasks involving the control and protection of train movements, which are performed decentrally, and
- *Mobile functions*
  Operational control performed by equipment in the vehicle which may be one-unit or multiple-unit. This also applies to a maintenance vehicle.

In order to implement these three functional groups (central, decentral, and mobile), it is necessary to have [3]:

- an operations control centre
- decentral operations control
- mobile operations control
- data communication
- station
- depot
- diagnostics system

2 Operations Control Centre

When a maglev system is put into long-distance operation, the control centre takes responsibility for all the higher-ranking operational tasks of a maglev high-speed line which includes its peripheral systems. This

calls for widespread automation of operations to be carried out, together with supervision, in the operations control centre. For example:

- planning
- disposition
- supervision
- control
- diagnosis
- operational statistics

Manual intervention in operational procedures, e.g. disposition and planning, is also carried out by the control centre.

3 Decentral Operations Control

Another fundamental subsystem of operations control is the wayside-installed decentral vehicle control. It is responsible for setpoint optimization, as well as route and vehicle protection. It communicates with its partners - propulsion unit, vehicles, guideway (switches) and the operations control centre.
Each decentral operations control has the task of controlling and protecting one maglev train within one substation section (for propulsion control). The guideway to be supervised can be a part of a comprehensive maglev system network in which multiple train operation is automatically performed according to a time schedule or to instructions from the control centre.
The components of decentral operations control are:

- decentral transmission
- decentral control
- decentral protection
- propulsion switch-off

4 Mobile Operations Control

To satisfy system requirements, some tasks of the operations control system are performed in the vehicle.
The principal task of this subsystem is to protect the vehicle. The vehicle safety equipment is in permanent contact with the decentral operation controls. Actual and required process variables are compared by the on-board equipment. In the event of one or the other system components failing, the vehicle safety equipment ensures that values are not exceeded. It intervenes in the process operation by enforcing a target braking to the next station or stopping point.

5 Data Communication

A trend-setting transportation system must be able to offer passengers, also during the actual journey, many possiblities for communication and for receiving information of all kinds – for it must be borne in mind that in the not-too-distant future these will be state-of-the-art features. To meet the high reliability and safety demands set for maglev train operation, as well as to cater for the large number of computer-controlled subsystems, a very high-capacity communication network is required for data exchange and for visual and aural information.

Mobile transmission

An extra-high frequency radio system, in the 40 GHz range, is provided to carry out mobile transmission tasks within the maglev system. Data is transmitted between guideway and train, for route control and protection, for propulsion operation as well as for passenger information and communication.

Stationary transmission

The principal task of operations control is to safeguard and control train movements. To achieve safe train control, each decentral operations control must be able to exchange data with its neighbouring decentral operations controls, approx. 30 km away, and with the operations control centre.
This requires a linking of all decentral operations controls with one another and with the control centre. A ring, which is based on a local area network, is used as communication system.

6 Station

Stations shall provide passengers with maximum comfort. There should be a clear and comprehensive system of information, easy-to-understand user directions and passenger access instructions. Station operations shall be integrated within the entire maglev system.
The safety level is responsible for station train despatch. Safety within the station mainly concerns the supervision and control of doors, and the detection of trains not running to schedule.

7 Depot

The same components shall be used for train handling in the depot as for open line operation.
As the distribution of decentral operation control corresponds to the distribution of propulsion units along the guideway, only one maglev train can be provided with propulsion and transmission per power substation section. In other words, only one vehicle can be controlled and safeguarded per power substation section

by decentral operations control. A depot must be provided with its own decentral operations control and power substation for propulsion control in order to provide independence from mainline traffic.
Depot operations can not be fully carried out according to a time schedule. A relatively large number of operations have to be manually executed via a work station of the operations control centre, which is, however, installed in the depot.

8 Diagnosis

A diagnostics system is a prerequisition for maintaining operational readiness of all maglev subsystems and associated components. In this way, operational efficiency is achieved. The fundamental aim is to prevent component failure leading to restrictions in operations, or at least to keep such restrictions to the shortest possible time.
Diagnostic tasks may be divided into 5 areas:

- collecting and storing process messages
- displaying current data in graphic form
- continuous supervision of process images
- drawing up maintenance and inspection instructions
- interpreting process images

9 Development Stage

The operations control system developed by Siemens for maglev trains can be used both for electrodynamic levitation and electromagnetic levitation. After a decision was made to use electromagnetic levitation for our Transrapid system, research using this form of levitation was successfully carried out in three areas:

- The development of an operations control system, purely at the safety and control level, which could be fully tested under realisitic conditions. Trials were carried out in the Transrapid Test Facility in Emsland in northern Germany. Only then was it possible to realize our aim to operate high-speed maglev trains.
- The demand for a site-independent operations control system, for functional changes in the vehicle and a further development of the computer system, resulted in a new operations control system, the programs of which are effected as site-independent logic. This system permits computers to be used on any maglev network. The special network topography and the site-specific parameters are deposited as configuration data. This second operations control system, developed in 1989, consists of fail-safe functioning microcomputer systems with very high availability. Continuous trial operations have been carried out in conjunction with the TR 07 vehicle at the Transrapid Test Facility in Emsland [4, 5].
- At present, the propulsion system at the Transrapid Test Facility permits one-train operation only. To perform tests on multiple-train operation, a longer guideway with additional power substations for propulsion control would be required [6].
  Therefore, a simulation of multiple-train operation has been provided at the Siemens laboratory in Brunswick to test, in particular, the interaction of subsystems when employed on a long stretch of line such as from Hamburg to Berlin.
  Our decentral operations controls meet the requirements of multiple-train operation. They protect each vehicle from collision by blocking the sections which are already occupied by other vehicles.
  The main components of the laboratory test facility in Brunswick are three physical decentral operations control installations which were used originally, and the communicaton links between them. Other operations control equipment are simulated – for testing intercommunication between the decentral components and for performing train operations with vehicles, guideway and propulsion units. By carrying out these simulated train operations, it has been possible to prove that the distributed control, safety and supervision of several decentral operations controls are able to successfully interact with one another within an information network.

REFERENCES

[1] Schnieder, E.: Die Betriebsleittechnik des TRANSRAPID in: Magnetbahn TRANSRAPID, MVP Versuchs- und Planungsgesellschaft für Magnetbahnsysteme mbH und TRANSRAPID International Gesellschaft für Magnetbahnsysteme, Darmstadt 1989, p. 60 - 64.

[2] Knigge, R.: Systembeschreibung, Siemens AG, Technischer Bericht TB06/1991.

[3] Siemens AG: Lastenhefte Forschungsvorhaben BMFT TV 9223 B, Technische Berichte 1993.

[4] Freitag, V.: Betriebsleittechnik für Magnetschnellbahnen in der Erprobung. Signal + Draht 84 (1992) 3, p. 67 - 72.

[5] Polifka, F.: Der Betrieb auf der TRANSRAPID-Versuchsanlage im Emsland (TVE), Eisenbahntechnische Rundschau 41 (1992) 11, p. 729 - 734.

[6] Miller, L.: Technologieprogramm TRANSRAPID, Eisenbahntechnische Rundschau 41 (1992) 11, p. 721 - 728.

Influence of JR Maglev on Environment

Nobuyuki Kokubun
Senior Engineer, Planning Department,
Maglev System Development Division,
Railway Technical Research Institute

Atsushi Honda
Senior Engineer, Linear Express Development Division,
Central Japan Railway Company

Morio Yasunami
Assistant chief, 7th construction division,
Kanto regional office,
Japan Railway Construction Public Corporation

I. Introduction

We are now newly constructing a test line in Yamanashi Prefecture for ascertaining the practical use of the superconducting magnetically levitated train, which is expected to be an epoch-making, ultra-highspeed mass-transportation system in the 21st century.

The fundamental research and development for this JR-type Maglev were started by Japan National Railways (JNR) at the beginning of 1960's. And they have fairly advanced. For example, in 1979, an unmanned vehicle attained a maximum speed of 517km/h on Miyazaki Test Track. And a manned vehicle attained a speed of 400km/h in 1987.

With the division and privatization of JNR in 1987, Railway Technical Research Institute (RTRI) took over JNR's business and continues running tests of vehicles on Miyazaki Test Track. However, Miyazaki Test Track is not suitable for testing the practical use of JR Maglev, because it is only 7km in length with a single track and it includes no tunnel section. So a new test line which has an overall length of some 40km has been needed.

In 1990, under guidance of Minister of Transport and with a state subsidy, RTRI, Central Japan Railway Company and Japan Railway Construction Public Corporation formed a consortium and started the construction of the new test line. The Yamanashi Test Line has a length of 42.8km including about 35km of tunnel sections. On the new test line, we intend to confirm the stable running at 550km/h and other matters to establish the actual service at 500km/h.

The environmental impact assessment for the construction was completed in September 1990. By January 1993, we have excavated about 4,000m in total.

In this paper, we mainly state the data of noise, vibration and the magnetic field measured in Miyazaki test track and all values predicted about trains running at 500km/h on the Yamanashi test line, and at last, about booming noise by micro-pressure waves.

II. Noises

The noise sources of ordinary trains are mainly classified as follows(Fig.1):

1) rolling noise caused by wheel and rail
2) current collecting noise caused by the pantograph and the trolley
3) aerodynamic noise caused by friction between the train body and the air
4) structure-borne sound

Since the Maglev vehicle begins to levitate at 100km/h, the rolling noise will never occur at 500km/h. And it has no pantograph or trolley, so it doesn't cause the current collecting noise. The structure-borne sound is comparatively small. So the noise caused by the Maglev vehicle is mainly the aerodynamic noise(Fig.2).

The MLU002, test vehicle on Miyazaki test track, is larger in cross-section and taller than the new test vehicle which we are developing for the Yamanashi new test line. And the MLU002 is different from the new test vehicle in shape of the head. We measured noise level of the MLU002 running at 300km/h. The place of measurement is 25m off the center of the track at the height of 1.2m above the ground level. The peak noise level was about 79dB(A)(slow) and its noise was caused by aerodynamics.

If the direct proportion law between noise level and 6th-powered vehicle speed is right, we can estimate the noise level of the MLU002 at 92dB(A), which is running at 500km/h.

To reduce the noise level of the new test vehicle for Yamanashi test line, we took care about some points as follows; First, we reduced the cross-section area and

height of the vehicle. Second, we cut down partial projection at auxiliary guide wheel and coupling section. Next, we improved the shape of the test vehicle-head. Finally, we made the surface of levitation and guidance coils flat. So we estimate that we can reduce the noise level of the new vehicle by about 10dB(A) in comparison with the MLU002. The noise level of new vehicle is estimated about 82dB(A) at peak when it runs at 500km/h and about 70dB(A) at 300km/h. Though we can't make easy comparison because of the difference in tone and so on, we suppose the new Maglev vehicle for Yamanashi is quieter than the Shinkansen and ordinary trains at the same speed.

III. Ground vibration

The load of the JR Maglev vehicle, which acts on the infrastructure and causes the ground vibration, is remarkably small in comparison with the ordinary trains. There are two causes. First, the new Maglev vehicle has a very light weight. It weighs only about half the newest Tokaido Shinkansen car. Second, ordinary train load is concentrated at small points of wheel, but the Maglev vehicle load is distributed during levitation.

We measured the vibration level of the MLU002 running at 300km/h. The place of measurement was 12.5m off the center of the track. Its level was about 45-50dB.

It is difficult to estimate ground vibration level accurately because the ground condition and structure form of the new Yamanashi test line are different from those of the Miyazaki. However, if the new Maglev vehicle for Yamanashi runs at 500km/h under the same situation as Miyazaki test track, we estimate the ground vibration at 60-65dB.

IV. Magnetic field

The word of "magnetic field" has two meanings, i.e., the direct magnetic field and the alternating magnetic field. The maglev train causes the alternating magnetic field around test line when it runs.

In Miyazaki test track whose viaduct has 8m height, the MLU002 causes only about 0.5 gauss at ground level. If the new Maglev vehicle for Yamanashi runs under the same situation as Miyazaki test track, we estimate the level of the magnetic field will be the same as the MLU002. And the new Maglev vehicle will make about 2 gauss magnetic field at the point which is 4m off the edge of the infrastructure, and on the same horizontal level of the new Maglev vehicle.

V. Booming noise by micro-pressure waves

When we decide the route of the train or the highway, it is difficult for us to avoid the tunnels, because there are many mountains in Japan. We have to care for booming noise by micro-pressure waves at the portal of the tunnels.

The micro-pressure waves of the tunnel is a phenomenon as follows; When a high-speed train enters into a tunnel, it generates compressed waves in the tunnel. The waves travel through the tunnel at the speed of sound and they burst as pulse when they arrive at the other portal of the tunnel. If the level of micro-pressure waves is too high, it generates booming noise at that portal of tunnel.

Since the Miyazaki test track has no tunnel, we have no data on micro-pressure waves of the Maglev trains.

We estimate the level of micro-pressure waves will be low enough even if the new maglev vehicle runs faster than Shinkansen, because we reduce the cross-section area of the new maglev train by about 35% and increase the tunnel cross-section area by about 15%(Fig3).

However, when the level of micro-pressure waves is not negligible, we would take measures such as the tunnel entrance hood or wave-absorptive method with the level shaft. The tunnel entrance hood is used for Shinkansen tunnel(photo 1). It is confirmed that the tunnel entrance hood which has 20m length can reduce the level of the micro-pressure waves by about 80%, and is effective against the micro-pressure waves.

VI. Post script

We will finish verification of the commercialization possibility of JR Maglev system by 1997 fiscal year, through enough running tests using the equipment.

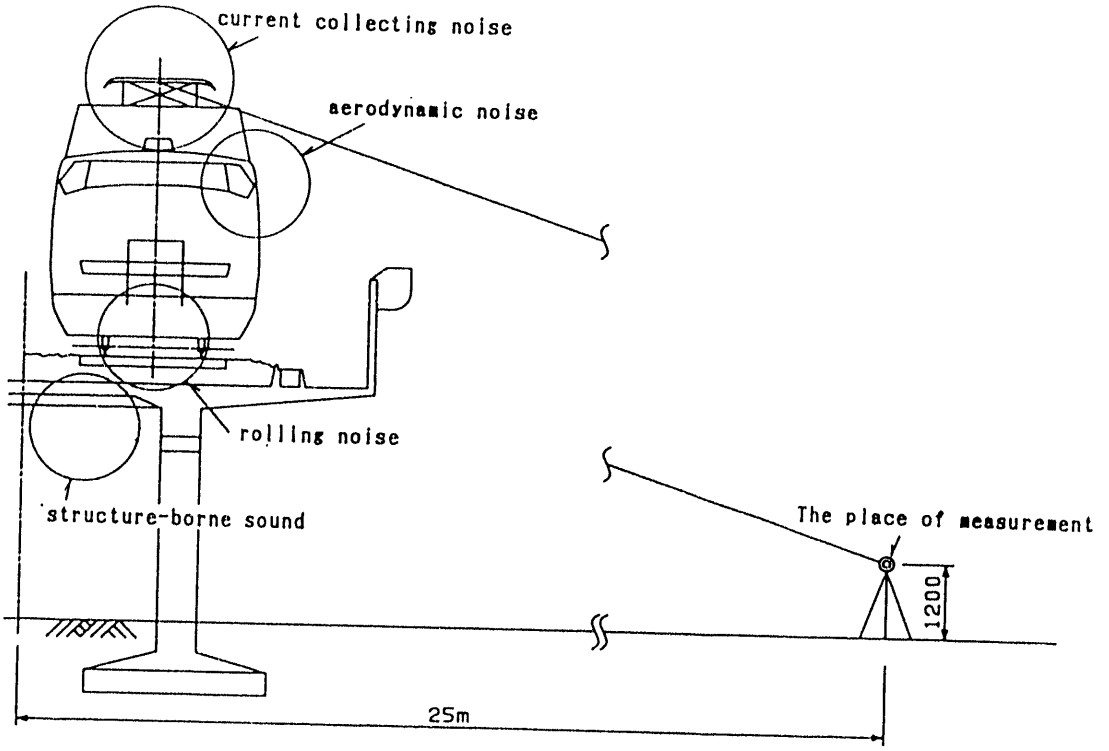

Fig 1. Noise sources of Shinkansen

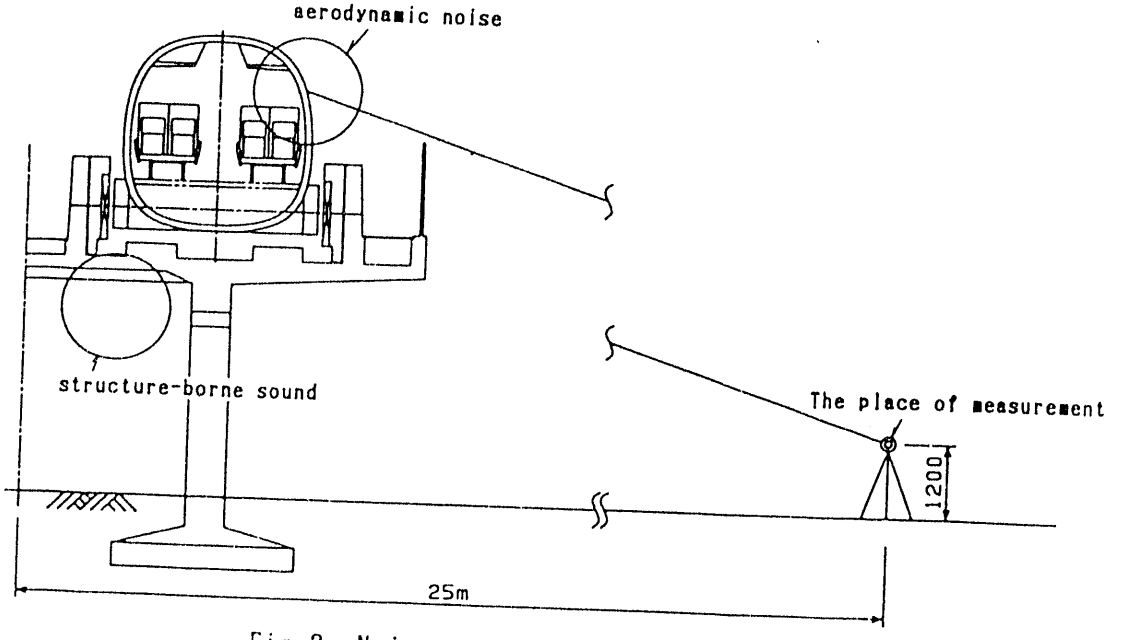

Fig 2. Noise sources of JR Maglev

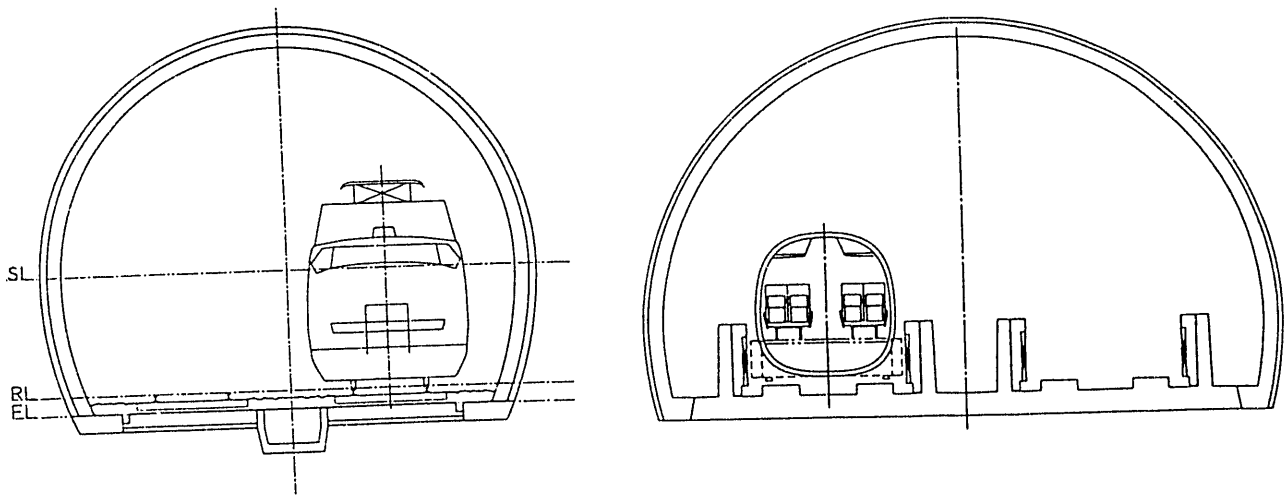

Fig 3. Comparison of tunnel cross-section

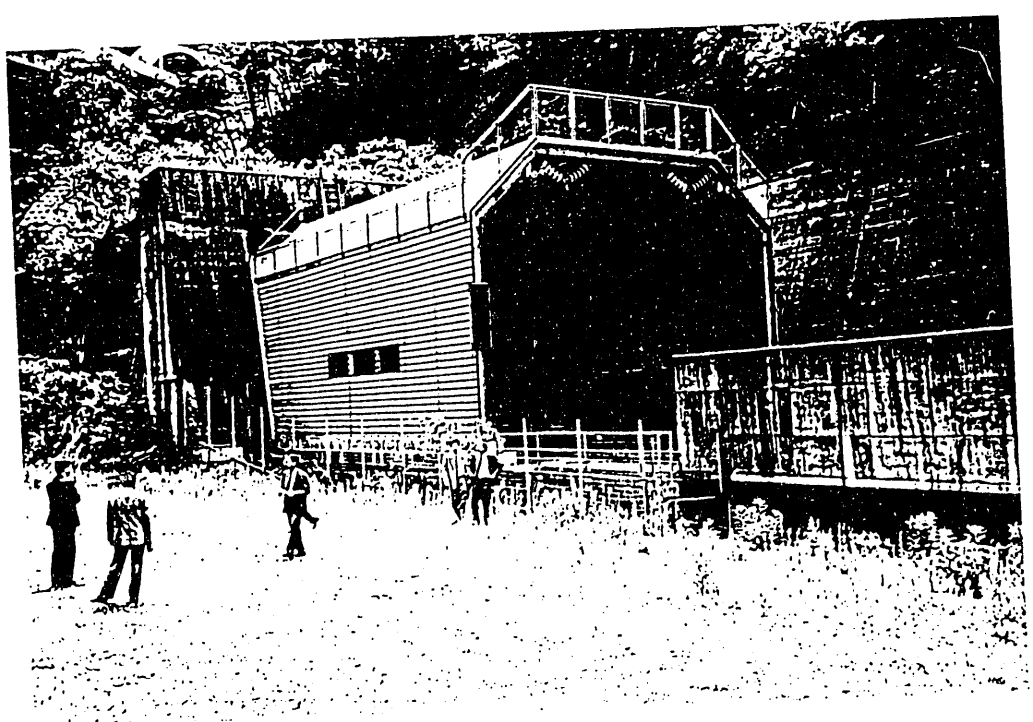

Photo 1. Example of tunnel entrance hood of Shinkansen

Train Control Systems for Superconductive Magnetic Levitation System

Kiyoto Kubota, Toyoji Tanaka, Yutaka Osada
Linear Express Development Division, Central Japan Railway Company

Shin Sasaki, Yoshinao Yokota
Maglev System Development Division, Railway Technical Research Institute

Abstract- The train control system of the JR Maglev, a high speed mass transportation system, is composed of traffic control system, drive control system, safety control system, train position detecting system and communication system.

On the basis of the train control system of the conventional railway systems in which train is driven automatically, the new train control system has been developed for the JR Maglev system.

I. Introduction

The JR Maglev train is driven by the linear synchronous motor with the primary side on the ground, which is composed of super conductive magnets on the vehicle and the ground coils.

In this paper, the structure and functions of the train control system will be discussed. The functions of the subsystems, such as the traffic control system, the drive control system and the safety control system, will also be described. The train position detection of high reliability and precision will be mentioned, whose output is used for synchronous control of the linear motor and assuring the system safety. Communication system between the vehicle and the facilities on the ground will be also discussed in this paper.

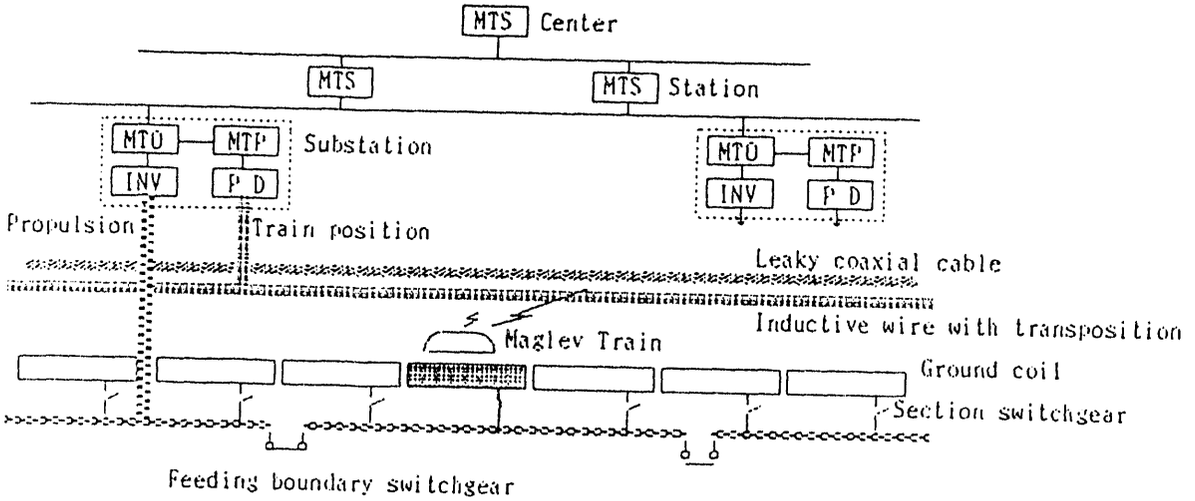

MTS:Maglev Traffic Control System
MTO:Maglev Train Operation System
(Train Operation Control System and Drive Control System)
MTP:Maglev Train Protection System
PD: Position Detector INV:Power Converter (Inverter)

Fig.1 Configuration of Train Control System

II. Structure of the train control system

The MTO and the MTP are installed at the power substation where converters are also provided. The MTS is installed at station yard and at the control center. Fig.1 shows the structure of the train control system.

III. Traffic control system

The traffic control system is divided into three parts, which are central traffic control system, local traffic control system and train operation control system. The functions and structures of these systems are shown in Fig.2.

A. Central traffic control system

The central traffic control system is installed at a command center and manages the data on the whole day train diagram and states of the operated trains. Its main functions are as follows.

a)This system generates or changes the train diagram. It also gives an alarm through the man-machine interface when a trouble occurs.

b)This system sends the train diagram to the local traffic control systems every morning before the train operation begins or whenever the diagram is changed.

B. Local traffic control system

The local traffic control systems are installed at each station and control the trains according to the train diagram delivered by the central traffic control system. Its main functions are as follows.

a)According to the diagram, the local traffic control system instructs the routes in the station area to the yard safety control system.

b)Comparing the actual arrival or departure time with the schedule, the local traffic control system calculates the actual train's running time between the stations.

c)The local traffic control system transfers the train operating data including the train running time and the train route to the train operation control system.

C. Train operation control system

The train operation control systems are installed at each substation and control the trains according to the data given by the local traffic control system. Its main functions are as follows.

a)Based on the position of the preceding train, the train operation control system determines the block section in which the following train has not its speed restricted. This system also orders a change of the boundary of block section according to the position of the trains.

b)On the basis of the safety area assured by the safety control system, the train operation control system generates the train speed command and transfers it to the drive control system. This system also monitors constantly the states of trains, inverters and equipment along the railroad and restricts the speed, acceleration or deceleration of the train if necessary.

IV. Drive control system

The drive control system is similar to the automatic train control facility of the automatic operational control system in conventional railway system. In the JR Maglev system with the primary side on the ground, the drive control system is installed at a power substation.

The drive control system controls inverters and section switchgears according to the speed command given by the train operation control system mentioned above. The main functions of the drive control system are as follows.

A. Speed control

The speed control unit generates a speed control curve, considering the speed command given by the train operation control system. Riding comfort for passengers, adaptation to the varying running resistance and precise stopping at the station are also important factors for deciding the speed curve.

In order to adjust the actual speed of the vehicle to the objective speed control curve, the speed control unit calculates the value of the current determined by the propelling- or braking-force considering the actual train speed given by the phase synchronous control unit and gives the current to the inverters.

B. Phase synchronous control

The phase synchronous control unit generates a detailed phase synchronous control signal which is necessary for the synchronous control of inverters. This signal is based on the phase signal given by the train position detecting unit which is a part of the safety control system and it is given to the inverters. The phase synchronous control unit calculates the speed of the vehicle from a very little change of the train-position, and gives the train position and speed to the speed control unit.

C. Section control

The section control unit controls the section switchgears according to the position of the vehicle under the no current -condition. In order to switch the feeding boundary switchgears under the no-current condition, the section control unit allows the safety control system to control the feeding boundary switchgears considering the states of the drive control system. The section control unit gives the starting- or stopping-timing signals to the inverters.

D. Safety brake control

When the drive control system receives the safety brake command from the safety control system, it stops the inverters, controls the dynamic brake or the coil-shortening brake.

V. Safety control system

The safety control system is in charge of block control, train speed check and route control. The safety control system determines the blocking area which is equal to the varying control area of the drive control system. This system monitors the speed and states of the train continuously and controls the safety brake if necessary. It works independently of the other subsystems.

A. Block control unit

Because an inverter can control only one train, we defined the control area of the drive control system as the blocking area. A few feeding boundary switchgears are provided between substations in order that interval between trains may be shorter by changing the blocking area. The block control unit is allowed to open one of these switchgears, and the opened switchgear determines boundary of block area. In this way an optimal train operation is realized. The following train is not allowed to move into the blocking area occupied with the preceding train.

B. Safety speed control unit

The safety speed control unit generates a safety speed curve under which the train can travel without collision or derailment. The curve is generated considering the distance between trains and route conditions. This unit monitors the actual speed of the train and confirms that its speed is under the safety speed limit. When the actual speed of the train exceeds the safety speed limit because of a failure of the normal regenerative brake system, the safety speed control unit commands the back-up brake, which is called the safety brake. Three types of the safety brakes are provided and one of them is selectively worked depending on the situation. The kinds of the safety brakes are as follows.

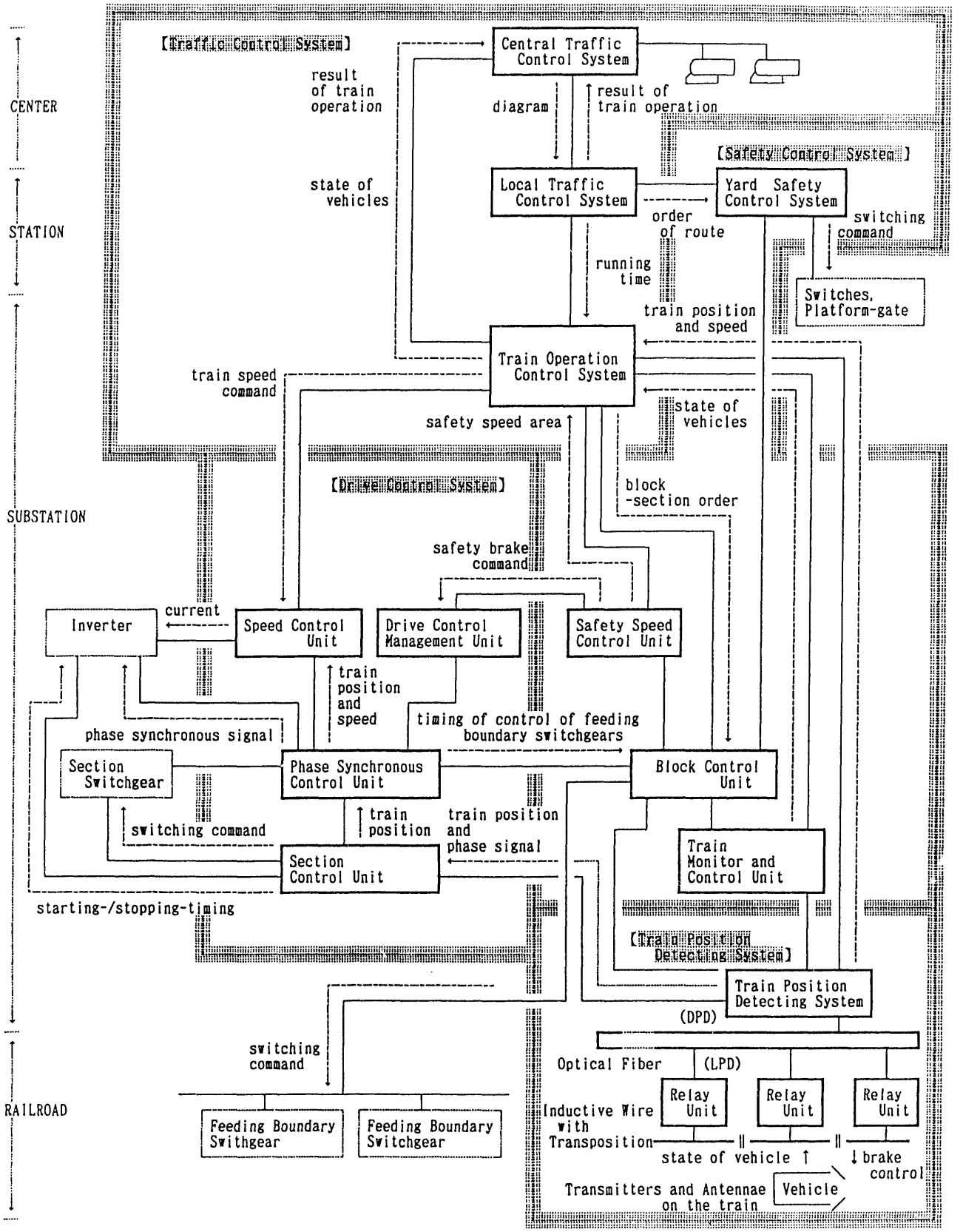

Fig. 2. Structure of the Train Control System

a)The dynamic brake (power consumption with resistance) and the wheel disc brake.

b)The coil shortening brake(propulsion coils are used as resistance) , the wheel disc brake and the aerodynamic brake.

c)The aerodynamic brake and the wheel disc brake.

C. Train monitor and control unit

The train monitor and control unit watches the states of the train and commands the safety brake in case of trouble. When the communication channel fails, this unit also commands the safety brake.

D. Yard safety control unit

The yard safety control unit is in charge of controlling the route switches and platform-gates. The interlocking device developed for the yard safety control has an additional function of controlling the doors on the vehicle, unlike the conventional one.

VI. Train position detection

Precise position detection of the vehicle is indispensable for the JR Maglev system to drive the vehicle with the linear synchronous motor whose primary side is on the ground. Precise train position data is used for the operational control, safety control and control of the section switchgears. In the Yamanashi test line, the inductive wire will be adopted as the position detecting component.

A. Structure and principle of the train position detection

The position detecting system is composed of the transmitting antenna on the vehicle, the inductive wire laid along the guideway and the Local Position Detectors (LPD) which are distributed along the inductive wire and it calculates the train position from the output signal of the inductive wire. The working principle of the train position detection is as follows.

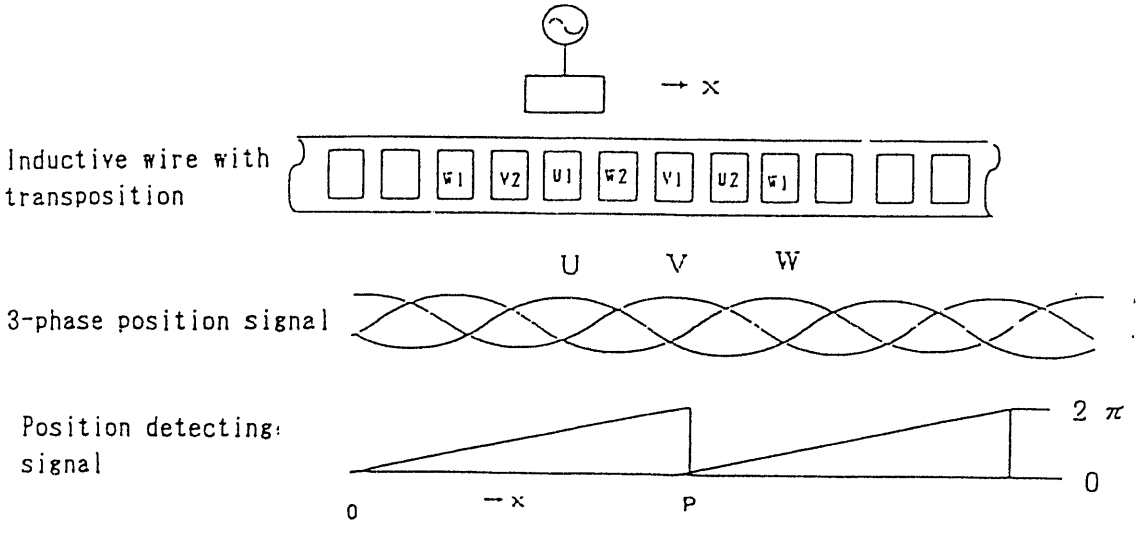

Fig.3. Principle of train position detection

The radio signal of 200 kHz is emitted from the vehicle. The inductive cable containing the inductive wires receives the signal which represents the train position. This cable in belt shape consists of 6 pairs of receiving loops whose transposing cycle P is equal to that of the propulsion coil on the ground. This cable is coated with polyethylene. As the vehicle travels, the output-voltage of the inductive wire varies in a sign curve shape. By processing this sign curve, the LPD makes the 3-phase alternating signal whose mutual lag is 2/3-pi and generates the position detecting signal which varies from 0 to 2-pi as the position of the vehicle does from 0 to P as shown in Fig.3.
The principle adopted in this process is essentially the same as the mechanism which makes a moving magnetic field from the 3-phase alternating current in a motor system. Thus the position of the vehicle is expressed in terms of the phase angle which changes from 0 to 2-pi and the counted number of P.
Precision of the train position detection depends on production- and construction-precision of the inductive cable and on the processing error range of the LPD. The standard deviation is expected to be about 30 mm.

B. Structure of the train position detecting system

The position detecting system (Fig.2) is composed of the transmitter on the vehicle, the inductive cable of laid 1 - 3 km long centrally in the guideway, the LPD and the position detector (DPD) installed at the power substation. Two LPDs are connected to both ends of the inductive cable and have a redundant structure. The LPD is composed of band-pass filters, position signal amplifiers, A/D converters, DSPs (Digital Signal Processor) and micro-computers. It detects the position of the vehicle by digital signal processing and sends this information to the DPD through the optical fiber. The DPD is composed of DSPs and micro-computers. It receives the position signal from the LPDs distributed between the neighboring power substations, traces the train, detects its position and velocity and gives these data to the drive control system, the traffic control system and the safety control system at the power substation.

VII. Communication system

The leaky co-axial (LCX) cable has been used in the Tokaido-shinkansen and the technology has already been completed. The data transmitting speed through LCX is 256 kbit/s. The LCX cable is used for telemetry or communication between the train and facilities on the ground. The antenna on the vehicle is always kept close to the LCX cable on the ground and a stable transmitting quality is attained. The vital information such as the brake command signal is transmitted through the inductive wire besides the LCX cable. The position of the LCX cable is determined on the basis of the pressure of air draft caused by the running train. The LCX cable is laid apart from the inductive cable in order to reduce the possibility of a complete failure of the channel between the train and the facilities on the ground. We are considering the adoption of the millimetric wave communication technique to increase the channel capacity in the future.

The facilities distributed along the guideway are controlled through the communication channel composed of the optical fiber. With adoption of the loop-type network, an equipment in the power substation can control lots of equipment outside of the substation through this network.

We discussed the structure and functions of the train control system in this paper. We shall construct a system for the Yamanashi test line on the basis of this structure.

Development of the system has been financially supported by the Japanese Government.

Maglev Demonstration Project
Site Location Study

Lawrence C. Lennon
Director of Planning
Berger, Lehman Associates, P.C.

I. Introduction

In November 1991, the New York State Thruway Authority (NYSTA) retained Berger, Lehman Associates, P.C. (BLA) with its sub-consultant Transrapid International (TRI) to conduct a Maglev Demonstration Project Site Location Study. The goal of this study was to identify four sites along the Thruway, each between 25 and 50 miles long, which might be suitable for the development of a maglev demonstration facility. This paper describes the site selection process and the four alternative sites proposed for consideration by NYSTA.

II. Study Area

The New York State Thruway, which extends 559 miles across the State, is the longest toll highway in the United States. The Thruway's 426 mile mainline connects New York City and Buffalo, the State's two largest cities. The study area encompasses the Thruway mainline (I-87/90), the New England Section (I-95) to the Connecticut State Line and the Berkshire Section (I-90) to the Massachusetts State Line.

III. Maglev Systems

Three maglev systems were used in the evaluation. These vehicle/guideway systems are the German Transrapid (TR07), the Japanese Linear Motor Car (MLU00X) and the U.S. Grumman (Configuration 002). They differ primarily in suspension technology (electromagnetic suspension vs. electrodynamic suspension), guideway magnets (superconducting vs. non-superconducting), guideway type (channel vs. T-type), and the ability of the passenger compartment to "tilt" when traversing horizontal curves (tilt vs. non-tilt). The Transrapid and Grumman vehicles were evaluated using tilt and non-tilt options.

IV. Methodology

The study was conducted in three phases. During the first phase, a database of existing conditions in the study area was developed along with a set of maglev design criteria. The database includes information on Thruway horizontal and vertical alignment, ROW widths and relevant land use and environmental data. The maglev design criteria covers guideway horizontal and vertical geometry including required superelevation and transitions.

During the study's second phase a screening of the study area was conducted to eliminate Thruway sections less suitable for facility development due to restrictive horizontal curvature. This was accomplished utilizing a series of templates which graphically presented tilt and non-tilt maglev horizontal curvature requirements at various speeds (See Table 1). These templates were superimposed on 1 inch=500 feet scale aerial photographs to identify speed restricted areas. Approximately half of the Thruway was eliminated from consideration based on this review. The Thruway was sub-divided into four corridors: New York City to Albany, Albany to Syracuse, Syracuse to Buffalo and the Berkshire Section.

The Thruway sections which were retained for further consideration after initial screening were evaluated to identify one preferred site in each of the four corridors. Sites were selected based on their ability to accommodate high speed maglev operations while minimizing adverse environmental impacts. Three of the four sites have both 25 mile and 50 mile long alignment options. The "Berkshire Section" is approximately 23 miles long.

Thus four sites were identified, one in each corridor. These sites encompass seven options when 25 and 50 mile alignment alternatives are considered.

V. Site Descriptions

Site 1 extends from Newburgh to Saugerties in Orange, Ulster and Greene Counties. The 50 mile long alignment option includes four existing Thruway service areas and two parking areas.

Site 2 extends from Utica to Syracuse in Herkimer, Oneida, Madison and Onondaga Counties. The 50 mile long alignment option includes three existing service areas and two parking areas.

Site 3 extends from Manchester to Rochester in Seneca, Ontario, Monroe and Genesee Counties. The 50 mile long alignment option includes four existing service areas and one parking area.

Site 4 is on the Berkshire Section in Albany, Rensselaer, and Columbia Counties. The 23 mile long alignment option includes two closed service areas. There are no parking areas along this alignment.

VI. Maglev Simulation

The model used to simulate maglev operations at the four alternative sites (seven alignment options) is based on a system of differential equations which describe the relationships between vehicle motion, resistance and thrust, and between voltage and current. It was previously developed by Transrapid International to evaluate alternative alignments and may be run for any maglev system for which basic power and resistance data are provided.

The model was used to generate a speed profile for each alignment option based on alignment-specific guideway geometry (i.e. grades, curves, superelevation), vehicle tilting capabilities, and selected passenger comfort criteria.

Primary among the passenger comfort criteria are acceptable lateral acceleration and jerk (i.e. rate of change in acceleration). The criteria utilized in this study are equivalent to those employed by Amtrak in their Northeast Corridor service.

The Amtrak criteria are conservative in that they assume that passengers may stand up and walk in the maglev throughout the trip and that railroad criteria are appropriate for maglev vehicles. Significantly higher levels of lateral acceleration and jerk are experienced regularly by airline passengers while seated. Higher acceptable levels are also proposed by some proponents of maglev. It is important to note that higher levels of acceptable lateral acceleration and jerk would permit higher maximum speeds on curves and thus higher average operating speeds.

The model was used to determine the operating characteristics (speed, energy use) of the three alternative maglev systems (Transrapid, Linear Motor Car, Grumman), two of which had tilt and non-tilt options (Transrapid and Grumman).

The simulation model was run in two modes: Type A simulation and Type B simulation. Type A simulation estimates a maglev's speed profile and energy consumption based on an operation designed to minimize energy consumption. This is accomplished by minimizing the number and magnitude of speed changes along a route. The result is a relatively constant speed profile.

Type B simulation is designed to minimize total travel time. This is accomplished using a more dynamic speed profile which is closer to the local speed constraints imposed by the guideway alignment. Under this operating scenario, both average speeds and energy consumption are higher than with Type A simulation.

In order to simplify the analysis, operations of the five maglev options (Transrapid tilt, Transrapid non-tilt, Grumman tilt, Grumman non-tilt, Linear Motor Car non-tilt) were simulated for the 50 mile alignment in the New York City to Albany corridor using both Type A and Type B operating scenarios. The remaining alignments were modelled for both tilt and non-tilt Transrapid Type A operations. This reduced the number of simulations while producing reasonable conclusions for all the potential maglev system-alignment combinations.

In general, Site 3 (Manchester to Rochester) offers the highest average speeds (215 mph-tilt, 180 mph-non-tilt) and highest maximum speed (275 mph-tilt, 205 mph-non-tilt) assuming energy efficient operational mode. Operating in a maximum speed mode, a speed of 300 mph may be achieved at this site.

Site 4 (Berkshire Section) has the most speed restrictive geometry. A non-tilting maglev has an average speed of 130 mph on this alignment assuming energy efficient operations. A tilting maglev would have an operating speed of 140 mph; a maximum speed of 200 mph could be achieved over a section less than 5 miles long assuming maximum speed operations.

Sites 1 (Newburgh to Saugerties) and 2 (Utica to Syracuse) fall between Sites 1 and 4 in terms of average operating speed and maximum speed. (See Tables 2, 3, and 4)

VII. Cost Estimates

Conceptual construction cost estimates were developed for four alternative sites, (seven alignment options). Each cost estimate contains a guideway cost estimate, vehicle cost estimate, and a support facility cost estimate.

The cost of a maglev support and maintenance facility including workshops, control and communications equipment, and general purpose maintenance vehicle is approximately $40,000,000. The required two-car maglev trainsets (two) will cost an additional $30,000,000. These costs are common to all alignment options.

Guideway costs were estimated using both "high" and "low" guideway profiles. The "high" profile dual guideway is designed to cross over most existing Thruway overpasses while compensating for some of the Thruway's grade changes. The "low" profile dual guideway is designed to reduce guideway construction costs by reducing average guideway column height. This is accomplished by reconstructing Thruway overpasses to allow the maglev to pass under. The cost of Thruway over-over modification, approximately $2,000,000 per overpass, is offset by guideway cost savings which vary by location based on reduced guideway height.

Generally a 50 mile long demonstration project with a dual guideway will cost approximately $1.3 billion while a 25 mile long project will cost approximately $740 million. It is important to note that these are approximate cost estimates prepared using small scale conceptual alignment plans and without detailed geotechnical or topographic data.

Within the limitations of this study there is no appreciable cost difference between alternative sites. All costs are given in 1992 dollars.

Implementation costs can be reduced by initially erecting a single guideway on piers capable of supporting a future dual guideway. The second guideway could be added at a later date when required. The 50 mile long single guideway would then cost approximately $870 million while a 25 mile long guideway would cost approximately $500 million.

TABLE 1

MAGLEV SCREENING GEOMETRY

Speed/Criteria	Non - Tilting Vehicle	Tilting Vehicle
300 MPH Operation		
Minimum Curve Radius	19,000 ft.	10,900 ft.
Spiral Length	1,000 ft.	2,000 ft.
Minimum Tangent Between Spirals	500 ft.	500 ft.
250 MPH Operation		
Minimum Curve Radius	13,300 ft.	7,600 ft.
Spiral Length	1,000 ft.	2,000 ft.
Minimum Tangent Between Spirals	400 ft.	400 ft.
200 MPH Operation		
Minimum Curve Radius	8, 500 ft.	4,800 ft.
Spiral Length	1,000 ft.	2,000 ft.
Minimum Tangent Between Spirals	300 ft.	300 ft.

TABLE 2

SIMULATION SUMMARY
50 MILE ALIGNMENTS
ENERGY EFFICIENT OPERATIONS

		Speed (mph)			
		Maximum		Average	
Site	Limits	Non - Tilt	Tilt	Non - Tilt	Tilt
1	Newburgh to Saugerties	160	215	135	175
2	Utica to Syracuse	180	240	150	185
3	Manchester to Rochester	205	275	180	215
4	Berkshire Section (1)	N.A.	N.A.	N.A.	N.A.

(1) Site 4 is 23 miles long.

TABLE 3

SIMULATION SUMMARY
SITE 1 (NEWBURGH TO SAUGERTIES)
50 MILE ALIGNMENT

Maglev System	Tilt Capability	Trip Time (min)		Speed (mph) Maximum		Speed (mph) Average	
		A (1)	B (2)	A	B	A	B
Grumman (002)	Tilt	16	15	215	260	185	200
	Non - Tilt	21	19	160	215	140	185
Transrapid (TR07)	Tilt	17	17	215	260	175	180
	Non - Tilt	22	19	160	220	135	155
Linear Motor Car (MLU00X)	Non - Tilt	22	19	160	215	140	160

NOTE:
(1) A = TYPE A - Energy Efficient Operation
(2) B = TYPE B - Maximum Speed Operation

TABLE 4

SIMULATION SUMMARY
50 MILE ALIGNMENTS
MAXIMUM SPEED OPERATIONS

		Maximum Speed (mph)		Distance (Miles)	
Site	Limits	Non - Tilt	Tilt	Non - Tilt	Tilt
1	Newburgh to Saugerties	225	250	<5	10
2	Utica to Syracuse	240	270	10	5
3	Manchester to Rochester	300	300	5	20
4	Berkshire Section (1)	200	225	5	<5

(1) Site 4 is 23 miles long.

The Environmental Impact of MAGLEV
A Comparative Study

Mark C McClintock
Rochester, New York

Abstract **- The rising economic and environmental cost of today's existing transportation infrastructure has necessitated the development of alternative transportation means. This study has been conducted to evaluate the environmental impact of a magnetic levitation system. It was found that maglev potentially operates at energy intensities less than that of airplanes or automobiles. Further reduction in energy use can be achieved by decreasing the operating speed of the maglev system. Associated decreases in emissions are found as well. The use of centralized power facilities for power generation will allow the use of alternative fuels and will produce power more efficiently than mobile sources such as jets or automobile engines. Constructing maglev along existing rights of way for highways and railways will substantially reduce the environmental impact of the system construction by localizing the construction impact to areas where an impact has already been made.**

I. Introduction

The automobile and the airplane have become extremely successful forms of transportation in the world today, and are now causing significant problems in congestion, air pollution and fuel consumption. Other environmental effects include land and resource consumption. Transportation accounts for significant portions of emitted carbon dioxide and other hazardous pollutants, and is the largest consumer of oil. To combat the increasing inefficiency and high environmental cost of transportation, magnetic levitation, or maglev, and other systems are being designed to transport people more efficiently than present transportation modes.

This study is conducted to evaluate the impact of an operational maglev system on the environment. It does not assume the use of any specific maglev design or route, but is intended to be as general as possible. The study is conducted by comparing maglev elements to similar elements of other transportation technologies and evaluating relative impacts. Data is collected from raw data published in tables, from previous studies on similar and related topics and from conversations with knowledgeable people. When extrapolation is necessary, the method is explained. No original laboratory studies are conducted due to lack of facilities. The data is presented in two sections: system operation and system construction. Finally, there is a brief analysis of several theoretical routes for illustration purposes.

Manuscript received March 17, 1993. This study was conducted independently.

II. Maglev System Operation

The purpose for the construction of a maglev system is to achieve superior performance over conventional transportation modes for short and medium range inter-city trips. The environmental impact of everyday operation of a maglev system is assessed and compared to other transportation modes. An evaluation of the economics associated with emissions control, fuel economy and local environmental impact is not possible in this report.

A. Energy Consumption

Energy consumption is of central importance to the environmental impact of a maglev system because fuel consumption and emissions are directly dependent on it. The energy required for travel per person per unit length is known as the energy intensity (EI). This is used to make inter modal energy consumption comparisons that are not dependent on vehicle size, trip length or number of passengers. Calculation of individual EI values are discussed below, and results are contained in fig. 1. The base figure is on-site energy consumption, and the net figure contains allowances for the efficiency of power generation and fuel shipments. Net fossil assumes only fossil fuel

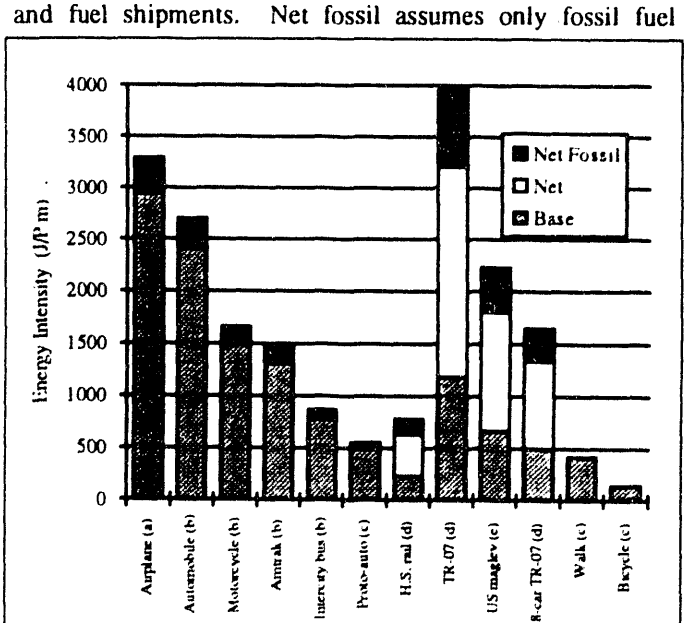

Sources: (a)[1]; (b)[2]; (c)[3]; (d)[4]; (e)[5,6,7,8].
Fig. 1. Energy intensities of primary inter city transportation modes.

powered generation, including coal, natural gas and petroleum. Energy consumption figures for fuel powered vehicles are computed from fuel consumption converted into energy using the energy equivalent figures listed in table 1.

The energy consumption for the Boeing 737 is computed from the following relation developed by John Harding of the U.S. DOT [1]. The total fuel, T, in liters consumed on a flight is:

$$T = 1249 \text{ li} + 3.72 \text{ li / km} \qquad (1)$$

Assuming a 61% load factor [2], and using the figures in table 1, we can calculate the energy intensity for the Boeing 737.

$$EI(D) = \frac{3.76\times10^{7} \text{ J / li}}{80 \text{ pass}}\left[\frac{1249 \text{ li}}{D} + 3.72 \text{ li / km}\right] \qquad (2)$$

where D is the travel distance in kilometers. This is plotted in fig. 2. The EI for the 737 changes dramatically depending on the length of the flight. For the EI contained in fig 1, a flight length of 483 kilometers (300 miles) is used because it is representative of the distances involved with maglev travel. The 737 is more fuel efficient than the fleet average for short haul air flight. It is used, however, because it represents the latest widely implemented air technology and the future of air travel and air fuel efficiencies in an aging airline fleet.

The automotive EI values represent a 1988 fleet highway average of 8.5 kilometers per liter (20.0 mpg), and occupancy of 1.7 passengers per car [2]. Several auto makers have concept cars in development that have mileage efficiency far in excess of current fleet averages. The Toyota advanced prototype from [3] is included to indicate the possible future for automobile fuel efficiency standards. This small and fuel efficient model achieves a theoretical 41.7 kilometers per liter (98 mpg). It is unrealistic to expect that we will see fleet averages in this neighborhood in the near future as large and aging vehicles continue to adversely effect the fleet average. However, the automobile fleet does have the potential for significant improvement over current standards. The Transrapid data is obtained from the National Maglev Initiative (NMI) [4]. The US maglev data

TABLE 1
Energy equivalent of fossil fuels.

kg coal	25.6 million J
m^3 dry natural gas	38.1 million J
liter kerosene (jet fuel)	37.6 million J
liter gasoline	34.8 million J
liter diesel	38.7 million J
liter crude oil	38.5 million J

Source: [2]

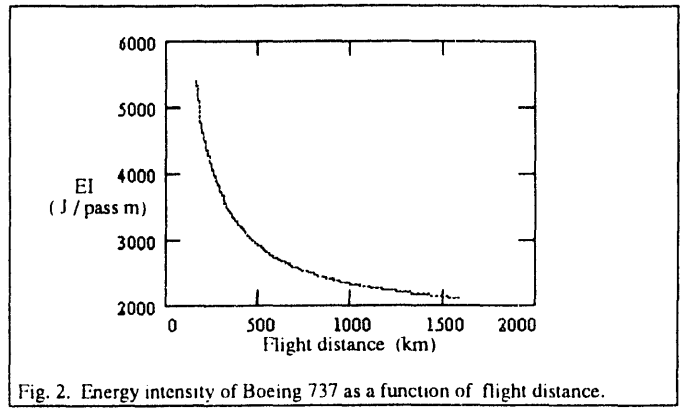

Fig. 2. Energy intensity of Boeing 737 as a function of flight distance.

is an average of data obtained from the four corporate members of the NMI and their most recent System Concept Definition (SCD) studies [5,6,7,8]. These values are for constant speed on a level grade. Actual vehicle EI's will be dependent on the route, how many stops are made, and how much hill climbing and acceleration and deceleration are necessary. The German system figures are included due to their experimentally verified nature, whereas the NMI figures are theoretical.

Table 2 gives the fossil fuel consumption and power output for US electric power utilities [9]. Using energy per unit fuel equivalents we calculate the efficiency of fossil fuel power plants to be 33%. We assume nuclear and hydro to be 100% efficient because their associated efficiency and environmental impact are not quantifiable in the same manner as fossil fuel powered generation. Their impact will be discussed later. With this allowance, we observe an overall power utility efficiency of 41%. Assuming another 10% loss in power transmission, the above figures come to 30% and 37% respectively. These are the efficiencies assumed in fig. 1.

Additional savings in energy will come from reduced congestion at airports due to fewer airplane takeoffs and landings. An original analysis of these savings is beyond the scope of this report. However, one was conducted by

TABLE 2
Power output, fuel consumption and efficiency of electric power utilities by type.

	Output 10^{18} J	Fuel Consumption	Energy equivalent of fuel 10^{18} J	Efficiency
Coal	5.62	675 bill kg	17.28	0.33
Petroleum	0.42	31.2 bill liter	1.09	0.39
Gas	0.95	78.9 bill m3	3.01	0.32
Nuclear	2.08	no data		
Hydro	1.01	no data		
Other[a]	0.04	no data		
Total	10.11		24.51	**0.41**
Total fossil	6.99		21.38	**0.33**

a. Other includes geothermal, wood, wind, waste and solar.
Source: [9]

Argonne National Laboratories [10] and predicts potential fuel savings of 1.1% - 3.9% based on a system wide 25% reduction in taxi/idle time. There will be a corresponding reduction in emissions.

High speed transportation at sea level is obtained at the cost of high aerodynamic drag. A detailed drag analysis is not possible here, however, a simple analysis is conducted for illustration purposes. To a good approximation, the aerodynamic drag is related to the square of the vehicle speed, and the magnetic drag is constant. For this analysis we will assume no grade, acceleration or head wind. The energy used for propulsion at constant speed is directly calculated from the force multiplied by a characteristic length. Therefore, the energy required per passenger meter is for propulsion is:

$$E_d(U) \approx cU^2 + m \qquad (3)$$

where the constant c is a function of vehicle frontal area, atmospheric density, the drag coefficient C_d and the number of passengers per of vehicle. The constant m is the magnetic drag. From [5], we will assume m to be 8% of $E_d(U)$ at 134 meters per second, although this will vary according to vehicle design and configuration. A constant vehicle energy consumption regardless of vehicle speed is required for maintenance of systems such as levitation, air conditioning and lighting. A reasonable assumption for this is 5 kilowatts per person, which we will call k [1]. This value divided by the speed gives the energy intensity for system maintenance. Therefore, the total vehicle energy intensity is:

$$EI(U) \approx (cU^2 + m) + k/U \qquad (4)$$

Fig. 3 shows a plot of $EI(U)$ vs U, and the substantial reduction in energy consumption if operating speeds are reduced. The system could be operated at about half the energy intensity by reducing operating speeds by approximately one third.

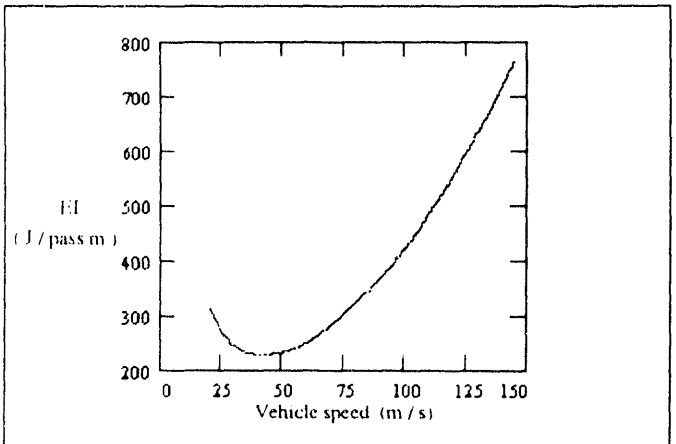

Fig. 3. EI as a function of speed for maglev vehicle.

B. Fuels and Power Production

One of the inherent advantages of maglev is the opportunity to use power that is centrally produced on a large scale. The efficiency of the combustion process on board airplanes, automobiles and other modes is already included in the base numbers of fig. 1. Designed for operation in more constant operating conditions and with the use of technologies such as fluidized bed combustion and steam turbines, power plants can operate at higher efficiencies than their smaller, space and weight constrained counterparts. Typically the thermal efficiency for automobiles is 25% [11], and for jet airplanes 20% - 30% [12].

By producing power centrally we have the option to use other forms of power such as coal, gas, nuclear power, hydro and experimental sources such as solar. Today fossil fuels, primarily coal, account for 69% of all domestic electricity production. Hydro-electric 10%, nuclear 21% and all other forms, including wind, wood, refuse, geothermal and solar less than 1% [2]. With the option to use alternative power sources, dependence on petroleum product in the transportation sector will decrease. This has environmental as well as political benefits including decreased dependence on foreign oil reserves. Our domestic oil reserves are limited and decreased consumption of these resources will hopefully postpone or eliminate the need to attempt oil exploration in ecologically sensitive areas such as the Alaska Wildlife Preserve. Albeit not without large capitol investment, existing power facilities may be upgraded with improved technology as it becomes available. New forms of power production may be incorporated into the transportation sector such as solar as it becomes cost effective.

Although non fossil fuel sources do not produce emissions in the same manner that fossil fuel plants do, they all have their own unique environmental problems. Hydro-electric power plants can be environmentally devastating to the communities both above and below the dam due to flooding of upstream land, and alterations of water flow patterns downstream. Although nuclear power produces very little gaseous emissions, it creates a small quantity of highly toxic waste where no suitable means for disposal have yet been implemented. Solar energy uses no fuel and has no emissions but necessitates the use of large quantities of land. Urban solutions include the use of rooftops and highway medians for the placement of solar collectors. At this time large scale power production by solar means is not cost effective, but this cost has been decreasing with advancements in solar technology.

The effect of power production for the use of maglev will be determined on a regional basis and on the characteristics of the maglev system. If a power plant is not operating at full capacity, a maglev system may be able to use the excess capacity thereby increasing the power plant's efficiency. However, if the maglev system exceeds a region's energy

capacity, the construction of new power plants will be necessary, with an associated negative environmental impact. Power use on the utility grid is by no means constant, and peak power demands can cause significant problems for power utilities. The power grid must be constructed to handle the peak power loads of the morning and evening, and must then operate at sub optimal conditions during the midday or overnight when demand is low. Maglev could effect this in either a positive or a negative sense. An analysis of ridership demand is beyond the scope of this paper, however, some pertinent points are made. If the maglev ridership is heaviest in the morning and evening, say a rush-hour demand, this could adversely effect the local power situation by aggravating the peak-trough nature of power demand. If the maglev system operates at a relative constant, a suitable power source should be able to be arranged that would not aggravate local conditions. Ideally, the peak maglev demand could be associated with low demand periods, and would benefit the power demand by smoothing out the peaks and troughs [13].

An increased emphasis is being placed on conservation when the need for more power is raised. Many utility planners believe that increased power demand by the construction of new industry and civilian development can be accommodated by an increase in conservation efforts. Cooperation by maglev planners with local power utilities in conservation efforts could have a substantial beneficial effect on local power situations.

Because maglev vehicles do not require on board energy production, no fuel is stored on board, and no filling of fuel needs to take place. This has several environmental advantages. In the case of accident, there is no fuel to be leaked to the environment. Storage facilities are not necessary and neither is the transfer of fuel to the vehicles. The transfer of fuel from storage tank to vehicle accounts for a significant portion of automobile emissions. Evaporation of gasoline can account for as much as 18% of automobile hydrocarbon emissions. Emissions will be discussed if further detail in the next section.

C. Emissions

Fig. 4 shows emissions on a kilogram per passenger meter basis for the six criteria emissions from utility power plants and from transportation. This data is taken from [14] and linearly scaled to be compatible with the EI values used in this report. Emissions for electric powered modes are calculated directly from kilograms of material per joule for electric utilities [14].

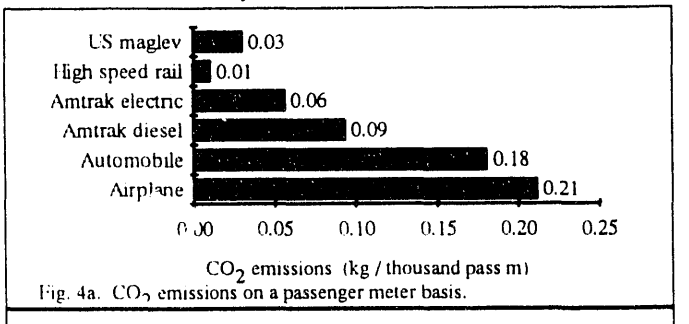

Fig. 4a. CO_2 emissions on a passenger meter basis.

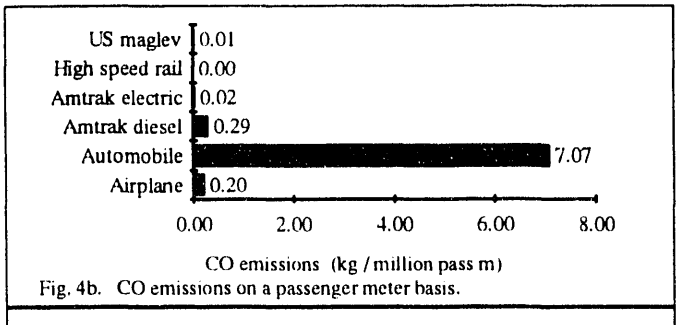

Fig. 4b. CO emissions on a passenger meter basis.

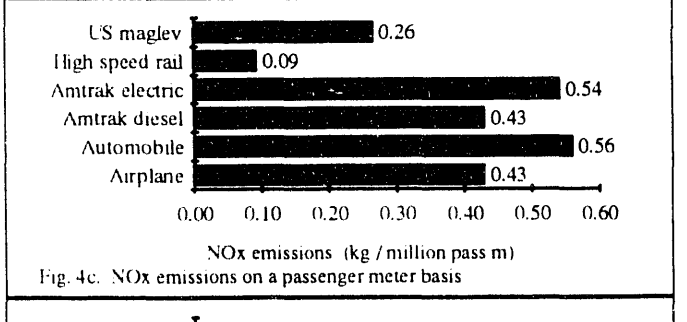

Fig. 4c. NOx emissions on a passenger meter basis

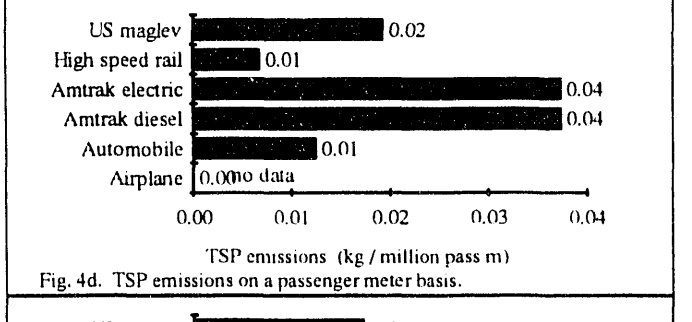

Fig. 4d. TSP emissions on a passenger meter basis.

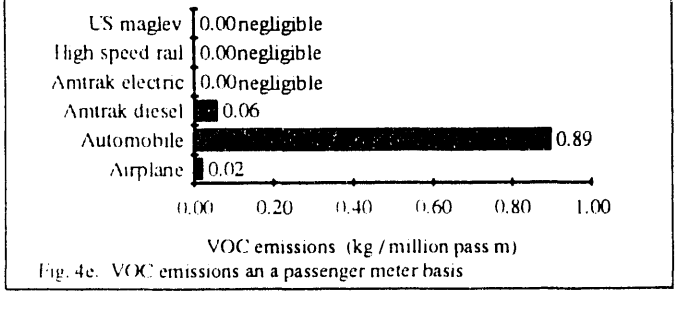

Fig. 4e. VOC emissions an a passenger meter basis

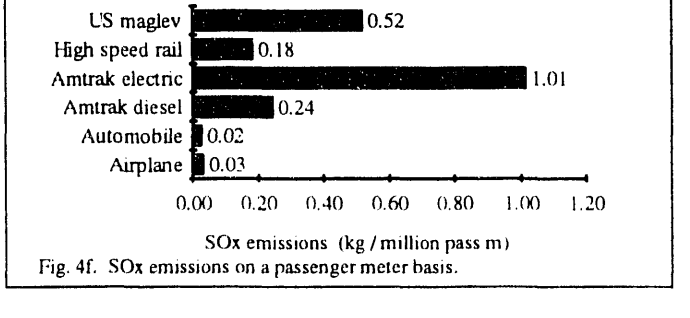

Fig. 4f. SOx emissions on a passenger meter basis.

Carbon monoxide, CO, is a colorless, odorless and potentially lethal gas that is the product of incomplete combustion. CO is responsible for headaches and decreased brain function and is a contributor to tropospheric ozone. Ozone, O_3, is produced through a complicated chemical chain of events in the presence of heat. It is a contributor to urban smog and causes a decrease in pulmonary function and capacity. The other two primary contributors to ozone are nitrogen oxides, NO_x, and non methane hydrocarbons, otherwise known as volatile organic compounds, VOC's [15]. In addition to ozone, NO_x is a component of smog and some members of this family are possible carcinogens, as are certain hydrocarbons. Carbon dioxide, CO_2, is not a health hazard directly. Life could not exist, as we know it, without CO_2. Since CO_2 has been emitted in unprecedented quantities by industrial processes, there has been significant buildup of CO_2 in the atmosphere causing what has become termed the "green house effect." This buildup of CO_2 in the atmosphere, together with other gasses, is causing the trapping of heat, and a potentially significant increase in temperature, causing planet wide atmospheric changes [16].

Oxides of sulfur, SO_x, are a natural product of fossil fuel combustion, and can be reactive with other chemicals and elements as either an oxidant or a reduction agent. SO_x is primarily responsible for acid rain, which has been responsible for widespread damage to forests and lakes and the defacement of many historically significant structures. Suspended particulates, TSP, is also a combustion product, and is responsible for respiratory dysfunction and disease [16].

Fig. 4 shows that a maglev system should cause a reduction in emissions over the airplane and especially the automobile in most areas. Because coal has a much higher sulfur content than oil, sulfur emissions will increase with the use of maglev.

D. Noise Pollution

Of major concern with a high speed vehicle traveling at ground level is the noise associated with it. Fig. 5 shows relative noise levels for various transportation modes and maglev. The figure shows maglev to be an order of magnitude less than the Japanese Shinkansen (bullet train), although significantly noisier than typical daily transportation modes. Data is from [17] and US maglev companies [5,6,7,8].

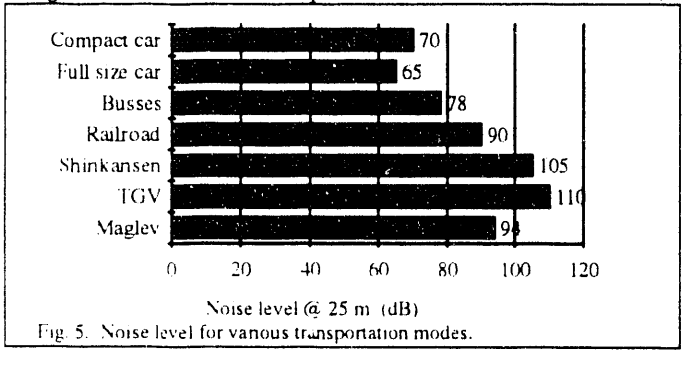

Fig. 5. Noise level for various transportation modes.

E. Magnetic Field Emission

The corporate members of the NMI have reported that electromagnetic fields (emf) from their vehicles drop to below 500 milligauss by 10 meters from the vehicle and below 100 milligauss by 20 meters. For comparison sake, some high power transmission lines emit as much as 500 milligauss at four meters. There is a lot that is still unknown about the connection of magnetic fields and health effects, and more study is necessary in this area. However, it seems that at this point maglev does not emit magnetic fields stronger than power lines, and possibly less than household appliances [18].

III. Maglev System Construction

Any construction project is by its very nature environmentally destructive. It will require the mining and manufacture of materials, the transporting of said materials and fuel, and will develop land previously undeveloped. Local wildlife populations will be displaced. It will effect wetlands and the local ecosystem. The construction will consume large quantities of fuel while access roads will take the construction effects out of the planned route and into surrounding areas. Part of the nature of a long and high speed project like the one we are discussing is that its route is relatively inflexible. It is problematic to alter the course of the guide way by a mile here and there to avoid ecologically sensitive areas or any other obstacle. The guide way will create an artificial barrier that will interrupt the migration of wildlife. However, maglev has relative strengths in many of these areas.

A. Rights of way and the guide way

It has been widely proposed to construct maglev along the existing rights of way of highways and railways. Because both of these systems are designed for much lower operating speeds than maglev, the maglev system, out of necessity, will be forced to be as flexible in its route as possible to allow it to closely follow the existing corridor. A tight correlation between the two routes will help to limit the environmental impact of the maglev system by localizing its impact to areas where an impact has already been made and the path largely cleared.

Due to maglev's high rate of speed, many designs call for the guide way to be elevated or subterranean. Current proposals widely employ elevated guide ways, and evaluation of a subterranean system is not pursued. An elevated guide way has several advantages to an at-grade guide way,

and a few costs. An elevated system will foremost be a visual blemish on the local scenery, as is the case of high voltage power lines, forming an imposing object and obstructing views. As an advantage of elevation, the 'footprint' of the guide way will be less than that of an at-grade guide way, using less ground space and possibly reducing certain aspects of the construction cost. A long continuous object such as a highway is virtually impassable for all but the largest animals. Median fencing or 'New Jersey Barriers' create an impassable wall; effectively cutting off migration routes and separating populations. Animal populations are forced to develop new food sources when trapped in seasonal feeding grounds off season [19]. Maglev proposals indicate that the guide way will be significantly elevated, allowing unobstructed passage of animals below the guide way. It is not clear yet how the passage of high speed vehicles will effect local animal populations.

Maglev is most desirable in populated corridors where congestion is causing the consideration of further airport construction. The Dallas airport is 7.20×10^7 square meters, enough land to construct a maglev corridor 25 meters wide and 2881 kilometers in length. Typical maglev corridor lengths are 500 kilometers to 1300 kilometers in length, creating a significant saving in land over the construction of new high volume airfields. This saving is increased if maglev is constructed on existing rights of way using previously developed land.

B. The construction energy deficit

The construction of a maglev system will consume millions of liters of fuel to power construction machinery before any fuel is saved by the operation of a more efficient alternative to the automobile and airplane. This 'fuel cost' is known as the *energy deficit*, and the time required to pay it off will depend on local system characteristics

According to [20], approximately 106.253 liters of fuel and lubricants are consumed for every million dollars of highway construction cost. If we apply this to a maglev system that will cost roughly $6 million per kilometer, we find that maglev construction will cost about 637,500 liters of fuel per kilometer. Over a 300 kilometer route this is 190 million liters of fuel. This is only an estimate. The fuel per dollar figure that is used to calculate this is based on highway construction and not elevated structures such as maglev. These figures are only included to illustrate that the construction of a maglev system will incur a significant energy deficit that should be considered in an environmental or energy analysis of the system.

IV. Hypothetical Route Scenario

For illustration purposes, four corridors are selected and route analyses are conducted making some realistic but hypothetical assumptions. Boston - New York - Washington D.C., Houston - Dallas and Los Angeles - San Francisco are analyzed. Annual air passenger figures are taken from [10], and it is assumed from [21] that twice the air traffic will represent the ground traffic. The ground mileage is the shortest route along major roads and the air mileage is point to point. It is assumed that there is a 50% penetration into the air and auto markets. Given those assumptions, the remainder of the data is directly calculated from the EI data and emissions data and is contained in table 3.

TABLE 3
Data on fuel savings and emission savings for hypothetical scenarios.

		Boston N.Y.	N.Y. D.C.	Houston Dallas	L.A. San Fran.
Ground distance	km	370	377	386	611
Air distance	km	306	338	362	563
Air passengers	thousands	3830	3210	2180	2010
Auto passengers	thousands	7660	6420	4360	4020
EI, air	J / pass m	4107	3904	3774	2231
Air travel					
Saved energy	trillion J	826	768	550	1032
Saved fuel	million li	22	20	15	27
Base fuel consumption	million li	128	113	79	128
Saved fuel	%	17	18	18	21
Auto travel					
Saved energy	trillion J	665	568	395	576
Saved fuel	million li	19	16	11	17
Base fuel consumption	million li	220	188	130	190
Saved fuel	%	9	9	9	9
Saved emissions	million kg				
CO_2	air	102	96	71	101
	auto	213	182	126	184
CO	air	0.110	0.102	0.075	0.107
	auto	10.0	8.5	5.9	8.7
NOx	air	0.068	0.076	0.060	0.084
	auto	0.425	0.363	0.254	0.368
SOx	air	-0.351	-0.298	-0.207	-0.302
	auto	-0.709	-0.605	-0.421	-0.614
VOC	air	0.012	0.011	0.008	0.011
	auto	1.26	1.08	0.75	1.09
TSP	auto	-0.014	-0.012	-0.008	-0.012

V. Conclusions

This study suggests several conclusions. The construction of any new system will inherently have an adverse effect on the environment, and therefore solutions employing the existing infrastructure are naturally a more desirable alternative. However, typical systems are designed to fit in with the existing infrastructure, thereby limiting the potential environmental threat of its construction. The construction of a maglev system along existing rights of way will have substantial environmental benefits over selecting a new right of way, and should have much less of an impact than the construction of new airports and highways.

Once in operation, a maglev system should help to reduce congestion at airports and roadways. It should be capable of transporting people short distances at speeds comparable to airplanes, and with an EI similar to or better than an automobile. SO_x emissions will increase, but this will be offset by an overall reduction in emissions. The use of centralized power facilities should reduce the dependence on oil in the transportation sector, and will give transportation the flexibility to use alternative energy sources. The precise effect of a maglev system on the electric power supply situation will be locally dependent on the maglev system and the power utilities. Maglev's high energy intensity is largely the result of its operating speed. If the operating speed is reduced, the energy intensity will also reduce. Maglev has the potential for a positive environmental impact if it is thoughtfully integrated with the existing transportation infrastructure.

VI. Recommendations

For the maglev system to have the most environmentally beneficial impact as possible, it is recommended that while the system be designed for speeds of 134 meters per second or more, that operating speeds of 100 meters per second should be considered in the interest of reduced energy consumption and noise. The system should be constructed as much as possible along the existing rights of way of railroads and highways for reduced impact. Efforts should be made to thoughtfully integrate maglev with the local power grid for maximum efficiency. A further study should be conducted to evaluate the magnitude of the energy deficit that will be incurred during the system construction, and how it compares with the prospected energy savings during operation.

VII. References

1. Thornton, Richard, 1993, Professor, MIT, personal communication with, Mar.
2. Kelly, James, "National transportation statistics, annual report, 1990," U.S. Department of Transportation, 1990.
3. Brown, L., Flavin, C., Postel, S., *Saving the planet*, World Watch Publication, Norton press, 1991.
4. Harding, John, 1993, U.S. Department of Transportation, Federal Railroad Administration, Chief NMI Scientist, personal communication with, Mar.
5. Deutsch, Lowell, 1993, Grumman Corporation, personal correspondence with, Feb., Mar.
6. Perkowski, Joe, 1993, Bechtel Corporation, personal correspondence with, Feb., Mar.
7. Samavadam, Gopal, 1993, Foster - Miller Incorporated,, personal correspondence with, Feb.
8. Kolm, Henry, 1993, Magneplane International, personal correspondence with, Feb.
9. Energy Information Administration, "Electric power annual," U.S. Department of Energy, 1992.
10. Johnson, L.R., Rote, D.M., Hull, J.R., Coffey, H.T., Daley, J.G., Giese, R.F., "Maglev vehicles and superconductor technology: integration of high-speed ground transportation into the air travel system," Argonne national laboratory, 1989.
11. Newton, K., Steeds, W., Garrett, T.K., *The Motor Vehicle*, Butterworths, England, 1983.
12. Treager, Irwine, *Aircraft Gas Turbine Engine Technology*, McGraw-Hill, 1979.
13. Arnold, Tom, 1993, Environmental Attorney, Arnold & Kangas, P.C., personal communications with, Mar.
14. Gordon, Deborah, *Steering a New Course: Transportation, Energy, and the Environment*, Island Press, 1991.
15. National Research Council, *Rethinking the ozone problem in urban and regional air pollution*, National Academy Press, 1991.
16. Springer, G., Patterson, D., *Pollution Formation and Measurement*, Plenum Press, 1973.
17. Gran, Richard, "Benefits of magnetically levitated high speed transportation for the United States," *Magnetic Levitation Technology and Transportation Strategies, SP-834*, Society of Automotive Engineers, 1990, pg 1-10.
18. "EMF studies show HSR, maglev fields trail other sources," *Maglev News*, vol 1, no 7, pg 8,9, Jan. 1993.
19. Woolsey, Henry, 1993, Massachusetts State Natural Heritage Program, personal conversations with, Feb.
20. Larson, Thomas, "Highway statistics 1990," U.S. Department of Transportation.
21. Lynch, Thomas, "Energy-related, environmental, and economic benefits of Florida's high-speed rail and maglev systems proposals," *Transportation Research Record*, 1255, 1990 pg 122-138.

Safety evaluation test for electromagnetic levitation transport system H-100

Takeshi Mizuma Yasuhiro Sato
Traffic Safety Division, Traffic Safety and Nuisance Research Institute , MOT.
Mitaka-shi,Tokyo,Japan 181

Eisuke Masada
Department of Electrical Engineering , The University of Tokyo
Bunkyo-ku,Hongo,Japan 113

Abstract - This paper reports test results on the support and guidance system , the propulsion system ,electrical equipment system and etc. obtained from basic tests conducted for safety evaluation on the Nagoya test track with electromagnetic levitation vehicle H-100.

I . Introduction

H-100 transport system is one of the normal conducting magnetic levitation transportation system ,supported and guided by magnetic force and driven by linear induction motors . The maximum speed achieved by it's urban transit type is on the order of 100 km/h . Since May 1991, the transport system has been tested by Chubu HSST Development on the testing track at Ohe, Nagoya. As the Ministry of Transport of Japan needs to set up ministerial ordinances as technical standards on safety and reliability before this kind of system is put into practical use, it has organized the "Committee for Investigation and Examination of Technical Evaluation Methods for Normalconducting Magnetic Levitation Transport System " (Chaired by Professor Eisuke Masada of the University of Tokyo). Safety evaluation methods and testing methods are currently examined , while test results are analyzed at the same time for evaluating safety.

This paper reports some examinations of the safety evaluation technique and the test results on the support and guidance system , the propulsion system , the electrical equipment system and etc. obtained from basic tests conducted forsafety evaluation.

II . Method of Safety Evaluation

The procedure for examination to make H-100 system practicable as a public transport and is under consideration by the above mentioned committee is shown in Figure 1 .

As an example , an excerpt of readjusted essential conditions regarding the support and guidance system is indicated in Table 1 .

Then ,problems to be examined to satisfy the essential conditions are extracted , and followed by examination of [1] the point of evaluation at which one's eyes are directed to evaluate the above problems to be examined [2] method of technological evaluation , and [3] criteria for evaluation. After completion of the above procedure , matters to be confirmed in future will be readjusted , items to be tested and method of test will be determined , and evaluation through testing will be executed. An example of test items thus determined for the support and guidance system is shown in Table 2.

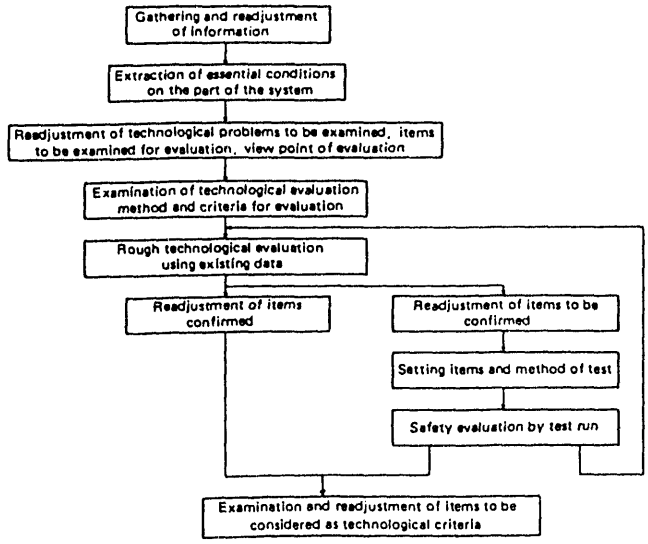

Fig. 1 Procedure of safety evaluation

III. Support and Guidance System

For the support and guidance system , the support force is obtained with the attraction between electromagnets and the rail , and the guidance force is obtained with restoring force. The running tests were conducted at up to the speed of 100 km/h on tracks including 100 m curve radius (100 mR) and 25 mR tracks. In order to evaluate the support and guidance gap , tolerance of the guidance gap , levitation force , and gap characteristics , measurements were taken on the levitation , guidance gap , levitation current. Figure 2

Table 1 Essential conditions regarding suspension and guidance system (extract)

(1) Regular operation (landing, standstill during floatation, propelling, braking)				
Essential conditions inside the suspension and guidance system				
	Conditions concerned in suspension and guidance	Hardware	(example)	Module is to be of construction that is capable of passing a section of track under prescribed condition without causing troubles under given load conditions and at a preset speed
		Control	(example)	Suspension control is to be capable of being performed maintaining levitation within preset range of fluctuations under prescribed conditions
	Condition concerned in riding quality	Train is capable of securing riding quality that will not give passengers unpleasant feeling by maintaining vibration acceleration within preset range under typical running condition.		
	Condition concerned in resistibility	To be capable of securing maintenance of operational functions to cope with incoming interfering electromagnetic waves, rails clogged with ice or snow, rust of rails, and expansion and contraction of track and rail, and so forth		
Essential conditions for other systems				
Inside the system	For propulsion system			
	For current collection system	(omitted)		
	For vehicle shell system			
	For signalling and safety system			
Exterior environment	Electromagnetic interference			
	Noise	(omitted)		
	Vibration			
(2) Abnormal operation (Failure of suspension and guidance system, earthquake, ice and snow, etc.)				
Securing safety				
	Rail and track system	Each of skid, rail, and track shall have sufficient strength for landing and running with skid and shall not cause derailment by running with skid		
	Module	Both the module itself and its part for fixing it shall have sufficient strength considering if contacting, absorbing, and falling should happen		
	Vehicle shell system	To be capable of with standing deceleration and impact generated when suspension system is in abnormal condition		
Safety control function				
	Process to come to a standstill	To be capable of landing with skid when train fails to operate		
	Changeover of failed part	To be capable of making quick response like detecting the failure immediately, switching to backup system, and cutting out failed part		
	Relation with other module	Failed magnet or module shall have no influence on the operation of sound magnet or module		

Table 2 Extract of prescribed test items for suspension and guidance system

1. Suspension and guidance system
(1) Confirmation of gap fluctuations for suspension and guidance
(2) Confirmation of lateral displacement of module and sliding skid
(3) Confirmation of riding quality and vibration acceleration
(4) Confirmation of suspension controllability when passing through rail joint, switch, and crossing
(5) Confirmation of detection performance of gap sensor and accelometer
(6) Confirmation of protective measures in case of failure
(7) Confirmation of nonreciprocal interference between suspension force and propulsion force
(8) Confirmation of suspension performance during power failure
(9) Confirmation of rail deformation by electromagnetic force for suspension
(10) Confirmation of the effect of electromagnetic noise on signalling and safety system
(11) Confirmation of strength and wear when the vehicle is sliding with skid

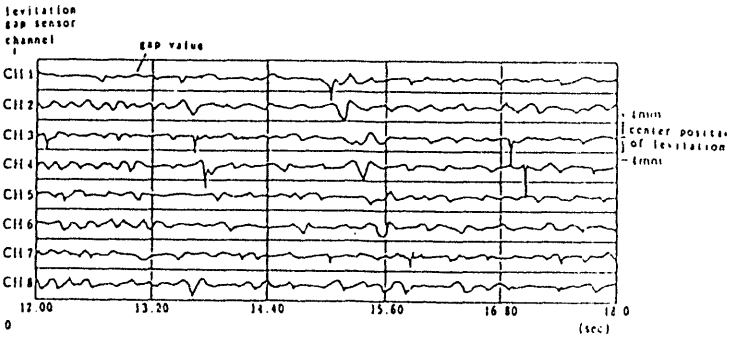

Fig.2 The levitation gap waveform at 100km/h running

shows levitation gap waveform measured during running test at 100 km/h .The following points were identified after the running tests on the straight track. 1) The levitation gap varied in proportionto the square root of the speed. 2) The maximum variation in the levitation gap was slightly larger with a full-loaded vehicle : approximately ± 3 mm with an empty-loaded vehicle against ± 4 mm with a full-loaded vehicle. There was still some room left against the maximum mechanical stroke of ± 6 mm , and the levitation gap was under control. 3) The maximum variation in the guidance gap was approximately 10mm with an empty-loaded vehicle , and 12 mm with a full-loaded vehicle . With some room left in the 15 mm maximum allowable variation , no contact was made between rail and guidance skids during the normal running. The guidance direction was also found under control.

Figure 3. shows the guidance gap waveform measured during the running on the 100 mR track. The following points were identified after the running test on the curved track.

1) The maximum variation in the guidance gap measured on the 100 mR track was slightly larger with a full-loaded vehicle : approximately ± 11 mm with an empty-loaded vehicle against ± 13 mm with a full-loaded vehicle.

2) The maximum variation in the guidance gap on the 25 mR curved track was approximately 31 mm with an empty-loaded vehicle , and 35 mm

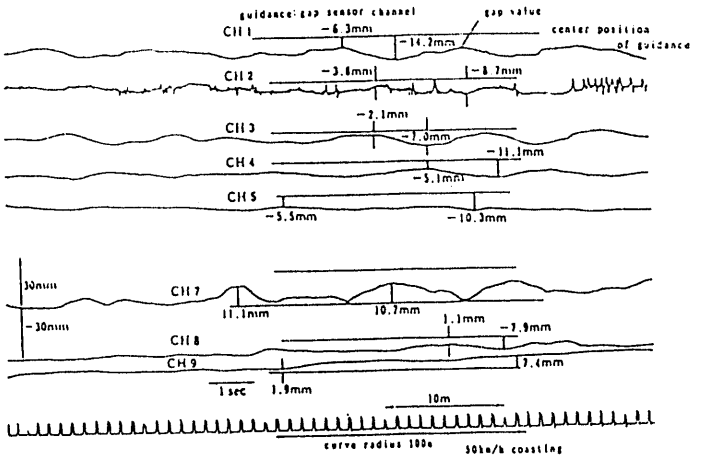

Fig.3 The guidance gap waveform of the curvature running at 100m radius

with a full-loaded vehicle. The figures deviated largely from the calculated 21 mm . Estimating the module-rail positions based on the measured gaps,the minimum possible gap between the guidance skids and rail is approximately 2 mm , and no contact should be made .

3) The maximum variation in the levitation gap measured on the curved track was approximately ±3mm , and the levitation gap was under control also on the curved track.

Summarizing all test results on support and guidance, including other support and guidance characteristic values measured at various experiment beams , turnouts or slopes , the levitation control is kept within the designed variation range , and it has been confirmed that there is no problem in obtain the levitation gap. As for the guidance control, the required force was confirmed , but the guidance gap was found greater than the calculated value on the 25 mR track , and the separation with the rail was sometimes narrowed . The contact, however, was made on the guidance skids, and no problem was found in achieving the strength. The remaining gap left for the contact has to be studied further.

IV. Propulsion System

The propulsion system applied here is one of the non-cohesion types obtained with linear induction motors . The test was designed primarily to check the braking performance at various speed levels up to 100 km/h, and the evaluation was made to check if the required deceleration rate was obtained while stopping the vehicle from high speed , if electric brakes and mechanical brakes operated in coordination , and if sufficient provisions were made against regeneration failure.

Figure 4 shows the waveform describing the

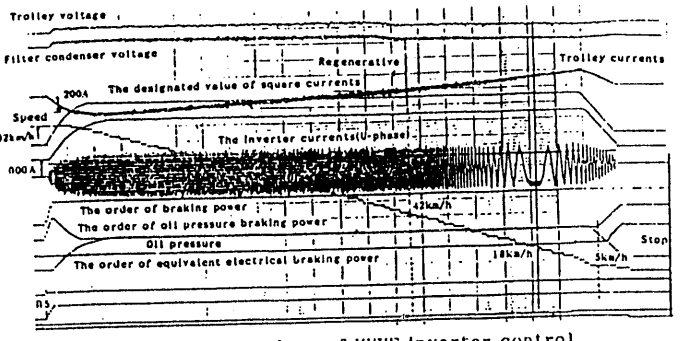

Fig.4 The waveform of VVVF inverter control in the regular braking at 100km/h

inverter control measured with the normal braking applied at 100 km/h . When the brakes were applied , if the designed electric brakes were provided, the mechanical brakes (driven by hydraulic) did not intervene (thus , not causing initial operation) , and the electric brakes provided all of the braking force all the way down to approximately 42 km/h as regenerative brakes, returning electric power to the contact line. It shifted to negative-phase brakes , when the vehicle reduced its speed below 18 km/h . The proportion of electric brakes was reduced below 5 km/h , applying the mechanical brakes to stop the vehicle in coordination of the both brakes. Furthermore, the following points were identified and confirmed in connection with the braking performance.

1) A failure of regeneration immediately triggered the mechanical brakes (with a few hundred seconds of delay) , without extending the braking distance greatly.

2) The electric brakes , when applied at a high speed, performed fairly constant deceleration rate, proving the braking function that was designed taking into consideration end effects.

3) Even when power failed (failure of power supplied from power substations) , the following sequence was confirmed : Electric brakes were activated within the speed range where regenerative electric currents returned into the power conduct line , and the emergency brake command was issued to apply mechanical brakes to stop the vehicle after the main circuit was cut off with the intervention of a low voltage detection device.

V. Electric Equipment System

Electric equipment for the magnetic levitation transportation system needs the following considerations :

1) Examining the capacity of equipment against regeneration failures as the magnetic levitation transportation system driven by the

linear motors makes the full use of the electric brakes.

2) Confirming if the protection devices works in the arranged ground system against line-to-ground fault.

3) Confirming that harmonics generated by the magnetic levitation transportation system should not be larger than that of the conventional railroad system.

Table 3 shows the braking time and ground fault currents at the time of ground fault with different ground system (of the substation). It has been confirmed that with any of these ground systems , the protection devices are activated to stop power supply at the substation after detecting ground failure.

Table 3 The braking time and the ground fault current

Grounded system		Braking time (ms)	Ground fault current
(-)High resistance ground system		61～65	(mA) 108～132
(-)Low resistance ground system		231～241	(A) 65～75
Resistance grounded neutral system	(+) Ground fault	386～444	(mA) 99～120
	(-) Ground fault	382～462	(mA) 106～132

Figure 5 shows the harmonic voltage distortion measured at the receiving end of the substation. According to this measurement , the difference of the voltage distortions found between without load and with the maximum currents (during power running) was only 3 % approximately , and the influence of harmonics generated by the vehicle running was small.

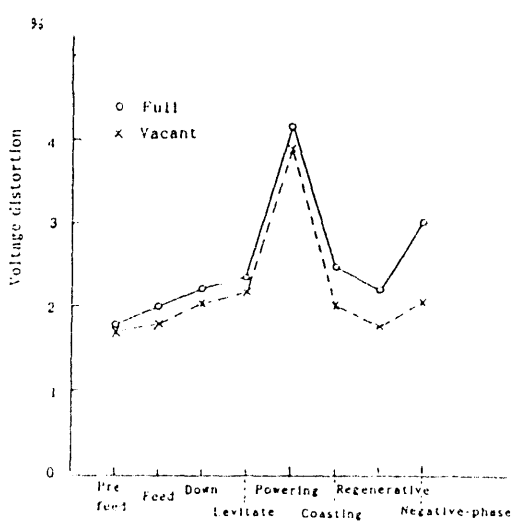

Fig. 5 The harmonic voltage distortion at the receiving end

Also , the resistance device switched by the chopper , installed as the regenerated power absorption device , was found effective if the voltage setting of switching was properly selected.

VI. Electric Power Consumption

The H-100 system, as the normal-conducting magnetic levitation transportation system, has various advantages derived from non-contact and non-cohesion characteristics. On the other hand , it has disadvantages in the electric power consumption due to the low efficiency caused by the linear induction motors, and due to the large quantity of auxiliary power required for continuous levitation controlled by the electromagnets.

Table 4 shows electric power consumption measured on the running pattern shown in the Figure 6. Compared with the conventional vehicle driven by the rotary induction motors with the VVVF inverter control, electric power consumption of the H-100 system is greater because of the higher auxiliary power requirement during coasting and low regenerative power . Compared with other new transportation systems (people mover) or monorail systems that employ rubber tires, however , electric power consumption per person required

Table 4 Measuring result of energy consumption

(Wh)

	powering	coasting	braking	
			regenerate	reverse
main circuit electric energy	3,298	- 27	- 236	218
PSU electric energy	299	517	210	
substation electric energy	4.2kWh	0.2kWh	0.2kWh	

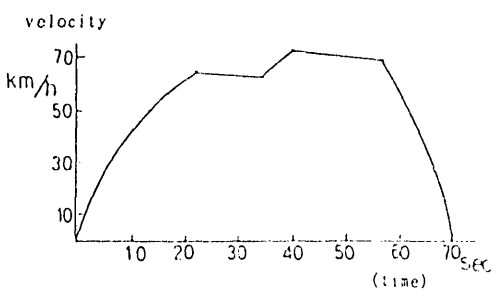

Fig. 6 The run curve for measuring energy consumption

for running is not expected to rise because (1) the weight of vehicle is lighter, (2) the time during the power running is shorter due to the low running resistance , and (3) the coasting time is longer due to the high acceleration and deceleration.

VII. Abnormal Vibration

The H-100 system uses chopper devices to control the electromagnetic currents for the levitation, and the VVVF inverter to control the propulsion with linear motors. The frequencies are different in the normal control range between the two , and they should not interfere each other . However, it has to be confirmed that abnormal vibration should be caused in relation with track system on the ground.

For the tests, (1) simulated speed signals were given while changing the inverter frequency, with the vehicle kept levitated still, to confirm that no vibration was made between the vehicle and the track (to check the possibility of resonance of the inverter frequency and the chopping frequency through the rail on the track) , and (2) with rail-fixing bolts loosened , the vehicle was levitated still and then driven, to check the possibility of resonance on the vehicle (relationship between the rail condition and the vehicle vibration).

Figure 7 shows the vertical vibration acceleration of modules with the bolts loosened when the vehicle was driven out of the levitated condition.

A various kinds of tests were conducted , and under some conditions , harmonics were found twice as much as the inverter frequency, superimposed on the vibration acceleration or levitation currents. Their absolute values , however , were very small and did not clearly appear as the vibration.

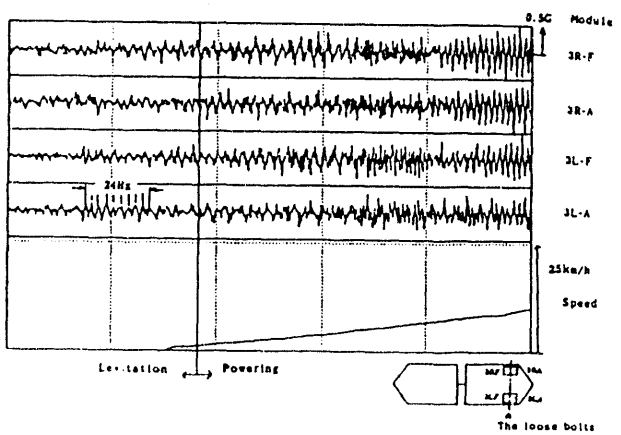

Fig.7 The vertical acceleration of each module on the rail with loose bolts

VIII. Conclusion

Some of the test results of the H-100 system obtained on the Nagoya test line have been presented in this paper. Basic safety factors such as the support and guidance system , propulsion system and electric equipment , have been proved fairly satisfactory . There remain some problems to be solved : guidance force and module behavior particularly on the sharp curve track (25 mR) , reduction of power consumption for propulsion , and improvements in the general riding quality. Furthermore , reliability and durability should be tested.

Then , overall safety and reliability of the H-100 system has been tested at the long-term running test now , in which safety against troubles and reliability and durability of the system are to be checked.

References

[1] Mizuma, et al. : Safety Evaluation Test of Model H-100 EMS Maglev Urban Transit System Japanese Railway Engineering August 1992, No. 120,pp6-10

[2] Mizuma,et al. : Safety evaluation test for electromagnetic levitation transportation system H-100 January 1993 , ISEM-Sapporo F-06 pp203

A Dynamic Computer Simulation of a High Speed Maglev Vehicle

Cam de Pierre
Advanced Programs, Hughes Aircraft Company, Fullerton, California

Abstract - The Maglev Performance Simulation (MPS) program is a computer simulation tool which provides performance assessment of high speed magnetically levitated transportation systems. Using MPS, a simulated maglev vehicle is made to traverse a hypothetical route. The performance of the vehicle, which is constrained by the comfort requirements of the passengers, the dynamics of the vehicle, the alignment of the route, and the desire to minimize energy costs is determined by the total trip time. Trip times for "standing" vs. "seat belted" comfort values are compared, then radii of curvatures are relaxed, and the trip times are compared with the initial route geometry. Speed vs. distance graphs are generated, illustrating speeds at different points in the route. Instantaneous propulsion power is provided in a power vs. distance graph and the total energy is calculated for the entire trip. A calculation is then made for the total energy consumption of a hypothetical maglev transportation system using 400 vehicles.

I. Introduction

The MPS program utilizes user defined inputs that characterize the alignment route and the maglev vehicle. The program allows flexibility in building any alignment route geometry and specifying a maglev vehicle with a wide variation of design parameters. The simulation process used was as follows. First, an alignment route geometry was defined in the program by inputting each geometrical segment making up the route. Second, the Linear Synchronous Motor (LSM) and the maglev vehicle were defined in the program by specifying a baseline set of characteristics. Third, ride comfort values were set to correspond to maximum limits for standing passengers and the simulation was run. Fourth, the ride comfort values were changed to correspond to maximum limits for seat belted passengers. A comparison of trip time was made between the two runs using standing and seat belted comfort values. Fifth, the standing ride comfort parameters were again used, but the radii of curvature for the route geometry were relaxed so that no radius of curvature was less than 1000 meters. A comparison was made with the original standing ride comfort values trip time. Sixth, the radii of curvature for the route geometry were relaxed so that no radius of curvature was less than 3000 meters and a comparison was again made with the original standing ride comfort values trip time. Seventh, the original alignment geometry and the standing ride comfort values were used to simulate the energy consumption of the LSM. Eighth, forward acceleration and braking limits were reduced to determine the net effect on the LSM energy consumption.

Manuscript received March 15, 1993. Work supported in part by National Maglev Initiative under contract DTFR 53-92-C-00003.

II. The Maglev System

The simulated maglev vehicle is approximately the size of a short range commercial jet and can carry over 100 passengers. The vehicle may traverse the guideway at speeds up to 134 meters per second (300 miles per hour) with a maximum banking angle of 45 degrees but must maintain the ride comfort values for either standing or seat belted passengers. The simulated maglev guideway uses a boxbeam design with an imbedded Linear Synchronous Motor (LSM). The LSM induces motion of the vehicle by reacting against the super-conducting magnets mounted on the vehicle. The levitation method is Electro-Dynamic Suspension (EDS) realized by repulsive forces between super-conducting magnets on the vehicle and embedded reaction coils in the guideway as the vehicle is moving. The speed of the vehicle is directly proportional to the frequency of the waveform impressed upon the LSM. The LSM is modeled in the simulation to provide limits on the vehicle dynamics, and to calculate energy expenditure.

III. The MPS Program

The Maglev Performance Simulation (MPS) is a modified version of the simulation program written by Professor J.E. Anderson and specifically redesigned for high speed maglev simulation. MPS permits the input of route data defined separately in the horizontal and vertical planes. These programs calculate the maximum speed through a curve given the maximum ride comfort values of acceleration and jerk. Curved guideways are obtained by solving numerically the second-order differential equations for yaw and pitch. For a plane curve, calculations are based on the exact solution of the differential equation of the curve. Combined vertical and horizontal curves cannot be solved exactly, so, the corresponding values for such a curve are determined by numerical solution of the differential equations for the space curve. Using the maximum speeds allowed through the curves and the power-limit of the LSM, as well as the comfort-limits on the passengers, the speed profile that will minimize the total trip time is determined. Using the characteristics of LSM and the aerodynamic and magnetic drag, as well as the dynamics of the vehicle, a power profile and the total energy to complete the route are determined.

(a) Route Alignment

A hypothetical route was constructed with a total curvilinear distance just under 800 kilometers, utilizing 52 horizontal and 52 vertical curves until 475 kilometers from terminal #1, at which point it is straight and level until reaching terminal #4.

The radii of curvatures are as small as 400 meters, and elevation grades are as high as 10%. There are two terminals at which the vehicle stops only momentarily in the simulation. Terminal #1 is where the vehicle starts from, terminal #2 is located 400 kilometers from terminal #1, terminal #3 is 470 kilometers from #1, and terminal #4 is where the vehicle ends its run.

(b) System Parameters

The system parameter inputs as shown in Table I allow the user to modify inputs for both the vehicle and the guideway [1]. Maximum Desired Cruise Speed, V_l, is the maximum allowable speed of the vehicle assuming ideal conditions. Vehicle Mass, M_v, is the total vehicle mass including passengers and baggage. Since the maglev vehicle is "flying" on a magnetic field, it is important to reduce the weight of the vehicle for efficient use of energy, in the same way that an airplane needs to be lightweight. Air Density, ρ, Drag Coefficient, C_d, and Frontal Area, A_f, are all used to calculate the aerodynamic drag resistance. The Width of Stator, W_s, is the width of the coil winding for the LSM. Pole Pairs per Vehicle, N_{pp}, refers to the number of super-conducting magnets on each sided of the vehicle that are synchronously linked to the excitation drive coils on the guideway. Air Gap Flux Density, B, is the magnetic inductance in webers per square meter (tesla). Magnetic Path Length of Vehicle, L_m, is the length from the first to the last super-conducting magnet. Length of Stator, L_S, is the length of the continuous magnetic drive coil attached to the guideway. Field Winding Pole Pitch, L_p, is the distance between magnetic poles of the LSM. R_L, L_{dm}, L_{qm}, L_L, R_f, L_f, and G_0, are all used for the calculation of power consumption for the LSM. The Number of Motors, N_m, is the number of LSM's. The Number of Phases, N_ϕ, indicates how many phases are in the LSM coil arrangement. Regeneration, fraction of output power, P_r, indicates what fraction of power used in magnetic braking is recovered back into the power grid. No regeneration capability was used in this simulation. Current Limit, I_l, puts a limit on the amount of current that can be supplied to the LSM. Total Volt-Amp (VI) Limit, P_l, gives the total available power at the source before multiplying by power factor.

(c) Ride Comfort Values

The ride comfort values given in Table II were used in the simulation. These are derived from the Department of Transportation's maximum allowable values for ride comfort for standing and seat belted passengers [2]. The "standing" ride comfort values are maximum allowed accelerations and jerks that standing passengers can tolerate. The "seat belted" ride comfort values are maximum allowed accelerations and jerks that seat belted passengers can tolerate.

Again, referring to Table II, the Total Banking Angle, ψ, indicates the maximum angle deviation of the passenger from level. Lateral Acceleration Limit, a_{ml}, is the sideways force on a passenger. Lateral Jerk Limit, j_{ml}, is the sideways rate of change of acceleration. Upward Acceleration Limit, a_{mu}, constrains the amount of "negative gravity" a passenger feels, and Downward Acceleration Limit, a_{md}, constrains the amount of "positive gravity" that the passenger feels. Vertical Jerk Limit, j_{mv}, prevents "bumpy" rides. Fore-Aft Acceleration Limit, a_{mf}, governs acceleration and deceleration of the vehicle. Fore-aft Jerk Limit, j_{mf}, governs the "smoothness" of acceleration and deceleration of the vehicle.

TABLE I
SYSTEM INPUT PARAMETERS

Maximum Desired Cruise Speed	V_l	m/s
Vehicle Mass	M_v	kg
Air Density	ρ	kg/m^3
Drag Coefficient	C_d	
Frontal Area	A_f	m^2
Maximum Grade	m_l	%
Width of Stator	W_s	m
Pole Pairs per Vehicle	N_{pp}	
Air Gap Flux Density	B	tesla
Magnetic Path Length of Vehicle	L_m	m
Length of Stator	L_s	m
Field Winding Pole Pitch	L_p	m
LSM Block Length Resistance	R_L	Ω
LSM Direct Magnetization Inductance	L_{md}	henries
LSM Quadrature Axis Magnet. Inductance	L_{qm}	henries
Block Length Inductance-no field	LL	henries
Resistance of Feeder Cable	R_f	Ω
Inductance of Feeder Cable	L_f	henries
Angle Between Current and Voltage	G_0	degrees
Number of Motors	N_m	
Number of Phases	N_ϕ	
Regeneration, fraction of output power	P_r	
Current Limit	I_l	amperes
Total Volt-Amp Limit	P_l	MVA

(d) Determination of Maximum Speed through Curves

Since a combined horizontal and vertical curve does not have an exact solution, it is necessary to split up the guideway curve into horizontal and vertical inputs, compute on the horizontal and vertical inputs separately, and then sort them together as a function of arc length. Each horizontal curve in the simulation is made up of a spiral section going into the curve, a constant curvature section, and another spiral section going out of the curve. The speed of the vehicle is constant as it transitions the curve. The spiral section of the curve is

TABLE II
RIDE COMFORT VALUES

		Standing	Seat Belted
Total Banking Angle	ψ	30 °	45 °
Lateral Accel. Limit	a_{ml}	0.16 g's	0.20 g's
Lateral Jerk Limit	j_{ml}	0.25 g's/sec	0.25 g's/sec
Upward Accel. Limit	a_{mu}	0.10 g's	0.10 g's
Downward Acc. Limit	a_{md}	0.30 g's	0.40 g's
Vertical Jerk Limit	j_{mv}	0.3 g's/sec	0.30 g's/sec
Fore-Aft Accel. Limit	a_{mf}	0.20 g's	0.6 g's
Fore-aft Jerk Limit	j_{mf}	0.25 g's/sec	0.25 g's/sec

constructed by the MPS to maintain a constant jerk. It can be shown analytically that the constant curvature section limits the speed of transition rather than the spiral section of the curve [4,5]. Thus maximum speed through the curve is given by

$$V_c = (a_{ml} R)^{1/2} \quad (1)$$

where a_{ml} is the comfort lateral acceleration, and R is the radius of curvature for the constant curvature section. If V_c exceeds the maximum allowable cruise speed, V_l then V_c is set to V_l. The vertical plane curves are similar to the horizontal curves, except that vertical offsets are much less than the horizontal offsets. Equation (1) can be used for maximum speed through vertical curves except that a_{mu} or a_{md} is substituted for a_{ml}, where a_{mu} is the comfort acceleration in the up vertical direction, and a_{md} is the comfort acceleration in the down vertical direction. Again, the speed of the vehicle is assumed to be constant through the curve, and the spiral transition part of the curve is assumed to maintain a constant jerk. If V_c exceeds the maximum allowable speed, V_l, then V_c is set to V_l.

IV. Maglev Performance

Performance is determined by total trip time and total energy to complete the route. Trip times were compared using "standing" vs. "seated belted" ride comfort values for the simulation run. Next, trip times were compared between the original route and relaxed radii of curvature routes using "standing" ride comfort values. Energy consumption for a run was compared as a function of decreasing acceleration and braking limits.

(a) Trip Times

The trip times (and average speeds) for "standing" and "seat belted" ride comfort values to travel from station #1 to station #4 on the route are given in Table III. Trip time is the total time interval to traverse the route. The trip time for seat belted passengers was reduced by 12% when compared to standing passengers. Since about half the route had no curves that effected trip time, the reduction in trip time considering only the curved sections of the route would be 24%, which is a substantial reduction.

(b) Vehicle Speed Profiles

Figures 1 and 2 show the vehicle speed vs. distance profile for "standing" and "seat belted" ride comfort values, respectively. These speed profiles give the instantaneous speed vs. distance of the vehicle for a given distance increment. Many of the curves that required slowing down in Fig. 1 were negotiated at maximum speed in Fig. 2. This accounts for the savings of 24% in trip time for the curved sections of the route.

(c) Radii of Curvature Relaxation

Two simulations were run after making the radii of curvature not less than 1000 meters and not less than 3000 meters, respectively. Table IV shows the total trip time for the redesigned routes compared to the initial route. Both

TABLE III
TRIP TIME COMPARISON

	Standing	Seat Belted
Total Trip Time	1h 59m 02s 7142 seconds	1h 45m 15s 6315 seconds
Average Speed	111.8 m/sec (250 mi/hr)	127 m/sec (284 mi/hr)
Trip Time Difference		13m 47s Faster
Average Speed Difference		15.2 m/sec Faster (34 mi/hr Faster)

initial and redesigned routes used the "standing" ride comfort values. Fig. 3 shows the speed profile of this new route for radii of curvature not less than 1000 meters. Fig. 4 shows the speed profile for radii of curvature not less than 3000 meters. Relaxing the radii of curvature to not less than 1000 meters gave a trip time reduction of 2.6%. Doubling this would give the trip time reduction for the curved sections, or 5.2%. Relaxing the radii of curvature even more to not less than 3000 meters gave a trip time reduction of 14.2%, or 28.4% for the curved sections alone. Thus, if radii of curvature relaxation is to be done, it is very advantageous to go to not less than 3000 meters, in terms of trip time reduction.

(d) Instantaneous Power

Fig. 1 shows the power profile for the vehicle from zero to 800 kilometers using the "standing" ride comfort values and the initial alignment route. The left y-axis scale is for the upper curve representing speed, and the right y-axis scale is for the lower curve representing instantaneous power. Note that the maximum required power for the vehicle was about 26 megawatts, even though the average required power per vehicle was only about 9.7 megawatts. The average was much lower than the 26 megawatts peak because very little or no power is used when slowing down to negotiate the next curve in the route. The vehicle coasts through a significant portion of the route making the overall average required power significantly less than the maximum peak power required. During the first 400 kilometers (the portion containing most of the curves) about 10.5 megawatts average power was required, whereas in the second 400 kilometers (mostly straight and level) it was 8.4 megawatts. Thus it can be seen that the actual power requirements do not vary much (about 20%) between a route with many tight curves, and a straight and level route, however, a price is paid in terms of reduced trip time for the route of many curves.

TABLE IV
REDESIGNED ROUTE ALIGNMENT TRIP TIME

	Original Alignment	No Radii of Curvature less than 1000 m	No Radii of Curvature less than 3000 m
Total Trip Time	1h 59m 02s 7142 secs	1h 55m 55s 6955 secs	1h 42m 09s 6129 secs
Average Speed	111.8 m/s (250 mi/hr)	114.8 m/s (256.6 mi/hr)	130.3 m/s (291.3 mi/hr)
Δ Time		3m 07s	16m 53s
Δ Speed		3 m/s (6.6 mi/hr)	18.5 m/s (41.3 mi/hr)

(e) Energy Demand for One Vehicle

The energy consumption for one vehicle to traverse the route in the forward direction from Terminal 1 to Terminal 4 is given in Table V. The energy required using the "standing" ride comfort values for acceleration and braking is indicated in the top row. The succeeding rows of the table show the energy requirements as the acceleration and braking values are reduced. The energy reduction from using an acceleration limit of 0.2g's and a braking limit of 0.2g's to using an acceleration limit of 0.16g's and a braking limit of 0.16g's amounts to a reduction of only about 5%. For the curved sections only, this would double, giving a reduction of about 10%.

(f) Energy Demand for 400 Vehicles

A full up system with a vehicle every 4 km in the 800 kilometer hypothetical route would require 200 vehicles one way, or 400 vehicle both ways. The total average demand power will be the average power per vehicle times the number of vehicles. If vehicle power usage is randomly distributed along the route, it would suffice to specify a power supply requirement that is three standard deviations greater than this total average demand power. For n independent data sets all with the same standard deviation, the standard deviation of the sum of the elements of all the sets is equal to the standard deviation of one set times the square root of n. For the simulated route with one vehicle, the power mean was 9.7 megawatts with a standard deviation of 7.8 megawatts. The total power required for a system of 400 vehicles would be 3880 megawatts with a standard deviation of 156 megawatts. Three standard deviations equals 468 megawatts and represents a reserve power requirement of 12%. Thus, for 400 vehicles the total energy required would be 3,880 megawatts (9.7 megawatts per vehicle) plus 468 megawatts (3 standard deviations), or a total maximum of 4348 megawatts. This is equivalent to the output of 2 or 3 average sized power generating stations, an average station producing between one and two thousand megawatts.

V. Conclusions

For the first half of the route containing the curved sections, seat belted passengers had a 24% reduction in trip time over standing passengers and radii of curvature not less than 3000 meters had a 28% reduction in trip time over the original alignment. Requiring both seat belted passengers and not less than 3000 meters radii of curvature will significantly reduce trip times on route alignments that contain many curves. Power requirements varied only about 20% between the first half of the route with many tight curves and the second half which was straight and level, but a price was paid in terms of reduced trip time for the first half. A four hundred vehicle fleet required a total of 4348 megawatts, 13% of which represents power reserve.

TABLE V
TOTAL ENERGY PER VEHICLE PER TRIP

Acceleration Limit	Braking Limit	Energy Required
0.20 g	0.20 g	69,984 megajoules (19,440 kWh)
0.16 g	0.20 g	69,253 megajoules (19,237 kWh)
0.20 g	0.16 g	66,838 megajoules (18,566 kWh)
0.16 g	0.16 g	66,153 megajoules (18,376 kWh)

References

[1] S. Brown, C. R. Dauwalter, F. Heger and M. Weinberg, "Final report, comparison of major parameters in electrodynamic and electromagnetic levitation transportation systems", (Maglev BAA #24), , Report R-2420, Charles S. Draper Laboratory, Inc., September, 1992.

[2] Peplar, R.D., et al, "Development of techniques and data for evaluating ride quality, Vol. II: Ride Quality Research," Report No. DOT-TSC-RSPD-77-1,II.

[3] "Guide for the Evaluation of Human Exposure to Wholebody Vibration," ISO Standard 2631/1 , International Organization for Standardization, 1985.

[4] Anderson, J.E., Geometry of curved PRT guideways, unpublished paper.

[5] Anderson, J.E., Transit System Theory, Lexington Books, D.C. Heath, 1978.

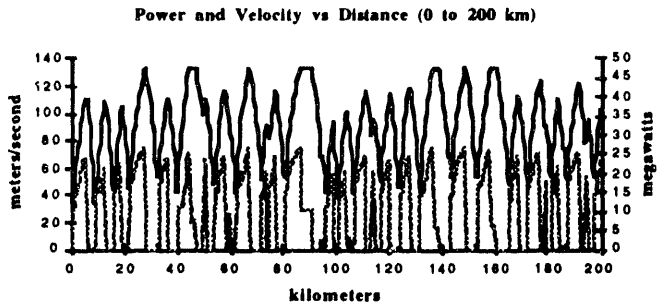

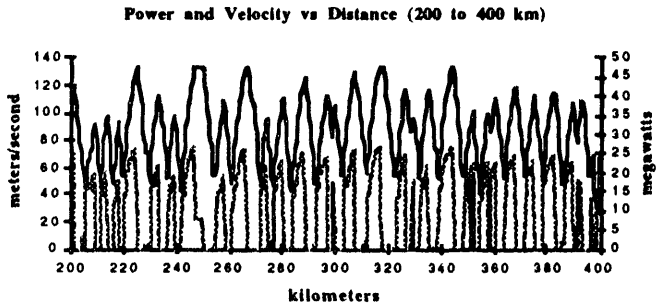

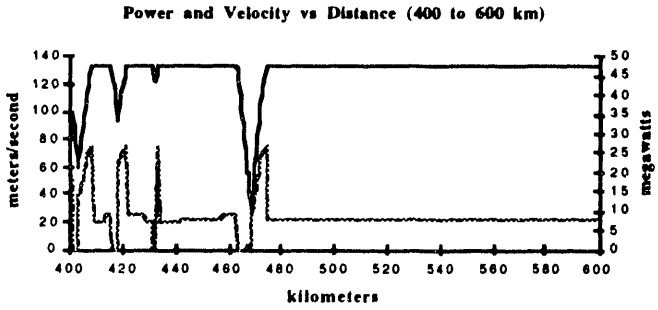

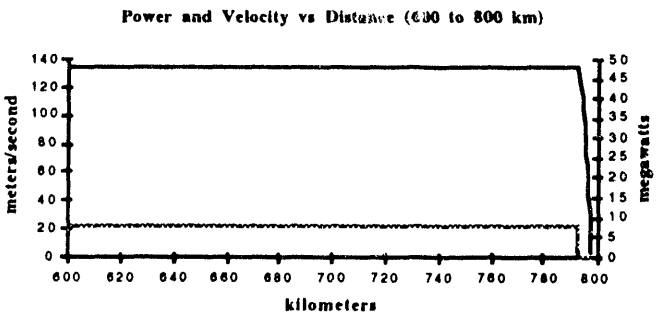

Fig. 1 "Standing" Ride Comfort Values

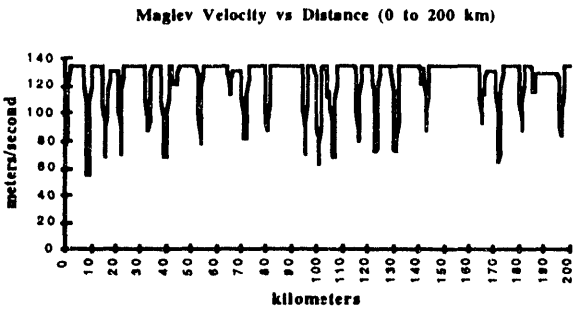

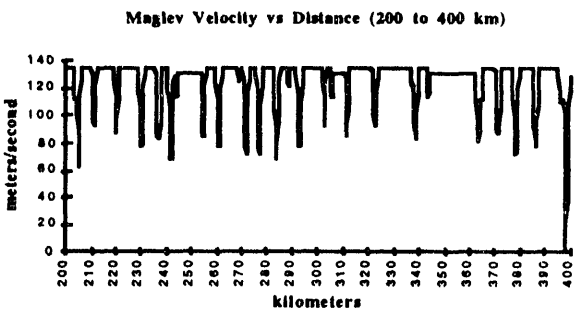

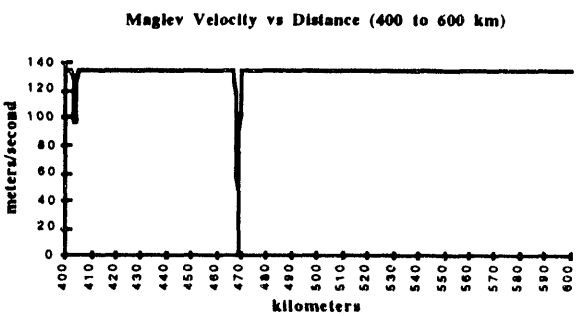

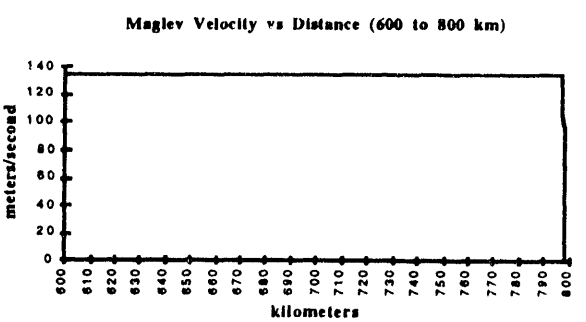

Fig. 2 "Seat Belted" Ride Comfort Values

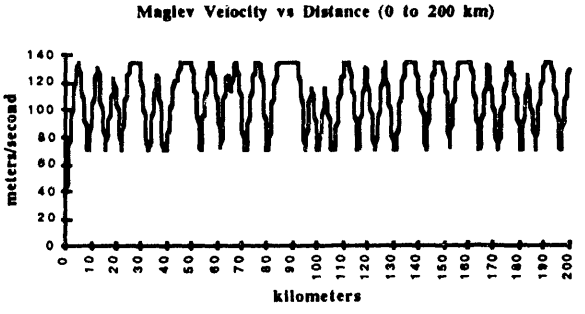

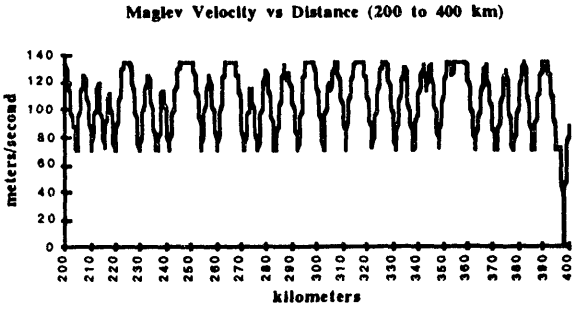

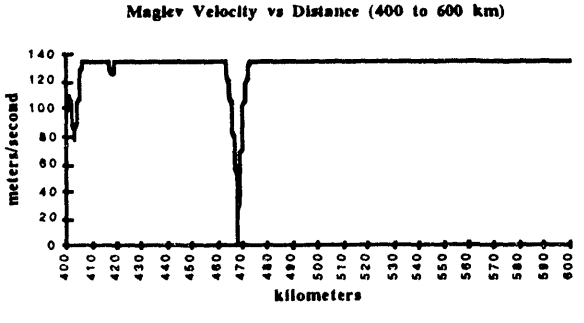

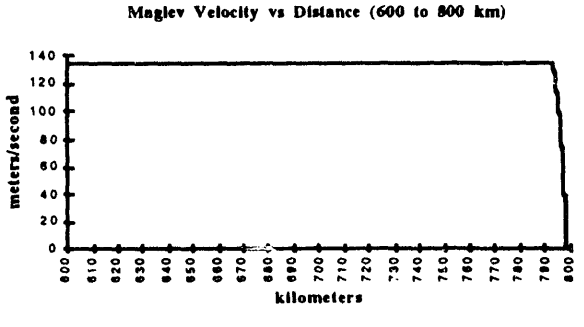

Fig. 3 No Radii Less Than 1000 Meters

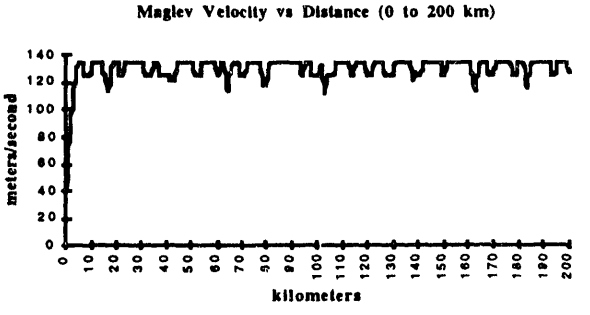

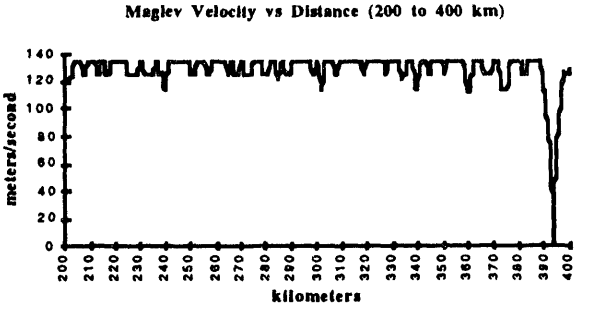

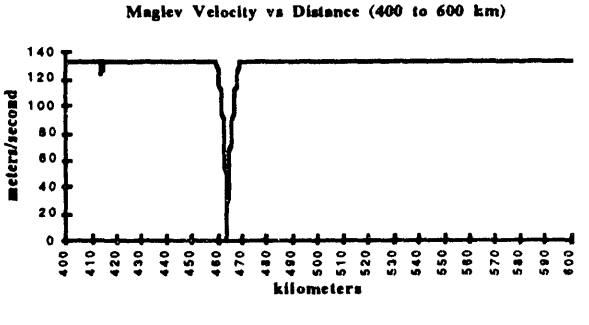

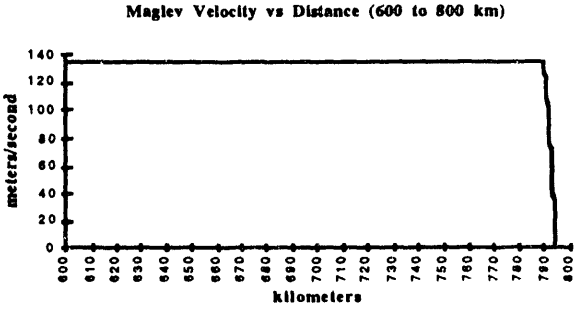

Fig. 4 No Radii Less Than 3000 Meters

Maglev Automated Preventive Maintenance System

Joseph S. Ng
Arthur L. Harris
Maurice E. Amoon

Product Support Division
Aerospace and Defense Sector
Hughes Aircraft Company, Fullerton, CA 92634

Abstract - When maglev technology is implemented, it must not only be operationally efficient and safe, but it must also be reliable and cost competitive to operate and maintain. Unexpected failures and high maintenance costs must be minimized.

This paper describes a system concept for an automated preventive maintenance system that provides predictions of degraded performance and imminent failures based on closely monitoring key system parameters. Data collected and monitored on each train are relayed to receivers at each station as the train passes through. This information is then analyzed at a central maintenance monitoring and control facility, and provides notification by alerts or warnings of impending failures in near real time to the trains. The maintenance control facility can also electronically provide diagnostic and technical manual information and instructional procedures to maintenance users throughout the system.

The system described provides an effective maintenance management system for the maglev train and minimizes maintenance costs as well as increasing system availability and sustaining maximum ridership.

I. Introduction

Maglev train systems offer the potential to be one of the key elements in the development of a new network of ground transportation systems. When implemented, this technology must not only be operationally efficient and safe, but it must also be reliable and cost competitive to operate and maintain. Operation and maintenance costs are the major elements in the life cycle cost of transportation systems including the maglev train. To maximize system availability and to ensure safe operation, vehicles are maintained on a predetermined schedule. Major components are replaced or overhauled at the projected limit of their projected service life. In some cases the projected life of a component may be far shorter than the actual service life. This method of maintenance results in premature replacement of serviceable parts and increases maintenance costs. On the other hand, from time to time a component may fail before it's projected life. This results in a catastrophic failure with service interruption, unscheduled maintenance and the potential for an impact on system safety.

To improve the cost effectiveness and reliability of the maglev train system, a maintenance concept must be developed to reduce or eliminate unscheduled maintenance, catastrophic failures and to maximize the useful life of the major components.

The Automated Preventive Maintenance System(APMS) is a state of art fault prediction and diagnostic system. APMS allows transportation systems such as the maglev train, conventional trains, trucks, and busses, to continuously monitor their operational status and predict failures in time to avoid costly unscheduled maintenance. The major benefits of APMS are to:

- Continuously monitor vehicle performance and provide status to a centralized maintenance support center.
- Limit or eliminate the number of catastrophic failures thereby minimizing service interruptions.
- Significantly improve the safety of the system.
- Predict failures before they occur.
- Minimize maintenance labor by only performing scheduled, just-in-time maintenance.
- Limit or eliminate down time.
- Provide real time or near real time readiness status of all vehicles.
- Provide a cost effective solution to system maintenance management.
- Minimize unnecessary replacement by permitting major components to be used to the limit of their useful life.
- Reduce the total number of trains required because of the higher availability of system assets, i.e., fewer spare vehicles.
- Reduce the requirement for special test equipment because of the extensive use of built in test and status monitoring systems.

II. System Architecture Requirements

The system design of the maglev automated preventive maintenance system must be tailored to the design of the maglev train. All functions critical to the safe and efficient operation of the maglev train must be identified and sensors installed and integrated to provide real time monitoring. The data from these sensors are then collected, stored, formatted and transmitted to a central facility for near real time analysis. Safety alerts and critical condition feedback to the trains is provided. All components of the system will provide accurate data in a reliable, cost effective manner. The system will provide a modular, flexible environment to allow expansion and reconfiguration as required, and be fully

integrated with the maglev command and control environment to be fully effective. The integrated communication system must have the capability to operate reliably in an electromagnetic environment and require no special licenses.

III. Architecture Overview

The APMS consists of three major sub-systems. They include the Status Monitor and Diagnostic Units, Network Status Interface Units and Maintenance Control Center as shown in Fig. 1.

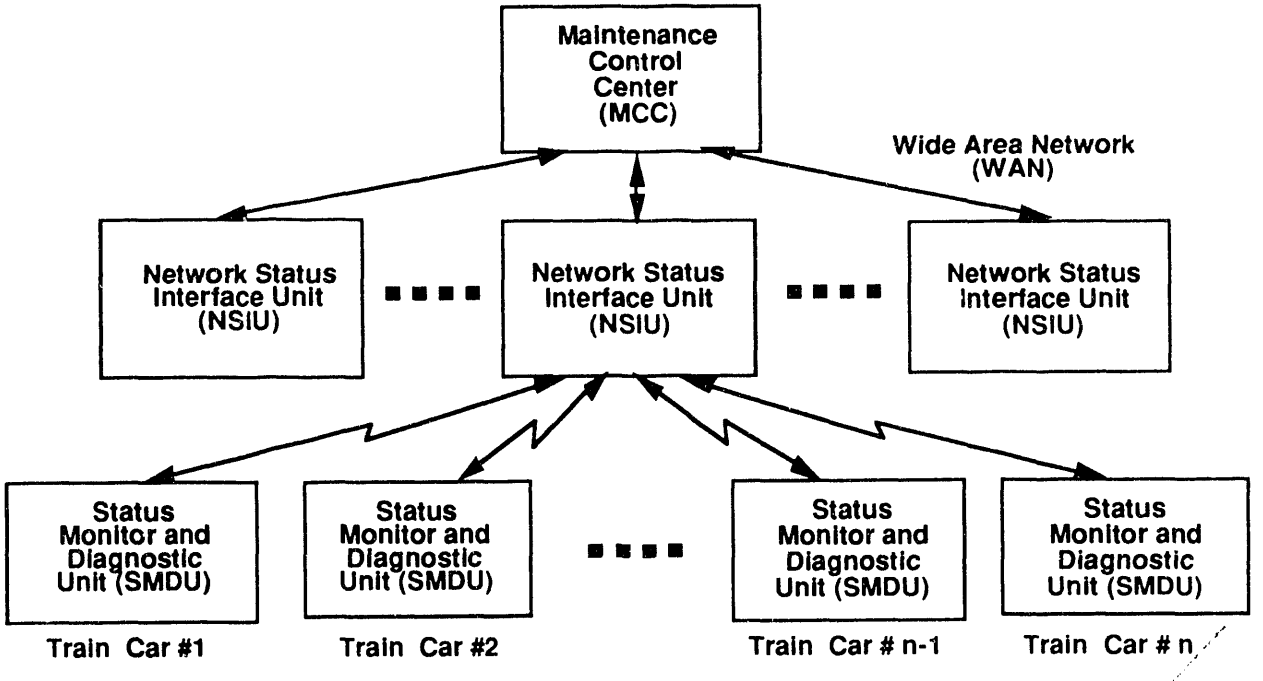

Figure 1. Automated Preventive Maintenance System Block Diagram

Network Status Interface Unit (NSIU) - The function of the NSIU is to communicate with the train mounted SMDU when the train is passing through the station or past a fixed monitoring location. The status information received from the train is forwarded to the MCC via a wide area network (WAN) for processing. If a message for a unique train address is sent from the MCC over the WAN, an NSIU will transmit that message to the train as it passes through stations.

Maintenance Control Center (MCC) - The MCC is the control center for the APMS system. By analyzing status and maintenance related data gathered from trains, the MCC prognostics processor determines the operational condition of the trains and automatically alerts the appropriate operation and maintenance crews that a repair activity is required and provides them with the pertinent data to facilitate the repair. The MCC also provides a maintenance support interface to the maglev train command and control system to ensure the current maintenance status is available to operations personnel. Additionally, the MCC provides a centralized repository for all maintenance related functions including a centralized diagnostic expert system, maintenance technical data manager, spares manager and maintenance scheduler.

Status Monitor and Diagnostic Unit (SMDU) - The SMDU is a vehicle mounted, microcomputer based monitoring subsystem. Included in this sub-system are sensors for vibration, acoustics, environmental conditions and analog and digital signals. The sensor data is processed and formatted by the microcomputer and stored in memory. A spread spectrum telemetry transceiver is interfaced to the microcomputer. When the vehicle passes through the station, the telemetry transceiver transmits the formatted SMDU data to the station equipment. The SMDU can also receive commands and/or message from the station equipment to control the vehicle or display messages to the operator.

IV. Status Monitor and Diagnostic Unit

The SMDU as shown in Fig. 2 monitors the condition of all maglev train systems and transmits the status data to the NSIU as the train passes through the station or other designated communication interface points. The SMDU provides monitoring coverage for propulsion, guidance, suspension, cryogenics, levitation, braking and all electronic controllers. Sensors are used to monitor the acoustic signature of critical train subsystems. Noise monitoring

technology utilizing digital signal processing is applied to detect abnormal sounds which might indicate a developing failure. The acoustic subsystem is built on expertise developed on underwater sonar signal analysis. Included are data sensors for vibration, shock, temperature and humidity which can be used to correlate intermittent malfunctions with the environmental conditions at the time of failure. Additionally, all recorded data are time and track position tagged to aid in evaluating operation.

A special version of SMDU will be used to monitor fixed resources such as power systems, controllers, switches, electronics and station equipment. These SMDUs will relay information to adjacent NSIUs over telephone lines or cellular phone connections.

All SMDUs will contain self test functions to ensure that reliable status data is transmitted to the MCC. Each car of the train and designated fixed resource will be equipped with an SMDU. Each SMDU will have its own unique identification address code. To minimize the possibility of interference, the SMDU transceiver utilizes spread spectrum communication technology to interface with the NSIUs.

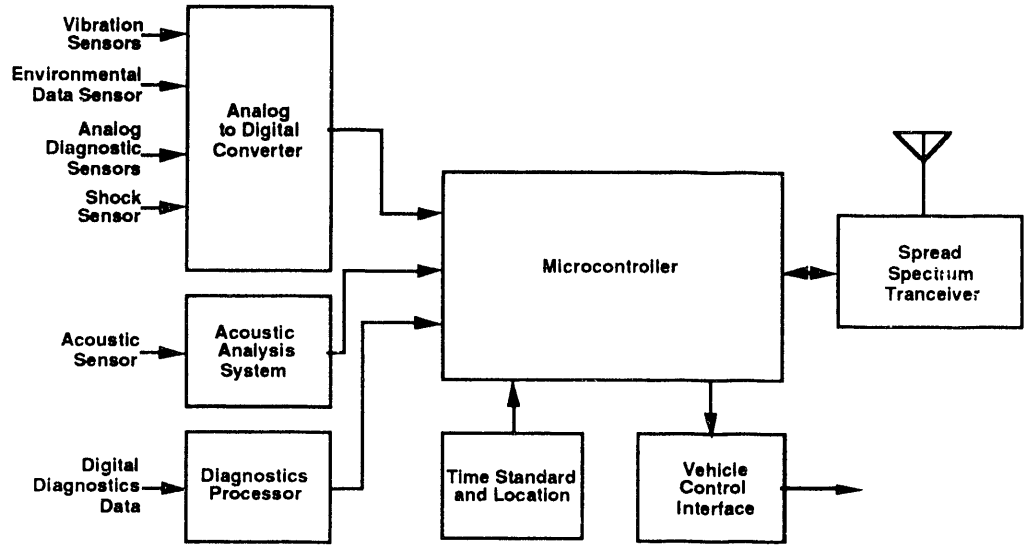

Figure 2. Status Monitor Diagnostic Unit Block Diagram

V. Network Status Interface Unit

The NSIU as shown in Fig. 3 is the communication interface to the train's SMDUs. The NSIUs are located in each station and at other designated points where communications with the trains are required. The NSIU's provide a two way interface to the MCC by transmitting monitored data to the MCC and receiving alert data from the MCC for retransmission to the maglev trains. The communication mode to the SMDUs will be accomplished via low power spread spectrum time-division-multiple-access (TDMA) technology devices. This mode provides secure, reliable communications and immunity from interference and does not require an FCC license. Communications with the MCC will be through the APMS via a wide area network.

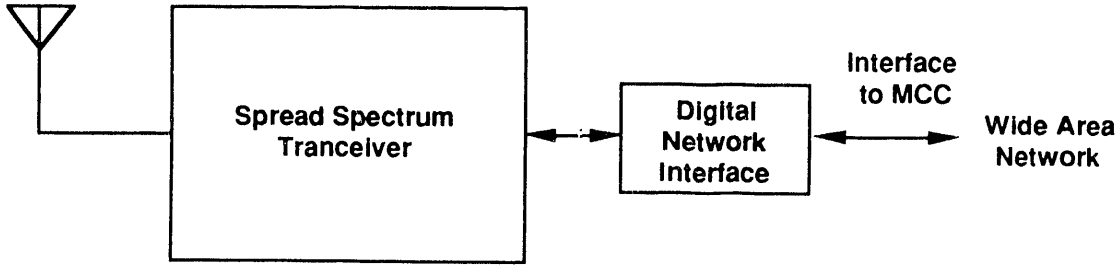

Figure 3. The Network Status Interface Unit (NSIU)

VI. Maintenance Control Center

The MCC as shown in Fig. 4 controls the operation of the maglev APMS. The hardware consists of an off-the-shelf computer interfaced to the maglev NSIU's, maintenance facility, and command and control system. The MCC software provides the following functionality:

- Status Monitor
- Prognostics Processor
- Diagnostic Expert System
- Interactive Technical Data Manager
- Spares Manager
- Maintenance Scheduler

Status Monitor- Through the APMS wide area network, the status monitor receives and stores all monitored train equipment operational status parameters from the SMDUs. All train and fixed resource failures are correlated to equipment serial number. A display of equipment status is provided for the on-duty maintenance manager. The status is continually updated and sent to the prognostics processor and maglev command and control system. The status monitor also controls all communications within the APMS.

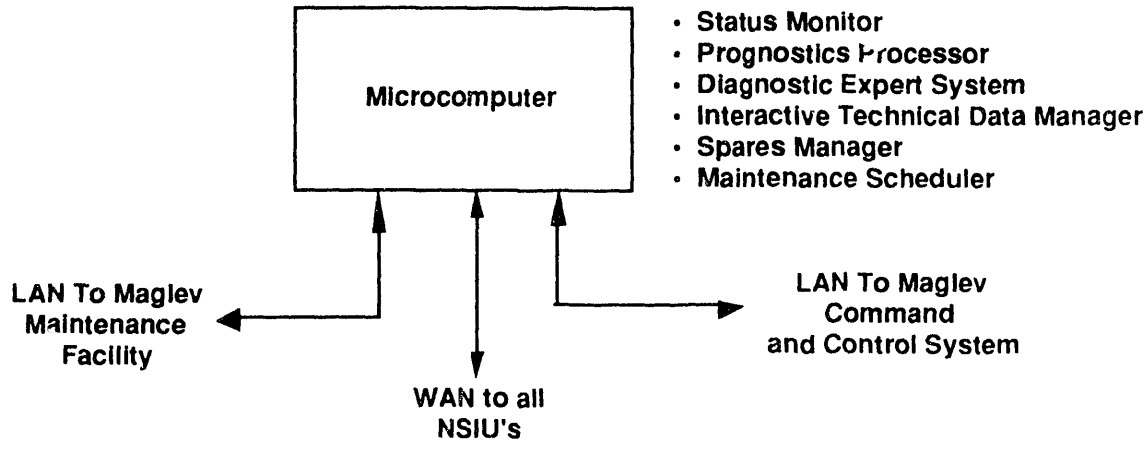

Figure 4. Maintenance Control Center

Prognostics processor-The prognostics processor's function is to predict expected failures in time to take corrective action to prevent them from becoming an operational problem. This is accomplished by continuously comparing baseline data signatures to collected near real time data over time. Robust statistical trending algorithms are used to analyze failures in all subsystems where degradation of performance can be followed. Acoustical analysis built on experience with underwater sonar systems and trend analysis on spectral data is used to predict failures that may have an acoustical signature. Vibration monitoring using background noise cancellation and digital signal processing techniques is used to detect changes indicating an imminent failure. Since false alarms can destroy confidence in the system as well as increase cost of operation, all predictions are verified by alternate methods as well as inserting operations and maintenance personnel for confirmation if possible.

Diagnostics Expert System-The diagnostic expert system provides an on-line troubleshooting capability for maintenance personnel throughout the maglev system. Maintenance personnel can access the expert level troubleshooting knowledge base from throughout the APMS by using a portable computer display or a data display on the equipment. The diagnostic expert system uses second generation artificial intelligence technology to provide assistance to the maintenance technician. A functional model of normal system operation is stored in the knowledge base and the inference engine (reasoning mechanism) generates an interactive procedure to verify correct operation. The maintenance personnel perform the tests and compare the results with data contained in the model to determine correct operation. The diagnostic expert system allows journeyman maintenance personnel to perform as well as experts to keep the trains running.

Interactive Technical Data Manager- The interactive technical data manager provides access to maglev technical data throughout the train system. The technical data is stored on a file server at the MCC and can be accessed at all maintenance locations as required. This approach streamlines the maintenance process by eliminating bulky technical manuals and ensures that up-to-date documentation is available throughout the system. Maintaining the data base is also much easier and more efficient than maintaining paper documentation because a change need only be entered

at the file server. The interactive technical data manager uses hypertext/hypermedia display techniques to achieve an interactive display-on-demand information system. Access to and navigation through the maintenance data is rapid and efficient.

Spares Manager - This function provides a tool for the effective management of maintenance spares. It allows maintenance personnel to fully control and report on the status of equipment, parts and supplies used in the maintenance of the maglev train system. It can provide spares usage reports including cost and flags major parts usage for analysis. Also provided are physical inventory checklists, parts on order status, equipment and parts cross references as well as identifying equipment using a specific part. The inclusion of the spares manager provides for the complete integration of all maintenance related functions at the MCC.

Maintenance Scheduler - The maintenance scheduler provides a tool for efficiently managing and coordinating maglev train maintenance personnel as well as providing reports on failure trends. It allows maintenance to be planned rather than constantly dealing with unexpected events. It has been shown that unplanned maintenance actions cost many times more than scheduled maintenance so a substantial cost savings can be realized by using this function at the MCC. The maintenance scheduler also provides a graphical display of failure trends so that detailed analysis can be performed. System status reports to management on repair costs, history, parts usage, maintenance distribution, downtime, catastrophic failures, and trends can also be generated.

VII. Summary

The maglev train requires an effective maintenance management system that minimizes operation and maintenance costs, and improves system availability. The automated preventive maintenance system (APMS) satisfies this requirement by anticipating failures and providing maintenance personnel with the information needed to repair them. APMS uses prognostics, artificial intelligence diagnostics, and electronic information delivery technology to provide an efficient maintenance management and aiding system. Maintenance personnel will require minimal formal training and their proficiency will be greatly improved through the use of these technologies. Special support equipment requirements will be greatly reduced, if not eliminated, because status monitoring and built-in-test diagnostics and maintenance data will be embedded in the maglev train system. Overall, system availability will be maximized and all repairs will be performed on a scheduled basis. Through implementation of APMS, the necessity of removing vehicles for unscheduled maintenance will be eliminated.

USING EXISTING INFRASTRUCTURE TO MAKE MAGLEV WORK IN THE UNITED STATES

by: C. Michael Gillam, P.E.

Edward E. Gilcrease, Jr., P.E.

May 20, 1993

Parsons Brinckerhoff Quade & Douglas, Inc.

If maglev systems are to be commercially and economically viable, they will have to access the centers of major metropolitan areas. The focus of this study was to investigate the feasibility of using existing railroad rights-of-way to access center-city terminals, in one of three possible methods:

- maglev vehicles traveling over existing railroad tracks with the use of steel guide wheels and some means of exterior propulsion (e.g. locomotive power.) A modification of this alternative would be to construct a "dual-mode" (or "at-grade") guideway, essentially a maglev guideway outfitted with standard rails at gauge;
- maglev vehicles transferring onto modified railroad flatcars (i.e., in "piggyback" fashion) and transported over existing railroad tracks with locomotive power; or
- constructing new grade-separated maglev guideways on existing railroad rights-of-way, either in an exclusive or shared right-of-way configuration.

As a result of using existing railroad corridors, certain mandated horizontal and vertical clearance requirements must be met. AREA clearance requirements were compared with those used by Amtrak for unrestricted operation on its nationwide system, with the finding that Amtrak clearance requirements were the most restrictive. This information was used to prepare a total of three summary clearance diagrams for maglev equipment. Because the Eastern U.S. Summary Clearance Diagram more correctly addresses the high platform station configuration, and high platforms are assumed for maglev operations (low platforms would necessitate a longer station dwell time), this diagram was used to assess the compatibility of present and planned maglev technologies with existing railroad infrastructure around the country.

The present and planned maglev technologies investigated include:

- Grumman "New York State" (Configuration 002) Maglev
- Transrapid Intercity (Transrapid 07) Maglev
- HSST Passive Intermediate Speed (HSST-300) Maglev
- Japan Railways Vertical Magnet (Configuration MLU 002) Maglev

Each of the four maglev technologies were superimposed upon the Eastern U.S. Summary Clearance Diagram in two

different modes of transportation - the "piggyback" and the "at-grade" modes. Their impacts upon the clearance diagram were evaluated, and advantages and disadvantages of each transportation mode were discussed.

The results of this preliminary feasibility analysis for the four maglev technologies and the two transportation modes were summarized with the finding that both the JR MLU 002 and the HSST-300 systems fit within the required clearance diagram. Both the HSST-300 and JR MLU 002 maglevs appear to be feasible in the "piggyback" mode, but only the JR MLU 002 might possibly work in the "at-grade" mode. The JR design has the significant advantage of being able, with minor modification, to run on existing rails on its own or to be accommodated on board a rail car carrier, but its development is at least ten years away and very little information was available during the course of the study on which to base meaningful conclusions.

At this time, the required clearance envelope for unrestricted operation on existing railroad corridors in the United States precludes use of the Grumman and Transrapid maglev systems in either the at-grade or piggyback modes due to their excessive width and wrap-around body designs. However, further investigation of individual corridors in the United States could identify facility and/or operational modifications that would permit use of these wider technologies to gain access to center city terminals.

As a result of the above discussion, the HSST-300 maglev technology was carried forward in this study for the investigation of a maglev-rail car carrier intermodal concept.

The maglev-rail car carrier intermodal concept would allow the selected HSST-300 maglev to transition from the high-speed maglev guideway to a modified rail car carrier for transport over existing corridors into center city terminals. Obviously, this transition location would be as close as possible to the terminal to minimize the travel time in the "piggyback" mode. This investigation showed that this transition process is technically feasible and can be achieved within a four-to-five minute time span with little or no passenger disruption. However, if this intermodal concept is furthered as a means of accelerating maglev implementation in the U.S., much more work would be necessary.

To assess the feasibility of maglev systems accessing existing center city terminals in the United States, information on 15 selected cities was reviewed. These cities anchor major metropolitan areas in some of the most heavily travelled transportation corridors on the west coast, midwest and east coast, and were thought to be good

candidates for some type of high speed guided ground transportation in the future. Special attention was paid to:

- the presence and location of existing transportation terminals and their effectiveness in serving the needs of the individual metropolitan area;
- the physical characteristics of the transportation corridors which serve those terminals;
- characteristics of adjacent land uses, and any proposed modifications;
- plans for major capital investment in transportation facilities (e.g., transit systems, multimodal facilities, major rehabilitation, etc.);
- restrictive horizontal and vertical curvature and clearances;
- length and height of existing station platforms and the presence of platform gaps;
- characteristics of current operating equipment;
- presence of electrification and power pickup arrangements; and,
- present and future interfaces with other transportation modes.

The individual urban areas were described in terms of their existing transportation infrastructure and future transportation plans and the feasibility of implementing maglev systems in these areas was assessed. In assessing these individual urban areas, certain assumptions regarding the viability of certain corridors which access the central business districts were made. Much of the proposed corridor discussion assumes the shared use of existing railroad right-of-way, an important component of any future high speed transportation network. Any proposed alignments that are addressed assumes acceptance of this shared right-of-way concept, and have not been discussed with the asset owners, adjacent land owners, city residents, environmental groups or appointed/ elected officials in the individual urban areas. Following are recommendations for those individual urban areas.

San Francisco

The existing CalTrain terminal at 4th and Townsend Streets does not serve the central business district (CBD) well, as it is geographically distant and has limited intermodal capability. This deficiency is being addressed in the study for a possible new terminal, but the construction cost estimate for either of the three alternatives may delay implementation of this worthwhile project. In an associated matter, the planned alignment for this terminal relocation project would severely constrain speeds into and out of the CBD. Should the proposed terminal project be delayed, an alternative location for a terminal station could be at the San Francisco International Airport. The CalTrain corridor to San Jose is well suited, for the most part, for higher speed operation. Numerous grade crossings

would require separation and some curve smoothing would be desirable.

Los Angeles

Los Angeles Union Passenger Terminal (LAUPT) is centrally located in downtown Los Angeles and is fast becoming a true intermodal terminal. As such, it deserves further consideration as a future high speed transportation terminal. The access into and out of LAUPT is rather circuitous and would have to be improved for a future high speed (HS) system. One question to be addressed in the near future will be LAUPT's ability to absorb future HS activity along with its present and proposed operations. The Southern Pacific Transportation Company (SPTC) San Fernando corridor appears to be rather well suited for higher speed operation, but has numerous grade crossings that would require separation in some fashion.

San Diego

The old Santa Fe Depot is well located within downtown San Diego, and is also becoming a true intermodal terminal. The railroad corridor which accesses the terminal from the north is constrained by existing land use and topographical features, consequently speeds would have to be adjusted accordingly. North of State Highway 52, the Interstate 5 alignment should be followed until the railroad corridor once again parallels Interstate 5.

St. Louis

The city appears to be furthering a planned intermodal facility just west of Union Station, however, a re-examination of the Union Station site should be made. The old terminal has undergone a dramatic renovation and has a tremendous unused capacity for additional transportation infrastructure. Using Union Station as the future intermodal terminal would also negate the need for an additional Metro Link station at Jefferson Avenue. If possible, the existing MacArthur Bridge should be used to cross the Mississippi River.

Chicago

Chicago Union Station (CUS) appears to be a natural choice for a future maglev terminal. There are no major physical restrictions, an extensive station renovation is being completed and the proposed Central Area Circulator project would provide easier interface with other activity centers and transportation modes. The SPTC/Amtrak/Santa Fe corridor which parallels the DesPlaines River appears to be well suited for higher speed technology. One area requiring further study would be the corridor's intersection with Conrail/Norfolk Southern (NS) trackage just south of the Chicago River. CUS' ability to absorb additional transportation operations would also require study.

Cleveland

The existing infrastructure and ambitious plans for Tower City Terminal make the terminal the restored focal point for intermodal transportation in Cleveland. The railroad alignments necessary for access to the terminal are more circuitous and will require extensive speed restriction. One primary focus of future study should be the improvement of these corridors for higher speed operation.

Buffalo

The existing Exchange Street Station is in a prime location to serve as a future maglev terminal. Its intermodal transportation capability is well documented, however, run-through flexibility should be improved. This improvement may be possible west of the station by constructing a southbound connection to the existing lakefront trackage which parallels State Highway 5.

Rochester

The existing intercity rail terminal in Rochester is in a fair location and could serve as a future maglev terminal. However, the trackage accessing the terminal from both the east and west has some constraining curvature and should be straightened if at all possible. Additional investigation into alternative terminal locations should occur at some future time.

Syracuse

Officials in Syracuse have recognized the inability of their existing rail terminal to serve as a future intermodal terminal and have initiated studies for a new site. However, there are some reservations about the location of the proposed Park Street site with respect to its proximity to downtown and Syracuse University. The possibility of sharing the Interstate 690 right-of-way north of downtown and reusing the old New York Central terminal should be re-examined.

Albany

It would be possible to have the maglev terminal in Rensselaer, which has adequate bus and taxi connections into the greater Albany area. However, other locations for an intermodal terminal are being discussed and it is too soon to tell if any of these garner support. Another issue which will impact the decision is the proposal to link a future intermodal terminal in Rensselaer with an extensive Riverfront development. For the most part, the corridor running through Albany / Rensselaer is suitable for higher speed operation.

New York City

Penn Station is the intermodal terminal facility in New York City and is undergoing an extensive improvement project. However, there are some problems in using

this terminal as a future maglev station. First, the tunnels under the Hudson and East Rivers are very narrow and would not allow wider equipment without modification. Second, Penn Station suffers today from the lack of operational capacity. Lastly, trains accessing Penn Station from the north must travel the Westside Connection which includes a very constrained curvature as it approaches the station. All of these issues must be addressed adequately before Penn Station could be used as a future maglev station. If maglev access into Penn Station is not possible for some reason, an alternative transfer station outside the city would have to be evaluated.

Pittsburgh

Penn Station is centrally located and could serve as a future maglev station. However, the hilly topography of the metropolitan area creates a difficult climate for high speed operation. Curves are tight and grades are steep and maglev (or other high speed technology) would have to overcome these with expensive structures and bridges.

Philadelphia

The 30th Street Station is ideally situated for use as a future maglev terminal. It is truly an intermodal facility and appears to have adequate capacity for additional transportation infrastructure. Obviously, the Northeast Corridor is perhaps the best corridor in the nation for further high speed improvements.

Boston

The intermodality and commercial activity present at the South Station Transportation Center, coupled with on-going improvements on the New Haven to Boston corridor, makes this an ideal location for a future maglev terminal.

Washington, D.C.

The unique mix of transportation modes, commercial activity and the relatively high speed Northeast Corridor makes Union Station the likely candidate for a future maglev terminal in Washington, D.C.

AUTHOR INDEX

END

DATE FILMED

11/12/93